

# FINAL REPORT

## A Chromium-Free Coating System for DoD Applications

SERDP Project WP-1341

MAY 2008

Dr. Wim J. van Ooij  
**University of Cincinnati**

This document has been approved for public release.



Strategic Environmental Research and  
Development Program

This report was prepared under contract to the Department of Defense Strategic Environmental Research and Development Program (SERDP). The publication of this report does not indicate endorsement by the Department of Defense, nor should the contents be construed as reflecting the official policy or position of the Department of Defense. Reference herein to any specific commercial product, process, or service by trade name, trademark, manufacturer, or otherwise, does not necessarily constitute or imply its endorsement, recommendation, or favoring by the Department of Defense.

**REPORT DOCUMENTATION PAGE**

*Form Approved  
OMB No. 0704-0188*

The public reporting burden for this collection of information is estimated to average 1 hour per response, including the time for reviewing instructions, searching existing data sources, gathering and maintaining the data needed, and completing and reviewing the collection of information. Send comments regarding this burden estimate or any other aspect of this collection of information, including suggestions for reducing the burden, to the Department of Defense, Executive Services and Communications Directorate (0704-0188). Respondents should be aware that notwithstanding any other provision of law, no person shall be subject to any penalty for failing to comply with a collection of information if it does not display a currently valid OMB control number.

**PLEASE DO NOT RETURN YOUR FORM TO THE ABOVE ORGANIZATION.**

<b>1. REPORT DATE (DD-MM-YYYY)</b> 30-01-2008	<b>2. REPORT TYPE</b> Final	<b>3. DATES COVERED (From - To)</b> SEP 2003 - JAN 2008
--	--------------------------------	--

<b>4. TITLE AND SUBTITLE</b>  Chromium-free Coating System for DoD Applications	<b>5a. CONTRACT NUMBER</b> DACA72-03-C-0019
	<b>5b. GRANT NUMBER</b> G100346-7200300000-1-1002189
	<b>5c. PROGRAM ELEMENT NUMBER</b>

<b>6. AUTHOR(S)</b>  van Ooij, Wim, Ph.D.	<b>5d. PROJECT NUMBER</b> WP-1341
	<b>5e. TASK NUMBER</b>
	<b>5f. WORK UNIT NUMBER</b>

<b>7. PERFORMING ORGANIZATION NAME(S) AND ADDRESS(ES)</b> University of Cincinnati Office of Sponsored Research Services 51 Goodman Drive, PO Box 21022, Cincinnati, OH 45221-0222	<b>8. PERFORMING ORGANIZATION REPORT NUMBER</b>
---	---

<b>9. SPONSORING/MONITORING AGENCY NAME(S) AND ADDRESS(ES)</b> USACE, HUMPHREYS ENGR CTR SPT ACTIVITY ATTN: CEHEC-CT 7701 Telegraph Road Alexandria VA 22315-3660	<b>10. SPONSOR/MONITOR'S ACRONYM(S)</b> USACE
	<b>11. SPONSOR/MONITOR'S REPORT NUMBER(S)</b>

**12. DISTRIBUTION/AVAILABILITY STATEMENT**

**13. SUPPLEMENTARY NOTES**

**14. ABSTRACT**

Several water-borne primer systems have been developed which can be applied on aluminium, hot-dip galvanized steel or cold-rolled steel. These primers do not require a metal pretreatment. They contain novel anti-corrosion pigments. Thus, they are completely chromium-free and have reduced VOC.

**15. SUBJECT TERMS**

coatings, adhesion, corrosion, silanes, aerospace, automotive.

<b>16. SECURITY CLASSIFICATION OF:</b>			<b>17. LIMITATION OF ABSTRACT</b>	<b>18. NUMBER OF PAGES</b> 1050	<b>19a. NAME OF RESPONSIBLE PERSON</b> W. J. van Ooij
<b>a. REPORT</b>	<b>b. ABSTRACT</b>	<b>c. THIS PAGE</b>			<b>19b. TELEPHONE NUMBER (Include area code)</b> 513-556-3194

# Table of Contents

<b>I.</b>	Cover Page	
<b>II.</b>	Contents	
<b>III.</b>	Acknowledgements	
<b>IV.</b>	Executive Summary	
<b>V.</b>	Objectives	
<b>VI.</b>	Background	
<b>VII.</b>	Materials and Methods	
	Introduction .....	1-3
	(A) Primers for CRS .....	3-9
	(B) Primer for HDG .....	9-12
	(C) Environmentally-Compliant Novolac Superprimers for Corrosion Protection of Aluminum Alloys .....	12-15
	(D) Epoxy-Acrylate Primer for Al Alloys .....	16-21
	(E) Neutron and X-Ray Reflectivity Characterization .....	21-29
<b>VIII.</b>	Results and Accomplishments	
	(A) Primers for CRS.....	30-64
	(B) Primer for HDG .....	65-81
	(C) Environmentally-Compliant Novolac Superprimers for Corrosion Protection of Aluminum Alloys .....	82-92
	(D) Epoxy-Acrylate Primer for Al Alloys .....	93-113
	(E) Packing Studies of the SERDP Primers; Novolac-Epoxy and Epoxy .....	114-130
	(F) Effect of Surface Cleaning on Silane/Primer Performance on CRS .....	131-138
	(G) Potential of Electrodeposition of Epoxy-Acrylate Primer .....	139-146
	(H) Silane and Primer Film Studies by Neutron and X-Ray Reflectivity Studies .....	147-178
<b>IX.</b>	Conclusions	
	<b>Appendix</b>	
<b>X.</b>	Supporting Data	
<b>XI.</b>	Technical Publications	
<b>XII.</b>	Other Technical Material	

## List of Tables

Table 8.1 List of Silanes used with trade names and chemical formulas	4
Table 8.2 Resins used in superprimer formulations	4
Table 8.3 Particles used in superprimer formulations	5
Table 8.4 Corrosion inhibitors used in the superprimer formulations	6
Table 8.5 Resins and compatible silanes	7
Table 8.6 The specific data of the epoxy dispersion used in the superprimer formulations	9
Table 8.7 Summary of the chemicals used in the development of the superprimer for HDG steel	11
Table 8.8 Properties of different superprimers	14
Table 8.9(a) Materials and the identity of the acrylic-epoxy based superprimer formulations	16
Table 8.9(b) Sources of chemicals	16
Table 8.10 Calculated neutron scattering length density (SLD) for the materials used in this study	23
Table 8.17 Formulation of epoxy-silane anticorrosion coating system	28
Table A.1 Comparison of performance of test results between control PRC Desoto MIL PRF and Superprimer formulation F	30
Table A.2 Summary of test results of the control, F-6 and F	34
Table A.3 Formulation chart of modified superprimers with particles/inhibitors	36
Table B.1 The specific data of the epoxy dispersion used in the superprimer formulations	65
Table B.2 Summary of the chemicals used in the development of the superprimer for HDG steel	66
Table B.3 Starting point recipe for the development of a functional superprimer for HDG steel	66
Table B.4 The controls and the formulations containing inhibitors	72
Table B.5 Chlorine and inhibiting atom concentrations in the scribed region of various scribed superprimer films on HDG exposed for 30 days in 3.5 wt% salt water	72
Table C.1 Properties of NP-1 formulations	91
Table E.1 Novolac-epoxy recipe used for packing study	114
Table E.2 Second set of packs of the novolac-epoxy primer	115
Table E.3 The two-pack novolac-epoxy system chosen for the third step of the packing study	116
Table E.4 Test results of the original draw-down applied primer coating on AA2024	116
Table E.5 Recipe for epoxy primer for HDG steel	117
Table E.6 Second set of packs of the epoxy primer	117
Table E.7 The three-pack epoxy system chosen for the third step of the packing study	118
Table E.8 Test results of epoxy primed panels prepared in different ways	119
Table E.9 MEK-double rub test results of different samples prepared from packs and sprayed onto AA2024	121

Table E.10 The recipe of NP-1 without and with zinc phosphate	122
Table E.11 Novolac-epoxy primers with DBTL	122
Table E.12 MEK-double rub results of different samples	123
Table E.13 Dry and wet adhesion test results of topcoated samples, novolac-epoxy primer on AA2024	124
Table E.14 MEK-double rub test results of differently cured novolac-epoxy primed samples	124
Table E.15 Example of the logic of the sample names	125
Table E.16 MEK double rub and adhesion test results for primed panels without topcoat	125
Table E.17 Adhesion test results for primed panels with topcoat	125
Table E.18 The larger scale packing study has been initiated by using the following pack system	126
Table E.19 The schedule of this study	127
Table E.20 Test results of epoxy primed HDG samples sprayed from 2 month old packs and cured differently	127
Table E.21 Recipe of the novolac-epoxy primer divided in packs	127

## List of Figures

Figure 8.11 Neutron reflectivity data of bis-amino silane exposed to d-NB	24
Figure 8.12 SLD profile of bis-amino silane when exposed to d-NB	24
Figure 8.13 C NMR spectra of AV3.4 mixture, neat bis-amino silane and neat VTAS	25
Figure 8.14 Primary reaction in neat bis-aminosilane and VTAS mixture	26
Figure 8.15 Si NMR spectrum of neat AV mixture in -75 to -40 ppm range	27
Figure 8.16 SLD profile of bis-amino silane under water conditioning at room temperature	27
Figure A.1 Aluminum panel coated with the PRC Desoto MIL-PRF yellow primer from military	31
Figure A.2 EIS Bode plot of formulation F coated on a CRS substrate and tested for 4 days	31
Figure A.3 EIS Bode plot of control PRC Desoto MIL PRF chromate-containing primer coated on a CRS substrate and tested for 4 days	32
Figure A.4 EIS Bode plot comparing the curves of F-6, F and the control Desoto PRC MIL PRF	33
Figure A.5 Salt spray result of F-6 after 2 weeks	34
Figure A.6 Impedance plots of bis-sulfur silane treated AA2024-T3 systems loaded with different amounts of silica nano-particles	38
Figure A.7 Salt immersion test after 7 days	39
Figure A.8 EIS impedance values of salt fog tested coatings with time	40
Figure A.9 EIS impedance values of salt fog tested coating with time of coating formulations containing alumina and with polyurethane topcoat	40
Figure A.10 Bode plot of F 10 without and with topcoat	41
Figure A.11 Bode plot of F 11 without and with topcoat	42
Figure A.12 Bode plot of F 12 without and with topcoat	43
Figure A.13 Salt spray results of F 10, F 11 and F 12 with and without topcoats after 3 weeks	44
Figure A.14 Salt fog test performance of F 28 after 0, 7 and 28 days	46
Figure A.15 Change in impedance values of F 28 coating with exposure time	47
Figure A.16 EIS impedance values of coating formulations F 13, F 14 and F 15 after being exposed to salt fog	49
Figure A.17 EIS Bode plots for 6 weeks of immersion of F 13, F 14 and F 15	51
Figure A.18 Salt spray results of formulations F13, F14 and F15 with and without topcoat after 6 weeks of testing	52
Figure A.19 Change in EIS impedance value of the coating formulations F20, F21, F24 and F25 with and without topcoat, after exposed to salt fog	53
Figure A.20 Salt spray test results of formulations F20, F21, F22, F24 and F25 without topcoats after 28 days of testing	53

Figure A.21 42 days EIS result for formulation with 40% zinc and 60% superprimer	55
Figure A.22 42 days EIS result for formulation with 70% zinc and 30% superprimer	56
Figure A.23 The salt spray result after 3 weeks of both 40% and 80% zinc formulations	56
Figure A.24 Comparison of the 6 week EIS result of a commercial chromate containing primer from carbozinc and zinc-rich superprimer	57
Figure A.25 500 hours salt fog result of commercial and zinc-rich superprimer	59
Figure A.26 200 hours salt fog result of zinc-rich primers with polyamide topcoat	59
Figure A.27 Zone 1 area in the scribe before immersion	61
Figure A.28 Zone 2 coated area before immersion	62
Figure A.29 Analysis over zone 2 with coated surface after immersion	63
Figure A.30 Zone 1 in the scribe after immersion	64
Figure B.1 Concept of the superprimer system	67
Figure B.2 Silanes used in the superprimer formulations	68
Figure B.3 ASTM B117 images of the three formulations compared to the starting point formulation F6	69
Figure B.4 Comparison of Bode plots of coatings with and without bis-benzene on day 10 of exposure to 3.5 wt% salt water	71
Figure B.5 IR spectra of superprimer films showing the effect of incorporation of the silanes bis-benzene and bis-sulfur	74
Figure B.6 The same IR spectra detailing the siloxane peak region	75
Figure B.7 The control and the best performing pigment containing coating	76
Figure B.8(a) SEM image of scribe – effect of 10% CZM	77
Figure B.8(b) EDX spectrum at the point in the scribe highlighted in figure B.8(a)	78
Figure B.9(a) SEM image of scribe – effect of 15% CZM	79
Figure B.9(b) EDX spectrum at the point in the scribe highlighted in figure B.9(a)	80
Figure C.1 Samples after salt water immersion for 30 days	83
Figure C.2 Samples after salt water immersion for immersion for 30 days	84
Figure C.3 EIS impedance data for novolac coatings	85
Figure C.4 Samples exposed in salt fog test	86
Figure C.5 Comparison of superprimer coatings and control exposed in salt fog test after 2000 hours	87
Figure C.6 Superprimer coating samples after subjected to bend test	88
Figure C.7 Scribe protection analysis of novolac superprimer using SEM/EDS	90
Figure C.8 Cross-sectional analysis of novolac superprimer using SEM/EDS	92
Figure D.1 Epoxy acrylate superprimer coating on AA2024 after 3500 hours of exposure to ASTM B117	94
Figure D.2 Epoxy-Acrylate superprimer coating on AA2024 after 317 days of Florida outdoor	

exposure	95
Figure D.3 Epoxy-acrylate superprimer with organic colorant added after 1000 hours of exposure in ASTM B117	102
Figure D.4 EIS measured during salt spray test (1000 hours)	103
Figure D.5 Contact angle changes during 1000 hours of salt spray test	103
Figure D.6 Setup of leaching-out experiment	109
Figure D.7 Leaching-out rate of Zn and P from superprimer coating, measured by ICP-MS	110
Figure D.8 Al <sub>2</sub> CuMg intermetallics in AA2024 with pitting after exposure to NaCl	111
Figure D.9 ToF-SIMS of bare AA2024 panels immersed in saturated zinc phosphate solution	111
Figure D.10(a) Scribe after exposure to 90 days of salt spray test	113
Figure D.10(b) Analysis of different area in the scribe by EDAX	113
Figure E.1 About 11 weeks of salt water immersion test results of novolac-epoxy primed AA2024 sprayed from fresh packs	119
Figure E.2 1536 hours of salt spray test results of novolac-epoxy primed AA2024 sprayed from fresh packs	120
Figure E.3 Generic structure of novolac epoxy resin	128
Figure E.4 The Epoxy-novolac based primer coating	128
Figure E.5 Samples after bend test and exposure to 3.5 wt% NaCl for 30 days	129
Figure E.6 Low Frequency impedance values of the inhibitor containing coatings measured during the exposure of these coatings in ASTM B117 salt spray test	129
Figure E.7 2000 hours of ASTM B117 salt spray exposure of the topcoated	130
Figure F.1 Etching effects of CRS by weight loss and ICP-MS measurements after cleaning at different pH values	131
Figure F.2 Surface morphology of CRS after cleaning at different pHs	132
Figure F.3 Calculated polar and dispersive components of as-cleaned CRS surface cleaned in different pH conditions based on contact angle measurements	133
Figure F.4 Schematic diagram of the mechanism of AV silane absorption onto CRS	134
Figure F.5 FTIR spectra of the 0.3 wt% AV silane coated CRS after curing at 100C for 60 minutes	135
Figure F.6 DC potentiodynamic curves	136
Figure F.7 EIS results of primer-coated CRS	137
Figure G.1 Thickness of the dip-coated coatings as a function of water content in the primer	139
Figure G.2 Samples prepared from the primers containing different contents of water after salt immersion test	139
Figure G.3 Water contact angle of the dip-coated coatings	140
Figure G.4 Variation of deposition voltage during cathodic electrodeposition at 30 mA	141
Figure G.5 Variation of deposition voltage during anodic electrodeposition at 30 mA	141

Figure G.6 Variation of deposition voltage and deposition current during anodic electrodeposition at 300 mA	142
Figure G.7 Stable deposition voltage as a function of deposition current when deposition current is below 100 mA	143
Figure G.8 Thickness of the coatings as a function of deposition current	143
Figure G.9 Samples electrodeposited at different currents after immersion test	144
Figure G.10 Water contact angle of the coatings as a function of deposition current	145
Figure G.11 Pencil hardness of the coating as a function of deposition current	145
Figure H.4 SLD profile of bis-amino silane under 80C water conditioning	148
Figure H.5 Scattering length density profiles of bis-sulfur silane films	148
Figure H.7 Refractive index of bis-sulfur silane	148
Figure H.6 SLD profile of mixed silane	149
Figure H.8(a) Reflectivity curves of bis-amino silane on silicon wafer dry	150
Figure H.8(b) SLD profiles corresponding to the reflectivity curves	150
Figure H.9 Best-fit SLD profiles of bis-sulfur silane film and bis-amino silane film	151
Figure H.10 Vapor-conditioning results for thick bis-sulfur silane films	152
Figure H.11 SLD profiles of thick bis-amino silane films	152
Figure H.12 Aging results for thin and thick bis-amino films	153
Figure H.13 Neutron reflectivity data from thick bis-sulfur silane	154
Figure H.14 Reflectivity data from thick bis-sulfur silane	154
Figure H.15 Neutron reflectivity data from thin bis-sulfur silane	155
Figure H.16 Reflectivity and SLD profile for thick mixed silane films	156
Figure H.17 Water penetration kinetic of bis-amino silane coatings	157
Figure H.19 The heavy water adsorption in the bis-sulfur silane film as a function of conditioning time	158
Figure H.20 Thickness increase of the bis-sulfur silane film as a function of water conditioning time	158
Figure H.21 IR spectra of the bis-amino silane film in as-prepared state and at equilibrium	159
Figure H.22 Normalized relative reflectance intensity of bis-amino silane	159
Figure H.23 IR spectra of the bis-sulfur film in as-prepared state and at equilibrium	159
Figure H.24 Normalized relative reflectance intensity of bis-sulfur silane	159
Figure H.28 C spectra of the neat AV3.4 mixture and 10 wt% AV3.4 water solution	162
Figure H.30 Possible reactions in the AV3.4 water solution	163
Figure H.31 Si NMR spectra after different aging times	164
Figure H.32 The Surface morphology of CRS after cleaning at different pHs	165
Figure H.33 Calculated polar and dispersive surface energy components	166
Figure H.34 Schematic diagram of the mechanism of AV silane adsorption on CRS	166
Figure H.35 DC potentiodynamic curves	167

Figure H.36 EIS results of primer-coated CRS	168
Figure H.38 X-Ray reflectivity and SLD profiles of the as-prepared AV films	169
Figure H.37 NR results showing the water response of AV mixtures with A/V ratios	170
Figure H.39 Scattering from the bulk film	171
Figure H.40 Neutron reflectivity data and best-fit SLD profiles of mixture	173
Figure H.41 D2O water vapor conditioning at room temperature	173
Figure H.42 Kinetic water uptake under saturated D2O vapor conditioning	174
Figure H.43 Liquid water contact conditioning	175
Figure H.44 Re-Dry state	175
Figure H.45 Aging of pure epoxy sample	176
Figure H.46 Aging of epoxy-silane sample	177
Figure H.47 SLD profiles of salt exclusion experiments on pure epoxy coating	177
Figure H.48 SLD profiles of salt exclusion experiments on epoxy-silane mixed coating	177

### **III. ACKNOWLEDGMENTS**

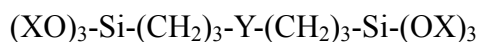
1. Prasan Harakuni, for running TOFSIMS spectra
2. Ohio Board of Regents (Columbus, Ohio) for matching funding
3. Nivin Mohamed Hussein for choosing this topic during her stay in Cincinnati
4. National Research Council (NRC) in Cairo, Egypt, for funding Nivin
5. Joel Johnson at the WP-AFB in Dayton, OH, for testing some of our coatings
6. Tammy Metroke of the University of Oklahoma for her help in obtaining the NMR data
7. Doug Kohls of the University of Cincinnati for his discussions
8. Jaraslaw Majewski, Erik Watkins and Hillary Smith of LANL for their help in acquiring the neutron and X-ray data
9. Jan Ilavsky and Byeongdu Lee at Argonne National Lab for their help in obtaining neutron and X-ray data
10. William Hamilton at ORNL for his help with the beam line
11. Michael Kent and Hyun Yim at Sandia National Labs for their help in acquiring the neutron data
12. Sushil Satija and Young-Soo Seo of NIST for their support
13. SERDP for providing the financial support for the project

## IV. EXECUTIVE SUMMARY OF WP1341, A CHROMATE-FREE PRIMER SYSTEM FOR DoD APPLICATIONS

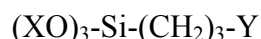
### Introduction

The objective of this project was to develop and test one or more primer systems that can be used on metals of interest to DoD, such as aluminum alloys, hot-dip galvanized steel (HDG) and cold-rolled steel (CRS). Primers are used as a basis for final paint systems on such metals. The corrosion protection of a painted metal comes primarily from the primer and not from the topcoat or the metal pretreatment under the primer. Therefore, the primer is a very important part of the integral paint system on a metal. Currently used primers contain organic solvents, chromate anti-corrosion pigments and other undesirable components from an environmental standpoint. Thus, our intent was to develop a number of primer systems that were largely water-based and did not contain anti-corrosion pigments based on chromates. Since such anti-corrosion pigments are not readily available, we had to invent and develop some new pigments that are compatible with the proposed primers. Such pigments are different for the different metals on which the primer is applied.

The basis of our proposed primer is the experience that we had developed at the University of Cincinnati in the period 1994-2000 with the use of organofunctional silanes for the corrosion protection of metals. Our group has pioneered such applications and we have filed many external publications and patents applications on this topic in that period. Especially bis-silanes (or dipodal silanes) of the type:



where Y is an organic group, were shown by us to be more effective for corrosion protection purposes than the more widely known mono-silanes of the type:



Such silanes were used as *pretreatments*, i.e., not as primers. In earlier work (an AFOSR MURI project) we have demonstrated that silane pretreatments can successfully replace the chromate pretreatment prior to priming a metal. In that project we achieved, for the first time, a 1000-h B-117 (salt spray test) resistance with a system that consisted of a silane pretreatment and a solvent-borne commercial chromate-free primer to which an experimental anti-corrosion pigment had been added. It was further demonstrated in that work that the function of the metal pretreatment (chromating for aluminum and HDG; phosphating for HDG and CRS) is primarily to improve the adhesion of the primer to the metal. The corrosion resistance of the painted metal stems from the activity of the anti-corrosion pigment (largely chromate) in the primer and from the adhesion between the pretreatment and the primer, *not* from the presence of chromate (or phosphate) in the pretreatment. The amount of chromate in the primer is about 1,000 times that in the pretreatment.

In the WP1341 project we used this finding and knowledge as a basis. The underlying idea in the project was to combine the silane metal pretreatment with the primer, resulting in a one-step primer in which the adhesion to the substrate is assured by the silane in the primer. Primers containing rather large amounts of silanes are not available commercially, thus they had to be developed by us from scratch. We termed such primers superprimers, because of their dual function. Although the initial objective, strictly speaking, was only to develop novel primer primers for DoD applications that were chromate-free (based on the relevant SERDP Statement-of-Need, SON, at the time), we extended this objective so as to include low VOC (i.e., water-borne), and containing effective chromate-replacing anti-corrosion pigments

Thus, in summary, we set out to develop one or more novel, anti-corrosion primers with the following characteristics.

- Basically consist of water-borne resin systems to which relatively large amounts of bis-silanes are added, which function as adhesion promoters to the substrate and crosslinkers for the resins
- Have low VOC (e.g., <100 g/L)
- Contain an effective, Cr-free anti-corrosion pigment
- Contain, optionally, additional additives such as nanoparticles, film formers, colorants, viscosity controllers, crosslinkers
- Contain no HAPs
- Can be applied on bare, i.e., cleaned-only, metal substrates, but should also work on pretreated metals
- Can be applied by all industrial techniques such as dipping, roll-coating, flow-coating, squeegee, draw-down bar, or spraying
- Work on more than one metal (with appropriate adjustment of the pigmentation system)
- Cures at room temperature (for use on Al) or at elevated temperatures for use on HDG and CRS
- Can be topcoated in about 6 hours (for use on Al with room-temperature cure)
- Should have good topcoat adhesion, both dry and wet
- Have the same or better corrosion performance as currently used solvent-based chromate-containing primers in combination with the standard chromate (or phosphate) pretreatment; target performances were resistance in the B-117 salt spray test of the primer only of 2000 hours for Al alloys, 1000 hours for HDG and 500 hours for CRS

### **Organization of the Project**

The organization of the project was as follows.

The PI (Wim van Ooij) led a group of graduate students at the University of Cincinnati who were each assigned a metal substrate for which to design and thoroughly test a primer for. The water-borne resin systems could be chosen from aqueous epoxy, acrylate, polyurethane dispersions or mixtures of one or more resins. The co-PI (Dale Schaefer) led another group which was responsible for the scientific evaluation of the silanes used and subsequently of model systems consisting of films of silanes and resins. This group used techniques such as neutron and X-ray scattering to determine water uptake and other properties of the films. The third group was

led by Guy Davis at Dacco SCI in Columbia, MD. This laboratory was responsible for exposure testing of candidate coatings by the B-117 and the Ford AGPE test. In addition, localized Electrochemical Impedance Spectroscopy (EIS) was performed while the test panels were being exposed. Finally, this group also exposed a number of coated panels at an outside site in Hawaii and another set in Florida. The table below is a complete listing of all participants in the project. It shows that the project has resulted in 6 PhD/MS theses at the University of Cincinnati, with one more completing in 2008.

## **Results**

As Table 1 shows, we initially worked on individual systems for the metals of DoD interest, but this distinction became more diffuse towards the end of the projects. Further, the system developed by Chetan Shivane for HDG was so complicated and user-unfriendly, that it was dropped before the end of the project. Therefore, the final results includes two different primer formulations - based on different types of resins - and a number of novel, anti-corrosion pigments. However, due to the availability of these pigments, the two systems can be used on almost any metal. Table 2 summarizes the achievements of the project, consisting of two workable superprimer formulations and six anti-corrosion pigments. The details of the formulations will be given in subsequent sections. The possible combinations of resins and pigments result in systems that can be used on essentially any metal or alloy of interest.

The observed performance and other achievements of the project are summarized in the list below.

- All chemicals used are commercially available, except for some of the pigments, which have to be synthesized
- The pot life of all systems is at least 6 hours
- Both primers can be formulated as two component packs with a shelf life of >6 months
- Both primers can be formulated to cure at room temperature in about two weeks, or in few minutes at elevated temperature; the difference is the type and level of curing agent added
- Primer films can be overcoated in about 6 hours
- The best performance obtained is 500 hours B-117 resistance on CRS, 2000 hours on HDG and 4000 hours on AA-2024-T3 and AA7075-T6, all for primers only; the performance with the topcoat was slightly less; in addition 12 months in salt water immersion of primers on AA7075-T6 with a clean scribe was obtained; the performance on CRS was much better in tests with a dry-out cycle included, such as the Ford AGPE test; the B-117 test is unsuited for primed CRS
- Outstanding performance during exposure in Hawaii and Florida was observed (topcoated); initially, films were observed to cure further during outdoor exposure
- It was shown that the SP-1 primer can be deposited by anodic electrodeposition, or a combination of cathodic and anodic electrodeposition; the films thus obtained showed improved corrosion performance as well as greater hardness and MEK values

- A novel test for the evaluation of the effectiveness of anti-corrosion pigments in primers was developed
- A new model for the mechanism of anti-corrosion pigments in primers on aluminum alloys was developed
- All silane films and silane-laced epoxy films absorb water. In most cases, the water uniformly occupies the bulk of the film. The bridging group controls the amount of water in the film. Bis silane films are the most hydrophobic
- The substrate does not play a key role for the water barrier properties of silanes
- Two absorption modes are observed: Henry's mode, which is related to the relaxation of the siloxane network and Langmuir's mode, which is related to the physical occupation of pre-existing free space. Langmuir absorption mode dominates the total absorption
- At elevated temperature, water conditioning leads to chemical reactions for all films studied. Bis-amino silane films show monotonic degradation. For bis-sulfur films, further condensation takes place, which improves the protective character. Pure bis-sulfur films above 1000 Å are robust
- Mixed silane films show unusual cure chemistry. The primary reaction in neat bis-amino-VTAS silane mixtures is the exchange of the hydrogen atom on secondary amine group of bis-amino silane with the acetoxy group of VTAS forming an amide complex and hydrolyzed VTAS. The primary reaction is followed by a series of hydrolysis and condensation reactions of bis-amino silane and VTAS and their reaction by-products
- The epoxy-silane mixed coating system has a layered structure. Silane is rich at the film-substrate interface and forms a highly condensed, hydrophobic interface. This interface accounts for the good adhesion and barrier properties of epoxy-silane coating system
- The condensed silane-rich interfacial layer in the epoxy-silane system is robust in a hydrothermal environment, whereas the bulk of the film is not. This result supports the idea that this special layer plays a key role of anti corrosion protection
- The presence of silane in an epoxy film leads to the exclusion of salt. This observation seems to be the most important factor accounting for the improved protection of silane-laced films
- Cleaning is critical to performance. The best performance results were obtained for the silane-coated and primer-coated CRS panels cleaned near the isoelectric point where the surface oxide is dense and spherical with the highest surface FeOOH/Fe<sub>2</sub>O<sub>3</sub> ratio. The nearly neutral surface, promotes hydrogen bonding of both silanols and secondary amine groups to the CRS surface.

### **Potential Applications and Licensing**

The PI has filed numerous invention disclosures with the University of Cincinnati (UC) on inventions resulting from this project. They have all been licensed to ECOSIL Technologies LLC, a company started by the PI in 2003. ECOSIL is now working with large companies such as PPG, Dow Corning and Sun Chemical on applications and sub-licensing. ECOSIL has production facilities in Fairfield, Ohio, and has recently teamed up with Calvary Industries, a

metal pretreatment company, also located in Fairfield, Ohio. ECOSIL and Calvary will manufacture the superprimer and pigments for industrial applications. One large customer for the superprimer is Wheatland Tube, a large tube manufacturing company in Chicago.

Major applications that we see for the technology developed in the WP1341 project include automobile bodies, automotive components, the coil coating industry and, especially, the aerospace industry

### External Testing of the Superprimers

The primers developed in this project have not yet been tested extensively by external laboratories. In a comparative program by researchers at the Navy in China Lake, CA, a 4000-hr B-117 resistance of some of our panels was reported. It had been anticipated to have the primers tested extensively at UDRI, a contractor for CTIO in Dayton, Ohio. The program was started, but prematurely discontinued because of a budget overrun. No report has been received on the preliminary data obtained. The PI is of the opinion that the most appropriate testing is that of exposure at outdoor sites. Therefore, the exposure at the Florida site, mentioned earlier, will be continued for an additional two years. Based on the results obtained, it will be decided how to develop this technology further for DoD applications. One option will be to submit an ESTCP proposal.

Table 1. Participants in the WP1341 Project

Name	Function	Responsibility and Tasks	Graduated
Wim van Ooij	PI	Guidance on developing formulations	n/a
Dale Schaefer	co-PI	Study mechanisms behind performance	n/a
Guy Davis	co-PI	Testing of candidate primers films	n/a
Trilok Mugada	graduate student	Initial primer for CRS; switched to Al	+
Chetan Shivane	graduate student	Epoxy Primer for HDG	+
Akshay Ashirgade	graduate student	Novolac primer for Al	+
Zhangzhang Yin	graduate student	Develop novel pigment systems for Al	2008
Paula Puomi	postdoctoral asst.	Practical applications including shelf life	n/a
Nivin Mohammed*	visiting scientist	Develop pigments for use on CRS	n/a
Liang Liu**	exchange student	Potential for electrodeposition of primers	n/a
Guirong Pan	graduate student	Characterization of silane films	+
Yimin Wang	graduate student	Characterization of silane films + cleaning	+
Peng Wang	graduate student	Characterization of silane + resin films	+

\* visitor from CRN in Cairo, Egypt in 2007; funded by the Egyptian Government

\*\* exchange visitor from Zhejiang University (Hangzhou, China) in 2007; not funded by the project

Table 2. Products developed or discovered in the WP1341 project

System	Description	Details
SP-1	epoxy-acrylate superprimer	works on Al, HDG and CRS
SP-2	novolac-epoxy superprimer	works on Al and HDG
Zinc phosphate/SiO <sub>2</sub>	pigment for SP-1 and SP-2	commercial, enhanced by SiO <sub>2</sub>
Cerium vanadate	pigment for SP-1	effective for Al and HDG
Cerium metasilicate	pigment SP-1	effective for Al
Cerium-exchanged SiO <sub>2</sub>	pigment for SP-1	very effective for Al
Ca/Mg phosphate on ZnO	pigment for SP	works in SP-1 on CRS
Ca/Zn borosilicate	Pigment	works in SP-1 on CRS

## V. OBJECTIVES

The objectives of the project were:

- To develop anti-corrosion primer systems for metals of interest to DoD that are chromate-free; metal substrates include aerospace aluminum alloys, such as AA2024-T3 and AA7075-T6, hot-dip galvanized steel (HDG) and cold-rolled steel (CRS)
- To develop primers that obviate the need for a chromate - or phosphate - metal pretreatment, i.e., can be applied on metals that are cleaned-only
- To replace the chromate-containing pigments with new pigments that provide equivalent corrosion protection as the currently used systems
- To test some commercial chromate-free pigments and to develop and test new ones
- To study the mechanism by which some of the chromate-free pigments provide corrosion protection
- To lower the VOC of the primer to less than 100 g/L; currently used systems have about 350 g/L, as they are solvent-based
- To study the water and electrolyte resistance of silane films and of films made of silanes mixed with resins; techniques to be used are neutron and X-ray reflectivity

## VI. BACKGROUND

The technology that we have developed in this project addresses the problem of chromate. Hexavalent chromium Cr(VI) is a known carcinogen. It also can cause respiratory and skin problems (dermatitis) to those exposed to it on a regular basis. Cr(VI) is a strictly regulated hazardous contaminant. OSHA has recently issued a new health standard for workplace exposures to Cr(VI) in February 2006. The new permissible exposure limit (PEL) has lowered the US health standard for Cr(VI) in electroplating to 5  $\mu\text{g}/\text{m}^3$ . This limit, already low on a global basis, may be lowered further in the next few years. The primary DoD impact of this PEL will be on the uncontrolled emissions from maintenance operations involving chromated metal and chromate solutions. This applies directly to maintenance operations such as sanding, stripping and painting on parts that have been coated with wash primer formulations. Wash primers are thin organic coatings used as anti-corrosion metal pretreatments. They are often used in situations where a fully blown conversion coating cannot be used due to infrastructure limitations. Wash primers consist of polyvinyl butyral resin, phosphoric acid, chromate and i-propanol.

The primers that we have developed in this project do not replace wash primers. A wash primer is a very thin coating with a limited capability for corrosion protection. They are applied on a direct-to-metal basis, i.e., they are sprayed on the bare, cleaned metal. The wash primer provides temporary corrosion protection and is then overcoated, first with a topcoat or with an epoxy primer followed by a topcoat. In the first case, the desired corrosion protection is not very stringent, as topcoats do not contain corrosion inhibitors. In the second case, the epoxy primer may have a high loading of anti-corrosion pigment such as chromates.

The main uses of chromate, Cr(VI), are: i) chromate solutions for electroplating of hard chromium coatings, ii) pigment such as zinc chromate or strontium chromate in primers, e.g., in aerospace, iii) chromate pretreatments of hot-dip galvanized steel or aluminum alloys. Our project has addressed to eliminate both ii) and iii). Of these two uses of Cr(VI) the amount used in paints as a pigment is about 1000x that of the use in metal pretreatment. That is because anti-corrosion primers can contain up to 30% by weight of chromate pigment. However, the workers are more likely to get in contact with the acid chromate solutions than with the solid pigment used in primers. On the other hand, sanding and tripping operations can lead to inhaling of dust containing chromates. This is one of the reasons why we have focused on the development of systems that can replace both sources of chromate by one process, namely a primer that does not require any metal pretreatment other than cleaning. Our primers do not contain chromate but we have developed replacement pigments that are just as effective as chromates.

## VII. MATERIALS AND METHODS

The materials used in this project were all commercially available. No synthesis of silane or resin molecules of any kind was performed. An exception to this statement was the synthesis of the anti-corrosion pigments cerium-exchanged silica, cerium silicate, Ca/Mg phosphate deposited on ZnO, and Ca/Zn borophosphate. They were all synthesized by mixing the raw materials in the desired ratios, evaporating them to dryness, washing them with DI water and then calcining them. More details are given in section IX, Results and Accomplishments.

The commercially available materials were a limited number of organofunctional silanes (viz., mainly bis-[triethoxy silyl] ethane and bis-[triethoxypropylsilyl] tetrasulfide), water-dispersed resins (epoxies, novolacs, acrylates and polyurethanes were used in this project; they all had about 50% dispersed solids) and optionally a series of additives, such as wetting agents, surfactants, co-solvents (film formers), colorants, curing agents, etc. They varied from system to system. More details can be found in the Results and Accomplishments section.

In addition to these chemicals, metal substrates were purchased, typically of 10 × 15 cm dimensions. They included the aluminum alloys AA2024-T3, AA7075-T6, hot-dip galvanized steel (20 μm zinc coating thickness), and cold-rolled steel of a standard quality.

With these ingredients, the following approach was adopted by the various students working in this project to arrive at a solution of the scientific questions addressed in this project (see section VI, Objectives)

- select a substrate (Al, HDG or CRS)
- select a resin for this substrate - the selection depended on the presumed application of the primer, and the allowable solvent content
- select a silane that might interact favorably with the resin system used
- select, optionally, a curing agent for the resin, depending on the end use of the primer
- select, optionally, an anti-corrosion pigment for the primer
- study the stability of the mixtures
- optimize the ratios of the ingredients in terms of pot life
- adjust the viscosity of the system in view of the planned application method (dipping, brushing or spraying)
- prepare the surface of the metal substrates by solvent and alkaline cleaning
- apply a film of the primer and cure it, either at room temperature for several days or at elevated temperature
- optionally, apply a topcoat over the primer film and cure it
- prepare films of control primers with and without topcoat on chromated or phosphated versions of the same substrate
- determine the properties and performance of the primers

- optimize the formulation of the primer with respect to performance, e.g., by a Design of Experiments, such as the Taguchi approach.
- study certain fundamental properties of the primer such as rate of water uptake, swelling characteristics, etc. (Schaefer's group)

The primer performance testing was performed by standard tests as much as possible. The test protocols included:

- Salt fog exposure of scribed panels - ASTM B-117 (up to 4000 hours)
- Salt water immersion tests of scribe panels - AASTM D-714 (up to 12 months)
- Paint adhesion testing by cross-cut and tape - ASTM D-3359-97
- MEK double rub test - ASTM D-4752-03 (a measure of crosslinking; minimum accepted value is 50)
- Nickel test - ASTM D-1886-03 (a measure of gouging or hardness)
- Pencil hardness test - ASTM D-3363-05 (another hardness criterion)

In addition, the following non-ASTM test were carried out.

- Ford APGE test; this is a cyclic accelerated test typically used on automotive coatings
- Electrochemical Impedance Spectroscopy (EIS) - the criterion here was the impedance of the primed metal at low frequencies and its behavior during continuous exposure to a salt solution
- Outdoor exposure of the topcoated panels; a leeward site on an Hawaiian island and one in Florida were selected; at the first site, exposure of some initial versions of a superprimer on CRS and Al were conducted for two years; in Florida the exposure was slightly less than one year
- Small-area EIS (using a two-electrode system) during exposure in the B-117, the Ford APGE and the outdoor tests was performed; these results provided information that was complementary to the scribe behavior that was visually observed and rated; this complementary information consisted of the stability of the primer-metal interface away from any defect; the criterion for failure here was a steep drop of the impedance after some time of exposure; in the Florida exposure of the most recent versions of the topcoated primers, it was observed that the impedance actually increased during the exposure, presumably as a result of further, slow crosslinking of the silane in the films during atmospheric exposure
- Neutron and X-ray reflectivity studies of very thin films of silanes films and, at a later stage, of epoxy-laced films were performed; these experiments were carried out by Schaefer's group at National Laboratories; details are given in Section IX, but the most significant results are that all silane films absorb liquid water or water vapor, i.e., are somewhat hydrophilic; a silane-epoxy film also absorbs water; however, the interface of such films is highly hydrophobic and does not absorb water; further, such films exclude salt from an electrolyte; it is believed that these properties are the underlying reasons for the extremely good corrosion performance and adhesion of superprimer films
- Nuclear Magnetic Resonance (NMR) using  $^1\text{H}$ ,  $^{13}\text{C}$  and  $^{29}\text{Si}$  was carried out in order to elucidate the chemistry in the liquid primer and in the solid films of the primer
- Time-of-Flight SIMS was carried out to understand the chemistry at the metal-primer interface of

the real systems, as opposed to the thin model films used by Schaefer's group

- Fourier Transform Infrared Spectroscopy in the ATR or RAIR mode of solid primer films was carried out to complement the NMR data

This approach led to the development of systems that met the objectives of this project, viz., primer systems that contained no chromate or HAPs and that are also much lower in VOC. The performance of these systems is at least equivalent to the currently used system, especially in outdoor exposure situations. We have systems tailored for Al alloys, for HDG and also for CRS. An enormous advantage of our systems is that they do not require any metal pretreatment (currently done by chromating, phosphating or by zirconium systems). We have also eliminated the chromate pigments from primers by developing new pigments, based on cerium or phosphates. Such pigments work surprisingly well, in fact better than expected. Our investigations indicated that such performance is due to the fact that our systems are hydrophilic, i.e., can absorb relatively large amounts of water. Thus, the pigments are leached out more effectively. This leaching effect is beneficial if the films are required to exhibit self-healing or defect-healing effects. It has no effect on the metal-primer interface.

The hydrophilicity of the primers does not impair the adhesion to the topcoat, nor does it affect the corrosion rate of the metal underneath the primer adversely. That is because our silane-resin combinations modify the resin films in three ways: i) the films have molecular voids which can reversibly absorb water without swelling of the films, ii) the resin-silane combination forms an interfacial layer which is very hydrophobic and does not absorb water; the water can, therefore, not reach the metal, and, iii) the presence of the silane in the films makes the films impervious to salt; although water can go in until a certain depth, any salt in the electrolyte is excluded. This combination of three anti-corrosion effects are unique

## **MATERIALS**

### **A. PRIMERS FOR CRS**

The following section gives information about the materials used for preparation of the superprimer. Procedures used for the preparation of the superprimer are discussed.

#### **Silanes**

Table 8.1 shows the list of silanes, which were experimented with, along with their trade names and chemical formulas. All the above silanes, except for VTAS, were obtained from GE Silicones. VTAS was obtained from Gelest Inc. (Tullytown, PA). The silanes were used without further purification. Some silanes were used in hydrolyzed state and the others in non-hydrolyzed state. A detailed explanation about the preparation of silane solutions is given in later sections of this summary during the introduction of the superprimer formulations.

Table 8.1: List of Silanes used with trade names and chemical formulas

TRADE NAME	CHEMICAL NAME	CHEMICAL FORMULA
A-1170	Bis(trimethoxysilylpropyl)amine	$(\text{OCH}_3)_3\text{Si}(\text{CH}_2)_3\text{NH}(\text{CH}_2)_3\text{Si}(\text{OCH}_3)_3$
A-1289	Bis(triethoxysilylpropyl]tetrasulfide	$(\text{OC}_2\text{H}_5)_3\text{Si}(\text{CH}_2)_3\text{S}_4(\text{CH}_2)_3\text{Si}(\text{OC}_2\text{H}_5)_3$
Y-9805	Bis(triethoxysilylpropyl]ethane	$(\text{OC}_2\text{H}_5)_3\text{Si}(\text{CH}_2)_2\text{Si}(\text{OC}_2\text{H}_5)_3$
TEOS	Tetraethoxysilane	$\text{Si}(\text{OC}_2\text{H}_5)_4$
A-Link 15	Nethyl-3-trimethoxysilylethylpropanamine	$\text{CH}_3\text{CH}_2\text{NHCH}_2\text{CH}(\text{CH}_3)\text{CH}_2\text{Si}(\text{OCH}_3)_3$
A-Link 25	Gamma-Isocyanatopropyltriethoxysilane	$\text{NCO}(\text{CH}_2)_3\text{Si}(\text{OC}_2\text{H}_5)_3$
VTAS	Vinyltriacetoxysilane	$\text{CH}_2=\text{CH}(\text{CH}_2)_2\text{Si}(\text{OCOCH}_3)_3$

Bis-amino (A-1170) and VTAS silanes are mixed in their pure state. The reaction is exothermic. The reaction mixture is allowed to stay on the shelf for at least 24 hours. This gives sufficient time for the reaction between the two silanes to go to completion. This mixture is water-soluble. But the order of mixing of water and silane does matter in this case. Addition of DI water at ordinary pH can result in immediate condensation of the amine content of the mixture resulting in threads of polymerized particles in the solution. To avoid this, the pH of the appropriate amount of DI water taken needs to be adjusted first around 3 to 4 using acetic acid. After this pH is adjusted, the required amount of the silane-reaction-mixture needs to be added slowly while stirring to DI water. Dilution of silane mixture by this method gives uniform clear silane solutions. So to 90 parts of DI water, the pH of which is adjusted to about 3 to 4, 10 parts of A-1170: VTAS (5:1) mixture is added slowly while stirring. After the clear solution is obtained, the solution is allowed about 4 hours of hydrolysis time. After these four hours the solution is good for coating or for use in coating formulations.

### Resins

**Table 8.2** is a list of resins that were used for formulation of superprimer. All of the resins were obtained from Resolution Performance Products (Houston, Texas). All the resins mentioned here are epoxy resins. Although other types of resins can be used for formulation of superprimers, this summary concentrates on the formulations based on water-based epoxy primers.

Table 8.2 Resins used in superprimer formulations

EPON 828 Resin-X-95
EPIREZ Resin 3510-W-60
EPIREZ Resin 3515-W-60
EPIREZ Resin 3540-WY-55

EPON 828 Resin-X-75 is a 95% DGEBA type epoxy resin solids in 5% xylene. It is a completely solvent-based resin whereas the rest of the resins in the table are completely water-based epoxy resins. EPI-REZ Resin 3510-W-60 is a waterborne dispersion of a low-molecular weight liquid Bisphenol-A epoxy resin EPON Resin 828-type. It has 60% solids in water and has no co-solvent. EPI-REZ Resin 3515-W-60 is a waterborne dispersion of a semi-solid Bisphenol-A epoxy resin. It has 63% percent solids in water and has no co-solvent. EPI-REZ Resin 3540-WY-55 is a waterborne dispersion of a solid Bisphenol-A epoxy resin (EPON 1007-type) with an organic co-solvent 2-propoxyethanol. It has 55% solids in water and 11% co-solvent.

All the resins were used in the obtained state without further dilution or modifications. Information about any other commercial resins or topcoats used for experiments in this summary is given at the time of their mentioning.

### Particles

**Table 8.3** shows a list of particles of nano-size that were included in the superprimer formulations. The particles were chosen on basis of their affinity towards silanes and the resins that were used in the superprimer formulations. All of the particles were used in the obtained state without further purification or dilution. They were added to the final superprimer formulation. Detailed explanations of mixing procedure are given in later sections.

Table 8.3 Particles used in superprimer formulations

NAME	TYPE	MANUFACTURER
Colloidal Silica	Silica nano-particles(suspension in water)	Cabot Corporation, Tuscola, IL
Aluminasol	Alumina nano-particles 10% by weight(suspension in water)	Nissan Chemical, Houston, TX
Carbosil	Carbon nanoparticles(Dry)	
Zinc Dust	Zinc nanoparticles(Dry)	U.S.Zinc, Houston, TX

### Inhibitors

A variety of corrosion-inhibiting pigments were tried in the superprimer formulations. The idea and the mechanism in which they work are discussed in the later chapters. Commercial inhibitors from many companies were obtained and tried. They were first tested for compatibility with the contents of the superprimers and then they were used in the final formulations with the recommended percentages. The following Table 8.4 shows the list of inhibitors that were compatible and were tried in the final formulations. All the inhibitors were used in the obtained state without further purification or dilution.

Table 8.4: Corrosion Inhibitors used in the superprimer formulations

NAME	COMPANY	TYPE
CZM	Molywhite,Cleveland,OH	Calcium Zinc Molybdate
M-119 LV	Cortec Corporation,St.Paul,MN	Trade Secret of the company
M-5120	Cortec Corporation,St.Paul,MN	Trade Secret of the company
M-118	Cortec Corporation,St.Paul,MN	Trade Secret of the company
Fluka-Sodium Vanadate	Sigma Aldrich	Sodium Meta Vanadate
SZP-391	Halox Pigments,Hammond,IN	Strontium Zinc Phosphate
Corrostayn 228	Wayne Pigment Corp,Milwaukee,WI	Trade Secret of the company
UC-Pigment	University of Cincinnati	Plasma Polymerized Pigment

### Metals/ Alloys

AA2024-T3 and cold-rolled steel panels with dimensions of 10 cm \* 15 cm \* 0.06 cm were purchased from Stillwater Steel Supply (Stillwater, OK). The sheets were cleaned with an uninhibited alkaline cleaner (AC 1055®, Brent America, Lake Bluff, IL). The metal substrates were first solvent scrubbed with red scotch-brite pads dipped in ethanol. Then they were cleaned and rinsed thoroughly with DI water to remove all the grit and dust caused by the scrubbing. Then the panels were ultrasonically cleaned with ethanol in an ultrasonic bath for 10 minutes each. The cleaned panels were further alkaline cleaned with 7.5 vol % of the AC 1055 aqueous solution at 60-70°C for 3-5 minutes. The cleaned panels were then rinsed in DI water. The panels were blow-dried with compressed air. The cleaned metal panels were checked for water-break-free surface. This water-break-free surface confirms that the surface was sufficiently clean for coatings to be applied.

### Superprimer formulations

This section gives detailed information about the superprimer. In the beginning it gives information about the method of selection of the components that go into the primer followed by initial formulation and their results. The developments that lead to the final formulation are discussed in detail. Test results including EIS and salt spray results are provided whenever necessary.

## Component Selection

The component selection for the formulation of a superprimer primarily targets on the kind of resin and the silanes/silane mixtures that are compatible with each other. The choice of resin can be any water-borne commercially available resin; an epoxy, polyurethane or acrylic-based. Even the choice of mixtures of two different resins is also a matter under current research. After the resin is chosen then a list of all the silanes which in theory would be compatible with the resin is made.

Table 8.5 shows the resin class and the compatible silane class. These silanes were checked for their compatibility with the resins by observing the properties such as the mixture's solution stability, viscosity, gel times, flow ability, pot life, dilution ability, proper wetting characteristics film forming capability etc. This thesis is mainly aimed at producing a superprimer using an epoxy-based resin. A detailed explanation of the formulations and the procedure for their preparation is given in the later sections.

Table 8.5: Resins and compatible silanes

RESIN	SILANE CLASS
Epoxy	Amine, Epoxy, Chloroalkyl, Mercapto
Polyester	Amine, Methacrylate, Styryl, Vinyl
Urethane	Amine, Alkaloamine, Epoxy, Isocyanate
Acrylic	Acrylic, Styryl, Epoxy

## Initial Formulations

This section discusses the gradual improvements that were made in the effort towards achieving the final superprimer formulations. The experimental results of the initial failed formulations were only provided as a comparison with final superprimer formulations.

To check if addition of an amine-functional silane would actually be able to cross-link/react with epoxy resin, a simple mixing trial was adopted. Bis-amino silane was mixed with EPON 828, a high solid DGEBA epoxy resin. A 2:1 ratio of amine silane and epoxy resin was mixed at slightly elevated temperature and at constant stirring. The two solutions were observed to be miscible with each other and the clear mixture was used for coating an alkaline-cleaned AA 2020 T3 panels. The solution gave rise to clear and tough films after an hour cure at 100°C. The mixed solution had a pot-life of only an hour. This observation proved that silane alone can be used as a curing agent for a resin and coatings can be obtained from it. The above mixture showed some excellent corrosion resistant characteristics like high modulus on an EIS-Bode plot and good salt immersion results, but the mixture was not water-reducible. The idea was to obtain a water-reducible primer so the work was shifted towards water-based epoxy resins.

EPI-REZ Resin 3510-W-60, a waterborne dispersion of a low molecular weight liquid Bisphenol-A epoxy resin EPON Resin 828-type, was obtained. Mixtures of it with Bis-amino silane were coated, but the coatings obtained had poor film characteristics such as improper curing ability and poor adhesion. Even after 3-week curing at room temperature the films were still found to be tacky and wet. EPI-REZ 3510-W-60 resin is a completely water-based resin with water as the only solvent and also the mixtures of it with amine silane contain only water as a solvent. The coatings formed from these resin-silane mixtures do require a lot of energy to drive the water from the film and give a dry film. This is the basic observed difference between the solvent-based and water-based coatings. Solvents usually require far less energy than water to evaporate, thus solvent-based coatings have far better curing and film characteristics than water-based coatings.

Following the above factor, EPI-REZ 3540-WY-55, water-based epoxy resin but with a co-solvent was chosen for trials. This resin contains 11% of 2-propoxyethanol as a co-solvent besides water. Formulations with EPI-REZ 3540-WY-55 showed some promising characteristics of a primer. So this particular resin was chosen to serve the purpose of a polymer in the superprimer definition. Bis-amino silane was chosen for the formulations. Although other mono-silanes could be compatible and be used for formulations, bis-silanes proved in previous occasions to work better than mono-silanes. Although bis-amino silane alone mixed well with the resin, the formulations showed low pot lives and gave brittle films. Bis-amino is a very basic silane, so, it gets subjected to immediate condensation in a higher pH environment of the resin. Even hydrolyzed solutions of bis-amino silanes require acetic acid to adjust the pH of the water solution. Their solutions in water are very unstable and gel up in a very short period of time.

For the purpose of obtaining solutions with comfortable shelf life before mixing, the idea of using silane mixtures was tried. Silane mixtures of bis-amino and vinyltriacetoxy silane have proven to give water soluble silane solutions with indefinite shelf life.

### **Preparation of Superprimer**

Part A: EPI-REZ 3540-WY-55-epoxy resin was used as obtained without further dilution.

Part B: 10% diluted solution of AV5 at pH 5. AV5 is mixture of A-1170 and VTAS mixed in the ratio of 5:1 by weight in pure state.

Preparation of Part B: A-1170 and VTAS silanes were mixed in their pure state. The reaction is exothermic. The reaction mixture was allowed to stay on the shelf for at least 24 hours. This gives sufficient time for the reaction between the two silanes to go to completion. This mixture is water-soluble. But the order of mixing of water and silane does matter in this case. Addition of DI water at ordinary pH can result in immediate condensation of the amine content of the mixture resulting in threads of polymerized particles in the solution. To avoid this, the pH of the DI water taken needs to be adjusted to around 3 to 4 using acetic acid. After this was adjusted, the required amount of the silane reaction mixture needs to be added slowly while stirring the DI water. Dilution of silane mixture by this method gives uniform clear silane solutions. This particular method of mixing is not uncommon in industries and pretreatment companies. So to 90 parts of DI water the pH of which was adjusted to about 3 to 4, 10 parts of A-1170: VTAS (5:1) mixture was added slowly while stirring. After the clear solution was obtained, the solution was allowed about 4 hours of hydrolysis time. After these four hours the solution is good for coating or for use in coating formulations.

Part C: Tetraethoxysilane, a common cross-linking silane with four hydrolysable alkoxy groups.

Weight Percentages: 80 % of Part A + 19 % of Part B + 1 % of TEOS

High Shear Mixing: A laboratory High Shear Mixer from Charles Ross Mixers and Blenders Company (Model LC 10) was purchased and used especially for mixing primer formulations. All the components mentioned above were mixed in the above weight ratio and high-shear mixed for 10 minutes at a speed of 2000 rpm.

Cleaning, Coating and Curing Method: After the formulations were mixed an incubation time of 30 minutes is allowed before coating. This would give enough time for the reaction between amine and epoxy groups to take place. The formulations can be coated using a drawdown bar, brushed or sprayed on. Formulations can be diluted to sprayable viscosity.

Aluminum alloy AA 2024-T3 panels were ultrasonically cleaned in ethanol for 5 minutes followed by alkaline cleaning at 65°C for 3 minutes in a 7% by volume Brent uninhibited alkaline cleaner solution in DI water. After alkaline cleaning the panels are thoroughly rinsed in DI water and then blow-dried. The panels were tested for water-break-free films indicating a clean surface. Carbon steel panels were first solvent-scrubbed using ethanol as solvent and scotch-brite pads to remove the dirt, corrosion products and expose clean, shiny metal-oxide surface. After the scrubbing, the panels were cleaned with water spray and then followed by ultrasonic cleaning in ethanol for 5 minutes. The final stages of cleaning included alkaline cleaning similar to the one followed for aluminum but at lower temperature of 55°C and for only 1 or 2 minutes. CRS is a very sensitive substrate so care was taken not to spoil the metal-oxide surface before coating with superprimer. After coating the panels were either cured for 1 hour at 100°C or for one week at room temperature.

## B. PRIMER FOR HDG

### Metal

HDG steel panels of 10 cm x 15 cm were purchased from Stillwater Steel Supply, Stillwater, OK. The zinc layer thickness on the material was about 20 µm. These metal panels were sheared into 5 cm x 7.5 cm or 7.5 cm x 10 cm sizes and cleaned before being coated.

### Water-borne dispersions of bisphenol A resins (major binders)

In the beginning of the study three different bisphenol A based resins were used. Two of them were: EPI-REZ 3540-WY-55 and EPI-REZ 5522-WY-55 which both are 55 % nonvolatile dispersions of a modified DGEBA epoxy resin in water and 2-propoxyethanol. The third one was a developmental epoxy dispersion, DPW-6520. This one is a 53 % solids, waterborne NEWGENT™ technology dispersion of a solid bisphenol-A epoxy resin with non-hazardous air pollutants (HAP's) co-solvents. All three were obtained from Resolution Performance Products, Houston, TX. The equivalent weight per epoxide (EEW), VOC-contents and other relevant data of the resins are listed in Table 8.6.

**Table 8.6. The specific data of the epoxy dispersion used in the superprimer formulations**

Epoxy dispersion	EEW	VOC, [g/L]	Solids content, %	Viscosity, cP
EPI-REZ 3540-WY-55	1600-2000	250	55	7000-17000
EPI-REZ 5522-WY-55	550-700	170	55	8000-19000
DPW-6520	500-600	74	53	1000-6000

### **Amine-based cross-linkers for the epoxy dispersions**

The use of two curing agents was investigated in this study. EPI-KURE 8290-Y-60, which is a water-reducible high molecular weight amine adduct cross-linker supplied as a 60% solids in 2-propoxyethanol and a developmental curing agent dispersion, DPC-6870, which is an aqueous dispersion of an amine adduct curing agent, were both procured from Resolution Performance Products, Houston, TX.

### **Silanes**

Mainly two silanes were used in this study. The bis-sulfur silane, bis[3-(triethoxysilyl)propyl]tetrasulfide, with the product name Silquest A1289 was obtained from GE Silicones, Wilton, CT. The bis-benzene silane, 1,4-bis(trimethoxysilyl)ethylbenzene, was obtained from Gelest Inc., Morrisville, PA. The starting superprimer formulation F6 contained, however, a water-based AV5 solution based on bis-amino silane, bis-[trimethoxysilylpropyl] amine and vinyltriacetoxysilane. Formulation F6 also contained a cross-linker silane TEOS, tetraethoxysilane. The bis-amino silane and the TEOS cross-linker were procured from GE Silicones, Wilton, CT. The VTAS was obtained from Gelest Inc., Morrisville, PA.

### **Non-chromate corrosion inhibitors**

As non-chromate corrosion inhibitors were studied, the following inhibitors were incorporated into the superprimer formulations:

- Molywhite CZM, a calcium-zinc molybdate corrosion inhibitor provided by Molywhite Pigments Group, Cleveland, OH
- Corrostayn 228, a synergistic corrosion inhibitor (based on Ca, Zn, P, Si, O) provided by Wayne Pigment Corp., Milwaukee, WI
- Phosguard J0806, a micronized zinc phosphate/molybdate corrosion inhibitor from Rockwood Pigments, Beltsville, MD
- Cerium exchange silica, prepared in our lab by Lin Yang et al.

### **Other pigments and fillers**

The effect of fillers and other special additives were studied either as such or in conjunction with corrosion inhibiting pigments in the superprimer formulations for HDG steel. These were:

- Tronox RF-K-2, a micronized rutile pigment coated with an aluminum compound for hydrophobicity. It was obtained from Kerr Mc Gee Pigments, Hamilton, OH
- Nanoactive S titanium dioxide, a 12-15 wt.-% suspension of titania in water, obtained from NanoScale Materials Inc., Manhattan, KS
- Alsibronz 06, a commercially available ultra-fine, chemically inert potassium aluminum silicate, provided by Englehard Corp., Iselin, NJ

A summary of the chemicals used in the development of the superprimer for HDG steel is shown in Table 8.7.

**Table 8.7. Summary of the chemicals used in the development of the superprimer for HDG steel**

<b>Superprimer components and chemicals for HDG steel</b>	
<b>Binders</b> Waterborne epoxy dispersions: EPI-REZ 3540-WY-55 EPI-REZ 5522-WY-55 DWP 6520	<b>Silanes</b> bis[3-(triethoxysilyl)propyl]tetrasulfide (bis-sulfur) 1,4-bis(trimethoxysilylethyl)benzene (bis-benzene) bis-[trimethoxysilylpropyl]amine (bis-amino silane) vinyl triacetoxysilane (VTAS)
<b>Crosslinkers</b> Epoxy-amine adducts: EPI-KURE 8290-Y-60 and DCP 6870	
<b>Anti-corrosive pigments</b> zinc phosphate (ZP) Corrostain 228 (Ca, Zn, P, Si, O) sodium metavanadate calcium zinc molybdate (CZM)	<b>Fillers and other pigments</b> titania barium sulfate mica Nanoactive S (titania dispersion)

### Sample preparation and cleaning

The HDG panels were first scrubbed using scotch-brite™. They were then ultrasonically cleaned in ethanol and acetone, successively for 10 minutes each, to remove impurities. This was followed by degreasing in a diluted (7 vol.-%) alkaline cleaner (Okemclean, provided by Oakite products, NJ) at 65 °C for 4 min, rinsed with tap water and blow-dried with compressed air to achieve a water-break-free surface.

The ingredients of the various superprimer formulations presented in this paper were mixed together and the dispersion was stirred vigorously in order to assure sufficient dispersion and homogenization of the mixture. The coating formulation was then applied on the cleaned HDG steel using a draw-down bar of 28 m. The coated panels were cured either at room temperature for 14 days or by using different curing conditions described in more detail in previous chapter.

### Tests and characterization

#### Tests

**Salt spray test according to the ASTM standard 1654-92** was used to evaluate the corrosion resistance of the superprimer coated HDG steel panels. This standard is similar to the well-known ASTM B-117 standard. The ASTM B-117 does not, however, include the scribing of the panels, which the ASTM 1654-92 describes. The salt spray testing was performed in a Singleton salt fog chamber at DACCO SCI, INC., Columbia, MD. Periodically the specimens were removed from the chamber and EIS measurements were taken using DACCO SCI's handheld corrosion sensors and a Gamry PC-4 potentiostat. These sensors allowed the EIS measurements to be taken under ambient conditions instead of immersion, which is usually required for traditional EIS.

**The Ford AGPE test** was also used to evaluate the corrosion performance of the coated panels. This test is a cyclic accelerated corrosion test including three cycles which are: 1) 15 minutes immersion in 5 % NaCl solution at room temperature; 2) 105 minutes ambient drying and 3) 2 hours in 90° humidity at 60°C. This test was also carried out at DACCO SCI and specimens were periodically removed from the test for EIS measurements as described above.

**Hawaii outdoor exposure test:** Some primed and topcoated panels were also tested outdoor by exposing them to the climate on the Maui beach of Hawaii. During the test EIS measurements were also recorded by the use of the handheld EIS instrument described earlier.

**Electron Impedance Spectroscopy (EIS)** measurements were carried out on HDG panels coated with the various supeprimer formulations. EIS measurements were recorded by using two equipments: 1) The DACCO SCI's handheld corrosion sensors with a Gamry PC-4 potentiostat and 2) a conventional set-up at UC, in which an area of 5.06 cm<sup>2</sup> of the coated panel is exposed to a corrosive 0.6 M NaCl electrolyte. Both measurements were made at frequencies ranging between 10<sup>-2</sup> to 10<sup>5</sup> Hz, with an AC excitation amplitude of 10 mV. For the latter measurements an SR810 frequency response analyzer connected to a Gamry CMS100 potentiostat was used. The set-up consisted of a standard calomel electrode used as the reference electrode with a graphite rod acting as the counter electrode. In this study EIS was primarily used to compare the low-frequency impedance values of the panels exposed to salt spray, Ford AGPE, outdoor or salt immersion testing. These results were compared in the form of Bode plots .

**MEK double rub test:** ASTM D4752-03 standard was utilized to measure the MEK double rub resistance of the coating. The test gives a rough idea of the extent of curing of most organic coatings.

## **C. ENVIRONMENTALLY-COMPLIANT NOVOLAC SUPERPRIMERS FOR CORROSION PROTECTION OF ALUMINUM ALLOYS**

### **Metal Substrate**

Aluminum AA 2024-T3 alloy substrates of 0.81 mm thickness were acquired from Stillwater Steel and Supply, Stillwater, OK. Chromate conversion coating (CCC) pretreated AA 2024-T3 substrates were obtained from ACT laboratories, Inc., Hillsdale, MI.

### **Water-based Resin Dispersions**

EPI-REZ™ 5003-W-55 resin, a nonionic aqueous dispersion of a polyfunctional aromatic epoxy resin with an average functionality of three, was acquired from Resolution Performance Products, Houston, TX. EPI-REZ 5003-W-55, also known as the bisphenol A novolac epoxy resin, is a solvent-free system intended for high performance applications which require maximum chemical and solvent resistance and/or elevated temperature service. NeoRez® R-972, a colloidal dispersion of aliphatic polyurethane, was acquired from DSM Neo-Resins, Wilmington, MA. It has good abrasion, chemical and UV resistance and is completely water reducible and contains 10 wt % VOC.

### **Silanes**

Organofunctional bis-silanes were used in this study for corrosion protection of AA 2024-T3 to obtain good adhesion to substrate as well as the topcoat. Silquest® A-1289 bis-[3-(triethoxysilyl) propyl] tetrasulfide or bis-sulfur silane ((OC<sub>2</sub>H<sub>5</sub>)<sub>3</sub>Si(CH<sub>2</sub>)<sub>3</sub>S<sub>4</sub>(CH<sub>2</sub>)<sub>3</sub>Si(OC<sub>2</sub>H<sub>5</sub>)<sub>3</sub>) was used in this study.

### **Crosslinkers and Curing Agents**

EPIKURE®™ Curing Agent 6870-W-53, a 53% solids, solvent-free, non-ionic aqueous dispersion of a modified polyamine adduct curing agent for the epoxy resin, was acquired from Resolution Performance Products, Houston, TX. NeoCryl® Crosslinker CX-100 is a 100% active polyfunctional

aziridine liquid crosslinker which produces a marked improvement in water, chemical, abrasion and humidity resistance.

### **Corrosion Inhibitors**

Alfa Aesar zinc phosphate, a technical grade zinc phosphate corrosion inhibitor was procured from Johnson Matthey, Ward Hill, MA.

### **Surfactants and Dispersants**

Surfynol MD 20 and Surfynol DF 110L defoamers were obtained from Air Products and Chemicals, Inc., Allentown, PA. BYK<sup>®</sup> P 104 S, a wetting and dispersing agent, which enhanced pigment dispersion was obtained from BYK-Chemie GmbH, Wesel, Germany.

### **Solvents and Cleaners**

Acetone, 99.5% pure was acquired from Tedia Company, Inc., Fairfield, OH. Methyl ethyl ketone (MEK) was acquired from Fisher Scientific, Fair Lawn, NJ. Okemclean alkaline cleaner was supplied by Chemetall Oakite, Romulus, MI.

### **Topcoats and Control Primers**

CA 7233 High solids chromated epoxy standard military primer and its activator component CA 7233 B, were procured from PRC DeSoto, Glendale, CA, and it conforms to military specification MIL-PRF-23377 H (Type I, class C). Desothane HS CA-8214/F36173, solvent-based camouflage gray polyurethane topcoat with a base component and an activator was also procured from PRC DeSoto, Glendale, CA. Defthane ELT MIL-PRF 85285 D, a gray military topcoat with a base component and an activator was procured from Deft Chemical Coatings, Irvine, CA.

### **Metal Surface Preparation**

Before primer coating, AA 2024-T3 panels were prepared by carrying out following cleaning steps:

- Dry scrubbing using scotch brite<sup>®</sup> for removal of superficial impurities and oxides
- Ultrasonic cleaning in ethanol for 8 minutes at room temperature to remove grease and oil
- Alkaline cleaning in Okemclean alkaline cleaner for 3-5 minutes or 0.5 M NaOH solution for 3-6 seconds at 60-65<sup>o</sup> C to enhance formation of aluminum hydroxide which helps adhesion to silane-based coatings
- Thorough rinsing in DI water till water break-free
- Blow-air drying

### **Formulation of Superprimer**

The compositions of superprimer through various stages of development are given in Table 1. After curing for 14 days at room temperature, the coatings made from these formulations were examined in tests such as solvent resistance, hardness and contact angle measurement. and their respective properties are mentioned in Table 8.8.

Formulation	Contact angle (RT)	MEK double rub		Pencil Hardness (RT)
		(RT)	(HT)	
ND-20	59°	60	300	1H
<b>N-1</b>	76°	60	300	1B
<b>NP-1</b>	79°	100	-	2H

Table 8.8

(a) Novolac epoxy resin and curing agent: The EPI-REZ 5003-W-55 novolac resin and EPIKURE 6870-W-53 cross-linker were mixed in different the weight ratios from 9:1 to 1:1. The two components were mixed in a beaker using a magnetic stirrer till the blend became homogenous. Coatings were made using the formulation on AA 2024-T3 sample. The formulation ND-20 showed the best performance in terms of contact angle and MEK double-rub values. Based on these initial findings, ND-20 was chosen as the base formulation for further modifications.

(b) Appropriate choice of silane: In this study, bis-sulfur silane was used in the novolac-based superprimer formulations to impart better water-barrier properties and corrosion resistance. Pure bis-sulfur silane formed an emulsified solution when mixed with novolac resin after 2-3 hours of continuous stirring. However, stirring was continued over a period of 24 hours to ensure a high degree of emulsification. The curing agent was added to the mixture of novolac resin and bis-sulfur silane and stirred vigorously till a homogenous solution was obtained. Polyurethane resin was added as the last ingredient. The formulations were then applied on cleaned AA 2024-T3 panels using a draw-down bar.

(c) Addition of polyurethane resin: It was observed that the novolac epoxy resin formed a hard coating when combined with the curing agent and was brittle at low temperatures. An aqueous polyurethane resin dispersion, NeoRez R-972 was used as a minor additive to enhance flexibility at low-temperatures. The amount in which polyurethane was added in the formulations was carefully controlled to avoid gelling or precipitation. As the polyurethane resins had high reactivity, the addition of polyurethane was preferably done in the end during the preparation of all the formulations containing it. Though the polyurethane by itself formed a very soft coating of hardness 5B, it appeared to have produced a synergistic effect on the enhancing the hardness of the NP-1 coating to 2H.

(d) Corrosion inhibitors: In this study the focus was on a class of inhibitors which have the potential to be effective on AA 2024 such as zinc phosphate and Corrostatin 228, a commercially produced synergistic mixture of zinc phosphate and calcium silicate. The inhibitor pigments were added before the addition of curing agent to the silane-resin mixture. This ensured proper dispersion and prevented coagulation of the pigment particles. Initial mixing was done by mechanical stirring for 30 to 45 minutes. Following this, the formulations were subjected to vigorous mixing in the high-shear blender at 2000 rpm for 10-12 minutes. From the observed double-rub values, it was found that the addition of pigments to the superprimer slightly lowered its solvent resistance.

(e) Minor additives: CX-100 addition further improved water and chemical resistance as well as enhanced adhesion to substrate. Surfynol MD 20 and Surfynol DF 110L defoamers were used to avoid foaming and to drive out air bubbles from the formulations. Defoamers were added in the amount of 1-2 wt.-% of the wet formulation. A wetting and dispersing agent, BYK P 104 S, was used to aid uniform dispersion and prevent agglomeration of the various pigments.

(f) Co-solvents: Solvents are used in coating formulations to facilitate rheological changes and improve stabilization of the individual components. They are also meant to extend the pot-life of the formulation and control viscosity before the application of coating. In these experiments, the solvents used in the formulations had to be VOC-free in order to maintain a low-VOC system. Water was the most commonly used solvent for superprimer formulations in this study. During spray-coating, water was used to dilute the formulations to the desired viscosity.

(g) High-shear Blender: A high shear blender/mixer manufactured by Ross Mixing Inc., Port St. Lucie, FL was used to mix the superprimer formulation. The micro-mixer/rotor assembly was used at speeds of 1000 rpm to 3000 rpm especially to obtain good dispersion of pigments in the superprimer formulation. The shearing effect produced by the micro-mixer helped in de-agglomeration of pigments and avoided precipitation. It also helped the blending of resin, silane and cross-linkers to form a macroscopically homogenous formulation.

### **Coating Application Methods**

The cleaned substrate samples were coated with the primer using a draw-down bar number R 14, which gave an average wet-film thickness of 25  $\mu\text{m}$ . The topcoat and control primers were also applied using the same draw-down bar. The superprimer formulations were also spray-coated using a SoftSpray HVLP Conversion Gun acquired from Wagner Spray Tech Corporation, Minneapolis, MN. The spray equipment set up consists of a spray gun, material and air hoses, a pressure pot containing the formulation and an air compressor. The viscosity of the formulation needs to be adjusted to enable spraying and avoid sagging. To avoid irregularities in the coating finish, the axis of the spray gun hose should always remain perpendicular to the substrate surface. The spraying pattern can be adjusted according to the application by turning the ears of the air cap into various positions. Multiple coats may be applied after the previous coats have been allowed to dry. A picture of the spray gun is shown in Figure.

### **Formulation for Spray Coating**

The original NP-1 formulation had to be modified in terms of viscosity and pigment dispersion. Poor dispersion of the pigments and high viscosity of the formulation could have affected the quality of the spray coating and clogged the spray gun nozzle. The viscosity was adjusted using solvents such as water and acetone. But acetone being volatile, did not serve the purpose of reducing the viscosity to the desired level as done by water. Hence, water was the only solvent used in spraying formulations. A finer grade of zinc phosphate from Alfa Aesar was used as corrosion inhibitor pigment. This pigment had a good dispersion in the water-based formulation. Surfynol MD-20 defoamer, BYK P-104 dispersing agent and CX-100 crosslinker were added in minor amounts.

### **Control Coatings**

CA 7233 High solids chromated epoxy standard military primer and its activator component CA 7233 B were mixed in the ratio 1:1 by volume and applied on chromate-pretreated AA 2024-T3 panels. The coatings were left to cure at room temperature. The topcoat Desothane HS CA-8214/F36173, mixed with its activator component in the volume ratio 3:1, was applied within 8-16 hr time frame after the application of the primer coating. This ensured good adhesion between primer and topcoat and avoided cracking of the topcoat. Both the control as well as the superprimer coatings was topcoated with Desothane topcoat. The topcoat Defthane ELT MIL-PRF 85285 D was used in coatings prepared for outdoor exposure test in Florida. The primer and the topcoat were applied using draw-down bars.

## D. EPOXY-ACRYLATE PRIMER FOR ALUMINUM ALLOYS

### Metal substrates

The aluminum alloys AA2024-T3 and AA7075-T6 substrates of 0.032 inch thickness used throughout all the studies were acquired from Stillwater Steel and Supply, Stillwater, OK. The CRS 1018 panels used in the last study reported were also from Stillwater Steel and Welding Supplies, LLC, Stillwater, OK. The HDG steel panels having a zinc coating thickness of ~ 20  $\mu\text{m}$  also used throughout the studies this year were from SSAB Tunnplat AB in Sweden.

### Superprimer components

Table 8.9 (a) & (b) lists the component and sources of acrylic-epoxy superprimer.

**Table 8.9(a)** Materials and the identity of the the acrylic-epoxy based superprimer formulations

Component	Identity
Zinc phosphate	Inhibitor
Silquest A-1289	Bis-sulfur silane
Maincote AE-58	Acrylic resin
Surfynol 104H	Surfactant
Daubond DC9010W55	Epoxy resin
Butyl cellusolve	Coalescing solvent
15% $\text{NaNO}_2$	Flash rust inhibitor
DI water	Viscosity modifier

### (b) Sources of chemicals:

Zinc phosphate(pigment)	available from Alfa Aesar, <a href="http://www.alfa.com">www.alfa.com</a>
Silquest A-1289	available from GE silicones, <a href="http://www.gesilicones.com">www.gesilicones.com</a>
Maincote AE-58	available from Rohm&Haas, <a href="http://www.rohmhaas.com">www.rohmhaas.com</a>
Surfynol 104H	available from Air Products, <a href="http://www.airproducts.com">www.airproducts.com</a>
DAUBOND DC9010W55	available from Daubert, <a href="http://www.daubertchemical.com">www.daubertchemical.com</a>
Butyl cellusolve	Available from Fisher Scientific or other chemical stores

## Silanes and other Chemicals

An Okemclean alkaline cleaner, provided by Oakite products, Berkley Heights, NJ was used to clean some of the panels. All primer formulations contained the bis-sulfur silane, bis[3-(triethoxysilyl)propyl]tetrasulfide, with the product name Silquest A1289 obtained from GE Silicones, Wilton, CT. Silquest<sup>®</sup> Y 9805 bis-[triethoxysilyl] ethane or BTSE,  $(OC_2H_5)_3Si(CH_2)_2Si(OC_2H_5)_3$  and Silquest<sup>®</sup> A-1170 bis-(trimethoxysilylpropyl) amine or bis-amino silane,  $OCH_3)_3Si(CH_2)_3NH(CH_2)_3Si(OCH_3)_3$ , and tetraethoxysilane (TEOS)  $(C_2H_5O)_4Si$ , were obtained from GE Silicones, South Charleston, WV. Vinyltriacetoxysilane (VTAS) was procured from Gelest Inc., Tullytown, PA.

CRS 1018 panels were used as substrate. Cleaning solutions of different pH-values were prepared by adjusting the amount of HCl and NaOH in the solution. The pH-values investigated were: 1.0, 3.6, 6.8, 8.5, 9.5, 10.5 and 12.4. The CRS substrate panels were first mechanically cleaned with Scotch Brite, rinsed with deionized (DI) water and blow-dried. The panels were then cleaned ultrasonically in acetone for 10 minutes to further degrease the panels. Thereafter, the CRS substrates were immersed in the cleaning solutions at the different pH-values mentioned above at 60°C for 3 minutes. After cleaning, the panels were immediately rinsed with DI water, blow-dried and stored in a desiccator until further characterization. The CRS panels cleaned, rinsed and dried as described above will hereafter be referred to as as-cleaned panels. The blank control panel was degreased as described above without using the final cleaning step.

For corrosion studies, a part of the as-cleaned panels were coated with silane and another part was coated with a silane-containing primer. A 10 wt.-% aqueous solution of bis-amino silane and VTAS in a weight ratio of 5:1 was used for silane coating of the CRS panels. To facilitate the hydrolysis process of this silane mixture, acetic acid was added to the DI water to adjust the pH to 5.5 prior to the addition of bis-amino silane/VTAS mixture. This AV silane mixture solution was aged for 4 hours at ambient temperature before it was applied to as-cleaned CRS by dipping for 30 seconds. The primer formulation used in this study contained 80 wt.-% epoxy resin, 10 wt.-% bis-sulfur silane, 9 wt.-% of AV silane and 1 wt.-% TEOS crosslinker. The primer formulation was applied by a draw-down bar to the panels. Both silane and primer-coated panels were cured at 100°C for 1 hour in air. The panels coated with the AV mixture solution are here after referred to as silane-coated panels and the panels coated with the silane-containing primer are referred to as primer-coated panels. The thickness of the primer coating was found to be around 8  $\mu m$ .

The properties of as-cleaned, AV-silane-coated and AV-silane-containing primer-coated CRS panels cleaned at different pH-values were characterized by ICP analysis, contact angle goniometry, Fourier Transform Infrared (FTIR) spectroscopy, SEM, DC polarization and Electrochemical Impedance Spectroscopy (EIS).

## Surface Cleaning of the Metals

The procedures of the surface cleaning of the aluminum alloys have varied slightly depending on the purpose of the study. For small sets of samples, the aluminum panels have been simply scrubbed with Scotch Brite and water in order to remove the oil from the panels. For larger studies the aluminum alloy panels were treated in the following way:

The AA2024-T3 panels were cleaned in the following way before primer coating:

- AA2024-T3 substrates were scrubbed by using ethanol and Scotch-brite pads

- ultrasonically cleaned in ethanol for about 8 min.
- alkaline cleaned in 0.5 M NaOH solution for 3-6 seconds at 60-65° C
- rinsed in DI water till water break-free, before
- drying the substrates with compressed air

The AA7075-T6 panels were cleaned in the following way before primer coating:

- AA7075-T6 substrates were rinsed with water and acetone
- scrubbed with Scotch-brite pads by using water
- rinsed with water
- ultrasonically cleaned in ethanol for about 8 min.
- finally rinsed with DI water, before
- drying the substrates with compressed air

After the review meeting in September, 2006, the surface preparation method used by the Air Force was adopted in the surface preparation of the AA2024 panels. This surface preparation method is described below:

**Air Force base cleaning and de-oxidizing procedure for aluminum alloy panels:**

1. Panels are scrubbed on both sides using a maroon “Scotch Brite” pad (approximately 120-grit equivalent) and a 10:1 mix of tap water / Brulin 815 GD (or equivalent) at room temperature.
2. Panels then receive a tap water rinse and are verified to be water break free; then they are immersed in de-ionized water and placed in a metal rack.
3. Each rack of panels receives a 5-minute immersion in the tap water / Brulin (10:1) circulating bath heated to a minimum of 142° F (see manufacturer’s instructions for various detergent mixtures and their bath temperatures).
4. Panels then receive a two-stage rinse.
  - a. Tap water immersion (10 dunks)
  - b. De-ionized water low-pressure spray
5. Panels are then immersed in a circulating De-Oxidizing bath for 2 minutes (see recipe below).
6. Panels again received a two-stage rinse.
  - c. Tap water immersion (10 dunks)
  - d. De-ionized water low-pressure spray

**De-Oxidizing Bath Recipe:**

- Butyl alcohol            35 vol.-%
- Isopropyl alcohol      25 vol.-%
- Phosphoric acid        18 vol.-%
- Deionized water        22 vol.-%

The degreasing of the HDG panels was done by using two methods. In the first one the panels are first scrubbed using Scotch-brite scrubs. They are then ultrasonically cleaned in ethanol and acetone,

successively, for 10 minutes each, to remove impurities. In the other procedure the HDG panels are scrubbed on both sides using a maroon “Scotch Brite” pad and a 10:1 mix of tap water / Brulin 815 GD (or equivalent) at room temperature. Then rinsed with tap water and subsequently with DI water. After degreasing the HDG panels in either way the panels were alkaline cleaned in a diluted (7% by volume in water) Okemclean alkaline cleaner at 65°C for 2 min and rinsed DI water, followed by blow-drying with compressed air.

The CRS substrate panels for the CRS cleaning study were first mechanically cleaned with Scotch Brite, rinsed with deionized (DI) water and blow-dried. The panels were then cleaned ultrasonically in acetone for 10 minutes to further degrease the panels. Thereafter, the CRS substrates were immersed in the cleaning solutions at the different pH-values at 60C for 3 minutes. After cleaning, the panels were immediately rinsed with DI water, blow-dried and stored in a desiccator until further characterization. The CRS panels cleaned, rinsed and dried as described above will hereafter be referred to as as-cleaned panels. The blank control panel was degreased as described above without using the final cleaning step.

### Superprimer mixing methodology and application

The methodology for mixing the primer formulations described here are for mixing the recipes as such.

**Formula:**

	grams
Mix the following	
<hr/>	
Zinc phosphate(pigment)	27.00
Silquest A-1289	5.75
Maincote AE-58	52.30
Surfynol 104H	1.20

Add in order with agitation, high speed shear blend for at least 10 minutes after all components are added

<hr/>	
Daubond DC9010W55	5.75
Butyl cellusolve	5.15
15% sodium nitrite solution	1.15
DI water	1.70
 Total	 100.00

In the studies this year the primers have been applied to the substrates by applying them with a draw-down bar producing a wet film thickness of 28 µm or higher. For spraying experiments two different spray guns have been used. The first spray gun procured for the SERDP project was a NB high-volume low-pressure (HVLP) spray gun from the Wagner Corporation, Minneapolis, MS. After visiting the Wright Patterson Air-Force base (WPAFB) in June 2006, we also bought the Millenium DeWilbiss spray gun in order

to be able to simulate the exact same spraying conditions used at the WPAFB.

Panels that were topcoated were topcoated within 24 hours of curing of the primer coating. The topcoat was usually applied by draw-down bar using a bar producing a topcoat film thickness close to 50  $\mu\text{m}$ . All panels primed and/or primed and topcoated were cured for least 14 days before testing. Some of the coated HDG steel panels were heat cured depending upon the topcoat and end-use application of the coating system.

### **Reference panels used in the studies**

The aluminum alloy and HDG chromate control panels had been pretreated with chromate and were coated with a standard military high solids chromate-containing epoxy primer, (CA 7233 + CA 7233B, blended in a ratio 1:1), which was obtained from PPG Industries, Glendale, CA. This primer conforms to military specification MIL-PRF-23377 H of Type I and class C. The topcoat used to topcoat the primed panels was a commercially available fluoropolymer-based military topcoat.

### **Test methods**

Test methods used to test the properties of the coated panels, e.g., the corrosion resistance of the coating system or the adhesion and mechanical properties of them, in the studies this year include the following methods:

- ASTM B-117 salt spray test
- ASTM D-714 salt water immersion
- ASTM D 3359 tape adhesion
- ASTM D 3912 chemical resistance
- ASTM D 4752 MEK double rub
- ASTM D 3363 pencil hardness
- ASTM G85 – SO<sub>2</sub> fog test
- Outdoor exposure (Hawaii)
- APGE cyclic Ford test

The exact description of the test conditions used in the above mentioned tests can be found in the ASTM standards or in the publications included in Appendix A.

### **Characterization methods**

Characterization methods used to understand the primer formulation chemistry, film formation chemistry and/or the corrosion protection mechanisms of the resulting primer films on the metals substrates studied includes the following techniques:

- DC polarization
- Electrochemical Impedance Spectroscopy (EIS)
  - Contact angle goniometry
  - IR spectroscopy
  - NMR spectroscopy
  - SEM/EDX
  - TOFSIMS
  - Ellipsometry

- Neutron and X-ray reflectivity
- Neutron scattering

The exact description of the measurement conditions used for the above mentioned techniques can in the publications included in Appendix A.

Certain bis-type silanes with the structure of  $(RO)_3Si(CH_2)_3-R'-(CH_2)_3Si(OR)_3$  provide excellent corrosion resistance on metals such as aluminum and steel. This section investigates the water barrier properties, water uptake kinetics and hydrothermal degradation of bis-amino silane (Bis-[trimethoxysilylpropyl]amine), bis-sulfur silane (Bis[3-(triethoxysilyl) propyl]tetrasulfide) and their mixture at the weight ratios of 1/3(amino/sulfur silane). These properties are critical to understand the origin of silane corrosion protection and the mechanism by which these films fail. The mixed silanes were also studied because they display better protection than either of the constituents alone. The results guide the improvement of superprimer formulations and identify potential vulnerabilities. The major conclusions are summarized at the end of the section.

## E. NEUTRON AND X-RAY REFLECTIVITY CHARACTERIZATION

### Water barrier properties

#### Sample preparation

A 1-wt % bis-sulfur silane solution was prepared by adding the silane to a mixture of DI water and ethanol. The ratio of silane/water/ethanol was (1/9/90) (w/w/w). After mixing with water the solution has to be hydrolyzed for some time to reach the “workable” condition. A uniform, transparent film can only be obtained from a solution that contains enough silanols generated by hydrolysis to accommodate subsequent condensation reactions. X-ray reflectivity (XR) of films spun at various hydrolysis times was employed to find the best hydrolysis time. Both the hydrolysis and condensation rates are pH-dependent, so the optimal hydrolysis time is actually controlled by pH. Under acidic conditions, fast hydrolysis is followed by slow condensation. An acidic solution, therefore, is more stable making it easier to obtain uniform films.

Since the natural pH of the bis-sulfur solution is around 6.5. Acetic acid was used to lower the pH to 4 to accelerate hydrolysis. The best hydrolysis time was found to be  $42 \pm 1$  hours for bis-sulfur silane. A 1% bis-amino silane solution was prepared similarly, but the pH was adjusted to 7.5 and the solution was aged  $18 \pm 1$  hours. The natural pH of bis-amino silane is above 10. Therefore, the solution is more stable at 7.5. The hydrolysis of bis-amino silane is much faster than bis-sulfur silane due to the catalytic effect of the secondary amine group.

The organic solvent used for the bis-amino solution was methanol because the hydrolysis product for bis-amino silane is methanol instead of ethanol. The mixture of bis-sulfur and bis-amino silane was made by mixing the above workable individual silane solutions at a bis-sulfur solution/bis-amino solution weight ratio of 3/1. The final solution contains 0.75-wt% bis-sulfur silane and 0.25-wt% bis-amino silane.

A 5 wt % silane solution was prepared in a similar way by adding the silane into a mixture of DI water and ethanol. The ratio of silane/DI water/ethanol was (5/5/90) (w/w/w). The mixture of bis-sulfur and bis-amino silane was made by mixing the “aged” individual silane solutions at a bis-sulfur solution/bis-amino solution weight ratio of 3/1. In the final solution, there will be 3.75 wt % bis-sulfur silane and 1.25 wt % bis-amino silane.

After the solution is properly aged, the film is deposited using a Laurell single-wafer spin processor.

During the first stage of study, silicon wafer substrates were used. The wafers are cleaned by immersion in a freshly prepared “piranha” solutions (conc.H<sub>2</sub>SO<sub>4</sub>/H<sub>2</sub>O<sub>2</sub> 30% =7/3 v/v) at room temperature for at least 30 minutes. After immersion, the substrates are rinsed repeatedly with de-ionized (DI) water. The silane solution is pipetted onto the wafers covering the whole surface. After one minute, the wafer is accelerated to 2000 rpm and held for 1 minute to spin off the excess solution and dry the film. The samples are dried in an oven for an hour at 80 °C or 180 °C.

To study the effect of the substrate on film properties, an Al layer was e-beam evaporated on a silicon wafer. The Al film thickness is around 200 Å and the roughness is about 10 Å. Silane films are then applied to the Al surface using the same spin-coating technique described above.

### **Characterization**

The water barrier properties of bis-amino, bis-sulfur silane and mixed silane films on Si wafers were assessed by neutron reflectivity (NR). NR is capable of probing structure, roughness and density of multiple layer coatings. The scattered beams from different interfaces of a multilayer structure interfere and give the reflectivity curve. The scattering power of each layer is called scattering length density (SLD), which is related to both coating mass-density and chemical structure. The measured scattering data are inverted to give the SLD profile normal to the film surface using the Parratt dynamic reflectivity formalism.

Deuterated solvents (D<sub>2</sub>O and deuterated nitrobenzene, d-NB) were used to challenge the silane coating films because of the high SLD, which enables NR to trace the solvent penetration in the silane films. The samples are conditioned and measured at equilibrium in saturated vapor. By varying the bridging functional group of silane, curing temperature, coating thickness and substrate type (Si/Al), the key factors determining the water barrier properties and anti corrosion performance were revealed.

### **Hydrothermal degradation properties**

#### **Sample preparation**

Samples are made according to previous section. Both 80 °C and 180 °C curing temperature were studied. Also both thin films deposited from 1% solution and thick films from 5% solution were prepared. Only silicon wafer substrates were investigated in the hydrothermal degradation study.

#### **Characterization**

The hydrothermal degradation properties of above silane films were studied by NR. Samples were first measured at as-prepared dry state to establish the virgin state. A sealed Teflon can containing water at 80°C was used to carry out accelerated aging. The samples were conditioned for 10 and 24 hours, and then measured in the re-dried state after each aging stage. The re-dry process takes about 12 hours in the presence of desiccant.

### **Kinetics of water absorption and transport**

#### **Sample preparation**

Samples are made according to previous section. Thick films deposited from 5% solution with 80 °C curing temperature and silicon wafer substrates were studied in this case.

#### **Characterization**

Kinetic studies of water transport in bis-silane films were performed in situ using NR and Reflection absorption Fourier transform infrared spectroscopy (FTIR-RA). For NR, measurements were carried out on bis-sulfur silane and bis-amino silane films in the presence of saturated D<sub>2</sub>O vapor. The time-resolved water ingress was calculated from the scattering length density (SLD) profile. Infrared

spectroscopy, because of its relatively quick response and the ability to identify the form of water absorption in silane films, was also used to monitor the water penetration progress, especially in the initial stage.

FTIR-RA measurements were conducted on a Perkin-Elmer Spectrum One spectrometer in mid-IR range (800 - 4000  $\text{cm}^{-1}$ ). All IR spectra were obtained with an incidence angle of  $45^\circ$  normal to the surface of the specimens with a spectral resolution of  $4 \text{ cm}^{-1}$ . For the dried and re-dried samples 64 scans were collected for each measurement. For the in situ sorption study, 16 scans were collected to ensure the rapid measurement in each run. In this case, the time for each spectra collection take approximately 1.5 minutes.

**Table 8.10: Calculated Neutron Scattering Length Density (SLD) for the materials used in this study.**

Material	Mass density ( $\text{g}/\text{cm}^3$ )	$10^6 \times \text{SLD}$ ( $\text{\AA}^{-2}$ )
Bis-amino silane monomer ( $\text{Si}_2\text{O}_6\text{C}_{12}\text{NH}_{31}$ )	1.04	0.299
Fully hydrolyzed bis-amino silane ( $\text{Si}_2\text{N}_1\text{C}_6\text{O}_6\text{H}_{19}$ )	1.04	0.522
Fully condensed bis-amino silane ( $\text{Si}_2\text{N}_1\text{C}_6\text{O}_3\text{H}_{13}$ )	1.04	0.816
$\text{D}_2\text{O}$	1.1	6.33
d-NB	1.204	5.55

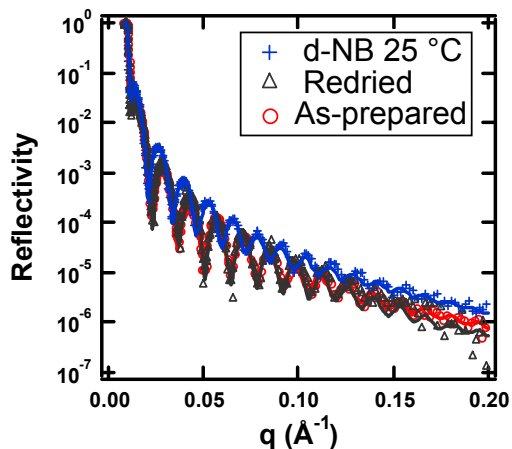


Figure 8.11. Neutron reflectivity data of bis-amino silane exposed to d-NB.

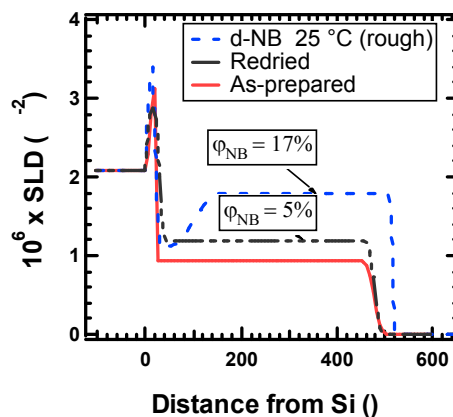


Figure 8.12 SLD profile of bis-amino silane when exposed to d-NB.

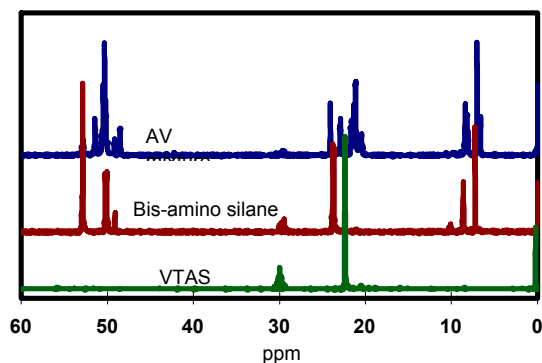


Figure 8.13.  $^{13}\text{C}$  NMR spectra of (a) AV3.4 mixture after 5-hour reaction time, (b) neat bis-amino silane, and (c) neat VTAS

## The AV silane system

### Objective

Coatings prepared with mixture of bis-[trimethoxysilpropyl]amine (bis-aminosilane, A) and vinyl triacetoxysilane (VTAS, V) are effective anti corrosion agents, but only under specific processing conditions. A water-miscible, stable and effective in anti-corrosion application can be achieved at A/V=3.4 (mol ratio).

This section focuses on the relationship between substrate-surface chemistry (cleaning), reaction mechanism, film structure and water-barrier properties of AV system. The major conclusions are summarized at the end of the section.

## **Chemistry of AV oil**

### **Sample preparation**

Neat bis-amino silane and VTAS were mixed at mol ratios (A/V) of 2, 3.4 and 5. After 4 hours from mixing of neat AV silane, 5-wt% water solutions of the AV mixtures were prepared by adding the neat AV into DI water while stirring. To retard condensation and to facilitate hydrolysis, an additional 0.12 wt% (of the total concentration) of glacial acetic acid was added to the water prior to the addition of neat silane mixtures. The diluted AV solutions were aged at ambient temperature for another 4 hours prior to spin coating.

### **Characterization**

$^{13}\text{C}$  and  $^{29}\text{Si}$  NMR were used to explore the reaction between bis-amino silane and VTAS.  $^{13}\text{C}$  NMR was used to determine the reaction between the amino and acetoxy functionalities.  $^{29}\text{Si}$  NMR was employed to monitor the hydrolysis and condensation reactions in water solution.

## **Cleaning**

### **Sample preparation**

The cleaning solutions of different pH were prepared by adjusting the amount of HCl and NaOH in the solution. The pH-values investigated were: 1.0, 3.6, 6.8, 8.5, 9.5, 10.5 and 12.4. The CRS substrate panels were first mechanically cleaned with Scotch Brite™, rinsed with deionized (DI) water and blow-dried. The panels were then cleaned ultrasonically in acetone for 10 minutes to further degrease the panels. Thereafter, the CRS substrates were immersed in the cleaning solutions at the different pH-values mentioned above at 60°C for 3 minutes. After cleaning, the panels were immediately rinsed with DI water, blow-dried and stored in a desiccator until further characterization. The blank control panel was also degreased as described above without immersing in cleaning solution.

For corrosion studies, some of the as-cleaned panels were dip-coated with silane and some were coated with a silane-containing primer. A 10 wt% aqueous solution of bis-amino silane and VTAS in a weight ratio of 5:1 was used for the silane coatings of the CRS panels. To facilitate the hydrolysis process, acetic acid was added to the DI water to adjust the pH to 5.5 prior to the addition of bis-amino silane/VTAS mixture. This AV mixture solution was aged for 4 hours at ambient temperature before it was applied to the as-cleaned CRS substrate. The AV silane coatings were applied by dipping the panels in the solution at room temperature for 30 seconds. The silane-coated panels were cured at 100°C for 1 hour in air.

The primer formulation contained 80-wt% epoxy resin, 10 wt% bis-sulfur silane, 9 wt% of AV silane and 1 wt% TEOS crosslinker. The primer formulation was applied by a draw-down bar. The primer-coated panels were cured at 100°C for 1 hour in air.

### **Characterization**

The etching rate of the CRS substrate was characterized by panel weight loss and by inductively coupled plasma mass spectroscopy (ICP-MS) of Fe in the cleaning solution. The contact angles were also measured for the panels cleaned under different pH solutions. Finally a 10 wt% bis-amino silane and VTAS mixture (3.4:1) was applied on the CRS panel surface and the corrosion resistance performance was investigated by DC potential measurements. A salt water immersion test (ASTM D714-56) was employed to evaluate the corrosion resistance of the primer-coated CRS panels. During salt water immersion, three fourths of a primer-coated CRS panel was immersed in aerated 0.6 M NaCl

solution at 25°C for one week.

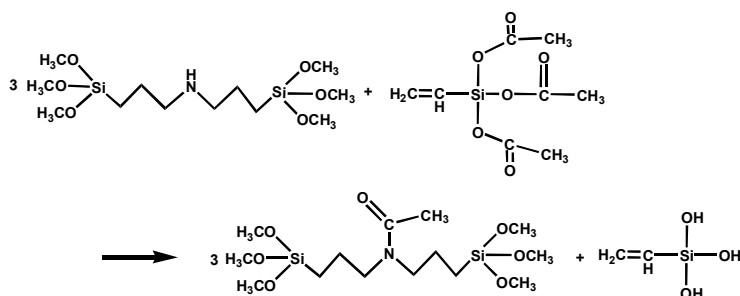


**Figure 8.14. Primary reaction in neat bis-aminosilane and VTAS mixture**

### Water barrier properties

#### Sample preparation

The Si wafers were cleaned by immersion in sulfuric acid/hydrogen peroxide (concentrated  $\text{H}_2\text{SO}_4/\text{H}_2\text{O}_2 = 7:3$  v/v) at room temperature for at least 30 min. After immersion, the substrates were rinsed repeatedly with deionized (DI) water and blow-dried.

The films were deposited using a Laurell single-wafer spin processor (North Wales, PA, USA). The silane solution was pipetted onto the wafer followed by one-minute stabilization to allow wetting and reaction with the substrate. The wafer was then accelerated to 2000 rpm or 3000 rpm and held for 30 s to spin off the excess solution and dry the film. To remove all traces of solvent and cure the film, the samples were then dried in an oven at 100 °C or 180 °C for 1 hour. The samples were kept in a desiccator until further measurements.

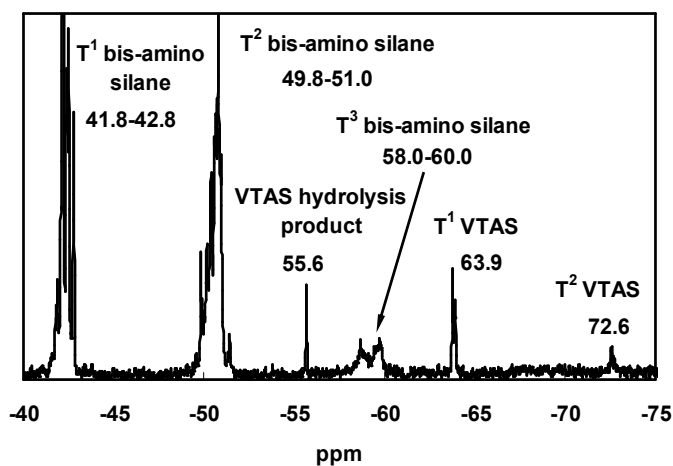


Figure 8.15.  $^{29}\text{Si}$  NMR spectrum of neat AV mixture. in -75 to -40 ppm range.

### Characterization

NR was utilized to investigate the water response of AV films. Samples are measured under similar conditions as described in the previous section.

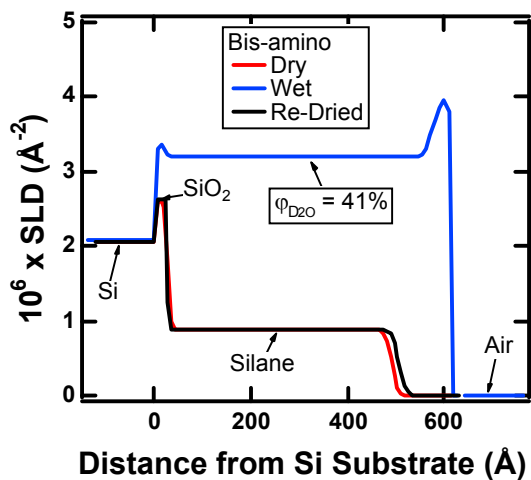


Figure 8.16. SLD profile of bis-amino silane under water conditioning at room temperature.

The background spectra on bare Si wafer were collected before each run under the same conditions. The background spectra were subtracted from each scan to obtain the IR spectra. The as-prepared dry state of the sample was measured with the desiccant present in the sealed sample chamber. During the D<sub>2</sub>O conditioning, the desiccant was removed and D<sub>2</sub>O water reservoir was put into the sealed sample chamber. FTIR was measured as soon as D<sub>2</sub>O is transferred into the sample holder. The FTIR-RA spectrum is repeatedly recorded at the designed time interval until the equilibrium state is confirmed by no further change.

## Epoxy-silane system

### Objective

Based on previous work, bis-silanes perform as coupling agents in anti-corrosion films, which make them promising alternatives to chromate metal pretreatment in metal-finishing industries. However, silane films have limitations in mechanical properties. Silane films thicker than 0.3 μm are subject to cracking; Epoxy resin has superior chemical and corrosion resistance as well as outstanding mechanical toughness. van Ooij et al. have established an excellent coating system with fairly high hardness based on mixture of epoxy (EPI-REZ™ 5003-W-55) and bis-silane (bis-sulfur).

The purpose of this work is to study the underlying mechanism of anti corrosion performance. The water barrier, hydrothermal degradation and salt exclusion properties of epoxy-silane coating system were investigated. The major conclusions are summarized at the end of the section.

## Water Barrier properties

### Sample preparation

In order to utilize reflectivity technologies as probes to investigate the water response of epoxy-silane coating system, high quality thin films are essential. It is difficult, however, to form high quality thin films from original water-born epoxy due to the large liquid particles in the emulsion. Films from water solutions do not form smooth enough films for reflectivity studies. Since the interactions among silane, epoxy and environment are the key factors of anti-corrosion performance, minor additives and surfactants will not affect the anti corrosion performance. Therefore we investigated films spun from solvents using the key epoxy components found in the water-borne emulsion. Both 4 MEK : 6 Toluene and 3 THF : 7 Toluene (V:V) are good solvent mixtures to form high quality film. The wafer cleaning procedure is the same as described in previous section. The coating solution formulation is shown in Table 8.17. Before mixing with epoxy and curing agent, Bis-sulfur silane should be properly aged (hydrolyzed) in ethanol. And the final mixed solution must not be older than 10 minutes to get smooth film.

**Table 8.17. Formulation of epoxy-silane anticorrosion coating system**

Novolic 5003	Bis-sulfur	Curing agent (polyamine)
75wt%	6wt%	19wt%

The samples are spun on 3 inch silicon slabs from 1% epoxy-silane solution by using a Laurell single-wafer spin processor. The mixture solution was pipetted onto the wafers covering the whole surface. After holding for one minute, the wafer is accelerated to 2000 rpm and held for 30 seconds to spin off

the excess solution and dry the film. The samples are dried in an oven for two hours at 90 °C and then at 120 °C for 30 minutes.

### **Characterization**

XR and NR were utilized to discover the film structure and to track the responses to water. The water barrier properties of pure epoxy and epoxy-silane mixture were assessed by NR. The samples are conditioned and measured kinetically and at equilibrium in saturated vapor in a sealed Al can. To understand the behavior of epoxy-silane system when directly contact with liquid water, the samples were also put in a liquid cell and interrogated by a neutron beam from the back (silicon side). By comparing the responses of pure epoxy and epoxy-silane samples, the role of silane can be interpreted.

### **Hydrothermal degradation**

#### **Sample preparation**

Samples are made according to previous section.

#### **Characterization**

For the hydrothermal degradation study, pure epoxy and epoxy-silane mixtures were first measured by NR in as-prepared dry state to establish the virgin condition. Hydrothermal aging is accelerated by immersing the samples in 80 °C water in a sealed container. The aging status is monitored after 10, 24 and 36 hours of exposure. The samples are re-dried for 4 hours in vacuum at 60 °C prior to assessment by NR.

### **Salt exclusion properties**

#### **Sample preparation**

Samples are made according to previous section.

#### **Characterization**

Anti corrosion performance is due to more complex aspects of the film than simple water barrier properties. The salt ions, especially chloride ions, play an important role in the metal corrosion. To investigate the salt exclusion behavior of the coating system, pure epoxy and mixed films were measured by NR at equilibrium in contact with pure H<sub>2</sub>O, saturated NaCl H<sub>2</sub>O solution and pure D<sub>2</sub>O liquid.

## VIII. RESULTS AND ACCOMPLISHMENTS

### A. PRIMERS FOR CRS

#### Test Results for Initial Formulations

**Table A.1** summarizes the test results of Superprimer formulation named ‘F’. The results are compared with a control primer. The control was a chromium containing primer from the Navy named PRC Desoto MIL-PRF, containing about 25 % wt of chromate. Figure A.1 shows the ASTM B117 Salt fog test results of the control and formulation F after 2 weeks. After 2 weeks the control did not show any corrosion in the scribe but superprimer F did. The corrosion resistance performance in other areas of the panel looked comparable. The corrosion of the scribe in formulation F coated panels was expected because the superprimer formulations do not have the so called self-healing effect of chromate-containing primers. EIS Results: Figures A.2 and A.3 show the EIS Bode plots of formulation F and the control. The plots show considerable difference in the film’s resistance and water penetrability of the coatings. The decrease in impedance values with due time indicates the decrease in resistance due to water penetration.

Table A.1: Comparison of performance of test results between control PRC Desoto MIL PRF and Superprimer Formulation F

	CONTROL	FORMULATION F
Salt spray	No corrosion in the scribe after 2 weeks	Corrosion in the scribe after 2 weeks
Salt immersion	Sustained for 1 month	Sustained for 1 month
Contact angle	69.5°	65.5°
EIS	6 ohm for 1 week	3 ohm for 2 days
Hardness	F	HB
Adhesion to Substrate	5B	4B
Paint Adhesion	5B	5B



Figure A.1: Yellow panel (left) is an aluminum panel coated with the PRC Desoto MIL-PRF Yellow primer from military. And the other panel is coated with formulation F

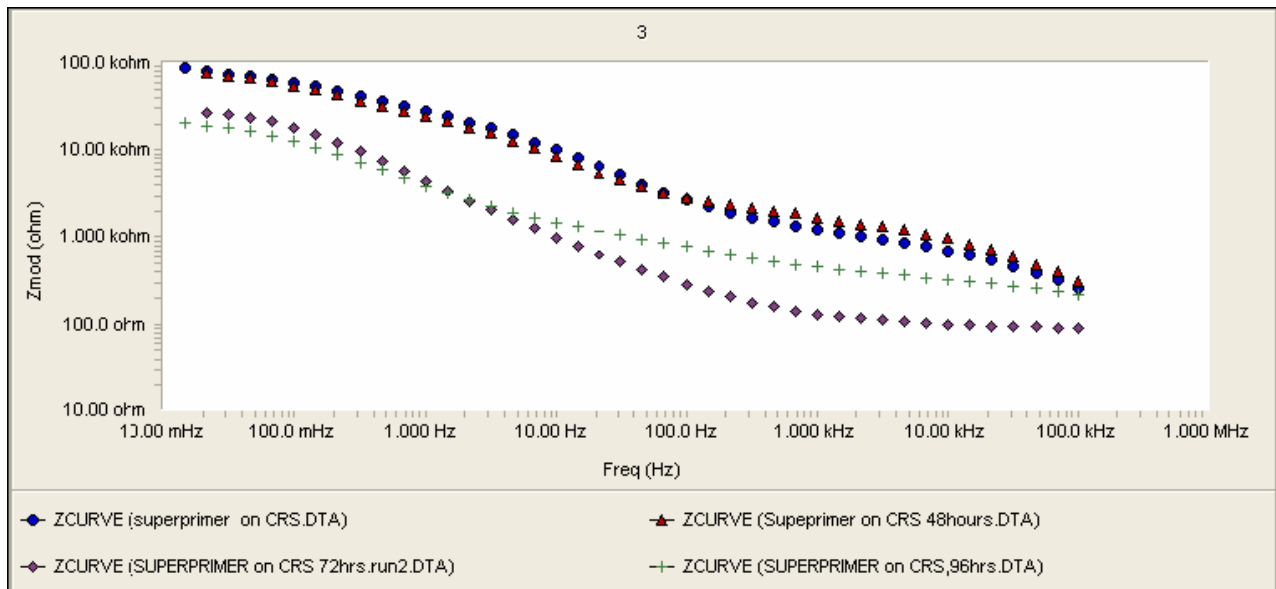


Figure A.2: EIS Bode plot of formulation F coated on a CRS substrate and tested for 4 days.

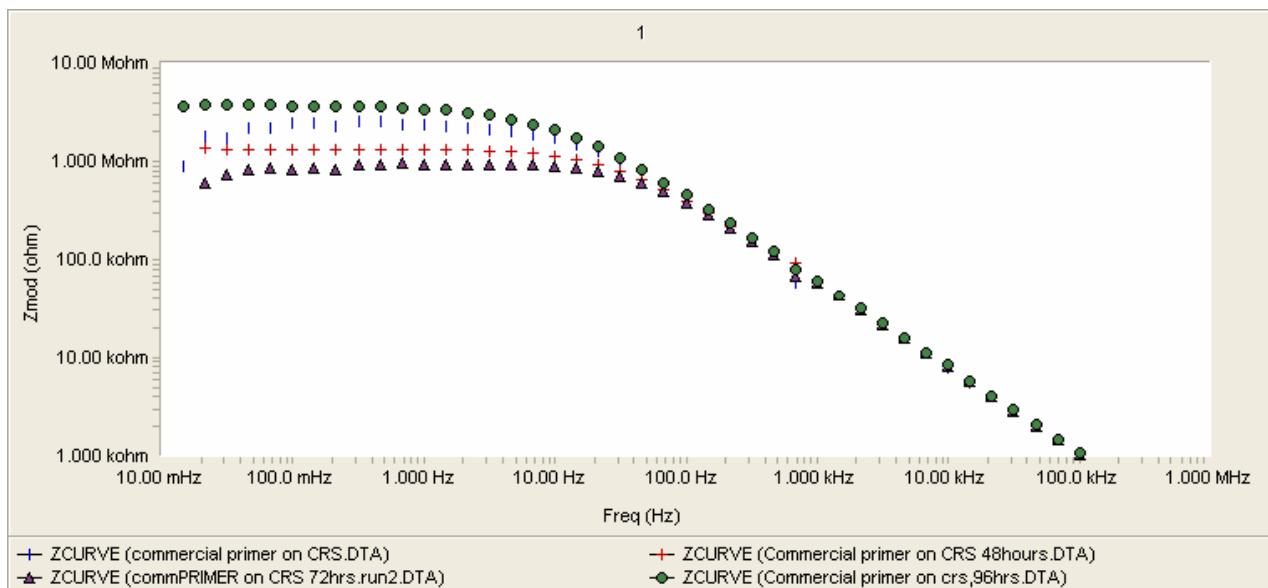


Figure A.3: EIS Bode plot of control PRC Desoto MIL PRF chromate-containing primer coated on a CRS substrate and tested for 4 days.

EIS plot of formulation F shows that the modulus values decrease with time. The figure also shows appearance of a second time constant which indicates appearance of a second conducting layer in due time. These two factors prove the hydrophilic nature of the formulation. Due to this nature, the coating seems to attract water molecules through its pores. The second conducting layer might be due to the complex molecular film formed by these and other hydrophilic groups in between the coating and the metal substrate. The EIS plot of the control did not show any signs of second time constant even though the modulus values decrease in due time.

### Improved Formulations

Although we were able to formulate successful coating formulations from silane resin combinations, the performance of superprimer formulation F was not up to par with the chromium containing controls. The coatings showed considerable hydrophilic nature. In an effort to improve the hydrophobicity of the coating, an addition of a known silane with extreme hydrophobic nature was sought. Bis-sulfur silane has been proven to be an efficient silane for use against corrosion protection in previous work. A new formulation F-6 was formulated and tested in this effort.

The following gives the information about the formulation. Formulation F-6:

The components and mixing procedure of Formulation F-6 are:

Part A: EPI-REZ 3540-WY-55 Epoxy resin

Part B: AV5 10 % in water at pH 6

Part C: TEOS

Part D: Bis-sulfur was used in pure as obtained state without further hydrolysis.

By weight:

Part A (80%) + Part B (9%) + Part C (1%) + Part D (10%)

\_ High-shear blended for 10 minutes at 2000 rpm. Bis-sulfur silane is not water-soluble. But solutions that were uniform to the visible eye were obtained after high shear mixing of the components. Even the coatings that were obtained from these coatings did not show any signs of immiscibility. The formulations did not separate into different layers in due time either.

\_ After allowing 20 minutes of incubation time, cleaned aluminum panels were either brushed or coated using a drawdown bar

\_ Panels cured at 100°C for 1 hour

### Test Results of Formulation F-6

The addition of hydrophobic sulfur silane improved the hydrophobic nature of the superprimer coating. Figure A.4 shows an EIS Bode plot comparing the modulus values of F-6, F and the control. The plot shows no drop in the F-6 curve even after 1 week of immersion. Whereas the EIS curves of formulation F were observed to drop with time. Figure A.5 shows an aluminum panel coated with F-6 and salt spray tested for 2 weeks. The picture shows no pitting in the un-scribed area and also no considerable corrosion in the scribe.

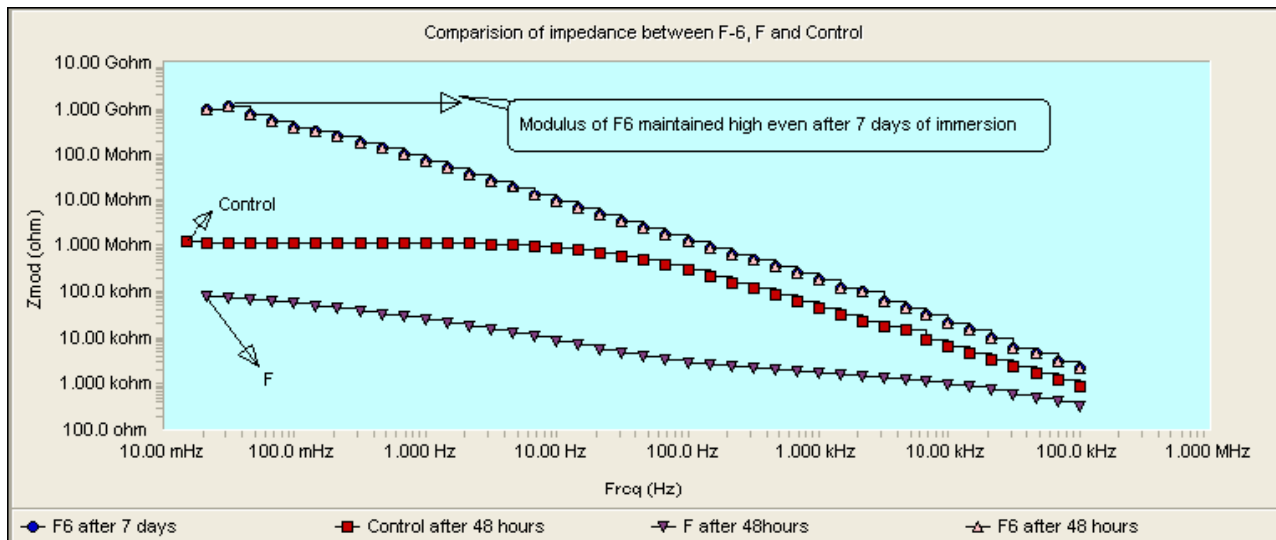


Figure A.4: EIS Bode plot comparing the curves of F-6, F and the control Desoto PRC MIL PRF



Figure A.5: Salt spray result of F-6 after 2 weeks

Table A.2 summarizes all the test results of F-6, F and control. Results of test such as hardness and tape adhesion showed considerable improvement in superprimer formulation F-6 in comparison to F.

Table A.2: Summary of test results of the control, F-6 and F

	CONTROL	FORMULATION F	FORMULATION F-6
Salt spray	No corrosion in the scribe after 2 weeks	Corrosion in the scribe after 1 week	Corrosion in scribe after 2 weeks
Salt immersion	Sustained for 1 month	Sustained for 1 month	Sustained for 2 months
Contact angle	69.5°	65.5°	78.4°
EIS	1 Mohm for 1 week	100 kohm for 2 days	1 Gohm for 1 week
Hardness	F	HB	F
Adhesion to substrate	5B	4B	5B
Paint Adhesion	5B	5B	5B

### **Additives to Primer**

The silane plus resin combinations can lead to coating formulations but to make it perform on par with chromate primers further additions need to be made. Detailed explanation of the idea, purpose and expectations of these additives in the primer were already given in the introduction sections. In this chapter, details about the mixing procedure of the additions, different kind of additives that were tried and their test results are given. There are primarily two important kinds of additives, nanoparticles and corrosion inhibitors. Many commercially available particles and inhibitors were tried and tested for corrosion performance. Test results by EIS and salt spray exposure are provided.

### **Pigments/Particles**

Particles and pigments are usually added to the paint to impart special characteristics or improve the coating properties of the primer/topcoat. Pigments, which are usually dry colorants, are used for coloring of paint, ink, plastic, fabric and other material. They can be natural, synthetic, organic and inorganic pigments. Pigments work by selectively absorbing some parts of the visible spectrum while reflecting others. Most of the nanoparticles have a catalytic effect on the chemical reactions occurring in the paint/primer systems. The particles for inclusion in the superprimer were also selected on the basis of their effect on the chemical reactions and curing of the primer.

Previous studies indicated that inclusion of silica particles improved the anti-corrosion performance of silane films. It was proposed that silane films that contained 5-ppm silica in them behaved as a cathodic barrier like cerium compounds. This type of activity is done with paint systems where the mechanical properties are improved by adding particles such as fillers, pigments and extenders in paint systems. The following particles were tried and tested in superprimer formulations:

- Silica
- Alumina
- Carbon Black
- Zinc Dust
- Corrosion Inhibitors

A separate section is devoted for formulation and testing results of zinc dust inclusion. The others are discussed below.

### **Silica, Alumina and Carbon Black**

The mixing procedure of superprimer with particles is not different from the procedure of silane and resin mixture. The particles are included along with other components and mixed using the high-shear mixer. The curing conditions were also not changed. The metal panels were cleaned in the same manner as mentioned before in the previous sections.

Table A.3 gives a detailed description of the components, their weight percentages in the mixtures and their corresponding formulation number. In some formulations there are no particle additions. Silanes such as A-link 25 and A-link 15 were tested to increase the cross-linking density of the films. Formulations numbered F 10 to F 12 are with alumina particles in increased weight percentages. F13 to F15 are with calcium zinc molybdate, a corrosion inhibitor from Molywhite

Corporation. Similar information about the additions in other formulations is clearly given in the table.

Table A.3: Formulation chart of modified superprimers with particles/inhibitors

FORMULATION (BY WEIGHT)	RESIN	AV5 (10%)	SULFUR SILANE	TEOS	ADDITION
F6	80	9	10	1	nil
F10	77.5	9	10	1	(Alumina) 2.5
F11	75	9	10	1	(Alumina) 5.0
F12	70	9	10	1	(Alumina) 10.0
F13	77.5	9	10	1	(CZM) 2.5
F14	75	9	10	1	(CZM) 5.0
F15	70	9	10	1	(CZM) 10.0
F16	80	9	10	nil	A-LINK-15
F17	80	9	10.9	nil	(A-link 25) 0.1
F18	80	9	10.9	nil	A-LINK-15 0.1
F19	80	9	10	1	BTSE (10%)
F20	78.8	9	10	1	(Cortec M119 LV)1
F21	78	9	10	0.5	Cortec M-5120(1%) + A-

					LINK-15(0.5)
F22	78	9	10	0.5	Cortec M-118(2%)+A-LINK-15(0.5)
F23	78	9	10	0.5	Sodium Vanadate 2%+A-LINK-15(0.5)
F24	75	9	10	0.5	Sodium Vanadate 5000 ppm+A-LINK-15(0.5)
					Halox SZP-391Strontium
F 25	77	9	10	0.5	Zinc Phosphosilicate 3%+A-LINK-15(0.5)
F26	80	9	10.5	0.5	nil
F27	77	9	10.5	0.5	Wayne Pigment Corp., Corrostain 3 %
F28	77	9	10.5	0.5	Carbon Black 3%
F29	77	9	10.5	0.5	UC Pigment 3%

### Results and Discussion

Previous work over modified silane films showed that increase in the percentage values of silica in the silane solutions actually decreased the performance against corrosion. Figure A.6

shows an EIS plot showing the effect of various amounts of silica in silane films. A probable theory for the mechanism of how the silica particles are acting towards the improvement of corrosion resistance performance was also given.

Figure A.6 combined with other test results proved that an optimized amount of silica is required for the best performance of the silane films. A similar observation is observed in case of superprimer formulations also. Formulations F 10, F 11 and F 12 have alumina nano-particles in increased weight percentages of 2.5, 5.0 and 10.0. A simple salt immersion test of AA 2024-T3 panels coated with the above three formulations showed that increased weight percentages of alumina in fact decreased the anti-corrosion performance. Figure A.7 shows salt immersion results after 7 days in 3.5% wt in DI water.

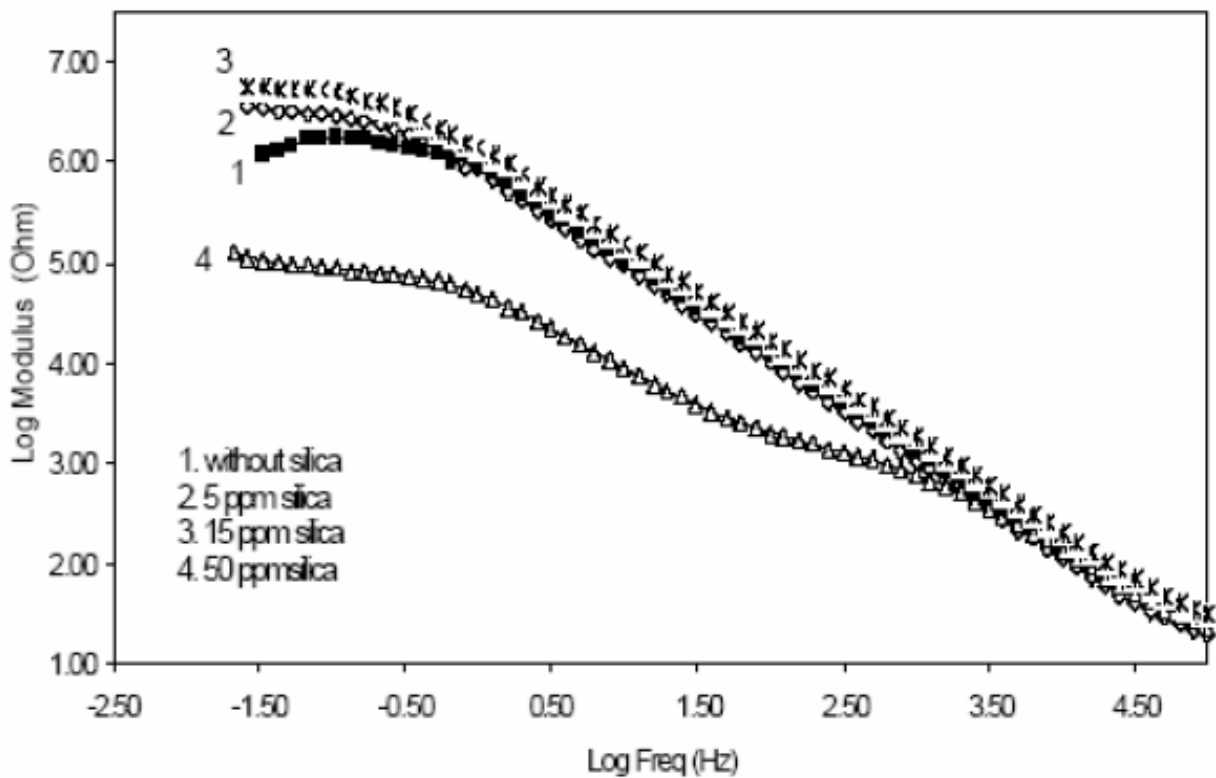


Figure A.6: Impedance plots of bis-sulfur silane treated AA2024-T3 systems loaded with different amounts of silica nano-particles

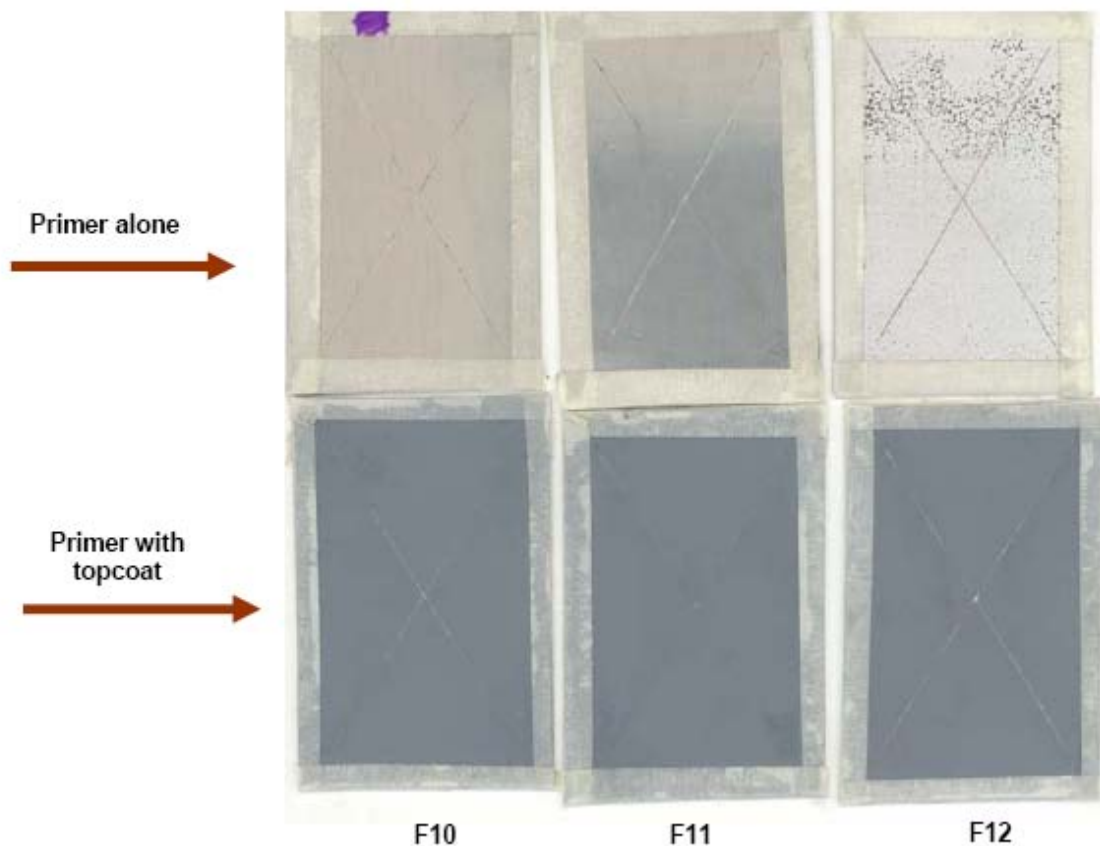


Figure A.7: Salt immersion test after 7 days. Formulations with increased weight percentages of alumina numbered F10, F11 and F12 in Formulation table.

EIS impedance values of the above coatings F10, F11 and F12 conformed to the above observation. Formulation F10 with 2.5 % alumina showed better impedance values with time. Figure A.8 shows EIS impedance values of salt fog-tested coatings with time. Impedance values of F10 were higher than F11 and F12 in most cases. Figure A.9 shows a similar plot with the same coatings but now with a topcoat over them. The topcoat used was a polyurethane based topcoat manufactured by DEFT. The impedance values of F10T and F11T, coating formulations of F10 and F11 with same topcoat showed similar performance.

Figures A.10, A.11 and A.12 show Bode plots of the coatings with and without topcoats tested. The numbers in the legend of the figures denote the number of days the panels has been exposed to the salt solution. Bode plots of coatings without topcoat show gradual decrease in the impedance values with time. All the three formulations behaved in the same way. This decrease in impedance values can be attributed to water penetration into the film with time. Bode plots of coatings with

topcoat showed varying results with time. The change in impedance values was not consistent with or linear with time. But the impedance values in all three cases were high, which showed an obvious fact that the water resistance of the coatings with topcoat is greater than the coatings without topcoat. The salt spray test results conformed to the observations made using EIS test. Figure A.13 shows salt spray results of F 10, F11 and F12 formulations with and without topcoat after 3 weeks of testing.

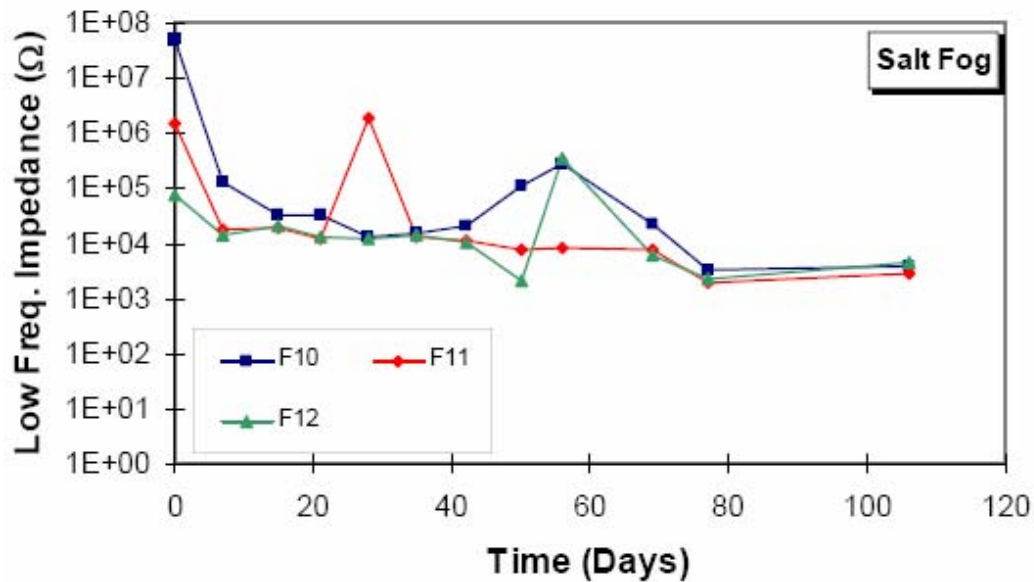


Figure A.8: EIS Impedance values of salt fog tested coatings with time.

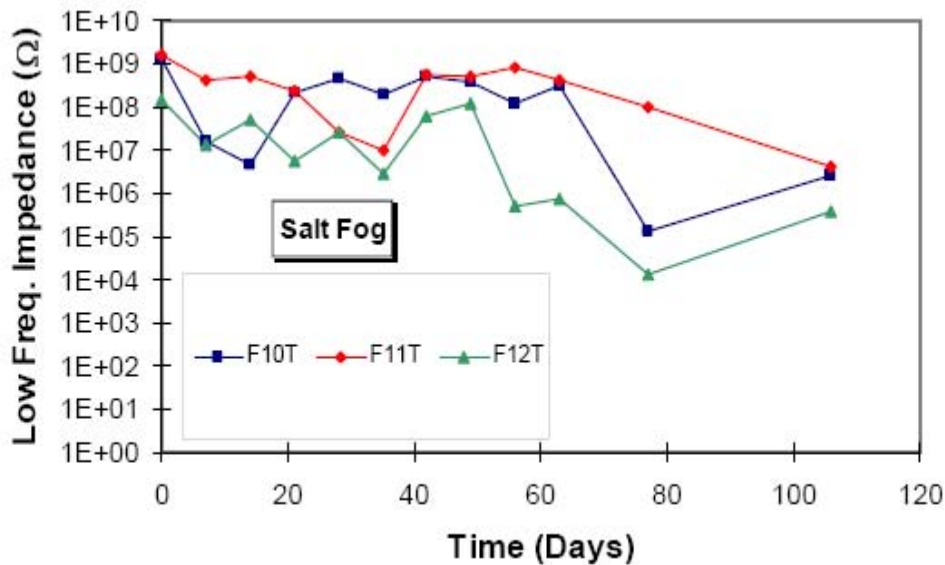


Figure A.9: EIS Impedance values of salt fog tested coating with time of coating formulations containing alumina and with polyurethane topcoat.

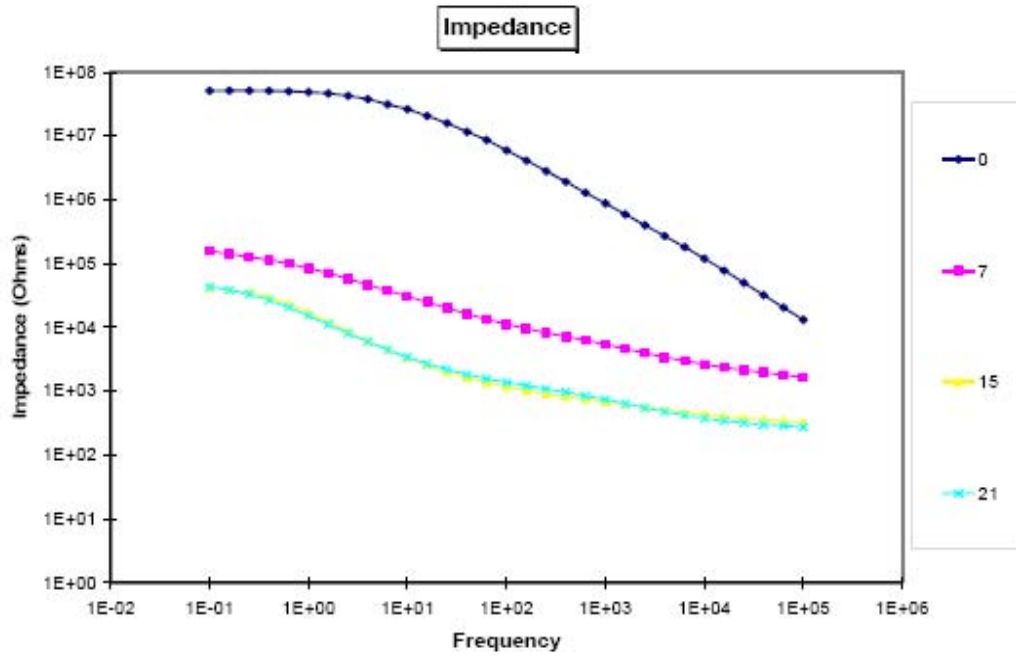
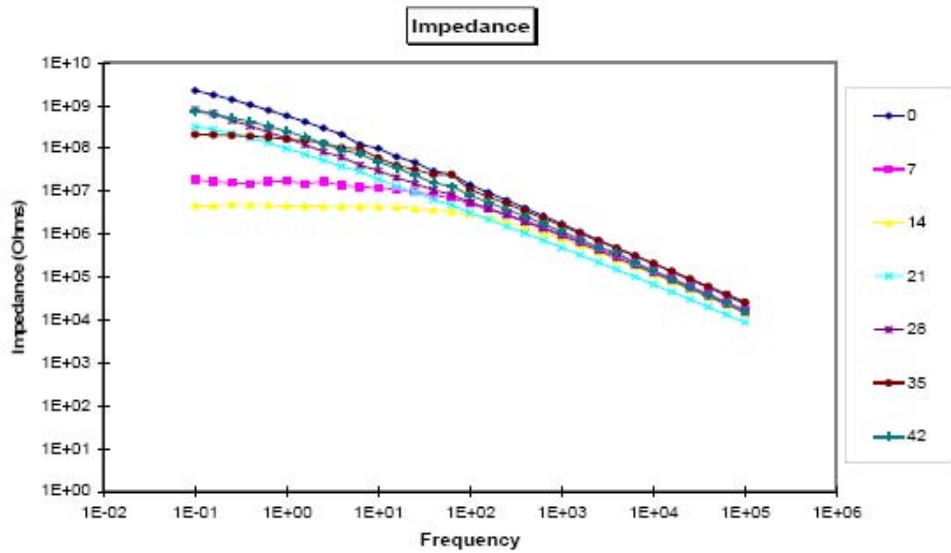


Figure A.10: Bode plot of F 10 without topcoat (above) with topcoat (below)



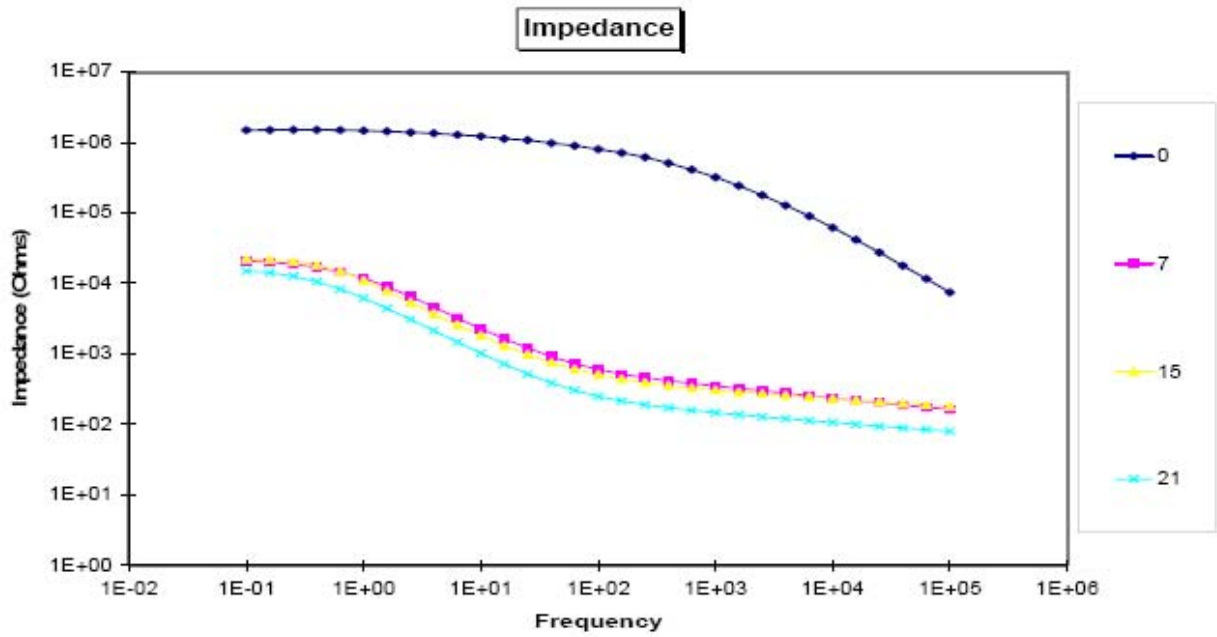
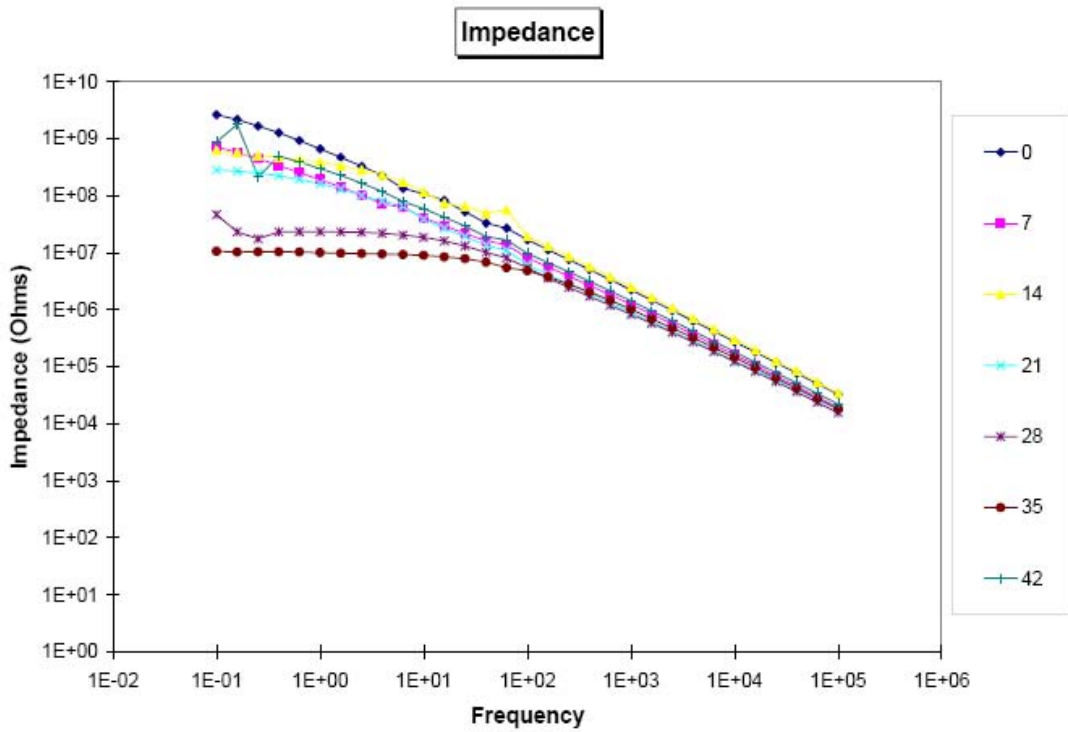


Figure A.11: Bode plot of F 11 without topcoat (above) with topcoat (below)



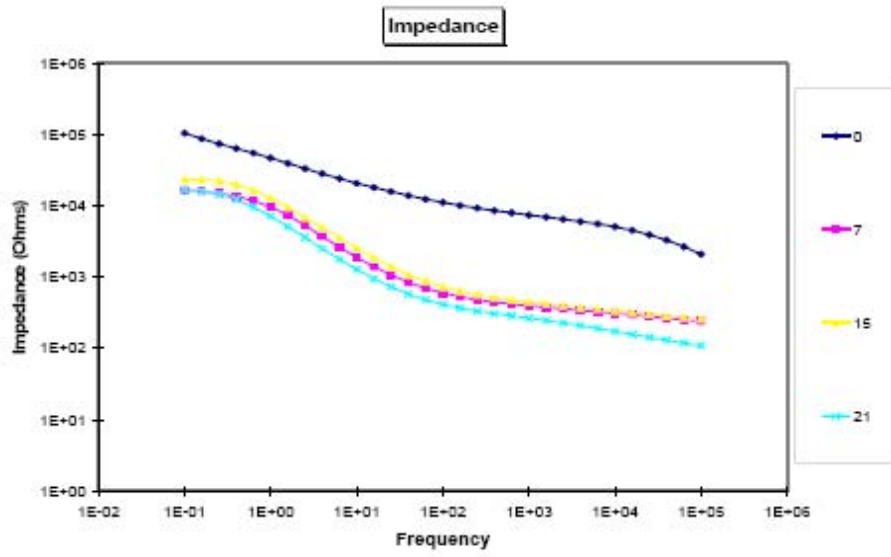
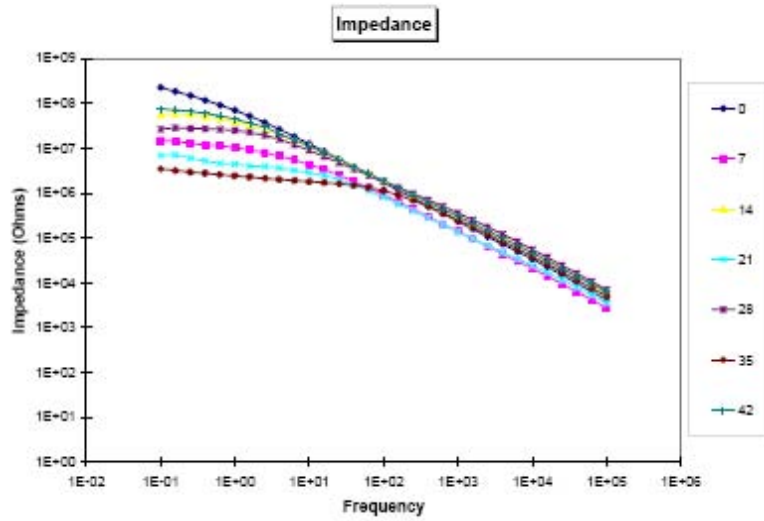
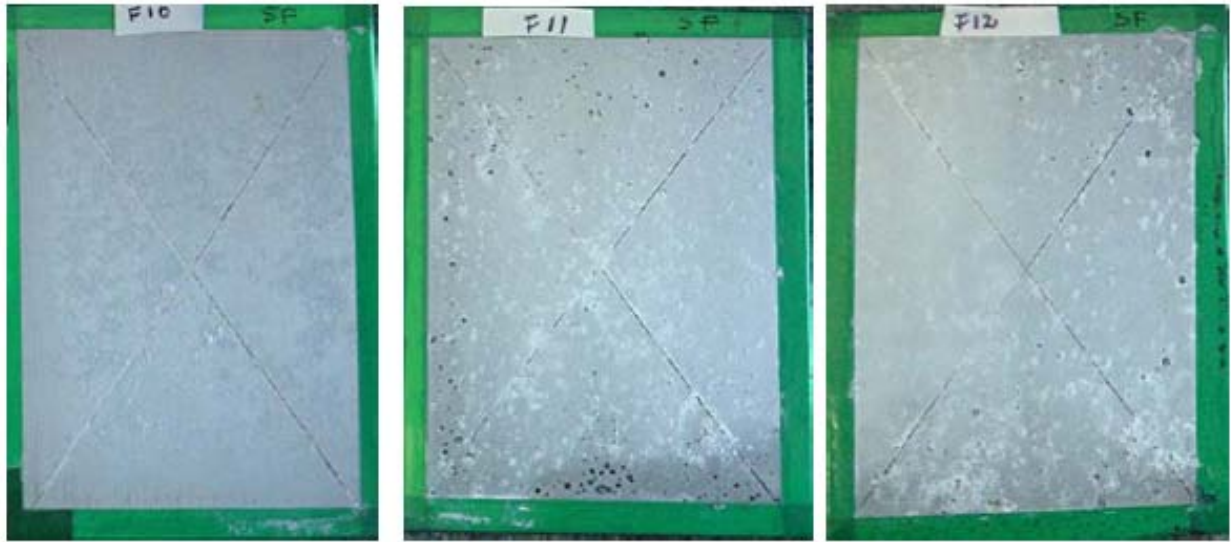


Figure A.12: Bode plot of F 12 without topcoat (above) with topcoat (below)





Salt Spray results of F 10, F11 and F12 without topcoat after 3 weeks



Control Salt Spray results of F 10, F11 and F12 with topcoat after 3 weeks

Figure A.13: Salt Spray results of F 10, F11 and F12 with and without topcoat after 3 weeks. The formulation information can be found from table A.3. Control is AA 2024 T3 panels with chromium pretreatment and epoxy primer with barium chromate.

The EIS Bode plots of the individual formulations containing alumina showed an appearance of a second time constant for longer immersion times. The 7 day curve of F10 was a rather flat when compared to curves of F11 and F12. The change in slope of the curves that indicates the appearance of a second time constant was more prominent in F11 and F12 than in F10. This

second time constant mentioned before indicates the appearance of a second hydrophilic layer beneath the topmost layer and above the metal oxide surface. This might indicate that water penetration through the films is less in case of F10 when compared to F11 and F12 for a short period of time. After 2 weeks all the 3 curves showed similar behavior in Figures A.10, A.11, and A.12.

This particular observation leads us to an explanation that can be given to behavior of the particles in the primer. According to researchers there is a critical amount of pigment that can be added to an organic coating system, beyond which the coating becomes more permeable or porous. Nano-particles are known to have a catalytic action on the chemical reactions in the primers. This observation was evident in case of formulations containing alumina, i.e., F10, F11 and F12. The pot life of a primer, which is the amount of time the primer stays at coat-able viscosity before gelling up after all the components are mixed. The pot lives are usually high for water-based primers when compared to solvent-based primers. In case of superprimer formulation F-6, it is close to a week. The pot-life changed with the kind of addition that is made to the primer. The weight of alumina in the formulations had an inverse linear relation with the pot-life.

The pot-life of the formulations decreased with increasing percentage of alumina. Similar behavior was found even in the case of inhibitor addition mentioned in the later part of the chapter. The factor that can influence the performance is that the particles being hydrophilic in nature obviously attract water into the films. This is evident in the poor performance of the formulation with higher percentages of alumina. A similar explanation is given as a mechanism for silica in silane films [3].

### **Carbon Black**

Carbon black is one of the oldest fillers used in the paint industry. It was used 27000 years ago for cave paintings, and in 2500 BC by the Egyptians in inks. It was also used for the printing process during the Middle Ages. The rubber industry is the biggest user of carbon blacks by a large margin, in comparison. The paint industry is only a modest user. The printing inks industry also uses significant quantities. Finer particle blacks are used for high-quality finishes such as in automotive paints on account of their higher jet-ness. Medium size blacks are used for intermediate quality paints, whereas the coarser pigments are used for decorative paints. For tinting purposes coarser grades are usually used as their lower strength meaning they are easier to control.

Carbon-black pigments are very fine particulates of sub-crystalline carbon fused into larger aggregates. It is a mixture of partially burned hydrocarbons. Carbon black is produced by partial combustion of natural gas. It is used as a black pigment for inks and paints, and is used in large amounts by the tire industry in the production of vulcanized rubber. Lampblack resembles carbon black, but is produced by burning liquid hydrocarbons, e.g., kerosene; it is often somewhat oily, is duller than carbon black, and may have a bluish undertone. It is sometimes used in making contact brushes for electrical apparatus. Any of various finely divided forms of carbon derived from the incomplete combustion of natural gas or petroleum oil and used to reinforce rubber and as an ingredient in inks, paints, crayons, and polishes.

Carbon blacks can be difficult to disperse as they have very small particles with a correspondingly large surface area. Improved dispersions can be attained by oxidizing the surface of the pigment or

by adding small quantities of organic groups such as carboxylic acids. Such groups decrease the pH of the aqueous extract and aid the wetting of the particles. The viscosity of the paint is affected by the inclusion of carbon particles. Particles of carbon form clusters that are often compared to a cluster of grapes, held together by forces ranging from weak physical attraction to chemical bonds. This structure affects the dispersibility, the jet-ness, gloss, and, above all, the viscosity of the paint. One of the problems with carbon black can be due to the absorption character of it. The light dusty form of carbon blacks allows them to be converted to an easy-to-disperse pellet form by the dry pelleting process. Over a period of time carbon blacks absorb active ingredients in a paint formulation, such as the metal soaps used as driers in air-drying alkyds. This absorption can lead to problems; however, doubling the dosage of drier content is a common way of compensating for this issue.

### **In the Superprimer**

Carbon black was tested as a pigment addition in the superprimer formulation. F28 is the formulation number corresponding to this formulation. 3% by weight of carbon black was introduced into the resin plus silane mixtures. The mixture was prepared using a high-shear blender similar to the other methods. The formulation was coated on AA 2024-T3 panels and was cured at 100°C for 1 hour. The coating resulted had an appearance of a glossy black paint. Performance tests like EIS and Salt Fog exposure were used to evaluate the coating. Figure A.14 shows the salt fog performance of the F 28 panel after 28 days. It can be observed from the figure that the performance showed no decrease for the first 7 days of exposure but gradually decreased after 28 days.

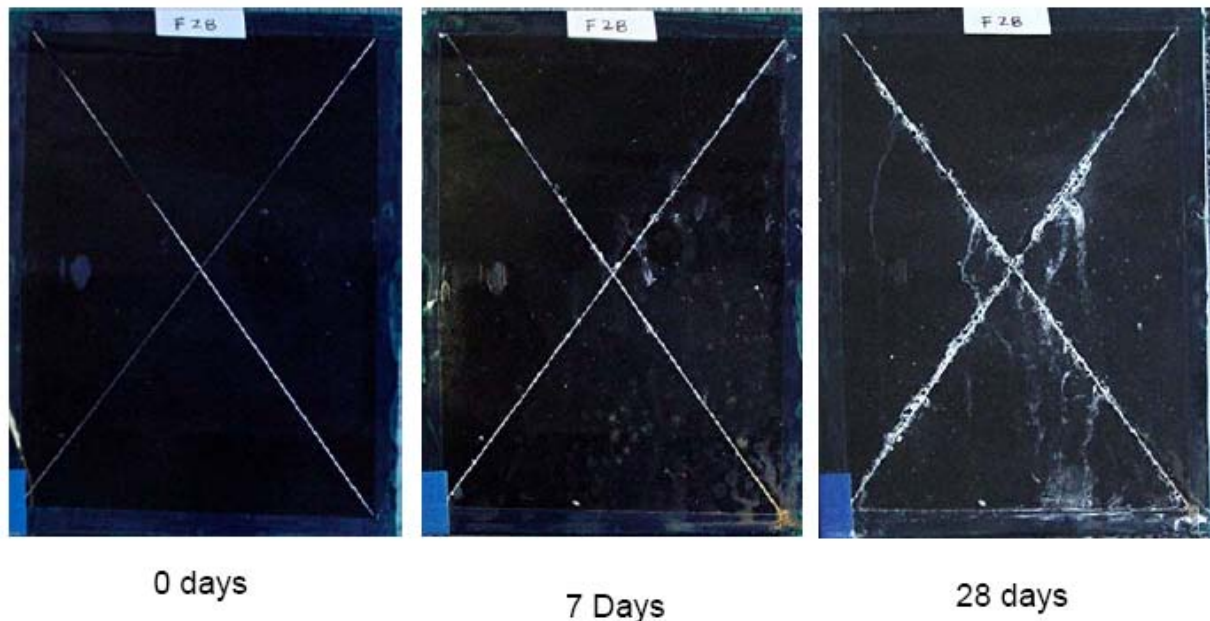


Figure A.14: Salt Fog test performance of F 28 after 0, 7 and 28 days. The formulation information can be found from table A.3.

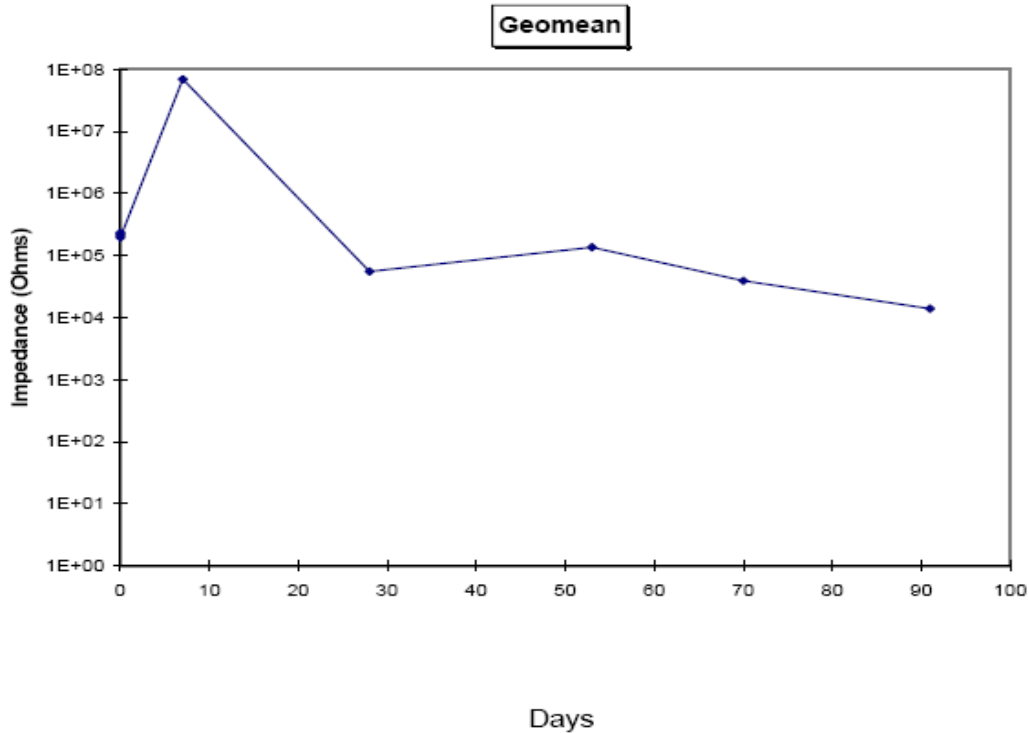


Figure A.15: Change in impedance values of F 28 coating with exposure time. The formulation information can be found from table A.3.

The observation in the salt fog conformed to the impedance change in Figure A.15. This figure shows an increase in the impedance values in the initial days of exposure. After 7 days the impedance showed a gradual decrease and the impedance values stabilized after 1-month exposure. The modulus value of the coating initially showed increase. This means that the resistance of the coating is increasing and the penetration of the corrosion causing species is difficult or slow. In due time the modulus values showed a decrease in their values and stabilized after 30 days. This shows that the coating's conductive nature improved with time or in other words the resistance of the coating decreased. This behavior can be explained by the penetration of water, oxygen and other corrosion causing species after long exposure times. After long exposure times the conducting species such as water penetrate through the coating and make the film more conductive. Initially the silane hydrolyzes thus increasing the resistance but after long periods of time the resistance drops due to passage of ions to the substrate. The same observation and deduction can be made from Figure that shows the individual impedance curves not clear.

### Corrosion Inhibitors

The idea of including a corrosion inhibitor is used to achieve what is called a 'self-healing' effect in superprimers. A few promising chromate replacements inhibitors have been derived from cerium and molybdenum salts. These are believed to inhibit corrosion by controlling the cathodic reaction by precipitating hydroxide/oxide layers at local regions of high pH [61-62]. Chromium containing primers have this property and it is this character that makes them so efficient. Corrosion inhibitors were loaded and tested in silane films before [3]. Some water-soluble silane

mixtures showed excellent corrosion behavior comparable to that of chromates. However, it was observed that alcohol-based silanes offer a higher corrosion resistance to the water-based silane systems. Vignesh et al showed that one of the ways to increase the corrosion performance of these silanes is to add corrosion inhibitors to the films that can leach out slowly. The results that are reported here for various organic and inorganic inhibitors were studied for the corrosion inhibition of AA2024-T3 alloys in 0.5 M NaCl solution. Examples are benzotriazole tolyltriazole and rare earth metal salts, e.g., cerium nitrate.

Many inhibitors were selected and tried by including them in the formulations. Formulations numbered F13, F14 and F15 in formulation table have calcium zinc molybdate in increasing weight percentages. Formulations F20 to F29 except for F26 and F28 are primers containing different kinds of corrosion inhibitors from different companies. Only those inhibitors that are recommended for their use in waterborne primer formulations were tested and tested. Chemical information of these inhibitors was provided in earlier sections.

### Results and Discussion

**Figure A.16** shows the change in impedance values with time of the formulations F13, F 14 and F 15. The curve of F15, which has the highest amount of calcium zinc molybdate (CZM) showed marginally higher values of impedance values than the formulations with lower weight percentages. Figure A.17 shows the salt spray results of the formulations with and without topcoat in Figure A.18. The results show that formulations with higher percentages of CZM performed better. This observation conformed to the EIS impedance plot above. The individual EIS Bode plots show that impedance values decrease at high magnitude for the first few days and then the modulus curves change at a very low magnitude. This observation might indicate that coating formulations containing corrosion inhibitors form insoluble corrosion products in due time that form or make the coating less accessible to water and other corrosion causing species.

The individual EIS plots of the above formulations with topcoat did not show much change in the impedance values with due time. But the performance results of formulations with and without topcoat showed similar behavior i.e., formulations with higher percentages of CZM performed better. Figure A.18 shows the test results of formulations with topcoat after 6 weeks of testing. Other corrosion inhibitors from companies like Cortec and Fluka were also tried. Figure A.19 and Figure A.20 show the EIS and salt spray results of the formulations F20, F21, F22, F24 and F 25. Figure A.19 shows that the impedance values of almost all the inhibitors formulations without topcoat are close by and decrease with time. The decrease in modulus values stabilizes after some time. This stabilization of the impedance values may be attributed to the fact that these inhibitors form insoluble corrosion products by reacting with corrosion causing elements.

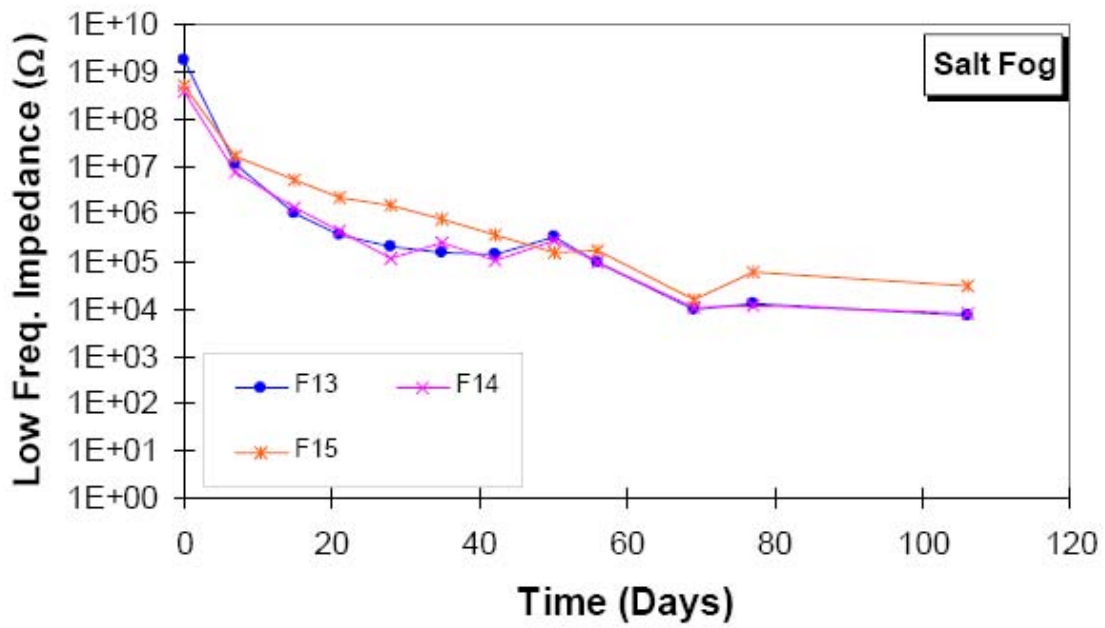
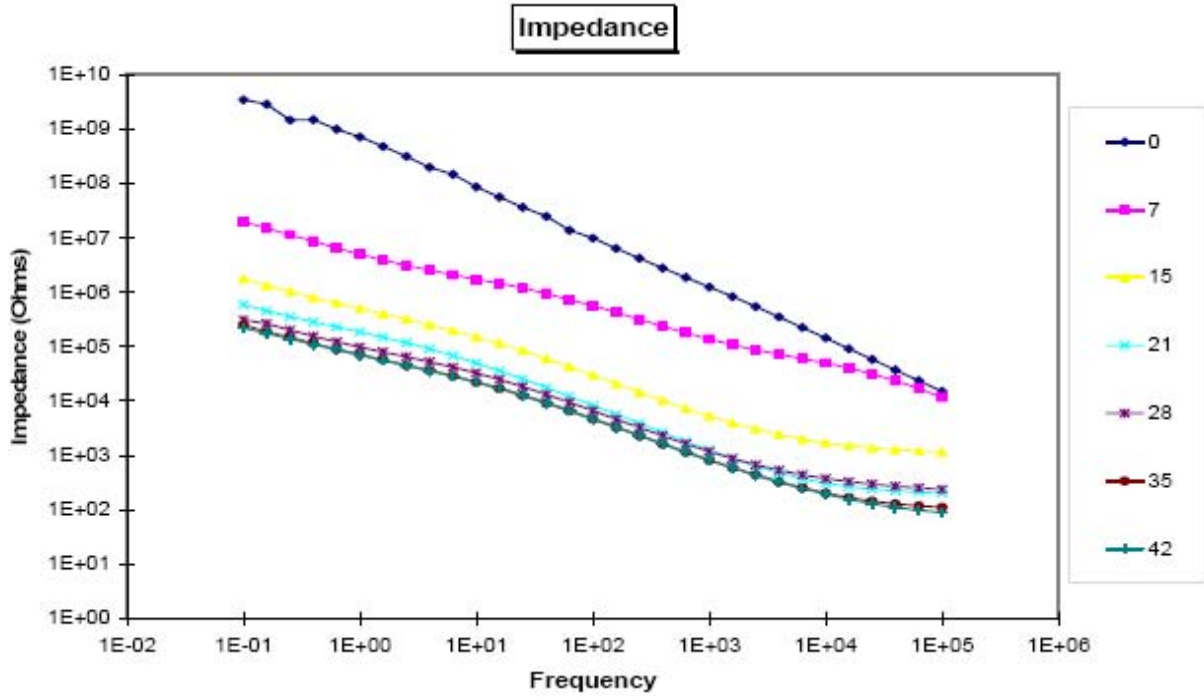
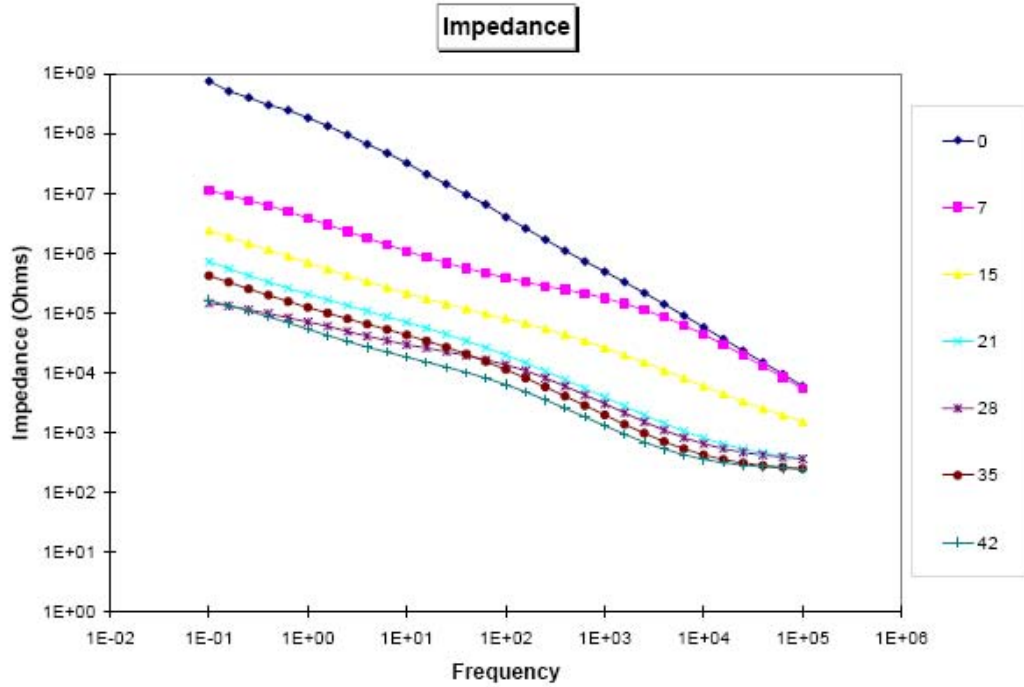


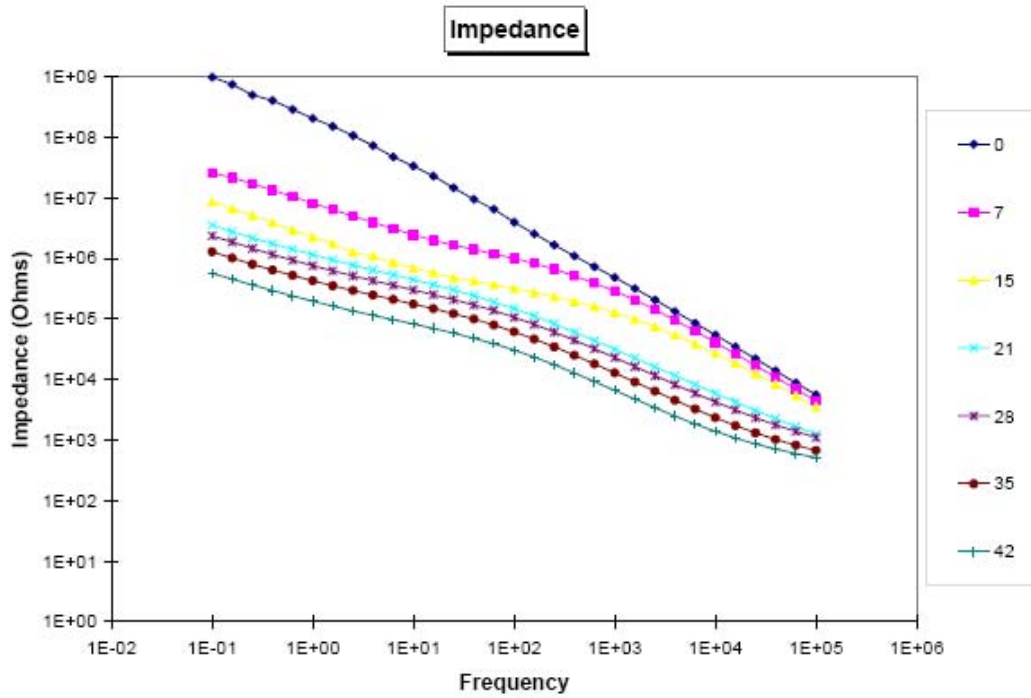
Figure A.16: EIS impedance values of coating formulations F13, F14 and F15 after being exposed to salt fog. The formulation information can be found from table A.3.



EIS Bode plots for 6 weeks of immersion of F 13

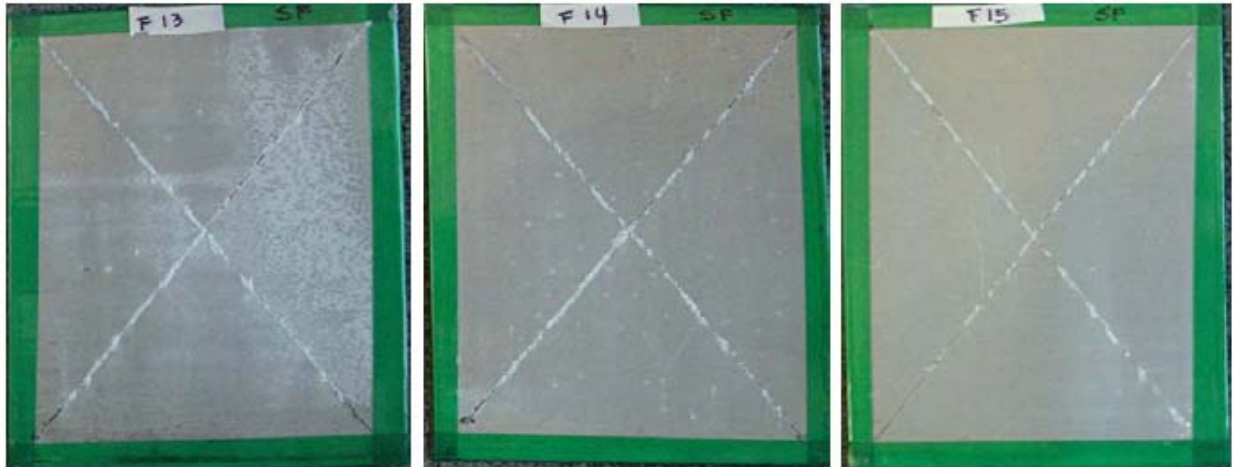


EIS Bode plots for 6 weeks of immersion of F14



EIS Bode plots for 6 weeks of immersion of F15

Figure A.17: EIS Bode plots for 6 weeks of immersion of F13, F14 and F15



Without topcoat (after 21 days of salt spray)



With topcoat (after 42 days of salt spray)

Figure A.18: Salt spray results of formulations F13, F14 and F15 with and without topcoat after 6 weeks of testing. Control is AA 2024 T3 panels with chromium pretreatment and epoxy primer with barium chromate.

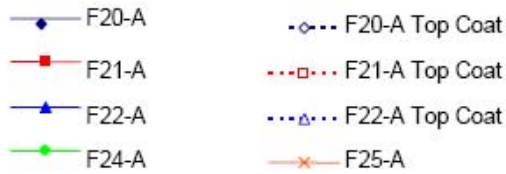
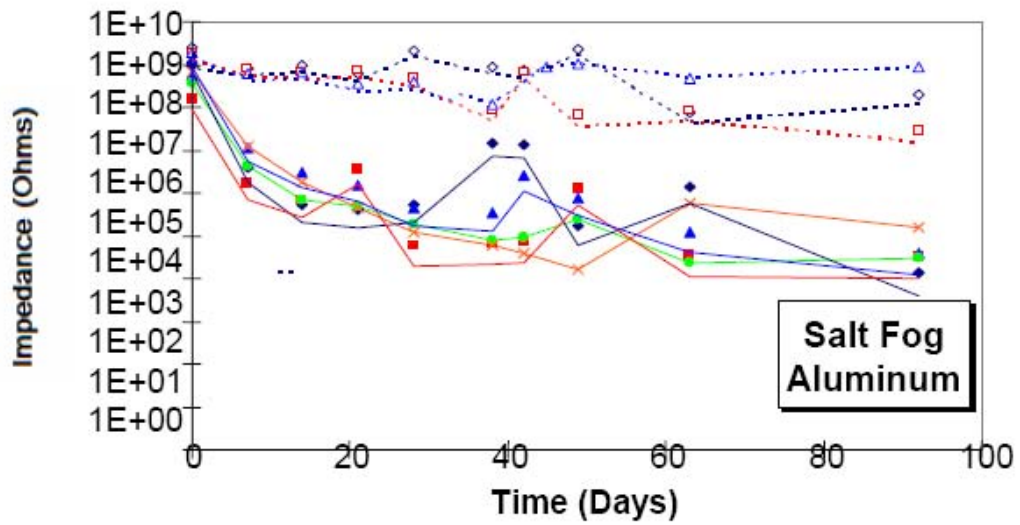


Figure A.19: Change in EIS impedance values of the coating formulations F20, F21, F24, F25 with and without topcoat, after exposed to salt fog.



Figure A.20: Salt Spray test results of formulations F20, F21, F22, F24 and F 25 without topcoats after 28 days of testing.

## **Zinc-Rich Superprimer**

Zinc-rich primers are as the name suggests primers with heavy loads of zinc metal dust in it. The zinc dust/powder is used as filler and is held in the coating by using a binder. Paints with zinc pigments contain about 80% by weight pigment of which 20% is oxide. Zinc-rich coatings contain 85-95% metallic zinc, by weight, in the dry coating with little or no oxide. Depending the type of binder used the primer can be organic or inorganic. Organic binder can be epoxy, polyurethane, acrylate etc. In inorganic zinc-rich primers the binders are usually silicates. The use of metallic zinc in primer formulations to achieve sacrificial protection of steel structures has been well established in the protective coating industry. The outstanding protective properties of metallic zinc-based primers are based on the sacrificial properties of these primers in combination with their barrier properties and physical characteristics.

The idea of zinc-rich primer started with the trials to test the superprimer's performance with particles in it. Zinc was used in it to formulate a zinc-rich superprimer. Zinc rich SUPERPRIMER is nothing but a zinc paint, which uses the superprimer as a binder and it, and would not include the pigments, color and nanoparticles. It is chromate-free, completely waterborne and has very low VOC in it. After several trials it was evident from the results that the waterborne superprimer formulation mentioned in the previous chapters had to be modified for best performance in the zinc-rich primers. The results and observation are discussed in the following chapters.

## **Formulation, Mixing and Coating**

The formulation of the zinc-rich primer is different from the usual superprimer with particles in it. The following shows information about the components and their mixing procedure:

- Part A: Superfine (grade 5) zinc dust at 70 % (by weight in the total formulation)
- Part B: WSP-1 (30% by weight in the total formulation) which contains 80% EPI REZ- 3540 resin + 19% (A1170: VTAS [5:1] ; 10% solutions in water) + 1% TEOS + defoamer [if needed]
- Part B is shear-blended for 10 minutes at 2100 rpm. Then Part A is added in small batches and blended for 20 minutes at 3000 rpm

The cleaning requirements for zinc-rich coatings are equally stringent as in conventional primers. Measures have to be taken to make sure that proper electrical contact is maintained in between the zinc in the coating and the steel substrate. Cleaning procedure is similar to the one in the previous chapters. Zinc-rich coatings can be applied using brush, drawdown or by a spraying method.

The zinc-rich superprimer coatings were cured at 100°C for 30 minutes and then letting the coating set at room temperature for 1 week. Zinc-rich primers work better performance-wise if the coatings were allowed to retain some moisture inside them for some time. This moisture retention will help form the zinc corrosion products and seal the pores of the coating. So for zinc-rich coatings a slight under-curing is preferred.

## **Results and Discussion**

In this section the test results using EIS, Salt Spray and SEM techniques are discussed. Percentage of Zinc Dust The percentage of zinc dust in the zinc-rich primers is critical and it determines the performance. It needs to be high enough for the primers to perform their function efficiently. Since these primers work on the basis of cathodic protection, it is necessary that the zinc metal particles

maintain electrical contact not only with the steel substrate but also with each other. So for the particles to be tight and intact in the coating over the substrate the percentage of zinc in dry zinc rich coating needs to be high.

Carbon steel panels were first solvent-scrubbed using ethanol as solvent and scotch-brite pads to remove the dirt, corrosion products and expose clean, shiny metal-oxide surface. After the scrubbing, the panels were cleaned with water spray and then followed by ultrasonic cleaning in ethanol for 5 minutes. The final stages of cleaning included alkaline cleaning similar to the one followed for aluminum but at lower temperature of 55°C and for only 1 or 2 minutes. CRS is a very sensitive substrate so care was taken not to spoil the metal-oxide surface before coating with superprimer. EIS and salt spray tests were used to analyze this effect. Figure A.21 shows EIS curves of a formulation containing 40% zinc 60% superprimer mixture for 0 to 42 days. Figure A.22 shows a similar result of formulation with 70% zinc and 30% superprimer.

Figure A.23 shows the salt spray result after 3 weeks of both 40% and 80% zinc formulations. The performance of 80% formulation was better than the one with 40%. It was not that evident from the comparison between both of their EIS curves. The significance of increasing modulus is explained here.

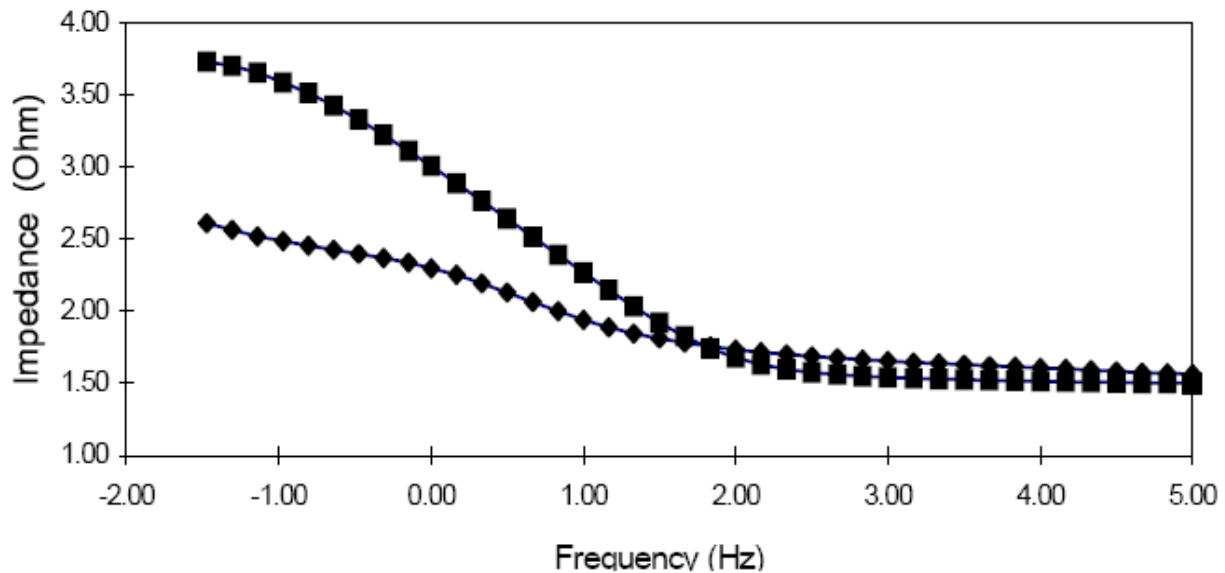


Figure A.21: 42 days EIS result for formulation with 40% zinc and 60% superprimer. The square block represents result for 42 days and the rhombus for 0 days.

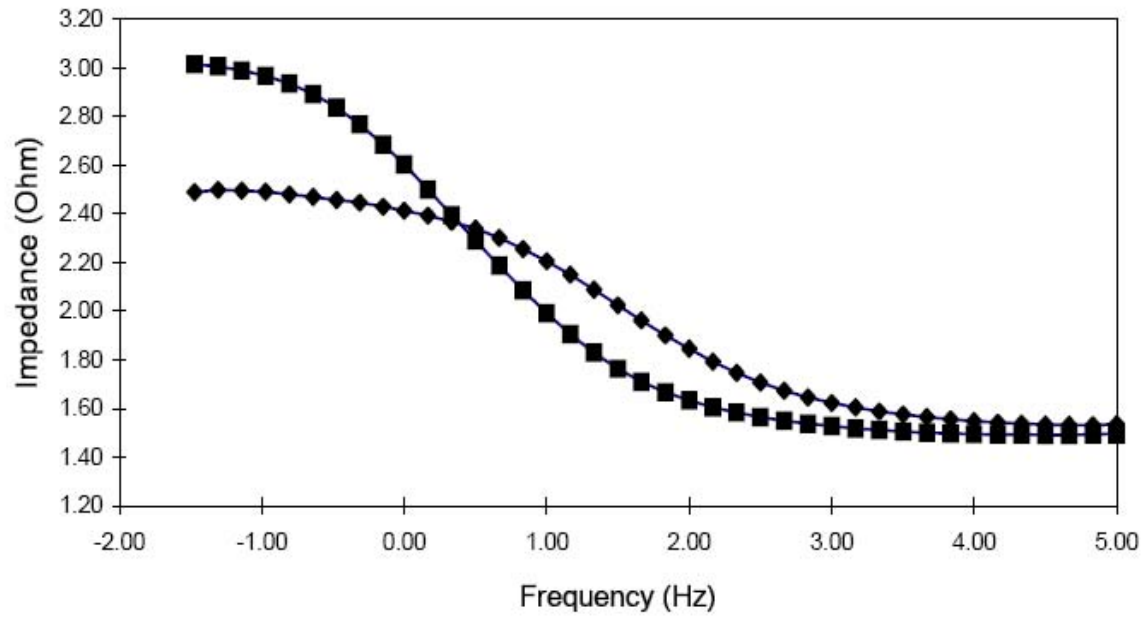


Figure A.22: 42 Days EIS result for formulation with 70% zinc and 30% superprimer. The square block represents result for 42 days and the rhombus for 0 days.

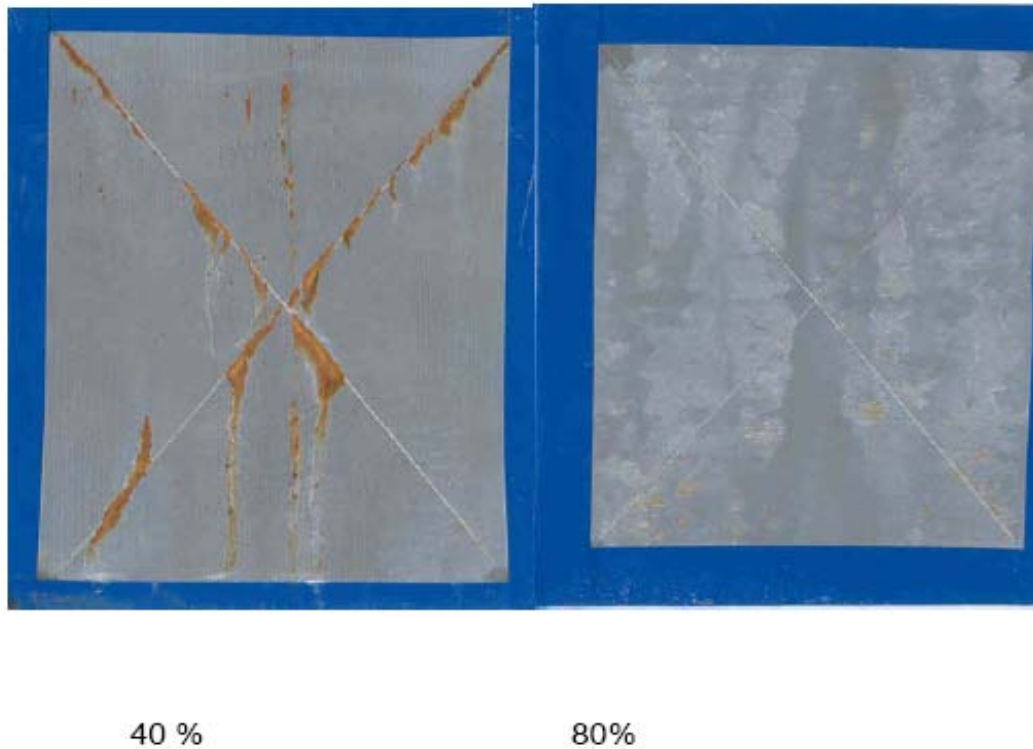


Figure A.23: The salt spray result after 3 weeks of both 40% and 80% zinc formulations.

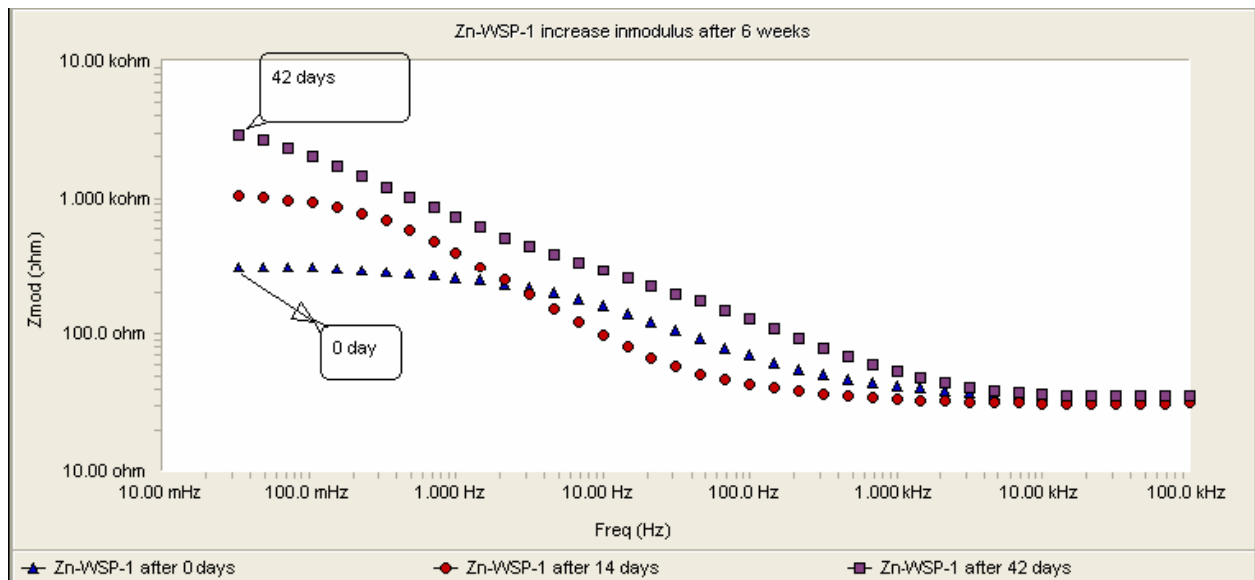
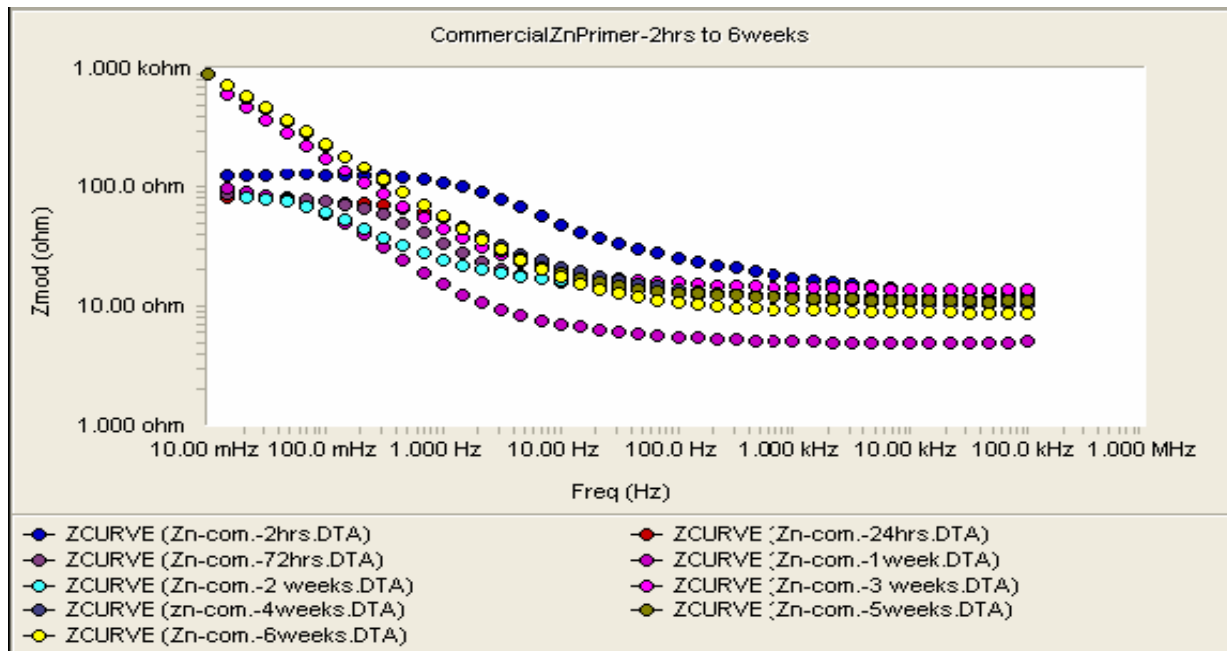


Figure A.24: 6 week EIS results of commercial and Zinc-rich superprimer.

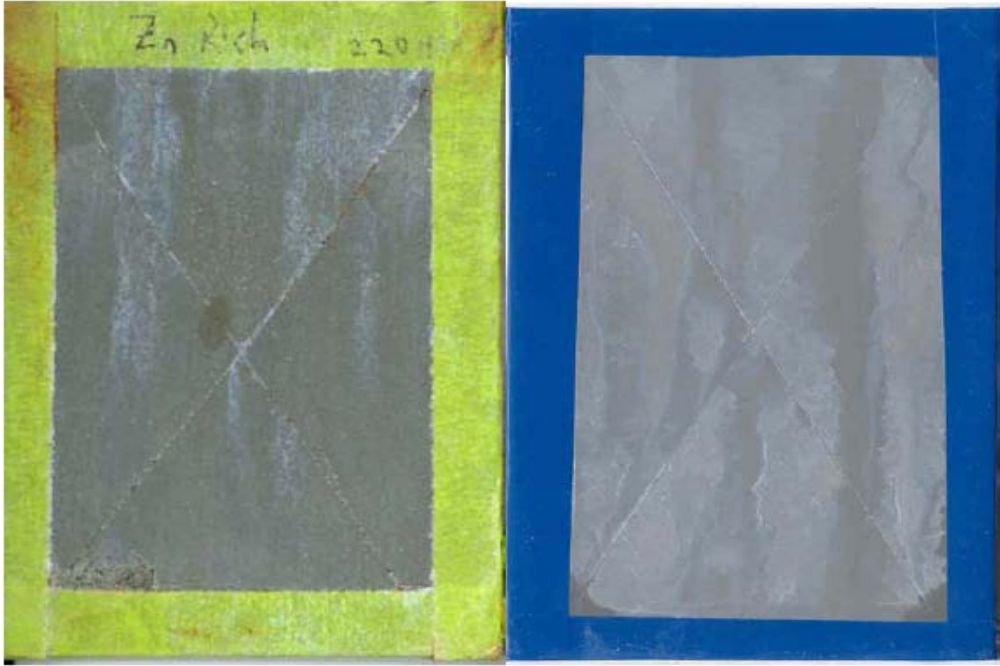
Figure A.24 shows a comparison of the 6-week EIS result of a commercial chromate containing primer from Carbozinc and zinc-rich superprimer. All the EIS impedance curves show an increase in the impedance values with due time. Because of the conductive metal zinc in zinc-rich coatings it has less resistance in the beginning. When the immersion time increases the zinc is corroded and forms its insoluble corrosion products. These corrosion products seal the pores and make the coating less permeable to water. In other words, this means an increase in the resistance. This behavior of the zinc rich coatings can be accounted for their increasing impedance behavior.

Salt fog results showed an equally good or better performance of the zinc-rich superprimer when compared to the commercial primer. Figure A.25 shows the comparison. However, the zinc-rich superprimer has the following advantages than most of the commercial primers:

- Completely water-reducible
- Easy clean-up
- Excellent adhesion to topcoat
- Low VOC
- Equal or better performance when compared to solvent-borne commercial paints
- Chromate-free
- Low solvent odor
- Pot life of close to 24 hours

Both primers performed equally well in terms of corrosion performance. No visible red corrosion products of steel were observed on the steel panels. In Figure A.25 white corrosion products of zinc were observed in the scribe. These white deposits of zinc hydroxide are highly insoluble to water and other species. The formation of these deposits is, in fact, an indication of good performance by the zinc-rich coatings. However, similar white corrosion products were not observed in the scribe of panels with both zinc rich coating and a polymer topcoat over it. Figure A.26 shows the 200-hour salt fog result of zinc rich primers with topcoat.

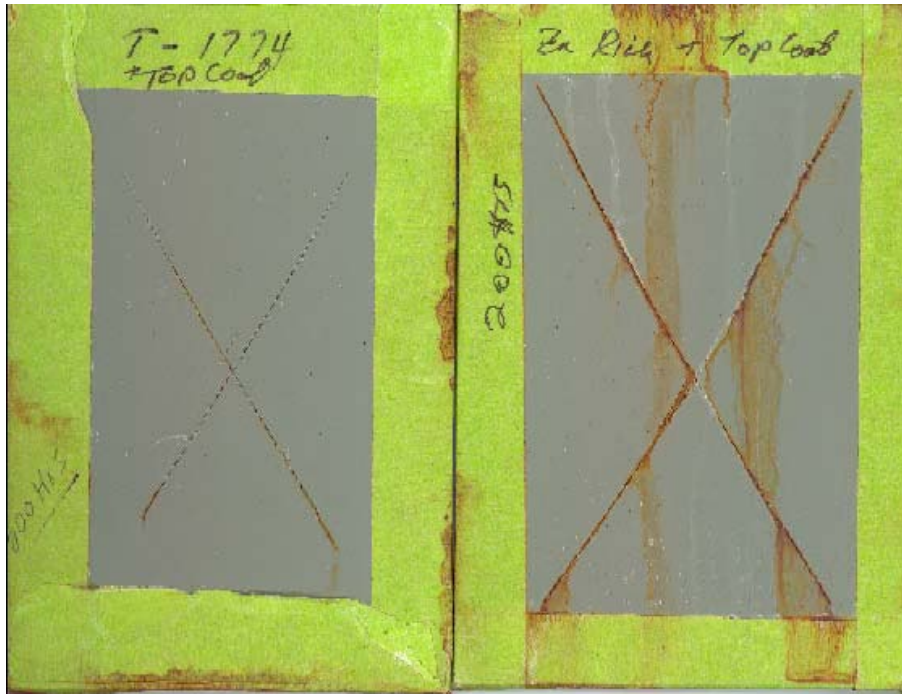
The noticeable difference between Figure A.25 and A.26 is the formation of red corrosion product of steel in the scribes of the panels with topcoat. Formation of zinc corrosion products at the scribe was not observed when the panels are coated with a topcoat. Thus the scribes of the panels were not protected. The reason for the zinc-rich primers to be not as efficient under the topcoat can be attributed to the fact that application of a topcoat over a zinc rich primer will actually decrease/cut-off the electrical contact between the zinc, iron and the environment (which acts as an electrolyte).



Commercial

Zinc-rich Superprimer

Figure A.25: 500 hours Salt fog result of commercial and zinc-rich superprimer.



Zinc-rich superprimer + Polyamide Topcoat

Commercial zinc-rich primer + Polyamide Topcoat

Figure A.26: 200 hours salt fog result of zinc-rich primers with Polyamide topcoat

As explained in the previous sections, a contact between the three is necessary for the corrosion protection action of the zinc. At the areas of a defect or a scribe only a small portion of zinc is exposed to the environment that can sacrifice itself and protect the steel. In the non-top coated panels a larger portion of the zinc surface is exposed and sacrificed, which will in turn help the steel underneath from getting corroded.

### **SEM Results**

An attempt was made to observe the corrosion protection of zinc using the EDS technique. The idea was to observe the formation of zinc corrosion products in the scribe with time. A 1 cm by 1 cm portion of a steel panel coated with zinc-rich superprimer was cut and scribed in the center. Analysis was done on two areas, one at the coating surface and one area in the scribe. First analysis was done in both the areas immediately after curing and another after 48 hours of immersion in 5% NaCl solution. The aim was to observe any traces of zinc that leached out from the coating to the scribe with time by forming zinc hydroxides.

Analysis of the coated areas before the immersion revealed the presence of only Si compounds. This Si is from the silane content in the zinc-rich coating. Analysis on the coated area after the immersion revealed the presence of zinc and traces of iron. To rectify this difference or strange observation further tests and studies need to be conducted. Analysis of scribed areas revealed some useful information. Before the immersion the only species detected were iron compounds. This is obvious because after a fresh scribe, formation of a shiny iron oxide layer is obvious. After the immersion, traces of zinc compounds were detected. This observation can be made using Figures A.27 to A.30.

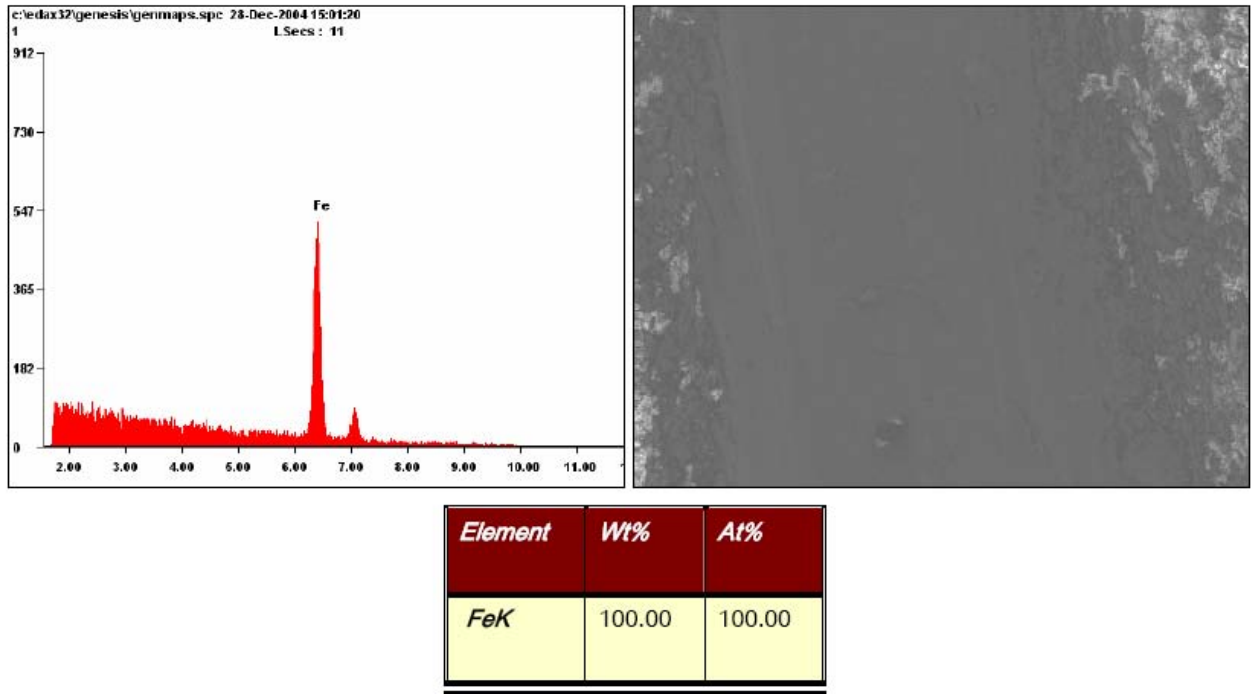
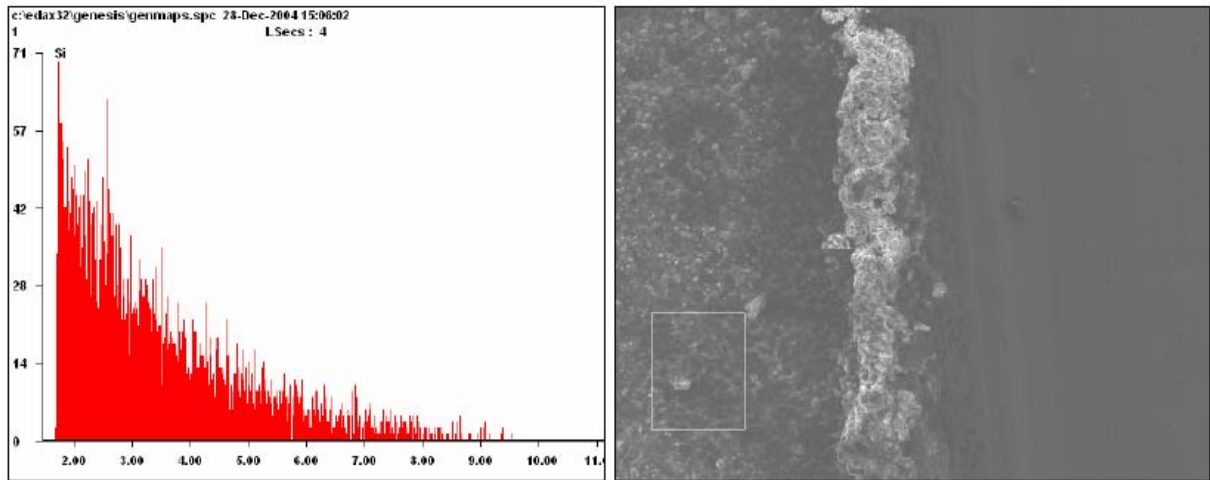
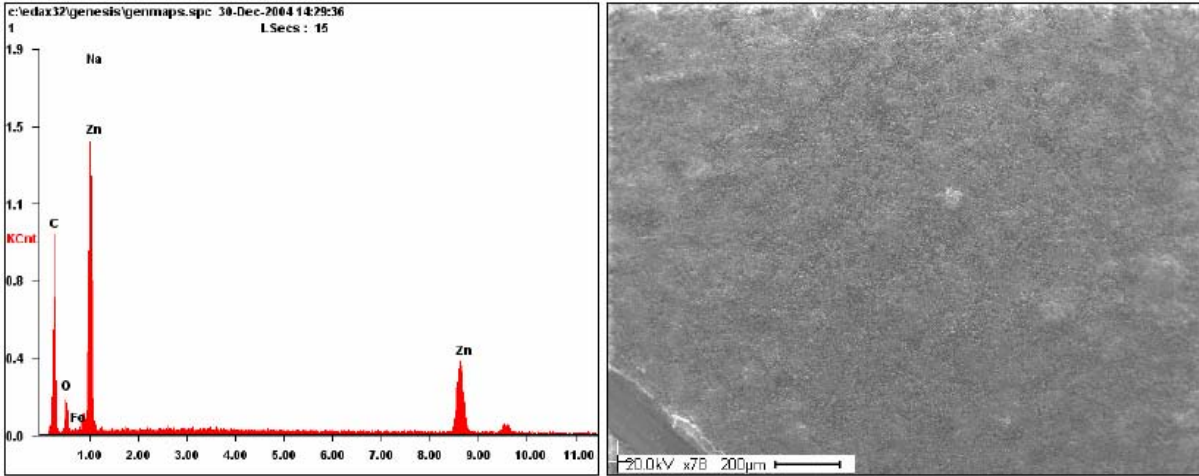


Figure A.27: Zone 1 area in the scribe before immersion.



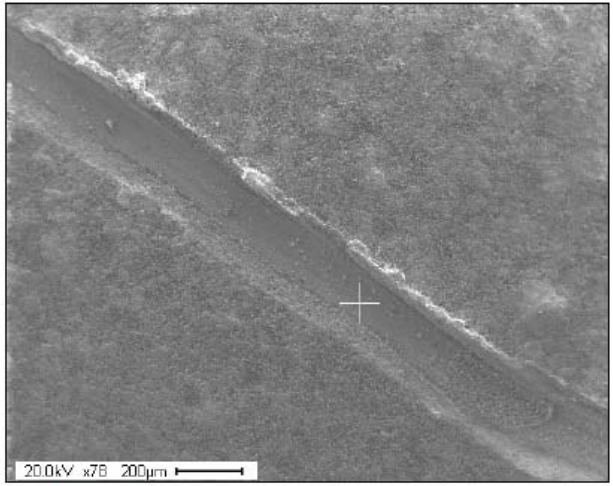
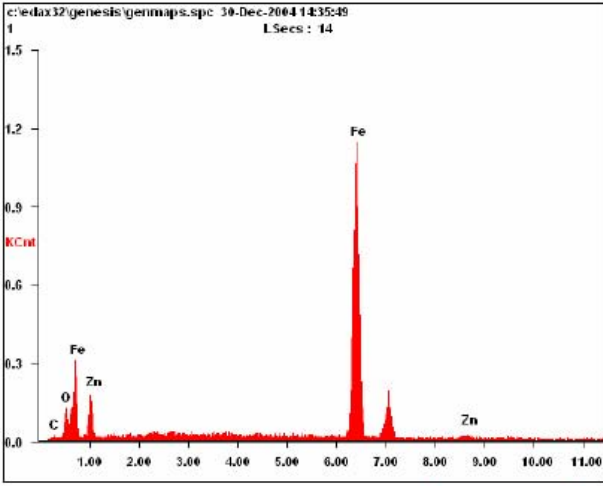
<i>Element</i>	<i>Wt%</i>	<i>At%</i>
<i>SiK</i>	100.00	100.00

Figure A.28: Zone 2 coated area before immersion



<i>Element</i>	<i>Wt%</i>	<i>At%</i>
<i>CK</i>	57.01	83.49
<i>OK</i>	05.85	06.43
<i>FeL</i>	02.01	00.63
<i>NaK</i>	00.00	00.00
<i>ZnK</i>	35.13	09.45

Figure A.29: Analysis over zone 2 with coated surface after immersion.



<i>Element</i>	<i>Wt%</i>	<i>At%</i>
<i>CK</i>	02.43	10.00
<i>OK</i>	02.02	06.24
<i>FeK</i>	88.37	78.32
<i>ZnK</i>	07.18	05.44

Figure A.30: Zone 1 in the scribe after immersion

## B. PRIMER FOR HDG

### Abstract

A novel chromate-free and low-VOC primer system for use on hot-dip galvanized (HDG) steel is presented and discussed. Essentially it consists of a mixture of organofunctional silanes, water-dispersed resins and additives such as inhibitors, nanoparticles and others. The primers do not require the use of a conversion coating and the curing temperature can be varied. With a suitable corrosion inhibitor added, a B-117 resistance of over 2000 hours is obtained for the primer without topcoat. Epoxy resins are typically used in the primer. With a careful selection of ingredient combinations, the possibilities are being explored of integrating the primer into a one-step, water-borne, fast-cure finishing system.

### Results

#### The starting point of the development work; formulation F6

The starting point for the development of a functional primer on HDG steel was a superprimer that had showed good results on AA 2024-T3. The recipe of this primer is shown in Table B.3. This formulation was based on the epoxy resin EPI-REZ 3540-WY-55, which has a high EEW of 1600-2000 (Table B.1), which means that the resin dispersion has less number of end epoxy groups per gram of resin and therefore a lower potential for cross-linking with a curing agent added. The formulation named F6, shown in Table B.3, was tested on HDG steel, but it failed on this substrate. Therefore, studies including the following steps were conducted on HDG to improve the starting point formulation, F6:

*Step 1:* Modifying and improving the F6 formulation to make it compatible with the HDG substrate.

*Step 2:* Search for epoxy resin and cross-linker combinations with low VOC but high performance.

*Step 3:* Search for compatible silanes for superprimers on HDG.

*Step 4:* Search for compatible inhibitors for superprimers on HDG.

Continuously during the above mentioned steps; cured superprimer components and also complete coatings were characterized using FTIR, contact angle and SEM/EDS.

**Table B.1. The specific data of the epoxy dispersion used in the superprimer formulations**

Epoxy dispersion	EEW	VOC, [g/L]	Solids content, %	Viscosity, cP
EPI-REZ 3540-WY-55	1600-2000	250	55	7000-17000
EPI-REZ 5522-WY-55	550-700	170	55	8000-19000
DPW-6520	500-600	74	53	1000-6000

**Table B.2. Summary of the chemicals used in the development of the superprimer for HDG steel**

<b>Superprimer components and chemicals for HDG steel</b>	
<b>Binders</b> Waterborne epoxy dispersions: EPI-REZ 3540-WY-55 EPI-REZ 5522-WY-55 DWP 6520	<b>Silanes</b> bis[3-(triethoxysilyl)propyl]tetrasulfide (bis-sulfur) 1,4-bis(trimethoxysilylethyl)benzene (bis-benzene) bis-[trimethoxysilylpropyl]amine (bis-amino silane) vinyl triacetoxysilane (VTAS)
<b>Crosslinkers</b> Epoxy-amine adducts: EPI-KURE 8290-Y-60 and DCP 6870	
<b>Anti-corrosive pigments</b> zinc phosphate (ZP) Corrostatin 228 (Ca, Zn, P, Si, O) sodium metavanadate calcium zinc molybdate (CZM)	<b>Fillers and other pigments</b> titania barium sulfate mica Nanoactive S (titania dispersion)

**Table B.3. Starting point recipe for the development of a functional superprimer for HDG steel**

<b>Formulation F6</b>
Part A: EPI-REZ 3540-WY-55 epoxy resin Part B: 10 % solution of AV5 (bis-amino and vinyltriacetoxy silane mixed in a ratio of 5:1) in water at pH 6 Part C: tetraethoxysilane TEOS Part D: bis-sulfur silane BS
Mix by weight: Part A (80 %) + Part B (9 %) + Part C (1 %) + Part D (10 %)
Shear blend for 8 minutes at 2200 rpm
Ready to use after 20 minutes incubation time

**Step 1; resins and cross-linker**

In the first step three new formulations were compared to the original formulation F6. In all three new formulations an epoxy amine-adduct cross-linker (EPI-KURE 8290-Y-60) was incorporated. The amount of cross-linker used was 10 wt.-%. In the two other formulations the original epoxy resin (EPI-REZ 3540-WY-55) was replaced by two low EEW epoxy resins; EPI-REZ 5522-WY-55 and DPW 6520, respectively. The formulations prepared were:

1. F6 : The original formulation made for AA2024-T3
2. F6 + 10 wt.-% cross-linker (EPI-KURE 8290-Y-60)
3. F6 substituted with low EEW epoxy resin EPI-REZ 5522-WY-55 + 10 wt.-% cross-linker
4. F6 substituted with low EEW epoxy resin DPW 6520 + 10 wt.-% cross-linker

The formulation and coating procedure for all the coating formulations were the same as for F6. However, curing conditions were varied, with the formulations being cured at 60°C for one hour followed by curing at 150°C for another hour. These coatings were tested in ASTM B117 salt spray and Ford APGE tests. The EIS curves were measured on the samples periodically as described in chapter 2. The panels were also exposed to outdoor testing at Hawaii. Figure B.3 shows the salt spray ASTM B-117 test results of the formulations described above. From Figure B.3 it can be seen that the third formulation performed better than the others. The summary of all the test results confirmed this result, i.e., formulation 3 outperformed formulations 2, 4, and the starting point formulation F6.

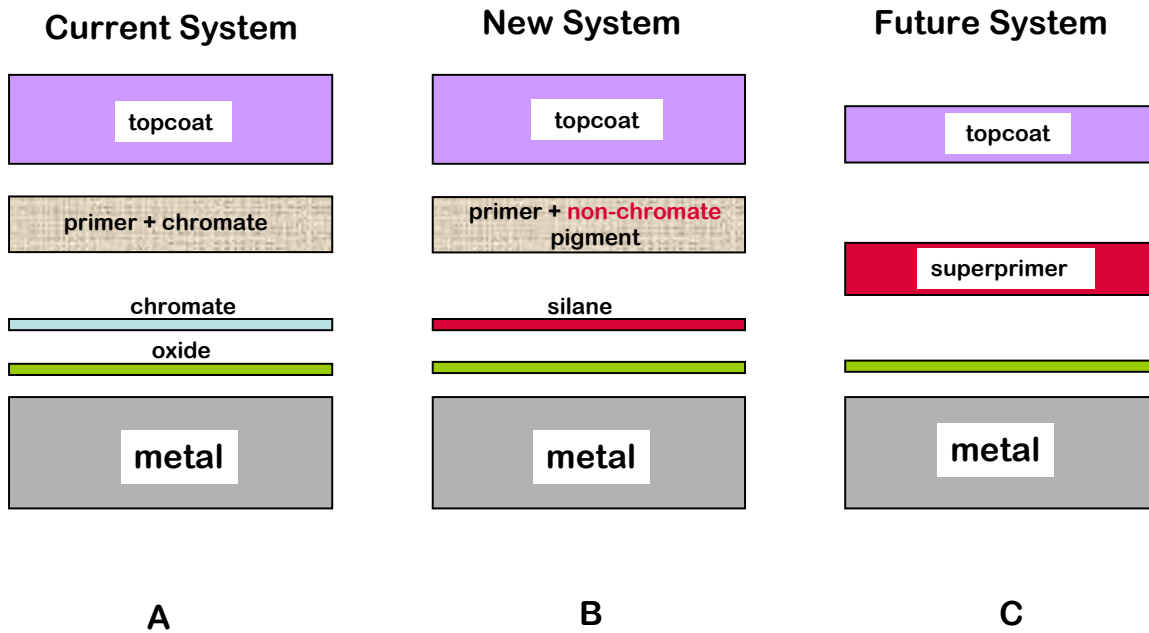
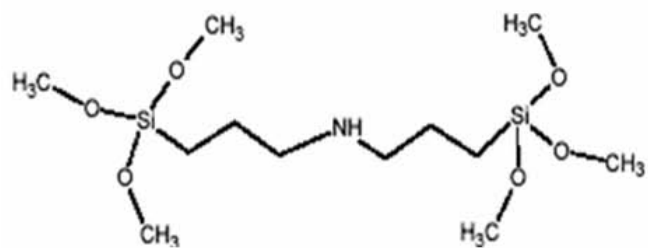
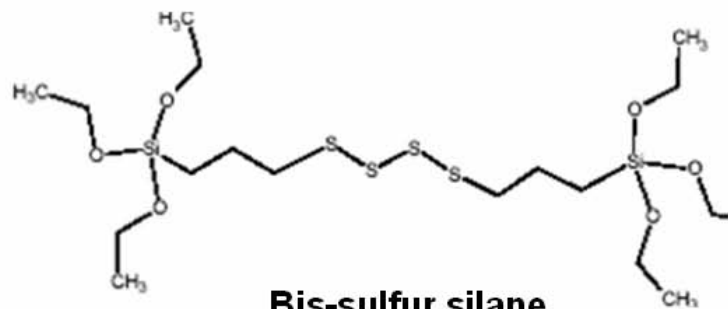


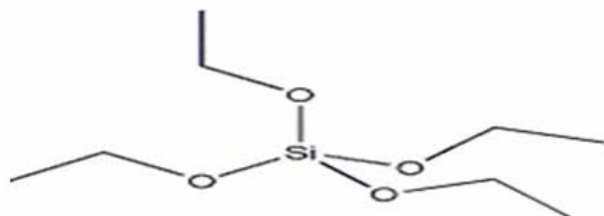
Figure B.1. Concept of the superprimer system



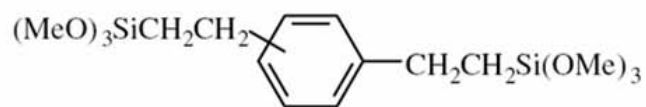
**Bis-amino silane**



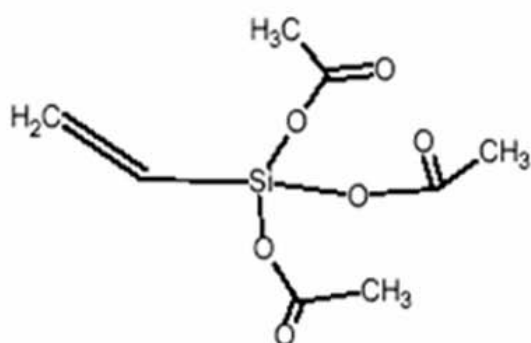
**Bis-sulfur silane**



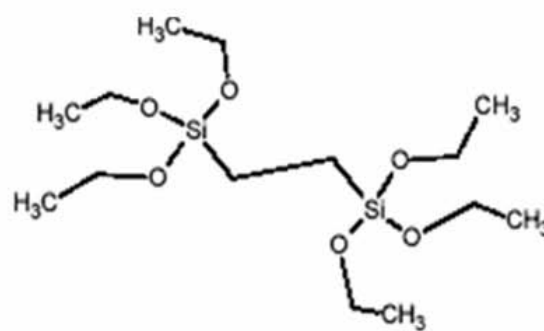
**TEOS**



**Bis-benzene silane**



**VTAS**



**BTSE**

Figure B.2. Silanes used in the superprimer formulations

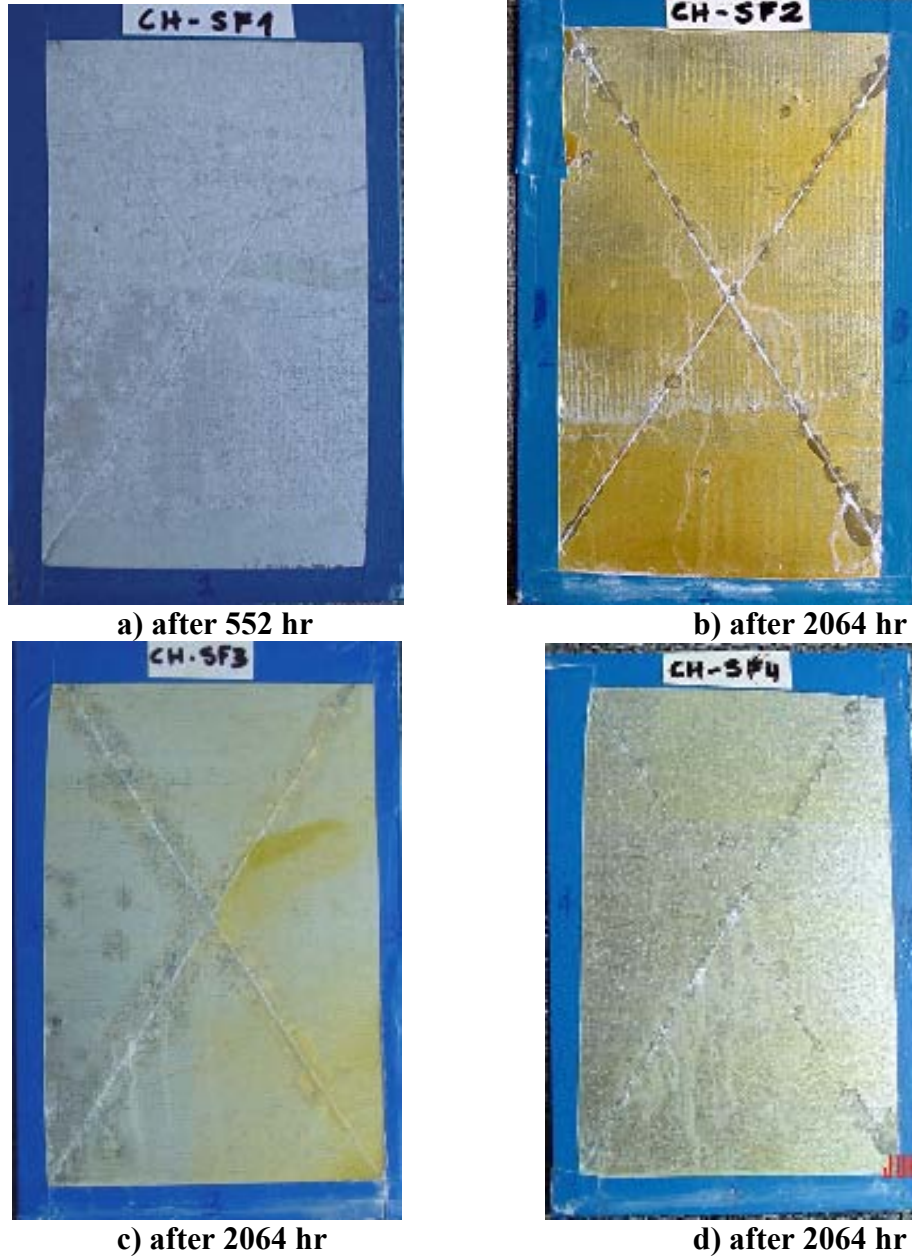


Figure B.3. ASTM B117 images of the three formulations compared to the starting point formulation F6: a) Formulation, F6: b) F6 + 10 wt.-% cross-linker (EPI-KURE 8290-Y-60); c) F6 substituted with low EEW epoxy resin EPI-REZ 5522-WY-55 + 10 wt.-% cross-linker and d) F6 substituted with low EEW epoxy resin DPW 6520 + 10 wt.-% cross-linker

### Step 2; ratios of resin DPW 6520 and cross-linker DPC 6870

The epoxy resin used in formulation 3 (EPI-REZ 5522-WY-55) and the cross-linker (EPI-KURE 8290-Y-60) used in step 1 both had a pretty high VOC-level. Therefore, the developmental work was continued with the DPW 6520 epoxy resin and a zero-VOC epoxy-amine adduct cross-linker, DPC 6870. These two together are known as the NEW-GEN system<sup>TM</sup>. Though the epoxy: amine

stoichiometric ratio of DPW 6520 and DPC 6870 is 70:30, combinations of the two components in various ratios ranging from 90:10 DPW 6520: DPC 6870 to 50:50 were formulated and subjected to various tests. It was observed that concentrations of DPC 6870 ranging between 20 – 35% gave reasonably good results in all the tests.

### **Step 3; the silanes bis-sulfur and bis-benzene**

The silanes for this study were carefully selected based on previous studies. The pure silanes selected were bis-sulfur and bis-benzene. Bis-sulfur silane has been used successfully in many superprimer formulations studied so far and has positive neutron reflectivity results. Bis-benzene silane, a non-functional organosilane has been shown to form highly hydrophobic pretreatments via immersion and electrodeposition.

The silanes were added to the combination of the low-VOC DPW 6520 epoxy resin and the zero-VOC cross-linker DPC 6870. The formulations with and without bis-sulfur silane in weight ratios were:

- Formulation A (without BS): 7:3 DPW 6520: DPC 6870
- Formulation B (with BS): 7:3:2 DPW 6520: DPC 6870: BS

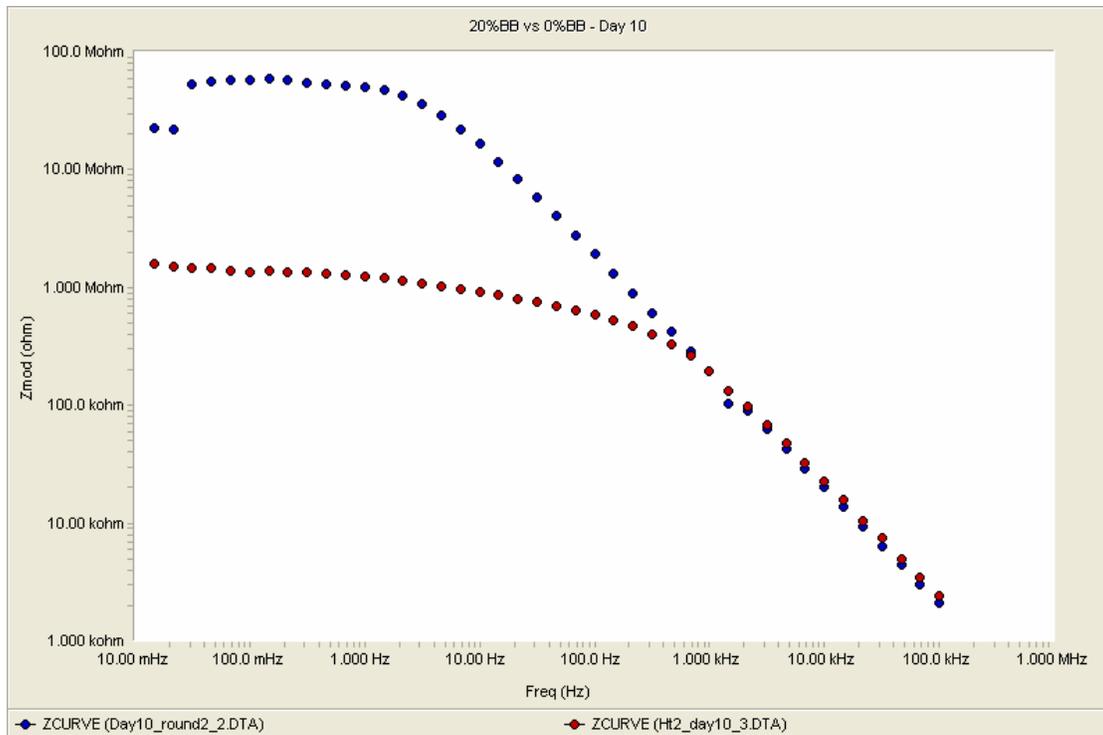
The incorporation of BS increased the contact angle and the MEK double rub results. The low frequency impedance values for both day 0 and day 30 were higher by decades for the BS containing coating compared to the coating without BS. Thus, the addition of BS resulted in an increase of the coating's resistance to water and organic solvents.

The formulations with and without bis-benzene silane in weight ratios were:

- Formulation C (without BB): 8:20 DPW 6520: DPC 6870
- Formulation D (with BB): 8:2:2 DPW-6520:DPC-6870:BB

The curing of these samples was also varied. The results of the various performance tests showed that the incorporation of bis-benzene improved the results of the coating. Figure B.4 shows the low frequency impedance plots of the coatings C and D on HDG cured at 60 °C for 1 hr and thereafter at 150 °C for 1 hr. It is clearly seen from Figure B.4 that the low-frequency impedance is high for the coating containing BB compared to the coating without silane. Figure B.4 also shows the images of the panels C and D after 35 days of EIS testing. The absence of discoloration in the bis-benzene incorporated film confirms the minimal water absorption and corrosion, already indicated by the Bode plot of Figure B.4. In summary, it was found that the incorporation of bis-benzene in the epoxy primer leads to increased:

- barrier property, i.e., increased low frequency impedance in EIS
- curing and solvent resistance, i.e., high MEK double rub and pencil hardness and
- hydrophobicity, i.e., increased contact angle with water.



**Panels under the O ring – After 35 days**

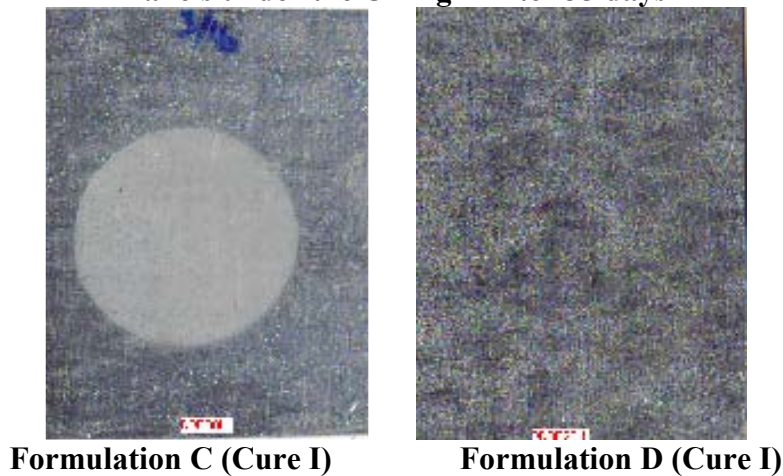


**Figure B.4.** Comparison of Bode plots of coatings with and without bis-benzene on day 10 of exposure to 3.5 wt% salt water. The images of the exposed are also shown below the impedance plots

**Step 4; the inhibitors**

A few commercially available non-chromate inhibitors, which had the potential to be effective on HDG steel were investigated in the fourth step of the study. The studied pigments were:

- zinc phosphate
- calcium zinc molybdate
- sodium metavanadate

- cerium based pigments (cerium exchange silica) and
- synergistic combinations of the above mentioned pigments

The pigments were added to the formulation based on the DPW 6520 epoxy resin, DPC 6870 cross-linker and bis-sulfur silane. The exact formulations of the controls and the pigment containing formulations are described in Table B.5. The first two formulations in Table B.4 (C1 and P2) were cured at 60°C for 1 hour, followed by 1 hour at 150°C. The rest were cured for 14 days at RT followed by a 10 minute curing at 150°C.

**Table B.4. The controls and the formulations containing inhibitors**

Formulation	DPW 6520 [g]	DPC 6870 [g]	Bis-sulfur [g]	Water [g]	Pigment Comp 1 [g]	Pigment Comp 2 [g]	Pigment Comp 3 [g]
C1, control*	8	2	1	0.5			
P2, CZM*	8	2	1	1	1.5 CZM		
C3, control	8	2	1	0.5			
P4, C 228	16	4	2	2	2 C 228	0.5 titania	0.5 mica
P5, Cerium	16	4	2	2	1 Ce silica	1 titania	1 mica
P6, mixture	16	4	2	2	1 Ce silica	1 C 228	1 ZP

\* C1 and P2 were cured at 60°C for 1 hour, followed by 1 hour at 150°C. The rest were cured for 14 days at RT followed by a 10 minute curing at 150°C.

**Table B.5.** Chlorine and inhibiting atom concentrations in the scribed region of various scribed superprimer films on HDG exposed for 30 days in 3.5 wt% salt water – EDX measurements to test efficacy of various inhibitors

Formulation/pigment	Chlorine concentration in the scribe (wt%)	Inhibiting atom concentration in the scribe (wt%)
732BS + 5% Corrostayn 228	15	0% P
732BS + 10% Corrostayn 228	4.01	0.18% P
732BS + 10% zinc phosphate	3.94	0.19% P
732BS + 10% calcium zinc molybdate	3.81	Mo overlaps with sulfur
732BS + 15% calcium zinc molybdate	2.38	Mo overlaps with sulfur
732BS + 10% Corrostayn + 1% NaVO <sub>3</sub>	2.77	0.26% V
No silane (73) + 10% zinc phosphate	3.75	0.17%P
High-temperature-cured (732BS) + 10% zinc phosphate	3.75	0.23% P

Figure B.7 shows the control and the best performing pigment containing superprimer coating after 2000 hr of ASTM B-117 salt spray testing. The coating that performed the best was the one containing 10 % Corrostayn 228 pigment and small amounts of titania and mica. The other pigments also performed quite well. They protected especially the scribe by inhibiting the formation of white rust and by preventing scribe creep. Of the tested pigments only the samples containing cerium exchanged silica showed a tendency towards blistering, as the silica particles are hydrophilic. It was also detected that the fillers titania and mica increase the barrier effect of the film, improves the hiding power of the film as well as aids pigment dispersion in the primer formulation.

SEM/EDX analysis was carried out on scribed pigmented superprimer coating in order to investigate the effectiveness of the different pigments for HDG steel. For this set of experiments six types of pigment combinations were added to the bis-sulfur containing superprimer formulation (7 g DPW 6520 + 3 g DPC 6870 +2 g bis-sulfur) as described below. The formulations were allowed to cure at RT for 14 days. They were then cross scribed and immersed in 3.5 wt% NaCl solution after which the scribes were kept under running water to remove external salt deposits. The pigments added to the bis-sulfur containing coating were:

1. 5% Corrostayn 228 (Corrostayn)
2. 10% Corrostayn
3. 10% zinc phosphate (ZP)
4. 10% calcium zinc molybdate (CZM)
5. 15% calcium zinc molybdate (CZM)
6. 10% Corrostayn 228 + 1% NaVO<sub>3</sub>

Further, the following two formulations were also analyzed: 10% ZP in 7g DPW + 3g DPC (no silane) and 10% ZP in 732 BS cured at 60°C, 1 hour and 150°C, 1 hour.

Figures B.8 and B.9 show an example of an analysis set of one of the studied pigment samples described above, namely the coating containing 15 % of CZM. The back scattered images are presented in Figures B.8(a) and B.9 (a) and the EDX analysis curves in Figures B.8(b) and B.9(b). Table B.5 shows the amount of chlorine in the scribe, which is directly proportional to the amount of zinc hydroxy chloride corrosion product formed on zinc in NaCl solutions and the amount of the inhibiting atom species for the pigment samples described above. Looking at the amount of chlorine in the scribes of Table B.5, the following order of effectiveness is seen among the inhibitors tested (starting from the poorest on left to the best on right):

5% Corrostayn < 10% Corrostayn < 10% ZP ~ 10% CZM < 15% CZM ~ 10% Corrostayn + 1% NaVO<sub>3</sub>

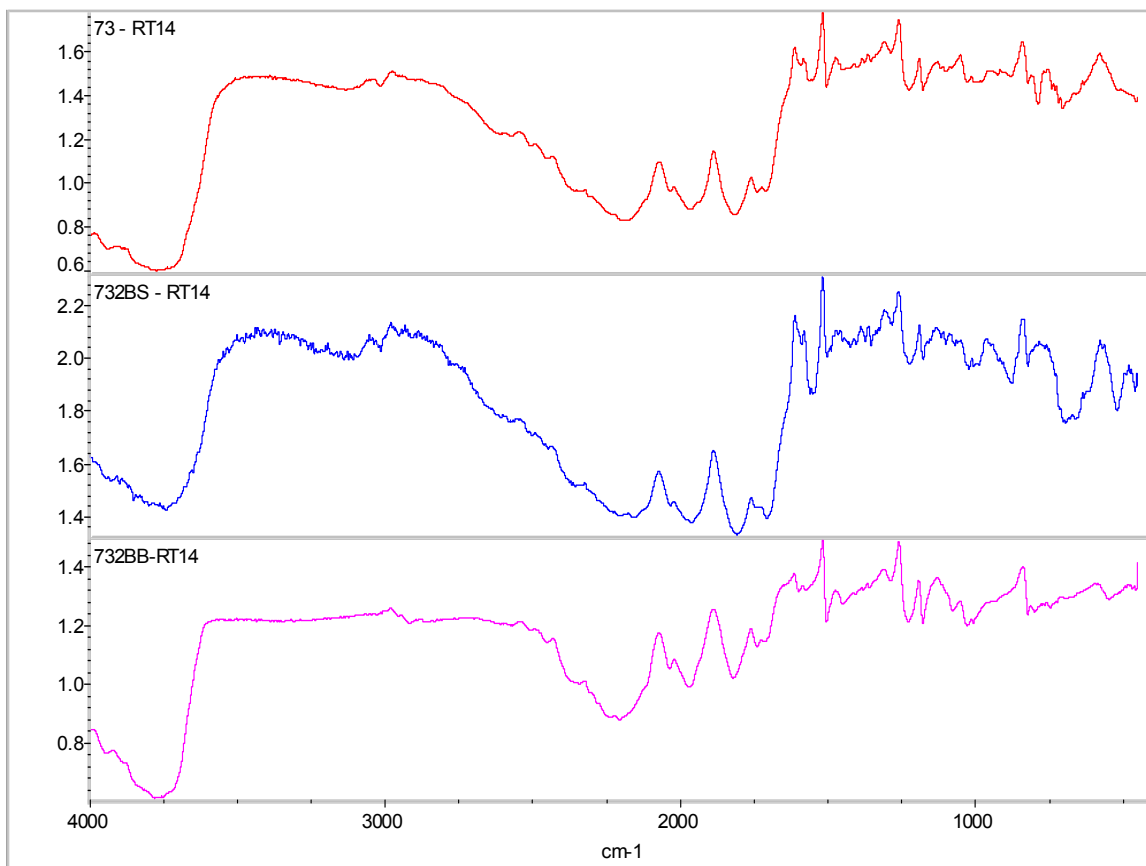


**Figure B.5.** IR spectra of superprimer films showing the effect of incorporation of the silanes bis-benzene and bis-sulfur

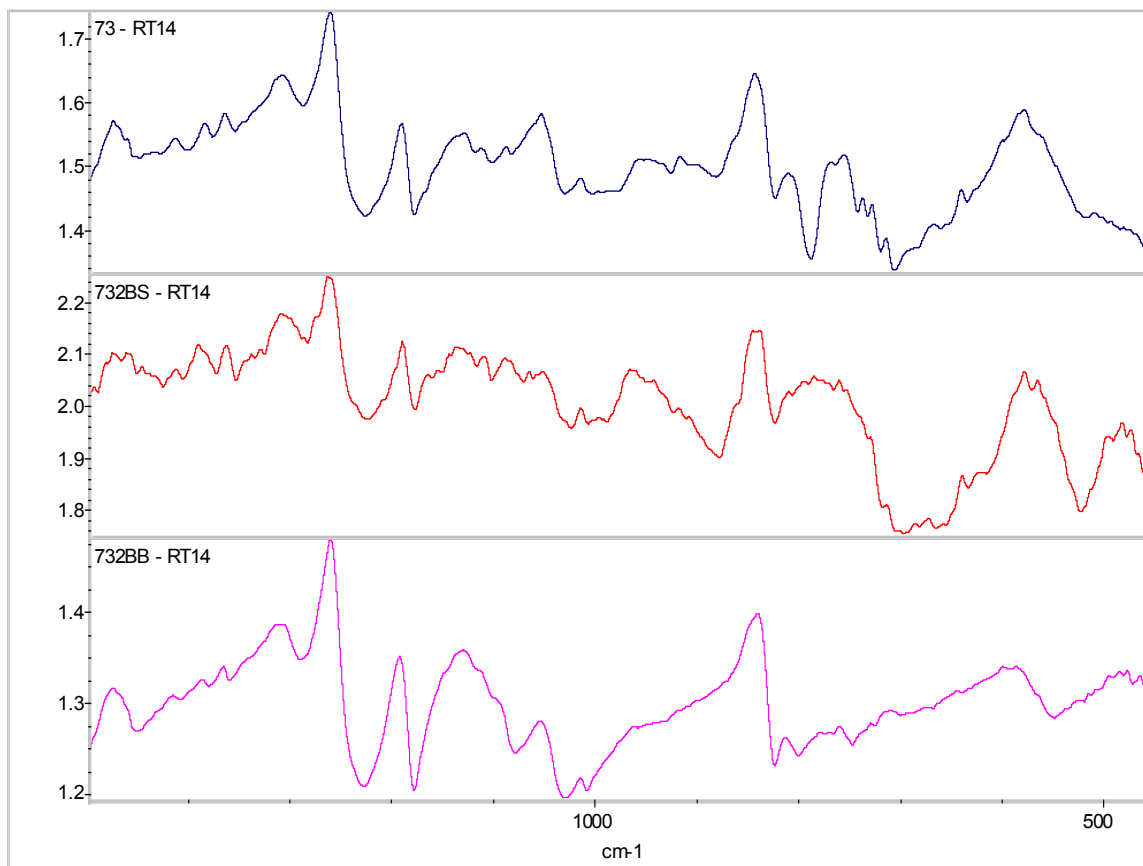


**Figure B.6.** The same IR spectra as in Figure 5 detailing the siloxane peak region



Figure B.7. The control (a) and the best performing pigment containing coating (b) after 2000 hr of ASTM B-117 salt spray testing. a) superprimer without pigments; b) superprimer with 10 % Corrostayn 228 pigment, and small amounts of titania and mica.



**Figure B.8 (a).** SEM image of scribe – effect of 10% CZM

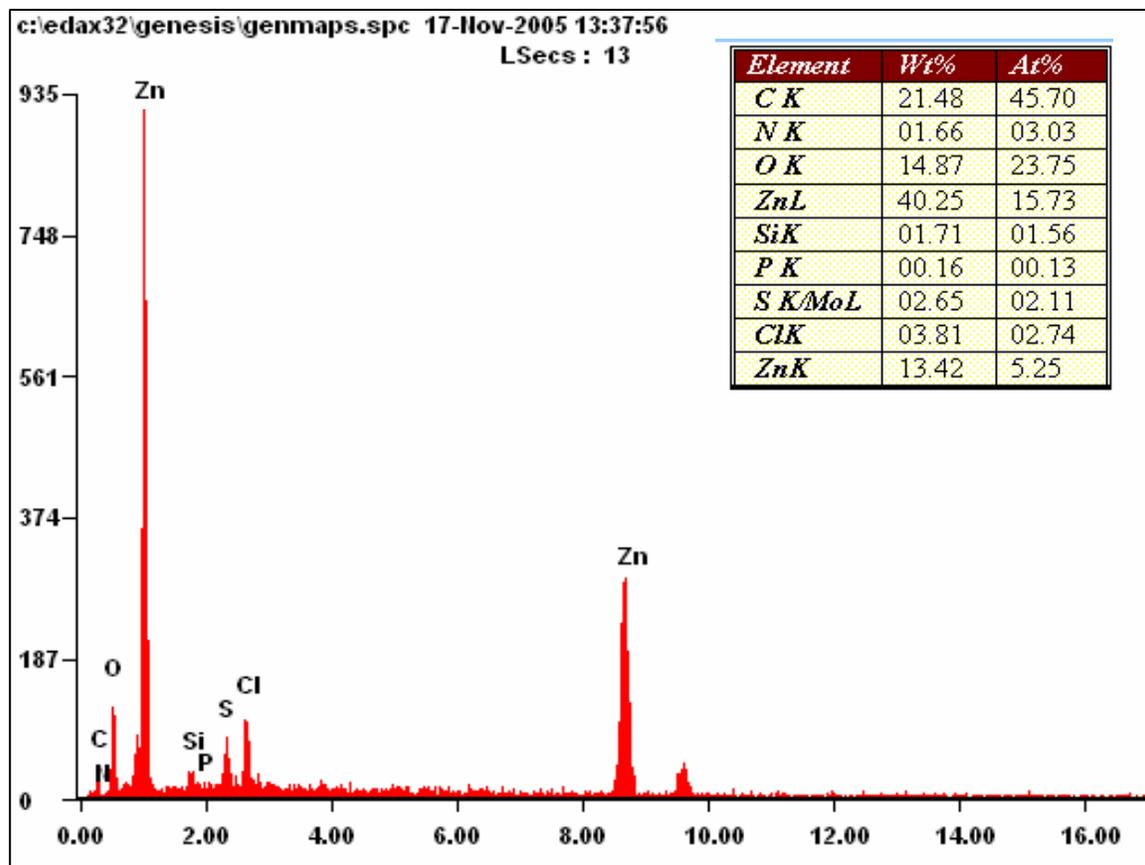
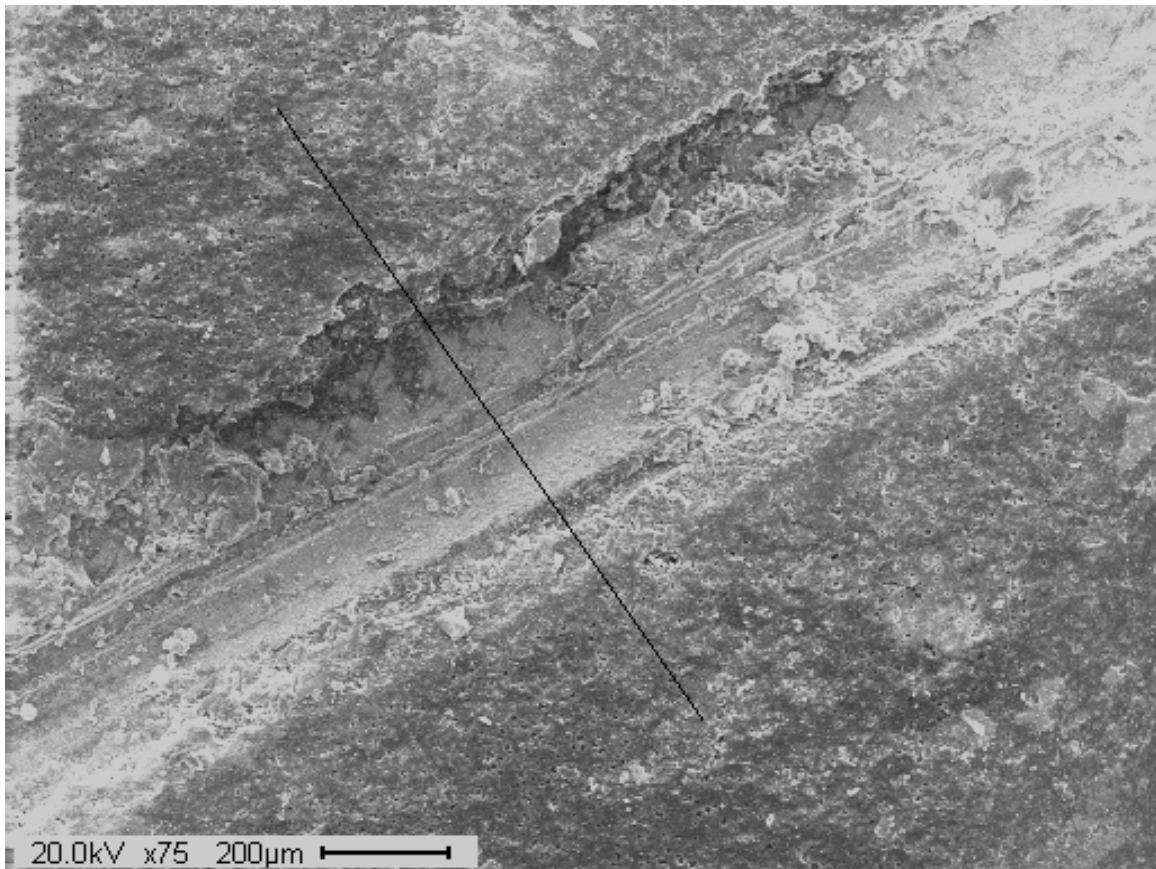
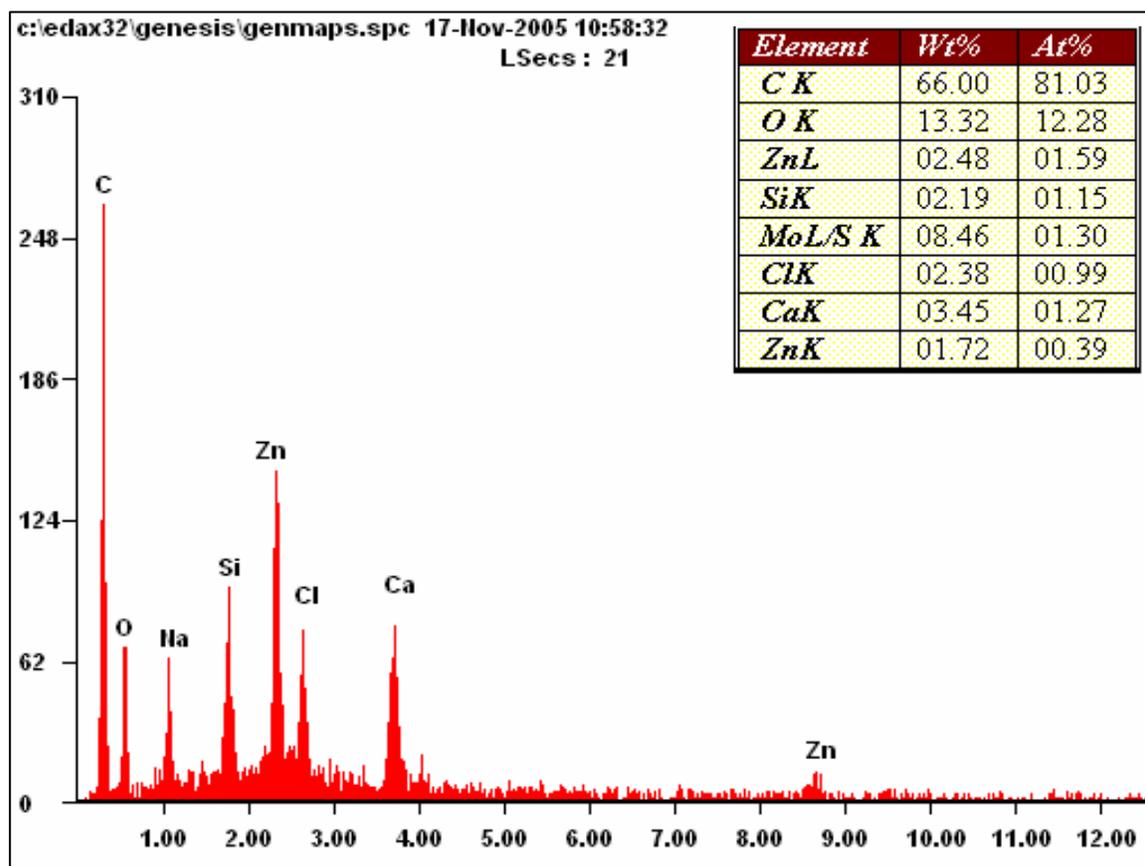


Figure B.8 (b). EDX spectrum at the point in the scribe highlighted in Figure 8 (a)



**Figure B.9 (a).** SEM image of scribe – effect of 15% CZM



**Figure B.9 (b).** EDX spectrum at the point in the scribe highlighted in Figure B.9 (a)

### Conclusions

The aim of this work was to start the developmental work of an effective anti-corrosive chromate-free, low-VOC, water-borne, direct-to-metal primer for hot-dip galvanized steel (HDG). The task was tackled by step-wise varying one or two components at a time. First the starting formulation F6 was modified by using an amine-adduct cross-linker and also by varying the resin in the

formulation. Step 2 improved the formulation with a low-VOC resin and a zero-VOC cross-linker. Step 3 investigated the use of three different silanes in the low-VOC coating system of step 2. Finally, in step 4, a set of pigment mixtures were incorporated in the bis-sulfur containing formulation developed in step 2.

The first and main conclusion of this study is that a silane-containing chromate-free low-VOC superprimer can be developed not only for aluminum alloys such as AA 2024-T3 but also for a more demanding substrate such as HDG steel. This superprimer coating survived 2000 hr in salt spray (Figure B.7), which is an unusual result for a chromate-free single layer coating on HDG steel. The second conclusion of this work is that a superprimer of this kind would hardly have been possible to develop without the use described synergism of the silanes and the chromate-free anti-corrosive pigments

Finally it is worth to mention that the results presented are only preliminary results of the beginning of the superprimer work on HDG steel. There is definitely more to be reported on this subject in the future.

## **C. ENVIRONMENTALLY-COMPLIANT NOVOLAC SUPERPRIMERS FOR CORROSION PROTECTION OF ALUMINUM ALLOYS**

### **Objective**

The following article focuses on the development of a novel, chromate-free, environmentally-benign superprimer system for the corrosion protection of aerospace aluminum alloys such as AA 2024-T3. The purpose is development, testing and characteristic study of a novel primer system which will integrate properties of silanes and novolac epoxy resins for the corrosion protection of AA 2024-T3 aerospace alloy. The superprimer under study is a novolac epoxy-based incorporated with bis-silanes, cross-linkers and other additives such as inhibitor pigments, surfactants and dispersants. Organofunctional bis-silanes are used in non-hydrolyzed forms to ensure better performance in terms of adhesion and corrosion protection. The surface pretreatment step is eliminated with the use of superprimer technology. The water-insoluble bis-silane addition imparts corrosion protection and the hydrophobicity to lend the system water-resistant properties. Due to the requirement of good low-temperature performance, polyurethane resin is added to the superprimer to impart flexibility. Cross-linkers (to boost room temperature) curing, surfactants (to improve adhesion) and dispersants (to improve pot-life) form an integral part of the superprimer system. Corrosion inhibitor pigments, nanoparticles and colorants are also incorporated in order to obtain a complete paint system.

In summary, this study deals with the development and evaluation of a superprimer coating with the following benefits:

- 1) Excellent corrosion protection and outstanding adhesion to the substrate as well as topcoats
- 2) Capable of replacing conventional chromate-based inhibitors with inorganic, non-toxic inhibitors
- 3) Able to eliminate the chromate conversion coating and other pretreatments on the AA 2024-T3 alloy
- 4) Excellent chemical resistance, water resistance and solvent resistance
- 5) Room-temperature curing with good high-temperature performance
- 6) Water-based, low-VOC and HAP free
- 7) Exceptional low-temperature properties such as flexibility

### **Performance Evaluation**

#### **Salt Water Immersion Test**

Salt water immersion test was carried out on coatings as a screening test to determine formulations showing promising performance. Figures C.1 and C.2 show images for coating formulations ND-20 (RT cured and HT cured), N-1 (RT cured and HT cured), and NP-1 with and without inhibitors after exposure in 3.5 wt.-% NaCl. The immersed coatings and the scribed surface were examined for evidence of corrosion or any other kind of deterioration. The coatings with NP-1 formulation without inhibitors suffered only minor scale white rusting with no discoloration or delamination. In the NP-1 formulation with zinc phosphate as inhibitor, scribes were mostly clean even after 60 days of salt water immersion. The salt water immersion test, thus, gave primary indications about the advantage of silane in enhancing corrosion resistance and water-barrier properties of the coating.



**ND-20  
RT cured**



**ND-20  
HT cured**



**N-1  
RT cured**



**N-1  
HT cured**

Figure C.1: Samples after salt water immersion for 30 days



NP-1 only



NP-1 with zinc phosphate  
corrosion inhibitor

Figure C.2: Samples after salt water immersion for 30 days

### **Electrochemical Impedance Spectroscopy**

Figure C.3 shows the Bode impedance plot for novolac formulation after 18 days of EIS testing. The impedance value at 1 mHz frequency was higher for N-1 than for ND-20. This showed the improvement in the corrosion resistance due to silane addition. A gradual decreasing trend in the impedance values was observed in both cases. However, the decrement of the impedance values was considerably greater in case of ND-20 formulation than in N-1 formulation. Also, at higher frequencies, the curve for ND-20 formulation shifted downwards which indicated electrolyte or water absorption by the coating possibly resulting in delamination. Occurrence of more than one time constant also confirmed that the coating layer was breached. In these curves, the modulus at high frequency (1 MHz) remains almost constant which points to the conclusion that there was no change in solution resistance. It means there was hardly any absorption of water or electrolyte by the coatings.

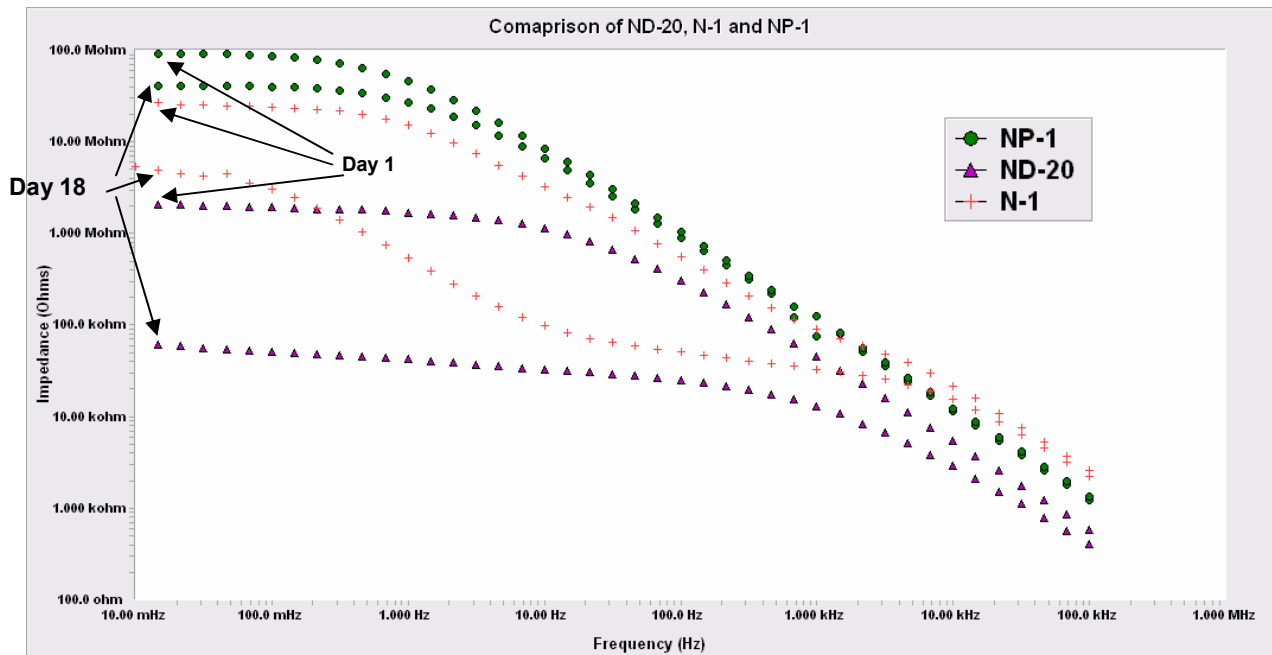


Figure C.3: EIS impedance data for novolac coatings

### Tape Adhesion Test

According to the ASTM 3359 standard, the adhesion of the superprimer can be classified as 4A as compared to 5A for the control coating. Topcoat adhesion to the superprimer was also excellent (classification 4A) for all the novolac formulations. However, topcoat adhesion depended on the time interval between the application of superprimer and the succeeding topcoat.

### ASTM B117 salt spray

ASTM B117 salt spray test was conducted on the novolac-based coatings and controls at DACCO SCI. Figures C.4 & C.5 show the images for novolac coatings and controls after 2000 hours of exposure in salt spray test. The ND-20 formulation showed substantial blistering and corrosion. In case of N-1, initial blistering was observed but the extent of corrosion was much lower. The performance for NP-1 coating was improved due to the synergistic effect produced by the silane, novolac resin and polyurethane resin. There was considerable white rust in the scribes with a hint of blistering. The rest of the coating remained clear of any corrosion or delamination. In the topcoated NP-1 coating with zinc phosphate, the inhibitor seemed to be less effective in the presence of a topcoat as a lot of white rust was visible in the scribes. The C1 coating showed no blistering or scribe creep which was expected. There was a slight hint of corrosion products on the scribes. The ineffectiveness of the chromate pigments in the presence of a topcoat was also clearly evident from the salt fog image for sample C2.



Figure C.4: Samples exposed in salt fog test

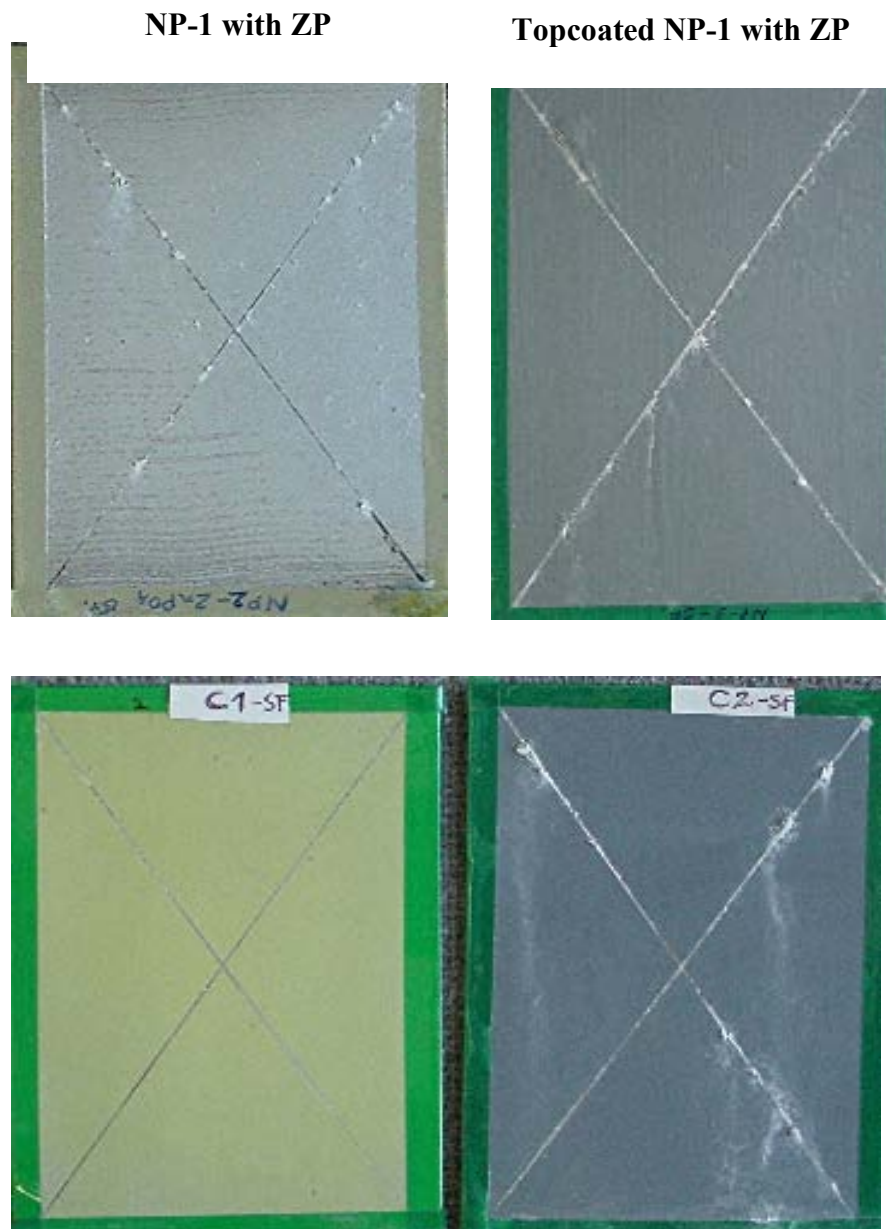


Figure C.5: Comparison of superprimer coatings and control exposed in salt fog test after 2000 hrs

### **Bend Test**

Figure C.6 shows images of superprimer coatings subjected to a room-temperature bend test and then exposure to 3.5 wt.-% NaCl solution for a period of 30 days. The ND-20 formulation showed huge cracks after bending because of its extreme brittleness. It also suffered from extensive corrosion on the cracks as well as the rest of the coating. The N-1 formulation was slightly less brittle after bending and only the cracked part of the coating suffered from corrosion. The NP-1

formulation showed no cracking at room temperature bending and remained intact even after exposure to salt water immersion. The bend test results confirmed the role of silane in providing corrosion protection and the flexibility and resistance to cracking imparted by the addition of polyurethane to the novolac-based superprimer.

### SEM/EDS Analysis

Scanning electron microscopy and energy dispersive X-ray analysis was carried out on superprimer formulations containing corrosion inhibitor pigments in order to test the effectiveness of pigments in terms of corrosion protection of the aluminum substrate. Cross-sectional analysis of a coated sample was also done to determine the phase distribution of the superprimer. The NP-1 superprimer coating with zinc phosphate inhibitor was chosen for SEM analysis as zinc phosphate was found to be the most effective inhibitor pigment from various corrosion tests. The NP-1 coating was used as reference or control. The coatings were cured at room temperature for 14 days. The coatings were scribed and exposed to 3.5 wt.-% salt water immersion test for a period of 30 days. The coatings were then washed to remove salt deposits and 1 mm x 1 mm samples of the scribed panels were prepared. The samples were sputtered with an Au-Pd target and analyzed using SEM/EDS.

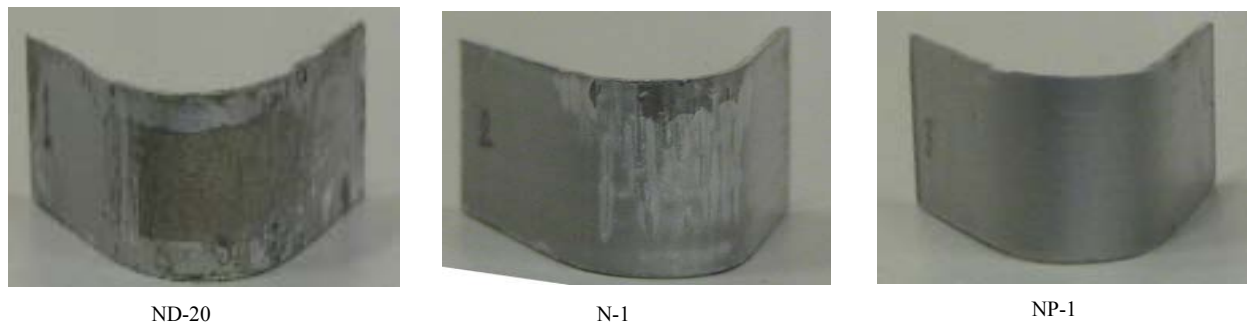
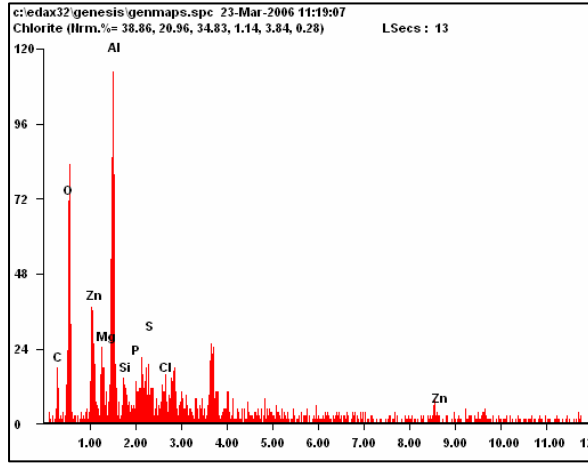
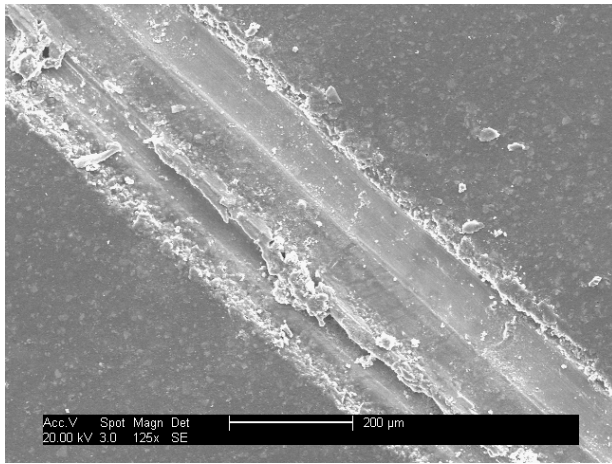


Figure C.6: Superprimer coating samples after subjected to bend test

Figure C.6 shows the backscattered SEM images of the scribed part of coating A with the distribution of various elements across the scribe obtained from a line scan. This sample had a visually clean scribe as seen from the SEM image with hardly any corrosion products on the scribe. Scans on the scribed part revealed high peaks of aluminum and oxygen and low peaks of zinc and chlorine. The amount of chlorine in the scribe is directly proportional to the amount of chloride corrosion product formed in NaCl solutions. In this case, the corrosion product if present would most probably be some complex of aluminum or copper or zinc hydroxy chloride. As the

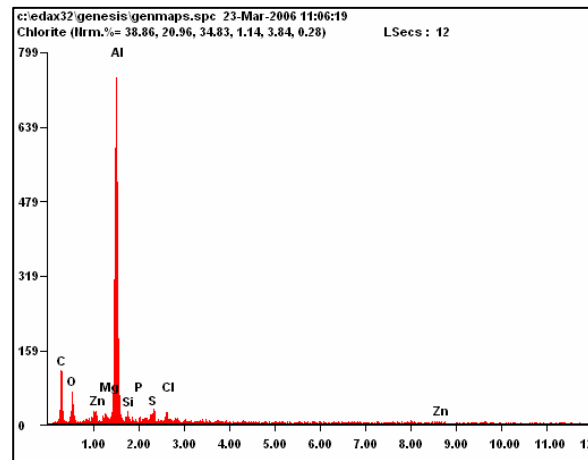
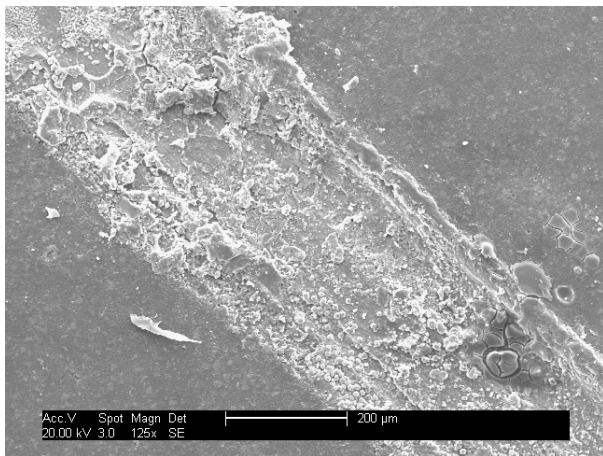
scribed part was approached in the scan, the chlorine content was actually found to be decreasing. The novolac resin had some amount of chlorine present due to epichlorohydrin. Based on the low amounts of chlorine and zinc in the scribe, it was concluded that the inhibitor was effective in protecting the scribe from corrosion keeping it free of corrosion products. The backscattered SEM images of the scribe region in coating which did not contain any inhibitor, showed that the scribe was very unclean with some deposits over the scribed part. High amount of chlorine was observed along the scribe. The low peaks for aluminum indicated that corrosion products were deposited on top of the exposed metals in the scribe. The absence of inhibitors led to corrosion of in the scribe. It could be certainly claimed that zinc phosphate works well in these water-based coatings

Figure C.7 provides cross-sectional view of the coating A, i.e. NP-1 coating with zinc phosphate inhibitors on AA 2024-T3. The line scan revealed that the distribution of the silane (Si) was fairly even along the cross-section. The SEM images also did not reveal any visible phase separation along the cross-section. The EDS scans and spot analysis also directed to the conclusion that the distribution of components was even. Huge chunks of inhibitor pigments were visible throughout the cross-section. However, the distribution of the pigments was uniform on a large scale.



<i>Elem</i>	<i>Wt</i>
<i>C</i>	17.
<i>O</i>	09.
<i>Al</i>	66.
<i>Si</i>	00.
<i>P</i>	00.
<i>S</i>	00.
<i>Cl</i>	00.
<i>Zn</i>	02.

SEM micrograph of coating NP-1 with protected scribe



<i>Elem</i>	<i>Wt</i>
<i>C</i>	75.
<i>O</i>	13.
<i>Al</i>	00.
<i>Si</i>	01.
<i>P</i>	00.
<i>S</i>	03.
<i>Cl</i>	03.
<i>Zn</i>	00.

SEM micrograph of coating NP-1 with un-protected scribe

Elemental distribution in the scribe

- Low Chlorine content
- High zinc content
- No corrosion products observed

- High Chlorine content
- Low zinc content
- Scribe covered with corrosion products

Figure C.7: Scribe protection analysis of novolac superprimer using SEM/EDS

## Summary

The experiments and performance test have demonstrated the following facts about the superprimer coatings:

- a) Incorporation of the silanes such as bis-sulfur, improves the anti-corrosion performance, water-barrier properties and adhesion characteristics of the novolac-based superprimer coatings.
- b) Corrostatin 228, zinc phosphate and sodium metavanadate have been effective in providing corrosion inhibition to the superprimer coatings on AA 2024-T3.
- c) The polyurethane resin enhances flexibility and low-temperature behavior of the novolac-based superprimer while further improving solvent resistance and adhesion.
- d) The complete topcoated superprimer system performs competitively vis-à-vis the topcoated control coating. This can be verified from the ASTM B117 salt spray test results.

Some prominent properties of the NP-1 formulation are mentioned in Table C.1. The next chapter gives the account of an effort made in this study to investigate the interaction of the superprimer components. A possible mechanism for the working of inhibitors in the superprimer was also investigated with the help of various characterization tools.

<b>Formulation</b>	<b>EPI-REZ 5003 (g)</b>	<b>EPIKURE 6870 (g)</b>	<b>Bis- sulfur silane (g)</b>	<b>NeoRez R-972 (g)</b>
<b>ND-20</b>	80	20		
<b>N-1</b>	72	18	10	-
<b>NP-1</b>	60	15	10	15

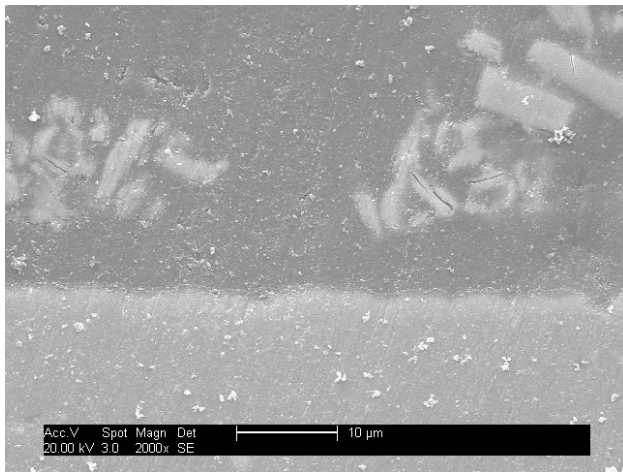
Table C.1

<b>Formulation</b>	<b>Contact angle (RT)</b>	<b>MEK double rub (RT) (HT)</b>		<b>Pencil Hardness (RT)</b>
<b>ND-20</b>	59°	60	300	1H
<b>N-1</b>	76°	60	300	1B
<b>NP-1</b>	79°	100	-	2H

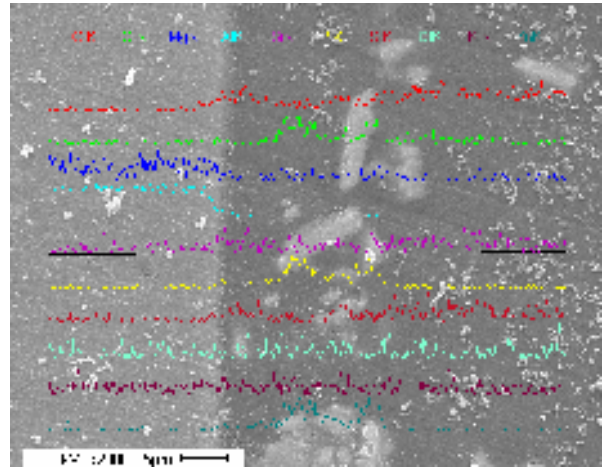
Table C.2

SEM/EDS analysis was performed to explore the role of corrosion inhibitors in corrosion protection of the substrate. TGA and DSC were used to study the thermal stability of the superprimer coatings. This chapter gives an account of the results and conclusion derived from the characterization of superprimer formulations discussed in earlier chapters.

SEM/EDS analysis verified the effectiveness of inhibitors in protecting exposed metal against corrosion. No corrosion products were observed in the scribe of NP-1 coating with inhibitors. High amount of crosslinking of the novolac resins and curing agent did not seem to affect leaching of inhibitors. Cross-sectional examination did not reveal any phase separation between the superprimer components suggesting an obvious interaction between them.



SEM micrograph of cross-sectional view of coating NP-1 on metals surface



Elemental distribution along the cross-section (from top to bottom in the micrograph)

Figure C.8: Cross-sectional analysis of novolac superprimer using SEM/EDS

## D. EPOXY-ACRYLATE PRIMER FOR Al ALLOYS

### Refinement and finalization of two superprimer formulations

The formulations of Novolac epoxy-based superprimer and epoxy-acrylate based superprimer have been finalized after refinement study. The following factors were studied and according to the results minor modifications were made to the formulation.

- a) Amount of co-solvent
- b) Amount of water
- c) Component ratio
- d) Amount of silane
- e) Addition of flush rust inhibitor

The formulations are sprayable and have a pot life of over 6 hours.

### Formulation

- 1) Novolac epoxy-based superprimer:

Part A:

Component	Parts in weight
Zinc phosphate	25
DI water	11
DPC-6870	13
Subtotal	49

Part B

Component	Parts in weight
EPI REZ 5003	52
Siquest A1289	5
Neorez R972	5
Subtotal	62

- 2) Epoxy-acrylate superprimer

Component	Parts in weight
Zinc phosphate	27.00
Silquest A-1289	5.75
Maincote AE-58	52.30
Surfynol 104H	1.20
Daubond DC9010W55	5.75
Butyl cellusolve	5.15
15% sodium nitrite solution	1.15
DI water	1.70
Total	100.00

### Performance

AA2024 coupon coated with epoxy-acrylate superprimer after 3500 hours of exposure to ASTM B117 is shown in Fig. D.1. Scribe showed some darkening but no obvious corrosion or blistering occurred.

Performance of novolac epoxy acrylate was reported in last year's report. Novolac epoxy superprimer coating passed 2000hours of ASTM B117 test.

The accelerated corrosion tests were performed by DACCO Scientific Inc.

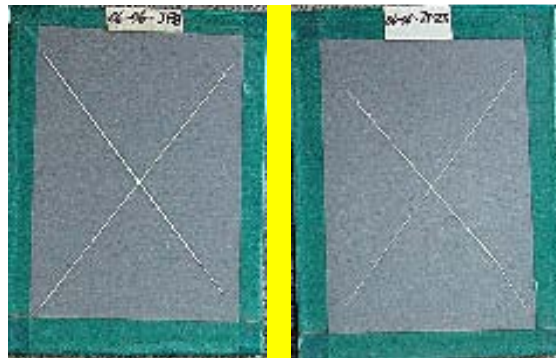
### Florida exposure test

To evaluate the performance of the superprimers in real working condition, epoxy-acrylate superprimer and novolac epoxy based superprimer were tested in outdoor exposure test at coastal area in Florida for 317 days. No corrosion or blistering was found on all the panels by visual inspection and no degradation was found on the panels coated with primer and topcoat as shown in the EIS test (Fig. D.2). The panels coated with superprimer + Defthane topcoat performed equivalently to the panels coated chromate conversion coating + Defthane topcoat.

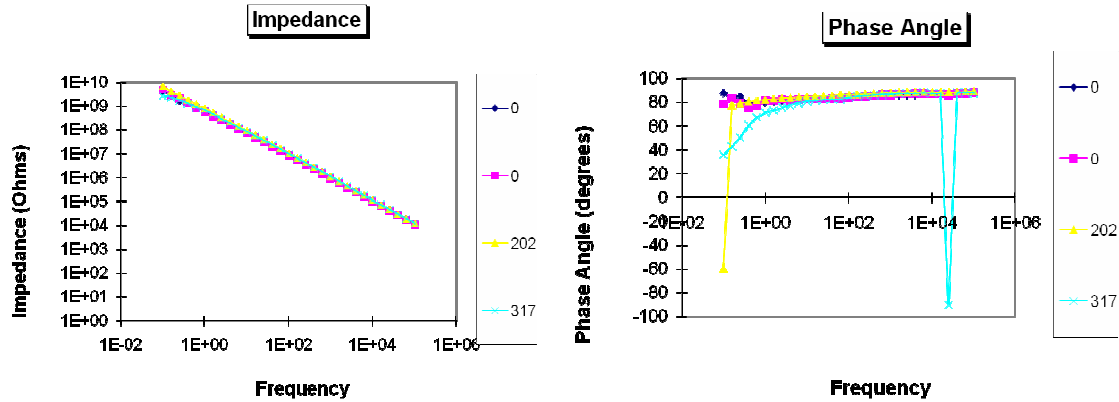


Fig. D.1 Epoxy acrylate superprimer coating on AA 2024 after 3500 hours of exposure to ASTM B117

(a) Image of the samples



(b) Impedance and contact angle: Epoxy-acrylate Superprimer + 30% ZP



(c) Impedance and contact angle: Chromate pretreatment + MIL-PRF-23377G

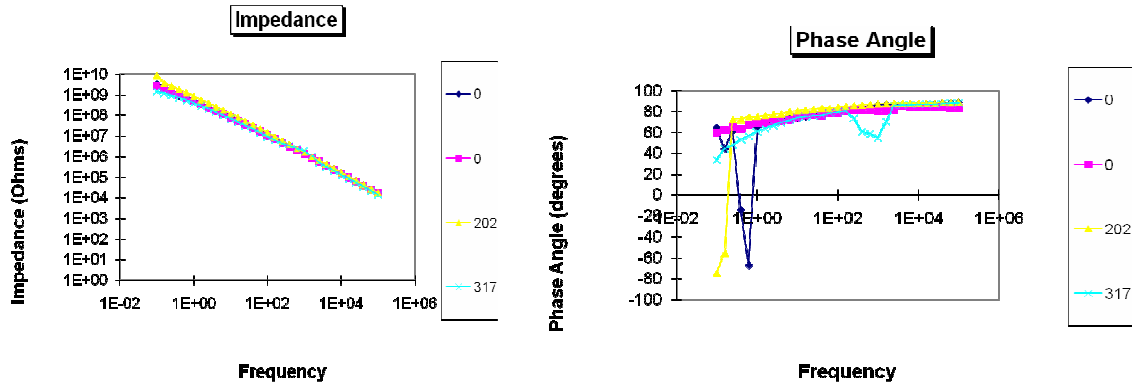


Fig. D.2 Epoxy-acrylate superprimer coating on AA2024 after 317 days of Florida outdoor exposure.

### Packing study of superprimers

Novolac epoxy acrylate superprimer:

Packing study of novolac epoxy superprimer has been carried out for 6 month. Coatings made from packs aged for 6 month showed adhesion inferior to that of freshly made coatings. Corrosion test of the panels are in progress.

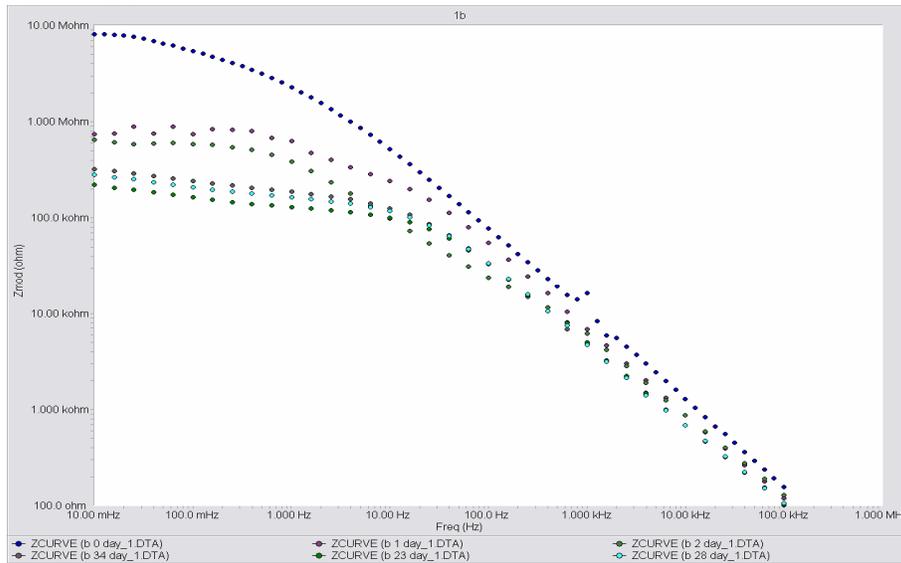
### Electrochemical impedance study

Electrochemical impedance spectroscopy (EIS) is used to study the effect of addition of silane and pigment on the properties of superprimer coating, and also the effect of chromate pretreatment. Coatings listed below were made and has been subjected to 30 days' EIS study. As indicated in impedance data, silane improved the barrier property of the superprimer coating and therefore reduced the degradation of the coating and corrosion. Equivalent circuit models will be constructed and interpreted.

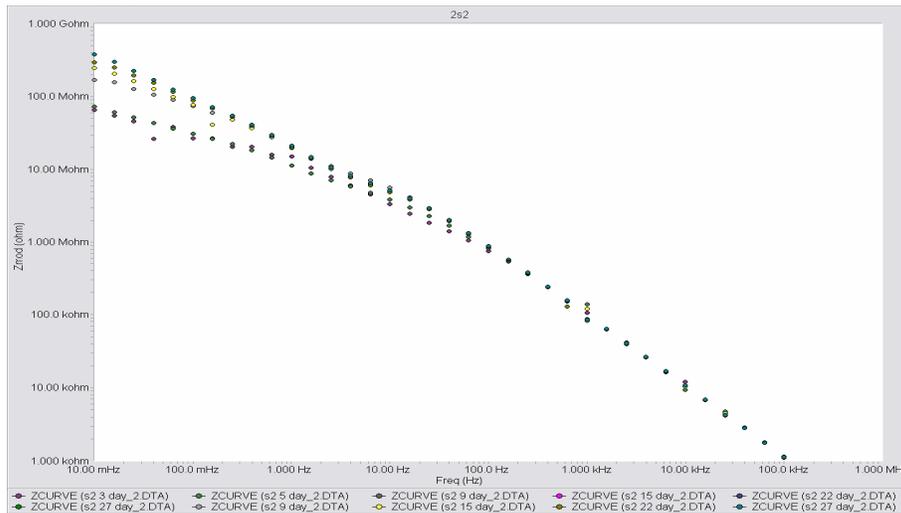
- Epoxy + Acrylate
- Epoxy + Acrylate + silane
- Epoxy + Acrylate + ZP

- Epoxy + Acrylate + Silane + ZP
- Epoxy + Acrylate + Silane + ZP + SiO<sub>2</sub>
- Chromate pretreatment + Epoxy + Acrylate
- Chromate pretreatment + Epoxy + Acrylate + ZP
- Chromate pretreatment + Industrial chromate primer

1) Epoxy + Acrylate  
0.6M NaCl

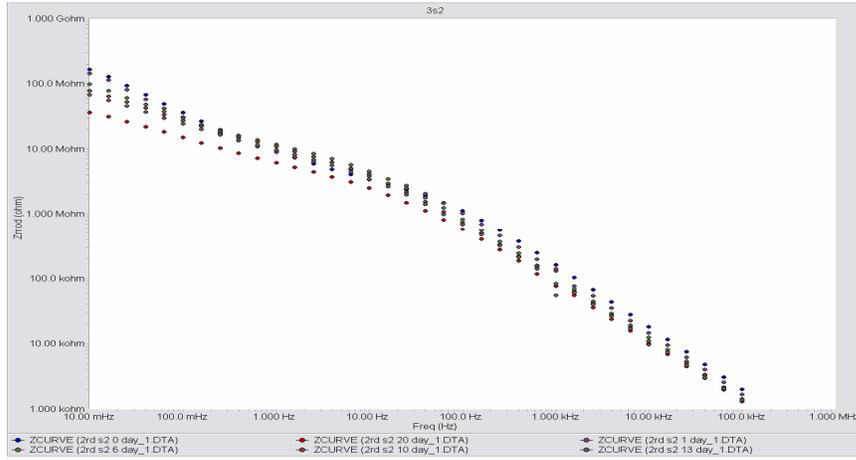


2) Epoxy + Acrylate + silane  
0.6M NaCl



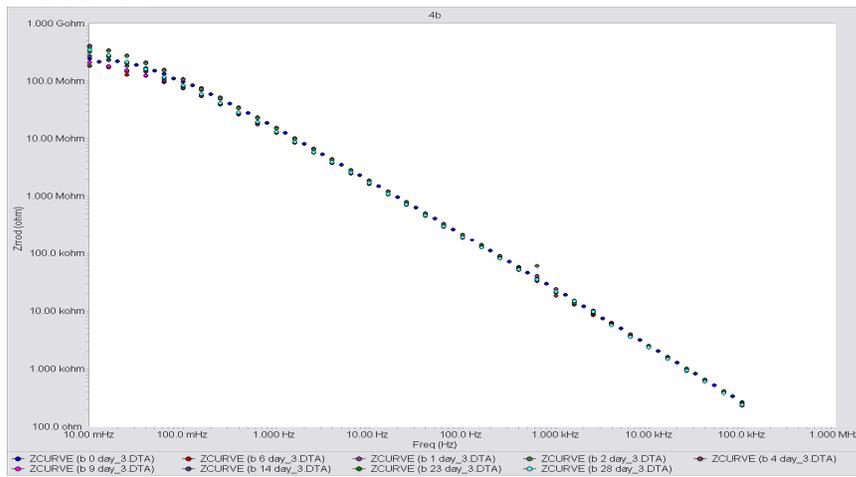
### 3) Epoxy + Acrylate + ZP

0.6M NaCl



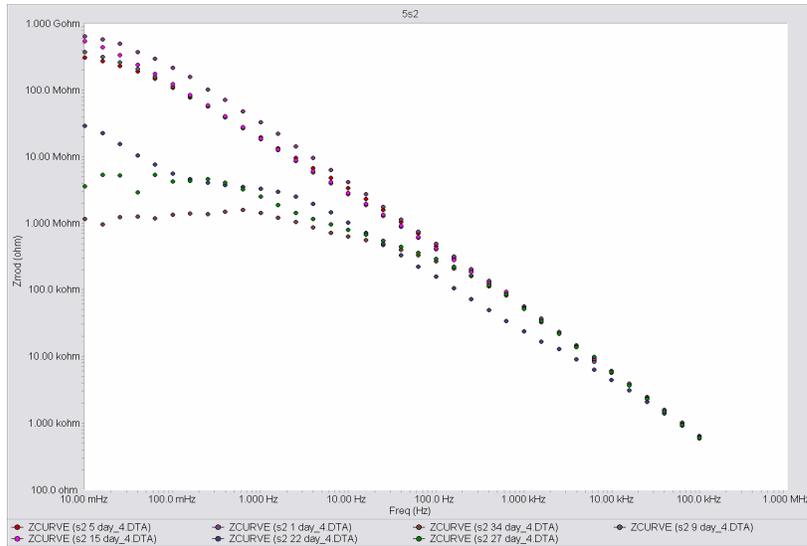
### 4) Epoxy + Acrylate + Silane + ZP

0.6M NaCl



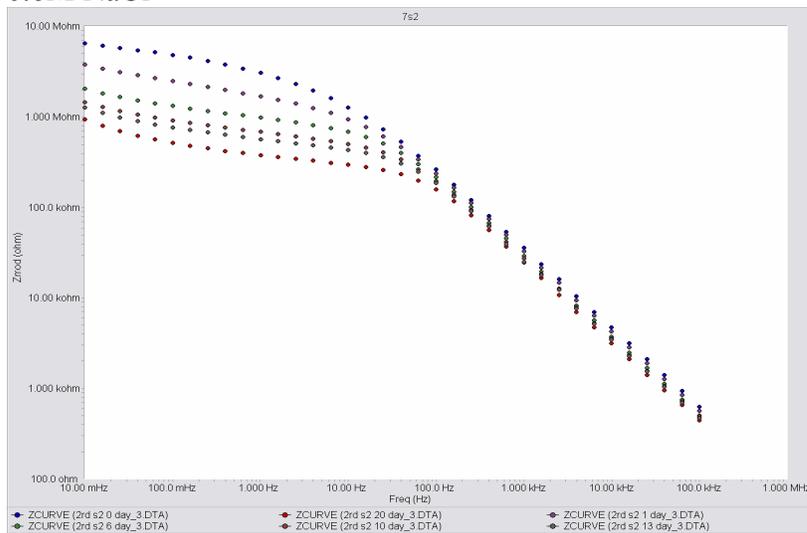
### 5) Epoxy + Acrylate +Silane +ZP+SiO2

0.6M NaCl



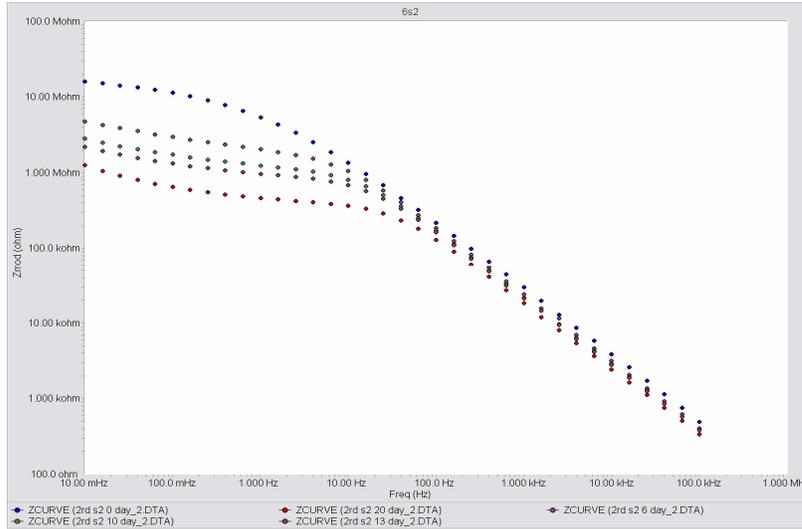
### 6) Chromate pretreatment + Epoxy + Acrylate

0.6M NaCl



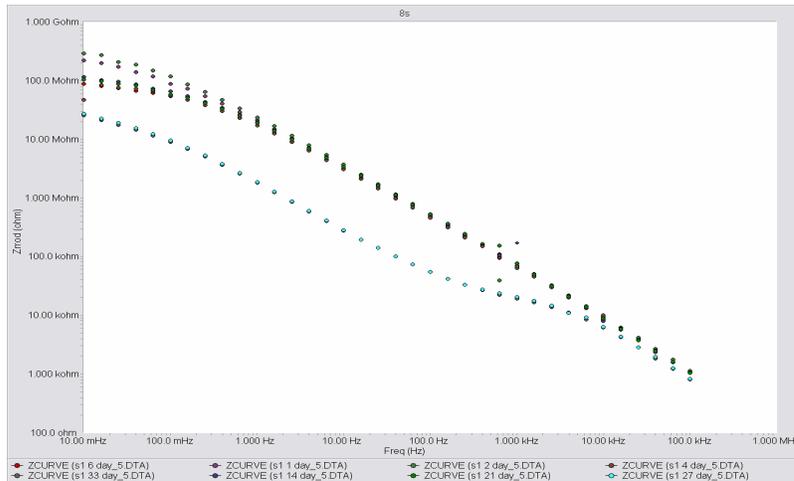
7) Chromate pretreatment + Epoxy + Acrylate + ZP

0.6M NaCl



8) Chromate pretreatment + Industrial chromate primer

0.6M NaCl



**A series of novel deposited pigments**

A series of novel shell/core structure pigments were made and tested on CRS. They are compounds containing two or more of Zn, Sr, Ca, Mg, phosphate and borate with ratio between the components varied. Different from other modified pigments, those pigments are deposited on to zinc oxide powders so they can replace the *filler + pigment* combination with higher efficiency and lower cost. The compound will also provide a stronger and wide-spectrum inhibition. Calcium magnesium phosphate and zinc magnesium borophosphate were the two found to provide anticorrosion protection comparable to chromate on CRS. The preparation of the pigments is elaborated below.

Preparation of phosphate pigments on zinc oxide:

1. Swelling of zinc oxide in distilled water for 3-4 hours.
2. Preparation of phosphates:
  - a. Magnesium carbonate and calcium hydroxide are dissolved in equal ratios in distilled water and then left to react with concentrated phosphoric acid according to the stoichiometric ratios to prepare Ca Mg phosphate.
$$6\text{Ca}(\text{OH})_2 + 6\text{Mg}(\text{CO}_3)_2 + 2\text{H}_3(\text{PO}_4)_2 \rightarrow (\text{Ca.Mg})_6(\text{PO}_4)_4 + 6\text{H}_2\text{O} + 12\text{CO}_2$$
3. Excess phosphoric acid is added to confirm the attachment to zinc oxide surface.
4. Prepared or bought phosphates from the market are added to the swelled zinc oxide from step 1.
5. The mixtures are added together with continuous stirring and at 100°C.
6. After 2 hours the mixture of the prepared pigment is then filtered, washed and dried.
7. The mixture is then calcined at 500°C for 2 hours.
8. Grinding of the pigment until it meets the requirement on particle size

Preparation of boro-phosphates

1. Magnesium carbonate and zinc oxide are mixed and dissolved in distilled water in the weight ratios 1Zn:4Mg for half an hour with continuous stirring.
2. Boric acid and phosphoric acid are added respectively in the weight ratios (2:6); the whole mixture is stirred for 2 hours at 100°C.
3. The mixture is filtered then washed very well to get rid of excess acids and dissolved byproducts.
4. Slow dehydration at 100°C overnight, then calcinations at 550°C for 4 hours.
5. Dry grinding or grinding in acetone until it meets the requirement on particle size

### **Cerium metasilicate**

Cerium metasilicate is a new pigment we synthesized and it was found to be effective on aluminum alloys. Epoxy/acrylate superprimer coating with 30 wt% CeSiO<sub>3</sub> provides about 2000 hrs of protection for AA2024-T3 panels in ASTM B117 test.

However, no than 10 wt% cerium metasilicate can be added into novolac epoxy-based superprimer otherwise the primer emulsion will turn into paste. Catalytic effect of Ce and Sn is now under study.

### **Circulating saltwater immersion test**

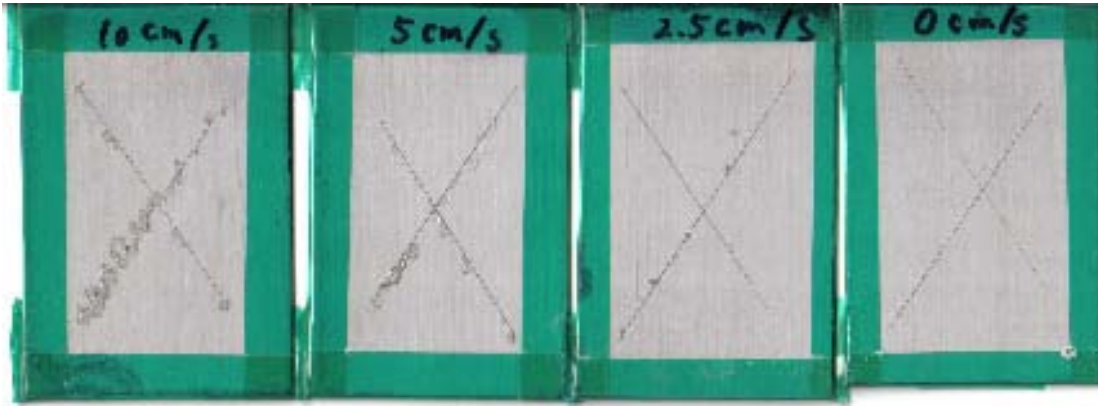
The flow rate of the media was found to have an effect on the performance of the primer and pigments. A circulating saltwater immersion test device with flow rate up to 10 cm/s was build. AA7075-T6 coated with the following recipes were tested under a flow rate of 0 cm/s, 2.5cm/s, 5cm/s and 10cm/s.

- a. L2 +20% ZP, without substrate pretreatment
- b. L2+20% barium chromate, without substrate pretreatment
- c. Cr (VI) pretreatment (Alodine 1200S) + Primer: MIL-PRF-23377G

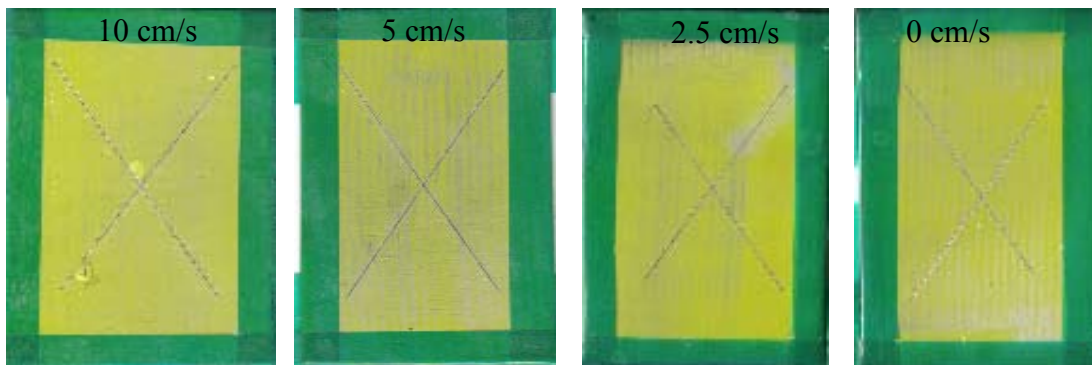
Results showed that the flow rate have a prominent effect on the performance of the coatings. This method can be included into the evaluation of the pigment as a fast and easy way to test the effectiveness of the pigment.

Substrate: AA7075-T6  
Coating: Superprimer and chromate-containing primers  
Temperature: 35 °C  
Flow rate: 0 cm/s, 2.5cm/s, 5cm/s and 10cm/s.

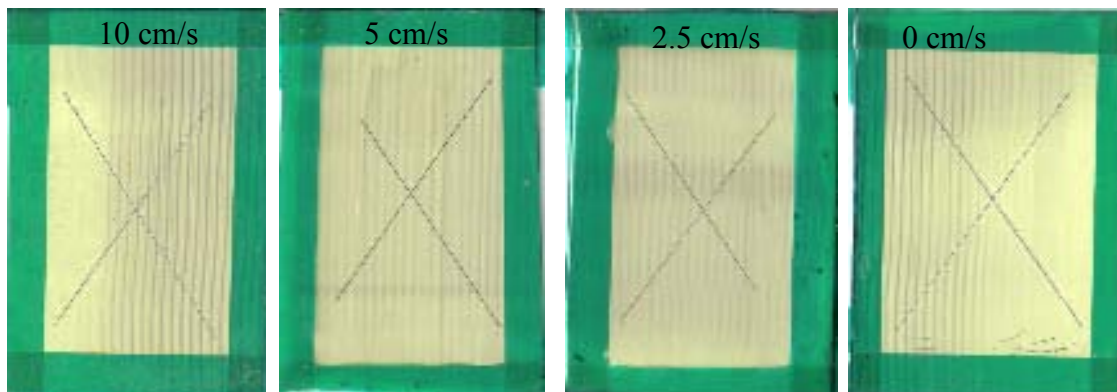
a. L2 +30% ZP, without substrate pretreatment



b. L2+30% Barium chromate, without substrate pretreatment



c. Cr (VI) pretreatment (alodine 1200S) + Primer: MIL-PRF-23377G



### **Nanoparticles as filler and Colorant**

Nanoparticles such as nano-size silica power, titania, and carbon black particles were attempted as fillers in the superprimer to improve performance of the coating.

A few inorganic and organic colorants were added to superprimer for visibility and aesthetic effect. Examples of colorant are iron oxide, carbon black and cobalt. Colored coatings were tested in salt spray to evaluate if the addition of those colorants will impair the performance of the superprimer coatings.

Nano-particle fillers were not found to improve the property of the coating and sometimes even acted adversely. Inorganic colorants should be added with care because most of them were found to impair the anticorrosion of the coating, while organic colorant were found to have minimal effect on the performance of the coating, probably due to the small amount of addition (a couple of drops of organic colorant is enough for 10 grams of superprimer).

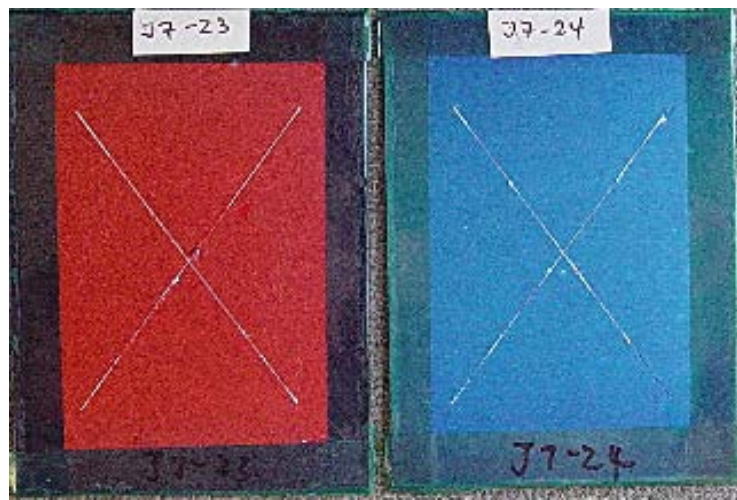


Fig. D.3 Epoxy-acrylate superprimer with organic colorant added after 1000 hours of exposure in ASTM B117. Substrate: AA2024.

### **Electrodeposition of superprimer**

As a new application method of superprimer, electrodeposition was explored with initial success. Electrodeposition is expected to provide a more uniform, controllable, better organized and less porous coating and better adhesion.

Electrodeposition of epoxy-acrylate superprimer has been experimented on HDG and CRS panels. Different deposition time and voltages have been attempted. Electrodeposited superprimer coating seemed to work better than spray-coated superprimer on HDG and CRS panels.

Electrodeposition conditions:

Voltage: -5V

Electrodeposition time: 15 minutes

Primer: epoxy-acrylate superprimer

Substrate: HDG panels



Figure D.4 EIS measured during salt spray test (1000 hours)

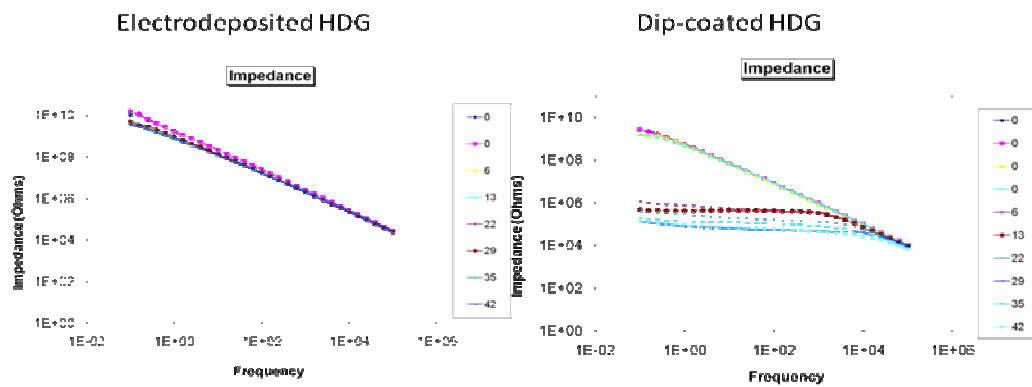
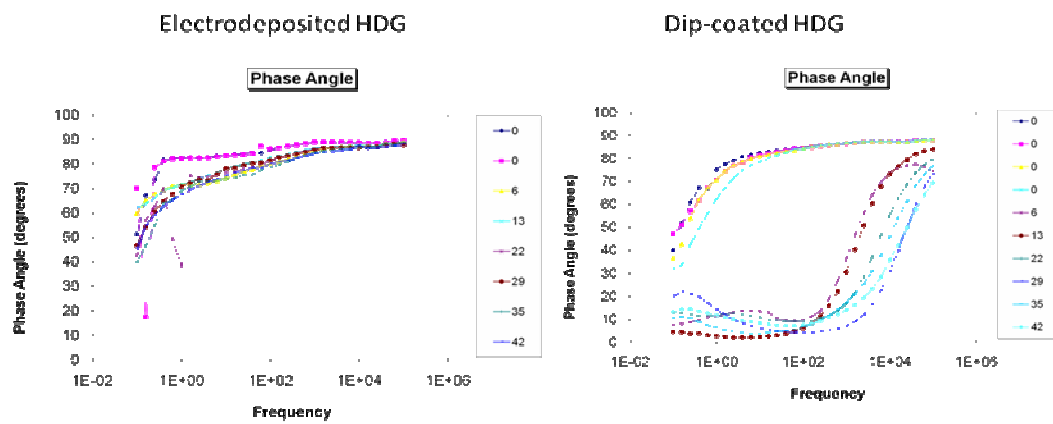
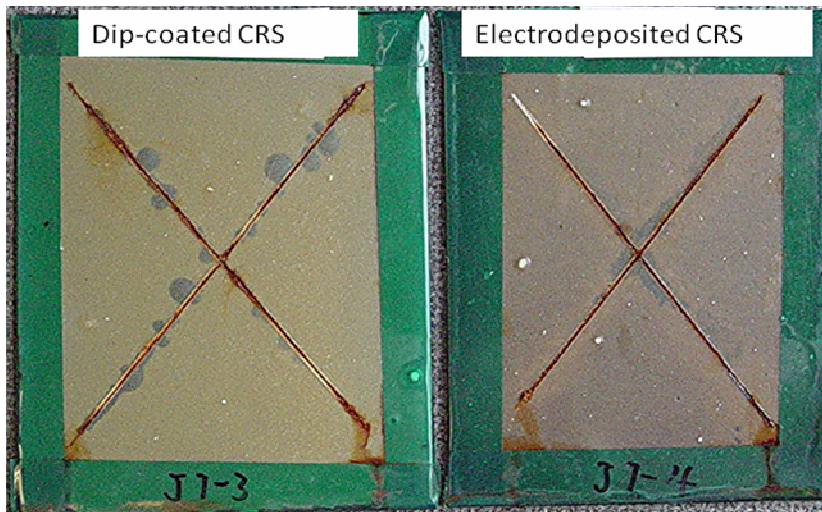


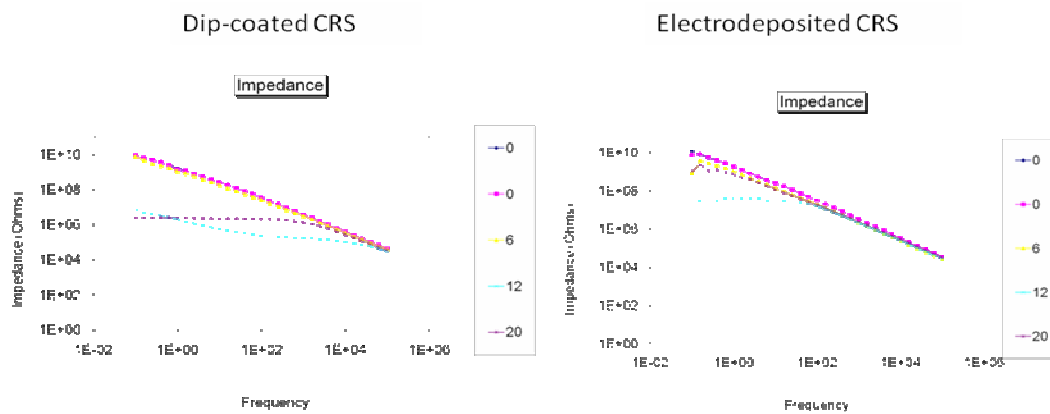
Figure D.5 Contact angle changes during 1000 hours of salt spray test



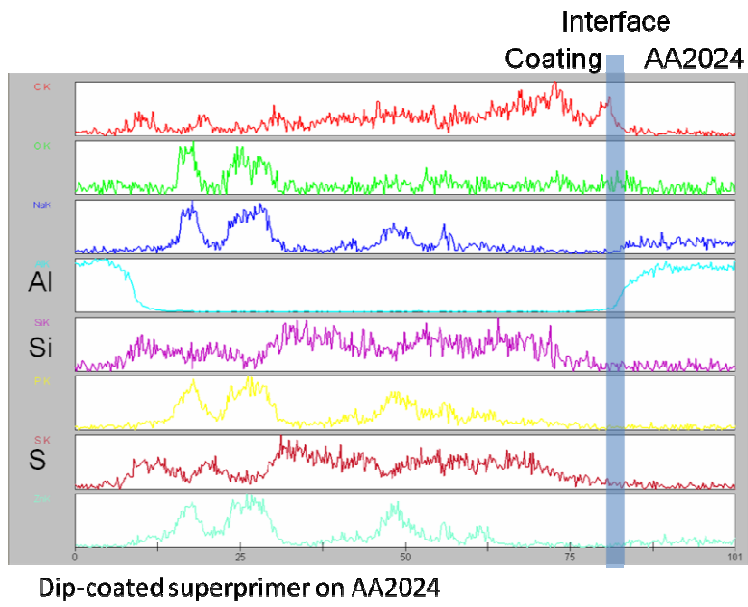
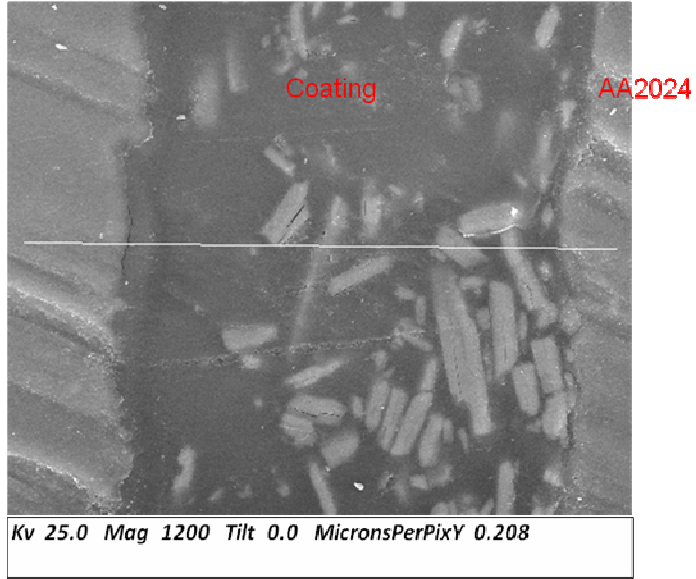
CRS:



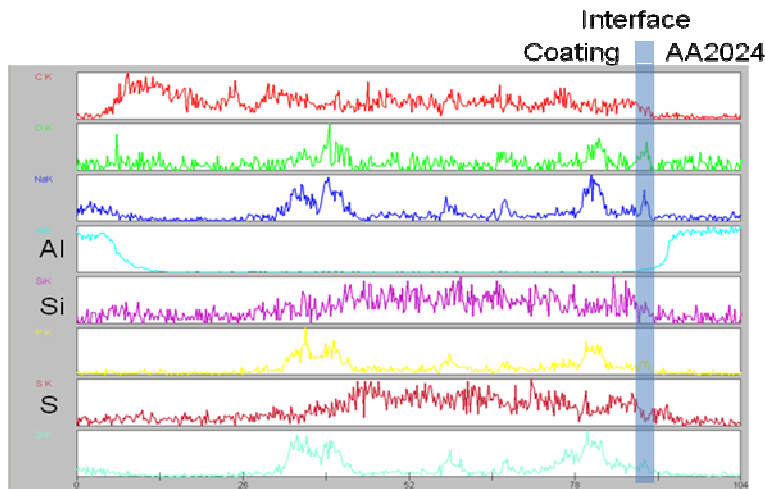
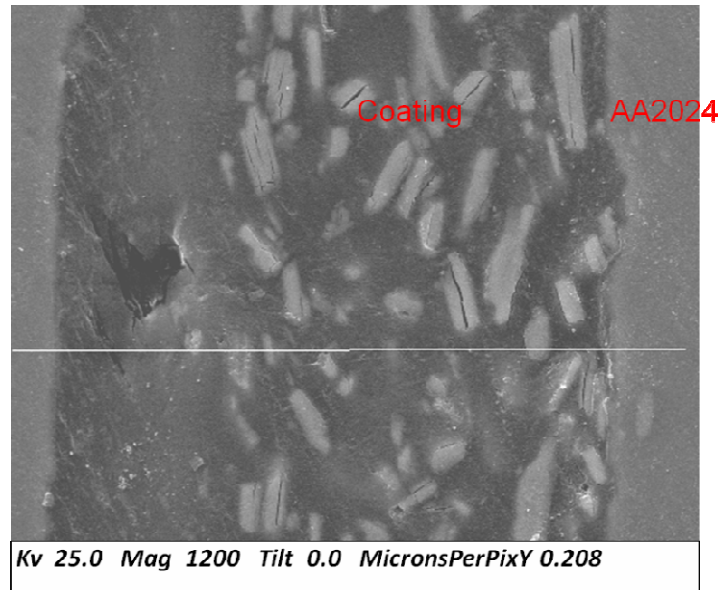
EIS measured during salt spray test



The cross-section of the two coatings were analyzed by using EDAX. Comparing the elemental line scan obtained from EDAX as shown in Fig. D.13, the electrodeposited coating seems to have a more uniform distribution of silane. Especially at the interface, the silane concentration in the electrodeposited coating seems to be higher than that of dip-coated coating.



Electrodeposited AA2024



Electrodeposited superprimer on AA2024

### Chrome(III) pretreatment evaluation

Chrome (III) pretreatment was evaluated. Chrome (III) pretreated AA2024 and AA7075 panels were tested in ASTM B117 test for 1300 hour. Chrome (III) provides protection comparable to Cr (VI) pretreatment for Al alloys. However, Chrome (III) pretreatment was not found to improve the performance of superprimer coated Al alloys.

#### Pretreatment:

Cr (III) pretreatment: METALAST TCP-HF

Cr (VI) pretreatment: ALODINE 1200S

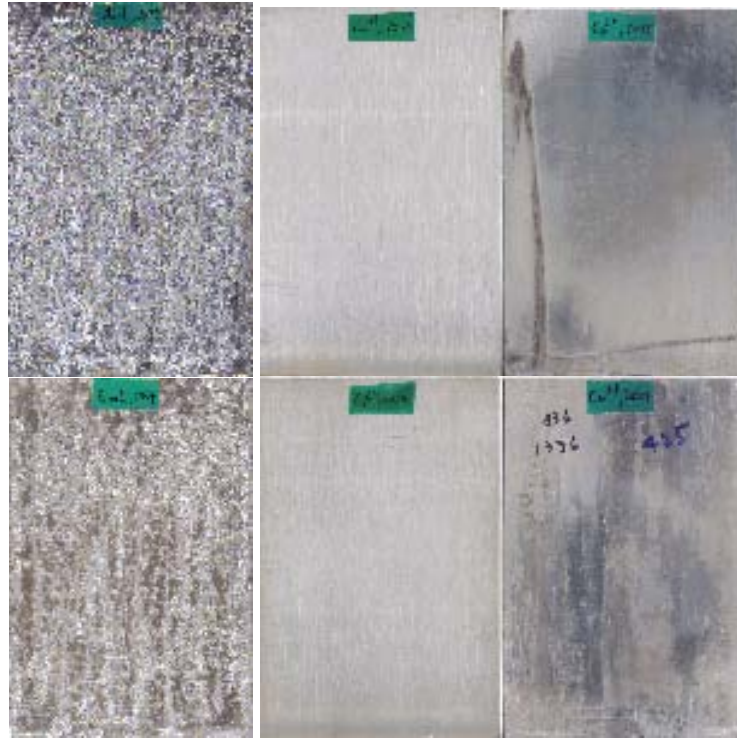
#### Substrate:

Aluminum alloy 2024-T3 and aluminum alloy 7075-T6 panels

**Exposure time:**

Untreated AA7075 panels: 65 hrs

Cr (III) and Cr (VI) treated panels: 1300 hrs



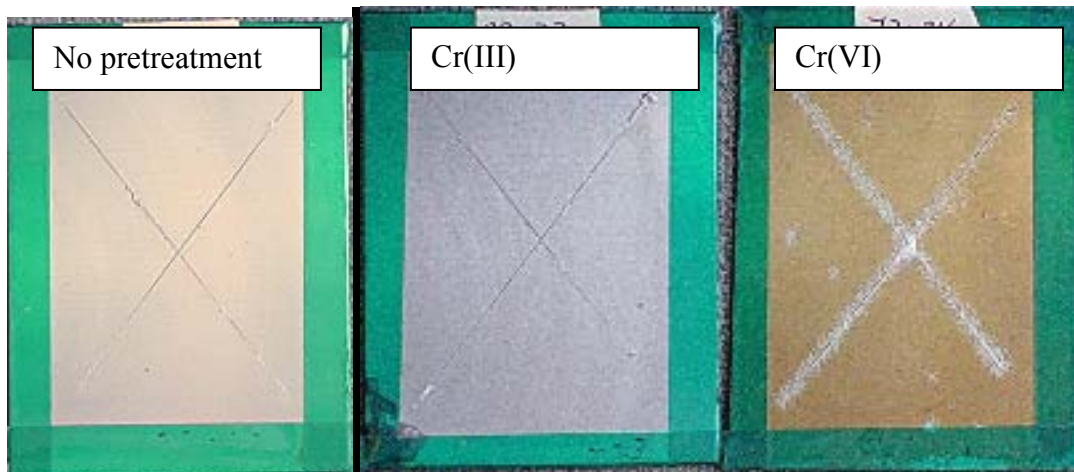
**Pretreatment:**

Cr (III) pretreatment: METALAST TCP-HF

Cr (VI) pretreatment: ALODINE 1200S

**Substrate:** Aluminum alloy 2024-T3

**Exposure time:** 2000 hours, ASTM B117



### Optimal time window to recoat/topcoat

Different topcoating time window (time between the primer and topcoat are applied), 4 hours, 1 day, 2 days and 5 days, were investigated in order to find out the optimal topcoating time. Though different topcoating time showed no impact on adhesion, a topcoating time window of 1 day or less seems to be the optimal, as shown in ASTM B117 test.

Different recoating time, 4 hours, 1 day, 2 days and 5 days, were investigated in order to find out the optimum topcoating time. The superprimer used was epoxy-acrylate superprimer and the topcoat was Defthane (MIL-PRF-85285D).

Dry and wet adhesion test (7 days' immersion in DI water) was preformed. All panels (topcoated after 4 hours, 1 day, 2 days and 5 days) exhibited good adhesion (5A or 5B).

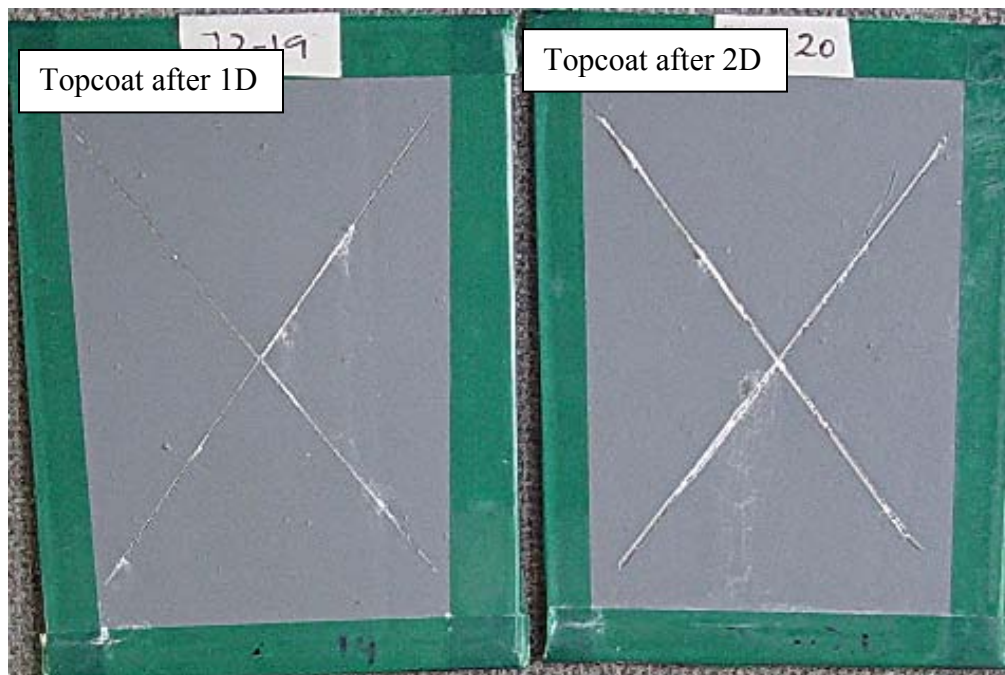
The panels are subject the ASTM B117 test. They have not show difference after 18 days. Final conclusions will be made after 2000hrs of salt spray test.

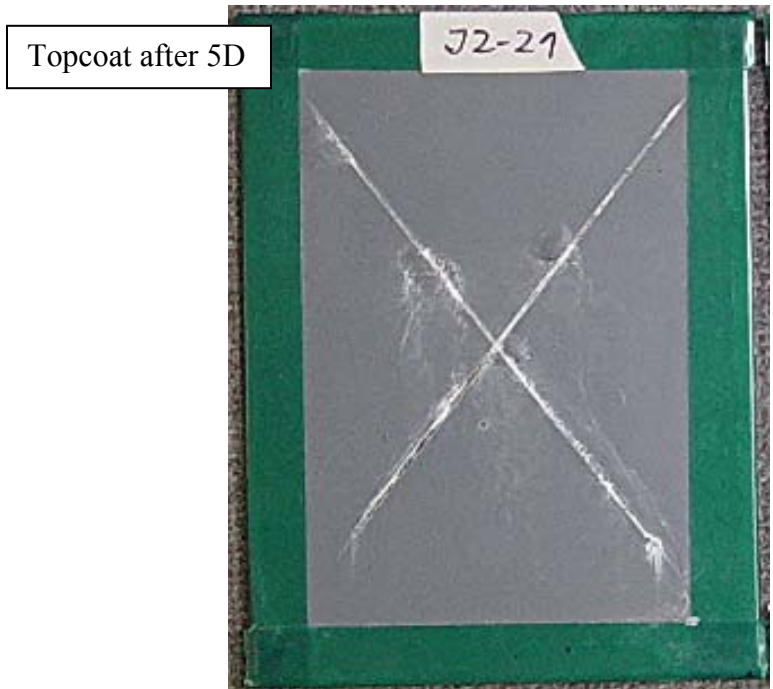
**Substrate:** AA2024-T3

**Exposure time:** 2000 hours

**Primer:** New L2 (epoxy-acrylate superprimer)

**Topcoat:** Defthane





**Status of the external testings**

- i. Testing performed by the Navy
- ii. Testing performed by CTIO at WPAFB

Epoxy-acrylate superprimer and novolac epoxy superprimer are under evaluation at WPAFB.

**Finished test:**

Crosshatch adhesion test: Both superprimer passed.  
 X cross adhesion test: Novolac epoxy superprimer passed. Epoxy-acrylate superprimer failed.  
 Lubricant and Jet fuel test: both superprimers passed.

**Tests in progress:**

Salt spray test: small blistering and darkening occurred on superprimer coatings after 300 hours. Another batch of superprimer coating cured for extended time will be tested.

**Leaching-out rate of pigment**

To verify the leaching-out of zinc phosphate from the coating, an experiment with setup as shown in Fig. D.6 was performed. A cylinder filled with DI water was placed vertically on a free-standing coating with acrylate-dominated layer exposed to DI water. The concentration changes of  $Zn^{2+}$  and  $PO_4^{3-}$  with time were measured using Inductively Coupled Plasma Mass Spectrometry (ICP-MS). ICP-MS confirmed that zinc phosphate leaches out from the acrylic layer and the leaching

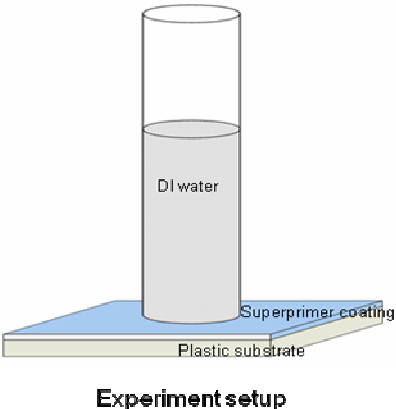


**Fig. D.6** Setup of leaching –out experiment

rate measured is shown in Fig. D.7. Notably, zinc leaches out faster and reached a higher concentration than phosphate did.

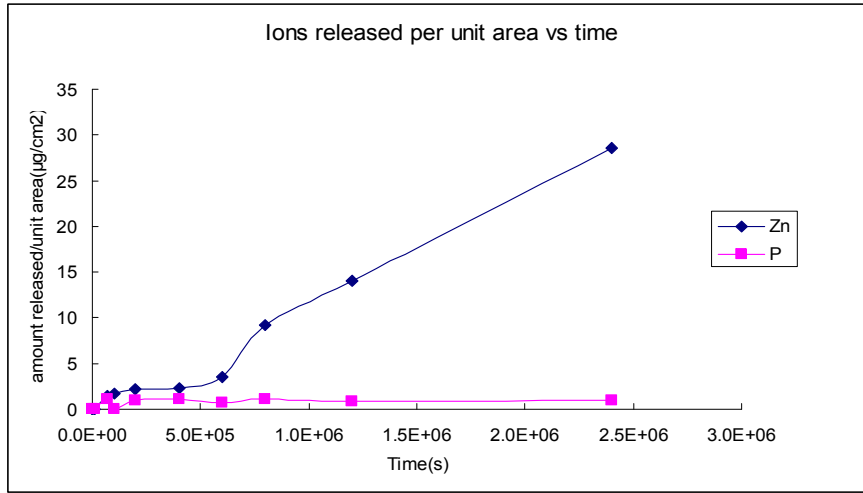


**Fig. D.7** Leaching-out rate of Zn and P from superprimer coating, measured by ICP-MS

Another experiment was designed to examine a relation between the corrosion rate and the turbulence of the environmental electrolyte. The results revealed that the corrosion rate of scribe on pigmented primer coating increases with flow rate of the electrolyte, which on the other hand demonstrated the effect of leached-out pigment on the scribe.

### Protection mechanism study

In order to find out how zinc phosphate works on aluminum, the following experiments were performed:

- 1) Compare a bare AA2024 panel immersed in Cl<sup>-</sup>-containing solution with and without zinc phosphate, especially the anodic and cathodic sites
- 2) Analyze the scribe after short term and long term of exposures to Cl<sup>-</sup>-containing solution
- 3) Study the interface between the zinc phosphate-pigmented coating and substrate

#### i. Bare AA2024 panels immersed in zinc phosphate solution

Bare AA2024 panels were immersed in blank 600ppm NaCl solution and 600ppm NaCl solution saturated zinc phosphate for 2 hours. SEM/EDAX (Fig.D.8) showed that pitting and Mg dissolution occurred at intermetallics Al<sub>2</sub>CuMg in NaCl solution w/o zinc phosphate. The Al matrix and intermetallics Al-Cu-Fe-Mn did not show corrosion.

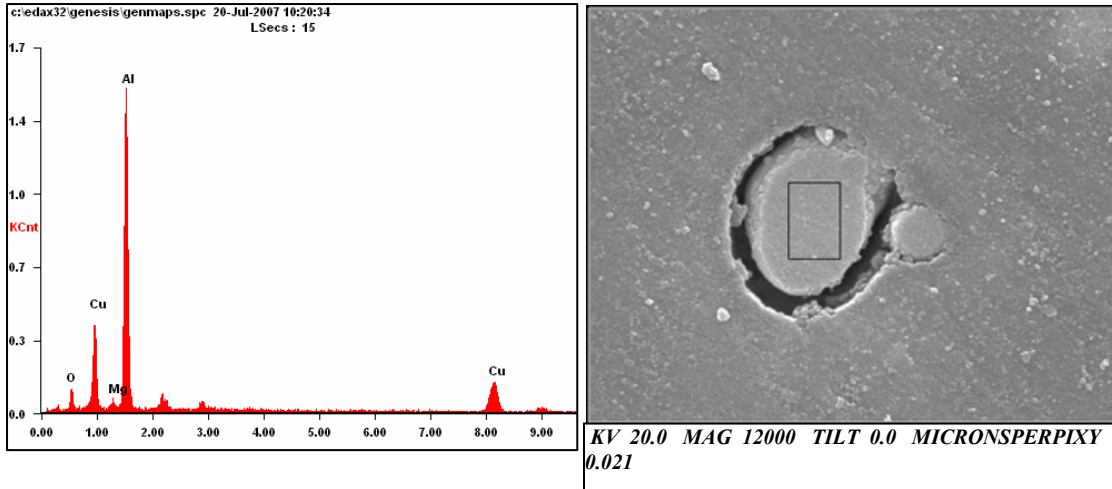
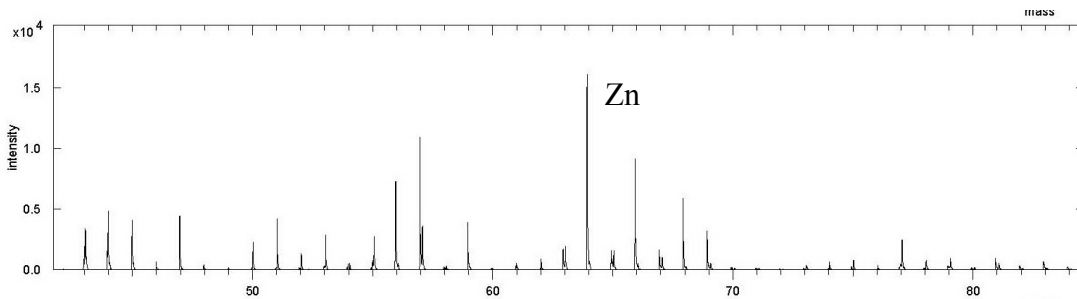


**Fig. D.8** Al<sub>2</sub>CuMg intermetallics in AA2024 with pitting after exposure to NaCl. Left: SEM image; Right: EDAX

No corrosion on matrix or intermetallics occurred on AA2024 immersed in NaCl solution containing zinc phosphate. However, EDAX using 20kv electron beam could not detect any zinc or phosphor on matrix or intermetallics of the immersed panel. Zinc and phosphate were detected on the surface of AA2024 by using ToF-SIMS, and the intensities of both species were fairly high, as shown in Fig. D.9.

Positive:



Negative:

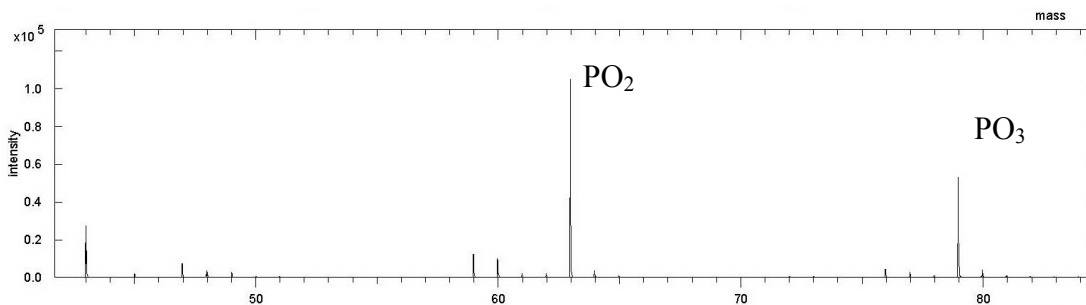


**Fig. D.9** ToF-SIMS of bare AA2024 panels immersed in saturated zinc phosphate solution

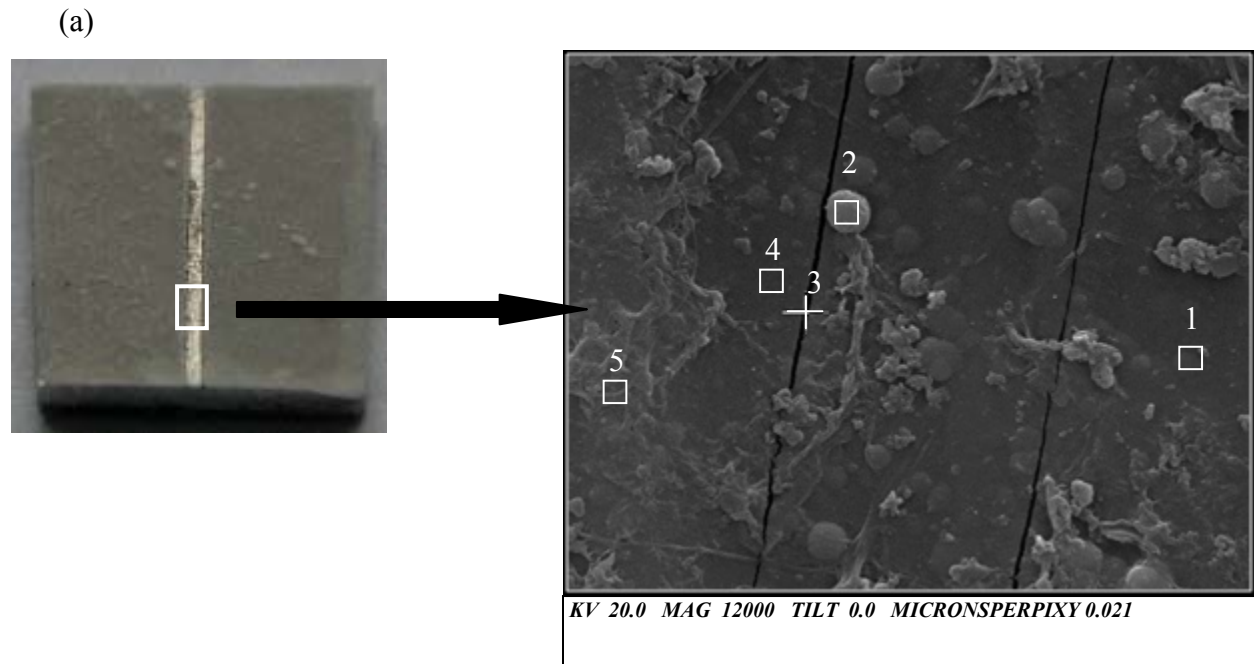
ii. Short term and long term of exposures to Cl-containing solution

AA2024 immersed in zinc phosphate-containing solution for 2 hours did not show any obvious pigment-involved reaction product or precipitated film, as discussed in previous section. Also as shown in Fig. 4, the scribe exposed to 30 days of salt water immersion showed a clean scribe but still the scribe did not indicate any reaction between the pigment and metal.

Fig. D.10a shows the scribe after exposure to 90 days of exposure to salt spray test (5% NaCl solution). The scribe appeared to be clean with original shining metal color after exposure. SEM found amorphous solids and cracks formed in the scribe. Fig. D.10b shows the composition of the amorphous solids, clean area, cracks.

The following conclusions about the effect of zinc phosphate can be made:

- a) Zinc phosphate reforms on aluminum surface in short terms. The film or deposition is too thin and can be only detected by SIMS.
- b) In the long run zinc can form relatively thick protective film on scribe. The major constituents of the film are Al, Zn, O. Si, P and Mg may also precipitates in the film.
- c) Large particles or clusters formed on intermetallics containing Mg which becomes the component of the protective clusters.
- d) Zinc seems to plays a greater role in the protection of the scribe than phosphate does. This can be due to the low leaching-out of phosphate in water (shown in Fig. D.7).
- e) The protective film formed on the scribe which consists of Al, Zn, O can be a hydrate when water is present. The cracks can form during the dehydration process.



(b)

Area 1			Area 2		
<i>Element</i>	<i>Wt%</i>	<i>At%</i>	<i>2 Element</i>	<i>Wt%</i>	<i>At%</i>
<i>OK</i>	09.29	16.00	<i>OK</i>	7.59	13.12
<i>NaK</i>	10.47	12.55	<i>NaK</i>	13.58	16.33
<i>MgK</i>	01.28	01.45	<i>MgK</i>	1.20	1.36
<i>AlK</i>	59.10	60.33	<i>AlK</i>	55.45	56.79
<i>SiK</i>	02.33	02.29	<i>SiK</i>	2.19	2.16
<i>ZnK</i>	17.52	07.38	<i>PK</i>	3.57	3.30
			<i>ZnK</i>	16.44	6.95

Area 3			Area 4			Area 5		
<i>Element</i>	<i>Wt%</i>	<i>At%</i>	<i>Element</i>	<i>Wt%</i>	<i>At%</i>	<i>Element</i>	<i>Wt%</i>	<i>At%</i>
<i>OK</i>	09.03	16.06	<i>OK</i>	09.46	16.70	<i>OK</i>	09.87	17.85
<i>AlK</i>	69.21	73.03	<i>AlK</i>	67.60	70.74	<i>AlK</i>	64.30	68.95
<i>PK</i>	02.94	02.71	<i>SiK</i>	02.05	02.06	<i>SiK</i>	03.00	03.09
<i>ZnK</i>	18.82	08.20	<i>PK</i>	03.07	02.80	<i>ZnK</i>	22.83	10.10
			<i>ZnK</i>	17.82	07.70			

**Fig. D.10** (a) Scribe after exposure to 90 days of exposure to salt spray test. Left: picture; right: SEM image

(b) Analysis of different area in the scribe by EDAX.

iii. Zinc phosphate in the coating

As discussed in Section 4.6.1.3, zinc or phosphate was not found on the interface (either coating side or metal side) through ToF-SIMS, which indicates that zinc phosphate did not forms protective film on aluminum in advance. The analysis on the scribe also did not found metallic soap product between zinc phosphate and acrylic or other binders as claimed by other authors as an inhibition mechanism on ferric substrates.

## E. PACKING STUDIES OF THE TWO SERDP PRIMERS; NOVOLAC-EPOXY AND EPOXY

### Packing of novolac-epoxy primer

Paints are usually divided into packs that are then mixed before applying the paint onto a substrate. Paint packs are stable for 12 months or more. The packing study of the novolac-epoxy and the epoxy primer were both done in a stepwise manner. The results of packing the novolac-epoxy primer is reported here along with a summary of the packing results obtained for the epoxy primer.

The recipe used for packing the novolac-epoxy primer is shown in Table E.1. This recipe was used for the packs, because it was the most suitable variation of the primer for spraying at the time of the beginning of the packing study.

**Table E.1.** Novolac-epoxy recipe used for packing study.

Ingredient	Abbreviation	Amount in [g]
EPI-REZ 5003 epoxy-novolac	novolac	52
EPIKURE 6870 crosslinker	crosslinker	13
Bis-sulfur silane	BS	5
NeoRez R-972 polyurethane	PU	5
Zinc phosphate	ZP	25
	Total	100
Water to reach 58 s viscosity flow		11
	Total	111

The first set of packs done showed that the following ingredient combinations were incompatible\*:

- Crosslinker and PU
- Crosslinker and BS
- Crosslinker, PU and BS
- Crosslinker and novolac-epoxy
- BS and water

\*Incompatible in this context means that the ingredients reacted with each other in such a way that the paint formulation could not be formulated anymore from the resulting packs.

Based on the results of the first set of packs, it was known that the combinations listed above were to be avoided in the second set of packs prepared. The second set of packs involved the pack systems presented in Table E.2.

**Table E.2** Second set of packs of the novolac-epoxy primer.

<b>System A</b>	<b>A1</b>	<b>A2</b>	<b>A3</b>
	PU	ZP	Crosslinker
	BS	Water	
		Novolac	
<b>System B</b>	<b>B1</b>	<b>B2</b>	<b>B3</b>
	PU	ZP	Crosslinker
	BS	Novolac	
	water		
<b>System C</b>	<b>C1</b>	<b>C2</b>	
	ZP	Novolac	
	Water	BS	
	Crosslinker	PU	
<b>System D</b>	<b>D1 same as C1</b>	<b>D2</b>	<b>D3</b>
		Novolac	PU
		BS	
<b>System E</b>	<b>E1 same as C1</b>	<b>E2</b>	<b>E3</b>
		Novolac	BS
		PU	
<b>System F</b>	<b>F1</b>	<b>F2</b>	
	Crosslinker	The rest	
	Water		

The method of testing the packs was simple. The packs were prepared and observations on the stability of the packs were done after aging the packs for about a month. The observations showed that packs A1 and B1, presented in Table E.2, resulted in odd dispersions which were not very usable after aging. All other packs appeared to be ok. The identical packs C1, D1 and E1 were also ok, except that they needed to be mixed in order to be usable.

In other words many of the pack systems seemed ok. Since a two-pack system is more desirable than a three-pack paint system, a two-pack system was chosen to the next step of the study. The following things were considered when choosing the packs system: System C has packs that are of almost equal weights, which results in an easy mixing ratio of the packs. Packs of system F are not of equal weight. Therefore, system C was chosen to the next step which consisted of spraying coatings from the fresh packs and 2,4 and 6 month old packs and testing the resulting coatings.

The packs of system C, shown in Table E.3 were scaled-up, prepared and the primer prepared from the fresh packs was sprayed onto AA2024 by using the new Millenium DeWilbliss spray gun. After leaving the panels to cure for 14 days at RT the following tests were done on the panels: EIS, adhesion (ASTM D3359), salt water immersion, salt-spray test, MEK double rub and chemical resistance.

**Table E.3** The two-pack novolac-epoxy system chosen for the third step of the packing study.

Pack C1	[g]	Pack C2	[g]
ZP	25	Novolac-epoxy	52
Water	11	BS	5
Crosslinker	13	PU	5
In all	49	In all	62

Table E.4 summarizes the comparison of the test results obtained from the primer formulation prepared from scratch and draw-down bar applied on AA2024 with the results obtained when the primer was prepared from fresh packs and sprayed onto AA2024.

**Table E.4** Test results of the original draw-down applied primer coating on AA2024 with the results obtained when the primer was divided into packs and sprayed onto AA2024.

Test	Primer applied by draw-down bar from the original recipe without using packs	Primer sprayed from fresh packs
Primer dry and wet adhesion to the substrate	Both 5B	Both 5B
Chemical resistance	Passed both	Passed both
Pencil hardness	2H	2B (new spray gun) 4H (old spray gun)
MEK double rub	> 60 rubs	< 10 rubs
30 days salt water immersion	Very good	Good
ASTM B-117	Fairly good after 2000 hrs	Still in test

When the test result in Table E.4 are compared with each other, it is observed that the results are essentially similar except for the MEK double rub result obtained for the primer sprayed from fresh packs. The MEK double rub was done from two different batches, packed and sprayed by two different persons in order to verify the result obtained. The result obtained remained, however, the same. The reason for the difference in the MEK results is most likely due to the fact that when the primer formulation is prepared from scratch, the bis-sulfur silane is predispersed or prehydrolyzed by letting it stir overnight with the resin and some. When spraying from fresh packs there is no time for this hydrolyzation of BS to occur. Therefore, the packs were aged for 6 weeks and then the primer formulation was again prepared from the packs and sprayed onto AA2024. The panels were left to dry and the MEK double rub test was done after 14 days of curing. The aging of the packs had no effect on the MEK double rub value, which meant that the bis-sulfur silane was unable to predisperse or hydrolyze in pack system C.

Even if pack system C failed to reproduce the desired results obtained before for the novolac-epoxy primer, it is worth to mention that the coatings sprayed from this pack system were more uniform and homogeneous than the coatings sprayed before. The average coating thickness was

50±5 µm, which meant a significant reduction in the variations in film thickness on one panel. The targeted thickness range of 25 µm was, however, not reached with this pack system. The packing study was continued by repacking the primer formulation using pack system E shown in Table E.2. The packs were prepared in three different ways and the resulting coatings were applied by draw-down bar onto AA2024. These panels are currently drying and will be tested after 14 days of curing, i.e., the packing study of the novolac-epoxy primer is still continuing.

### Packing of epoxy primer

The packing of the epoxy primer was done in a similar way as for the novolac-epoxy primer. Since the recipe of this primer is very similar to the novolac-epoxy primer, it was detected in the first set of packs that the same ingredient combinations as for the novolac-epoxy primer were also incompatible for this primer. These combinations were therefore again avoided in preparing the second set of packs. The second set of packs was done based on a recipe that was essentially similar to the one shown in Table E.5. The second set of pack systems prepared for this primer is listed in Table E.6.

Table E.5 Recipe for epoxy primer for HDG steel.

Epoxy primer for HDG steel
EPI-REZ 6520 epoxy 27 g
Ancarez Ar 550 epoxy 16 g
EPIKURE 6870 crosslinker 11 g
Bis-sulfur silane (BS) 11 g
NeoRez R-972 PU 4 g
Corrostayn 228 pigment 11 g
NaVO <sub>3</sub> pigment 1 g
Water 21 g
Total 100 g

Table E.6 Second set of packs of the epoxy primer.

System A	A1	A2	A3
	Acrylate/PU	ZP	Crosslinker
	BS	Water	
		Epoxy	
		Ancarez Ar	
System B	B1	B2	
	ZP	Epoxy	
	Water	Ancarez Ar	
	Crosslinker	BS	
		Acrylate/PU	
System C	C1	C2	C3
	ZP	Epoxy	Acrylate/PU
	Water	Ancarez Ar	

	Crosslinker	BS	
<b>System D</b>	<b>D1 same as C1</b>	<b>D2</b>	<b>D3</b>
		Epoxy	BS
		Ancarez Ar	
		Acrylate/Pu	
<b>System E</b>	<b>E1</b>	<b>E2</b>	
	Crosslinker	The rest	
	Water		

Only one pack system; system C, containing the polyurethane minor binder was usable after aging the packs. This pack system is presented in more detail in table E.7.

**Table E.7** The three-pack epoxy system chosen for the third step of the packing study.

<b>Pack 1</b>	<b>[g]</b>	<b>Pack 2</b>	<b>[g]</b>	<b>Pack 3</b>	<b>[g]</b>
Corrostayn 228	14.4	EPI-REZ 6520-WH-53	36	NeoRez R-972 PU resin	4.8
NaVO <sub>3</sub>	1.0	Ancarez Ar 550	21.6	Water	4.8
Water	28	Bis-sulfur silane	14.4	Sum	9.6
EPIKURE crosslinker 6870	14.4	Sum	72.0		
Sum	57.8				

Since fairly good ASTM B-117 test results had been obtained earlier with the epoxy primer on AA2024 (see Figure E.2a), the packing study was decided to be done by using AA2024 instead of HDG steel. The epoxy formulation was prepared from the fresh packs shown in the above Table E.6 and sprayed onto AA2024 by using the DeWilbliss spray gun. The coated panels were left to dry for 14 days at RT and tested with the same set of tests as used for the novolac-epoxy primed AA2024 panels. The MEK double rub and the pencil hardness values for the epoxy primed panels were surprisingly poor. This was further investigated by comparing the MEK double rub and the pencil hardness values on different epoxy primed panels prepared in different ways this year. The obtained results on different panels are summarized in Table E.8.

**Table E.8** Test results of epoxy primed panels prepared in different ways.

Formulation preparation method	Curing cond.	MEK double rubs	Pencil hardness
From the fresh packs (system C)	14 RT	< 10	6B
From scratch by prehydrolyzing BS	Room temp	~ 25	Not tested
From scratch by prehydrolyzing BS	150°C, 20 min. (on HDG steel)	> 100	6H (hardest possible)
From scratch without prehydrolyzing BS	150°C, 20 min. (on HDG steel)	> 100	H (acceptable)

As the results reported in Table E.8 are studied, it is obvious that the epoxy primer has to be heat cured whether or not the formulation is prepared from scratch or from packs. Therefore, the packing study will be continued by using HDG steel panels which can be heat cured after spraying the primer from packs. Also for the epoxy primer it is worth to mention that the variations in film thickness from panel to panel and within one panel were reduced significantly by adjusting the spray conditions used.

**Further developments in the packing of the primers**

**Packing of novolac-epoxy formulation**

The test results for the novolac-epoxy primed panels sprayed from fresh packs were otherwise good, but the primer showed very poor MEK double rub values. Water immersion test results of for novolac-epoxy primer sprayed from fresh packs are shown in Fig. E.1 and the corresponding salt spray test results are presented in Figure E.2.



**Figure E.1.** About 11 weeks of salt water immersion test result of novolac-epoxy primed AA2024 sprayed from fresh packs.

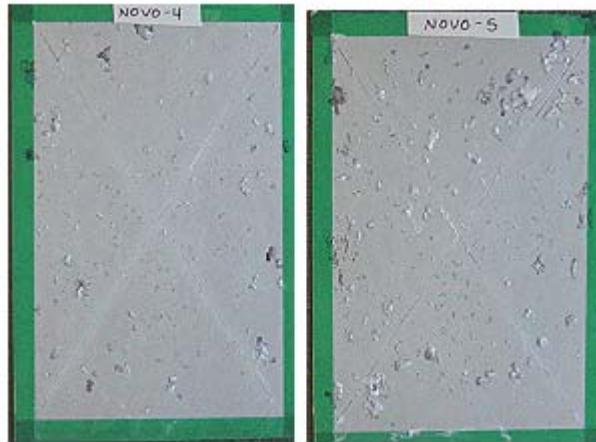


**Figure E.2.** 1536 hours of salt spray test result of novolac-epoxy primed AA2024 sprayed from fresh packs.

As can be seen from Figure E.2 the condition of the scribes is very good but the quality of the primer coating is poor. The poor MEK results of the novolac-epoxy primed AA2024 panels sprayed from fresh packs may be due to the fact that in the fresh packs the bis-sulfur silane does not have any time to pre-dissolve or hydrolyze. Therefore, after aging the packs (shown in Table E.3) for 6 months they were sprayed onto AA2024 again and tested. However, the MEK double rub value did not improve.

Therefore, pack system C was prepared again with a smaller amount of ZP (15 g) and larger amounts of BS and PU (10 g each). Also pack systems similar to the C packs were prepared, but the BS was kept in a separate pack, which contained a small amount of ethanol for dissolving the BS and aiding in hydrolyzing it. These packs were then mixed and primed onto AA2024, but still the MEK double rub value did not improve.

Next it was investigated if the curing time of the primer coating could be the solution to the poor MEK values of the novolac-epoxy primer prepared from the packs. Therefore, all old samples of this primer (prepared from scratch or from packs) were gathered and tested. The results are presented in Table E.9.

Table E.9. MEK-double rub test results of different samples prepared from packs and sprayed onto AA2024:

<b>Sample</b>	<b>Prepared</b>	<b>Tested</b>	<b>How aged/cured</b>	<b>MEK rubs</b>
NOVO (from fresh packs)	10/03/06	11/01/06	Aged for ~1 month	5
NOVO (from fresh packs, John)		11/02/06	Aged for ~1 month	5
NOVO (from 6 week-old packs)	11/15/06	01/25/07	Aged for 2 months and 10 days	5
NOVO (from 6 week-old packs) + <b>TOPCOAT</b>	11/15/06	01/25/07	Aged for 2 months and 10 days	> 100
NOVO (from fresh packs)	10/03/06	01/25/07	Aged for ~4 months	45
NOVO (from fresh packs, John)		01/25/07	Aged for ~4 months	25
NOVO (from fresh packs)	10/03/06	01/26/07	Aged ~4 months and HT at 70°C 15 min.	70

As can be seen from Table E.9, aging and heat curing of the coated panels improves the curing of the coating, but not necessarily in a very consistent way. The topcoated samples were intended to be put through other tests, but as they were cut to smaller pieces, the topcoat simply came off from the primer, which indicated that if the primer is not cured properly then the topcoat delaminates from the primer.

Since hydrolyzing the BS silane in the packs did not solve the problem. The next step was to investigate if the ZP in the coating interferes with the film formation and curing of the coating. Furthermore, the preparation method of the primer was investigated in order to find out how much difference there is between primer coatings prepared from scratch and from packs.

NP-1 is the optimized formulation that Akshay developed. The recipe of NP-1 without and with zinc phosphate is shown in Table E.10. Akshay's coding; N = novolac, P = PU.

Table E.10. The recipe of NP-1 (novolac-epoxy primer) without and with zinc phosphate

Ingredient	NP-1 without ZP [g]	NP-1 with ZP [g]
EPI-REZ 5003 novolac-epoxy	60	52
EPIKURE 6870 crosslinker	15	13
BS	10	8
NeoRez R-972 PU	15	12
Pigments	-	15
Total	100	100

Addition of water to the formulation:

For draw-down bar formulation: 6.5 g

For spray formulation: 11 g

When the formulation is prepared from scratch then the novolac-epoxy resin, water, BS and possible pigment are left stirring overnight. The next day first the crosslinker and then the PU are mixed in. For this part of the study samples with dibutyl tin dilaurate (DBTL) were also prepared according to recipes shown in Table 1.11. N-1 is the version of NP-1 without PU.

Table E.11. Novolac-epoxy primers with DBTL.

Ingredient	N-1 + DBTL [g]	NP-1 + DBTL [g]	NP-1+ZP+DBTL from scratch [g]	NP-1+ZP+DBTL from packs [g]
EPI-REZ 5003 novolac-epoxy	72	60	52	52
EPIKURE 6870 crosslinker	18	15	13	13
BS	10	10	8	8
NeoRez R-972 PU	-	15	12	12
Pigments	-	-	15	15
Dibutyl tin laurate, DBTL	0.05 5 drops	0.05 5 drops	0.04 4 drops	0.05 5 drops

Table E.12 shows MEK-double rub results of different samples prepared from scratch and applied by draw-down bar onto AA2024.

Table E.12. MEK-double rub results of different samples. RT = room temperature

Sample	Comment	Prepared	Tested	How aged/cured	MEK rubs
NP-1	Primed	01/24/07	020807	14 days RT	< 5
NP-1	Primed	01/24/07	020807	14 days RT + 15 min 70°C	< 5
NP-1	Primed	01/24/07	Panel left for aging		
NP-1+ZP	Primed	01/24/07	020807	14 days RT	< 5
NP-1+ZP	Primed	01/24/07	020807	14 days RT + 15 min 70°C	< 5
NP-1+ZP	Primed	01/24/07	Panel left for aging		
N-1 + DBTL	Primed	01/25/07	021307	18 days RT	< 5
N-1 + DBTL	Primed	01/25/07	021307	18 days RT + 20 min 70°C	< 5
NP-1 + DBTL	Primed	01/30/07	021307	14 days RT	< 5
NP-1 + DBTL	Primed	01/30/07	021307	14 days RT + 20 min 70°C	< 5
NP-1+ZP+DBTL from scratch	Primed	01/30/07	021307	14 days RT	< 5
NP-1+ZP+DBTL from scratch	Primed	01/30/07	021307	14 days RT + 20 min 70°C	< 5
NP-1+ZP+DBTL from packs	Primed	01/30/07	021307	14 days RT	< 5
NP-1+ZP+DBTL from packs	Primed	01/30/07	021307	14 days RT + 20 min 70°C	< 5

As can be detected from Table E.12, no matter how the the novolac-epoxy primer is prepared (from scratch or packs, with or without ZP or with or without catalyst) it does not cure sufficiently in 14 days RT and apparently it does not even help to put it for 20 minutes in 70°C.

The only logical explanation to the discrepancy between MEK results obtained earlier in the SERDP project and to the results shown in Table E.12, is that before this the panels were aged much longer than 14 days before they were tested for MEK double rub.

Next it was studied how the insufficient curing of the primer affects the dry and wet adhesion test results of this primer with topcoat. The results are shown in Table E.13, and as can be seen from the results the wet adhesion of the primed and topcoated samples suffers, if the primer coating does not cure properly as such or under the topcoat.

Table E.13. Dry and wet adhesion test results of topcoated samples, novolac-epoxy primer on AA2024.

Sample	Dry adhesion	Wet adhesion
NP-1 + DBTL from scratch	5B	0B
NP-1+ZP+DBTL from scratch	5B	0B
NP-1+ZP+DBTL from packs	5B	0B

The general conclusion from results presented above was that the novolac-epoxy primer prepared from scratch or packs does not cure properly at room temperature and therefore we experience lack of adhesion between the primer and the topcoat. Therefore, samples NP-1 and NP-1+ZP (recipes shown in Table E.10) were cured in different ways. The MEK double rub test results are shown in Table. E.14.

Table E.14. MEK-double rub test results of differently cured novolac-epoxy primed samples.

Sample	How aged/cured	MEK rubs
NP-1	2 h at 70°C	~30
NP-1 + ZP	2 h at 70°C	<10
NP-1	overnight at 70°C	~80
NP-1 + ZP	overnight at 70°C	>100
NP-1	2 h at 90°C	~45
NP-1 + ZP	2 h at 90°C	<30

Table E.14 shows that if the samples are cured overnight at 70°C or after a shorter time at a higher temperature the primer coating cures more thoroughly, which results in improved MEK double rub test results. After this result, the next question was; does the topcoat stick better to the more thoroughly cured primer? To answer the question topcoated panels were prepared with the Desothane HS topcoat that we received directly from the supplier with Donna Ballards' help. The AA2024 panels for this study were pretreated according to the Air Force surface preparation method and these panels were painted with the novolac-epoxy primer prepared from fresh and more than 6 month old packs. As application method both draw-down bar and spraying application were used and before topcoating the panels were cured either in high or room temperature.

**Summary of parameters:**

Age of packs: new and >6 month old

Application method: draw down bar vs. sprayed

Curing of primer coating: RT (14 days at RT) or HT (3 hours at 100°)

Without and with topcoat. Topcoated are designated by TP.

The logic of naming the samples is described in Table E.15 and the test results of the samples without topcoat are shown in Table E.16 and with topcoat in Table E.17.

**Table E.15 Example of the logic of the sample names.**

Sample	Applied by	Age of packs	Cured at	Topcoat
N RT	Draw-down bar	N=new	RT	None
O RT	Draw-down bar	O=old	RT	None
NS RT	S=spraying	N=new	RT	None
OS RT	S=spraying	O=old	RT	None

**Table E.16 MEK double rub and adhesion test results for primed panels without topcoat.**

Sample	MEK	Dry adh.	Wet adh.
N RT	<10	5B	5B
O RT	40	5B	2B
NS RT	<10	5B	5B
OS RT	<10	5B	0B
N HT	15	5B	5B
O HT	25	5B	0B
NS HT	105	4B	4B
OS HT	95	5B	5B

Conclusions based on Table E.16:

- The room-temperature cured ones have in general poor MEK-values (which was already known)
- When it comes to the high temperature cured samples the sprayed ones have better MEK results than the draw-down bar applied.
- Dry adhesion of all tested samples is good.
- The primer films applied from fresh packs both by draw-down bar and spraying show good wet adhesion to the substrate
- The primers films applied from 6 month old packs have in general bad wet adhesion, except for the film sprayed and cured at HT.

**Table E.17 Adhesion test results for primed panels with topcoat.**

Sample	Dry adh.	Failure interface	Wet adh.	Failure interface
N RT TP	5B	-	0B	Metal-primer
O RT TP	4B	-	3B	-
NS RT TP	5B	-	5B	-
OS RT TP	5B	-	0B	Metal-primer
N HT TP	0B	Metal-primer	0B	Metal-primer
O HT TP	4B	-	0B	Metal-primer
NS HT TP	2B	Metal-primer	5B	-
OS HT TP	0B	Metal-primer	0B	Metal-primer

Conclusions based on Table E.17:

- The RT cured samples have at least good dry adhesion.
- Well, this time the reason for the failure in dry adhesion of the high-temperature cured samples could not be insufficient cleaning of the substrate. Therefore, the result is true and something during the HT curing weakens the adhesion between the metal and the HT cured primer.
- When it comes to wet adhesion only the primer film sprayed from fresh packs which has been either RT or HT cured performs well. The rest fail.
- This means that the application method and the age of the packs affect the wet adhesion.
- Sprayed samples perform better than draw-down bar applied and the films applied from fresh packs perform much better than the films from old packs.

### Packing of the epoxy formulation

The packing study of the epoxy primer was continued on HDG steel by spraying the formulation (Table E.18) prepared from 2 month old packs, according to the time-table shown in Table E.19. These panels were tested after curing the coated panels in the following way:

1. for 14 days at RT, sample name: ECO 7
2. for 14 days at RT + 10 min at 100°C, sample name: ECO 1
3. for 14 days at RT + 20 min at 100°C, sample name: ECO 5

The test results of the above mentioned samples are shown in Table E.20. The results were again not encouraging.

**Table E.18.** The larger scale packing study has been initiated by using the following pack system.

Pack 1	[g]	Pack 2	[g]	Pack 3	[g]
Corrostayn 228	14.4	EPI-REZ 6520-WH-53	36	NeoRez R-972 PU resin	4.8
NaVO <sub>3</sub>	1.0	Ancarez Ar 550	21.6	Water	4.8
Water	28	Bis-sulfur silane	14.4	Sum	9.6
EPIKURE 6870 crosslinker	14.4	Sum	72.0		
Sum	57.8				

**Table E.19.** The schedule of this study.

Date	Termed	Event	Comments
10/11/06	Fresh packs	Spraying of fresh packs onto AA2024	Viscosity 29 s, low, coatings still ok
12/21/06	2 month old	Spraying of 2 month old packs onto HDG	Viscosity 45 s, fairly ok coatings
2/23/07	4 month old	Spraying of 4 month old packs	
4/23/07	6 month old	Spraying of 6 month old packs	
10/23/07	12 month old	Spraying of 12 month old packs	

**Table E.20.** Test results of epoxy primed HDG samples sprayed from 2 month old packs and cured differently.

Sample	Curing	Dry adhesion	Wet adhesion	Chem. res. HCl	Chem. res. NaOH	MEK double rub
ECO 7	14 days RT	3B	0B	No pass	Pass	< 2
ECO 1	14 days RT + 10 min 100°C	0B	0B	Pass	Pass	< 5
ECO 5	14 days RT + 20 min 100°C	1B	0B	Pass	pass	< 10

Based on the discouraging results shown in Table E.20, it was decided not to put any more effort in the packing study of this primer. Earlier in the SERDP project a lot of effort had already been put into developing this epoxy primer to a more robust primer, however, without much success. Therefore it was logic to drop it from further studies.

#### 1.4 WP-1341 action item 2; discussion of the novolac-epoxy coating for DoD implementation

The packed version of the novolac-epoxy primer was selected for the DoD applications on aluminum alloy substrates. The recipe of this primer divided in packs is shown in Table E.21.

Table E.21. Recipe of the novolac-epoxy primer divided in packs.

Pack 1	Weight percentage
Zinc phosphate; ZP	22
Deionized water	13
EPIKURE 6870 amine adduct curing agent	11
Pack 2	
EPI-REZ 5003-W-55 epoxy, novolac-epoxy	45
Silquest A-1289 bis-sulfur silane; BS silane	4.5
Neo-Rez R-972 polyurethane; PU	4.5

This primer was developed from a previous superprimer, which was based on a simple epoxy resin, which also consisted of a hydrophobic bis-sulfur silane; a silane crosslinker, tetraethoxysilane (TEOS) and a hydrophilic silane mixture based on bis-amino silane and a vinyltriacetoxysilane. This starting formulation was modified with the novolac-epoxy resin mainly in order to obtain improved adhesion and corrosion resistance. The structure of the novolac-epoxy is shown in Figure E.3.

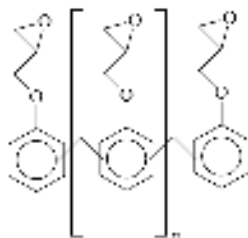


Figure E.3. Generic structure of novolac epoxy resin

The composition of the novolac-epoxy primer was developed in steps. First an optimum resin:curing agent ratio was sought out experimentally by ranging the ratio from 1:1 to 9:1. The experimental results showed that the optimum ratio of resin:curing agent was 4:1 for a primer coating on AA2024-T3. Secondly the type of silane was studied. The hydrophobic bis-sulfur silane proved to give good results and especially good results when used together with a small amount of polyurethane resin. The salt spray test result showing the performance of the novolac-epoxy primer on AA2024 without BS silane, with BS silane and with BS silane and polyurethane is presented in Figure E.4.

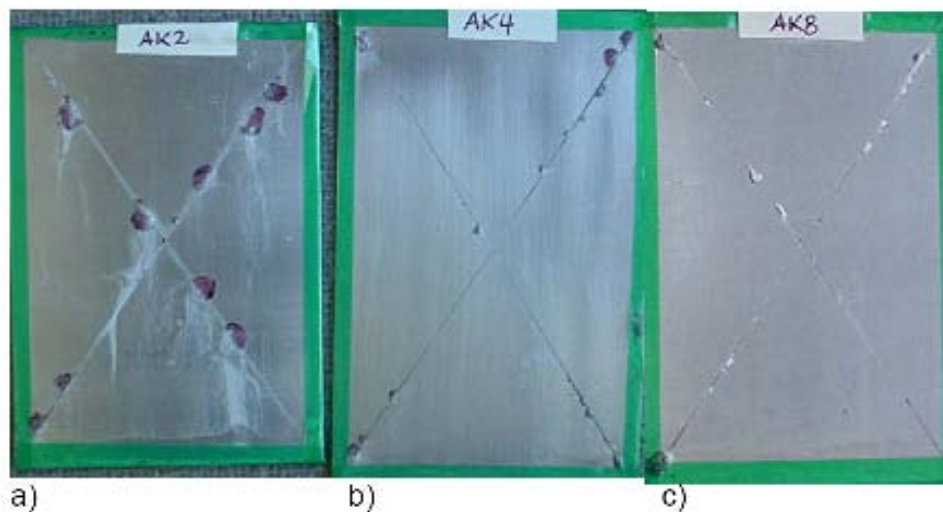


Figure E.4. The epoxy-novolac based primer coating a) without bis-sulfur silane after 1000 hrs, b) with bis-sulfur silane after 1500 hrs and c) with bis-sulfur silane and polyurethane after 2000 hrs of exposure in ASTM B-117 salt spray test.

In order to investigate the flexibility of the coatings, the three coatings shown in Figure E.4 were subjected to a bend test. After bending the specimens were immersed in 3.5 wt.-% NaCl for 30 days. The results of the test are shown in Figure E.5.

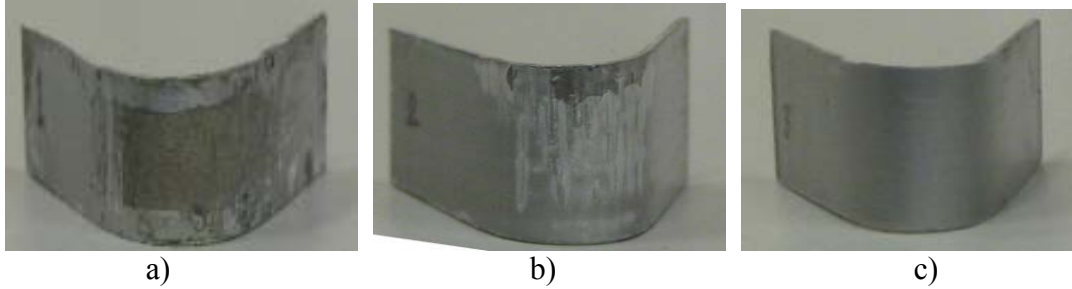


Figure E.5. Samples shown in Figure 2 after bend test and exposure to 3.5 wt.% NaCl for 30 days; the novolac-epoxy primer a) without BS silane, b) with BS silane and c) with BS silane and polyurethane.

From Figure E.5 it is very clear that the polyurethane together with the BS silane in the novolac-epoxy primer both improve flexibility and corrosion resistance. A selected combination of pigments was investigated for this novolac-epoxy primer containing both BS silane and polyurethane. The impedance result of the pigment testing is shown in Figure E.6.

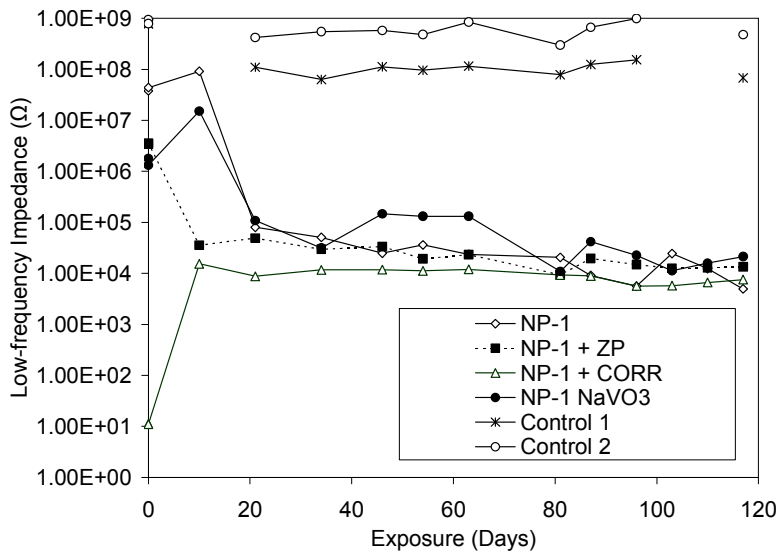
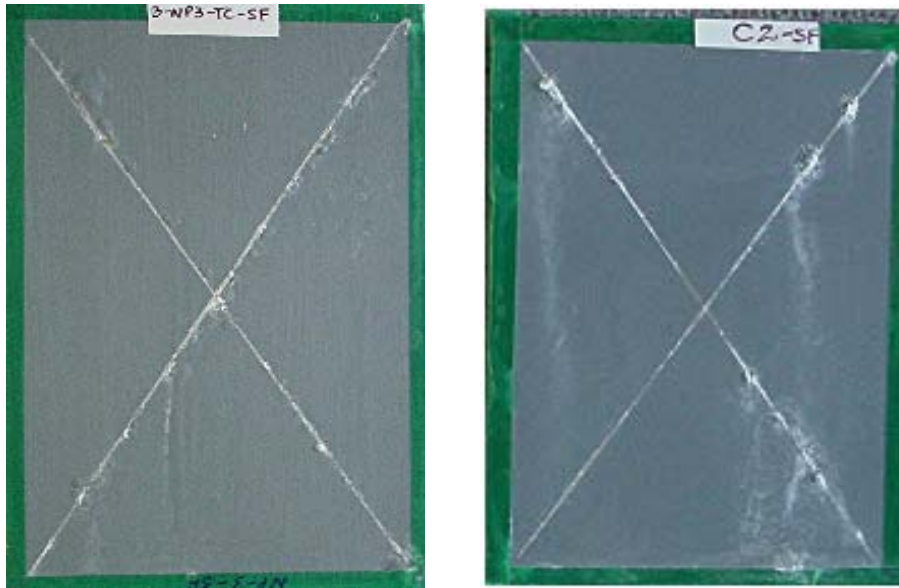


Figure E.6. The low frequency impedance values of the inhibitor containing coatings measured during the exposure of these coatings in ASTM B117 salt spray test.

Many of the chromate-free anticorrosion pigments performed fairly well in this coating. When these pigment containing coatings were tested with a topcoat, the best result was obtained with the zinc phosphate containing primer shown in Figure E.7, compared with the topcoated chromate containing control primer.



a) b)  
Figure E.7. 2000 h of ASTM B-117 salt spray exposure of the topcoated a) novolac-epoxy primer containing BS, PU and zinc phosphate and b) chromate-containing primer control.

As shown by Figure E.7 the performance of the selected topcoated novolac-epoxy primer is comparable with the control. Therefore, this formulation was subjected to a study, where the purpose was to divide the components of the primer into two packs. The packs shown in Table 1 appeared to be stable for about 6 months. However, a drop in the performance of the resulting coating was observed after preparing the primer from 6 month old packs. The performance of the primer prepared from fresh packs was, however, on the same level as the performance of the corresponding primer prepared from scratch. This was especially observed for wet adhesion test results. A drop in salt spray test result was, however, observed if the primer coating was not let to dry long enough before testing.

The primer shown in Table E.21 is currently being tested at UDRI at the WPAFB. All wet adhesion test results were good, but the salt spray test results were poor, probably due to insufficient curing of the primer in the complete coating system. Most likely the curing time of the primer can be improved by adjusting the resin: crosslinker ratio and/or by adding a small amount of a quick coalescing solvent to the existing formulation. These two measures to speed up the cure are currently being investigated.

## F. EFFECT OF SURFACE CLEANING ON SILANE/PRIMER PERFORMANCE ON CRS

### Introduction

Silane coatings have emerged as one of the most promising candidates for replacement of currently used chromate treatments in metal finishing to improve adhesion to metal substrates and corrosion performance. A mixture of bis-[trimethoxysilylpropyl]amine (bis-amino silane, A) and vinyl-triacetoxysilane (VTAS, V) has emerged as an outstanding candidate among water-based silanes with comparable corrosion protection performance to the organic solvent-based silanes on many metal substrates which exhibits broader compatibility with paints than most silanes.

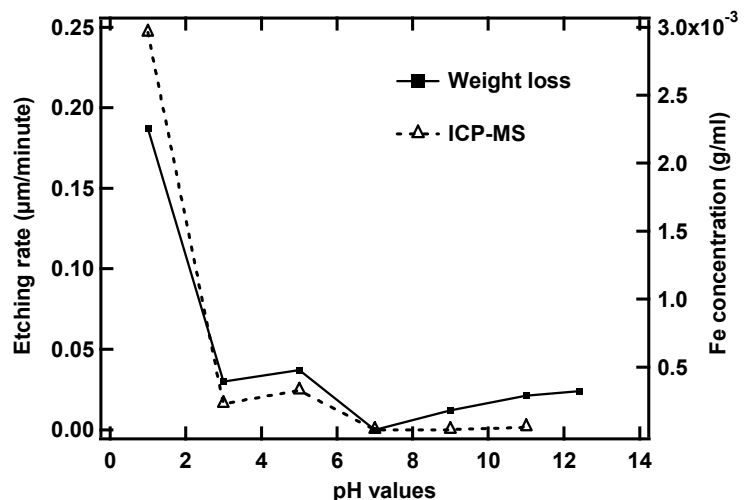
The adhesion and structure of the silane coating is very sensitive to the surface oxide as well as to the surface cleaning procedures of the metal substrate. Recently the effect of the metal surface cleaning on silane adsorption has been recognized. When a silane solution is applied on the metal surface, silanol (-SiOH) groups absorb instantly on the metal surface through hydrogen bonds. During the subsequent curing and drying process, the condensation reactions occur between surface hydroxyl group and silanol group at the silane-metal interface. The SiOMe contribute to the strong bonding and corrosion resistance of the silane coating to the metal substrate. The amount of hydroxyl groups on the metal surface is directly related to the cleaning conditions of the metal substrate and the anti-corrosion performance of metals. The present work aims at understanding the relationship between the surface cleaning pH and the corrosion performance of silane and primer-coated cold-rolled steel (CRS).

### Results and discussion

#### Etching rate

Figure F.2 shows the etching rate of the as-cleaned CRS panels and the  $^{56}\text{Fe}$  concentration in the solution after cleaning at different pH values. The etching rate determined from the weight loss of the panels and the  $^{56}\text{Fe}$  concentrations in the solution after cleaning follow a similar trend. Both results suggest that the etching rate of CRS in acidic conditions is much higher than in alkaline conditions with the maximum etching rate of CRS observed at pH~1.0. The minimum etching rate is found around zero in neutral cleaning conditions (pH~6.8). The etching rate of CRS increases on both sides of the neutral conditions with the acidic side increasing more steeply.

Figure F.1 Etching effects of CRS by weight loss and ICP-MS measurements after cleaning at different pH values



### 3.2 Surface morphologies of as-cleaned CRS surfaces

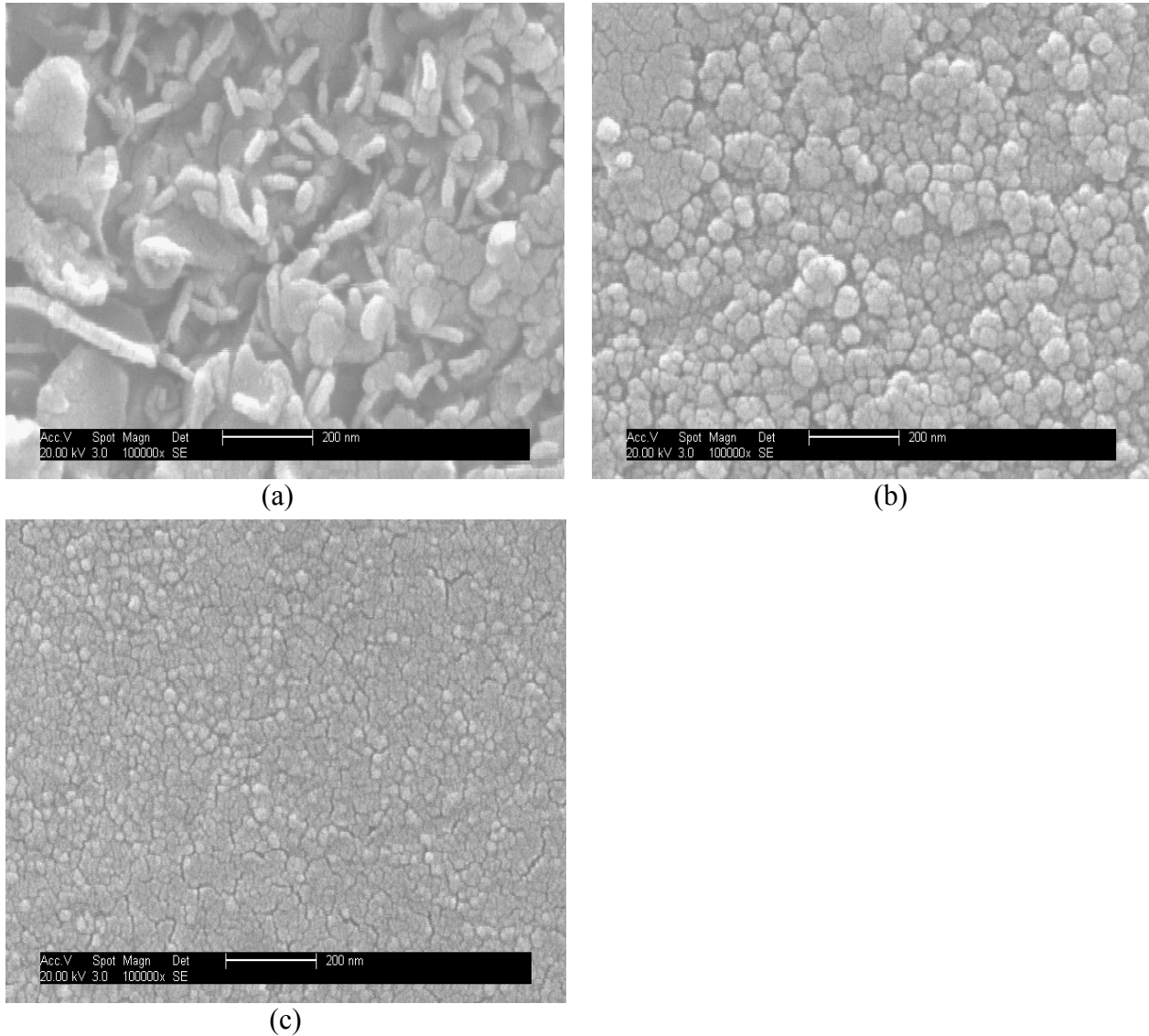


Figure F.2 shows the surface morphology of CRS after cleaning at different pHs (pH~1.0, pH~9.5 and pH~12.4).

Very distinguished surface oxide morphologies are observed for CRS cleaned under different pHs and re-exposed to air. Coarse, loose and platelet surface oxide morphology was observed on CRS surface cleaned in strong acidic conditions (pH~1.0), which may be related to rapid dissolution of the Fe surface in strong acidic conditions mentioned above. A fine, dense and spherical surface oxide morphology was detected on the CRS surface cleaned in alkaline environments (pH~9.5 and pH~12.4) as shown in figures F.4 (b) and F.4(c) which suggest that the alkaline cleaning condition facilitates the formation of a fine and dense surface oxide layer after exposure to air.

The coarse and loose surface oxide layer formed on CRS after cleaning in strongly acidic condition is inferior for the formation of a dense bonding layer between silane and CRS. The fine and dense surface oxide formed on CRS after cleaning in alkaline condition, on the other hand, is desirable for the formation of dense bonding layer between CRS and silane.

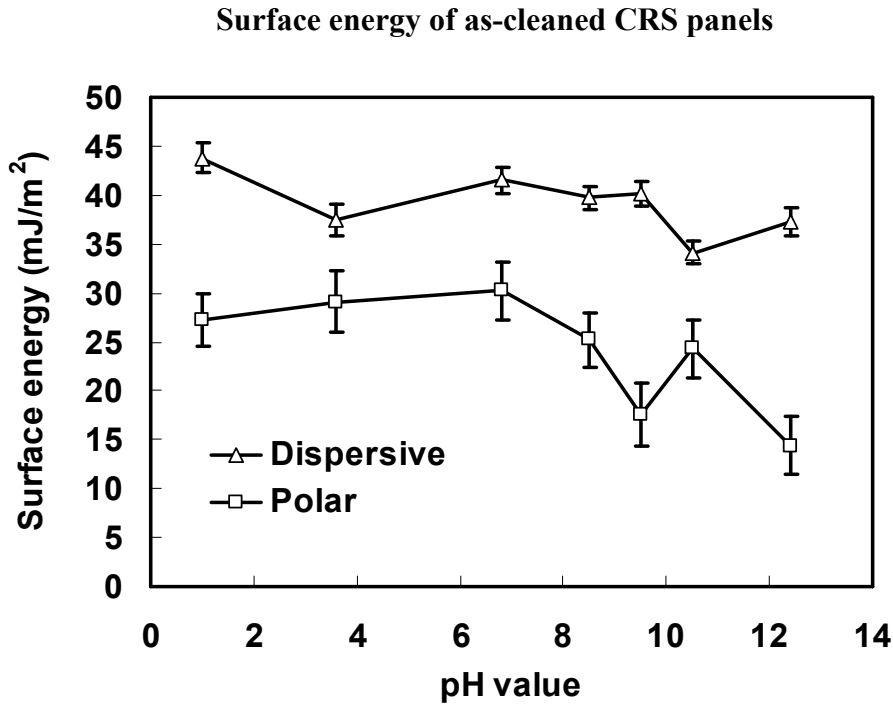
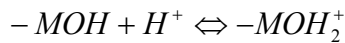
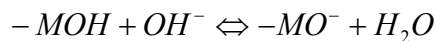


Figure F.3 Calculated polar and dispersive components of as-cleaned CRS surface cleaned in different pH conditions based on contact angle measurements

Figure F.3 shows the dispersive and polar components of the as-cleaned CRS panels after cleaning in different pH conditions. It is detected that the dispersive component is relatively constant over the whole pH range, whereas the polar component has two minima over the whole pH range; one at pH~9.5 and another at pH~12.4. The minimum at pH~9.5 is understandable given the reported isoelectric point (IEP) of CRS, which is around 9-10. In aqueous solutions, the surface hydroxyl groups may remain undissociated, in which case the pH of the aqueous solution is the same as the IEP of the surface oxide. If the pH is less than the IEP, the surface will acquire a positive charge:



If the pH of the solution is greater than the IEP, the surface will acquire a negative charge:



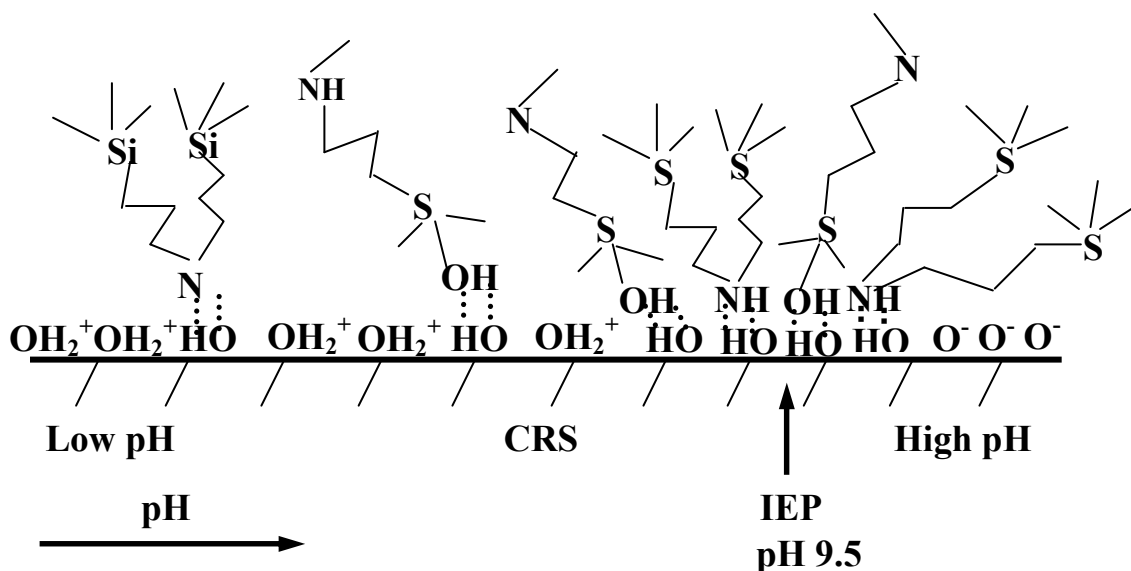


Figure F.4 Schematic diagram of the mechanism of AV silane absorption onto CRS

The surface charge and the isoelectric point of CRS are schematically depicted in Figure 4. The hydrolyzed AV silane solution contains weakly acidic silanol groups and strongly basic secondary amine groups. During the coating process, the AV silane can absorb on CRS via hydrogen bonding both through silanol groups and secondary amine groups. Strong alkaline or acidic cleaning of CRS results in a charged surface as shown in Figure F.4, which is less favorable as a basis for the absorption of silane via hydrogen bonding for silanols and/or secondary amine groups. However, at near neutral conditions close to the IEP of CRS both these species are able to absorb through hydrogen bonding, which leads to increased bonding of AV silane onto CRS at mild alkaline pH around 9.5. *Our study also shows that a thicker silane layer is observed on CRS cleaned at pH~9.5.* The thicker layer at pH~9.5 agrees with the above explanation due to the abundant bonds formed between the functional groups of AV silane and the CRS surface close to IEP as discussed above.

#### Fourier-Transform Infrared Reflection-Absorption (FTIR-RA) Spectroscopy analysis of silane-coated CRS

The FTIR-RA spectra of the silane-coated panels after curing at 100°C for 60 minutes are shown in Figure F.5. The band at 1020  $\text{cm}^{-1}$  is assigned to the short-chain or cyclic siloxane (Si-O-Si), whereas the band at 1100  $\text{cm}^{-1}$  is assigned to long and branched-chain siloxane. The peaks at 1560  $\text{cm}^{-1}$  and 1610  $\text{cm}^{-1}$  are assigned to the hydrogen-bonded and free -NH, respectively. The peak at 920  $\text{cm}^{-1}$  is most likely due to silanol (Si-OH) groups.

Some changes are observed for the AV silane films after curing on CRS cleaned at the different pH values, as shown in Figure F.9(b). The long-chain siloxane peaks at about 1100  $\text{cm}^{-1}$  increase in intensity for the panels cleaned at pH~1.0 and pH~9.5 which indicates further crosslinking of silanols during curing. For the panel cleaned at pH~12.4, however, the increase in long-chain siloxane peak is not observed as compared with the coating before curing. In the meantime, the

intensity of the hydrogen bonded -NH peaks at  $1560\text{ cm}^{-1}$  decrease after curing regardless of cleaning pH. During curing at  $100^\circ\text{C}$ , the silanol groups hydrogen bonded with -NH groups condense between themselves. As a result, the hydrogen-bonded -NH groups are liberated and the hydrogen-bonded -NH peak at  $1560\text{ cm}^{-1}$  decreases.

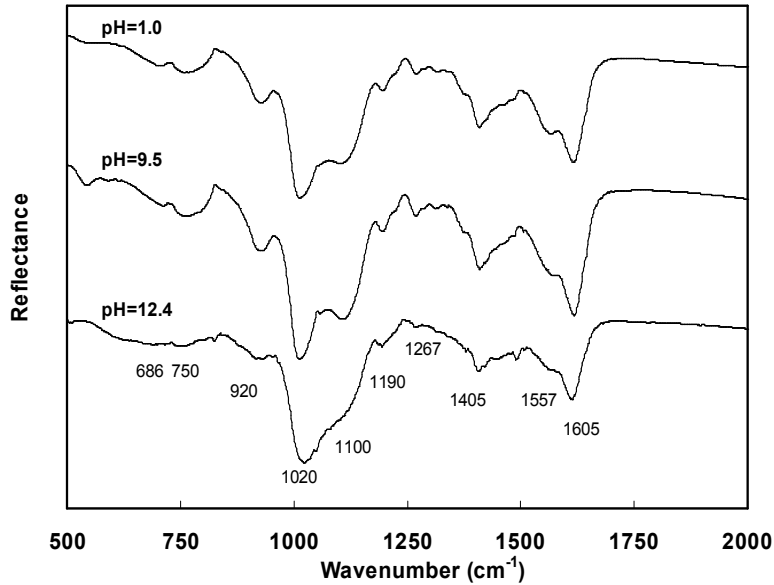


Figure F.5. FTIR spectra of the 0.3 wt.-% AV silane coated CRS after curing at  $100^\circ\text{C}$  for 60 minute

### DC potentiodynamic results of CRS panels

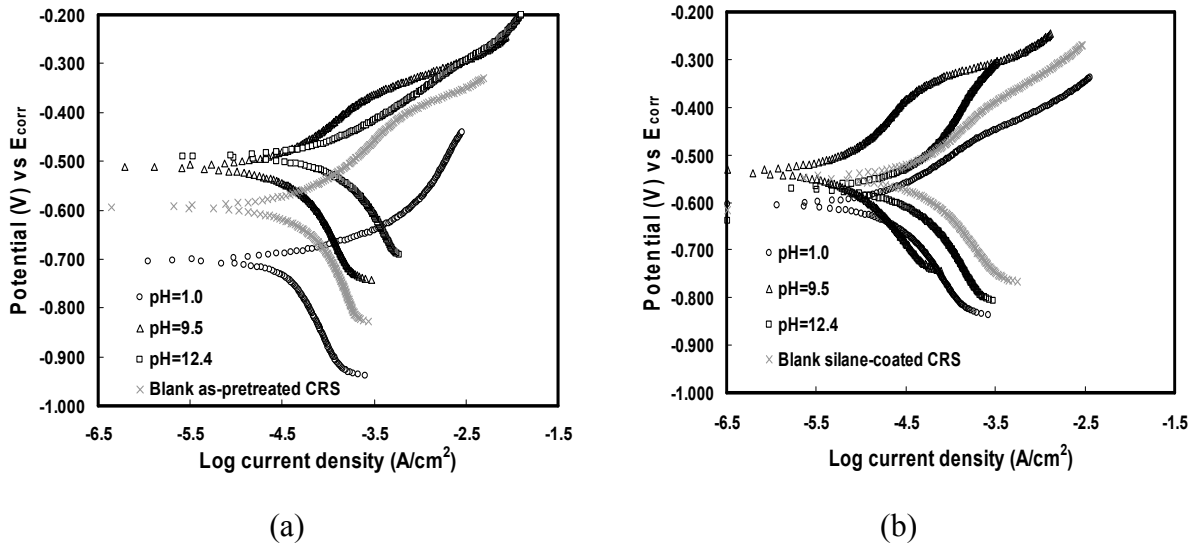


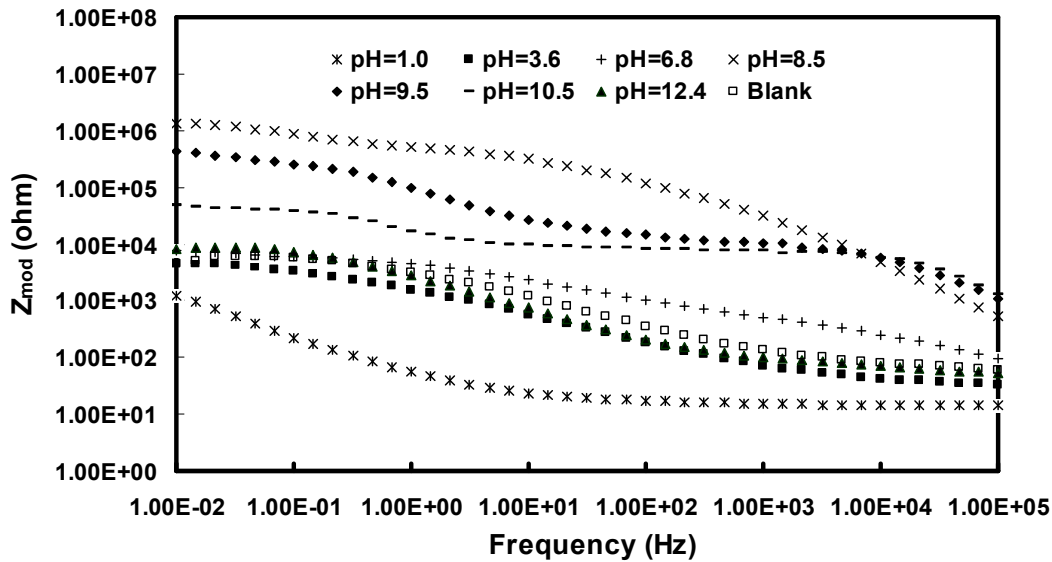
Figure F.6. DC potentiodynamic curves of the (a) as-cleaned CRS panels (b) silane-coated at different pH values

DC potentiodynamic measurements were performed on the as-cleaned CRS panels. Differences in the DC polarization results of these samples indicate differences in the stability of the surface oxide layer formed after cleaning. The stability of the surface oxide layer is further related to the composition, density and thickness of the layer. Figure F.6(a) shows the DC polarization results for the CRS cleaned at different pH values. Comparing with the blank control panel, it was found that the cathodic reaction is suppressed whereas the anodic reaction on CRS surface is promoted after cleaning in acidic conditions. On the other hand, the anodic reaction was suppressed and the cathodic reaction was promoted for CRS cleaned in mild alkaline conditions (pH~9.5). For the panels pretreated in strongly alkaline condition (pH~12.4), however, both the anodic and the cathodic reaction are promoted. The lowest  $I_{\text{corr}}$  value for CRS cleaned in mild alkaline condition (pH~9.5) suggests that a dense and stable oxide layer has been formed on CRS. The porous surface is probably accountable for the high current density in the strongly acidic condition (pH~1.0) and the abundant grain boundary of fine grain structure is most likely the cause for the high  $I_{\text{corr}}$  in strongly alkaline conditions (pH~12.4).

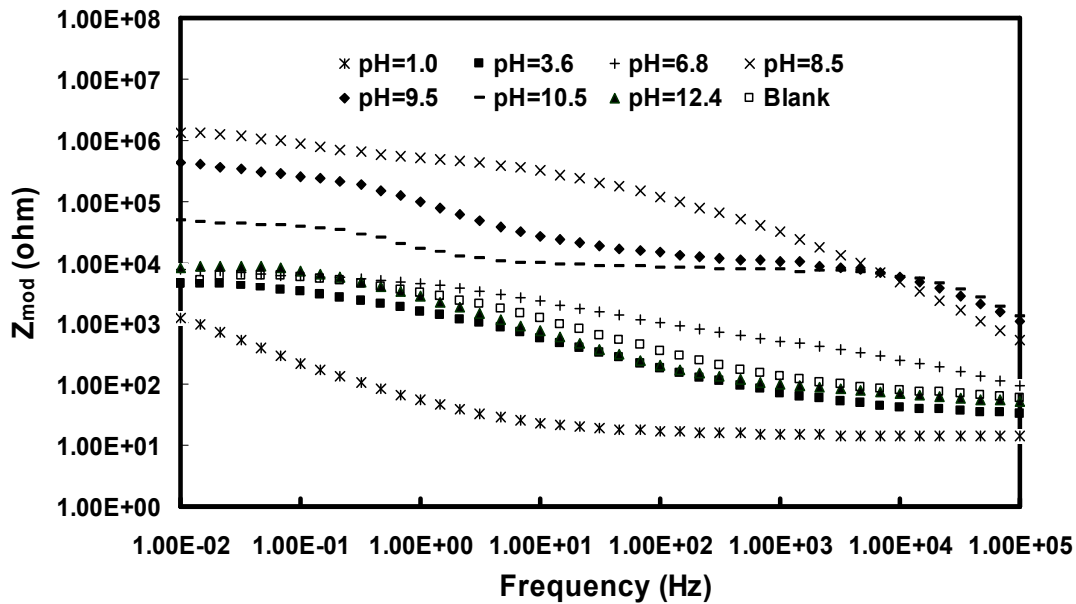
Figure F.6(b) shows the DC potentiodynamic curves of the silane-coated CRS panels cleaned at different pH values. Comparing with the shape of the curves shown in Figure F.6(a), the shape of the DC polarization curves of the silane-coated CRS panels remain the same. The decrease in  $I_{\text{corr}}$  after coating with silane indicates that the silane coating is densely and strongly bonded to the CRS surface and serves as an effective barrier against electrolyte. However, such a significant reduction in current density is not observed for the silane-coated blank panel or for the silane-coated panels cleaned at pH~1.0 and pH~12.4 compared with the corresponding as-cleaned panels. Comparing with the uncoated (as-cleaned) CRS blank panel, no reduction in current density is observed on blank CRS panels after silane deposition indicating cleaning is very essential for the achievement of good bonding and anti-corrosion performance for silane coatings.

### **Electrochemical Impedance Spectroscopy (EIS) of primer-coated CRS panels**

The EIS measurements were performed on primer-coated CRS maintained in 0.6 M NaCl solution for the following periods of times: 0, 1, 2, 7 and 14 days. Figures F.7(a) and F.7(b) show the Bode plots of impedance and phase angle curves of primer-coated CRS panels cleaned in different conditions at the beginning of the EIS experiment on day 0. It was found that the impedance modulus of the CRS panels cleaned in mild alkaline conditions (pH~8.5 to 10.5) were around  $10^4$  to  $10^6 \Omega$  and were up to 2 decades of magnitude higher than for the panels cleaned in the other conditions. This result agrees well with the DC polarization test results.



(a)



(b)

Figure F.7 EIS results of primer-coated CRS on (a) day 0 and (b) day 14 in 0.6 M NaCl solution.

More importantly, the primer-coated CRS panel cleaned at pH~9.5 reveals two time constants in the phase angle plot, one at low and another at high frequencies, while the panels cleaned in the other conditions possess only one time constant at intermediate frequencies (Figure F.7b). The presence of an extra time constant in the low frequency range has usually been assigned to the formation of a layer between the coating and the metal oxide on a metal surface. The difference in the time constant behavior supports the conclusion that the formation of bonds between the coating and the CRS surface is most abundant after cleaning in mild alkaline (pH~9.5) conditions.

## **Conclusions**

CRS was cleaned in different pH values in order to investigate which condition would produce the best surface for the AV silane and the AV-silane-containing primer to bond to CRS. Both the as-cleaned surfaces and the as-cleaned silane-coated surfaces were characterized with several analytical methods and the corrosion performance of the as-cleaned, silane-coated and primer-coated panels were evaluated by electrochemical methods and/or salt water immersion exposure testing.

The best performance results were obtained for the silane-coated and primer-coated panels cleaned in mild alkaline conditions (pH~9.5) near the isoelectric point of CRS. SEM and surface energy examination of CRS cleaned in mildly alkaline cleaning condition detected a fine, dense, spherical surface oxide morphology, the highest surface FeOOH/Fe<sub>2</sub>O<sub>3</sub> ratio and a nearly neutral surface which promoted hydrogen bonding of both silanols and secondary amine groups to the CRS surface. This resulted in the most abundant number of bonds and a thicker silane film. Moreover, the FTIR examination indicated that acidic (pH~1.0) and mild alkaline cleaning conditions (pH~9.5) result in the formation of long-chain siloxane whereas the strong alkaline cleaning condition (pH~12.4) inhibits the long-chain siloxane formation.

## G. POTENTIAL OF ELECTRODEPOSITION OF EPOXY-ACRYLATE PRIMER

**Try to reduce coating thickness:**

**Experimental:**

Skip the polishing in detergent 815 during the sample pretreatment before deposition.

**Results:**

(1) Coating thickness:

Dip-coated samples, 80°C curing for 4.5 h.

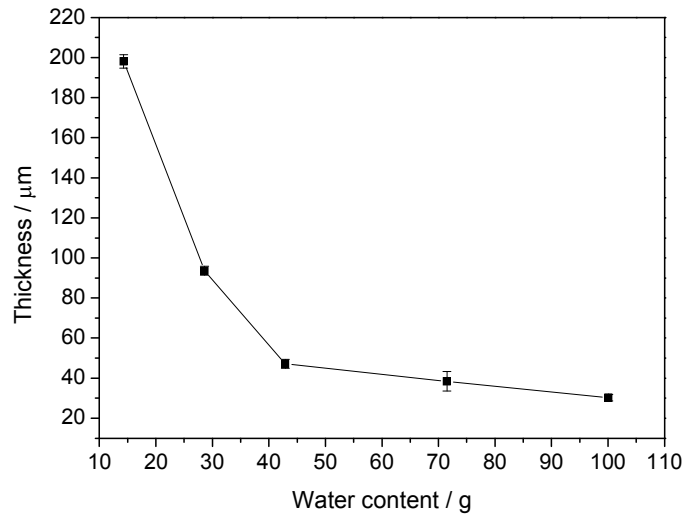


**Fig.G.1 The thickness of the dip-coated coatings as a function of water content in the primer (Maincote AE-58 150 g)**

(2) Salt immersion test:1

All the samples perform good after 7 days salt immersion test.

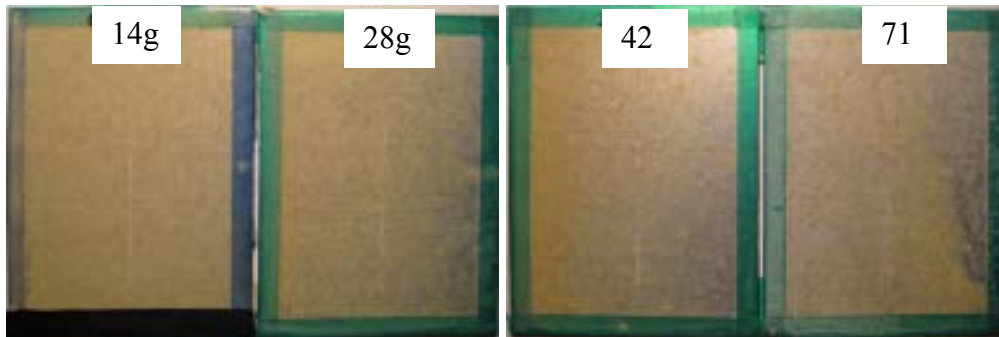


**Fig.G.2 The samples prepared from the primers containing different content of water (Maincote AE-58 150 g) after salt immersion test (55°C, 5% NaCl, 7 days)**

(3) Water contact angle:

All of the samples have the water contact angle around 80 °.

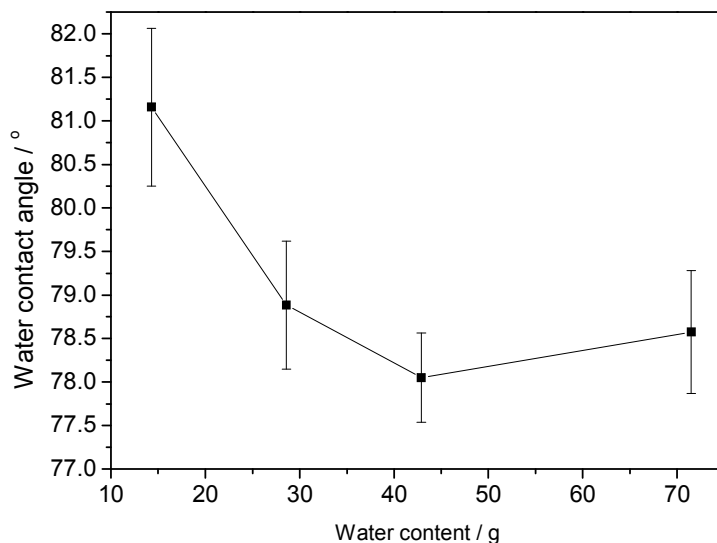


**Fig. G.3 The water contact angle of the dip-coated coatings as a function of water content in the primer (Maincote AE-58 150 g)**

(4) Pencil hardness:

All of the dip-coated samples prepared from the primers containing different content of water perform the pencil hardness around 4B.

#### **Discussion:**

The coating thickness can be reduced by reducing the viscosity of the primer, which can be simply achieved via diluting the primer with water. It seems that the dilution would not deteriorate the coatings' corrosion resistance.

However, the stability of the primer solution after dilution should be further concerned.

#### **Effect of deposition current in the coating electrodeposition from diluted primer**

##### **Experimental:**

Use the primer formula as in part 1. Add water up to 100 g (Maincote AE-58 150 g). The rest procedures are the same as in part 1.

##### **Results:**

(1) The variation of deposition voltage during the electrodeposition:

Cathodic case:

During the cathodic electrodeposition, the deposition voltage goes up. The typical curve is shown as follows.

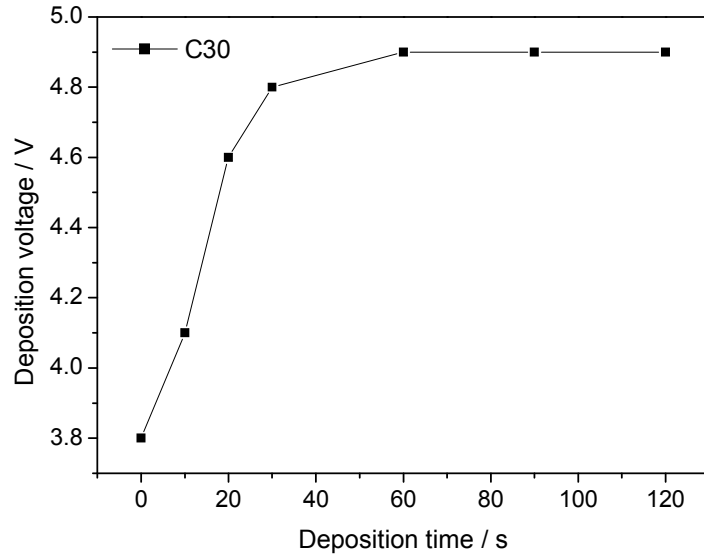


**Fig. G.4 The variation of deposition voltage during the cathodic electrodeposition at 30 mA**

Anodic case:

When the deposition current is below 100 mA, the deposition voltage only slightly goes up during the electrodeposition process. The typical curve is shown as follows.

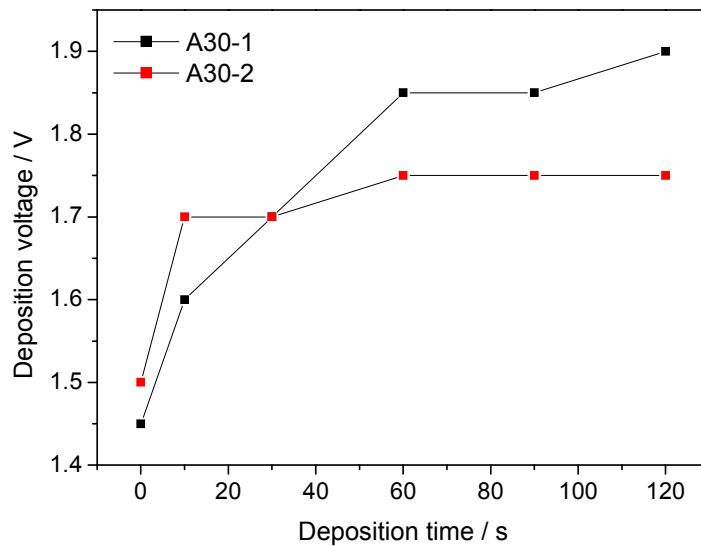


**Fig. G.5 The variation of deposition voltage during the anodic electrodeposition at 30 mA (2 duplicate samples)**

However, when the deposition current reaches up to 300 mA, a sharp increase in the deposition voltage can be observed. The deposition voltage may reach up to 30 V, which is the maximum voltage of the power supply. Afterward, the deposition voltage remains constant and the deposition current starts to decrease.

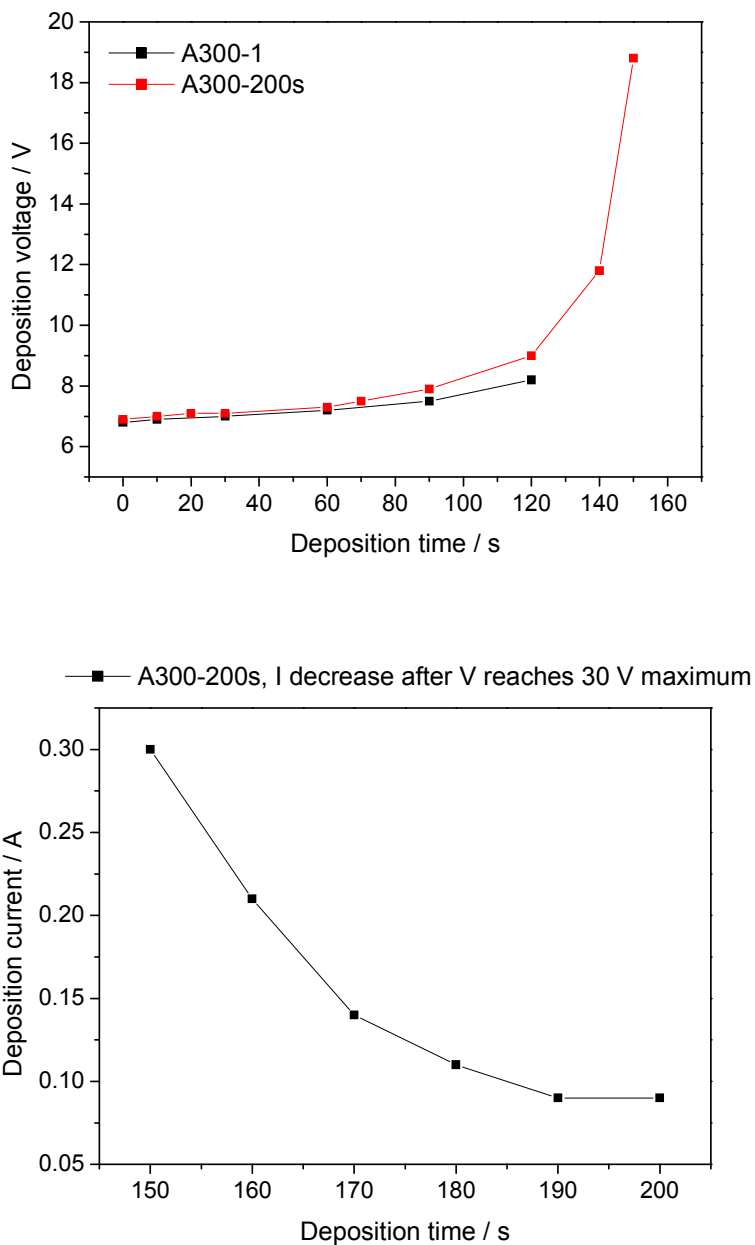


**Fig. G.6** The variation of deposition voltage and deposition current during the anodic electrodeposition at 300 mA

The relationship between the deposition voltage and the deposition current when the deposition current is below 100 mA:

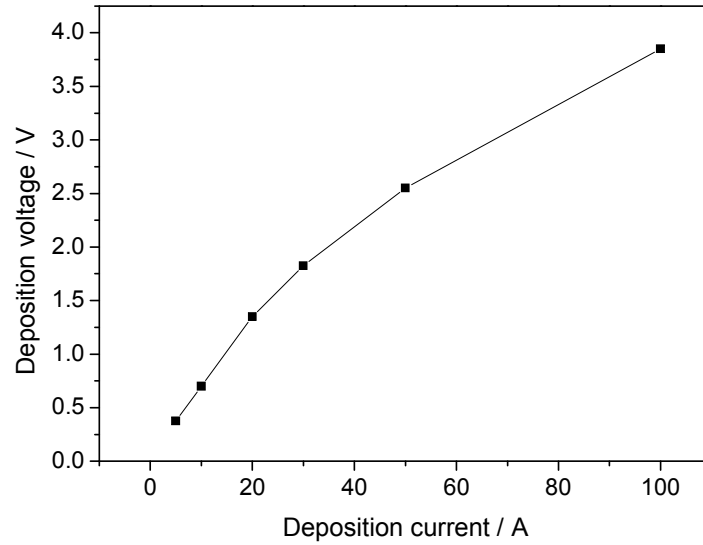


**Fig. G.7** The stable deposition voltage as a function of the deposition current when the deposition current is below 100 mA

(2) Coating thickness:

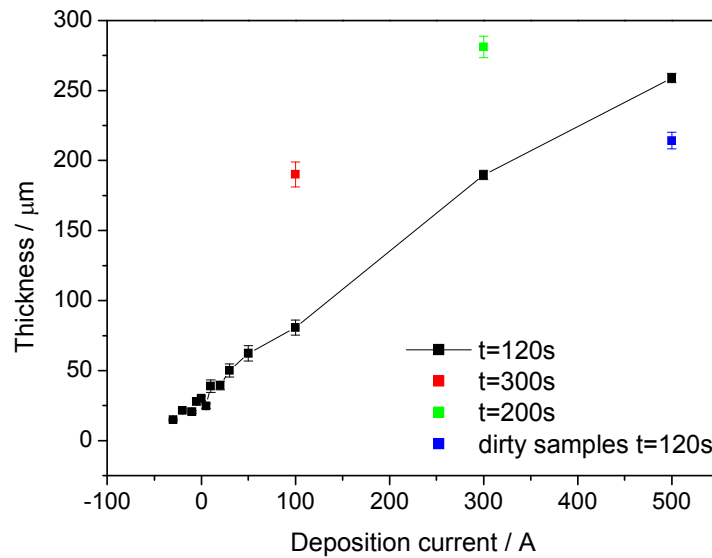


**Fig. G.8** The thickness of the coatings as a function of deposition current

(3) Salt immersion test:

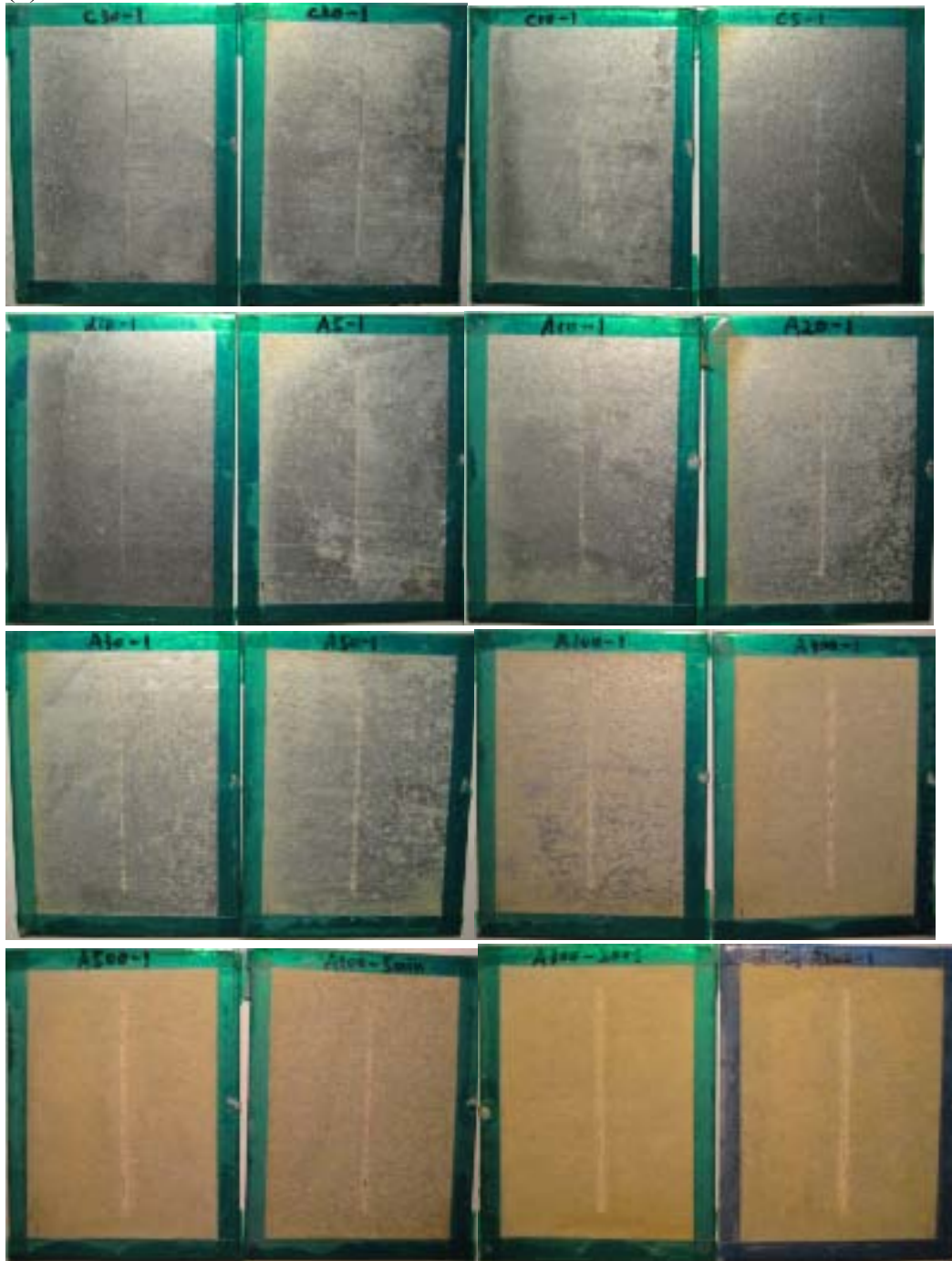


**Fig. G.9 The samples electrodeposited at different currents after salt immersion test (55°C, 5% NaCl, 7 days)**

The cathodically electrodeposited samples perform uniform corrosion after salt immersion test. However, in the anodically electrodeposited samples, only the A5 sample performs serious



As the deposition current increases, the obtained coatings become harder and harder. Moreover, the hardness of all the coatings significantly increases after salt immersion test, indicating the silane in the coatings further condense during the salt immersion.

**Discussion:**

The deposition voltage variation during the electrodeposition indicates that high anodic deposition current could lead to thick resistant coatings.

The corrosion resistance of the coatings seems not to be significantly improved by anodic electrodeposition, because the dip-coated sample also perform good after salt immersion test.

However, anodic electrodeposition at high current may lead to the poor adhesion of the obtained coatings. That's probably because the serious zinc dissolution and the lack of silane in the coating/metal interface.

The variations of the thickness, the water contact angle, and the pencil hardness of the coatings are similar as in the last report, and can be explained by the same reason.

**Plan**

Focus on the cathodic + anodic electrodeposition. Leave the engineering aspects aside (thickness, roughness, throwing power, etc.). Use the diluted primer formula. Try two anodic deposition currents, i.e. 30 mA and 300 mA, to see the benefit of cathodic pretreatment. Prepare much more duplicate samples for cathodic delamination, salt immersion, salt spray, EIS, IR, water contact angle, pencil hardness, thickness, SEM/EDX (cross section), SIMS measurements.

## H. SILANE AND PRIMER FILM STUDIES BY NEUTRON AND X-RAY REFLECTIVITY STUDIES

### The bis-amino and bis-sulfur silane systems

Certain bis-type silanes with the structure of  $(\text{RO})_3\text{Si}(\text{CH}_2)_3\text{-R}'\text{-(CH}_2)_3\text{Si(OR)}_3$  provide excellent corrosion resistance on metals such as aluminum and steel. This section investigates the water barrier properties, water uptake kinetics and hydrothermal degradation of bis-amino silane (Bis-[trimethoxysilylpropyl]amine), bis-sulfur silane (Bis[3-(triethoxysilyl) propyl]tetrasulfide) and their mixture at the weight ratios of 1/3(amino/sulfur silane). These properties are critical to understand the origin of silane corrosion protection and the mechanism by which these films fail. The mixed silanes were also studied because they display better protection than either of the constituents alone. The results guide the improvement of superprimer formulations and identify potential vulnerabilities. The major conclusions are summarized at the end of the section.

### Project Accomplishments

#### Bis-amino silane film

NR offers nanometer resolution in the SLD profile perpendicular to the substrate surface. NR can easily examine interfaces that are buried within a sample. The SLDs of the materials used in this study are shown in table H.1.

The crosslink density profile within the film was probed using solvent swelling in deuterated nitrobenzene based on the assumption that the equilibrium volume fraction of a swelling solvent depends on the local cross-link density. The interaction of silane with water was also studied by exposing silane to water at room temperature and under hydrothermal conditions. Since the silanes are expected to work primarily as water barriers, understanding of water-silane interaction is essential for optimizing the properties of the film.

We first examined bis-amino silane films in the dry state. Then the films were then exposed to saturated deuterated-nitrobenzene (d-NB) and saturated  $\text{D}_2\text{O}$  vapor at room temperature and neutron reflectivity data were collected in this “wet state.” Then the samples were re-dried in a desiccator and new NR measurements were performed in the re-dried state.

When swollen in d-NB, the NB does not penetrate the film substrate interface indicating this region is heavily crosslinked (Figures H.1 and H.2). Water, however, uniformly penetrates the bulk film (Figure H.3) and even shows a slight excess at the two interfaces.

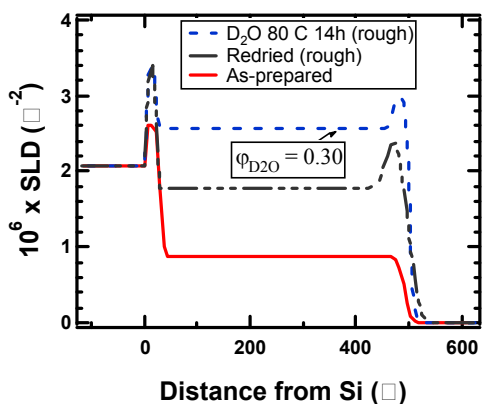


**Figure H.4. SLD profile of bis-amino silane under 80 °C water conditioning.**

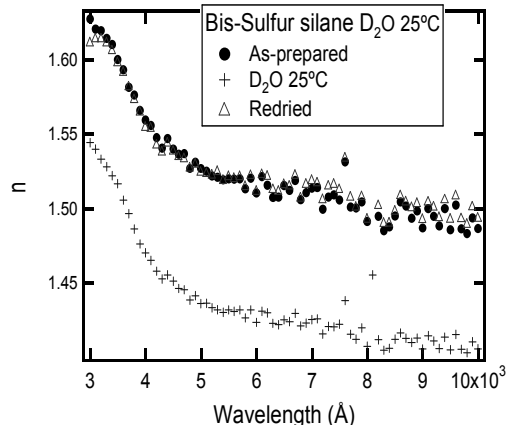


**Figure H.7. Refractive index,  $n$ , of bis-sulfur silane film following  $D_2O$  conditioning at room temperature obtained from ellipsometry measurement.**

Figure H.4 shows the behavior of bis-amino film under 80°C water conditioning. Two important observations should be noticed from these data. First, the bis-amino silane films conditioned with  $D_2O$  at 80°C show a large increase in reflectivity, as well as a  $D_2O$ -rich layer near both the air-side surface and the substrate-side interface. Second, after drying, the SLD remains elevated relative to that of the as-prepared sample indicating deuterium is still present after redry. In addition, the film was found to be rough in both the swollen and re-dried states. Both of these observations indicate that a chemical change occurred upon heating in saturated  $D_2O$  at 80°C. Several reactions appear possible. Some deuterium must be incorporated in the re-dried film either in the form of  $-ND$  or  $-Si-OD$ . Since, based on the SLD value in the dry state, we conclude the film is highly condensed, it is unlikely that  $Si-OD$  is present. Therefore we conclude that there is exchange of the amino protons.

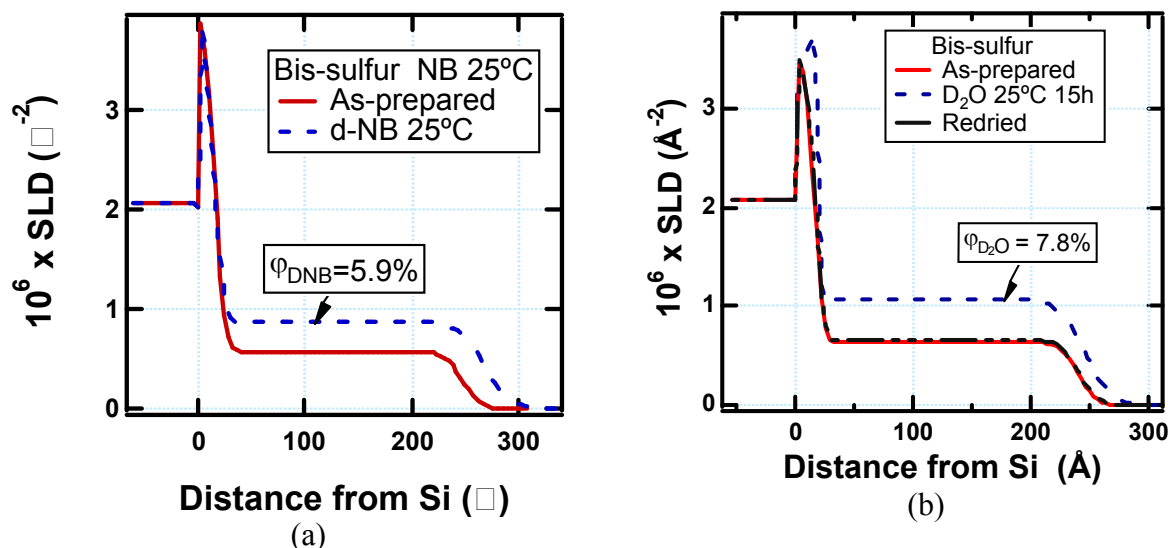


**Figure H.5. Scattering length density profiles of bis-sulfur silane films after exposure to (a): d-NB; (b):  $D_2O$  at room temperature.**

### Bis-sulfur films

For bis-sulfur films, the same experimental procedures were carried out as bis-amino silane films. NR data were obtained for the films as-prepared, after exposure to saturated D<sub>2</sub>O vapor, and after re-drying. Variation in the structure normal to the substrate was also examined by swelling the film with deuterated nitrobenzene (d-NB), a non-reacting swelling agent.

Figure H.5 shows the SLD profiles of bis-sulfur silane after exposure to d-NB and D<sub>2</sub>O at room temperature. The profiles show no altered chemical composition near the substrate or the air surface as was observed for bis-amino silane films. Also based on the measured SLD of the film, bis-sulfur silane does not fully condense at room temperature—about 15% uncondensed groups remain in the as-prepared film. These unhydrolyzed groups lead to poor wetting and non-uniform films. Although bis-sulfur silane film is not fully condensed, it swells less in water (7.8%) than bis-amino silane (41%) because of the hydrophobic nature of bridging group.

Also, bis-sulfur films swell more in d-NB than in water even though the volume fraction of the water is greater. Apparently NB swells the polymer chain whereas water resides in the free volume. NB is therefore a better solvent than water or possibly water enhances condensation of the residual ethoxy groups, which would counteract chain expansion.

### Mixed silane films

The D<sub>2</sub>O conditioning results for mixed silane are shown in Figure H.6. At room temperature, the

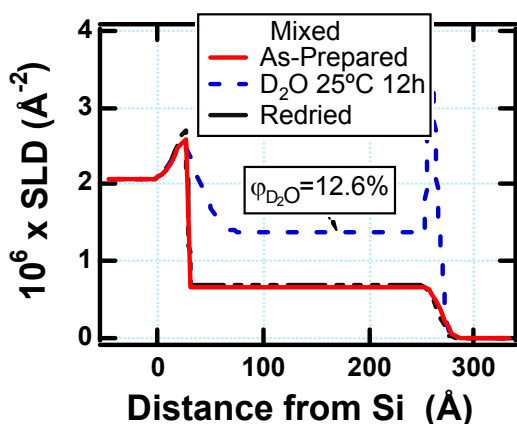


Figure H.6a. SLD profile of mixed silane at 25°C.

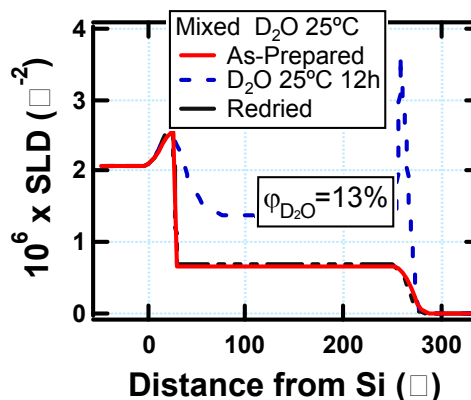
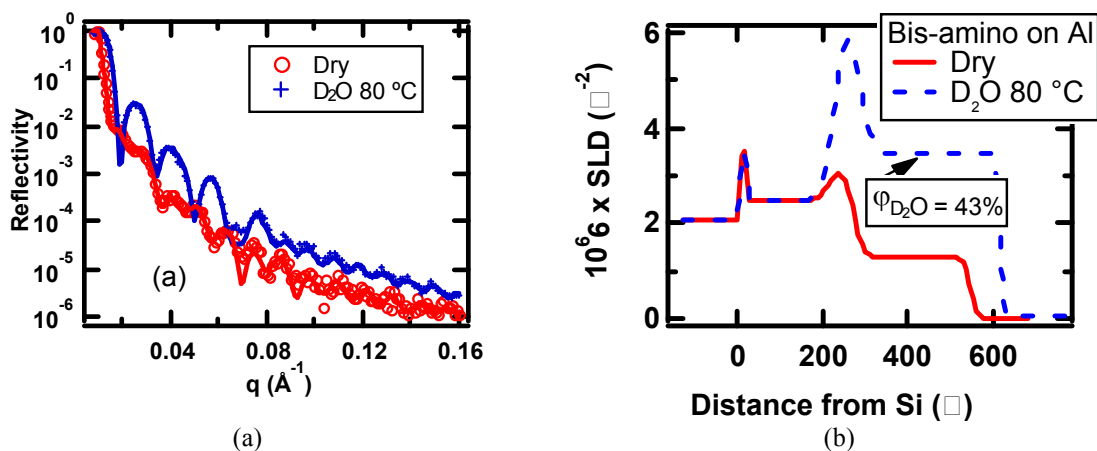


Figure H.6a. SLD profile of mixed silane at 80°C.



**Figure H.8. (a) The reflectivity curves of bis-amino silane on silicon wafer dry and after exposure to D<sub>2</sub>O; (b) The SLD profiles corresponding to the reflectivity curves in (a).**

calculated volume fraction of free water is 12.6%. We conclude that, at least for silicon wafer substrates and the thickness of films we used, the water barrier ability of mixed silane

is not enhanced but roughly that of both components weighted by their volume fraction. Surprisingly the thickness of the “swollen” films decreases compared to the as-prepared state. In addition, the SLD of the redried film is higher than the as-prepared state. The shrinkage is likely due to the condensation of unhydrolyzed ethoxy groups.

We previously demonstrated that bis-amino silane film is highly condensed and most, if not all, of the alkoxy groups have been transformed to  $-\text{Si}-\text{O}-\text{Si}-$  bonds. Therefore, the shrinkage of the mixed silane film is mainly due to the transformation of the alkoxy groups to  $-\text{Si}-\text{O}-\text{Si}-$  bonds. Comparing the result of bis-sulfur silane and mixed silane, we conclude that condensation is accelerated in the mixed film. Bis-amino silane, acts as a catalyst in the hydrolysis of bis-sulfur silane. This effect might account for the enhanced performance of mixed silane compared to individual silanes.

Since bis-amino silane has both catalytic effect and hydrophilic effect, a thicker film is needed for the catalytic effect to dominate the hydrophilic effect. Temperature also accelerates the hydrolysis of residual ethoxy group. Therefore, both temperature and thickness effects were investigated.

Film thickness information and optical constants were also obtained from ellipsometry (Figure H.7). The variation of optical constants following the hydrothermal conditioning confirmed the results of neutron reflectivity. AFM showed that the roughness of silane film deposited using spin coating is about 10 Å. The roughness of bis-amino silane is smaller than bis-sulfur silane, and mixed silane is in between.

### Al substrates

Aluminum was sputtered on silicon wafer. The resulting film is around 200 Å and the roughness is about 10 Å. Silane films were then applied to Al surface using the procedures developed for bare silicon wafers. The reflectivity curves from silane film on Al-on-silicon substrate do not have equally spaced peaks (Figure H.8a). Instead, double peaks are obtained because of the contribution of both Al layer and silane film.

A six-layer model (silicon, silicon oxide, aluminum, aluminum oxide, silane, air) was required to fit the data (Figure H.8b). Similar to the result we obtained on silicon wafer substrate, water completely penetrates up to the interface between aluminum and silane. Apparently the postulated barrier properties of silane films are associated with either thick films or more complex aspects of the film.

### Effect of curing temperature

The vapor-conditioning results for bis-sulfur silane cured at 180 °C are shown in Figure H.9a. Compared to film cured at 80 °C (not shown), the thickness of the as-prepared state is smaller and the SLD is higher. The calculated volume fraction of D<sub>2</sub>O in the swollen film is 2% compared to 7.8% for films cured at 80 °C. These observations indicate that a denser film is formed when cured at 180 °C.

The denser film obtained at 180 °C is due to: elimination of water and ethanol enclosed in the film, further condensation of residual silanol group and breakdown of tetrasulfide bonds into shorter

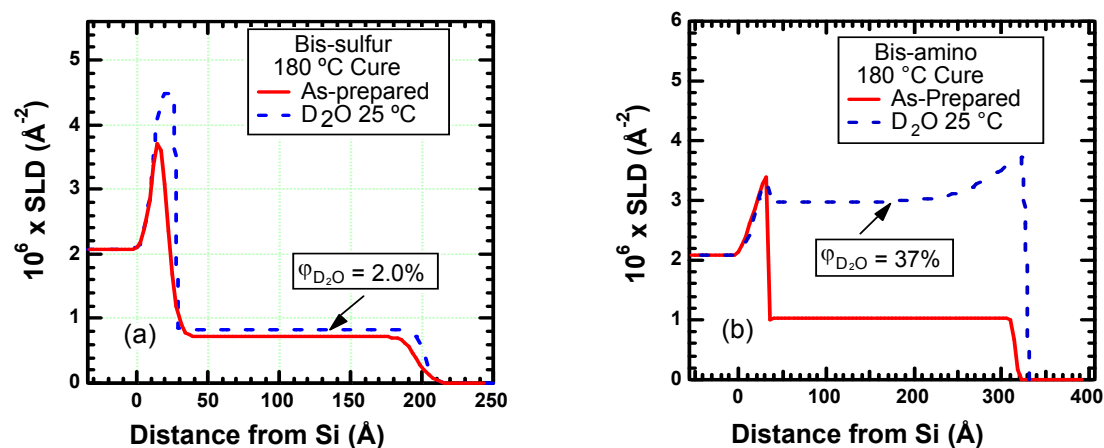


**Figure H.9. Best-fit SLD profiles of (a) bis-sulfur silane film; (b) bis-amino silane film cured at 180 °C as-prepared, after exposure to D<sub>2</sub>O vapor at room temperature.**

leakage. All of these processes result in a higher crosslink density and lower thickness.

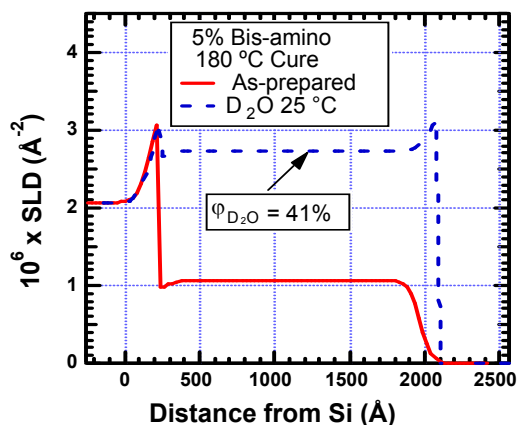


**Figure H.11. SLD profiles of thick bis-amino silane film cured at 180 °C as-prepared, after exposure to D<sub>2</sub>O vapor at room temperature.**

film cured at both 80 °C and 180 °C. Film thickness is more important for bis-sulfur than for bis-amino films. For thick bis-sulfur films cured at 80 °C we observe a significant increase in reflectivity of the conditioned film compared to dry film (Figure H.10a), indicating enhanced absorption of water. The calculated volume fraction of D<sub>2</sub>O in the swollen film is 11%, substantially higher than the 7.8% absorbed in thin films. The SLD of the dry film (not shown) is lower than that of thin films. The lower SLD of dry film and the increased water absorption in the swollen film indicate that the thick films deposited at 5% are less dense (greater free volume) than 1% films cured at the same temperature.

For thick bis-sulfur films cured at 180 °C (Figure H.10b), the water-conditioned reflectivity curve

is

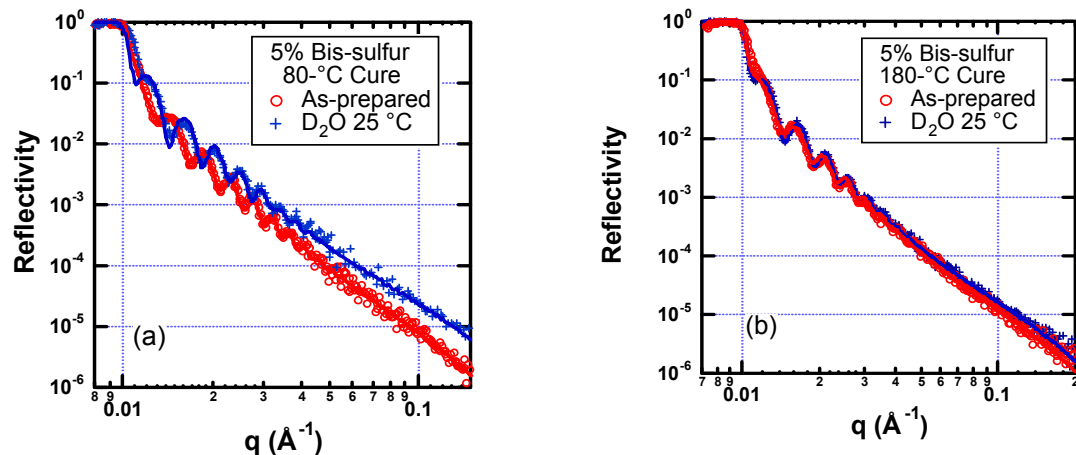


**Figure H.10. Vapor-conditioning results for thick bis-sulfur silane films cured at (a) 80 °C; (b) 180 °C. Thicker, less dense films are obtained at 5% compared to 1% precursor solutions. Greater change in reflectivity is observed for the 80-°C film when exposed to water vapor.**

Figure H.9b shows the SLD profiles of bis-amino silane film cured at 180 °C and water-vapor conditioned at room temperature. In contrast to bis-sulfur silane film, substantial absorption of D<sub>2</sub>O is observed based on the increased reflectivity relative to the as-prepared film. The calculated volume fraction of D<sub>2</sub>O in the swollen film ( $\phi_{D_2O} = 37\%$ ) is close to the film cured at 80 °C ( $\phi_{D_2O} = 41\%$ ). This observation confirms the conclusion from the previous study that is-amino silane is fully condensed at the curing temperature of 80 °C. Increased temperature does not affect the bulk structure of the film or the amount of water absorbed.

Higher concentration and lower spin speed are used to obtain thicker films. Figure H.10 shows the water-conditioning results for thick bis-sulfur silane

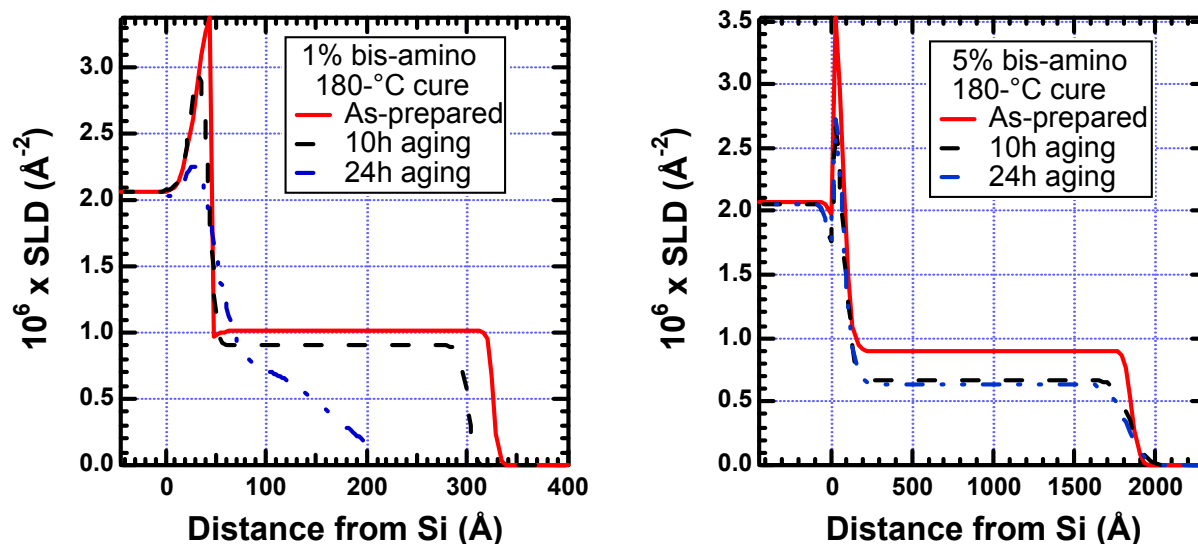


**Figure H.12. Aging results for thin (1%) and thick (5%) bis-amino films cured at 180°C.**

almost the same as the as-prepared film. There is almost no absorption of water. Previous work on thin bis-sulfur silane showed that films cured at 180 °C are denser compared to films cured at 80 °C and the water volume fraction reduced from 7.8% to 2%. For the 5% film, the water volume fraction is reduced to almost zero when the curing temperature is 180 °C.

The vapor-conditioning results for thick bis-amino cured at 180 °C is shown in Figure H.11. The water volume fraction is 41%, similar to the value obtained from thinner 1% bis-amino silane films on both silicon wafer and Al substrates. So, for bis-amino silane film, increasing thickness and cure temperature has no effect on its water-barrier properties. Under any preparation conditions, water penetrates up to substrate and the films absorb about 40% water.

### Hydrothermal degradation

Neutron reflectivity data were obtained for the films as-prepared and also after 10 and 24-hours exposure to 80 °C liquid water and subsequent re-drying. We found that bis-sulfur films are much more robust than bis-amino films in hot water.

### Bis-amino silane

SLD profiles in Figure H.12 shows that bis-amino films degrade in hot water regardless of film thickness. The SLD drops and the film surface erodes.

### Bis-sulfur silane

#### Effect of curing temperature

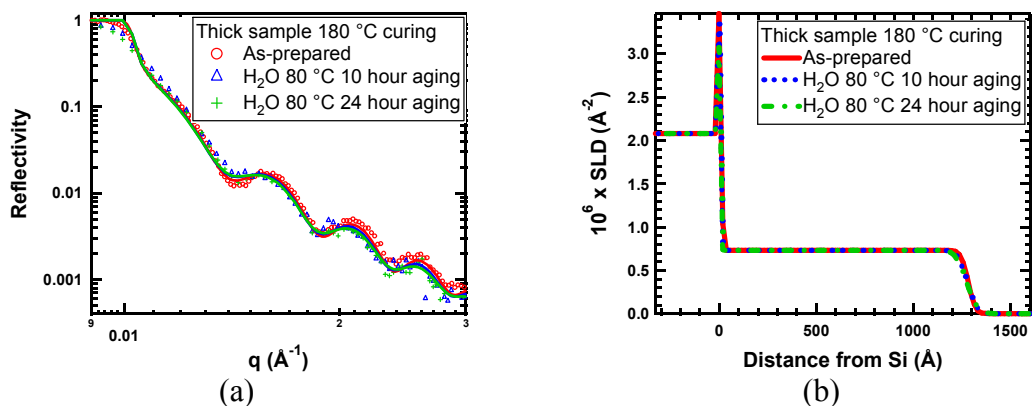


**Figure H.14. (a) Reflectivity data from thick bis-sulfur silane film cured at 180°C, as-prepared and after aging in 80°C liquid H<sub>2</sub>O for 10 and 24 hours. The curves through the data points correspond to the best fits using model SLD profiles. (b) Best-fit SLD profiles corresponding to the curves through the data in (a). The data indicate that the film is robust.**

Two thick films deposited from 5% bis-sulfur silane solution and cured at different temperatures (180°C and 80°C) were measured to investigate the influence of curing temperature. The reflectivity data after each aging stage for the sample cured at 80°C were shown in Figure H.13. The corresponding data for 180°C-cured sample are shown in Figure H.14.

For the 80°C-cured film (Figure H.13), the fringes are less distinct after 10 and 24 hours aging, which indicates an increase of roughness. The SLD profiles also show a broader SLD transitional region at the film-air interface. However, the thickness and SLD of middle of the film remain unchanged, which indicates that the bulk of the film is robust under accelerated aging. The aging process neither hydrolyzes nor densifies the film.

For the 180°C-cured film (Figure H.14), there are no noticeable changes even after 24-hours aging (Figure H.14). Neither the thickness nor SLD of bulk film changes. Even the top surface remains as smooth as the virgin state.

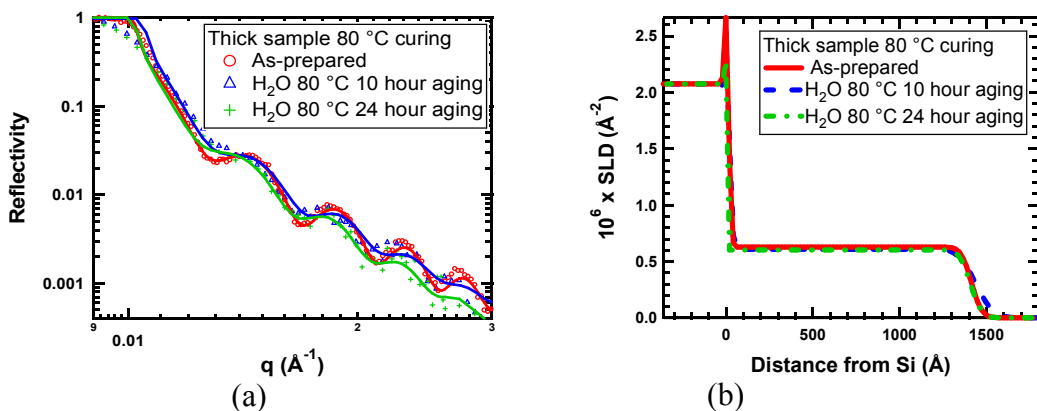


**Figure H.13. (a) Neutron reflectivity data from thick bis-sulfur silane cured at 80°C, as-prepared and after aging in 80°C liquid H<sub>2</sub>O for 10 and 24 hours. (b) Best-fit SLD profiles corresponding to the curves through the data in (a). The data indicate minor alteration of the surface region on accelerated aging.**

The possible reactions in bis-sulfur silane films cured at 180 °C that lead to denser films are: elimination of water and ethanol retained in the film, further condensation of residual silanol groups and breakdown of polysulfide bonds to shorter linkage. Elevated curing temperature (180 °C) also improves hydrothermal stability to bis-sulfur films due to the higher crosslink density. The degradation rate is related to the crosslink density profile in the film. Higher crosslink density regions have a lower degradation rate.

Although it is expected that 80°C-cured films are vulnerable because of the insufficient condensation, our observations show that the 80°C-cure is sufficient to provide good hydrothermal stability to bis-silane films except for the top surface. The elevated curing temperature leads to increased condensation and therefore further enhances the durability of both the bulk film and the surface.

### Effect of film thickness

Films of two different thicknesses, deposited from 1% and 5% bis-sulfur silane solution and cured at 180°C, were measured to investigate the influence of film thickness on the hydrothermal stability. The reflectivity data at each aging stage of the thin sample (deposited from a 1% bis-sulfur silane solution) are plotted in Figure H.15. The results for thick sample (deposited from a 5% bis-sulfur silane solution) are shown in Figure H.14.

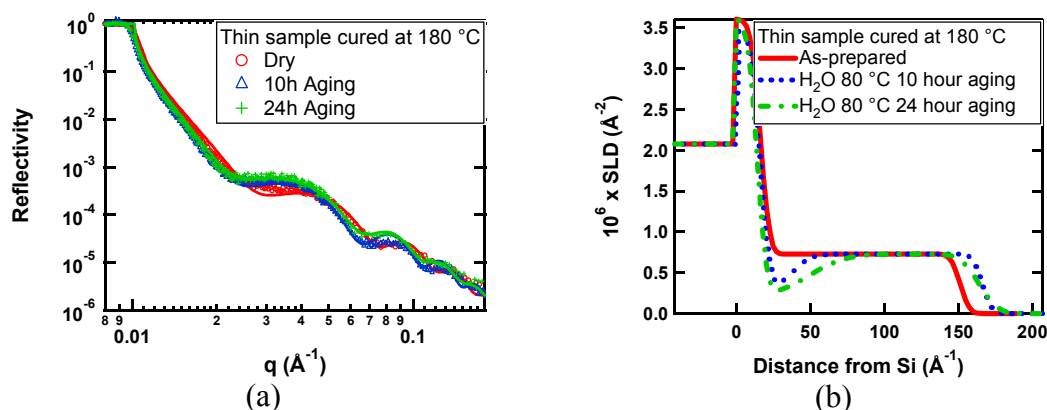


**Figure H.15. (a) Neutron reflectivity data from thin bis-sulfur silane film cured at 180°C, as-prepared and after aging in 80°C liquid H<sub>2</sub>O for 10 and 24 hours. (b) Best-fit SLD profiles corresponding to the curves through the data in (a). The data indicate considerable reconstruction of the film-substrate interface. The fits are not particularly good. A number of different structures were evaluated before settling on the two-layer-film model, which is the simplest structure that adequately represents the data.**

For the thin sample cured at 180°C (Figure H.15), one-uniform-layer structure was observed. The thickness of thin film is  $135 \pm 5$  Å, which is 10% of the thickness of the thick film. The SLD of thin film is  $(7.3 \pm 0.3) \times 10^{-7}$  Å<sup>-2</sup>, which indicates a fully condensed state. However, after aging, changes occur near the film-silicon interface and at the top surface. After 10-hours aging, the total thickness of the film increases 10% due to the degradation and swelling of the film-silicon

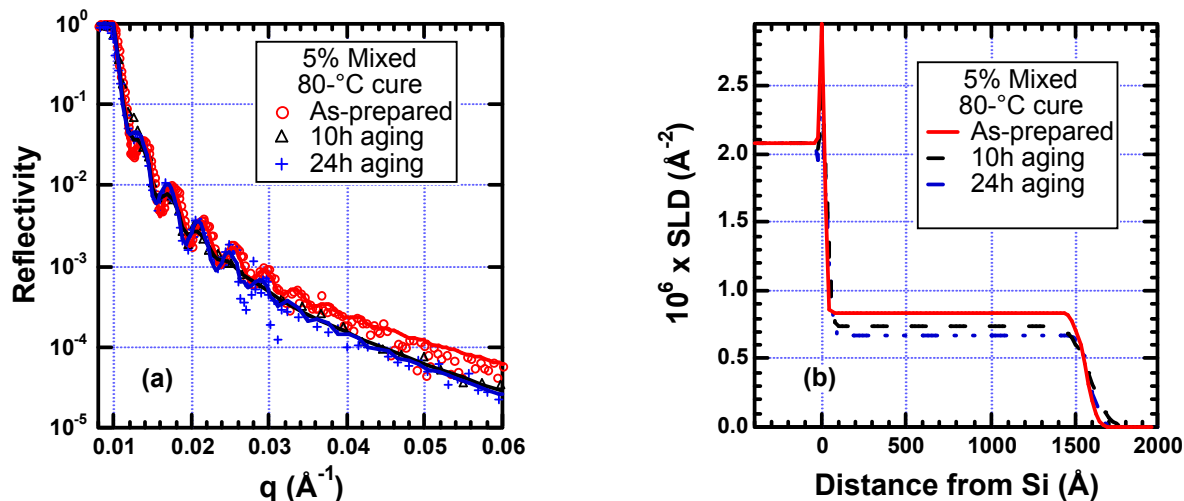


**Figure H.16. Reflectivity (a) and SLD profile (b) for thick mixed silane films cured at 80 °C. Degradation is observed due to the presence of bis-amino silane.**

interface. Although most of the film retains its original SLD, a low SLD ( $2.8 \pm 0.5 \times 10^{-7} \text{\AA}^{-2}$ ) region appears at the film-substrate interface. The width of this region is  $20 \pm 5 \text{\AA}$ . The gradient between this region and bulk film indicates that this is a transitional region rather than a sharp interface. If the density decrease is the only cause of the SLD drop, the 62% SLD drop means that 62% of interfacial material is lost after 10 hours aging.

After 24 hours aging, the width of affected interfacial area increases from  $20 \pm 5 \text{\AA}$  to  $35 \pm 5 \text{\AA}$ . The SLD decreases further to  $2.0 \pm 0.3 \times 10^{-7} \text{\AA}^{-2}$ , which indicates the density of interface drops another 11%. At the same time, the top surface becomes rough.

These phenomena indicate that for thin bis-sulfur film, the film-substrate interface is more vulnerable than bulk film. The interface is damaged during the hydrothermal degradation and about 73 % of the material is lost after 24-hours aging. It is reasonable to believe that the failure will occur at the substrate interface for thin bis-sulfur film under hydrothermal conditions.

Compared with the stability of thick, high-temperature-cured bis-sulfur film, we conclude that a thickness greater than 1000  $\text{\AA}$  is essential to achieve hydrothermal stability of bis-silane films.

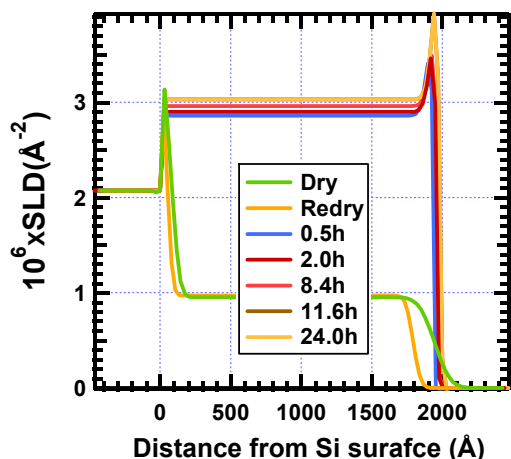


**Figure H.17. Water penetration kinetic of bis-amino silane coatings (a) SLD profile as a function of water conditioning time (b) Fraction of absorbed water as a function of exposure time.**

profiles as the function of water conditioning time. During the water conditioning, water rapidly occupies 30 vol% in 0.5 hour and slowly increases to 33 vol% over the next 11.1 hours and reaches equilibrium after 11.6 hours of D<sub>2</sub>O conditioning. The thickness increase is delayed and reaches equilibrium at 24 hours. The total thickness increase after equilibrium is 2.3%.

The large difference between the volume of water absorption and swelling of the film implies that about 30 vol% of D<sub>2</sub>O is accommodated in the molecule-level free space in the as-prepared film. In the first 0.5 hours, Langmuir absorption mode, which is related to the physical occupation of existing free space, dominates the water absorption. After first 0.5 hours, Henry's mode, which related to the relaxation of the siloxane network, dominates.

### Bis-sulfur silane film

Figure H.18 shows the neutron reflectivity of the bis-sulfur silane in the as-prepared state, the water conditioned state at different times and the re-dried state. As with bis-amino silane, the SLD of the bis-sulfur silane increase rapidly in first 0.5 hour. After 0.5 hour, little SLD increase is observed during the prolonged D<sub>2</sub>O conditioning. Finally, equilibrium is reached in 6 hours, which shows that that the bis-sulfur silane film reaches equilibrium more rapidly than that of the bis-amino silane film mentioned above (11.6 hours, Figure H.19). The total water absorption at equilibrium is 4.6 vol%, which is much less than the 33 vol% observed for bis-amino silane.

The thickness increase during the D<sub>2</sub>O conditioning is plotted against the water conditioning time as shown in Figure H.20. The thickness increase is much more sluggish than the SLD increase. The calculated thickness increase after the saturation is about 0.45%. Most D<sub>2</sub>O is physically accommodated in the free space of the film instead of swelling the bis-sulfur silane film. That is, Langmuir's mode dominates initial stage of the water absorption, while Henry's mode dominates after first 0.5 hours.

### Mixed silane films

For mixed amino-sulfur films degradation is enhanced compared to neat bis-sulfur films. Fig.H.16 shows the reflectivity and SLD profile for mixed films containing bis-sulfur and bis-amino in a 3/1 weight ratio. Although mixed films show improved corrosion protection compared to either neat bis-amino or neat bis-sulfur, the presence of bis-amino leads to a susceptibility to hydrothermal degradation.

### Kinetics of water adsorption

#### Results from NR

#### Bis-amino silane film

Neutron reflectivity of a 2000-Å bis-amino silane films was recorded *in situ* during D<sub>2</sub>O conditioning. SLD profiles of the coating were obtained from the best fit of individual reflectivity curves. Figure H.17 shows the reflectivity and corresponding SLD

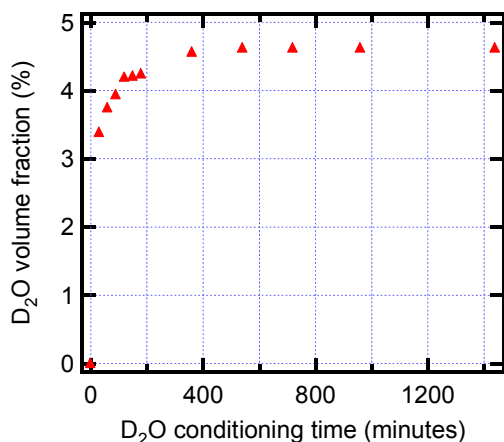


**Figure H.19.** The D<sub>2</sub>O absorption in the bis-sulfur silane film as the function of the D<sub>2</sub>O conditioning time. The film is saturated with D<sub>2</sub>O water in 6 hours. No further change in SLD is observed after 6 hours water conditioning.

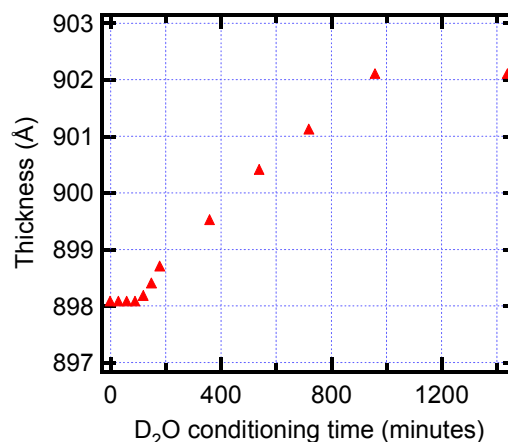


**Figure H.20.** Thickness increase of the bis-sulfur silane film as the function of the water conditioning time. Note that the thickness increase is slower than the SLD increase as shown in Figure 19

### Results from FTIR-RA

Fourier transform reflection-absorption infra red spectroscopy (FTIR-RA) was also employed to trace the water ingress in the films in the initial stage (especially within the first 30 minutes) of conditioning.

#### Bis-amino silane film

The IR spectra of D<sub>2</sub>O-conditioned bis-amino silane in the as-prepared state and at equilibrium after 1210 minutes of D<sub>2</sub>O conditioning are shown in Figure H.21.

By plotting the normalized intensity increase of the D-O-D bending vibration peak at 1340 cm<sup>-1</sup> against the D<sub>2</sub>O conditioning time, water absorption profiles are obtained (Figure 22). Equilibrium absorption is reached at around 1150 minutes.

FTIR analysis agrees with the NR experiment. The diffusion of D<sub>2</sub>O follows Fickian's behavior with a slight deviation in the intermediate stage of diffusion. The deviation may result from of the relaxation of the molecular chains and swelling of the films (Henry absorption).

#### Bis-sulfur silane film

The IR spectra of D<sub>2</sub>O-conditioned bis-amino silane film in the as-prepared state and at equilibrium of D<sub>2</sub>O conditioning are shown in Figure H.23. By plotting the normalized intensity increase of the D-O-D bending vibration peak at 1340 cm<sup>-1</sup> against the D<sub>2</sub>O conditioning time, water absorption profiles are obtained (Figure H.24).

Fickian's behavior is also observed at the beginning of the ingress. However, larger deviation from the Fickian behavior is observed near the equilibrium state due to the interaction between the D<sub>2</sub>O and the siloxane network.

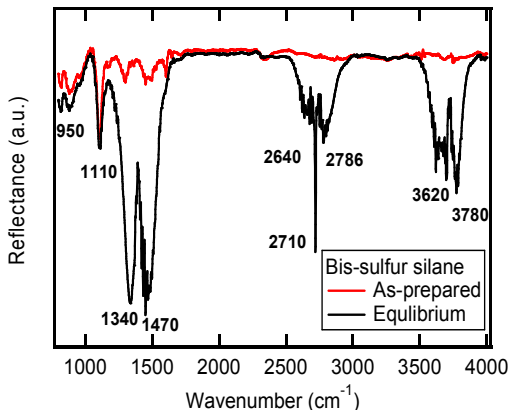


**Figure H.23.** The IR spectra of the bis-sulfur film in as-prepared and equilibrium state.

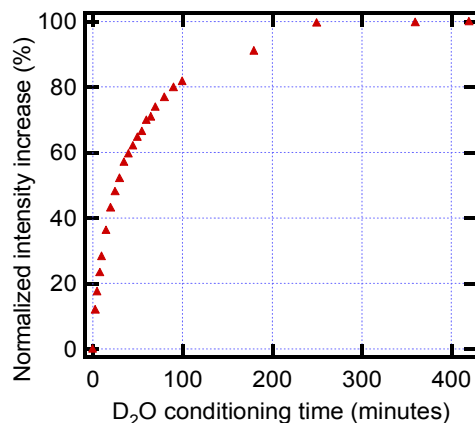


**Figure H.24.** Normalized relative intensity increase of bis-sulfur silane film during D<sub>2</sub>O conditioning. The equilibrium of the D<sub>2</sub>O absorption is reached at around 250 minutes.

### Conclusions regarding the bis amino and bis sulfur systems

1: Bridging group is the key factor that controls the water-barrier properties of silane films. Bis-sulfur silane is not as condensed as bis-amino silane, but it swells less in water because of the hydrophobic nature of bridging group. By contrast, bis-amino film is more hydrophilic since the secondary amine group hydrogen bonds with water. Bis-amino silane films show monotonic

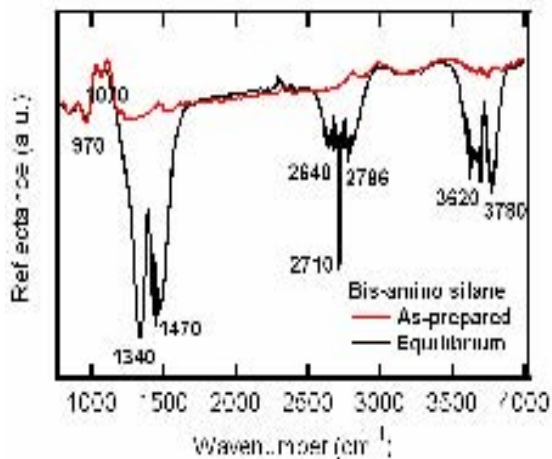


**Figure H.21.** The IR spectra of the bis-amino silane film in as-prepared state and at equilibrium.

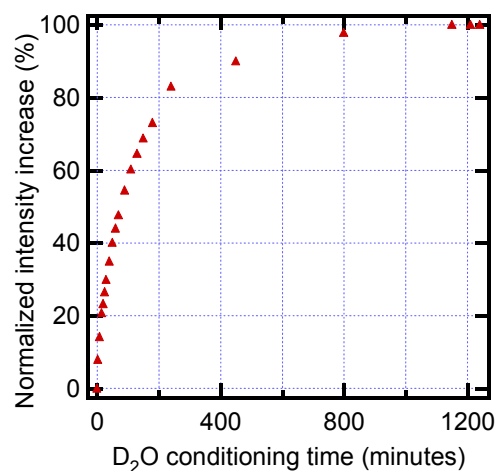


**Figure H.22.** Normalized relative reflectance intensity increase of the 1340 cm<sup>-1</sup> IR peak of bis-amino silane film during D<sub>2</sub>O conditioning.

degradation no matter how thick the films are. For bis-sulfur films, thickness becomes the key factor. Thicker films (above 1000 Å) are robust whereas thin films are not.

2: At elevated temperature, water-conditioning leads to further chemical reactions for all films studied. After re-drying following room-temperature conditioning, the reflectivity curves of bis-

amino, bis-sulfur as well as the mixed film all return to the as-prepared profile indicating no chemical reaction occurs at room temperature. With 80-°C water-vapor conditioning, however, the reflectivity of the redried film remains elevated relative to the as-prepared film due to formation of Si-O-Si- and Si-OD in bis-sulfur silane and the exchange of the amine proton with a deuteron in bis-amino silane.

3: The improved anti-corrosion performance of the mixed film is traced to modification of the chemistry in both the film and the precursor solution. Based on the enhanced shrinkage that occurs following water-vapor conditioning of the mixed film, condensation is accelerated in the mixed silane. Regarding to the precursor solution, bis-amino silane may act as a catalyst in the hydrolysis of bis-sulfur silane leading to more silanols groups in the solution, which in turn improves the wettability of the solution. Because of the bis-amino silane in the mixed silane, however, degradation takes place during 80 °C water conditioning.

Although the redried films show enhanced shrinkage in the mixed film, the vapor-swollen state does not show any unusual character. The mixed silane film swells to an extent that is only slightly less than that of both components weighted by their volume fraction. Thickness and roughness of mixed silane in the swollen state is also between that of bis-amino silane and bis-sulfur silane. Contact angle, however, does track corrosion performance in that the mixed silane has the highest contact angle. Presumably the chemistry discussed above leads to an air surface that favors hydrophobicity in the mixed film.

4: The substrate does not play a key role for the water barrier properties of silanes. The films deposited on Al substrate and silicon wafer have similar bulk properties and top surface morphology. We conclude that a 200-Å silane film is thick enough that the substrate does not affect the top surface or the bulk structure.

5: Higher curing temperature leads to denser film for bis-sulfur and mixed silane, whereas the temperature effect on bis-amino silane film is negligible. This result confirms that bis-amino silane is highly condensed at a curing temperature of 80 °C. Further increasing in cure temperature does not affect the bulk structure of the film.

6. Although it is expected that an 80-°C cured bis-sulfur films are vulnerable to degradation due to insufficient condensation, our observations show that an 80-°C cure is sufficient to provide good hydrothermal stability except for the top surface. Elevated curing temperature increases condensation and therefore further enhances durability.

7: Film thickness is an important variable that controls water-barrier performance: Bis-sulfur silane deposited at 5% concentration and cured at 80 °C is more porous compared to the thinner film deposited at 1% concentration. As a result, the thicker film absorbs more water. Bis-sulfur silane provides an adequate barrier to water penetration only for films cured at 80 °C whose thickness exceeds 1200 Å. Therefore, for bis-sulfur silane films, both larger thickness and higher cure temperature are critical for effective water-barrier properties. By contrast, bis-amino films show no performance improvement with increased thickness and curing temperature.

8: In situ water conditioning study indicates that bis-amino silane film absorbs substantially more D<sub>2</sub>O (33 vol%) than the bis-sulfur silane film (4.6 vol%) at equilibrium. Bis-sulfur silane film reaches equilibrium more rapidly than bis-amino silane film. Two absorption modes are observed in both films, Henry's mode, which related to the relaxation of the siloxane network and Langmuir's mode, which is related to the physical occupation of existing free space. Langmuir

absorption mode dominates the total absorption of both films.

9: The thickness increase of both bis-amino silane and bis-sulfur silane film is much smaller than expected based on the volume of D<sub>2</sub>O absorbed, which implies that the most of water resides in the free space instead of swelling the film. The Langmuir absorption mode dominates the D<sub>2</sub>O absorption process. The increase of the film thickness lags behind the water absorption indicating the Langmuir absorption is more rapid than the absorption via the Henry absorption mode.

10: FTIR analysis agrees with the NR experiment. Bis-sulfur silane film reaches equilibrium more rapidly than bis-amino silane film. The diffusion of D<sub>2</sub>O in both films follows Fickian's behavior with slight deviation at the intermediate stage of diffusion. The deviation from Fickian kinetics may result from the relaxation of the molecular chain and swelling of the films.

11: The above study of the water penetration and absorption in bis-amino silane and bis-sulfur silane films indicates both films are susceptible to water. Water penetrates rapidly into the films. This result indicates the interfacial bonding between silane and substrate must be critical in anti-corrosion performance and also raises concern regarding the long-term susceptibility of the silanes to hydrolytic degradation. Development of silane and polymer mixture (primer) coating may increase the long-term stability of the films.

## **The AV silane system**

### **Objective**

Coatings prepared with mixture of bis-[trimethoxysilpropyl]amine (bis-aminosilane, A) and vinyl triacetoxysilane (VTAS, V) are effective anti corrosion agents, but only under specific processing conditions. A water-miscible, stable and effective in anti-corrosion application can be achieved at A/V=3.4 (mol ratio).

This section focuses on the relationship between substrate-surface chemistry (cleaning), reaction mechanism, film structure and water-barrier properties of AV system. The major conclusions are summarized at the end of the section.

## **Project Accomplishments**

### **NMR study of AV chemistry**

#### **Neat AV mixture**

<sup>13</sup>C NMR spectra show that the primary reaction in neat AV3.4 silane mixture is the exchange of the hydrogen atom on secondary amine group of bis-amino silane with the acetoxy group of VTAS forming an amide complex and hydrolyzed VTAS. The primary reaction is followed by a series of condensation and hydrolysis reaction of bis-amino silane and VTAS and their reaction by-products.

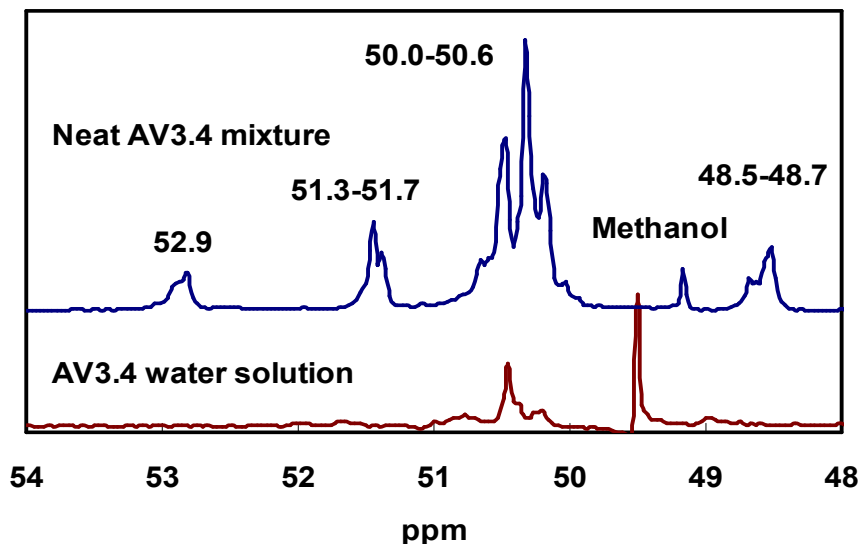


**Figure H.28.**  $^{13}\text{C}$  spectra of the neat AV3.4 mixture and 10 wt% AV3.4 water solution collected after 5-hour hydrolysis in water.

Figure H.25 compares the  $^{13}\text{C}$  liquid NMR spectra in 0-60 ppm region of AV3.4 silane mixture after 5 hours from mixing. New peaks occur after mixing in 48-53 ppm and 18-25 ppm range. The NMR spectra indicate that the primary reaction is exchange of the acetoxy group on VTAS with the secondary amine hydrogen, forming an amide complex as shown in Figure H.26. The stoichiometric ratio of primary reaction is therefore 3. When bis-amino silane and VTAS are mixed near the stoichiometric ratio (AV3.4), the reaction in the mixture is near completion.

Figure H.27 shows the  $^{29}\text{Si}$  NMR spectrum of neat AV mixture in -75 to -40 ppm range, which indicates that the primary reaction is followed by the condensation between silanol groups on the reacted VTAS from the primary reaction. The water generated from the VTAS condensation then further hydrolyzes bis-amino silane and produces methanol. The condensation between hydrolyzed bis-amino silane generates additional water. The hydrolysis and condensation products of bis-amino silane and VTAS are observed in neat AV3.4 mixture.

#### **AV silane in water solution**

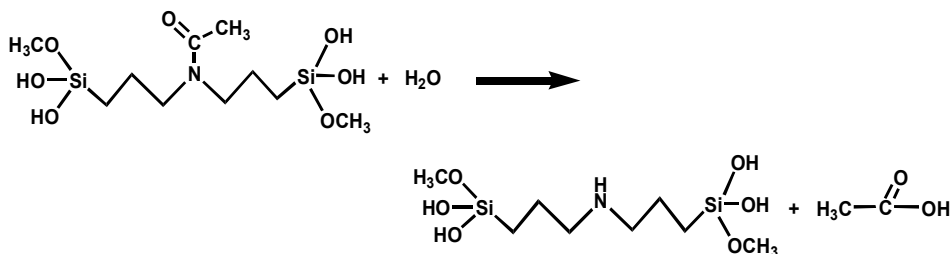
$^{13}\text{C}$  and  $^{29}\text{Si}$  spectra of the neat AV3.4 and 10 wt% AV3.4 water solution were shown in Figure H.28 and Figure H.29 respectively.  $^{29}\text{Si}$  NMR spectra were also recorded as the function of hydrolysis time from 80 minutes to 1740 minutes in order to monitor the hydrolysis and condensation of AV silane in water solution. The spectra are shown in Figure H.31.

In water solution, the amide complex formed in the neat AV mixture decomposes into bis-amino silane and acetic acid (Figure H.30). Bis-amino silane condenses into higher condensation products ( $T^2$  and  $T^3$ ). The lowest condensation product of bis-amino silane ( $T^1$ ) is absent. Time-resolved  $^{29}\text{Si}$  NMR reveals that the intermediate condensation product of bis-amino silane ( $T^2$ ) dominates due the high hydrolysis rate of bis-amino silane in the initial stage of hydrolysis. As hydrolysis time increases, the hydrolysis rate of neat bis-amino silane decreases, and the higher condensation

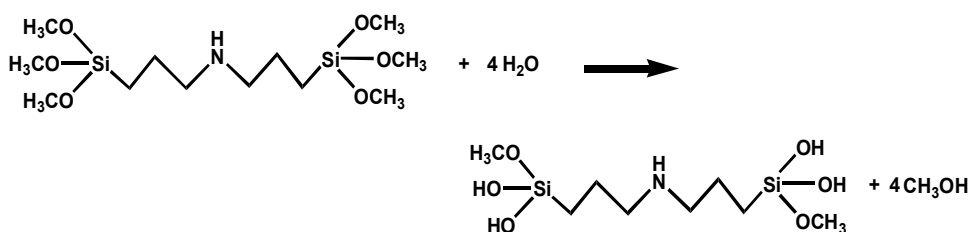
products ( $T^3$ ) increases at the cost of the intermediate condensation products ( $T^2$ ) as well as the uncondensed hydrolysis product of bis-amino silane.

The condensation products of VTAS are absent in the AV solution even when all the VTAS is hydrolyzed at 1740 minutes, which indicates the hydrolyzed VTAS is stabilized in the water solution. The weakly acidic silanol group (-OH) on hydrolyzed VTAS forms hydrogen bonds ( $NH \cdots OH$ ) with the strongly basic secondary amine group (-NH) on bis-amino silane. The OH group of VTAS is thus stabilized by secondary amine group and the condensation between the silanol groups of bis-amino silane and VTAS is retarded. The decrease of the solution pH by release of the acetic acid through the decomposition of the amide complex in the water solution also contributes to the stability of the AV solution.

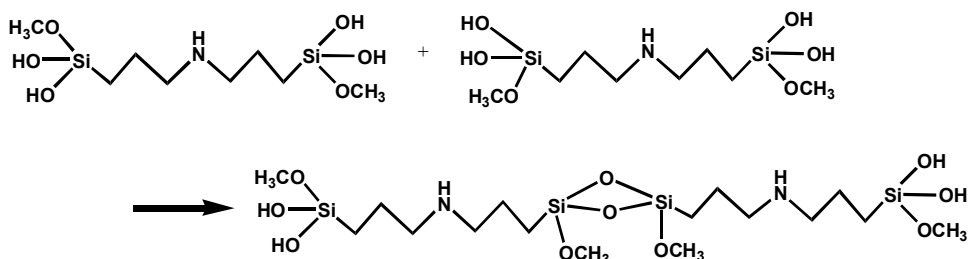
Figure H.32 shows the surface morphology of CRS after cleaning at different pHs. Distinct surface oxide morphologies are observed for CRS cleaned under different pHs and re-exposed to air. Coarse, loose and platelet surface oxide morphology was observed on CRS surface cleaned in strong acidic conditions (pH~1.0), which may be related to rapid dissolution of the Fe surface. A fine, dense and spherical surface oxide morphology was detected on the CRS surface cleaned in alkaline environments (pH~9.5 and pH~12.4) as shown in Figures H.32 (b) and H.32(c) which suggest that the alkaline cleaning condition facilitates the formation of a more protective surface oxide layer after exposure to air.



**Decomposition of amide complex in water solution**



**Hydrolysis of bis-amino silane**



**Condensation of bis-amino silane**

**Figure H.30. Possible reactions in the AV3.4 water solution, (a) Decomposition of amide complex in water solution, (b) Hydrolysis of bis-amino silane, (c) Condensation of bis-amino silane.**

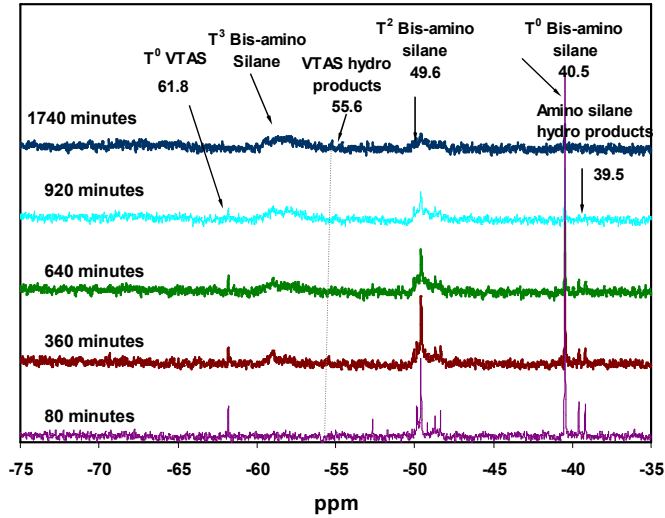


Figure H.31.  $^{29}\text{Si}$  NMR spectra after different aging times.

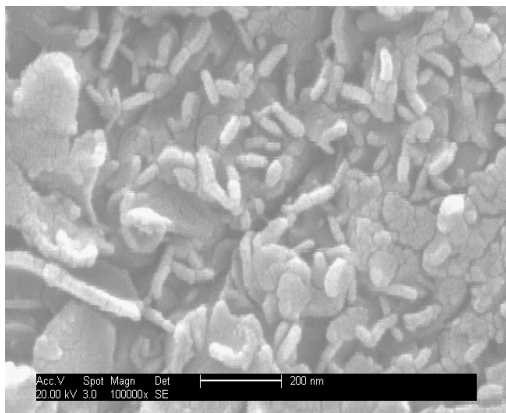
### Cleaning of cold-rolled Steel (CRS)

#### Surface morphologies of as-cleaned CRS surfaces

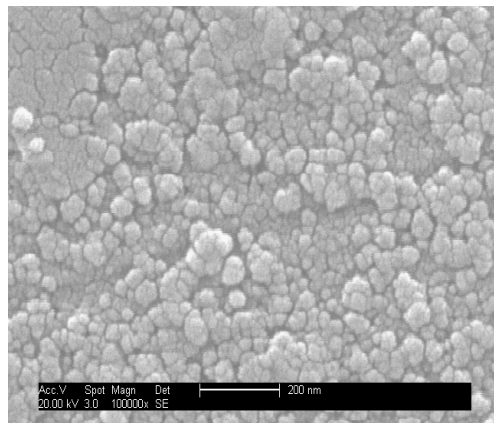
The coarse and loose surface oxide layer formed on CRS after cleaning in strongly acidic condition is inferior for the formation of a dense bonding layer between silane and CRS. The fine and dense surface oxide formed on CRS after cleaning in alkaline condition, on the other hand, is desirable for the formation of dense bonding layer between CRS and silane.

Figure H.33 shows the dispersive and polar components of the surface energy after cleaning in different pH conditions. It is detected that the dispersive component is relatively constant over the whole pH range, whereas the polar component has two minima over the whole pH range; one at pH~9.5 and another at pH~12.4. The minimum at pH~9.5 is understandable given the reported isoelectric point (IEP) of CRS, which is around 9-10. In aqueous solutions, the surface hydroxyl groups may remain undissociated, in which case the pH of the aqueous solution is the same as the IEP of the surface oxide.

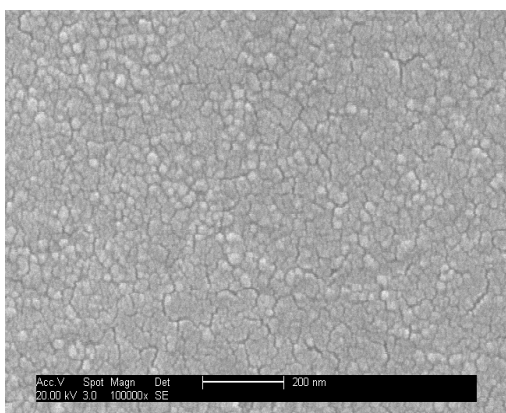
The surface charge and the isoelectric point (IEP) of CRS are schematically depicted in Figure H.34. The hydrolyzed AV silane solution contains weakly acidic silanol groups and strongly basic secondary amine groups. During the coating process, the AV silane can absorb on CRS via



(a)



(b)

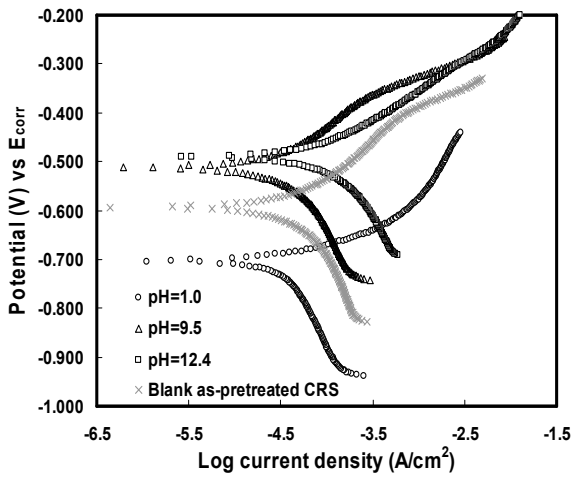


(c)

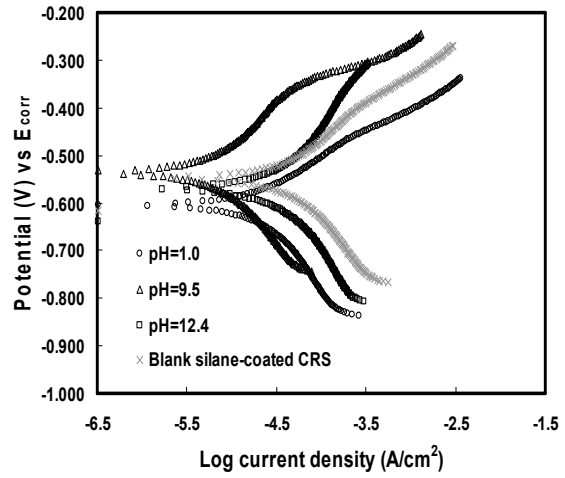
**Figure H.32 The surface morphology of CRS after cleaning at different pHs (pH~1.0, pH~9.5 and pH~12.4).**

hydrogen bonding both through silanol groups and secondary amine groups. Strong alkaline or acidic cleaning of CRS results in a charged surface as shown in Figure H.34, which is less favorable for the absorption of silane via hydrogen bonding of silanols and/or secondary amine groups. However, at near neutral conditions close to the IEP of CRS both these species are able to absorb through hydrogen bonding, which leads to increased bonding of AV silane onto CRS at mild alkaline pH around 9.5.





(a)



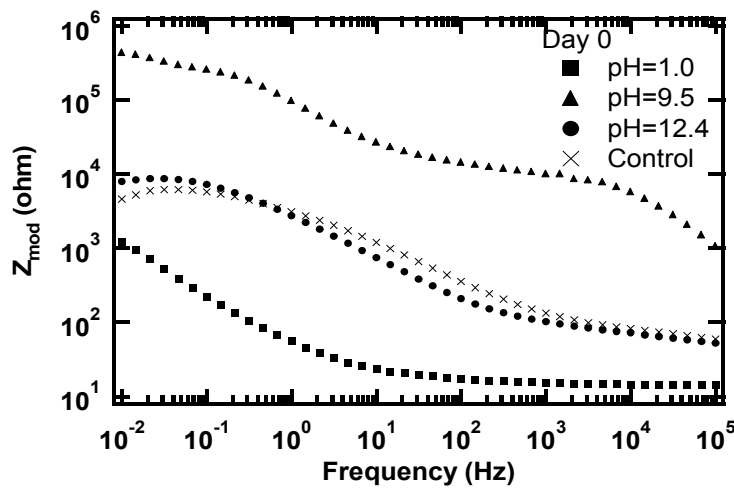
(b)

**Figure H.35. DC potentiodynamic curves of the (a) as-cleaned CRS panels (b) silane-coated at different pH values.**

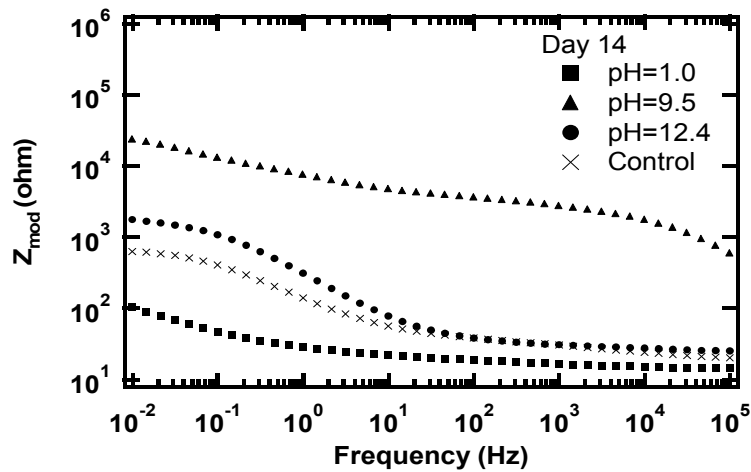
Figure H.35(b) shows the DC potentiodynamic curves of coated CRS panels cleaned at different pH values. Compared with the curves shown in Figure H.35(a), the shape of the DC polarization curves of the silane-coated CRS panels remains the same. The decrease in  $I_{\text{CORR}}$  after coating with silane indicates that the silane coating is dense and strongly bonded to the CRS surface, serving as an effective barrier against electrolyte. Cleaning is essential for the achievement of good bonding and anti-corrosion performance for silane coatings.

Figures H.36(a) and (b) show the Bode plots of impedance curves of primer-coated CRS panels cleaned under different pH conditions. Data are shown immediately after cleaning and after 14 days of salt immersion. The impedance moduli of the CRS panels cleaned in mild alkaline conditions (pH~9.5) are around  $10^5$  to  $10^6 \Omega$  and are 2 decades higher than for the panels cleaned in the other conditions. This result agrees well with the DC polarization test results.

More importantly, the primer-coated CRS panel cleaned at pH~9.5 reveals two time constants, one at low and another at high frequencies. The presence of an extra time constant in the low frequency range has usually been assigned to the formation of a layer between the coating and the metal oxide on a metal surface. The difference in the time constant behavior supports the conclusion that the formation of bonds between the coating and the CRS surface is most abundant after cleaning in mild alkaline (pH~9.5) conditions.



(a)



(b)

**Figure H.36 EIS results of primer-coated CRS on (a) day 0 and (b) day 14 in 0.6 M NaCl solution.**

After 14 days of salt-water immersion (Figure H.36b) the low-frequency modulus drops by one or two orders. However, the panels cleaned in mildly alkaline conditions (pH~9.5) still have higher impedance than those cleaned in all other conditions. For the panels cleaned at pH~9.5, the second time constant still exists, indicating survival of the bonding layer between the primer coating and the substrate after 14 days of immersion. For the control panels and those cleaned in acidic (pH~1.0) as well as in strongly alkaline (pH~12.4) conditions, only one time constant was observed after 14 days as on day 0.

### Water barrier properties of AV films

#### NR study of the water resistance of AV silanes

Figure H.37 shows the neutron SLD of AV coatings after water conditioning at room temperature. By comparing the SLD of the as-prepared state and the water-conditioned state, the volume-percent water can be calculated. Less water penetrates the coating near the stoichiometric ratio ( $A/V = 3.4$ ). Compared to the as-prepared state, the SLDs of the  $D_2O$ -conditioned films increase substantially with very small thickness increase, regardless of  $A/V$  ratio. All  $D_2O$ -conditioned films show enhanced SLD on both the air-side surface and the Si substrate interface implying a D-rich region attributed to  $D_2O$  absorption and D-exchanged protonated amino groups near the substrate, respectively.

The SLDs of the re-dried films almost return to their original as-prepared (dry) values after re-dry, which suggests the films are quite stable in water vapor. The small SLD increase between the dry and re-dried states may result from a chemical reaction resulting in the incorporation of deuterium into the film during conditioning.

### X-ray reflectivity (XR) on AV films

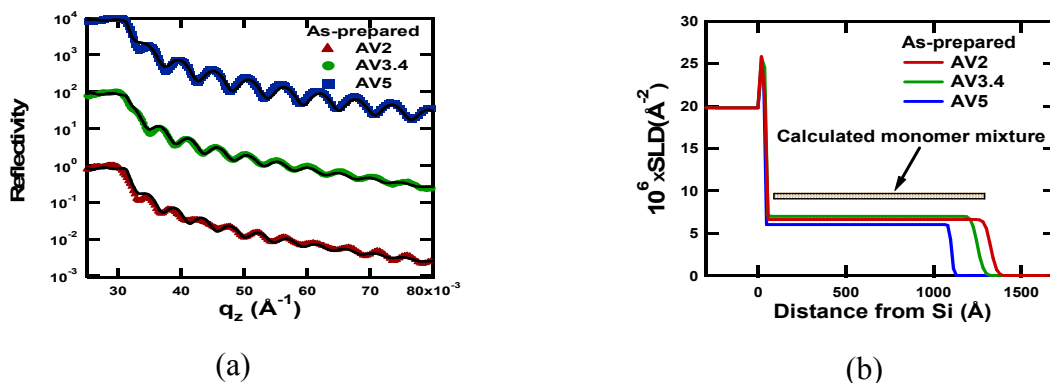
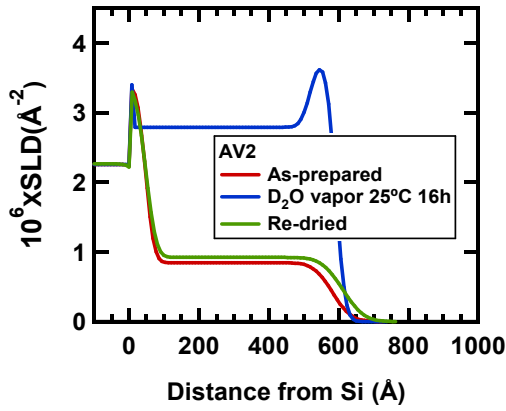
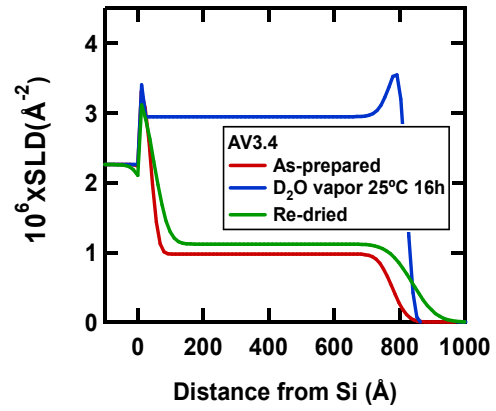


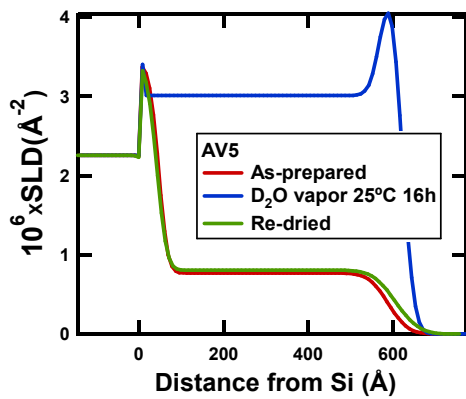
Figure H.38. X-ray reflectivity and SLD profiles of the as-prepared AV films at different  $A/V$  ratios.



(a)



(b)



(c)

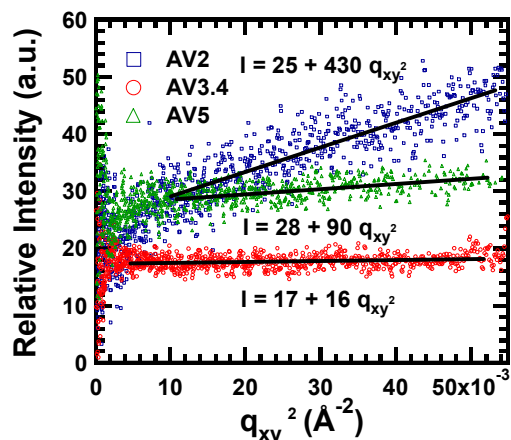
**Figure H.37. NR results showing the water response of AV mixtures with A/V ratios. Minimum water absorption is observed near the stoichiometric film (A/V = 3.4).**

Figure H.38(a) shows the XR data of as-prepared films as a function of A/V ratio. Figure H.38(b) shows the SLD profile. A typical SLD profile can be divided into three regions: the wafer substrate, the native surface oxide and the silane film. The bottom surface of the native  $\text{SiO}_2$  layer is designated as zero distance.

According to the best-fit SLD profiles, all the films have a nominal thickness of around  $1200 \text{ \AA}$ . The experimentally determined SLDs ( $6 \times 10^{-6} - 8 \times 10^{-6} \text{ \AA}^{-2}$ ) for different AV ratios are substantially less than the calculated SLDs of both the monomer mixtures and all-possible reaction products. Since the monomer densities were employed in the SLD calculation, these results imply that the film densities are below that of the monomer precursors. The reaction between bis-amino silane and the VTAS must produce considerable void space either in the form of pores or molecular-level free volume. The density of the films can be estimated as  $0.69 \text{ g/cm}^3$ ,  $0.80 \text{ g/cm}^3$  and  $0.65 \text{ g/cm}^3$  for AV2, AV3.4 and AV5, respectively.

### Grazing incidence small angle scattering (GISAXS)

In order to understand the nature of the ~30-vol% void space detected in the as-prepared films, grazing incidence small angle scattering (GISAXS) was performed. GISAXS is sensitive to fluctuations in electron density in the length-scale range  $< 100 \text{ \AA}$ .



**Figure H.39.** The scattering from the bulk film obtained by subtracting the surface scattering from the total scattering.

The scattering from the bulk film obtained by subtracting the surface scattering from the total scattering are shown in Figure 39 after normalizing the intensity by the beam path length in the film. The lowest scattered intensity is observed for AV3.4, implying that the near-stoichiometric film is the most uniform. AV3.4 also shows the weakest  $q$ -dependence. AV2 film shows highest intensity and weakest  $q$ -dependence, both of which imply that it is most homogeneous.

### Conclusions regarding the AV System

- $^{13}\text{C}$  NMR spectra show that the primary reaction in neat AV3.4 silane mixture is the exchange of the hydrogen atom on secondary amine group of bis-amino silane with the acetoxy group of VTAS forming an amide complex and hydrolyzed VTAS. The primary reaction is followed by a series of hydrolysis and condensation reactions of bis-amino silane and VTAS and their reaction by-products.
- In water solution, the amide complex formed in the neat AV mixture decomposes into bis-amino silane and acetic acid. Bis-amino silane condenses into higher condensation products ( $T^2$  and  $T^3$ ). The lowest condensation product of bis-amino silane ( $T^1$ ) is absent.
- Time-resolved  $^{29}\text{Si}$  NMR reveals that the intermediate condensation product of bis-amino silane dominates due to the high hydrolysis rate of bis-amino silane in the initial stage of hydrolysis. As hydrolysis time increases, the hydrolysis rate of neat bis-amino silane decreases, and the higher condensation products increase at the cost of the intermediate condensation products as well as the uncondensed hydrolysis product of bis-amino silane. The condensation products of VTAS are absent in the AV solution even when all the VTAS is hydrolyzed at 1740 minutes, which indicates the hydrolyzed VTAS is stabilized in the water solution.
- Based on the NMR results and previous observations on the stability of the AV mixture, a model of the AV solution stabilization is proposed. The weakly acidic silanol group ( $-\text{OH}$ ) on hydrolyzed VTAS forms hydrogen bonds ( $\text{NH}\cdots\text{OH}$ ) with the strongly basic secondary amine group ( $-\text{NH}$ ) on bis-amino silane. The OH group of VTAS is thus stabilized by secondary amine group and the condensation between the silanol groups of bis-amino silane and VTAS is retarded.

The decrease of the solution pH by release of the acetic acid through the decomposition of the amide complex in the water solution also contributes to the stability of the AV solution.

5. The best performance results were obtained for the silane-coated and primer-coated CRS panels cleaned near the isoelectric point of CRS. At the IEP, the surface oxide is dense and spherical with the highest surface FeOOH/Fe<sub>2</sub>O<sub>3</sub> ratio. The nearly neutral surface, promotes hydrogen bonding of both silanols and secondary amine groups to the CRS surface. FTIR indicates that acidic (pH~1.0) and mild alkaline cleaning conditions (pH~9.5) result in the formation of long-chain siloxane whereas the strong alkaline cleaning condition (pH~12.4) inhibits the long-chain siloxane formation.

6. The structure of AV films was studied with XR and GISAXS, and the interaction of water in the films was also explored with NR as function of A/V mol ratio. The XR experiments show that considerable void space exists in as-prepared films regardless of AV ratio. The void space is minimized near the stoichiometric ratio due to higher crosslink density at stoichiometry. GISAXS indicates that the void space exists as molecular-level density fluctuations.

7. On water exposure one penetrant population is dissolved in polymer matrix and the other physically occupies unrelaxed void space. Most of the water is accommodated in void space of film during water-vapor conditioning with the least amount being absorbed near stoichiometry. A small SLD change and irreversible thickness change in redried film implies chemical interaction of the film with water. The largest degree of chemical alteration between the as-prepared and the redried states is observed near the stoichiometric A/V ratio. The chemical alteration is attributed to reaction of water with the amide complex.

## **Epoxy-silane system**

### **Objective**

Based on previous work, bis-silanes perform as coupling agents in anti-corrosion films, which make them promising alternatives to chromate metal pretreatment in metal-finishing industries. However, silane films have limitations in mechanical properties. Silane films thicker than 0.3 μm are subject to cracking; Epoxy resin has superior chemical and corrosion resistance as well as outstanding mechanical toughness. van Ooij *et al.* have established an excellent coating system with fairly high hardness based on mixture of epoxy (EPI-REZ™ 5003-W-55) and bis-silane (bis-sulfur).

The purpose of this work is to study the underlying mechanism of anti corrosion performance. The water barrier, hydrothermal degradation and salt exclusion properties of epoxy-silane coating system were investigated. The major conclusions are summarized at the end of the section.

## **Project Accomplishments**

### **Water barrier properties**

#### **Film structure**

Neutron reflectivity (NR) experiments were carried out on SPEAR at Lujan Center, Los Alamos National Lab. Figure 40 gives the structure of epoxy-silane film in the as-prepared dry state. Based on the known SLDs of the constituents and the measured SLD profile (Figure H.40b), the mixed epoxy-silane film is not uniform normal to the substrate surface. Based on the drop in the SLD near the substrate a highly condensed silane-rich layer exists at the film-substrate interface.

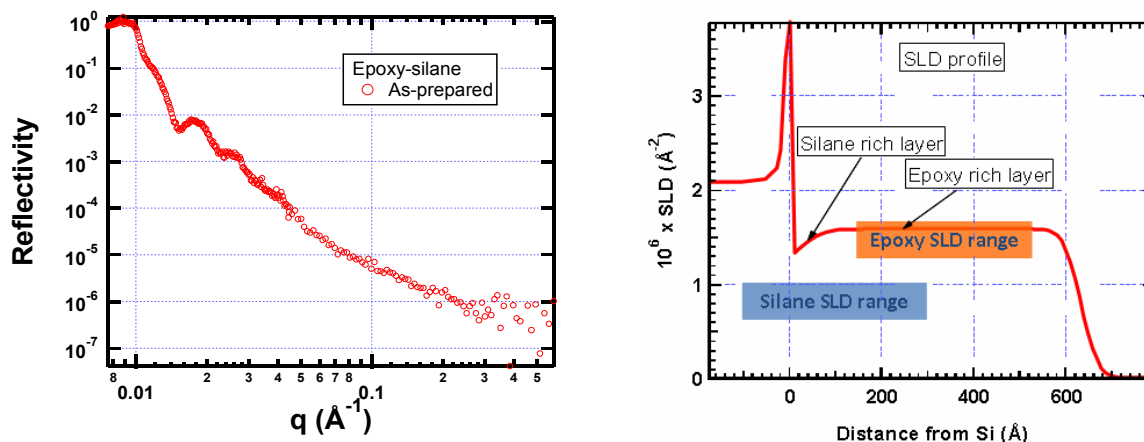


**Figure H.40. Neutron reflectivity data and best-fit SLD profiles of mixture of EPI-REZ™ 5003-W-55, bis-sulfur and curing agent in the as-prepared state.**

### Response to water

#### Vapor conditioning

The SLD profiles of pure epoxy and epoxy-silane mixture samples, dry and at equilibrium with saturated D<sub>2</sub>O vapor, are shown in Figure H.41. For both samples, there is no significant film swelling. A water rich top layer was observed for both cases. The water concentration is lower for the mixed sample (3% volume) than for pure epoxy sample (6% volume). Moreover, for the mixed sample, the condensed silane-rich layer at the film-substrate interface is hydrophobic. The SLD of this layer only slightly increases after the whole coating reaches equilibrium with heavy water vapor. The silane layer provides good adhesion and water barrier properties, which is a significant factor leading to the favorable anti-corrosion performance of this epoxy-silane system.

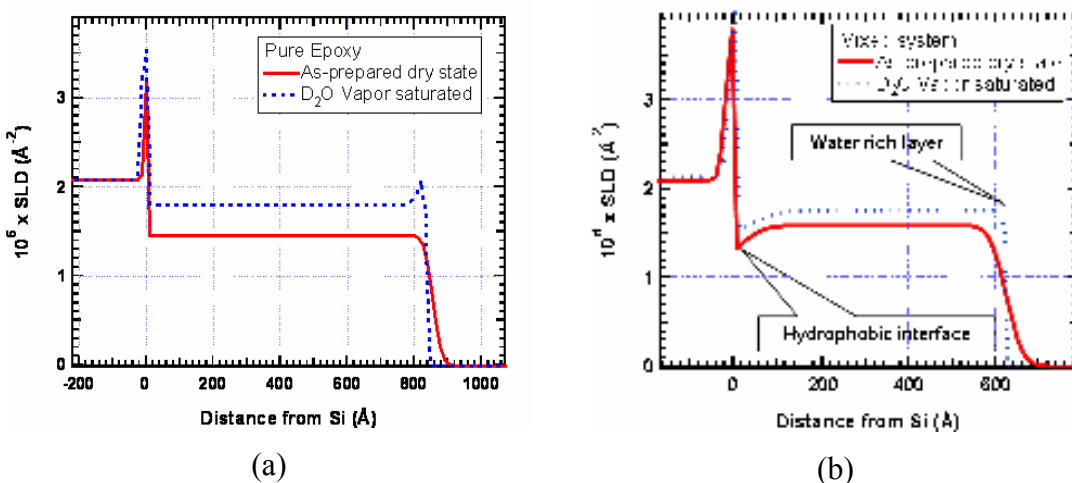


**Figure H.41. D<sub>2</sub>O vapor conditioning at room temperature (a) pure epoxy; (b) epoxy-silane**

A kinetic study of water absorption in saturated D<sub>2</sub>O vapor environment was also carried out at LANL. Rapid NR scans were performed to track the water uptake process. As shown in Figure 42

both pure and mixed systems reach equilibrium within half an hour. This result indicates that the overall hydrophobicity of bulk film is low. Water enters film readily and penetrates the entire bulk film in a short period. It is believed that the highly condensed hydrophobic silane-rich interfacial layer provides the critical anti corrosion protection.

### Liquid water contact

As shown in Figure H.43, when treated with liquid D<sub>2</sub>O, similar behavior was observed as the case of D<sub>2</sub>O vapor conditioning. The thicknesses of the film remains constant. More water is absorbed, however, when directly contact with liquid water. The D<sub>2</sub>O volume fractions are 10vol% and 6vol% for pure and mixed film respectively, which indicates that the mixed film is more hydrophobic because of the presence of bis-sulfur silane. Liquid D<sub>2</sub>O penetrates the entire film for pure epoxy sample while the mixed film retains the hydrophobic silane-rich layer located at the SiO<sub>2</sub>-film interface.

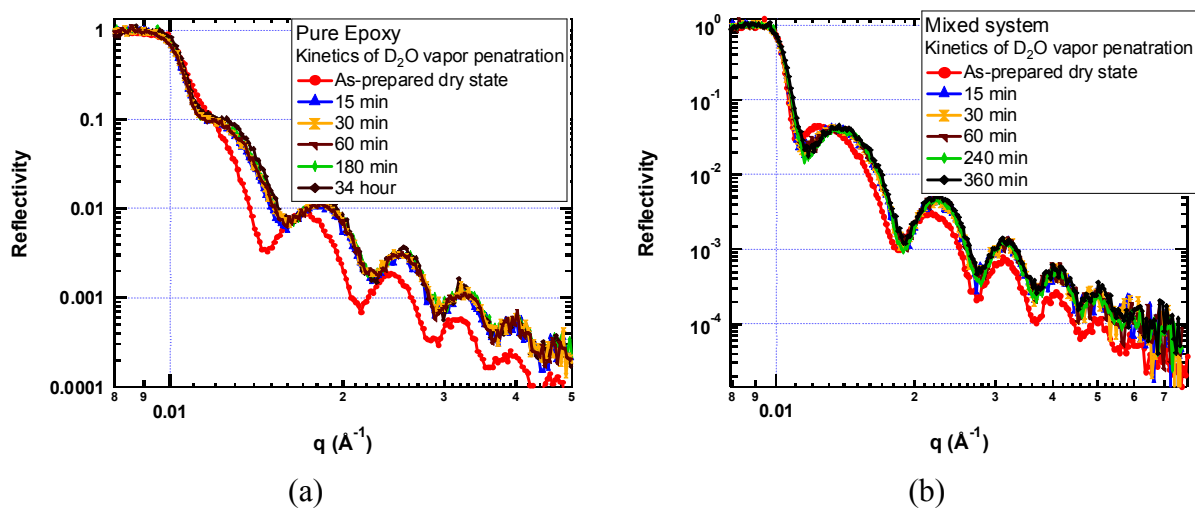
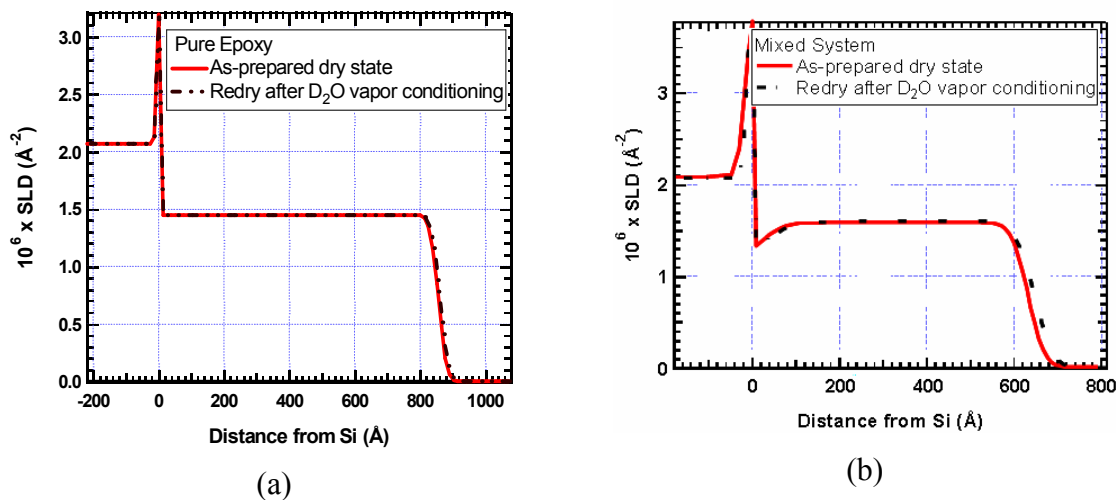


Figure H.42. Kinetic water uptake under saturated D<sub>2</sub>O vapor conditioning (a) pure epoxy; (b) epoxy-silane mixture

### The re-dried state

Figure H.44 gives the SLD profiles of re-dry state. According to these SLD profiles, the films recover both physically and chemically after exposure to water vapor. The SLDs return to the as-prepared dry state and there is no significant thickness change.



**Figure H.44. Re-dry state (a) pure epoxy; (b) epoxy-silane mixture**

### Hydrothermal degradation

Neutron reflectivity data were obtained for the films as-prepared and also after 10, 24 and 36 hours exposure to 80 °C liquid water and subsequent re-drying (Figures H.45 and H.46). We found that

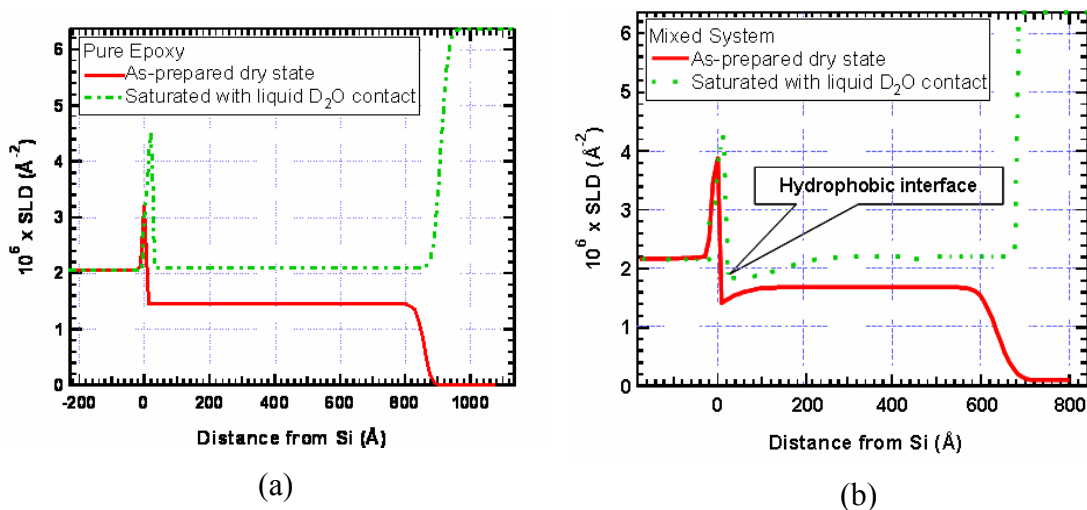


**Figure H.43. Liquid water contact conditioning (a) pure epoxy; (b) epoxy-silane mixture**

neither pure epoxy nor epoxy-silane anti corrosion film is robust in hot water

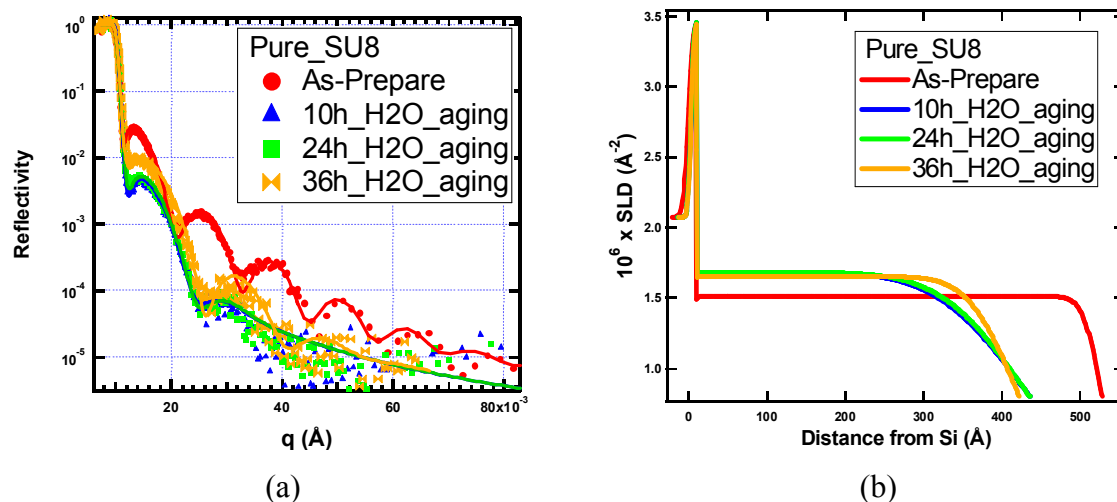


**Figure H.45. Aging of pure epoxy sample in 80 °C liquid water. (a) experimental reflective curves; (b) best-fit SLD profiles**

### Pure epoxy

The experimental NR curves and best-fit SLD profiles of different periods of aging as presented in Figure H.45. Fast degradation occurs in the first 10 hours. The film shrinks 20%. The overall film density drops 10%. After that, the system reaches a stable plateau up to 24 hours of aging. After 24 hour, the thickness and SLD of pure epoxy film begins to drop slowly, which indicates that mass loss occurs both at the surface and in the films.

### Mixed epoxy-silane system

As shown in Figure H.46, the mixed film behaves differently from pure epoxy films. The bulk film swells and its SLD drops, but there is integrated no mass loss of the bulk film until 24 hours of aging. After 24 hours, the bulk film begins to shrink, but the SLD remains constant, which indicates that the top of the film starts to degrade. The highly condensed silane-rich interfacial layer is robust even after 36 hours of exposure. This result supports the idea that this special layer plays a key role of anti corrosion protection.

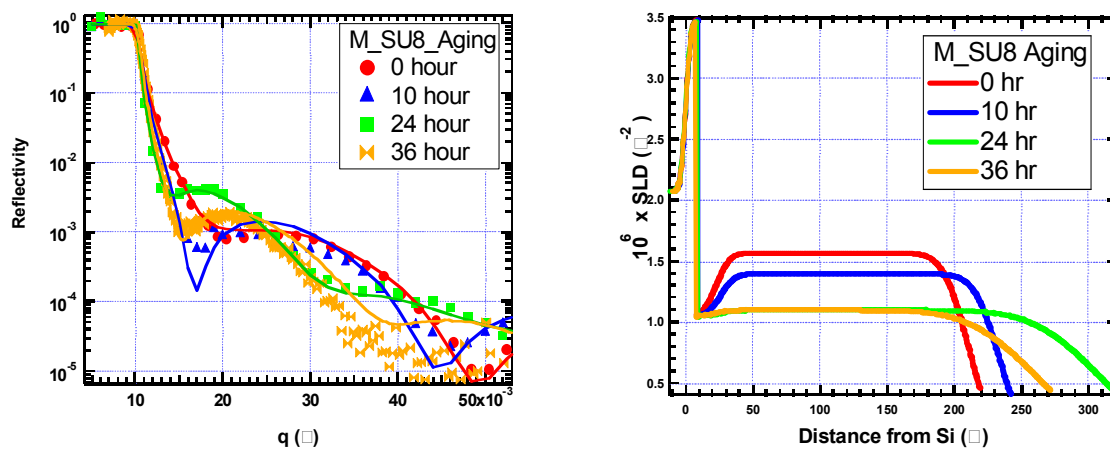


**Figure H.46. Aging of epoxy-silane sample in 80 °C liquid water. (a) experimental reflective curves; (b) best-fit SLD profiles**

reflective curves; (b) best-fit SLD profiles.

### Salt exclusion

#### Pure epoxy

Pure epoxy is not a salt barrier. After conditioning with saturated NaCl solution, the salt fraction inside the film is 2vol%, which can be calculated by the SLD profile shown in Figure H.47. The SLD increase at the film-substrate interface is caused by the salt accumulation. After re-dry, the SLD of the coating film does not return to the as-prepared value, which means there 2vol% salt remains in the pure epoxy film. There is also a salt rich layer at the top surface for re-dried state, which results from salt crystallization on the surface in the re-dry process.

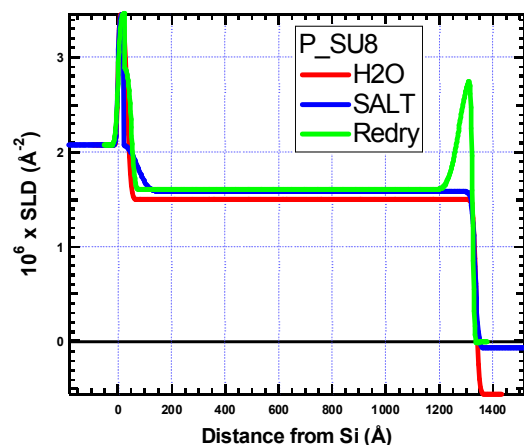


Figure H.47. SLD profiles of salt exclusion experiments on pure epoxy coating.

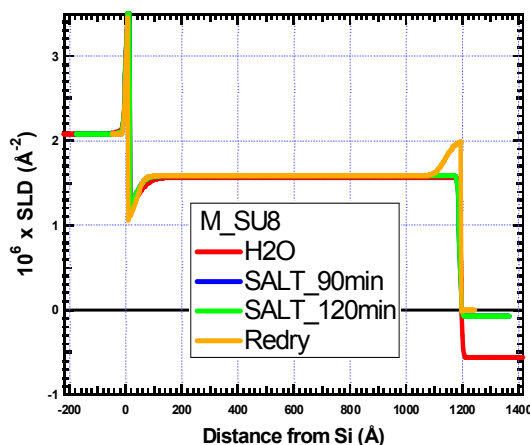


Figure H.48. SLD profiles of salt exclusion experiments on epoxy-silane mixed coating.

#### Epoxy-silane mixed film

By contrast to the pure epoxy system the epoxy-silane mixture is a salt barrier. After conditioning with saturated NaCl solution, salt is excluded from the film. According to the SLD profiles shown in Figure H.48, the SLD of film remains unchanged. After re-dry, the SLD of the coating film recovers the as-prepared value, which again indicates there is no salt in the film after salt solution treatment. The salt-rich layer on top surface is due to the crystallization of salt when re-dried.

#### Conclusions regarding the epoxy-silane system

1. The epoxy-silane mixed coating system has a layered structure. The bis-sulfur silane is rich at the film-substrate interface and forms a highly condensed, hydrophobic interface. This interface accounts for the good adhesion and water barrier properties of epoxy-silane coating system. The water is absorbed physically inside molecular level free space inside the film without swelling the film. After re-dry, the film recovers the original virgin state.
2. The bulk film of neither pure epoxy nor the epoxy-silane mixture is a water barrier. When exposed to water vapor or liquid, water penetrates the film and saturates the film in half an hour. The water is stopped by the interfacial silane-rich layer.
3. Neither pure epoxy nor epoxy-silane is robust under hydrothermal aging. Pure epoxy film

shrinks after aging. The overall film density drops 10% in the first 10 hours of aging. The system has a stable plateau between 10 to 24 hours of aging. After 24 hour, the mass loss continues both at surface and in the bulk of film. The mixed film behaves differently from pure epoxy. The bulk film swells without mass loss until 24 hours of aging. After 24 hours, the bulk film begins to shrink, the top of the film starts to degrade. The condensed silane-rich interfacial layer is robust even after 36 hours of exposure to a hydrothermal environment. This result supports the idea that this special layer plays a key role of anti corrosion protection.

4. The presence of silane in an epoxy film leads to the exclusion of salt. This observation seems to be the most important factor accounting for the improved protection of silane-laced films.

## IX. CONCLUSIONS

### Overview of achievements of this project

The overall result of this project is that we have developed two primer systems consisting of bis-silanes and water-dispersed resin systems, optionally containing anti-corrosion pigments. Some of these chromate-free pigments were also developed in this project. Such primers are novel and patented by The University of Cincinnati with subsequent exclusive licensing to ECOSIL Technologies LLC. The latter now has the capability to manufacture the primers and supply them to military and commercial customers.

The utility of the outcome of this project is that the combination of metal pretreatment (phosphating, chromating) and anti-corrosion primer in many areas of industry and military operations can be replaced with one of our primers. Currently there is much research effort spent on a worldwide scale to develop new metal pretreatments that can replace the chromate pretreatment. Examples of products that are commercially available are trivalent chromium, Cr(III), and various zirconium-containing products. Such products individually work reasonably well, but on a continuous line they suffer from the drawback that they are much less robust than a chromating line. For instance, when a line stalls, the metal part is oxidized. The chromating bath is so acidic that this oxide is easily removed. This is not the case on an Cr(III) line or a zirconate line, since these baths have higher pH values. The same argument can be made for contamination by oils or other organic materials. In a Cr(VI) line, such oils are removed by the acidic chromate solutions, but not by the chromate replacements. In summary, the newer treatments are less robust than the chromating process. Therefore, the results with the newer treatments are generally disappointing. No treatment has been put forward that has the same overall universal properties as Cr(VI).

Much less development work has been performed in the field of primers or anti-corrosion pigments. Our products are unique, therefore. We have developed anti-corrosion pigments that were tailored for water-borne primers. The understanding of the mechanism by which pigments work has been improved in this project. For instance, zinc phosphate is a known pigment, but its performance in commercial solvent-borne epoxy primers is not outstanding. However, in our superprimers, it rivals, and often exceeds, the performance of chromates. The hydrophilicity of films formed from water-based polymers is used to our advantage. The degree of leaching of the phosphate from our primers is much greater than from solvent-borne coatings, in which they have been tested before. A saturated zinc phosphate solution, even in a 5% NaCl solution, was found by us to be an extremely effective inhibitor of the corrosion of AA2024-T3 and AA7075-T6 alloys, despite the extremely low concentration of  $Zn^{2+}$  and  $PO_4^{3-}$  in a concentrated solution. The strong inhibiting performance of zinc phosphate is one of the important findings of this project. The effectiveness of zinc phosphate in coatings made from water-borne coatings is another result of the project.

The relatively high hydrophilicity of our coatings is not an impediment to their performance. We have found, in reflectivity studies by neutrons and X-rays, that the water absorbed by our coatings is absorbed in molecular voids of the coatings. As a result, the adhesion of the coatings is not impaired by the water absorption. That is because the superprimer films do not swell appreciably in water.

Another remarkable property of our primer films, which is different from current commercial primer films, is that in films formed mixtures of silanes - added without hydrolysis - and water-dispersed resins such as epoxies or epoxy-acrylates, the interface region close to the metal is very hydrophobic.

This hydrophobicity increases further with time after deposition of the films. Although we do not fully understand the mechanism of the formation of this region, it can be stated that this film acts as a built-in protection against corrosive attack by water and electrolyte ingress into the films.

The figure below gives a tentative but plausible explanation of the formation of that hydrophobic region. The silane hydrolyzes and condenses throughout the entire primer film, as a result of the high level of water contained in it and later during ingress of water into the hydrophilic coating. Since the silane in the primer is diluted by resin, it cannot form a three-dimensional siloxane network, but it forms siloxane nanoparticles instead. These particles are hydrophobic, but the concentration is too low to affect the bulk of the primer film, however. Due to phase separation effects, the siloxane concentration will be higher in a region close to the interface. Their concentration can become so high that a thin region effectively becomes a barrier to water or electrolyte diffusion and the metal is protected even in situations of long immersion in water or salt solutions.

Another possibly very important finding of this work is that it has been found feasible to deposit the primer films, after only minor modification of the formulation by using electrodeposition (see contribution by Liang Liu). The significance of this finding is that it may be possible to eventually simplify the pretreatment line in the automobile industry. Such a line currently is about 800 meters long and consists of about 15 steps or operations, viz., several zinc phosphating and a number of electrocoat steps. Since our primer technology does not require zinc phosphating, it may be possible to reduce such a line to about 5-6 steps consisting of cleaning, rinsing, electrodeposition and curing of the film. However, as Liang Liu's report indicates, the optimum conditions for this technology have not yet been established. Considerably more work needs to be done. However, it has been demonstrated that a combination of cathodic followed by anodic electrodeposition yields films with better corrosion protection of metals such as HDG, than by dipping and curing alone. For the automobile industry, electrodeposition is and remains the technology of choice because of the high throwing power of the process.

The mechanism of the improved deposition process has not yet been studied in any detail, but it has been shown that in the cathodic step the silane migrates to the metal surface, where it hydrolyzes and condenses as a result of the water decomposition, which increases the pH. The resin dispersion, which is anionic, is not much affected by this pH increase. However, during the subsequent anodic deposition step in the same bath, the anionic resin precipitates on the silane-coated metal which is now the anode. The result is a crosslinked polymer film with a strong interfacial silane enrichment, as if the coating had been deposited in a two-step process, viz., a silane bath first followed by a dip in superprimer mixture.

Other findings in this project which are worth mentioning are the following.

- A simple but effective test for the performance of an anti-corrosion pigment in a primer has been developed. We have thus far tested it in primers made from water-borne systems only, but there is no reason why it would not work for any primer. The test consists of scribing a primed panel as usual and then exposing it to a flowing salt water bath. The flow rate is controlled and varied between 0 and 20 cm/min. The condition of the scribe (i.e., presence of corrosion products) is evaluated after 30 days. Those pigments with the least rust after 30 days are the most effective. Some pigments do well at slower flow rates, but fail at the higher flow rates. Chromate is still effective at 20 cm/min.

- Several new pigments for use in water-borne primers on cold-rolled steel (CRS) were discovered in the last stages of the project. This is also significant, as there not many chromate-free primers for water-borne primers on the market. The pigments are mixed phosphates or borophosphates and work especially well with our epoxy-acrylate superprimers. Such systems do not form flash rust, a known problem with water-borne systems on CRS. They could be developed as a result of our understanding of the mechanism of our primers and pigments such as zinc phosphate. An important conclusion of these studies was that there is a balance or relationship between the hydrophilicity (water uptake) of the primer coating and the solubility of the pigment. Therefore, pigments like strontium chromate did not work too well in our superprimers on CRS, as their solubility was too high. The mixed phosphate pigments were optimized in solubility so that the corrosion-inhibiting active ions ( $\text{Ca}^{2+}$  and  $\text{PO}_4^{3-}$ ) were leached out at an optimized rate.
- A final result obtained late in the project is that the primers can be divided up in two formulations that can be mixed shortly before application by dipping, rolling, brushing or spraying. The two individual formulations (the "packs") have a shelf life of at least 6 months when stored at room temperature. After mixing the primer has a pot life of at least 6 hours. Thus, these conditions come very close to industrial or military requirements.
- Earlier in the project we had reported on a series of novel chromate-free pigments specifically for use of the primers on aluminum alloys. Later on they were also found to be effective on hot-dip galvanized steel (HDG). In addition to the finding that micronized zinc phosphate, a commercial material, can replace chromates in water-borne primers on Al and HDG when mixed with silica, we have also developed the following new pigments: cerium-exchanged silica, cerium vanadate, and cerium silicate.

The conclusions from the work done by co-PI Schaefer, who studied the background mechanisms of the performance of silane films and, subsequently, of films containing silanes and resins, are the following.

- All silane films and silane-laced epoxy films absorb water. In most cases, the water uniformly occupies the bulk of the film. The bridging group controls the amount of water in the film. Bis silane films are the most hydrophobic.
- The substrate does not play a key role for the water barrier properties of silanes.
- Two absorption modes are observed: Henry's mode, which is related to the relaxation of the siloxane network and Langmuir's mode, which is related to the physical occupation of pre-existing free space. Langmuir absorption mode dominates the total absorption.
- At elevated temperature, water conditioning leads to chemical reactions for all films studied. Bis-amino silane films show monotonic degradation. For bis-sulfur films, further condensation takes place, which improves the protective character. Pure bis-sulfur films above 1000 Å are robust.
- Mixed silane films show unusual cure chemistry. The primary reaction in neat bis-amino-VTAS silane mixtures is the exchange of the hydrogen atom on secondary amine group of bis-amino silane with the acetoxy group of VTAS forming an amide complex and hydrolyzed VTAS. The primary reaction is followed by a series of hydrolysis and condensation reactions of bis-amino silane and

VTAS and their reaction by-products.

- The epoxy-silane mixed coating system has a layered structure. Silane is rich at the film-substrate interface and forms a highly condensed, hydrophobic interface. This interface accounts for the good adhesion and barrier properties of epoxy-silane coating system.
- The condensed silane-rich interfacial layer in the epoxy-silane system is robust in a hydrothermal environment, whereas the bulk of the film is not. This result supports the idea that this special layer plays a key role of anti corrosion protection.
- The presence of silane in an epoxy film leads to the exclusion of salt. This observation seems to be the most important factor accounting for the improved protection of silane-laced films.
- Cleaning is critical to performance. The best performance results were obtained for the silane-coated and primer-coated CRS panels cleaned near the isoelectric point where the surface oxide is dense and spherical with the highest surface FeOOH/Fe<sub>2</sub>O<sub>3</sub> ratio. The nearly neutral surface, promotes hydrogen bonding of both silanol groups and secondary amino groups to the CRS surface.

Economic feasibility of the primers and pigments developed in WP1341

All the components of our primers are readily commercially available, with the exception of the cerium or phosphate pigments mentioned above, if used. We have not made a detailed economic analysis of the primers in this project, because there are too many uncertainties. However, in products currently marketed by ECOSIL Technologies LLC that are based on this technology, the products cost roughly the same as currently used solvent-borne products that require a chromate pretreatment (of HDG). Thus the technology is certainly feasible and economically viable.

The uncertainties mentioned above relate to the size of the shipment. Components in our primers that are relatively expensive are the silanes. The resin dispersion are comparable in price to the solvent-based ones. So, where our process is of lower cost is in the absence of organic solvents, the absence of a metal pretreatment (other than cleaning, which is the same as in current technology). Where our products are more expensive, is in the use of the silanes, which are absent in currently used primers. The zinc phosphate pigment is of the same cost level as chromate pigments, the cerium-based pigments are a factor 2 more expensive. Where our technology also scores more favorably is in the cost of waste disposal. Our primer solutions do not contain toxic components and, therefore, do not require any special processing or treatment prior to disposing of them as waste.

Although the silanes were mentioned as the factor with the highest cost, typically costing between \$30-50 per kg, the actual cost of the primer will depend appreciably on the amount of silane added. Silanes differ considerably in cost, depending the type. Typical silane prices are \$20-\$60 per kg, if bought in small amounts. These prices will drop considerably, e.g., more than by 50%, for large quantities, starting at 200-L drums. Thus, the cost of the primer depends, to a large degree, on the type of silane used, the amount added and the volume of the primer sold.

### **General attractiveness**

The attractiveness of the systems developed here are obvious. They contain much less VOC than currently used primers in many industries and in military devices, aircraft, vehicles, ships, etc.. The main objective of the project, eliminating chromate from anti-corrosion primers, has been fully met.

Both the chromate pretreatment and the chromate pigment have been eliminated or replaced with other materials. The performance in salt spray testing, salt immersion and outdoor exposure, as well as adhesion and chemical resistance is practically equivalent. Therefore, they can find applications in the automotive industry (components, not car bodies, which would require electrodeposition, see earlier), aerospace (military and commercial aircraft), coil coating lines and even on ship hulls. For all these applications we have novel, chromate-free pigments available. Further, the exact formulation and the curing conditions for each of these applications need to be optimized. The flexibility of our process allows such optimizations to be performed.

### **Unresolved issues**

Before our results can be routinely applied in some of the areas suggested above, more work needs to be performed. Some of these experiments are already being handled by and at ECOSIL Technologies. At this stage, some of the unresolved issues are the following.

- We need more outdoor exposure data; due to a glitch in the sample handling by DACCO SCI, our panels were only exposed for slightly over 300 days instead of more than one year; on the other some preliminary primer versions were exposed, with good results, for over two years in Hawaii.
- The electrodeposition process of the primer, which has huge applications in the automotive industry, needs to be sorted out and developed further; there are so many variables here that we have not been able to complete this task in the project; it was not one of our objectives at the start of the project to include electrodeposition as one of the methods of application; however, in another project we discovered the benefits of electro-assisted deposition of silanes by themselves, so we tried the process on the complete primer formulation and obtained encouraging results.
- We need more data on certain properties of the primers such as resistance to many chemicals, oils and lubricants; so far the resistance against NaOH and HCl in standard ASTM tests has been tested with positive results.
- An issue not addressed in this project is how the primers (or the topcoated primers) can be removed or repaired. After complete cure, silanes are very resistant to solvents, so it will not be easy to remove the primers for repainting or repair.
- The data that needs to be collected as per bullets 1, 3 and 4 could conceivably form the topic of an ESTCP project. However, the PI of project WP1341 will retire from the University of Cincinnati on September 1, 2008, so he will not be available to prepare such an ESTCP or work on it.
- The transition situation for this technology is good, as ECOSIL Technologies LLC is already in place. ECOSIL is the exclusive licensee of the University of Cincinnati for this technology and is ready to manufacture and sell or sub-license to commercial and military customers. ECOSIL is working in JDAs with companies like PPG and Dow Corning on large applications in the coil coating, automotive and aerospace industries.

## **X. SUPPORTING DATA**

This section contains data not included in section VIII. Results and Accomplishments (from Sect. IX). Since almost all of the data collected in this project were included in University theses, we have decided to include the complete theses in this section. Links are provided to the following theses.

**Trilok Mugada** - MS - superprimer for cold-rolled steel

**Chetan Shivane** - MS - superprimers for hot-dip galvanized steel

**Akshay Ashirgade** - MS - superprimers for aluminum alloys

**Zhangzhang Yin** - PhD - draft thesis on pigments in superprimers for aluminum alloys

**Guirong Pan** - PhD - water uptake of silane films (neutron scattering)

**Yimin Wang** - PhD - reactions between silanes (neutron and X-ray scattering)

**Peng Wang** - PhD - study of silane-resin films (neutron and X-ray scattering)

# UNIVERSITY OF CINCINNATI

Date: April 12, 2006

I, Trilok Ranjan Mugada,  
hereby submit this work as part of the requirements for the degree of:  
Master Of Science

in:

Material Science And Engineering

**It is entitled:**

"SUPERPRIMER": Chromate-free Coating System for DoD Applications

\_\_\_\_\_  
\_\_\_\_\_  
\_\_\_\_\_

**This work and its defense approved by:**

Chair: Dr. William van Ooij  
Dr. Relva C. Buchanan  
Dr. Jude Iroh  
\_\_\_\_\_  
\_\_\_\_\_

# **“SUPERPRIMER”: Chromate-Free Coating System For DoD Applications**

A dissertation submitted to the

Division of Research and Advanced Studies

of the University of Cincinnati

In partial fulfillment of the

requirements for the degree of

**MASTER OF SCIENCE**

In the Department of Chemical and Materials Engineering

of the College of Engineering

By

**TRILOK RANJAN MUGADA**

B.Tech, Chemical Engineering

Jawaharlal Nehru Technological University, India, August 2001

**Committee Chair: Dr. William J. van Ooij**

## ABSTRACT

The idea of this research topic was to develop a novel, environmentally benign coating system for metal alloy structural components in DoD systems. The coating was chromate-free and contained little or no volatile organic compounds (VOC's). The integrated organosilane system replaced the chromate system entirely including all chromate pretreatment and all corrosion-inhibiting chromate pigments. The complete system and also most or all of its components were water-borne. The term used to denote this particular primer is "superprimer." This primer was based on organofunctional silanes that possess an extraordinary ability to protect metals against corrosion. The proposed work integrated organosilanes into a full water-borne coating system. The objective was to replace the current system (metal pretreatment, primer and topcoat) with no sacrifice of corrosion performance.

Chapter 1 gives a brief overview on important concepts including corrosion and its control, significance of chromium in corrosion control and its use, silane technology, idea of the superprimer and the objective of this thesis.

Chapter 2 gives information about the materials used for preparation of the superprimer.

Procedures used for the testing and preparation of the superprimer are discussed.

Chapter 3 gives detailed information about the superprimer. In the beginning it gives information about the choice of selecting the components that constitute the primer followed by initial formulation and their results. The developments that led to the final formulation are discussed in detail. Test results including EIS and salt spray results are provided whenever necessary.

The silane plus resin combinations can lead to coating formulations but in order to make it perform on par with chromate primers further additions need to be made. Detailed explanation of the idea, purpose and expectations of these additives in the primer are already given in Chapter 1. In Chapter 4, details about the mixing procedure of the additions, different kind of additives tried and their test results are given. There are primarily two important kinds of additives, nanoparticles and corrosion inhibitors. Many commercially available particles and inhibitors were tried and tested for corrosion performance. Test results by EIS and salt spray are provided.

Zinc-rich primers are as the name suggests primers with heavy loads of zinc metal dust in it. The zinc dust/powder is used as filler and is held in the coating by using a binder. Paints with zinc pigments contain about 80% by weight pigment of which 20% is oxide. Zinc-rich coatings contain 85-95% metallic zinc, by weight, in the dry coating with little or no oxide. Depending the type of binder used the primer can be organic or inorganic. Organic binders can be epoxy, polyurethane, acrylate etc. In inorganic zinc-rich primers the binders are usually silicates. Chapter 5 starts with a

brief explanation on the uses, application, and mechanism of action and the idea of zinc-rich primers. It also includes the idea of the zinc-rich superprimer, the formulations, test results etc.

Chapter 6 discusses the characterization work that was done in the final stages of this thesis work. The NMR characterization technique was used in the trials to investigate the chemical structural characteristics and changes in the superprimer formulations. For this NMR instruments at Oklahoma State University in Stillwater, OK were used. Both carbon and silicon NMR analysis were applied.

Chapter 7 summarizes the conclusions of this thesis.

Chapter 8 discusses the recommendations for future work.



## ACKNOWLEDGMENTS

I would like to express my sincere thanks and appreciation to my advisor Dr. William J. van Ooij for giving me an opportunity to work with him in his group and guiding me through this thesis. What I learned from him in the past three years has shaped my career and thus my future. Each and everything of his; his zeal toward work, his lectures in class and group meetings, his suggestions, and his emails containing constructive criticism of my work will all be permanent guidelines for whatever I do in my future work.

I appreciate the SERDP-DoD of the U.S government for the funding of this project. I am grateful for the funding of this project through the DoD's SERDP, the Strategic Environmental Research and Development Program.

I sincerely thank my committee members Dr. R. C. Buchanan and Dr. Jude Iroh for spending time to review my thesis.

I thank my senior group members Dr. Danqing Zhu, Matthew Stacy, Vignesh Palanivel, and Anuj Seth, who are still an encouragement. Their works, including their published literature on silanes, have been my guides for the preparation towards this project.

I appreciate the efforts of my friend Mr. Chetan Shivane, without which this thesis might still be unfinished.

I also thank Dr. Tammy Metroke of Oklahoma State University for the help and guidance with the characterization work in this thesis.

Working and learning in our silane lab could not have been more fun without my lab partners and friends Akshay, Shekar, Naveen, Jasspreet, Karthik, Senthil, Kris, Ramki, Madhu Ranjan, Anna, Lin, Hrishi, G.K, Karuna, Seetharam, Pan and Yimin. I specially thank Shashi and Prasan who assisted Dr. Van Ooij during my tenure and with whom I shared an office.

I wish to thank my then employers Mr. Kenneth Mazzochi, Mr. William Hand and all others at Park Nameplate, Dover, NH, for their support and for understanding my priority towards this thesis.

Finally, I am forever indebted to my family and friends who have been the cornerstones of my life.

## TABLE OF CONTENTS

List of Tables.....	14
List of Figures.....	15
CHAPTER 1: INTRODUCTION .....	20
1.1 Corrosion.....	20
1.1.1 Definition.....	20
1.1.2 Theory.....	20
1.1.3 Corrosion Control and its Significance.....	25
1.2 Corrosion in the Department of Defense.....	27
1.2.1 Coating Technology in DoD.....	31
1.2.2 Chromium: Use, Mechanism, Advantages and Disadvantages.....	34
1.2.2.1 Use and Methods.....	34
1.2.2.2 Mechanism.....	46
1.2.2.3 Advantages of chromate conversion coatings.....	48
1.2.2.4 Disadvantages of chromate coatings.....	49
1.3 Superprimer.....	50
1.3.1 Definition.....	50

1.3.2 Background and Origin.....	50
<b>CHAPTER 2: MATERIALS AND TESTING PROCEDURES.....</b>	<b>61</b>
<b>A. Materials.....</b>	<b>61</b>
A.2.1 Silanes.....	61
A.2.2 Resins.....	62
A.2.3 Particles.....	63
A.2.4 Inhibitors.....	63
A.2.5 Metals/ Alloys.....	64
<b>B. Testing Procedures.....</b>	<b>65</b>
B.2.1 Electrochemical Impedance Spectroscopy.....	65
B.2.2 Salt Spray Test (ASTM B 117).....	65
B.2.3 NMR Spectroscopy.....	66
B.2.4 Infrared Spectroscopy.....	71
B.2.5 Scanning Electron Microscopy (SEM/EDX).....	76
B.2.6 Film Hardness Test.....	77
B.2.7 Tape Adhesion Test.....	78
B.2.8 Solvent Resistance Test .....	79
<b>CHAPTER 3: SUPERPRIMER: FORMULATION, PREPARATION AND TEST RESULTS.....</b>	<b>80</b>

3.1 Choice of the components.....	80
3.1.1 Chemistry .....	81
3.2 Initial Formulations and Results.....	82
3.2.1 Formulations.....	82
3.2.2 Results.....	84
3.3 Superprimer Formulation.....	85
3.4 Test Results.....	88
3.5 Improved Formulations.....	90
3.6 Test Results of Formulation F-6.....	91
3.7 Conclusion.....	92
CHAPTER4: ADDITIVES TO PRIMER.....	93
4.1 Pigments/Particles.....	93
4.1.1 Silica, Alumina and Carbon Black.....	94
4.2 Results and Discussion.....	95
4.3 Corrosion Inhibitors.....	102
4.3.1 Results and Discussion.....	103
4.4 Conclusion.....	106

<b>CHAPTER 5: ZINC RICH SUPERPRIMER.....</b>	<b>108</b>
<b>5.1 Uses and Applications.....</b>	<b>108</b>
<b>5.2 Mechanism.....</b>	<b>117</b>
<b>5.3 Zinc – Rich Superprimer.....</b>	<b>120</b>
<b>5.3.1 Formulation, Mixing and Coating.....</b>	<b>120</b>
<b>5.3.2 Results and Discussion.....</b>	<b>121</b>
<b>5.4 Conclusion.....</b>	<b>126</b>
<b>CHAPTER 6: CHARACTERIZATION .....</b>	<b>128</b>
<b>6.1 NMR Characterization.....</b>	<b>130</b>
<b>6.1.1 Objective and Sample Preparation.....</b>	<b>130</b>
<b>6.1.2 Observations.....</b>	<b>132</b>
<b>6.2 IR Characterization.....</b>	<b>134</b>
<b>6.2.1 Equipment and Sample Preparation.....</b>	<b>136</b>
<b>6.2.2 IR Spectra.....</b>	<b>135</b>
<b>CHAPTER 7: CONCLUSIONS.....</b>	<b>138</b>
<b>CHAPTER 8: RECOMMENDATIONS FOR FUTURE WORK.....</b>	<b>143</b>
<b>REFERENCES.....</b>	<b>145</b>

Appendix.....	151
Tables.....	152
Figures.....	168

## LIST OF TABLES

Table 2.1: List of Silanes used with trade names and chemical formulas

Table 2.2 Resins used in superprimer formulations

Table 2.3 Particles used in superprimer formulations

Table 2.4: Corrosion Inhibitors used in the superprimer formulations

Table 3.1: Resins and compatible silanes

Table 3.4.1: Comparison of performance of test results between control PRC Desoto MIL PRF and Superprimer Formulation F

Table 3.6.1: Summary of test results of the control, F-6 and F

Table 4.1.1: Formulation chart of modified superprimers with particles/inhibitors

Table 6.1: Peak assignments in the carbon spectrum of commercial resin;

Spectra for the component silanes AV5 and bis-sulfur are shown in Figures 6.3 and 6.4. Refer to Figure 6.1

Table 6.2: Table showing the change in intensities at certain peak of Figure 6.5 varies with time.

Time is shown in the Y-axis of the table and the peak values in the X-axis of the table.

Table 6.3: Solid State NMR spectrum of cured superprimer coating shown in Figure 6.6

Table 6.4: Peak assignments for bands in IR spectra

## LIST OF FIGURES

Figure 1.1: A typical corrosion mechanism

Figure 1.2: Heavy Corrosion Environment

Figure 1.3: Corroded C-141 aircraft

Figure 1.4: Corroded aircraft part

Figure 1.5: Corroded navy pier

Figure 1.6: Typical coating system in DoD

Figure 1.7: Corrosion repair in DoD

Figure 1.8: Commercial blue-bright, iridescent and golden yellow, olive drab, matte black and bronze chromating examples

Figure 1.9: Chromate coating's self-healing mechanism

Figure 1.10: Silane mechanism over a metal

Figure 1.11: Superprimer: adsorption of superprimer on metal

Figure 1.12: Superprimer: crosslinking of resin by bis-silane

Figure 3.1: Schematic showing the probable reactions between epoxy-epoxy and epoxy-tertiary amine

Figure 3.1.2: Reaction between a primary amine and an epoxy group

Figure 3.2.1 Bode Plot of, 1: Blank uncoated Al 2024 T3 sample, 2: Coated with AMME silane and cured at 110°C, 3: A 1:8 mixture of polyurethane resin and AMME silane, 4: A 1:10 mixture of polyurethane resin and AMME silane

Figure 3.2.2: 1: A 1:2 mixture of EPON 828 resin with A-1170 unhydrolyzed silane coated on AA 2024 T3 panel cured at 110°C, 2: Same mixture as in 1, but cured a RT for a 48 hours,3: Al panel coated with silane alone, 4: Blank uncoated panel

Figure 3.4.1: Yellow panel (left) is an aluminum panel coated with the PRC Desoto MIL-PRF Yellow primer. The other panel is coated with formulation F

Figure 3.4.2: EIS Bode plot of formulation F coated on a CRS substrate and tested for 4 days

Figure 3.4.3: EIS Bode plot of control PRC Desoto MIL PRF chromate containing primer coated on a CRS substrate and tested for 4 days

Figure 3.6.1: EIS Bode plot comparing the curves of F-6, F and the control Desoto PRC MIL PRF

Figure 3.6.2: Salt spray result of F-6 after 2 weeks

Figure 4.2.1: Impedance plots of bis-sulfur silane-treated AA2024-T3 systems loaded with different amounts of silica nano-particles

Figure 4.2.2: Salt immersion test after 7 days. Formulations with increased weight percentages of alumina numbered F10, F11 and F12 in formulation table

Figure 4.2.3: EIS Impedance values of salt fog tested coatings with time

Figure 4.2.4: EIS Impedance values of salt fog tested coating with time of coating formulations containing alumina and with poly-urethane topcoat

Figure 4.2.5: Bode plot of F 10 without topcoat and with topcoat

Figure 4.2.6: Bode plot of F 11 without topcoat and with topcoat

Figure 4.2.7: Bode plot of F 12 without topcoat and with topcoat

Figure 4.2.8: Salt Spray results of F 10, F11 and F12 with and without topcoat after 3 weeks. The formulation information can be found in Table 4.1.1

Figure 4.2.9: Salt Fog test performance of F 28 after 0, 7 and 28 days. The formulation information can be found in table 4.1.1

Figure 4.2.10: Change in impedance values of F 28 coating with exposure time. The formulation information can be found in table 4.1.1

Figure 4.2.11: EIS impedance curves of F28. The formulation information can be found in table 4.1.1

Figure 4.3.1: EIS impedance values of coating formulations F13, F14 and F15 after being exposed to salt fog. The formulation information can be found from table 4.1.1.

Figure 4.3.2: EIS Bode plots for 6 weeks of immersion of F13, F14 and F15. The formulation information can be found from table 4.1.1.

Figure 4.3.3: Change in impedance values of coatings put under salt fog testing

Figure 4.3.4: Individual impedance plots of formulations F13, F14 and F15 with topcoat

Figure 4.3.5: Salt spray results of formulations F13, F14 and F15 with topcoat after 6 weeks of testing

Figure 4.3.6: Change in EIS impedance values of the coating formulations F20, F21, F24, F25 with and without topcoat, after exposed to salt fog

Figure 4.3.7: Salt Spray test results of formulations F20, F21, F22, F24 and F 25 without topcoats after 28 days of testing

Figure 5.1 Schematic of the zinc-iron couple and the half cell reactions

Figure 5.2 Comparison between a conventional primer and the zinc rich coatings

Figure 5.3: 42 Days EIS result for formulation with 40% zinc and 60% superprimer. The square block represents result for 42 days and the rhombus for 0 days

Figure 5.4: 42 Days EIS result for formulation with 70% zinc and 30% superprimer. The square block represents result for 42 days and the rhombus for 0 days

Figure 5.5: The salt spray result after 3 weeks of both 40% and 80% zinc formulations

Figure 5.6: 6 week EIS results of commercial and zinc-rich superprimer

Figure 5.7: 500 hours Salt fog result of commercial and zinc-rich superprimer

Figure 5.8: 200 hours salt fog result of zinc-rich primers with polyamide topcoat

Figure 5.9: Zone 1 area in the scribe before immersion

Figure 5.10: Zone 2 coated area before immersion

Figure 5.11: Analysis of zone 2 with coated surface after immersion

Figure 5.12: Zone 1 in the scribe after immersion

Figure 6.1: Structure of Epirez 3540

Figure 6.2: Epirez 3540-wy-55 resin

Figure 6.3: C-13 spectrum of AV5

Figure 6.4: C13 spectrum of bis-sulfur silane

Figure 6.5: Solid C13 spectrum of cured superprimer

Figure 6.6: <sup>29</sup>Si NMR spectrum of the cured coating

Figure 6.7: IR spectrum of 10% AV5 coated AA 2024T3 panel cured at RT and at 100°C for 1 hour

Figure 6.8: IR spectrum of bis-sulfur silane film

Figure 6.9: IR spectrum of Epirez 3540 resin and F6 coatings cured at 100°C + F6 superprimer formulation

Figure 6.10: IR spectrum of F6 cured at 100°C

Figure 6.11: Cure trend of F6 formulation with time

Figure 7.1: Hawaiian outdoor exposure testing results over F-6 base formulation primer coatings over carbon steel with topcoat. After 141 days of testing.

Figure 7.2 AA 2024-T3 coated with F-6 superprimer with topcoat submitted to outdoor exposure of 141 days at Hawaii. Both before (left), and after (right) are shown.

Figure 7.3: Outdoor exposure sight in Hawaii

Figure 7.4: Panel arrangement at Hawaii outdoor exposure center

Figure 7.5: Rack location at Hawaii exposure center

## **CHAPTER 1: INTRODUCTION**

This chapter gives a brief overview of important concepts including corrosion and its control, significance of chromium in corrosion control and its use, silane technology, idea of the superprimer and the objective of this thesis.

### **1.1 Corrosion**

#### **1.1.1 Definition**

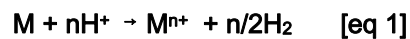
Corrosion is an electrochemical reaction process which leads to continuous loss of metal or metal alloys. Energy is needed to extract metals from their mineral state to the pure state. The same amount of energy is emitted during the formation of its chemical compounds or in other words during the process of corrosion.[1] Corrosion returns the metal to its combined state in chemical compounds that are similar or even identical to the minerals from which the metals were extracted. Thus corrosion has been called extractive metallurgy in reverse [2-4]. An attempt has been made in the next few paragraphs to explain the science behind the corrosion process in simple terms.

#### **1.1.2 Theory**

It is a natural law for materials to exist in the lowest energy state possible. This law applies to metal atoms also, which is the reason why they exist in mineral or chemically compounded state

instead of their pure metal state. Every metal surface (except in the case of noble metals such as gold) has a layer of its own oxide on top with pure metal alloy underlying this oxide surface. The formation of an oxide on a pure metal or metal alloy surface is instantaneous. So even in the case of scratches and damages, a metal surface metal oxide will be formed almost instantaneously from the underlying metal upon exposure to atmosphere. This formation of oxide is due to a normal chemical reaction.

Every chemical reaction requires a driving force or in technical terms, energy in some form. The energy required for a certain reaction to proceed forward is called its potential. Consider the following common reaction between a metal and an acid as an example,



Each reactant in the above reaction is reacting with the other to form another more stable form of its own, in the exposed conditions. Metal is reacting to form a metal salt as a product which is more stable than metal itself when exposed to this particular acid. Similarly hydrogen, which was at first in an acid, reacts to form hydrogen and liberate itself into a more stable form of hydrogen gas. These reactions/stabilizations of materials in any conditions happen/occur by transfer of their electrons. Since transfer of electrons involves transfer of charge and transfer of charge is termed

as current, the potential/driving force which makes the reaction happen is given an electrical term of Electrochemical Potential.

Every material bears a certain amount of charge on it. Increase in the amount of this charge by transfer of electrons from it is called the oxidation/anodic reaction. Acceptance of electrons from other materials is called the reduction/cathodic reaction. In every reaction one reactant passes through oxidation and the other through reduction. So each of the reactions has some potential attached to it. The above reaction can be divided into 2 reactions. A schematic is shown in Figure

1.1:



The  $e_c$  and  $e_a$  mentioned above are the potential of each of these half reactions. The reactions are called as half-cell reactions and the potentials are half-cell electrode potentials or redox potentials. The potential required for the complete reaction to happen will be the sum of the half-cell electrode potentials. This information is very useful in detecting the reaction mechanisms when two or more reactants are involved.

$$E = e_a + e_c$$

This electrochemical potential can be related to the most basic free energy change using the equation:

$$\Delta G = -FE \quad [\text{eq 4}]$$

At standard state or when reactants react in standard amount at a standard known temperature the above relation would be,

$$\Delta G_0 = -FE_0 \quad [\text{eq 5}]$$

Where  $E_0$  and  $G_0$  are standard values for any reaction/reactant,  $n$  is the number of electrons or equivalents involved in the reaction and  $F$  is Faraday's constant, 96,500 coulombs per equivalent.

Thus we have a fundamental relationship, in which a charge,  $nF$ , taken reversibly at equilibrium through a potential  $E_0$ , corresponds to an energy change  $\Delta G_0$ .

When reactants react at conditions different from the standard conditions the potential or the driving of the reaction to proceed will change. This change can be monitored using the following reaction,

$$E = E^0 + (2.303RT/nF) \times \text{Log} (A) \quad [\text{eq 6}]$$

Where  $E$  = the total potential (in mV) developed between the sensing and reference electrodes.

$E^0$  = is a constant which is characteristic of the particular ISE/reference pair (It is the sum of all the liquid junction potentials in the electrochemical cell)

2.303 = the conversion factor from natural to base10 logarithm.

R = the Universal Gas Constant (8.314 joules/K/mole).

T = the Absolute Temperature.

n = the charge on the ion (with sign).

F = the Faraday Constant (96,500 coulombs).

Log (A) = the logarithm of the activity of the measured ion

In the right half of the above reaction the terms T and A denote the dependence of a reaction potential on temperature (T) and concentration (A).

Corrosion involves similar chemical reactions. Availability of reactants at cathode, anode and an electrolyte to allow the movement of electrons will drive the chemical reaction forward and repeat itself. This combination is the reason behind the continuous deterioration of corroding metal. For this particular reason corrosion is termed as an electrochemical reaction instead of just a chemical reaction.

### 1.1.3 Corrosion Control and its Significance

Nature's simple low energy law is acting as a starting point for corrosion. Corrosion is involved in many aspects of life and has both direct and indirect effects on most of them. From a common stain in a kitchen sink to a major aircraft accident can be caused by corrosion. CC technologies and NACE international study shows that the cost of corrosion in US alone is 280 billion dollars per year. The major industry getting affected by this is the Department of Defense which includes Army, Navy and Air force. Plans for control or prevention of this corrosion are no doubt a matter of greatest concern.

It was mentioned in the previous section that as long as reactants and oxidation species are available, the corrosion of any metal is going to continue until its complete deterioration. Controlling the environment by removing/decreasing the corrosion causing species in it can be one method. Limiting and prevention of metal exposure to the corrosion causing species are other options. Corrosion protection by organic/inorganic coatings has been in use for several decades and has been proven to be a very effective option.

Organic coatings have been extensively used as barrier coatings which prevent the entry of water and ions and inhibit the cathodic reduction reaction from taking place [5]. These coatings form a cross-linked net-like sheet structure over the substrate and this coating adheres to the metal substrate. The efficiency of the coatings depends on the ability of the coatings to prevent the

corrosion causing species like water and oxygen from seeping through the coatings to the metal underneath. Thus it depends mainly on the cross-linking density of the coating itself and also its adhesion to the metal. Bolger and Michaels [6] showed that a good interfacial adhesion at the metal coating interface is very important for good corrosion performance. Coating delamination failures are mainly due to formation of corrosion causing formation of hydroxyl at the metal-coating interface. These hydroxyl ions initiate the cathodic reactions and hence drive the corrosion reactions forward. This phenomenon was demonstrated by Dickie and Floyd [7].

So, it is first necessary that the coating prevents the passage of these species to the metal. If for a reason the coating fails to prevent the passage, the interface or the metal surface should be passive for these species to react. This condition of the passivity on any metal surface depends on conditions like pH and the stability of the surface. The metal oxide itself can be passive but it again depends on the pH of the environment. The metal oxide can be turned to a more passive layer by making it react with other compounds. These compounds are called inhibitors and they can be organic or inorganic. Organic inhibitors were extensively studied by several authors [5-7]. Most of the organic inhibitors are in the form of weak acids and their derivatives from insoluble salts at the metal surface [5]. This insoluble passive insulating layer prevents the electrochemical reactions to take place and inhibit corrosion. Inorganic corrosion inhibitors such as chromates, phosphates and recently, cerium salts have been widely used for corrosion control of various

metals and alloys. These corrosion inhibitors work in the same way by the formation of passivating hydroxide/oxide films and suppressing the cathodic reaction by limiting the diffusion of the electrolyte, oxygen and water to the substrate. It will also limit the transfer of electrons to the metal interface. Inorganic inhibitors are active corrosion inhibitors that undergo reduction at active corrosion sites (pits, precipitates or inclusions) to form insoluble oxides.

There are many methods like the above which are used and there are many other options that are still under development and have a huge prospect. This corrosion problem and the cure for it as a whole give a very large scope for an extensive research and study.

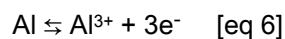
## **1.2 Corrosion in the Department of Defense**

The Department of Defense (DoD) acquires, operates and maintains a vast array of physical assets, ranging from vehicles, aircraft, ships, and other material to wharves, buildings and other stationary structures that are subject to corrosion. It maintains equipment and infrastructure worth billions of dollars in many environments where corrosion is causing military assets to deteriorate, shortening their useful service lives. A typical heavy corrosion environment is shown in Figure 1.2. The resulting increase in required repairs and replacements drives up costs and takes critical systems out of action, reducing mission readiness. In 2001, a government-sponsored study estimated the costs of corrosion for military systems and infrastructure at about \$20 billion

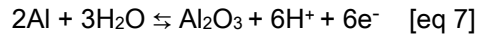
annually and found corrosion to be one of the largest components of life-cycle costs for weapon systems. Typical examples of corrosion are shown in Figures 1.3 – 1.5

The metals used by DoD include Cold Rolled Steel, Hot Rolled Steel, electro-galvanized steel, Hot Dip Galvanized, titanium zinc sheets, galvalume sheet, galvanized sheet, aluminum alloys, 1XXX, 2XXX, 3XXX, 5XXX, 6XXX, 7XXX, copper, brass, nickel and magnesium alloys. But primarily aluminum alloy AA 2024 T3 finds its use in the aircraft industry and carbon steel is still found to have a major usage in the construction side. This thesis primarily concentrated the testing and trials on these two substrates. In the next few paragraphs of this section an understanding of the corrosion of these two metals is given.

Aluminum and aluminum alloys have been used as aerospace materials especially in commercial airplanes due to their high strength/stiffness to weight ratio, mechanical properties and corrosion resistance. The aluminum oxide formed on the surface is very stable in ordinary conditions. The conditions where the oxide is stable and unstable can be easily derived using a Pourbaix diagram. According to it the oxide layer is stable in the pH ranges of 3.9 and 8.6. At conditions lower than this pH range aluminum oxidizes to aqueous cations following the reaction



When the pH is in between the range 3.9 – 8.6 aluminum converts to aluminum oxide in the presence of cathodic reaction-deoxidizer.



When the pH is above this range the aluminum changes to soluble anions



According to the above information the aluminum metal is not susceptible to corrosion (passive to corrosion) as long the conditions are in oxide forming stage. When the conditions shift to either of the sides the aluminum metal/oxide layer is susceptible to corrosion. Factors like pH and concentration play a major role in determining the conditions. Their dependence is already explained in the previous sections.

The passive oxide film is susceptible to localized breakdown leading to loss of the underlying aluminum metal. If the localized attack occurs at an open surface it is called pitting corrosion. These corrosion forms can lead to structural breakdown by acting as sites of crack initiation. The following review helps in understanding pitting corrosion as it is the main form of corrosion in aircraft aluminum alloys [3].

Pitting corrosion has been studied in great depth by several authors [8-9]. Frankel [10] suggested various stages of pitting to explain localized corrosion initiation and growth. He reported that any of these stages is important involving passive film breakdown, growth of metastable pits and growth of larger stable pits. The second and the final stages are associated with the understanding of pit initiation, growth and repassivation of the metal surface. It was suggested that localized corrosion is controlled by factors relating to stabilization and growth of pits rather than the influence of the passive film which is secondary in nature [10].

The most widely used aircraft aluminum alloy is the AA2024-T3 alloy. Many researchers [8-10, 11] have done extensive work in order to understand the corrosion mechanism of AA2024-T3 alloy. The AA2024-T3 alloy is made up of Al, 3.8-4.9 Cu, 1.2-1.5 Mg, 0.3-0.9 Mn, 0.5 Si, 0.5 Fe, 0.1 Cr, Zn and Ti. The heterogeneous distribution of the copper-aluminum phases in the alloy is the cause of the low resistance of the alloy. These second phase particles give added mechanical strength to the aluminum matrix but they are undesirable for corrosion resistance of the alloy. Pitting is the major form of corrosion but corrosion forms such as intergranular and stress corrosion also occur.

According to Buchheit et al., there are many second-phase particles that are formed in AA2024-T3 alloy [12]. He suggested that the concentration of copper in second phase particles and the local depletion of copper in certain micro-structural areas establish a local galvanic cell that

results in localized attacks [12]. They are called S phases as they are characterized by spherical shape. Literature suggests two major types of second phase particles: Al-Cu-Mg which is called the S phase characterized by high copper content and Al-Cu-Fe-Mn second phase particles. The formation and the distribution of these second phase particles lead to the poor corrosion resistance properties of the AA2024-T3 alloy [12].

Iron can exist in the oxidation states of +2 and +3, which complicate the Pourbaix diagram. At above neutral conditions the iron forms a protective layer which makes the iron passive. In the lower and neutral conditions it corrodes because the oxide is not formed. For better understanding and more information about the reaction of iron at different conditions the reader is referred to [1].

### **1.2.1 Coating Technology in DoD**

Defense equipment and infrastructure are exposed to the harshest environments and are high prone to be corroded easily and also quickly. Most of the defense equipment is very expensive and the need to maintain them in their best shape is imperative. Corrosion of the equipment could in fact be the main reason for their deterioration and poor performance. So the department uses an efficient state-of-the-art-three-layer coating technology for most of their equipment. Figure 1.6 shows a schematic of this technology and Figure 1.7 shows an example of a typical corrosion repair in DoD.

Painting and coating operations fall into three primary categories. These categories are:

- Surface preparation/Conversion coating
- Priming
- Painting (including cleaning and maintenance);

Surfaces must be treated before painting for corrosion control and to ensure proper paint adhesion. Most services also employ some type of Chemical Agent Resistant Coating (CARC) to protect equipment from chemical attack and exposure. Surface preparation typically involves cleaning and preparing the surface, treating the surface and changing its characteristics, and rinsing and cleaning the treated surface. The current pre-treatment technique used is primarily chromate conversion coating. The thickness of this coating layer ranges from 0.06  $\mu\text{m}$  to 2  $\mu\text{m}$ . This layer is of prime importance to the corrosion protection and adhesion of the next coating layer, i.e., primer above it. The method and mechanism is discussed in more detail in the next section. But this chromate conversion can lead to wastewater treatment requirement and hazardous waste disposal issues because it is a known fact that chromium is declared a prominent carcinogenic and its use is facing extension.

The primer, which is the second layer, is usually comprised of a pigmented organic resin matrix.

The thickness of this layer can vary from 5-20  $\mu\text{m}$ . The pigmented formulation may be formulated

with chromates or not in the resin matrix. The main purpose of this layer is to improve corrosion performance and also act as an intermediate between the organic top-coat and the inorganic pretreatment. This particular organic layer acts as a bridge between the two end layers. The use of chromium is also frequent in this layer. Some DoD primers contain about 20 – 25 % by weight of chromate as pigments in them. These pigments leach out from the primer layer and form a passivating layer on the metal in place of scratches and damages. Besides the use of chromium the primers have other issues like air quality issues. Some of the current coatings contain high concentrations of Volatile Organic Compounds (VOC's) and Hazardous Air Pollutants (HAPs).

The final layer is a topcoat which is supposed to be flexible, have a matte finish and be chemically resistant with maximum exterior durability. The topcoat also provides the aircraft with decoration and camouflage. A typical topcoat is made of polyurethane resin and the thickness varies between 50 and 200  $\mu\text{m}$ .

Painting operations can vary greatly depending on the facility and the end-use of the item to be painted, but most opportunities for painting, deal with the lowering of VOC emissions during paint application and paint equipment cleaning. Examples of opportunities in the area of painting include low-VOC paints, waterborne paint systems, powder coat paint systems, automatic and non-solvent gun cleaning equipment, as well as equipment and methods to improve the application of paint.

## 1.2.2 Chromium: Use, Mechanism, Advantages and Disadvantages

### 1.2.2.1 Use and Methods

The following information can be obtained from multiple websites A.1, A.2, A.3 listed in the appendix, and from literature ref [23-24]. Chromate films are chemical conversion coatings, in the process of which the substrate metal participates in the coating reaction and becomes a component of the coating; and it has a profound influence on the properties of the coating [13-14].

Among the metals commercially chromated are zinc and cadmium electroplates; zinc die castings; hot-dipped galvanized steel; aluminum (in almost every conceivable form); and sometimes copper and silver alloys. Chromate coatings improve corrosion resistance and appearance of metals and adhesion of organic topcoats [14].

The chromating process involves a chemical reaction between the metal surface and an aqueous solution containing chromates and some activator ions. The activators can be sulfates, chlorides, fluorides, phosphates and complex cyanides. Usually chromating process can be substrate specific but some solutions can be used on different kinds.

The solutions for chromating are acidic. A simplified reaction proceeds along the following lines.

Metal at the interface is dissolved by the acid and enters the solution as metal ions. There is a

local rise in pH (lowering acid content) in the immediate vicinity of the interface. Basic metal ions combine with chromate ions to form a compound that is insoluble at the local (higher) pH. This compound precipitates on the metal surface as an adherent coating. Reaction by-products enter the main solution.

Coatings formed by the reaction are of necessity built up from the inside out. Since coatings can only be produced by the interaction of the solution with the metal, the solution must diffuse through prior layers of coating and reaction products must diffuse outward [13-14].

This inward-outward diffusion of solution can have a detrimental effect on thicker coatings. They may be powdery and loosely adherent. And solution trapped in the coating interstices can lower final corrosion resistance [13].

Because the chromating process involves a continuous chemical reaction, the depletion of the solution content is obvious. It is necessary to maintain solution concentration steady so that uniform coating properties can be maintained over the entire working life of a chromating bath. In the next following paragraphs a few types of chromating processes have been discussed. Figure 1.8 shows an example of commercially available chromating types.

### **Zinc and Cadmium Electroplate**

A typical cycle used to chromate electroplated work follows these steps:

1. Electroplate.
2. Rinse (multiple rinses may be employed).
3. Optional dip in 0.25-0.50 pct nitric acid.
4. Chromate.
5. Cold rinse.
6. Leach (if required).
7. Cold rinse.
8. Warm-air dry off.

Plated parts are to be chromated are placed on racks or in stainless steel baskets convenient for the dipping step. Corrosion resistance depends on the particular chromate selected. Appearance also is a consideration. Plated parts are to be chromated with a minimum thickness of 0.006 mm. An average of 0.0012 mm is consumed by the chromating process, leaving 0.0048 mm, which is required for satisfactory corrosion resistance.

#### **Clear Bright.**

This is one of the earliest types of chromating process in which the solution was a concentrated (100 g/liter chromic acid) solution that did a certain amount of chemical polishing. The solution consists of chromates, sulfates and buffers such as borates or acetates, and, it deposits a gold

film which can be removed by a subsequent immersion in dilute alkali (leaching, sometimes called bleaching). This coating was once very popular for wire goods such as refrigerator racks since the polishing of the chromate produces an appearance similar to that of chromium.

To use this process on zinc plate, the process was modified. The two-step process has been largely replaced by more dilute, single-dip processes. This greatly reduces the cost of maintaining a highly concentrated solution and the cost of waste-treating the spent chromate. The double-dip process, i.e., chromate plus alkali leach, is still often used on cadmium plate.

### **Blue Bright**

Single-dip solutions for passivating zinc plate and providing a degree of stain resistance are used in both rack and barrel plating. Plated fasteners, steel stampings and wire goods are now commonly chromated in these solutions. The baths consist of chromates, fluorides and large amounts of nitric acid. The concentrated proprietary products are available in liquid form (which contains nitric acid) or as a granular powder (to which the user adds nitric acid).

Working solutions will contain only about one g/liter of chromic acid (or even less), about one percent of the amount in the former baths. Naturally, the cost of preparing these and of subsequent waste treatment is considerably lower.

Chromate films from this type of bath can be dyed a variety of colors with organic dyes. This can serve as identification, especially for screws, nuts and small parts. These solutions are specific for zinc electroplate and will not work on cadmium or other types of zinc.

### **Gold Films**

Gold chromate films are produced by solutions containing chromates with sulfate or chloride activators produce gold colors. These films contain considerably higher amount of hexavalent chromium than clear films, and the gold color can be due to this reason. Corrosion resistance is better. Baths of this type can be used for zinc, cadmium and some zinc die castings.

### **Olive Drab**

The olive drab in chromate films is achieved by inclusion of organic acid modifier. The higher corrosion resistance of these coatings can be due to the same reason. These are applied to zinc and cadmium electroplates from baths similar to those used for gold coatings. The color is not especially pleasing, however, and coatings of this type are functional rather than decorative.

### **Black**

The black color in chromate films can be achieved by the incorporation of a soluble silver salt into a gold chromate solution which produces a deposit of black silver chromate. This coating has excellent corrosion resistance and a jet black matte appearance, with good light absorbance.

These products should find some applications in coating parts for solar collectors. The use of a

silver salt tends to make the process expensive and sensitive to chloride contamination. The sensitivity to chlorides can be an issue when the chloride baths are used in the chromating process.

### **Zinc Die Castings**

Zinc-die-castings are extensively used in decorative and functional automotive applications. Parts such as carburetors and fuel pumps are highly susceptible to the ravages of water-gasoline corrosion, which is a particularly aggressive combination. Without chromate protection, a gelatinous precipitate of zinc hydroxide quickly fouls small orifices and ventures. A gold chromate deposit prevents this problem.

A typical cycle for chromating Zamak die castings is as follows:

1. Deburr (mechanical or thermal).
2. Alkali clean.
3. Cold rinse.
4. Acid activation (dilute sulfuric or phosphoric acid, often with included fluorides).
5. Cold rinse.
6. Warm rinse.
7. Warm-air dry.

## **Hot-Dipped Galvanized Steel**

Hot-dipped galvanized steel coils can be susceptible to the formation of white zinc corrosion products during their storage. To prevent this they might need to be chromated at the mill. Or they can be chromated on high-speed coil-coating lines as a pre-paint treatment, to provide corrosion resistance and excellent paint adhesion. Unfortunately the first process is no substitute for the second. The mill process is intended only for passivation and is an inferior adhesive coat for paint. It is also extremely difficult to remove, so that galvanized steel that is ultimately to be painted should be specified *without* mill chromate passivation (it should be oiled instead).

## **Mill Chromate**

Typically, two types of mill chromating are used. One has a fluoride activator, while the other is based on reduced (trivalent) chromium. The process involves flooding of the solutions over the coil after it comes from the galvanizing pot (after water quench). The chromate solution is dilute (1 g/liter) and is not rinsed, but squeegeed off. A thin film remains, it reacts with the zinc and the coating is dried in place. Coatings are clear, colorless and intended to provide protection until sheet is fabricated, often under outdoor storage conditions at construction work sites.

## **Paint-Base Chromate**

Applied on high-speed coil-coating lines, these are chromate solutions of moderate concentration (10 g/liter) with complex fluoride activators. New coil-coating lines can handle widths of metal up

to 152 cms wide and run at 1.5 m/sec. Coil is painted in-line by reverse-roll-coat methods and subsequently fabricated into residential siding and architectural building panels.

### **Gold Chromate**

Gold chromates of this type used for zinc plate and Zamak are sometimes used on galvanized steel stampings and hardware.

### **Aluminum**

Chromates for aluminum fall into two categories: chrome-phosphates, primarily those used on architectural aluminum extrusions to provide a paint-bonding coat, and chrome oxides applied to almost every type of aluminum, i.e., sheet, coil, stampings and castings. Purposes: paint bonding and corrosion resistance.

### **Chrome Phosphate**

Baths for applying chrome phosphate consist of chromate ions, phosphates and fluorides. Although the solution contains chromium in the hexavalent form (Cr (vi)) chemical reduction takes place on the metal at the point of application, so that the chromium in the coating is essentially all trivalent chromium (III) phosphate. Most lines for applying this type of chromate spray it on cleaned aluminum extrusions, but some dip lines are in operation. Since the chromate coating itself contains no hexavalent chromium, it is common practice to use a passivating hexavalent chromium rinse as the final step in the treatment. A typical cycle would be:

1. Alkali clean
2. Rinse
3. Chromium-phosphate
4. Rinse
5. Hexavalent chromium rinse (seal)

Paint is customarily applied in-line by electrostatic spray and then baked producing a finished extrusion ready for assembly into window casings and such. This process produces remarkable adhesion. Corrosion resistance is also excellent if the final seal and paint are properly selected.

The coating has an almost colorless to pale green appearance, making it very suitable for the application of white and pastel colors (no bleed through).

### **Chrome Oxide**

Chrome oxide treatments deposit a chromate film ranging in color from nearly colorless through gold to brown. Baths contain chromates, fluorides, nitrates and an accelerator, which may be ferricyanide or a metal from group 7 or 8 of the periodic table. Ferri-cyanide-accelerated baths are fastest, developing the most coating for a given time. They are also quite easily controlled and rejuvenated. The main objection to ferricyanide baths is the complex cyanide radical in the subsequent rinse water, which is difficult to remove or destroy, and decomposes to cyanide in the presence of ultraviolet light.

Gold chromate films are used both with and without paint. Unpainted, they give corrosion protection on aluminum stampings, tubular products, extrusions, die castings and aluminum heat exchangers. As a base for paint, the gold chromates afford both adhesion and corrosion resistance to coil-coated sheet used for residential siding and building panels. Unlike the chrome-phosphate, chrome oxide coatings are rich in hexavalent chromium and need no additional seal to develop their maximum corrosion resistance.

### **Process Parameters**

In general, the operation and control of a chromate processing solution are simplicity itself.

Treatment times, whether by spray or dip, are relatively short, ranging from a few seconds (for a bright dip on zinc plate) to a maximum of five minutes (for the heaviest coatings on aluminum).

Temperature requirements are also moderate: most solutions operate at or near room temperature and few require temperatures above 54°C.

The solutions are aggressive, especially those that contain fluorides. Satisfactory acid-resistant materials are stainless steel (316 ELC), polyethylene, polypropylene, PVC and rubber.

The usual chemical control of a chromating solution consists of a titration to determine hexavalent chromium, and pH measurements to regulate acidity. Titration of total acid is sometimes used, but the build-up of reaction products makes pH a more reliable choice.

Chromate films should not be dried at elevated temperature, since they rupture (mud cracking) and lose protective value. For films on zinc, drying temperature should be below 54°C, while aluminum can tolerate temperatures to about 82°C with no adverse effects.

## **Testing**

All chromates are intended to increase the service life of the finished article and this implies improved corrosion resistance. Accelerated tests have been developed in an attempt to predict service life and to compare various treatments. The most common of these is exposure to salt fog (ASTM B-117).

When evaluating results, comparing results between different test sites or recording results, give particular attention to the following:

1. Use of good quality sodium chloride in the test solution, and pH adjust.
2. Measure atomization rate (amount of salt solution sprayed).
3. Specify what constitutes a significant surface. A significant surface is customarily exposed at an angle of 15° from vertical. This may be particularly difficult in the case of odd-shaped parts or small screws. In these cases, the angle or position of exposure must be agreed upon, since it is of paramount importance and results are otherwise not

- comparable. Companies or trade associations may specify how parts are to be positioned.
4. Specify what constitutes corrosion, e.g., a white pinpoint, heavy white corrosion products or red rust. If possible, have photographs or examples to illustrate degrees of corrosion.
  5. Specify if parts are to be observed at periodic intervals (e.g., 24 hours) and tested until failure, or exposed for a certain time (e.g., 168 hours), then evaluated and rated after completion.

These points are directed to the salt spray test but are valid for other corrosion tests as well.

All corrosion tests are subject to interpretation. Outdoor exposure tests are among the most reliable, but even these really measure only what happens under a very specific set of conditions in a single environment; they should not be interpreted as "real world performance".

## **EPA**

Chromium, whether in hexavalent or trivalent form, is classified as hazardous waste by EPA.

Chromate-containing effluents are also regulated on the federal, state and local level. Rinse waters and spent solutions must be treated to remove chromium before discharge.

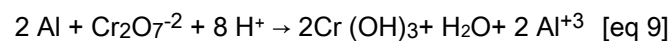
Most commonly, hexavalent chromium is reduced to the trivalent form with sodium metabisulfite.

The trivalent chromium is then precipitated by pH adjustment with alkali such as liquid caustic or

lime. The precipitated solids containing the chromium are mechanically separated from the liquid by settling or filtration. They can then be removed (by a certified waste hauler) to an approved landfill.

#### 1.2.2.2 Mechanism

The CCC formation involves destabilization of the passive oxide film by fluoride, followed by reduction of chromate by the exposed aluminum. Figure 1.9 shows a schematic of the mechanism of chromium coatings.



Exposure to chromate-containing CCC solution results in the reduction of the hexavalent chromium to trivalent chromium which is retained in the chromate conversion coating. In summary the mechanism of chromate inhibition of aluminum (AA2024-T3) is that chromate is a very soluble, high-valence oxidizing ion with a lower-valence which is insoluble and creates an extremely protective oxide/hydroxide film. The formation of an insoluble trivalent chromium oxide/hydroxide film stops the localized corrosion in AA2024-T3 alloy.

Chromate conversion coatings in addition to their excellent corrosion properties, adhesion and paintability are noted for their ability to self-heal if damaged by mechanical or chemical action provided they are not severe. This behavior was observed by several researchers [13-14] when

the coating was subjected to an aqueous environment. Self-heal or active protection involves release of soluble chromate ions from the coating, transport through the solution and subsequent action at the site of damage, namely the pits. This active corrosion protection is different from passive or barrier corrosion protection which is a thickened oxide/hydroxide film at the metal surface. This property allows the structure or component to withstand minor mechanical or chemical damage on the coating sustained during service without having maintenance.

According to researchers in the Fontana Corrosion Research Center at Ohio State University [8-10] there is direct and indirect evidence supporting the idea that a leached-out chromate ion results in the dynamic repair by interacting with the defects or pits in the coating. On the basis of their experimentation Buchheit et al., were able to establish testable criteria and place a set of guidelines for the self-healing ability of chromates. A schematic of this explanation of chromate mechanism is shown in Figure 1.9.

They are:

- 1) The coating must contain a reservoir of inhibiting compound which can be released when needed.
  
- 2) The inhibitor must be water-soluble and be released into the contact solution.

3) The leached-out inhibitor must be able to diffuse out of the coating and be transported through the solution.

4) The transported inhibitor must act on damaged or exposed areas and inhibit further corrosion.

Given these distinct characteristics chromate conversion coatings have been and still are the most widely used surface pretreatment process in the aircraft industry.

### **1.2.2.3 Advantages of chromate conversion coatings**

1) CCC gives excellent corrosion protection to the metal substrate (passes 336 hours of standard salt spray test- ASTM B117)

2) They improve adhesion between many paint and metals

3) They exhibit active corrosion protection, i.e., the self healing effect

4) They are visible to the naked eye so they are used in decorative coating industries

5) Chromate coatings are easy to apply and are economically viable

6) They are completely water-based surface treatments without any organic solvent

#### 1.2.2.4 Disadvantages of chromate coatings

The major disadvantage associated with the chromates is not its performance or properties but its toxic carcinogenic effects. Chromate and chromate-containing compounds have been limited since 1982 by the Environmental Protection Agency through several acts. In Europe, for example, a directive was issued by their environmental board to eradicate the use of chromium by 2003, but it has now been delayed to 2007. Because of this a green corrosion inhibitors revolution has taken shape in the last decade to replace chromates [15]. The EPA states that the hexavalent chromium Cr<sup>6+</sup> whose properties make it an excellent corrosion inhibitor is environmentally unsafe. It is believed that the strong oxidation properties of chromates have brought much scrutiny concerning its use. The Cr<sup>6+</sup> undergoes reduction which eventually damages the DNA cells. Chromate exposure through inhalation, ingestion and skin contact is the most common ailment resulting in lung cancer. The environmental burden of using chromate has greatly affected the aerospace industry due to its dependence on using aluminum alloys. Thus it becomes imperative that chromates be replaced by environmentally benign coatings that offer the same performance levels of the chromates. The next section discusses one of the promising environmentally acceptable treatments.

## 1.3 SUPERPRIMER

### 1.3.1 Definition

The silane research group of Dr. William van Ooij defines this coating system to be, *'a chromate free, low or no VOC, no HAP, completely water-reducible universal coating system which is a direct onto metal coating and does not require an extra conversion coating. It will eliminate the use of chromium in the form of both conversion coating and in the form of pigments in the current coating practice. Their use will be replaced by an integrated organosilane system in combination with a compatible polymer. Further additions of particles and corrosion inhibiting pigments including color will be made to give the coating system a shape of a complete ready to commercial primer.* Van Ooij's research gave it the generic name 'SUPERPRIMER'.

### 1.3.2 Background and Origin

#### 1.3.2.1 Silane Pretreatments: Performance and Promise

Silanes, technically called as organofunctional trialkoxy silanes have been known and used as adhesion promoters for decades in various industries [16-23]. They are very efficient in binding two unlike materials like organic and inorganic materials together; hence the name coupling agent is given to it. This property of silanes allows them to be efficient in many areas like reinforced plastics, fiber reinforced thermoplastics, electric cables of cross-linked polyethylene, adhesion

promoters in resins and coatings, sealant primers, shell molds, brake linings, polishers, adhesives, printing oils, etc [24-36].

This ability of silanes is due to their unique chemical structure. The ability of silanes to act as adhesion promoters is attributed to their unique chemical structure. Organofunctional silanes have a general formula  $X_3\text{-Si-(CH}_2)_n\text{-Y}$  where Y represents an organofunctional reactive group and X is a hydrolyzable ester group which is capable of reacting with inorganic materials. The functional groups can be a vinyl, sulfur or an amine group and many others which can interact with organic materials such as polymers. A schematic of silane mechanism is shown in Figure 1.10.

Plueddemann et al. [16] studied in great depth the ability of silanes to improve properties of glass/polymer composites. He was able to demonstrate that the mechanical properties of the glass/polymer composites can be enhanced with the application of silane coupling agents like vinyl, amine or methacrylate silanes. Plueddemann proposed various theories to explain the silane solution chemistry and its bonding mechanisms to the inorganic material. According to him the alkoxy ester groups need to be hydrolyzed with water to form silanol groups (Si-OH). These silanol groups are expected to form strong covalent bonds with a hydrated inorganic material. The silanol groups undergo condensation reactions on contact with an inorganic/metal surface leading to the formation of siloxane chains and metallo-siloxane bonds at the interface. The presence of

more active silanol groups in the hydrolyzed silane mixture is important in order to get good reactivity at the surface and subsequently more metallo-siloxane bonds are formed. The bonding of reactive groups to polymers has also been studied in great depth [37-38]. The good adhesion of the silane to the polymer is attributed to the chemical reactions that occur between the functional group in the silane and the reactive functional group in the polymer.

In order to understand the theory and application of this silane coupling agents many researchers conducted various analytical and characterization techniques and studied film properties like structure, morphology and interaction with metals and polymers. They also varied process parameters like pH, rate of hydrolysis, method of application, curing and choice of solvent [37-39].

The application of silanes towards corrosion protection of metals was not studied in detail until Van Ooij et al. [40-45], who initiated research in this area. Initially corrosion performance of mono-silanes was investigated. Petrunin studied the corrosion protective properties of silanes coupling agents such as  $\gamma$ -GPS and  $\gamma$ -APS on aluminum surfaces. Duquensay [46] treated aluminum alloys with silanes such as  $\gamma$  GPS. All authors were convinced of the formation of a covalent bond that forms at the interface.

Van Ooij and his coworkers concentrated on the corrosion inhibiting property of silanes to establish a suitable environmentally acceptable surface treatment. They were able to prove that silanes can protect metals especially aluminum and steel from all forms of corrosion, such as

uniform, galvanic, pitting, crevice corrosion and stress corrosion cracking to name a few. Recent research activities of this group are focused on inhibiting microbiologically induced corrosion and corrosion fatigue cracking by silanes. During the initial stages of research on silanes, Subramanian and Van Ooij [45] measured corrosion properties of mono-silanes and bis-silanes films deposited on steel and aluminum. They found that the bis-type silanes gave better corrosion performance as compared with the mono-silanes. They used potentiodynamic direct current polarization tests to confirm this behavior. Later Electrochemical Impedance Spectroscopy (EIS) was used to characterize and explain the corrosion behavior of these bis-silane films [45].

Zhu and Van Ooij further developed a number of silane systems for bare metal corrosion and surface pretreatment. An electrochemical study of silane mixtures of bis-sulfur and bis-amino silane showed better corrosion resistance than an individual silane system [11]. Further, the effect of hydrolysis time, and curing temperature was investigated to explain the corrosion mechanism of the silane films. They suggested that the corrosion inhibiting properties of the silane film were due to the high hydrophobicity of the fully cross-linked film. They also developed completely water-based silane systems without the use of solvent to further the potential of using silanes as effective corrosion-inhibiting systems.

Palanivel and Van Ooij further developed modified silane systems for improved corrosion protection for aluminum alloys [3]. They showed that additions of particles to silane films at an

optimum level increase the performance. They also showed that self-healing ability of chromate films can be imitated in silanes by addition of corrosion inhibitors.

The above research took the silane research group's study further into areas of primer development and to the idea of a primer with the unique abilities. The next section discusses the origination of this idea. An attempt is made to develop a primer whose single coating would perform equally well when compared to the two layer conversion coating plus primer system.

#### **1.3.2.2 Superprimer Idea and the Objective of this Thesis**

When used as a corrosion protection treatment without paint, a silane film has limitations in that its film thickness cannot be greater than about 0.3  $\mu\text{m}$ . Silane films are brittle when deposited at greater thickness. Although such thin films provide a remarkable level of protection against various forms of corrosion, they are easily damaged. Therefore a necessity to develop a coating with a greatly enhanced film build came up. The increased film build will be the result of the incorporation of nanoparticles, which will interact strongly with the silane molecules. Brittleness of the films will be controlled by incorporating one or more polymer resins to improve film toughness. Success in this task will generate metal treatment systems that are more robust and can be used as self-priming coatings, superprimers, or as metal pretreatments.

The proposed coating will comprise the following components.

**A:** One or more of an organofunctional silane preferably selected from the class of bis-silanes which Van Ooij and co-workers found to be considerably more effective than mono-silanes [8-10, 28]. They have also discovered that mixtures of two silanes are often markedly more effective than either silane alone. Examples of bis-silanes that they have used successfully in a variety of corrosion and bonding applications are (X = CH<sub>3</sub> or C<sub>2</sub>H<sub>5</sub> (methoxy or ethoxy) :

- bis-[triethoxysilyl]ethane: (XO)<sub>3</sub>-Si-CH<sub>2</sub>CH<sub>2</sub>-Si-(OX)<sub>3</sub>
- bis-[triethoxysilylpropyl]amine: (XO)<sub>3</sub>-Si-(CH<sub>2</sub>)<sub>3</sub>-NH-(CH<sub>2</sub>)<sub>3</sub>-Si-(OX)<sub>3</sub>
- bis-[triethoxysilylpropyl]ethylenediamine: (XO)<sub>3</sub>-Si-(CH<sub>2</sub>)<sub>3</sub>-NH-CH<sub>2</sub>CH<sub>2</sub>-NH-(CH<sub>2</sub>)<sub>3</sub>-Si-(OX)<sub>3</sub>
- bis-[triethoxysilylpropyl] urea: (XO)<sub>3</sub>-Si-(CH<sub>2</sub>)<sub>3</sub>-NH-CO-NH-(CH<sub>2</sub>)<sub>3</sub>-Si-(OX)<sub>3</sub>.

**B:** A low-molecular weight water-soluble polymer or copolymer selected from the generic class of epoxy, polyester, polyurethane or acrylate.

**C:** A reinforcing filler material, preferably of nanoparticle size, of the metal oxide type that adsorbs silanes. Examples are zinc oxide, aluminum oxide, iron oxide, magnesium oxide and silica. The particle size is of the order of 50-100 nm. The pigment will be dispersed into the coating by solgel methods or by high-shear blending.

**D:** A water-soluble inhibitor for corrosion protection of metals. This component is variable in that it is selected on the basis of the substrate. A range of inhibitors is available for metals such as steels, aluminum alloys, zinc, and brass. The inhibitor will be leachable from the coating at a controlled rate.

**C:** Additional components such as emulsifiers, surfactants, film builders, UV absorbers, or thickeners. These agents are present in low concentrations, e.g., of the order of 0.5% solids. The UV absorber can be a pigment such as ZnO or TiO<sub>2</sub>.

The functional group R in the silane will be selected so that it reacts with functional groups in the polymer backbone. Attempts to exploit the linkage between soft and hard phases to generate tough films by nano-phase reinforcement [48-49] will be made. The novelty of the design of this primer is that we add enough silane so that, in addition to crosslinking with the polymer, the silanes will also crosslink with itself and form a three-dimensional siloxane network, interpenetrated with the cross-linked polymer. The result will be a polymer-toughened siloxane film. The mechanical strength is further improved by incorporation of the nanoparticle reinforcing filler. These particles are bonded to themselves and to the polymer by the silane.

The nanoparticles will improve the scratch resistance of the coating and lower its permeability to electrolyte. Nanoparticles can also accelerate the cure of the coating by catalytic effects, as

Palanivel and Van Ooij in their recent experiments have shown [3]. The bis-silane is clearly playing multiple roles, which presumably account for the effectiveness of these films. Linkage to the polymer (through the R-group) provides toughening. Crosslinking of the bis-silane with itself leads to a hydrophobic network with extremely low water permeability. Finally, the silane anchors the film to the metal substrate by formation of the interfacial conversion product.

Van Ooij and co-workers in their prior research have identified the hydrophobicity of the film as critical to performance. Other factors, such as porosity, oxide bonding, and corrosion inhibition are present as well, but hydrophobicity is the key. [50, 13-15, 51] Hydrolyzed silanes are very hydrophilic due to the silanol groups. As a result, they readily adsorb on hydrophilic surfaces, such as metals, glass or metal oxide powders. After adsorption and curing they become hydrophobic, as they lose water and crosslink to Si-O-Si units, which are hydrophobic. The transition from hydrophilic to hydrophobic is what makes silanes so unique. No other surface treatment or coupling agent shows this behavior.

Because of the dominant influence of hydrophobicity, any coating system must completely encapsulate (or dissolve) any hydrophilic resin molecules, which are necessarily somewhat hydrophilic to assure dispersion in the carrier fluid. After curing, a transition must take place that renders the entire film highly hydrophobic. In other words, it is crucial that phase separation between the siloxane and the resin be avoided or at least restricted to nanometer dimensions. An

attempt to specifically study the phase behavior of various silane-resin combinations will be made.

The proposed technology is compatible with conventional corrosion inhibition strategies. The function of a conventional inhibitor is to provide corrosion protection in nicks and scratches in the coating. The initial primer film is densely cross-linked, an addition of a water-soluble inhibitor to the coating that will leach out very slowly due to the extreme hydrophobicity of the film. This approach gives great flexibility in selecting the inhibitor. Optimizing the inhibitor based on the target substrate can be made. The inhibitor replaces the defect-healing capabilities of chromates used in conventional metal primers. Palanivel and Van Ooij already have published results that confirm the validity of this concept [3]. Of the other additives; the UV absorber is built-in if we use zinc oxide (a UV absorber) as the nanoparticles. Silanes are known to adsorb on zinc oxide. TiO<sub>2</sub> (a UV scatterer) can also be used. Nanoparticles of various types (SiO<sub>2</sub>, Fe<sub>2</sub>O<sub>3</sub>, and CuO) can be generated by *in-situ* sol-gel methods from alkoxy compounds. These particles can play a number of roles such as reinforcement, pigmentation and UV protection. Figures 1.11 and 1.12 give a schematic of superprimer adsorption on a metal and its crosslinking in the film.

In summary, this primer will provide outstanding corrosion protection for most metals, by itself or with an overcoat. It can function as a self-priming coating if used at the maximum coating weight, which we estimate to be about 20-30  $\mu\text{m}$ . Since the film can be tailored to specific substrates, it

can be used as stand alone coating on aircraft, ships, missiles, munitions and support equipment.

It will be water-based, environmentally compliant and simple enough to be applied by semiskilled workers. Coating maintenance will be straightforward as the film can be overcoated and cured.

Overall, the coating system that will be developed here will meet the following requirements:

- The coating is devoid of chromates or other toxic components
- The coating protects various metals against all common forms of corrosion, including localized attack such as pitting, stress corrosion cracking (SCC) and corrosion fatigue cracking (CFC)
- The coating adheres very well to the metal and is paintable by all common paint systems such as epoxies, polyesters, acrylates, and polyurethanes
- The chemicals used in the coating mixture are all water-soluble (low VOC)
- The film thickness is variable and ranges from 1 to 20  $\mu\text{m}$
- The coating cures thermally at or near room temperature
- The coating can withstand mechanical deformation such as deep drawing, i.e., the coating is flexible
- The coating is UV resistant without over-coating
- The coating can be applied by dipping, wiping, spraying or brushing
- The coating is translucent allowing direct inspection of both the film and substrate

- The coating is thermally stable to at least 250°C for one hour
- The coating is very hydrophobic (surface energy typically that of silanes, i.e., ~25 mJ/m<sup>2</sup>)

## CHAPTER 2: MATERIALS AND TESTING PROCEDURES

The following chapter gives information about the materials used for preparation of the superprimer. Procedures used for the testing and preparation of the superprimer are discussed.

### A. Materials

#### A.2.1 Silanes

Table 2.1 shows the list of silanes which were experimented with, along with their trade names and chemical formulas.

All the above silanes, except for VTAS, were obtained from GE Silicones. VTAS was obtained from Gelest Inc. (Tullytown, PA). The silanes were used without further purification. Some silanes were used in hydrolyzed state and the others in non-hydrolyzed state. A detailed explanation about the preparation of silane solutions is given in later chapters while introducing superprimer formulations.

Bis-amino (A-1170) and VTAS silanes are mixed in their pure state. The reaction is exothermic.

The reaction mixture is allowed to stay on the shelf for at least 24 hours. This gives sufficient time for the reaction between the two silanes to go to completion. This mixture is water-soluble. But the order of mixing of water and silane does matter in this case. Addition of DI water at ordinary pH can result in immediate condensation of the amine content of the mixture resulting in threads

of polymerized particles in the solution. To avoid this, the pH of the appropriate amount of DI water taken needs to be adjusted first around 3 to 4 using acetic acid. After this pH is adjusted, the required amount of the silane-reaction-mixture needs to be added slowly while stirring to DI water. Dilution of silane mixture by this method gives uniform clear silane solutions. This particular method of mixing is not uncommon in industries and pretreatment companies. So to 90 parts of DI water the pH of which is adjusted to about 3 to 4, 10 parts of A-1170:VTAS (5:1) mixture is added slowly while stirring. After the clear solution is obtained, the solution is allowed about 4 hours of hydrolysis time. After these four hours the solution is good for coating or for use in coating formulations.

### **A.2.2 Resins**

The following Table 2.2 is a list of resins which were used for formulation of superprimer. All of the resins were obtained from Resolution Performance Products (Houston, Texas). All the resins mentioned here are epoxy resins. Although other types of resins can be used for formulation of superprimers this thesis concentrates on the formulations based on water-based epoxy primers.

EPON 828 Resin-X-75 is a 95% DGEBA type epoxy resin solids in 5% xylene. It is a completely solvent-based resin whereas the rest of the resins in the table are completely water-based epoxy resins. EPI-REZ Resin 3510-W-60 is a waterborne dispersion of a low-molecular weight liquid Bisphenol A epoxy resin EPON Resin 828-type. It has 60% solids in water and has no co-solvent.

EPI-REZ Resin 3515-W-60 is a waterborne dispersion of a semi-solid Bisphenol A epoxy resin. It has 63% percent solids in water and has no co-solvent. EPI-REZ Resin 3540-WY-55 is a waterborne dispersion of a solid Bisphenol A epoxy resin (EPON 1007-type) with an organic co-solvent 2-propoxyethanol. It has 55% solids in water and 11% co-solvent. All the resins were used in the obtained state without further dilution or modifications. Information about any other commercial resins or topcoats used for experiments in this thesis is given at the time of their mentioning.

### **A.2.3 Particles**

The following Table 2.3 shows a list of particles of nano-size which were included in the superprimer formulations. The particles were chosen on basis of their affinity towards silanes and the resins that were used in the superprimer formulations. All of the particles were used in the obtained state without further purification or dilution. They were added to the final superprimer formulation. Detailed explanations of mixing procedure are given in later chapters.

### **A.2.4 Inhibitors**

A variety of corrosion-inhibiting pigments was tried in the superprimer formulations. The idea and the mechanism in which they work are discussed in the later chapters. Commercial inhibitors from many companies were obtained and tried. They were first tested for compatibility with the

contents of the superprimers and then they were used in the final formulations with the recommended percentages. The following Table 2.4 shows the list of inhibitors which were compatible and were tried in the final formulations. All the inhibitors were used in the obtained state without further purification or dilution.

#### **A.2.5 Metals/ Alloys**

AA2024-T3 and cold-rolled steel panels with dimensions of 10 cm \* 15 cm \* 0.06 cm were purchased from Stillwater Steel Supply (Stillwater, OK). The sheets were cleaned with an uninhibited alkaline cleaner (AC 1055®, Brent America., Lake Bluff, IL). The metal substrates were first solvent scrubbed with red scotch brite pads dipped in ethanol. Then they were cleaned and rinsed thoroughly with DI water to remove all the grit and dust caused by the scrubbing. Then the panels were ultrasonically cleaned with ethanol in an ultrasonic bath for 10 minutes each. The cleaned panels were further alkaline cleaned with 7.5 vol % of the AC 1055 aqueous solution at 60-70°C for 3-5 minutes. The cleaned panels were then rinsed in DI water. The panels were blow-dried with compressed air. The cleaned metal panels were checked for water-break-free surface. This water-break-free surface confirms that the surface was sufficiently clean for coatings to be applied.

## **B. Testing Procedures**

### **B.2.1 Electrochemical Impedance Spectroscopy**

*Electrochemical Impedance Spectroscopy measurements (EIS)* were employed to evaluate the corrosion performance and film properties of the coatings on metal panels in a 0.6 M NaCl solution (pH 6.5). The EIS measurements were carried out using an SR810 frequency response analyzer connected to a Gamry PC-3 potentiostat. The measured frequency range was from  $10^{-2}$  to  $10^5$  Hz, with AC excitation amplitude of 10 mV. SCE was used as the reference electrode and coupled with a graphite counter electrode. The surface area exposed to the electrolyte was 5.16 cm<sup>2</sup>.

### **B.2.2 Salt Spray Test (ASTM B 117)**

*ASTM B117 (Salt spray (fog) test, SST)* this test was employed to evaluate bare corrosion protection of silane-treated metals without topcoats. According to the specifications, 5% salt solution (NaCl) is atomized in a salt spray chamber at 35°C with the solution pH around 7. The tested panels were placed at an angle of 45° in the chamber, exposing the panel to salt fog for a certain length of time.

### B.2.3 NMR Spectroscopy

*NMR Spectroscopy* was done on superprimer formulations both in liquid and dry forms. For testing in dry form, fine powder was obtained by scraping the coatings from the metal panels after coating and curing. These scrapings from the coatings were made into a very fine powder by grounding it manually using a mortar and pestle. Liquid formulations were also tested directly without further modifications. NMR spectroscopy was done at Oklahoma State University, Stillwater, OK. The following brief explanation is given with the help of the information published in A.4.

NMR spectroscopy is an efficient analytical technique which can be used for characterization of different kinds of solid and liquid materials. Within a sample specific NMR active nuclei can be observed, which provides a unique level of selectivity for NMR spectroscopy technique. Solid-state and liquid-state NMR spectrometers can be used to discriminate between the reactant components and final superprimer mixture. Liquid-state NMR spectroscopy can be an efficient method to determine molecular structure and conformation. It can be used for both qualitative and quantitative analysis of specific components in a mixture, and, it also provides a sensitive method to quantify impurities, reaction products, or residual solvents including water. In most of the cases this type of spectroscopy the sample size can be only a few milligrams of material while solid-state NMR experiments may require approximately 50 mg of material.

Subatomic particles, electrons, protons and neutrons can be imagined as spinning on their axes.

The spins of these particles in most of the atoms like  $^{12}\text{C}$ , are paired against each other, such that the nucleus of the atom results in no overall spin. However, in some atoms (such as  $^1\text{H}$  and  $^{13}\text{C}$ ) the nucleus does possess an overall spin. The net spin can be determined by the number of neutrons and the number of protons; when they are both even, the nucleus has no spin. In the other case when the number of neutrons plus the number of protons is odd, then the nucleus has a half-integer spin (i.e.  $1/2$ ,  $3/2$ ,  $5/2$ ) the final case would be if the number of neutrons and the number of protons are both odd, then the nucleus has an integer spin (i.e., 1, 2, 3).

Much of the quantum mechanics depends on the overall spin  $I$ . A nucleus with spin  $I$  will have  $2I + 1$  possible orientations whereas a nucleus with spin  $1/2$  will have 2 possible orientations. When an external magnetic field is not applied the energy levels have equal energy, but in the presence of the magnetic field the energy levels split and each level is given a magnetic quantum number  $m$ .

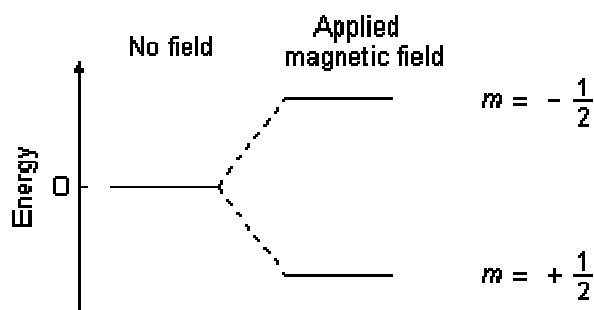
Sometimes the nuclei of isotopes contain an odd number of electrons and/or an odd number of neutrons, in which case the mechanical spin phenomena exhibited by them is associated with angular momentum which is characterized by a nuclear spin quantum number  $I$  such that,

$I = 1/2n$ , where  $n$  is an integer 0,1,2,3...etc.

Some nuclei like that of  $^{12}\text{C}$  and  $^{16}\text{O}$ , fall into the category in which the  $I$  value is equal to 0. In this case there is no angular momentum or the mechanical spin phenomena. Nuclei for which  $I = 1/2$  include  $^1\text{H}$ ,  $^{19}\text{F}$ ,  $^{13}\text{C}$ ,  $^{31}\text{P}$  and  $^{15}\text{N}$ , while  $^2\text{H}$  and  $^{14}\text{N}$  have  $I = 1$ .

When atomic nuclei associated with a charge spin on their axes they generate a small electric current and a certain amount of magnetic field is associated with it. This magnetic dipole moment varies with each element. When a finite amount of external magnetic field is applied, a certain amount of torque is experienced by the nuclear magnet which tries to align itself with the external magnetic field. For example, a nucleus with  $1/2$  spin has two possible orientations, one in the direction of the applied field with low energy and one against the field with high energy. The orientation with low energy will be more populated than the higher energy one.

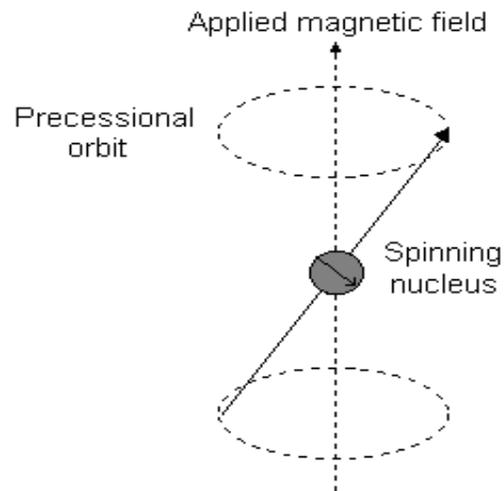
### Energy levels for a nucleus with spin quantum number $1/2$



On application of electromagnetic radiation with enough frequency, the oriented nuclei of the lower energy state spin-flip to the higher energy state after the absorption of a definite amount of

energy/radiation. During the process of this transition the nuclei is said to be in resonance with the applied radiation. Hence the procedure is named as nuclear magnetic resonance.

The spin-flip transition of every nucleus does not occur at the same frequency even if the magnetic dipole moment is the same. It depends on the number of rotating electrons which determines the amount of shielding experienced by a certain nuclei. So the greater the number of electrons in an environment the greater the shielding will be on a nuclei. So the number of electrons will play a part in the magnetic field of the nuclei making each nucleus nuclear magnetic resonance signal unique.



The resulting shift in the NMR signal for a given nuclei is called as the Chemical Shift. The protons or carbons adjacent to electronegative atoms will be de-shielded and moved to a higher chemical shift . The chemical shift is defined by the equation shown below:

$$\text{Chemical Shift } (\Delta) = (\text{shift observed/oscillator frequency}) \times 10^6 \text{ ppm}$$

The factor of  $10^6$  is introduced into the equation to give a simple whole number scale for convenience.

For both  $^1\text{H}$  and  $^{13}\text{C}$  NMR, the NMR absorption of the molecule tetra methyl silane ( $(\text{CH}_3)_4\text{Si}$ ) is set to be zero. When compared with other organic molecules the carbons and protons of this molecule are more shielded. The length of the scale for  $^1\text{H}$  NMR is 0-12 ppm and for  $^{13}\text{C}$  nuclei it is 0-220 ppm.

The nucleus of  $^{29}\text{Si}$  NMR has very low sensitivity so the spectrum gives rise to sharp lines. Its wide chemical shift range helps to determine the chemical environment in silicon compounds. At -90 ppm a background signal due to the glass tube and the probe is observed .

One further feature of proton NMR is the fact that the intensity of the absorbance of a given class of nuclei (with a certain chemical shift) is proportional to the number of protons giving rise to the signal; that is, the area under a given peak (the integration) is directly proportional to the number of that type of protons in the molecule. Integrations are typically given as simplest whole-number

ratios, hence, acetic acid,  $\text{CH}_3\text{COOH}$ , will have two peaks in the proton NMR, one at  $\Delta = 2$ , area = 3, and a second at  $\Delta = 12$ , area = 1. Methyl acetate,  $\text{CH}_3\text{COOCH}_3$ , will also have two peaks in the proton NMR, one at  $\Delta = 2$ , area = 1, and a second at  $\Delta = 4$ , area = 1 (the *relative areas* of both peaks are the same, but each one represents three hydrogens).

#### **B.2.4 Infrared Spectroscopy**

*RAIR characterization* was used to study the chemical structures of the deposited silane films.

The reflection-absorption infrared spectroscopy spectra was obtained using a BIO-RAD FTS-40 FT-IR spectrometer equipped with a BIO-RAD variable angular 32 reflectance attachment at an angle of  $75^\circ$ . The spectra were acquired for 256 scans using  $4\text{cm}^{-1}$  resolution. These tests were performed at the Chemistry Department, University of Cincinnati, Cincinnati, Ohio.

Coates in [52] gave the best explanation for IR spectroscopy by stating that the vibrational spectrum of a molecule is considered to be a unique physical property and is characteristic of the molecule. As such, the infrared spectrum can be used as a fingerprint for identification by the comparison of the spectrum from an “unknown” with previously recorded reference spectra. This is the basis of computer-based spectral searching. In the absence of a suitable reference database, it is possible to effect a basic interpretation of the spectrum from first principles, leading to characterization, and possibly even identification of an unknown sample. [52]

All types of matter absorb energy when exposed to electromagnetic radiation. Energy in light or electromagnetic radiation exists in form of photons. The amount of energy depends on the frequency of the radiation. The radiation is divided into Microwave, Infrared, Visible and Ultraviolet regions. On the high-energy side of the complete spectrum lies the ultraviolet and on the low-energy side is the infrared. The portion of the infrared region is most useful for analysis of organic compounds.

The energy possessed by any molecule can be distributed into rotational, vibrational, electronic and translational energies. The sum of these energies gives the total energy. The translational energy relates to the displacement of molecules in space as a function of normal thermal motions of matter. Rotational energy, which gives rise to its own form of spectroscopy, is observed as the tumbling motion of a molecule, which is the result of absorption of energy in the microwave region.

The electronic component of the energy is linked to the energy transitions of electrons as they are distributed throughout the molecule and this energy is observed only when the radiation is in visible or ultraviolet portions. The vibrational energy component corresponds to the energy associated with the molecule when the component atoms vibrate about their mean center of their chemical bonds.

The following explanation is from the information published on A.5.

Photon energies associated with this part of the infrared are not large enough to excite electrons, but may induce vibrational excitation of covalently bonded atoms and groups. The covalent bonds in molecules are not rigid sticks or rods, such as found in molecular model kits, but are more like stiff springs that can be stretched and bent.

The energy of a photon of light is given by the Planck-Einstein equation:

$$E = h\nu \quad [\text{eq 10}]$$

Where:

$h$  = Planck's constant ( $4 \times 10^{-13}$  kJ / mol)

$\nu$  = frequency of light ( $\text{s}^{-1}$ )

The relationship between frequency and wavelength of light is:

$$\nu = c / \lambda \quad [\text{eq 11}]$$

Where:

$c$  = speed of light ( $3 \times 10^{10}$  cm/s)

$\lambda$  = wavelength of light (cm)

A molecule will not absorb all incoming light, but only that light which has energy equal to a quantized transition within the molecule. Depending upon the energy of the incident light, several electronic (or nuclear) transitions are allowed as described below.

- exciting a molecule from one rotational level to another - microwaves
- exciting a molecule from one vibrational level to another - infrared
- exciting a molecule from one electronic level to another - UV/Vis

The larger the energy gap between levels, the higher the frequency ( $\nu$ ) and the smaller the wavelength ( $\lambda$ ) must be for the incoming radiation.

The infrared radiation excites the component atoms in a molecule to a vibration state. This excitation causes the bond in between the component atoms to stretch and bend. The frequency of the radiation at which a bond bends or stretches is unique and can be found from simple formulas. From a simple statement of Hooke's Law we can express the fundamental vibrational frequency of a molecular ensemble according to equation:

$$\nu = \frac{1}{2\pi c} \sqrt{\frac{\kappa}{\mu}} \quad [\text{eq 12}]$$

Where  $n$  = fundamental vibration frequency,  $k$  = force constant, and  $m$  = reduced mass. The reduced mass,  $m = m_1 \cdot m_2 / m_1 + m_2$ , where  $m_1$  and  $m_2$  are the component masses for the chemical bond under consideration. This simple equation provides a link between the strength (or springiness) of the covalent bond between two atoms (or molecular fragments), the mass of the interacting atoms (molecular fragments) and the frequency of vibration. Although simple in concept, there is a reasonably good fit between the bond stretching vibrations predicted and the values observed for the fundamentals. [52]

Infrared spectroscopy involves the absorption of infrared light causing chemical bonds to bend and stretch. Infrared light has wavelengths ( $l$ ) between 2.5 and 25 mm and wave numbers ( $N^\circ$ ) between 4000 and 400  $\text{cm}^{-1}$

$$N^\circ (\text{cm}^{-1}) = 1 / l (\text{cm}) \quad [\text{eq 13}]$$

The wave number is directly proportional to the energy so it increases with the wave number.

Determining stretching frequencies for bonds, Hooke's Law can be used to estimate the wave number of light that will be absorbed by different types of chemical bonds.

$$N^\circ = 4.12 * (K / m)^{1/2} \quad [\text{eq 14}]$$

Where:

$K$  = force constant (in  $\text{N} / \text{cm}$ )

- for single bond:  $K = 5 \text{ N/cm}$
- for double bond:  $K = 10 \text{ N/cm}$
- for triple bond:  $K = 15 \text{ N/cm}$

$m = M_1 M_2 / (M_1 + M_2)$  ( $M_1$  and  $M_2$  are molar masses of atoms involved in bond) [52].

### **B.2.5 Scanning Electron Microscopy (SEM/EDX)**

*Scanning Electron Microscopy (SEM/EDX)* was used for micro structural characterization and analysis of the precipitates and compounds such as cerium in panels and along scribes of panels.

The Scanning Electron Microscope is an incredible tool for observing objects of interest at a micro-level. It is very different from the conventional light microscopes which use a series of glass lenses to bend light waves and create a magnified image. The magnified images given by the SEM are created by the use of electrons instead of light waves. The SEM shows very detailed 3-dimensional images at much higher magnifications than is possible with a light microscope. The images created without light waves are shown in black and white. Extreme care has to be taken during the sample preparation because the samples have to withstand the vacuum inside the microscope. Biological specimens are dried in a special way that prevents them from shriveling. Because the SEM illuminates them with electrons, they also have to be made to conduct electricity. The sample is placed inside the microscope's vacuum column through an air-tight door. After the air is pumped out of the column, an electron gun emits a beam of high energy

electrons. This beam travels downward through a series of magnetic lenses designed to focus the electrons to a very fine spot. Near the bottom, a set of scanning coils moves the focused beam back and forth across the specimen, row by row. As the electron beam hits each spot on the sample, secondary electrons are knocked loose from its surface. A detector counts these electrons and sends the signals to an amplifier. The final image is built up from the number of electrons emitted from each spot on the sample. EDX was used to characterize the presence of compounds and elements in corroded AA2024-T3 at an accelerating voltage of 20 kV. A Hitachi S- 3200 N SEM machine was used for the analysis.

#### **B.2.6 Film Hardness Test**

ASTM D 3363 Pencil Hardness testing method was used to observe the hardness values of the primer films. This test uses lead pencils with a broad range of hardness values. The softest to hardest is in the order of 2B - B - HB - F - H - 2H - 3H - 4H - 5H - 6H. The scratch resistance is equal to the hardness value of the pencil which makes a scratch and a gauge hardness value of the primer films is equal to the hardness value of the pencil which removes the film. In previous research on silanes [3] fifteen indentation experiments were performed on bis-sulfur silane-treated samples using MTS Nanoindenter XP and the patented Continuous Stiffness

Measurement (CSM) technique, the details of which are best discussed in reference [53]. Those techniques were not used for testing primer films here.

Similarly, Ellipsometry experiments were performed over a wide range of wavelengths of 300-800 nm with angle of incidence at 60, 65, 70, 75 degrees respectively. The Psi and the delta values were calculated and a computer was used for data acquisition. Further information about ellipsometry can be referred to [54]. Those techniques will not be useful for use on primer films.

### **B.2.7 Tape Adhesion Test**

*Crosscut adhesion tape test (ASTM D3359)* was used to assess the adhesion of coating films to metallic substrates by applying and removing pressure. A cutting tool device having a cutting edge angle between 15 and 30° was chosen, that will make several cuts simultaneously. Cuts were made on the coating in one steady motion with sufficient pressure on the cutting tool. After making two such cuts at 90° the grid area was brushed and a 2.5 cm wide semi-transparent pressure-sensitive tape was placed over the grid. The tape was rubbed with an eraser on the end of a pencil. After 30 s of application, the tape was removed rapidly and the grid inspected according to the ASTM standards. The amount of coated area retained under the tape corresponds to the adhesion efficiency of the primer. The more coated material removed by the tape, the poorer the adhesion of the coating to the substrate.

### **B.2.8 Solvent Resistance Test**

The ASTM D 4752 test for evaluating the solvent resistance of the primer films was performed.

This test method is used to determine the degree of cure of a baked film by the paint film resistance to a specified solvent. The Solvent Rub Test is usually performed using methyl ethyl ketone (MEK) as the solvent. The MEK resistance applies to paints, topcoats and primers.

This test involves rubbing the surface of a baked film with cheesecloth soaked with MEK until failure or breakthrough of the film occurs. The type of cheesecloth, the stroke distance, the stroke rate, and approximate applied pressure of the rub are specified. The rubs are counted as a double rub (one rub forward and one rub backward constitutes a double rub). The test is used widely in the paint industry because it provides a quick relative estimation of degree of cure without having to wait for long-term exposure results.

## **CHAPTER 3: SUPERPRIMER: FORMULATION, PREPARATION AND TEST RESULTS**

This chapter gives detailed information about the superprimer. In the beginning it gives information about the choice of picking of the components that go into the primer followed by initial formulation and their results. The developments that lead to the final formulation are discussed in detail. Test results including EIS and salt spray results are provided whenever necessary.

### **3.1 Choice of the components**

Following the background information provided in Chapter 1 about the superprimer, the choice of components that has to be made primarily targets on the kind of resin and the silanes/silane mixtures that are compatible with the particular resin chosen. The choice of resin can be any water-borne commercially available resin primarily an epoxy, polyurethane or acrylic-based. Even the choice of mixtures of two different resins is also a matter under current research. After the resin is chosen then a list of all the silanes which in theory would be compatible with the resin is made. Table 3.1 shows the resin class and the compatible silane class.

These silanes were checked for their compatibility with the resins by observing their mixture solution stabilities, viscosity changes, gel times, flow abilities etc. Since the basic aim was to formulate a primer which can be coated over a metal substrate, the requirements of a solution for

it to pass for a primer are taken into consideration. These requirements include pot lives, solution viscosity, dilution ability, proper wetting characteristics and film forming capability. This thesis is mainly aimed at producing a superprimer using an epoxy-based resin. A detailed explanation of the formulations and the procedure for their preparation is given in the later sections.

### **3.1.1 Chemistry**

The basic idea of the superprimer as mentioned in Chapter 1 is to form a primer out of a resin and a silane combination. Other additions to it are to enhance the performance characteristics of this primer. This primer would not require any additional pretreatment application and can be used as a direct on to metal coating.

When an epoxy-based resin is chosen, silanes or silane mixtures that contain amino groups are preferred. The amino groups in silanes such as bis-amino may react and open the epoxy ring in the resin and lead to cross-linking. Self cross-linking of both the silane and resin to themselves is also expected to occur although it was not demonstrated here. This cross-linking is enhanced while the curing/drying of the films over the substrate. The following list shows the chemical reactions that occur in an epoxy resin and amino silane combination.

Figures 3.1.1 and 3.1.2 show model reactions between an epoxy group and a tertiary aliphatic amine and primary amines, respectively.

The OH groups on the metal oxide surface may undergo a condensation reaction with the OH groups of the resin and thus lead to adhesive bonds between the resin and the surface. OH groups follow a condensation reaction to also allow cross-linking in the coatings.

## **3.2 Initial Formulations and Results**

### **3.2.1 Formulations**

This section discusses about the gradual improvements towards final superprimer formulations.

The experimental results of the initial failed formulations were only provided as a comparison with final superprimer formulations.

To check if addition of an amine-functional silane would actually be able to cross-link/react with epoxy resin, a simple mixing trial was adopted. Bis-amino silane was mixed with EPON 828, a high solid DGEBA epoxy resin. A 2:1 ratio of amine silane and epoxy resin was mixed at slightly elevated temperature and at constant stirring. The so obtained clear liquid was used for coating on alkaline-cleaned AA 2020 T3 panels. The solution gave rise to clear and tough films after an hour cure at 100°C. The mixed solution had a potlife of only an hour. This observation proved that silane alone can be used as a curing agent for a resin and coatings can be obtained from it.

Although the above mixture showed some excellent corrosion resistant characteristics like high modulus in EIS plot and good salt immersion results, the mixture was not water-reducible. The

idea was to obtain a water-reducible primer so the work was shifted towards water-based epoxy resins. EPI-REZ Resin 3510-W-60, a waterborne dispersion of a low molecular weight liquid bisphenol A epoxy resin EPON Resin 828-type, was obtained. Mixtures of it with amine-functional silanes like bis-amino were tried but observed to have poor film characteristics such as improper curing ability and poor adhesion. Even after 3-week curing at room temperature the films were still found to be tacky and wet.

EPI-REZ 3510-W-60 resin is a completely water-based resin with water as the only solvent and also the mixtures of it with amine silane contain only water as a solvent. The coatings formed from these resin-silane mixtures do require a lot of energy to drive the water from the film and give a dry film. This is the basic observed difference between the solvent-based and water-based coatings. Solvents usually require far less energy than water to evaporate, thus solvent-based coatings have far better curing and film characteristics than water-based coatings.

Following the above factor, EPI-REZ 3540-WY-55, water-based epoxy resin but with a co-solvent was chosen for trials. This resin contains 11% of 2-propoxyethanol as a co-solvent besides water.

The formulations showed a promising way towards a complete coating.

### 3.2.2 Results

EIS results were used to evaluate the film characteristics of the coatings. The impedance values in Bode plots gives information about the resistance of the film and water penetration through the film with time.

The thicknesses of silane pretreatment films are usually in the nano-meter scale. The thickness usually increases with concentration of the silane mixtures. But as the thickness increases the films become brittle. The idea of superprimer actually began with the thought to make thick silane films flexible enough so as not to break at higher thicknesses. Addition of a compatible polymer to silane solutions which would react with the silane to give flexible, tough and highly cross-linked film was tried.

Bayer PU 410, water-based polyurethane resin was found to be compatible with AMME silane.

The effect of increasing the resin content with silane on film properties was observed using EIS.

Figure 3.2.1 shows a Bode plot of a few of the initial formulations and their comparison with silane pretreatments. An increase in modulus value is observed with the increase in resin content of silane + resin mixtures.

This observation gave us an idea for mixing of formulations. In the next result we show an EIS result of a resin + silane mixture of an epoxy + amino silane and comparison of the film properties

with silane pretreatment alone. The EIS result of the silane + resin mixture showed high film modulus and an equally good performance in a salt immersion test. The salt immersion results of these panels are not discussed here.

The above two results and similar others led us to believe that thicker pretreatment films can in fact be achieved and primer films which do not require a conversion coating can be obtained from silane + resin combinations.

### **3.3 Superprimer Formulations**

As mentioned in the previous sections those initial water-based superprimer formulations with EPI-REZ 3510 showed some poor film characteristics. Formulations with EPI-REZ 3540-WY-55 showed some promising characteristics of a primer. So this particular resin was chosen to serve the purpose of a polymer in the superprimer definition.

Bis-amino silane was chosen for the formulations. Although other mono-silanes could be compatible and be used for formulations, bis-silanes proved in previous occasions to work better than mono-silanes [11]. Although bis-amino silane alone mixed well with the resin, the formulations showed low pot lives and gave brittle films. Bis-amino is a very basic silane so it is subjected to immediate condensation in a higher pH environment of the resin. Even hydrolyzed

solutions of bis-amino silanes require acetic acid to adjust the pH of the water solution. Their solutions in water are very unstable and gel up in a very short period of time.

For the purpose of obtaining solutions with comfortable shelf life before mixing, the idea of using silane mixtures was tried. Silane mixtures of bis-amino and vinyltriacetoxysilane have proven to give water soluble silane solutions with indefinite shelf life [11].

#### *Parts and Preparation of Superprimer*

Part A: EPI-REZ 3540-wy-55 epoxy resin was used as obtained without further dilution.

Part B: 10% diluted solution of AV5 at pH 5. AV5 is mixture of A-1170 and VTAS mixed in the ratio of 5:1 by weight in pure state.

*Preparation of Part B:* A-1170 and VTAS silanes were mixed in their pure state. The reaction is exothermic. The reaction mixture was allowed to stay on the shelf for at least 24 hours. This gives sufficient time for the reaction between the two silanes to go to completion. This mixture is water soluble. But the order of mixing of water and silane does matter in this case. Addition of DI water at ordinary pH can result in immediate condensation of the amine content of the mixture resulting in threads of polymerized particles in the solution. To avoid this, the pH of the DI water taken needs to be adjusted to around 3 to 4 using acetic acid. After this was adjusted, the required amount of the silane reaction mixture needs to be added slowly while stirring the DI water.

Dilution of silane mixture by this method gives uniform clear silane solutions. This particular method of mixing is not uncommon in industries and pretreatment companies. So to 90 parts of DI water the pH of which was adjusted to about 3 to 4, 10 parts of A-1170: VTAS (5:1) mixture was added slowly while stirring. After the clear solution was obtained, the solution was allowed about 4 hours of hydrolysis time. After these four hours the solution is good for coating or for use in coating formulations.

Part C: Tetraethoxysilane, a common cross-linking silane with four hydrolyzable alkoxy groups.

*Weight Percentages:* 80 % of Part A + 19 % of Part B + 1 % of TEOS

*High Shear Mixing:* A laboratory High Shear Mixer from Charles Ross Mixers and Blenders Company (Model LC 10) was purchased and used especially for mixing primer formulations. All the components mentioned above were mixed in the above weight ratio and high-shear mixed for 10 minutes at a speed of 2000 rpm.

*Cleaning, Coating and Curing Method:* After the formulations were mixed an incubation time of 30 minutes is allowed before coating. This would give enough time for the reaction between amine and epoxy groups to take place. The formulations can be coated using a drawdown bar, brushed or sprayed on. Formulations can be diluted to sprayable viscosity.

Aluminum alloy AA 2024-T3 panels were ultrasonically cleaned in ethanol for 5 minutes followed by alkaline cleaning at 65°C for 3 minutes in a 7% by volume Brent uninhibited alkaline cleaner solution in DI water. After alkaline cleaning the panels are thoroughly rinsed in DI water and then blow dried. The panels were tested for water-break-free films indicating a clean surface.

Carbon steel panels were first solvent-scrubbed using ethanol as solvent and scotch-brite pads to remove the dirt, corrosion products and expose clean, shiny metal-oxide surface. After the scrubbing, the panels were cleaned with water spray and then followed by ultrasonic cleaning in ethanol for 5 minutes. The final stages of cleaning included alkaline cleaning similar to the one followed for aluminum but at lower temperature of 55°C and for only 1 or 2 minutes. CRS is a very sensitive substrate so care was taken not to spoil the metal-oxide surface before coating with superprimer.

After coating the panels were either cured for 1 hour at 100°C or for one week at room temperature.

### **3.4 Test Results**

Table 3.4.1 summarizes the test results of Superprimer formulation named 'F'. The results are compared with a control primer. The control was a chromium containing primer from the Navy named PRC Desoto MIL-PRF, containing about 25 % wt of chromate.

*Salt Spray:* Figure 3.4.1 shows result of control and formulation F after 2 weeks. After 2 weeks the control did not show any corrosion in the scribe but superprimer F did. The corrosion resistance performance in other areas of the panel looked comparable. The corrosion of the scribe in formulation F coated panels was expected because the superprimer formulations do not have the so called self-healing effect of chromate-containing primers.

*EIS Results:* Figures 3.4.2 and 3.4.3 show the EIS Bode plots of formulation F and the control. The plots show considerable difference in the film's resistance and water penetrability of the coatings. The decrease in impedance values with due time indicates the decrease in resistance due to water penetration.

EIS plot of formulation F shows that the modulus values decrease with time. The figure also shows appearance of a second time constant which indicates appearance of a second conducting layer in due time. These two factors prove the hydrophilic nature of the formulation. Due to this nature the coating seems to attract water molecules through its pores. The second conducting layer might be due to the complex molecular film formed by these and other hydrophilic groups in between the coating and the metal substrate. The EIS plot of the control did not show any signs of second time constant even though the modulus values decrease in due time.

### 3.5 Improved Formulations

Although we were able to formulate successful coating formulations from silane resin combinations, the performance of superprimer formulation F was not upto par with the chromium-containing controls. The coatings showed considerable hydrophilic nature. In an effort to improve the hydrophobicity of the film an addition of a known silane with extreme hydrophobic nature was sought. Bis-sulfur silane has been proven to be an efficient silane for use against corrosion protection in previous work [11]. A new formulation F-6 was formulated and tested in this effort.

The following gives the information about the formulation.

#### *Formulation F-6*

The components and mixing procedure of Formulation F-6 are:

Part A: EPI-REZ 3540-WY-55 Epoxy resin

Part B: AV5 10 % in water at pH 6

Part C: TEOS

Part D: Bis-sulfur was used in pure as obtained state without further hydrolysis.

By weight:

Part A (80%) + Part B (9%) + Part C (1%) + Part D (10%)

High-shear blended for 10 minutes at 2000 rpm. Bis-sulfur silane is not water soluble. But solutions which were uniform to the visible eye were obtained after high shear mixing of

the components. Even the coatings which were obtained from these coatings did not show any signs of immiscibility. The formulations did not separate into different layers in due time either.

After allowing 20 minutes of incubation time cleaned aluminum panels were either brushed or coated using a drawdown bar

Panels cured at 100°C for 1 hour

### **3.6 Test Results of Formulation F-6**

The addition of hydrophobic sulfur silane improved the hydrophobic nature of the superprimer coating. Figure 3.6.1 shows an EIS Bode plot comparing the modulus values of F-6, F and the control. The plot shows no drop in the F-6 curve even after 1 week of immersion. Whereas the EIS curves of formulation F were observed to drop with time.

Figure 3.6.2 shows an aluminum panel coated with F-6 and salt spray tested for 2 weeks. The picture shows no pitting in the unscribed area and also no considerable corrosion in the scribe.

Table 3.6.1 summarizes all the test results of F-6, F and control. Results of test such as hardness and tape adhesion showed considerable improvement in superprimer formulation F-6 in comparison to F.

### 3.7 Conclusions

Silanes or silane solutions at high concentrations can be used for coating purposes by modifying silanes with resins. Primer formulations were obtained by silane plus resin combinations, called by a generic term 'superprimers'. Formulations were developed and tested from low concentrations of resin followed by increased percentages of resin. A completely water-soluble superprimer formulation was developed using a waterborne resin and water-soluble silane solutions. Hydrophobicity and anti-corrosion performance of the superprimer were improved by inclusion of hydrophobic silane into the formulation. Test results including EIS and salt spray exposure showed that improved superprimer formulation had very good anti-corrosion performance. In the next chapter additions to superprimer will be discussed. Additions like nano-size particles and corrosion inhibiting pigments added to give specific qualities will be discussed in detail along with the formulations and test results.

## CHAPTER 4: ADDITIVES TO PRIMER

The silane plus resin combinations can lead to coating formulations but to make it perform on par with chromate primers further additions need to be made. Detailed explanation of the idea, purpose and expectations of these additives in the primer were already given in Chapter 1. In this chapter details about the mixing procedure of the additions, different kind of additives were tried and their test results are given. There are primarily two important kinds of additives, nanoparticles and corrosion inhibitors. Many commercially available particles and inhibitors were tried and tested for corrosion performance. Test results by EIS and salt spray exposure are provided.

### 4.1 Pigments/Particles

Particles and pigments are usually added to the paint to impart special characteristics or improve the film properties to the primer/paint coating. When in use for coloring of paint, ink, plastic, fabric and other material, a pigment is a dry colorant, usually an insoluble powder. There are both natural and synthetic pigments, both organic and inorganic ones. Pigments work by selectively absorbing some parts of the visible spectrum (see light) whilst reflecting others. Most of the nanoparticles have a catalytic effect on the chemical reactions occurring in the paint/primer systems. The particles for inclusion in the superprimer were also selected on the basis of their effect on the chemical reactions and curing of the primer. Previous studies indicated that inclusion of silica particles improved the anti-corrosion performance of silane films [3]. It was proposed that silane

films formed from the 5 ppm silica-containing silane solution behaves as a cathodic barrier like cerium compounds [55-56]. This type of activity is done with paint systems where the mechanical properties are improved by adding particles such as fillers, pigments and extenders in paint systems [57]. The following particles were tried and tested in superprimer formulations:

- Silica
- Alumina
- Carbon Black
- Zinc Dust
- Corrosion Inhibitors

A separate chapter is devoted for formulation and testing results of zinc dust inclusion. The others are discussed in this Chapter.

#### **4.1.1 Silica, Alumina and Carbon Black**

The mixing procedure of superprimer with particles is not different from the procedure of silane and resin mixture. The particles are included along with other components and mixed using the high-shear mixer. The curing conditions were also not changed. The metal panels were cleaned in the same manner as mentioned before in chapter 3.

Table 4.1.1 gives a detailed description of the components, their weight percentages in the mixtures and their corresponding formulation number. In some formulations there are no particle additions. Silanes such as A-link 25 and A-link 15 were tested to increase the cross-linking density of the films. Formulations numbered F 10 to F 12 are with alumina particles in increased weight percentages. F13 to F15 are with calcium zinc molybdate, a corrosion inhibitor from Molywhite Corporation. Similar information about the additions in other formulations is clearly given in the table.

## **4.2 Results and Discussion**

Previous work over modified silane films [3] showed that increase in the percentage values of silica in the silane solutions actually decreased the performance against corrosion. Figure 4.2.1 shows an EIS plot showing the effect of various amounts of silica in silane films. A probable theory for the mechanism of how the silica particles are acting towards the improvement of anti-corrosion performance was also given.

Figure 4.2.1 combined with other test results proved that an optimized amount of silica is required for the best performance of the silane films. A similar observation is observed in case of superprimer formulations also. Formulations F 10, F 11 and F 12 have alumina nano-particles in increased weight percentages of 2.5, 5.0 and 10.0. A simple salt immersion test of AA 2024-T3 panels coated with the above three formulations showed that increased weight percentages of

alumina in fact decreased the anti-corrosion performance. Figure 4.2.2 shows salt immersion results after 7 days in 3.5% wt in DI water.

EIS impedance values of the above coatings F10, F11 and F12 conformed to the above observation. Formulation F10 with 2.5 % alumina showed better impedance values with time.

Figure 4.2.3 shows EIS impedance values of salt fog-tested coatings with time. Impedance values of F10 were higher than F11 and F12 in most cases.

Figure 4.2.4 shows a similar plot with the same coatings but now with a topcoat over them. The topcoat used was a polyurethane based topcoat manufactured by DEFT. The impedance values of F10T and F11T, coating formulations of F10 and F11 with same topcoat showed similar performance.

Figures 4.2.5, 4.2.6 and 4.2.7 shows Bode plots of the coatings with and without topcoats tested over for a period of time. The numbers in the legend of the figures denote the number of days the panels has been exposed to the salt solution. Bode plots of coatings without topcoat show gradual decrease in the impedance values with time. All the three formulations behaved in the same way. This decrease in impedance values can be attributed to water penetration into the film with time. Bode plots of coatings with topcoat showed varying results with time. The change in impedance values was not consistent with or linear with time. But the impedance values in all

three cases were high, which showed an obvious fact that the water resistance of the coatings with topcoat is greater than the coatings without topcoat.

The salt spray test results conformed to the observations made using EIS test. Figure 4.2.8 shows salt spray results of F 10, F11 and F12 formulations with and without topcoat after 3 weeks of testing.

The EIS Bode plots of the individual formulations containing alumina showed an appearance of a second time constant for longer immersion times. The 7 day curve of F10 was a rather flat when compared to curves of F11 and F12. The change in slope of the curves which indicates the appearance of a second time constant was more prominent in F11 and F12 than in F10. This second time constant mentioned before indicates the appearance of a second hydrophilic layer beneath the topmost layer and above the metal oxide surface. This might indicate that water penetration through the films is less in case of F10 when compared to F11 and F12 for a short period of time. After 2 weeks all the 3 curves showed similar behavior in Figures 4.2.5, 4.2.6, and 4.2.7.

This particular observation leads us to an explanation that can be given to behavior of the particles in the primer. According to researchers [58] there is a critical amount of pigment that can be added to an organic coating system, beyond which the coating becomes more permeable or

porous. Nano-particles are known to have a catalytic action on the chemical reactions in the primers [59-60]. This observation was evident in case of formulations containing alumina, i.e., F10, F11 and F12. The pot life of a primer is defined as the amount of time the primer stays at coat-able viscosity before gelling up after all the components are mixed. The pot lives are usually high for water-based primers when compared to solvent-based primers. In case of superprimer formulation F-6, it is close to a week. The pot-life changed with the kind of addition that is made to the primer. The weight of alumina in the formulations had an inverse linear relation with the pot-life. The pot-life of the formulations decreased with increasing percentage of alumina. Similar behavior was found even in the case of inhibitor addition mentioned in the later part of the chapter.

The factor that can influence the performance is that the particles being hydrophilic in nature obviously attract water into the films. This is evident in the poor performance of the formulation with higher percentages of alumina. A similar explanation is given as a mechanism for silica in silane films [3].

### **Carbon Black**

Carbon black is one of the oldest fillers used in the paint industry. It was used 27000 years ago for cave paintings, and in 2500 before Christ by the Egyptians in inks. It was also used for the printing process during the middle Ages.

The rubber industry is the biggest user of carbon blacks by a large margin, in comparison. The paint industry is only a modest user. The printing inks industry also uses significant quantities. Finer particle blacks are used for high-quality finishes such as in automotive paints on account of their higher jet-ness. Medium size blacks are used for intermediate quality paints, whereas the coarser pigments are used for decorative paints. For tinting purposes coarser grades are usually used as their lower strength meaning they are easier to control.

Carbon-black pigments are very fine particulates of sub-crystalline carbon fused into larger aggregates. It is a mixture of partially burned hydrocarbons. Carbon black is produced by partial combustion of natural gas. It is used as a black pigment for inks and paints, and is used in large amounts by the tire industry in the production of vulcanized rubber. Lampblack resembles carbon black, but is produced by burning liquid hydrocarbons, e.g., kerosene; it is often somewhat oily, is duller than carbon black, and may have a bluish undertone. It is sometimes used in making contact brushes for electrical apparatus. Any of various finely divided forms of carbon derived from the incomplete combustion of natural gas or petroleum oil and used to reinforce rubber and as an ingredient in inks, paints, crayons, and polishes.

Carbon blacks can be difficult to disperse as they have very small particles with a correspondingly large surface area. Improved dispersions can be attained by oxidizing the surface of the pigment

or by adding small quantities of organic groups such as carboxylic acids. Such groups decrease the pH of the aqueous extract and aid the wetting of the particles.

The viscosity of the paint is affected by the inclusion of carbon particles. Particles of carbon form clusters which are often compared to a cluster of grapes, held together by forces ranging from weak physical attraction to chemical bonds. This structure affects the dispersibility, the jet-ness, gloss, and, above all, the viscosity of the paint.

One of the problems with carbon black can be due to the absorption character of it. The light dusty form of carbon blacks allows them to be converted to an easy-to-disperse pellet form by the dry pelleting process. Over a period of time carbon blacks absorb active ingredients in a paint formulation, such as the metal soaps used as driers in air-drying alkyds. This absorption can lead to problems; however, doubling the dosage of drier content is a common way of compensating for this issue.

### *In the Superprimer*

Carbon black was tested as a pigment addition in the superprimer formulation. F28 is the formulation number corresponding to this formulation. 3% by weight of carbon black was introduced into the resin plus silane mixtures. The mixture was prepared using a high-shear blender similar to the other methods. The formulation was coated on AA 2024-T3 panels and was

cured at 100°C for 1 hour. The coating resulted had an appearance of a glossy black paint.

Performance tests like EIS and Salt Fog exposure were used to evaluate the coating.

Figure 4.2.9 shows the salt fog performance of the F 28 panel after 28 days. It can be observed from the figure that the performance showed no decrease for the first 7 days of exposure but gradually decreased after 28 days.

The observation in the salt fog conformed to the impedance change in Figure 4.2.10. This figure shows an increase in the impedance values in the initial days of exposure. After 7 days the impedance showed a gradual decrease and the impedance values stabilized after 1 month exposure. The modulus value of the coating initially showed increase. This means that the resistance of the coating is increasing and the penetration of the corrosion causing species is difficult or slow. In due time the modulus values showed a decrease in their values and stabilized after 30 days. This shows that the coating's conductive nature improved with time or in other words the resistance of the coating decreased. This behavior can be explained by the penetration of water, oxygen and other corrosion causing species after long exposure times. After long exposure times the conducting species such as water penetrate through the coating and make the film more conductive. Initially the silane hydrolyzes thus increasing the resistance but after long periods of time the resistance drops due to passage of ions to the substrate.

The same observation and deduction can be made from Figure 4.2.11 which shows the individual impedance curves not clear.

### 4.3 Corrosion Inhibitors

The idea of including a corrosion inhibitor is used to achieve what is called a 'self-healing' effect in superprimers. A few promising chromate replacements inhibitors have been derived from cerium and molybdenum salts. These are believed to inhibit corrosion by controlling the cathodic reaction by precipitating hydroxide/oxide layers at local regions of high pH [61-62]. Chromium-containing primers have this property and it is this character which makes them so efficient. The detailed explanation of this effect was given earlier in Chapter 1. This effect can also be seen in the left side panel of Figure 3.4.1. Corrosion inhibitors were loaded and tested in silane films before [3]. Some water-soluble silane mixtures showed excellent corrosion behavior comparable to that of chromates [63]. However, it was observed that alcohol-based silanes offer a higher corrosion resistance to the water-based silane systems [64]. Vignesh et al [3] showed that one of the ways to increase the corrosion performance of these silanes is to add corrosion inhibitors to the films which can leach out slowly. The results that are reported here for various organic and inorganic inhibitors were studied for the corrosion inhibition of AA2024-T3 alloys in 0.5 M NaCl solution. Examples are benzotriazole [65-66], tolyltriazole [67] and rare earth metal salts, e.g., cerium nitrate [67-69].

Many inhibitors were selected and tried by including them in the formulations. Formulations numbered F13, F14 and F15 in formulation table have calcium zinc molybdate in increasing weight percentages. Formulations F20 to F29 except for F26 and F28 are primers containing different kinds of corrosion inhibitors from different companies. Only those inhibitors which are recommended for their use in waterborne primer formulations were tested and tested. Chemical information of these inhibitors was provided in Chapter 2.

#### **4.3.1 Results and Discussion**

Figure 4.3.1 shows the change in impedance values with time of the formulations F13, F 14 and F 15. The curve of F15 which has the highest amount of calcium zinc molybdate (CZM) showed marginally higher values of impedance values than the formulations with lower weight percentages.

Figure 4.3.2 shows the salt spray results of the formulations with and without topcoat in Figure 4.3.5. The results show that formulations with higher percentages of CZM performed better. This observation conformed to the EIS impedance plot above. The individual EIS Bode plots show that impedance value decrease at high magnitude for the first few days and then the modulus curves change at a very low magnitude. This observation might indicate that coating formulations

containing corrosion inhibitors form insoluble corrosion products in due time which form or make the coating less accessible to water and other corrosion causing species.

The individual EIS plots of the above formulations with topcoat did not show much change in the impedance values with due time. But the performance results of formulations with and without topcoat showed similar behavior i.e., formulations with higher percentages of CZM performed better. Figure 4.3.5 shows the test results of formulations with topcoat after 6 weeks of testing.

Other corrosion inhibitors from companies like Cortec and Fluka were also tried. Figure 4.3.6 and Figure 4.3.7 show the EIS and salt spray results of the formulations F20, F21, F22, F24 and F 25.

Figure 4.3.6 shows that the impedance values of almost all the inhibitors formulations without topcoat are close by and decrease with time. This decrease in modulus values stabilize after some time. This stabilization of the impedance values may be attributed to the fact that these inhibitors form insoluble corrosion products by reacting with corrosion causing elements. The mechanism by which these corrosion inhibitors work follows next.

Metal oxide or corrosion product over metal substrates like aluminum and steel delaminates easily from the surface to expose fresh metal, thus allowing for continued corrosion. Under normal atmospheric conditions (without inhibitors present), the corrosion products does not form an adherent or so-called 'passive' layer on the metal surface. It is also well established that most

organic coating films are not sufficiently impermeable to water and oxygen to prevent corrosion based on barrier properties alone. Effective corrosion inhibition by coatings therefore requires other protection mechanisms. When a coating film containing corrosion inhibitors becomes exposed to moisture, component ions of the inhibitors for example molybdate ions in case of Calcium Zinc Molybdate will pass into solution and migrate to the metal surface due to the controlled solubility characteristics of these pigments. The ability of these ions like molybdate ions to stabilize a thin, adherent and protective layer on iron and other metals is the key to the effectiveness of corrosion inhibitors. The oxide layer effectively insulates (i.e. passivates) the metal from attack and halts the corrosion process. The passivating properties of molybdates, zinc compounds, vanadium compounds etc are well recognized and documented in the field of corrosion science [70].

The main aim of using the corrosion inhibitors was to imitate the self-healing characteristic of chromates. This particular character of chromates like it is explained in chapter 1 allows the chromates to leach out of the coating and form insoluble chromium corrosion products over the scribes, scratches or any other kind of mechanical damages and protect them from further damage. The same kind of behavior was tried to achieve in the superprimer by addition of corrosion inhibitors. Though the performance of the coatings improved in un-scribed areas most of the cases but none of the corrosion inhibitors tried gave the superprimer a self-healing

capability. None of the coating formulations with corrosion inhibitors showed nil-corrosion in the scribe. Visible corrosion was observed in all the cases. This means that the inhibitors so far tried were not able to imitate the chromates in this aspect. It is one of the areas research still needs to be continued. Trials to find the right inhibitor still need to be done extensively.

#### **4.4 Conclusions**

Particles and corrosion inhibitors were added to silane plus resin mixtures to provide superprimer with better film properties and anti-corrosion performance. Alumina, carbon black and zinc were tried as particle inclusions along with commercially available corrosion inhibitors. EIS and salt spray standard tests were used to monitor the film properties and anti-corrosion performance simultaneously.

Test results showed that alumina addition to superprimer enhances the anti-corrosion performance. Increasing levels of alumina leads to decrease in the corrosion performance. Increase in porosity and hydrophylicity with increase in the amount of particles is considered to be the likely explanation behind this observation.

Carbon black was loaded as a pigment in the superprimer formulations. EIS and salt fog tests conformed to a single observation that the coatings resistance increased initially and the conductive nature of the coating increased with the exposure time. The performance of the

coating decreased with the increased in the conductive nature of the coating. A probable explanation of formation of hydrophilic hydroxyl complexes of the coatings components is given for the observation.

Corrosion inhibitors were tried to provide enhanced corrosion protection to the superprimer. This idea was put to trial so as to imitate the self-healing characteristic of the chromate primers. Test results showed that the corrosion performance did increase and primer coated surfaces showed less pitting and general corrosion in un-scribed areas. But the inhibition could not protect the scribed areas. Visible corrosion was found in most of the formulations. Quest for the right inhibitor still needs to be continued and this particular area gives scope for further research.

## CHAPTER 5: ZINC-RICH SUPERPRIMER

Zinc-rich primers are as the name suggests primers with heavy loads of zinc metal dust in it. The zinc dust/powder is used as filler and is held in the coating by using a binder. Paints with zinc pigments contain about 80% by weight pigment of which 20% is oxide. Zinc-rich coatings contain 85-95% metallic zinc, by weight, in the dry coating with little or no oxide. Depending the type of binder used the primer can be organic or inorganic. Organic binder can be epoxy, polyurethane, acrylate etc. In inorganic zinc-rich primers the binders are usually silicates. In the next few sections a brief explanation on the uses, application, mechanism of action and the idea of zinc-rich primer is described.

### 5.1 Uses and Applications

The amount of zinc in zinc pigments is not sufficient to permit galvanic protection by zinc. However, the zinc/zinc-oxide combination serves as an inhibitor for atmospheric, in both primer and finish coats [1]. The zinc-pigmented coatings show excellent adhesion, coverage and are very effective coatings for rural and mild industrial atmospheres but zinc-rich coatings are used and preferred for more aggressive atmospheres.

The use of metallic zinc in primer formulations to achieve sacrificial protection of steel structures has been well-established in the protective coating industry. The outstanding protective properties

of metallic zinc-based primers are based on the sacrificial properties of these primers in combination with their barrier properties and physical characteristics.

The majority of the zinc-based primers are formulated with either the inorganic silicate binders or with epoxy resin systems. In the United States the zinc silicates are predominantly used as primers for new buildings, such as for offshore structures and bridges. The only time zinc epoxy primers are used in service is for touch-up of coatings applied during fabrication, where severe damage to bare metal has occurred. Conversely, in Europe zinc epoxies are prevalingly used, particularly in the North Sea offshore industry based in U.K. and Norway [71].

Zinc primers are found to be useful in many areas of an industry. Zinc primers are strongly suggested for use in the conditions where there is frequent wetting by salt water, condensation, splashing, spray or frequent immersion and in the areas where there is chemical exposure with pH range 5 to 10 [1]. DoD also is a major consumer of zinc-rich primers. Some of the zinc primers used by DoD are A-9-73, MIL-P-21035, MIL-P-24441, MIL-P-26915B, TT-P-641, TT-P-645A, TT-P-645B, TT-P-1046A and TT-P-1757.

A-9-73, MIL-P-21035, MIL-P-26915B are zinc-dust primers used for ferrous metals, marine use, severe atmospheric exposures (when topcoated), regalvanizing welds, bridges, steel pipes, chemical plants (when properly topcoated) or architectural equipment.

MIL-P-24441 is a polyamide epoxy zinc Primer for use where excellent adhesion is needed on solvent-cleaned steel or for a marine environment protective coating.

TT-P-641 Type II is a zinc dust primer for steel or galvanized metal surfaces.

TT-P-645A is a zinc chromate primer for metal surfaces.

TT-P-645B is a zinc alkyd primer for steel or aluminum.

TT-P-1046A is a zinc rich primer for bare ferrous metals, marine use, bridges, steel pipes, chemical plants (when top-coated), and where there are severe atmospheric exposures (when top-coated).

In the case of application, zinc-pigmented coatings differ from zinc-rich coatings. Zinc-pigmented coatings can be applied using brush, roller, or spraying and they do not have stringent substrate cleaning requirements. In some formulations they can be even applied over rusted surfaces unlike for zinc-rich coatings where the substrate surface needs to be very clean before coating.

Application conditions and requirements for zinc-rich coatings such as those mentioned needs to be more clean and precise. The metal surface for zinc-rich coatings before application needs to be extremely clean. Any traces of organics, dust, grease, etc., which prevent the contact between the iron and zinc need to be removed from the surface in order to maintain electrical contact

between the two metal surfaces. The importance of the contact in performance will be clearer after the explanation in the mechanism section.

In the next section we will discuss two main types of primers.

According to the Steel Structures Painting Council Zinc (SSPC), zinc-rich primers employed in coating films at loadings that insure the film conductivity, will form an efficient anode of a galvanic couple with steel, sacrificially corroding itself, and overriding local cell activity on the steel which becomes entirely cathodic and protected.

The concept is easily adaptable to practical coating systems, and such primers are the most efficient of all. Zinc-rich primers based on both organic and inorganic vehicles are widely and successfully employed. They are discussed in the following

#### **A. ORGANIC ZINC-RICH PRIMERS**

Organic zinc-rich primers are used where resistance under coating damages is necessary, for which reason they are used under exterior topcoats and finishes and where decorative colors and finishes are provided by topcoats. For applications requiring resistance to water immersion, salt, high humidity and mild chemical fumes zinc-rich coatings are used as an efficient option. These applications include highway bridges, chemical process plant equipment, sewage and water treatment plants, marine structures, ship hulls, ballast tanks, ship structures and many others.

However they are not suitable for environments of  $\text{pH} < 5$  or  $> 10$ , where the zinc is more readily dissolved.

The pigment volume concentration (P.V.C) of the organic zinc-rich primers is usually high. This allows it to maintain zinc particle to zinc particle contact within its continuum and contact between pigment and substrate to ensure electrical conductivity within the film and across the interface.

Because of these requirements the paints are formulated at a pigment volume concentration slightly above the critical pigment volume concentration (C.P.V.C). The coatings made from these primers should also display sufficient adhesion at these loadings. Usually chlorinated rubber, epoxy/polyamides, high molecular weight linear epoxies and epoxy ester systems are used as binders. The coatings will display properties which vary and depend on the vehicle type.

When the P.V.C is adjusted to values just higher than the C.P.V.C the primer will achieve the tightest particle to particle concentration and zinc encapsulation with the binder is reduced. When different particles sizes are used at optimized values it may also assist here to provide more uniform packing, resulting in better particle contact and ultimate galvanic protection. Too high of pigment volume concentration might effect the coating's adhesion to the substrate. If zinc were the only pigment used the fixation for P.V.C would be very simple, but usually the formulations are very complicated and they include anti-gassing agents, thixotropes, anti-settling agents, extenders, etc. Sometimes even small amounts of oil-absorbent materials decrease the C.P.V.C

value but not the P.V.C value due to which the coating might become very porous. But optimized amounts might help maintain a P.V.C:C.P.V.C, ratio by reducing the amount of zinc required, thus obtaining a strong film. This provides enough film and film/substrate conductivity for good protection.

Application of organic zinc-rich primers needs to be done with care. Proper mixing and agitation is a must to ensure homogenous film to be formed. Sometimes even with the use of the best thixotropes settlement of zinc is possible. Due to this zinc encapsulation might be possible which might result in nullification of cathodic protection.

## **B. INORGANIC ZINC-RICH PRIMERS**

Post-cured organic zinc-rich paints, though comparably are difficult to apply and require very precise surface preparation, they are more resistant. Some water-based zinc-rich coatings are initially applied as suspension of zinc dust in a sodium silicate solution and then after the water has evaporated the coating is washed with an acid phosphate solution which will convert the zinc to insoluble silicates and phosphates [1]. But self-cured zinc-rich coatings are formulated in such a way that the carbonic acid that is formed by dissolving of carbon-dioxide from air will cure the coatings by the same chemistry as for the post-cured coatings. Before application of topcoats on organic zinc-rich primers, they need to be washed to remove the excess acid, but rinsing and washing are usually not necessary for self-cured coatings [1].

Silicates which are used as binders in inorganic zinc-rich paints react with zinc to form primary bonded zinc silicate matrices. In organic zinc rich primers the particles do not react but are held within a polymer matrix. Vehicles may generally be classified as either alkaline silicates (water solutions of sodium, potassium, lithium, or quaternary ammonium silicates) or alkyl silicates which may be ethyl silicate (the most common) or higher alkyl or alkoxy homologues.

### **INORGANIC VS ORGANIC**

For inorganic zinc-rich primers the zinc levels can be lower than that required for organic zinc-rich primers without sacrificing the performance. Zinc levels of 70% by weight can be enough to give good performance. Whereas for organic primers, the percentage levels of the zinc should be considerably high to ensure good performance.

Inorganic zinc-rich primers are better than organic rich primers as far as performance is concerned. They are strong, hard, and resistant to impact and abrasion. They are quite resistant to heat. The performance of inorganic primer films does not deteriorate with age but organic zinc-rich primers do. Weathering may actually improve their physical properties.

Inorganic types are better than the organic adhesion-wise also. It is also suspected that it might be due to the formation of primary valency linkages with the substrate as well as the zinc. The mechanism of adhesion at this point is unknown. But the surface preparation requirements of

inorganic zinc-rich primers are exceptionally higher than the organic primers (particularly with the alkaline silicate systems). A commercial blast is the very minimum acceptable, and a white or near white blast with a typical surface profile of 1 to 2 mils being more usual and often mandatory. Alkyl silicates are rather more tolerant of poorly blasted substrates than the water-based type, probably reflecting their higher organic content and lower surface energies.

The inorganic zinc-rich coatings can be considered as better and safer coatings than organic type even though they are incompatible with poorly prepared surfaces. Sometimes the organics may mislead the applicator by adhering to poorly prepared substrates but in fact in the areas where there is no proper contact with the pure surface a good performance cannot be expected. Inorganics require such contact (through good surface preparation) not only for protection, which may be initially difficult to determine, but also for good initial adhesion, which is easy to determine. If an inorganic sticks, it should protect. If an organic sticks, protection is still an open question.

### **Secondary Mechanisms**

If cathodic protection were the sole mechanism of zinc-rich primers, they would rapidly break down as zinc was consumed. In practice, this is not the case. As zinc corrodes, its corrosion products (depending upon the environment) tend to polarize the reaction, coating the zinc and bridging the voids within the film, thereby packing them so that the primer is sealed from the

environment. The film is slowly transformed from a zinc-rich primer to a barrier primer, and, in this state, it is maintained until the zinc is again exposed by some abuse. The zinc will then corrode again and be healed with corrosion product (providing that the agents of physical or chemical abuse have been removed). These phenomena are primarily responsible for long term zinc-rich protection.

Zinc-rich primers are normally applied at approximately 25  $\mu\text{m}$ . Some compositions form good films at thicknesses up to 150  $\mu\text{m}$ , while others may severely mud-crack at these high builds.

The porosity of zinc-rich films (particularly the inorganic ones) can lead to problems because of air occlusion during top coating. The resultant bubbling and pin-holing of applied top-coats may necessitate the use of mist coats, thinned finish coats or tie coats before finish coat application.

Careful formulation of solvent system and pigmentation of the finish coat can mitigate this problem, and many manufacturers carefully tailor finish coats for bubble-free application over the zinc-rich primers.

#### **CHROMIUM USE IN ZINC PRIMERS**

The use of chromium in zinc-rich primers is not uncommon. Zinc chromate pigments can be added to primers made of several different resin types, such as epoxy, polyurethane, alkyd and others. Some of the primers used by DoD contain chromate in them. Chromium proves its

efficiency in corrosion protection in these primers too. Zinc salts added to chromates form  $ZnCrO_4$ , a cathodic inhibitor, which is more effective than the simple summation of the individual cathodic effects of  $Zn^{2+}$  and  $CrO_4^{2-}$  taken alone [1].

Zinc chromate is simply a corrosion-resistant pigment that is added to certain coatings. In the case of a wash primer, the phosphoric acid actually reacts with the metal, whereas in the case of zinc chromate this is not the case. In dry, low-humidity weather the zinc chromate does not do anything other than remain in the coating. On the other hand, when the humidity in the air increases or on rainy day moisture from the air penetrates the primer coating and slightly dissolves the zinc chromate. The dissolved zinc chromate solution now does react with the underlying metal surface and forms a passive layer (like a blanket) that prevents corrosion. As soon as the weather becomes dry again the zinc chromate no longer plays a role at least until the next time it rains, when the process is repeated. If there are frequent cycles of high and low humidity the zinc chromate will eventually be depleted and soon after one might start to see corrosion of the metal. However the use of chromium is avoided in these primers, too, because of their ill effect on life.

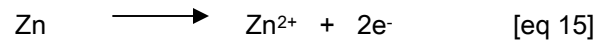
## **5.2 MECHANISM OF CORROSION PROTECTION OF ZINC-RICH PAINTS**

From the early 1800's cathodic protection has developed rapidly and its use has become widespread. New materials such as sacrificial alloys of magnesium and aluminum and superior

impressed current anodes together with developments in electrical and electronic engineering have allowed great advances in the techniques. Cathodic protection is now established as an essential engineering service with a sound and comprehensive scientific background. The mechanism of zinc cathodic protection comes into this category.

The basic principle of corrosion protection is simple. A metal dissolution is reduced through the application of a cathodic current. Cathodic protection is often applied to coated structures, with the coating providing the primary form of corrosion protection. The CP current requirements tend to be excessive for uncoated systems. Cathodic protection has probably become the most widely used method for preventing the corrosion deterioration of metallic structures in contact with any forms of electrolytically conducting environments, i.e. environments containing enough ions to conduct electricity such as soils, seawater and basically all natural waters. Cathodic protection basically reduces the corrosion rate of a metallic structure by reducing its corrosion potential, bringing the metal closer to an immune state. The two main methods of achieving this goal are by either using *sacrificial anodes* with a corrosion potential lower than the metal to be protected using an impressed current provided by an external current source. Zinc-rich primers mechanism of corrosion protection comes into the sacrificial anode category.

As the basic reason of zinc is lower than iron in the electrochemical series zinc acts as a sacrificial anode in the galvanic couple of iron and zinc. In a common galvanic couple between iron and zinc the following will be the anodic reaction:



Zinc in the above reaction oxidizes to zinc ions. Whereas at the cathode the following reaction happens:



The idea of cathodic protection is to artificially shift the potential of a metal so that it becomes either immune or passive. In natural soils and waters it is normal to shift the potential of steel to the immune region whereas for steel in concrete it is preferable to re-establish passivity.

In sacrificial anode cathodic protection, a galvanic cell is set up by connecting the steel to a more reactive metal, usually zinc. The zinc then undergoes the anodic reaction and corrodes whilst the steel is rendered entirely unreactive because the whole surface undergoes the cathodic reaction mentioned above and the iron no longer dissolves. This may also be thought of as the anodic sites on the steel being shifted to the zinc.

Conventional primers contain a polymer network which prevents the electrolyte penetration and thus corrosion. Zn-rich primers have loads of zinc dust in them and a binder which keeps all this zinc metal dust in tact, thus providing a way to coat the zinc metal over steel and protect it from corroding.

The corrosion products of zinc are usually zinc hydroxides formed at the anodic sites. These corrosion salts of zinc which are insoluble by nature form near or in the pores and thereby shielding the underlying surface from the atmosphere. These deposits prevent the penetration of moisture and other corrosive species from reaching the substrate. This prevents the underlying steel from getting corroded.

### **5.3 ZINC-RICH SUPERPRIMER**

The idea of zinc-rich primer started with the trials to test the superprimer's performance with particles in it. Zinc was used in it to formulate a zinc-rich superprimer. Zinc rich SUPERPRIMER is nothing but a zinc paint which uses the superprimer as a binder and it would not include the pigments, color and nanoparticles. It is chromate-free, completely waterborne and has very low VOC in it. After several trials it was evident from the results that the waterborne superprimer formulation mentioned in the previous chapters had to be modified for best performance in the zinc-rich primers. The results and observation are discussed in the following chapters.

### 5.3.1 FORMULATION, MIXING AND COATING

The formulation of the zinc-rich primer is different from the usual superprimer with particles in it.

The following shows information about the components and their mixing procedure:

- Part A: Superfine (grade 5) zinc dust at 70 % (by weight in the total formulation)
- Part B: WSP-1 (30% by weight in the total formulation) which contains 80% EPI REZ-3540 resin + 19% (A1170: VTAS [5:1] ; 10% solutions in water) + 1% TEOS + defoamer [if needed]
- Part B is shear-blended for 10 minutes at 2100 rpm. Then Part A is added in small batches and blended for 20 minutes at 3000 rpm

The cleaning requirements for zinc-rich coatings are equally stringent as in conventional primers.

Measures have to be taken to make sure that proper electrical contact is maintained in between the zinc in the coating and the steel substrate. Cleaning procedure is similar to the one in the previous chapters. Zinc-rich coatings can be applied using brush, drawdown or by a spraying method.

The zinc-rich superprimer coatings were cured at 100°C for 30 minutes and then letting the coating set at room temperature for 1 week. Zinc-rich primers work better performance-wise if the

coatings were allowed to retain some moisture inside them for some time. This moisture retention will help form the zinc corrosion products and seal the pores of the coating. So for zinc-rich coatings a slight under-curing is preferred.

### **5.3.2 RESULTS AND DISCUSSION**

In this section the test results using EIS, Salt Spray and SEM techniques are discussed.

#### ***Percentage of Zinc Dust***

The percentage of zinc dust in the zinc-rich primers is critical and it determines the performance.

It needs to be high enough for the primers to perform their function efficiently. Since these primers work on the basis of cathodic protection, it is necessary that the zinc metal particles maintain electrical contact not only with the steel substrate but also with each other. So for the particles to be tight and intact in the coating over the substrate the percentage of zinc in dry zinc rich coating needs to be high.

Carbon steel panels were first solvent-scrubbed using ethanol as solvent and scotch-brite pads to remove the dirt, corrosion products and expose clean, shiny metal-oxide surface. After the scrubbing, the panels were cleaned with water spray and then followed by ultrasonic cleaning in ethanol for 5 minutes. The final stages of cleaning included alkaline cleaning similar to the one followed for aluminum but at lower temperature of 55°C and for only 1 or 2 minutes. CRS is a

very sensitive substrate so care was taken not to spoil the metal-oxide surface before coating with superprimer.

EIS and salt spray tests were used to analyze this effect. Figure 5.3 shows EIS curves of a formulation containing 40% zinc 60% superprimer mixture for 0 to 42 days. Figure 5.4 shows a similar result of formulation with 70% zinc and 30% superprimer.

Figure 5.5 shows the salt spray result after 3 weeks of both 40% and 80% zinc formulations. The performance of 80% formulation was better than the one with 40%. It was not that evident from the comparison between both of their EIS curves. The significance of increasing modulus is explained here.

Figure 5.6 shows a comparison of the 6-week EIS result of a commercial chromate containing primer from Carbozinc and zinc-rich superprimer. All the EIS impedance curves show an increase in the impedance values with due time. Because of the conductive metal zinc in zinc-rich coatings it has less resistance in the beginning. When the immersion time increases the zinc is corroded and forms its insoluble corrosion products. These corrosion products seal the pores and make the coating less permeable to water. In other words, this means an increase in the resistance. This behavior of the zinc rich coatings can be accounted for their increasing impedance behavior.

Salt fog results showed an equally good or better performance of the zinc-rich superprimer when compared to the commercial primer. Figure 5.7 shows the comparison. However, the zinc-rich superprimer has the following advantages than most of the commercial primers:

- Completely water-reducible
- Easy clean-up
- Excellent adhesion to topcoat
- Low VOC
- Equal or better performance when compared to solvent-borne commercial paints
- Chromate-free
- Low solvent odor
- Pot life of close to 24 hours

Both primers performed equally well in terms of corrosion performance. No visible red corrosion products of steel were observed on the steel panels. In Figure 5.7 white corrosion products of zinc were observed in the scribe. These white deposits of zinc hydroxide are highly insoluble to water and other species. The formation of these deposits is, in fact, an indication of good performance by the zinc-rich coatings. However, similar white corrosion products were not observed in the scribe of panels with both zinc rich coating and a polymer topcoat over it. Figure 5.8 shows the 200 hour salt fog result of zinc rich primers with topcoat.

The noticeable difference between Figure 5.7 and 5.8 is the formation of red corrosion product of steel in the scribes of the panels with topcoat. Formation of zinc corrosion products at the scribe were not observed when the panels are coated with a topcoat. Thus the scribes of the panels were not protected. The reason for the zinc-rich primers to be not as efficient under the topcoat can be attributed to the fact that application of a topcoat over a zinc rich primer will actually decrease/cut-off the electrical contact between the zinc, iron and the environment (which acts as an electrolyte). As explained in the previous sections, a contact between the three is necessary for the corrosion protection action of the zinc.

At the areas of a defect or a scribe only a small portion of zinc is exposed to the environment which can sacrifice itself and protect the steel. In the non-top coated panels a larger portion of the zinc surface is exposed and sacrificed, which will in turn help the steel underneath from getting corroded.

### ***SEM Results***

An attempt was made to observe the corrosion protection of zinc using the EDS technique. The idea was to observe the formation of zinc corrosion products in the scribe with time.

A 1 cm by 1 cm portion of a steel panel coated with zinc-rich superprimer was cut and scribed in the center. Analysis was done on two areas, one at the coating surface and one area in the

scribe. First analysis was done in both the areas immediately after curing and another after 48 hours of immersion in 5% NaCl solution. The aim was to observe any traces of zinc that leached out from the coating to the scribe with time by forming zinc hydroxides.

Analysis of the coated areas before the immersion revealed the presence of only Si compounds. This Si is from the silane content in the zinc-rich coating. Analysis on the coated area after the immersion revealed the presence of zinc and traces of iron. To rectify this difference or strange observation further tests and studies need to be conducted.

Analysis of scribed areas revealed some useful information. Before the immersion the only species detected were iron compounds. This is obvious because after a fresh scribe, formation of a shiny iron oxide layer is obvious. After the immersion, traces of zinc compounds were detected. This observation can be made using Figures 5.9 to 5.12.

## **5.4 CONCLUSIONS**

Zinc-rich Superprimer can be a promising replacement for solvent-based chromate containing zinc-rich primers. A successful formulation was optimized after running trials with different percentages of the components. EIS and salt spray results were used to test the formulations. It was proven that a higher percentage of zinc is needed for better corrosion performance. Higher percentage of zinc ensures proper electrical contact in between the zinc particles and the steel

substrate. This electrical contact is needed because zinc performs according to sacrificial anode mechanism.

EIS and salt spray results proved that zinc-rich superprimer formulations performs equally well or better than a commercial chromate containing zinc-rich primer. However the superprimer has the advantage of being completely water-based with very low VOC and additionally it is chromate-free. It is very comfortable to work with and because it is water-soluble the effort in cleaning issues is reduced.

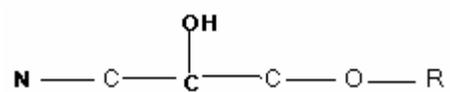
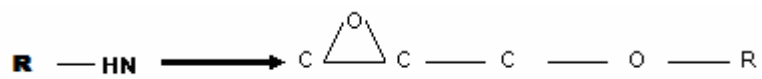
The superprimer showed excellent adhesion to a topcoat and had no adhesion issues. However it was observed both in the cases of the superprimer and a commercial primer that the scribes are not protected when used with topcoat. This observation was attributed to the fact that using a topcoat actually reduces the amount of exposed zinc on a substrate. The amount of zinc exposed is critical in the performance wise for a zinc-rich coating. So for the zinc-rich coatings to perform efficiently they need to be used without a topcoat.

## CHAPTER 6: CHARACTERIZATION

This chapter discusses the characterization work that was done in the final stages of this thesis work.  $^{13}\text{C}$  NMR and IR characterization techniques were used to investigate the chemical structural characteristics and changes in the superprimer formulations. NMR equipment in Chemistry Department at Oklahoma State University was used.  $^{29}\text{Si}$  NMR spectra were recorded on a Varian Inova 600 MHz spectrometer using a Varian broadband probe. Spectra were collected with a 1-pulse experiment using a 9 ms pulse width with a 30 seconds pulse delay and 472 scans. All chemical shifts were referenced to Tetra Methoxy Silane. Both carbon and silicon NMR analysis were tried. The RAIR spectra were obtained by using a Spectrum One FTIR spectrometer from Perkin Elmer, Wellesley, MA. A variable angle diffuse reflectance accessory was used with the incidence angle being fixed at  $80^\circ$ . The scanning range was from  $4000\text{ cm}^{-1}$  to  $450\text{ cm}^{-1}$  and 64 scans of each film were taken.

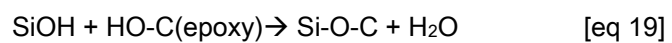
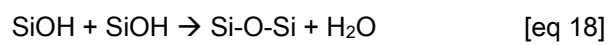
Characterization was aimed at observing the possible or expected chemical reactions in the coating system. They are:

Secondary amine NH and Epoxy reaction



[eq 17]

Silane condensation reactions





## 6.1 NMR Characterization

### 6.1.1 Objective and Sample Preparation

It was our intention to gather information on the chemical reactions in the superprimer coating by using the NMR technique both before and after coating. In this view, samples were tested using the carbon NMR technique both in liquid and solid form. Individual components of the superprimer including the silanes and the resins were tested in as-obtained liquid form for reference and then the final superprimer solution prepared in the following way was tested. Cured coatings of superprimer were scraped from metal surfaces, powdered and tested for solid-state NMR.

The following is the primer formulation under focus:

#### *Formulation F-6*

The components and mixing procedure of Formulation F-6 are:

Part A: EPI REZ 3540-WY-55 Epoxy resin

Part B: AV5 10 % in water at pH 6. Bis-amino and vinyltriacetoxysilane mixed in 5:1 volume ratio and then diluted with water.

Part C: TEOS

Part D: Bis-sulfur silane

By weight:

Part A (80%) + Part B (9%) + Part C (1%) + Part D (10%)

High-shear blended for 10 min. at 2000 rpm

After allowing 20 minutes of incubation time, cleaned aluminum panels were either brushed or coated using a drawdown bar

Panels cured at 100° C for 1 hour

<sup>13</sup>C NMR spectra were taken of the primary components and the final formulation. Analysis was done by comparing the spectra for the appearance of new peaks which might show the progress of the chemical reactions that could happen in the final formulation. Liquid <sup>13</sup>C NMR was done on AV5, bis-sulfur, 3540 resin and the F6 formulation.

Solid  $^{13}\text{C}$  NMR was done on a cured coating of the completed formulation. Cured coatings made on the aluminum in the above fashion were scraped using an ordinary blade and then the scrapings were ground to a powder form using mortar and pestle. An NMR spectrum was taken of solid powders.  $\text{Si}^{29}$  NMR was done on liquid samples only.

### 6.1.2 Observations

#### *Epirez wy 55 3540 Resin*

The chemical structure of the typical DGEBA resin is shown in Figure 6.1. This is a water-based epoxy resin with 2-propoxyethanol as a co-solvent. The peaks observed and their assigned bonds are mentioned in Table 6.1. Figure 6.2 shows the spectrum.

The superprimer was prepared by the usual mixing procedure mentioned in the previous chapters. No additions of particles or inhibitors were made to it. The mixture was analyzed initially, after 16 hours and after 8 days after mixing. The NMR peaks taken with time are shown in Figure 6.5 and Table 6.2. This was done to monitor the hydrolysis of the silanes in it.

The initial spectrum of the superprimer mixture contains resonances due to the component resin, solvent, and silanes. A small peak at 49.3 ppm due to MeOH is present initially and increases in intensity with time, indicating that hydrolysis of the bis-amino silane continues with time.

The relative intensities of the ethanol peaks at 57.5 and 17.7 ppm, initially decrease and then increase with time as compared with the intensities of the ethoxy peaks at 58.4 and 18.5 ppm, indicating that hydrolysis of the bis-sulfur silane continues with time. Initially the decrease in peak sizes might be caused because of the evaporation of ethanol that is present as solvent in the coatings. With time the intensities increase which might be due to formation of ethanol by the hydrolysis of bis-sulfur silane.

The intensity of the 69 ppm C-OH peak decreases with time, though a clear reaction product is not observed. The intensities of the epoxide peaks do not appear to change with time.

#### *Cured Superprimer Coating*

Solid state NMR spectra of the cured coating were collected and the peak assignments observed are shown in Table 6.3 and the spectrums shown in Figure 6.6.

The spectrum showed peaks due to the resin and unreacted bis-sulfur. The unreacted bis-sulfur was also observed in the  $^{29}\text{Si}$  NMR spectra of the coating, as T<sup>0</sup> (non-hydrolyzed), T<sup>1</sup>, T<sup>2</sup>, and T<sup>3</sup> peaks accounted for approx. 35.5, 9.1, 12.2, and 43.0 % of the total peak area.  $^{29}\text{Si}$  NMR spectrum of the cured coating is shown in Figure 6.7.

Only two successful conclusions about hydrolysis of bis-amino and bis-sulfur silanes could be drawn from the NMR tests so far. Peaks at around 70 ppm could not be positively assigned to

either Si-O-C or C-O-C because they were observed in both resin and the final formulation. This makes it uncertain to relate the observation to the cross-linking of the epoxy groups. However further tests using the IR technique are conducted to determine this observation.

## **6.2 IR Characterization**

### **6.1.1 Equipment and Sample Preparation**

The chemical structures of the superprimer coatings and the component silanes and resins on aluminum AA 2024 T3 were studied by reflection-absorption infrared (RAIR) spectroscopy. The RAIR spectra were obtained by using a Spectrum One FTIR spectrometer from PerkinElmer, Wellesley, MA. A variable angle diffuse reflectance accessory was used with the incidence angle being fixed at 80°. The scanning range was from 4000  $\text{cm}^{-1}$  to 450  $\text{cm}^{-1}$  and 64 scans of each film were taken.

Coatings of the superprimer and also its component resin and silanes were made on aluminum panels. The IR absorbance spectra were taken on coatings at different cure conditions. The conditions are specified whenever necessary in the next section. Coatings were made from water-diluted 10% silane mixture of bis-amino and VTAS (5:1) and pure bis-sulfur silane. Spectra were also taken of coatings made from only resin and complete superprimer formulation F6. Peak assignments were made in detail for each spectrum in the following section.

## 6.2.2 IR Spectra

### *AV5 Coatings*

Bis-amino and vinyltriacetoxo silanes are mixed in 5:1 volume ratio. A 10% diluted solution was prepared in water at pH 6. Cleaned aluminum 2024 T3 panels were dip-coated and cured at 100°C for 1 hour. The IR spectrum taken over such a sample is shown in Figure 6.8. Important peak assignments are shown in the figure and also mentioned in Table 6.4. Important peaks for Si-O-Si, Si-O-Me and secondary amines which are peculiar for the silane mixture are found and noted. Peaks for OH groups are also found which can be from silane hydrolysis and formation of alcohol.

### *Bis-sulfur Coatings*

Pure bis-sulfur silane coatings were dip-coated on aluminum panels and cured at 100°C for 1 hour. The IR spectrum with peak assignments taken of such a sample is shown in Figure 6.9. Peaks for Si-O-Si and Si-O-Si can also be seen here. Any peaks showing the presence of sulfur bonds are not prominent because unlike oxygen containing bonds, C-S and C-S-H vibrations tend to give weak absorptions in the infrared spectrum. The higher mass of sulfur, compared with oxygen, results in the characteristic group frequencies occurring at noticeably lower frequencies than the oxygen-containing analogs [33].

### *Resin and Superprimer Coatings*

The commercial EPIREZ 3540 wy-55 resin used in the superprimer formulation (F6) was coated using a drawdown bar on a cleaned aluminum panel. The superprimer formulation F6 which contains 80% resin, 10.5% bis-sulfur silane, 9% AV5 (105 diluted) and 0.5% tetraethoxysilane was prepared and coated using a drawdown bar. The resin coating was cured at 100°C for 1 hour. Superprimer coatings were cured both at 100°C for different timings and also at RT for a number of days. The time and conditions are mentioned whenever necessary while discussing the spectra. The IR spectrum with peak assignments of the resin coating is shown in Figure 6.10. The IR spectra of the F6 formulation at different curing conditions are shown in Figures 6.11 and 6.12.

EPIREZ 3540 is a water-based DGEBA resin showed characteristic epoxy peaks at  $\sim 1259\text{ cm}^{-1}$  and at  $\sim 890\text{ cm}^{-1}$ . A combination of peaks at  $\sim 1600$  and  $1500\text{ cm}^{-1}$  shows the aromatic nature of the resin. A broad peak in the range of  $3600\text{ cm}^{-1} - 3200\text{ cm}^{-1}$  shows the hydrogen bonding in the resin. Peaks in the same range are observed also in Figures 6.10 and 6.11 of the superprimer spectra cured at different conditions. Superprimer is a multi-component mixture hence the spectra showed a few peaks which are related to other bonds present in the primer. Peaks observed in the range of  $1130\text{ cm}^{-1} - 1000\text{ cm}^{-1}$  prove the presence of siloxane linkages (Si-O-Si) obtained from condensation of both the silanes. Siloxane linkages to metal (Si-O-Me) which improve the

adhesion are also observed in the range  $1000\text{ cm}^{-1} - 900\text{ cm}^{-1}$ . Some peaks in the range of  $1150-1050\text{ cm}^{-1}$  might also be due to an alkyl substituted C-O-C stretch which results from the crosslinking of epoxy groups. Some peaks around  $950\text{ cm}^{-1}$  might also be due to condensation reactions between silanol SiOH and C-OH groups which lead to Si-O-C linkage.

To observe the cure trend IR spectrum was taken over F6 coated sample at different cure occasions. In Figure 6.12 spectra of F6 coatings cured at  $100^{\circ}\text{C}$  for 1, 2 and 3 hours and at room temperature for 1 hour and 5 days are shown. A marginal increase in the intensity of peaks in the range for Si-O-Si and Si-O-Me linkages are observed in between the spectrum cured at RT for 1 hour and at RT for 5 days. This shows that silanes in the superprimer hydrolyze and condense and thus crosslink better with time than in the fast cure conditions. This can be explained by the fact that a reasonable amount of sulfur silane in the coating is present in its pure unhydrolyzed state at the time of coating. This silane hydrolyzes with the moisture in air while curing at room temperature. Condensation reactions happen with due time and thus increase the cross-linking of the films. Increase in the intensity of the peaks which show the Si-O-Me linkages in the range  $1000\text{ cm}^{-1} - 900\text{ cm}^{-1}$  is also observed.

## CHAPTER 7: CONCLUSIONS

Silanes or silane solutions at high concentrations can be used for coating purposes by modifying silanes with resins. Primer formulations were obtained by silane plus resin combination, called 'superprimer'. Formulations were developed and tested from low concentrations of resin followed by increased percentages of resin. A completely water-soluble superprimer formulation was developed using a waterborne resin and water-soluble silane solutions. The hydrophobicity and anti-corrosion performance of the superprimer were improved by inclusion of hydrophobic silane into the formulation. Test results over the coatings formed by base formulation including EIS and salt spray exposure showed that the improved superprimer formulation has very good anti-corrosion performance. The coatings passed 2 weeks of ASTM B117 salt spray. Outdoor exposure testing was also done at a testing center in Hawaii. Coatings from the base formulations with topcoat over steel panels were exposed. Figure 7.1 and Figure 7.2 show the tested panels both before and after exposure. The coatings over carbon steel showed filiform corrosion in the scribed areas, whereas the coatings over aluminum panels showed no signs of visible corrosion as of yet. Figure 7.3 shows the aerial view of the exposure sight in Florida. And figure 7.4 shows how the panels are exposed at the sight. Figure 7.5 shows the position of the panels at the exposure center. Additions such as nano-size particles and corrosion inhibiting pigments added to give specific qualities were discussed in detail along with the formulations and test results.

Particles and corrosion inhibitors were added to silane plus resin mixtures to provide superprimer with better film properties and anti-corrosion performance. Alumina, carbon black and zinc were tried as particle inclusions along with commercially available corrosion inhibitors. EIS and salt spray standard tests were used to monitor the film properties and anti-corrosion performance simultaneously. Coatings from formulations F10 which contains about 2.5 % by weight of alumina, showed good anti corrosion performance. These coatings without any topcoat passed 500 hours in salt spray testing, and passed 1000 hours in salt spray when tested with topcoat. Similarly, coatings from inhibitor formulations namely calcium zinc molybdate (F-15 with 10% by weight), passed 500 hours in salt spray testing without a topcoat, and 1000 hours with topcoat. These two formulations can be recommended as suitable primer formulations for aluminum.

Also, test results over different formulations showed that alumina addition to superprimer enhances the anti-corrosion performance. However, increasing level of alumina leads to decrease in the corrosion performance. Increase in porosity resulted by the increase in the amount of particles can be considered as a possible explanation behind this observation. But, the loaded percentages are far below the CPVC value of the alumina in a coating. Alumina used here was a water-based paste and by nature alumina is considered to be very hydrophilic. So, the increase in its weight percentage can actually increase the hydrophilicity of the coatings and

hence decrease the performance. And this was quite evident from the performance test results of F10, F11 and F12 coatings both with and without topcoat.

Carbon black was loaded as a pigment in the superprimer formulations. EIS and salt fog tests conformed to a single observation that the coatings resistance increased initially and then decreased with time. The conductive nature also of the coating increased with the exposure time. The performance of the coating decreased with the increased in the conductive nature of the coating. A possible explanation of formation of hydrophilic hydroxyl ions migrating to the substrate through the coatings is given for the observation.

Corrosion inhibitors were tried to provide enhanced corrosion protection to the superprimer. This idea was put to trial so as to imitate the self-healing characteristic of the chromate primers [3]. Test results showed that the corrosion performance did increase and primer-coated surfaces showed less pitting and general corrosion in un-scribed areas. But the inhibition could not protect the scribed areas. Visible corrosion was found in most of the formulations. The search for the right inhibitor which can provide the scribe protection still needs to be continued and this particular area gives scope for further research.

A zinc-rich superprimer can be a promising replacement for solvent-based chromate-containing zinc-rich primers. A successful formulation was optimized after running several trials with different

percentages of the components. EIS and salt spray test results were used to analyze the formulations. It was proven that higher percentage of zinc is needed for better corrosion performance. Higher percentage of zinc ensures proper electrical contact in between the zinc particles and the steel substrate. This electrical contact is needed because zinc performs according to a sacrificial anode mechanism. A chromate-free, completely water-based, very low VOC zinc rich superprimer formulation was obtained which performed equally better with a commercially available zinc-rich primer. Salt spray results proved this observation. The developed zinc rich superprimer has better ease to work with, easy to clean and has comfortable potlife. These factors coupled with its good performance can be an excellent promise as coatings for steel.

EIS and salt spray results proved that zinc-rich superprimer formulations performs equally or better than a commercial chromate containing zinc-rich primer. However the superprimer has the advantaged of being completely water-based with very low VOC (~50 g/l) and additionally it is chromate-free. It is very comfortable to work with and being water-soluble reduces the effort and cost in cleaning issues.

The superprimer showed excellent adhesion to topcoats. However it was observed both in the cases of superprimer and commercial primer that the scribes were not protected when used with topcoat. The reason was attributed to the fact that using a topcoat actually reduces the amount of

exposed zinc on a substrate. The amount of zinc exposed is critical for the performance of a zinc-rich coating. So for the zinc-rich coatings to perform efficiently they need to be used without a topcoat.

Characterization using IR and NMR techniques proved that hydrolysis of the component silanes takes place with time. A two-step cure starting with a room temperature then force curing it at a certain higher temperature might be show promise towards increased adhesion to the substrate.

This is due to the observed fact that the component silane which exists in its pure state undiluted state hydrolysis in due time and its cross-linking within the coating and adhesion to the substrate increase gradually with time.

Si-O-Si chemical linkages from silanol-silanol condensation, Si-O-Me from silanol-hydroxy condensation and Si-O-C from silanol-epoxy condensation were expected to occur in the coating system. The peaks with reasonable intensity for the first two linkages were observed. A possible overlap of the peaks in IR range  $1000\text{ cm}^{-1}$  –  $900\text{ cm}^{-1}$  made it hard prove the possible reactions of epoxy-silanol crosslinking which occurs at around  $950\text{ cm}^{-1}$ .

## CHAPTER 8: RECOMMENDATIONS FOR FUTURE WORK

This thesis work is one of the three initial works on the superprimer idea. Other works include solvent-borne superprimer idea. This thesis concentrated its work primarily on trying to find the aimed coating system with an epoxy resin as a base. The work was started from scratch just by simple mixing of solutions. Many important things were realized during the course of this work. Much more can be achieved and researched with further work. Here are a few recommendations which might help the future work in this area.

It is suggested to use the equivalent weight method to determine the required ratio between the resin and its curing agent (reactive agent like silane in the system) for its complete reaction. This simple method requires one to find the weight per epoxide chain of the resin that is being used and to mix it with an equivalent amount of the curing agent that will react with the whole epoxide. This sort of method might decrease the cumbersome trial and error methods commonly used. Many factors like pot life of the material, viscosity, etc., can be controlled once the ratio for complete reaction is known, i.e., for example less curing agent can be used to increase the pot life and flexibility of the coating. This method is commonly used for high-solids coatings in automotive industries and it is worth trying here too.

Further increasing the amount of solvent in the superprimer system for better curing ability of the system can be a valuable trial. This can be simply tried by using hydrolyzed bis-sulfur system in ethanol rather than using pure silane alone. NMR results revealed that there is a lot of unreacted sulfur silane left in the superprimer coatings.

It is also suggested to use a high epoxide containing resin, which are available commercially.

High molecular weight epoxies might have better effect on the performance of the coatings.

Similar trials can be made for zinc-rich superprimer work also. Addition of solvent based bis-sulfur silane into the binder of the superprimer can be a valuable trial. This way of inclusion of solvent in the system will increase the curing ability and hence the performance of the zinc-rich coatings.

Care should be taken not to include too much of silane as it is expected that too much of silane can encapsulate the zinc particles and decrease its performance in the coatings.

Further optimization of the percentage of zinc can be a trial worth doing.

## References

1. Denny A. Jones, "Principles and Prevention of Corrosion", 2nd ed., Prentice Hall, New York, 1996.
2. J.H Payer, W.K. Boyd, D. B. Dipplod, and W.H. Fisher, Mater. Perform., May-Nov. 1980.
3. Vignesh Palanivel, M.S. Thesis, University of Cincinnati, Department of Materials Science and Engineering, 2003.
4. A.N. Onal and A. A. Aksut, Anti-Corr Met and Mat, 47, 339 (2000)
5. J.C. Bolger and A.S. Michaels, Inter. Conv. For. Poly. Coatings, Weiss and Cheever, ed., Elsevier, New York (1968)
6. R.A. Dickie and F.L. Floyd, Poly Mat for Corrosion Control, ACS Symposium Series, Washington, 1, (1987)
7. K. Aramaki, CORROSION SCIENCE, 44, 886 (2002)
8. R.G. Buchheit, R.K. Boger, M.W. Donohue, Proceedings of the Symposium on Seawater Corrosion, Electrochem Soc., Pennington, NJ, 99-26, 205 (2000)
9. G.S. Frankel and W. Zhang, Electrochem. Solid-State Lett., 3, 268 (2000)
10. Plueddemann, E. P., "Silane Coupling Agents", 2nd ed., Plenum Press, New York, 1991.

11. D. Zhu, Ph. D. Dissertation, University of Cincinnati, Department of Materials Science and Engineering, 2002
12. R.G. Buchheit, L.P. Montes, M.A. Martinez, J. Michael, P.F. Hlava, J. Electrochem.Society, 12, 4424 (1999)
13. P. Campestri, A. Hovestad, Electrochimica Acta, 47, 1097 (2002)
14. P. Schmutz, G.S. Frankel, J. Electrochem. Soc., 146, 4461 (1999)
15. D. Zhu, and W.J. Van Ooij, Corros. Sci., in press, 2002
16. R.G. Buchheit, R.K. Boger, M.W. Donohue, Proceedings of the Symposium on Seawater Corrosion, Electrochem Soc., Pennington, NJ, 99-26, 205 (2000)
17. D. Zhu, Ph. D. Dissertation, University of Cincinnati, Department of Materials Science and Engineering, 2002
18. H. Woo, P.J. Reucroft, R.J. Jacob, J. Adh. Sci. Tech., 7, 681 (1993)
19. J.M. Chovelon, L.E.L. Aarch, M. Charbonium, M. Romand, J. Adh, 50, 43 (1995)
20. P. Walker, J. Adh. Sci. Tech, 5, 279 (1991)
21. W.J. van Ooij and T. F. Child. CHEMTECH, 28, 26 (1998)
22. V. Subramanian, Ph. D. Dissertation, University of Cincinnati, Department of Materials Science and Engineering, 1999.

23. G. P. Sundararajan, M. S. Thesis, University of Cincinnati, Department of Materials Science and Engineering, 2000.
24. W.J. van Ooij, Proc. Adv. Techniques for Replacing Chromium (Johnstown, PA: Concurrent Technologies, Corp) 421 (1996)
25. A.Sabata, W.J. van Ooij, H.K. Yasuda, Surf. Interface Anal., 20, 485 (1993)
26. V. Subramanian, W.J. van Ooij, CORROSION, 54, 204 (1998)
27. Underhill, P. R., and Duquesnay, D. L., K. L. Mittal (Ed.), Silanes and Other Coupling Agents, K. L. Mittal Ed., VSP, Utrecht, 2, 149 (2000)
28. Petrunin, M. A., Nazarov, A. P., and Mikhailovski, Yu. N., J. Electrochem. Soc., 143, 251 (1999)
29. F. Mansfeld, F.J. Ferez and Wang, Thin Solid Films, 270, 417 (1995)
30. Beccaria, A. M., and Chiaruttini, L., Corros. Sci., 41, 885 (1999)
31. Van Ooij, W. J., Zhu, D., Sundararajan, G. P., Jayaseelan, S. K., Fu Y., and Teredesai, N., Surf. Engg. 16, 386 (2000)
32. H. Leidheiser Jr, M. De Costa and R.D. Granata, Corrosion, 43, 382 (1987)
33. John Coates, Encyclopedia of Analytical Chemistry, 2000, John Wiley & Sons Ltd, Chichester.

34. Morris, E., Stoffer, J.O., O'Keefe, T.J., Yu, P., and Lin, X., Polym. Mater. Sci. Eng., 81, 167 (1999)
35. 30. R.M.A.Azzam and N.M.Bashara, Ellipsometry and polarized light, North Holland Pub.Company, (1977)
36. J.H. Osborne, K. Y. Blohowaik, S. R. Taylor, C. Hunter, G. Bierwagon, B. Carlson, D. Bernard, M. S. Donely, Prog Org Coat, 41, 217 (2001)
37. K. Aramaki, Corr. Sci, 43, 2201 (2001)
38. Osterholtz, F. D., and Pohl, E. R., J. Adhesion Sci. Technol.6, 127 (1992)
39. Parkhill, R. L., Knobbe, E.T. and Donley, M.S., Progress in Organic Coatings, 41, 261 (2001)
40. Narayanan R, El-Sayed MA, J Am Chem Soc. 2003 Jul 9;125(27):8340-7.
41. Jiang Y.; Decker S.; Mohs C.; Klabunde K.J., Journal of Catalysis, Volume 180, Number 1, November 1998, pp. 24-35(12).
42. M.A. Arenas, A. Conde, J.J. Damborenea, CORROSION SCIENCE, 44, 520 2002)
43. R.L. Parkhill, E.T. Knobbe and M.S. Donley, Prog Org Coat, 41, 261 (2001)
44. D. Zhu, and W.J. Van Ooij, J. Adhesion Sci. Technol, 16, 1235 (2002)
45. D. Zhu, and W.J. Van Ooij, Prog. Org. Coatings, in press

46. R. Rungta, *Metal Finishing*, 95, 114 (1997)
47. A.N. Onal and A. A. Aksut, *Anti-Corr Met and Mat*, 47, 339 (2000)
48. K. Aramaki, *Corr. Sci*, 45, 210 (2003)
49. R.G. Buchheit, S.B. Mamidipally, P. Schmutz, H. Guan, *Proceedings of NACE International*, Houston, TX, 67-92 (2000)
50. Oliver, W.C., and Pharr, G. M., *J. of Mater. Res.*, 7, 1564 (1992)
51. Mercer, A D., *Mater. Perform.* Vol. 29, no. 6, pp. 45-49. June 1990
52. J.M. Keijman, PCE '99 CONFERENCE, 10-12 March 1999, The Brighton Centre, Brighton, England.
53. Application notes on EIS, available online at [www.Gamry.com](http://www.Gamry.com)
54. Tait W. S., *An Introduction to Electrochemical Corrosion Testing for Practicing Engineers and Scientists*, Pair O Docs Publications, Racine, WI (1994)
55. Murray J. N., *Prog Org Coat*, 30, 225 (1997)
56. Kendig M. and Scully J., *Corrosion* 46, 22 (1990)
57. Bonora P.L., Deflorian F., and Fedrizzi L., *Electrochim Acta* 41, 1073 (1996)
58. Davis G.D. and Dacres C.M., U.S. Patent 5,859,537, January 12, 1999. Davis G.D. and Dacres C.M., U.S. Patent 6,054,038, April 25, 2000. Davis G.D. and Dacres C.M., U.S.

Patent 6,313,646, November 6, 2001. Davis G.D., Dacres C.M., and Krebs L.A., U.S.

Patent 6,328,878, December 11, 2001

59. Mansfeld F., *Corrosion* 37, 301 (1981)
60. Kendig M., Mansfeld F., and Tsai S., *Corros. Sci.* 23, 317 (1983)
61. Kendig M. and Scully J., *Corrosion* 50, 527 (1989)
62. Scully J.R., *J. Electrochem. Soc.* 136, 979 (1989)
63. Tait W.S., *J. Coat. Technol.* 61, 57 (1989)
64. Murray J.N. and Hack H.P., *Corrosion90*, Paper 140, NACE 1990
65. Grandle J.A. and Taylor S.R., *Corrosion* 50, 792 (1994)
66. Meade C.L., *Metal Finishing* 98, 540 (2000)
67. Altmayer F., *Metal Finishing*, 97, 584 (1999)
68. Baldwin K.R., Smith C.J.E., *Aircraft Engineering and Aerospace Technology: An International Journal*, 71, 3, 239-244 (1999)
69. Böhm S., Sullivan J.H., Worsley D. A., *Materials and Corrosion* 52, 540 (2001)
70. Bierwagen G., Tallman D., Li J., He L., Jeffcoate C., *Prog Org Coat*, 46, 149 (2003)
71. Hospadaruk V., Huff J., Zurilla R.W., and Greenwood H.T., *Trans. SAE* 87, 755 (1978)

## APPENDIX

A.1 <http://www.techsolve.org/p2iris/metalfinish/1058-s.htm>

A.2 <http://www.pfonline.com/articles/pfd0020.html>

A.3

[http://wrrc.p2pays.org/p2rx/subsection.cfm?hub=445&subsec=2&nav=2&CFID=35148&CFTOKEN=](http://wrrc.p2pays.org/p2rx/subsection.cfm?hub=445&subsec=2&nav=2&CFID=35148&CFTOKEN=86950217)

[N=86950217](http://wrrc.p2pays.org/p2rx/subsection.cfm?hub=445&subsec=2&nav=2&CFID=35148&CFTOKEN=86950217)

A.4 <http://www.shu.ac.uk/schools/sci/chem/tutorials/molspec/nmr1.htm>

A.5 <http://www.chemistry.ccsu.edu/glagovich/teaching/472/ir/em.html>

A.6

[www.acq.osd.mil/log/mppr/senior\\_steering/Dunmire%20MTSSG%20Slides%20REV1%20Oct%20](http://www.acq.osd.mil/log/mppr/senior_steering/Dunmire%20MTSSG%20Slides%20REV1%20Oct%2012.ppt)

[012.ppt](http://www.acq.osd.mil/log/mppr/senior_steering/Dunmire%20MTSSG%20Slides%20REV1%20Oct%2012.ppt)

## TABLES

**Table 2.1: List of Silanes used with trade names and chemical formulas**

TRADE NAME	CHEMICAL NAME	CHEMICAL FORMULA
A-1170	Bis(trimethoxysilylpropyl)amine	$(\text{OCH}_3)_3\text{Si}(\text{CH}_2)_3\text{NH}(\text{CH}_2)_3\text{Si}(\text{OCH}_3)_3$
A-1289	Bis(triethoxysilylpropyl]tetrasulfide	$(\text{OC}_2\text{H}_5)_3\text{Si}(\text{CH}_2)_3\text{S}_4(\text{CH}_2)_3\text{Si}(\text{OC}_2\text{H}_5)_3$
Y-9805	Bis(triethoxysilylpropyl)]ethane	$(\text{OC}_2\text{H}_5)_3\text{Si}(\text{CH}_2)_2\text{Si}(\text{OC}_2\text{H}_5)_3$
TEOS	Tetraethoxysilane	$\text{Si}(\text{OC}_2\text{H}_5)_4$
A-Link 15	Nethyl-3-trimethoxysilylethylpropanamine	$\text{CH}_3\text{CH}_2\text{NHCH}_2\text{CH}(\text{CH}_3)\text{CH}_2\text{Si}(\text{OCH}_3)_3$
A-Link 25	Gamma-Isocyanatopropyltriethoxysilane	$\text{NCO}(\text{CH}_2)_3\text{Si}(\text{OC}_2\text{H}_5)_3$
VTAS	Vinyltriacetoxysilane	$\text{CH}_2=\text{CH}(\text{CH}_2)_2\text{Si}(\text{OCOCH}_3)_3$

**Table 2.2 Resins used in superprimer formulations**

EPON 828 Resin-X-95
EPIREZ Resin 3510-W-60
EPIREZ Resin 3515-W-60
EPIREZ Resin 3540-WY-55

**Table 2.3 Particles used in superprimer formulations**

<b>NAME</b>	<b>TYPE</b>	<b>MANUFACTURER</b>
Colloidal Silica	Silica nano-particles(suspension in water)	Cabot Corporation, Tuscola, IL
Aluminasol	Alumina nano-particles 10% by weight(suspension in water)	Nissan Chemical, Houston, TX
Carbosil	Carbon nanoparticles(Dry)	
Zinc Dust	Zinc nanoparticles(Dry)	U.S.Zinc, Houston, TX

**Table 2.4: Corrosion Inhibitors used in the superprimer formulations**

<b>NAME</b>	<b>COMPANY</b>	<b>TYPE</b>
CZM	Molywhite, Cleveland, OH	Calcium Zinc Molybdate
M-119 LV	Cortec Corporation, St. Paul, MN	Trade Secret of the company
M-5120	Cortec Corporation, St. Paul, MN	Trade Secret of the company
M-118	Cortec Corporation, St. Paul, MN	Trade Secret of the company
Fluka-Sodium Vanadate	Sigma Aldrich	Sodium Meta Vanadate
SZP-391	Halox Pigments, Hammond, IN	Strontium Zinc Phosphate
Corrostayn 228	Wayne Pigment Corp, Milwaukee, WI	Trade Secret of the company
UC-Pigment	University of Cincinnati	Plasma Polymerized Pigment

**Table 3.1: Resins and compatible silanes**

<b>RESIN</b>	<b>SILANE CLASS</b>
Epoxy	Amine, Epoxy, Chloroalkyl, Mercapto
Polyester	Amine, Methacrylate, Styryl, Vinyl
Urethane	Amine, Alkaloamine, Epoxy, Isocyanate
Acrylic	Acrylic, Styryl, Epoxy

Table 3.4.1: Comparison of performance of test results between control PRC Desoto MIL PRF and Superprimer Formulation F

	CONTROL	FORMULATION F
<b>Salt spray</b>	No corrosion in the scribe after 2 weeks	Corrosion in the scribe after 2 weeks
<b>Salt immersion</b>	Sustained for 1 month	Sustained for 1 month
<b>Contact angle</b>	69.5°	65.5°
<b>EIS</b>	6 ohm for 1 week	3 ohm for 2 days
<b>Hardness</b>	F	HB
<b>Adhesion to Substrate</b>	5B	4B
<b>Paint Adhesion</b>	5B	5B

Table 3.6.1: Summary of test results of the control, F-6 and F

	CONTROL	FORMULATION F	FORMULATION F-6
Salt spray	No corrosion in the scribe after 2 weeks	Corrosion in the scribe after 1 week	Corrosion in scribe after 2 weeks
Salt immersion	Sustained for 1 month	Sustained for 1 month	Sustained for 2 months
Contact angle	69.5°	65.5°	78.4°
EIS	1 Mohm for 1 week	100 kohm for 2 days	1 Gohm for 1 week
Hardness	F	HB	F
Adhesion to substrate	5B	4B	5B
Paint Adhesion	5B	5B	5B

**Table 4.1.1: Formulation chart of modified superprimers with particles/inhibitors**

<b>FORMULATION (BY WEIGHT)</b>	<b>RESIN</b>	<b>AV5 (10%)</b>	<b>SULFUR SILANE</b>	<b>TEOS</b>	<b>ADDITION</b>
F6	80	9	10	1	nil
F10	77.5	9	10	1	(Alumina) 2.5
F11	75	9	10	1	(Alumina) 5.0
F12	70	9	10	1	(Alumina) 10.0
F13	77.5	9	10	1	(CZM) 2.5
F14	75	9	10	1	(CZM) 5.0
F15	70	9	10	1	(CZM) 10.0
F16	80	9	10	nil	A-LINK-15
F17	80	9	10.9	nil	(A-link 25) 0.1
F18	80	9	10.9	nil	A-LINK-15 0.1
F19	80	9	10	1	BTSE (10%)
F20	78.8	9	10	1	(Cortec M119 LV)1
F21	78	9	10	0.5	Cortec M-5120(1%) + A-

					LINK-15(0.5)
F22	78	9	10	0.5	Cortec M-118(2%)+A-LINK-15(0.5)
F23	78	9	10	0.5	Sodium Vanadate 2%+A-LINK-15(0.5)
F24	75	9	10	0.5	Sodium Vanadate 5000 ppm+A-LINK-15(0.5)
F 25	77	9	10	0.5	Halox SZP-391 Strontium Zinc Phosphosilicate 3%+A-LINK-15(0.5)
F26	80	9	10.5	0.5	nil
F27	77	9	10.5	0.5	Wayne Pigment Corp., Corrostain 3 %
F28	77	9	10.5	0.5	Carbon Black 3%
F29	77	9	10.5	0.5	UC Pigment 3%

Table 6.1: Peak assignments in the carbon spectrum of commercial resin;

Spectra for the component silanes AV5 and bis-sulfur are shown in Figures 6.3 and 6.4. Refer to

Figure 6.1

PEAK POSITION	COMPONENT	ASSIGNMENT
156.8	Resin	Phenyl
143.4	Resin	Phenyl
127.9	Resin	Phenyl
114.3	Resin	Phenyl
72.9	Propoxyethanol	
72.1	Propoxyethanol	
70.2	Resin	Internal C-O-C
69.1	Resin	Internal C-OH
61.2	Propoxyethanol	
50.4	Resin	Epoxide
44.3	Resin	Epoxide
41.6	Resin	Quaternary C

31.1	Resin	(CH <sub>3</sub> ) <sub>2</sub>
22.8	Propoxyethanol	
10.5	Propoxyethanol	

Table 6.2: Table showing the change in intensities at certain peak of Figure 6.5 varies with time.

Time is shown in the Y-axis of the table and the peak values in the X-axis of the table.

ppm	49.3	17.9	57.5	18.6	58.5
Initial	2.4	35.9	32.1	170.7	119.8
16 hours at RT conditions	11.8	11.8	11.3	118.3	103.8
8 Days at RT conditions	12.38	37.34	46.6	105	89.1

Table 6.3: Solid State NMR spectrum of cured superprimer coating shown in Figure 6.6

PEAK	COMPONENT	ASSIGNMENT
158.5	Resin	Phenyl
145.4	Resin	Phenyl
129.3	Resin	Phenyl
116.3	Resin	Phenyl
70.7	Resin	Internal C-O-C
59	Bis-sulfur silane	OCH <sub>2</sub> CH <sub>3</sub>
42.7	Resin (possible bis-sulfur overlap?)	Quaternary carbon
32.2	Resin	(CH <sub>3</sub> ) <sub>2</sub>
24.1	Resin	SCH <sub>2</sub> CH <sub>2</sub> CH <sub>2</sub> Si(OR) <sub>3</sub>
18.8	Resin	OCH <sub>2</sub> CH <sub>3</sub>
11.1	Resin	SCH <sub>2</sub> CH <sub>2</sub> CH <sub>2</sub> Si(OR) <sub>3</sub>

Table 6.4: Peak assignments for bands in IR spectra

FUNCTIONAL GROUP	MOLECULAR MOTION	WAVENUMBER (CM <sup>-1</sup> )
alkanes	C-H stretch	<sup>29</sup> 50-2800
	CH <sub>2</sub> bend	~1465
	CH <sub>3</sub> bend	~1375
	CH <sub>2</sub> bend (4 or more)	~720
alkenes	=CH stretch	3100-3010
	C=C stretch (isolated)	1690-1630
	C=C stretch (conjugated)	1640-1610
	C-H in-plane bend	1430-12 <sup>90</sup>
	C-H bend (monosubstituted)	~990 & ~910
	C-H bend (disubstituted - E)	~970
	C-H bend (disubstituted - 1,1)	~890
	C-H bend (disubstituted - Z)	~700
	C-H bend (tri-substituted)	~815
alkynes	acetylenic C-H stretch	~3300

	C,C triple bond stretch	~2150
	acetylenic C-H bend	650-600
	C-H stretch	3020-3000
	C=C stretch	~1600 & ~1475
	C-H bend (mono)	770-730 & 715-685
	C-H bend (ortho)	770-735
	C-H bend (meta)	~880 & ~780 & ~690
aromatics	C-H bend (para)	850-800
	O-H stretch	~3650 or 3400- 3300
alcohols	C-O stretch	1260-1000
	C-O-C stretch (dialkyl)	1300-1000
ethers	C-O-C stretch (diaryl)	~1250 & ~1120
	C-H aldehyde stretch	~2850 & ~2750
aldehydes	C=O stretch	~1725
ketones	C=O stretch	~1715

	C-C stretch	1300-1100
carboxylic acids	O-H stretch	3400-2400
	C=O stretch	1730-1700
	C-O stretch	1320-1210
	O-H bend	1440-1400
esters	C=O stretch	1750-1735
	C-C(O)-C stretch (acetates)	1260-1230
	C-C(O)-C stretch (all others)	1210-1160
acid chlorides	C=O stretch	1810-1775
	C-Cl stretch	730-550
anhydrides	C=O stretch	1830-1800&1775- 1740
	C-O stretch	1300-900
amines	N-H stretch (1 per N-H bond)	3500-3300
	N-H bend	1640-1500
	C-N Stretch (alkyl)	1200-1025
	C-N Stretch (aryl)	1360-1250

	N-H bend (oop)	~800
amides	N-H stretch	3500-3180
	C=O stretch	1680-1630
	N-H bend	1640-1550
	N-H bend (1°)	1570-1515
alkyl halides	C-F stretch	1400-1000
	C-Cl stretch	785-540
	C-Br stretch	650-510
	C-I stretch	600-485
nitriles	C,N triple bond stretch	~2250
isocyanates	-N=C=O stretch	~2270
isothiocyanates	-N=C=S stretch	~2125
imines	R <sub>2</sub> C=N-R stretch	1690-1640
nitro groups	-NO <sub>2</sub> (aliphatic)	1600-1530&1390- 1300
	-NO <sub>2</sub> (aromatic)	1550-1490&1355- 1315

mercaptans	S-H stretch	~2550
sulfoxides	S=O stretch	~1050
sulfones	S=O stretch	~1300 & ~1150
sulfonates	S=O stretch	~1350 & ~11750
	S-O stretch	1000-750
phosphines	P-H stretch	2320-2270
	PH bend	1090-810
phosphine oxides	P=O	1210-1140

# FIGURES

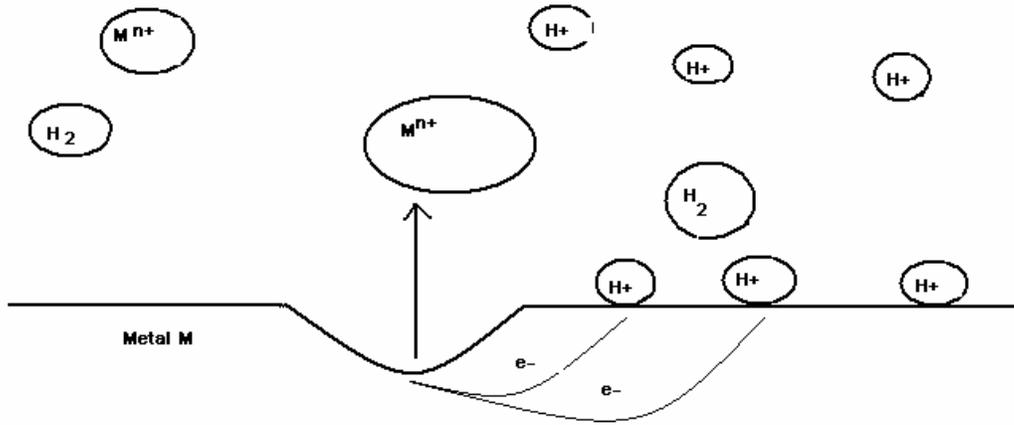


Figure 1.1: A typical corrosion mechanism



Figure 1.2: Heavy Corrosion Environment [A.6]



Figure 1.3: Corroded C-141 aircraft. [A.6]



Figure 1.4: Corroded aircraft part. [A.6]

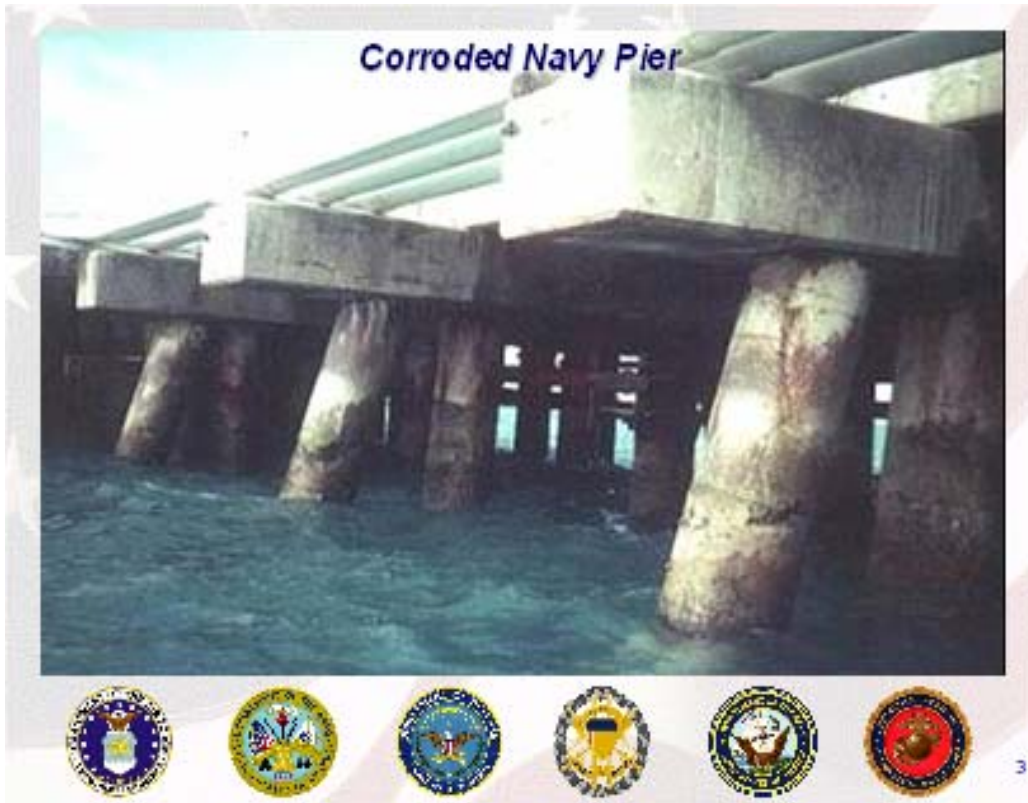


Figure 1.5: Corroded navy pier. [A.6]

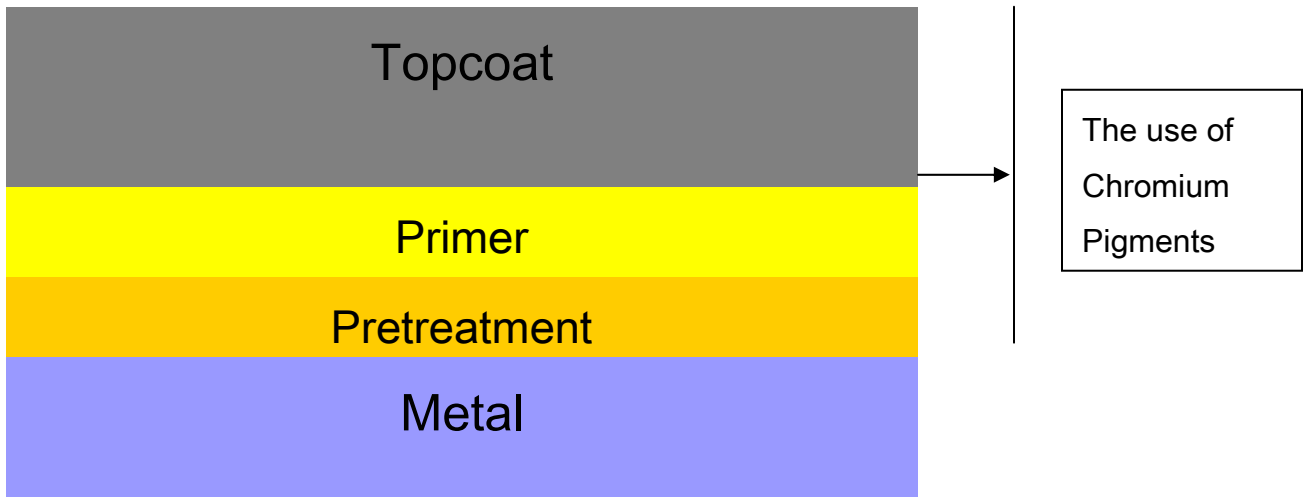


Figure 1.6: Typical coating system in DoD



Figure 1.7: Corrosion repair in DoD. [A.6]



Figure 1.8: Commercial blue-bright, iridescent and golden yellow, olive drab, matte black and  
bronze chromating examples

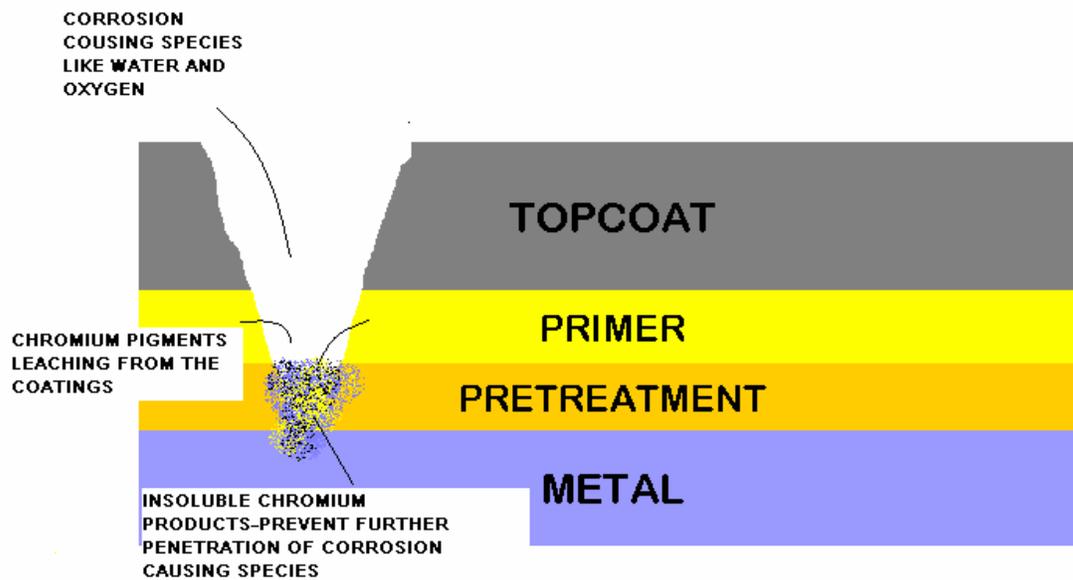


Figure 1.9: Chromate coating's self-healing mechanism

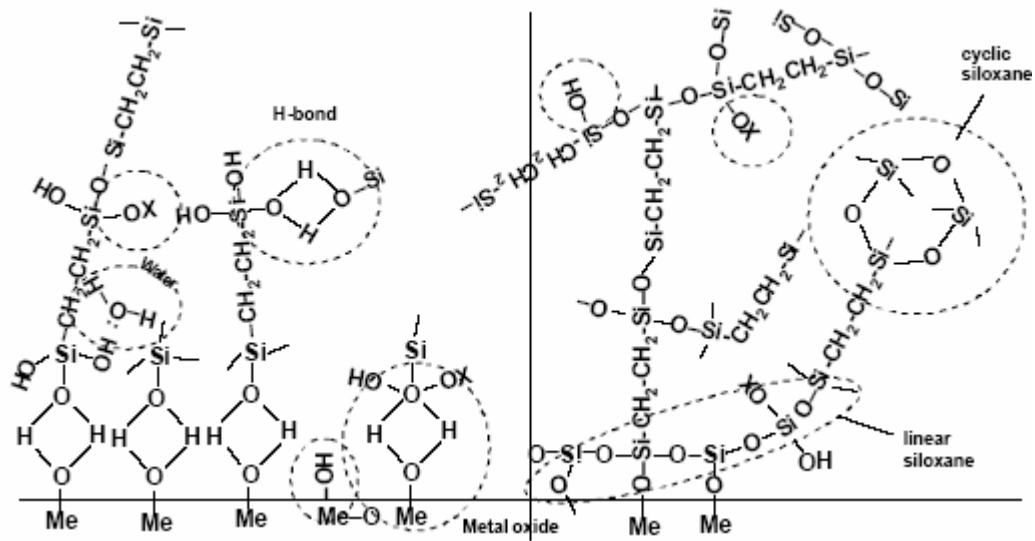


Figure 1.10: Silane mechanism over a metal

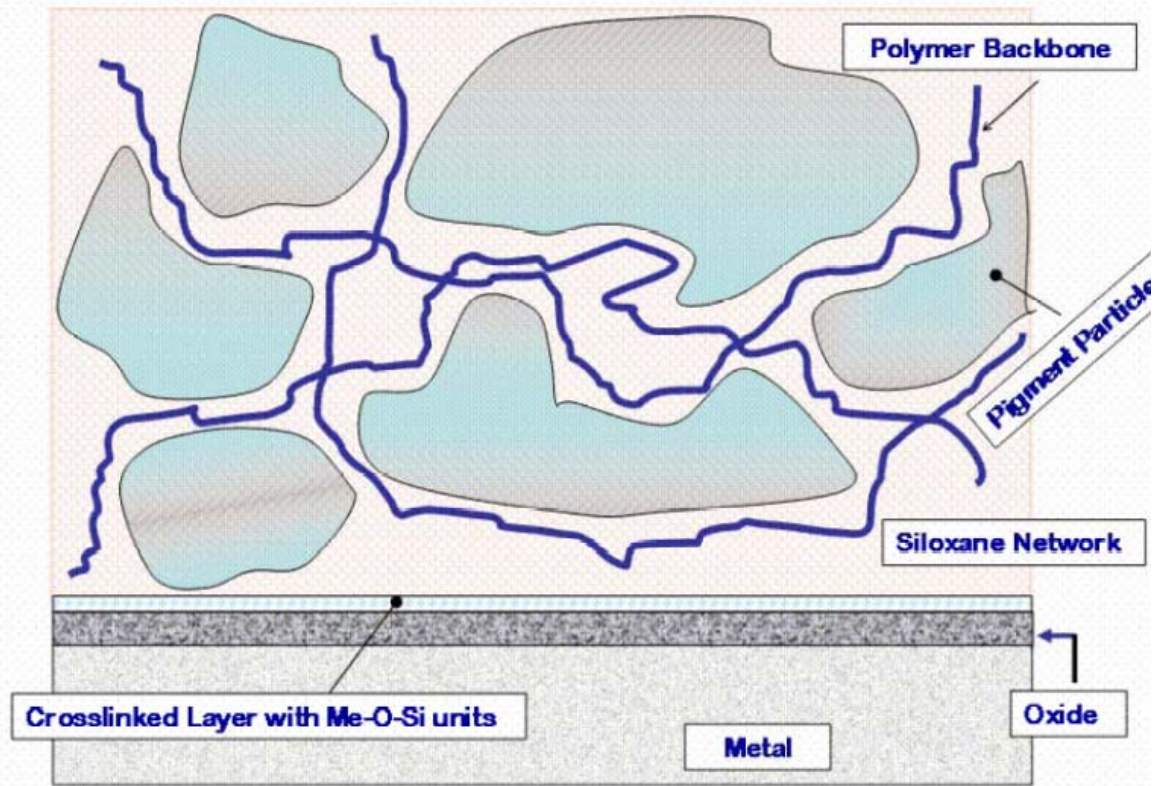


Figure 1.11: Superprimer: adsorption of superprimer on metal [Van Ooij, SERDP review, 2004]

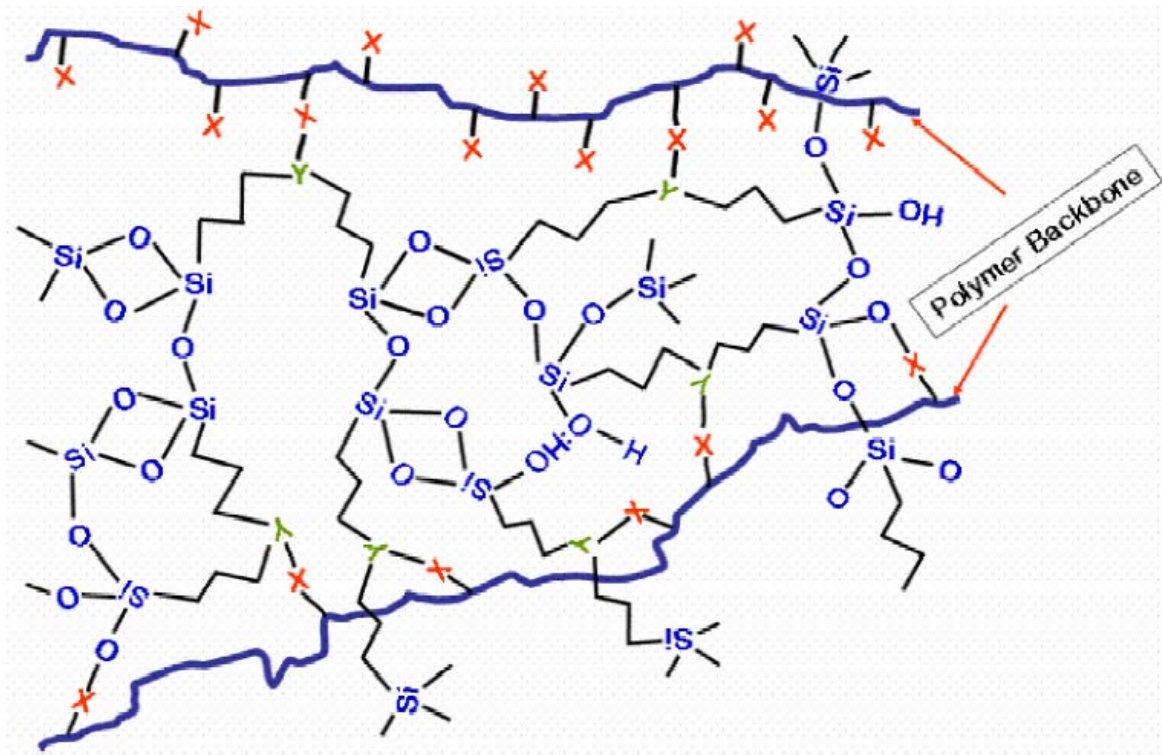
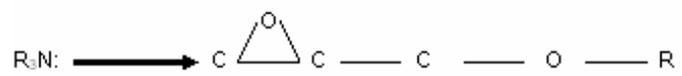
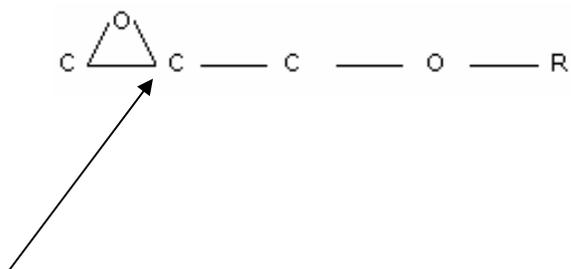
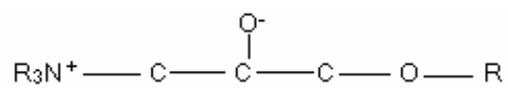


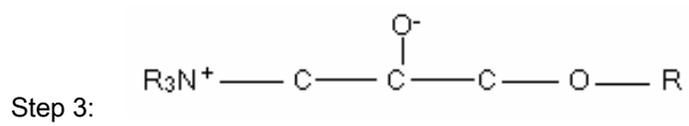
Figure 1.12: Superprimer: crosslinking of resin by bis-silanes [Van Ooij, SERDP review, 2004]

Step 1:

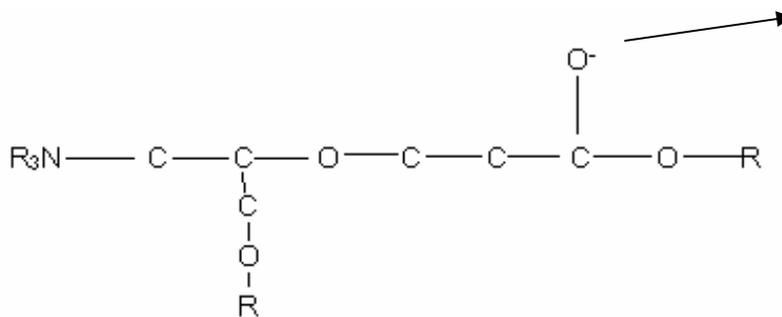


Step 2:





Further  
polymerization



Step 4:

Figure 3.1: Schematic showing the probable reactions between epoxy-epoxy and epoxy- tertiary amine.

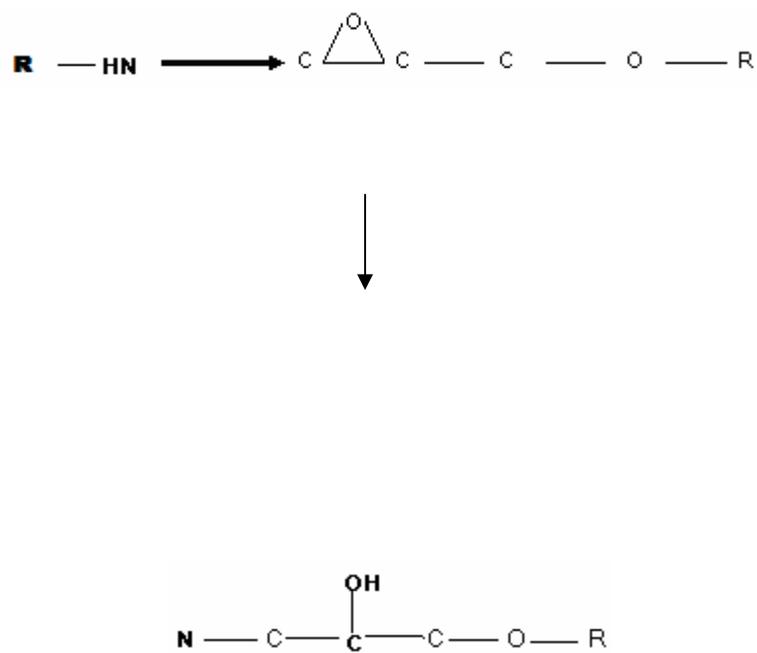


Figure 3.1.2: Reaction between primary amine and an epoxy group

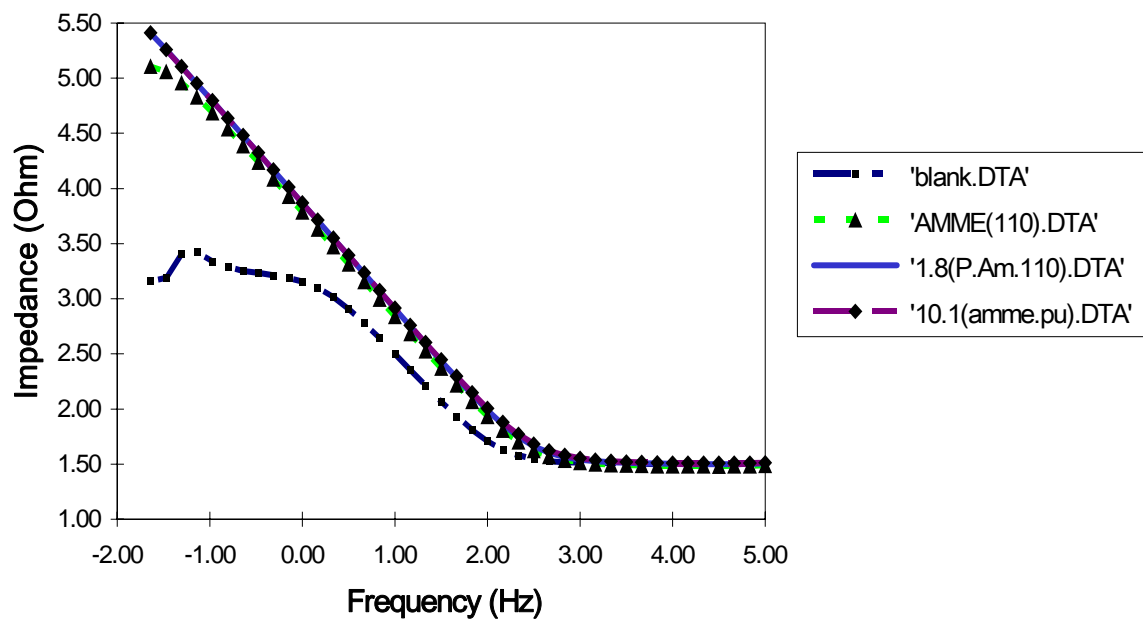


Figure 3.2.1 Bode Plot of, 1: Blank uncoated Al 2024 T3 sample, 2: Coated with AMME silane and cured at 110°C, 3: A 1:8 mixture of polyurethane resin and AMME silane, 4: A 1:10 mixture of polyurethane resin and AMME silane.

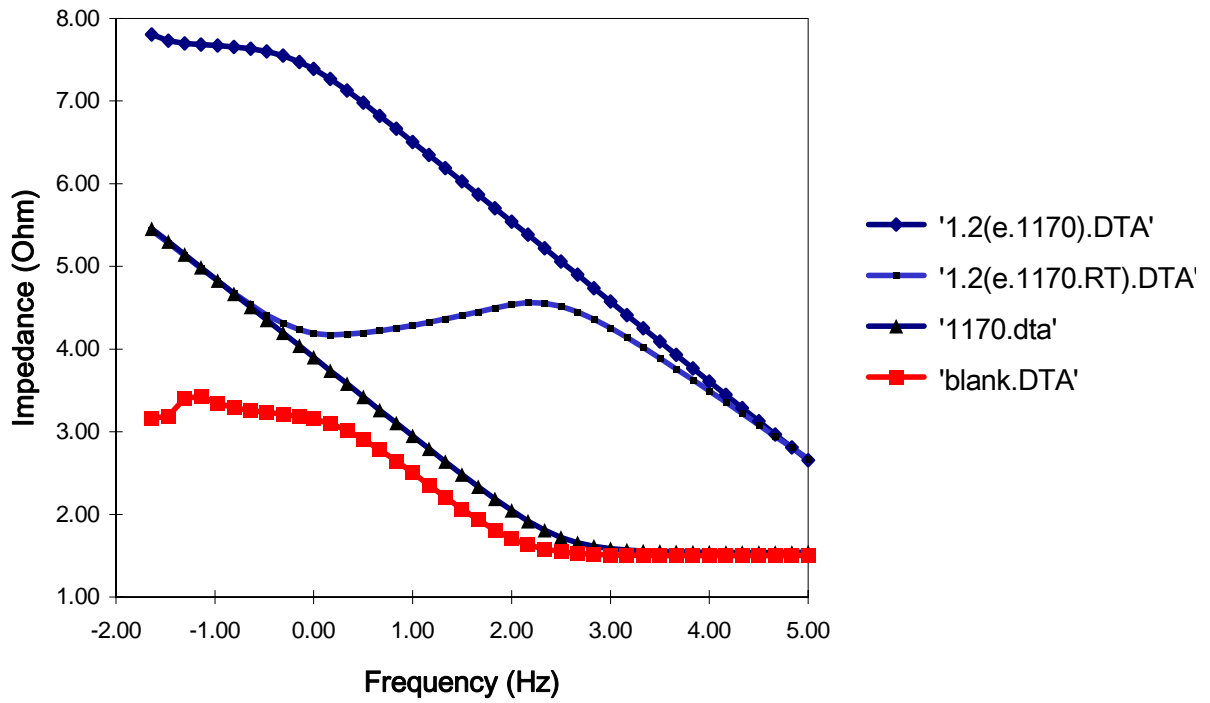


Figure 3.2.2: 1: A 1:2 mixture of EPON 828 resin with A-1170 unhydrolyzed silane coated on AA

2024 T3 panel cured at 110°C, 2: Same mixture as in 1, but cured a RT for a 48 hours,3: Al panel

coated with silane alone, 4: Blank uncoated panel



Figure 3.4.1: Yellow panel (left) is an aluminum panel coated with the PRC Desoto MIL-PRF

Yellow primer from military. And the other panel is coated with formulation F

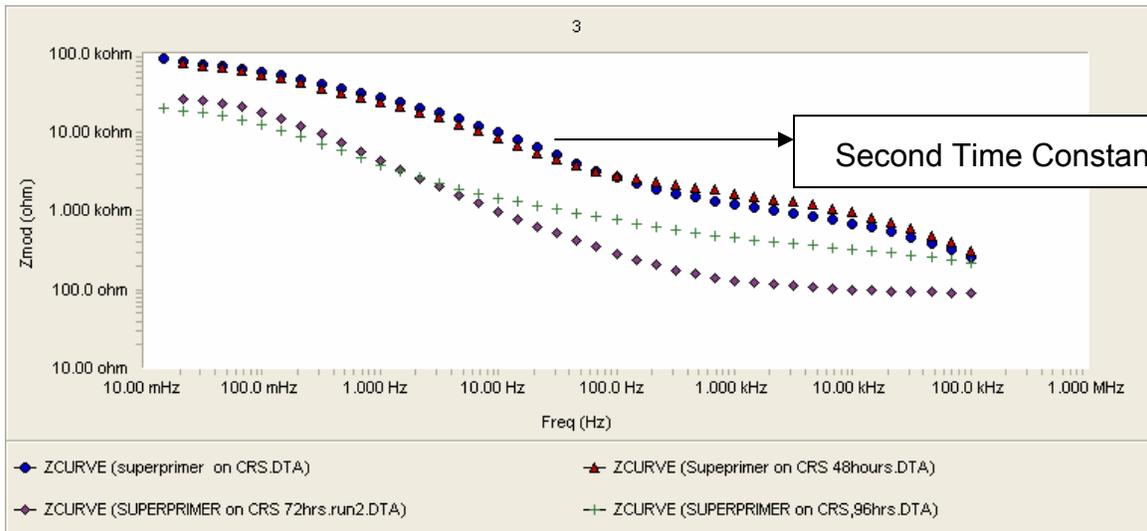


Figure 3.4.2: EIS Bode plot of formulation F coated on a CRS substrate and tested for 4 days.

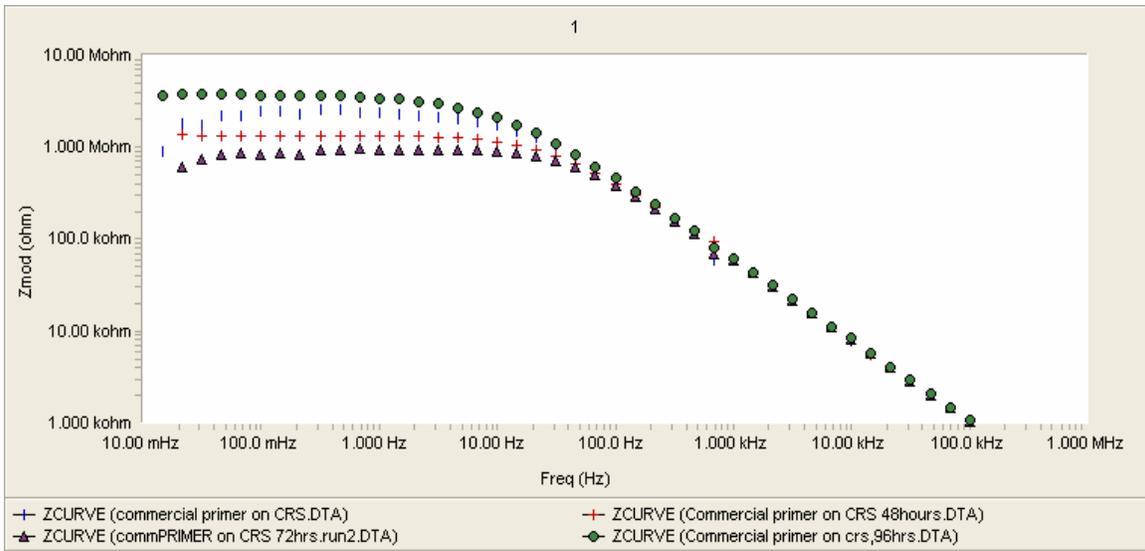


Figure 3.4.3: EIS Bode plot of control PRC Desoto MIL PRF chromate-containing primer coated on a CRS substrate and tested for 4 days.

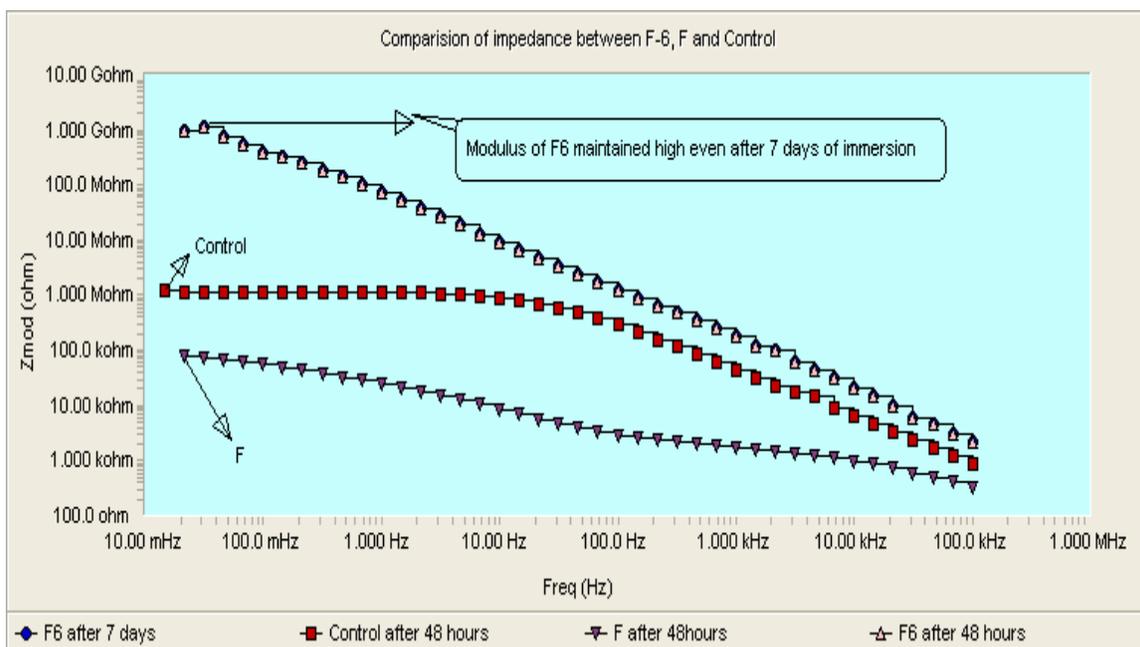


Figure 3.6.1: EIS Bode plot comparing the curves of F-6, F and the control Desoto PRC MIL PRF



Figure 3.6.2: Salt spray result of F-6 after 2 weeks

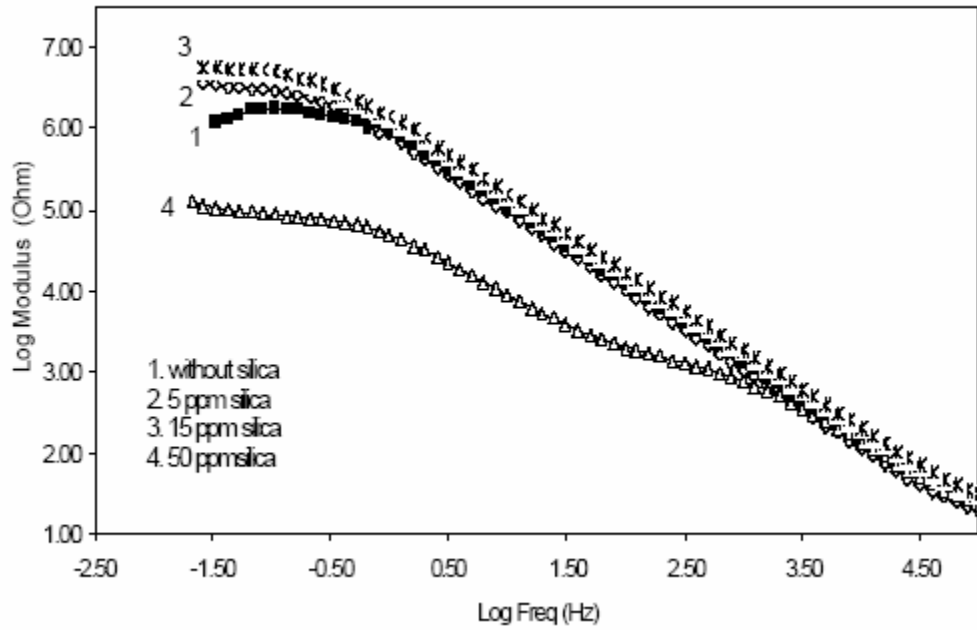


Figure 4.2.1: Impedance plots of bis-sulfur silane treated AA2024-T3 systems loaded with different amounts of silica nano-particles

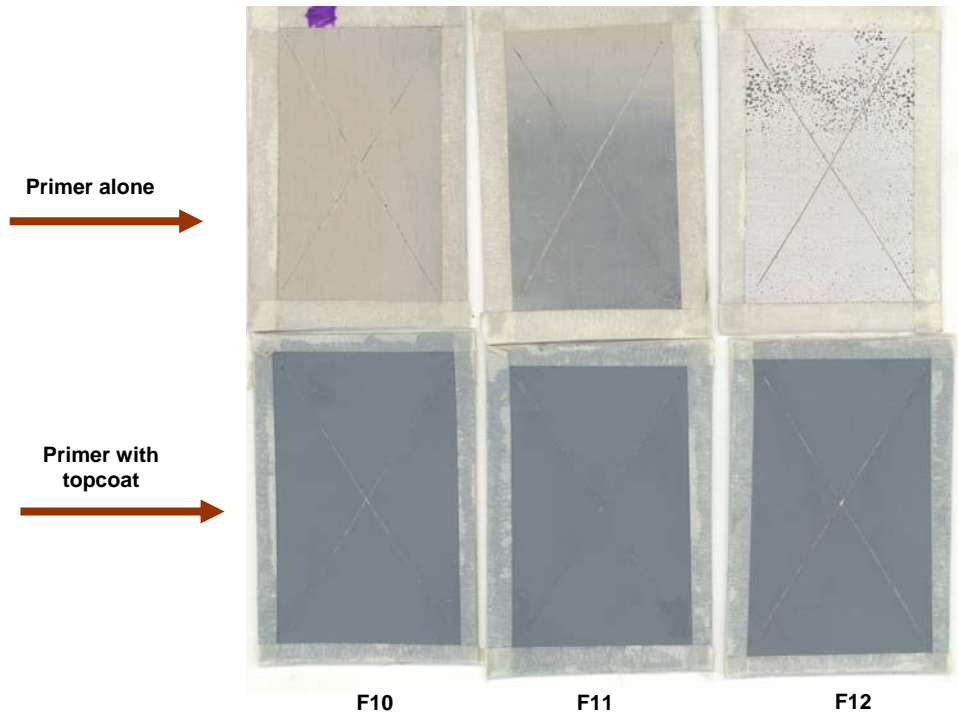


Figure 4.2.2: Salt immersion test after 7 days. Formulations with increased weight percentages of alumina numbered F10, F11 and F12 in Formulation table.

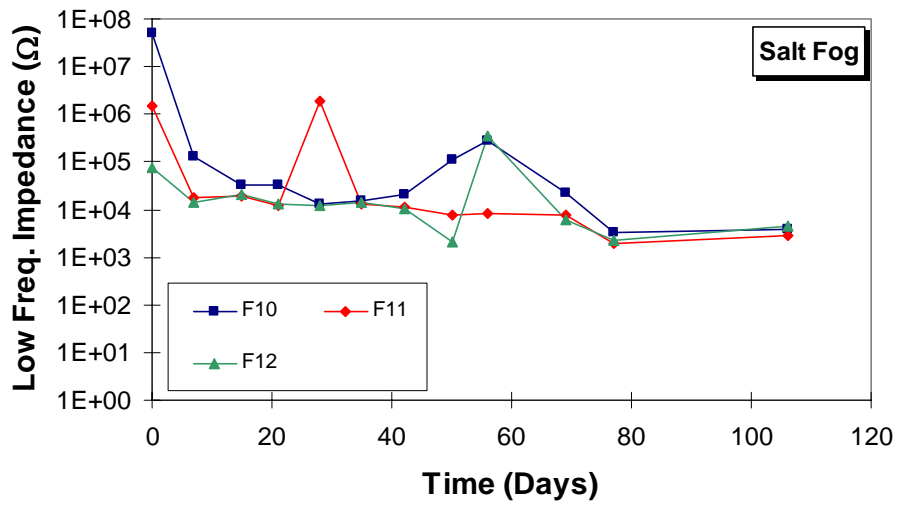


Figure 4.2.3: EIS Impedance values of salt fog tested coatings with time.

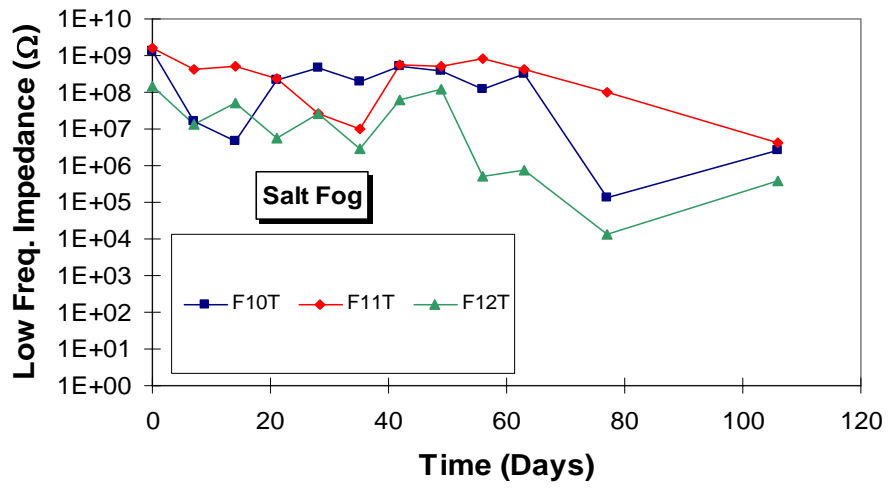


Figure 4.2.4: EIS Impedance values of salt fog tested coating with time of coating formulations

containing alumina and with poly-urethane topcoat.

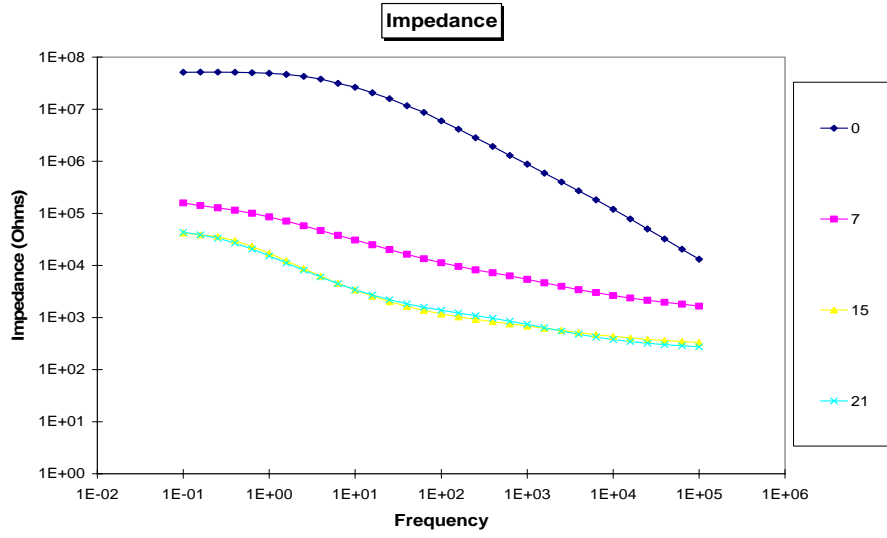
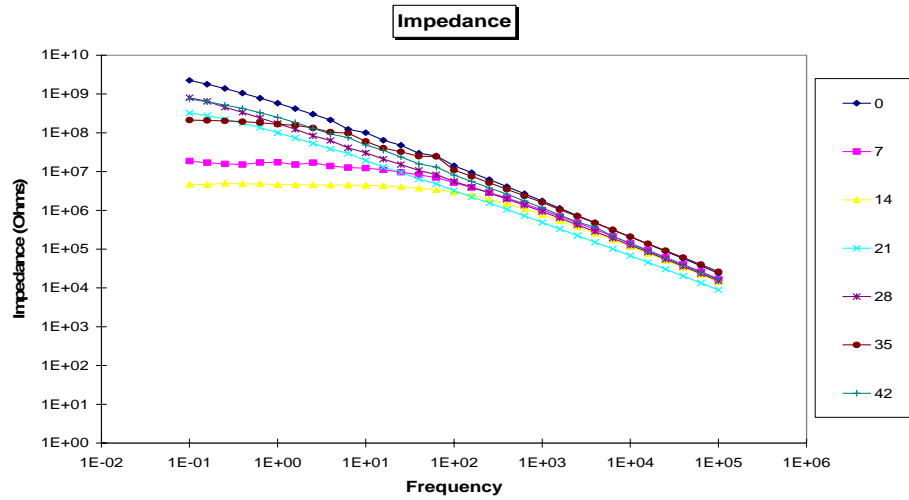


Figure 4.2.5: Bode plot of F 10 without topcoat (above) with topcoat (below)



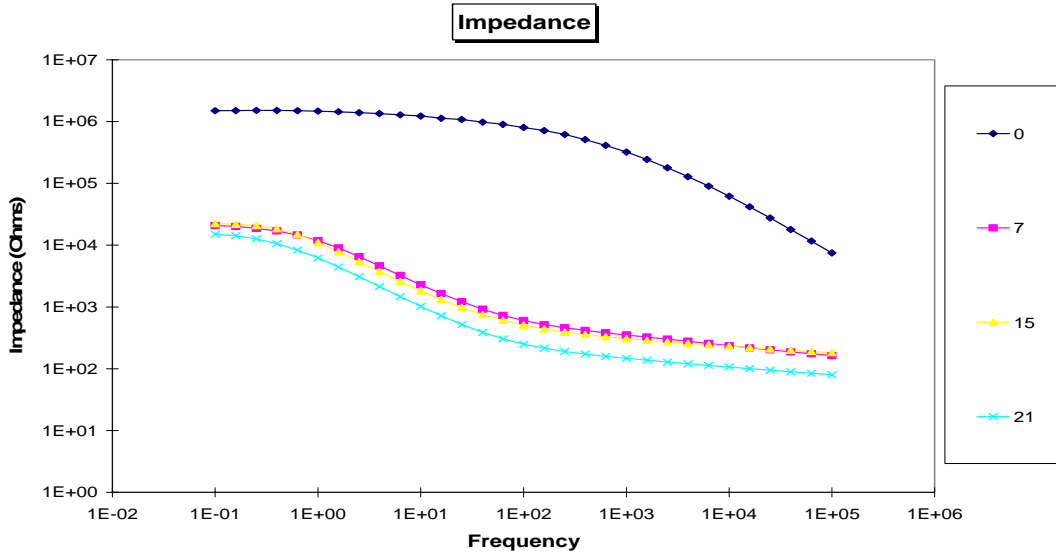
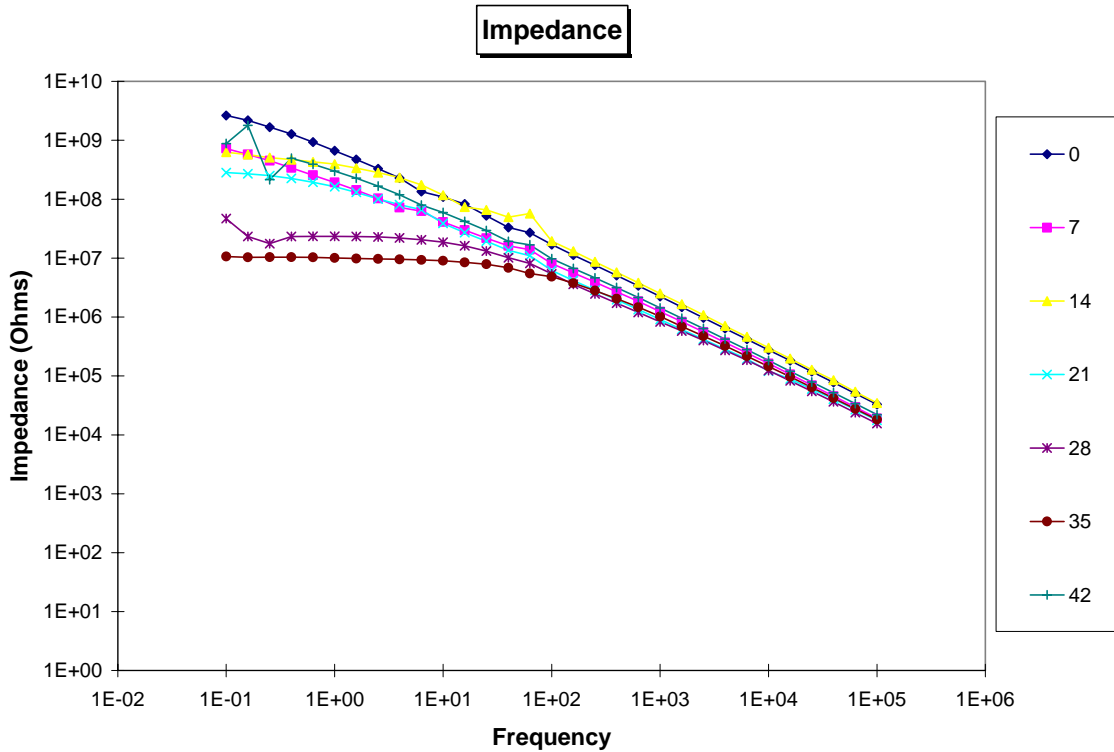


Figure 4.2.6: Bode plot of F 11 without topcoat (above) with topcoat (below)



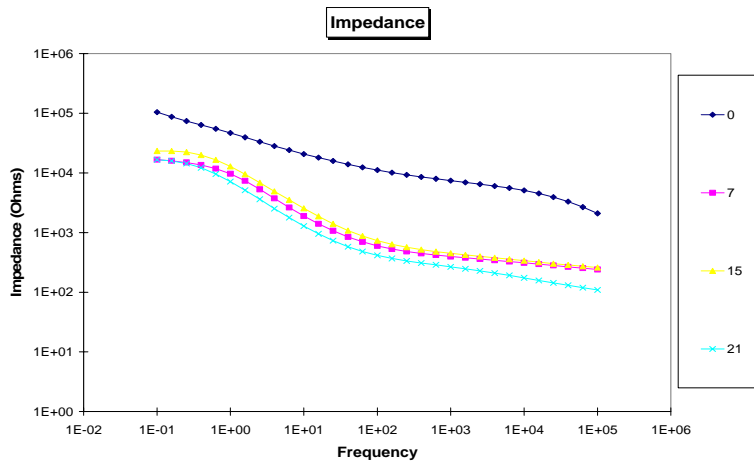
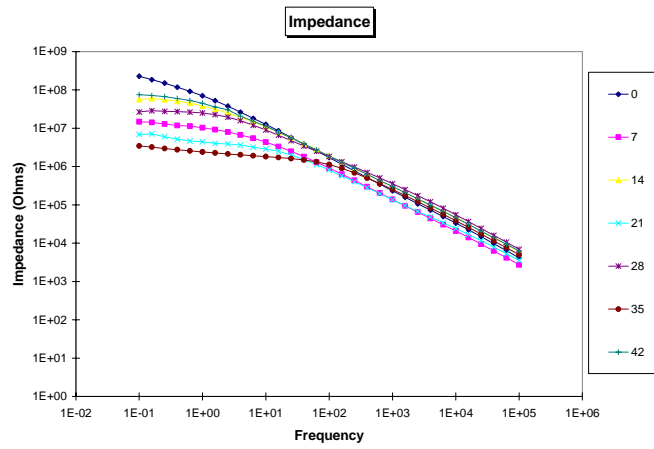
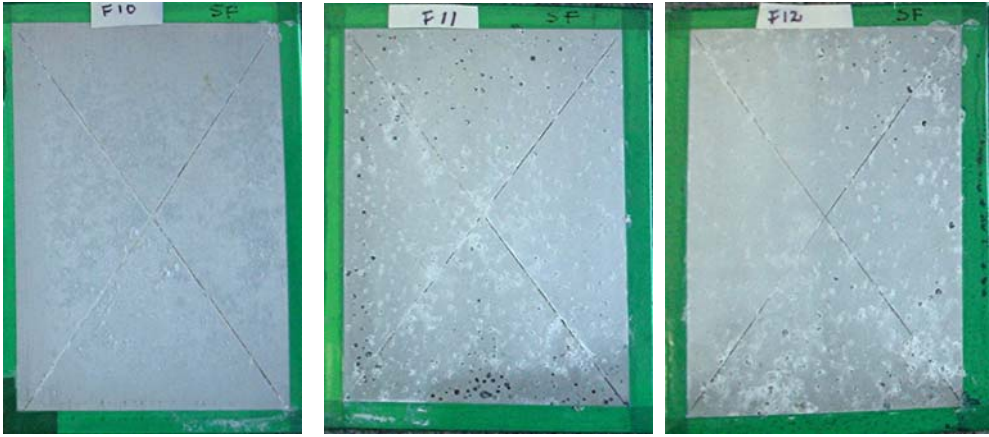


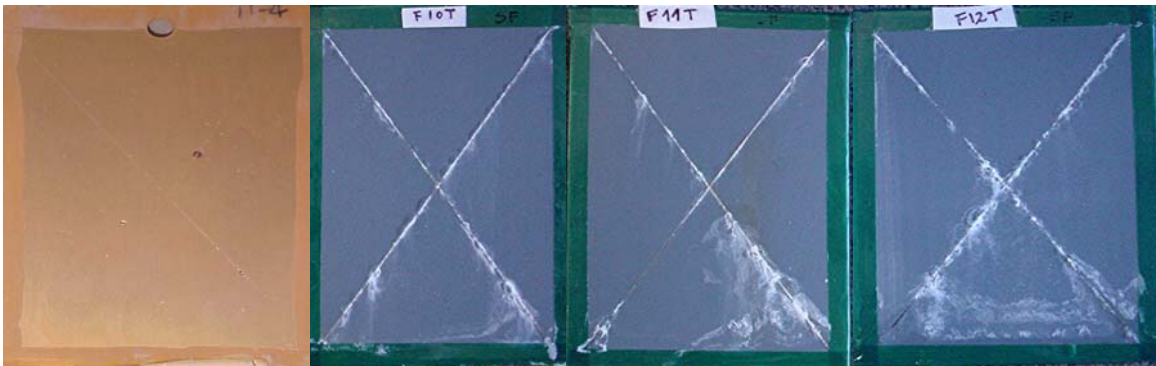
Figure 4.2.7: Bode plot of F 12 without topcoat (above) with topcoat



(below)



Salt Spray results of F 10, F11 and F12 without topcoat after 3 weeks



Control      Salt Spray results of F 10, F11 and F12 with topcoat after 3 weeks

Figure 4.2.8: Salt Spray results of F 10, F11 and F12 with and without topcoat after 3 weeks. The formulation information can be found from table 4.1.1. Control is AA 2024 T3 panels with chromium pretreatment and epoxy primer with barium chromate.

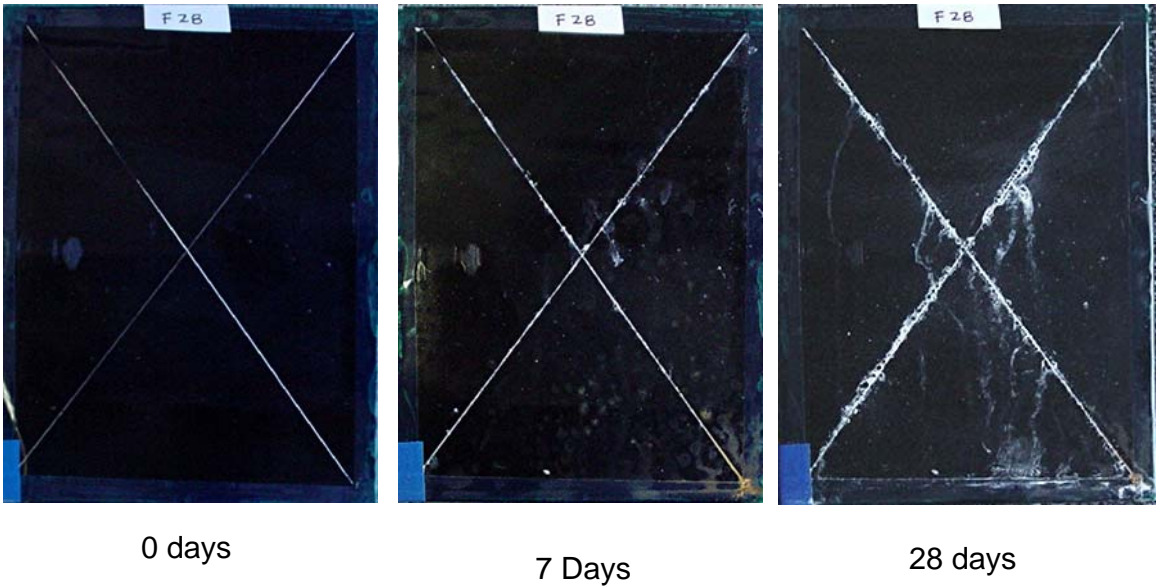


Figure 4.2.9: Salt Fog test performance of F 28 after 0, 7 and 28 days. The formulation information can be found from table 4.1.1.

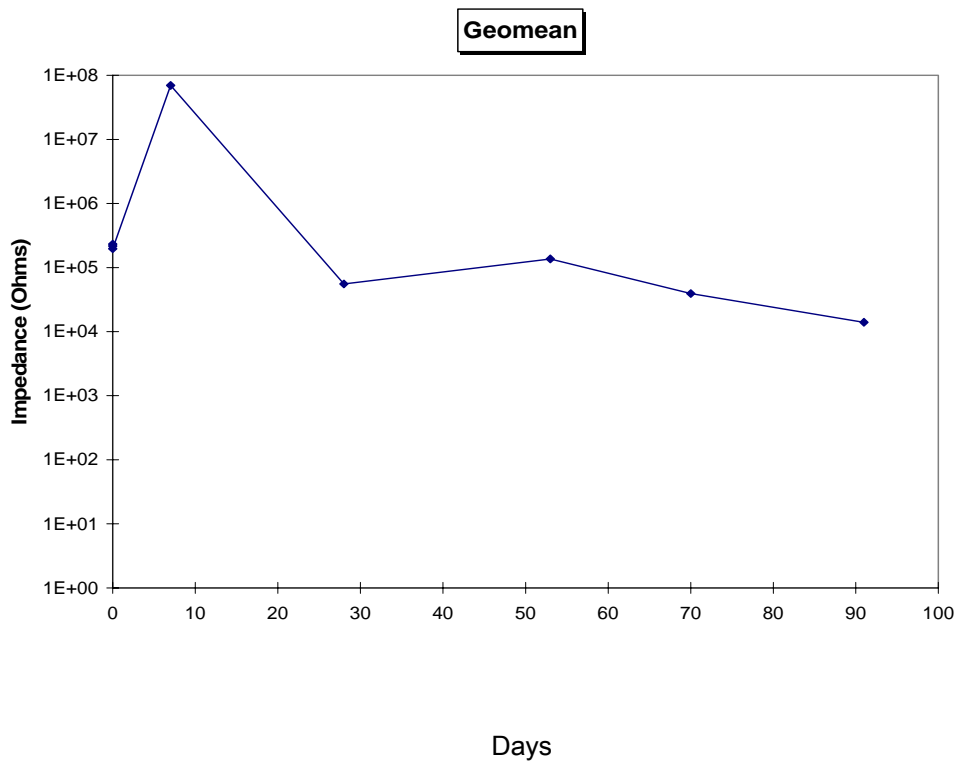


Figure 4.2.10: Change in impedance values of F 28 coating with exposure time. The formulation information can be found from table 4.1.1.

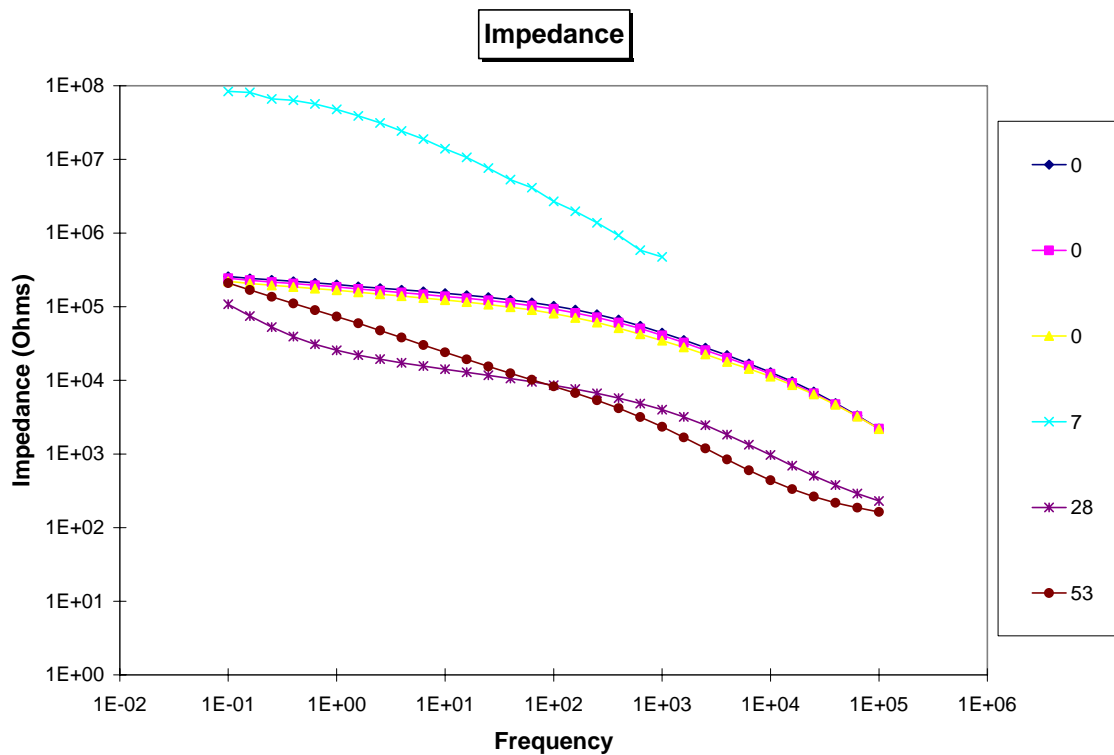


Figure 4.2.11: EIS impedance curves of F28. The formulation information can be found from table

4.1.1.

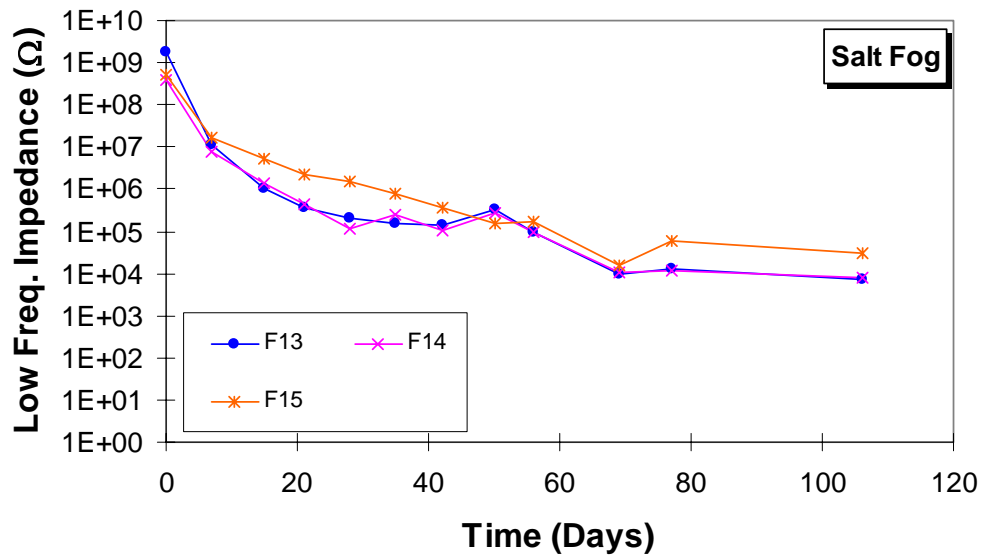
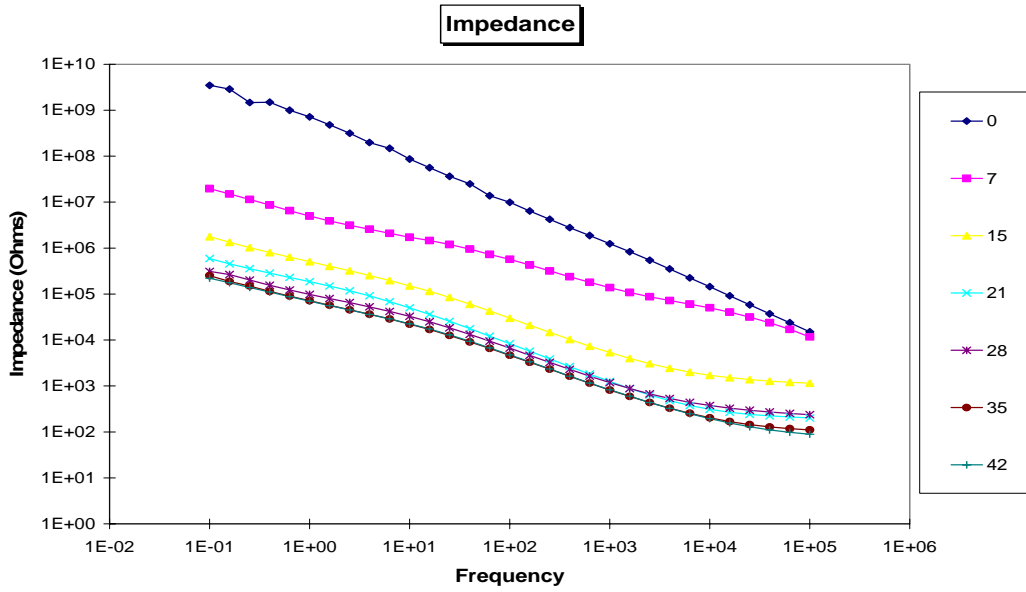
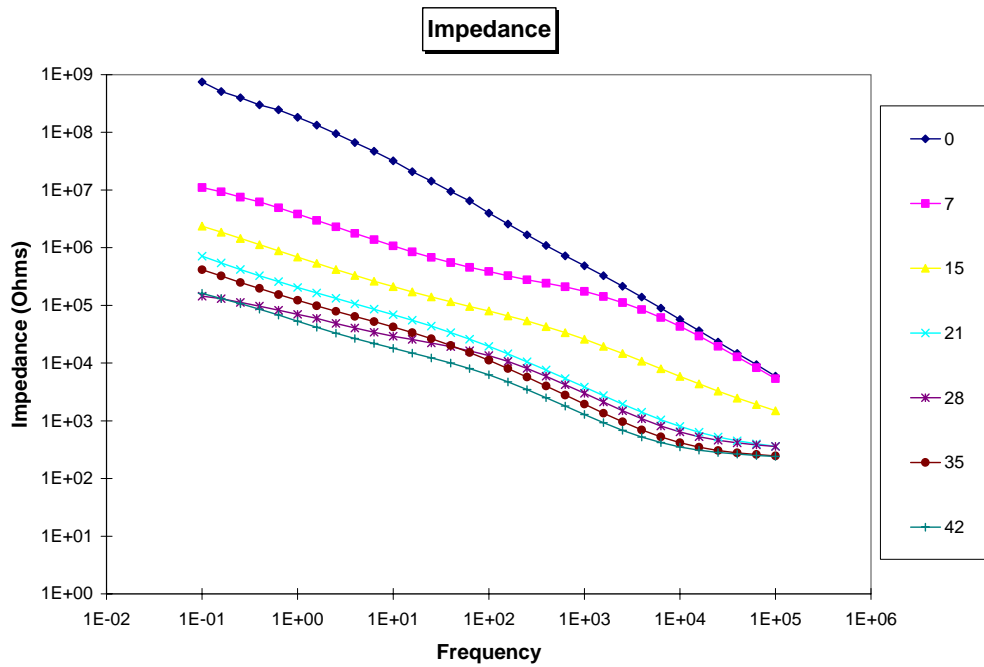


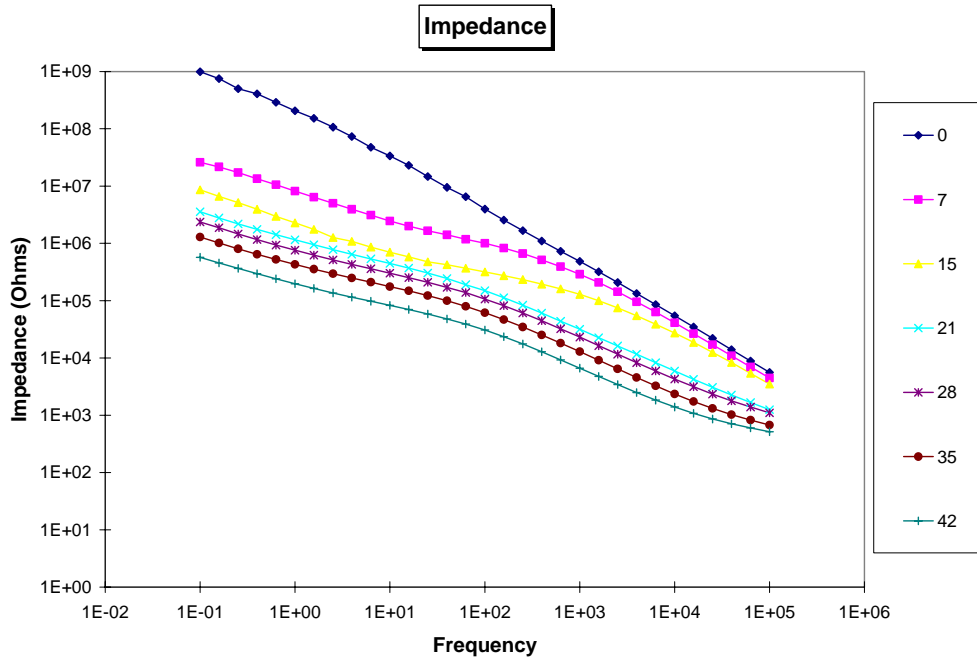
Figure 4.3.1: EIS impedance values of coating formulations F13, F14 and F15 after being exposed to salt fog. The formulation information can be found from table 4.1.1.



EIS Bode plots for 6 weeks of immersion of F 13



EIS Bode plots for 6 weeks of immersion of F14



EIS Bode plots for 6 weeks of immersion of F15

Figure 4.3.2: EIS Bode plots for 6 weeks of immersion of F13, F14 and F15

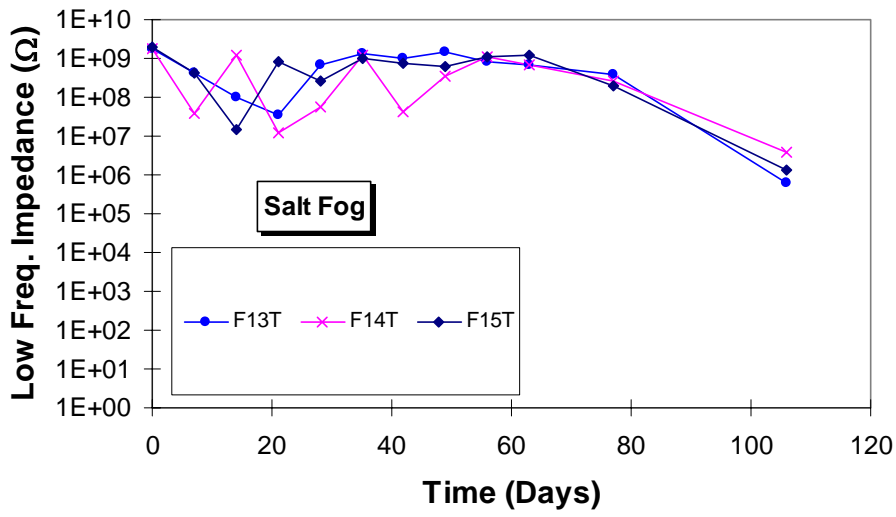
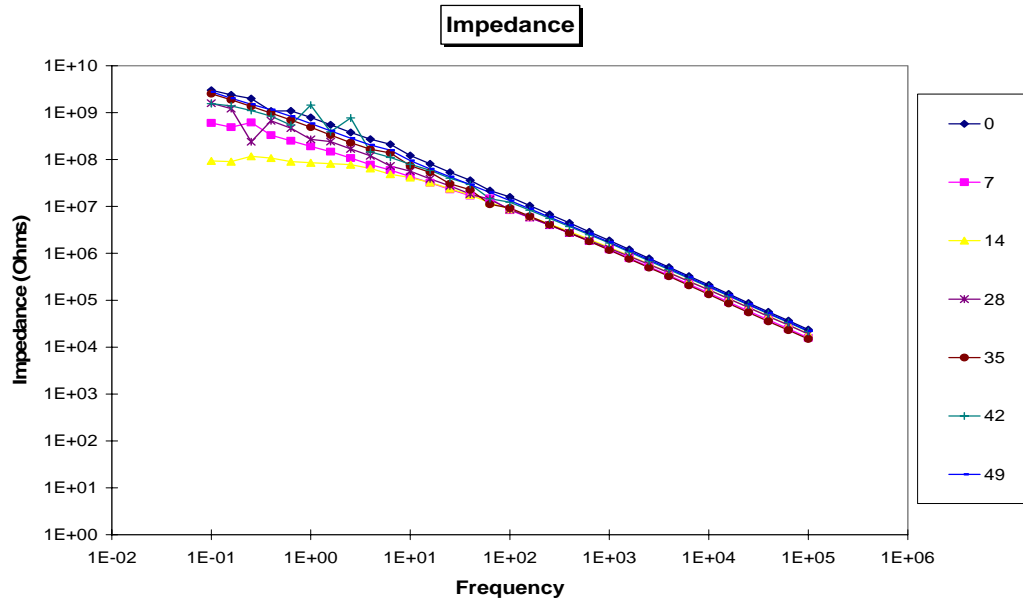
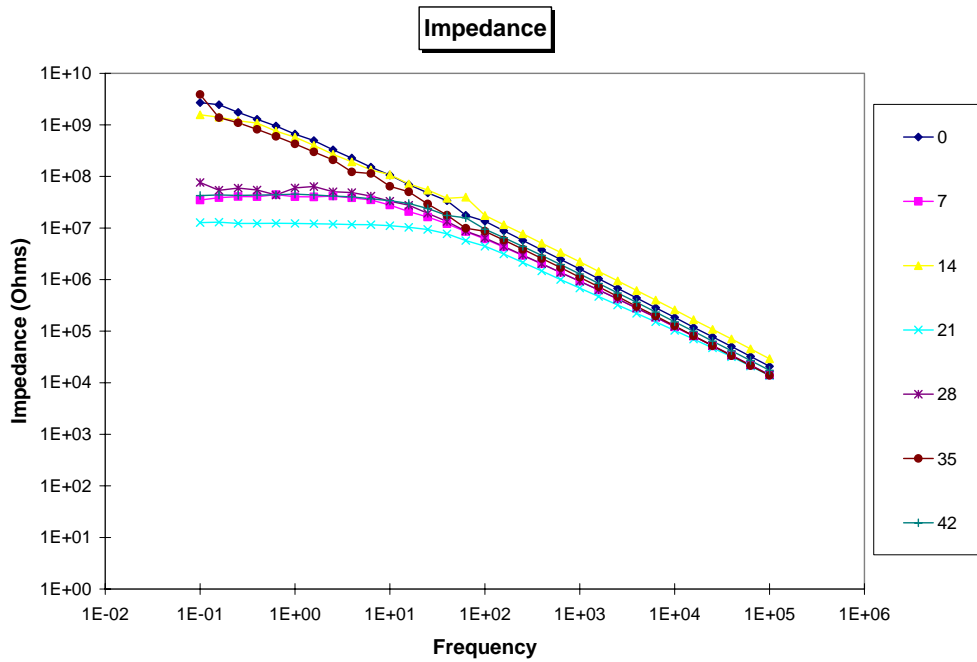


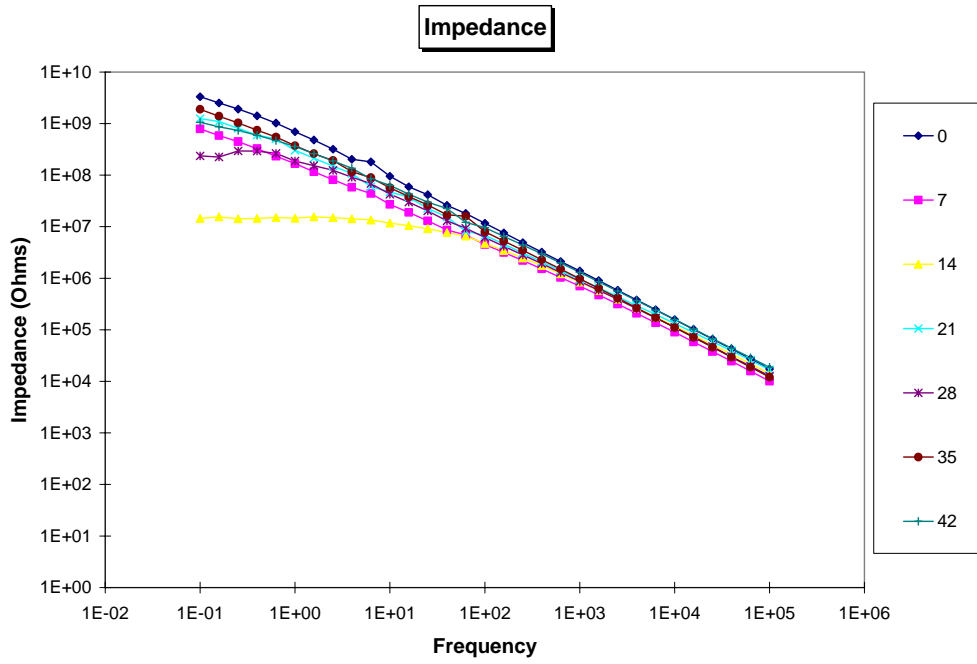
Figure 4.3.3: Change in impedance values of coatings put under salt fog testing



Individual impedance plots of formulations F 13 with topcoat

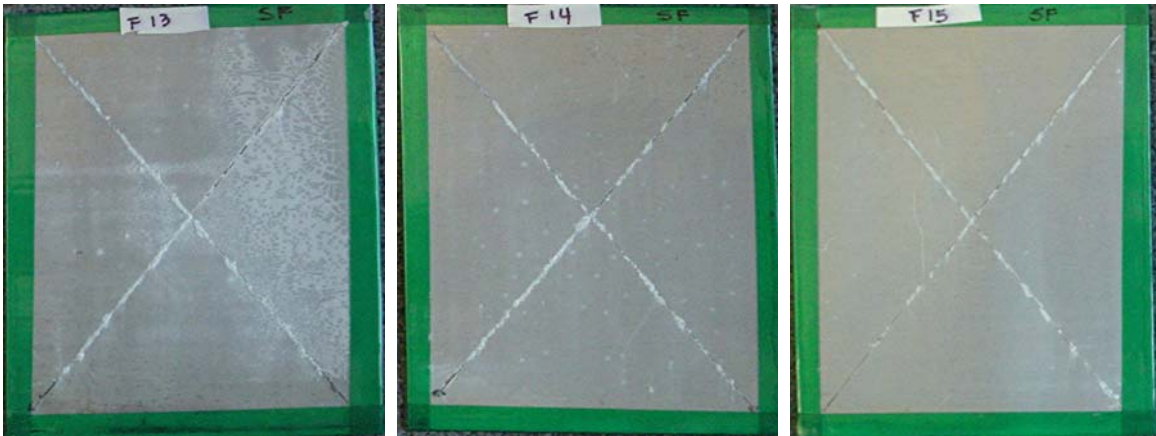


Individual impedance plots of formulations F 14 with topcoat

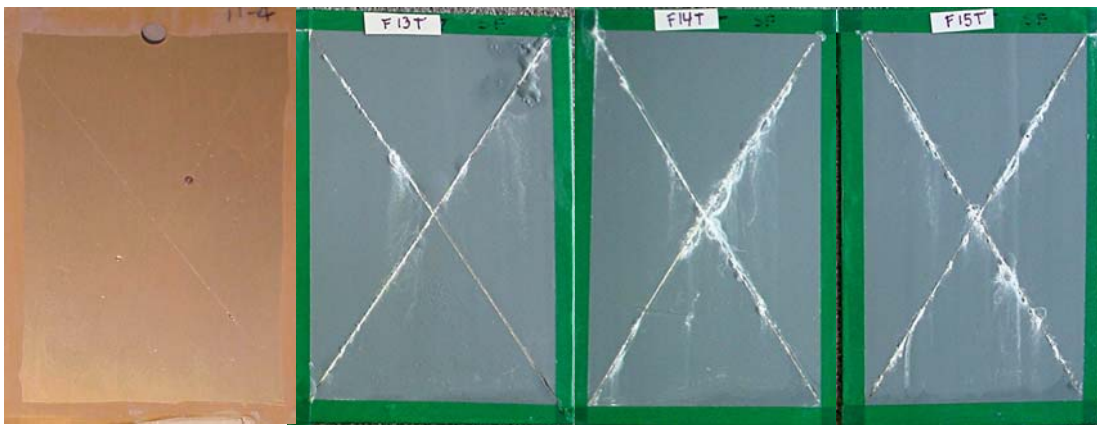


Individual impedance plots of formulations F 15 with topcoat

Figure 4.3.4: Individual impedance plots of formulations F13, F14 and F15 with topcoat.



Without topcoat (after 21 days of salt spray)



With topcoat (after 42 days of salt spray)

Figure 4.3.5: Salt spray results of formulations F13, F14 and F15 with and without topcoat after 6 weeks of testing. Control is AA 2024 T3 panels with chromium pretreatment and epoxy primer with barium chromate.

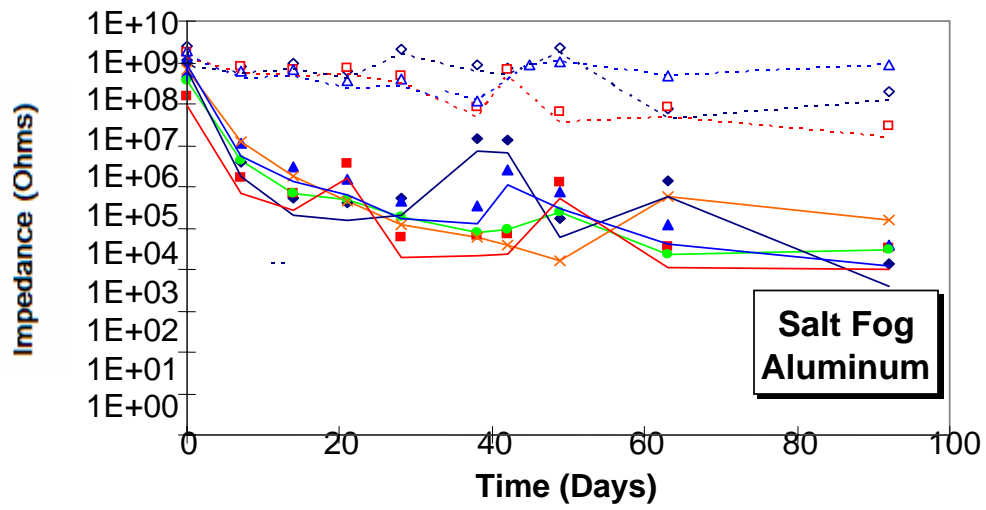


Figure 4.3.6: Change in EIS impedance values of the coating formulations F20, F21, F24, F25

with and without topcoat, after exposed to salt fog.

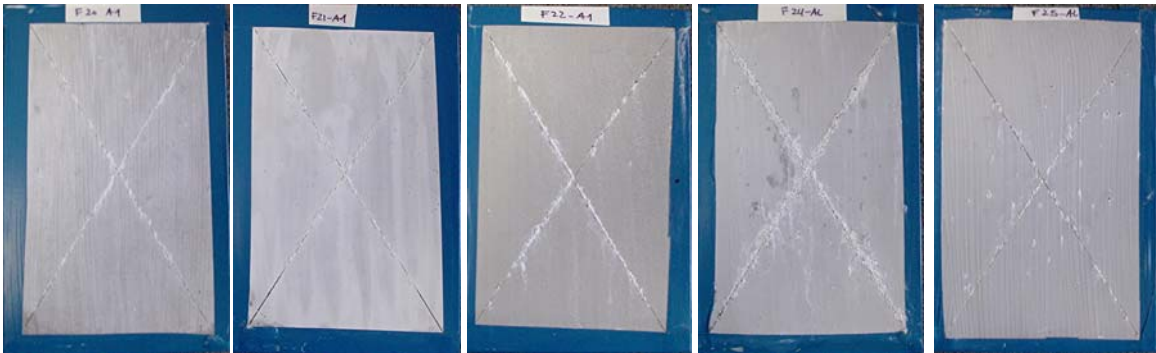


Figure 4.3.7: Salt Spray test results of formulations F20, F21, F22, F24 and F 25 without topcoats after 28 days of testing.

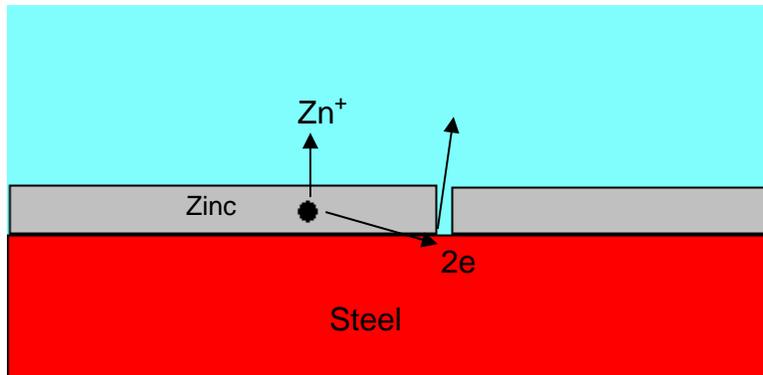


Figure 5.1

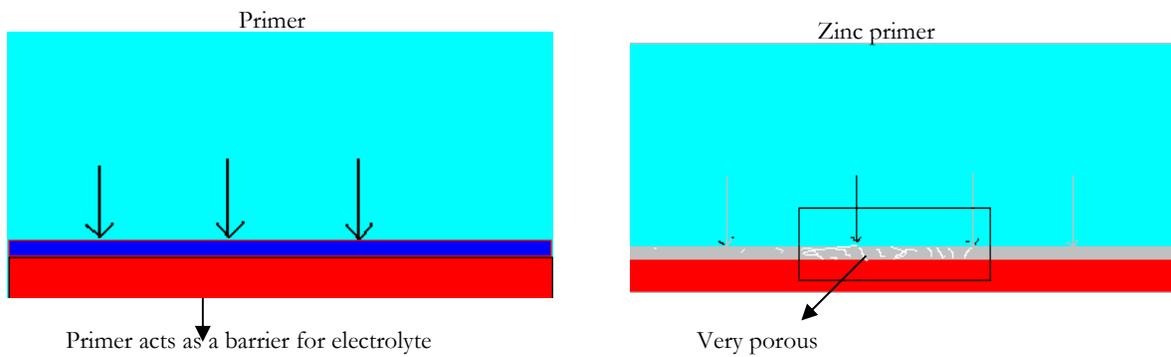


Figure 5.2

Figure 5.1 shows a schematic of the zinc-iron couple and the half cell reactions.

Figure 5.2 shows the comparison between a conventional primer and the zinc rich coatings.

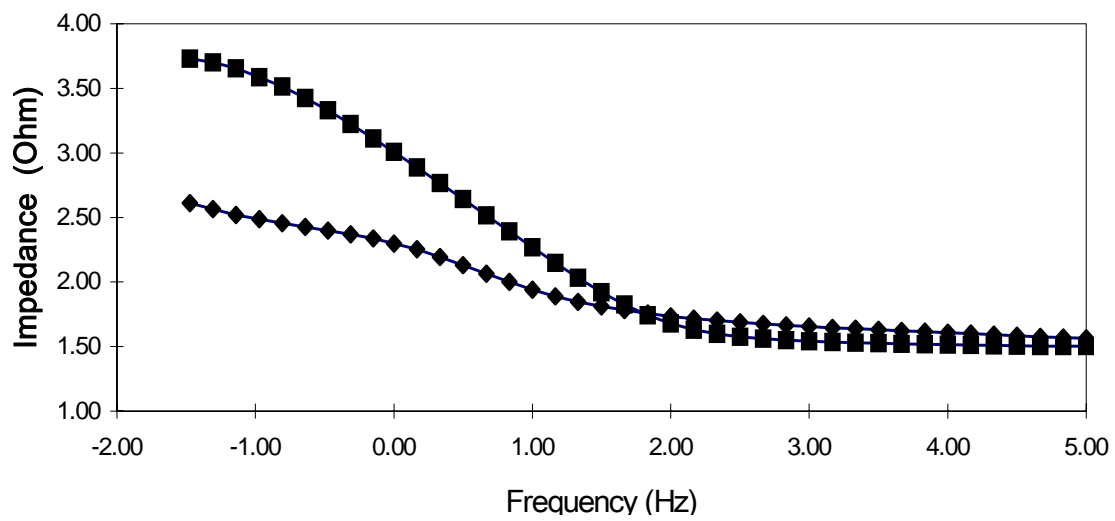


Figure 5.3: 42 days EIS result for formulation with 40% zinc and 60% superprimer. The square block represents result for 42 days and the rhombus for 0 days.

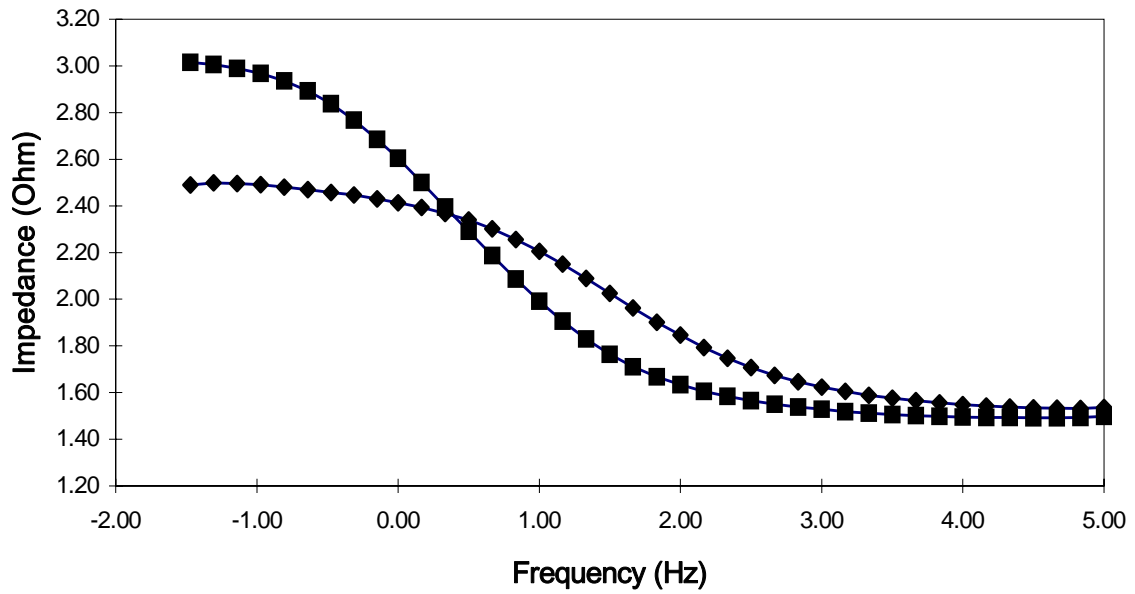


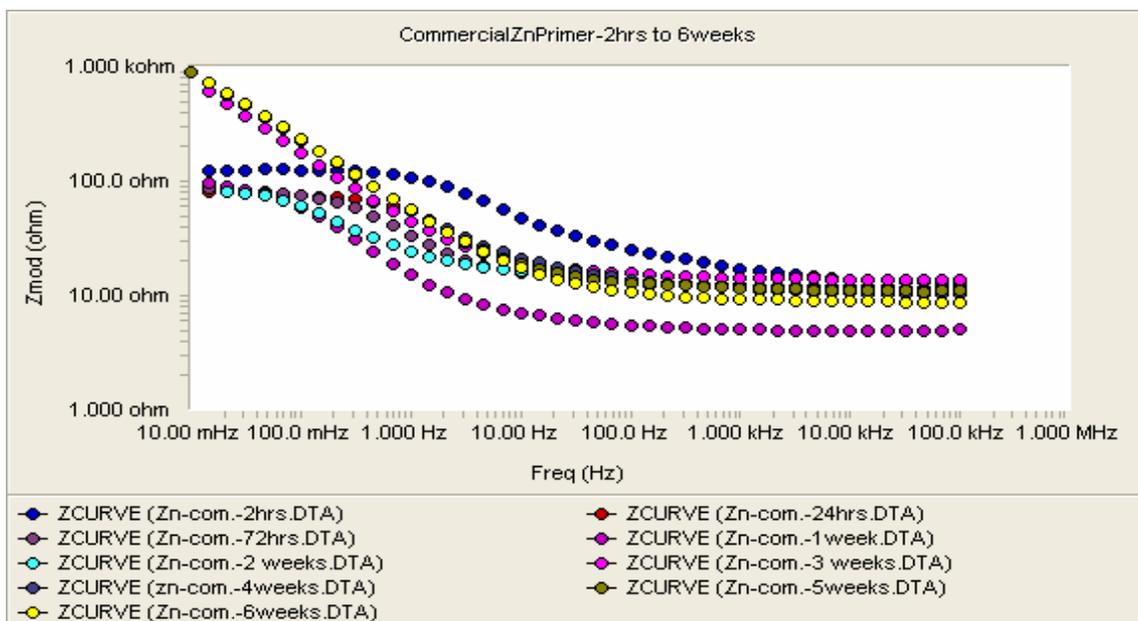
Figure 5.4: 42 Days EIS result for formulation with 70% zinc and 30% superprimer. The square block represents result for 42 days and the rhombus for 0 days.



40 %

80%

Figure 5.5: The salt spray result after 3 weeks of both 40% and 80% zinc formulations.



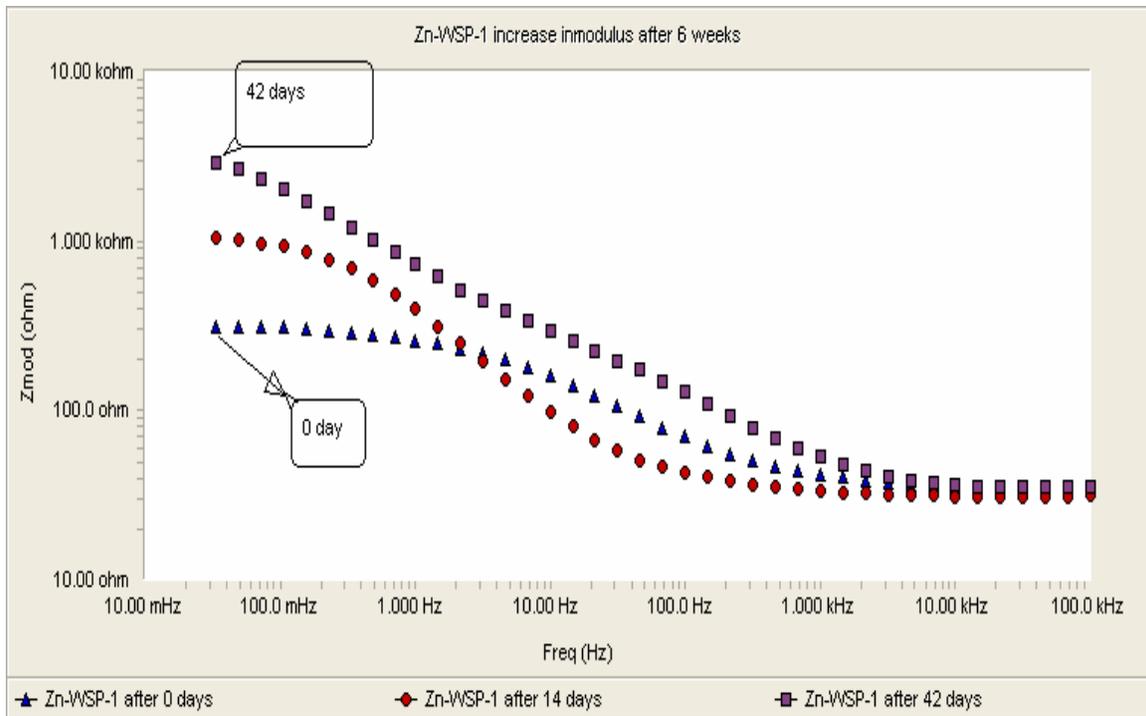


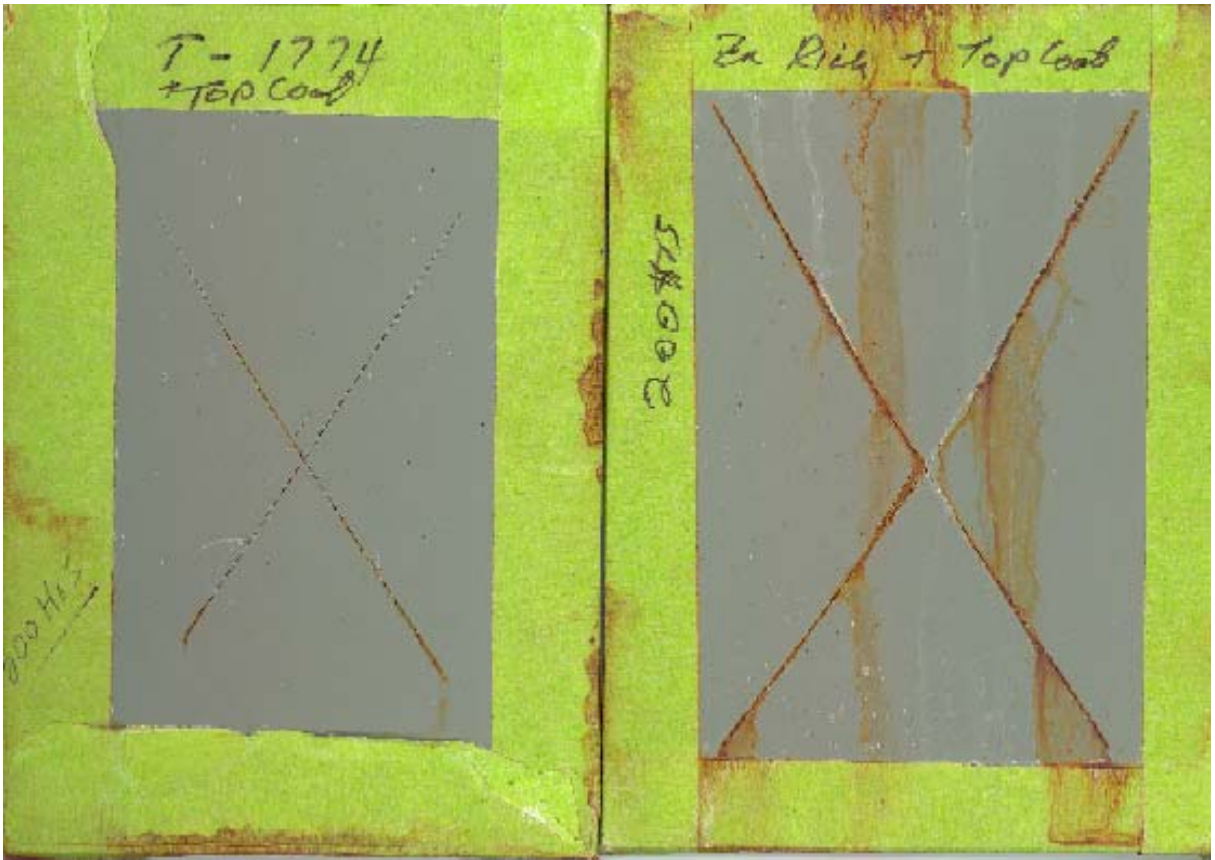
Figure 5.6: 6 week EIS results of Commercial and Zinc-rich superprimer.



Commercial

Zinc-rich Superprimer

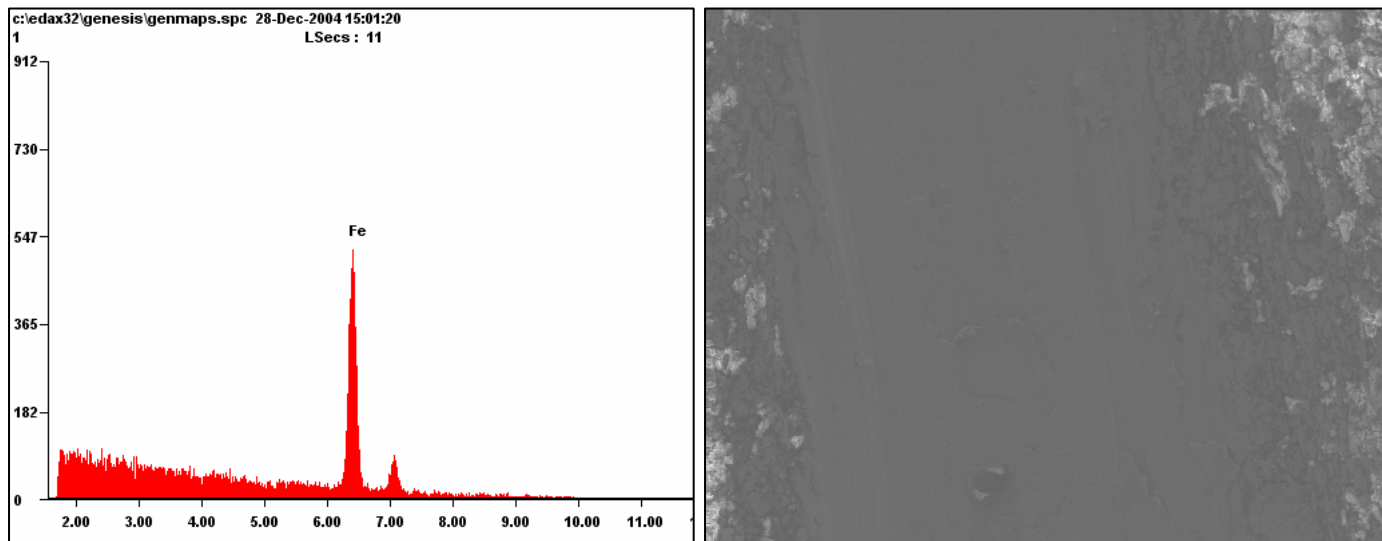
Figure 5.7: 500 hours Salt fog result of commercial and zinc-rich superprimer.



Zinc-rich superprimer + Polyamide Topcoat

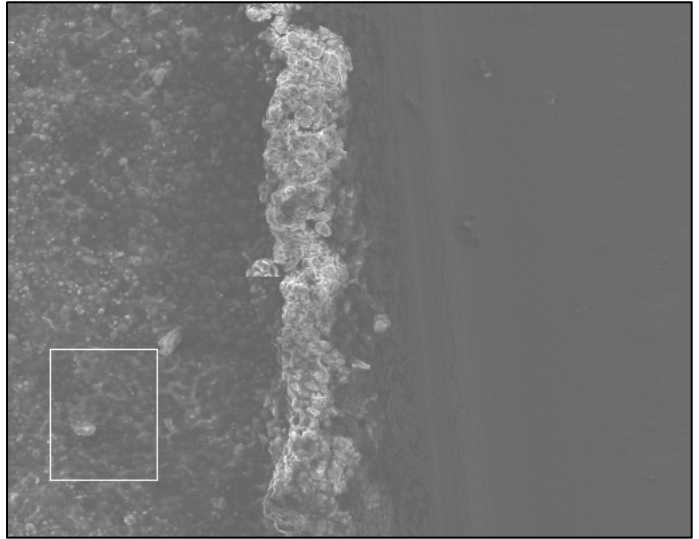
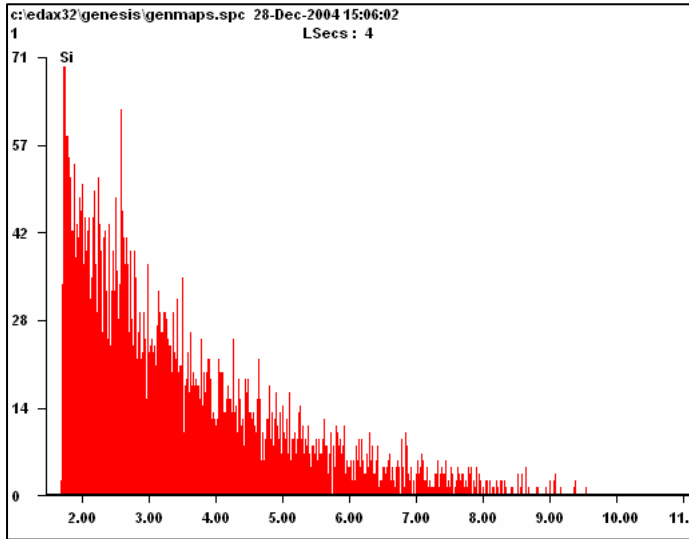
Commercial zinc-rich primer + Polyamide Topcoat

Figure 5.8: 200 hours salt fog result of zinc-rich primers with Polyamide topcoat



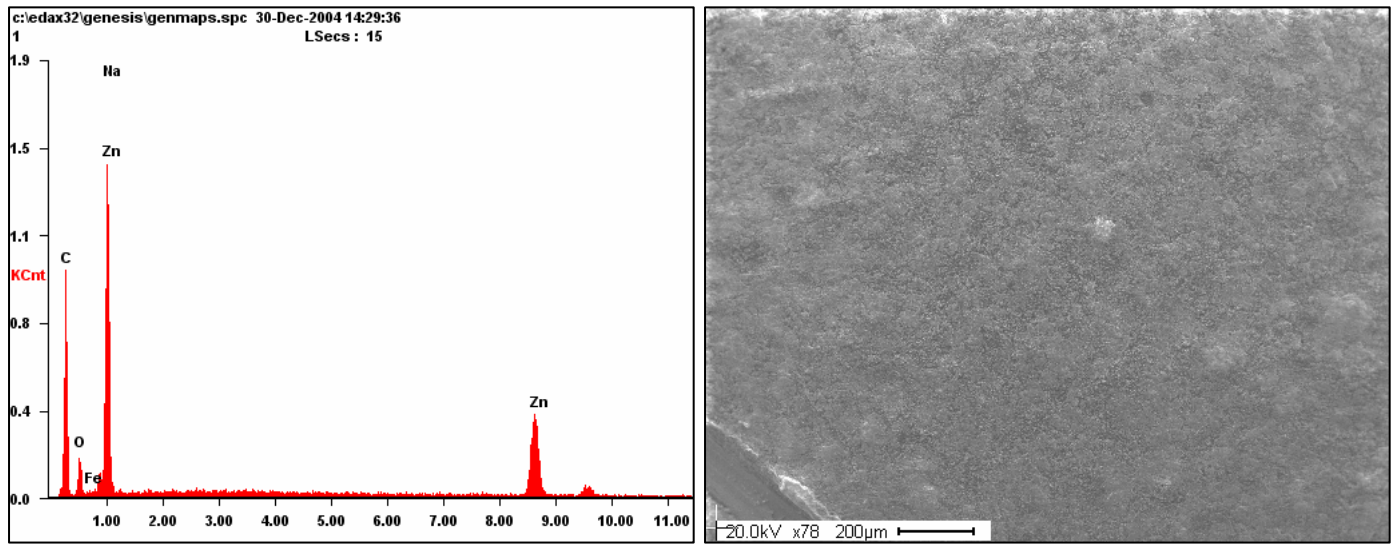
<i>Element</i>	<i>Wt%</i>	<i>At%</i>
<i>FeK</i>	100.00	100.00

Figure 5.9: Zone 1 area in the scribe before immersion.



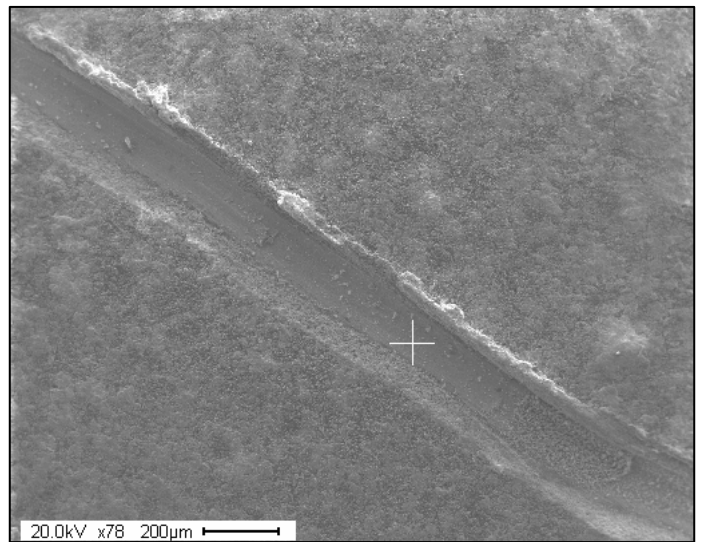
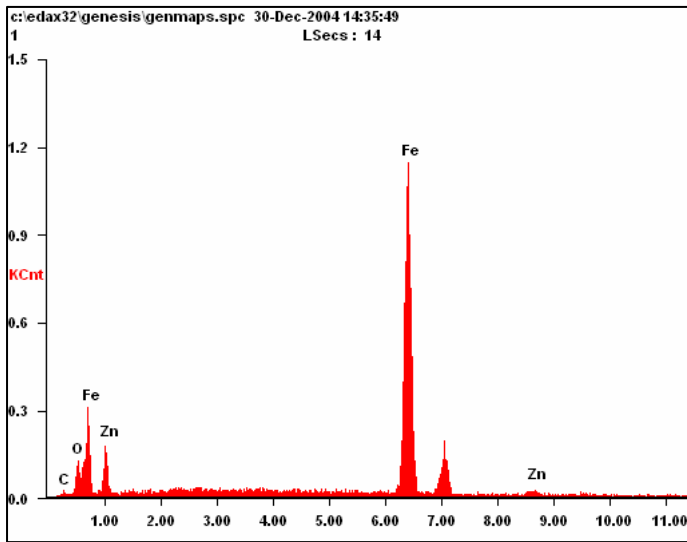
<i>Element</i>	<i>Wt%</i>	<i>At%</i>
<i>SiK</i>	100.00	100.00

Figure 5.10: Zone 2 coated area before immersion



<i>Element</i>	<i>Wt%</i>	<i>At%</i>
<i>CK</i>	57.01	83.49
<i>OK</i>	05.85	06.43
<i>FeL</i>	02.01	00.63
<i>NaK</i>	00.00	00.00
<i>ZnK</i>	35.13	09.45

Figure 5.11: Analysis over zone 2 with coated surface after immersion.



<i>Element</i>	<i>Wt%</i>	<i>At%</i>
<i>CK</i>	02.43	10.00
<i>OK</i>	02.02	06.24
<i>FeK</i>	88.37	78.32
<i>ZnK</i>	07.18	05.44

Figure 5.12: Zone 1 in the scribe after immersion

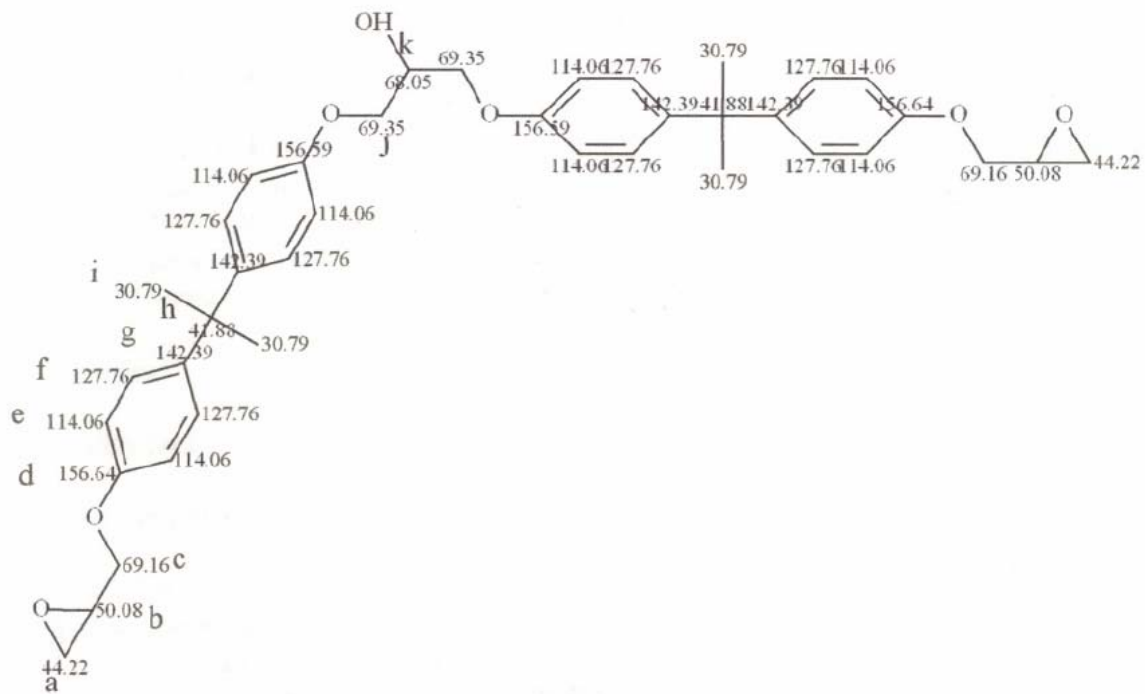


Figure 6.1: Structure of Epirez-3540-wy-55

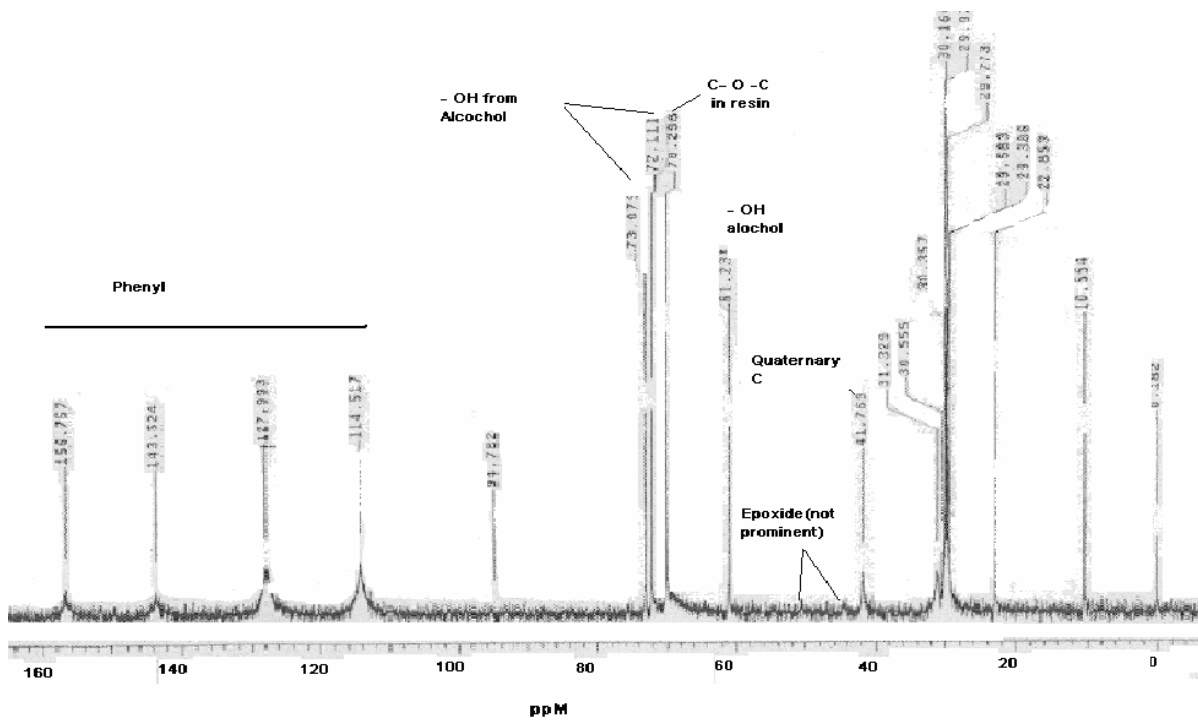


Figure 6.2: C<sup>13</sup>NMR spectrum Epirez-3540-wy-55 Resin

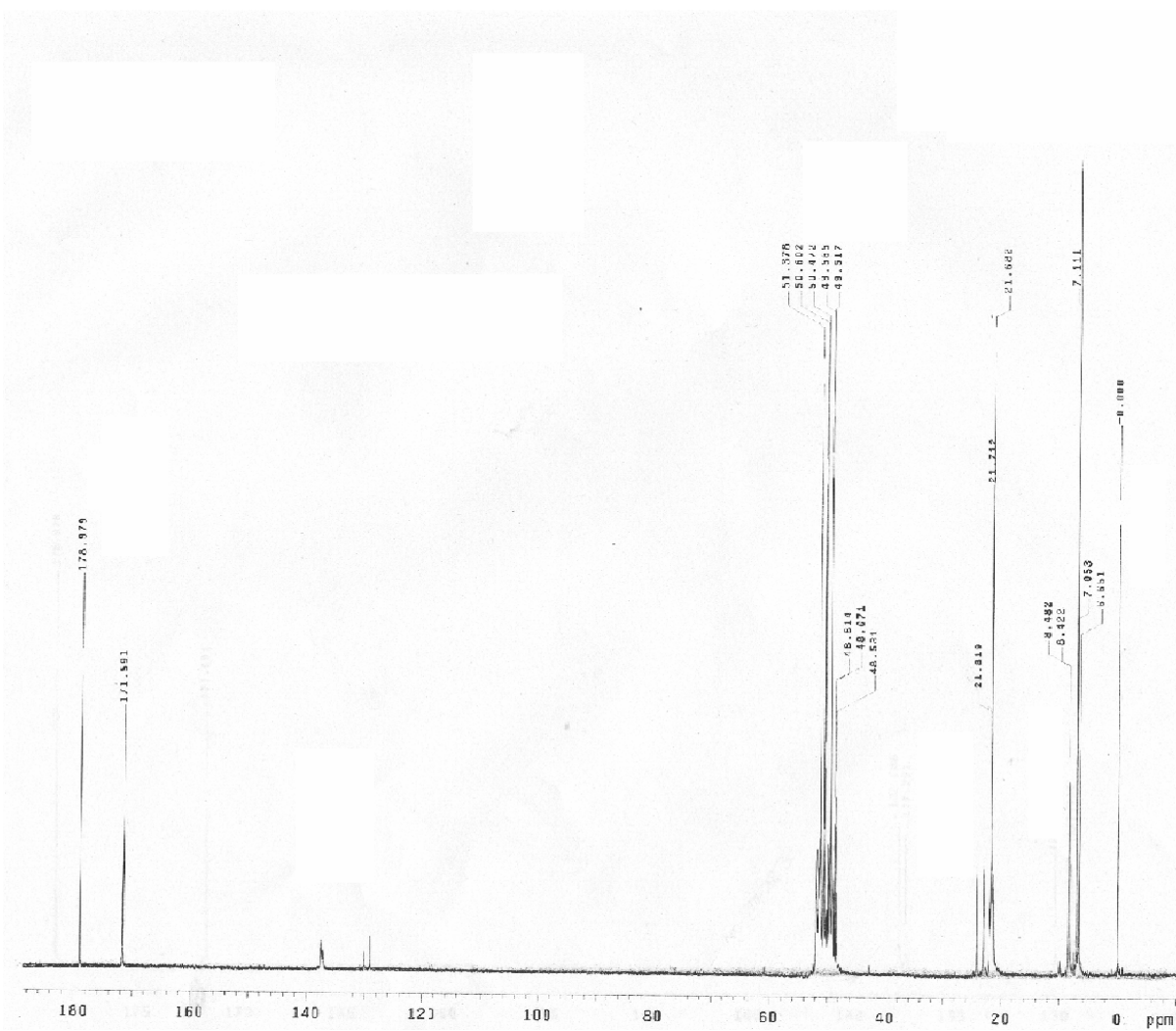


Figure 6.3:  $^{13}\text{C}$  spectrum of AV5

A1289

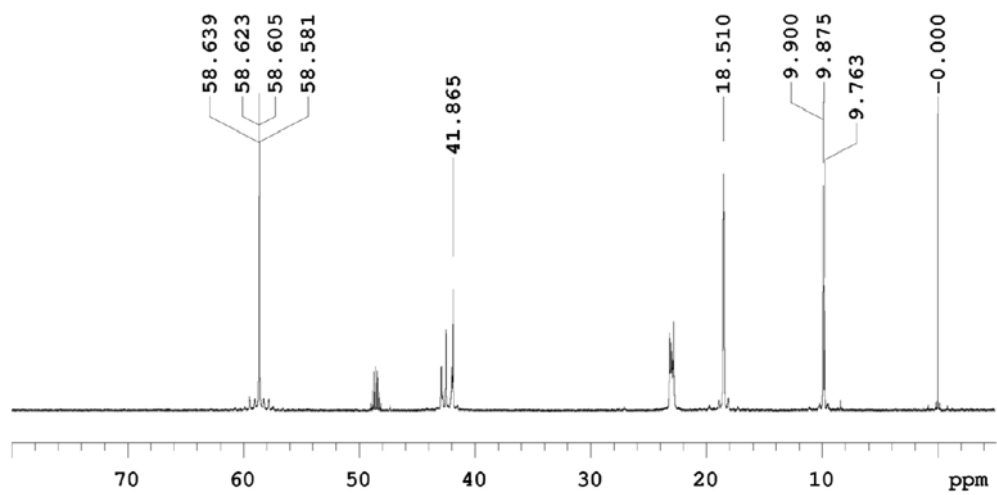
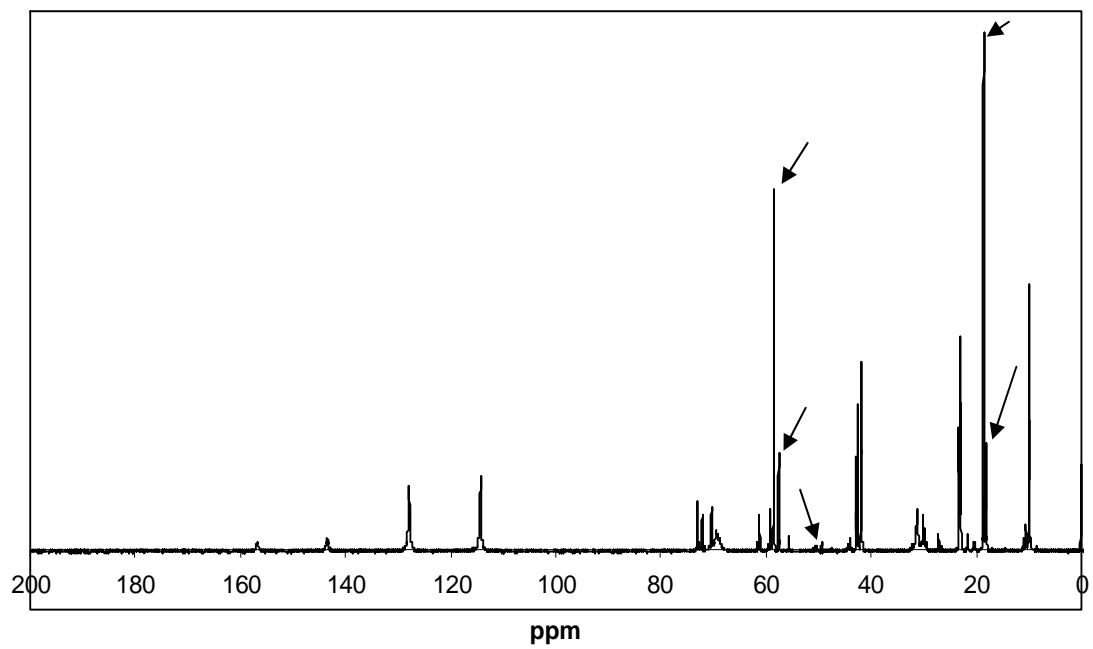
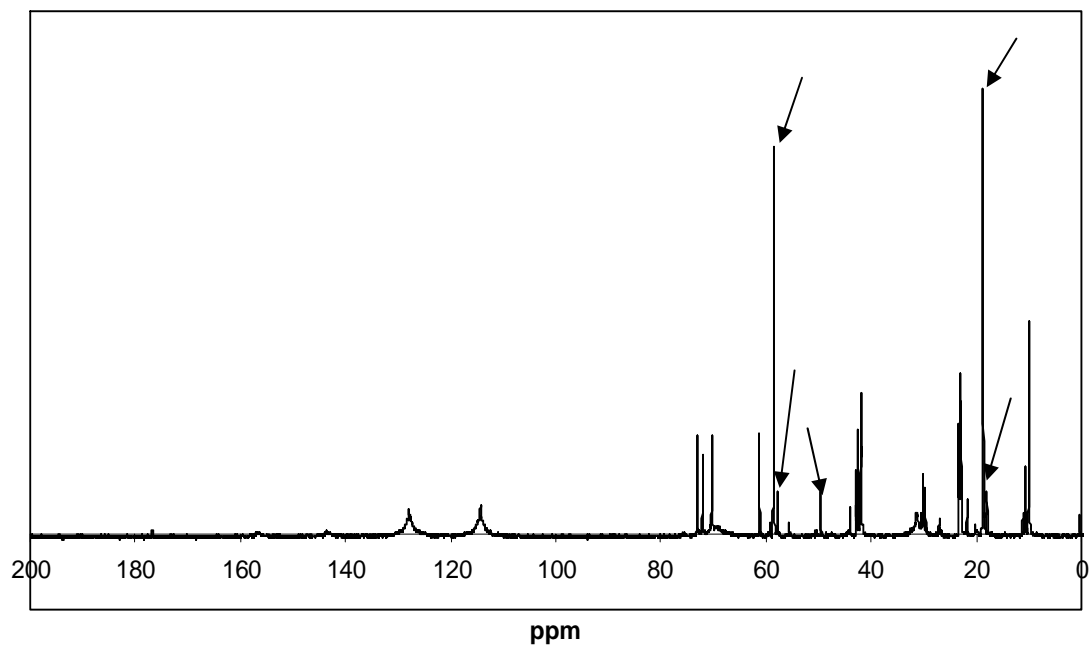


Figure 6.4:  $^{13}\text{C}$  spectrum of bis-sulfur silane

Initial



After 16 hours



After 8 Days

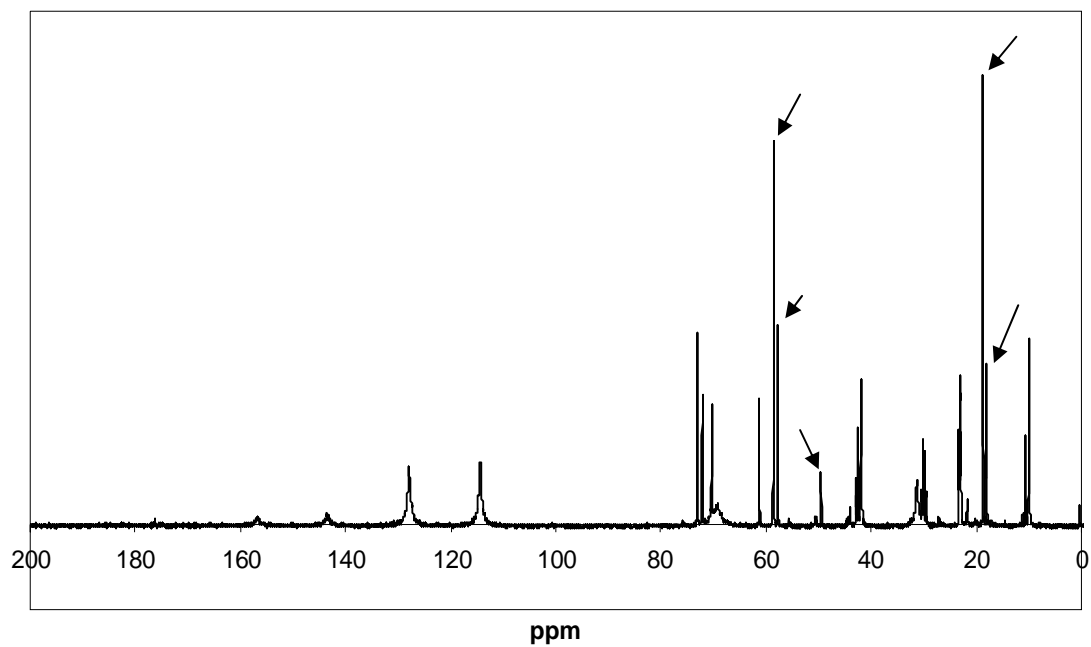


Figure 6.5:  $\text{C}^{13}$  NMR peaks over liquid superprimer formulation at time Initial (after mixing), after 16 hours and after 8 days.

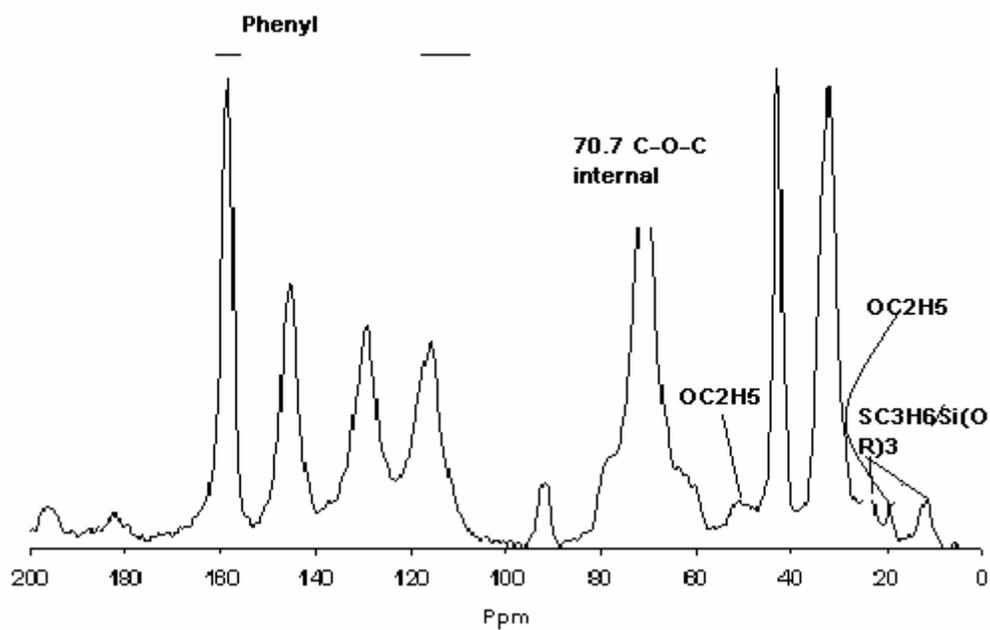


Figure 6.6: Solid  $^{13}\text{C}$  spectrum of cured superprimer

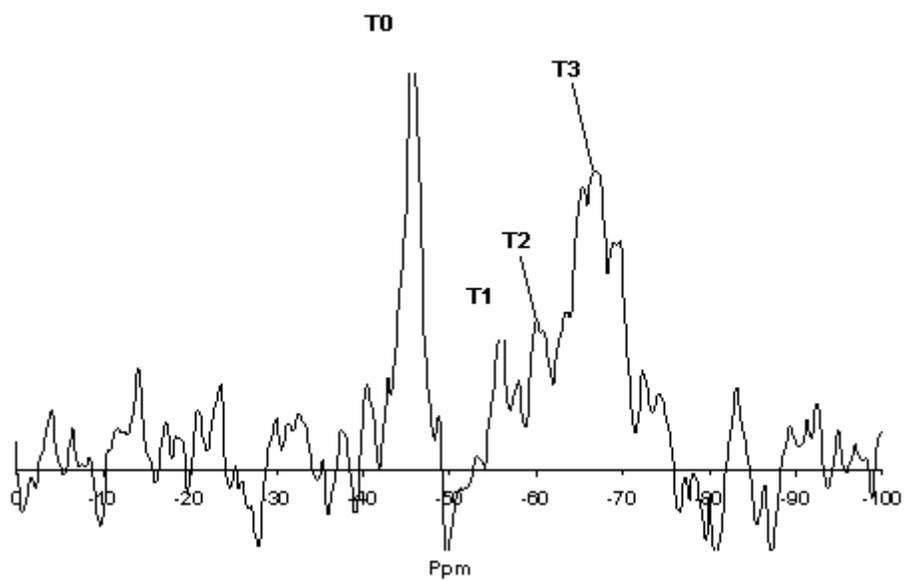


Figure 6.7:  $^{29}\text{Si}$  NMR spectrum of the cured coating

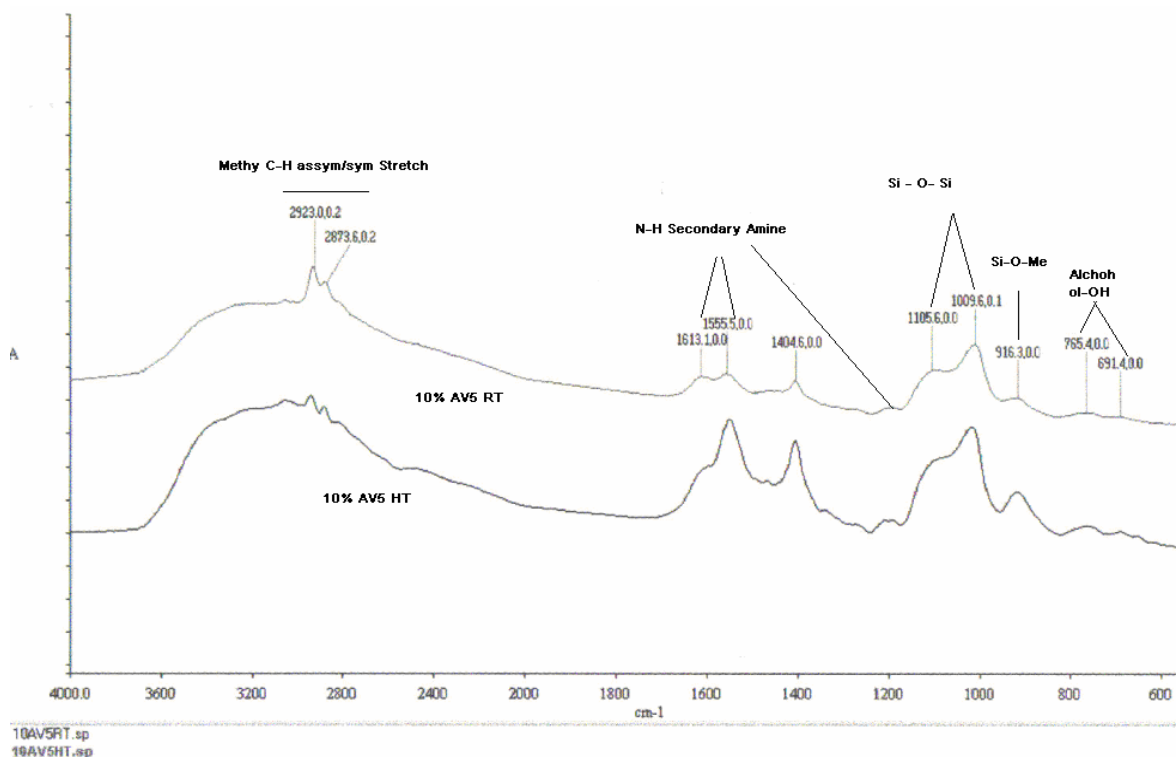


Figure 6.8: IR spectrum of 10% AV5 coated AA 2024T3 panel cured at RT and at 100°C for 1 hour.

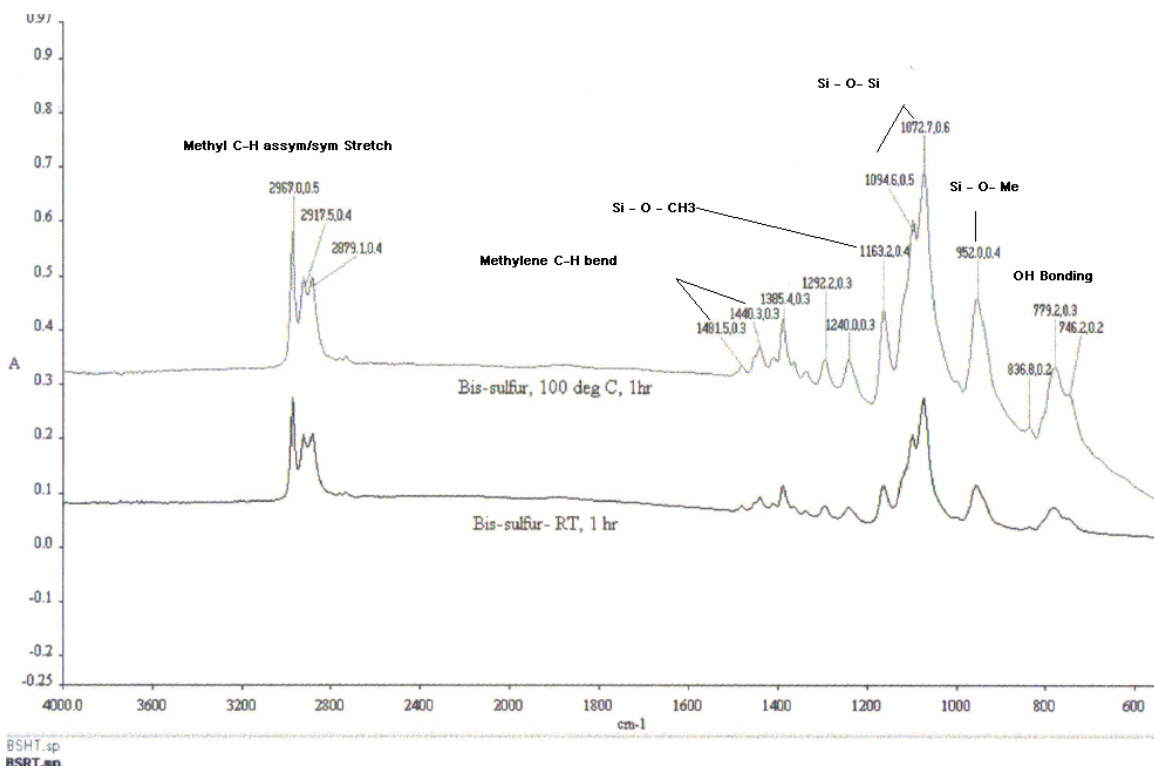


Figure 6.9: IR spectrum of bis-sulfur silane

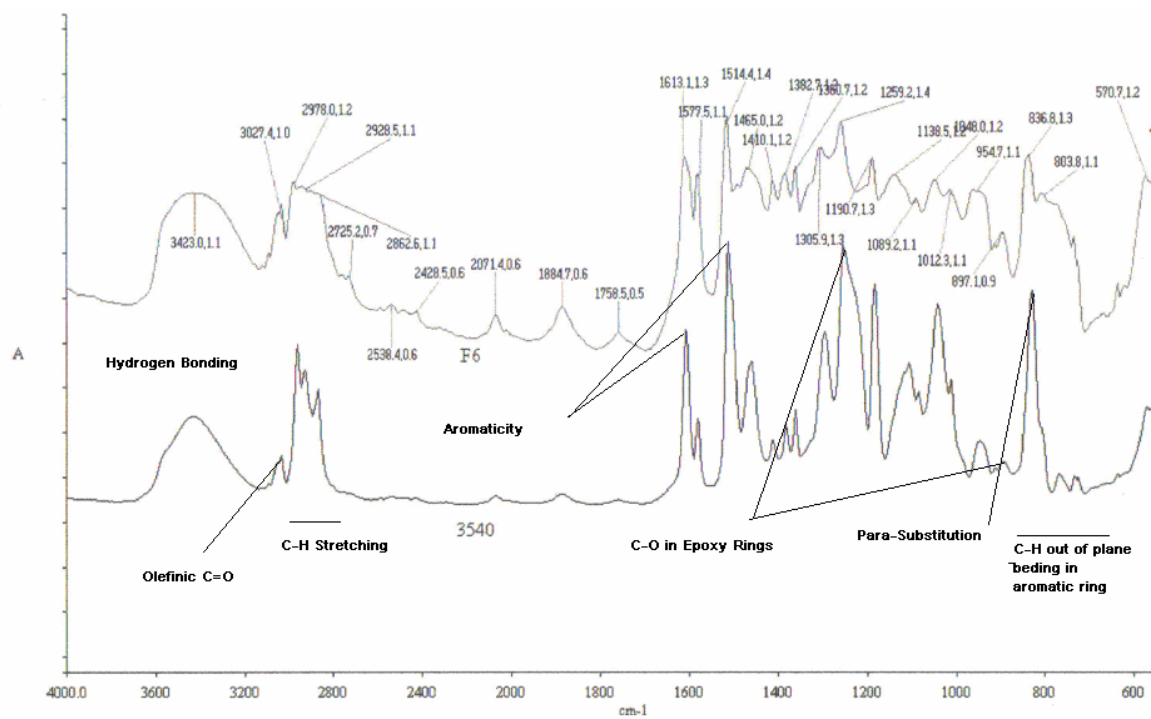


Figure 6.10: IR spectrum of 3540 resin and F6 coatings cured at 100°C + F6

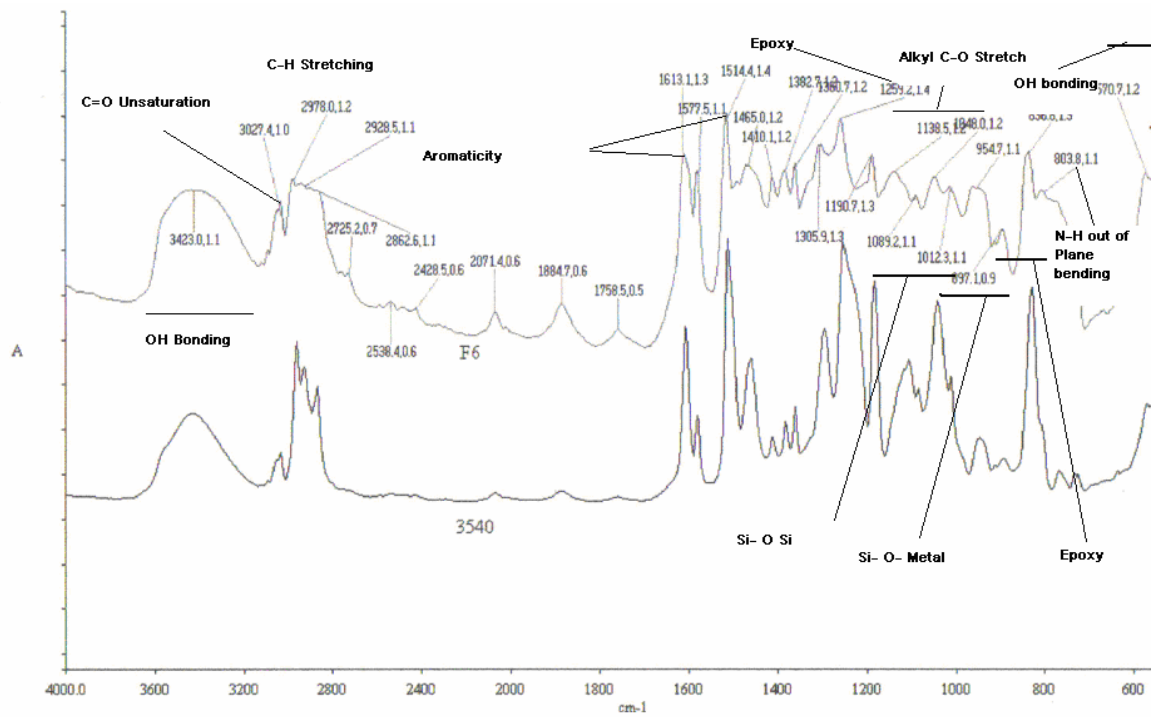


Figure 6.11: IR spectrum of F6 cured at 100°C.

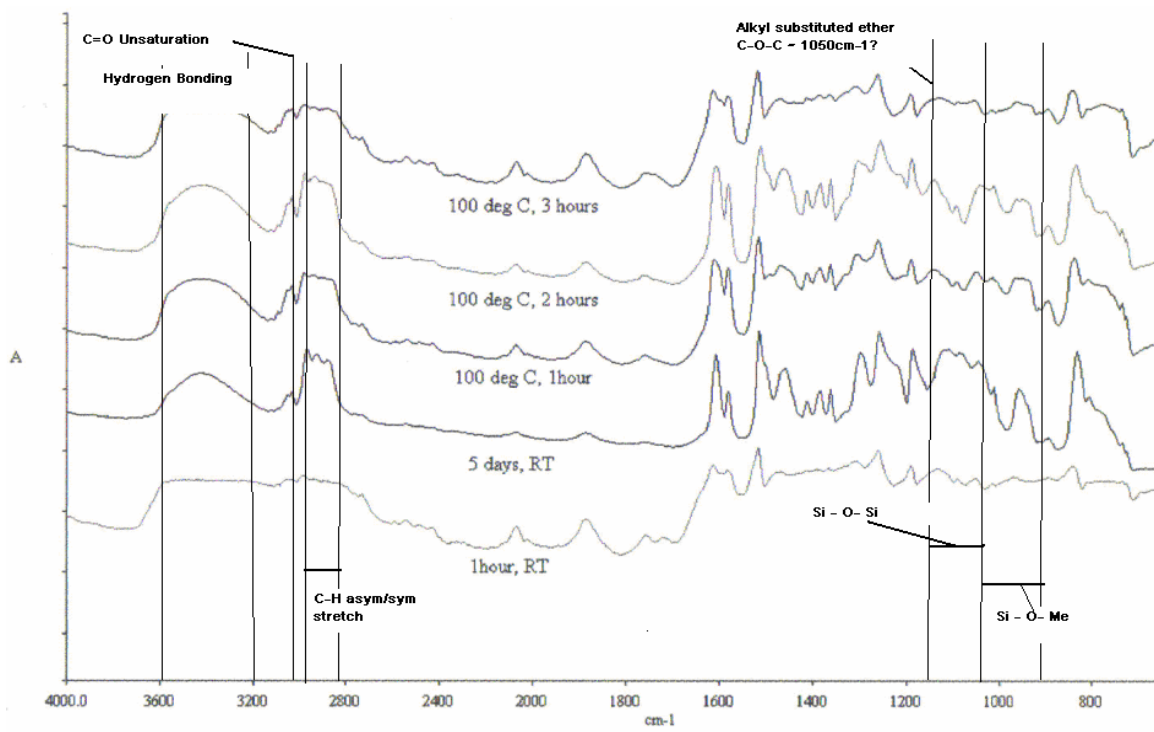
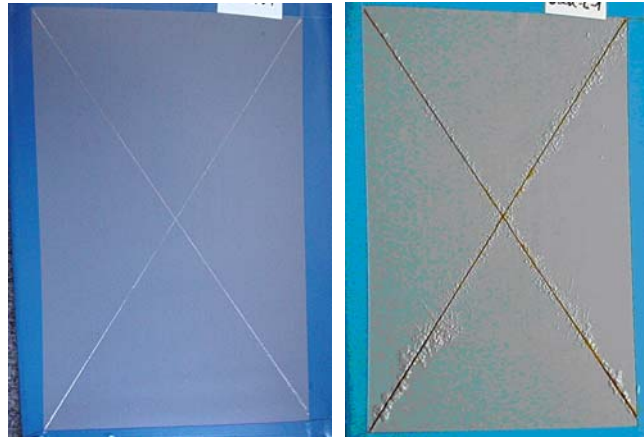


Figure 6.12: Cure trend of F6 formulation with time.



Before exposure

After Exposure

Figure 7.1: Hawaiian outdoor exposure testing results over F-6 base formulation primer coatings over carbon steel with topcoat. After 141 days of testing.

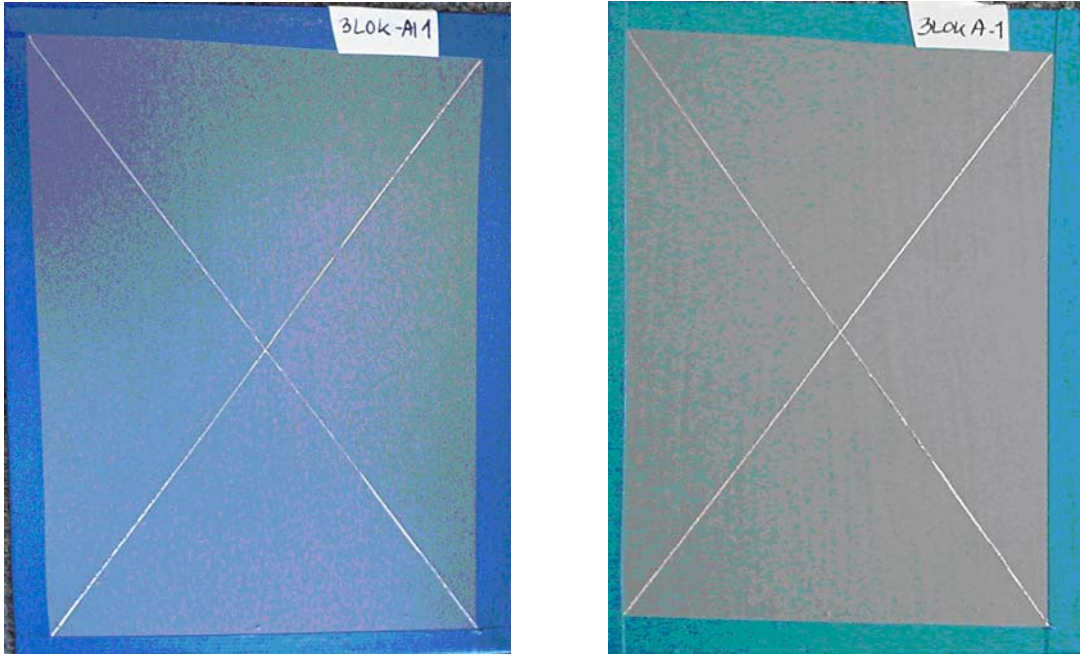


Figure 7.2 AA 2024-T3 coated with F-6 superprimer with topcoat submitted to outdoor exposure of 141 days at Hawaii. Both before (left), and after (right) are shown.



Figure 7.3: Outdoor exposure sight in Hawaii



Figure 7.4: Panel arrangement at Hawaii outdoor exposure center



Figure 7.5: Rack location at Hawaii exposure center

# UNIVERSITY OF CINCINNATI

**DATE: 02/15/2006**

---

I, **Chetan Shivane** \_\_\_\_\_ ,

hereby submit this as part of the requirements for the degree of:

**Master of Science**

---

in:

**Materials Science and Engineering**

---

It is entitled:

**Environment-Friendly Anti-Corrosion ' Superprimers' for HDG**

---

---

---

**Approved by:**

---

**Wim J. van Ooij**

---

**Stephen J. Clarson**

---

**Relva C. Buchanan**

---

---

# **Environment-Friendly Anti-Corrosion ‘Superprimers’ for HDG**

A thesis submitted to the Division of Research and Advanced Studies at the University of Cincinnati in partial fulfillment of the requirements for the degree of

## **MASTER OF SCIENCE**

in the

Chemical and Materials Engineering Department, College of Engineering

February, 2006

by

**Chetan Shivane**

B.Tech., Jawaharlal Nehru Technological University (Hyderabad, India)

**Thesis committee**

**Dr. W. J. van Ooij (chair), Dr. Stephen J. Clarson, Dr. Relva C. Buchanan**

**Chemical and Materials Engineering Department**

**University of Cincinnati**

## **ABSTRACT**

This work deals with the development and study of a one-step direct-to-metal coating to prevent corrosion of hot-dip galvanized steel (HDG). Environmental concerns have led to legislations demanding the replacement of highly toxic hexavalent chromate compounds, which are widely used as inhibitor pigments in the primer coatings as well in the pretreatment layers as chromate conversion coatings (CCC). Legislations have also been imposed on the use of a large number of widely used organic solvents in primer coatings, as these solvents have been categorized as volatile organic compounds (VOC), which can damage the protective atmospheric ozone layer. This work addresses the former concern by using non-chromate inhibitor pigments instead of chromate pigments. Further, the requirement of CCC is obviated by inclusion of silane coupling agents in the primer, which leads to improved adhesion and anti-corrosion performance by the primer. Such direct-to-metal primer coatings have been named in earlier studies in our group as 'superprimers'. The latter concern is addressed by the use of water-borne dispersion binders and cross-linkers, which mainly involve the use of VOC-exempt water as the solvent. This study seeks to develop and study bisphenol-A epoxy-based low-VOC, chromate-free, anti-corrosion superprimers for HDG.

Chapter 1 presents the introduction, literature review and background for this work, while Chapter 2 deals with the experimental part – materials and testing. The development and performance testing aspects of this study are dealt within Chapters 3 and 4. Chapter 3 presents the enhanced anti-corrosion performance imparted by the inclusion of bis-sulfur and bis-benzene silanes and also the polyurethane and polyacrylate minor binders in the primer formulations. It

also presents the benefits gained by incorporation of the non-chromate inhibitors, mainly phosphate, molybdate or vanadate - based pigments in the coating formulations.

Optimization studies of superprimer formulations using the Taguchi design of experiments approach is presented in Chapter 4. It also presents the successful anti-corrosion performance of these optimized coatings and their comparison with chromated control coatings.

Chapter 5 presents characterization studies of superprimer coatings and its component coatings using IR, solid-state  $^{13}\text{C}$  NMR and SEM/EDX studies. The deductions from these studies allowed the explanation of the results of the MEK double rub test (solvent resistance), contact angle tests with water and thermogravimetric analysis and the anti-corrosion performance of the superprimer coatings in general. Chapter 6 presents the conclusions and suggestions for future work.

Also presented independently as an appended chapter (APPENDIX), is a to-be-published study delineating the formulation and performance attributes of an optimized silane-epoxy-resin formulation as a passivating pretreatment for HDG. This formulation can be considered as a spin-off of the superprimer work as it is similar to a diluted form of the superprimer, however, with the concentration of the silane exceeding that of the resin.



## ACKNOWLEDGMENTS

I am grateful to my academic advisor Professor Wim J. van Ooij, for giving me the opportunity to work on this project and for his invaluable advice and guidance throughout the course of this work. I also thank my thesis committee members, Prof. Stephen J. Clarson and Prof. Relva C. Buchanan for taking the time to review my thesis and provide suggestions. My thanks to Dr. Dale W. Schaefer for his valuable comments and suggestions.

I am thankful to the Strategic Environmental Research and Development Program (SERDP) for providing financial support for this study and Donna Ballard of the Air Force Research laboratories for providing status reviews and suggestions to the project. I am also thankful to Dr. Guy Davis of DACCO SCI, INC., Columbia, MD, for providing the facility and support for performance testing of coatings and Dr. Tammy Metroke of the Department of Chemistry, Oklahoma State University, for her invaluable help with NMR studies. My thanks to Sumeet for operating SEM/EDX and Sachit for his help with the thermogravimetric analysis.

I express my gratitude to all of my research group-mates, past and present: Trilok, Anuj, Senthil, Shekhar, Naveen, Prasan, Akshay, Kris, Karthik, Jaspreet, Lin, John, Youngchul, Rick, Pankaj, Abhay, Danqing and Paula, for their support and encouragement. My special thanks to Trilok for initiating me in this project, to Anuj for his help with the Taguchi analysis and to Paula (Dr. Paula Puomi) for patiently reviewing my thesis.

I am obliged to my room-mates Pannu, Nag, Hem, Sireesha and Priyanka for their understanding and support throughout my stay at UC and making my stay an enjoyable one.

I am thankful to the entire faculty and my friends at UC for making the UC experience an educating and uplifting one.

Finally, I express my deepest gratitude to my parents and my sister for their unwavering love and support through thick and thin. Without their understanding and encouragement, this work would not have been possible.

# TABLE OF CONTENTS

<b>LIST OF TABLES</b> .....	<b>9</b>
<b>LIST OF FIGURES</b> .....	<b>11</b>
<b>1. INTRODUCTION</b> .....	<b>20</b>
1.1 CORROSION OF METALS .....	20
1.2 HOT-DIP GALVANIZED STEEL .....	21
1.3 CORROSION PREVENTION BY ORGANIC COATINGS.....	22
1.4 THE SUPERPRIMER .....	25
1.5 SOLVENT-BASED PRIMERS AND THEIR ALTERNATIVES .....	27
1.6 WATER-BORNE COATINGS .....	28
1.7 BISPHENOL-A EPOXY RESINS AND THEIR WATER-BORNE VARIATIONS .....	30
1.8 CURING AGENTS FOR BISPHENOL-A EPOXIES – WATER-BORNE EPOXY-AMINE ADDUCTS .....	33
1.9 POLYURETHANE AND POLYACRYLATE DISPERSIONS .....	35
1.10 CHROMATES AND THEIR ALTERNATIVES .....	36
1.11 SILANES .....	39
1.12 DESIGN OF EXPERIMENTS USING THE TAGUCHI APPROACH .....	40
1.13 THESIS OBJECTIVE – SUMMARY .....	41
1.14 REFERENCES .....	43
<b>2. EXPERIMENTAL</b> .....	<b>46</b>
2.1 MATERIALS.....	46
2.1.1 Water-borne dispersions of bisphenol-A (major binders).....	46
2.1.2 Minor binders.....	47
2.1.3 Amine-based crosslinkers for the epoxy dispersions.....	47
2.1.4 Non-chromate corrosion inhibitors.....	48
2.1.5 Other pigments and fillers.....	48
2.1.6 Surfactants and dispersants .....	49
2.1.7 Silanes .....	49
2.1.8 Solvents .....	50
2.1.9 Metal .....	50
2.1.10 Topcoat and control primers.....	50
2.2 SUBSTRATE PREPARATION AND CLEANING .....	51
2.3 FORMULATION PREPARATION .....	51
2.4 PERFORMANCE EVALUATION TESTS AND CHARACTERIZATION STUDIES.....	51
2.4.1 Salt water immersion test.....	51
2.4.2 Electrochemical Impedance Spectroscopy (EIS).....	52
2.4.3 The ASTM B117 .....	53
2.4.4 The Ford AGPE test.....	55
2.4.5 Hawaii outdoor exposure test .....	55
2.4.6 The Machu test.....	56
2.4.7 Tape adhesion test.....	56
2.4.8 MEK double rub test .....	57
2.4.9 Pencil hardness test.....	57
2.4.10 Infrared spectroscopy.....	57
2.4.11 NMR spectroscopy .....	58
2.4.12 SEM/EDX.....	61
2.4.13 Contact angle measurements .....	62
2.4.14 Chemical resistance .....	64
2.4.15 Thermogravimetric analysis (TGA).....	64
2.5. REFERENCES .....	65

<b>3. WATER-BORNE BISPHENOL-A SUPERPRIMER - IMPROVEMENTS.....</b>	<b>68</b>
3.1 STEP 1: MODIFYING AND IMPROVING FORMULATION F6 TO SUIT HDG SUBSTRATE .....	73
3.2 STEP 2: SEARCH FOR LOW-VOC, HIGH-PERFORMANCE SYSTEMS.....	75
3.3 STEP 3: SILANES, MINOR BINDERS, INHIBITORS, CO-SOLVENTS AND ADDITIVES .....	77
3.3.1 Silanes.....	77
3.3.2 Minor binders.....	83
3.3.3 Inhibitors.....	85
3.3.4 Co-solvents.....	87
3.3.4 Cross-linker for silanes – DBTL .....	89
3.3.5 Specialty barrier pigment for superprimers – leafing aluminum paste.....	90
3.4 SUMMARY.....	91
3.5 REFERENCES .....	92
<b>4. OPTIMIZED SUPERPRIMER .....</b>	<b>94</b>
4.1 BACKGROUND .....	94
4.2 TEST RESULTS AND OBSERVATIONS .....	102
4.2.1 Salt water immersion results.....	102
4.2.2 MEK double rub test .....	102
4.2.3 Machu test.....	103
4.2.4 Topcoat – wet adhesion test .....	103
4.2.5 EIS test - comparison of low-frequency impedances.....	104
4.3 ANALYSIS – OPTIMIZATION PLOTS .....	104
4.4 ASTM B117 AND FORD TESTS - COMPARISONS BETWEEN OPTIMIZED FORMULATIONS AND CONTROLS .....	107
4.5 REFERENCES .....	113
<b>5. CHARACTERIZATION OF SUPERPRIMERS.....</b>	<b>114</b>
5.1. REACTION CHEMISTRIES .....	114
5.2. FTIR ANALYSIS .....	119
5.2.1. Bis-sulfur vs bis-benzene.....	119
5.2.2. DPW 6520 vs Ancarez AR 550.....	121
5.2.3. DPC 6870.....	122
5.2.4. ECO-CRYL 9790.....	123
5.2.5. NeoRez R 972.....	124
5.2.6. Epoxy dispersion and ECO-CRYL 9790 (9:1 mixture) .....	124
5.2.7. Epoxy dispersion and NeoRez R 972 (9:1 mixture).....	125
5.2.8. Epoxy-amine curing - effect of high curing temperature .....	126
5.2.9. Epoxy-amine – effect of the type of silane.....	126
5.2.10. Polyurethane and silane.....	128
5.2.11. Polyacrylate and silane.....	128
5.3. <sup>13</sup> C NMR ANALYSIS .....	128
5.3.1. NMR of Resins, silanes, and curing Agents.....	129
5.3.2 Possible curing reactions.....	130
5.3.3 NMR analysis as a function of cure time.....	131
5.4. MEK DOUBLE RUB, CONTACT ANGLE AND ACID-BASE TESTS .....	134
5.5. THERMOGRAVIMETRIC ANALYSIS .....	136
5.6. SEM/EDX ANALYSIS.....	14040
5.6.1 Inhibitor testing.....	140
5.6.2 Cross-sectional phase distribution.....	142
5.7. BIS-SULFUR VS BIS-BENZENE – DIFFERENCE IN ADHESION, AN EXAMPLE.....	142
5.8. SUMMARY OF CHARACTERIZATION .....	143
5.9 REFERENCES .....	144
<b>6. CONCLUSIONS AND SCOPE FOR FURTHER RESEARCH.....</b>	<b>146</b>
<b>TABLES.....</b>	<b>149</b>

***FIGURES..... 182***  
***APPENDIX: SILANE-EPOXY-INHIBITOR PRETREATMENT FOR HDG ..... 304***

## LIST OF TABLES

- 2.1 Comparison of four commercial water-borne epoxy resin dispersions
- 2.2 Steps in the FORD AGPE cyclic test
- 3.1 Formulation F6 on AA2024-T3 - the precursor for this work
- 3.2 Adhesion ability of silanes on various inorganic substrates
- 3.3 VOC levels of a few superprimer components
- 3.4 New-Gen systems - properties vs. curing conditions
- 3.5 Superprimer with and without bis-sulfur – comparison of contact angle and MEK double rub values
- 3.6 Superprimer with and without bis-benzene – comparison of MEK double rub and pencil hardness values at two curing conditions
- 3.7 Superprimer with and without bis-benzene – contact angle values
- 3.8 Superprimer with and without DBTL - Pencil hardness values
- 4.1 Factors and levels in an L9 orthogonal array
- 4.2 L9 orthogonal array for set A (OA1)
- 4.3 L9 orthogonal array for set B (OA2)
- 4.4 L9 orthogonal array for set C (OA3)
- 4.5 L9 orthogonal array for set D (OA4)
- 4.6 MEK double rub values for formulations in OA4, before and after immersion in 3.5 wt.-% salt water
- 4.7 Machu test ratings for formulations in OA4
- 4.8 Optimized formulation levels for OA1
- 4.9 Optimized formulation levels for OA2

- 4.10** Optimized formulation levels for OA3
- 4.11** Optimized formulation levels for OA4
- 4.12** All the four optimized formulations tabulated together
- 4.13** Comparison of a few properties of the optimized formulations vis-à-vis the solvent-based, chromated, epoxy-polyamide control primer
- 5.1** RAIR Peak assignments for bis-benzene film
- 5.2** RAIR Peak assignments for bis-sulfur film
- 5.3** RAIR Peak assignments for films of the two epoxy dispersions – DPW 6520 and Ancarez AR550
- 5.4** RAIR Peak assignments for the film of epoxy-amine adduct crosslinker, DPC 6870
- 5.5** RAIR Peak assignments for the film of polyacrylate dispersion, ECO-CRYL 9790
- 5.6** RAIR Peak assignments for the film of polyurethane dispersion, NeoRez R 972
- 5.7** Solid-state  $^{13}\text{C}$  NMR peak assignments for the solid-state
- 5.8** Contact angle and MEK double rub values for room temperature and high-temperature-cured films of water-borne epoxy superprimer and its components
- 5.9** TGA weight loss temperatures and total weight loss of various superprimer films and its components
- 5.10** Chlorine and inhibiting atom concentration in the scribe region of various scribed superprimer films on HDG exposed for 30 days in 3.5 wt% salt water – EDX measurements to test efficacy of various inhibitors

## LIST OF FIGURES

- 1.1 Corrosion chemical reactions on iron, in aqueous environments
- 1.2 Schematics showing the progress from a conventional coating system to a superprimer-based coating system
- 1.3 Epoxide ring opening (cross-linking) by various cross-linkers
- 1.4 Chemical structures of commonly used silanes in superprimers
- 2.1 (a) Bode plots for a damaged coating on a metal
- 2.1 (b) Nyquist plot for a damaged coating on a metal
- 2.2 A general electro-chemical cell set-up for EIS measurements
- 2.3 A schematic of a salt-spray test chamber
- 2.4 The salt spray chamber at DACCO SCI, INC., that was used for this study
- 2.5 Steps in the Ford AGPE cyclic corrosion test
- 2.6 Location and set-up for outdoor corrosion testing of coated HDG panels in Hawaii
- 2.7 Examples of low-frequency impedance curves of the three corrosion tests: ASTM B117, Ford AGPE and outdoor exposure at Hawaii, for comparison of the severity of these tests
- 2.8 Vibration modes of bonds in a  $\text{SO}_2$  molecule subjected to excitation by IR radiation
- 2.9 Calculated IR peaks with the corresponding vibration modes for a  $\text{SO}_2$  molecule subjected to excitation by IR radiation
- 2.10 Example of an IR spectrum - propanoic acid
- 2.11 Ray diagram and mirror set-up in a specular reflectance attachment used in IR spectroscopy

- 2.12 Illustration of nuclear spin, its values and its governing equation
- 2.13 The two spin states of a nucleus subjected to an external magnetic field  $B_0$
- 2.14 Absorption of IR radiation leading to conversion of nuclear spin states, due to energy difference between the two spin-states
- 2.15 Interfacial tensions at various interfaces for a liquid droplet on a solid surface in air
- 2.16 The contact angle goniometer, VCA Optima 2000
- 2.17 Video snap-shots of the liquid droplet being dispensed, shown along with the markers used for calculation of the contact angle values
- 2.18 Basic principle and conditions behind the working of a thermogravimetric analyzer
- 2.19 Example of a TGA curve showing the thermal degradation regimes of an epoxy composite
- 3.1 Failure of F6 on HDG – low-frequency impedance curve and exposed panel image in the Ford test
- 3.2 Low-frequency impedance curves for F6 and its three modifications for HDG, in the B117 and Ford tests
- 3.3 Ford test - exposed HDG panels coated with the three F6 modifications
- 3.4 B 117 test - exposed HDG panels coated with F6 and its three F6 modifications
- 3.5 Hawaii outdoor exposure test results for top-coated formulations 1, 2 and 3
- 3.6 Comparison of the three tests: B117, Ford test and outdoor exposure at Hawaii, for the formulations 1, 2 and 3 shown respectively in each plot
- 3.7 Effect of the epoxy-amine ratio on important coating properties

- 3.8** Coating without bis-sulfur – Bode impedance plots on day 0 and day 30 of 3.5 wt% salt water exposure
- 3.9** Coating with bis-sulfur – Bode impedance plots on day 0 and day 30 of 3.5 wt% salt water exposure
- 3.10** Comparison of bode plots of coatings with and without bis-benzene on day 10 of exposure to 3.5 wt% salt water. The images of the exposed are also shown below the impedance plots
- 3.11** Machu test exposed panels showing the effect of incorporation of hydrolyzed BTSE in superprimer coatings
- 3.12** Bode plots for superprimer coating without any minor binder – on days 1, 3 and 10 of exposure
- 3.13** Bode plots for superprimer coating with polyurethane minor binder – on days 1, 3 and 10 of exposure
- 3.14** Bode plots for superprimer coating with polyacrylate minor binder – on days 1, 3 and 10 of exposure
- 3.15** HDG panels with coatings with and without 15% CZM inhibitor – after 2000 hours of exposure
- 3.16** Coated HDG panels with various inhibitors – after 1350 hours of B117 test exposure
- 3.17** Low-frequency impedance curves showing the absence of any deterioration in anti-corrosion performance of superprimers upon incorporation of the co-solvents acetone and Archer-RC

- 3.18** Images of B117 test-exposed panels after 35 days of exposure, showing the absence of any deterioration in anti-corrosion performance of superprimers upon incorporation of the co-solvents acetone and Archer-RC
- 3.19** Images of B117 test-exposed panels, after 1350 hours of exposure, showing the absence of any deterioration in anti-corrosion performance of superprimers upon incorporation of DBTL
- 3.20** HDG panels coated with superprimers with and without leafing aluminum paste after exposure to 30 days of salt water immersion and 3 days of Machu test
- 4.1** Coatings in OA4 after 3 days of exposure in the Machu test
- 4.2** Tape adhesion test results - Effect of silane on wet-adhesion of primer with topcoat and substrate. 1\_1 and 2\_1 formulations do not have any silane and show poor adhesion. 2\_6 and the rest of the tested formulations having silane component and thereby show excellent adhesion
- 4.3** Low-frequency impedance values of the coatings in OA1, on day 1 and day 30 of exposure in EIS
- 4.4** Low-frequency impedance values of the coatings in OA2, on day 1 and day 30 of exposure in EIS
- 4.5** Low-frequency impedance values of the coatings in OA3, on day 1 and day 30 of exposure in EIS
- 4.6** Low-frequency impedance values of the coatings in OA4, on day 1 and day 30 of exposure in EIS
- 4.7** Optimization plot for OA1
- 4.8** Optimization plot for OA2

- 4.9** Optimization plot for OA3
- 4.10 (a)** Optimization plot for Factor 1 of OA4
- 4.10 (b)** Optimization plot for Factor 2 of OA4
- 4.10 (c)** Optimization plot for Factor 3 of OA4
- 4.10 (d)** Optimization plot for Factor 4 of OA4
- 4.11** Images of HDG panels coated with the four optimized coatings and the two chromated controls, all without topcoat and 2000 hours of exposure in the B117 test
- 4.12** Images of HDG panels coated with the four optimized coatings and the two chromated controls, all with topcoat and 2000 hours of exposure in the B117 test
- 4.13** Images of HDG panels coated with the four optimized coatings and the two chromated controls, all without topcoat and 59 cycles of exposure in the Ford cyclic test
- 4.14** Images of HDG panels coated with the four optimized coatings and the two chromated controls, all with topcoat and 59 cycles of exposure in the Ford cyclic test
- 4.15** Low-frequency impedance curves of HDG panels coated with the four optimized coatings and the two chromated controls, all without topcoat and 2000 hours of exposure in the B117 test
- 4.16** Low-frequency impedance curves of HDG panels coated with the four optimized coatings and the two chromated controls, all with topcoat and 2000 hours of exposure in the B117 test

- 4.17** Low-frequency impedance curves of HDG panels coated with the four optimized coatings and the two chromated controls, all without topcoat and and 59 cycles of exposure in the Ford cyclic test
- 4.18** Low-frequency impedance curves of HDG panels coated with the four optimized coatings and the two chromated controls, all with topcoat and and 59 cycles of exposure in the Ford cyclic test
- 5.1** RAIR spectrum of neat bis-benzene film on day 7 of RT cure
- 5.2** Stacked RAIR spectra of neat bis-benzene films for comparison at various curing stages
- 5.3** RAIR spectrum of bis-sulfur film on day 7 of RT cure, with annotated peaks
- 5.4** Stacked RAIR spectra of bis-sulfur films for comparison at various curing stages
- 5.5** RAIR spectrum of DPW 6520 film, with annotated peaks
- 5.6** RAIR spectrum of Ancarez AR550 film, with annotated peaks
- 5.7** Stacked RAIR spectra of DPW 6520 films for comparison at various curing conditions
- 5.8** Stacked RAIR spectra of Ancarez AR 550 films for comparison at various curing conditions
- 5.9** Comparison of the RAIR spectra of DPW 6520 and Ancarez AR 550 films on day 14 of room temperature curing
- 5.10** RAIR spectrum of DPC 6870 film, with annotated peaks
- 5.11** Stacked RAIR spectra of DPC 6870 films at various curing conditions
- 5.12** RAIR spectrum of ECO-CRYL 9790 film, with annotated peaks, on day 0 of room temperature curing

- 5.13** RAIR spectrum of ECO-CRYL 9790 film, with annotated peaks, on day 0, after high temperature curing
- 5.14** Stacked RAIR spectra of ECO-CRYL 9790 films for comparison at various curing conditions
- 5.15** RAIR spectrum of NeoRez R 972 film, with annotated peaks
- 5.16** Stacked RAIR spectra of NeoRez R 972 films for comparison at various curing conditions
- 5.17** Stacked RAIR spectra of films of a 9:1 mixture of Ancarez AR 550 and ECO-CRYL 9790 respectively, at various curing conditions
- 5.18** Stacked RAIR spectra of films of a 9:1 mixture of DPW 6520 and ECO-CRYL 9790 respectively, at various curing conditions
- 5.19** Comparison of the RAIR spectra of films of the two 9:1 epoxy-polyacrylate mixtures on day 14 after high temperature curing
- 5.20** Stacked RAIR spectra of films of a 9:1 mixture of Ancarez AR 550 and NeoRez R 972 respectively, for comparison at various curing conditions
- 5.21** Stacked RAIR spectra of films of a 9:1 mixture of DPW 6520 and NeoRez R 972 respectively, for comparison at various curing conditions
- 5.22** Comparison of the RAIR spectra of films of the two 9:1 epoxy-polyurethane mixtures on day 14 after high temperature curing
- 5.23** Comparison of the RAIR spectra of a 7:3 mixture of DPW 6520 and DPC 6870 respectively on day 14 of room temperature curing and day 14 after high temperature curing

- 5.24** The same RAIR spectra as in Figure 5.23 detailing the region in and around the characteristic epoxy peak at  $915\text{ cm}^{-1}$
- 5.25** RAIR spectra of superprimer films showing the effect of incorporation of the silanes bis-benzene and bis-sulfur
- 5.26** The same RAIR spectra as in Figure 5.25 detailing the siloxane peak region
- 5.27** Silanes - representative structures and calculated peak positions
- 5.28** DPW 6520 - representative structures and calculated peak positions
- 5.29** ECO-CRYL 9790 - representative structures and calculated peak positions
- 5.30** Neorez R 972 - representative structures and calculated peak positions
- 5.31** Liquid  $^{13}\text{C}$  NMR spectrum for DPW 6520 along with representative DGEBA
- 5.32** Five major cross-linking reactions in the superprimers under study
- 5.33** Solid-state  $^{13}\text{C}$  spectra for NMR solid sample 1 (7 3 2)
- 5.34** Solid-state  $^{13}\text{C}$  spectra for NMR solid sample 2 (7 3 2 BB)
- 5.35** Solid-state  $^{13}\text{C}$  spectra for NMR solid sample 3 (7 3 2 8290)
- 5.36** Solid-state  $^{13}\text{C}$  spectra for NMR solid sample 4 (7 3 2 ECO)
- 5.37** Solid-state  $^{13}\text{C}$  spectra for NMR solid sample 5 (7 3 2 PUD)
- 5.38** Solid-state  $^{13}\text{C}$  spectra for NMR solid samples 6 (PIG) and 7 (PIG\_HT)
- 5.39** TGA-curves of the eight analyzed samples
- 5.40 (a)** SEM image of scribe – effect of 5% Corrostain 228
- 5.40 (b)** EDX spectrum at the point in the scribe highlighted in Figure 5.45 (a)
- 5.41 (a)** SEM image of scribe – effect of 10% Corrostain 228
- 5.41 (b)** EDX spectrum at the point in the scribe highlighted in Figure 5.46 (a)
- 5.42 (a)** SEM image of scribe – effect of 10% zinc phosphate

- 5.42 (b)** EDX spectrum at the point in the scribe highlighted in Figure 5.47 (a)
- 5.43 (a)** SEM image of scribe – effect of 10% CZM
- 5.43 (b)** EDX spectrum at the point in the scribe highlighted in Figure 5.48 (a)
- 5.44 (a)** SEM image of scribe – effect of 15% CZM
- 5.44 (b)** EDX spectrum at the point in the scribe highlighted in Figure 5.49 (a)
- 5.45 (a)** SEM image of scribe – effect of 10% Corrostatin 228 + 1% NaVO<sub>3</sub>
- 5.45 (b)** EDX spectrum at the point in the scribe highlighted in Figure 5.50 (a)
- 5.46 (a)** SEM image of scribe – effect of silane absence
- 5.46 (b)** EDX spectrum at the point in the scribe highlighted in Figure 5.51 (a)
- 5.47 (a)** SEM image of scribe – effect of high temperature cure
- 5.47 (b)** EDX spectrum at the point in the scribe highlighted in Figure 5.52 (a)
- 5.48 (a)** SEM image of the cross-section of superprimer coating on HDG. Notice the line on which the EDX line scan was taken
- 5.48 (b)** EDX line spectra on the line shown in Figure 5.48 (a), revealing the relative elemental distribution

# 1. INTRODUCTION

This thesis focuses on the development and study of an effective anti-corrosive non-chromate, low-VOC, water-borne, optimized, direct-to-metal primer for hot-dip galvanized steel (HDG). The introduction chapter discusses the corrosion of metals and its protection by organic coatings and details on HDG. It then goes on to delineate the differences between conventional primers and superprimers, solvent-borne and water-borne coatings, chromates and their replacements. It also discusses the components of superprimers with emphasis on the type of components used specifically for this study. It then gives a brief on the formulation optimization procedure followed in this study and finally ends with a summary of the thesis objective.

## 1.1 Corrosion of metals

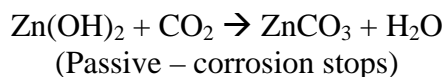
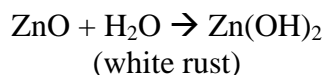
Corrosion refers to the electrochemical degradation (chemical, mechanical and electrical properties) of metals due to reactions with the elements of their environment. It is a major source of revenue loss for all types of industries worldwide, in terms of equipment problems, lost time, maintenance costs and workplace hazards. In a study made by CC Technologies Laboratories, Inc., Dublin, Ohio, in cooperation with NACE International and funded by the Federal Highway Administration in 1998 [1], the total direct cost of corrosion in USA was determined to be \$276 billion per year, which is 3.1 percent of the U.S. gross domestic product (GDP). During corrosion, the metal surface becomes the host to anodic and cathodic reaction sites (half cell reactions). The anodic reaction generates electrons and causes metal dissolution, while cathodic reactions such as hydrogen liberation, consume these electrons and aid the completion of the electrochemical corrosion reaction. A schematic of the corrosion process on iron along with the possible half cell reactions depending on the type of environment is shown in Figure 1.1. There

are many forms of corrosion based on the prevailing combination of environmental factors or factors intrinsic to the metal, such as the presence of ions, presence and concentration of oxygen, gradients in ion/oxygen concentration in the electrolyte, external or residual stress, static/dynamic stress, high temperature, radiation, biomass, corrosive chemicals in the environment, impurities or inclusions in the metal and metal coupling (galvanic corrosion). Corrosion can be avoided or minimized by proper material selection, environmental control, substrate design and substrate modification by use of barrier or conductive coatings. Many references are available which describe the corrosion mechanisms of different metal substrates in different environments and methods to prevent corrosion. Some of them are found in references 2, 3 and 4.

## **1.2 Hot-dip galvanized steel**

Hot-dip galvanized steel (HDG) is widely used in automobiles, electrical home appliances and construction industry due to the corrosion resistance imparted in addition to the mechanical strength of steel. About 3.1 million tons of galvanized steel was produced in North America in 2004, with an average growth rate of 1.9% since 1997 [5]. The zinc layer is metallurgically bonded to steel by dipping steel parts into baths of molten zinc, by either a continuous process (sheet galvanized steel) or a batch process (batch-galvanized steel). The zinc layer serves as a sacrificial layer, providing cathodic protection to the steel substrate. The normal corrosion life cycle of zinc consists of the formation of zinc oxide, followed by its basic hydroxide (white rust) and finally basic carbonate. The last compound forms a protective, relatively impermeable layer, thereby protecting the zinc beneath. This layer is usually formed after one year of outdoor exposure. The first two compounds, i.e., ZnO and Zn(OH)<sub>2</sub> form porous, unprotective films.

Also, the hydroxide ('white rust') layers are prone to be washed away by water. The oxide-hydroxide layer starts forming usually 24 hours after the hot zinc layers have been coated and rolled [6]. Nevertheless, the zinc layer is slowly, but eventually, consumed by corrosion, especially in humid storage conditions and in absence of sufficient carbondioxide. An organic coating or a passivating treatment on this zinc coating (duplex coatings) provides barrier protection to the zinc layer and thereby greatly extends its service life. Prevention of white rust by an additional coat also enhances the appearance of the steel. The series of chemical reactions occurring during corrosion of the zinc layer are:



In order to effectively prevent corrosion, the organic coating has to successfully adhere to the galvanized steel substrate. Not all paints adhere well to galvanized steels. The superprimers formulated in this study, as will be discussed later, achieve excellent adhesion via proper surface cleaning procedures and incorporation of silanes.

### **1.3 Corrosion prevention by organic coatings**

Organic coatings prevent corrosion by one or more of the three following mechanisms: a) barrier effect: creating a barrier to the transport and thereby preventing access of corrosive electrolyte, ions and oxygen to the metal surface; b) cathodic effect: cathodic prevention of the metal by utilizing the galvanic potential difference between the metal and the coating material, e.g., zinc-

rich coatings and, c) inhibitor effect: slow release of inhibitors or passivating species from coating onto the metal surface. Protective coatings are a major method of corrosion prevention and in USA in 1998, of the total costs of methods and services, viz., \$121.4 billion, protective coatings singly contributing \$108.6 billion [1].

Conventional coating systems in general consist of three or more layers of coatings.

- i. *Pretreatment*: Improves the adhesion between the metal and the upper coating layers and/or passivates the metal surface against corrosion. So far, conversion coatings of chromate (CCC) or zinc phosphate or anodized coatings (in case of aluminum alloys) have been used widely, especially the first one, i.e., CCCs because of their excellent anti-corrosive properties. However many alternatives are being explored because of the toxic nature of chromates used in CCCs. Most notable amongst these alternatives are silane pretreatments.
- ii. *Primer*: This is the most important layer in case of anti-corrosive coatings. It provides barrier properties and active corrosion prevention. The general components of an organic primer are its binder such as epoxies, polyurethanes, alkyds polyesters, silicones, polyacrylates etc., hardeners, which depends on the binder in use, anticorrosive inhibitors which are inorganic pigments or organic compounds like chromates, phosphates, nitrites, tolytriazoles, etc., other pigments, mainly colorants like titania etc., fillers such as mica, barium sulfate, etc., and additives, mainly, surfactants and dispersants.
- iii. *Topcoat*: This layer provides durability to the coating system by imparting improved abrasion resistance, hardness, protection against sunlight, radiation or other environmental factors. It is mainly made-up of polyurethanes, polyacrylates, alkyds or polyesters and can be applied in one or more layers, wherein each layer may be different from the other in terms of the polymer used.

The primer or topcoat is a two-pack system if the hardener or activator portion is provided separately and has to be added and mixed with the resin portion before application to the substrate. It is a one-pack system if the hardener and binder are all provided together as a single 'pack', i.e., already mixed, and hence can be directly applied to the substrate.

This study concentrates on the second layer of the coating system, i.e., the primer. As has been mentioned earlier, this study seeks to modify the primer in such a way that the pretreatment layer can be disposed. A primer layer in general should possess good properties of wet and dry adhesion to the substrate, chemical and solvent resistance, barrier properties, resistance to osmotic blistering and active protection of the metal against corrosion by effective inhibitor leaching and further, based on the application, mechanical properties such as flexibility, hardness, abrasion resistance, etc. More information on organic coatings can be found in references 7 and 8.

Organic coating technologies have been evolving towards environmentally friendly systems. This evolution is being driven by two major environmental concerns:

- a) Elimination of the highly effective, but toxic hexavalent chromate pigments. Chromates are widely used in conversion coatings and as corrosion inhibitors in primers. Chromate replacements are being sought for these applications.
- b) Reduction or elimination of Volatile Organic Content (VOC) in coatings systems. The VOC in coatings is due to the extensive use of solvents such as xylene, alcohols and ethers, which are classified as VOC by the Environmental Protection Agency (EPA), as they work towards

the degradation of the protective ozone layer present in the upper parts of troposphere. Alternatives for these high-VOC solvent-borne coatings are being developed. The main routes being pursued are development of water-borne coatings, high solid coatings, UV/radiation-cured coatings, powder coatings and use of VOC-exempt solvents other than water, for example, acetone, tertiary butyl alcohol or parachlorobenzotrifluoride. For a list of VOC-exempt solvents see reference 9. The work in thesis addresses these concerns. More background information on these issues will be provided later in this chapter.

## **1.4 The Superprimer**

The superprimer concept was introduced by Dr. Van Ooij, et al. at the University of Cincinnati [10]. The main difference between a conventional primer and a superprimer is that the latter coating has no pretreatment layer and invariably has silanes in its formulations. Further, in this study VOC-exempt solvents (water and acetone) replace the conventional VOC solvents and non-chromate inhibitors replace chromate pigments leading to low-VOC, non-chromate water-borne superprimers. The concept of superprimer – a single layer, direct-to-metal primer, obviating the need for a pretreatment layer, had its origins in the quest towards alternatives for chromate conversion coatings. Silane-based pretreatments, notably bis-silane based pretreatments, as will be explained later, were shown to be competitive replacements for chromate conversion coatings. They provide good corrosion protection to the metal substrate by improving adhesion between the primer and the substrate and by imparting hydrophobicity to the metal surface. When mixed with conventional primers or binders, these silanes were shown to impart excellent corrosion protection as was first shown by Van Ooij, et al. [10]. The schematics

for a conventional system, a system with silane pretreatment and the superprimer system are shown in Figure 1.2.

The concept of superprimers is rather new. However, more methodical studies on superprimers based on different binder systems and non-chromate pigments were carried out by Van Ooij et al. over the last couple of years [11-16]. The types of superprimer formulated and studied so far have been: a) a room-temperature-cured water-borne acrylate-epoxy-silane based superprimer for AA2024-T3 substrate [11,12], b) a room-temperature-cured solvent-borne epoxy-isocyanate-silane-based superprimer for hot-dip galvanized steel [13,16] and, c) a room-temperature-cured water-borne epoxy-silane system for AA2024-T3 substrates [14].

In each of the superprimer formulations mentioned above, a few combinations of binders and pigments were found to be effective for each type of substrate. There are many factors that not only determine the extent of corrosion protection imparted by a superprimer for a particular type of substrate, but also other properties such as hardness, solvent resistance, flexibility, abrasion resistance, etc. The main factors involved, not necessarily independent, are i) the basic chemistry of the binder system, i.e., binder(s) with or without crosslinker(s), ii) the type and concentration of the silane(s) used, the extent of the crosslinking in the film, iii) the nature and extent of carrier solvent - whether it is an organic solvent or water, iv) the type and concentration of anticorrosive pigments, colorants, fillers etc., v) the curing method used - room temperature or high temperature and vi) the type and concentration of performance enhancing additives like surfactants and dispersants. These factors have to be varied and optimized to formulate

superprimers with specific properties. The water-borne non-chromated superprimers formulated for this study have some or all of the components mentioned below:

- A. *The organic polymer binder*: water-borne epoxy dispersions of bisphenol-A epoxy (major binder), polyurethane and polyacrylates (minor binders)
- B. *Cross-linker/hardener*: water-borne epoxy-amine adducts
- C. *Silanes*: bis-sulfur silane, bis-benzene and bis-[triethoxysilyl]ethane (BTSE)
- D. *Non-chromate pigments and fillers*: calcium zinc molybdate, zinc phosphate, corrostain 228, cerium exchange silica, mica and titania
- E. *Co-solvents*: acetone
- F. *Other additives* – surfactants and dispersing agents

In formulating a non-chromate, low-VOC, water-borne superprimer, the first four components are of great significance. Each of these four classes along with the terms non-chromate, water-borne will be elucidated to some extent later in this chapter. The details about each chemical used in particular will be discussed in the next chapter.

## **1.5 Solvent-based primers and their alternatives**

Solvent-based primers are of two types: a) monomers or low-molecular weight polymers dissolved or dispersed in an organic solvent such as xylene, alcohols, glycols, ethers, etc., which chemically react (cure) after application to the substrate by a mechanism specific to the monomer type and thereby polymerize, or, b) pre-polymerized high molecular-weight molecules dispersed or dissolved in an organic solvent, which cure by solvent evaporation. The type of solvent

medium for a particular type of binder is determined on the basis of the solubility parameter for that particular solvent or solvent blend measured and calculated in accordance with the ASTM D 3132 standard. Organic solvents or solvent blends provide many advantages such as customized solubility and evaporation rates and in general lower surface tensions (20 – 30 mN/m) [17]. The latter property is of utmost importance in determining the wettability of the coating. In order that the substrate be wetted by the coating formulation, its surface tension has to be less than or equal to the surface energy of the substrate. The surface energy values for some substrates and solvents are given in reference 17. But most of the organic solvents used as carriers harm the ozone layer and are classified as VOCs (volatile organic compounds) and emit HAPs (hazardous air pollutants). They can be harmful to humans via skin contact and inhalation. Thus, organic solvents in coatings are undesirable from an occupational hygiene and ecological perspective. These concerns and consequently the legislations being imposed by the EPA are causing the coatings world to look for safer, environmentally friendly alternatives. The options being explored and commercialized are: a) decreasing the solvent content to less than 3 - 4% (low-solvent, high-solids coatings), b) use of water as the carrier medium (water-borne dispersions or emulsions), c) use of VOC-exempt solvents, d) solvent-free powder coatings, e) radiation curing. In this work the water-borne coatings option has been explored and will be discussed in brief in the next section.

## **1.6 Water-borne coatings**

Use of water as an alternative carrier medium has significant shortcomings. Firstly, the polar nature of water is in contrast with the nature of most of the high performance binders, which are non-polar, although many water-soluble binders are also available which have polar groups, e.g.,

polyesters. This means that water cannot act as a true solvent for these binders and only dispersions or emulsions are possible. Even the formulation of stable dispersions or emulsions requires the use of surfactants to reduce the energy differential at the binder-water interface. Secondly, the high surface tension of water (72 mN/m) poses difficulties in achieving good wettability on many a substrate. For metals, the surface energy is around 25 - 45 mJ/m<sup>2</sup>. This again calls for the use of surfactants to reduce the energy differential at the coating-substrate interface. Thirdly, water-borne coatings are more sensitive to surface preparation. Organic impurities on metal substrates lower the surface energy of the substrate and thereby increase the energy differential between the coating and the substrate, causing wettability problems. In the case of solvent-borne coatings, organic impurities on the surface are dissolved to an extent by the non-polar solvent present in them. However, this is not the case for water-borne coatings, so more rigorous surface cleaning procedures have to be followed. Finally, water-borne coatings in general need longer drying times due to the lower evaporation rate of water vis-à-vis most of the conventional organic solvents.

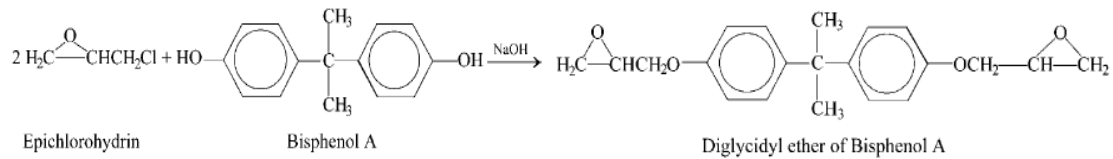
Despite all the disadvantages associated with water-borne coatings, they remain a strong contender to overtake the position of solvent-borne coatings in the world coatings market. The surfactant technology is advanced enough to overcome the aforementioned wettability problems. Specialized additives, fillers, corrosion inhibitors and other pigments are available which greatly improve the anti-corrosive performance of these coatings. The carrier used - water, is inexpensive and safe, is VOC-free and non-toxic. Water-borne coatings neither have the problem of high viscosity as in high-solids coatings nor do they require specialized equipment for application and curing, as in the case of powder coats or radiation cured coatings. The current

technology for production of water-borne coatings, with major inputs from applied surfactant science, has generated competitive dispersions and emulsions for a whole gamut of competitive coatings on a variety of substrates [18]. With improvements in technology further cost reductions and performance improvements can be expected.

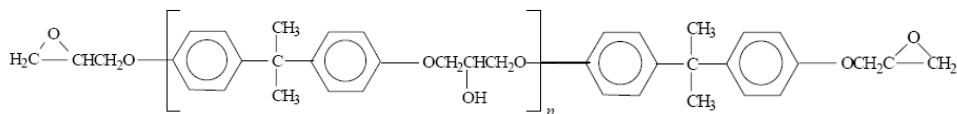
Proprietary 'self-emulsifiable' resins made by reacting surfactants with the polymer are available commercially [18]. However, another approach, more widely used, in order to dissolve or disperse or emulsify an inherently insoluble binder in water, binder salts are first prepared by reacting the binder with its respective pH counterpart. If the binder has acidic groups, it is reacted with a base (usually amines) and if the binder has basic groups it is reacted with acids. Based on this procedure, it is possible to dissolve low molecular weight (< 20,000) polymers, disperse medium molecular weight (< 200,000) polymers and emulsify high molecular weight (> 200,000) polymers [19]. Many a binder has been modified for conversion into a water-borne coating. For anticorrosive coatings most notable of these binders are bisphenol-A and bisphenol-F-based epoxies, polyurethanes, poly(meth)acrylates, and styrene-acrylate co-polymers. In this study water-borne dispersions of solid bisphenol-A epoxies have been used as the major binder, while polyurethane and acrylate dispersions have been used as minor binders.

## **1.7 Bisphenol-A epoxy resins and their water-borne variations**

Bisphenol-A epoxy resins are reaction products of epichlorohydrin and of bisphenol-A. The simplest of these resins is diglycidyl ether of bisphenol-A (DGEBA) as shown by the reaction below:



The generalized structure for a bisphenol-A epoxy resin is given by



Where n ranges from 0 (for DGEBA) to 24. The higher the value of n, the higher the molecular weight and the higher the epoxy equivalent weight (EEW), which is the total molecular weight per epoxide molecule. Apart from bisphenol-A resins, there are few other bisphenol-A analogs of commercial importance, such as the resins derived from halogenated bisphenol-A which have inherent flame-retardant properties and the novolac epoxy resins (bisphenol-F) derived from reaction between epichlorohydrin and phenol-formaldehyde. The latter resins have higher epoxy functionality and hence are capable of high crosslink densities and high temperature stabilities. More information on the various major epoxy resins is available in reference 20.

Bisphenol-A epoxies and all epoxy resins in general have excellent electrical, thermal, and chemical resistance. They show excellent adhesion on many substrates and can be crosslinked using a variety of hardeners, as will be discussed later. They harden quickly and have a high abrasion resistance. Epoxies in general are less flexible. However, the rate of hardening and the trade-off between flexibility and hardness can be altered using the right type and amount of hardener and the curing temperature. Its features of excellent adhesion and compatibility with many corrosion-inhibiting pigments and fillers make it an ideal choice as binders for anti-

corrosive primers. However, they do not show good UV resistance, hence a top-coat, made usually of polyurethanes, polyacrylates or alkyds, is applied over them to provide durability.

Water-borne coatings of epoxies available commercially, are usually one of the following two types of two-component systems [21]: a) Type I: liquid epoxy resin + curing agent, b) Type II: water-borne dispersion of solid epoxy particles + water-dispersed or reducible curing agent. In the older type I epoxy dispersions, the liquid epoxy resin is emulsified in water upon addition of the curing agent (usually a polyamine/amide or their epoxy-adducts). In this type, the dispersion particles contain both the epoxy and amine components. The epoxy-amine curing reaction is shown in Figure 1.3. These dispersions do not have flow and coalescence problems. They do not require additional coalescents, which are high in VOC, and hence have low VOC (0-120 g/L). This type of dispersions has high reactivity because of their low EEW (175-240 g/epoxide-equivalent) and hence a low pot-life (1-3 hours). Also these coatings do not lacquer dry (drying by water evaporation) and require the curing reaction to reach significant levels to reach a tack-free state. Hence the drying times for liquid epoxy systems are high (around 6 hours).

In the newer type II epoxy dispersions, solid epoxies are supplied pre-dispersed at 50-55% solids in water and co-solvent. To aid in processing and to overcome the poor flow and coalescence of solid epoxies, 5-10% glycol ether is added to the dispersions thereby eliminating any possibility for zero-VOC formulations (VOC ~ 240 - 360 g/L). The curing agent must migrate from the aqueous phase into the dispersed epoxy particles for the curing reaction to occur. These systems have longer pot-lives > 4 hours, higher EEW: 450-750 g/epoxide-equivalent and hence reactivity is lower), shorter dry times, as they lacquer dry. The films formed are relatively more flexible

than those formed by type I systems. The pot-life in most of the type II systems is not signaled by a visible change in viscosity. It is the time in which the local curing reactions are complete and cured particles are formed which fail to coalesce completely to a non-porous film at ambient curing temperatures. In other words, the pot-life ends at a point wherein the minimum film forming temperature exceeds the ambient.

New products have emerged in the market, which claim to combine the attributes of shorter dry times, longer pot lives and low VOCs, for example, DPW-6520 from Resolution Performance Products and Ancarez AR 550 from Air products. Some of them also claim to indicate a visible end of pot life. These novel epoxy dispersions and some type II dispersions have been used as major binders in this study. More details on the specific approaches taken to achieve water-borne epoxy systems are shown in Chapter 11 of reference 7.

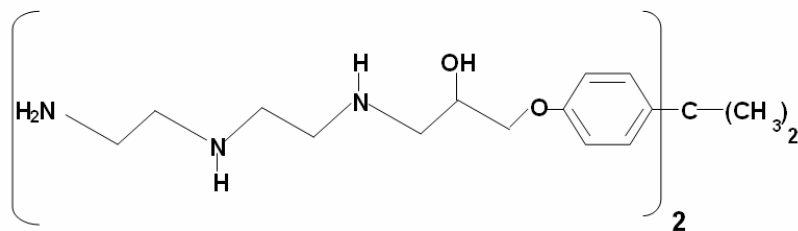
## **1.8 Curing agents for Bisphenol-A epoxies – water-borne epoxy-amine adducts**

Polyamines, polyamides, organic acids, anhydrides, boron trifluoride and tertiary amine catalysts are among the more frequently used curing agents for epoxy resins. The curing agents open up the oxirane ring and act as bridges, binding the epoxy polymers into a dense three-dimensional network. The general structures resulting from the reaction between an epoxy ring and different curing agents are shown in Figure 1.3. Among the five types of curing agents mentioned above, the first two types, i.e., polyamines and polyamides, are widely used in case of anticorrosive primers. Water-borne polyamines have been used as the hardeners in this study and hence are

discussed briefly ahead. More information on the curing agents for epoxy resins can be found in reference 20.

Polyamines are classified based on the number of active hydrogen atoms present on the amine groups - primary, secondary or tertiary. The first two classes cross-link by an addition mechanism, while the latter class, which are Lewis bases, i.e., electron pair donors cross-links by a catalytic mechanism. They are also categorized based on the structure of amine compounds – aliphatic, aromatic, alicyclic and heterocyclic. The two classifications lead to a total of 12 generic types.

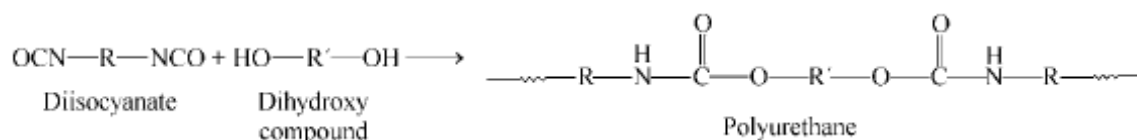
Most of the amines, may irritate skin, possess a noxious odor or emit corrosive fumes. Hence they are mostly sold as modified variations with reduced vapor pressures and tendency to irritate, under many proprietary names. One approach to formulate amine cross-linkers with higher equivalent weight and lower toxic hazard is to make ‘amine-adducts’ made by reacting standard liquid bisphenol-A epoxy with excess of a multifunctional amine. A variety of amines can be used to provide adducts with a range of cure rates and pot lives. A simple epoxy amine adduct is shown below. In this study water-borne epoxy-amine adducts have been used as the curing agents.



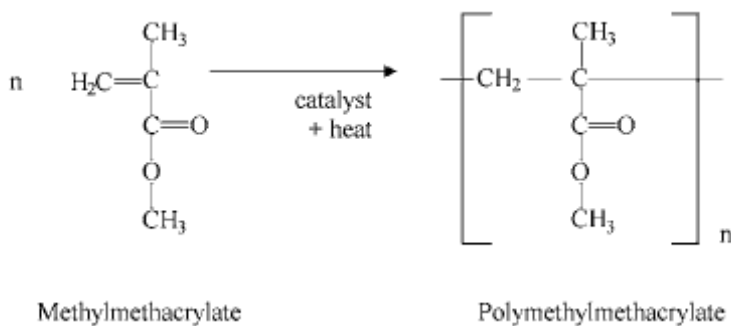
For low temperature curing (below 5 °C), modified amines such as amine-Mannich bases (methylolphenyl + excess polyamine) [22] and amine terminated amines (multifunctional amine + aliphatic mono- or di-carboxylic acids) [23] can be used.

## 1.9 Polyurethane and polyacrylate dispersions

In this study water-borne polyurethane and polyacrylate dispersions were used as support binders, i.e., as the minor components, which are usually less than 5 wt-% of the total formulation. Polyacrylate-based coatings are known for their hardness, gloss, weatherability, fast dry or tack-free time and crosslink ability, from reactive monomer functionality - OH, acid or epoxy groups, etc., while polyurethane-based coatings are known for their flexibility, abrasion resistance, acid rain resistance, gloss retention and impact resistance. The basic reactions for formation of polyurethanes and polyacrylates and their structures are shown below. More information on these compounds can be found in references 7, 8 and 20.



### Basic polyurethane reaction



### Polyacrylate formation

The above-mentioned ‘support-binders’ were introduced in the epoxy-amine matrix in order to study their effect on the corrosion preventability of the films formed. The study was carried with the expectation that some of the possible reactions between the functional groups present in the polyurethane, polyacrylate, epoxy, amine and silane components can lead to more densely cross-linked, inter-cross-linked or interpenetrating networks (IPNs), forming films with better barrier and chemical resistance properties. Possible reactions between the different components of the superprimer are presented in Chapter 5.

### **1.10 Chromates and their alternatives**

Hexavalent chromate compounds have been the workhorse of anti-corrosive coatings for years. They are highly efficient in preventing corrosion and are cost-effective and hence have been in wide usage in passivating treatments such as chromate conversion coatings and as anticorrosive pigments in primers.

For chromate conversion coatings (CCCs), the hexavalent chromate compounds are deposited onto the metal substrate (Al and steel alloys) from either acidic e.g., Alodine process or alkaline solutions containing hexavalent chromate compounds and other film-enhancing compounds such as fluorides and ferricyanides. Chromate treatments have been developed for many metal substrates. In case of metals such as iron or steel where no direct chromate rinse has been successful, a chromate rinse succeeds some other rinse, usually a phosphate rinse. Details on chromate bath compositions for specific substrates can be found in reference 4.

CCC formation involves electrochemical reduction of chromate followed by inorganic polymerization to build the conversion film [24-26]. Specifically, this process involves reduction of Cr(VI) in solution to form hydrated  $\text{Cr}(\text{OH}_2)_6^{3+}$ . This species hydrolyzes in the locally alkaline region at the alloy-solution interface forming hydrated chromium hydroxide,  $\text{Cr}(\text{OH}_2)_3(\text{OH})_3$ . This hydrate then polymerizes by forming Cr(III)-OH-Cr(III) linkages forming a so-called polymer “backbone.” Simultaneously, chromate binds via oxygen ligands forming Cr(VI)-O-Cr(III) linkages, which are characteristic of chromium chromate conversion coatings [25].

CCCs of today are easily applied and offer excellent corrosion resistance, including a self-healing ability. CCCs are also easily painted. The ‘self-healing’ or ‘self-repair’ ability refers to the ability of chromate pigments or conversion coatings to rebuild the protective chromate layers even in areas where they have been damaged. This ability of chromate pigments stems from the reservoir of Cr(VI), which can convert to Cr(III) and again form the protective chromate film in damaged areas.

As corrosion inhibitor, the hexavalent chromate is added as leachable pigments to the primers, thereby providing active corrosion protection. Strontium chromate has the ideal solubility to be used as a corrosion inhibiting pigment in primers. Chromates are very effective inhibitors of Fe, Mg, Al, Cu and Zn corrosion.  $\text{CrO}_4^{2-}$  is a typical oxidant passivator of the anodic and cathodic type, and passivates independent of dissolved oxygen. In contrast with  $\text{NO}_2^-$  and  $\text{MoO}_4^{2-}$ , chromates, are effective in moderately acidic conditions as well [27].

However for the past few years strong concerns have arisen due to the carcinogenic nature of these compounds. The molecular debris associated with conversion of the valence state of chromate from hexavalent to trivalent cause critical changes in the DNA structure and is the reason behind its carcinogenic nature [28]. In order to discourage and eventually eliminate the use of these highly toxic compounds, stringent legislations have been imposed by various environmental organizations world-wide. Thereby the coatings industry has been exploring alternatives towards non-chromate pretreatments and inhibitors.

Many alternatives have been explored, both for CCCs and chromate inhibitors, but none of them have individually stood up to the performance levels achieved by the chromates. However, there have been instances of non-chromate complete systems which have performed better than the chromated systems. Thus, to compare chromated with non-chromated systems, it is advisable to consider the performance of all the layers taken together, rather than the individual layers [29].

For CCCs, some of the main alternatives explored have been zinc phosphate CCs, cerium-based CCs, vanadate-based CCs, manganese-based CCs, and last but not the least silane-based pretreatments. A critical review of the aqueous chemistry of the hexavalent chromium along with alternate chemistries is presented in reference 30. The last of the coatings mentioned, i.e., silane-based pretreatments especially in conjunction with non-chromate inhibitors, have shown performance comparable to CCCs along with excellent adhesion properties [31]. A brief discussion about the utility of silanes for corrosion prevention is mentioned below. This class of compounds forms the cornerstone of this study.

All commercial corrosion inhibitor pigments belong to a few generic families of inorganic salts of  $A_m^{n+}B_n^{m-}$ , or basic salts of  $A_m^{n+}B_{n-z}^{m-}OH_z^-$  general formula, where  $n, m = 2$  or  $3$ , and  $A^{n+}$  is Zn(II), Ca(II), Sr(II), Al(III), Ba(II), Mg(II), while  $B^{m-}$  is  $CrO_4^{2-}$ ,  $PO_4^{3-}$ ,  $MoO_4^{2-}$ ,  $BO_2^-$ ,  $(SiO_3^{2-})_n$ ,  $n > 1$ ,  $HPO_3^{2-}$ ,  $P_3O_{10}^{5-}$ ,  $NCN^{2-}$ ,  $CO_3^{2-}$  or various combinations of the same. Additionally,  $OH^-$  is a constituent of basic salts. Sodium nitrite ( $NaNO_2$ ), although not available as a pigment grade (due to its excess solubility), is an effective corrosion inhibitor for iron. Sinko has written an excellent review on the various available replacements for chromate inhibitors, their mechanisms and their pros and cons [32]. In this study, some of these non-chromate pigments were used as corrosion inhibitors. Also, aromatic organic nitrogen compounds like tolyltriazole, benzotriazole etc. can be used as corrosion inhibitors. Some of these organic inhibitors in conjunction with inorganic inhibitors have been used earlier in superprimers on AA2024 alloy [33]. However, they are not a part of this study.

### 1.11 Silanes

Trialkoxysilanes have been standing as the prime contender as alternatives for chromate conversion coatings ever since its anticorrosive properties were first demonstrated using organo-functional di-podal silanes or ‘bis-silanes’ [34]. Bis-silanes, which have two legs of alkoxy groups i.e., two trialkoxy silyl groups, general formula,  $(OR)_3Si(CH_2)_nR'(CH_2)_nSi(OR)_3$  where  $R'$  = organo-functional group and  $R$  = alkyl group, were shown to be more effective in preventing corrosion than mono-silanes which have the general formula,  $R'(CH_2)_nSi(OR)_3$ . The latter class of silanes have a single leg of alkoxy groups and are typified by  $\gamma$ -Aminopropyltriethoxy silane ( $\gamma$ -APS), which is the most widely used silane in the industry.

Trialkoxysilanes, in general, form hydrophobic films in two steps: firstly, the *hydrolysis* of the ester (-OR) groups to hydroxyl (-OH) groups in the presence of water, i.e., formation of the hydrophilic silanol groups (SiOH) and secondly the *condensation* of the silanol groups upon themselves (self-condensation) to form the hydrophobic siloxane (-Si-O-Si-) network and onto the metal substrate to form the hydrolytically unstable metallo-siloxane (-Me-O-Si-) interface. These reactions are shown in Chapter 5. The metallo-siloxane groups are in a reversible equilibrium with silanol and metal-hydroxide groups. Hence, to maintain the adhesion of the silane film to the metal and for adequate corrosion protection, the silane film should be made hydrophobic enough to prevent water permeation into the metallo-siloxane layer. Reference 35 gives a good account of the chemistry and use of silanes as coupling agents. Bis-silanes, due to the presence of a higher density of -OR groups as compared with mono-silanes, form denser and less porous layers of both metallo-siloxane (Me-O-Si) and siloxane (Si-O-Si) bonds on metals and hence their superior adhesion and water-barrier properties vis-à-vis mono-silanes. Apart from their use as replacements for CCCs, silanes have been used as a main component of the superprimers [11 - 16]. They increase the adhesion of these direct-to-metal superprimers and also improve their barrier properties. The silanes widely used in superprimer formulations are shown in Figure 1.4.

## **1.12 Design of experiments using the Taguchi approach**

The design of experiments (DOE) using the Taguchi approach can economically satisfy the needs of problem solving and product or process design optimization projects in the manufacturing industry. By applying this technique, engineers, scientists, and researchers can significantly reduce the time required for experimental investigations. In this study fractional

factorial experiments have been performed using L9 Taguchi orthogonal arrays in order to find the optimum combination of factors (binder, hardener and silanes) and levels (concentration) of each factor. An orthogonal array is a characteristic mathematical combination of factors and levels used in fractional factorial experiments. Many types of orthogonal arrays are available and choosing a particular array depends on the complexity of the experiment at hand. L9 orthogonal arrays are used for experiments involving four factors and three levels. If the conventional complete experiments route is taken, then in this case, to find the optimum formulation,  $3^4$ , i.e., 81 experiments have to be performed.

However by using the L9 orthogonal array and the Taguchi approach, the optimum formulation can be found by conducting just nine experiments, i.e., only nine combinations of factors and levels as given by the L9 orthogonal array. This study used a simplified Taguchi approach and thereby is limited to the optimization of factor levels via observation of coating property trends with changing levels of each factor. It neither dwells into the nature and extent of interaction between the factors nor does it look into the effect of noise factors, if any. Such a simplified approach has been used successfully used earlier in similar studies [12, 36]. Further comparison tests of these optimized formulations were carried out along with chromated controls. More general information on design of experiments, principles behind the use of orthogonal arrays and the complete Taguchi approach can be obtained from references 37 - 40.

### **1.13 Thesis objective – summary**

This study seeks to formulate a superprimer which satisfies the following requirements:

- a) By definition of the superprimer, it should obviate the requirement of a pretreatment – conversion or otherwise, i.e., this superprimer should be directly applied onto the bare metal substrate, which was galvanized steel in this study.
- b) It should show excellent adhesion to the substrate as well as with topcoats via incorporation of silanes.
- c) It should not contain any hexavalent chromate-based inhibitors.
- d) It should exhibit good barrier properties and solvent and chemical resistance
- e) It should provide active corrosion protection by incorporation of suitable non-chromate inhibitors
- f) It should minimize the use of solvents containing VOC and hence should be low in VOC
- g) It should be predominantly water-borne with some VOC-exempt co-solvents, if any.

This study also seeks to formulate a superprimer whose composition has been optimized with respect to the properties mentioned above. A Taguchi design of experiments approach has been followed to achieve this optimization. Therefore, in brief, the main objective of this thesis is to formulate *an effective anti-corrosive non-chromate, low-VOC, water-borne, optimized superprimer for hot-dip galvanized substrates* (Chapters 3 and 4). The chemicals and testing procedures are introduced in Chapter 2.

This study also characterizes the superprimer and its components using FTIR, NMR and SEM/EDX and tries to elucidate the chemistry and mechanisms underlying the anti-corrosive properties of the superprimer (Chapter 5). Conclusions and scope for future work are discussed in Chapter 6.

The APPENDIX, presents a separate to-be-published study on the preparation and characterizations of a silane-epoxy-inhibitor passivating pretreatment for HDG. This formulation can be considered as a spin-off of the superprimer work as it is similar to a diluted form of the superprimer, however, with the concentration of the silane exceeding that of the resin.

## 1.14 References

1. Report by CC Technologies Laboratories, Inc. to Federal Highway Administration (FHWA), Office of Infrastructure Research and Development, *Corrosion Costs and Preventive Strategies in the United States*, Report FHWA-RD-01-156, September 2001. Available at <http://corrosioncost.com/>
2. Jones D.A., *Principles and Prevention of Corrosion*, Prentice-Hall, Inc., Upper Saddle River, NJ (1996)
3. Fontana M. G., *Corrosion Engineering*, 3<sup>rd</sup> ed., McGraw-Hill, Denver, CO (1986)
4. Shreir, L.L., Jarman, R.A., Burstein, G.T., *Corrosion*, 3<sup>rd</sup> ed., 1-2, Elsevier, San Diego, CA (1994)
5. [www.galvinfo.com](http://www.galvinfo.com), *International Lead Zinc Research Organization*
6. Malone J.F., *Mat. Perf.*, 31, 5 (1992)
7. Wicks Z., Jones F. N., Pappas S.P., *Organic coatings Science and technology*, 2<sup>nd</sup> ed., Wiley-Interscience, New York, NY (1999)
8. Lambourne, R., Strivens, T.A. *Paints and Surface Coatings-Theory and Practice*, 2<sup>nd</sup> ed, Woodhead publishing, Cambridge, England (1999)
9. [www.epa.gov](http://www.epa.gov), Code of Federal Regulations # 40 C.F.R. 51.100(s), *Definitions*
10. Seth A., Van Ooij W. J., *J. Mat. Engg. Perf.* 13, 292 (2004)

11. Seth A., Van Ooij W. J., submitted for publication in *Silane and Other Coupling Agents*, Vol 4., K. L. Mittal, eds., 2006
12. Seth A., Van Ooij W. J., Submitted for publication in the ACS Volume based on *New Developments in Coatings Tech.*, P. Zarras, B. C. Benicewicz, T. Wood, B. Richey, Eds. 2005
13. Suryanarayanan K., *M.S.Thesis, University of Cincinnati* (2005).
14. Mugada T., *M.S. Thesis, University of Cincinnati*, to be published in 2006
15. Seth A., Van Ooij W. J., Metroke T., Apblett A., Submitted for publication in *Prog. Org. Coat.*, G. P. Bierwagen, Eds., 2005
16. Suryanarayanan K., Metroke T., Van Ooij W. J., submitted for publication in *Silane and Other Coupling Agents*, Vol 4., K. L. Mittal, eds., 2006
17. Orr E.W., *Performance Enhancement in Coatings*, Hanser Publishers, Munich, Germany (1998)
18. Wegmann A., *J. Coat. Technol.*, 65, 27 (1993)
19. Dören K., Freitag W., Stoye D., *Water-borne Coatings: the Environmentally Friendly Alternative*, Hanser publishers, Munich, Germany (1994)
20. Licari J. J., *Coating Materials for Electronic Applications - Polymers, Processes, Reliability, Testing*, William Andrew Publishing/Noyes, New York, NY (2003)
21. Dubowik D. A., Ross G. C., *Novel Water-borne Epoxy Resin Technology for Zero-VOC 2K Coatings*, [www.pcimag.com](http://www.pcimag.com) (2000)
22. Weinmann D. J., Dangayach K., Smith C., *J. Coat. Technol.* 68, 29 (1996)
23. Brady R.F. Jr., Charlesworth J.M., *J. Coat. Technol.* 65, 81 (1993)
24. Osborne J.H., *Prog. Org. Coat.*, 41, 217 (2001)

25. Xia L., McCreery R.L., *J. Electrochem. Soc.* 145, 3083 (1998)
26. Zhang W., Buchheit R.G., *J. Electrochem Soc.* 149, B357 (2002)
27. Szklarska-Smialowska Z., Staehle R.W., *J. Electrochem. Soc.*, 121, 9 (1974)
28. O'Brien P.O., Kortenkamp A., *Transit. Metal Chem.*, 20, 636 (1995)
29. Duartea R. G., Bastosa A.C., Castela A.S., Ferreira M.G.S., *Prog. Org. Coat.*, 52, 320, (2005)
30. Kendig M.W., Buchheit R.G., *Corrosion*, 59, 5 (2003)
31. Palanivel V., Huang Y., Van Ooij W.J., *Prog. Org. Coat.*, 53, 153-168 (2005)
32. Sinko J., *Prog. Org. Coat*, 42, 267, (2001)
33. Yang L., Seth A., Simhadri N., Van Ooij W. J., submitted for publication in the *Silane and Other Coupling Agents*, Vol 4., K. L. Mittal, eds., 2005, Canada; June 22 – 24 (2005)
34. Van Ooij W.J., Child T., *Chemtech* 28, 26 (1998).
35. Plueddemann E.P., *Silane Coupling Agents*, 2<sup>nd</sup> ed., Plenum Press, New York, NY (1991)
36. Puomi P., H.M. Fagerholm H.M., Rosenholm J.B., Sipila R., *Surface and Coatings Technology*, 115, 70 (1999)
37. *NIST/SEMATECH e-Handbook of Statistical Methods*, available at <http://www.itl.nist.gov/div898/handbook>
38. ASQ statistics division, *Improving Performance Through Statistical Thinking* (2000)
39. Taguchi G., Chowdhury S., Wu Y., *Taguchi's Quality Engineering Handbook*, Wiley-Interscience, New York, NY (2004)
40. Tracton A.A., *Coatings Technology Handbook*, 3<sup>rd</sup> ed., Marcel Dekker, New York, NY (2005)

## 2. EXPERIMENTAL

The following write-up describes all the materials, which were a part of all the coating systems prepared or used in this study. It also describes the substrate preparation methods, performance testing methods and characterization techniques used to understand the mechanisms underlying the coating performance.

### 2.1 Materials

#### 2.1.1 Water-borne dispersions of bisphenol-A (major binders)

- *Developmental Epoxy Dispersion DPW-6520*, A 53%-solids, water-borne NEWGEN™ technology dispersion of a solid bisphenol-A epoxy resin with a non-HAPS co-solvent with a VOC of 74g/L and equivalent weight per epoxide of 500-600, from Resolution Performance Products, Houston, TX.
- *EPI-REZ 5522-WY-55 Resin* is a 55%-nonvolatile dispersion of a modified DGEBA epoxy resin in water and 2-propoxyethanol with a VOC of 170g/L and equivalent weight per epoxide of: 550-700. It has excellent chemical and corrosion resistance even for ambient temperature cures. It was obtained from Resolution Performance Products, Houston, TX.
- *EPI-REZ 3540-WY-55 Resin* is a 55%-nonvolatile dispersion of a modified DGEBA epoxy resin in water and 2-propoxyethanol with a VOC of 240g/L and equivalent weight per epoxide of 1600-2000. It was obtained from Resolution Performance Products, Houston, TX.
- *Ancarez AR550*, a water-borne solid epoxy resin dispersion delivered at 55% solids in water. It has zero VOC and does not gel instantaneously with ECO-CRYL 9790 and NeoRez R-972 (introduced below), unlike many other epoxy dispersions. Its equivalent weight per epoxide is 1600. It was obtained from Air Products and Chemicals, Inc., Allentown, PA.

The equivalent epoxide weight (EEW) of an epoxy resin is the weight of resin in grams which contains one gram equivalent of epoxy, while HAPS refers to hazardous air pollutants. A comparison between the different epoxy dispersions used in this study has been tabulated in Table 2.1.

### **2.1.2 Minor binders**

Minor binders refers to the polyurethane and polyacrylate resin dispersions, which were added in minor amounts (5-10 wt-%) to the superprimer formulations.

- *ECO-CRYL 9790*, an acrylic resin dispersion supplied at 42% solids in water, 2-propoxyethanol, xylene and triethylamine, from Resolution Performance Products, Houston, TX.
- *Neorez R-972* is a colloidal dispersion of aliphatic polyurethane at 34% solids in N-Methyl-2-Pyrrolidone (NMP) and triethylamine. It has good abrasion and chemical resistance. It was obtained from NeoResins Inc., Wilmington, MA.

### **2.1.3 Amine-based crosslinkers for the epoxy dispersions**

- *Developmental Curing Agent Dispersion DPC-6870*, an aqueous dispersion of an amine adduct curing agent (Zero VOC), also from Resolution Performance Products, Houston, TX.
- *EPIKURE 8290-Y-60*, a water-reducible, high molecular weight amine adduct supplied at 60% solids in 2-propoxyethanol (high VOC – 890 g/L) designed for used in two-package, water-borne coatings systems exhibiting excellent chemical and corrosion resistance as well

as long-term water and humidity resistance over a variety of substrates, from Resolution Performance Products, Houston, TX.

#### **2.1.4 Non-chromate corrosion inhibitors**

- *Molywhite CZM*, a calcium-zinc molybdate corrosion inhibitor provided by Molywhite Pigments Group, Cleveland, OH.
- *Corrostayn 228*, a synergistic corrosion inhibitor, containing Ca, Zn, P, Si, O atoms, possibly calcium zinc phospho-silicate, provided by Wayne Pigment Corp., Milwaukee, WI
- *Phosguard J0806*, a micronized zinc phosphate/molybdate corrosion inhibitor from Rockwood Pigments, Beltsville, MD
- *Cerium-exchanged silica* was prepared in our labs by Lin Yang. Its details cannot be disclosed at this time, due to IP issues.
- *Sodium meta-vanadate*, of chemical grade was obtained from Fluka industries, Switzerland.

#### **2.1.5 Other pigments and fillers**

- *Tronox RF-K-2*, a micronized rutile pigment coated with an aluminum compound for hydrophobicity. It was obtained from Kerr Mc Gee Pigments, Hamilton, OH
- *NanoActive S Titanium di-oxide*, a 12-15% by weight suspension of titania in water, obtained from NanoScale Materials Inc., Manhattan, KS
- *Alsibronz 06*, a commercially available ultra-fine sized, chemically inert potassium aluminum silicate platelets, provided by Englehard Corporation, Iselin, NJ

- *Stapa Hydrolac*, leafy aluminum paste containing petroleum distillate, obtained from Eckart America, Louisville, KY.

### 2.1.6 Surfactants and dispersants

- *Surfynol MD 20*, a micro-defoamer obtained from Air Products and Chemicals, Inc., Allentown, PA
- *BYK® P 104 S*, a wetting and dispersing additive which improves pigment wetting and stabilizes pigment dispersion. Used in amine-neutralized aqueous coatings; incompatible with mineral spirits. Prevents flooding of titanium dioxide in combination with other color pigments. It is a solution of a lower molecular weight unsaturated polycarboxylic acid polymer with a polysiloxane copolymer in xylene and 2,6-dimethyl-4-heptanone. It was obtained from BYK-Chemie GmbH, Wesel, Germany.

### 2.1.7 Silanes

- *Bis-sulfur silane* or bis [3-(triethoxysilyl)propyl]tetrasulfide, obtained from GE Silicones, Wilton, CT; product name: Silquest® - A1289.
- *Bis-benzene silane* or 1,4-bis(trimethoxysilylethyl)benzene obtained from Gelest Inc., Morrisville, PA.
- *BTSE* or bis-[triethoxysilyl]ethane, obtained from GE Silicones, Wilton, CT; product name: Silquest® Y 9805.
- *Bis-amino silane* or bis-[trimethoxysilylpropyl] amine, obtained from GE Silicones, Wilton, CT; product name: Silquest®-A1170.
- *VTAS* or vinyltriacetoxysilane, obtained from Gelest Inc., Morrisville, PA

- *TEOS* or tetraethoxysilane, obtained from GE Silicones, Wilton, CT

The chemical structures of these silanes were shown earlier in Figure 1.4.

### **2.1.8 Solvents**

- *Deionized water*, obtained from our lab supply.
- *Acetone – 99.9% pure* from Fisher Scientific, Raleigh, NC

### **2.1.9 Metal**

- *Hot-dipped sheet galvanized steel (HDG)* panels of 10 cm x 15 cm were purchased from Stillwater Steel Supply, Stillwater, OK. The zinc layer thickness on the material was about 20 microns. These metal panels were usually sheared into 5 cm x 7.5 cm or 7.5 cm x 10 cm sizes and cleaned before being coated.

### **2.1.10 Topcoat and control primers**

- *High solids chromated epoxy standard military primer CA 7233* along with its activator component CA 7233 B, blended in a ratio 1:1. Conforms to military specification MIL-PRF-23377 H (Type I, class C), obtained from PPG Industries, Glendale, CA.
- *Desothane HS*, solvent-based gray polyurethane topcoat. Base component and activator blended in a ratio of 3:1, obtained from PPG Industries, Glendale, CA.
- *Devguard* primer obtained from ICI Devco Coatings, Cleveland, OH, a non-chromate alkyd primer was also used as a control primer in some experiments. The primer was applied with a

28  $\mu\text{m}$  draw-down bar, and the primer was allowed a curing time of 2 days at room temperature.

## **2.2 Substrate preparation and cleaning**

The HDG panels were first scrubbed using Scotch-brite™ scrubs. They were then ultrasonically cleaned in ethanol and acetone successively for 10 minutes each to remove impurities. This was followed by degreasing in a diluted (7% by volume in water) alkaline cleaner Okemclean, provided by Oakite products, Berkley Heights, NJ, at 65°C for 4 min and rinsed with tap water, followed by blow-drying with compressed air to achieve a water-break-free surface.

## **2.3 Formulation preparation**

As the formulation procedure is different for each type of formulation, it will be explained at various instances in Chapters 3 and 4 wherever it is required.

## **2.4 Performance evaluation tests and characterization studies**

**2.4.1 Salt water immersion test** is a simple but very useful test to measure anti-corrosiveness and water resistance of organic films. In this test, coated and cross-scribed panels were immersed into a 0.6 M NaCl solution and their performance was monitored over time. The coatings were periodically checked for any scribe creep, corrosion or blistering. The usual immersion time was 30 days. However, it could be extended if the coatings did not show any substantial deterioration.

**2.4.2 Electrochemical Impedance Spectroscopy (EIS)** is a very useful coating evaluation technique. It can be used to determine the degradation of coatings due to onset of corrosion and extent of corrosion of bare as well as coated metals. It is a tool which enables the study of the nature, course and extent of coating degradation. Coating degradation aspects like delamination at various interfaces, perforation, blistering, etc., can be studied in single-coat or multi-coat systems. In this study, however, EIS has been used mainly as a performance evaluation tool for evaluating coating performance via comparison of low-frequency impedance, and not for a mechanistic study, except in the Appendix chapter on the non-chromate pretreatment.

The vicinity of the surface of a corroding metal in an electrolyte is polarized to what is known as a steady-state electrical double layer (EDL). In this state the metal ions leave the surface of the metal leaving negative charge due to excess electrons behind on the metal. In one of the proposed EDL models, a layer of water molecules adsorbed on the metal surface separates the excess electron layer on the metal surface from the hydrated metal ions present in the vicinity of the metal in the electrolyte. Reduction of electrochemically active species such as hydrogen ions, etc., use up some of the electrons on the metal, creating charge imbalance and thereby releasing more metal ions into the electrolyte in order to achieve charge stabilization and continue corrosion. In any case, this separated opposite charge model of the corroding metal acts as a capacitor. The adsorbed water acts as a dielectric. The electrolyte present has electrical resistance. The presence of coating(s) on top of the metal surface creates more interfaces. The coating material, too, is a dielectric, creating another capacitor in parallel. Porosity in coatings creates electrolyte pathways and the extent of porosity determines the electrical resistance of the coating.

So, a coated, corroding metal surface can be modeled as a circuit consisting of capacitors and resistors. When alternating current over a wide range of frequency is passed through a corroding coated or uncoated metal and the output from it, can be presented mainly in two ways: a) zode plot - impedance vs frequency and b) Nyquist plot – real component of impedance vs imaginary component. When this output is compared with the theoretical output plots of the same type from an appropriate representative circuit model, useful information on the nature and extent of corrosion and coating degradation, if any, can be obtained. Figures 2.1 (a) and 2.1(b) show the Bode plots and Nyquist plots, respectively, for a damaged coating, while Figure 2.2 shows a general cylinder-electrodes set-up for used for EIS study. However, only Bode magnitude plots have been studied in this work. These figures have been obtained from reference 1. More information on the utility and theory of EIS can be found in references 2 - 6.

Electrochemical Impedance Spectroscopy measurements were carried out on HDG panels coated with the various supeprimer formulations. An area of 5.06 cm<sup>2</sup> of the coated panels area was exposed to aerated 0.6 M NaCl electrolyte. An SR810 frequency response analyzer connected to a Gamry CMS100 potentiostat was used for the purpose. Measurements were made at frequencies ranging between 10<sup>-2</sup> to 10<sup>5</sup> Hz, with an AC excitation amplitude of 10 mV. A standard calomel electrode was used as the reference electrode with a graphite rod acting as the counter electrode.

**2.4.3 The ASTM B117** salt spray test is used widely in the coatings industry to evaluate the corrosion resistance of coated metal substrates. In this test, cross-scribed coated panels of HDG, coated with primer, with or without topcoat, were exposed to 5% salt solution (NaCl) atomized

in a salt spray chamber at 35°C with the solution pH around 7. To be more precise, this test is the ASTM 1654-92. The actual B117 test does not involve scribing of the panels. However both tests are known by the 'B117' name in the industry. The exposed panels are periodically checked for corrosion in the scribe, formation of blisters and delamination in the general coating area and near the scribe. Thus, this test evaluates the corrosion protection and adhesion performance of the coatings. Various scribed HDG panels coated with supeprimer, with and without Desothane HS topcoat and scribed were subjected to this test.

In this study, these tests were performed in the salt spray chamber at DACCO SCI, INC., Columbia, MD. Specimens were placed in a certified Singleton salt fog chamber according to ASTM B 117. Periodically they were removed from the chamber and EIS measurements were taken using DACCO SCI's handheld corrosion sensors [7] and a Gamry PC-4 potentiostat. These sensors allowed the EIS measurements to be taken under ambient conditions instead of immersion, which is required for the traditional EIS that has been correlated with long-term coating performance [8-14]. The EIS spectral frequency range was 0.1 to 100,000 Hz. The low-frequency impedance reported below was the geometric mean of the impedances from the lowest frequency decade (0.1 to 1 Hz). A schematic of a typical salt fog chamber is shown in Figure 2.3 [15], along with the image of the salt spray chamber at DACCO SCI, that was used for testing the panels in this study (Figure 2.4).

The veracity of the correspondence of B117 test results to actual outdoor exposure behavior of coatings has been widely debated. However, B117 remains the most widely used accelerated test for performance evaluation in the industry. Other accelerated tests, mainly, cyclic tests have been

suggested as better alternatives. Some of these tests, such as the Prohesion test, Ford APGE test and other tests developed by the automobile industry are gaining acceptance. The Ford APGE test has also been used for performance evaluation in this study, and is described below. More information on some of the accelerated tests in use can be found in references 16 - 19.

**2.4.4 The Ford AGPE test** is a cyclic accelerated corrosion test. These tests were also carried out at DACCO SCI, INC., Columbia, MD. The cyclic corrosion test was developed for the evaluation of perforation resistance of automotive painted steels [20-22]. A Blue M VP100 Humidity Chamber was used for the purpose. A daily cycle is given in Table 2.2. On weekends, the panels are kept in the humidity chamber. Other automotive companies have similar cyclic tests, differing in detail of exposure conditions. The exposure period was 100 cycles. Periodically, the specimens were removed and EIS measurements were taken using the procedure described above. This test is the most aggressive when compared with the B117 test and the outdoor exposure test (to be discussed below). Various HDG panels coated with supeprimer and Desothane HS topcoat were cross-scribed and subjected to this test. An image of the Ford AGPE set-up and cycle at DACCO SCI is shown in Figure 2.5.

**2.4.5 Hawaii outdoor exposure test:** Some panels were tested by outdoor exposure on the Maui beach of Hawaii. HDG panels (10 cm x 15 cm) coated with superprimer formulations, topcoated with PRC Desoto topcoat and cross-scribed, were exposed on the beach, which is located on the leeward side of the island. The annual temperature here ranges from 20 to 25°C, with high humidity. The only disadvantage of an outdoor exposure test is the long observation

times needed, usually > 2 years. So far exposure data is available for less than a year of exposure on a few panels. An image of the test location and set-up is shown in Figure 2.6. In this case too, local impedance readings were taken periodically. A comparison of the intensities of the three tests is shown in the Figure 2.7. In general, the steeper the slope of low-frequency impedance plot, the faster the interface is degrading.

**2.4.6 The Machu test** is an accelerated corrosion test for painted HDG widely used in Europe [23]. The solution used in this test directly attacks the paint-metal interface due to the presence of the oxidizer  $H_2O_2$  and the test results are claimed to correlate with 500 hours of ASTM B117 salt spray test [23]. It is especially useful for galvanized steels. The painted panels are cross-scribed on the surfaces, and then immersed in a solution of 5% NaCl + 0.6%  $H_2O_2$  at 37°C for two days. On the second day 0.6%  $H_2O_2$  is added to maintain the peroxide levels. After 2 days of immersion, the panels are taken out and adhesive tape is used to pull off the delaminated paints. Alternatively, a knife can be used to lightly scrape off the paint in delaminated areas along the scribe lines. The extent of delamination around the scribe is a measure of paint adhesion and corrosion performance of the entire system [24].

**2.4.7 Tape adhesion test** (to measure wet adhesion): HDG Panels with cured superprimer coatings were immersed in DI water for 7 days and were subjected to tape adhesion tests according to the ASTM D3359-97 standard, to measure the adhesion of the superprimer to the substrate. This test involves pulling the specified tape off cross-hatched immersed parts of the coating and check the extent of coating material that is removed in order to quantify adhesion.

Similar tests were also carried out on panels with superprimers topcoated with Desothane HS topcoat, in order to test the adhesion at the topcoat-primer interface.

**2.4.8 MEK double rub test:** The MEK double rub test is a method for determining the extent of curing and drying of coatings. This test involves repetitive rubbing of a coating using cheese cloth dipped in MEK until the coating material is removed from the coating surface. It was carried out on cured formulations according to the ASTM D4752-03 standards. This test is particularly useful for room temperature-cured coatings. It was used here for performance evaluation as well as for characterization studies.

**2.4.9 Pencil hardness test** is a simple and quick way of estimating the extent of cure and drying of a film. Cured films of various compositions are allowed sufficient curing time. In this study, it was 14 days for room-temperature-cured coatings. The test was carried out in accordance with the ASTM D3363-00 standard. This test involves scratching a coating using pencils of increasing hardness. The coatings hardness is indicated by the first pencil which can gouge it. This test is particularly useful for room-temperature-cured coatings.

**2.4.10 Infrared spectroscopy** involves FTIR spectrometers, which record the interaction of IR radiation with a sample, measuring the frequencies at which the sample absorbs the radiation and the intensities of the absorption. Determining these frequencies allows identification of the sample's chemical make-up, since chemical functional groups are known to absorb radiation at specific frequencies. A particular type of bond vibrates or stretches to absorb energy only when exposed to a radiation of a characteristic frequency. However different groups can have

overlapping ranges of excitation frequencies, giving rise to some ambiguity. The intensity of the absorption is related to the concentration of the component. Intensity is generally reported in terms of percent transmittance, the amount of light that passes through it or its counterpart, absorbance. Information about the characteristic excitation frequencies of various groups/bonds can be found from references 25 and 26. Figures 2.8 and 2.9 show the type of vibrational modes for SO<sub>2</sub> and a calculated spectrum for the same, respectively. Figure 2.10 shows an actual IR spectrum for propanoic acid. These images have been obtained from reference 27.

The chemical structures of the various coatings on HDG steel were studied by reflection absorption infrared (RAIR) spectroscopy. The RAIR spectra were obtained by using a Spectrum One FTIR spectrometer from Perkin Elmer, Wellesley, MA. A fixed-angle specular reflectance accessory was used with the incidence angle fixed at 80°. The scanning range was from 4000 cm<sup>-1</sup> to 450 cm<sup>-1</sup> and 64 scans of each film were taken. Figure 2.11 shows the ray diagram for IR measurements using a specular reflectance accessory.

**2.4.11 NMR spectroscopy** is a very valuable tool to characterize in detail the organic chemistry of a liquid or solid system. It is the only technique that can provide detailed information on the exact three-dimensional structure of molecules in solution. In this study, NMR has been used to study the occurrence of various possible reactions between the components of a formulation, both in the uncured liquid state and in the cured, partially cured or dried solid-state. This study complements the IR study and can take care of the ambiguity that can arise from IR spectroscopy in some cases.

Nuclei with an odd atomic number ( $^1\text{H}$ ,  $^{13}\text{C}$ ,  $^{15}\text{N}$ , etc.) have nuclear spin (Figure 2.12). In the absence of a magnetic field these nuclei point in random directions, but in the presence of a magnetic field they will align either parallel or anti-parallel to the magnetic field (Figure 2.13). The parallel orientation is lower in energy. When a nucleus is exposed to the right combination of magnetic field and electromagnetic radiation it flips from parallel to anti-parallel orientation. The absorption of energy required for flipping is detected by the NMR spectrometer. Depending on the environment of a nucleus and the interactions it makes, a specific amount of energy will be required to make it resonant (Figure 2.14). Figures 2.12 – 2.14 were obtained from reference 28.

A NMR spectrometer consists of four parts: magnet, RF generator, detector, and computer. The magnet surrounds the sample, generating a magnetic field of 1-20 Tesla. The RF generator emits a precise frequency of light (radio frequency). The detector (probe) measures sample's absorption of RF energy and the computer analyzes the signal from the detector to produce a spectrum

The variation of nuclear magnetic resonance frequencies of the same kind of nucleus, due to variations in the electron distribution, is called the chemical shift. The size of the chemical shift is given with respect to a reference frequency or reference sample, usually a molecule like trimethylsilane (TMS) with a barely distorted electron distribution. The chemical shift ( $\delta$ ) is usually expressed in parts per million (ppm) by frequency, because it is calculated from:

$$\delta = \frac{\text{difference in precession frequency between two nuclei}}{\text{operating frequency of the magnet}}$$

Since the numerator is usually in hertz, and the denominator in megahertz,  $\delta$  is expressed in ppm. The detected frequencies (in Hz) are usually referenced against TMS, which is given the chemical shift of zero. The operating frequency of a magnet is calculate from the Larmor equation  $\omega = \gamma * B_0$ , explained in Figure 2.13.

$^1\text{H}$ ,  $^{13}\text{C}$ ,  $^{29}\text{Si}$  NMR are some types of NMR spectroscopy used frequently.  $^1\text{H}$  (proton NMR) examines the characteristics of  $^1\text{H}$  (99.9% of the total natural H availability). The number of peaks equals the number of chemically different  $^1\text{H}$ , while the area of the peaks is proportional to the number of  $^1\text{H}$  nuclei absorbing at that particular frequency. The chemical shift indicates the functional groups interacting with that  $^1\text{H}$ , while the splitting of the peaks (the number of smaller peaks a signal is split into) equals the number of other  $^1\text{H}$  interacting with a certain  $^1\text{H}$  minus one.

$^{13}\text{C}$  NMR can be used to study reactions such as epoxy ring opening, condensation with silanols and other reactions involving the C atoms. It examines the characteristics of  $^{13}\text{C}$  (1% of the total natural C availability), with the number of peaks being equal to the number of chemically different  $^{13}\text{C}$  states. The chemical shift indicates the functional groups interacting with that  $^{13}\text{C}$ . Similar is the case of  $^{29}\text{Si}$  NMR which can be used to study silane hydrolysis, condensation and other reactions involving Si atoms. Other advanced techniques include multi-dimensional NMR spectroscopy (2D, 3D, 4D) which allows larger molecules to be studied. Common techniques here include COSY (gives distance through covalent bonds) and NOESY (gives distance through space). More information on the NMR theory and techniques can be obtained from references 29-31.

The NMR equipment at the Chemistry Department of Oklahoma State University was used for these studies. Liquid-state  $^{13}\text{C}$  NMR and solid-state  $^{13}\text{C}$  NMR studies were carried out on various formulations in collaboration with Dr. Tammy Metroke.

Liquid-state  $^{13}\text{C}$  NMR spectra were collected using a Varian Inova 400 MHz spectrometer. Spectra were collected using a Varian broadband probe and a single pulse sequence using a 10.2  $\mu\text{s}$  pulse width with a 3-second pulse delay and 2000 scans. All chemical shifts were referenced to TMS.

Solid-state NMR experiments were performed on dried samples using a Chemagnetics CMX-II 300 MHz (7.06 T) spectrometer. A Chemagnetics triple resonance probe was used for data collection. Resonance frequency for  $\text{C}^{13}$  NMR was 75.6 MHz. All peaks were referenced to an external TMS standard. The spectra were collected using a quasi-adiabatic CP/MAS pulse sequence using a 1 s pulse delay, a 5  $\mu\text{s}$  pulse width, a 1 ms contact time, and 2000-3600 scans. Magic angle spinning was carried out in 5 mm zirconia rotors spinning at 5 kHz. The same samples used for solid-state  $^{13}\text{C}$  NMR studies were subjected to solid-state  $^{29}\text{Si}$  studies. However, the silane content in the formulations studied (10 – 20 wt %) was not enough for detection and the spectra could not be recorded. Hence, solid-state  $^{29}\text{Si}$  NMR has not been used for characterization studies in this work.

**2.4.12 SEM/EDX:** A Philips XL 30 environmental scanning electron microscope (ESEM) was used in this study. This is a flexible scanning electron microscope with a large chamber. It can be

used for conventional high vacuum imaging, or in the environmental mode, can be used to examine wet or non-conducting samples. Samples can be examined in an atmosphere of up to 1.3 kPa of water vapor pressure.

The back-scattered and secondary electron images were complemented by appropriate quantified chemical information from EDX (as point scans or line scans) to achieve mainly two purposes. Firstly, they were used to detect the efficacy of an inhibitor. Coatings with different type and concentrations of inhibitors were scribed and immersed in 3.5 wt% NaCl solution for 30 days. The coatings were then cleaned with running water. The scribe and its vicinity were then observed using SEM/EDX for the presence of corrosion products and corrosion-inhibiting species and their concentrations were studied. Secondly, these studies were also used to analyze the phase separation or stratification in the superprimer, and thereby propose a model of the superprimer. The operating voltage was 25 kV.

**2.4.13 Contact angle measurements** characterize the interfacial tension between a solid and a liquid drop. The technique provides a simple method to generate a great amount of information for surface analysis. This test was also mainly used in characterization studies in order to measure the extent of hydrophobicity of a variety of cured films on HDG. In general, the greater the contact angle, the more the water-barrier property (lower wettability) of the film and corrosion protection imparted by it. A contact angle of greater than or equal to  $90^\circ$  is an indication of total hydrophobicity.

The spreadability of a liquid droplet and hence its shape on a solid surface is governed by the forces at all the interfaces, as given by the Young's equation:

$$\gamma_{SL} = \gamma_S - \gamma_L \cos\theta$$

where  $\gamma_{SL}$  is the interfacial tension between the liquid and the surface,  $\gamma_S$  is the interfacial tension between the surface and the vapor, while  $\gamma_L$  is the interfacial tension between the liquid and its vapor.  $\theta$  is the contact angle. These forces are depicted in Figure 2.15. Contact angle can be measured or calculated by two methods; goniometry and tensiometry. Analysis of the shape of a drop of test liquid placed on a solid is the basis for goniometry. The contact angle in this case is a function of the droplet thickness ( $\sim$  radius), the liquid viscosity and density, apart from surface tension. Hence these variables have to be controlled in order to standardize the measurements and get accurate readings. Also the surface tension values of the liquids that are dispensed have to be provided in order to accurately calculate the contact angle. Tensiometry directly measures the interfacial forces acting at various interfaces in order to calculate the contact angle. Each method has its own advantages and disadvantages. In this study, goniometry was used to directly measure the contact angle from the shape of the droplet and these values were used as a measure of hydrophobicity of the coatings. Surface energy calculations were not a part of this study. More information on these methods can be obtained from reference 32.

Contact angle measurements were performed on a contact angle goniometer VCA2000 manufactured by AST Products, Inc., Billerica, MA. The basic elements of a goniometer include a light source, sample stage, lens and image capture. The contact angle can be assessed directly by measuring the angle formed between the solid and the tangent to the drop surface. A water drop of controlled volume was dispensed on the coated panels from a syringe. Contact angle

measurements were made by analyzing the image of the dispensed liquid drop using the software accompanying the goniometer. The equipment set-up and a screenshot of a water droplet being dispensed are shown in Figures 2.16 and 2.17.

**2.4.14 Chemical resistance:** This test was also mainly used in characterization studies in order to determine the resistance of a coating to 6 N HCl and 6 N NaOH solutions. This is a simple test which involves exposure of a cured coating to these acidic and basic solutions for one day. Deterioration of the coating can be observed as a color change or formation of perforation in the coating. The tests were carried out in accordance with the ASTM D3912 standard.

**2.4.15 Thermogravimetric analysis (TGA)** involves measurement of weight change as a function of time or temperature. Evaluation of fillers, bound water, unbound water, antioxidants, thermal stability, etc., is possible by using this analytical route. In this study this method was used to evaluate the thermal stability of various coatings, in order to study the effect of the type of silane addition, addition of pigments and increase of curing period. As the thermal stability of a coating is dependent on the extent of curing in the coating sample, comparison of thermal stabilities of various samples can give an idea of the extent of various cross-linking reactions (epoxy-amine, siloxane, etc.) in the coating.

The instrument used for the study was TGA 2950 from Texas instruments, Dallas, TX. Three milligrams of the coating film was taken on a platinum pan and studied in a temperature range of 25°C to 350°C with a heating rate of 10 °C /min. The coating samples were also isothermally heated for 5 minutes at 350 °C. The samples were heated in an atmosphere of nitrogen. Figure

2.18 shows the basic principle of a TGA instrument [33]. Figure 2.19 shows a TGA curve for an epoxy adhesive subjected to this study [34]. More information on thermal analysis techniques can be obtained from reference 35.

The next chapter provides an account of the performance evaluation studies and the pertinent results.

## 2.5. References

1. Application notes on EIS, available online at [www.Gamry.com](http://www.Gamry.com)
2. Tait W. S., *An Introduction to Electrochemical Corrosion Testing for Practicing Engineers and Scientists*, Pair O Docs Publications, Racine, WI (1994)
3. Jones D. A., *Principles and Prevention of Corrosion*, 2<sup>nd</sup> edn., Prentice-Hall, New York, NY, (1996) p. 556
4. Murray J. N., *Prog Org Coat*, 30, 225 (1997)
5. Kendig M., J., *Corrosion* 46, 22 (1990)
6. Bonora P.L., Deflorian F., Fedrizzi L., *Electrochim Acta* 41, 1073 (1996)
7. Davis G.D., Dacres C.M., U.S. Patent 5,859,537, January 12, 1999. Davis G.D. and Dacres C.M., U.S. Patent 6,054,038, April 25, 2000. Davis G.D. and Dacres C.M., U.S. Patent 6,313,646, November 6, 2001. Davis G.D., Dacres C.M., and Krebs L.A., U.S. Patent 6,328,878, December 11, 2001
8. Mansfeld F., *Corrosion* 37, 301 (1981)
9. Kendig M., Mansfeld F., Tsai S., *Corros. Sci.* 23, 317 (1983)
10. Kendig M., Scully J., *Corrosion* 50, 527 (1989)

11. Scully J.R., *J. Electrochem. Soc.* 136, 979 (1989)
12. Tait W.S., *J. Coat. Technol.* 61, 57 (1989)
13. Murray J.N., Hack H.P., *Corrosion90*, Paper 140, NACE 1990
14. Grandle J.A., Taylor S.R., *Corrosion* 50, 792 (1994)
15. Meade C.L., *Metal Finishing* 98, 540 (2000)
16. Altmayer F., *Metal Finishing*, 97, 584 (1999)
17. Baldwin K.R., Smith C.J.E., *Aircraft Engineering and Aerospace Technology: An International Journal*, 71, 3, 239-244 (1999)
18. Böhm S., Sullivan J.H., Worsley D. A., *Mat. and Corr.* 52, 540 (2001)
19. Bierwagen G., Tallman D., Li J., He L., Jeffcoate C., *Prog Org Coat*, 46, 149 (2003)
20. Hospadaruk V., Huff J., Zurilla R.W., Greenwood H.T., *Trans. SAE* 87, 755 (1978)
21. Ford Laboratory Test Method, BI-23-1, April 30, 1981
22. Holubka J.W., Chun W., Dickie R.A., *J. Adhes.* 30, 173 (1989)
23. Machu W., Hlawiczka S., *Metalloberfläche* 27, 409 (1974)
24. Zhu D., Van Ooij W.J., *J Adhes Sci Technol* 16, 1235 (2002)
25. Socrates G., *Infrared Characteristic Group Frequencies*, John Wiley & Sons Inc., New York, NY (2001)
26. Coates J., *Encyclopedia of Analytical Chemistry* (Ed) R.A. Meyers, John Wiley & Sons Ltd, New York, NY (2000)
27. *Chemistry 112 Laboratory: Infrared Spectroscopy—An Introduction*, available online at [http://employees.oneonta.edu/kotzjc/LAB/IR\\_Intro.pdf](http://employees.oneonta.edu/kotzjc/LAB/IR_Intro.pdf)
28. NMR lectures by K.D. Bishop, available online at [chemistry.umeche.maine.edu/CHY431/NMR](http://chemistry.umeche.maine.edu/CHY431/NMR)

29. Ibbett R.N. (ed), *NMR Spectroscopy of Polymers*, Chapman and Hall Inc., New York, NY (1993).
30. Bruch M. D. (ed.), *NMR Spectroscopy Techniques*, Marcel Dekker Inc, New York, NY, (1996).
31. Duer M.J. (ed), *Solid-state NMR spectroscopy: Principles and Applications*, Blackwell Science, Ames, IA (2002)
32. Rajagopalan R., Hiemenz P.C., *Principles of Colloid and Surface Chemistry (3<sup>rd</sup> ed.)*, Marcel Dekker Inc, New York, NY, p. 248 (2000)
33. Article on thermal analysis, available online at [www.bolton.ac.uk](http://www.bolton.ac.uk)
34. Article on *Formulating B-Staged Epoxy Adhesives* available online at <http://www.specialchem4adhesives.com/resources>
35. Brown M.E., *Introduction to Thermal Analysis: Techniques and Applications*, Springer, Washington, DC (2001)

### **3. WATER-BORNE BISPHENOL-A SUPERPRIMER - IMPROVEMENTS**

This chapter discusses a part of my work, mainly formulations and results, under the project *Chromate-free coating systems for DoD applications* funded under the Strategic Environmental Research and Development Program (SERDP). This is a four-year project which started in September 2003 and will end in September 2007. I worked on this project for one complete year, viz., 2005. When I started working on this project, 16 months of project time had already elapsed. The focus of the earlier work was on developing a superprimer for AA2024-T3 alloy. A successful water-borne epoxy based superprimer formulation (Table 3.1) which showed 2000 hours of salt spray resistance in the B117 test had been developed and some effective corrosion inhibitors were identified by Trilok Mugada. More information on this work can be found in reference 1.

Now, the focus was to develop a superprimer for hot-dip galvanized steel (HDG) as it is a major material required in many defense applications. The first step was, to try out the earlier superprimer for AA2024-T3 (F6) on HDG. However, this formulation failed on HDG. Figure 3.1 shows the Ford cyclic test result for the formulation F6 on HDG after 15 cycles of exposure (15 days).

The failure of F6 on HDG can be attributed to two major characteristics of the substrate of concern:

- a) *Zinc is more corrosive than aluminum*: The zinc layer on steel works by a sacrificial mechanism. As such it is very susceptible to corrosion. A coating on HDG – a so-called ‘duplex coating’, should subjugate the original corrosion tendency of the zinc layer as well as

the extra corrosion tendency imparted by the galvanic difference between zinc and steel. This, of course, does not mean that the purpose of zinc on steel is defeated. It only means that the services of the zinc layer on steel are delayed. How far these services are delayed determines the efficacy of the coating in question.

- b) *Zinc is a difficult metal to adhere to:* Even in case of successful coupling agents as silanes, zinc can pose adhesion problems. As can be seen in the series shown in Table 3.2, zinc lies in the bottom half of the series on adhesion of silanes with various inorganic substrates [2].

There are ways to overcome these problems. The following methods may lead to better anti-corrosion coatings/superprimers, if incorporated:

- a) *Proper surface treatment of the HDG substrate:* Proper surface treatment is an essential requirement of any substrate to be coated as it serves to improve the wettability of the coating and consequently its adhesion to the substrate. Firstly, in case of the HDG or zinc substrates, both the naturally forming zinc oxide-hydroxide or zinc-hydroxycarbonate layers are very hydrophobic with average liquid penetration contact angles of 88.6° and 86.2° respectively [3]. Also, most manufacturers of HDG provide surface treatment to the substrates, to prevent the formation of wet storage stain. This further increases the hydrophobicity of the substrate and does not provide a suitable anchor to the organic coating. Thus, for any HDG substrate which is older than 24 hours, with or without storage surface treatment, and which has to be provided with an organic coating, a proper surface treatment procedure to remove these hydrophobic layers and provide spreadability and adhesion, is essential. These organic impurities can be removed using

solvents such as acetone and ethanol. Further, mechanical cleaning of the surface using sand-blasting or other means such as scrubbing by use of abrasive material (sand paper or Scotch-brite™) can remove the hydrophobic oxide-hydroxide or hydroxyl-carbonate layers on the substrate.

Secondly, as mentioned in Chapter 1, adhesion of silanes to inorganic substrates, proceeds via hydrogen bonding between the hydroxyls in silanols (Si-OH) and the hydroxyls in the metal-hydroxide (Me-OH). The metallo-siloxane bond is then formed by elimination of water. Thus, a high concentration of metal bonded surface hydroxyls increase the possibility of a dense metallo-siloxane layer and hence superior adhesion of the silane film to the metal. This hydroxyl concentration can be increased by treatment with an alkaline cleaner [4]. Thus if silanes are incorporated in the primer, an alkaline treatment will improve adhesion. However, zinc is amphoteric and an aggressive alkaline cleaner without an inhibitor cannot be used. But the inhibitor may deposit on the substrate and reduce adhesion. These concerns have been addressed in the cleaning procedure followed for HDG substrates in this study and the procedure has been described in Section 2.2 of Chapter 2. The general industrial procedures for cleaning HDG can be obtained from reference 5.

*b) Proper choice of silane:* Silane forms the core component of the superprimer and a judicious choice of the silane ensures an effective superprimer. Firstly, it is advisable to choose a ‘bis’ or a dipodal silane instead of a monosilane, as these silanes form tighter networks and may offer up to  $10^5$  times greater hydrolysis resistance than mono-silanes, making them particularly appropriate for primer applications [2]. Even in the case of bis-silanes, the type of functional

group, the linker length (number of carbon atoms linking the two trialkoxy ends of a di-podal trialkoxy silane) of the silane and hydrolytic stability of the bonds formed (Si-O-Si and Me-O-Si) by that particular silane are very important. Reference 2 gives an account of these factors and their importance while selecting a silane coupling agent. In the silanes used in F6, bis-amino silane for example, had hydrophilic secondary amino groups, which have a tendency to become protonated in the presence of water and the positive charge on these groups attract detrimental ions like  $\text{Cl}^-$ ,  $\text{SO}_4^{2-}$ , etc., which accelerates corrosion of the metal substrate [6]. Further neutron reflectivity studies of bis-amino silanes films confirmed that they are very hydrophilic and tend to degrade in the presence of boiling water [7]. The same studies with bis-sulfur films showed that they are hydrophobic, more resistant to the action of boiling water and seem to show reconstruction of the siloxane and metallo-siloxane bonds upon drying.

c) *Incorporation of cross-linker and catalyst:* Formulation F6 did not have any cross-linker, neither for the epoxy resin nor for the silanes. The type of cross-linkers for epoxy resins and their importance in forming a densely cross-linked film with increased water and solvent barrier properties has been discussed in Chapter 2. Cross-linkers (hardeners) for binder resins are an indispensable part of any primer formulation. Catalysts for cross-linking silanes are mainly tin compounds such as dibutyltin dilaurate (DBTL), dibutyldiacetoxin, or titanates such as titanium propoxide or tertiary amines such as benzyldimethylamine. They accelerate the cross-linking between the silanols or silanols and metal-hydroxyls especially in room temperature curing [8]. These catalysts for silanes are of special importance in water-free environments but can also be of significance in water-borne coatings. However, they need to be added in low concentrations, as they can affect topcoat adhesion and chemical resistance of the coatings.

- d) *Using an epoxy with higher reactivity:* As mentioned in Chapter 2, the epoxy equivalent weight of an epoxy resin determines its reactivity and the extent of cross-linking achievable through hardener addition. In formulation F6, the epoxy resin used EPI-REZ 3540-WY-55 has a higher EEW of 1600-2000, which means lower number of end epoxy groups per gram of the resin dispersion and lower potential for cross-linking via epoxy ring-opening when a curing agent is added. If this epoxy resin dispersion can be replaced by another resin with lower EEW, more cross-linked films can be achieved. However, the EEW of the epoxy resin should not be too low, as the high reactivity can lead to low pot lives (time to gel) of the primer formulations.
- e) *Curing temperature:* A high curing temperature usually leads to better films. The high temperature drives out water from the formulation and accelerates curing reactions. Even for some types of silanes, like the bis-sulfur silane, high curing temperatures of 180°C, which was used in these studies, can lead to resilient films as confirmed by the neutron reflectivity studies mentioned above in reference 7. However, this may not be the case for every silane, as the same studies with bis-amino films showed no improvement in high-temperature-cured bis-amino films. In certain cases there may be side reactions like porosity formation due to excess release of volatile matter from the coating upon heating or any associated decomposition or degradation reactions at the high temperature. A high curing temperature may not be feasible from a substrate point of view. For example, in case of AA2024-T3, curing at high temperatures can lead to a change in morphology and concentration of the intermetallic  $\text{Cu}_2\text{Al}$  precipitates and this can alter the mechanical properties of the substrate which may be undesirable. However, in the case of HDG, the higher curing temperature is not of concern from this point of view. So, depending on

the equipment availability, economic feasibility and the type of coating desired, a high-temperature cure can be chosen to achieve improved coatings.

Severall of the above mentioned routes were tried on various superprimer formulations in this study. The work carried out in this project over the past year can be divided into five steps:

*Step 1:* Modifying and improving the F6 formulation to make it compatible with the HDG substrate

*Step 2:* Search for low-VOC high performance systems – epoxy and cross-linker combinations

*Step 3:* Search for compatible minor binders, silanes, inhibitors, zero-VOC solvents and catalysts for superprimers on HDG

*Step 4:* Taguchi optimization – for optimized room-temperature-cured or room temperature+ high-temperature-cured superprimers

*Step 5:* This step continues simultaneously with the above four steps. It includes characterization of various coatings – individual components, simple mixtures as well as complete superprimer films using SEM/EDX, NMR, MEK double rub, contact angle, EIS and TGA

The first three steps are described in this chapter, while Chapter 4 presents step 4 and Chapter 5 discusses step 5.

### **3.1 Step 1: Modifying and improving formulation F6 to suit HDG substrate**

The first task of improving the F6 formulation was attempted from the resin and cross-linker and the curing temperature perspective. Firstly, 10% of a water-dispersible epoxy-amine adduct

cross-linker, EPIKURE 8290-Y-60 was added to the F6 formulation and named F6+10%8290. Further, the higher-EEW EPI-REZ 3540-WY-55 epoxy resin was substituted in two formulations with two lower-EEW resins, namely DPW 6520 and EPI-REZ 5522-WY-55 (Table 2.1). In brief, three modified formulations were made and tested along with F6. They were:

1. *F6* : The original formulation made earlier for AA2024-T3
2. *F6 + 10% 8290*: F6 formulation with 10% by weight of EPIKURE 8290-Y-60 added
3. *5522 substituted F6 + 10% 8290*: The above formulation with the low-EEW EPI-REZ 5522-WY-55 substituting the original EPI-REZ 3540-WY-55 epoxy dispersion.
4. *DPW 6520 substituted F6 + 10% 8290*: The second formulation above with the low-VOC, higher-EEW epoxy dispersion DPW-6520 substituting the original EPI-REZ 3540-WY-55 epoxy dispersion.

The formulation and coating procedure for all the coating formulations was the same as for F6. However, the curing conditions were varied, with the formulations being cured at 60°C for one hour followed by curing at 150°C for another hour. These step-curing conditions were used as a high curing temperature drives the epoxy-amine curing reactions to completion. However, to avoid possible thermal-shock and fissures in coatings, a step-cure is advisable. Curing at 60°C may also increase the extent of silane hydrolysis as the water present in the formulation does not evaporate-out at this temperature. The local low-frequency impedance curves for the above mentioned formulations in the ASTM B 117 and Ford APGE tests are shown in Figure 3.2. The images of formulations 2, 3 and 4 after 56 cycles of exposure in the Ford test are shown in Figure 3.3, while the images of formulations 1, 2, 3, 4 exposed to ASTM B117 test are shown in Figure

3.4. In the latter figure, the image of formulation 1 is shown after only 23 days (552 hours) of exposure, because it already had started to chalk throughout the coating surface by this time. The rest of the formulations performed quite well even after 2000 hours of exposure. The general trend seen in these two tests is  $1 \ll 2 \sim 4 < 3$  (worse to better). Figure 3.5 shows the Hawaii outdoor exposure test results for topcoated formulations 1, 2, 3 after 178 days of exposure. The formulations were topcoated with the gray polyurethane topcoat, Desothane HS, before subjecting them to the high temperature cure. These results include the low-frequency impedance curves and the images of the exposed panels. All the three images of the panels look good, with minimal scribe creep or corrosion. However the impedance curve drops most rapidly for formulation #1, with formulation #3 again slightly outperforming formulation #2, confirming the effect of the cross-linker and advantage of the lower EEW resin (5522-WY-55) over the higher-EEW resin, EPI-REZ 3540-WY-55. Figure 3.6 compares the three test: ASTM B117, Ford AGPE and Hawaii outdoor exposure for formulations 1,2 and 3. Formulation 4 could not be tested because of lack of HDG panels at that time. All the three formulations confirm the same trend of aggression in the tests, i.e., Ford > B 117 > Hawaii outdoor exposure.

### **3.2 Step 2: Search for low-VOC, high-performance systems**

The above modifications mentioned in step 1 gave outstanding improvement in performance. However, the cross-linker utilized EPIKURE 8290-Y-60 had a substantially high VOC level (~856 g/L). Also, one of the substitute epoxy dispersions, EPIKURE 5522-WY-55, was a bit on the higher side of the VOC levels (~170g/L). So, a combination of water-borne epoxy dispersion and cross-linker was needed which had low VOC levels but would deliver the same improved performance as its predecessor. DPW 6520 epoxy (used earlier in step 1; VOC ~ 70g/L) and

DPC 6870 epoxy-amine adduct cross-linker (zero-VOC), together known as the NEW-GEN systems™, were chosen. Calculated VOCs of some resins, silanes and cross-linkers are shown in Table 3.3.

Although the epoxy:amine stoichiometric ratio of DPW 6520 and DPC 6870 was 70:30, combinations of the two components in various ratios ranging from 90:10 DPW 6520: DPC 6870 to 50:50 were formulated and subjected to various tests. A concentration of DPC 6870 between 20 and 35% gave reasonably good results in all the tests. The test results are summarized in Table 3.4.

It is advisable that coating stoichiometry be based on intended end uses and not always stick to the theoretical stoichiometric ratio, since a wide variety of performance properties may be obtained through variation of the epoxy-to-hardener ratio. For example, the theoretical stoichiometric ratio for EPI-REZ 5522-WY-55 and EPIKURE 8290-Y-60 is 80:20. However, the effect of the deviation from this ratio on various performance attributes is shown in Figure 3.7. These important, interesting plots have been obtained from the technical data sheet for EPI-REZ 5522-WY-55 [9]. The glass transition temperature ( $T_g$ ) for epoxy-amine mixtures is highest at the stoichiometric ratio indicating the cross-link density of the film. The increase in  $T_g$  of various epoxy-amine mixtures with increasing curing temperature indicates the effect of curing temperature in driving the curing reaction to completion. Also an increase in amine content directly leads to increased water saturation levels and water diffusion coefficients. This is due to the polar nature of amine groups and water. The amount of water absorbed or diffusing through the film can also have an effect on the leaching rates of inhibitors in these films. The effect of

epoxy-amine ratio on the microstructure, water absorption and cross-link density of films and the significance of curing temperatures can be obtained from references 10 – 12.

### **3.3 Step 3: Silanes, minor binders, inhibitors, co-solvents and additives**

This section presents a collation of various experiments which show-case the effect of addition a few silanes, minor binders, inhibitors, co-solvents and additives. These experiments were carried out individually at different times and were not a part of a single planned study. Hence, a systemic comparison between all the formulations is not available. However, the levels of each component were based on preliminary EIS studies, all of which have not been presented here. Only a few salient formulations which show the advantage offered by incorporation of a particular component individually in the coating formulations are presented here. Optimization of the levels of each component is presented in Chapter 4. A larger, more comprehensive and systematic comparison using the MEK double rub, contact angle and chemical resistance tests is presented in Chapter 5.

#### **3.3.1 Silanes**

As mentioned before silanes are the cornerstone of this study. Apart from their major contribution of providing adhesion to the substrate as well as to the topcoat, a silane can also improve other properties like hydrophobicity (water-barrier), solvent resistance, hardness and abrasion resistance. The presence and extent of these improvements depends on the choice of the silane. Bis-amino silane, although very effective as a pretreatment under primers, was phased out from the study due to the negative neutron reflectivity reports [7] and its tendency to attract detrimental anions [6]. Bis-sulfur silane has been used successfully in many superprimer

formulations studied so far and had positive neutron reflectivity reports [7]. It was one of the silanes incorporated in this study. Bis-benzene silane, a non-functional organosilane has been shown to form highly hydrophobic pretreatments via immersion and electrodeposition [13]. This was another silane which was used in this study and the results, as will be shown below, were very encouraging. Suryanarayanan and Van Ooij [14], had shown that a combination of a hydrolyzed silane and a non-hydrolyzed silane gives the best performance in a solvent-borne epoxy-isocyanate system on HDG. To test whether the same effect is observed in a water-borne epoxy-amine primer system, it was decided to try a hydrolyzed silane in one of the superprimer systems. As the bis-amino silane was ruled out, a substitute was being searched. Zhu et al. had created stable hydrolyzed solutions of BTSE silane in water (unpublished) and had used them successfully as pretreatments on AA 2024-T3. Thus, hydrolyzed BTSE was finalized upon as the third silane to be tried out in this study. Shown below are some results of experiments with superprimer systems with the above three silanes incorporated individually into the systems.

**a) Bis-sulfur silane**

The formulations compared in this experiment were:

Formulation	DPW 6520 [g]	DPC 6870 [g]	Bis-sulfur [g]
Formulation A (no bis-sulfur)	7	3	
Formulation B (with bis-sulfur)	7	3	2

The components were mixed using a spatula till they became homogeneous. They were then applied onto the cleaned HDG metal panels using a draw-down bar of 28  $\mu\text{m}$  and cured at room temperature for 14 days. Table 3.5 gives the contact angle and MEK double rub values of both the formulations. For both the tests, we can see that values are substantially higher for

formulation B. This shows the improved resistance against water penetration viz., the contact angle increase) and solvent action viz., MEK resistance that addition of bis-sulfur silane provides to the epoxy primer.

Figure 3.8 and 3.9 show two EIS Bode plots: for formulation A and formulation B on day 0 and day 30 of the test, respectively. We can clearly observe that the low-frequency impedance values for both day 0 and day 30 are higher by decades for formulation B vis-à-vis formulation A. This result again underscores the improved water-barrier property and hence increased corrosion resistance that bis-sulfur silane imparts to the epoxy primer.

**b) Bis-benzene silane**

The formulations compared in this experiment were:

Formulation	DPW 6520 [g]	DPC 6870 [g]	Bis-benzene [g]
Formulation A (no bis-benzene )	8	2	
Formulation B (with bis-benzene )	8	2	2

The components were mixed using a spatula until they became homogeneous. They were then applied on the cleaned metal panels using a draw-down bar of 28 µm.

The coatings were then cured at one of the three different conditions:

- Cure I: Step curing: curing in an oven at 60 °C for 1hr, followed by 150 °C for 1hr
- Cure II: Room temperature (RT) curing for 14 days
- Cure III: RT curing for 14 days + curing at 150 °C for 10 minutes

The results of various performance evaluation tests are shown in Figure 3.10 and Tables 3.6 and 3.7. The improvement in performance with the incorporation of bis-benzene is obvious in each test.

The low-frequency impedance is, largely, a measure of the extent of corrosion reaction undergoing underneath the film, at the film-metal interface. The higher the low-frequency impedance, the more resistant to corrosion the metal is. In the EIS Bode plots shown here, we can see that the low-frequency impedance is very low for the film without the silane vis-à-vis the film with the silane. This reinforces the positive effect on corrosion resistance that incorporation of the silane imparts to the film.

After 35 days of EIS testing, the EIS cylinders were removed from the panels, cleaned in running water to remove deposited salt, if any, and their images were taken, which are shown along with the Bode plots in Figure 3.10. If we observe the two panels, we can notice significant discoloration of the panel having the coating without any silane. This discoloration is due to the water absorbed by the film and the corrosion reaction going on underneath the film. The absence of this discoloration in the silane-incorporated film confirms the minimal water absorption and corrosion.

As explained in the test procedure for the MEK double rub test, this test is an indication of solvent resistance and extent of curing of the coating. The higher the MEK double rub value, the higher is the solvent resistance and cure of the coatings. We can observe in the table that the MEK double rub values are higher for the formulation with the bis-benzene silane at both room temperature and high temperature curing compared with the formulation without any silane.

Further, the increase in MEK double rub value is very high in case of the bis-benzene incorporated formulation, indicating the positive effect that bis-benzene has on the curing of the superprimer, especially at high-temperature curing.

The significance of the pencil hardness test has been mentioned earlier. The bis-benzene-incorporated superprimer shows a high degree of hardness for both room temperature and high temperature curing. Coating hardness not only measures the extent of cure, but is also an important mechanical property and many an application requires the coating to possess hardness greater than or equal to a certain specified level, depending on the application. Generally, the higher the hardness, the better it is.

Thus in brief, the incorporation of bis-benzene in epoxy primers leads to increased barrier property, i.e., increased low-frequency impedance in EIS, increased curing and solvent resistance i.e. MEK double rub test and hardness and increased hydrophobicity, i.e., increased contact angle with water.

### **c) Hydrolyzed BTSE**

The formulations prepared for this study are shown in the table below. The hydrolyzed BTSE was prepared by taking a 1:1 vol/vol mixture of water and BTSE and subjecting the mixture to stirring on a magnetic stirrer for 3 days at 300 rpm. The components should be added in the order mentioned above. They were mixed vigorously using a spatula until they became homogeneous. They were then applied on the cleaned metal panels using a 28  $\mu\text{m}$  draw-down bar. All the formulations were cured at room temperature for 14 days.

Formulation	DPW 6520 [g]	hydrolyzed BTSE [g]	Water [g]	Pigments	DPC 6870 [g]
Formulation 1 (Commercial control)	A commercial non-chromated alkyd based primer – Devguard 4651				
Formulation 2 (without hydrolyzed BTSE)	8		1.5	1 g phosguard + 0.25 g titania + 0.25 g mica	2
Formulation 3 (with hydrolyzed BTSE)	8	2		1 g phosguard + 0.25 g titania + 0.25 g mica	2

The Machu test results shown in Figure 3.11 are obvious. Formulation 1 (commercial control) and Formulation 2 (control without silane) show either scribe and edge delamination and significant amount of white rust. However, the superprimer with hydrolyzed BTSE does not show any delamination and white rust, indicating the superior adhesion and anticorrosion properties of the hydrolyzed BTSE-based superprimer.

Thus, in brief, the incorporation of hydrolyzed BTSE in an epoxy primer greatly improves the adhesion of the primer to the substrate and hence its overall protection against corrosion. It also seems to improve the dispersion of the pigments in the coating, which can be noticed in the difference in appearance of coatings 2 and 3.

Thus the three silanes: bis-sulfur, bis-benzene and hydrolyzed BTSE improved the corrosion resistance of water-borne epoxy primer films when incorporated individually in the superprimer formulations.

### 3.3.2 Minor binders

The possibility of interactions between different classes of binders was the reason behind the incorporation of 'minor binders', i.e., binders in less than 10% of the total formulation weight; epoxy dispersions were the major binders used throughout this study. The minor binders tried out were all low-VOC resins. Only the results of incorporation of water-borne polyurethane and acrylate dispersions are shown here. The possible reactions between these binders and the epoxy and silane components are shown in Chapter 5. Two other minor binders tried out were vinylidene-di-chloride-acrylic copolymer, which purportedly reduces oxygen and water permeability, and water-dispersible long-chain alkyds in order to exploit the possible reaction expected between C=C in the alkyd and the bis-sulfur silane. However, the former drastically increased the hydrophilicity of the superprimer showing a reduced contact angle with water and the formulations with the latter (alkyd) failed to cure at both at room temperature and high temperature conditions. Hence systematic studies of these binders were not carried out and their results are not discussed here.

A point to be noted here is that in formulations involving the use of the polyurethane and polyacrylate minor binders, an additional water-borne dispersion, Ancarez AR 550 is incorporated. This dispersion is involved because, unlike DPW 6520, this dispersion does not gel with the aforementioned minor binder. DPW 6520 shows instantaneous gelling when either of the two dispersions are added to it. But the former epoxy dispersion is of a higher EEW and has a tendency towards foaming and hence is not a good choice to use as the sole epoxy binder in a formulation. So, in formulations involving polyurethane and polyacrylate minor binders, a combination of the epoxy dispersions Ancarez AR550 and DPW 6520 was used. The minor

binder was first added to Ancarez AR550. This mixture is then added to DPW 6520 and no gelling was observed. Chapter 5 attempts to explain the difference in behavior of these two dispersions.

The coating formulations prepared for this experiment are shown below. All the ratios are in weight (grams of each component). The components should be added in the order mentioned as mentioned in the table below. They were mixed using a spatula until they became homogeneous. They were then applied on the cleaned metal panels using a 28  $\mu\text{m}$  draw-down bar. All the formulations were step-cured: 60 °C for 1 hour, followed by 1hour at 150 °C. Such step-curing will reduce the thermal shock and the consequently spalling which may be induced in a coating.

Formulation	Ancarez AR 550 [g]	Neo-Rez R 972 [g]	ECO-CRYL 9790 [g]	Bis-sulfur [g]	Surfynol MD 20	DPW 6520 [g]	DPC 6870 [g]
Formulation 1 (simple bis-sulfur based)				10		80	20
Formulation 2 (with polyurethane)	35	10		10	0.05 ml	30	20
Formulation 3 (with polyacrylate)	35		5	10	0.05 ml	30	20

Formulations 2 and 3 have very low VOC ~ 35 g/L. Figures 3.12, 3.13 and 3.14 show the EIS bode plots for formulations 1, 2 and 3 respectively for days 1, 3 and 10. We can see the average higher impedance value for formulations B and C vis-à-vis formulation A, indicating the improved water-barrier property and subsequently anti-corrosion tendency of superprimers with the inclusion of polyurethane or polyacrylate dispersions as minor binders. The addition of these

minor binders also necessitates the addition of Ancarez AR 550 epoxy dispersion, as this obviates the instantaneous gelling tendency observed when NeoRez R-972 or ECO-CRYL 9790 is directly added to DPW 6520. Addition of a defoamer is advisable while including Ancarez AR 550, as it is susceptible to foaming. Surfynol MD 20 is appropriate for this purpose.

### **3.3.3 Inhibitors**

The various commercially available non-chromate inhibitor pigments have been discussed briefly in Chapter 1. In this study the focus was on a class of inhibitors which have the potential to be effective on HDG, namely phosphates (zinc phosphate - ZP), molybdate (calcium zinc molybdate - CZM), vanadates (sodium meta-vanadate), cerium-based pigments (cerium-exchanged silica – Ce Silica) and synergistic combinations of these such as the commercially available Corrostain 228 – corrostain, and other combinations of the aforementioned inhibitors. Equations describing the probable mechanism of their protective action are presented in Chapter 5.

The formulations made for this study with inhibitors are shown in the table below. In the formulations shown in the table, Formulations 1 and 2 were step cured: 60 °C for 1 hour, followed by 1 hour at 150 °C. Formulations 3-6 were also step cured: 14 days at RT followed by a 10 minute curing at 150 °C. The components should be added in the order in which they appear in the table. They were mixed using a spatula until they became homogeneous. When pigments are present, especially hard-to-disperse pigments like titania, it is advisable to use shear blender for mixing, as it will aid the dispersion of the pigments. However, in this experiment, the

formulations were not shear-blended as the shear-blender in our lab was non-functional at that time. They were then applied on the cleaned metal panels using a 28 µm draw-down bar.

Formulation	DPW 6520 [g]	Bis-sulfur [g]	Water [g]	Pigment Comp 1 [g]	Pigment Comp 2 [g]	Pigment Comp 3 [g]	DPC 6870 [g]
Formulation 1 (control 1 - without any inhibitor)	16	2	1				4
Formulation 2 (with 15% CZM)	16	2	2	3 CZM			4
Formulation 3 (control 2 – without any inhibitor)	16	2	1				4
Formulation 4 (10% Corrostayn 228)	16	2	2	2 Corrostayn	0.5 titania	0.5 mica	4
Formulation 5 (5% Cerium-exchanged silica)	16	2	2	1 Ce silica	1 titania	1 mica	4
Formulation 6 (a mixture of three inhibitors)	16	2	2	1 Ce silica	1 Corrostayn	1 ZP	4

Figures 3.15 and 3.16 shows the images of the various pigmented formulations on HDG exposed to the salt fog test. Notice the condition of the scribe in each of the formulations. Comparing formulations 1 and 2, we can see that due to the presence of CZM in formulation 2, it does not show white rust as seen in formulation 1. Unlike formulation 3, formulations 4, 5 and 6 do not exhibit any scribe creep or due to the inhibitors present in them.

Thus, we have found inhibitors which work either individually or in combination with other inhibitors. These inhibitors are: Corrostayn 228, Molywhite CZM, zinc phosphate (Phosguard) and cerium-exchanged silica. However, the last one shows a tendency towards blistering, as the silica particles are hydrophilic. The presence of fillers like titania (Tronox Rf-K-2) and mica

(Alsibronz 06) increase the barrier effect of the film and also improves its hiding power. The presence of titania suspension (nanoactive S) increases the hiding power of the film as well as aids pigment dispersion in the primer formulation.

### 3.3.4 Co-solvents

Zero-VOC co-solvents, apart from water, are an intrinsic part of any low-VOC formulations. They not only act as a carrier medium, but also serve in aiding rheological changes and evaporation rate. The viscosity and drying time of the formulations can be modified (increased or decreased) by using an organic co-solvent. They can also serve in prolonging the pot-life of the formulation. Two zero-VOC solvents, namely acetone and Archer RC have been tested in this experiment. The formulations prepared for this experiment are shown in the table shown below. The components should be added in the order mentioned. They were mixed vigorously using a spatula until they became homogeneous. They were then applied on the cleaned metal panels using a 28  $\mu\text{m}$  draw-down bar. All the formulations were cured at room temperature for 14 days.

Formulation	DPW 6520 [g]	Bis-sulfur [g]	Water [g]	Acetone [g]	Archer RC [g]	Pigments	DPC 6870 [g]
Formulation 1 (with acetone and water)	16	2	1	1		3 g ZP + 1 g nano titania suspension	4
Formulation 2 (with only water)	16	2	2			3 g ZP + 1 g nano titania suspension	4
Formulation 3 (with water and Archer RC)	16	2	1		1	3 g ZP + 1 g nano titania suspension	4

Figures 3.17 and 3.18 show the low-frequency impedance curves and images of the co-solvent included superprimers coated onto HDG, along with the only water-based control. As can be seen from the B117 plots and images, the substitution of water with an organic co-solvent such as acetone or Archer RC does not deteriorate the performance of the epoxy films as we do not observe any significant difference in the impedance curves and scribe conditions. Further the addition of the organic co-solvent facilitates the manipulation of the primers rheology, making the primer more workable. For example, the primer can be made less viscous (by adding acetone) or more viscous (by adding Archer). If pigments are added to the system, the co-solvent can aid their dispersion (acetone) or prevent settling (Archer). Also, the room temperature drying of the superprimer can be accelerated by addition of an organic co-solvent (acetone). There are many other promising co-solvents, VOC exempt or otherwise, which can offer similar advantages and can be compatible with an epoxy-based superprimer. Some examples include solvents such as p-chlorobenzotrifluoride (obtained as oxsol-100 from Kowa Chemicals, Japan), 2-butoxyethanol, or a mixture of these. In the formulations, the presence of NanoActive S, nano titania suspension does not only act as pigmenting additive. It provides more water to the pigmented primer system and also seems to aid the dispersion of the other.

In brief, two co-solvent + water-based superprimer systems have been demonstrated to provide equivalent corrosion resistance properties as the water-based superprimer. The two solvents (in fact co-solvents) are zero-VOC solvents. Their use provides superior workability vis-à-vis a water-based superprimer and also can provide a control over the primers curing or drying rate.

### 3.3.4 Cross-linker for silanes – DBTL

As has been mentioned before, catalysts for cross-linking silanes accelerate the cross-linking between the silanols and also between silanols and metal hydroxyls, especially in room temperature curing. In this experiment a tin-based catalyst dibutyltindilaurate (DBTL) has been tested for cross-linking capability and its adverse effect on corrosion resistance imparted by the superprimers, if any. The formulations prepared for this experiment were:

Formulation	DPW 6520 [g]	Bis-sulfur [g]	Water [g]	DBTL	Pigments	DPC 6870 [g]
Formulation 1 (control – without DBTL)	16	2	2		3 g ZP + 1 g nano titania suspension	4
Formulation 2 (with DBTL)	16	2	2	0.2 ml	3 g ZP + 1 g nano titania suspension	4

The components should be added in the order mentioned above. They were mixed using a spatula until they became homogeneous. They were then applied on the cleaned HDG metal panels using a 28  $\mu\text{m}$  draw-down bar. The formulations were cured for 14 days at room temperature.

As seen in Table 3.8, we observe an increase in film hardness with the addition of DBTL, which is an indication of the extent of cross-linking. Superprimers with and without DBTL coated onto HDG and subjected to ASTM B117 test for 1350 hours are shown in Figure 3.19. From the salt spray images, we can see that the corrosion protection ability of the films is not affected as the scribe conditions (creep and corrosion) are similar for both the panels. In fact, it is slightly better

for formulation 2. Thus, addition of a small amount of DBTL to a room temperature-cured water-borne epoxy superprimer increases its hardness without affecting its ability to protect the metal against corrosion.

### 3.3.5 Specialty barrier pigment for superprimers – leafing aluminum paste

Leafing aluminum paste consists of flat or spherical aluminum particles with fatty acid lubricant (for example, stearic acid) layers, which reduce its density enabling the pigment to float and thereby form a layer at the top of the coating. They have been used regularly in topcoat formulations on automotive bodies as opalescent pigments which enhance the appearance. Apart from their cosmetic purposes, leafing aluminum paste provides excellent barrier protection against moisture and oxygen. More information on leafing aluminum paste can be obtained from reference 15.

In this experiment, the effect of incorporation of aluminum paste in superprimers has been tested.

The formulations made for this study were:

Formulation	DPW 6520 [g]	Bis-sulfur [g]	Water [g]	Stapa Hydrolac – leafy aluminum [g]	Pigments	DPC 6870 [g]
Formulation 1 (control – without aluminum paste)	16	2	3		2 g ZP + 0.5 g titania + 0.5 g mica	4
Formulation 2 (with aluminum paste)	16	2	1	1	0.4 g ZP	4

The components should be added in the order mentioned above. They were mixed using a spatula until they became homogenous. They were then applied on the cleaned metal panels using a 28  $\mu\text{m}$  draw-down bar. The formulations were cured for 14 days at room temperature.

Figure 3.20 shows the images of superprimer formulations with and without the leafing aluminum pigment coated on HDG and subjected to 30 days of salt water immersion test followed by the Machu test, which are very aggressive conditions of testing. We can observe that the overall appearance of the formulation 2 is very good. It has a metallic luster and the aluminum paste floats to the surface of the film and increases its barrier property. The presence of zinc phosphate in formulation 2 also provides scribe protection. Aluminum paste as a pigment is much less prone to flocculation vis-à-vis other pigments like zinc phosphate. On the other hand, the control formulation (1), without the pigment shows a lot of tiny blisters throughout the coating. Notice the presence of spots in formulation 1 and their absence in formulation 2. Thus we can see that even in water-borne epoxy superprimers, leafing aluminum paste provides the same advantages as in other superprimers. It provides a metallic luster to the film and significantly increases its barrier property. It can also be combined with corrosion inhibitors and colorants to provide scribe protection to the film and enhance its appearance.

### **3.4 Summary**

The experiments described above have demonstrated that:

- a) Incorporation of the silanes bis-sulfur, bis-benzene and hydrolyzed BTSE improve the anti-corrosion performance of water-borne bisphenol-A superprimers by improving the adhesion and barrier properties of the coatings.

- b) Incorporation of polyacrylate (ECO-CRYL 9790) and polyurethane (NeoRez R 972) water-borne dispersions improve the anti-corrosion performance of water-borne bisphenol-A superprimers by improving the barrier properties of the coatings.
- c) Corrostain 228, cerium-exchanged silica, zinc phosphate and calcium zinc molybdate are effective anti-corrosive pigments for HDG in water-borne bisphenol-A superprimers.
- d) Acetone and Archer RC, when used as co-solvents in water-borne bisphenol-A superprimers, facilitate their processing without adversely affecting its anti-corrosion properties.
- e) DBTL expedites room-temperature curing of water-borne bisphenol-A superprimers and lead to increased hardness without adversely affecting its anti-corrosion properties.
- f) Incorporation of leafing aluminum pigment in water-borne bisphenol-A superprimers, significantly enhances the appearance and barrier property of the coating thereby leading to improved anti-corrosion performance of the coatings.

The next chapter discusses the variables and process used for optimization of low-VOC non-chromated formulations along with comparison studies with chromated systems.

### **3.5 References**

1. Mugada T., *M.S. thesis, University of Cincinnati*, to be published in 2006
2. Arkles B., Larson G. (eds), *Silicon Compounds: Silanes and Silicones*, a product catalogue by Gelest Inc., Morrisville, PA, p 168 (2004)
3. Muster T.H., *Corros. Sci.*, 46, 2337–2354 (2004)
4. Shirai K., *Langmuir*, 18, 6623 (2002)

5. Dunham K.J., *Preparing Hot-dip galvanized steel surfaces for painting and powder coating: a primer*, Metal finishing, 20 (September 2002)
6. Zhu D., *Ph.D. thesis, University of Cincinnati* (2005)
7. Pan G., Schaefer D.W., submitted for publication in the *Silanes and Other Coupling Agents*, Vol 4., K. L. Mittal, eds., 2005, Canada; June 22- 24, 2005
8. Kanan S., *Langmuir*, 18, 6623 (2002).
9. Product bulletin# SC: 1559-01, on Epi-Rez 5522-WY-55 obtained from [www.resins.com](http://www.resins.com)
10. Grave C., McEwan I., Pethrick R. A., *J. App. Poly. Sci.*, 69, 2369 (1998)
11. Vanlandingham M.R., Eduljee R.F., Gillespie Jr J. W., *J. App. Poly. Sci.*, 71, 699 (1999)
12. Meyer F., Sanz G., Eckieza A., Mondragon I., Mijovic J., *Polymer*, 36, 1407 (1995)
13. Chandrasekaran S., *M.S. thesis, University of Cincinnati*, to be published in 2006
14. Suryanarayanan K., *M.S. thesis, University of Cincinnati* (2006 )
15. George W., *Handbook of Fillers - A Definitive User's Guide and Databook*, 2<sup>nd</sup> ed. ChemTec Publishing, Toronto, Canada (2000)

## 4. OPTIMIZED SUPERPRIMER

### 4.1 Background

The previous chapter gave an account of the experiments with various components. After those experiments, a set of chemicals which showed potential was identified under each component, i.e., major binder, minor binder, cross-linker and silane. However, we still did not have exact knowledge as to what the concentration of each component should be in order to achieve optimized performance. This chapter presents optimization of four different types of coating formulations (with the same type of inhibitor) vis-à-vis the first four of the aforementioned five components. Optimization of inhibitors was done using SEM/EDX studies and is presented in Chapter 5. Optimization of coating formulations involves many variables as discussed below.

Firstly, the appropriate performance parameters have to be chosen i.e., we have to set our objectives and expectations from the experimental outcome. Each formulation needs to be subjected to various tests in order to determine the performance attributes of concern. For example, water-barrier property via contact angle test or EIS low-frequency impedance, solvent resistance via MEK double rub test, wet-adhesion of primer or topcoat via tape adhesion tests or Machu test, scribe protection or effective leaching of inhibitor in order to prevent corrosion via salt water immersion test or Machu test etc. In this study, the performance tests utilized were: salt water immersion test, Machu test, EIS, topcoat adhesion test and MEK double rub test.

Secondly, the number of chemicals, i.e., factors to be used in a formulation and the concentrations i.e., levels of each chemical to be considered, have to be decided. The chemicals and their concentrations have to be decided based on prior experience and knowledge about the

system at hand. Some theoretical knowledge and preliminary testing gives an idea of the concentration range of a particular chemical, in which the optimum concentration may be present. In this study some of these preliminary investigations had been presented in Chapter 3. Testing all the possible combinations in each set of factors and levels can give rise to one type of optimized superprimer. In this study four such sets of four factors and three levels have been chosen, which will give rise to four types of optimized superprimers. These then again have to be subjected to final comparative tests to decide the best amongst them. The sets tested were:

- a) Set A - Simple silane-based water-borne epoxy superprimer system – one epoxy + one amine and three silanes. This set is expected to give the optimum combination of silanes in a superprimer. The three silanes and their levels and the epoxy-amine ratios were chosen based on the experiments described in Chapter 3 and prior theoretical knowledge of the components.
- b) Set B - Water-borne epoxy superprimer system with polyurethane and acrylate minor binders – two epoxies + one amine, one polyurethane, one polyacrylate and one silane. This set is expected to give optimum combinations of the two minor binders - polyurethane and polyacrylate. All the levels and components were chosen based on the experiments described in Chapter 3 and prior theoretical knowledge of the components.
- c) Set C - Water-borne epoxy superprimer system with polyurethane minor binder - two epoxies, one amine, one polyurethane, and one silane. This set is expected to give the optimum ratio of the combinations of the two epoxies Ancarez AR 550 and DPW 6520 and also the optimum level of the polyurethane binder in such a system. All the levels and

components were chosen based on the experiments described in Chapter 3 and prior theoretical knowledge of the components.

- d) Set D - Room-temperature-cured water-borne epoxy superprimer system – one epoxy + one amine, another amine, two silanes. This set is expected to give the optimum combinations of the two silanes - bis-benzene and bis-sulfur and the two cross-linkers DPC 6870 (higher levels) and EPIKURE 8290-Y-60 (lower levels taken, as it has high VOC) in a room-temperature-cured system. All the levels and components were chosen based on the experiments described in Chapter 3 and prior theoretical knowledge of the components.

Note: Sets A, B and C were step cured at room temperature for fourteen days followed by a short high temperature cure at 135 °C for thirty minutes, while set D was just room temperature-cured for 14 days. The additional high temperature cure was used in the case of sets A, B and C as it was seen in the previous chapter that such a cure significantly improves the MEK double rub values and contact angles of the coatings, i.e., the barrier property of the coatings are improved.

Finally, the number of formulations to be tested has to be decided. The basic, direct approach will be the full factorial approach, which involves testing all possible combinations of factors and levels. In the sets chosen for this study which involve four factors and three levels, a total of  $3^4$  i.e 81 combinations are possible. If there are more factors and more experiments, then accordingly, it will require testing more combinations. This obviously is a very laborious, expensive and time-consuming approach and in some cases it may be practically impossible to test the large number of total set of samples. A much less expensive and quicker approach involves the statistical routes and fractional factorial design of experiments. Fractional factorial

design is a factorial experiment in which only an adequately chosen fraction of the treatment combinations required for the complete factorial experiment is selected to be run.

The Taguchi approach for fractional factorial design of experiments, developed and pioneered by Genichi Taguchi is a widely used 'off-line quality control method' because it is a method of ensuring good performance in the design stage of products or processes [1]. Taguchi methods allow estimation of the effects and interactions of several factors. Thereby it provides methods for optimization of factors and their levels. Taguchi designs differ from the classical fractional design as he introduced several noteworthy new ways of conceptualizing an experiment that are very valuable, especially in product development and industrial engineering, and of special importance are the concepts of parameter design - to minimize the variation in product quality) and tolerance design, i.e., how, and when, tightened tolerances for a product or a process are to be specified so that quality and performance or productivity are enhanced. He also advocated using inner and outer array designs to take into account two types of factors. The *design factors* or the main factors (inner), which in the case of coatings are the component chemicals, the curing temperature or curing cycle, etc. The *noise factors* (outer), which are the less controllable or uncontrollable factors, for example, in the case of coatings it can be moisture or ambient temperature if the coatings are being cured at room temperature.

In this study Taguchi fractional factorial experiments have been performed using L9 Taguchi orthogonal arrays in order to find the optimum combination of factors (binders, hardeners and silanes) and levels (concentration) of each factor. An orthogonal array is a characteristic mathematical combination of factors and levels used in fractional factorial experiments. Many

types of orthogonal arrays are available and choosing a particular array depends on the complexity of the experiment at hand. L9 orthogonal arrays are used for experiment involving four factors and three levels. Genichi Taguchi published a booklet of design nomograms [2] which may be used as a design guide. Thus, in this study instead of the 81 formulations which have to be tested if the normal full factorial route is taken, only 9 formulations need to be tested when a L9 orthogonal array is used. The L9 orthogonal array specifies which particular 9 of those 81 combinations need to be tested. The L9 orthogonal array presenting those nine combinations of factors (1, 2, 3, 4) and levels (1, 2, 3) is shown in Table 4.1. All the four factors (at the levels specified in each cell) in a row form one specific combination, which has to be formulated and tested.

This study takes a simplified Taguchi approach and thereby is limited to the optimization of factor levels via observation of coating property trends with changing levels of each factor. It neither dwells into the nature and extent of interaction between the factors, nor does it look into the effect of noise factors, if any. Such a simplified approach has been used successfully earlier in similar studies [3,4]. These optimized formulations have been further tested using the ASTM B117 and the Ford test for comparison amongst themselves.

The outcomes are also expected to answer some questions like:

- Is a hydrolyzed silane required in a water-borne superprimer?
- Is a combination of polyurethane and polyacrylate minor binders synergistic or antagonistic?
- If a combinations of silanes is used then what the optimized ratio for that system, what is the optimized ratio of epoxies when two epoxies are used in a system?, and finally,

- What is the optimized epoxy-amine ratio for a system?

Also to be noted here is the fact that all the formulations had 5 wt-% of zinc phosphate inhibitor and 5 wt-% of titania. The pigments were added in order to check the leaching efficiency of the zinc phosphate in each coating formulation. This was indirectly observed by the extent of scribe protection against corrosion in the Machu test and the salt water immersion test.

The factors and levels in each of the four sets, along with their respective orthogonal arrays (OA) are described below:

➤ **Set A – OA1:**

- *Factor 1 (DPW+DPC):* Includes three mixtures of DPW 6520 (DPW) and DPC 6870 (DPC) i.e., three different epoxy-amine stoichiometric ratios. *Level 1:* 8 g DPW + 2 g DPC; *level 2:* 7.5 g DPW + 2.5 g DPC; *level 3:* 6.5 g DPW + 3.5 g DPC
- *Factor 2 (BS):* Three levels of bis-sulfur silane (BS). *Level 1:* 0 g; *level 2:* 1 g; *level 3:* 2 g
- *Factor 3 (1:1 Hydrolyzed. BTSE):* Three levels of hydrolysed BTSE. The hydrolysed BTSE was prepared by stirring a 1:1(v/v) mixture of water and neat BTSE on a magnetic stirrer (300 rpm) for 72 hours. *Level 1:* 0 g; *level 2:* 0.5 g; *level 3:* 1 g
- *Factor 4 (BB):* Three levels of bis-benzene silane (BB). *Level 1:* 0 g; *level 2:* 1 g; *level 3:* 2 g

The OA1 matrix is shown in Table 4.2. All the chemicals, except DPC 6870 were added along with the inhibitor and filler or hiding agent. They were mixed vigorously using a spatula till they

became homogeneous. DPC 6870 was then added and the formulation was again stirred vigorously.

➤ **Set B – OA2:**

- *Factor 1 [(1:1 Ancarez : DPW) + DPC]:* Three different mixtures of two epoxy dispersions (Ancarez AR 550 and DPW 6520 in the ratio 1:1 by weight) and DPC 6870. *Level 1:* 8.5 g of 1:1 Ancarez : DPW + 1.5g OF DPC; *level 2:* 8 g of 1:1 Ancarez : DPW + 2 g OF DPC; *level 3:* 7.5 g of 1:1 Ancarez : DPW + 2.5 g of DPC
- *Factor 2 (ECO-CRYL):* Three levels of ECO-CRYL 9790 (ECO-CRYL) polyacrylate dispersion. *Level 1:* 0g; *level 2:* 0.25g; *level 3:* 0.5g
- *Factor 3 (PU):* Three levels of Neorez R-972 polyurethane dispersion (PU). *Level 1:* 0g; *level 2:* 0.5g; *level 3:* 1g
- *Factor 4 (BB):* Three levels of bis-benzene silane (BB). *Level 1:* 0g; *level 2:* 1g; *level 3:* 2g

The OA2 matrix is shown in Table 4.3. Ancarez, DPW and BB were added along with the inhibitor and filler or hiding agent. They were mixed vigorously using a spatula till they became homogeneous. DPC 6870 and NeoRez R-972 or ECO-CRYL 9790 was then added and the formulation was again stirred vigorously.

➤ **Set C – OA3:**

- *Factor 1 (Anca + DPW):* Three mixtures of Ancarez AR 550 (Anca) and DPW 6520 (DPW). *Level 1:* 4g of Ancarez AR 550 and 4g of DPW 6520; *level 2:* 3g of Ancarez AR 550 and 5g of DPW 6520; *Level 1:* 2g of Ancarez AR 550 and 6g of DPW 6520

- *Factor 2 (DPC):* Three levels of DPC 6870 (DPC). *Level 1:* 1.5g; *level 2:* 2g; *level 3:* 3g
- *Factor 3 (PU):* Three levels of Neorez R-972 polyurethane dispersion (PU). *Level 1:* 0 g; *level 2:* 0.5 g; *level 3:* 1 g
- *Factor 4 (BS):* Three levels of bis-sulfur silane (BS). *Level 1:* 0 g; *level 2:* 1 g; *level 3:* 2 g

The OA3 matrix is shown in Table 4.4. Ancarez, DPW and BS were added along with the inhibitor and filler or hiding agent at 5% of the total formulation weight. They were mixed vigorously using a spatula till they became homogenous. DPC 6870 and NeoRez R-972 or ECO-CRYL 9790 was then added and the formulation was again stirred vigorously using a spatula.

➤ **Set D – OA4:**

- *Factor 1 (5522+DPC):* Three mixtures of EPI-REZ 5522-WY-55 epoxy dispersion (5522) and DPC 6870 (DPC). *Level 1:* 8g 5522 + 2g DPC; *level 2:* 7.5g 5522 + 2.5g DPC; *level 3:* 7g 5522 + 3g DPC
- *Factor 2 (8290-Y-60):* Three levels of EPIKURE 8290-Y-60 (8290-Y-60) water dispersible, solvent based epoxy-amine adduct crosslinker. *Level 1:* 0g; *level 2:* 0.5g; *level 3:* 1g
- *Factor 3 (BS):* Three levels of bis-sulfur silane (BS). *Level 1:* 0.5 g; *level 2:* 1 g; *level 3:* 1.5 g
- *Factor 4 (BB):* Three levels of bis-benzene silane (BB). *Level 1:* 0.5 g; *level 2:* 1 g; *level 3:* 1.5 g

The OA4 matrix is shown in Table 4.5. 5522, BS and BB were added along with the inhibitor and filler or hiding agent They were mixed vigorously using a spatula till they became

homogenous. DPC 6870, and 8290-Y-60 were then added and the formulation was again stirred vigorously.

For all the sets, the formulations were applied on the cleaned HDG panels using a 28  $\mu\text{m}$  draw-down bar. Also, as mentioned earlier, the inhibitor used was zinc phosphate in 5% of the total formulation weight while the filler or hiding agent was titania in 5% of the total formulation weight. Sets A, B and C cured at room temperature for 14 days followed by a short high temperature cure at 135  $^{\circ}\text{C}$  for 30 minutes, while the formulations in set D were cured at room temperature for 14 days. Five replicates of each formulation were made for the five performance tests. As there were a total of 36 formulations in the four sets, a total 180 panels were coated for this study.

## **4.2 Test results and observations**

### **4.2.1 Salt water immersion results**

All the 36 formulations were subjected to the salt water immersion test for 30 days. However, none of the panels showed any scribe corrosion or deterioration during this period of time. Hence this test was not able to differentiate the performance of any of the formulations.

### **4.2.2 MEK double rub test**

All the formulations in the sets A, B and C, which were high-temperature-cured showed excellent MEK double values of  $>300$ . Hence this test was not able to differentiate the formulations in these matrices. However, in the Set D (OA4), in which the formulations were

cured at room temperature, significant differences were observed within the formulations. The MEK double rub values for all the formulations in OA4 are shown in Table 4.6.

### **4.2.3 Machu test**

None of the formulations in the high-temperature-cured matrices OA1, OA2 and OA3 showed substantial scribe corrosion, creep or delamination even when the test was extended to the third day. No deterioration was observed for these panels even in the region away from the scribe. However, all these formulations deteriorated beyond recognition by the end of day 4 of the test. Hence this test did not turn out to be a differentiating test for the formulations in sets A, B and C. Similar results were observed for the room-temperature-cured formulations in the matrix OA4 when the test was conducted for two days. However, when the test was extended to three days, these panels showed substantial deterioration. The images of these panels are shown in Figure 4.1. Based on the extent of delamination, i.e., the amount of delaminated area under the coating and the overall appearance of the coating, each coating was ranked on a scale of 0 to 10. The rankings of each coating in this matrix for this test are shown in Table 4.7.

### **4.2.4 Topcoat – wet adhesion test**

All the formulations were coated and allowed a drying time of 6 hours before the polyurethane topcoat, Desothane HS, was coated over them. The formulations were then allowed to cure according to the curing conditions of the set. After completion of curing, all the topcoated formulations were immersed in DI water for 7 days. They were then subjected to the tape adhesion test. The tests were carried out according ASTM D 3359, test method B, with cross-hatch. Only two of the 36 formulations showed poor adhesion and both of them contained no

silane (formulations 1\_1 and 2\_1). Formulation 1\_1 showed an adhesion of 2B (~25% delamination) and formulation 2\_1, also showed an adhesion of 2B (~25% delamination), however, it was more deteriorated with blisters being observed on the coating surface. Both formulations showed areas of delamination both at the primer-metal and primer-topcoat interfaces. None of the other 34 formulations showed any delamination (adhesion level 5B). These results underline the great role that silanes play in imparting adhesion of primers to both the metal as well as the topcoat. Images of the formulations 1\_1 and 2\_1 subjected to this test are shown in Figure 4.2. Also shown in the same figure is the image of formulation 2\_6 which was subjected to the same test but showed no delamination, similar to the other 33 panels.

#### **4.2.5 EIS test - comparison of low-frequency impedances**

After curing, all the 36 formulations were subjected to an EIS study and their low-frequency impedance was noted before and after immersion in 3.5 wt.-% NaCl for 30 days. The low-frequency impedance is a measure of the water-barrier property of the coating. Bar plots showing the low frequency impedance values of all the coatings in matrices OA1, OA2, OA3 and OA4 are shown in Figures 4.3, 4.4, 4.5 and 4.6, respectively. These test results are analyzed using optimization plots shown in the section below.

#### **4.3 Analysis – optimization plots**

Optimization plots were drawn for analysis of the previous test results. The values obtained were normalized to a scale of 100, with the highest value obtained for the test in matrix being taken as 100 and the other values were scaled accordingly. For example., in case of OA4, a value of 100

was given to low the low-frequency impedance value of formulation 4\_6, as it had the highest value after 30 days and the low-frequency impedance values for other formulations was scaled accordingly. Similarly, the other values for all the tests and formulations were normalized on a scale of hundred. The same level for a factor is present in three formulations of a matrix. This gives rise to three normalized values for each test and factor level. The average of these three test values for a level was calculated and this is the average response of a factor level to a specific test. Then plots were drawn showing the variation of these average response values with the level of each factor. Such plots were drawn for each test on the formulations in matrix and the plots were superimposed. Based on these plots the optimum level for each factor was chosen. The combination of the optimum level of each factor forms the optimum formulation. For OA1, OA2 and OA3 only the 30-day low-frequency impedance values were taken as the differentiating parameter, as the other tests were not able to differentiate them. However for OA4, MEK double rub, 30-day low-frequency impedance and Machu test results were taken as the differentiating parameter. The optimization plots and the deduced optimized formulations for each matrix are shown below.

### **OA1 optimization plots**

As the 30-day low-frequency impedance is the only differentiating parameter in this matrix, all the plots for each factor have been superimposed. The optimization plots are shown in Figure 4.7. The optimized levels for each factor which taken together form the optimized formulation for this set is shown in Table 4.8.

In this case, as there is just one differentiating test, we can directly choose the ‘best level’ for a given factor, i.e., the level with the highest value of average response (for low-frequency impedance). In the optimized formulation for OA1, shown in Table 4.8, we can see that the level of hydrolyzed BTSE is zero, i.e., it leads to the conclusion that there is no requirement of a hydrolyzed silane in a water-borne epoxy superprimer. This is probably due to the large amount of water already present in the water-borne formulation. Thereby, the neat silane (at least a part of it) itself becomes hydrolyzed. However, in a solvent-borne formulation, as there is no intrinsic water, hydrolyzed silane has to be added.

### **OA2 optimization plots**

Again as the 30-day low-frequency impedance is the only differentiating parameter in this matrix, all the plots for each factor have been superimposed. The optimization plots are shown in Figure 4.8. The optimized levels for each factor which taken together form the optimized formulation for this set is shown in Table 4.9.

The optimized formulation deduction route is the same here as was done for OA1. An important observation in this formulation is that the optimized level of PU is zero, i.e., ECO-CRYL and PU are antagonistic and ECO-CRYL aids performance better than PU. This antagonistic behavior was seen while preparing the formulations containing PU and ECO-CRYL. These formulations showed a tendency to form precipitates which had to be vigorously stirred in order to become redissolved into the formulation. Another reason may be a probable strong tendency of phase separation between the two minor binders.

### **OA3 optimization plots**

In this case too as the 30-day low-frequency impedance is the only differentiating parameter in this matrix, all the plots for each factor have been superimposed. The optimization plots are shown in Figure 4.9. The optimized levels for each factor which taken together form the optimized formulation for this set is shown in Table 4.10

### **OA4 optimization plots**

In this matrix, as there are three differentiating parameters, the average response vs factor level plot for each factor have been drawn separately. Here , the optimized level for each factor is the level which shows good value of average reponse for each test (not necessarily the best value). The optimization plots for each factor in OA4 is shown in Figures 4.10 (a) - 4.10 (d). The optimum formulation is shown in Table 4.11.

The four optimum formulations are summarized in Table 4.12. These four optimum formulations were subjected to the ASTM B117 and the Ford cyclic test. Also subjected to the same tests were chromated controls. All the formulations subjected to these two tests along with the results shown in the next section.

## **4.4 ASTM B117 and Ford tests - comparisons between optimized formulations and controls**

I) *Optimized formulations subjected to these two tests:*

Optimum formulations with and without Topcoat: *OA1opt, OA2Opt, OA3opt, OA4opt*, i.e., the four optimized formulations show in Table 4.12 subjected to curing conditions used in that

matrix, without any topcoat; and *OA1opt-TC*, *OA2Opt-TC*, *OA3opt-TC*, *OA4opt-TC*, i.e., optimized formulations with topcoat. The polyurethane topcoat Desothane HS was applied after the primer was allowed a drying time of 6 hours. The primer along with the topcoat was then allowed to cure at the curing conditions used in that matrix. All these formulations had 10 wt-% of Corrostatin 228 and 1 wt-% of sodium meta-vanadate. As will be shown in Chapter 5, this combination of inhibitors shows the best inhibitive action of all the inhibitors tested for this study.

## II) *Chromated controls*

- i. *BP*: Solvent-borne chromated epoxy primer on bare HDG. BP stands for bare HDG+ control primer.
- ii. *BPT*: Desothane HS polyurethane topcoat on solvent-borne chromated epoxy primer on bare HDG. BPT stands for bare HDG + control primer + topcoat
- iii. *CP*: Solvent-borne chromated epoxy primer on chromated-HDG. i.e., HDG having a chromate conversion coating. CP stands for chromated HDG + control primer
- iv. *CPT*: Desothane HS polyurethane topcoat on solvent-borne chromated epoxy primer on chromated- HDG. CPT stands for chromated HDG + control primer + topcoat.

In brief, six panels, four optimum formulations and two controls, with and without topcoat were subjected to ASTM B117 and Ford cyclic tests. Figures 4.11 and 4.12, shows the images of formulations with and without topcoat respectively, after they had been subjected to 2000 hours, in fact, 86 days which equals 2064 hours of the B117 test, while Figures 4.15 and 4.16 show the corresponding low-frequency impedance curves. Similarly, Figures 4.13 and 4.14, shows the

images of formulations with and without topcoat respectively, after they had been exposed to 59 cycles of the Ford cyclic test, while Figures 4.17 and 4.18 show their corresponding low-frequency impedance curves.

Observation of the B117 test images for both the topcoated and non-topcoated formulations, indicate similar level of anticorrosive performance provided by the four optimized formulation vis-à-vis the chromated epoxy-polyamide control primer. The performance of the chromated controls, both with and without the chromate pretreatment, is excellent, as expected. The high organic solvent content (VOC = 340 g/L) in the control provides the resistance against water penetration, because water is polar while organic solvents are predominantly non-polar. Further, organic solvents dissolve the binders well and increase coalescence, thereby forming better films. Simultaneously, the high amount of the highly effective strontium chromate inhibitor (upto 30 wt.-%) in it provides active corrosion protection as confirmed by the clean scribes. However, the four low-VOC non-chromated optimized primers with Corrostain 228 and sodium meta-vanadate also show minimal scribe corrosion, and none of these formulations show any blistering or delamination, neither near scribes nor within the coating area.

The Ford test images of the topcoated and non-topcoated coatings again reveal the same conclusions. However, as the Ford test is more aggressive vis-à-vis the B117 test we do see some substantial amount of white rust in the scribes in both the optimized coatings and the controls, with the controls performing slightly better than the rest. Only the OA1opt formulation has started showing some signs of red rust (corrosion of the steel beneath the zinc layer). However,

none of the formulations show much delamination or blistering. Table 4.13 summarizes some of the performance attributes of the optimized superprimers and the control primer.

The low-frequency impedance curves, especially of the non-topcoated optimized formulations and more specifically the B117 curves, seem to be indicating that the controls are much better than the optimized ones, as the impedance drops much faster for the latter than the former. However, here, we need to understand the meaning of the low-frequency impedance. Low-frequency impedance is mainly an indicator of the water absorption tendency of a coating. As the coatings made in this study are water-borne, they contain many polar groups which tend to attract water. Further, the presence of the amine cross-linker, which is again hydrophilic, increases the hydrophilicity of the coatings.

However, this phenomenon of water penetration cannot be avoided if water-borne coatings are formulated. The best alternative is to make the coating resistant to the degrading action of water. Water absorption in general leads to negative effects, such as swelling, blistering and delamination of coatings. The inclusion of silanes and minor binders in the formulations serves this purpose. They subjugate the swelling and blistering tendency by forming inter-crosslinked or interpenetrating networks. Also, the presence of silanes greatly enhances the adhesion with the substrate as well as with the topcoat. The better low-frequency impedance curves for formulations OA2opt and OA3opt compared with optimized formulations 1 and 4, especially in the Ford test, points towards the positive effect of the polyacrylate and polyurethane minor binders respectively on the water-barrier property of the coatings. Further, the presence of effective inhibitors (non-chromate inhibitors in this case) in sufficient amounts can totally

subjugate the corrosive effect of deleterious ions which can find pathways to the metal substrate through water.

Thus, water penetration can be turned to our advantage by use of suitable inhibitors, provided an appropriate 'water-resistant' (not necessarily water-repelling) film is present. This has been achieved in this study and observed in the B117 and Ford test results of the optimized coatings - relatively lower values of low-frequency impedance, but near-clean scribes and no delamination or blistering. It was discussed in the first chapter that it is advisable to compare complete systems rather than individual layers. In this aspect, another objective achieved in this study is the performance of the complete systems: primer + topcoat, which rivaled the performance of conventional chromate pretreatment + chromated primer + topcoat system. The similar performance levels of the chromated and non-chromated complete systems can be observed in the tested panel images as well as the low-frequency impedance curves.

Nevertheless, as always, there is scope for further improvement and in this case it is via incorporation of higher amounts of inhibitors. Synergistic combinations of inhibitors and their minimum working amounts have been determined and are shown in this study, earlier in Chapter 3 and later in Chapter 5 in the SEM/EDX studies. However, the present concentrations are around 15% and higher amounts (up to 30 wt. %) of the right pigment can lead to much better results. The objective can be clean scribes, even in the Ford test. But increasing the pigment amount would require better dispersing conditions and alternative diluents (other than water). Better dispersion of pigments require the use of mechanical agitation - ball mills and shear

blenders. The latter has already been sporadically and successfully tried. Also determining the right type and amount of dispersing agents needs to be done.

Pigments have a strong tendency to absorb oil or water. The oil absorption per gram of a pigment can be mostly obtained from its technical data sheet. This absorption thickens the formulation and increases its viscosity beyond the working range. Thus, the formulation has to be further diluted. But the diluent, usually a solvent, has to be chosen carefully, as it can hinder the cross-linking of the film. For solvent-borne coatings, a wide variety of choices are available. But for water-borne coatings, the choices are limited. The first obvious choice would be water. But the use of water beyond a point for this purpose is fraught with disadvantages. Excess water may destabilize the various dispersions on which the water-borne coating is based, i.e., epoxy dispersion, polyurethane dispersion, polyacrylate dispersion, pigment dispersion, etc. Water has a poor coalescing action and hence excess water can lead to porous films or films with reduced cross-link densities. Finally, the presence of excess adsorbed water on pigments may cause blistering problems.

One type of alternative for this is the use of VOC-exempt solvents acetone, parachlorobenzotrifluoride or tertiary butyl alcohol. Acetone has already been tried, but again, use of excess amounts of it may not be useful as acetone evaporates quickly. So, alternative VOC-exempt solvents have to be explored. The second type of alternative involves the use of reactive diluents like butyl glycidyl ether (BGE) or cresyl glycidyl ether. These reactive diluents usually have one epoxide end group and therefore cannot form cross-links in the network. However, they chemically react with the film network. By chemically attaching to the network,

the reactive diluents become a permanent and stable part of it. However, there are some diluents like diglycidyl ether of polypropylene glycol, which have more than one epoxide end group and hence can also cross-link. Some of the commonly used diluents in epoxy systems can be found in reference 5. Usually a combination of these benefits may be obtained by using a blend of diluents, reactive or non-reactive or both, instead of a single diluent.

These improvements and the routes to achieve them should be the course for the future work..

These suggestions for future work along with some others will be mentioned in Chapter 6.

The next chapter gives an account of our attempts at understanding the chemistry of the superprimers.

## 4.5 References

1. *NIST/SEMATECH e-Handbook of Statistical Methods*, available at <http://www.itl.nist.gov/div898/handbook>
2. Taguchi G., Konishi S., *Orthogonal Arrays and Linear Graphs*, ASI press Dearborn, MI (1987)
3. Seth A., Van Ooij W.J., submitted for publication in the ACS symposium series volume based on *New Developments in Coatings Tech.*, Zarras P., Benicewicz B. C., Wood T., Richey B., Eds. 2005
4. Puomi P., Fagerholm H.M., Rosenholm J.B., Sipila R., *Surf. and Coat. Tech.*, 115 (1999)
5. Peters S. T., *Handbook of Composites*, Chapman & Hall, London, UK (1998) p 48.

## 5. CHARACTERIZATION OF SUPERPRIMERS

### 5.1. Reaction chemistries

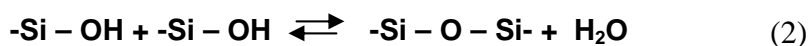
We start with a synopsis of potential reactions between the components of our primers. Pigments are not considered at this stage. Some of the presented reactions have been collated from literature while others are proposed reactions. The general chemical structure of each component can be found in Chapter 1. Later during the chapter, we will try to conclude whether some of these reactions are occurring in our systems.

#### *Silane hydrolysis and condensation*

(a) Hydrolysis:

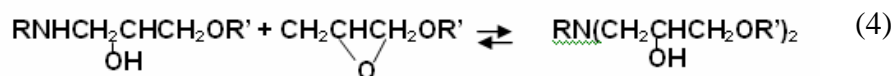


(b) Condensation:



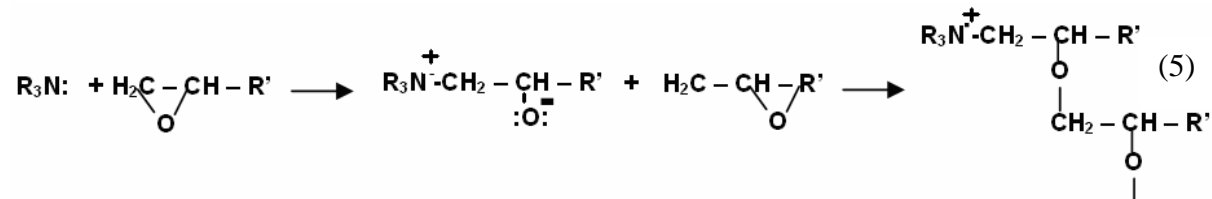
#### *Epoxy-amine reactions:*

(a) With primary and secondary amines present in DPC 6870 and Epicure 8290-Y-60



Obtained from reference 1.

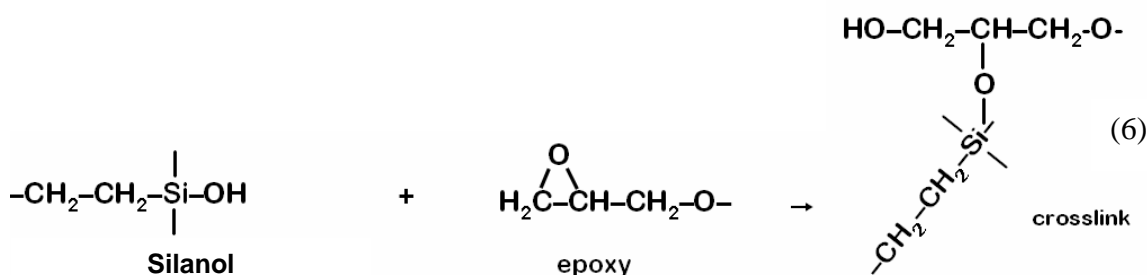
(b) With triethylamine (present in ECO-CRYL 9790 and NeoRez R972)



Obtained from reference 2.

***Binder-silane reactions:***

(a) Epoxy + silane

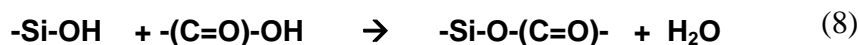


Obtained from reference 3.



This is a proposed reaction. The  $-CH-OH$  group is present in the epoxy resin in the repeating unit. It is also formed when the epoxy ring is opened by a cross-linking reaction, for example, by the amine.

(b) Acrylate-silane



The  $-(C=O)-OH$  group is present in the polyacrylates, more specifically, in co-polymers of acrylate-acrylic acid such as ECO-CRYL 9790, which is a carboxyl-functional acrylic latex.

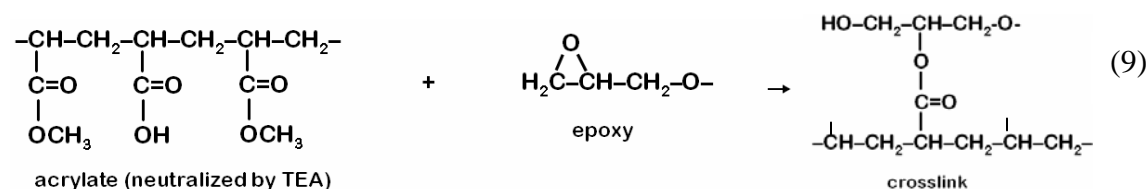
The above reactions was obtained from reference 4.

(c) Polyurethane-silane

No primary reaction between polyurethane and non-functional/sulfur-functional silane was traced in literature. There may be a possibility of hydrogen bonding between the NH groups in the polyurethane and the hydroxyl groups in the hydrolyzed silane. However, the NH groups in polyurethane may show a preference for intra-molecular hydrogen bonding with the OH groups present along the polyurethane chain. Bafna et al., in our group have shown in an unpublished work that the addition of BTSE to a polyurethane-based superprimer leads to increased adhesion of the primer with the substrate and improved anti-corrosion performance. However, no chemical reaction between the polyurethane and the silane has been traced as yet. The polyurethane and siloxane networks most probably form an interpenetrating network amongst themselves i.e., no primary cross-linking reaction, with the silane component contributing to the increased adhesion.

***Polyacrylate-epoxy reaction:***

(a) Epoxy ring opening



This is a proposed reaction and may occur at high temperatures [5].

(b) Formation of -C-O-C- linkage



The -(C=O)-OH groups are present in ECO-CRYL 9790 carboxyl-functional acrylic latex, while the -CH-OH groups are present in the epoxy resin. This is a proposed reaction.

***ECO-CRYL 9790 self-cross-linking:***

Formation of -C-O-C- linkage due to intra-cross-linking between the carboxyl groups of the carboxyl –functional polyacrylate



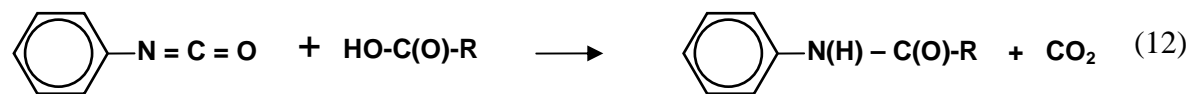
This is a proposed reaction.

***Polyurethane-epoxy reaction:***

Isocyanate and epoxy resins react with each other. However, a reaction between urethane and epoxy was not traceable. Though polyurethane may decompose to form isocyanates and alcohols and the isocyanate can participate in reactions, this decomposition reaction is significant only above 200°C [6].

***Polyacrylate-polyurethane reaction:***

A fully formed polyurethane cannot react with a polyacrylate. However if there is any free isocyanate in the polyurethane, it can react with the polyacrylate as shown below [7]:



However, in water-borne polyurethanes, there is no free isocyanate, as it can vigorously react with the water in the dispersion to form amine and carbon-di-oxide. So this reaction is not possible when a water-borne polyacrylate and polyurethane are used.

***Hydrogen Bonding***

Even if there is a lack of primary bonding between any of the components, significant secondary bonding, especially hydrogen bonding may be present, due to the presence of amine, hydroxyl

and carbonyl groups. The main sources of hydrogen bonding in superprimers are the hydroxyl groups, which are present in silanols, epoxies and acrylates and primary or secondary amines which are present in the epoxy-amine adduct cross-linker and polyurethane. These hydrogen bonds are present either intra-molecularly or inter-molecularly or both and either between the same species (OH - OH or NH - NH) or different species such as NH - OH, N-H - (C=O) or O - H - (C=O).

***Adhesion to the substrate***

(a) Epoxy adhesion on zinc

Epoxy resins bond to the surface by two main mechanisms, depending on the type of hydroxyl groups present on the substrate. At sites on the substrate where physisorbed water is present, epoxy groups can replace this water and become adsorbed onto the surface. In ambient conditions on the zinc oxide-surface, these sites constitute the minority [8]. At other sites, which constitute the majority in ambient conditions, where chemisorbed hydroxyl groups are present, i.e., metal-hydroxyl groups, reaction 13 will occur.

1. With an organic acid polymer



2. With an organic base polymer



In the case of epoxy-amine adducts, both the above reactions occur, as NH, NH<sub>2</sub> and the –OH groups are present [9]. Further, nitrogen also shows a strong tendency towards adsorption in metals and this will increase the adhesion, too.

(b) Silane adhesion on zinc

Trialkoxy silanes hydrolyze to silanols and these silanols become attached to the metal substrate after forming hydrogen bonds with the metal-hydroxyl groups according to reaction 13. This reaction can be simply rewritten as shown below:



Where 'Me' stands for the metal, in this case, zinc. In case of functional silanes, such as sulfur silane or amino silanes, additional adhesion may be provided due to the strong adsorbing tendency of sulfur and amine groups [9].

## 5.2. FTIR analysis

RAIR spectra of 28  $\mu\text{m}$  thick coatings of main neat components present in the optimum formulations along with some of their mixtures have been recorded and analyzed in order to understand the component and their reaction chemistries at various curing conditions. The peak assignments were made using references 10 - 15.

### 5.2.1. Bis-sulfur vs bis-benzene

Neat silanes – bis-benzene and bis-sulfur were spread uniformly on clean HDG panels and excess silane allowed to flow out by keeping the panels at a slanted position. In this comparison, we wanted to monitor the extent and rate of siloxane (Si-O-Si) formation in the two silanes, viz., bis-benzene (BB) and bis-sulfur (BS). Figure 5.1 shows the spectrum for BB with peak annotations, with Table 5.1 showing the peak assignments. Figure 5.2 shows the stacked spectra of BB, on day 0, day 3 and day 7 of the room-temperature cure. Similarly, Figure 5.3 shows the

spectrum for BS with peak annotations, with Table 5.2 showing the peak assignments. Figure 5.4 shows the stacked spectra of BS, on day 0, day 3 and day 7 of the room-temperature cure.

If we observe the stacked spectra, we notice that neither of the silanes have cross-linked completely in atmosphere during the period of exposure. In fact, a substantial amount of the methoxy (in BB) and ethoxy (in BS) remains, as seen by their strong and sharp peaks. Secondly, we observe that BB forms siloxane networks faster than BS. In other words, hydrolysis and condensation rates for BB are higher than for BS. The peaks for long chain Si-O-Si in case of BB start appearing right from the first day and are very clearly visible by the 7<sup>th</sup> day (circled for highlighting). However, in the case of BS, they are overlapped by the stronger Si-O-C peak at 1091 cm<sup>-1</sup>. They are indicated by an arrow. By the 7<sup>th</sup> day, the same Si-O-C peak broadens into the 1086-1040 cm<sup>-1</sup> region of long chain Si-O-Si indicating the formation of these chains. However, the overlapping points towards the lower concentrations of the Si-O-Si network. Further, there is a small peak at 880 cm<sup>-1</sup> in the case of BB that is missing in the case of BS. This peak corresponds to the silanol groups. This further strengthens the lower hydrolysis rate in case of BS. There may be a higher proportion of shorter siloxane chains vis-à-vis the long chains in case of BS. However, the corresponding siloxane peaks overlap with peaks from the ethoxy source. This slower hydrolysis and consequently slower condensation in the case of BS can be attributed to the presence of the highly hydrophobic sulfur atoms, which prevent its easy hydrolysis. In short, bis-sulfur silane forms lower amount of siloxane, with a higher proportion of short chains than bis-benzene.

### 5.2.2. DPW 6520 vs Ancarez AR 550

Each resin was coated on two cleaned HDG panels. One of the panels was allowed to cure at room temperature and the IR spectra were recorded periodically, while the other panel was cured at high temperature, viz., at 60 °C for one hour followed by another hour at 150 °C and the IR spectrum was recorded. This film was further allowed to cure at room temperature for 14 days and the IR reading was taken again. This procedure has been followed for all the films made for the IR studies which have either the epoxy, polyacrylate and polyurethane resins.

The individual spectrum of the two epoxies on day 14 of curing along with the peak annotations are shown in Figures 5.5 and 5.6. The peak assignments for these two spectra have been combined and are presented in Table 5.3. Comparing the stacked spectra of these films in Figures 5.7 and 5.8, we do not see any discernible change in the chemistry of the resins DPW 6520 (DPW) and Ancarez AR 550 (Anca) at different curing stages, except the loss of water at a higher curing temperature or curing time, indicated by a change in the baseline of the spectra. Less free water can mean stronger spectra and a higher baseline. A point to note here and in the spectra coming ahead, are the various curing conditions used and their notations, wherever applicable. RT0, RT3, RT7 and RT14 stands for the spectra of a coating taken of the day 0, day 3, day 7 and day 14 of exposure to ambient laboratory conditions, respectively. 60+150 stands for high temperature step curing at 60 °C for one hour followed by another hour at 150 °C, while 60+150+RT14 extends the former curing cycle by another step by exposing the coating for an additional cure at ambient laboratory conditions for 14 days.

The comparison of the IR spectra of the two epoxies on day 14 is shown in Figure 5.9. The main difference between DPW 6520 and Ancarez AR 550 is the presence of a small amount of acetone and propylene glycol monomethyl ether as a coalescent, a total of less than 5 wt.-%, in the former. This can lead to the observation of a stronger OH and ether band in DPW vis-à-vis Ancarez. This difference can be observed in the overlapping of the O-H ( $3500\text{-}3200\text{ cm}^{-1}$ ) and C-H ( $3000\text{-}2850\text{ cm}^{-1}$ ) bands in case of DPW, while these bands are separately visible in case of Ancarez. Also, DPW has a lower EEW than Ancarez and therefore more number of epoxide groups per gram. However, the increased epoxide is not visible in the epoxide peak at  $919\text{ cm}^{-1}$ , probably due to overlapping by other vibrations. The lower epoxide peak at  $919\text{ cm}^{-1}$  in DPW may also be due to opening of a part of the epoxide rings by hydroxyl groups in polypropylene glycol or any other proprietary additives in the dispersion.

### 5.2.3. DPC 6870

Figure 5.10 shows a spectrum of DPC with peak annotations and Table 5.4 gives the peak assignments for the same. Figure 5.11 shows the comparison of the DPC spectra at different curing stages. We do not see any major differences at any temperatures except that the peaks corresponding to the benzenic overtones ( $2000\text{-}1600\text{ cm}^{-1}$ ) are visible in the case of higher temperature-cured films, which is of little consequence.

The spectra for the epoxy-amine adduct DPC 6870 (DPC) are very complex with much overlapping. It is difficult to interpret whether the amine is aromatic or aliphatic. Primary amines show a dual peak in the region  $3400\text{-}3250\text{ cm}^{-1}$ , while secondary amines show a single peak in that region. However, the peaks due to secondary and primary amines are also overlapped with other peaks from the di-substituted benzene (present in the epoxy part) and aliphatic chain

vibrations and no clear differentiation is possible. There is no indication to the presence of significant amount of epoxy groups. Although a very small peak at  $920\text{ cm}^{-1}$  (epoxide group) is visible, it is very minor. So the epoxide groups in the epoxy-amine adduct are almost completely opened up by the amines. Aromatic compounds are seen, but they do not point to the presence of aromatic amines and they are most probably only due to the substituted benzene rings in the cross-linked epoxy part of the epoxy-amine adduct. DPC 6870 is designed for room temperature curing and may be mainly composed of aliphatic amines, as aromatic amines generally require higher temperatures for curing. Also, as the structure for an epoxy-amine adduct indicates, it should have both primary and secondary amine groups.

#### **5.2.4. ECO-CRYL 9790**

Figures 5.12 and 5.13 show the spectra for ECO-CRYL 9790 (Eco) films on day 14 of room temperature cure and 60 + 150 high temperature cure respectively, while Figure 5.14 shows the stacked spectra for ECO-CRYL films at different curing conditions. The peak assignments are shown in Table 5.5. The main difference observed when comparing the stacked spectra is the disappearance of the band in the region  $3500\text{--}3250\text{ cm}^{-1}$ . That points towards the reduction of hydrogen bonding between the hydroxyl groups in polyacrylate, especially the intermolecular hydrogen bonding. This loss of bonding is accompanied by the appearance of a peak at  $1650\text{ cm}^{-1}$ , which corresponds to intramolecular hydrogen bonding between the carboxylic acid groups of the polyacrylate. Another difference is again the visibility of the benzenic overtones (due to xylene) which were masked earlier probably due to the higher baseline. This is not of significance. The final difference is the appearance of a small peak at  $1801\text{ cm}^{-1}$ , which can be attributed to the cross-linking between the hydroxyl groups of the polyacrylate, to form the –

(C=O)-O-(C=O)- bond, as shown in reaction 11 on polyacrylate self-cross-linking. This peak falls in the region of benzenic overtones, but is not in the usual position for a benzenic overtone and hence has been attributed to polyacrylate self-cross-linking. Overall, high temperature curing leads to some self-cross-linking in ECO-CRYL, along with changes in hydrogen bonding.

### **5.2.5. NeoRez R 972**

Figure 5.15 shows the peak annotations for NeoRez R972 polyurethane dispersion (PUD) while the corresponding peak assignments are shown in Table 5.6. Observation of the stacked spectra of PUD films (Figure 5.16) reveals no differences between them. So there is little difference in the PUD films at various curing conditions, except the drying of the film.

### **5.2.6. Epoxy dispersion and ECO-CRYL 9790 (9:1 mixture)**

Figures 5.17 and 5.18 show the stacked spectra of 9:1 mixtures of Ancarez : Eco and DPW: Eco respectively at different curing conditions. In case of mixtures individual peak assignments have not been made and only the wave numbers of interest have been studied. There is no change observed in the DPW-based mixture with changing curing conditions. However, there is an increase in the intermolecular hydrogen bonding in the Ancarez-based mixture with increasing time ( $3500 - 3200 \text{ cm}^{-1}$ ). Figure 5.19 shows a comparison of the two mixtures after 60 + 150 + RT14 curing. The difference between the two is highlighted by the circle. The peak at  $1136 \text{ cm}^{-1}$  corresponding to the C-O stretch in the epoxide ring is shortened with respect to its adjacent peak in the case of the DPW-based mixture but not in case of the Ancarez-based mixture. This adjacent peak corresponds to the C-N vibration in TEA and it remains constant, as TEA acts as a catalyst. This shows that the catalytic cross-linking of epoxide by TEA is more pronounced in

the case of the DPW-based mixture, because of the lower concentration of epoxide rings in DPW-based mixture vis-à-vis Ancarez-based mixture. This difference between the two mixtures is observed right from the start, i.e., even in RT0 mixtures. This implies that the epoxide opening reaction is instantaneous and it points to the catalytic ring opening by TEA. This deduction also supports the observation of instantaneous gelling when ECO-CRYL (which has TEA) is added to DPW. But this gelling is not observed in case of Ancarez, probably due to its much lower reactivity and thereby lower epoxide ring content. There is no indication of the epoxy opening by the polyacrylate here. As this should be a rather slow reaction as it is not a catalytic reaction, a change in epoxide content should be observed between the first and fourteenth day of curing, which is not observed in the spectra. Hence, epoxy ring opening by the acrylate (reaction 9) is ruled out. Also the formation of -C-O-C- linkage between the epoxy and the polyacrylate (reaction 10) was not seen.

### **5.2.7. Epoxy dispersion and NeoRez R 972 (9:1 mixture)**

Figures 5.20 and 5.21 show the stacked spectra of 9:1 mixtures of Ancarez : PUD and DPW : PUD respectively at different curing conditions. Figure 5.22 shows a comparison of the two mixtures after 60 + 150 + RT14 curing. The observations here are similar to the observations made in the earlier section. The catalytic effect of TEA (reduction of epoxide peak) is visible in case of DPW, as PUD also has some TEA, and its effect is not seen in Ancarez-based mixtures. The curing condition does not make much difference. The only differences observed were in the amount of intermolecular hydrogen bonding which is indicated by the extent of depression in the broad band near  $3200\text{ cm}^{-1}$ , and which seems to decrease at high temperature cure, but again increases upon extended curing at room temperature. No reaction was observed between the

epoxy groups and the secondary amine groups in the polyurethane. This may be due to the reduced reactivity of these secondary amine groups because of intra-molecular hydrogen bonding with the adjacent carbonyl groups [16].

### **5.2.8. Epoxy-amine curing - effect of high curing temperature**

As the complexity of the formulation increases, the peak at  $1139\text{ cm}^{-1}$  becomes a less reliable indicator for epoxide concentration, as it can easily be masked by vibrations from other sources. In Figure 5.23, we see that there is no difference in the  $1136\text{ cm}^{-1}$  peak at the two curing conditions. However, when we zoom in to the range of  $960 - 840\text{ cm}^{-1}$ , to observe the characteristic epoxide peak, which is surprisingly weak in case of DPW at  $920\text{ cm}^{-1}$ , (Figure 5.24), we can observe the difference between the two curves. The epoxide peak in case of room-temperature-cured coating is higher than for the high-temperature-cured coating. This proves that higher curing temperatures push the epoxy-amine reaction towards completion. Note that the scales for the two full curves happen to be similar and hence the difference is not masked even though we are not looking at relative differences. The degree of difference in curing is difficult to measure. However, the difference should be significant, as will be seen in the MEK double rub results, later in this chapter.

### **5.2.9. Epoxy-amine – effect of the type of silane**

Figure 5.25 shows the stacked spectra of 3 coating formulations cured for 14 days at room temperature, namely, 73 – RT14 (7:3 DPW:DPC by weight), 732BS (7:3:2 DPW:DPC:BS by

weight) and 732BB (7:3:2 DPW:DPC: BB by weight). The main objective here is to observe the extent and if possible the nature (long or short) of siloxane formation when the type of silane is changed in a superprimer. Figure 5.26 shows the same stacked spectra as in Figure 5.25, but zoomed in to the region of  $\sim 1500 - 500 \text{ cm}^{-1}$ , so as to observe siloxane formation. In this region, two peaks are of concern. The peak at  $\sim 1128 \text{ cm}^{-1}$  corresponds to the vibration from short siloxane chains as well as C-N stretch from secondary amine and hence seen even in 73 – RT14. The peak at  $\sim 1056 \text{ cm}^{-1}$  corresponds to long chain siloxane vibrations. In fact the region  $1085 - 1040 \text{ cm}^{-1}$  corresponds to this, and C-H bending of the 1, 4 substituted benzene + symmetric C-O-C stretching of the aromatic ether. The last two sources are the same for all three formulations, which may be slightly higher in 732BB, because of the higher benzene content.

Now, if we observe the relative heights of the  $1128 \text{ cm}^{-1}$  peak against the  $1056 \text{ cm}^{-1}$  peak in the three formulations, we notice that the  $1128 \text{ cm}^{-1}$  peak is much higher than the  $1056 \text{ cm}^{-1}$  peak for 732BB-RT14, slightly higher for 732BS-RT14 and shorter in case of 73-RT14. Thus, there is ample indication of short chain siloxane formation both for BB and BS. However, it is much higher for bis-benzene. Also the  $1128 \text{ cm}^{-1}$  peak for 732BB is very broad and overlaps with the  $1085-1040 \text{ cm}^{-1}$  region which corresponds to long chain siloxane formation. However, long chain siloxane formation is not significant because both in the case of 732BB and 732 BS, the  $1056 \text{ cm}^{-1}$  peak does not change much and definitely not as much as the  $1128 \text{ cm}^{-1}$  peak. In brief, more siloxane is formed in bis-benzene-based superprimers than bis-sulfur-based superprimers, and the amount of short chain siloxanes is higher than long chain siloxanes in both cases. It cannot be confirmed whether -Si-O-C- linkages are formed between the silanol groups and CH-

OH in the epoxy, as these Si-O-C- peaks overlap with the Si-O-C- peaks from the unhydrolyzed silane, which is substantial even after 14 days of curing.

#### **5.2.10. Polyurethane and silane**

As no primary reaction is expected between these two components, this mixture has not been analyzed. The only interaction expected is the secondary reaction, i.e., hydrogen bonding between the hydroxyl group in silanol and the amine and/or carbonyl groups in the polyurethane. We observe a characteristic broad band in the  $3600\text{-}3200\text{ cm}^{-1}$  corresponding to these intra-molecular and inter-molecular hydrogen bonding. But this broad band overlaps with the band corresponding to the hydroxyl groups.

#### **5.2.11. Polyacrylate and silane**

Seth [4] has analyzed a mixture of ECO-CRYL and bis-sulfur silane (7:1.5 by weight) using FTIR. He detected the formation of hydrogen bonds between the carboxylic acid groups and silanol groups. They were found to be reversible. With the passage of time, a silicon ester, i.e., SiO(C=O) linkage was formed between these two groups, with elimination of water (reaction 8). This reaction was found to be very slow.

### **5.3. $^{13}\text{C}$ NMR analysis**

$^{13}\text{C}$  NMR analysis, mainly solid-state  $^{13}\text{C}$  NMR was performed on various superprimer formulations as a function of curing time. The solid-state analysis, as will be explained later, required some liquid state  $^{13}\text{C}$  NMR studies of individual components. These results of  $^{13}\text{C}$

analysis complement the IR analysis. The seven coating formulations which were analyzed by solid-state  $^{13}\text{C}$  NMR are described below:

- 1) **7 3 2** - 7 g DPW 6520 + 3 g DPC 6870 + 2 g bis-sulfur
- 2) **7 3 2 BB** -7 g DPW 6520 + 3 g DPC 6870 + 2 g bis-benzene
- 3) **7 3 2 8290** - 7 g DPW 6520 + 3 g EPI-KURE 8290 + 2 g bis-sulfur
- 4) **7 3 2 Eco** - 2.6 g Ancarez AR 550 + 4.4 g DPW 6520 + 3 g DPC 6870 + 2 g bis-sulfur + 0.4 g ECO-CRYL 9790
- 5) **7 3 2 PUD**- 2.6 g Ancarez AR 550 + 4.4 g DPW 6520 + 3 g DPC 6870 + 2 g bis-sulfur + 0.4 g NeoRez R972
- 6) **PIG** - 3 g Ancarez Ar 550 + 5 g DPW 6520 + 3 g DPC 6870 + 2g bis-sulfur + 1g acetone + 2 g pigments (1: 3 titania: zinc phosphate)
- 7) **PIG\_HT** - 3g Ancarez Ar 550 + 5g DPW 6520 + 3g DPC 6870 + 2 g bis-sulfur + 1 g acetone + 2 g pigments (titania, zinc phosphate) and cured at 60° C, 1 hour, and 150 °C, 1 hour.

All the samples were cured at room temperature conditions for up to 43days, except sample 7, which was high temperature-cured at 60°C for one hour, followed by 150°C for another hour.

### 5.3.1. NMR of resins, silanes, and curing Agents

Representative chemical structures for all the component materials were prepared based on knowledge of the chemical structures disclosed by the manufacturer. Approximate  $^{13}\text{C}$  NMR peak positions were calculated using ChemWindow software. The representative structures with the calculated peak positions for resonance of each type of carbon atom are shown in Figures 5.27 – 5.30. The individual component materials were analyzed using liquid-state  $^{13}\text{C}$  NMR. For

these materials, the observed NMR spectra contained resonances similar to those calculated by the software. Liquid-state NMR spectra generally comprise narrow spectral resonances due to the rapid isotropic motion of the individual molecules in the liquid. In contrast, solid-state NMR spectra comprise relatively broad resonances due to chemical shift anisotropy caused by an averaging of molecular structures due to the static nature of the sample. Due to the broad, overlapping nature of the solid-state NMR spectra, peak assignments were made based on the observed resonances in the liquid-state spectra.

As an example, the liquid-state  $^{13}\text{C}$  NMR spectrum of neat DPW 6520 is shown in Figure 5.31. The chemical structure of the DGEBA backbone is shown in the same figure. Peak assignments are made as shown in the figure.

### **5.3.2 Possible curing reactions**

The curing reactions between DPW and DPC are primarily expected as epoxide-amine reactions between DPW and DPC. Mainly, five general reactions are anticipated to occur during curing as shown in Figure 5.32. Reaction I is between an epoxy group and an amine generating C-OH and N-H (secondary amine) functionalities. Reaction II is condensation between a C-OH group on DGEBA and a Si-OH group from a hydrolyzed silane. This reaction was observed after long curing times,  $\geq 21$  days at room temperature. Reaction III is between a secondary amine and an alkoxy (methoxy/ethoxy) group of a non-hydrolyzed silane generating a tertiary amine. Reaction IV is between a secondary amine and an epoxy group and reaction V is catalytic cross-linking in epoxy resin by TEA (present in ECO-CRYL 9790 and NeoRez R 972).

### 5.3.3 NMR analysis as a function of cure time

Solid-state  $^{13}\text{C}$  NMR analysis was performed for the seven coatings on day 4, day 21 and day 43 (~ 0.5, 3 and 6 weeks). The coatings were allowed to dry at room temperature. For the high-temperature-cured sample 2, NMR analysis was performed only on day 4. Also for the 7 3 2 Eco sample, NMR spectra were collected only on days 4 and 21.

Figures 5.33 – 5.37 show the solid-state  $^{13}\text{C}$  NMR spectra for the samples under investigation as a function of cure time. The general peak assignments are presented in Table 5.7. In general, the epoxy-amine (EA) curing reactions produced new peaks at ~ 70.6 (C-O-C, DGEBA), 62.4 (C-OH, DGEBA and EA), 58 (C-O-Si, epoxy-silane), 51.2 (C-NH, EA), 42.7, 34.1, and 23.7 ppm. The last three peaks are unassigned. The peak at approximately 58 ppm is broad and is observed as an increase in the width of the 62.4 ppm peak. While these peaks are observed in all of the spectra collected, the relative intensities of each varied and depended on the coating system. No evidence of non-reacted epoxide groups at 50 and 44 ppm was observed. This may be because of the relatively lower concentrations of the non-reacted epoxide groups and the overlapping of these peaks by other stronger peaks.

Sample 1 (7 3 2): Figure 5.33 shows the solid-state  $^{13}\text{C}$  NMR spectra for this coating. In this coating, reactions I and II appear to dominate, resulting in the formation of C-OH and N-H groups, as observed by the increase in intensity of the 62.4 ppm peak during the cure time. The broadening of the C-OH peak of 62.4 ppm at approximately 58 ppm due to growth of the C-O-Si peak indicates hydrolysis and subsequent condensation of bis-sulfur during the curing period.

Sample 2 (7 3 2 BB): Figure 5.34 shows the solid-state  $^{13}\text{C}$  NMR spectra for this coating. Reaction I appears to dominate this coating. No significant broadening is seen near the 58 ppm region. Another important observation is the little change observed between the day 21 and day 43 NMR spectra of this coating. This is presumably due to the faster hydrolysis and crosslinking of bis-benzene and thereby faster achievement of equilibrium siloxane concentrations vis-à-vis bis-sulfur (as seen in IR studies). This explanation is also supported by the observations from TGA (seen later), which show that 732 BB has higher thermal stability (more cross-linked networks) than 732, but the thermal stability in the latter does not change much with an increased curing time. Thus, 732 BB is more cured than 732 at shorter cure times.

Sample 3 (7 3 2 8290): Figure 5.35 shows the solid-state  $^{13}\text{C}$  NMR spectra for this coating. Products from reactions I, II, and III are observed in the  $^{13}\text{C}$  NMR spectra of this coating at all stages of the cure time. C-OH, C-O-Si, and N-H bonds are formed. Additionally, a peak at 53.9 ppm is observed due to tertiary amine formation. This is due to the nature of the Epikure 8290 curing agent as compared to DPC 6870. Epikure 8290 comprises a higher amine equivalent weight, indicating a more reactive curing agent. The C-N-C bond may be formed either due reactions III or IV. However, the peak assignments for the carbon atoms in C-N-C reaction product are closer to 53.9 ppm in reaction III than in reaction IV. Hence, reaction III seems more favorable than reaction IV. However, more detailed studies may be needed to confirm this hypothesis

Sample 4 (732 ECO): Figure 5.36 shows the solid-state  $^{13}\text{C}$  NMR spectra for this coating. Reaction I appears to dominate this formulation. Broadening near the 58 ppm region is much less

than seen in the sample 732. Further the intensity difference between 70.6 (C-O-C) and 63.2 peaks (C-OH) peaks is also less than in sample 732. This may be due to the formation of the C-O-C network due to the presence of TEA in ECO-CRYL 9790. This catalytic curing of epoxy by TEA (reaction V) was also observed in IR studies. This can also account for the improved water and solvent barrier properties, i.e., contact angle and MEK double rub tests, shown ahead, which is observed upon addition of such small amounts of polyacrylate to the superprimer. Thus the addition of polyacrylate slightly hinders silane hydrolysis but initiates catalytic curing of epoxy.

Sample 5 (732 PUD): Figure 5.37 shows the solid-state  $^{13}\text{C}$  NMR spectra for this coating. Reactions I and II dominate this coating formulation as C-OH, C-O-Si, and N-H peaks are produced. The Si-O-C formation is not hindered much as in 732 ECO. However, effect of catalytic curing of epoxy resin (reaction V) is also not observed significantly as in the 732 ECO case.

Sample 6 (PIG): Figure 5.38 shows the solid-state  $^{13}\text{C}$  NMR spectra for this coating. The spectra are similar to 732 with reactions I and II dominating. However upon close observation, apart from the similar broadening of 62.4 peaks in 732 and 3 + PIG, we see a slight peak at 58 ppm in the day 4 spectra of this sample. This difference is not seen in later readings. The additional initial hydrolysis in case of 3 + PIG may be due to the additional water in the formulation (which is added in order to decrease the increased viscosity upon pigment addition). However, after the water dries off, sample 3 + PIG exhibits similar behavior as 732. Thus addition of pigments slightly affects silane hydrolysis, but does not affect epoxy-amine cross-linking.

Sample 7 (PIG\_HT): Figure 5.38 shows the solid-state  $^{13}\text{C}$  NMR spectrum for this coating. The width of 62.4 peak of this spectrum (broadening due to Si-O-C) is same as sample 3 + PIG on day 4. However epoxy-amine crosslinking is much increased (higher 62.4 peak vis-à-vis 70.6). Thus, high temperature curing does not significantly affect silane hydrolysis. However, it enhances epoxy-amine cross-linking.

In brief, these solid-state  $^{13}\text{C}$  NMR studies have shown that a) bis-benzene-based superprimers cure faster than bis-sulfur based super-primers, b) EPIKURE 8290-Y-60 forms films with epoxy resins, which are more cross-linked than when DPC-6870 is used. Even the secondary amines in the reaction product of EPIKURE 8290-Y-60 with epoxides further cross-link the epoxy or the silanols, c) catalytic cross-linking of the epoxide groups due to TEA present in the minor binders is more evident when the polyacrylate ECO-CRYL 9790 is used compared with the polyurethane NeoRez R 972, d) addition of pigments slightly increases silane hydrolysis, but does not affect epoxy-amine cross-linking and, e) high temperature curing does not significantly affect silane hydrolysis but enhances epoxy-amine cross-linking.

#### **5.4. MEK double rub, contact angle and acid-base tests**

The MEK double rub, contact angle and acid and base resistance test were carried out various formulations cured at two conditions: room temperature curing for fourteen days and high temperature cure at 60°C, 1 hour followed by 150°C, 1 hour. The results for the contact angle and MEK double rub tests are shown in Table 5.8.

Observation of Table 5.8 reveals that, a general trend of higher contact angle and MEK double rub values at the higher curing temperature. There are, however, a few exceptions especially in the case of contact angle of samples, 9Ancarez+1Eco, 9DPW+1Eco, 9DPW+1PUD, which show a decrease in contact angle with increased temperature. The last two formulations are rather quick to gel, which may be because of free neutralizing monomeric amine present in the ECO or PUD). These three formulations show a tendency to emit vapors, when heated. The resulting micropores on the surface in the former formulations may be the reason behind the reduced contact angle. However, when a combination of the two epoxies (Ancarez and DPW) are taken, this problem is not seen. This observation is confirmed by the MEK and contact angle test results for the last two formulations in Table 5.8 which involve a mixture of the two epoxies. Their contact angle and MEK resistance do not deteriorate at high curing temperatures.

Individually bis-benzene shows much higher contact angle both for room temperature and high temperature curing. When comparing the formulations: 732BS, 732 BB and 7311, we reach the conclusion that in the case of room-temperature-cured formulations bis-benzene is a much better option as it shows both higher contact angle as well as much higher MEK rub values. However, as will be seen later, bis-sulfur shows much higher adhesion to substrates than bis-benzene. So for room-temperature-cured formulations, the best formulation should be a combination of bis-sulfur and bis-benzene for good adhesion as well as hydrophobicity and solvent resistance. This, has been confirmed with the optimization studies, with the 1: 1 mixture of bis-sulfur and bis-benzene. As can be seen from the formulation, 7311 shows properties intermediate to both 732 BS and 732 BB. For high-temperature-cured coatings, the differences between the advantages imparted by each silane diminish, most probably due to the extra curing between the epoxy and

the amine of the coatings, as seen earlier. Therefore, in this case, bis-sulfur is a good option, as it is cheaper. The improved hydrophobicity upon adding bis-sulfur or bis-benzene is expected as they are both quite hydrophobic. Also, the increased MEK double rub and contact angle values with bis-benzene can be attributed to its greater tendency towards the formation of siloxane which was already confirmed by IR studies.

Also the decreased contact angle with increasing amine content, but without the silane, can be observed from formulations 71 and 73 in Table 5.3. This decrease is due to the polar nature of the amine groups, but is counter-balanced by the hydrophobicity provided by the silanes.

In the acid and base resistance tests, using the 6M HCl and NaOH solutions, respectively, none of the formulations shown in the Table 5.8 failed, except the films of neat silanes (bis-sulfur and bis-benzene) cured at either room temperature or high temperature. These films turned black and were destroyed. This was not surprising, as the low chemical resistance of individual silane films is a known fact. The superprimer formulations did not, however, show any signs of deterioration. Moreover, the epoxy-amine adduct cross-linker DPW did not fail even in the acid test, probably due to the presence of the epoxy groups.

## **5.5. Thermogravimetric analysis**

These studies were carried out in order to compare the thermal stabilities of various components and formulations. The effect of the silane added, effect of cross-linker and pigment were studied. In all, eight samples were analyzed using TGA. Their TGA curves are shown in Figure 5.4 and their equal % weight loss temperatures are shown in Table 5.9. In Figure 5.39, the curve for each

of the sample below is indicated by its name and its corresponding serial number, as shown below:

1. DPW – DPW 6520 (14 day room temperature cure)
2. 732BB – 7g DPW 6520 + 3 g DPC 6870 + 2 g bis-benzene (14 days room temperature cure)
3. 732BB old – 7 g DPW 6520 + 3 g DPC 6870 + 2 g bis-benzene (two months room temperature cure)
4. 732BS – 7 g DPW 6520 + 3 g DPC 6870 + 2 g bis-sulfur (14 days room temperature cure)
5. 732BS old – 7 g DPW 6520 + 3 g DPC 6870 + 2 g bis-sulfur (two months room temperature cure)
6. 73 – 7 g DPW 6520 + 3 g DPC 6870 (14 days room temperature cure)
7. Oa3 n - 2.6 g Ancarez AR 550 + 4.4 g DPW6520 + 3 g DPC6870 + 2 g bis-sulfur + 0.4 g NeoRez R972 – No pigments (two months room temperature cure)
8. Oa3 w - 2.6 g Ancarez AR 550 + 4.4 g DPW6520 + 3 g DPC6870 + 2 g bis-sulfur + 0.4 g NeoRez R972 + 1 g zinc phosphate + 0.4 g titania – with pigments (two months room temperature cure)

The TGA curves reveal the order of thermal stability of the 8 samples as:

73 ~ 732BB ~ 732BB old > DPW > oa3 w > 732BS old > 732BS > oa3n

The weight loss in all formulations upon heating is due to two main causes: firstly, due to the evaporation of water and other solvents, which were entrapped or are created due to

condensation reactions, and secondly, due to degradation of chemical bonds, which depends on the bond strengths of all the bonds involved. The bond strengths for C-C, C-O, C-H, N-H, O-H, C-N, Zn-O, S-S and Si-O bonds are 349, 286, 370, 355, 426, 293, 284, 205 and 443.7 kJ/mol respectively [17- 20].

The cross-linked epoxy-amine product (73) provides the highest thermal stability. Addition of the silanes in general reduces the thermal stability of the formulation. The decrease in thermal stability is minimal when bis-benzene is used. However, when bis-sulfur is used, the decrease in thermal stability is substantial. These observations can be easily explained by the facts observed in IR studies that bis-sulfur forms less siloxane with shorter chains than bis-benzene. The short monomers have low thermal stabilities. The bond strength of a C-O bond is 286 kJ/mol, while that of a Si-O bond is 443.7 kJ/mol [17]. Thus the presence of the ethoxy or methoxy groups in non-condensed states leads to a decreased thermal stability. However, as we have seen for bis-benzene, the siloxane concentration is higher (still there may be some amount of unhydrolyzed silane) and therefore the observed higher thermal stability of BB-based formulations, equal to that of the 73 formulation. Another reason for the lower thermal stability of the bis-sulfur based formulation 732BS is the low bond energy of the S-S groups, which has the lowest energy value of most of the bonds occurring in superprimer systems (205 kJ/mol).

Increased curing times have a pronounced effect in increasing the thermal stability of superprimer formulations. This can be again explained on the basis of increased siloxane formation with increased curing times. The increase in thermal stability with increased curing time is, however, greater in the case of 732BS than 732BB. This indicates that bis-benzene silane

in 732BB is already cross-linked enough by the end of 14 days and hence not much change is observed upon extending the curing time to two months. However, the cross-linking for bis-sulfur is hardly complete by 14 days and the cross-linking increases significantly when the curing time is extended. However, the thermal stability at the end of two months for 732BS (i.e., 732S old) is still much lower than 73 and 732BB.

Another observation has been the slight decrease in thermal stability with the addition of pigments (oa3 n vs oa3 w). In general, the thermal stability of epoxy paints decrease in the presence of inorganic pigments. This was observed in the case of epoxy-siloxane resin system with polyamide cross-linker, which showed decreased thermal stability upon addition of titania [21]. The loss in thermal stability was explained as due to electrostatic interaction between dispersed metal oxide particles and polymeric chain of the paint, which develop strain among bonds and lead to decomposition of paints at lower temperatures. The same explanation may justify the lower thermal stability in oa3w compared with oa3n.

Weight loss of the coating samples may not always imply bond dissociation. It can also be a result of bond-forming reactions, for e.g., in these cases, mainly condensation of silanols to form siloxane, accompanied by evolution of alcohol i.e., ethanol in case of bis-sulfur-based superprimers and methanol in case of bis-benzene superprimers. However, to attribute the exact cause of weight loss and the contribution of each cause, additional information obtained from evaluation of the effluent gases using chromatography or mass spectrometry will be required. This can be a part of the future work.

## 5.6. SEM/EDX analysis

Scanning electron microscopy and energy dispersive X-ray analysis was carried out on pigmented superprimer formulations in order to a) test the effectiveness of different pigment combinations in order to prevent corrosion of HDG and b) to study the cross-sectional phase distribution of the superprimer.

### 5.6.1 Inhibitor testing

To a 732BS formulation (7 g DPW 6520 + 3 g DPC 6870 +2 g bis-sulfur), six types of pigments or pigment combinations were added, as described below. The formulations were allowed to cure at RT for 14 days. They were then cross scribed and immersed in 3.5 wt.% NaCl solution for 30 days, after which the scribes were kept under running water for 30 seconds to remove external salt deposits, if any. 1 mm x 1 mm specimens of these scribed panels were then sputter coated with a Au-Pd film and analyzed using SEM/EDX. The pigments added to the 732BS system were:

- a) 5% Corrostayn 228 (corrostayn)
- b) 10% Corrostayn 228
- c) 10% zinc phosphate (ZP)
- d) 10% calcium zinc molybdate (CZM)
- e) 15% calcium zinc molybdate
- f) 10% Corrostayn 228 + 1% NaVO<sub>3</sub>

Two other formulations which were tested were:

- g) 10% zinc phosphate in 7g DPW + 3g DPC (no silane)

- h) 10% zinc phosphate in 732 BS cured at 60 °C, 1 hour and 150°C, 1 hour (high-temperature-cured)

Figures 5.40 to 5.57 give the backscattered images of the scribe region [figures(a)] along with the corresponding EDX spectra of a point in the scribe [figures (b)] for the above samples. Table 5.10 shows the amount of chlorine in the scribe which is directly proportional to the amount of zinc hydroxy chloride corrosion product formed on zinc in NaCl solutions, and the amount of the inhibiting atom species for the same samples. These values were obtained by averaging the values of the respective atomic concentrations in the scribes at three different points. Looking at the amount of chlorine in the scribes, the following order of effectiveness is seen among the inhibitors tested:

5% corrostain < 10% corrostain < 10% ZP ~ 10% CZM < 15% CZM ~ 10% corrostain + 1% NaVO<sub>3</sub>

It could be argued that the inclusion of silane leads to a decrease in the leaching rates of pigments because the silane may get adsorbed on the surface of the pigments and form a film which can reduce the leaching rate of the pigment. However this is not observed, as both 10% ZP and no silane 10% ZP formulations show a similar level of Cl concentration. This may be explained by assuming that water will adsorb preferentially to the silanes on pigment surfaces, which in turn may prevent the silane film from being formed on the pigments. Further, if the results of 10% ZP and 10% ZP HT are compared, it is observed that high temperature curing does not have a significant affect on the leaching rate of pigments.

### 5.6.2 Cross-sectional phase distribution

Figure set 5.48 provides cross-sectional elemental distribution information of the superprimer 7311 with 10% ZP (7 g DPW + 3 g DPC + 1 g bis-sulfur + 1 g bis-benzene + 1.2 g zinc phosphate). Figure 5.48 (a) shows the backscattered image with the line on which a line scan was taken, while Figure 5.48 (b) shows the EDX line scans for the elements C, P (in the inhibitor), S (in bis-sulfur silane) and Si (in the two silanes). The line scan reveals that the distribution of the elements is slightly irregular. However, there is no major phase separation observable.

### 5.7. Bis-sulfur vs Bis-benzene – difference in adhesion, an example

We had seen in earlier studies that both bis-sulfur and bis-benzene silanes provide good adhesion on HDG surface. This is because adhesion on metals is mainly due to the formation of metallo-siloxane bonds. However, the difference in the adhesive powers of the two silanes can be observed when a polymeric substrate is used (where in the metallo-siloxane bonds are not possible). 732 BS and 732 BB films were coated onto Teflon<sup>®</sup> petridishes and removed after 7 days. 732 BB films were coherent but cleanly stripped from the substrate. However, 732 BS films stuck on to the substrate and could be removed partially and with great difficulty. This observation demonstrates the additional adhesion imparted by bis-sulfur. So, a combination of bis-benzene and bis-sulfur in a superprimer can provide good adhesion as well as good film cross-linking. However, this enhanced adhesion, presumably due to the adsorption of sulfur atoms on the substrate, apart from the metallo-siloxane bonds, needs to be confirmed on a zinc substrate and the adhesion mechanism needs further study with surface analysis tools like Time-of-Flight Secondary Ions Mass Spectroscopy (TOFSIMS). This study is beyond the scope of this work and is presented as a suggestion for future work.

## 5.8. Summary of characterization

- a) In the superprimers studied, bis-benzene silane forms more siloxane with longer chains than bis-sulfur silane. However, bis-sulfur silane is capable of providing better adhesion. A combination of bis-sulfur and bis-benzene silanes provides a good synergism of barrier and adhesion properties to the superprimer. Apart from siloxane networks, there are indications that silanes also form inter-crosslinked networks (Si-O-C-C-linkage) with the epoxy-amine network in the superprimer. However this needs to be confirmed further. The thermal stability of superprimers is in general reduced due to the presence of uncondensed silanes. This reduction is minimal for bis-benzene but substantial for bis-sulfur. The presence of silanes does not lead to reduced leaching of inhibitors in superprimers.
  
- b) High temperature curing improves the epoxy-amine cross-linking which in turn leads to improved hydrophobicity and solvent resistance. However, it does not affect siloxane formation significantly. High temperature curing also does not appear to decrease the inhibitor leaching. In general high-temperature-cured superprimers form coatings with better overall properties than room-temperature-cured superprimers.
  
- c) The minor binders, polyurethane and polyacrylate, form interpenetrating networks with epoxy-amine and siloxane networks through hydrogen bonding of various functional groups. The triethylamine present in these minor binder dispersions also has a catalytic effect on the epoxy-amine cross-linking. The addition of a minor binder can afford a reduction in the amine cross-linker level, which can increase the hydrophobicity of the

film without affecting its solvent resistance, especially for high-temperature-cured coatings. The minor binders do not affect the thermal stability of the superprimers significantly.

- d) The continuation of epoxy-amine cross-linking and silane condensation reactions have been detected in superprimers even when the curing was extended into the second month.
- e) The poor chemical resistance of the silanes does not affect the chemical resistance of the epoxy-amine superprimers formulated for this study. They showed good chemical resistance in 6 M HCl and NaOH tests.
- f) The distribution of various components in the epoxy-amine superprimers is fairly homogenous with no major phase separation.
- g) 15% calcium zinc molybdate and a combination of 10% Corrostatin 228 and 1% sodium meta-vanadate in epoxy-amine superprimers, provide good corrosion inhibition on HDG steel.

## 5.9 References

1. Talbot J.D.R., *J. Poly. Sci.*, 42, 3579 (2004)
2. Licari J.J., Hughes L.A., *Handbook of Polymer Coatings for Electronics – Chemistry, Technology and Applications*, 2<sup>nd</sup> ed., William Andrew publishing/Noyes, New York, NY (1990)

3. Xue G., *Die Angewandte Makromolekulare Chemie*, 151, 85 (1987)
4. Seth A., *Ph.D.Thesis, University of Cincinnati*, to be published in 2006
5. Hegedus C.R., Pepe F. P., Dickenson J.B., Walker F.H. *Water-Borne Acrylic-Epoxy Coatings*, available at [www.airproducts.com](http://www.airproducts.com)
6. Fabris H.J., *Adv. Urethane Sci. and Technol.* 4 89 (1976)
7. Evtushenko Y.M., Ivanov V.M., Zaitsev B.E., *J. Anal. Chem.*, 57, 439 (2002)
8. Nakazawa M., Somorjai G.A. *App.Surf. Sci.*, 84, 309 (1995)
9. Sugama T., Kukacka L. E., and Carciello N., *J. Mater. Sci.*, 19, 4045 (1984)
10. Socrates G., *Infrared Characteristic Group Frequencies*, John Wiley & Sons Inc., New York, USA (2001)
11. Coates J., *Encyclopedia of Analytical Chemistry* (Ed) R. A. Meyers, John Wiley & Sons Ltd, New York ,10815 (2000)
12. IR wizard of University of Potsdam, available at <http://www.chem.uni-potsdam.de/cgi-bin/irwiz2.pl>
13. Matinlinna J.P., Areva S., Lassila L.V.J., Vallittu P.K., *Surf. Interface Anal.*; 36, 1314 (2004)
14. Cherdoud-Chihani A., Mouzali M., Abadie M. J. M., *J. App.Poly. Sci.*, 87, 2033 (2003)
15. Puomi P., Fagerholm H. M., *J. Adhes Sci Technol*, 15, 509 (2001)
16. Wicks D.A., Yeske P.E., *Prog. Org. Coat*, 30, 265 (1997)
17. Chiang C., Ma C.M., Wang F., Kuan H., *Euro. Poly. Jour.*, 39, 825 (2003)
18. *N-H and C-H bond strengths*, available online at [www.newton.dep.anl.gov](http://www.newton.dep.anl.gov)
19. *Basic concepts of chemical bonding*, available online at <http://wine1.sb.fsu.edu>
20. *Sartomer Cure Concepts, Volume 5*, available online at [www.sartomer.com](http://www.sartomer.com)
21. Rodriguez M.T., Gracenea J.J., Kudama A.H., Suay J.J. *Prog. Org. Coat.*, 50, 62 (2004)

## 6. CONCLUSIONS AND SCOPE FOR FURTHER RESEARCH

In brief, environment-friendly, chromate-free, low-VOC, anti-corrosion superprimers have been formulated and optimized. These superprimers provide excellent corrosion protection – 2000 hours of salt fog resistance, and their performance rivals that of the commercially used solvent-borne chromated, epoxy - polyamide primers used currently. They can effectively replace the state-of-art primers, are direct-to-metal i.e., they do not require any passivation or pretreatment layer and at the same time are environmentally benign.

When incorporated in water-borne bisphenol-A - polyamine primer systems, bis-sulfur and bis-benzene silanes, yielded enhanced corrosion protection on hot-dip galvanized steel. Incorporation of small amounts of the water-borne polyurethane or polyacrylate dispersions (~ 5-10% by weight of the formulation) further improved the corrosion protection imparted by the superprimers. The addition of phosphate, molybdate and vanadate based non-chromate inhibitors provided self-healing abilities to the superprimers, i.e., active corrosion protection of the metal in the regions where the coating is damaged.

A Taguchi design of experiments technique was used to identify four types of water-borne epoxy-amine superprimer systems optimized vis-a-vis various performance attributes for an anti-corrosive primer. They are: a) simple silane-based superprimer, b) superprimer with polyacrylate minor binder, c) superprimer with polyurethane minor binder and d) room temperature-cured superprimer. The comparison of these superprimers, having 10% of the synergistic zinc-phosphosilicate based Corrostain 228 inhibitor and 1% sodium meta-vanadate with commercially available chromated controls in standard accelerated corrosion tests revealed nearly comparable

anti-corrosion performance to the commercial chromated controls. In complete systems, i.e., systems with an additional polyurethane topcoat layer, the optimized systems show anti-corrosive performance equal to the chromated complete systems. In other performance aspects such as solvent resistance and hardness, the optimized superprimer formulations showed performances superior to the chromated control primer. The optimized superprimer formulations were very low in VOC levels and were also totally chromate-free. In general, superprimers were formulated with VOC-levels as low as 30 g/L, with zero chromate content and which survived 2000 h of exposure in the B117 test. They met all the requirements mentioned in the objective for this study.

Based on this work, of all the primers formulated, the primers which are recommended finally as anti-corrosion primers for HDG are OA2opt and OA3opt (Table 4.12) in applications where high temperatures curing is feasible and OA4opt in cases where only room temperature curing is possible. The formulation procedure for these formulations, the inhibitor used, the application procedure and a synopsis of their properties has been presented in Chapter 4. The formulation should be preferably mixed using a high-shear blender at 3000 rpm for 10 minutes. The formulations mentioned were prepared for application using a draw-down bar, which is similar to the primer application procedure in the coil-coating industry, which uses a blade application process. However, for applications such as anti-corrosive primers for automotive bodies, where spraying is used, dilution of these superprimers with a combination of water and other solvents may be needed. Commercialization of these systems should involve separation of the superprimers into stable packs - two-pack or three-pack systems for long storage lives. Further studies and testing can be carried out for optimizing the solvent content in such a superprimer, in

order to achieve increased pot lives and favorable viscosity, without deteriorating the performance.

Characterization studies of superprimer formulations and/or its components carried out using FTIR and solid-state  $^{13}\text{C}$  NMR elucidated, to an extent, the underlying chemistry of the superprimer formulations. These results have been summarized in section 5.8 of Chapter 5. Some of the deductions from these studies explained the contact angle, MEK double rub values and thermal stabilities of superprimer formulations/components. SEM/EDX studies identified the minimum amount of effective inhibitor(s). They also disclosed the fairly homogeneous distribution of the components in superprimer films. In brief, environmentally friendly (low-VOC, non-chromate), one-step, water-borne epoxy-amine anti-corrosion superprimers for hot-dip galvanized steel were developed and studied.

Further research can be focused on Inductively Coupled Plasma – Mass spectroscopy studies (ICP-MS) in order to determine the leaching rate of various inhibitors in superprimer formulations and the effect of each component and curing conditions on their leaching rates. Surface and interface studies can be carried out using TOFIMS to elucidate the difference in adhesion mechanisms of bis-sulfur and bis-benzene with zinc, if any.  $^{29}\text{Si}$  NMR studies can further elucidate and confirm the siloxane crosslinking reactions and its influencing factors. Rheology studies using advanced rheometers can be carried out to study the effect of various organic co-solvents (in low amounts) and dispersants in improving pigment dispersion at high pigment levels that are usually found in commercial primer formulations.

**Table 2.1.** Comparison of four commercial water-borne epoxy resin dispersions

<b>Epoxy dispersion</b>	<b>EEW (g/epoxide-equivalent)</b>	<b>wt% solids and viscosity</b>	<b>VOC</b>	<b>Additional comments</b>	<b>Supplier</b>
EPI-REZ 3540-WY-55	1600 - 2000	55% and 7000 – 17000 cP	250 g/L	5522 and DPW resins perform better	Resolution Performance Products
EPI-REZ 5522-WY-55	550 - 700	55% and 8000 – 19000 cP	170 g/L	Good corrosion resistance; cures well at room temperature too	Resolution Performance Products
DPW 6520	500 - 600	55% and 1000 – 6000 cP	74 g/L	Very good for low- VOC formulations esp. for high temperature curing	Resolution Performance Products
Ancarez AR 550	1300	55% and 100 cP	0 g/L	Does not gel with polyacrylate and polyurethane dispersions unlike the other three resins	Air Products

**Table 2.2.** Steps in the FORD AGPE cyclic test

<b>Step#</b>	<b>Procedure</b>
<b>1</b>	15 minutes immersion in 5% NaCl solution at room temperature
<b>2</b>	105 minutes ambient drying
<b>3</b>	22 hours in 90% humidity at 60 °C

**Table 3.1.** Formulation F6 on AA2024-T3 - the precursor for this work

<b>Formulation F6</b>
<b>Part A:</b> EPI-REZ 3540-WY-55 epoxy resin
<b>Part B:</b> 10 % solution of AV5 (bis-amino and vinyltriacetoxy silane mixed in a ratio of 5:1) in water at pH 6
<b>Part C:</b> tetraethoxysilane TEOS
<b>Part D:</b> bis-sulfur silane BS
Mix by weight: Part A (80 %) + Part B (9 %) + Part C (1 %) + Part D (10 %)
Shear blend for 8 minutes at 2200 rpm
Ready to use after 20 minutes incubation time
Pigmented F6 formulations: 3% Corrostayn 228, 10% CZM gave > 2000 hours of salt fog resistance on AA2024-T3

**Table 3.2.** Adhesion ability of silanes on various inorganic substrates [2]

	SUBSTRATES
EXCELLENT	Silica
	Quartz
	Glass
	Aluminum (AlO(OH))
	Alumino-silicates (e.g. clays)
	Copper
GOOD	Tin (SnO)
	Talc
	Inorganic Oxides (e.g. Fe <sub>2</sub> O <sub>3</sub> , TiO <sub>2</sub> , Cr <sub>2</sub> O <sub>3</sub> )
	Steel, Iron
	Asbestos
	Nickel
	Zinc
	Lead
SLIGHT	Marble, Chalk (CaCO <sub>3</sub> )
	Gypsum (CaSO <sub>4</sub> )
	Barytes (BaSO <sub>4</sub> )
	Graphite
POOR	Carbon Black

**Table 3.3.** VOC levels of a few superprimer components

<b>Component</b>	<b>~ VOC (g/L)</b>
EPI-REZ 3540-WY-55	250
EPI-REZ 5522-WY-55	176
EPIKURE 8290-Y-60	856
Bis-sulfur silane	< 55
F6 formulation	206
F6 + 5% EPIKURE 8290-Y-60	236
F6 + 10% EPIKURE 8290-Y-60	265
DPW-6520	74
DPC-6870	None

**Table 3.4.** New-Gen systems™ – properties vs. curing conditions. Refer section 3.2 of this thesis

<b>Curing Conditions</b>	<b>Cure I (Room temperature curing)</b>	<b>Cure II (60 °C, 1hr)</b>	<b>Cure III (60 °C, 1hr+ 100 °C, 1hr)</b>
<b>MEK Double Rub test</b>	Poor-less than 40	Average: from 40- 200	Excellent: 250-1200
<b>Dry Adhesion</b>	Excellent-5B	Excellent-5B	Excellent-5B
<b>Flexibility (180° bend test)</b>	Very poor in general	Better than Cure I. Still some crazing observed	Excellent – Increases upto 30%DPC then decreases
<b>Day 1- Low- frequency Impedance</b>	A max of 100 kΩ	A max of 1MΩ	A maximum of 1GΩ, the rest lie b/w 1- 20MΩ
<b>Pencil hardness</b>	4H-5H	4H-5H	~ 6H
<b>3.5wt% Salt water Immersion</b>	Poor-scribe corrosion and creep started from day4 of immersion	Poor – scribe corr. Started by day 7 at most ratios	No corrosion during the first week

**Table 3.5.** Superprimer with and without bis-sulfur - comparison of contact angle and MEK double rub values. Refer p 78 of this thesis.

<b>Formulation</b>	<b>Contact angle with water</b>	<b>MEK double rub test value</b>
Formulation A	32.5	50
Formulation B	50	170

**Table 3.6.** Superprimer with and without bis-benzene – comparison of MEK double rub and pencil hardness values at two curing conditions. Refer p 79 of this thesis.

<b>Formulation</b>	<b>MEK</b>		<b>Pencil Hardness</b>	
	<b>Cure II</b>	<b>Cure III</b>	<b>Cure II</b>	<b>Cure III</b>
Formulation A	7	400	2H	4H
Formulation B	16	1000	5H	5H

**Table 3.7.** Superprimer with and without bis-benzene – contact angle values. Refer p 79 of this thesis.

<b>Formulation</b>	<b>Contact Angle test</b>
Formulation A (Cure III)	65°
Formulation B (Cure III)	80°

**Table 3.8.** Superprimer with and without DBTL - Pencil hardness values. . Refer p 89 of this thesis.

<b>Formulation</b>	<b>Pencil hardness</b>
Formulation 1	2H
Formulation 2	5H

**Table 4.1.** Factors and levels in an L9 orthogonal array

<b>Coating#</b>	<b>Factor 1</b>	<b>Factor 2</b>	<b>Factor 3</b>	<b>Factor 4</b>
<b>1</b>	Level 1	Level 1	Level 1	Level 1
<b>2</b>	Level 1	Level 2	Level 2	Level 2
<b>3</b>	Level 1	Level 3	Level 3	Level 3
<b>4</b>	Level 2	Level 1	Level 2	Level 3
<b>5</b>	Level 2	Level 2	Level 3	Level 1
<b>6</b>	Level 2	Level 3	Level 1	Level 2
<b>7</b>	Level 3	Level 1	Level 3	Level 2
<b>8</b>	Level 3	Level 2	Level 1	Level 3
<b>9</b>	Level 3	Level 3	Level 2	Level 1

**Table 4.2.** L9 orthogonal array for set A (OA1)

<b>Coating</b>	<b>DPW + DPC</b>	<b>BS</b>	<b>1:1 Hydr. BTSE</b>	<b>BB</b>
<b>OA1_1</b>	8 + 2	0	0	0
<b>OA1_2</b>	8 + 2	1	0.5	1
<b>OA1_3</b>	8 + 2	2	1	2
<b>OA1_4</b>	7.5 + 2.5	0	0.5	2
<b>OA1_5</b>	7.5 + 2.5	1	1	0
<b>OA1_6</b>	7.5 + 2.5	2	0	1
<b>OA1_7</b>	6.5 + 3.5	0	1	1
<b>OA1_8</b>	6.5 + 3.5	1	0	2
<b>OA1_9</b>	6.5 + 3.5	2	0.5	0

**Table 4.3.** L9 orthogonal array for set B (OA2)

<b>Coating</b>	<b>(1:1 Ancarez : DPW) + DPC</b>	<b>Ecocryl</b>	<b>PU</b>	<b>BB</b>
<b>OA2_1</b>	8 + 1.5	0	0	0
<b>OA2_2</b>	8 + 1.5	0.25	0.5	1
<b>OA2_3</b>	8 + 1.5	0.5	1	2
<b>OA2_4</b>	8 + 2	0	0.5	2
<b>OA2_5</b>	8 + 2	0.25	1	0
<b>OA2_6</b>	8 + 2	0.5	0	1
<b>OA2_7</b>	7.5 + 2.5	0	1	1
<b>OA2_8</b>	7.5 + 2.5	0.25	0	2
<b>OA2_9</b>	7.5 + 2.5	0.5	0.5	0

**Table 4.4.** L9 orthogonal array for set C (OA3)

<b>Coating</b>	<b>Ancarez + DPW</b>	<b>DPC</b>	<b>PU</b>	<b>BS</b>
<b>OA3_1</b>	4 + 4	1.5	0	0
<b>OA3_2</b>	4 + 4	2	0.5	1
<b>OA3_3</b>	4 + 4	3	1	2
<b>OA3_4</b>	3 + 5	1.5	0.5	2
<b>OA3_5</b>	3 + 5	2	1	0
<b>OA3_6</b>	3 + 5	3	0	1
<b>OA3_7</b>	2 + 6	1.5	1	1
<b>OA3_8</b>	2 + 6	2	0	2
<b>OA3_9</b>	2 + 6	3	0.5	0

**Table 4.5:** L9 orthogonal array for set D (OA4)

<b>Coating</b>	<b>5522 + DPC</b>	<b>8290-Y-60</b>	<b>BS</b>	<b>BB</b>
<b>OA4_1</b>	8 + 2	0	0.5	0.5
<b>OA4_2</b>	8 + 2	0.5	1	1
<b>OA4_3</b>	8 + 2	1	1.5	1.5
<b>OA4_4</b>	7.5 + 2.5	0	1	1.5
<b>OA4_5</b>	7.5 + 2.5	0.5	1.5	0.5
<b>OA4_6</b>	7.5 + 2.5	1	0.5	1
<b>OA4_7</b>	7 + 3	0	1.5	1
<b>OA4_8</b>	7 + 3	0.5	0.5	1.5
<b>OA4_9</b>	7 + 3	1	1	0.5

**Table 4.6.** MEK double rub values for formulations in OA4, before and after immersion in 3.5 wt.-% salt water

<b>Formulation</b>	<b>Before immersion in salt water</b>	<b>After 30 days of Immersion in salt water</b>
4_1	10	28
4_2	380	240
4_3	320	230
4_4	90	190
4_5	90	170
4_6	180	175
4_7	280	220
4_8	320	215
4_9	100	17

**Table 4.7.** Machu test ratings for formulations in OA4

<b>Formulation</b>	<b>Ranking /10</b>
4_1	6.5
4_2	8
4_3	4
4_4	7.5
4_5	3.5
4_6	4
4_7	4.5
4_8	3
4_9	4.5

**Table 4.8.** Optimized formulation levels for OA1

<b>Factor</b>	<b>Best level (value)</b>
DPW + DPC	3 (6.5 +3 .5)
BS	2 (1)
1:1 hydr BTSE	1 (0)
BB	3(2)

**Table 4.9.** Optimized formulation levels for OA2

<b>Factor</b>	<b>Best level (value)</b>
(1:1Anca + DPW) + DPC	2 (8+ 2)
Ecocryl	2 (0.25)
PU	1 (0)
BB	2 (1)

**Table 4.10.** Optimized formulation levels for OA3

<b>Factor</b>	<b>Best level(value)</b>
Ancarez + DPW	2 (3+5)
DPC	3 (3)
PU	2 (0.5)
BS	3 (2)

**Table 4.11.** Optimized formulation levels for OA4

<b>Factor</b>	<b>Best level (value)</b>
5522 + DPC	1(8 + 2)
8290	2 (0.5)
BS	2 (1)
BB	2 (0.5)

**Table 4.12.** The four optimized formulations

<b>OA (optimized)</b>	<b>Factor 1</b>	<b>Factor 2</b>	<b>Factor 3</b>	<b>Factor 4</b>
<b>OA1opt</b>	50% DPW + 27% DPC	7.7% bis-sulfur	0% hydrolyzed BTSE	15.3% bis-benzene
<b>OA2opt</b>	35.5% Ancarez + 35.5% DPW + 17.75% DPC	2.25% Ecocryl	0% PUD	9% bis-benzene
<b>OA3opt</b>	22.2% Ancarez + 37% DPW	22.2% DPC	3.7% PUD	14.9% bis-sulfur
<b>OA4opt</b>	64% 5522 + 16% DPC	4% 8290	8% bis-sulfur	8% bis-benzene

Note: The concentration of each component is presented as % of total formulation weight

**Table 4.13.** Comparison of a few properties of the optimized formulations vis-à-vis the solvent-based, chromated, epoxy-polyamide control primer

<b>Formulation</b>	<b>VOC (g/L)</b>	<b>Pot-life (hours)</b>	<b>Chemical resistance 6M NaOH / HCl</b>	<b>Topcoat adhesion</b>	<b>MEK double rub</b>	<b>Hardness</b>
<b>OA1opt</b>	45	~3.5	Pass	5B	> 300	4H
<b>OA2opt</b>	30	~3	Pass	5B	> 300	4H
<b>OA3opt</b>	40	~3	Pass	5B	> 300	4H
<b>OA4opt</b>	145	~3	Pass	5B	260	3H
<b>Chromated Control primer</b>	340	~5	Pass	4B	300	3H

**Table 5.1.** RAIR Peak assignments for neat bis-benzene film; refer to Figure 5.1

<b>Wave number</b>	<b>Associated structure</b>
2967	Assymmetric stretching of O-CH <sub>3</sub>
2845	Symmetric stretching of O-CH <sub>3</sub>
1901, 1603	Benzenic overtones
1456	CH <sub>2</sub> scissoring / CH <sub>3</sub> assymmetric / C=C stretching of the 1,4-substituted benzene
1204	-O-CH <sub>3</sub> bending
1126	Si-O-C asymmetric stretching + -Si-O-Si- small chains
1059	<i>Long -Si-O-Si- chains + C-H bending of the 1,4 substituted benzene</i>
1009	<i>-Si-O-Si- small chains</i>
882	<i>Si-OH, Si-O stretching</i>
833	-O-CH <sub>3</sub> out of plane deformation
706	CH <sub>2</sub> rocking + C-H stretching of the di-substituted benzene
474	Inorganic silicates

**Table 5.2.** RAIR Peak assignments for neat bis-sulfur film; refer to Figure 5.3

<b>Wave number</b>	<b>Associated structure</b>
2974	CH <sub>3</sub> asymmetric stretching
2926	CH <sub>2</sub> asymmetric stretching
2886	CH <sub>3</sub> symmetric stretching
1482	CH <sub>2</sub> symmetric bending
1442	CH <sub>2</sub> asymmetric bending
1390	CH <sub>3</sub> symmetric bending
1296	CH <sub>2</sub> wagging
1243	CH <sub>2</sub> -S wagging
1167	O-C <sub>2</sub> H <sub>5</sub> bending
1123	-Si-O-Si- <i>small chains</i> + Si-O-C asymmetric deformation
1085	Si-O-C asymmetric stretching + Si-O-Zn bond + -Si-O-Si- <i>small chains</i>
960, 787	Si- O-C <sub>2</sub> H <sub>5</sub> symmetric stretching
479	Inorganic silicates + S-S stretch in polysulfides +Si- O- C <sub>2</sub> H <sub>5</sub> symmetric deformation

**Table 5.3.** RAIR Peak assignments for DPW 6520 and Ancarez AR 550; refer to Figure 5.5 and Figure 5.6

Wave number (cm <sup>-1</sup> )	Associated structure
3590 - 3400	Intramolecular hydrogen bonding between hydroxyl groups
3550 – 3230	Intermolecular hydrogen bonding between hydroxyl groups
3500 – 3300	O–H stretching (includes the OH groups from the epoxy)
3000 – 2850	C–H stretching from aliphatic groups + CH <sub>3</sub> asymmetric stretching
2700-2400	from hydride vibrations, such as from silanes (Si-H), thiols and sulfides (S-H), phosphines (P-H), arsines (As-H), boranes (B-H), etc. These are a part of the surfactants/dispersants used in the system and are proprietary
2000-1650	Weak overtone and combination bands. Characteristic of substitution pattern (from substituted benzene)
1518, 1584, 1615	Asymmetric stretching of C=C of the 1,4-substituted benzene
1471	CH <sub>2</sub> scissoring / CH <sub>3</sub> asymmetric / C=C stretching of the 1,4-substituted benzene
1305	CH <sub>2</sub> twisting and wagging + C-H deformation vibration from secondary alcohol bounded (CHOH in the epoxy part of the adduct)
1261	Asymmetric C-O-C stretching of the aromatic ether and vibration of the epoxide ring
1191	C-H bending (benzenic)
1136	C-O stretching of the epoxide ring
1052	C-H bending of the 1,4 substituted benzene + symmetric C-O-C stretching of the aromatic ether
919	Characteristic vibration of the epoxide group
844	C-H stretching of the 1,4 substituted benzene + CH <sub>2</sub> rocking of the epoxide group
738	CH <sub>2</sub> rocking + C-H stretching of the di-substituted benzene
584, 480	Disulfides S-S stretch usually a constituent of surfactants

**Table 5.4.** RAIR Peak assignments for the film of epoxy-amine adduct crosslinker, DPC 6870; refer to Figure 5.10

Wave number (cm <sup>-1</sup> )	Associated structure
3590 - 3400	Intramolecular hydrogen bonding between hydroxyl groups
3550 - 3230	Intermolecular hydrogen bonding between hydroxyl groups
3500 - 3300	O–H stretch
3450 - 3200	N–H stretch (from the amines)
3000-2850	C-H stretch from the alkanes or aliphatic chains+ CH <sub>3</sub> asymmetric stretching
2700-2400	Peaks not visible in this region. Due to the hydrides in the proprietary surfactants/dispersants
2000 - 1600	Weak overtone and combination bands from di-substituted benzene (benzene fingers)
1613	C=C stretching in the benzene ring
1516	C=C stretching in the benzene ring (goes along with the 1613 peak)
1474	CH <sub>2</sub> scissoring / CH <sub>3</sub> asymmetric / C=C stretching of the 1,4-substituted benzene
1313	CH <sub>2</sub> twisting and wagging + C-H deformation vibration from secondary alcohol bounded (CHOH in the epoxy part of the adduct)
1259	Asymmetric C-O-C stretching of the aromatic ether and vibration of the epoxide ring
1191	C-H bending (benzenic)
1056	C-H bending of the 1,4 substituted benzene + symmetric C-O-C stretching of the aromatic ether
1127	C-N stretching of the aliphatic secondary amine
840	C-H stretching of the 1,4 substituted benzene + CH <sub>2</sub> rocking of the epoxide group + N-H wag of the aliphatic secondary amine

**Table 5.5.** RAIR Peak assignments for the film of polyacrylate dispersion, ECO-CRYL 9790; refer to Figure 5.12 and Figure 5.13

Wave number (cm <sup>-1</sup> )	Associated structure
3590 - 3400	Intramolecular hydrogen bonding between hydroxyl groups
3550 - 3230	Intermolecular hydrogen bonding between hydroxyl groups
3500 - 3300	O–H stretching (includes the OH groups from the epoxy)
3000 - 2850	C–H stretching from aliphatic groups + CH <sub>3</sub> asymmetric stretching
2700-2400	from hydride vibrations, such as from silanes (Si-H), thiols and sulfides (S-H), phosphines (P-H), arsines (As-H), boranes (B-H), etc. These are a part of the surfactants/dispersants used in the system and are proprietary
1946, 1872	Weak overtone and combination bands. Characteristic of substitution pattern (from substituted benzene)
1801	C=O stretch in $-(CO)-O-(CO)-$
1742	C=O stretch
1712	C=O stretch conjugated with a C=C from xylene
1675	C=O stretching vibration in intramolecularly bonded acid groups of the polyacrylate
1603	C=C stretching in the benzene ring
1583	C=C stretching in the benzene ring after conjugation with the carbonyl groups
1496	=C-H and ring C=C strong vibration from the di-substituted benzene.
1457	CH <sub>2</sub> scissoring / CH <sub>3</sub> asymmetric / C=C stretching of the 1,4-substituted benzene (in xylene)
1402	C-H asym. deformation vibration in ester group
1277	Primary alcohol OH in-plane bend
1190	C-N stretch (TEA) + C-H bending (benzenic) + -O-CH <sub>3</sub> bending + strong C-O stretch
944	C-O stretching vibration in ester groups
909	-O-CH <sub>3</sub> out of plane deformation
770	C-O-C deformation vibration in ester group + C-C rocking in CH <sub>2</sub>
707, 692	CH <sub>2</sub> deformation in vinylidene groups (if present as additive) + OH in alcohol, out-of-plane bend
553, 570	C-C skeletal vibrations from aliphatic chains + OH in alcohol, out-of-plane bend

**Table 5.6.** IR Peak assignments for the film of polyurethane dispersion, NeoRez R 972; refer to Figure 5.15

Wave number (cm <sup>-1</sup> )	Associated structure
3590 - 3400	Intramolecular hydrogen bonding between hydroxyl /secondaryamine groups
3550 - 3230	Intermolecular hydrogen bonding between hydroxyl groups / secondary amine groups
3500 - 3300	O-H stretching (free / adsorbed water)
3450 - 3200	N-H stretch (from the amines)
2700-2400	From hydride vibrations, such as from silanes (Si-H), thiols and sulfides (S-H), phosphines (P-H), arsines (As-H), boranes (B-H), etc. These are a part of the surfactants/dispersants used in the system and are proprietary
1747	C=O stretch
1558	Weak N-H deformation vibrations
1470	CH <sub>2</sub> scissoring / CH <sub>3</sub> asymmetric stretching
1273	Asymmetric C-O-C stretching + CH <sub>2</sub> wagging
1200	C-N stretch (TEA) + strong C-O stretch
1150	C-O stretching vibration in ester groups
1085	-O-CH <sub>3</sub> out of plane deformation
786	C-O-C deformation vibration + C-C rocking in CH <sub>2</sub>

**Table 5.7.** Solid-state  $^{13}\text{C}$  NMR peak assignments for the solid-state  $^{13}\text{C}$  NMR studied samples; refer to Figures 5.33 - 5.38 for the spectra

Peak	Component	Assignment
189.22		Spinning side bands
175.2		Spinning side bands
151.6	Epoxy resin	Phenyl
138.04	Epoxy resin	Phenyl
121.4	Epoxy resin	Phenyl
107.8	Epoxy resin	Phenyl
83.8	unassigned	Unassigned
70.6 (slight peak)	Epoxy resin	C-O-C in the DGEBA backbone
62.1	Epoxy resin	C-OH in the DGEBA backbone
58 (appears as broadening of 62.4 peak)	Epoxy-silane	<u>C</u> -O-Si
51.2	Epoxy-Amine product (EA) in the crosslinkers and the resin-crosslinker reaction product.	<u>C</u> -NH
53.6	Unhydrolyzed silane – secondary amine reaction product	<u>C</u> -N-C tertiary amine product
42.3	Epoxy-Amine product (EA)	unassigned
34.2	Unassigned	unassigned EA reaction product
22.9	Epoxy-Amine product (EA) in the crosslinkers and the resin-crosslinker reaction product	unassigned EA reaction product
15.2, 10.5, 8.2	Unassigned	Unassigned

**Table 5.8.** Contact angle and MEK double rub values for room temperature and high-temperature-cured films of water-borne epoxy superprimer and its components

Coating formulation/component	Contact angle in degrees (room temp cured 14 days)	Contact angle in degrees (60+150 cure)	MEK double rub (room temp cured 14 days)	MEK double rub (60+150 cure)
Ecocryl (Eco)	66	83	30	40
Neorez R972 (PUD)	65	75	30	100
DPW 6520 (DPW)	63.1	85	35	45
Ancarez AR 550 (Anca)	42	54	15	25
bis-sulfur (BS)	63	80.5	NA	NA
Bis-benzene (BB)	65	93	NA	NA
DPC 6870 (DPC)	< 30	60	40	70
9 g Anca + 1 g PUD	49	62	45	45
9 g Anca+ 1 g Eco	73	66	50	100
9 g DPW + 1 g Eco	78	70	30	50
9 g DPW + 1 g PUD	79	65.5	45	45
7 g DPW + 1g DPC	43	70.5	25	70
7 g DPW + 3 g DPC	32.5	66	50	300+
7 g DPW + 3 g DPC + 2 g BS	50	77	170	300+
7 g DPW + 3 g DPC + 2 g BB	72	78	290	300+
7 g DPW + 3 g DPC + 1 g BB + 1 g BS	64.5	77.5	250	300+
3 g Anca + 5 g DPW + 3 g DPC + 2 g BS + 0.5 g PUD	51.8	74	150	300+
3 g Anca + 5 g DPW + 3 g DPC + 2 g BS + 0.5 g Eco	59.5	75	240	300+

Note: The top 7 rows present the individual components used in the studied superprimer along with the abbreviations, which are used in the mixtures presented from row# eight

**Table 5.9.** TGA weight loss temperatures and total weight loss of various superprimer films and its components

<b>Formulation#</b>	<b>Notation</b>	<b>5% wt loss temperature (°C)</b>	<b>10% wt loss temperature (°C)</b>	<b>15% wt loss temperature (°C)</b>	<b>Total weight loss%</b>
<b>1</b>	DPW	250	285	325	22.5
<b>2</b>	732bb	255	330	347	18
<b>3</b>	732bb old	260	335	350	17.5
<b>4</b>	732bs	195	225	240	40
<b>5</b>	732bs old	190	220	230	37
<b>6</b>	73	320	330	340	18
<b>7</b>	Oa3 n	180	205	230	40
<b>8</b>	Oa3 w	175	210	260	35.5

**Table 5.10.** Chlorine and inhibiting atom concentrations averaged over three points in the scribed region of various scribed superprimer films on HDG, exposed for 30 days in 3.5 wt% salt water - EDX measurements to test efficacy of various inhibitors

<b>Formulation/pigment</b>	<b>Chlorine concentration in the scribe (wt%)</b>	<b>Inhibiting atom concentration in the scribe (wt%)</b>
732BS + 5% Corrostatin 228	15	0% P
732BS + 10% Corrostatin 228	4.01	0.18% P
732BS + 10% zinc phosphate	3.94	0.19% P
732BS + 10% calcium zinc molybdate	3.81	Mo overlaps with sulfur
732BS + 15% calcium zinc molybdate	2.38	Mo overlaps with sulfur
732BS + 10% Corrostatin + 1% NaVO <sub>3</sub>	2.77	0.26% V
No silane (73) + 10% zinc phosphate	3.75	0.17% P
High-temperature-cured (732BS) + 10% zinc phosphate	3.75	0.23% P

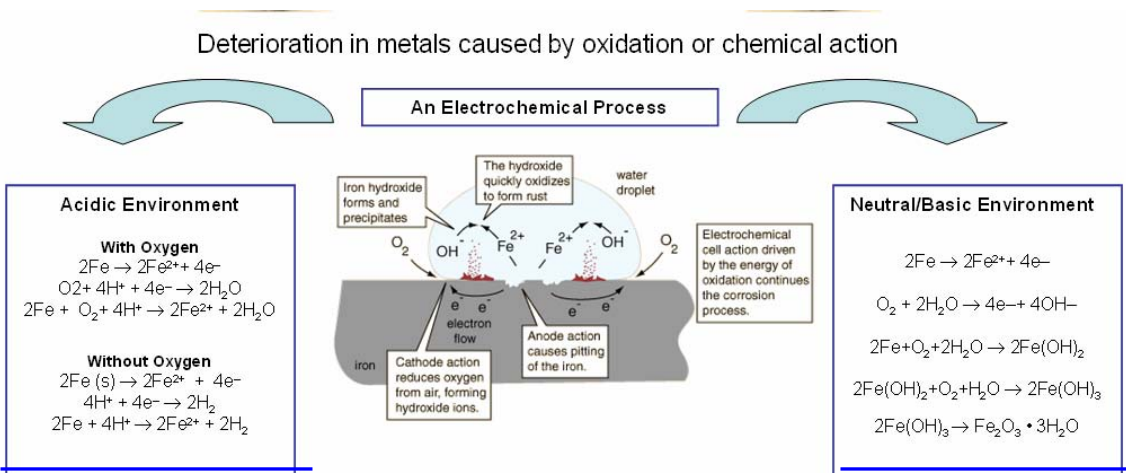


**Figure 1.1.** Corrosion chemical reactions on iron, in aqueous environments

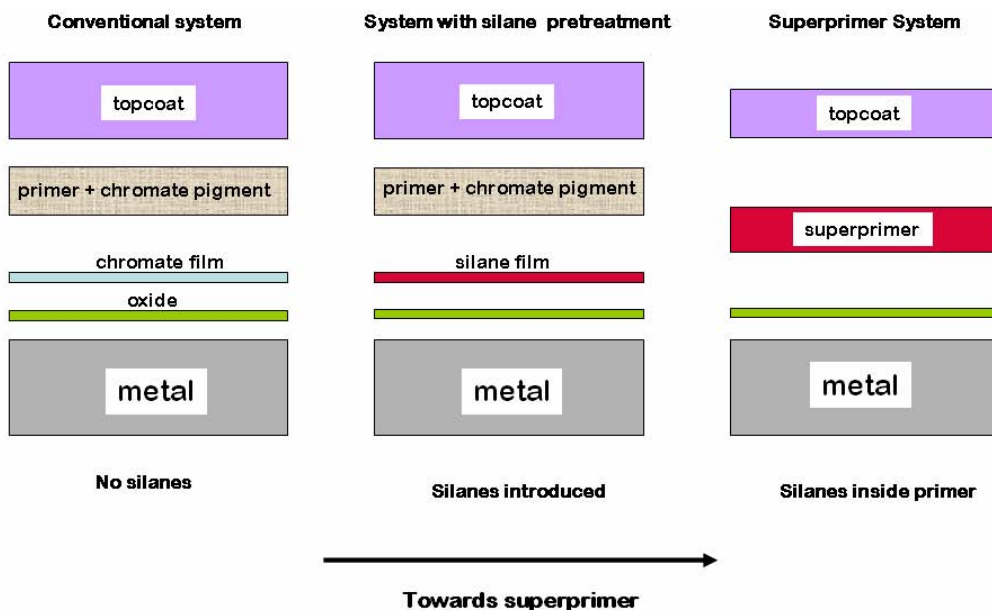


**Figure 1.2.** Schematics showing the progress from a conventional coating system to a superprimer-based coating system



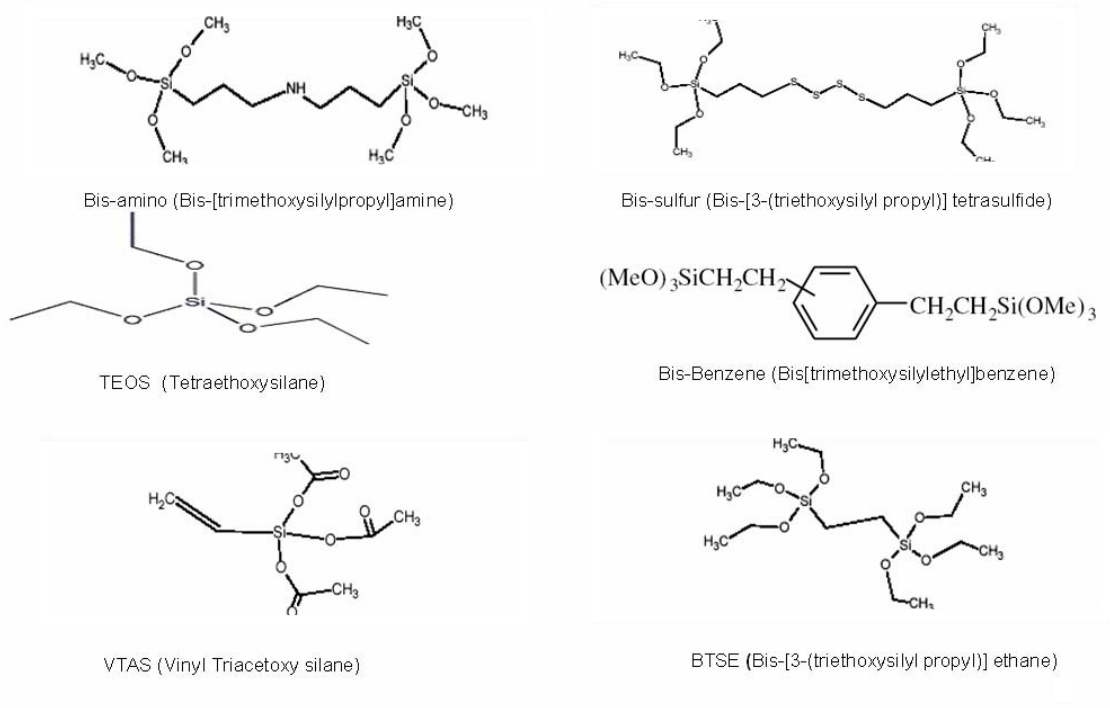
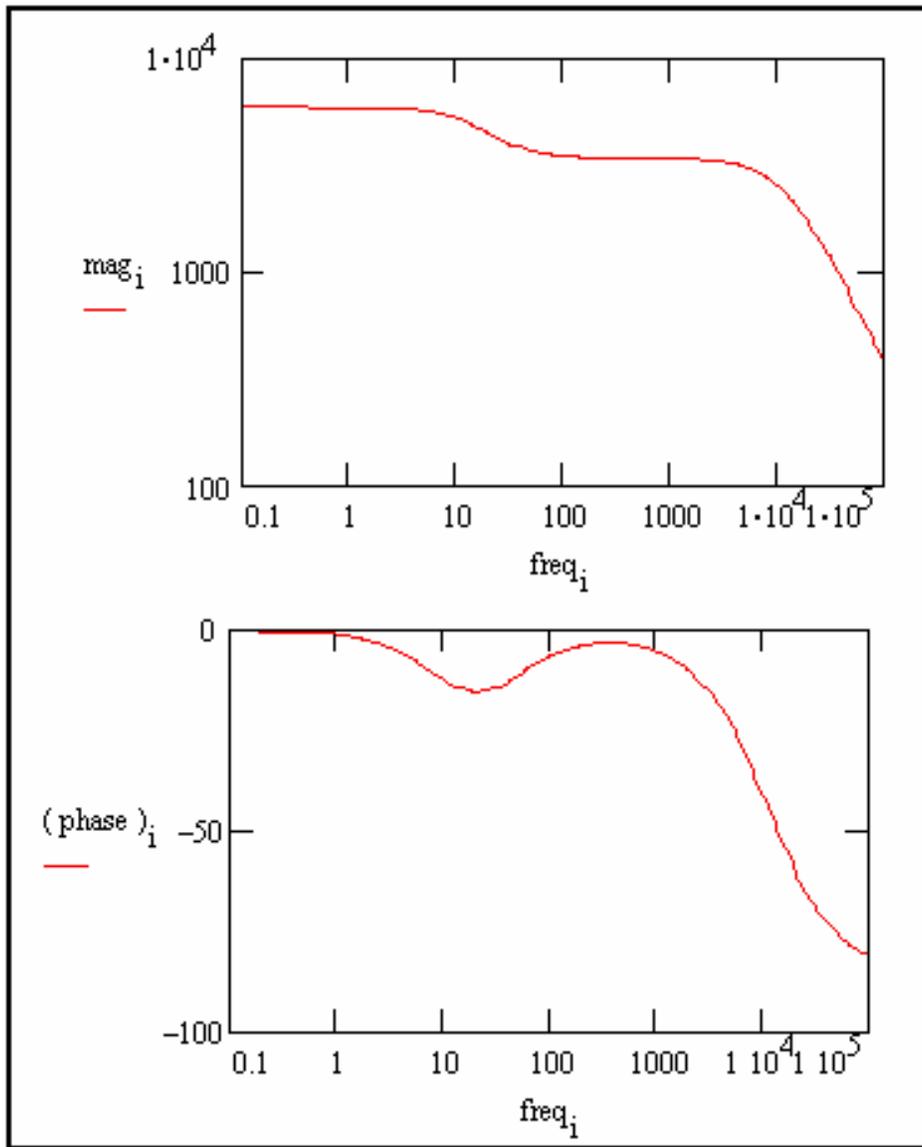
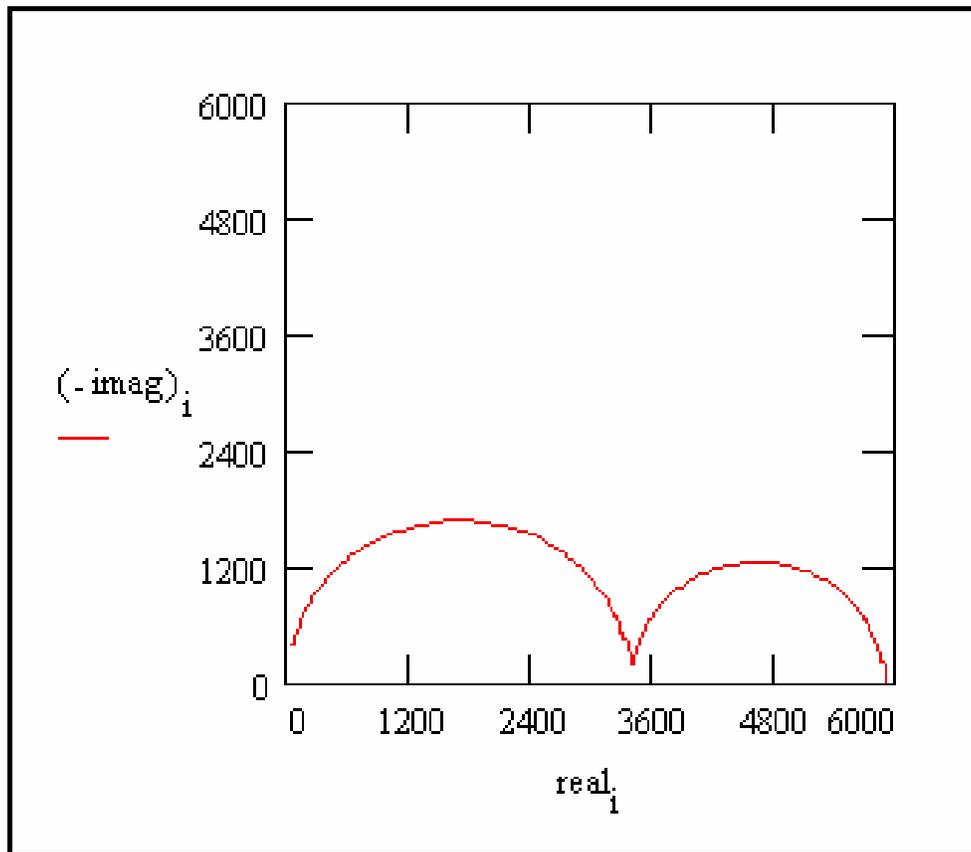


**Figure 1.4.** Chemical structures of commonly used silanes in superprimers



Note:  $\text{mag}_i$  represents the magnitude of the impedance vector, while  $(\text{phase})_i$  represents the phase angle of the same vector

**Figure 2.1 (a).** Bode plots for a damaged coating on a metal

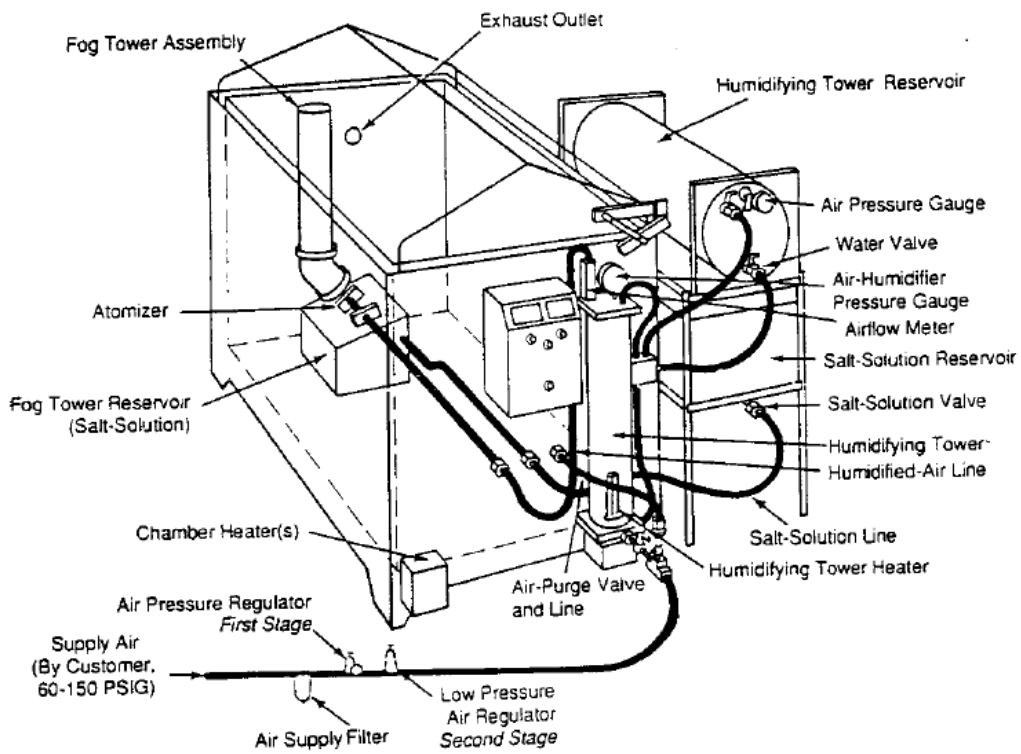


Note:  $(-imag)_i$  represents the imaginary part of the impedance vector, while  $real_i$  represents the real part of the same vector. Nyquist plots do not contain information on frequency.

**Figure 2.1 (b).** Nyquist plot for a damaged coating on a metal



**Figure 2.2.** A general electrochemical cell set-up for EIS measurements



Note: The panels are positioned on brackets inside the chamber, either on the floor or on the walls, or both.

**Figure 2.3.** A schematic of a salt-spray test chamber



**Figure 2.4.** The salt spray chamber set-up at DACCO SCI, INC.

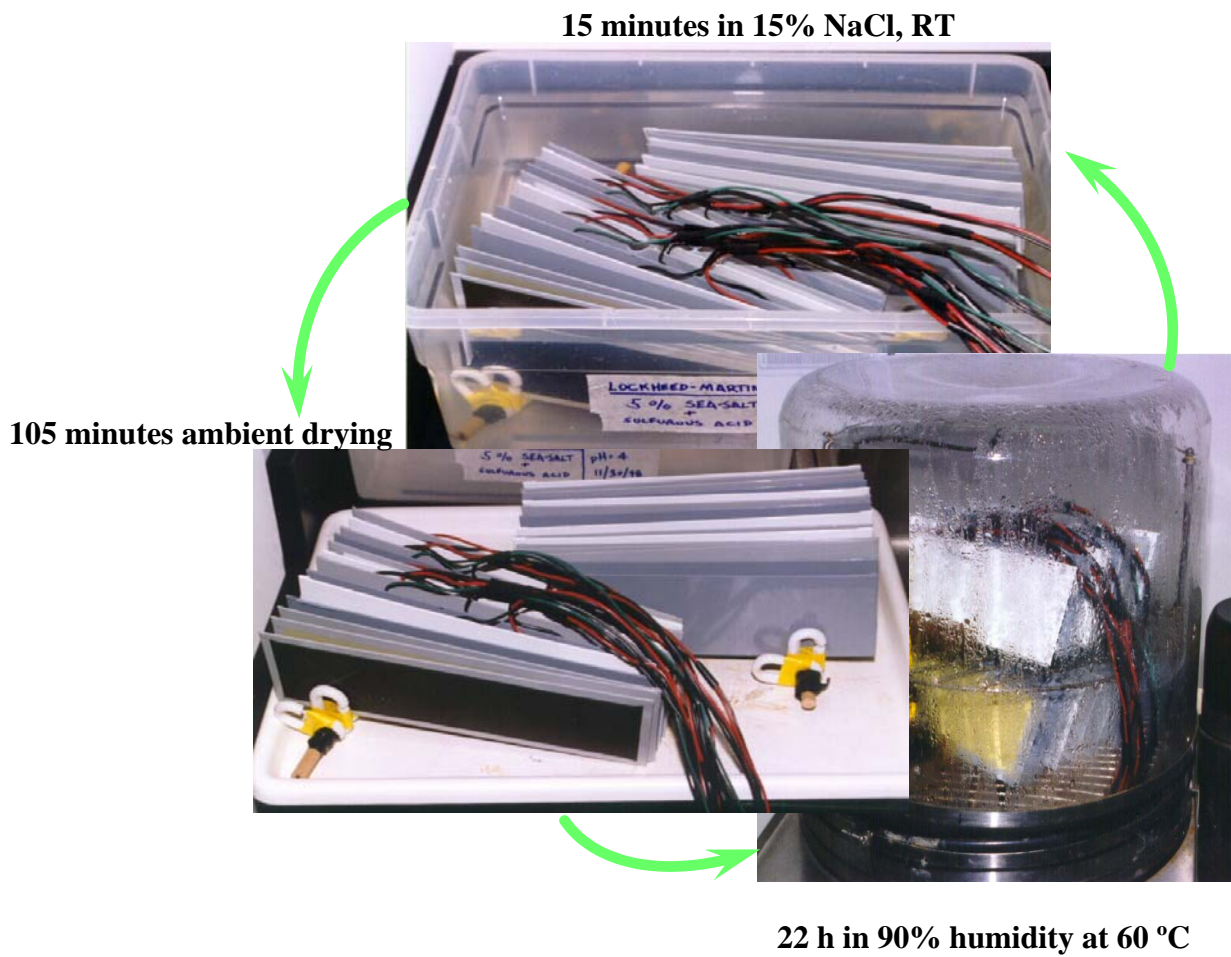
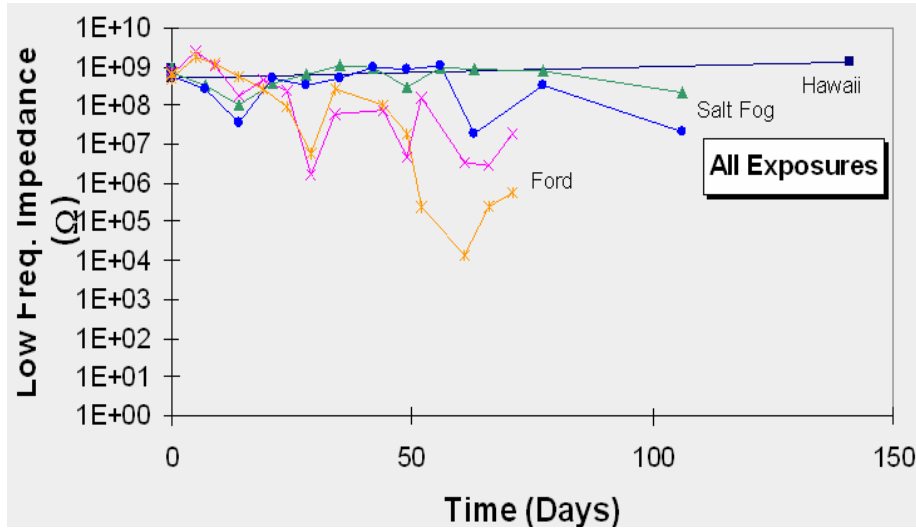


**Figure 2.5.** Steps in the Ford AGPE cyclic corrosion test



**Figure 2.6.** Location and set-up for outdoor corrosion testing of coated HDG panels, in Hawaii



Severity of tests: Ford > Salt fog > Hawaii

Note: The impedance measurements are made in the area of the intact coating, away from the scribe region.

**Figure 2.7.** Examples of low-frequency impedance curves of the three corrosion tests: ASTM B117, Ford AGPE and outdoor exposure at Hawaii, for comparison of the severity of these tests

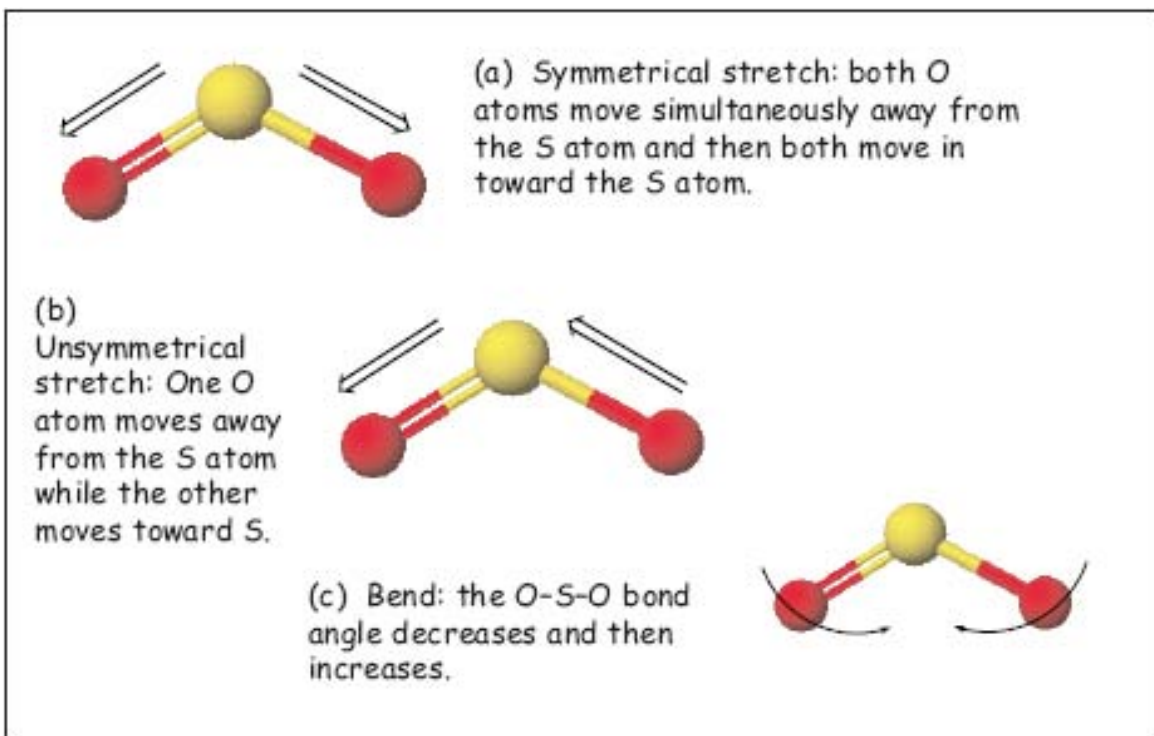


**Figure 2.8.** Vibration modes of bonds in a  $\text{SO}_2$  molecule subjected to excitation by IR radiation

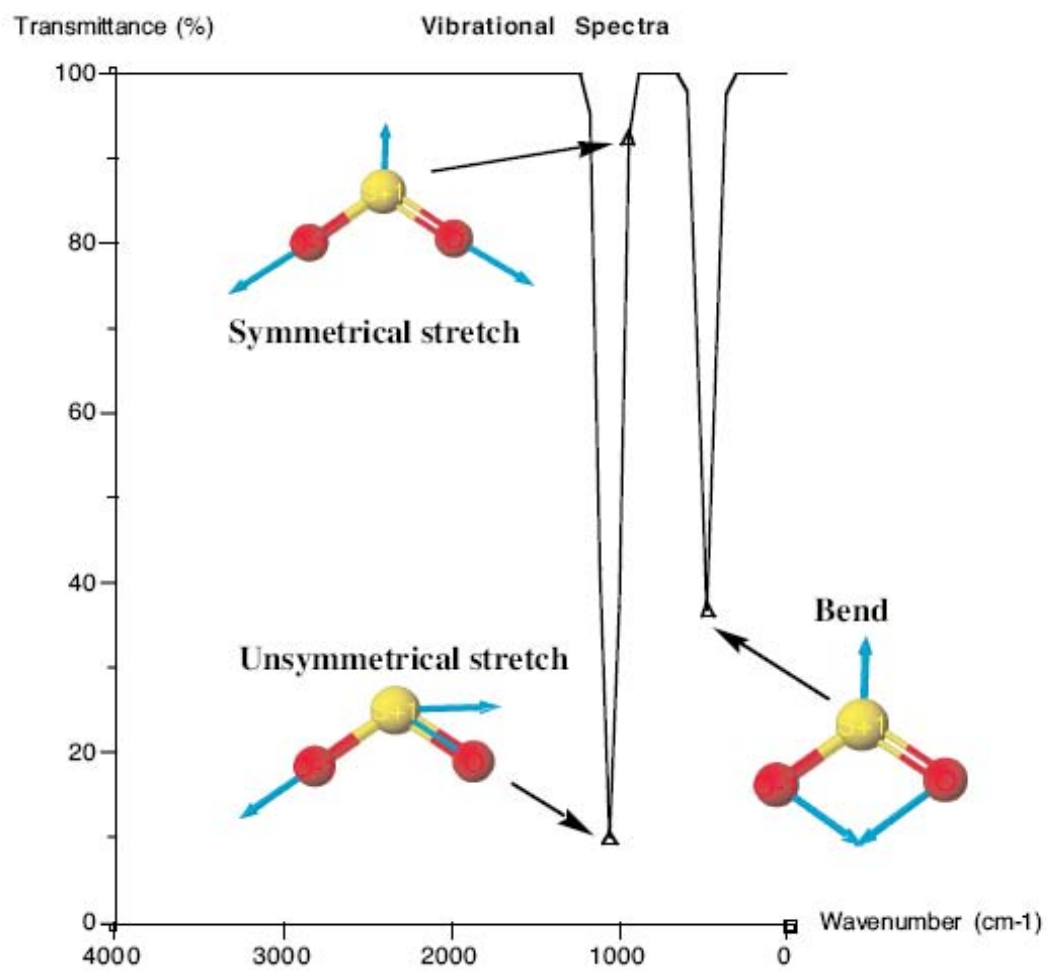
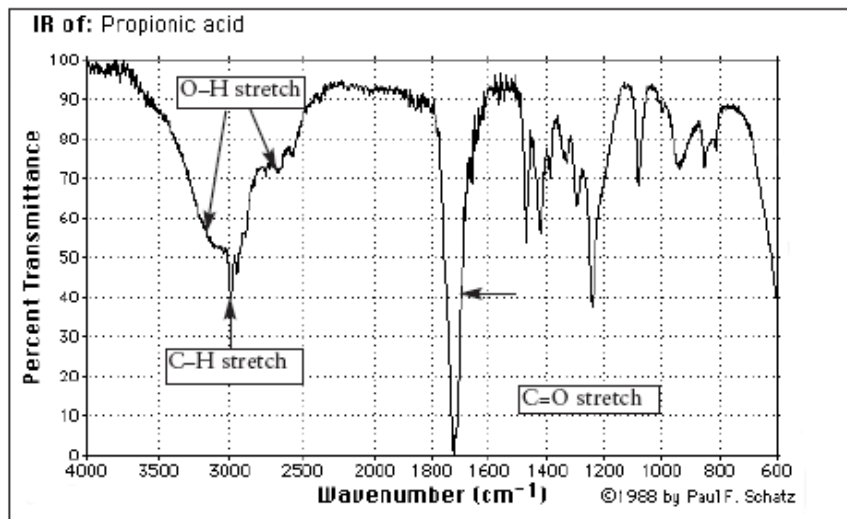


**Figure 2.9.** Calculated IR peaks with the corresponding vibration modes for a SO<sub>2</sub> molecule subjected to excitation by IR radiation

*Propanoic Acid*



An organic acid is characterized by the  $\text{-CO}_2\text{H}$  group (the carboxylic acid group). This group has a very clear infrared fingerprint. Here you see the strong, broad O-H stretching band (overlapping the C-H stretch) and the sharp, strong C=O band.

Propanoic acid - structure

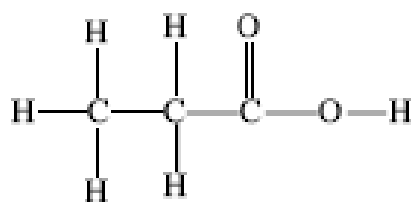


**Figure 2.10.** Example of an IR spectrum - propanoic acid

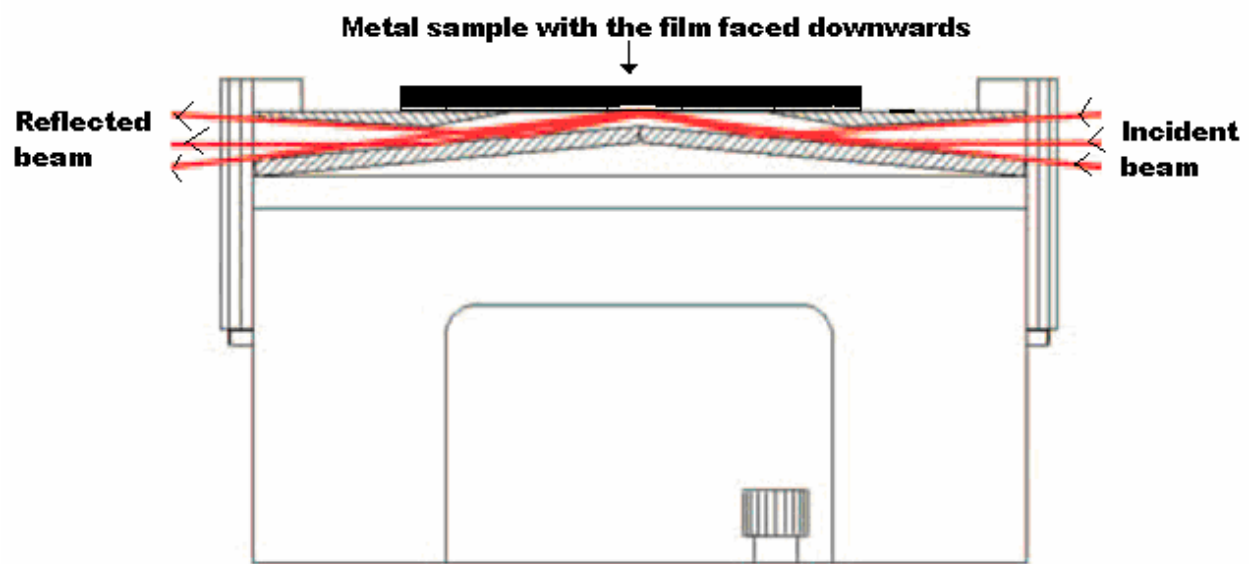


**Figure 2.11.** Ray diagram and mirror set-up in a specular reflectance attachment used in IR spectroscopy

Nuclear spin

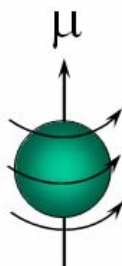
$$\mu = \gamma I \hbar$$

$\mu$  - magnetic moment

$\gamma$  - gyromagnetic ratio

$I$  - spin quantum number

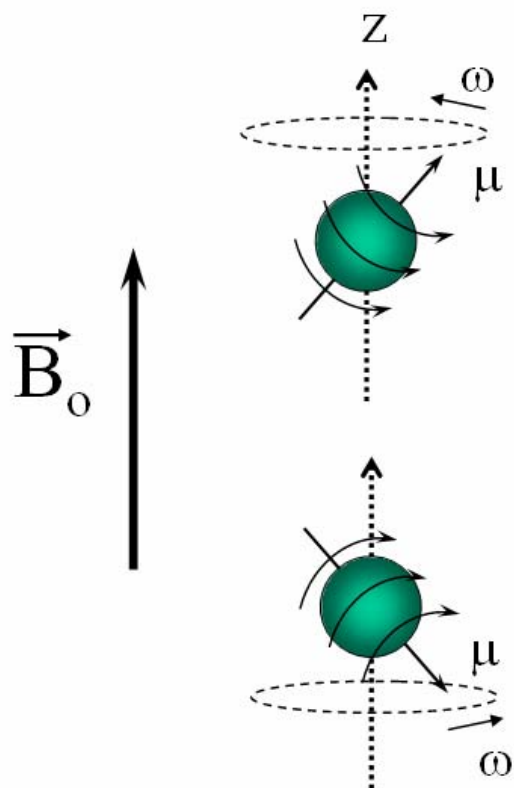
$\hbar$  - Planck's constant



$I$  is a property of the nucleus

Mass #	Atomic #	$I$
Odd	Even or odd	$1/2, 3/2, 5/2, \dots$
Even	Even	0
Even	Odd	1, 2, 3

**Figure 2.12.** Illustration of nuclear spin, its values and its governing equation



$$\omega = \gamma B_0 = \nu/2\pi$$

$\omega$  - resonance frequency  
in radians per second,  
also called Larmor frequency

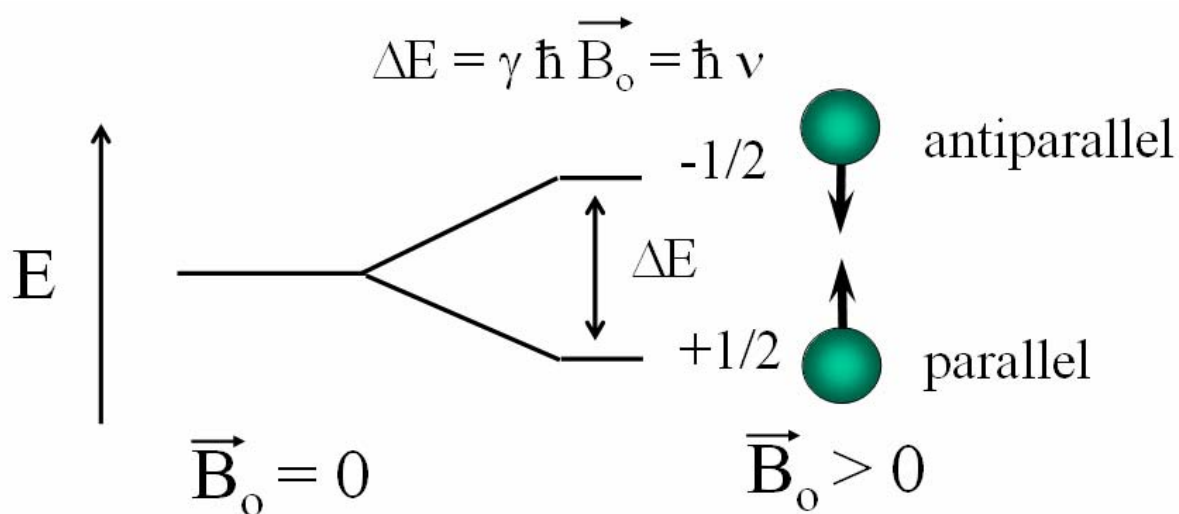
$\nu$  - resonance frequency  
in cycles per second, Hz

$\gamma$ - gyromagnetic ratio

$B_0$  - external magnetic  
field (the magnet)

Spin 1/2 nuclei will have two  
orientations in a magnetic field  
+1/2(parallel) and -1/2 (anti-parallel)

**Figure 2.13.** The two spin states of a nucleus subjected to an external magnetic field  $B_0$



Therefore, the nuclei will absorb light with energy  $\Delta E$  resulting in a change of the spin states.

**Figure 2.14.** Absorption of IR radiation leading to conversion of nuclear spin states, due to energy difference between the two spin states

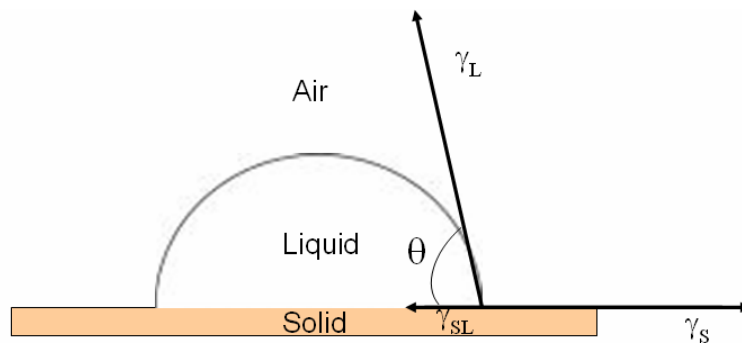


**Figure 2.15.** Interfacial tensions at various interfaces for a liquid droplet on a solid surface in air



**Figure 2.16.** The contact angle goniometer, VCA Optima 2000

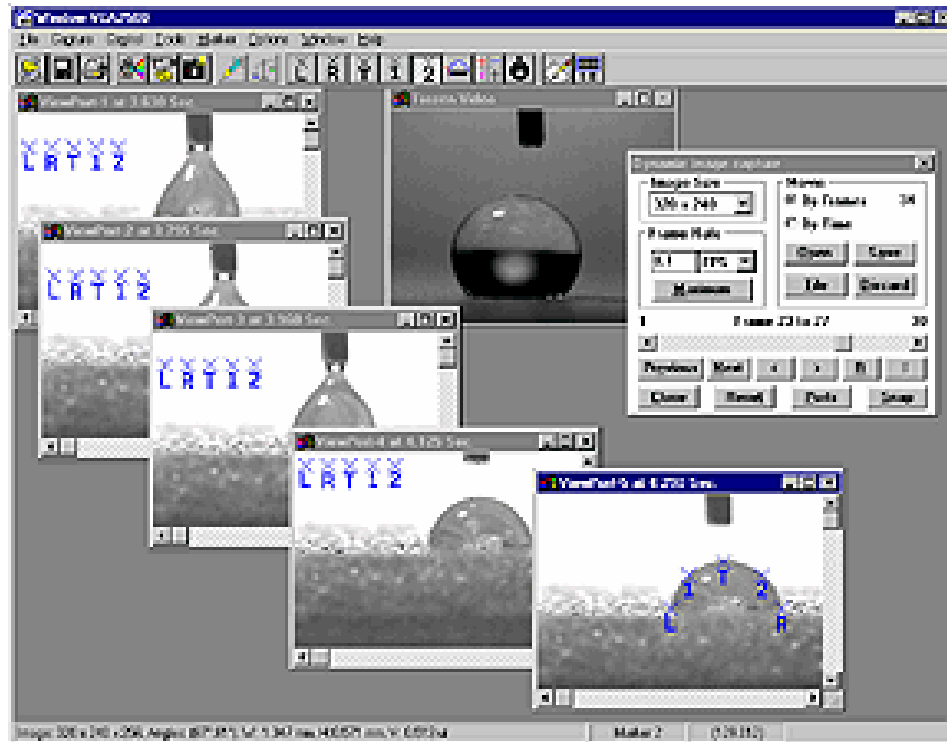


**Figure 2.17.** Video snap-shots of the liquid droplet being dispensed, shown along with the markers used for calculation of the contact angle values

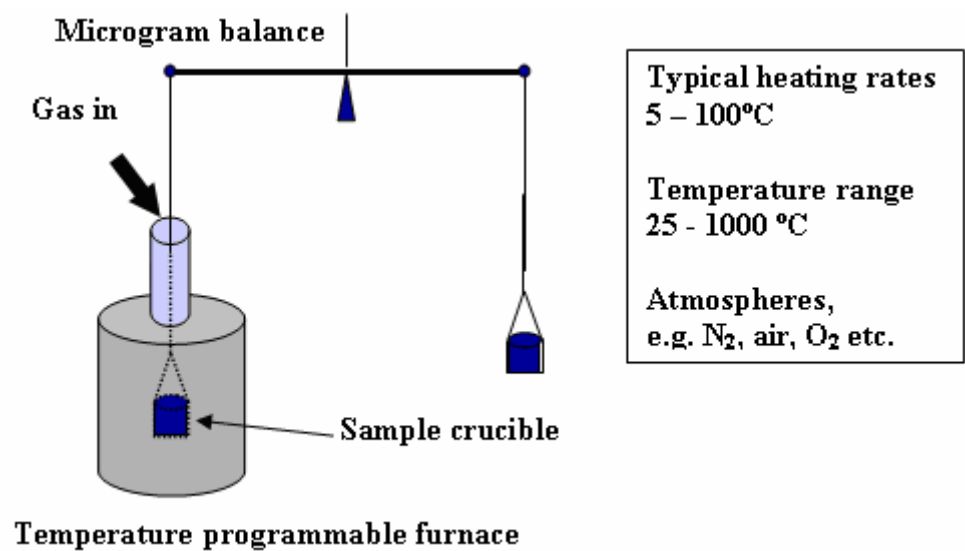


**Figure 2.18.** Basic principle and working conditions of a thermogravimetric analyzer

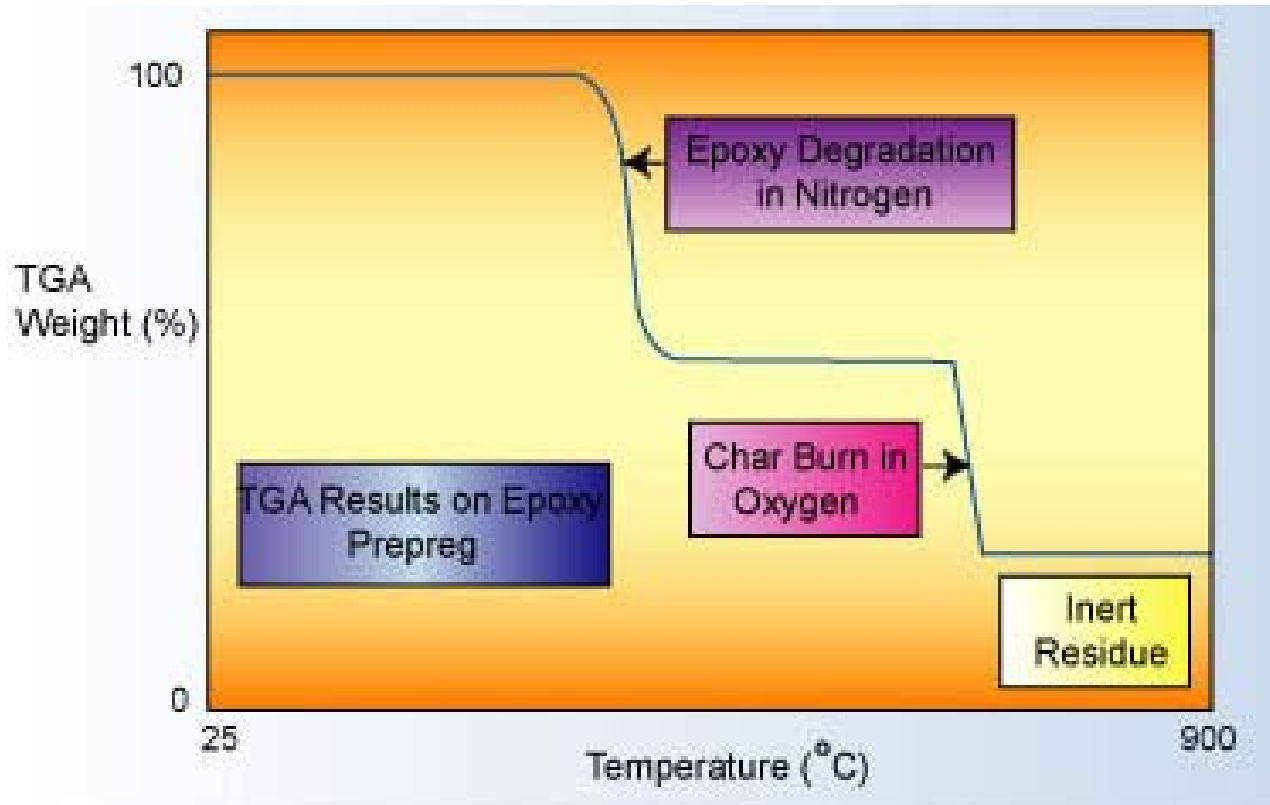
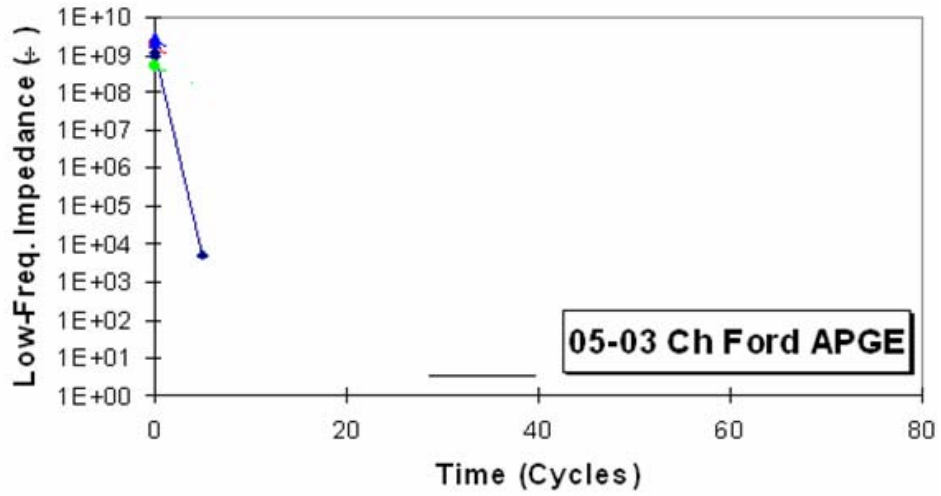


**Figure 2.19.** Example of a TGA curve showing the thermal degradation regimes of an epoxy composite



After 15 cycles

**Figure 3.1.** Failure of formulation F6 on HDG - low-frequency impedance curve and exposed panel image in the Ford test; formulation details in Table 2.1, p 150

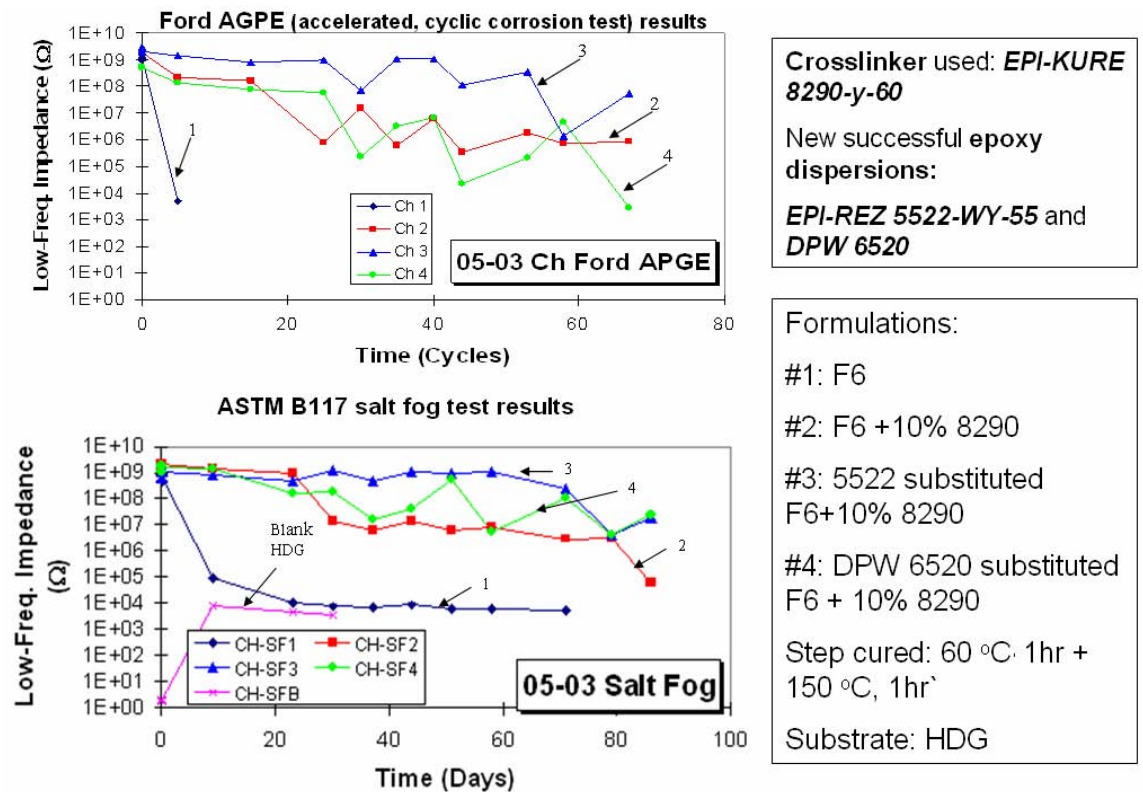


**Figure 3.2.** Low-frequency impedance curves for F6 and its three modifications for HDG, in the B117 and Ford tests; formulation details on p 74

Ford AGPE (accelerated, cyclic corrosion test) images(after 56 cycles)

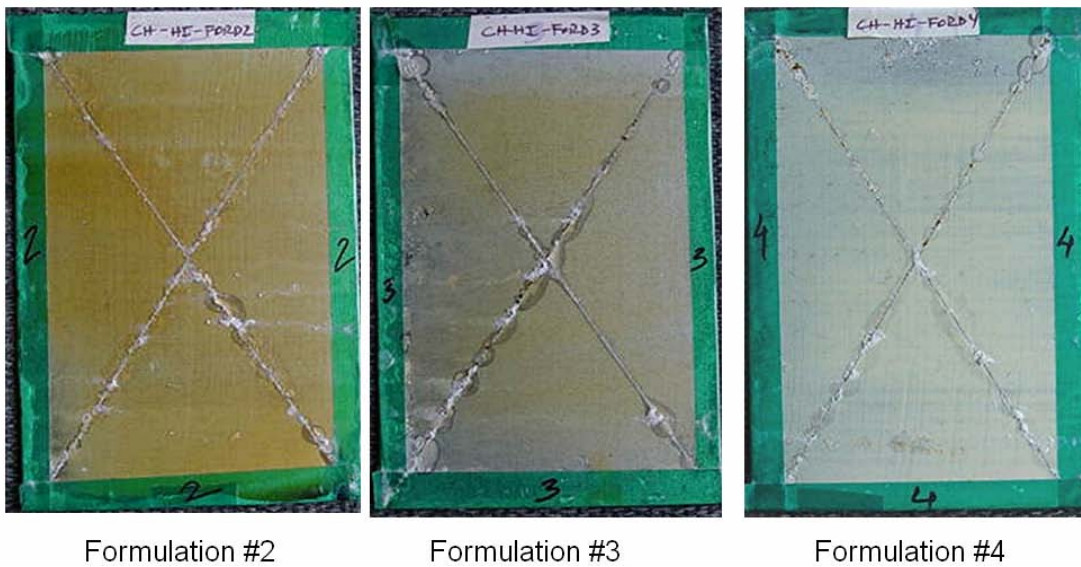


**Figure 3.3.** Ford test - exposed HDG panels coated with the three F6 modifications; formulation details on p 74



#1: After 23 days (552 hours)



#2: After 86 days (2064 hours)



#3: After 86 days (2064 hours)



#4: After 86 days (2064 hours)

**Figure 3.4.** B 117 test - exposed HDG panels coated with F6 and its three F6 modifications; formulation details on p 74

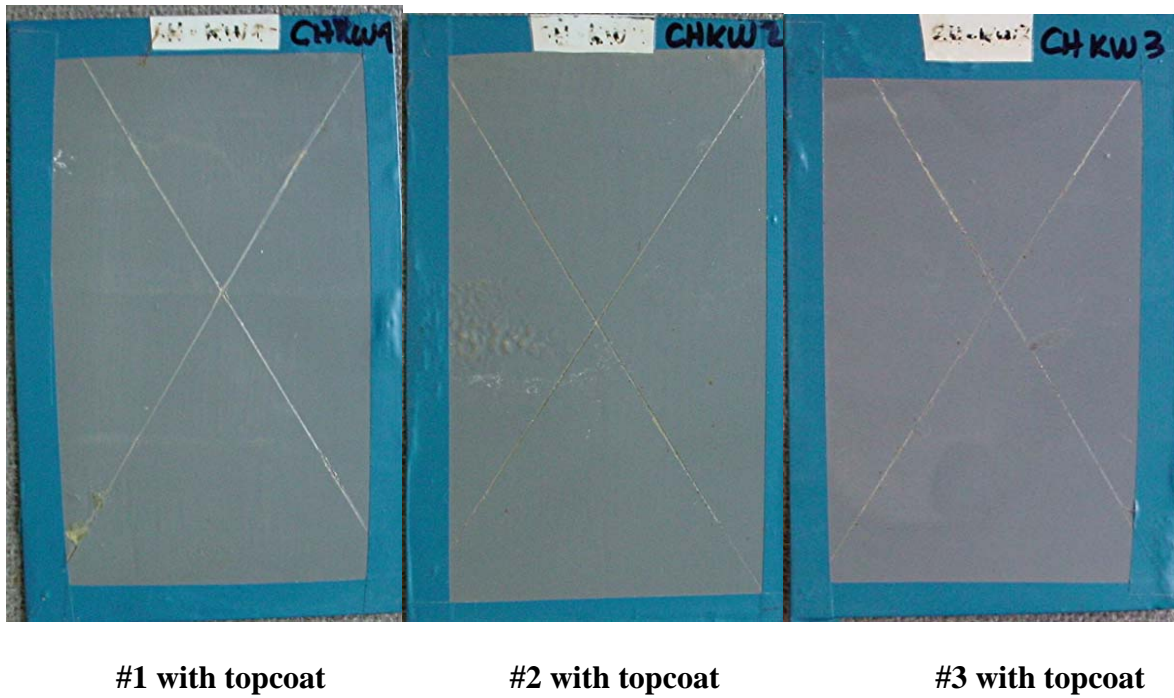
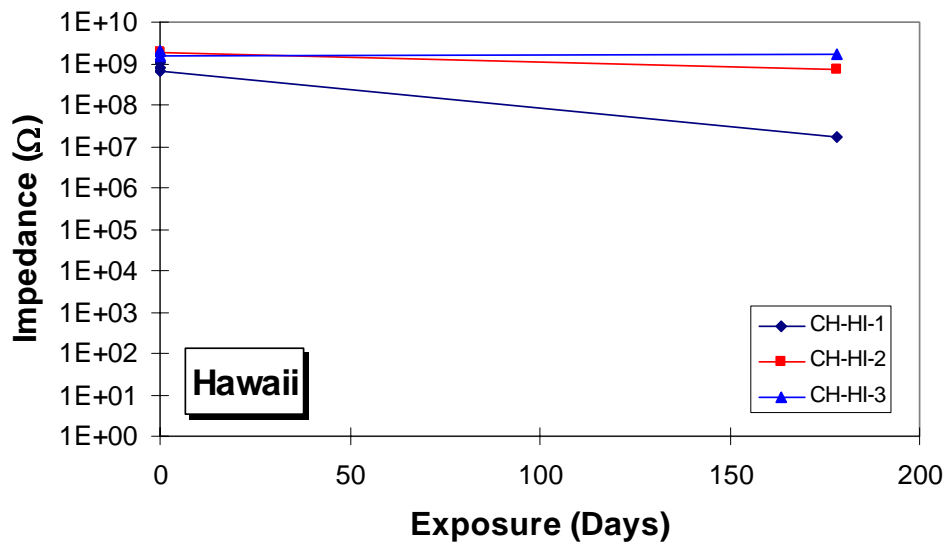


**Figure 3.5.** Hawaii outdoor exposure results – 178 days of exposure. F6 and two of its modified and formulations with topcoated; formulation details on p 74

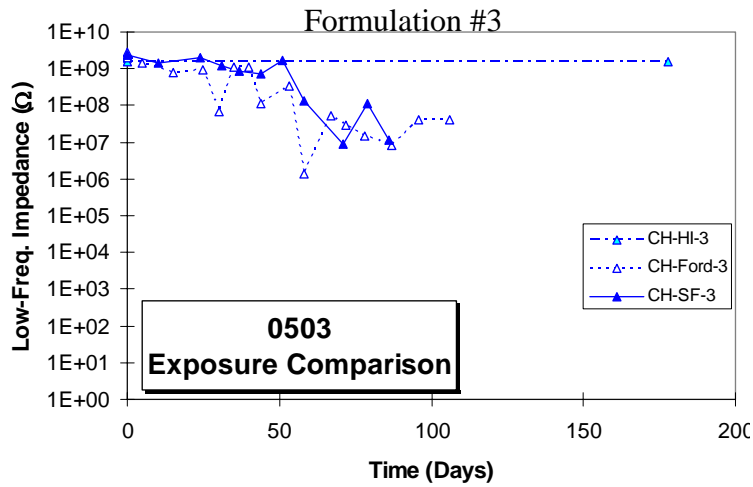
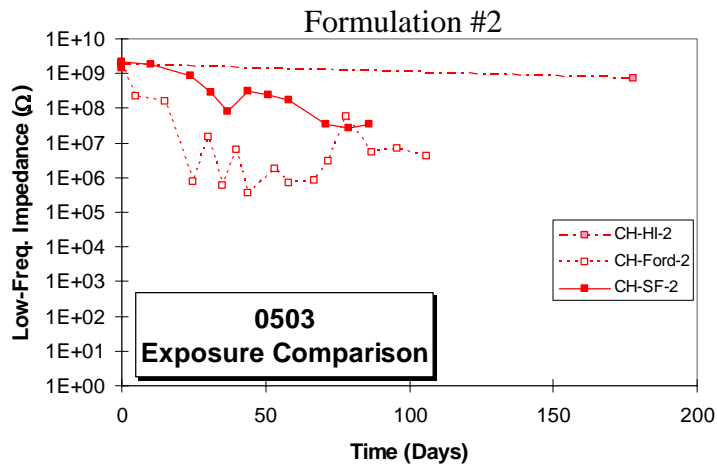
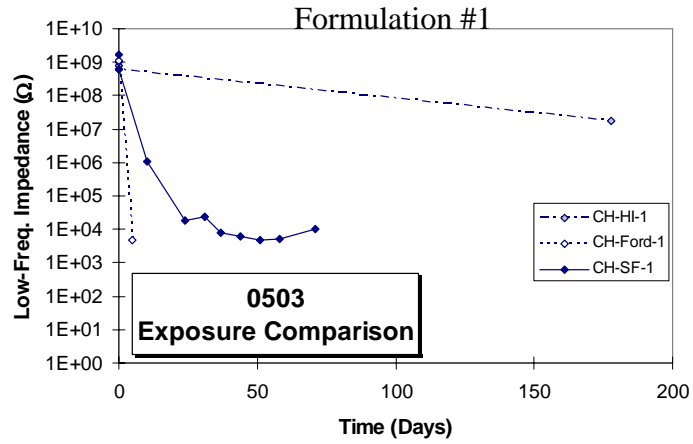
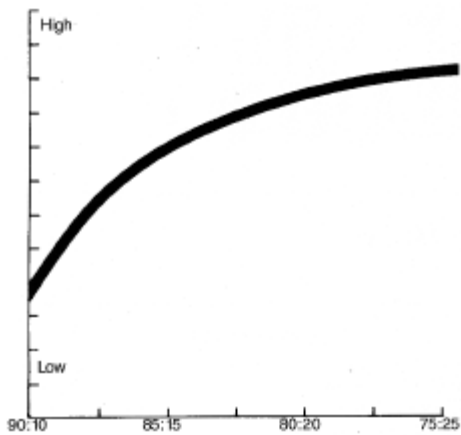
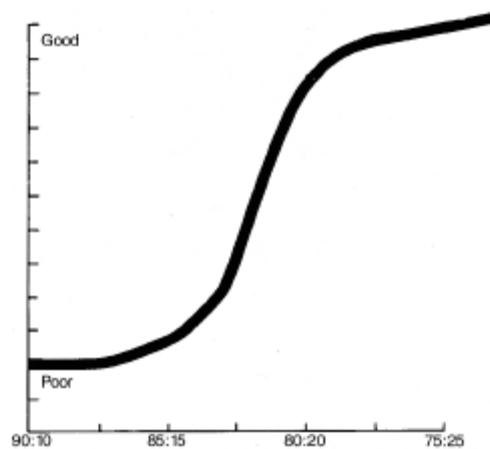


**Figure 3.6.** Comparison of the three tests: B117, Ford test and outdoor exposure at Hawaii; formulation details on p 74



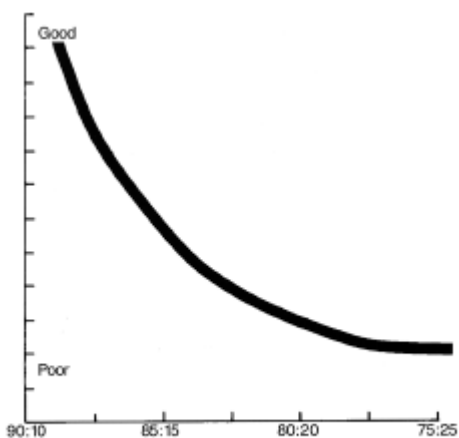
Epoxy: Curing Agent, solids

**Hardness development**



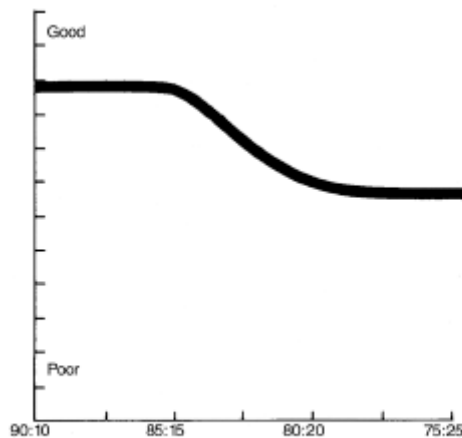
Epoxy: Curing Agent, solids

**Solvent resistance**



Epoxy: Curing Agent, solids

**Acid resistance**



Epoxy: Curing Agent, solids

**Salt fog resistance**

Note: Theoretical stoichiometric ratio in this case is 80:20

**Figure 3.7.** Effect of the epoxy : amine ratio (EPI-REZ 5522-WY-55 : EPIKURE 8290-Y-60) on important coating properties [9]

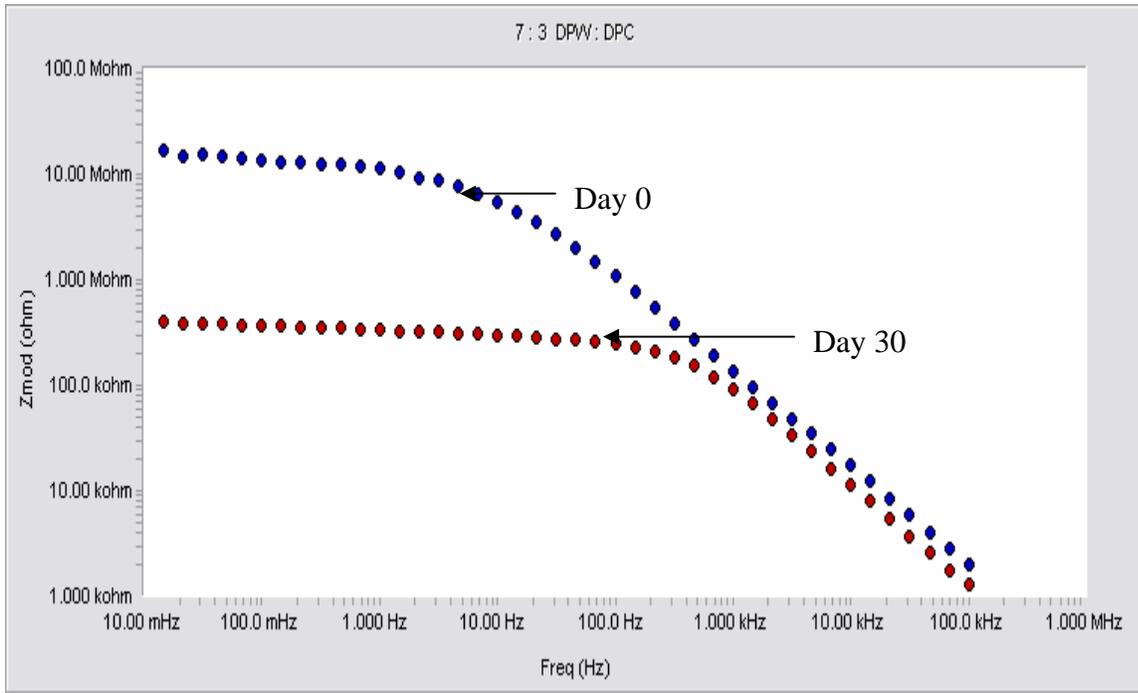


**Figure 3.8.** Coating without bis-sulfur – Bode impedance plots on day 0 and day 30 of 3.5 wt% salt water exposure; formulation details on p 78

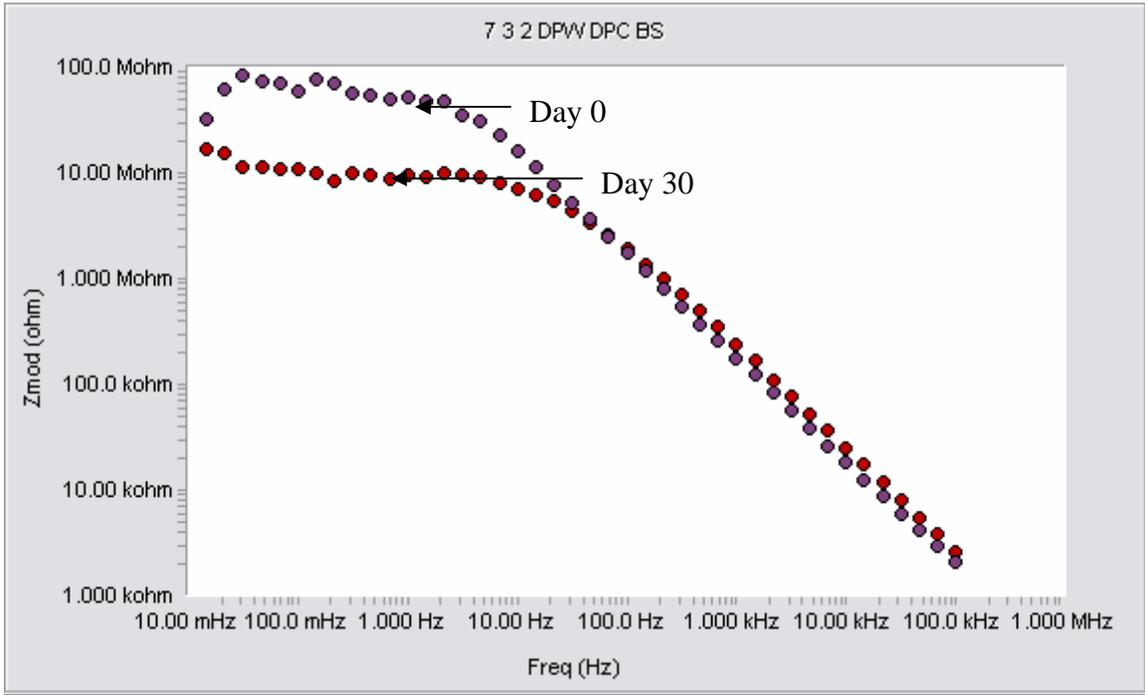
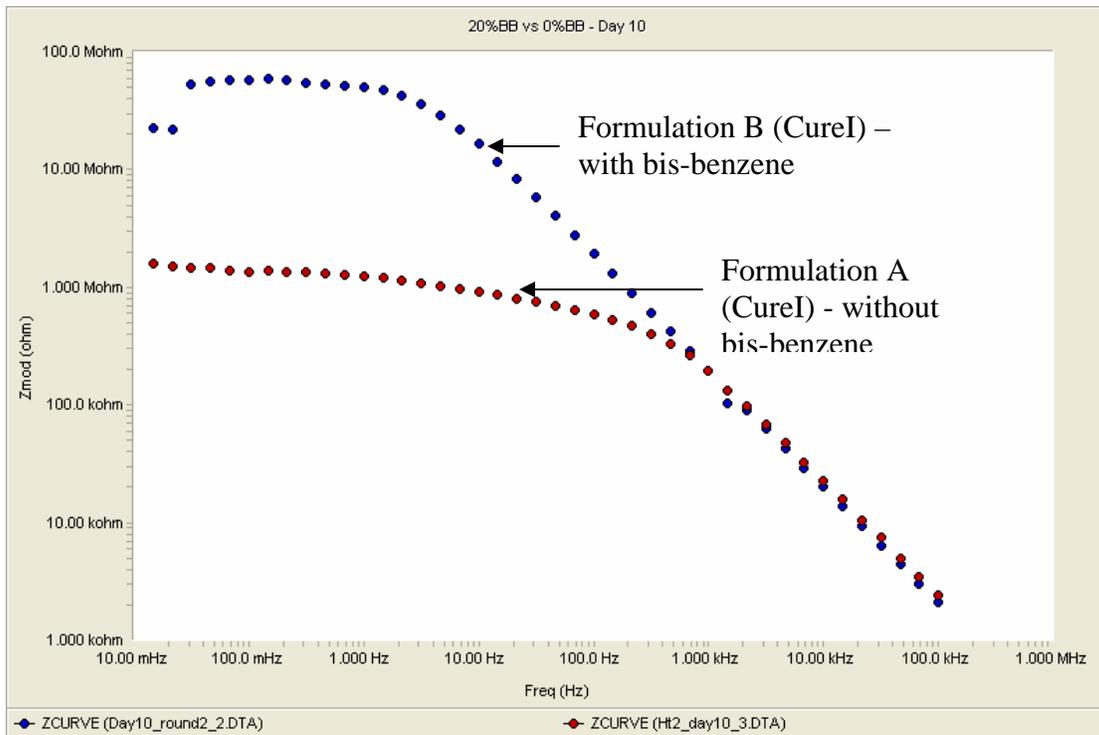
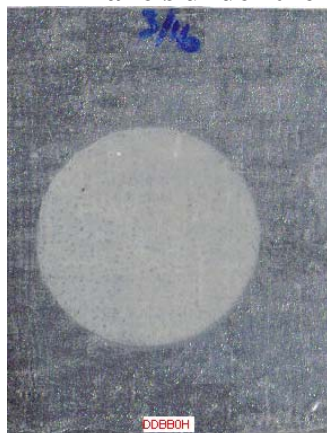


**Figure 3.9.** Coating with bis-sulfur – Bode impedance plots on day 0 and day 30 of 3.5 wt% salt water exposure; formulation details on p 78



**Panels under the O ring – After 35 days**



**Formulation A (CureI)**



**Formulation B (CureI)**

**Figure 3.10.** Comparison of bode plots of coatings with and without bis-benzene on day 10 of exposure to 3.5 wt% salt water. The images of the exposed are also shown below the impedance plots; formulation details on p 79

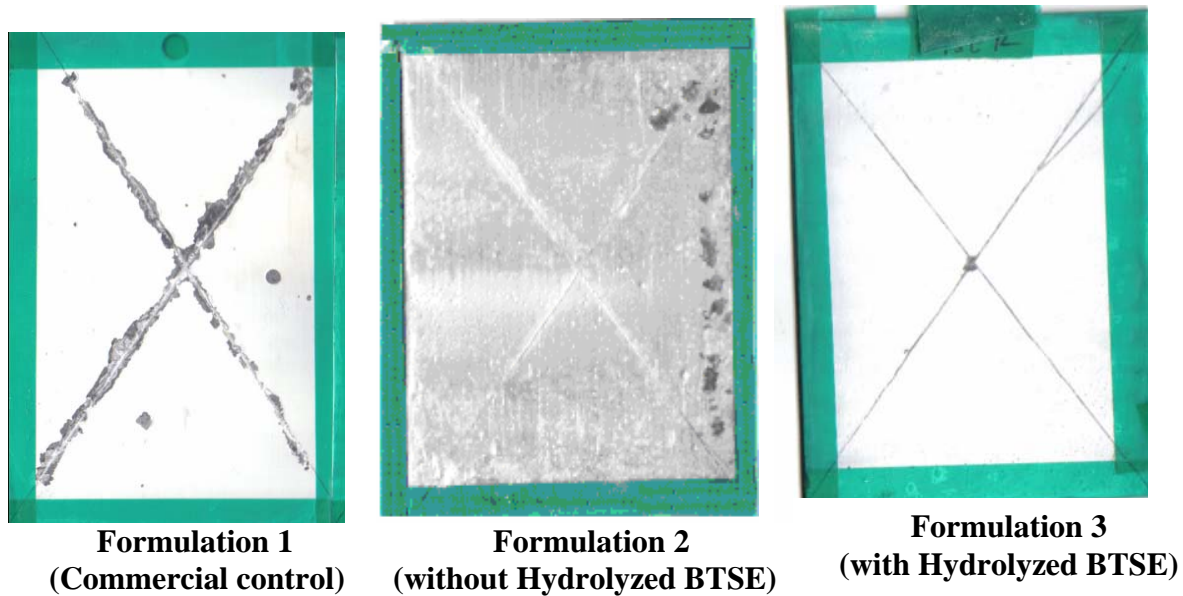


**Figure 3.11.** Machu test exposed panels showing the effect of incorporation of hydrolyzed BTSE in superprimer coatings; formulation details on p 82

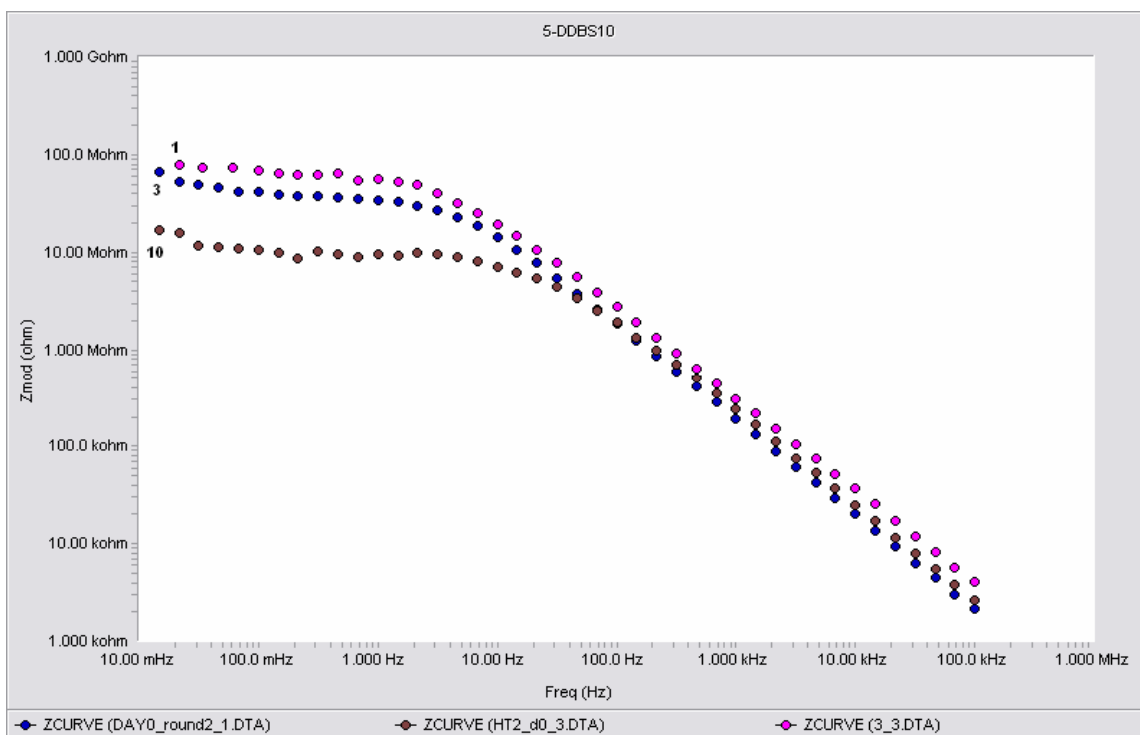


**Figure 3.12.** Bode plots for superprimer coating without any minor binder (Formulation 1) – on days 1, 3 and 10 of exposure; formulation details on p 84

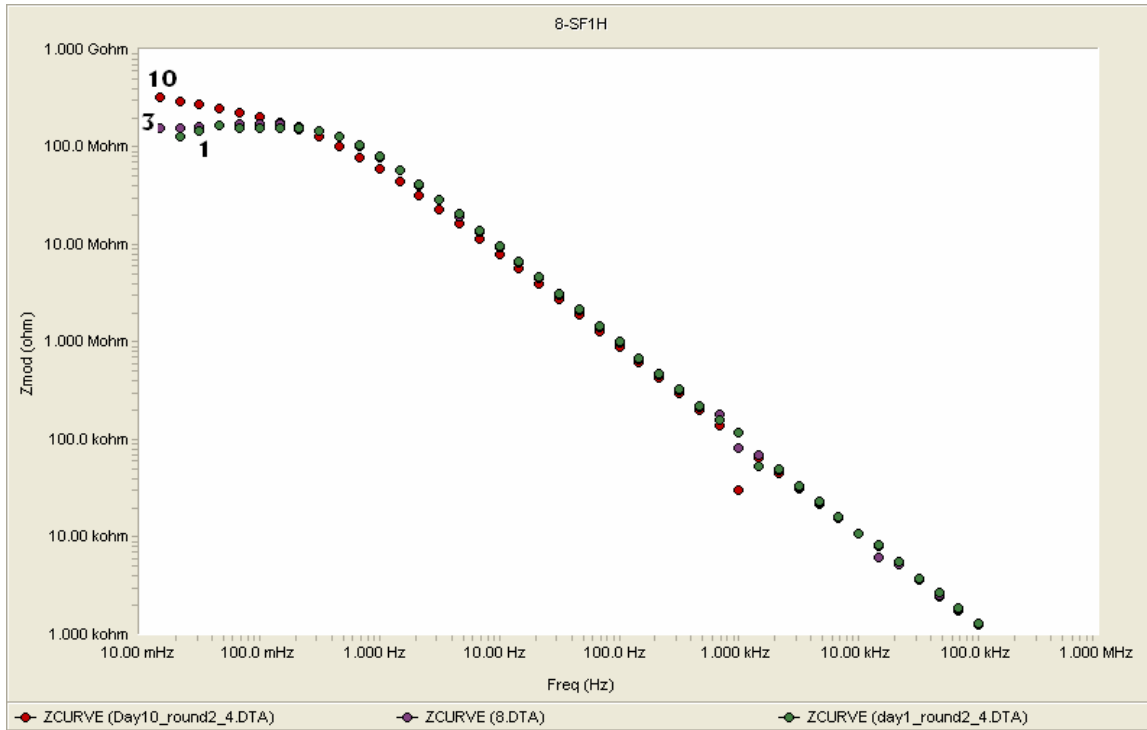


**Figure 3.13.** Bode plots for superprimer coating with polyurethane minor binder (Formulation 2) – on days 1, 3 and 10 of exposure; formulation details on p 84

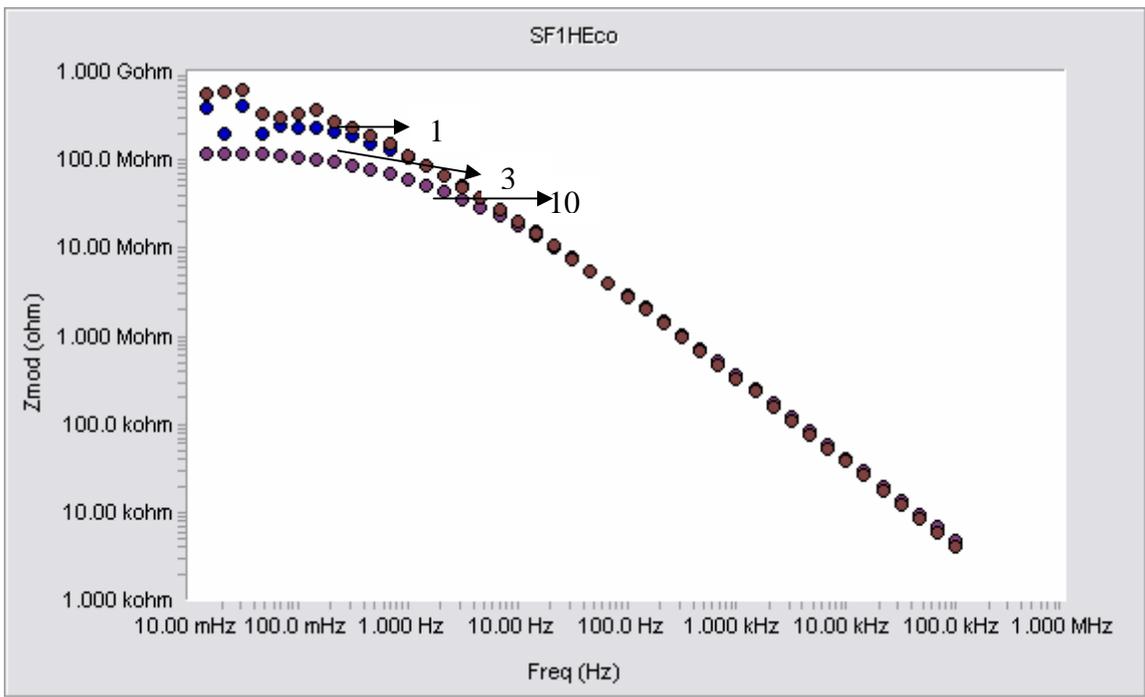


**Figure 3.14.** Bode plots for superprimer coating with polyacrylate minor binder (Formulation 3) – on days 1, 3 and 10 of exposure; formulation details on p 84

Coated HDG panels after 2000 hours of ASTM B117 test



Formulation 1  
(control 1 – without any inhibitor):



Formulation 2  
(with 15% CZM)

**Figure 3.15.** HDG panels with coatings with and without 15% CZM inhibitor – after 2000 hours of exposure; formulation details on p 86



Formulation 3  
(control 2 – without any inhibitor):



Formulation 4  
(with 10% corrostain 228)



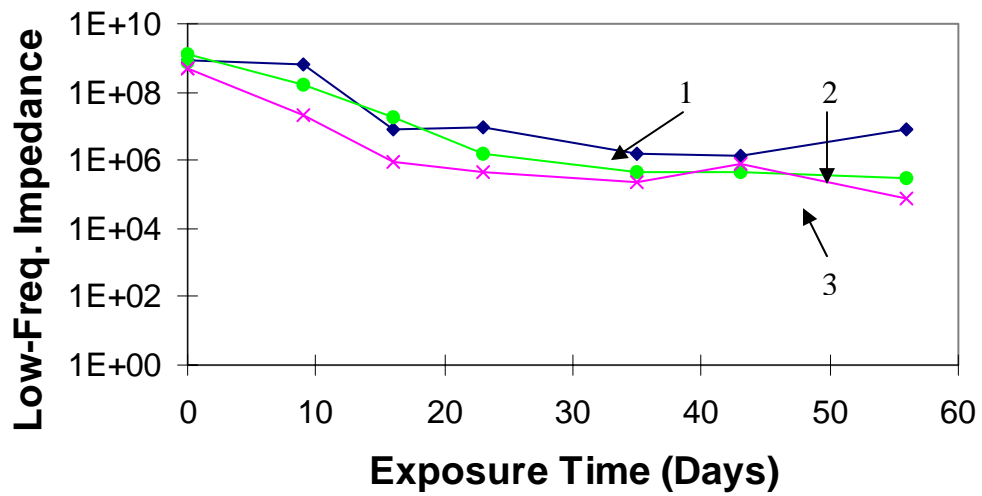
Formulation 5  
(with 5% cerium exchange silica )



Formulation 6  
(with a mixture of ZP, corrostain)

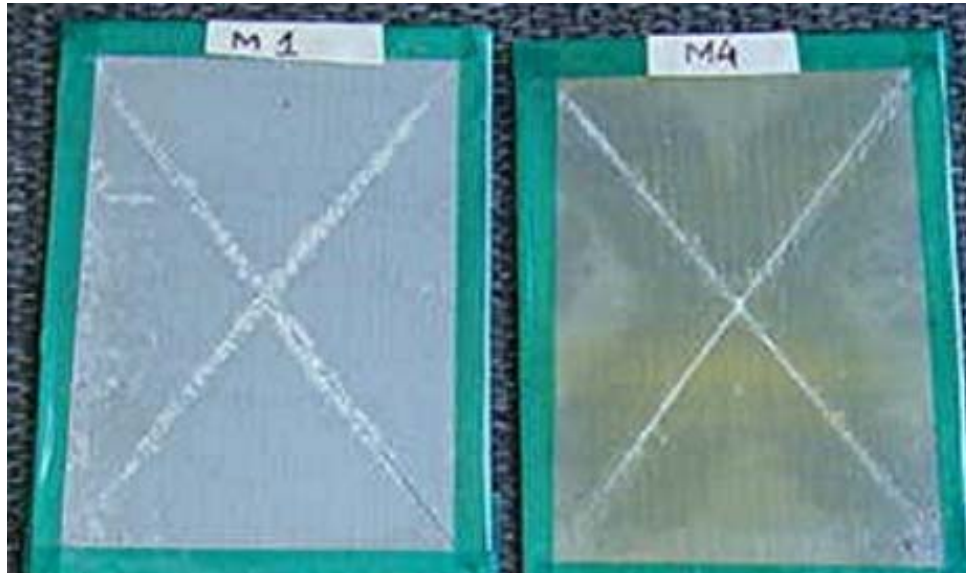
**Figure 3.16.** Coated HDG panels with various inhibitors – after 1350 hours of B117 test exposure; formulation details on p 86

1350 hours of ASTM B117 exposure



1- without any co-solvent; 2 – with acetone as co-solvent; 3 –Archer RC as co-solvent

**Figure 3.17.** Low-frequency impedance curves showing the absence of any deterioration in anti-corrosion performance of superprimers upon incorporation of the co-solvents acetone and Archer RC; formulation details on p 87



**Formulation 1**

**Formulation 2**

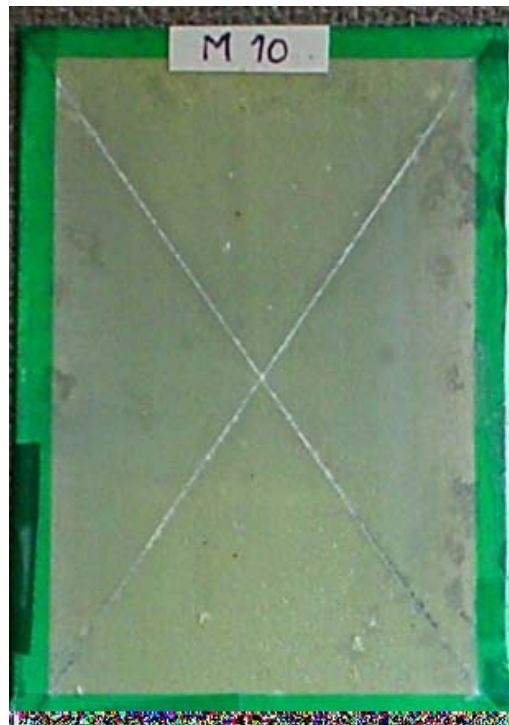


**Formulation 3**

**Figure 3.18.** Images of B117 test-exposed panels after 35 days of exposure, showing the absence of any deterioration in anti-corrosion performance of superprimers upon incorporation of the co-solvents acetone and Archer RC; formulation details on p 87



**Formulation 1  
(without DBTL)**



**Formulation 2  
(with DBTL)**

**Figure 3.19.** Images of B117 test-exposed panels, after 1350 hours of exposure, showing the absence of any deterioration in anti-corrosion performance of superprimers upon incorporation of DBTL; formulation details on p 89



Formulation 1  
(without aluminum paste)



Formulation 2  
(with aluminum paste)

**Figure 3.20.** HDG panels coated with superprimers with and without leaving aluminum paste after exposure to 30 days of salt water immersion and 3 days of Machu test; formulation details on p 90

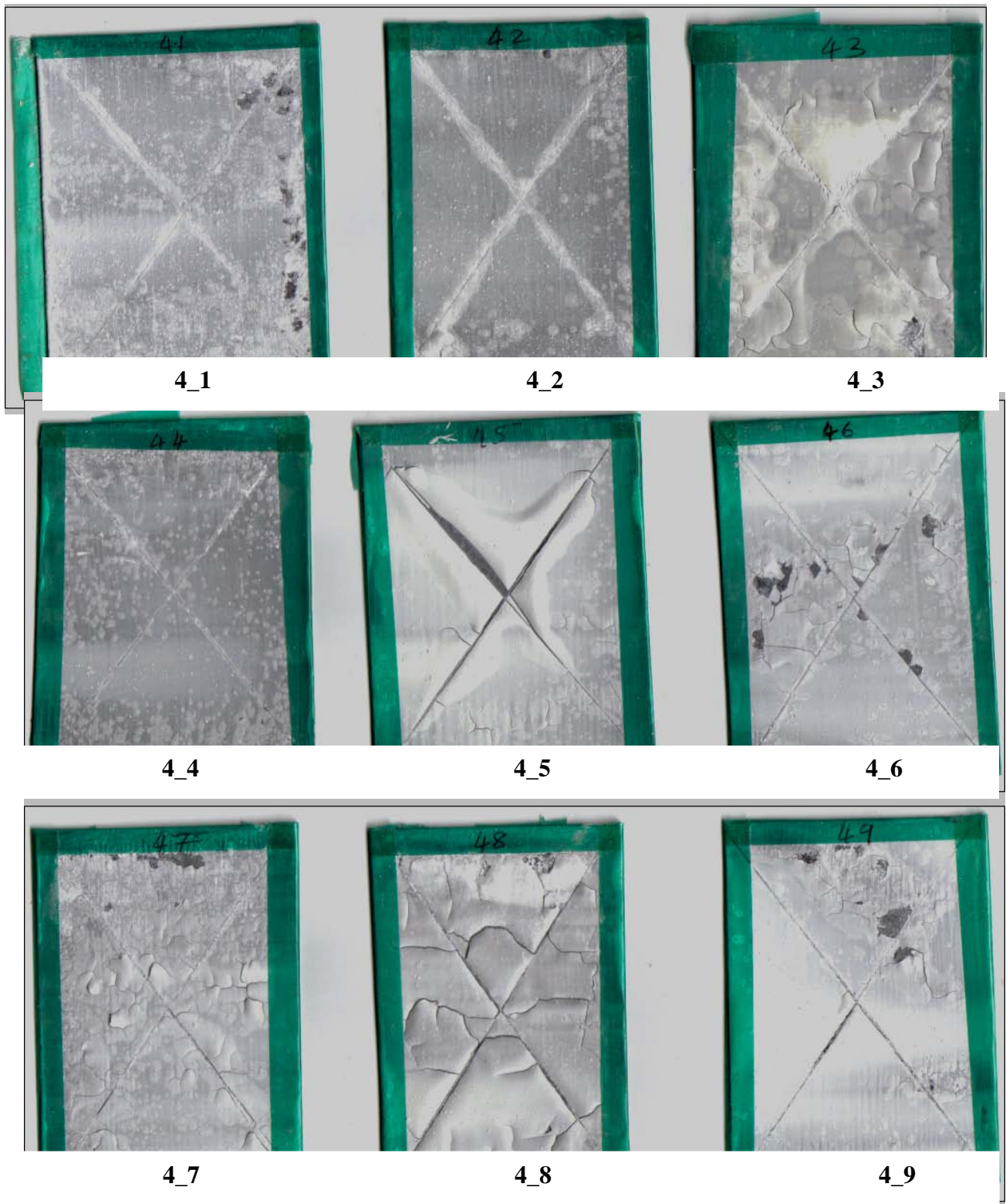


**Figure 4.1.** Coatings in OA4 after 3 days of exposure in the Machu test; formulation details in Table 4.5 on p 162



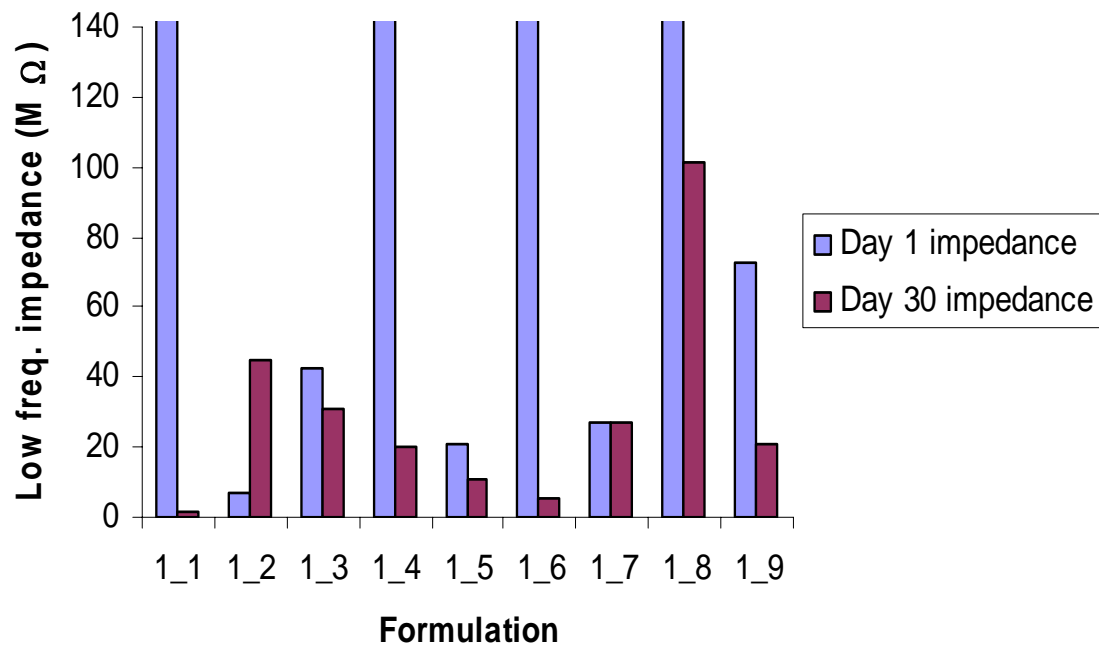
1\_1

2\_1

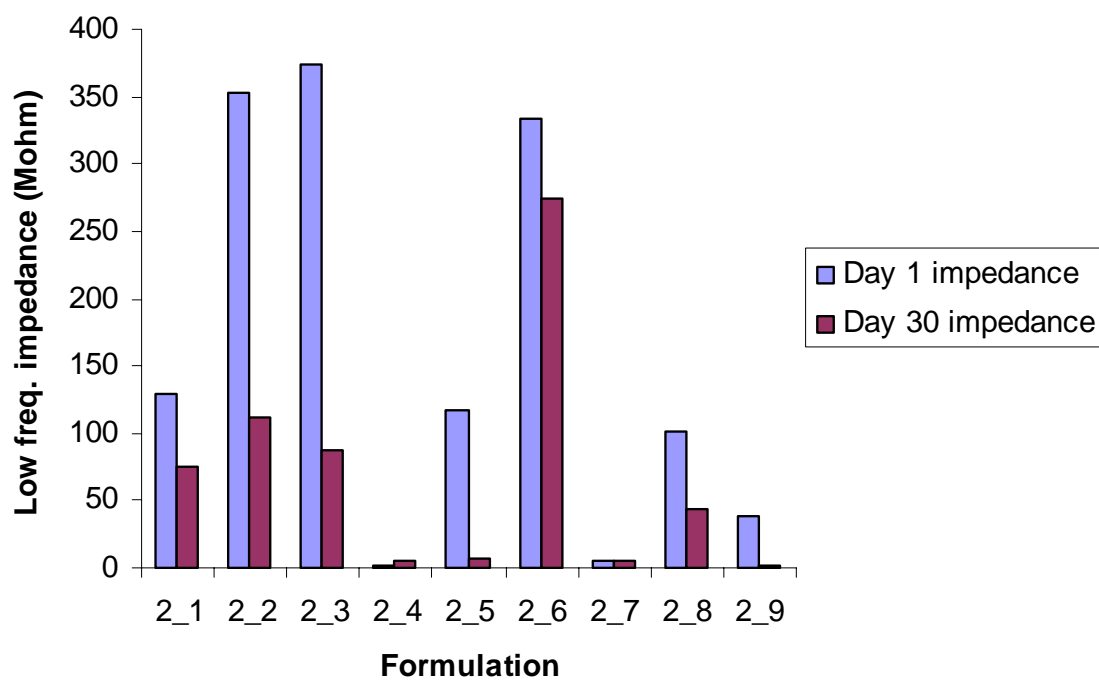


2\_6 ( and the rest of the formulations)

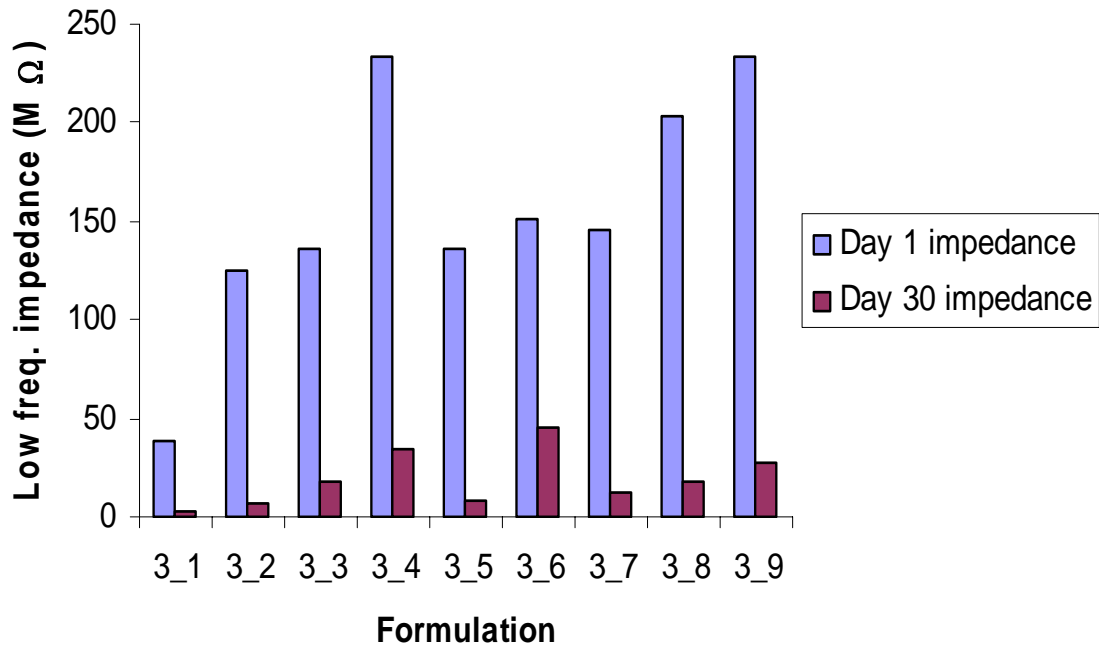
**Figure 4.2.** Tape adhesion test results - Effect of silane on wet-adhesion of primer with topcoat and substrate. 1\_1 and 2\_1 formulations do not have any silane and show poor adhesion. 2\_6 and the rest of the tested formulations having silane component and thereby show excellent adhesion



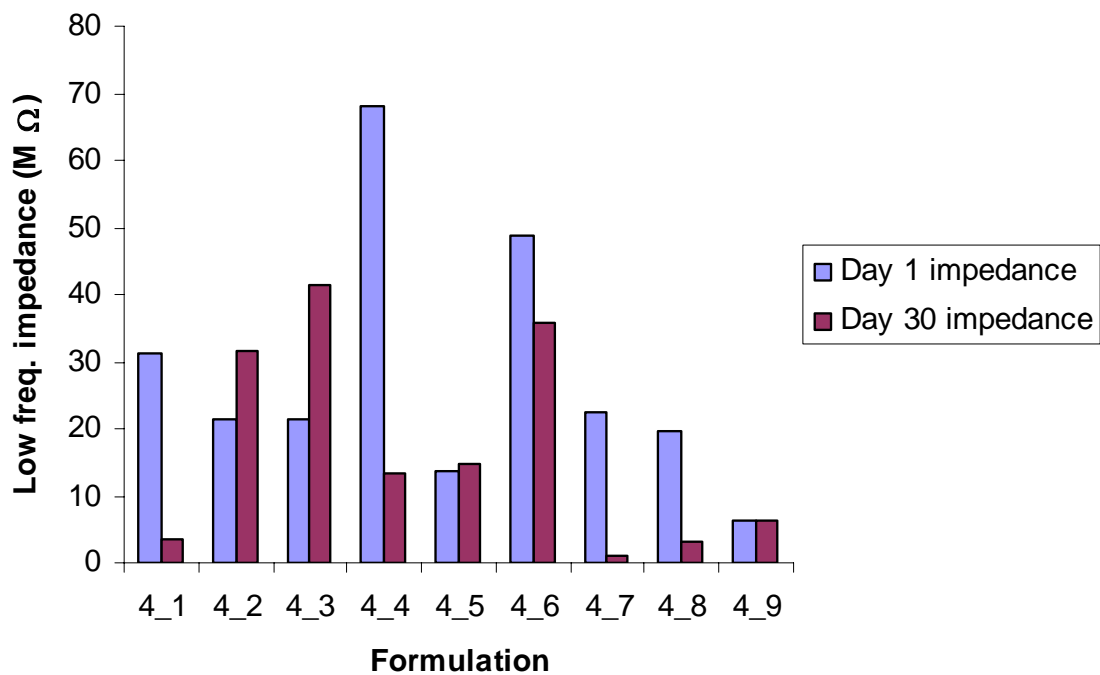
**Figure 4.3.** Low-frequency impedance values of the coatings in OA1, on day 1 and day 30 of exposure in EIS



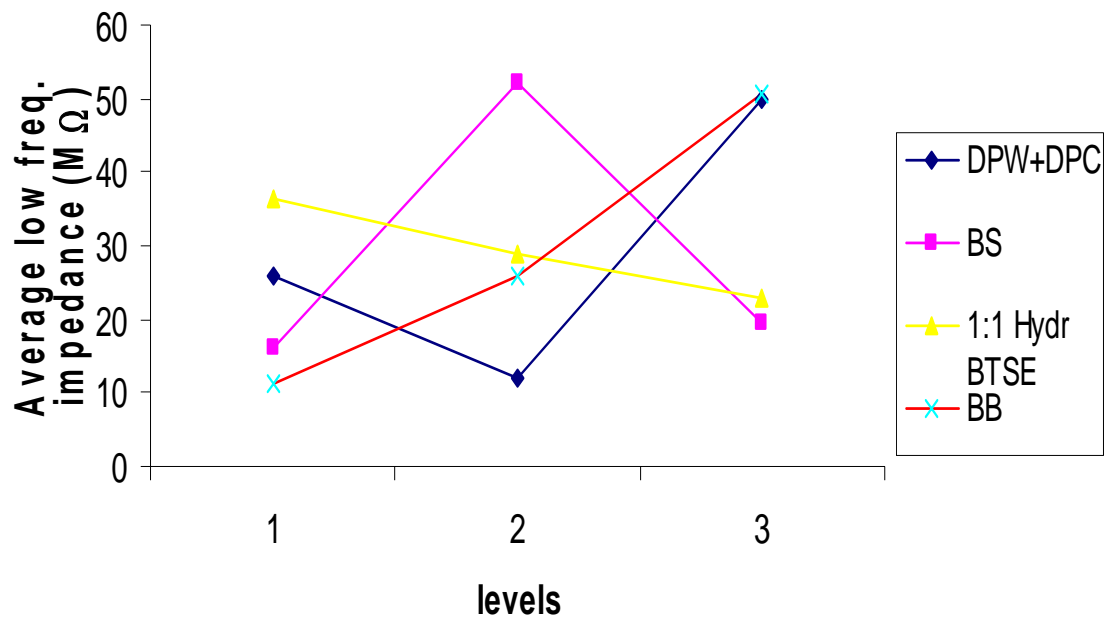
**Figure 4.4.** Low-frequency impedance values of the coatings in OA2, on day 1 and day 30 of exposure in EIS



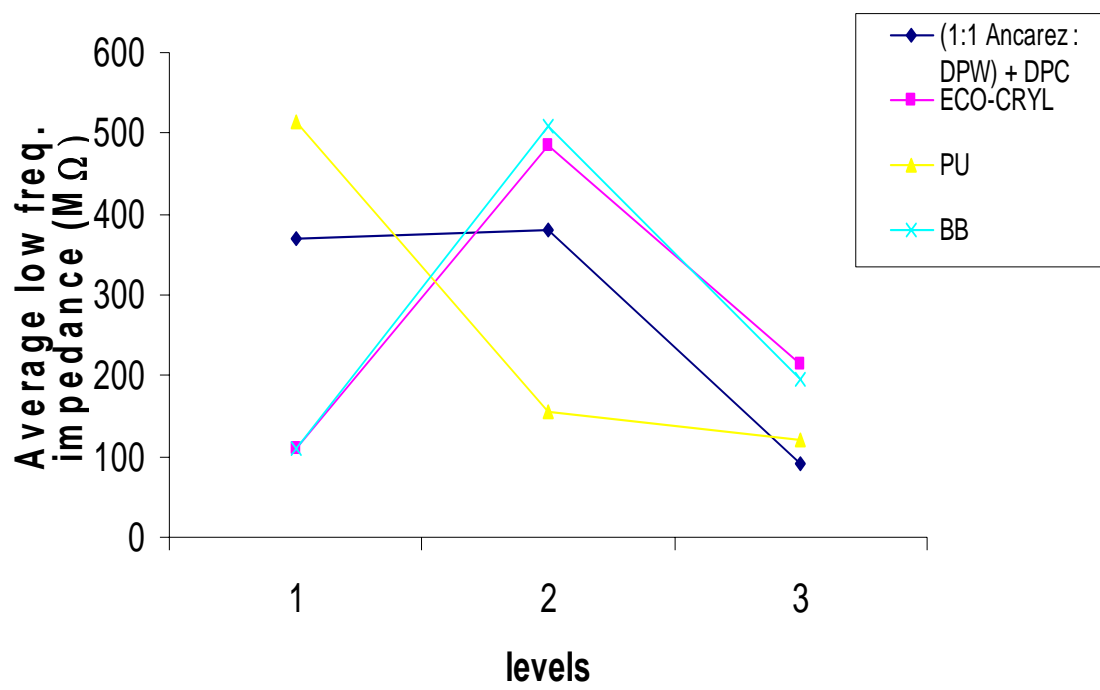
**Figure 4.5.** Low-frequency impedance values of the coatings in OA3, on day 1 and day 30 of exposure in EIS



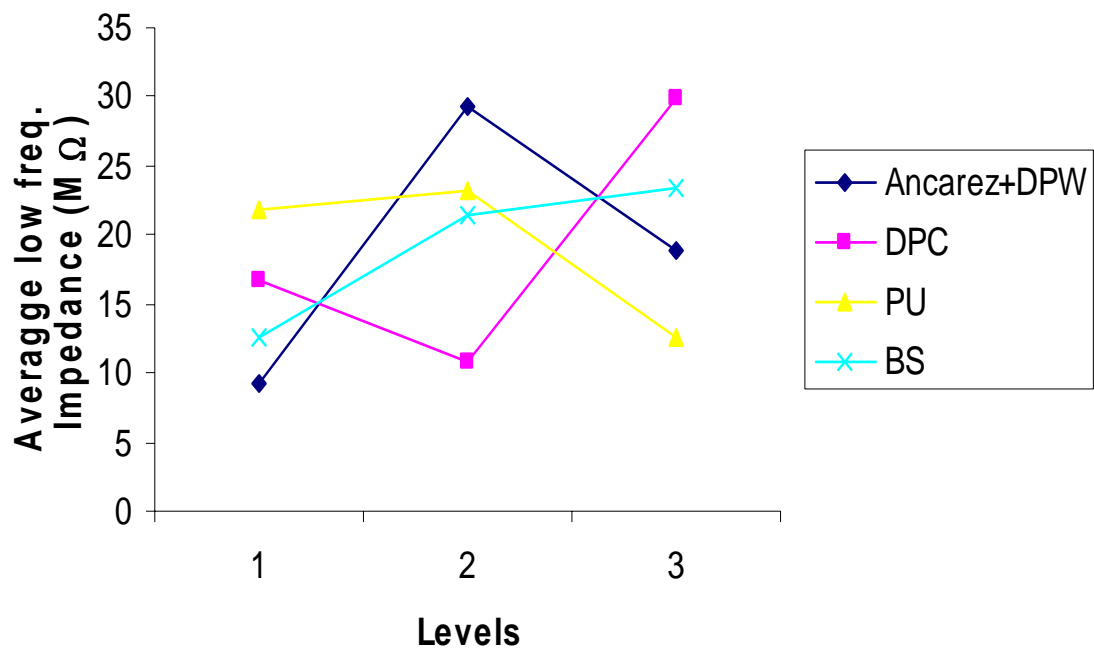
**Figure 4.6.** Low-frequency impedance values of the coatings in OA4, on day 1 and day 30 of exposure in EIS



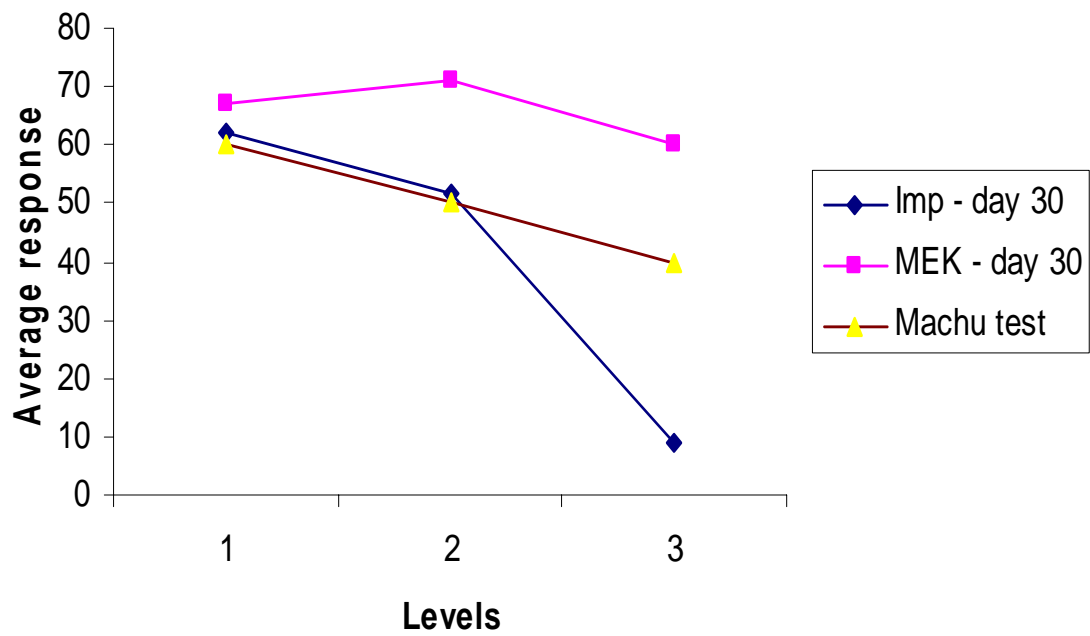
**Figure 4.7.** Optimization plot for OA1



**Figure 4.8.** Optimization plot for OA2

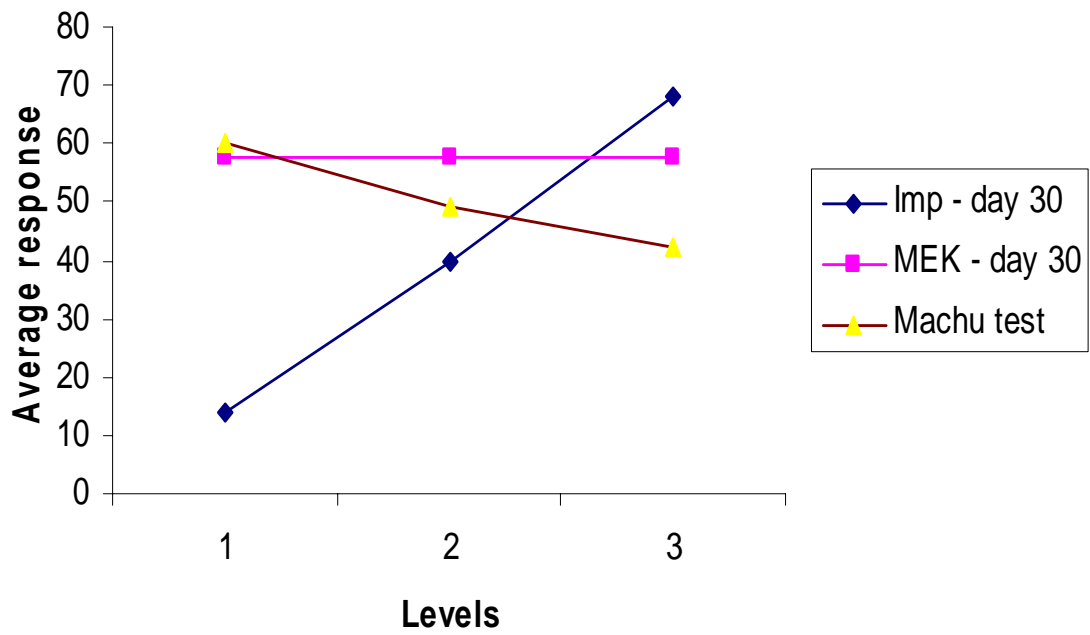


**Figure 4.9.** Optimization plot for OA3



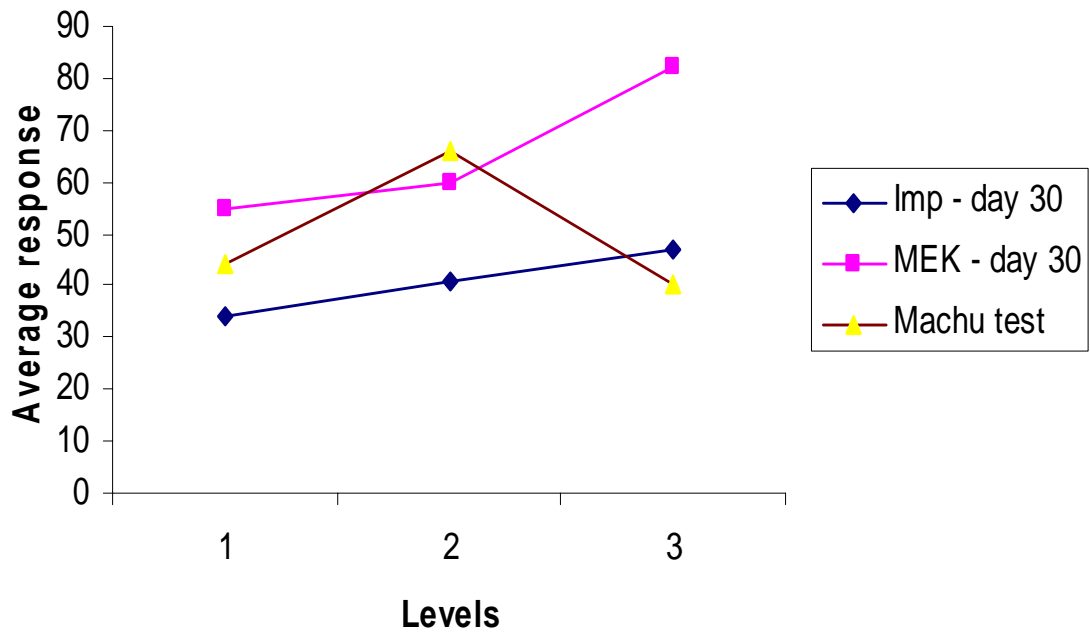
Optimum level for this factor: level1 (8+2)

Figure 4.10 (a). Optimization plot for Factor 1 of OA4



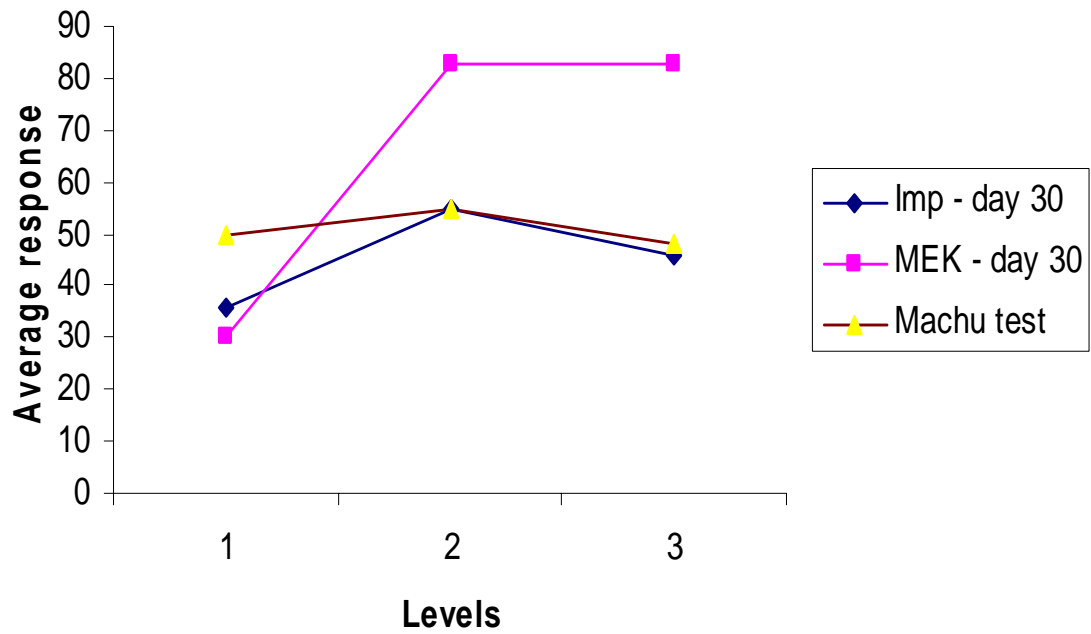
Optimum level for this factor: level 2 (0.5)

Figure 4.10 (b). Optimization plot for Factor 2 of OA4



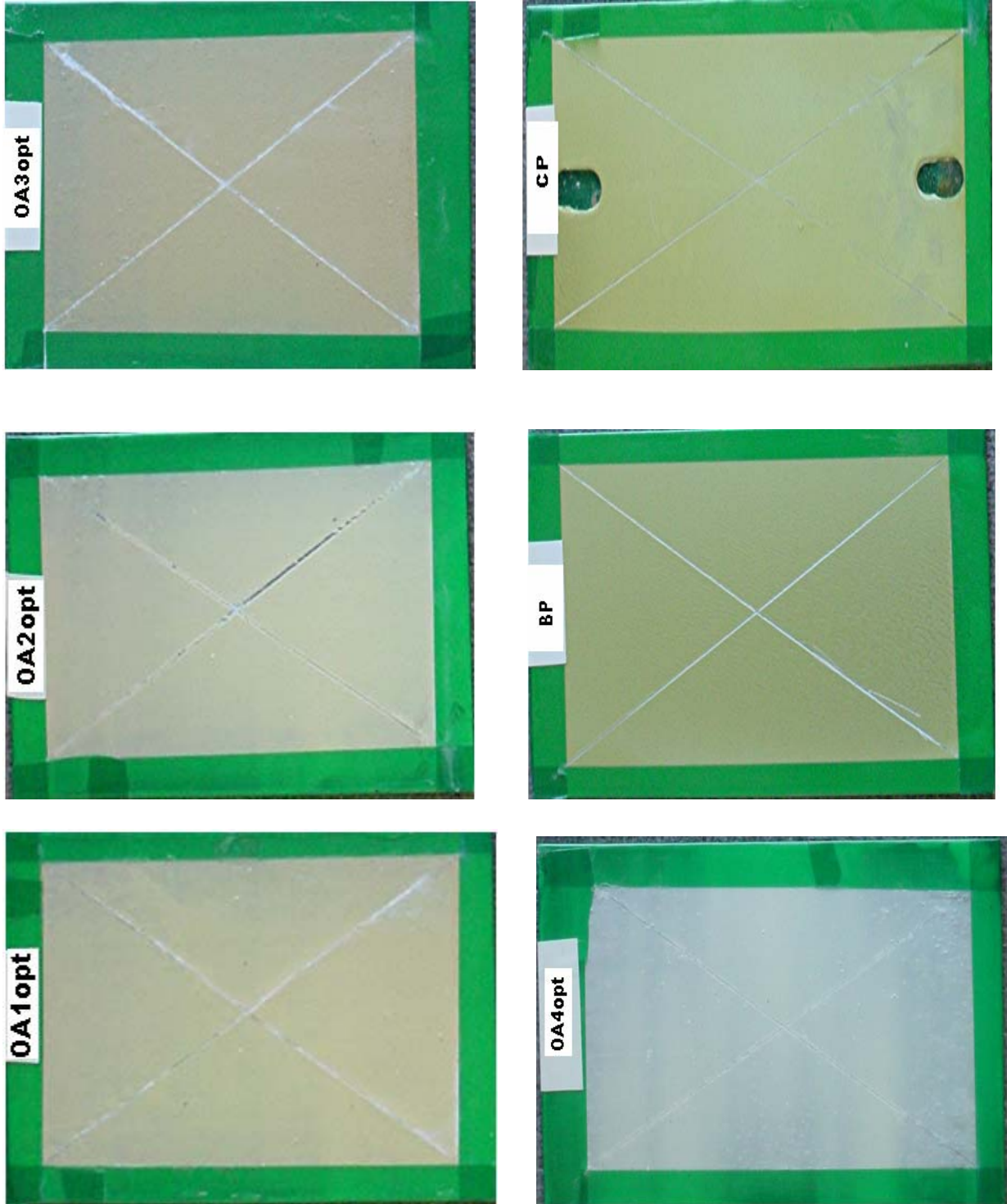
Optimum level for this factor: level 2 (1)

Figure 4.10 (c). Optimization plot for Factor 3 of OA4



Optimum level for this factor: level 2 (0.5)

**Figure 4.10 (d).** Optimization plot for Factor 4 of OA4



**Figure 4.11.** Images of HDG panels coated with the four optimized coatings and the two chromated controls, all without topcoat and 2000 hours of exposure in the B117 test

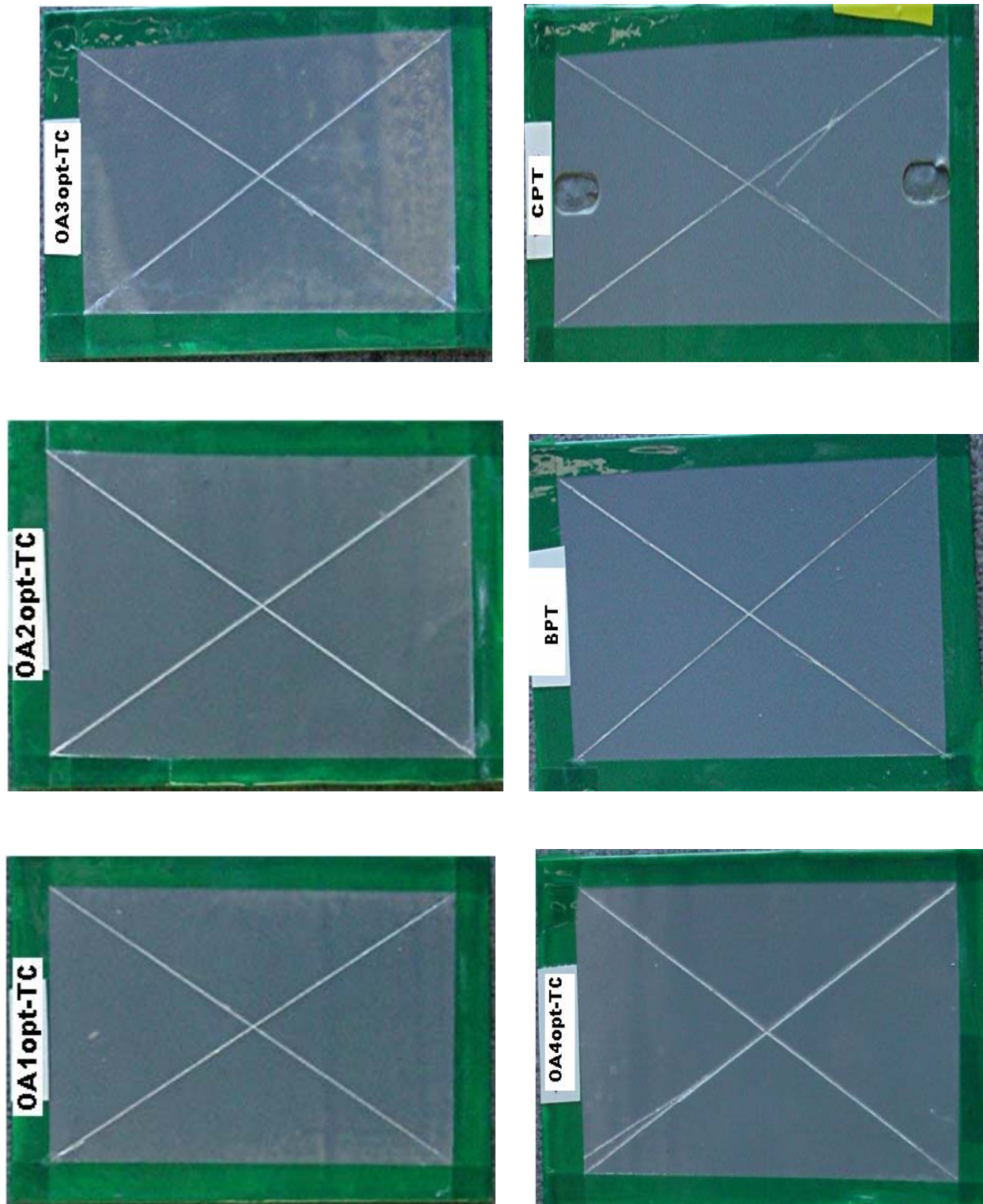


**Figure 4.12.** Images of HDG panels coated with the four optimized coatings and the two chromated controls, all with topcoat and 2000 hours of exposure in the B117 test

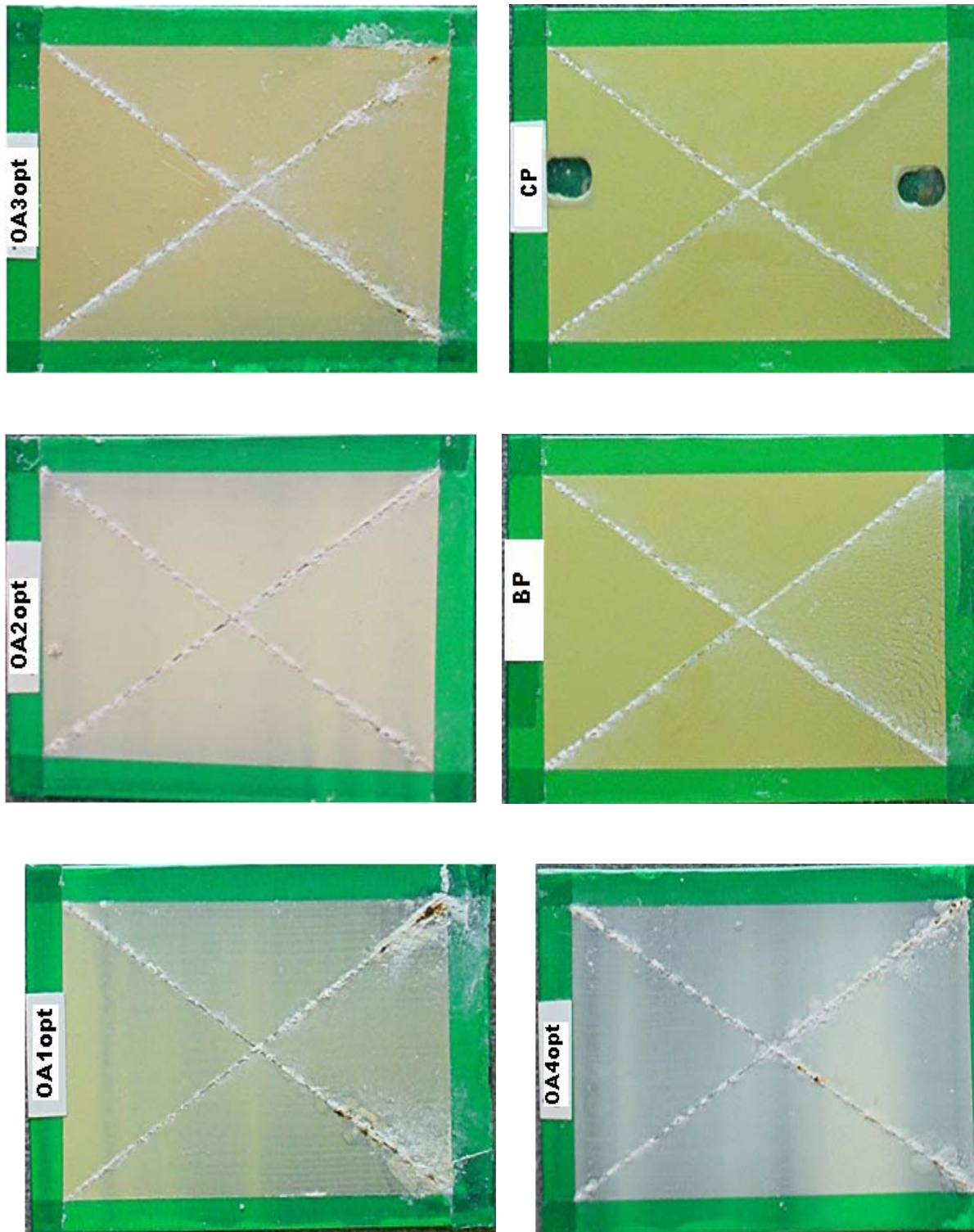


**Figure 4.13.** Images of HDG panels coated with the four optimized coatings and the two chromated controls, all without topcoat and 59 cycles of exposure in the Ford cyclic test

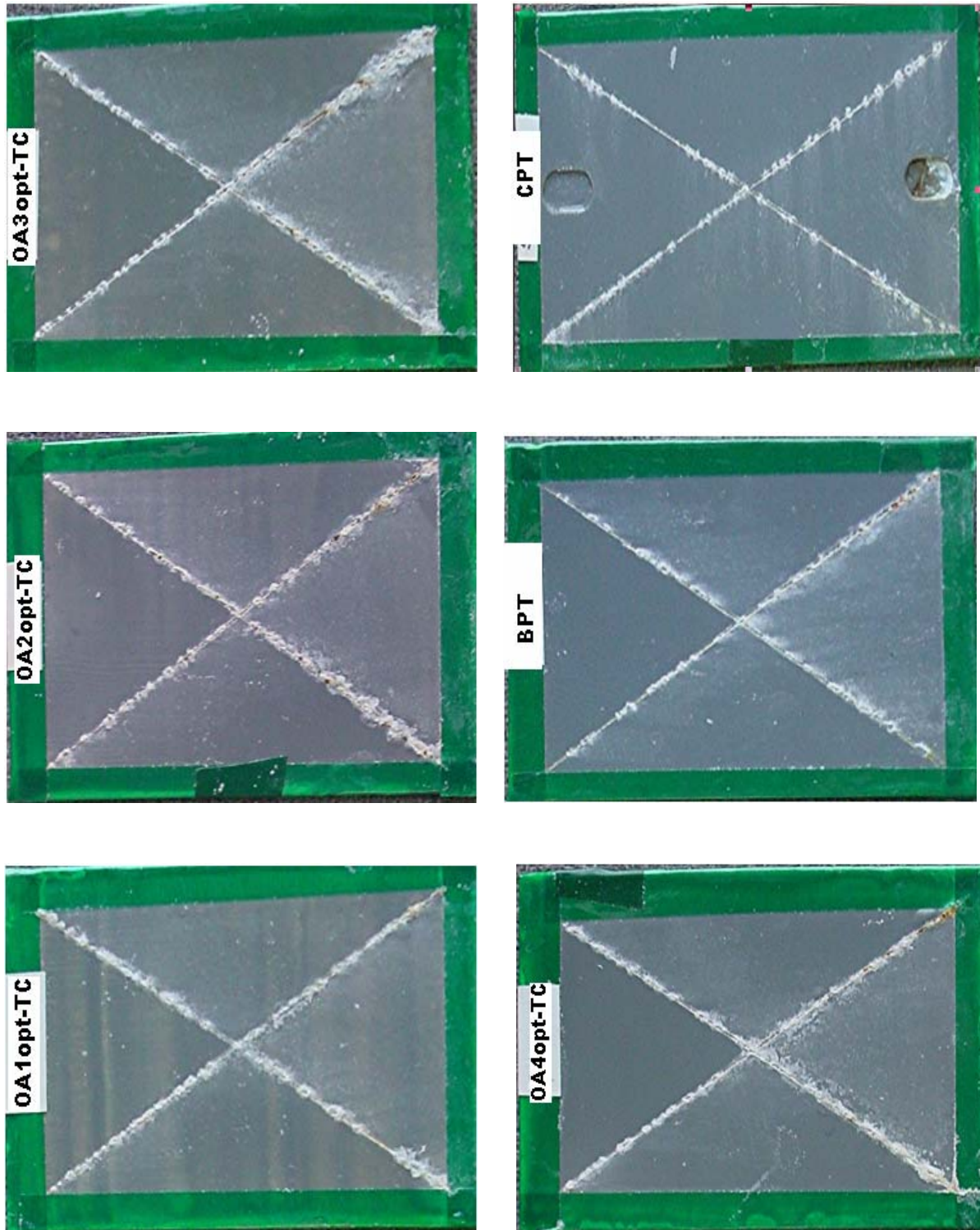


**Figure 4.14.** Images of HDG panels coated with the four optimized coatings and the two chromated controls, all with topcoat and 59 cycles of exposure in the Ford cyclic test

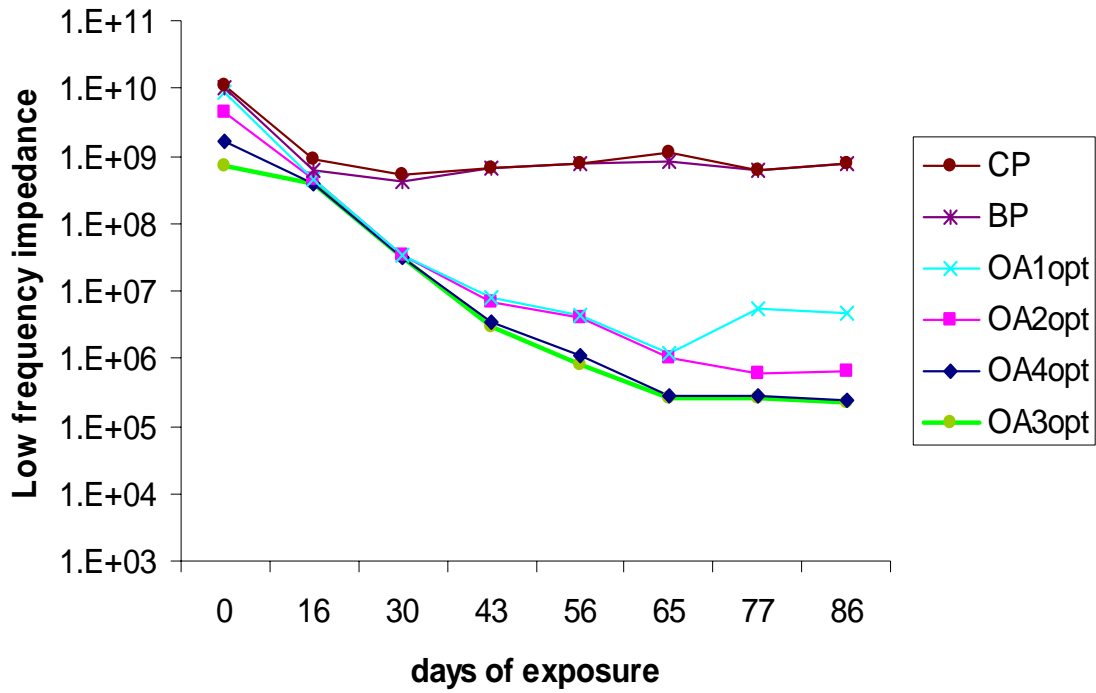


**Figure 4.15.** Low-frequency impedance curves of HDG panels coated with the four optimized coatings and the two chromated controls, all without topcoat and 2000 hours of exposure in the B117 test

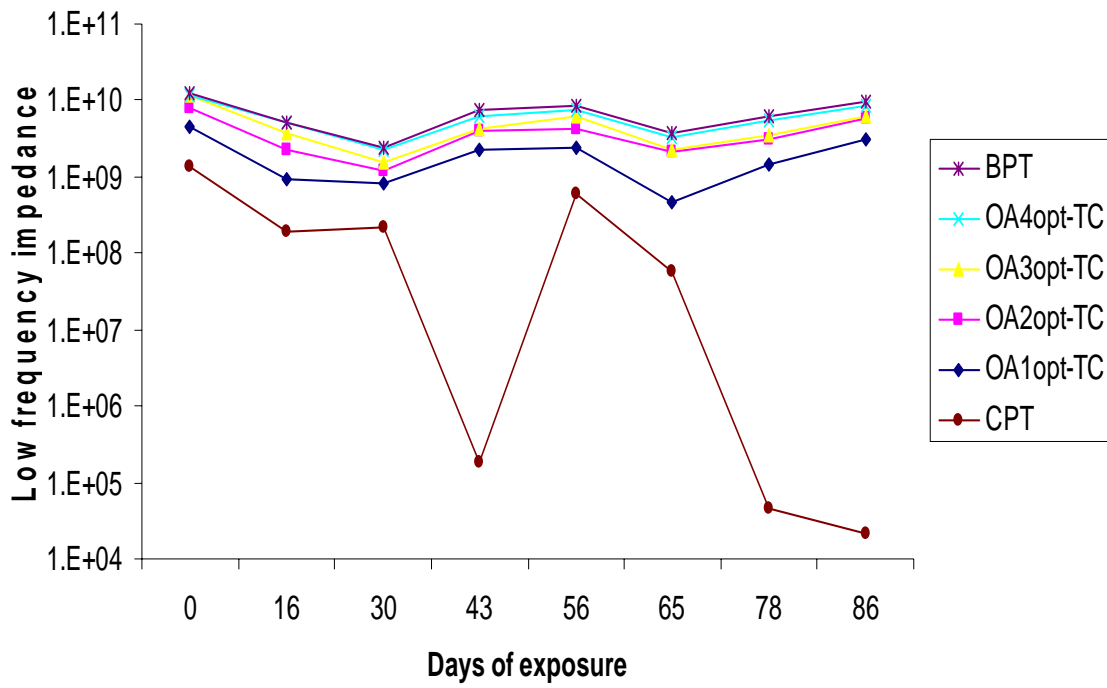


**Figure 4.16.** Low-frequency impedance curves of HDG panels coated with the four optimized coatings and the two chromated controls, all with topcoat and 2000 hours of exposure in the B117 test

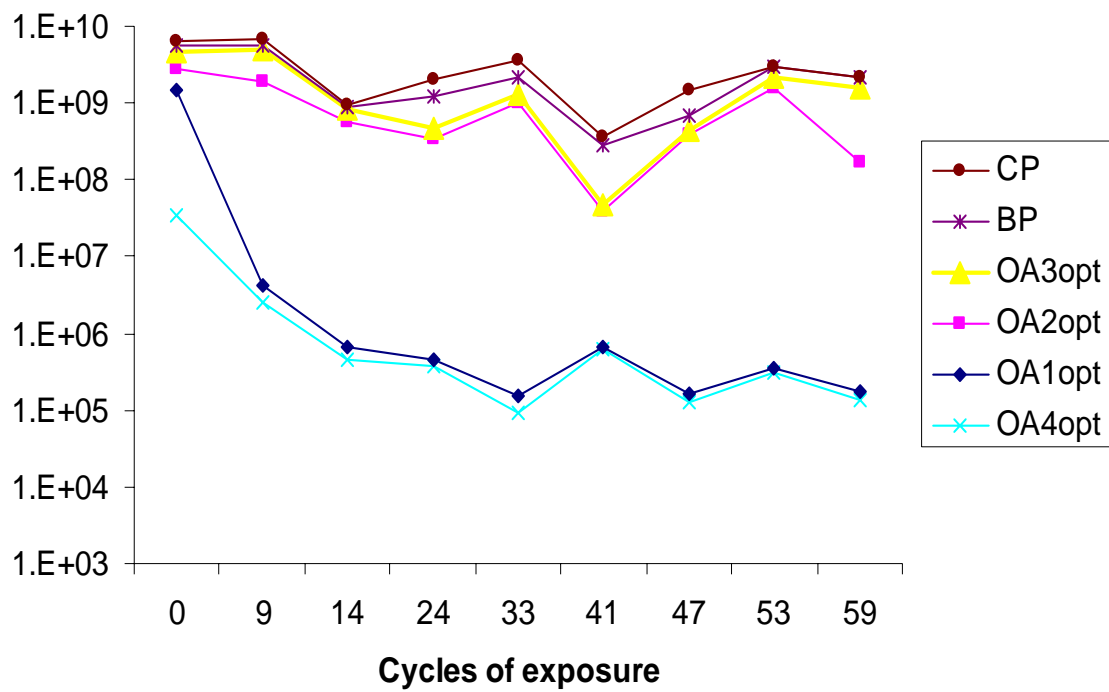


**Figure 4.17.** Low-frequency impedance curves of HDG panels coated with the four optimized coatings and the two chromated controls, all without topcoat and and 59 cycles of exposure in the Ford cyclic test

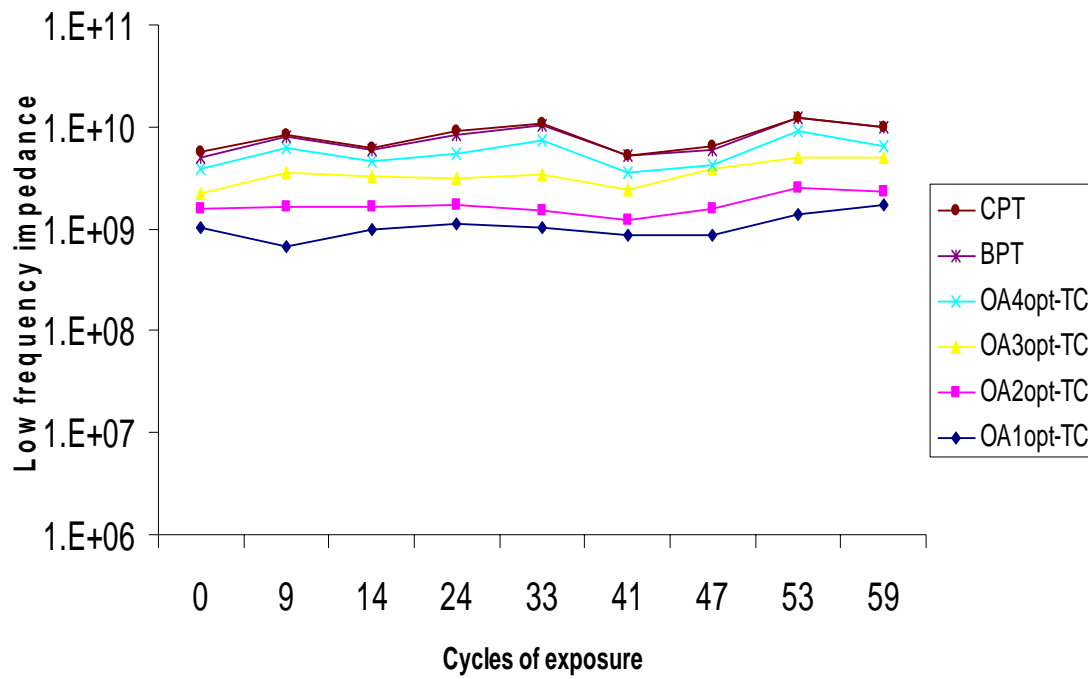


**Figure 4.18.** Low-frequency impedance curves of HDG panels coated with the four optimized coatings and the two chromated controls, all with topcoat and and 59 cycles of exposure in the Ford cyclic test

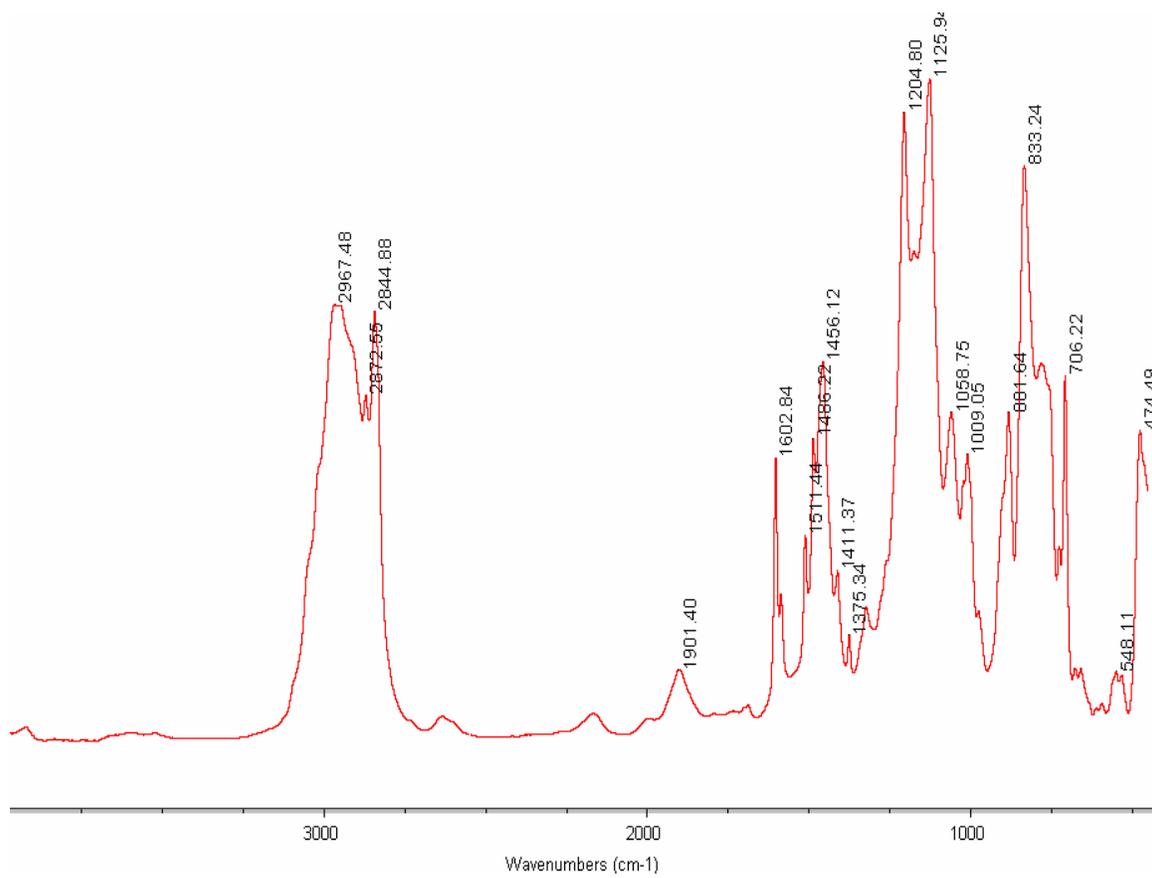


**Figure 5.1.** RAIR spectrum of neat bis-benzene film on day 7 of RT cure, with annotated peaks; refer Table 5.1 for peak identification

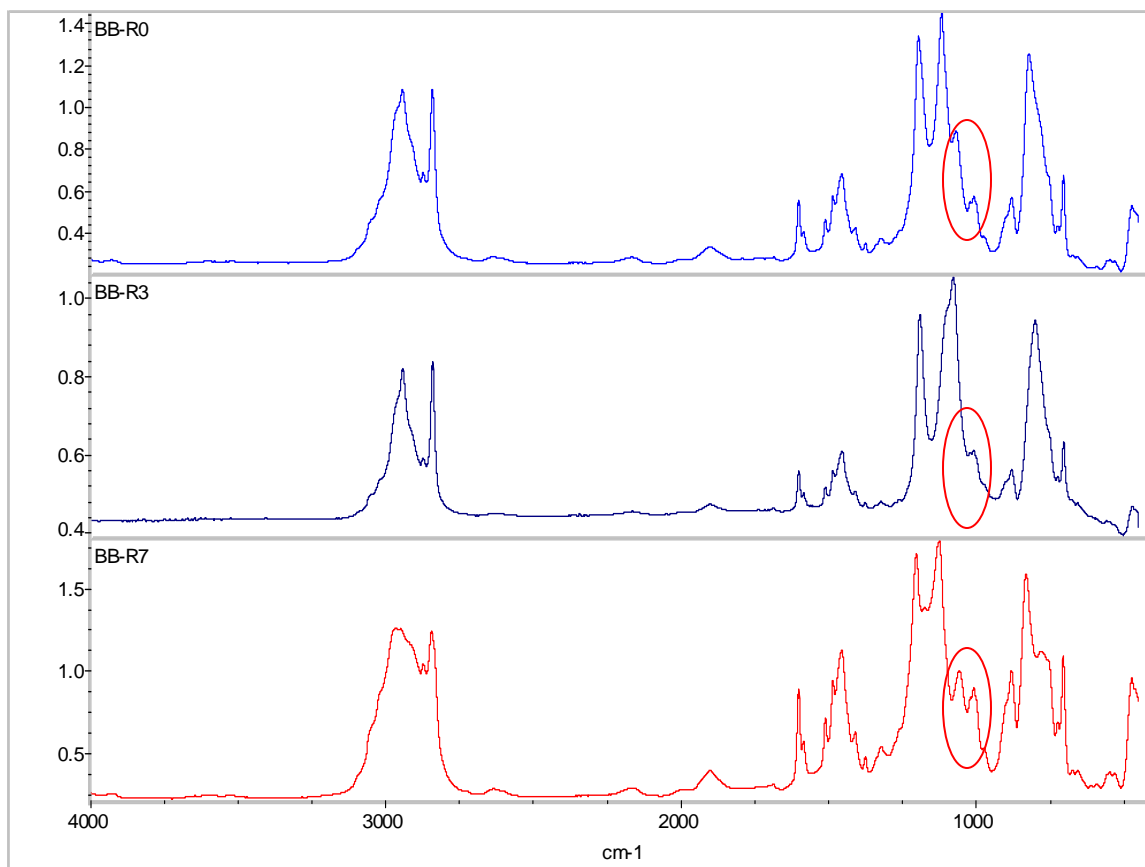


**Figure 5.2.** Stacked RAIR spectra of bis-benzene films for comparison at various curing stages; refer Table 5.1 for peak identification

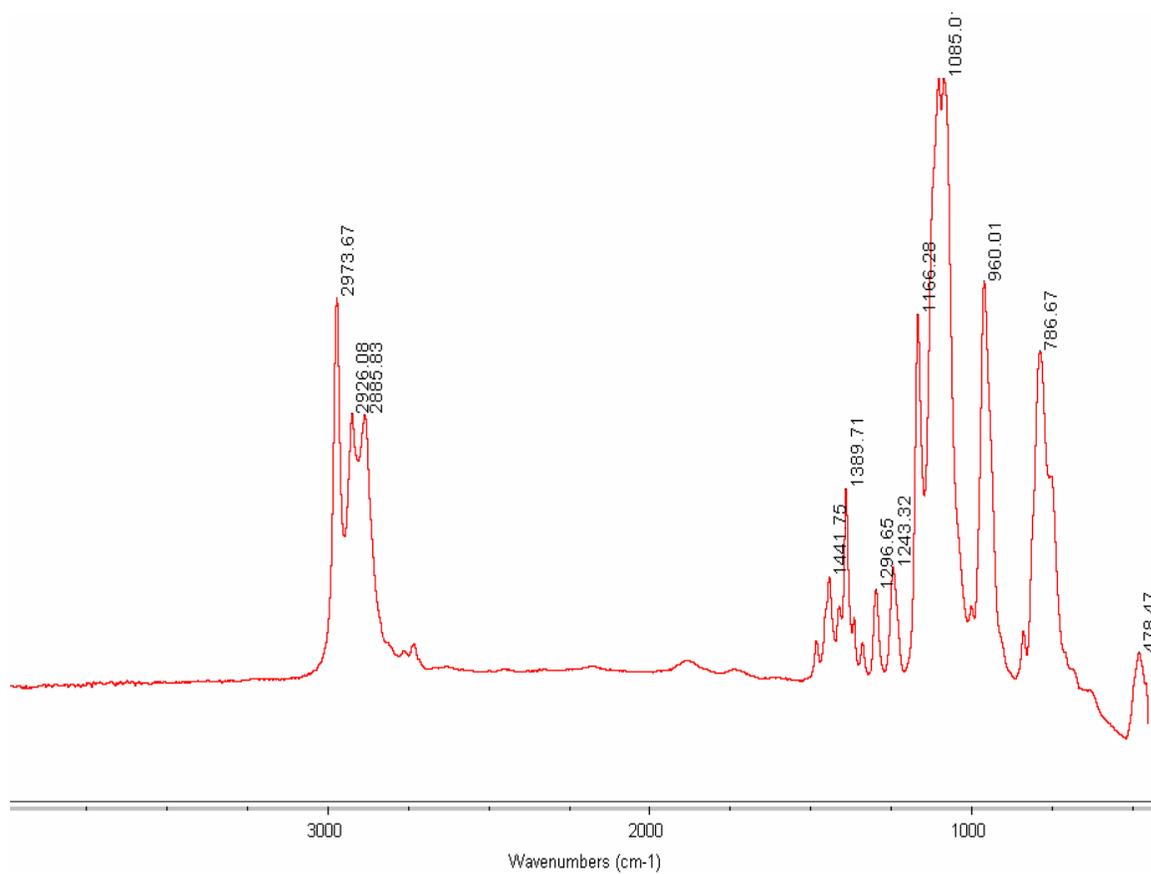


**Figure 5.3.** RAIR spectrum of neat bis-sulfur film on day 7 of RT cure, with annotated peaks; refer Table 5.2 for peak identification

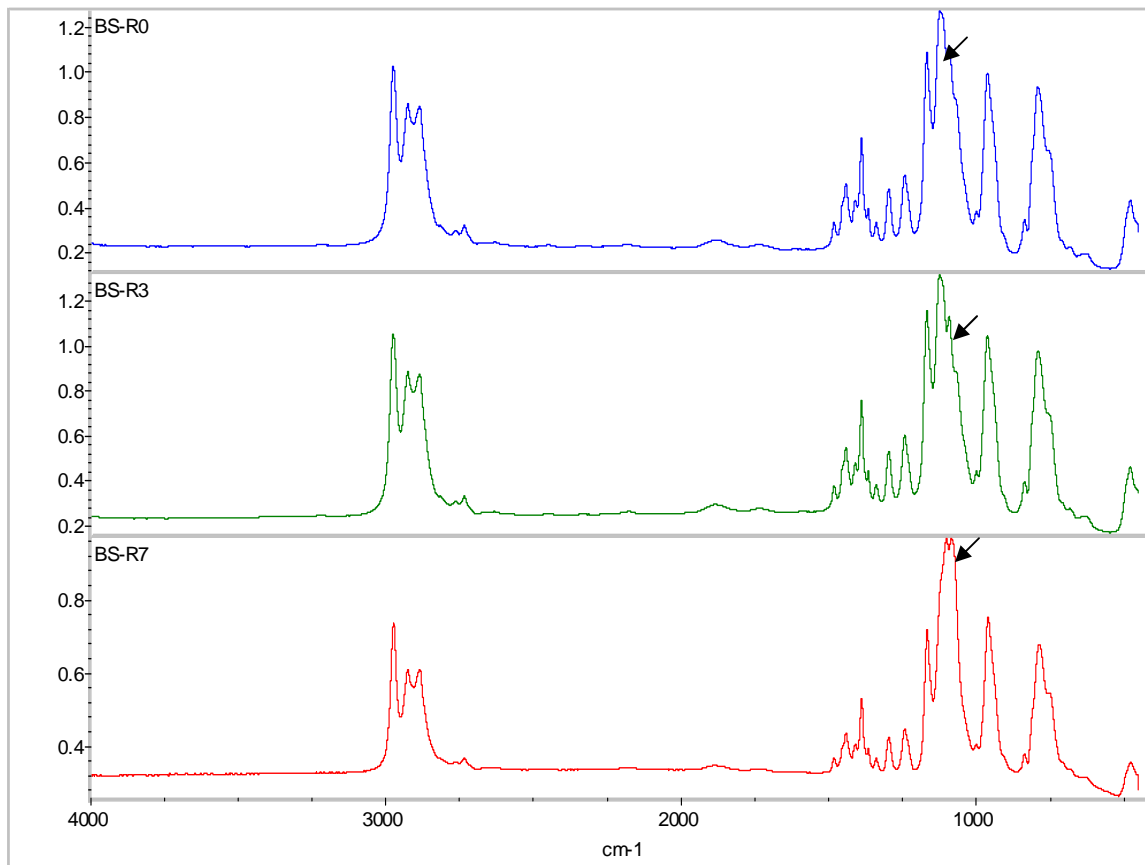


**Figure 5.4.** Stacked RAIR spectra of neat bis-sulfur films for comparison at various curing stages; refer Table 5.2 for peak identification

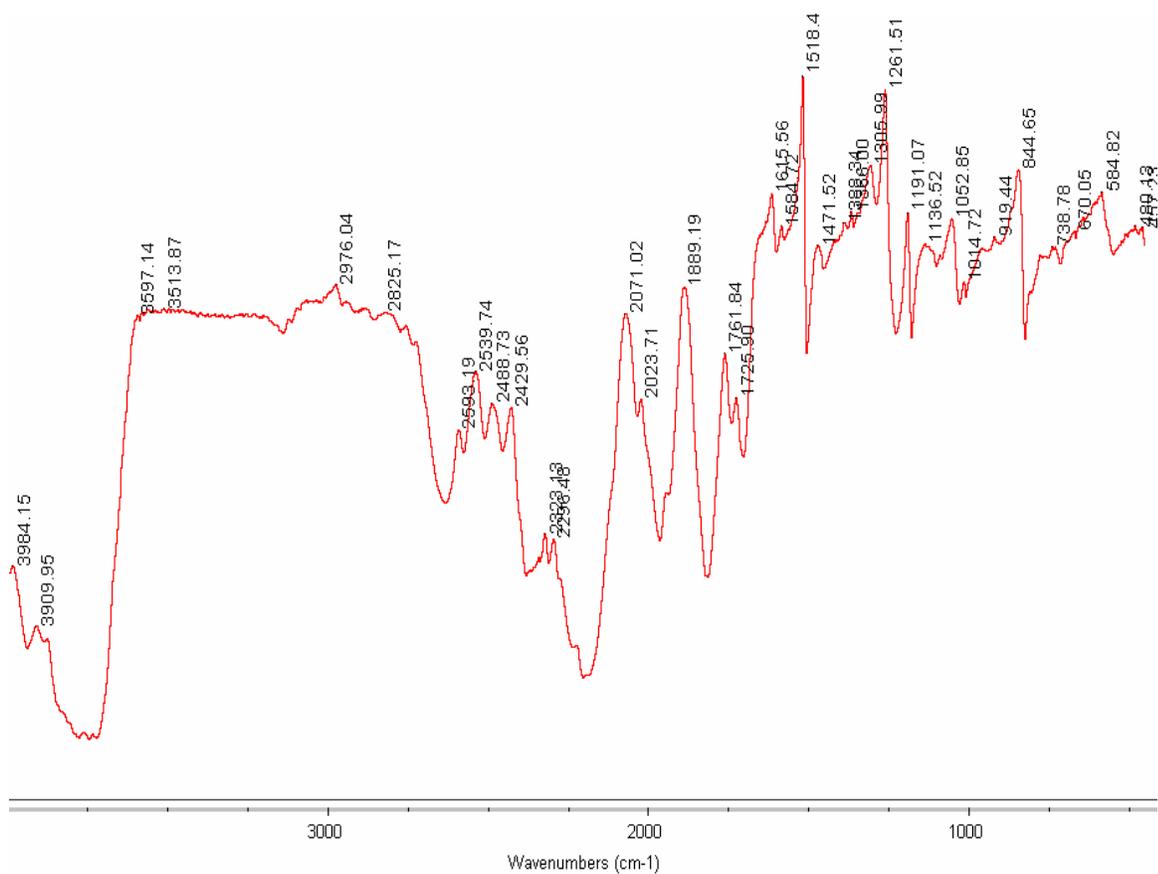


**Figure 5.5.** RAIR spectrum of DPW 6520 film, with annotated peaks; refer Table 5.3 for peak identification

Ancarez - RT14

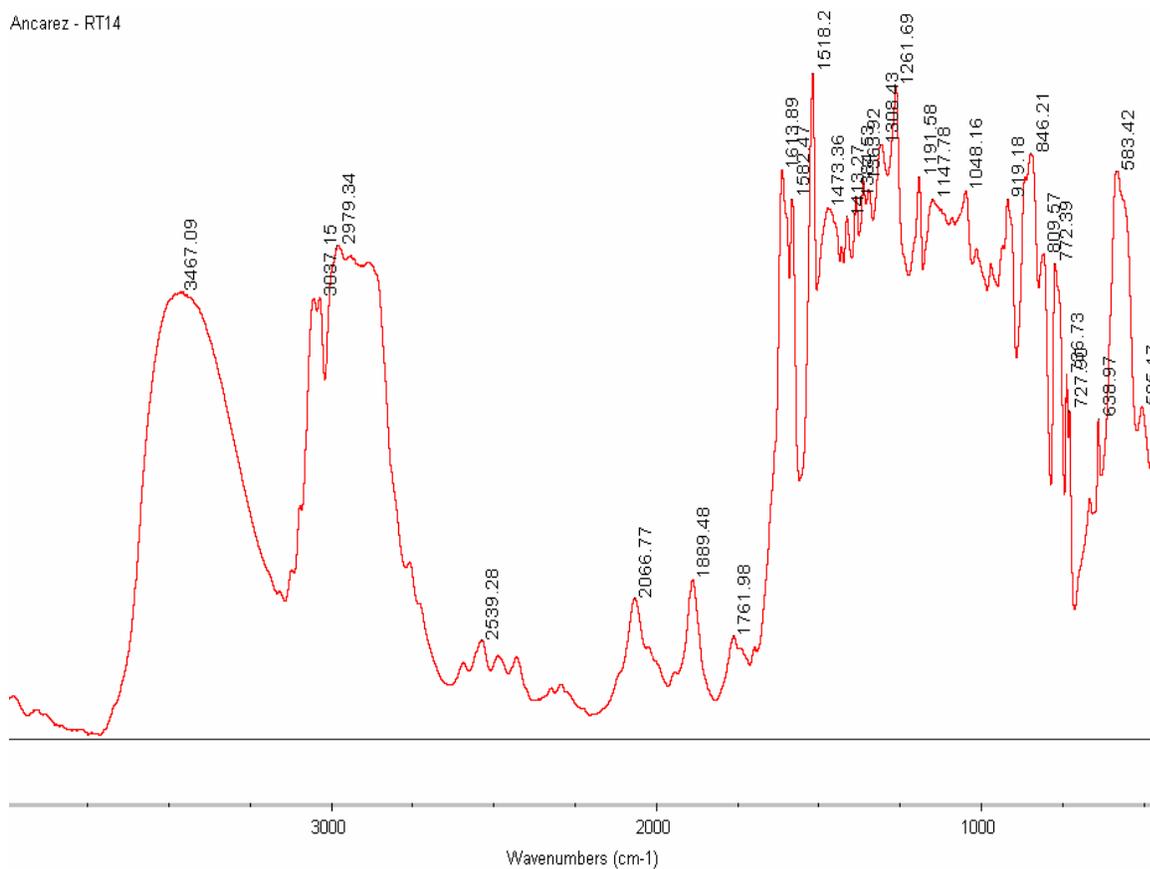


**Figure 5.6.** RAIR spectrum of Ancarez AR 550 film, with annotated peaks; refer Table 5.3 for peak identification

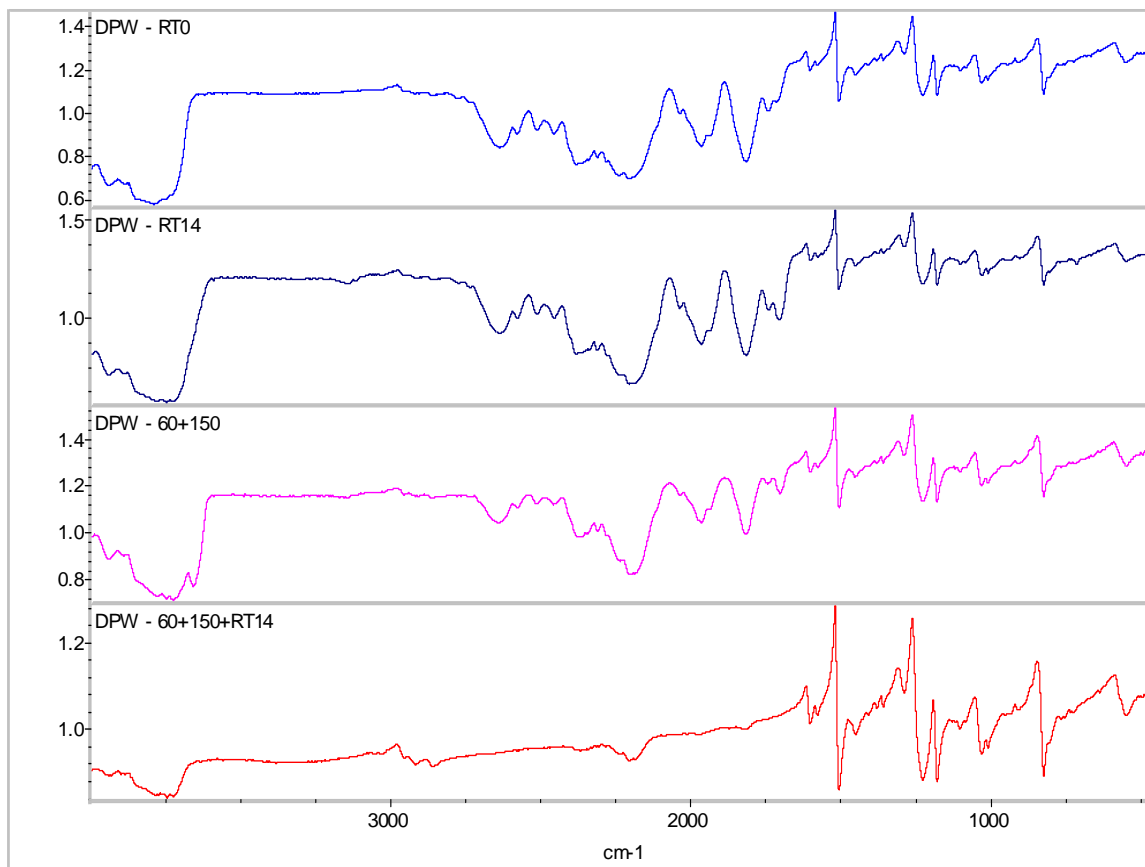


**Figure 5.7.** Stacked RAIR spectra of DPW 6520 films for comparison at various curing conditions; refer Table 5.3 for peak identification

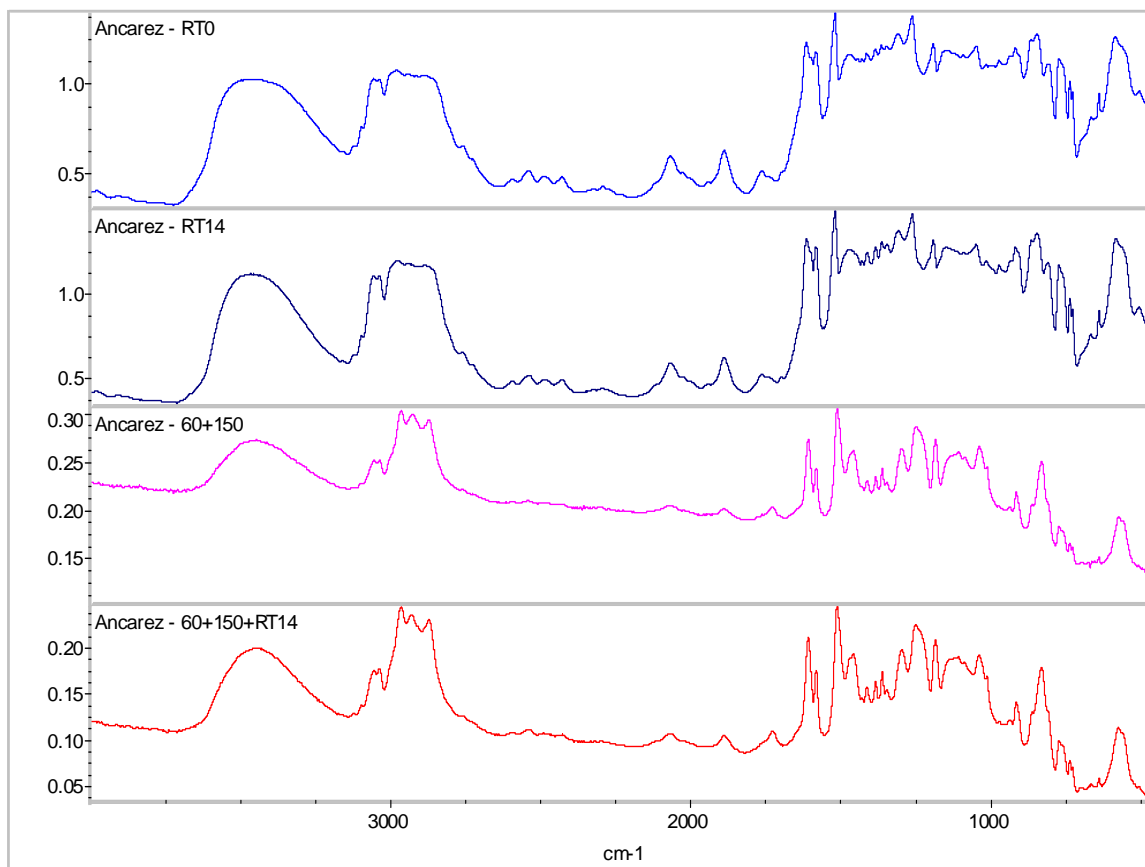


**Figure 5.8.** Stacked RAIIR spectra of Ancarez AR 550 films for comparison at various curing conditions; refer Table 5.3 for peak identification

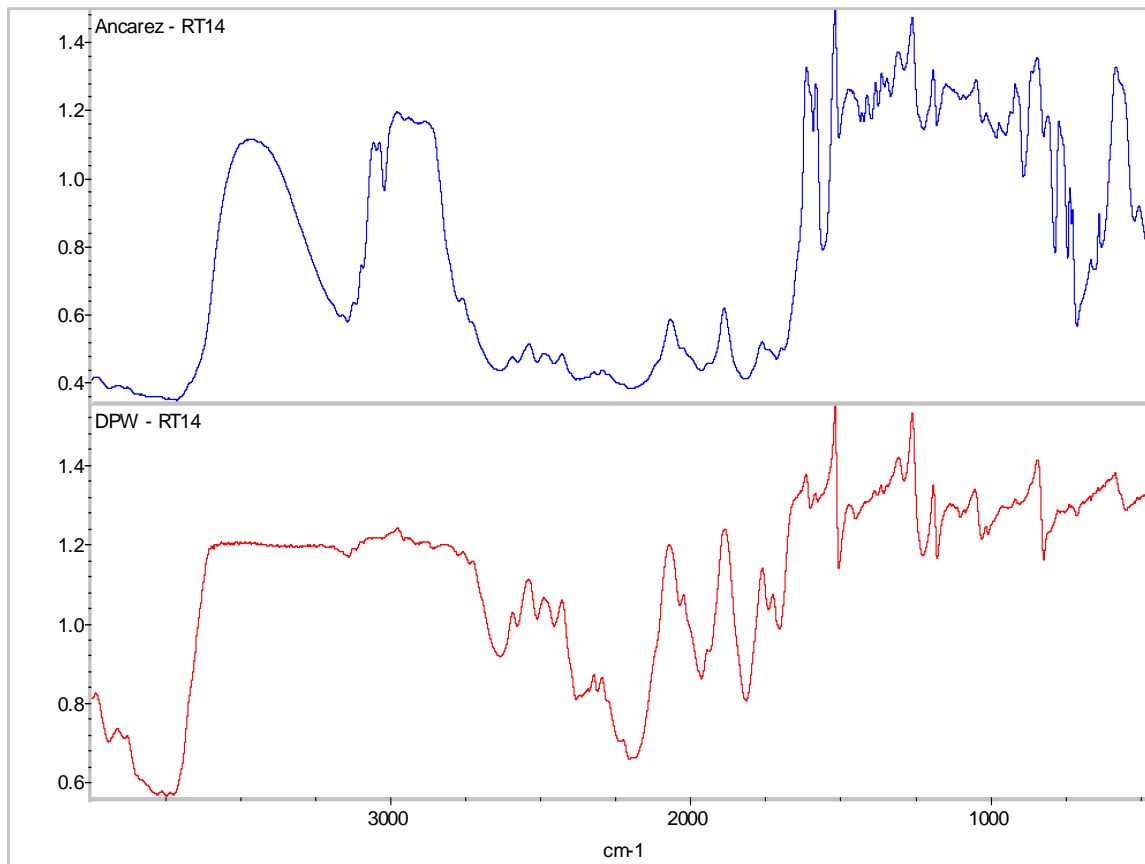


**Figure 5.9.** Comparison of the RAIR spectra of DPW 6520 and Ancarez AR 550 films on day 14 of room temperature curing; refer Table 5.3 for peak identification

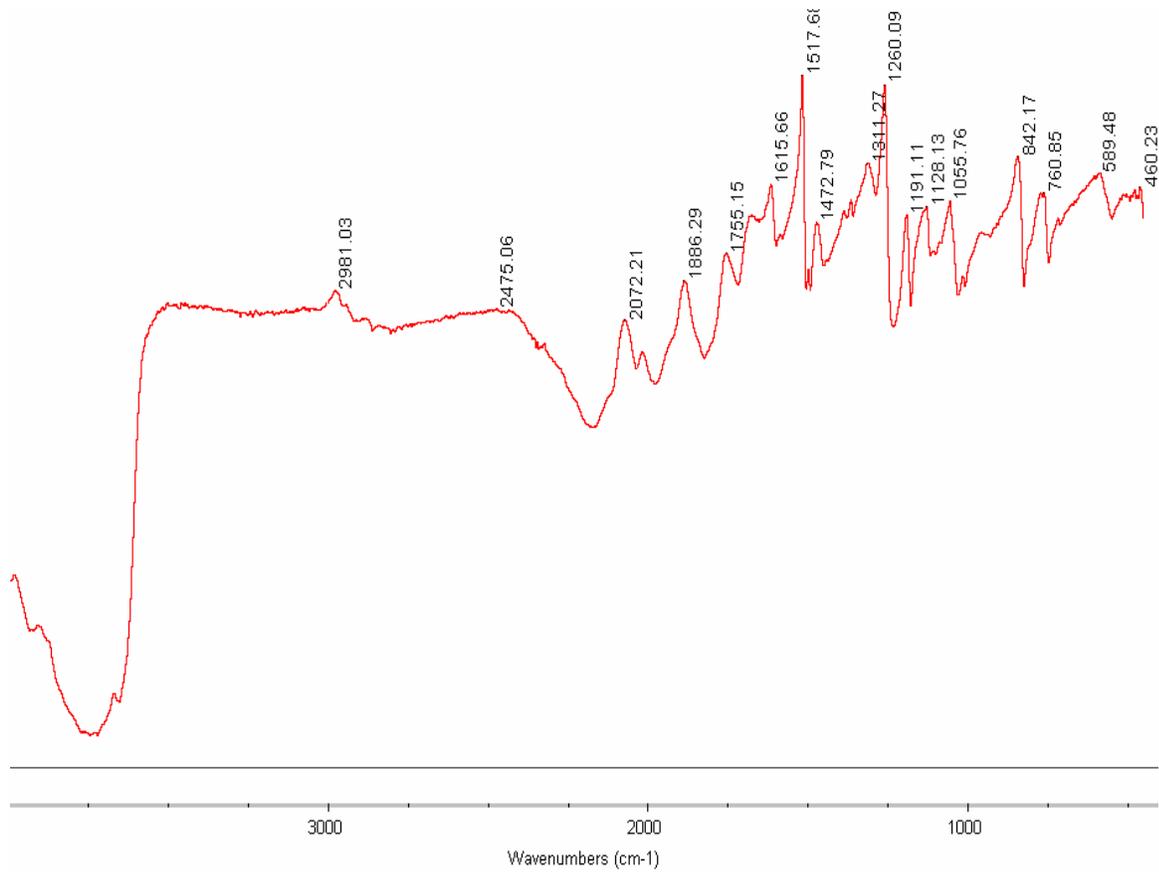


**Figure 5.10.** RAIR spectrum of DPC 6870 film, with annotated peaks; refer Table 5.4 for peak identification

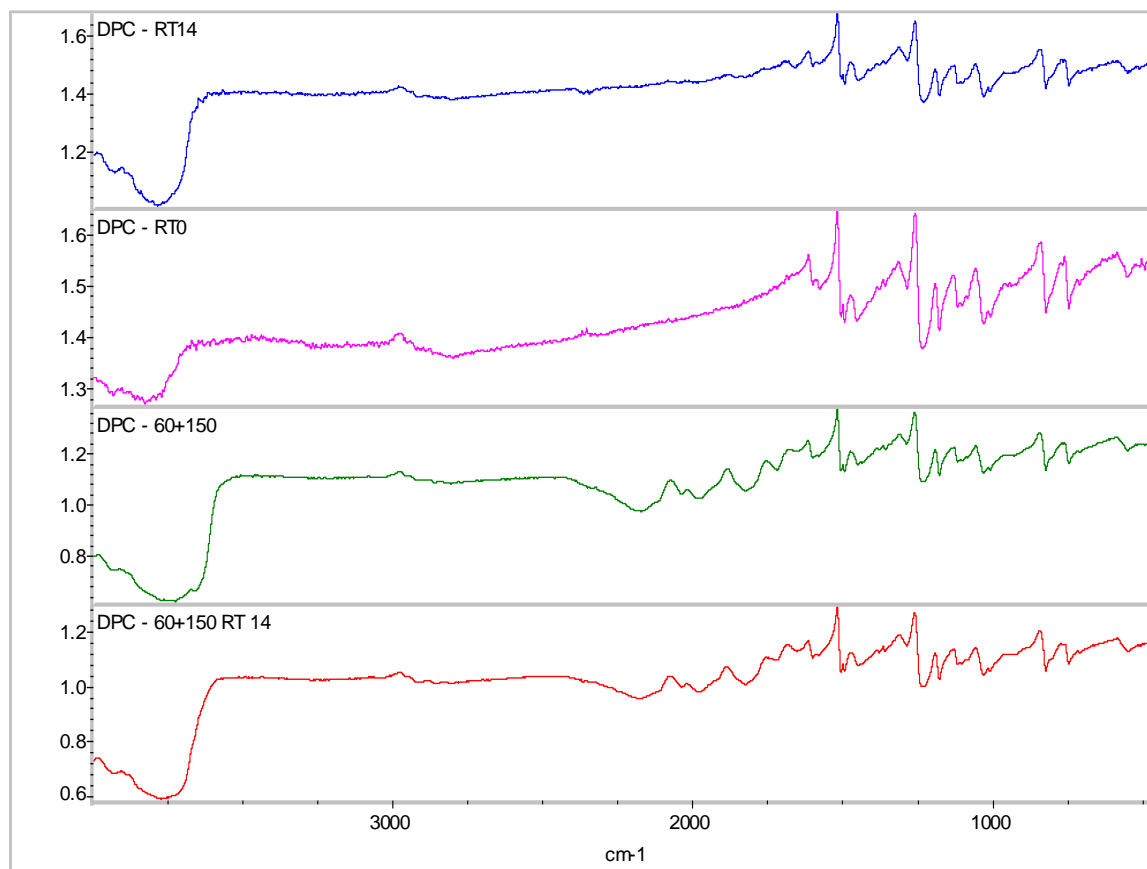


**Figure 5.11.** Stacked RAIR spectra of DPC 6870 films for comparison at various curing conditions; refer Table 5.4 for peak identification

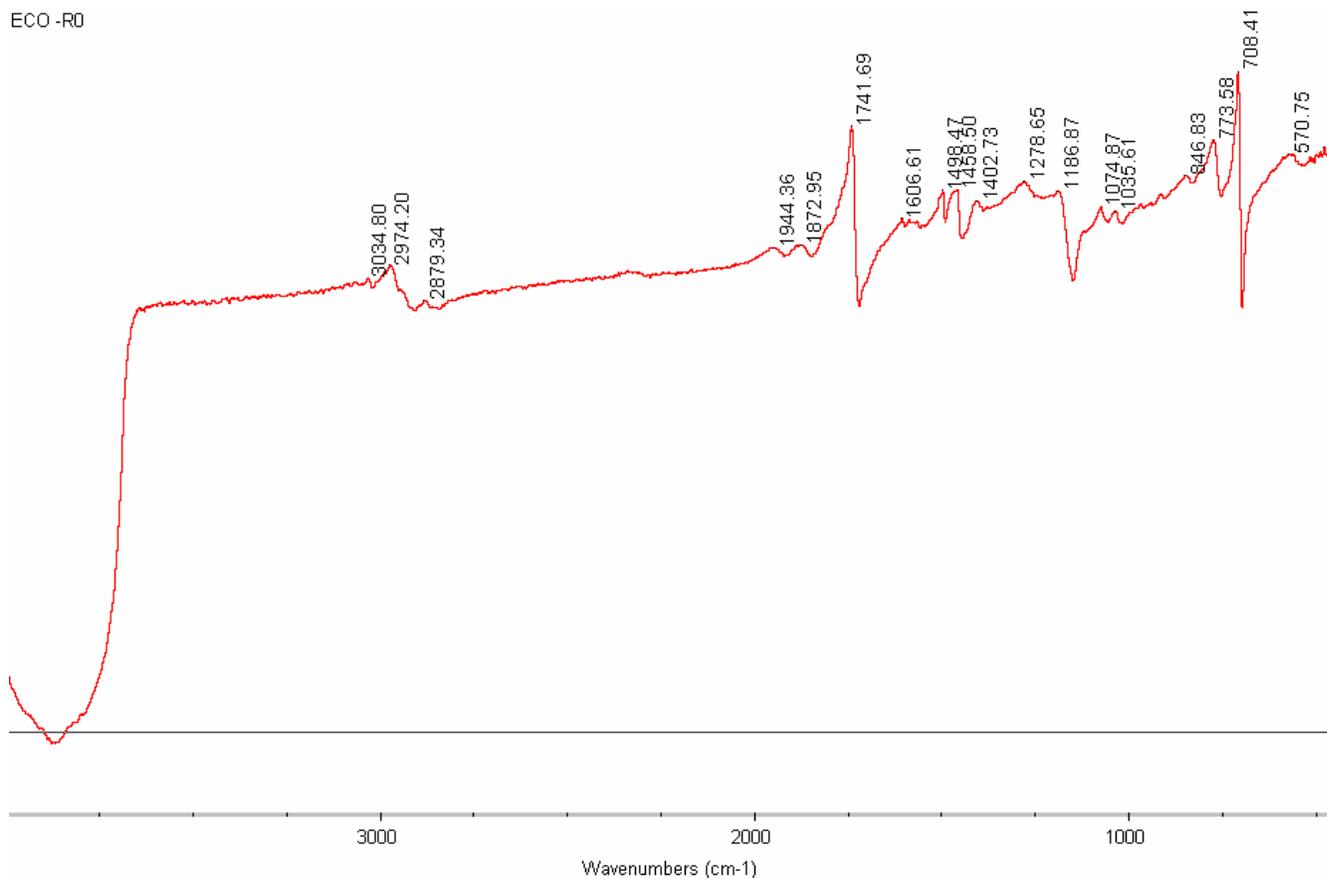


**Figure 5.12.** RAIR spectrum of ECO-CRYL 9790 film, with annotated peaks, on day 0 of room temperature curing; refer Table 5.5 for peak identification

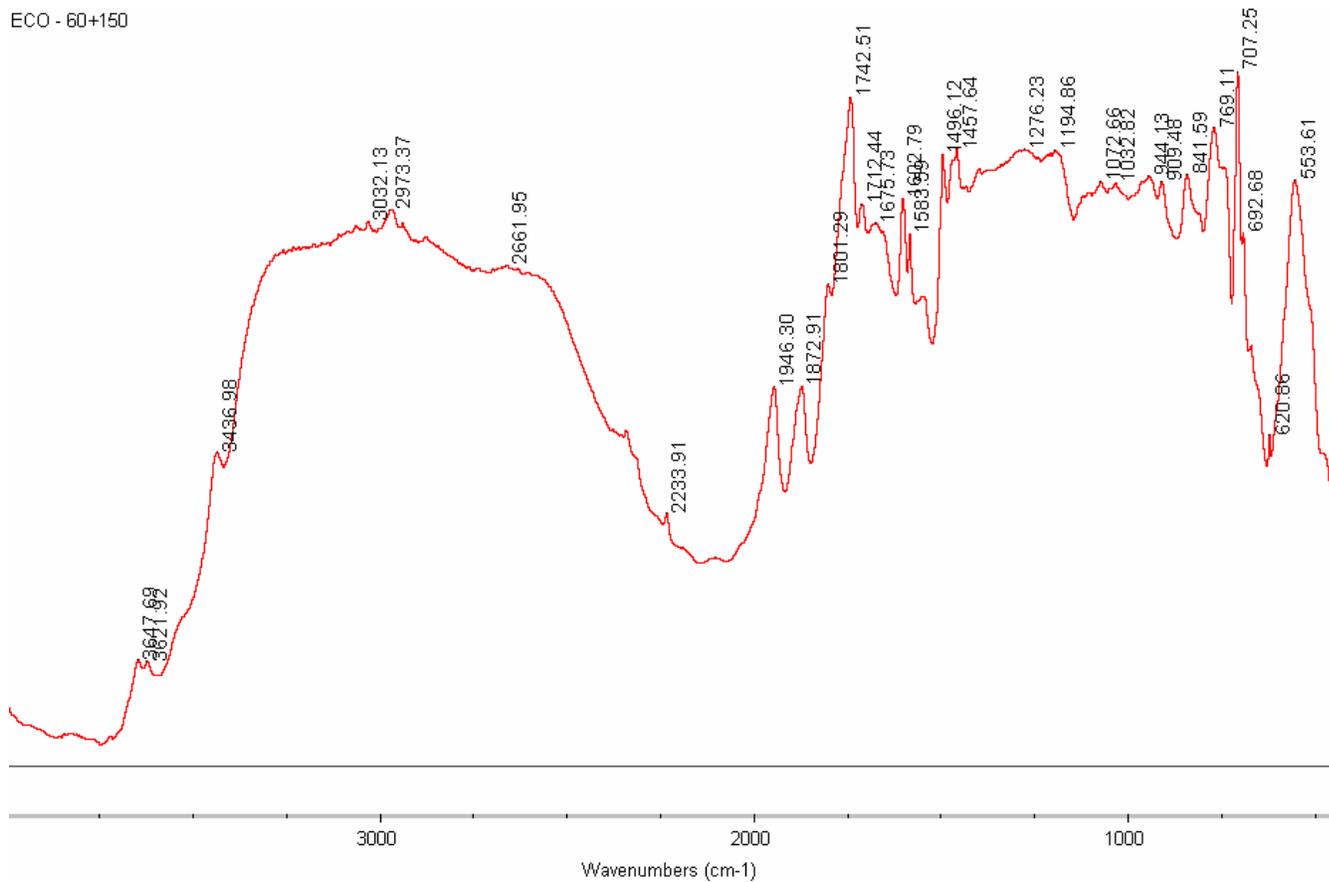


**Figure 5.13.** RAIR spectrum of ECO-CRYL 9790 film, with annotated peaks, on day 0, after high temperature curing; refer Table 5.5 for peak identification

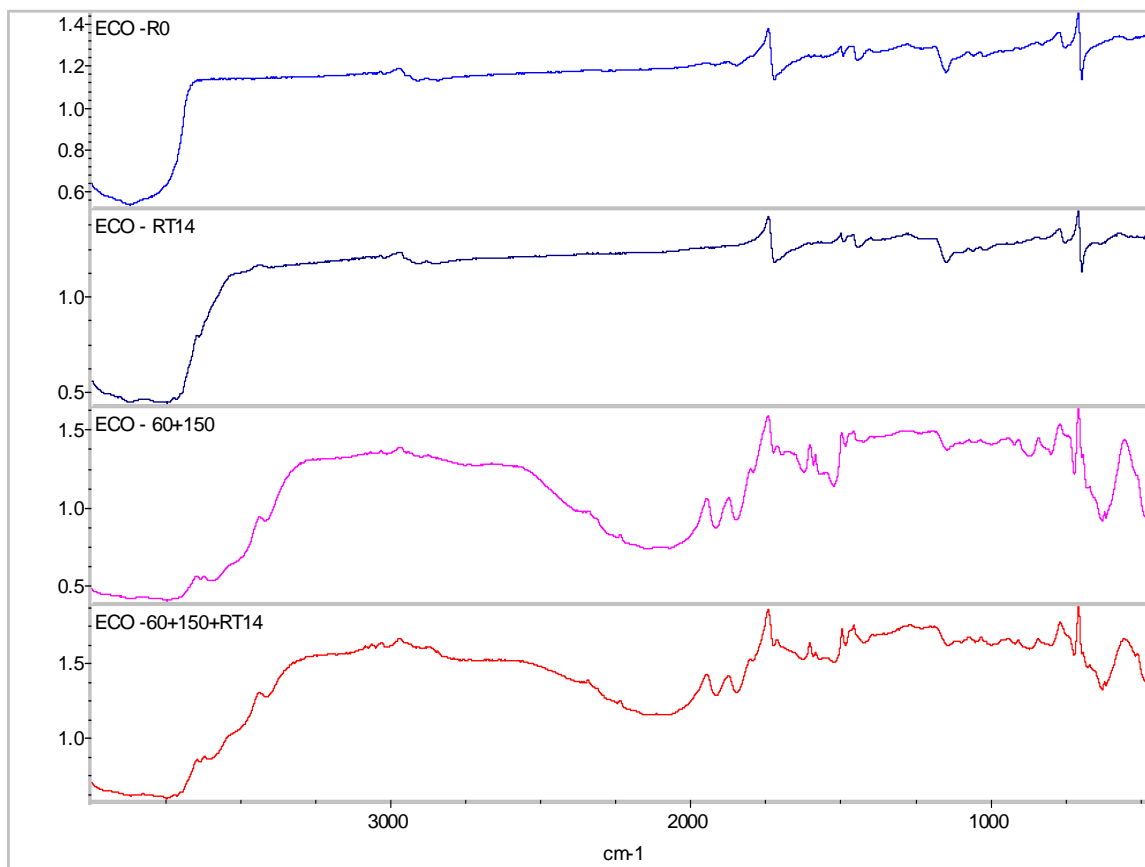


**Figure 5.14.** Stacked RAIR spectra of ECO-CRYL 9790 films for comparison at various curing conditions; refer Table 5.5 for peak identification

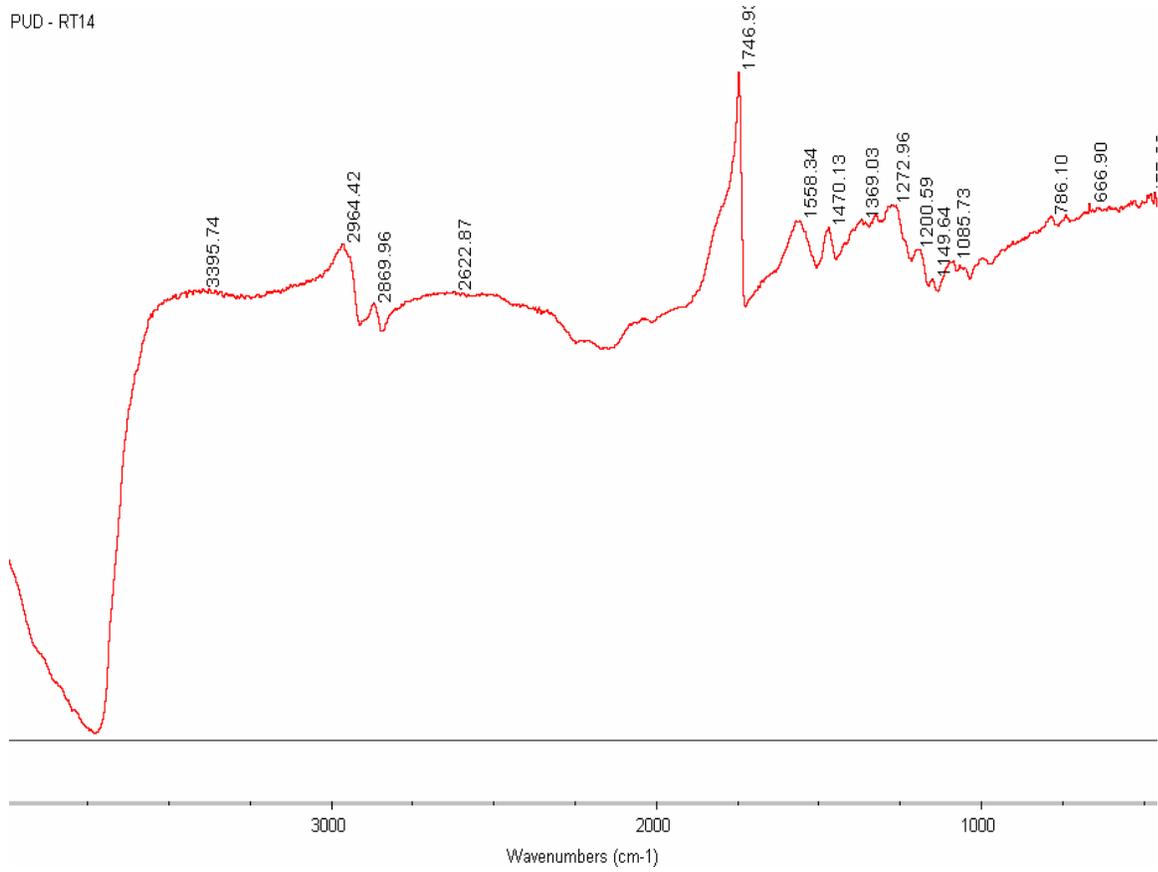


**Figure 5.15.** RAIR spectrum of NeoRez R 972 film, with annotated peaks; refer Table 5.6 for peak identification

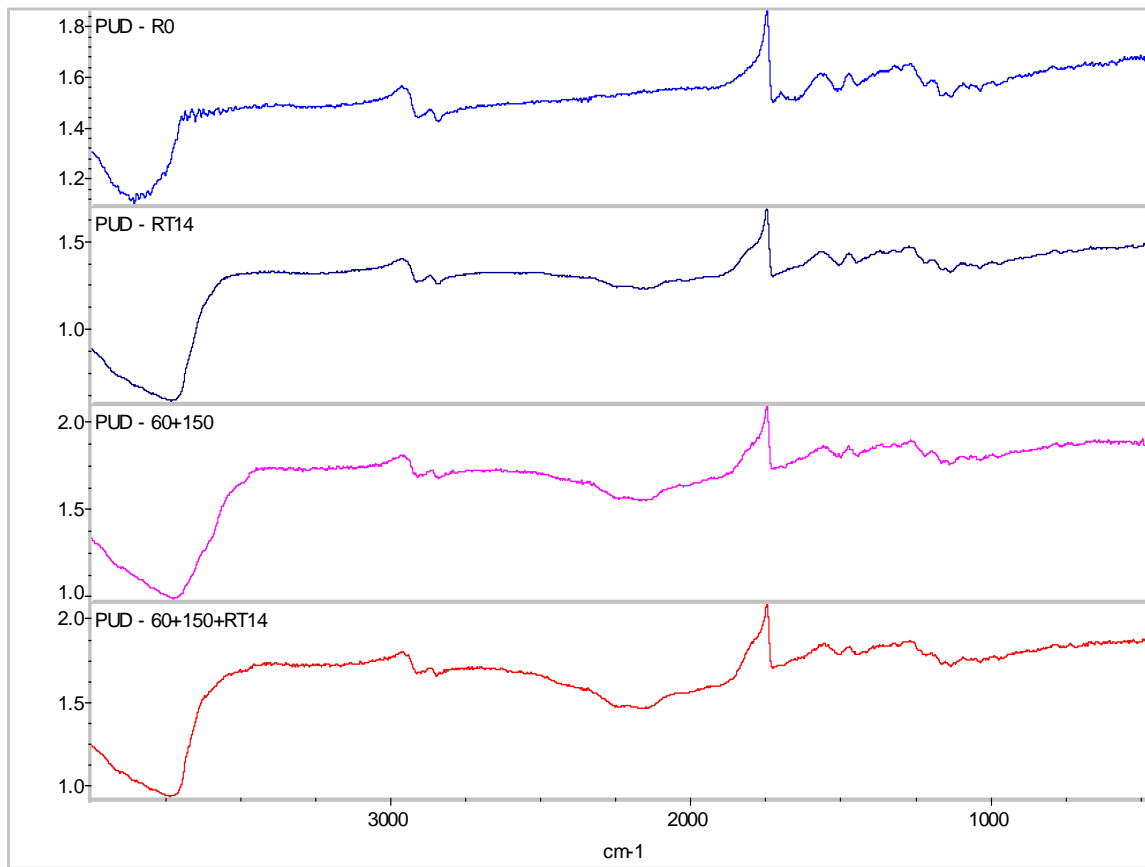


**Figure 5.16.** Stacked RAIR spectra of NeoRez R 972 films for comparison at various curing conditions; refer Table 5.6 for peak identification

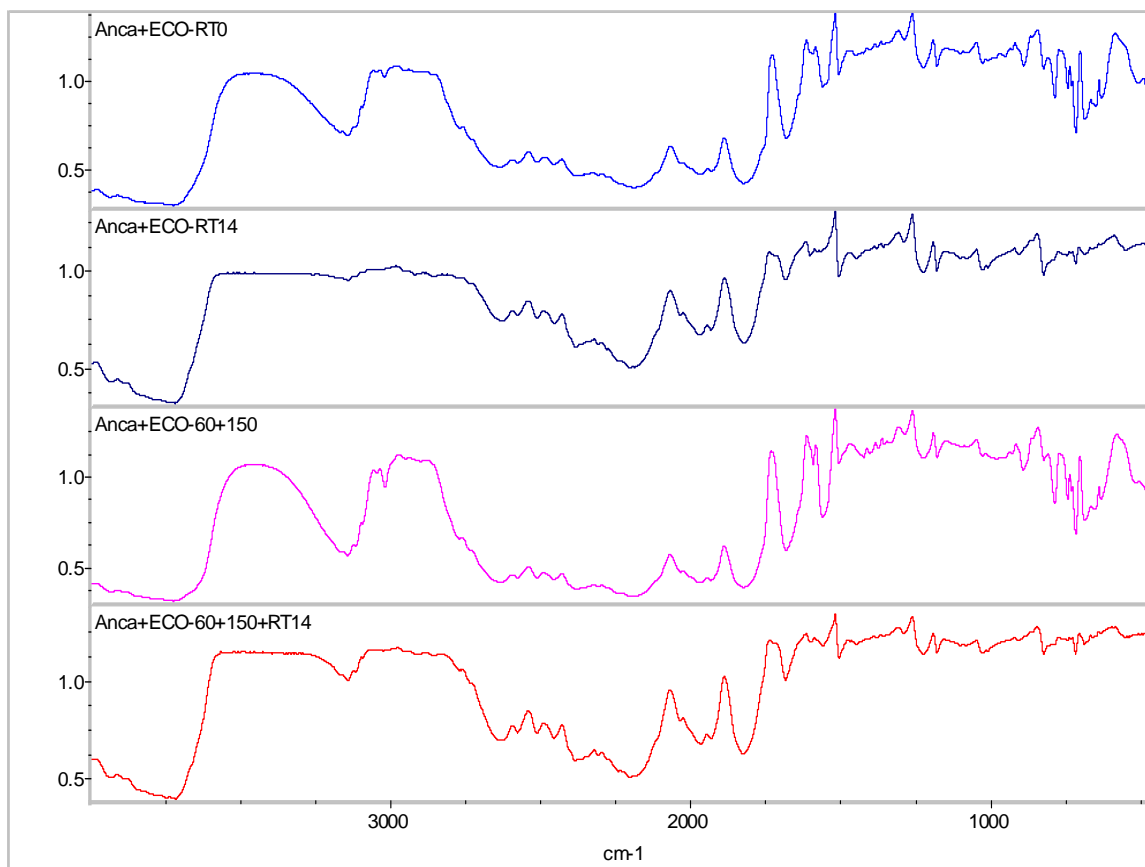


**Figure 5.17.** Stacked RAIR spectra of films of a 9:1 mixture of Ancarez AR 550 and ECO-CRYL 9790 respectively, for comparison at various curing conditions

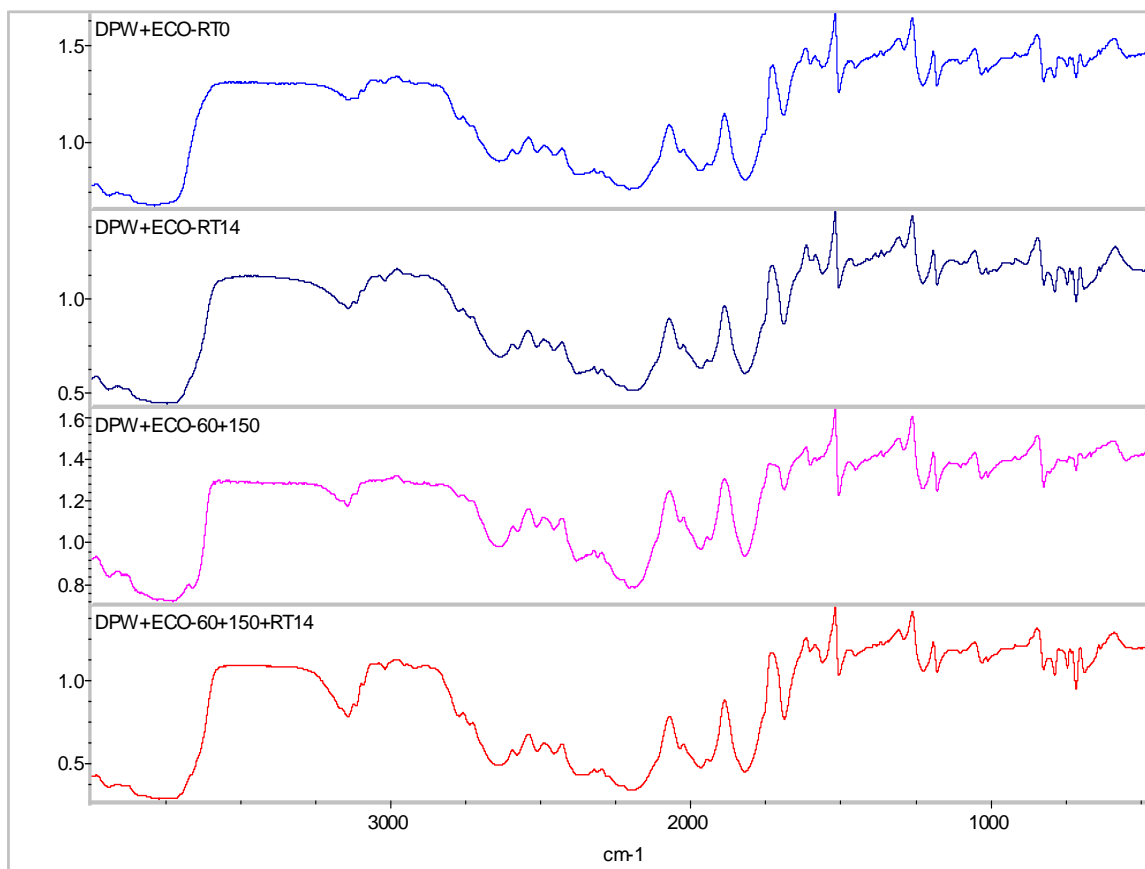


**Figure 5.18.** Stacked RAIR spectra of films of a 9:1 mixture of DPW 6520 and ECO-CRYL 9790 respectively, for comparison at various curing conditions

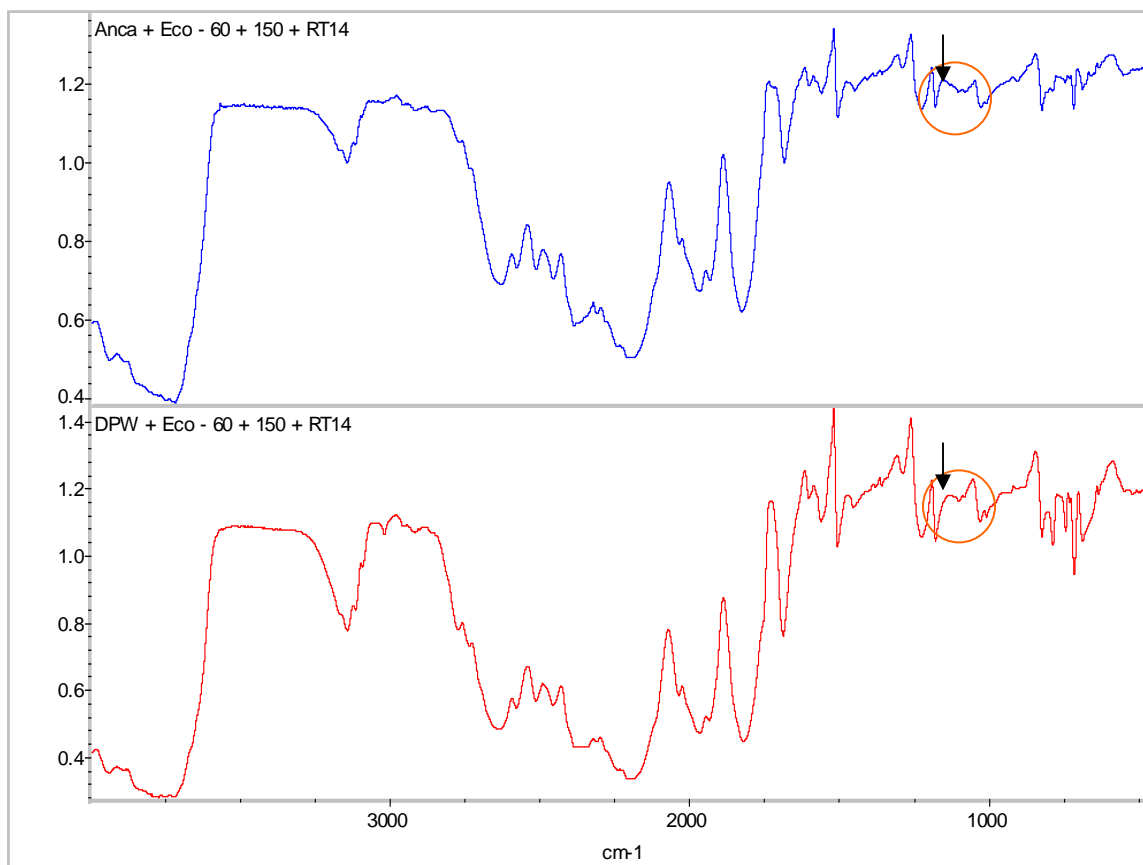


**Figure 5.19.** Comparison of the RAIIR spectra of films of the two 9:1 epoxy-polyacrylate mixtures on day 14 after high temperature curing

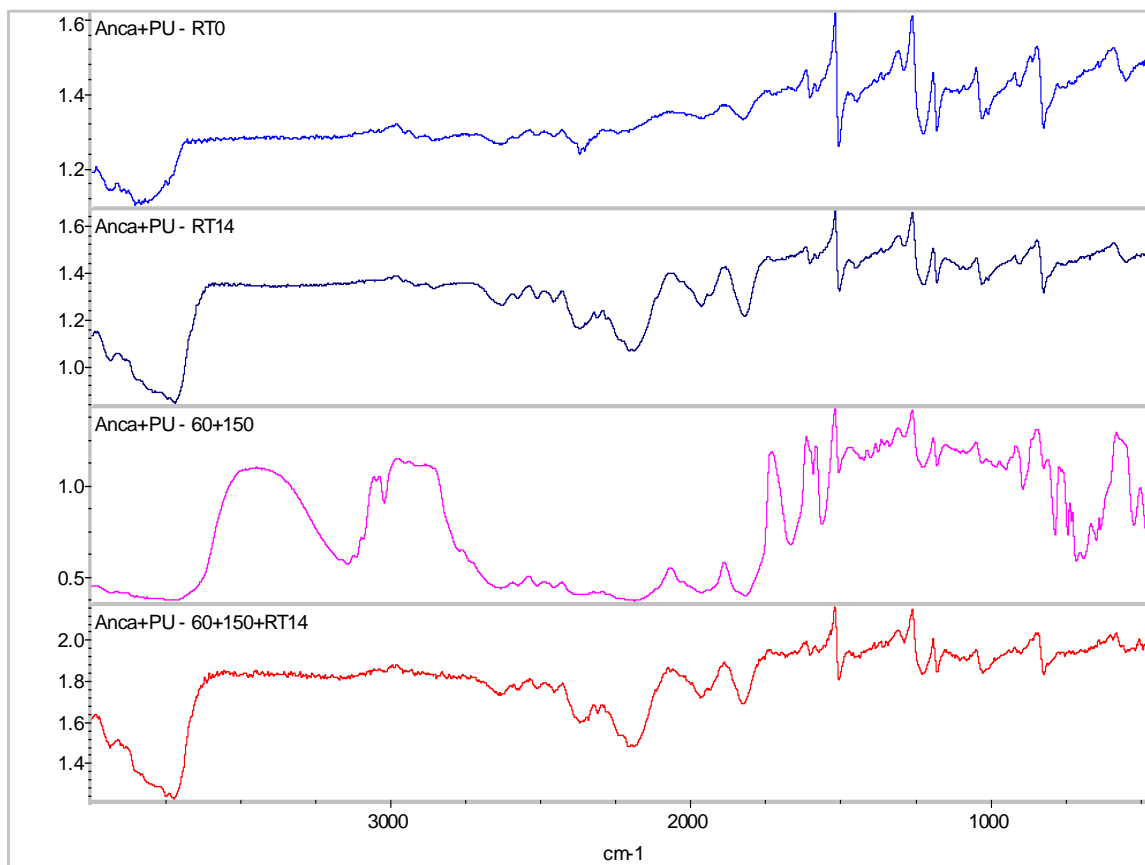


**Figure 5.20.** Stacked RAIIR spectra of films of a 9:1 mixture of Ancarez AR 550 and NeoRez R 972 respectively, for comparison at various curing conditions

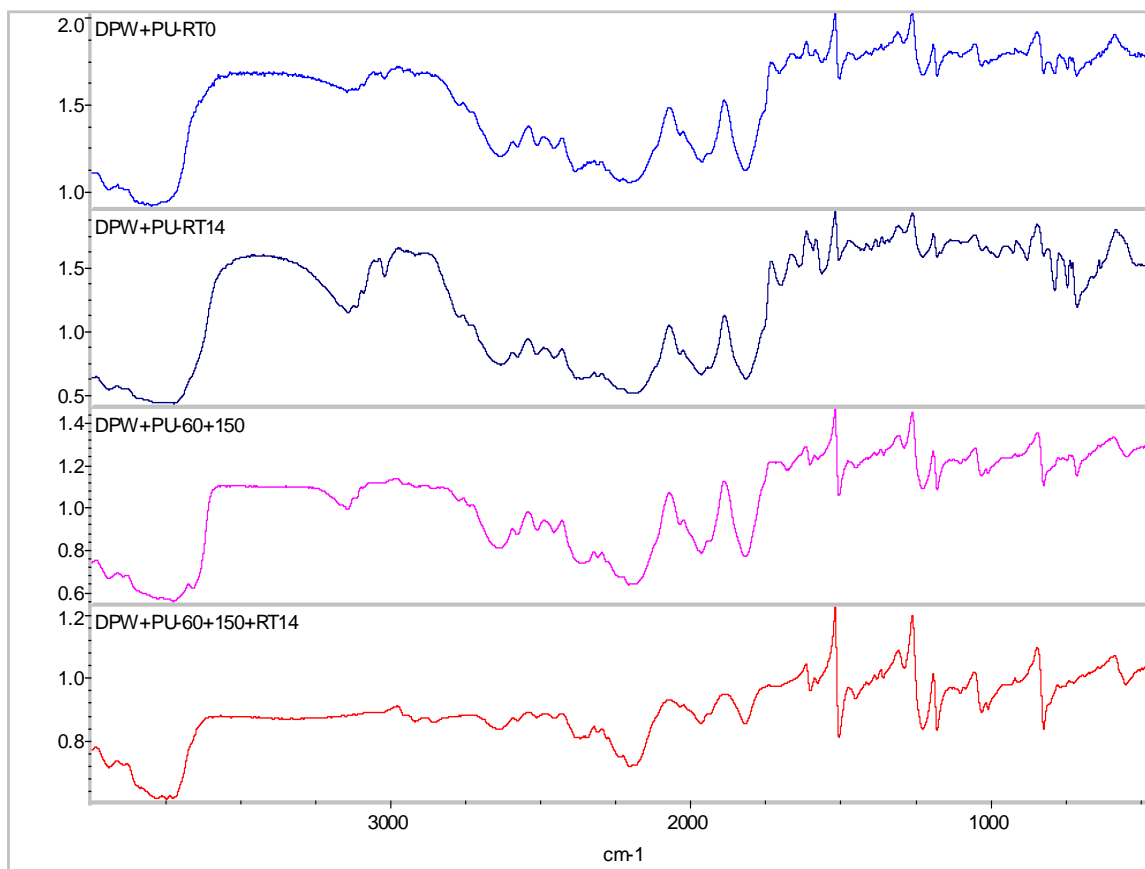


**Figure 5.21.** Stacked RAIR spectra of films of a 9:1 mixture of DPW 6520 and NeoRez R 972 respectively, for comparison at various curing conditions

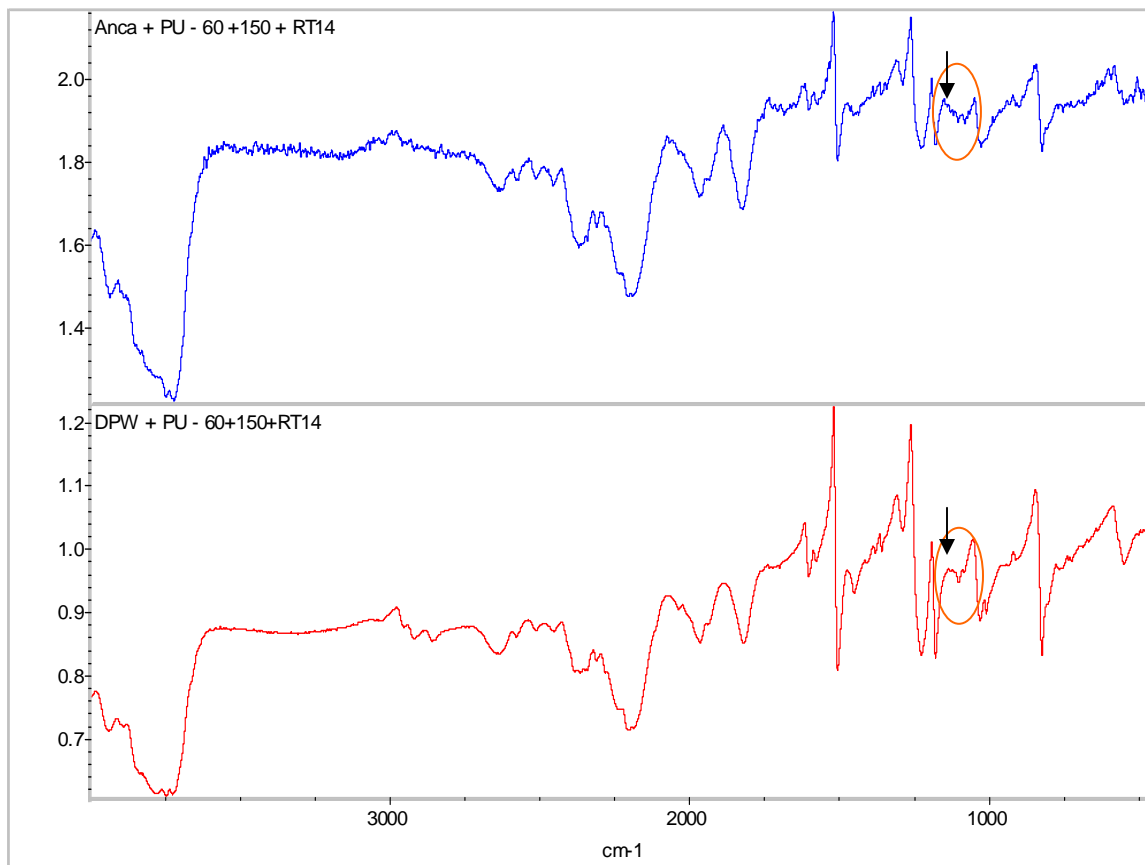


**Figure 5.22.** Comparison of the RAIIR spectra of films of the two 9:1 epoxy-polyurethane mixtures on day 14 after high temperature curing

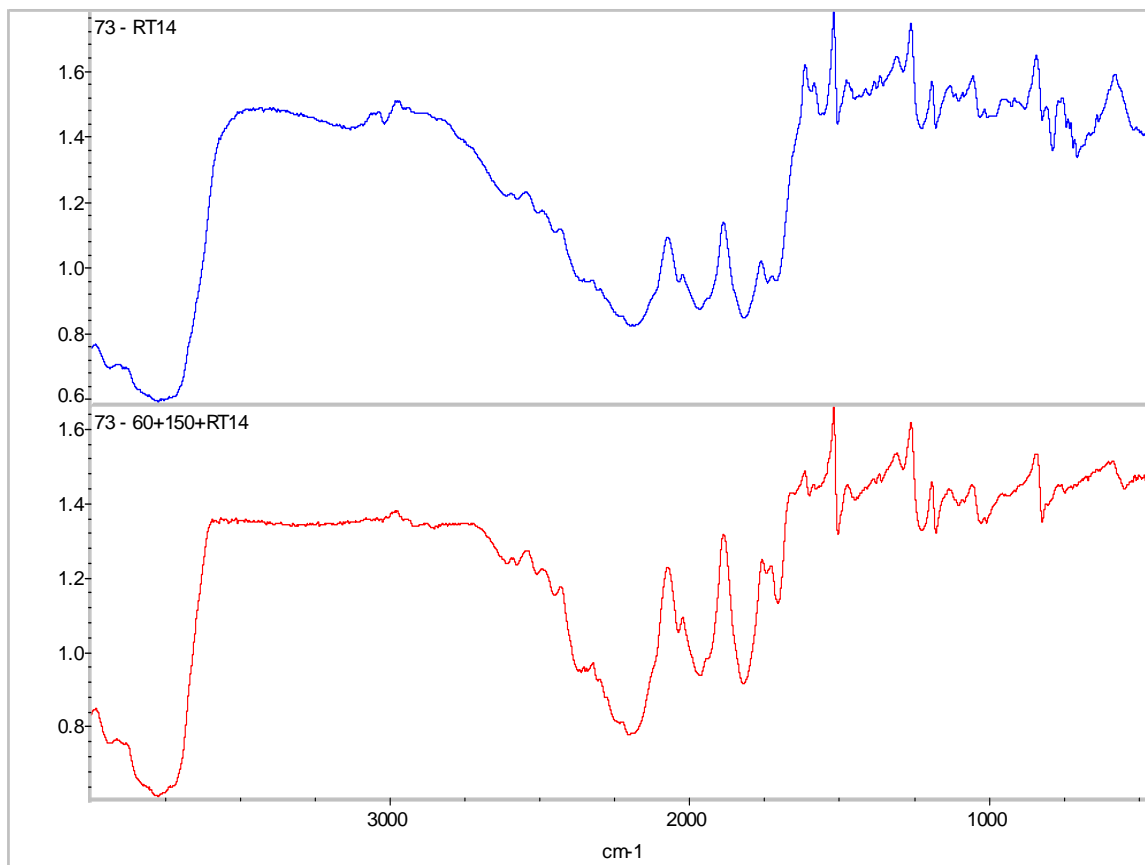


**Figure 5.23.** Comparison of the RIR spectra of a 7:3 mixture of DPW 6520 and DPC 6870 respectively on day 14 of room temperature curing and day 14 after high temperature curing

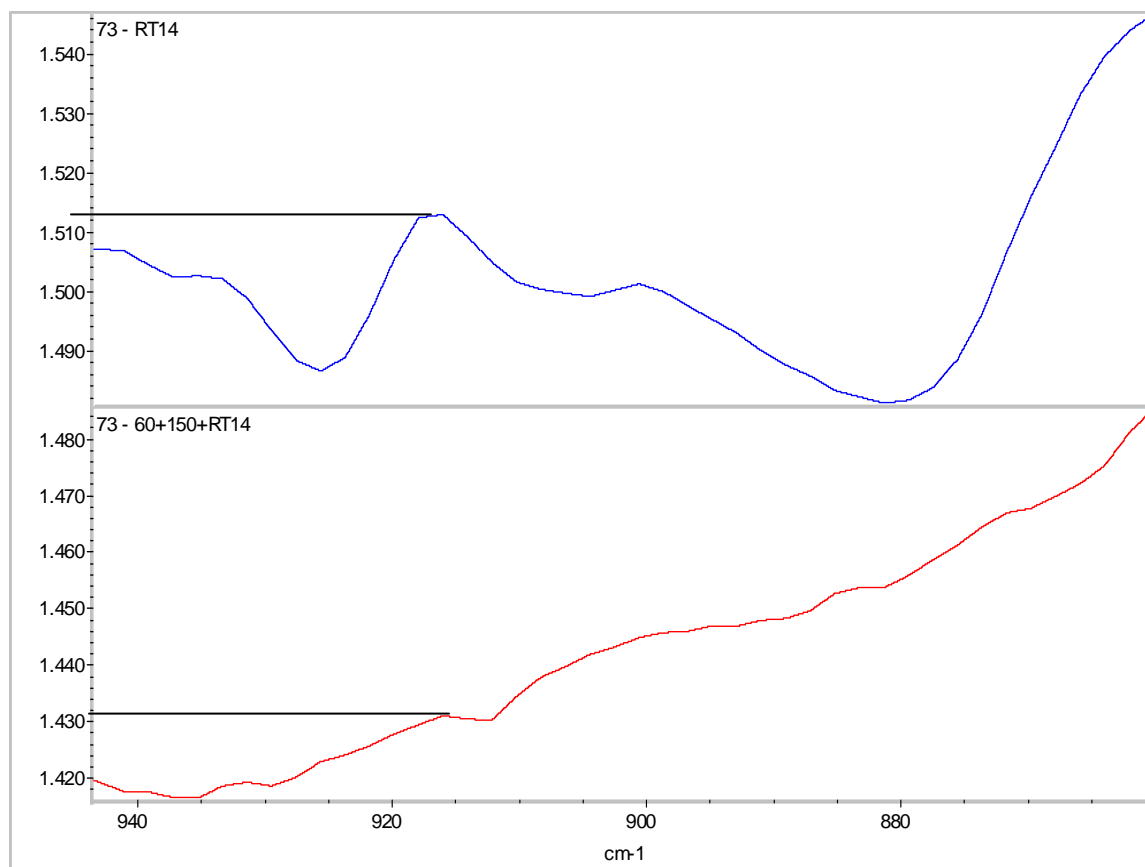


**Figure 5.24.** The same RAIR spectra as in Figure 5.23 detailing the region in and around the characteristic epoxy peak at  $915\text{ cm}^{-1}$

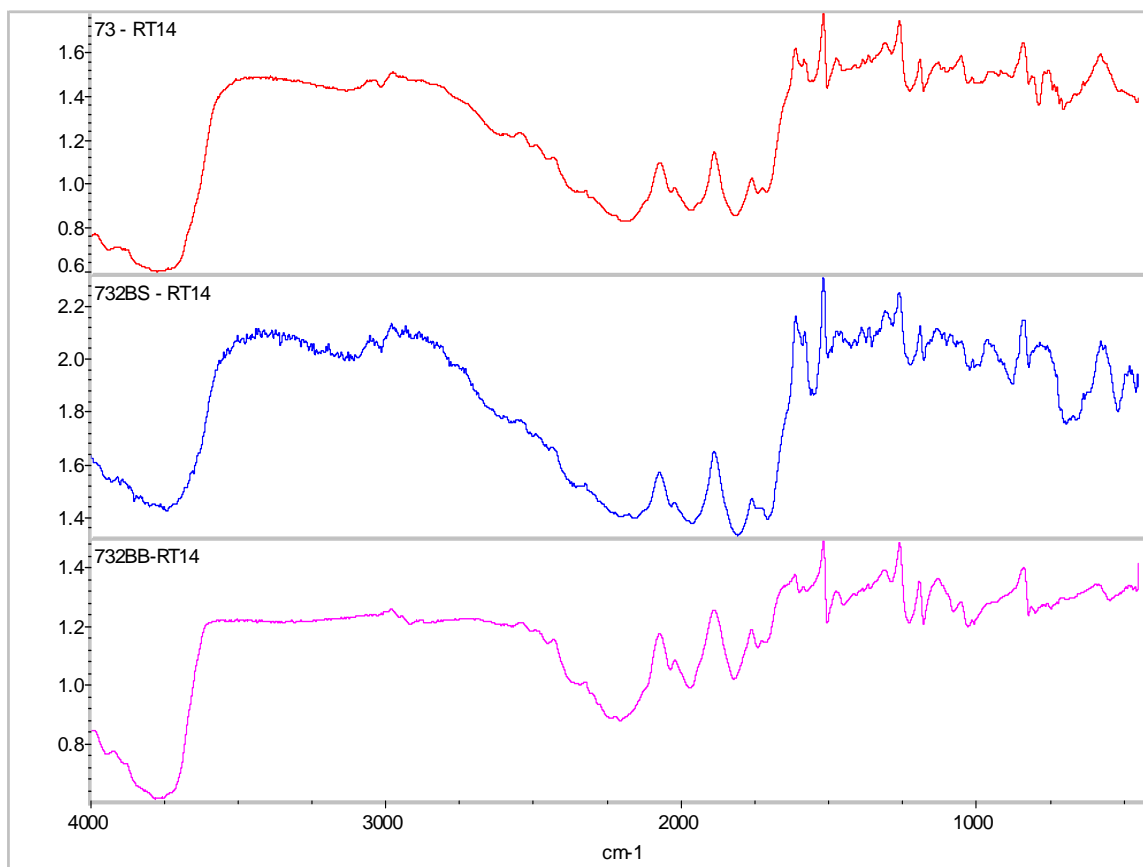


**Figure 5.25.** RAIR spectra of superprimer films showing the effect of incorporation of the silanes bis-benzene and bis-sulfur

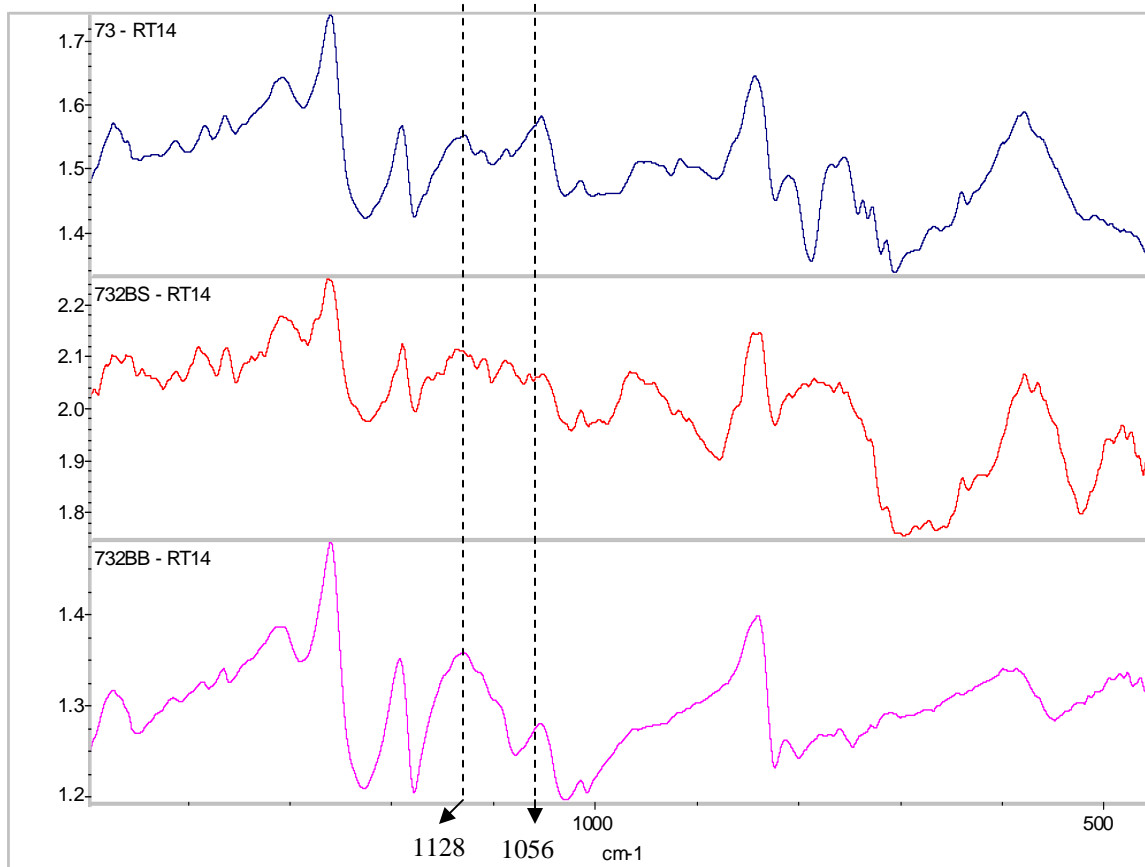
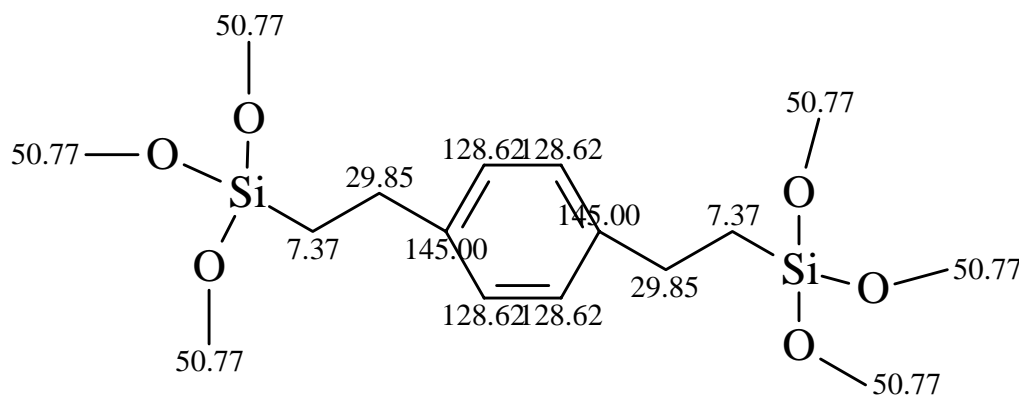


**Figure 5.26.** The same RAIR spectra as in Figure 5.25 detailing the siloxane peak region

### Bis-benzene silane



### Bis-sulfur silane

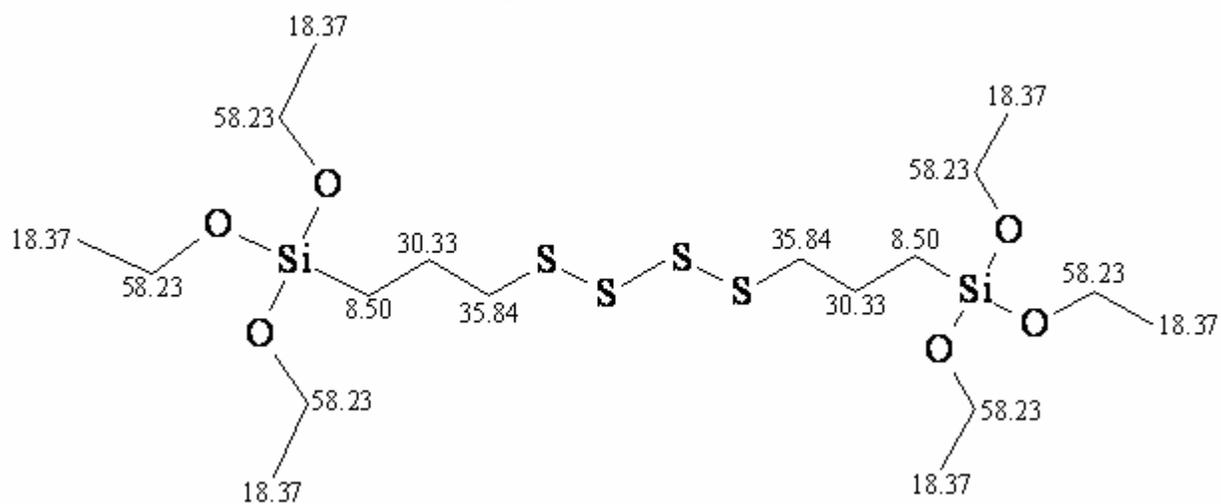


**Figure 5.27.** Silanes - representative structures and calculated peak positions

### Simple bisphenol A epoxy resin

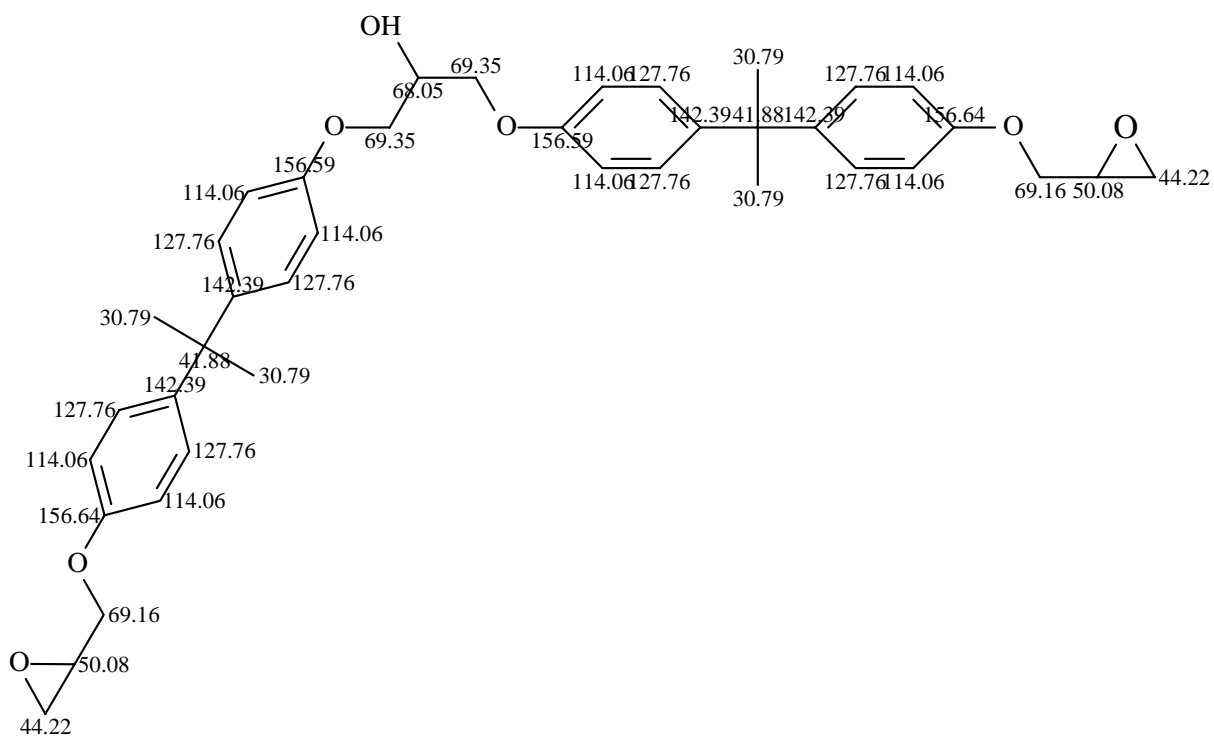


**Figure 5.28.** DPW 6520 - representative structure and calculated peak positions

**Representative carboxyl-functional polyacrylate**

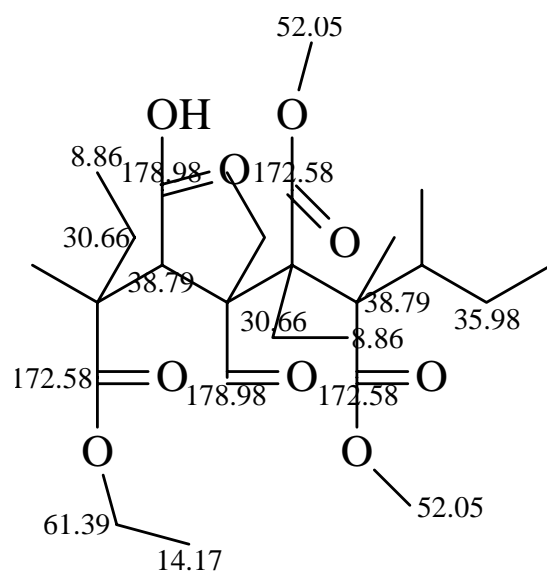


**Figure 5.29.** Ecocryl 9790 - representative structure and calculated peak positions

**Representative polyurethane**

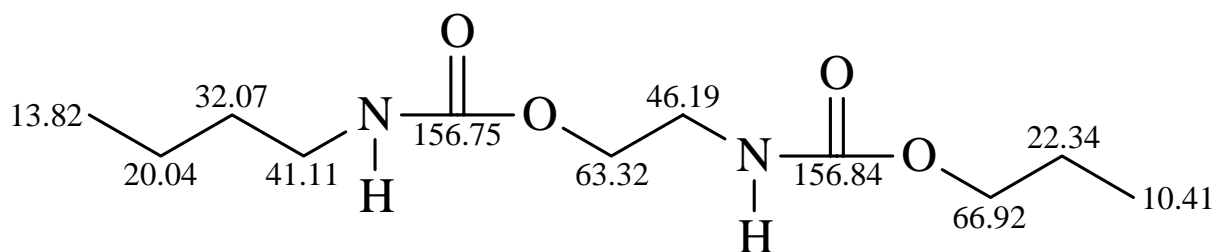


**Figure 5.30.** Neorez R 972 - representative structures and calculated peak positions

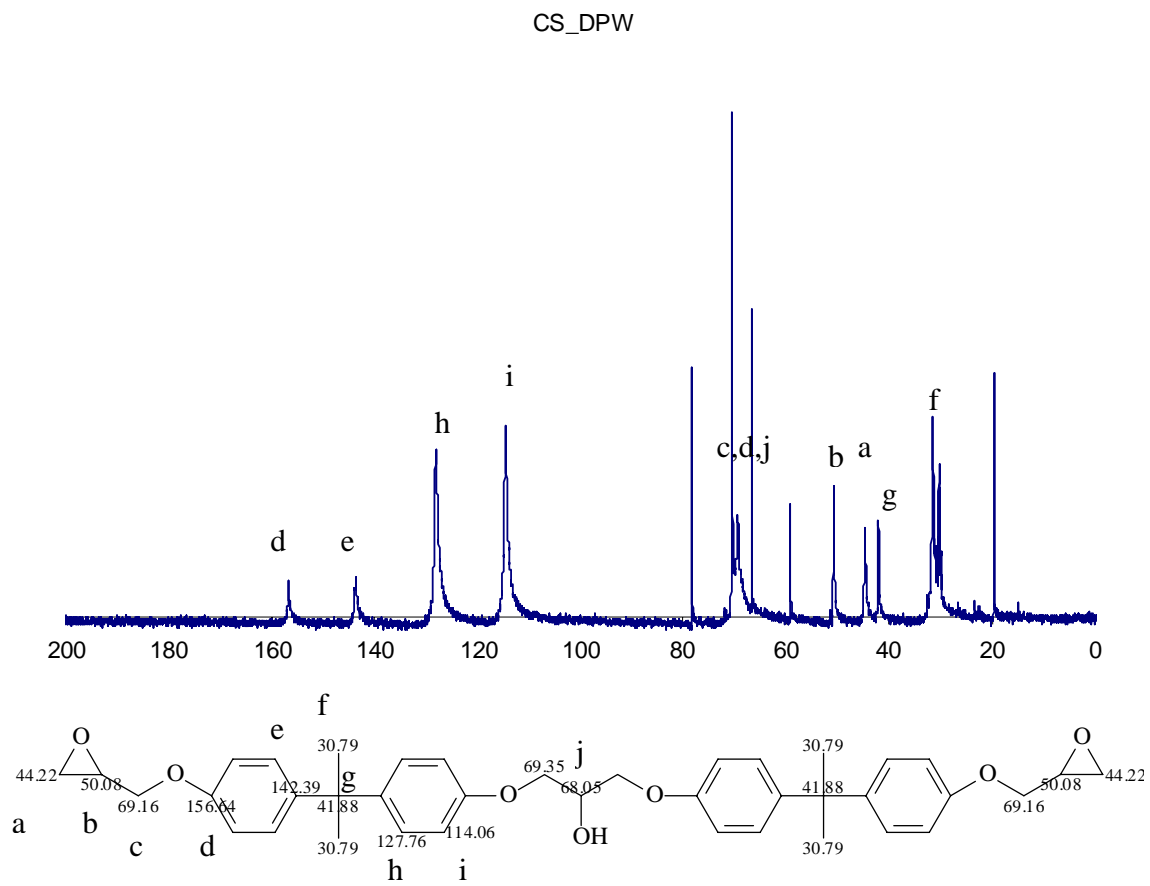


**Figure 5.31.** Liquid  $^{13}\text{C}$  NMR spectrum for DPW 6520 along with representative DGEBA

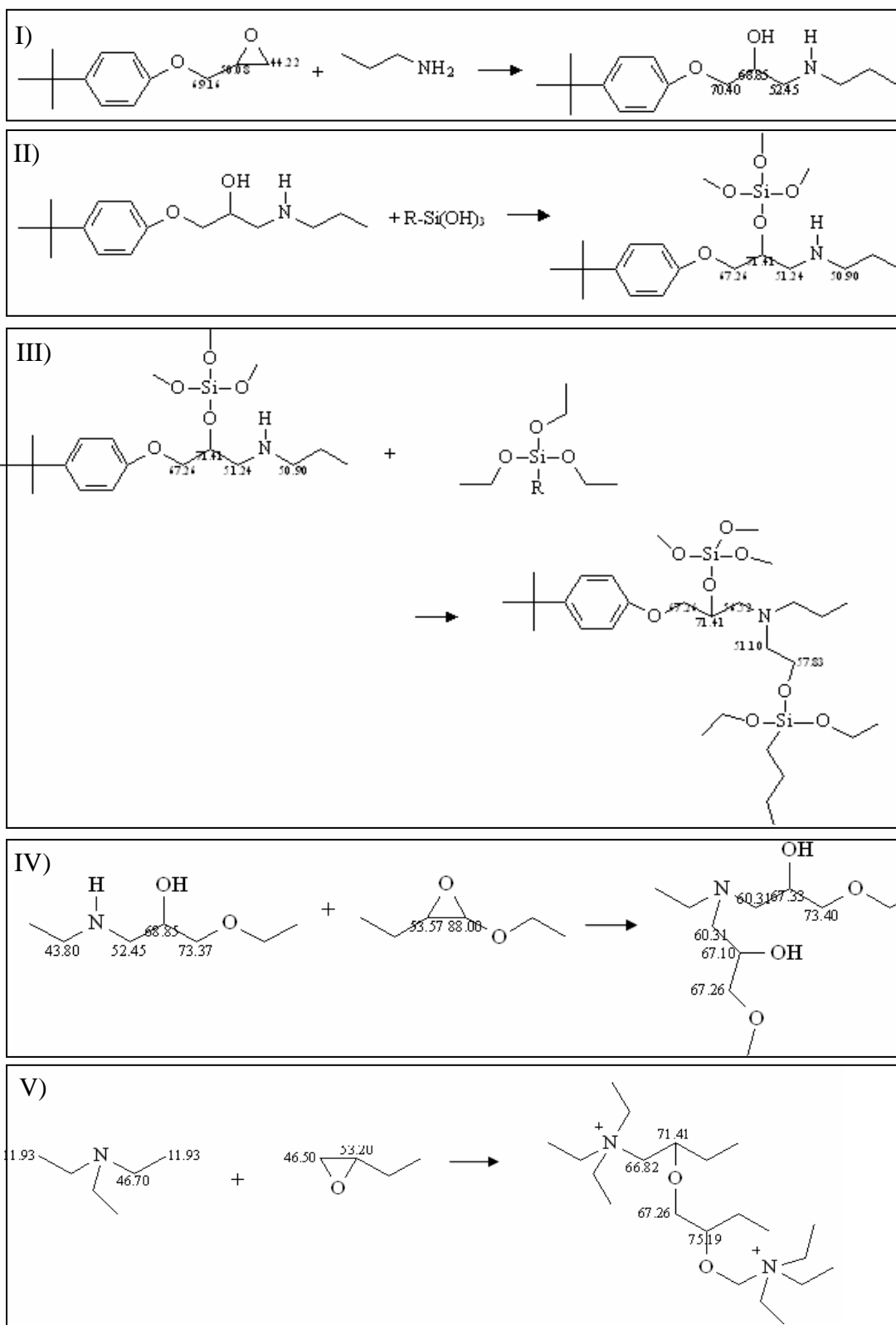


**Figure 5.32.** Five major cross-linking reactions in the superprimers under study

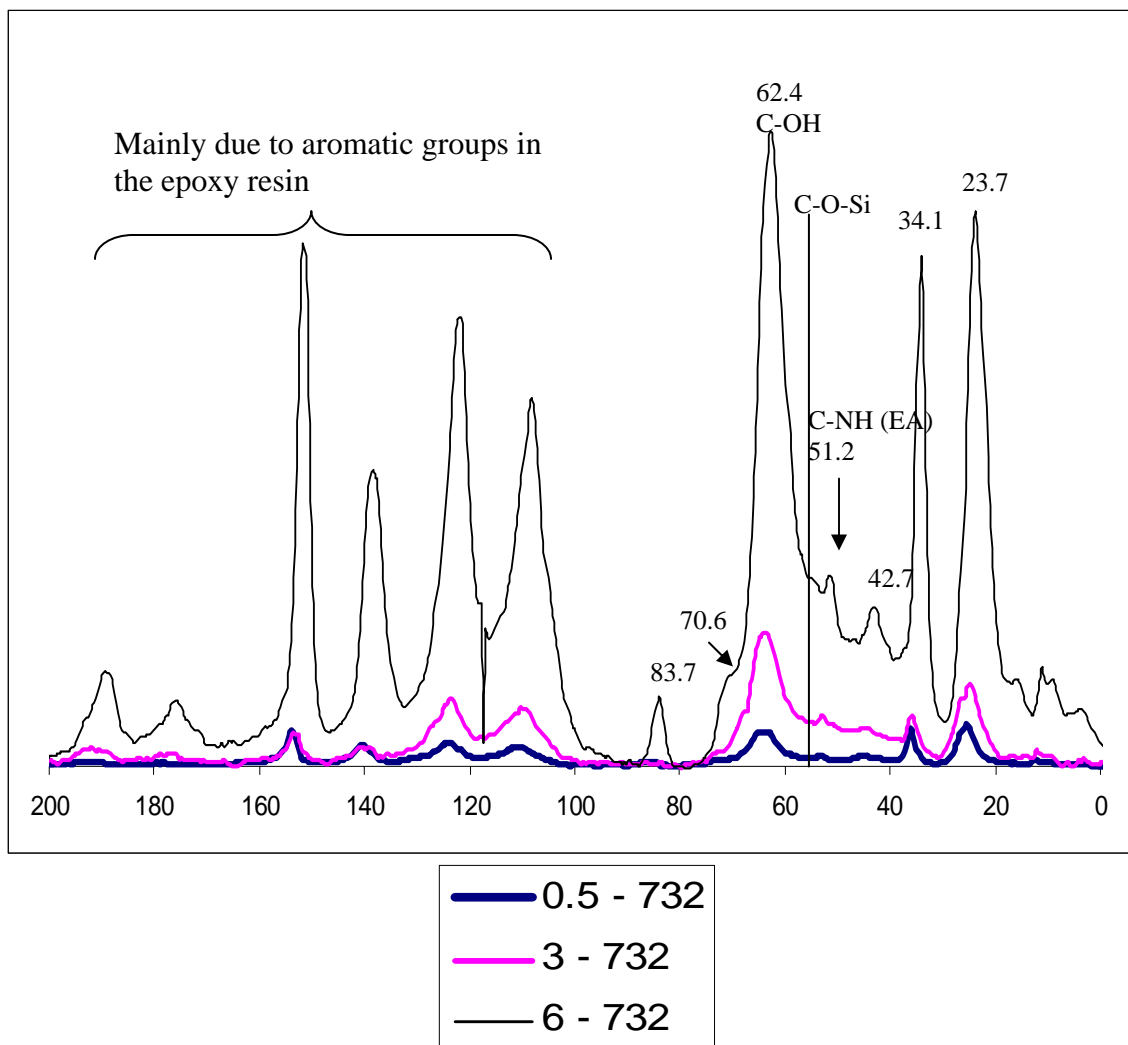


**Figure 5.33.** Solid-state  $^{13}\text{C}$  spectra for NMR solid sample 1 (7 3 2); refer Table 5.7 and p 129 for peak identification and formulation details, respectively

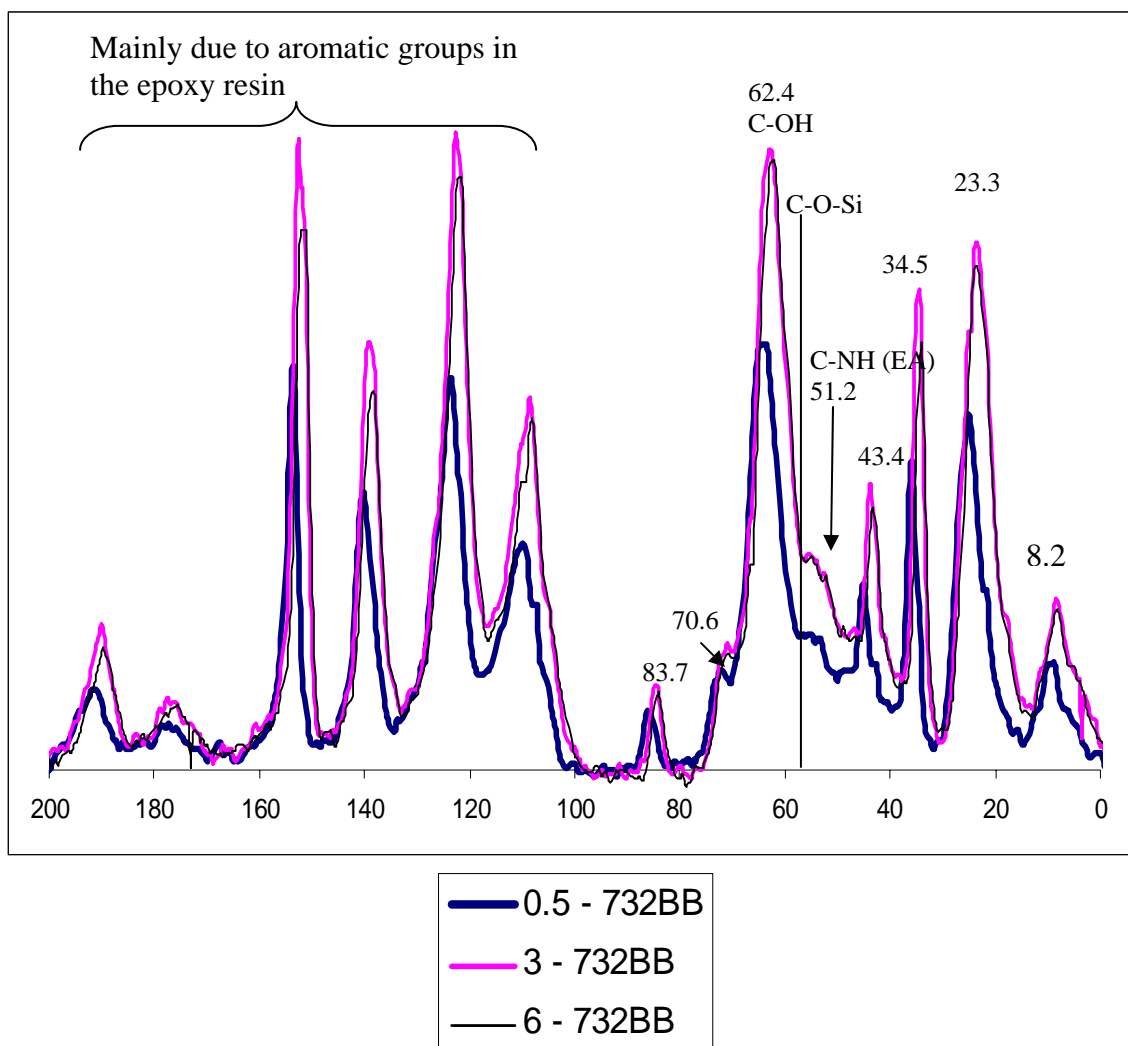


**Figure 5.34.** Solid-state  $^{13}\text{C}$  spectra for NMR solid sample 2 (7 3 2 BB); refer Table 5.7 and p 129 for peak identification and formulation details, respectively

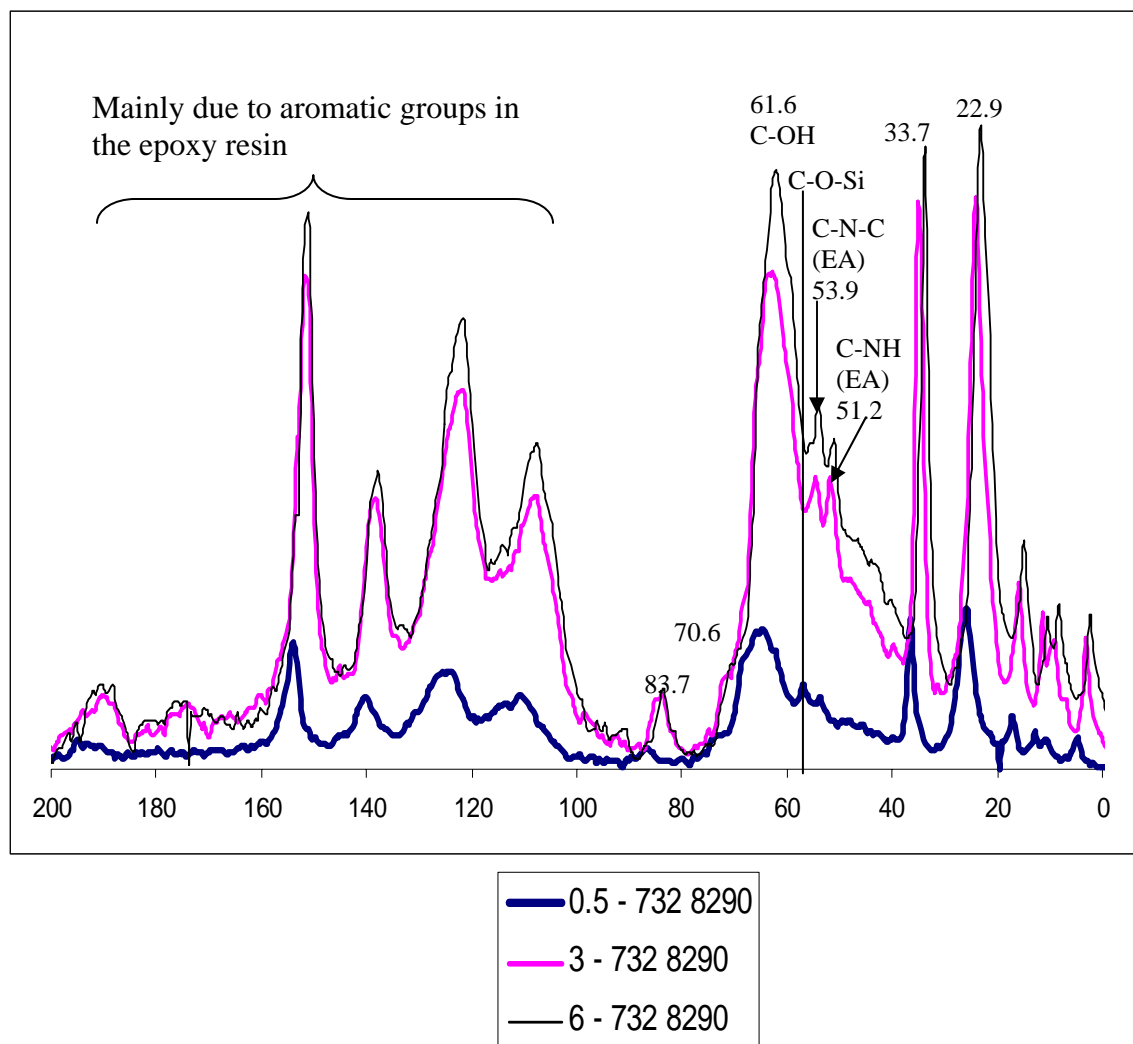


**Figure 5.35.** Solid-state  $^{13}\text{C}$  spectra for NMR solid sample 3 (7 3 2 8290) ; refer Table 5.7 and p 129 for peak identification and formulation details, respectively

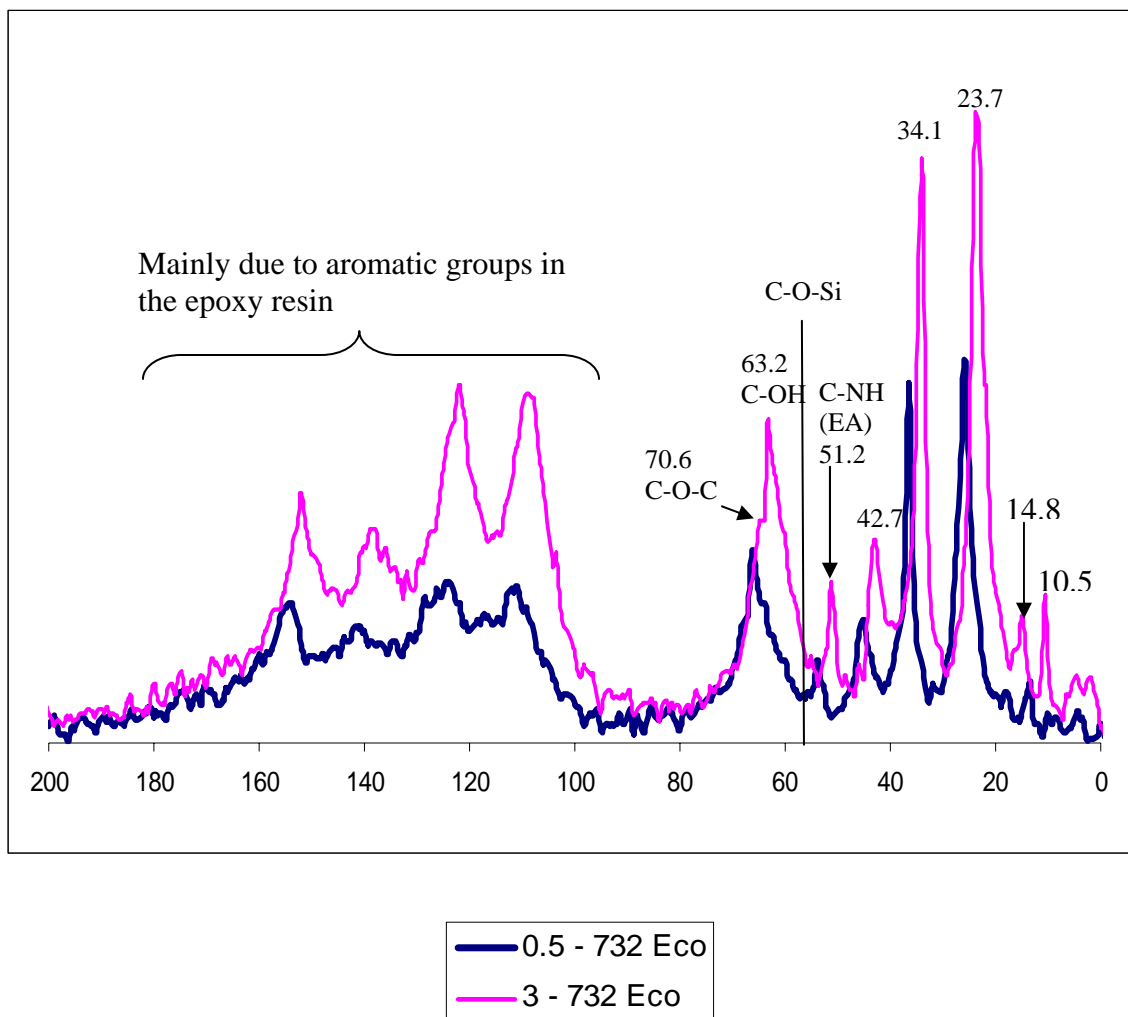


**Figure 5.36.** Solid-state  $^{13}\text{C}$  spectra for NMR solid sample 4 (7 3 2 ECO) ; refer Table 5.7 and p 129 for peak identification and formulation details, respectively

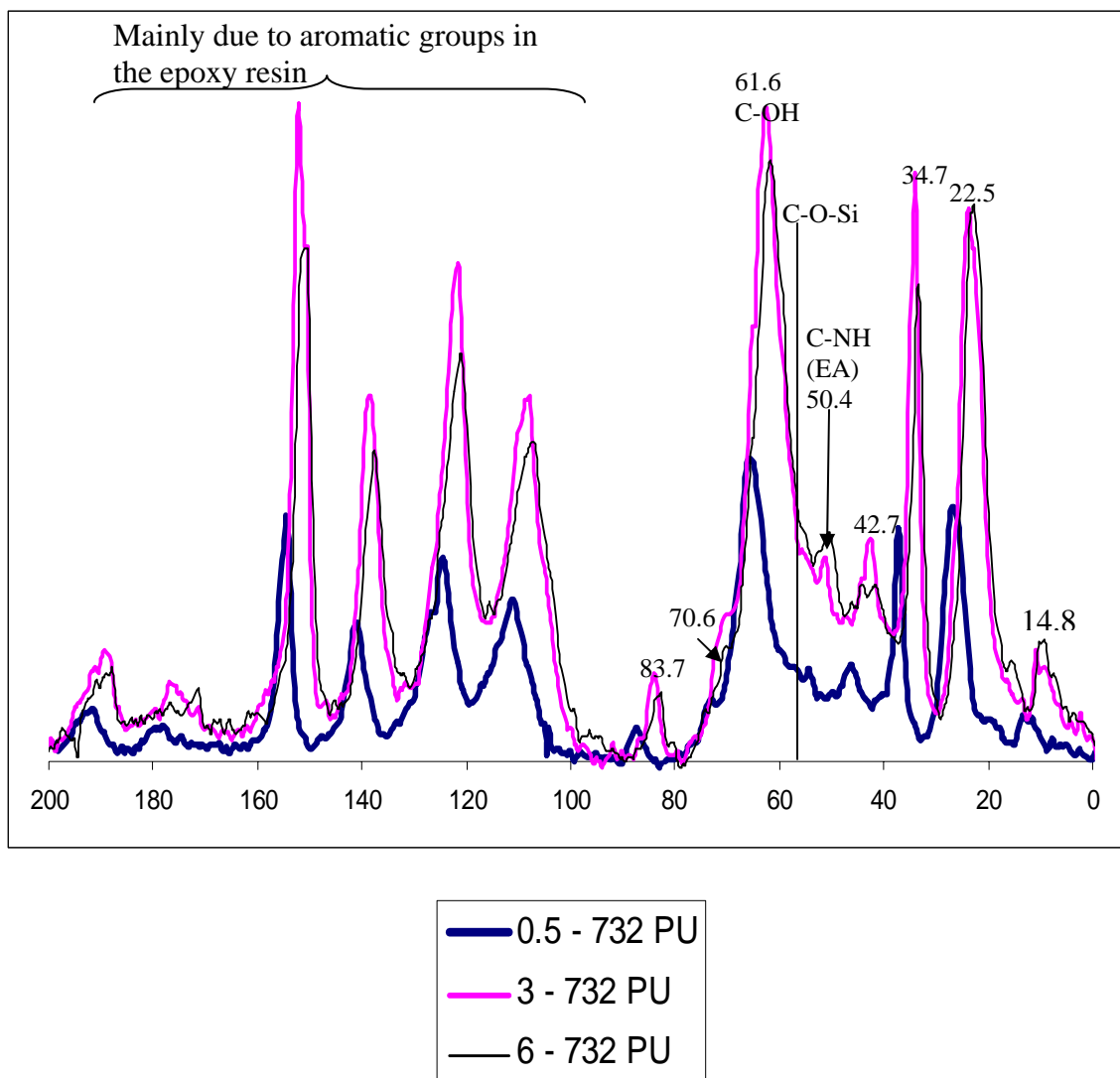


**Figure 5.37.** Solid-state  $^{13}\text{C}$  spectra for NMR solid sample 5 (7 3 2 PUD) ; refer Table 5.7 and p 129 for peak identification and formulation details, respectively

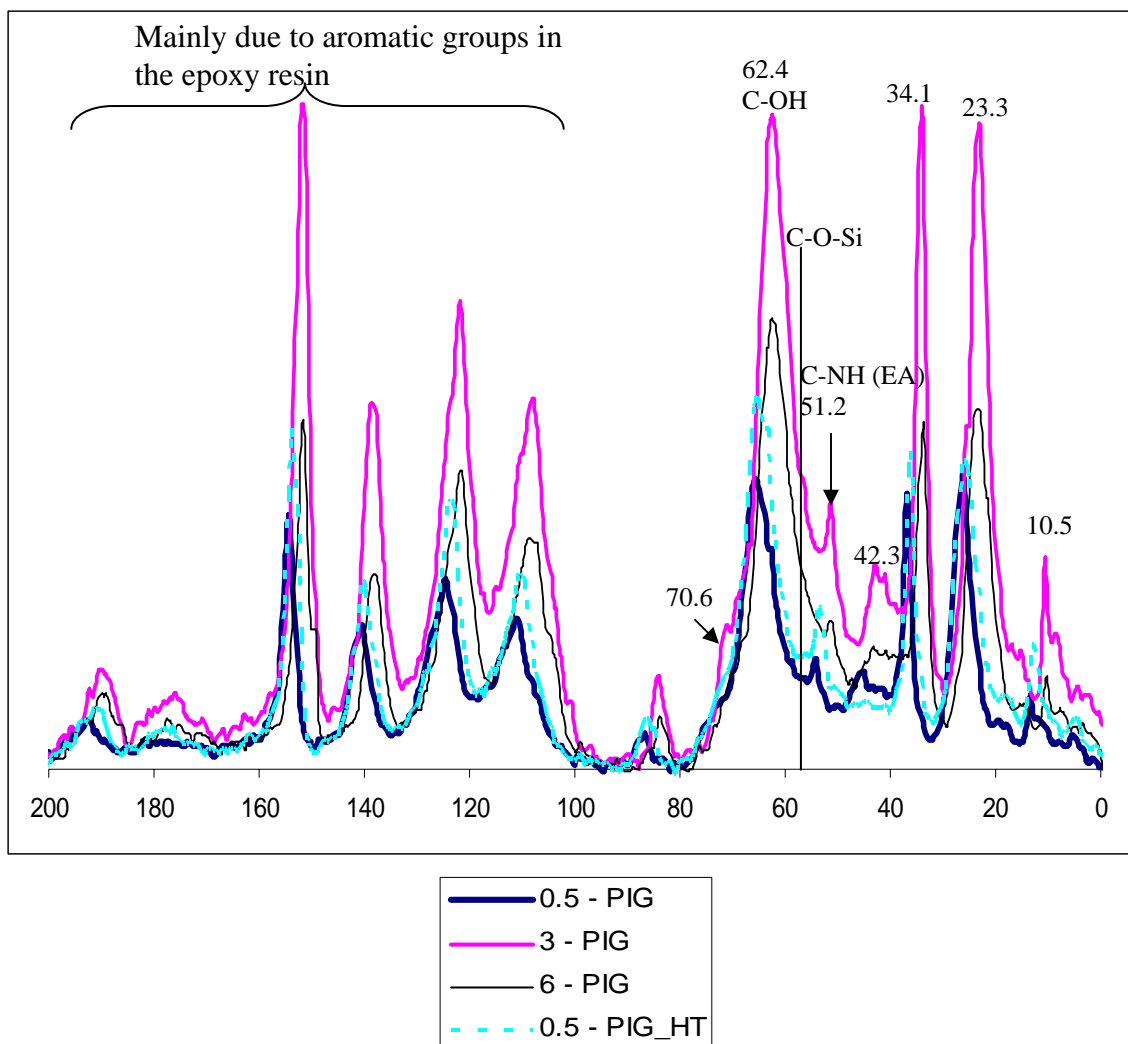


**Figure 5.38.** Solid-state  $^{13}\text{C}$  spectra for NMR solid samples 6 (PIG) and 7 (PIG\_HT) ; refer Table 5.7 and p 129 for peak identification and formulation details, respectively

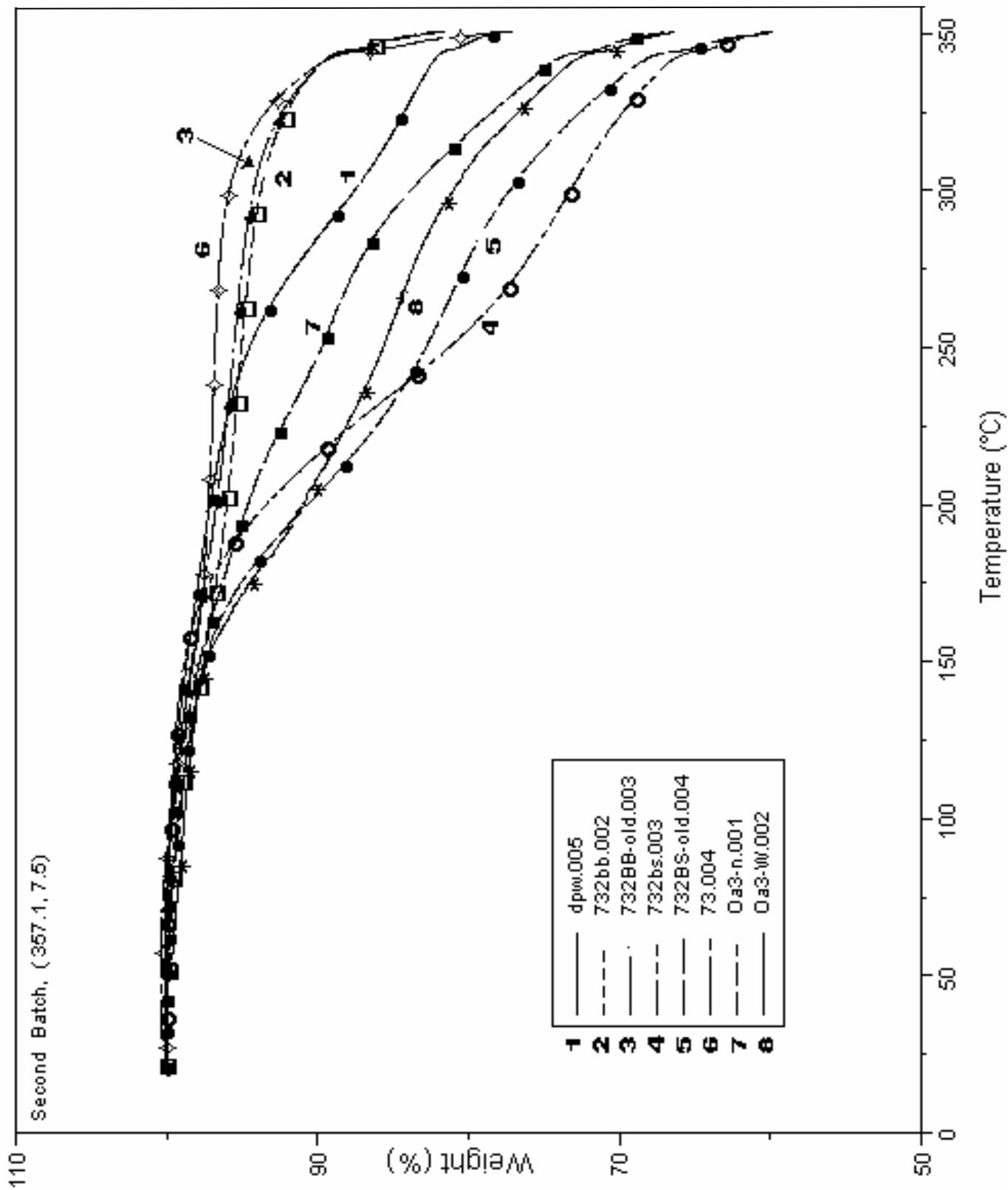
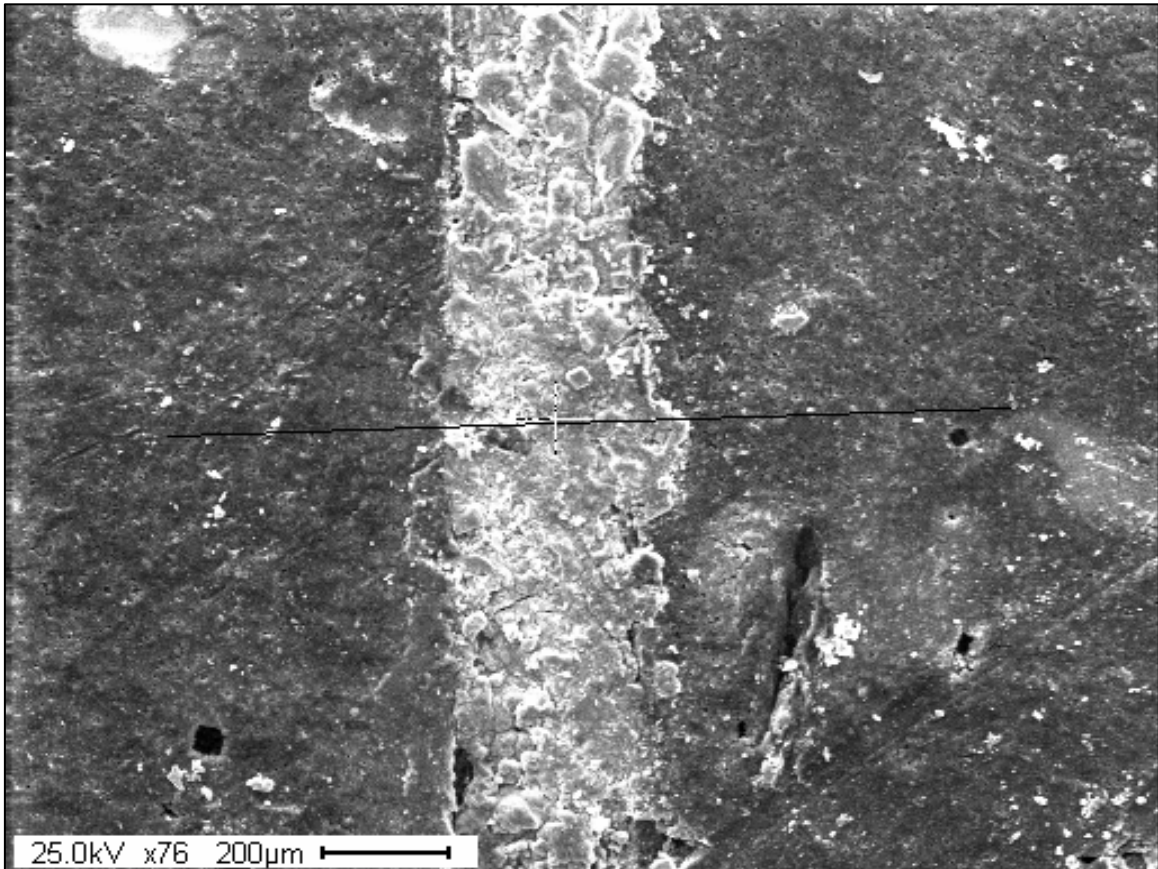


Figure 5.39. TGA curves of the eight analyzed samples; refer p 137 for sample identification



**Figure 5.40 (a).** SEM image of scribe – effect of 5% Corrostatin 228

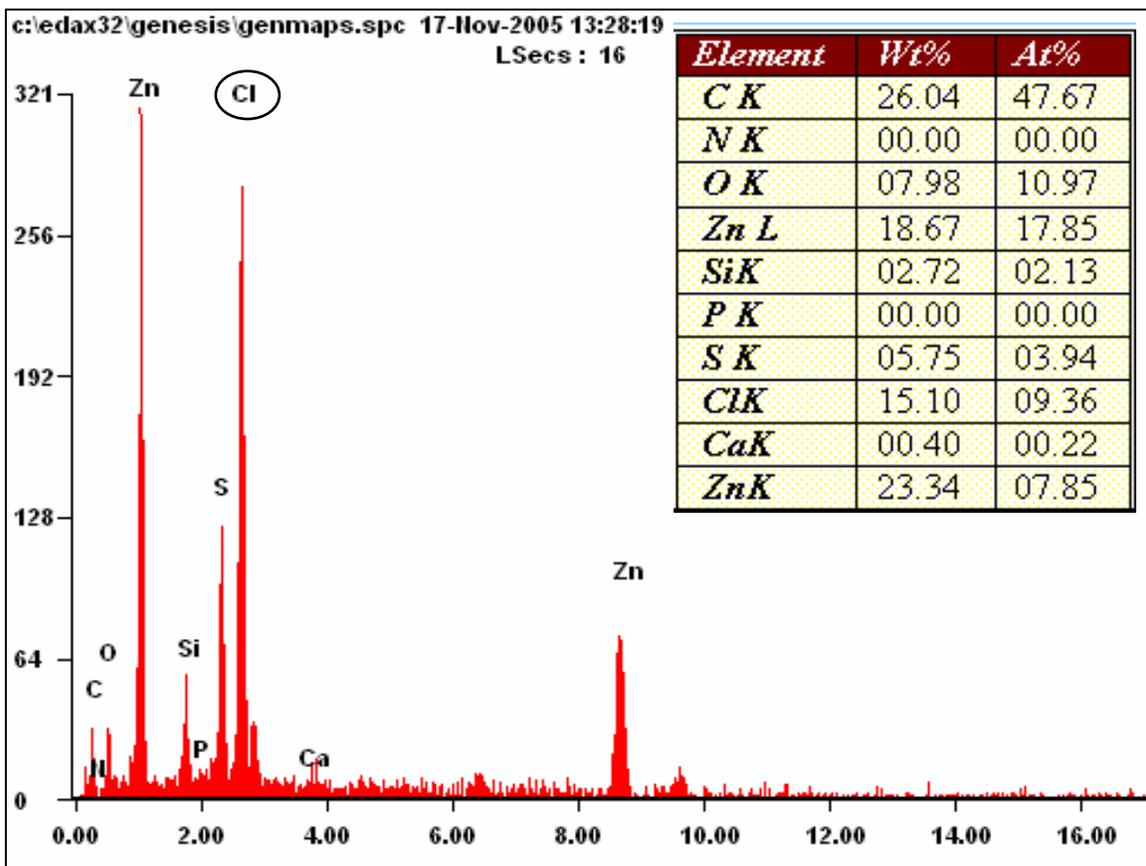
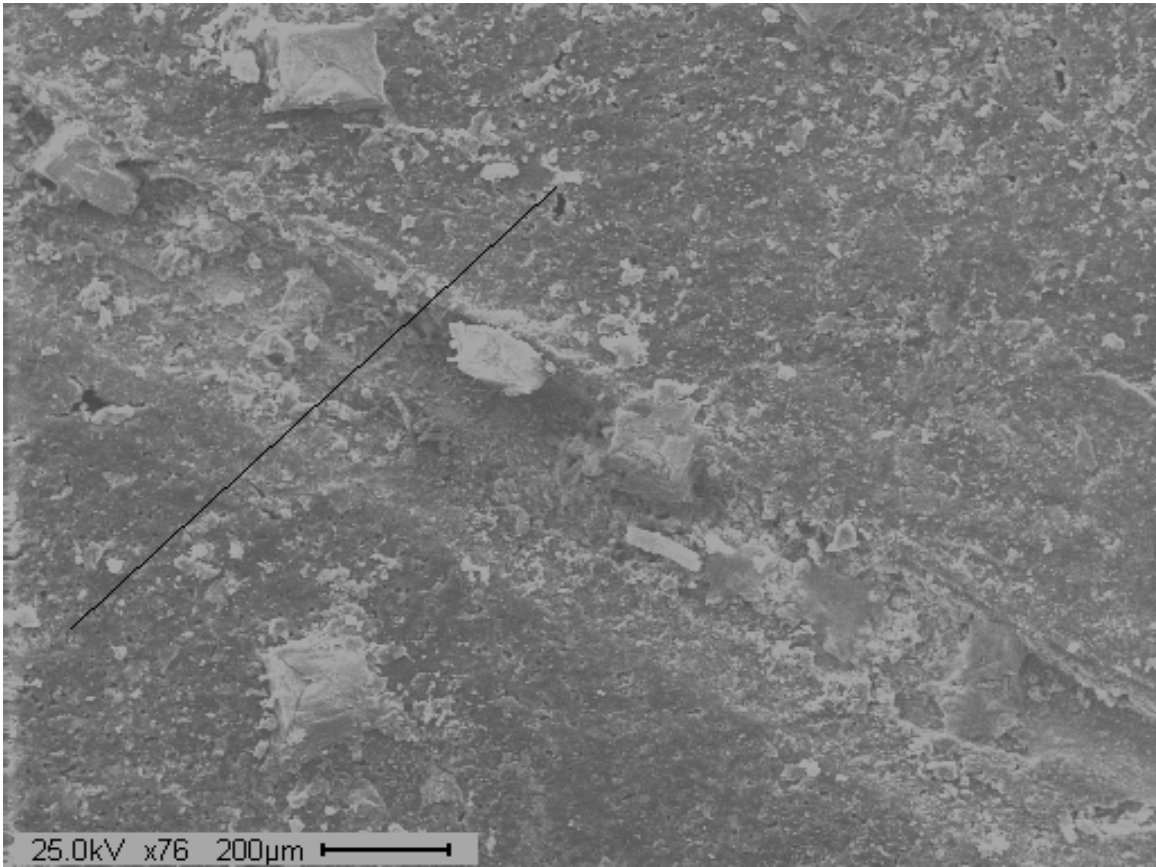


Figure 5.40 (b). EDX spectrum at the point in the scribe highlighted in Figure 5.45 (a)



**Figure 5.41 (a).** SEM image of scribe – effect of 10% Corrostain 228

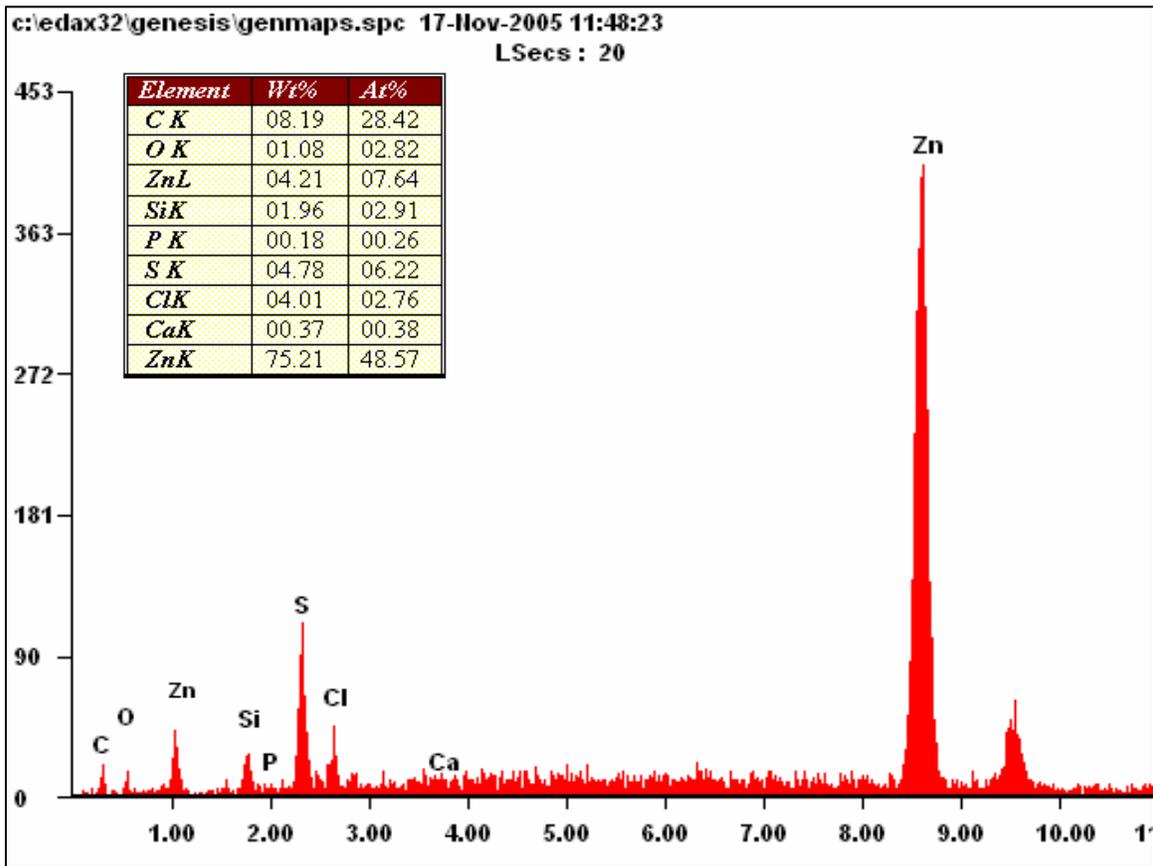
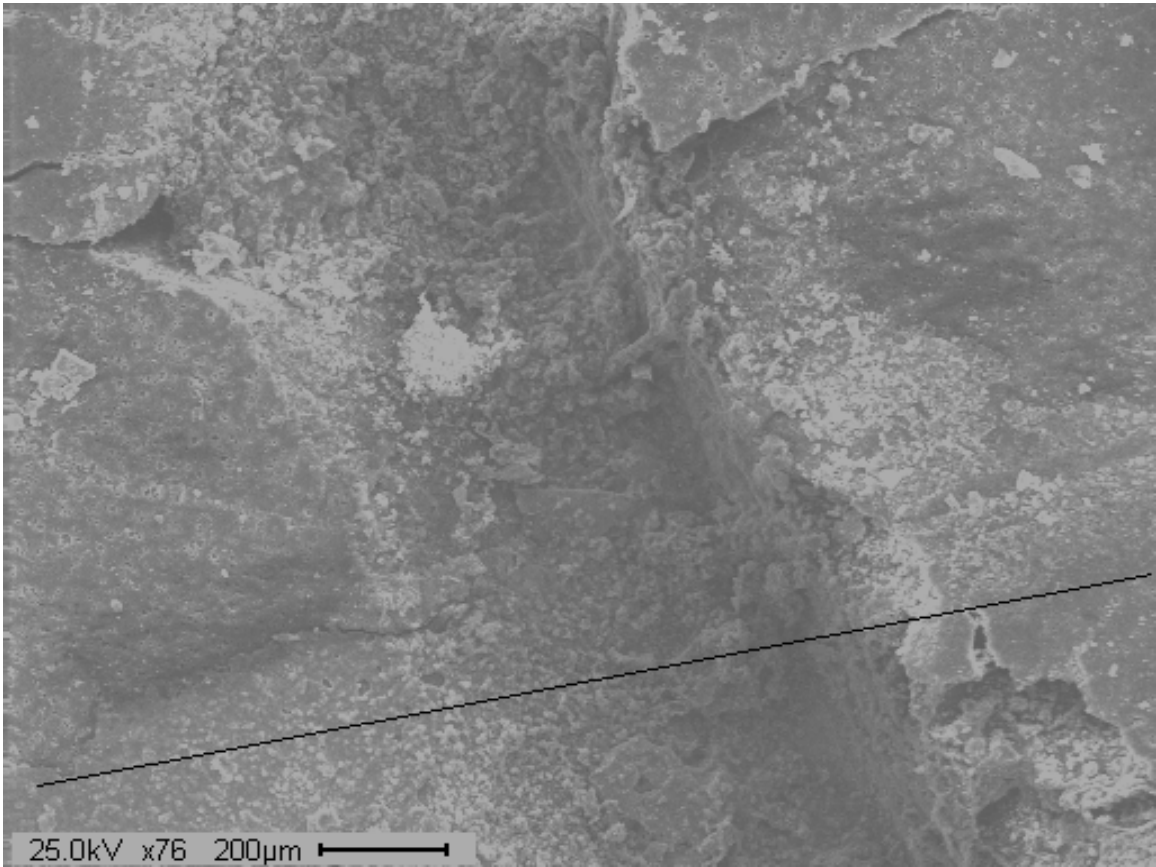


Figure 5.41 (b). EDX spectrum at the point in the scribe highlighted in Figure 5.46 (a)



**Figure 5.42 (a).** SEM image of scribe – effect of 10% zinc phosphate

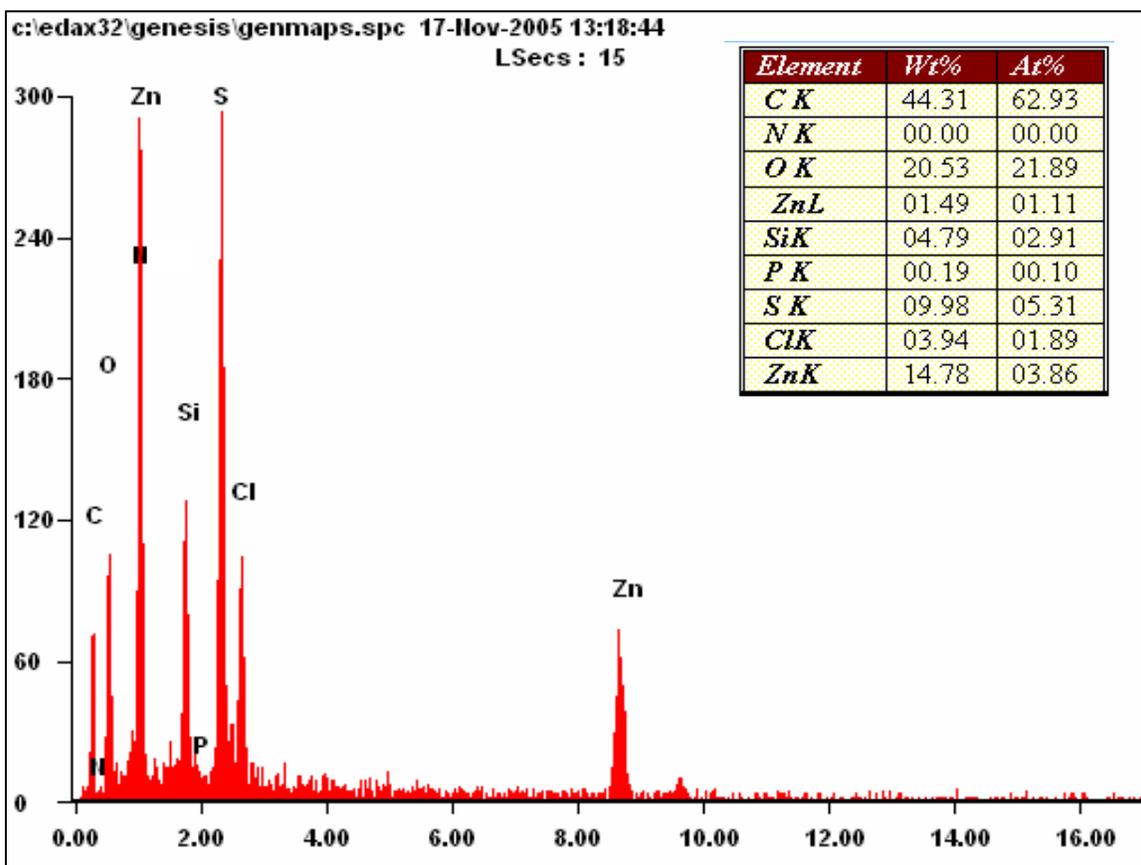
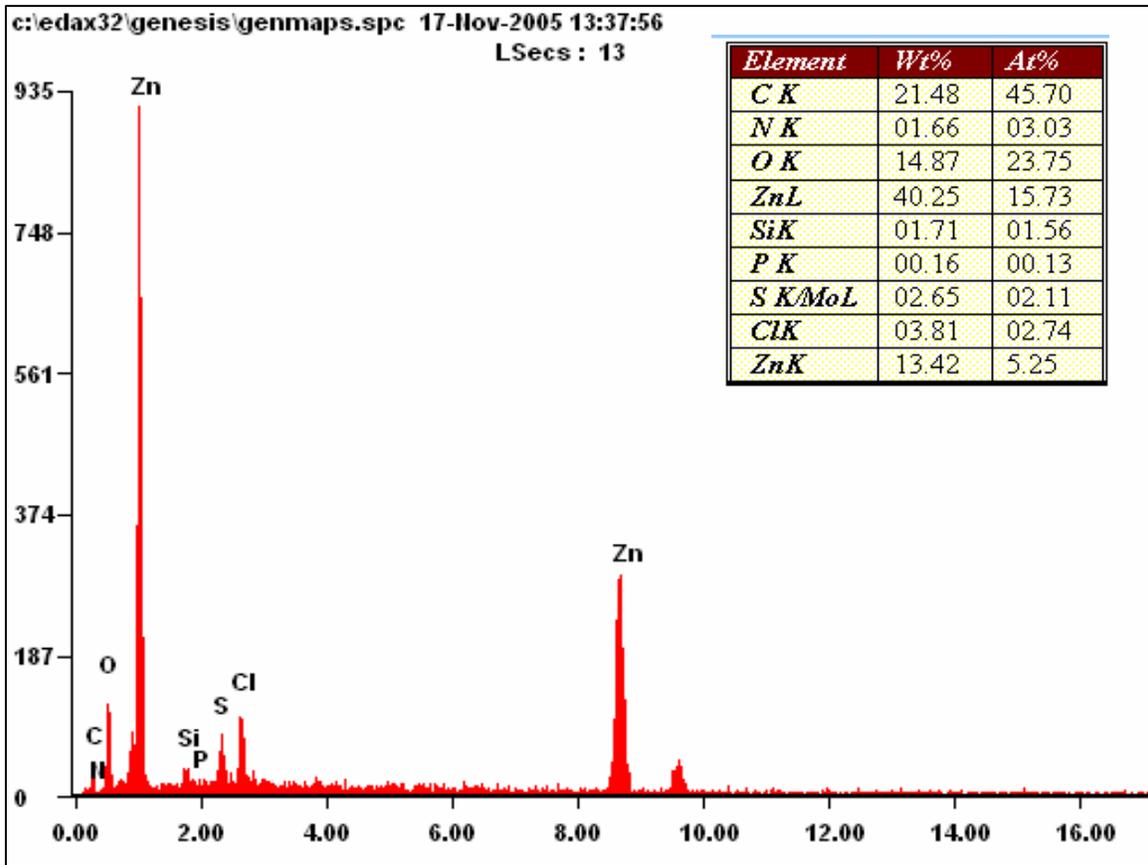


Figure 5.42 (b). EDX spectrum at the point in the scribe highlighted in Figure 5.47 (a)



**Figure 5.43 (a).** SEM image of scribe – effect of 10% CZM



**Figure 5.43 (b).** EDX spectrum at the point in the scribe highlighted in Figure 5.48 (a)

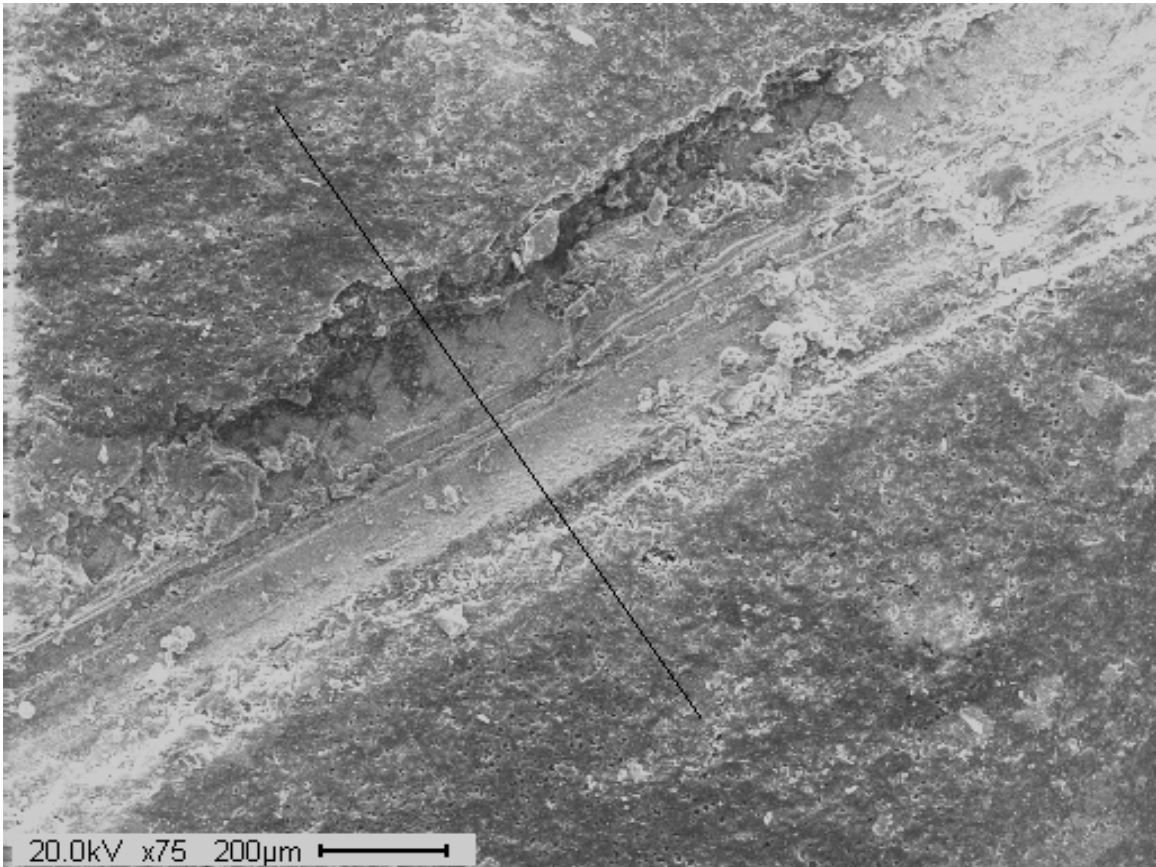


**Figure 5.44 (a).** SEM image of scribe – effect of 15% CZM

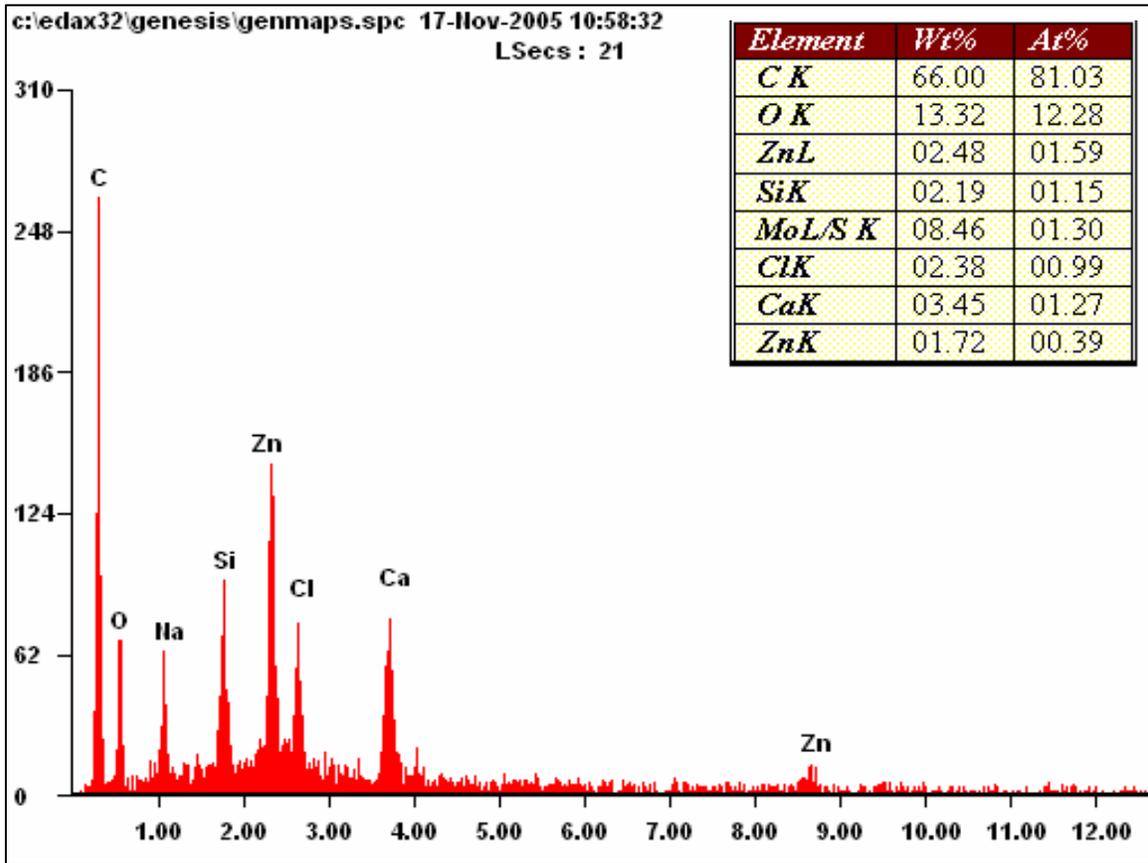


Figure 5.44 (b). EDX spectrum at the point in the scribe highlighted in Figure 5.49 (a)



**Figure 5.45 (a).** SEM image of scribe – effect of 10% Corrostain 228 + 1%  $\text{NaVO}_3$

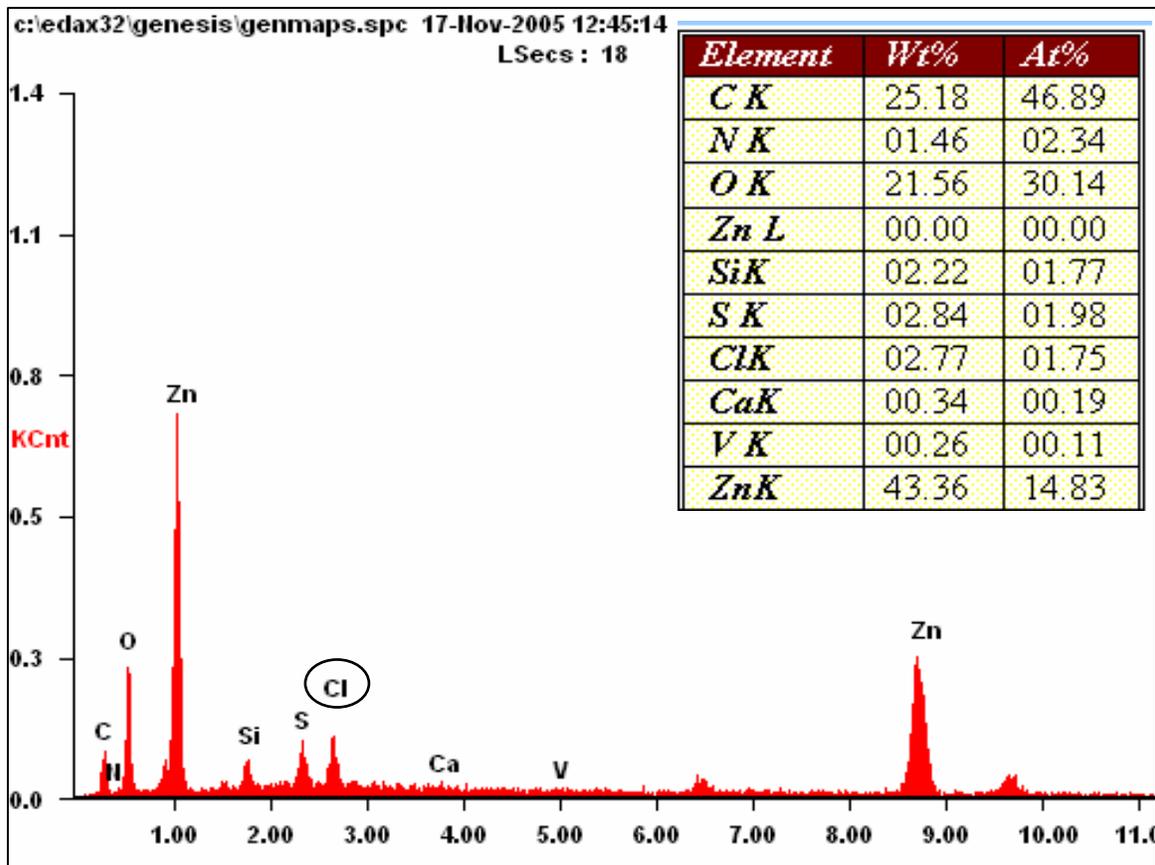
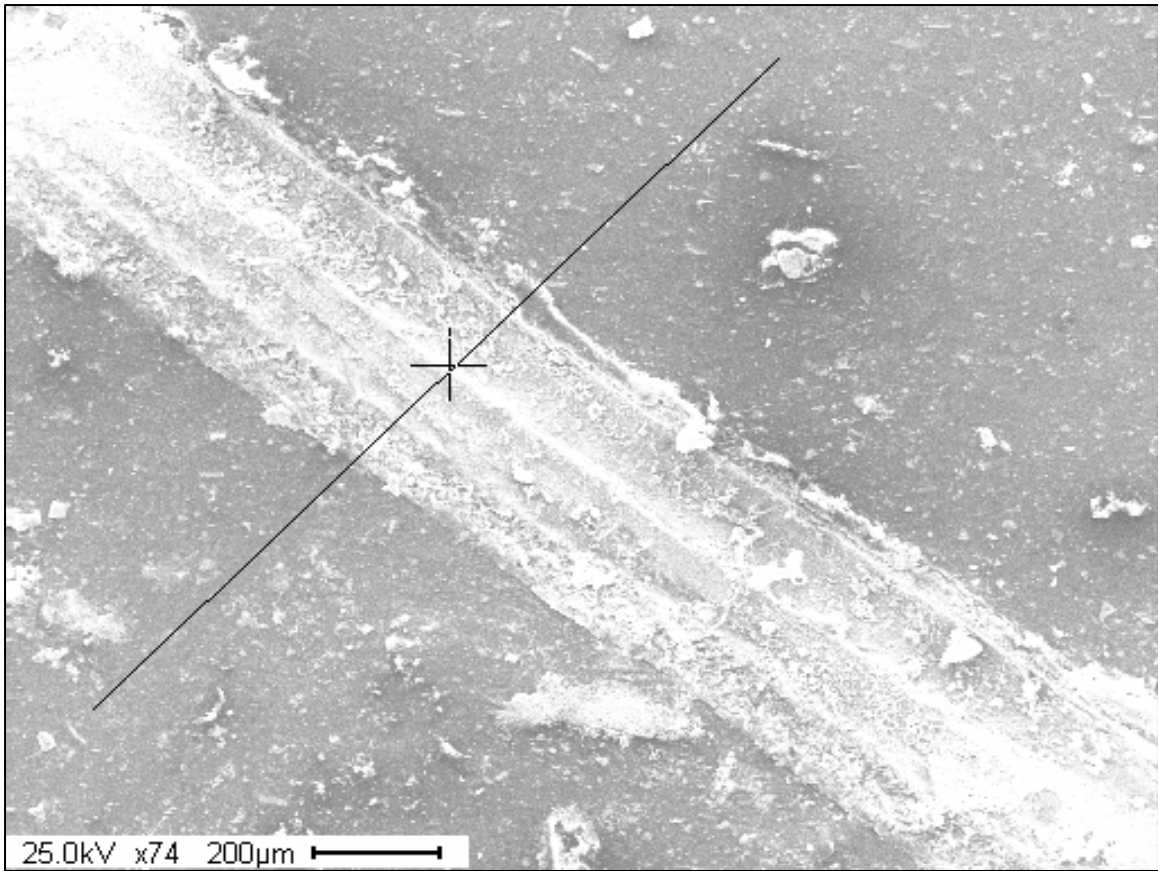


Figure 5.45 (b). EDX spectrum at the point in the scribe highlighted in Figure 5.50 (a)

**Figure 5.50 (a)**



**Figure 5.46 (a).** SEM image of scribe – effect of silane absence

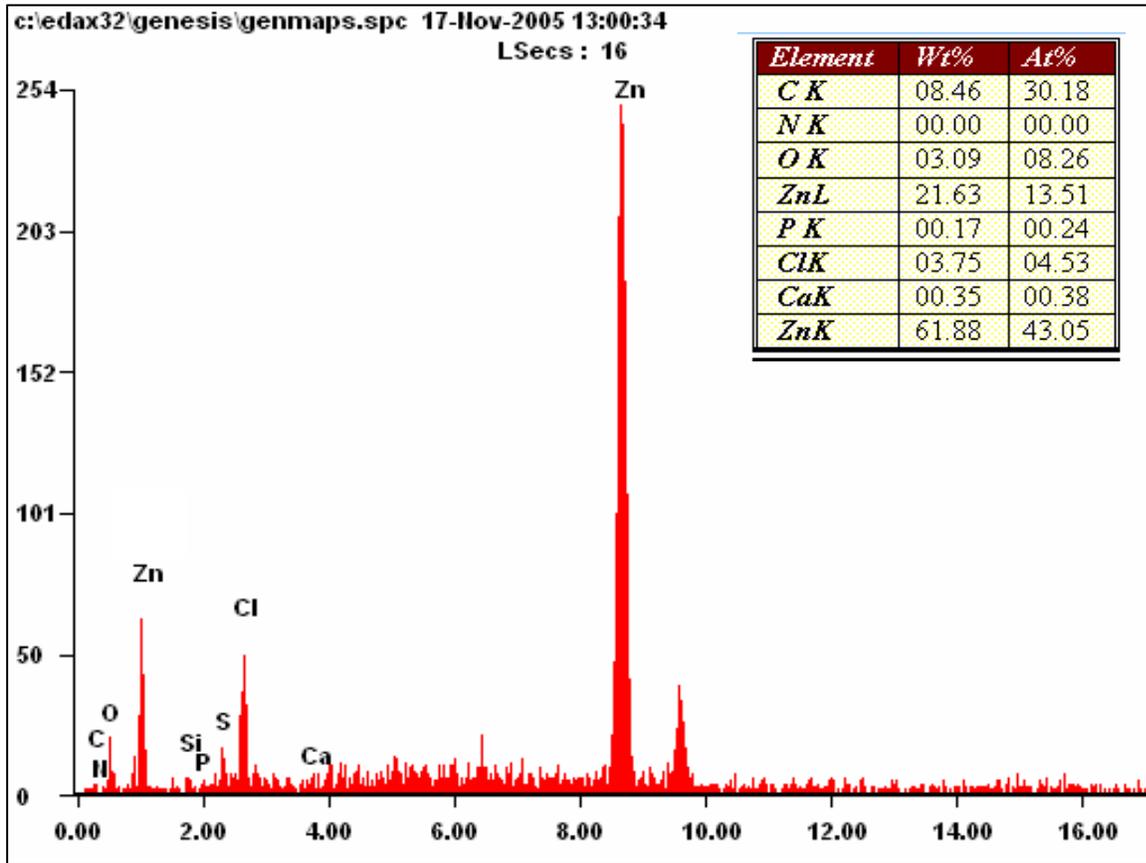
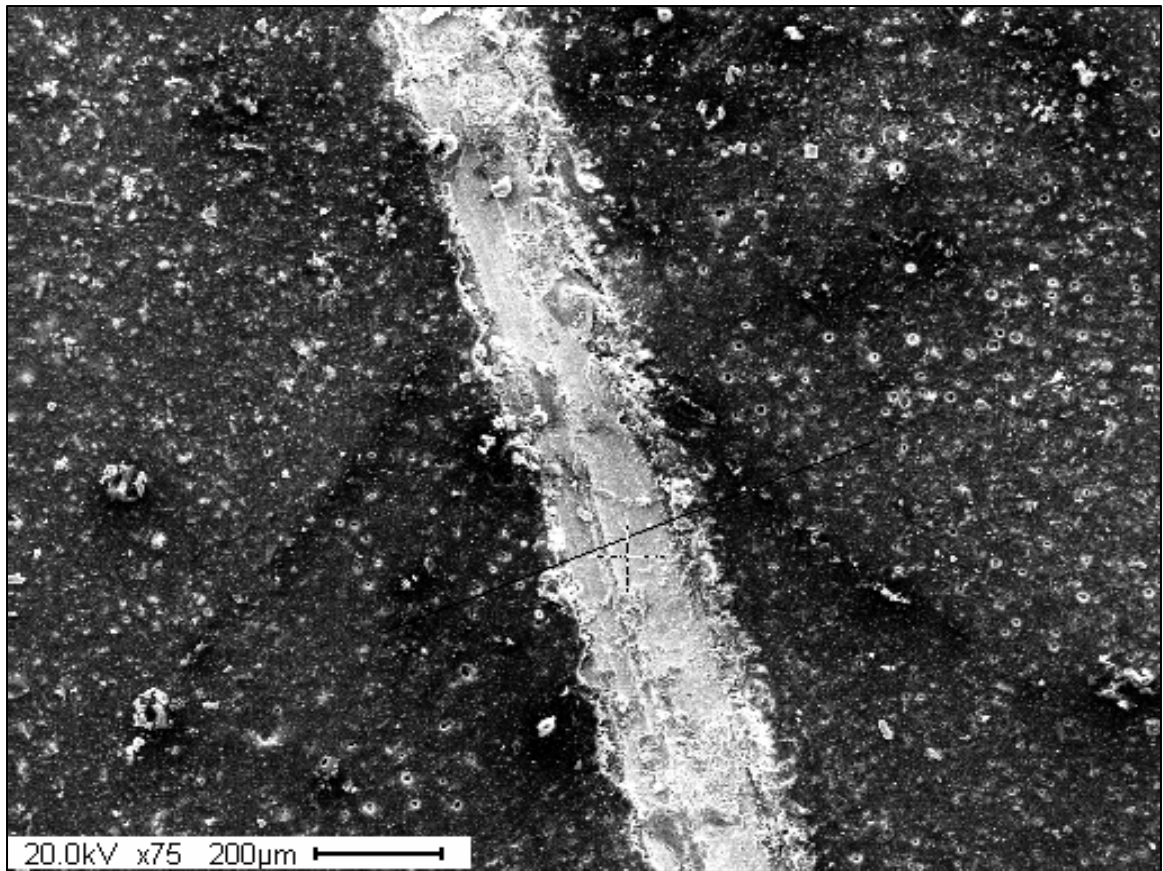


Figure 5.46 (b). EDX spectrum at the point in the scribe highlighted in Figure 5.51 (a)



**Figure 5.47 (a).** SEM image of scribe – effect of high temperature cure

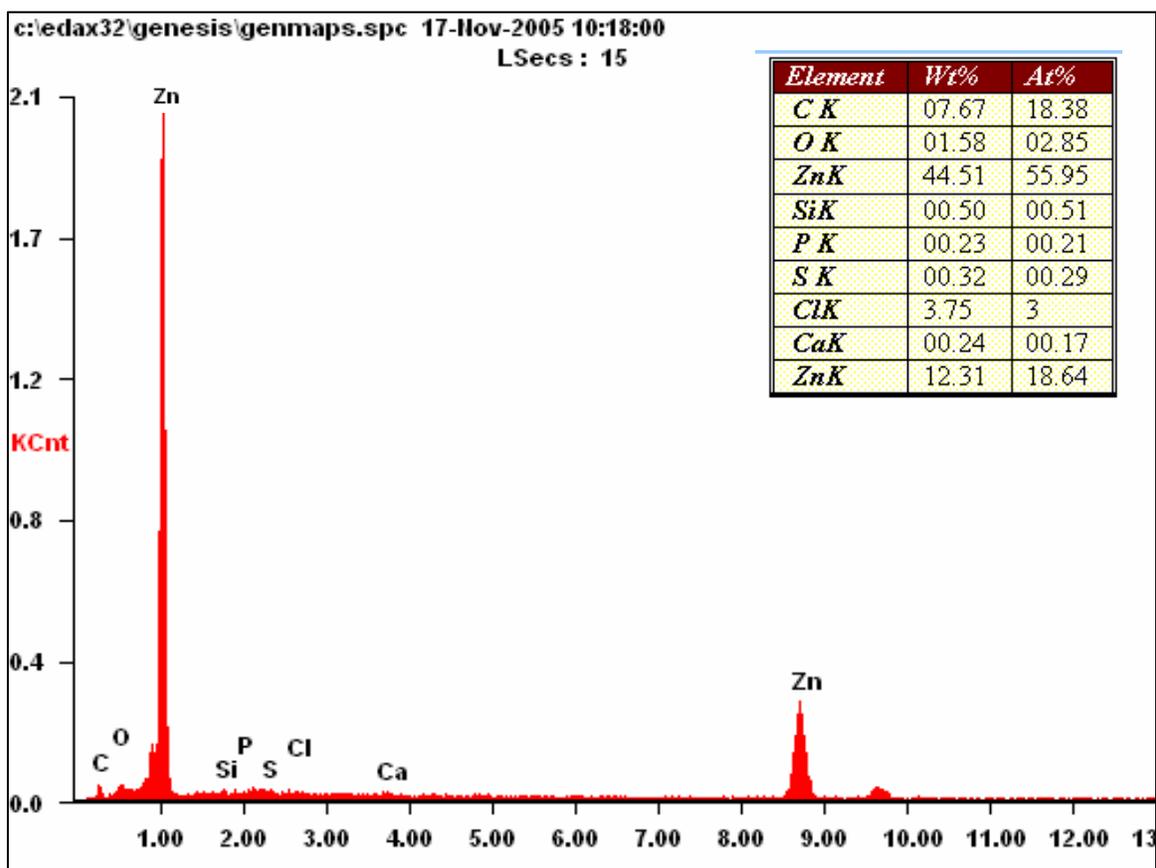
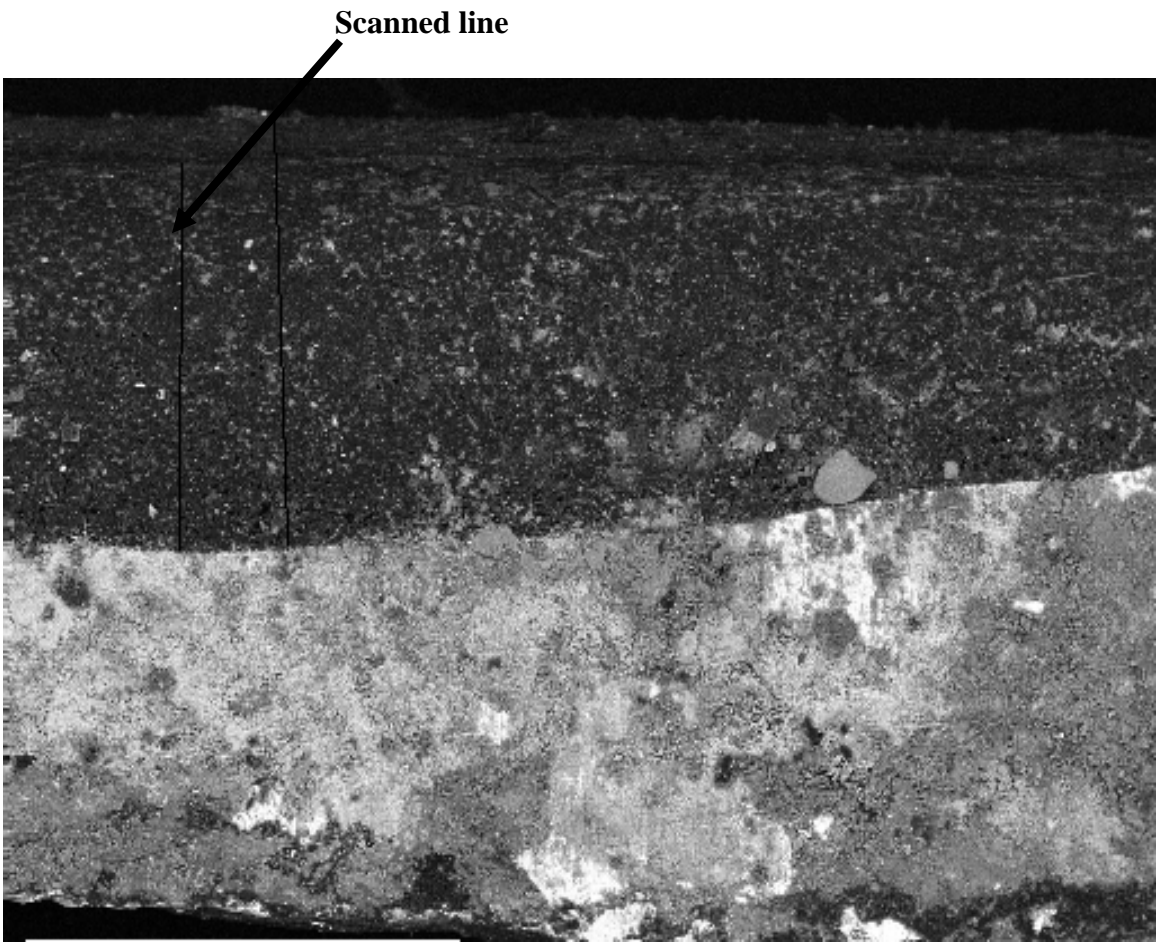
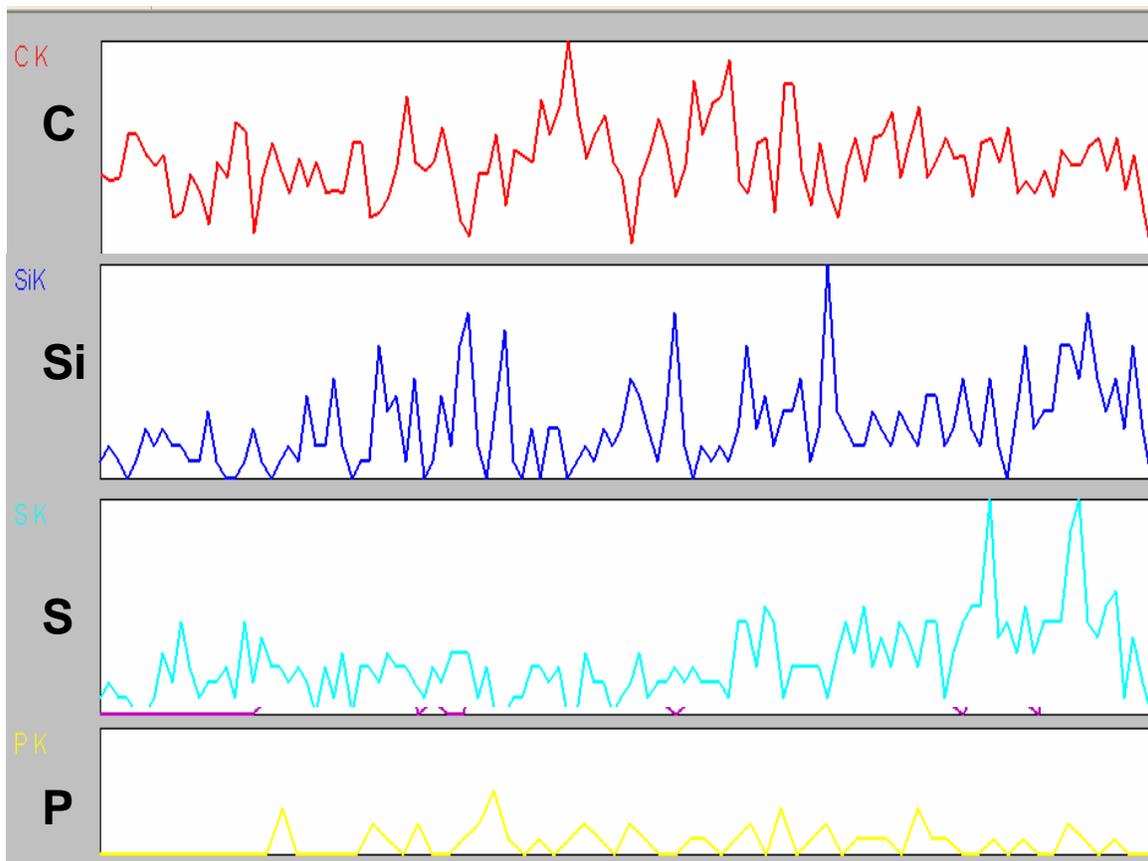


Figure 5.47 (b). EDX spectrum at the point in the scribe highlighted in Figure 5.52 (a)



**Figure 5.48 (a).** SEM image of the cross-section of superprimer coating on HDG. Notice the line on which the EDX line scan was taken starting from bottom, towards the top.



**Figure 5.48 (b).** EDX line spectra on the line shown in Figure 5.48 (a), revealing the relative elemental distribution

## **APPENDIX: SILANE-EPOXY-INHIBITOR PRETREATMENT FOR HDG**

As mentioned in the introduction, this chapter presents a to-be-published study delineating the formulation and performance attributes of an optimized silane-epoxy-resin formulation as a passivating pretreatment for HDG. This chapter is complete in itself and is independent of the previous chapters. However, this chapter presents a study of the development and properties of a formulation that can be considered as a spin-off of the superprimer work, as it is similar to a diluted form of the superprimer, however, with the concentration of the silane exceeding that of the resin. Hence this work has also been included in this thesis.

### **Abstract**

Bis-silane films have proved to be environmentally benign, non-toxic and competent replacements for chromates as pre-treatments for corrosion protection of metallic substrates. So far the best performances have been shown by solvent-based silanes, having high volatile organic content (VOC). Amongst the water-based silanes, AV5, a 5:1 mixture of bis-[trimethoxysilylpropyl] amine (A1170) and vinyltriacetoxysilane, has shown great promise for aluminum-based alloys. However, its performance in case of more susceptible substrates like hot-dip galvanized steels (HDG) and cold-rolled steels is below par. The aim of this work was to improve the suitability of AV5 as a pretreatment for hot-dip galvanized steel. This silane mixture was modified with an additive for cross-linking and toughening, and a corrosion inhibitor for self-healing. The concentration levels were optimized for the best performance after testing formulations with all the nine possible combinations of factor levels. Electrochemical Impedance Spectroscopy (EIS), Direct Current Polarization (DCP), and salt immersion were the performance tests utilized for this screening. The efficacy of inhibitive action was confirmed using the scratch cell test. The chemical nature of the the improved system vis-à-vis the base silane system (AV5) was investigated using IR spectroscopy

**Keywords:** Organofunctional Silanes, VOC, Corrosion, HDG, Coatings, Chromate.

\* submitted for publication in the *Silane and Other Coupling Agents*, Vol 4., K. L. Mittal, eds., 2005, Canada; June 22 – 24 (2005)

## 1. Introduction

Hot-dip galvanized steel (HDG) is widely used in automobiles, electrical home appliances and construction industry due to the corrosion resistance imparted to the mechanical strength of steel. The zinc layer serves as a sacrificial layer, providing cathodic protection to the steel substrate. However, the zinc layer is eventually consumed by corrosion. An organic coating or

\* To whom correspondence should be addressed; email vanooiwj@email.uc.edu

a passivating treatment on this zinc coating provides barrier protection to the zinc layer and thereby greatly extends its service life. Prevention of white rust by the additional coat also enhances the appearance of the steel.

Trialkoxysilanes have been suggested as alternatives for chromate conversion coatings ever since their anticorrosive properties were first demonstrated using organo-functional di-podal silanes or 'bis-silanes' [1]. Apart from providing corrosion protection, they also perform as a coupling agent, promoting adhesion between the organic coating and the metallic substrate. Bis-triethoxysilylethane (BTSE) [2] and bis-triethoxy tetrasulfide (bis-sulfur) [3] are the two bis-silanes that have proven to be competent pretreatments especially for aluminum alloys. However, these silanes are hydrophobic and solvent-based, so for their hydrolysis they are typically dissolved in a 95:5 by volume mixture of ethanol and water. Bis-amino silane is a water-based silane and hence has low-VOC content. However, it does not provide sufficient corrosion protection due to the water and anion attracting tendency of the secondary amines in the bis-amino films [4]. Puomi, et al., have characterized various solvent-based silane pretreatments on HDG [5-6].

In several cases, mixtures of silanes have proven to be more effective than single silanes, especially in case of galvanized steel, where the more hydrophobic silanes fail to sufficiently wet the zinc oxide layer on HDG. Van Ooij, et al., have worked on such mixtures comprising bis-amino silane [7-8]. One such successful mixture was a 3:1 v/v mixture of bis-sulfur silane and bis-amino silane [7]. This mixture has shown excellent performance as a pretreatment on HDG. However, the mixture is predominantly solvent-based.

Another range of mixtures are the bis-amino silane + vinyltriacetoxysilane (VTAS, a monosilane) systems [8]. These mixtures, in ratios of 1:1 (bis-amino:VTAS) and up by volume, have stable shelf lives even when they have been diluted by water, unlike either of the silanes individually. One mixture denoted as AV5, a 5:1 mixture, is especially stable. A 5% solution of AV5 in water has a shelf life of more than a year. Water-based silane mixtures hydrolyze quickly unlike their solvent-based counterparts. Further, the aforementioned solution has a natural pH of 6, which falls within the region of ZnO stability. Zinc oxide is stable in the pH range of 6 and higher, while for hydrolysis of silanes, the lower the pH, the better it is. This brings the silane deposition window for zinc substrates to a pH value of 6-9 [9]. Also, AV5 films show good adhesion to many primers.

Despite the advantages associated with AV5, i.e., a stable shelf life, quick hydrolysis, low-VOC, good wetting of substrate and prevention of zinc dissolution in HDG, and good adhesion with a broad variety of paints and coatings, its hydrophilicity remains a deficiency in terms of corrosion protection as stand-alone films. It is the aim of this study to capitalize upon the strengths of AV5 and mitigate its weakness. The water-barrier aspect of the films is improved by incorporating a water-borne epoxy dispersion. An additional aspect considered in this study is the self-healing ability of silane films. This has been imparted by incorporation of small amounts of an inhibitor,

which enables the films to be used as stand-alone coatings i.e., without any primer, similar to chromate films.

For the past few years alternatives to replace the toxic hexavalent chromate inhibitors are being explored and no inhibitor has been developed so far which rivals the effectiveness of chromate [10]. Palanivel, et al., have introduced organic molecules and inorganic cerium salts into AV5 films with some degree of success [11]. Vanadates are a relatively new class of inhibitors. Buchheit, et al., have shown the effectiveness of vanadates as vanadate conversion coatings [12] and Al-Zn-decavanadate hydrotalcite pigment in epoxy primers on Al alloys [13]. Hence, a vanadate compound was used as an inhibitor in our work. The compound used here was shown to be effective in AV5 on AA2024-T3 substrates [14].

The formulations were tested for their anti-corrosion performance by DCP, EIS, salt water immersion, the Machu test and the ASTM B117 salt spray test. The chemical structure of the optimized system was analyzed using infrared spectroscopy.

## **2. Experimental**

### **2.1 Silanes**

Bis-[3-(trimethoxysilyl)propyl]amine (bis-amino silane), with the trade names of Silquest A1170<sup>®</sup> was provided by OSi Specialties (Tarrytown, NY) and vinyltriacetoxysilane (VTAS) was obtained from Gelest Inc. (Morrisville, Pa). The silanes were used without further purification. Their structures are shown in Figure 1. A mixture of water-based silane mixture AV5 was obtained by mixing the bis-amino silane and VTAS in 5:1 ratio by volume. The AV5 was further diluted by mixing 5 vol% of AV5 and 95 vol% of distilled water. This solution was

aged at its natural pH of 6 while being stirred on an electromagnetic stirrer at 300 rpm for 3 hrs to hydrolyze the silane solution.

## **2.2 Water-borne Epoxy Dispersion**

A modified DGEBA type water-borne epoxy dispersion was introduced to improve the water-barrier properties of the AV5 solution. It was obtained from Resolution Performance Products, Houston, Texas. A water-borne epoxy dispersion provides several advantages: compatibility with water-based silane system, low-VOC, and the possibility of a dense IPN (interpenetrating network) or a combination of interpenetration and crosslinking between the siloxane and epoxy networks. The epoxy used was chosen from a host of commercially available water-borne epoxy dispersions, based on preliminary salt immersion results.

## **2.3 Corrosion Inhibitor**

Sodium meta-vanadate was used as an inhibitor for the study. It is marketed by Fluka industries, Switzerland as a chemical.

**2.4 Commercial Alkyd Primer:** Devguard primer obtained from ICI Devco Coatings Cleveland, OH, a non-chromate alkyd primer was used as a primer on the uncoated, plain AV% coated and optimized formulation coated panels in the Machu test. The primer was applied with a 28  $\mu\text{m}$  draw-down bar, and the primer was allowed a curing time of 2 days at room temperature.

## **2.5 Optimization Matrix and Formulation Procedure**

Three levels of concentration were chosen for the epoxy (1%, 2% and 3%) and the inhibitor (100 ppm, 150 ppm and 200 ppm) based on preliminary salt-water immersion studies. Also formulated were plain 5% AV5 solution (L00) as a control and a L20 for IR study. The

formulation matrix is shown in Table 1. The formulation procedure for plain 5% AV5 solution has already been shown in section 2.1. In case of resin and inhibitor modifications, the resin and inhibitor are added in desired concentrations to the unhydrolyzed (un-aged) 5% AV5 solution, and the silane-resin-inhibitor system was then aged while being stirred at 300 rpm on a magnetic stirrer for three hours.

## **2.6 Metal Substrate and Surface Treatment**

Hot-dipped sheet galvanized steel panels of 10 cm x 15 cm were purchased from Stillwater Steel Supply, Stillwater, OK. The zinc layer thickness on the substrates was about 20 microns. These HDG panels were ultrasonically cleaned in ethanol and acetone successively for 10 minutes each to remove impurities. This was followed by degreasing in a diluted (7% by volume in water) alkaline cleaner (Okemclean, provided by Oakite products, NJ) at 65 °C for 4 min, rinsed with tap water and blow-dried with compressed air to achieve a water-break free surface. The cleaned substrates were dip-coated in the aged formulations for 1 minute, followed by curing in a furnace at 150 °C for 80 minutes.

## **3. Characterization and Testing**

### **3.1 Direct Current Polarization (DCP)**

DCP measurements were made on uncoated as well as coated HDG panels. Before taking the measurements, the coated panels were immersed for three hours in a 3.5 wt% NaCl solution, in order to achieve a steady state open-circuit potential. A standard calomel electrode and platinum mesh were used as the reference electrode and counter electrode, respectively. The data were recorded over the range of  $E_{\text{corr}} \pm 0.25\text{V}$  (SCE), where  $E_{\text{corr}}$  is the equilibrium corrosion potential or open circuit potential of the tested samples. The scan rate was 1 mV/s.

### **3.2 Electrochemical Impedance Spectroscopy (EIS)**

EIS measurements were carried out on HDG panels coated with the formulations mentioned in the Table 1. An area of 5.06 cm<sup>2</sup> of the coated panels area was exposed to a corrosive 0.6 M NaCl electrolyte. An SR810 frequency response analyzer connected to a Gamry CMS100 potentiostat was used for the purpose. Measurements were made at frequencies ranging between 10<sup>-2</sup> to 10<sup>5</sup> Hz, with an AC excitation amplitude of 10 mV. A standard calomel electrode was used as the reference electrode with a graphite rod acting as the counter electrode

### **3.3 Salt Water Immersion Test**

Salt water immersion test is a non-standardized but very useful test to measure anti-corrosiveness and water resistance of organic films. In this test, coated and cross-scribed panels were immersed into a 0.6 M NaCl solution and their performance was monitored over time. The coatings were periodically checked for any scribe creep, corrosion or blistering. The usual immersion time was 30 days. However it could be extended if the coatings did not show any substantial deterioration.

### **3.4 Scratch Cell Test**

A scratch cell was used to test the efficacy of the corrosion inhibitive action of the inhibitors in films. A scratch cell is meant to duplicate a scratch defect in a coating. Buchheit, et al., had utilized a scratch cell to test the inhibitive action of an Al-Zn-decavanadate hydrotalcite (HT-V) pigment [12]. In this study, a simplified model of that scratch cell was used as shown in Figure 9a.

### **3.5 Machu Test**

The Machu test is an accelerated corrosion test for painted HDG widely used in Europe. The solution used in this test directly attacks the paint-metal interface due to the presence of the

oxidizer  $\text{H}_2\text{O}_2$  and the test results are claimed to correlate with 500 hours of ASTM B117 salt spray test [15]. It is especially useful for galvanized steels. The painted panels are cross-scribed on the surfaces, and then immersed in a solution of 5% NaCl + 0.6%  $\text{H}_2\text{O}_2$  at 37 °C for two days. On the second day 0.6%  $\text{H}_2\text{O}_2$  is added to maintain the peroxide levels. After 2 days of immersion, the panels are taken out and adhesive tape is used to pull off the delaminated paints. Alternatively, a knife can be used to lightly scrape off the paint in delaminated areas along the scribe lines. The extent of delamination around the scribe is a measure of paint adhesion and corrosion performance of the entire system [16].

### **3.6 ASTM B 117 Test**

This test was employed to evaluate the bare corrosion protection of silane-treated metals without topcoats. According to the specifications, a 5% NaCl solution is atomized in a salt spray chamber at 35°C with the solution pH around 7. The tested panels were placed at an angle of 45 degrees in the chamber and exposed to the salt fog for the test period.

### **3.7 Infrared Spectroscopy**

The chemical structures of the silane films on HDG steel were studied by reflection absorption infrared (RAIR) spectroscopy. The RAIR spectra were obtained by using a Spectrum One FTIR spectrometer from Perkin Elmer, Wellesley, MA. A variable angle diffuse reflectance accessory was used with the incidence angle being fixed at 80°. The scanning range was from 4000  $\text{cm}^{-1}$  to 450  $\text{cm}^{-1}$  and 64 scans of each film were taken.

## 4. Results and Discussion

### 4.1 Direct Current Polarization

The DCP curves were plotted for each of the coated panels on the first and fourteen days of immersion in 0.6M NaCl solutions. Gamry Echem-Analyst™ software was used to obtain the values of open circuit corrosion potential ( $E_{\text{corr}}$ ) and corrosion current ( $I_{\text{corr}}$ ). Figures 2 and 3 show the variation of the  $E_{\text{corr}}$  and  $I_{\text{corr}}$  values respectively with each formulation.

The  $E_{\text{corr}}$  is a very important parameter. It determines how actively the zinc corrodes while cathodically protecting the steel. The  $E_{\text{corr}}$  value for HDG with the L23 coating increased during immersion, perhaps due to the substrate modification by leaching of the inhibitor. On day 14, the  $E_{\text{corr}}$  of L23 was about 70 mV lower than the plain AV5 (L00 coat) and showed the lowest  $E_{\text{corr}}$  (-1.1 V) among all the coatings. This means that at the weak areas, i.e., scratches, scribes, edges, etc. the zinc continues to protect the steel cathodically, however before the cathodic action is required the barrier effect due to the passivation of its surface with the inhibitor comes into action and hence the zinc dissolution rate is lowered. In other words, in the presence of L23, zinc consumption is minimal and a thinner zinc coating can be sufficient for imparting cathodic protection for a longer time period. Also, the effective leaching of the inhibitor in L23 coupled with the higher hydrophobicity of L23 film (observed in EIS studies) leads to a corresponding low  $I_{\text{corr}}$  value at the end of 14 days. As  $I_{\text{corr}}$  is directly proportional to the corrosion rate (equation 1), it implies that L23 shows the least corrosion rate of all the formulations.

$$\text{Corrosion rate (MPY)} = I_{\text{corr}} \cdot \Delta\varepsilon/\rho \cdot 2.54 \times 10^{-4} \text{ [cm/year]} \quad (1)$$

Where MPY is the corrosion rate in cm/year,  $I_{\text{corr}}$  is the current at open circuit corrosion potential in A/cm<sup>2</sup>,  $\Delta\varepsilon$  is the equivalent weight of the substrate in g/eq, and  $\rho$  is the density of the substrate in g/cm<sup>3</sup>.

All the silane formulations behaved the same on the first day of immersion, indicated by their relatively close  $E_{\text{corr}}$  and  $I_{\text{corr}}$  values, but the L3x series is marginally better than the rest. On day 14 the following trends were observed in each series. In the L1x series, the  $E_{\text{corr}}$  first increased then decreased with inhibitor concentration. In the L2x series, we observed an increase in  $E_{\text{corr}}$  with increase in inhibitor concentration, while in the L3x series, the  $E_{\text{corr}}$  was relatively stable and independent of the inhibitor concentration. The  $I_{\text{corr}}$  trend in each series was complementary in each case, i.e., the  $E_{\text{corr}}$  increased with a decrease in  $I_{\text{corr}}$  and vice versa.

The  $E_{\text{corr}}$  (and subsequently the  $I_{\text{corr}}$ ) depends on several factors, viz.,

- a) The density and nature of the passivation layer at the metal interface. In formulations having just the silane, a metallo-siloxane (Me-O-Si) layer is formed at the metal interface. However, with the incorporation of varying concentrations of epoxy in each formulation, the chemical nature of the interfacial layer as well as the crosslink-density may change. This change in surface chemical has a direct effect on  $E_{\text{corr}}$  values.
- b) The film density, i.e., extent of crosslinking and/or interpenetration of the epoxy/siloxane networks. This affects the amount and rate of electrolyte ingress.
- c) The critical pigment volume concentration (CPVC) of the films. The CPVC of any binder, in this case the silane solution, is that volume of the pigment beyond which the film becomes porous. Below CPVC, as the pigment concentration increases, the porosity of the cured film decreases and correspondingly, its barrier property increases.
- d) Leaching rate of an inhibitor. The leaching rate of the inhibitor in a film should neither be too high nor too low. For a cathodic inhibitor (such as the vandate compound used here), to show a significant  $E_{\text{corr}}$  drop and thereby be effective, sufficient amount of inhibitor should leach

out before excess electrolyte ingress occurs and the corrosion reaction becomes too aggressive. But at the same time, the leaching rate should not be too high so as to cause blistering in the film. A high leaching rate also has the risk of the inhibitor being consumed quickly over time. The leaching rate of the same inhibitor varies with the nature of the film.

Some sort of interaction among some or all of these factors can be attributed to explain each and every one of the observed aforementioned trends. However, further investigation needs to be done with respect to the nature of the interfacial layer, the film chemistry and the pigment leaching, before attributing any mechanism exactly.

DCP curves for the blank panel, L00 and L23 (the best in DCP) are shown in Figure 4. The improved performance is obvious. The effect of the inhibitor is obvious in the case of L23. The inhibitor effectively passivates the zinc layer under the film as observed by the  $E_{\text{corr}}$  rise with time. The  $I_{\text{corr}}$  of L23 does not vary much and remains at a very low value. The L00 film on the other hand is good on day 1. However its hydrophilic nature and lack of any inhibitors leads to a rapid increase of  $I_{\text{corr}}$  and a drop in potential towards the  $E_{\text{corr}}$  of corroding zinc as the Me-O-Si interfacial layer is hydrolytically unstable and dissolves quickly. As expected, the blank HDG panel corrodes heavily. Its  $E_{\text{corr}}$  does not change with time, as the nature of the corroding layer does not change. It remains as such, i.e., plain corroding zinc.

#### **4.2 Electrochemical Impedance Spectroscopy:**

Impedance and phase angle measurements of the coatings were taken over a course of 25 days and Bode plots were obtained on days 0, 1, 3, 7, 14, 21 and 25. The low-frequency impedance moduli for each formulation on day 1 and day 25 of measurement were obtained from the Bode plots. The low-frequency impedance gives a measure of the barrier property of a coating. Its

variation for each formulation is shown in Figure 5. References 17-21 give information on the application of EIS techniques to study corrosion process under paints.

From Figure 5, we can clearly observe that at the end of 14 days, four coatings L11, L23, L32 and L33 stand out. However, as seen before, DCP results show that L23 by far outperforms the rest vis-à-vis the passivation of the surface. Surface passivation in these cases is due to film barrier property as well as the leaching of the pigment. This result is confirmed by salt-water immersion results, as will be shown later in section 4.3.

The change in Bode plots over time for L00 and L23 is shown in Figure 6. The impedance modulus vs. frequency and the phase angle vs. frequency plots are shown separately. In case of a metal with a porous coating, there are two maxima, one representative of the coating and the other is the corrosion reaction. The low-frequency region gives information on the corrosion reaction, while the high frequency region gives information on the coating. From the Bode plots we can see that the low-frequency impedance modulus for L00 decreases rapidly over time. Also, in the low-frequency region phase angle increases at every frequency, while in the high frequency region, a decrease in phase angle is observed which indicates the increase of the corrosion reaction and simultaneously, a decrease in coating condition (water uptake, bond dissociation especially the Me-O-Si bonds, etc). L23, in contrast, maintains a high low-frequency impedance throughout. Its Bode plots remain stable throughout the course of electrolyte exposure. In the Bode phase plot for L23, the low-frequency maximum is very low and starts appearing only towards the end of the exposure period, while the high frequency maximum shows a high phase angle, indicating a low corrosion rate and integrity of the coating (no water uptake and no bond dissociation).

A model for fitting the EIS curves [19-20] (Figure 7) was set up using the Gamry EchemAnalyst™ software. EIS fits were obtained for the 14<sup>th</sup> day L00 and L23 curves. The obtained fits were within the minimum required levels for the goodness of fit. Coating and corrosion parameters were obtained from these fits. The values of the different parameters for L00 and L23 are shown in Table 2. We can notice that the value of the pore resistance for L23 is much higher than the pore resistance value for L00, indicating low porosity in the L23 film. The coating capacitance of L23 is lower than that of L00, indicating less water uptake by L23. Similarly, the capacitance of the exposed metal for L23 is lower than that of L00, indicating less moisture and corrosion products at the metal surface underneath the L23 film. Finally, the polarization resistance of the L23 film is more than 30 times higher than that of the L00 film. As the polarization resistance is inversely proportional to the corrosion current and hence the corrosion rate, it implies that at the end of 14 days, the corrosion rate of the zinc underneath the L23 film more than thirty times lower than that of the zinc underneath the L00 film. This difference will only widen with increasing exposure time (as confirmed by DCP results), as the L00 film rapidly deteriorates with exposure time, while the L23 film maintains its integrity as shown in the Bode plots of Figure 5.

### **4.3 Salt Water Immersion Test**

The images of the coated panels immersed in 0.6 M NaCl solutions are shown in Figure 8. We can clearly see the difference between the panels. The uncoated control is heavily corroded and so is the plain AV5, i.e., L00. L00 shows heavy scribe corrosion and creep. L11, L32 and L33, which came close to L23 in EIS studies, did not perform well both in this test as well as in DCP test. The leaching rate of inhibitor in these films was not good enough to prevent scribe corrosion. Only L23 performed well.

#### **4.4 Scratch Cell Test**

As mentioned before, a scratch cell is meant to simulate a scratch. The exposed area under the blank panels acts as a large scratch. The images shown in Figure 9 are after two days of testing period. As evident from the heavy corrosion of the first two images of blank panels, both blank-on-blank and blank-on-L00 do not show any scratch protection. Blank-on-L23 shows very little corrosion, however indicating the effective leaching of the inhibitor from the L23 film.

#### **4.5 Machu Test**

Figure 10a shows the Machu test panel images for L00 and L23. L00 was totally corroded, the corrosion proceeding even to the red rust stage, while L23 showed only some white rust. The Machu test results for the uncoated control, L00 and L23 panels, each further coated with a commercial alkyd primer (Devoe primer) are shown in Figure 10b. Blank panels show heavy scribe creep. There is very little difference between the L00 and L23 panels (only one or two pits of red rust in L00) at the end of two days. The differences may accentuate on further exposure. Therefore, the L23 system performs as well as, if not better than the L00 system as a pretreatment underneath other paints as well.

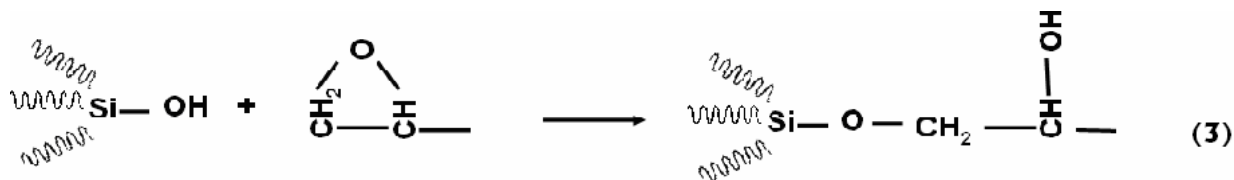
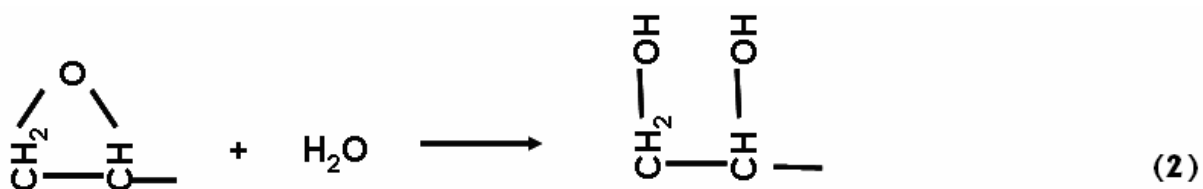
#### **4.6 ASTM B 117 Test**

The Salt fog test results for the first 100 hours show a considerable difference in performance in the AV5 films by incorporating the epoxy and the inhibitor. Figure 11 shows the salt fog test images of L00 (plain AV5), L03 and L23 (the optimized formulation with the epoxy and the inhibitor), coated onto cleaned HDG panels. As we can see clearly, the L00 shows substantial white rusting throughout the panel surface within 8 hours of exposure. With the incorporation of inhibitor in L03, the panel shows improved resistance towards corrosion, with some white rust

appearing at around 25 hours. However, the optimized coating L23 shows no signs of corrosion even after 100 hours of exposure.

#### 4.6 Infrared Spectroscopy

Absorption spectra were recorded for L00, L20 and L23 films on HDG. They are shown in Figure 12. Table 3 gives the assignment for the IR peaks [22, 23]. In the cured film, we can encounter secondary amines, due to the presence of bis-amino silane, vinyl groups due to the presence of VTAS and epoxy rings because of the water-borne epoxy addition. Upon hydrolysis, the methoxy groups remain in equilibrium with the silanol groups. Hence we can expect these two species. Metallo-siloxanes and siloxanes are formed from the condensation of silanol groups. Xue studied reactions occurring in aqueous solutions of an epoxy silane,  $\gamma$ -glycidoxypropyltrimethoxysilane [22]. He concluded that in aqueous solutions, the epoxy rings can be opened up via hydrolysis by water and also hydrolysis by silanol groups, with the kinetics of the former dominating the latter due to the higher amount of water in the solution. Similarly, in our case, hydrolysis of the epoxy ring by water and silanol is quite possible as shown in equations 2 and 3, respectively.



There is a sharp peak at  $1485\text{ cm}^{-1}$ , which corresponds to the C-H bending in methylene ( $-\text{CH}_2$ ). This may be attributed to the formation of methylene in the SiOCC structure during the epoxy ring opening by silanols. However, if this is so, then another peak at around  $950\text{ cm}^{-1}$  corresponding to the SiOCC structure should be observed [22], which is not the case. Hence, the  $1485\text{ cm}^{-1}$  must be due to methylene groups already present in the epoxy additive and not due to epoxy ring opening by silanols. Even if the epoxy ring opening by silanols occur it must be minimal, as the kinetics of silanol opening the epoxy are expected to be much slower than water opening the epoxy, due to the larger concentration of water present.

However, the peak due to the C – OH group overlaps with the peak due to the Si-OH groups. Further we do not see any SiOCC peak at  $950\text{ cm}^{-1}$  in the spectra of L00 and L23, minimizing the possibility of epoxy ring opening via reaction with silanol groups. If the epoxy ring is opened by water, we should observe secondary alcohol ( $-\text{CH}_2\text{OH}$  – peak at  $1100\text{ cm}^{-1}$ ), tertiary alcohol ( $-\text{CHOH}$ -peak  $1150$ ), methyne ( $>\text{CH}$ -:  $2900\text{-}2880\text{ cm}^{-1}$  for C-H stretch and  $1350\text{-}1330\text{ cm}^{-1}$  for C-H bend). The first two group peaks for the alcohols overlap with the siloxane and metallo-siloxane peaks. There is a very weak peak for the methyne C-H stretch peak at  $2900$  (in L20 and L23 and obviously absent in L00). There is no C-H bend peak visible at  $1350\text{-}1330\text{ cm}^{-1}$ . So we have either overlapping or weak peaks as evidence for epoxy hydrolysis by water.

The epoxy ring may also be opened up by the secondary amine of the bis-amino silane, as shown in Figure 13. This can cause a peak at  $1090\text{-}1130\text{ cm}^{-1}$  due to the C-N stretch. However, only a very small peak is observed in this range for L00 and L23. Ambiguity remains in this regard due to overlapping group frequencies and the presence of weak peaks.

We observe a weak peak at  $1280\text{ cm}^{-1}$  in L20 and L23, an indication of unhydrolyzed epoxy. So, the IR study is useful in leading us to the conclusion that some epoxy is hydrolyzed by water and

some remains unhydrolyzed. Further investigation via liquid and solid  $\text{Si}^{29}$  and  $\text{C}^{13}$  NMR can confirm the nature of epoxy opening, crosslinking by amine and the presence of unhydrolyzed epoxy.

We do not observe any noticeable difference between the IR spectra of L20 and L23, except the sharpening of the Si-O-Si and Metal-O-Si peaks. The inhibitor may have had a catalytic effect on the condensation of the silanols, as was proposed by Daniels, et al., in the case  $\gamma$ -glycidoxypropyltrimethoxysilane, which showed increased dimerization in the presence of colloidal silica particles [24].

## **5. Conclusions**

An improved and optimized water-based silane passivation treatment for galvanized steels has been developed. It is easy to prepare, has higher hydrophobicity, low porosity, lower VOC, good self-healing property and also performs efficiently as a pretreatment, providing good paint adhesion. Most of the epoxy added is hydrolyzed while at least a part of it remains unhydrolyzed. However the exact nature of network formation needs further investigation.

## **6. Acknowledgement**

We acknowledge the Strategic Environmental Research and Development Program (SERDP) for their partial financial support of this project. We are also thankful to Dr. Danqing Zhu for her valuable discussions.

## References

1. W. J. van Ooij, T. Child, Chemtech 28 (1998) 26.
2. V. Subramanian, W. J. van Ooij, Corrosion 54 (1998) 204.
3. W. J. van Ooij, SIP seminar, Oslo, Norway, March, 2004.
4. V. Subramanian, Ph. D. Dissertation, University of Cincinnati, Department of Materials Science and Engineering, Cincinnati, OH (1999).
5. P. Puomi, H. M. Fagerholm, J. Adhes Sci Technol 15 (2001) 509.
6. P. Puomi, H. M. Fagerholm, J. Adhes Sci Technol 15 (2001) 869.
7. W. J. van Ooij, D.Q. Zhu, G. Prasad and S. Jayaseelan, Y. Fu, and N. Teredesai Surf Eng, 16 (2000) 386.
8. D.Q. Zhu, W. J. van Ooij, Electrochim Acta 49 (2004) 1113.
9. W. Yuan and W. J. van Ooij, J. Colloid Interface Sci. 185 (1997) 197.
10. J. Sinko, Prog Org Coat 42 (2001) 267.
11. V. Palanivel, W. J. van Ooij Prog Org Coat 53 (2005) 153.
12. H. Guan, R.G. Buchheit, Corrosion 60 (2004) 284.
13. R. G. Buchheit, H. Guan and F. Wong, Prog Org Coat 47 (2003) 174.
14. L. Yang, N. B. Simhadri and W.J.van Ooij, presented at the conference on Silane and other coupling agents, Toronto, Canada, 2005
15. W. Machu, S. Hlawiczka, Metalloberflache 27 (1974) 409.
16. D. Zhu, W.J. van Ooij, J Adhes Sci Technol 16 (2002) 1235.
17. W. S. Tait, An Introduction to Electrochemical Corrosion Testing for Practicing Engineers and Scientists, Pair O Docs Publications, Racine, WI (1994).

18. D. A. Jones, Principles and Prevention of Corrosion, 2<sup>nd</sup> edn., Prentice-Hall, New York (1996) 556.
19. J. N. Murray, Prog Org Coat, 30 (1997) 225.
20. M. Kendig and J. Scully, Corrosion 46 (1990) 22.
21. P.L. Bonora, F. Deflorian, and L. Fedrizzi, Electrochim Acta 41 (1996) 1073.
22. G. Xue, Die Angewandte Makromolekulare Chemie, 151 (1987) 85.
23. J. Coates, Encyclopedia of Analytical Chemistry (Ed) R. A. Meyers, John Wiley & Sons Ltd, New York (2000) 10815.
24. M. W. Daniels, J. Sefcik, L. F. Francis and A. V. McCormick, J. Colloid Interface Sci. 15 (2001) 509.

## Figure Captions

- Figure 1: Chemical structures of bis-amino silane and VTAS
- Figure 2: The open circuit corrosion current of the coated panels and uncoated control on the first and 14<sup>th</sup> day of immersion
- Figure 3: The open circuit corrosion potentials of all the coated panels and uncoated control on the first and 14<sup>th</sup> day of immersion.
- Figure 4: DCP curves for uncoated control, L00 and L23 on the first and 14<sup>th</sup> days of immersion
- Figure 5: EIS low-frequency impedance moduli of coated panels on the first and 25<sup>th</sup> days of the test
- Figure 6: Comparison of the Bode plots and phase angle of L00 and L23. Also shown is the appearance of the panels under the O-ring of the EIS cylinder, at the end of the testing period.
- Figure 7: Equivalent Circuit Model for EIS data fitting for immersed L00 and L23 panels.  $R_{so}$  is the uncompensated solution resistance,  $C_c$  is the silane coating capacitance,  $R_{po}$  is the pore resistance of the silane film,  $R_p$  is the polarization resistance and  $C_f$  is the capacitance of the exposed metal.
- Figure 8: Images of the panels immersed in 0.6 M NaCl solution for 30 days. Images of L11, L23, L32 and L33 are shown as they had close low-frequency impedance moduli. The performance of the panels not shown was below par.
- Figure 9(a): Schematic of the set-up of the scratch cell test.
- Figure 9(b): Scratch cell test results: Images of the panels placed on the upper side (uncoated controls) in the set-up with corresponding lower side panels

- Figure 10(a): Machu test results for HDG panels coated with L00 and L23
- Figure 10 (b): Machu test results for the uncoated control, L00 and L23 panels, coated with a commercial alkyd primer
- Figure 11: ASTM B117 results for the L00, L03 and L23 panels
- Figure 12: IR spectra for the L00, L20 and L23 with peak assignments indicated. Refer to Table 2 for the values of peak assignments
- Figure 13: Epoxy ring opening by the secondary amine of the bis-amino silane and the consequent inter-cross-linking between the epoxy and bis-amino siloxane networks

**Table 1**

Table of all formulations made compared in this study

Formulation	Concentration of Resin (% wt.)	Inhibitor (ppm)
L <sub>00</sub>	0	0
L <sub>11</sub>	1	100
L <sub>12</sub>	1	150
L <sub>13</sub>	1	200
L <sub>21</sub>	2	100
L <sub>22</sub>	2	150
L <sub>23</sub>	2	200
L <sub>31</sub>	3	100
L <sub>32</sub>	3	150
L <sub>33</sub>	3	200
L <sub>20</sub>	2	0

**Table 2**

Coating and corrosion parameters of L00 and L23 obtained from EIS modelling

Parameter	L00	L23
$R_{po}$	31.92 $\Omega$	420.4 $\Omega$
$R_p$	299.4 $\Omega$	9160 $\Omega$
$C_c$	4.14 $\mu\text{F}$	1.422 $\mu\text{F}$
$C_f$	734.9 $\mu\text{F}$	10.55 $\mu\text{F}$

**Table 3**

Table 3: Peak assignments for the IR spectra of L00, L20 and L23 shown in Figure 11

Group Frequency (wavenumber $\text{cm}^{-1}$ )	Assignment
3570 – 3200 (broad)	Due to hydrogen bonded –OH grps, Si-OH groups manifest at a higher frequency than C-OH groups
3390, 1250-1150	$\begin{array}{c} \text{Si-N-Si} \\   \\ \text{H} \end{array}$ NH single band at 3390
2970-2950/ 2880 -2860	-CH <sub>3</sub> Methyl C-H asym/sym stretch
2900-2880	Methylene C-H stretch
2840 (sharp), 1190	Si-O-CH <sub>3</sub>
1650-1550	Secondary amine, NH bend
1600, 1410	Si-CH=CH <sub>2</sub>
1485-1445	methylene C-H bend
1190-1130	Secondary amine CN stretch
1130-1000	Si-O-Si
1000 – 900	Si-O-Metal

Figure 1

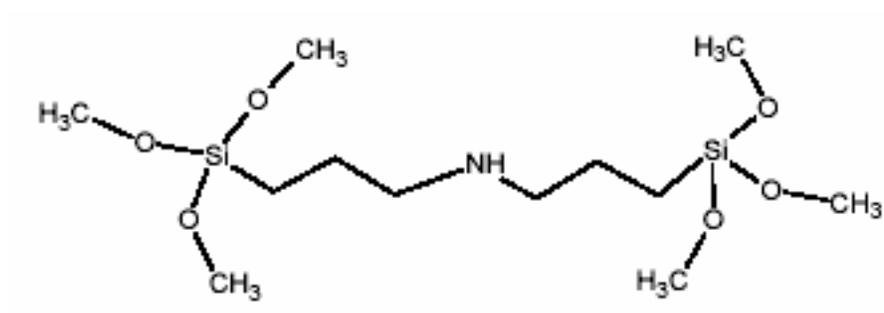
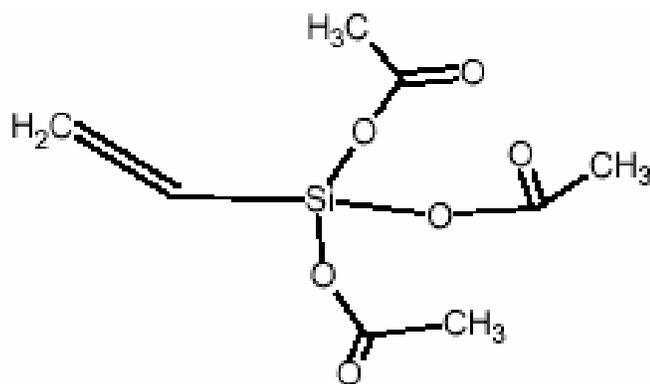
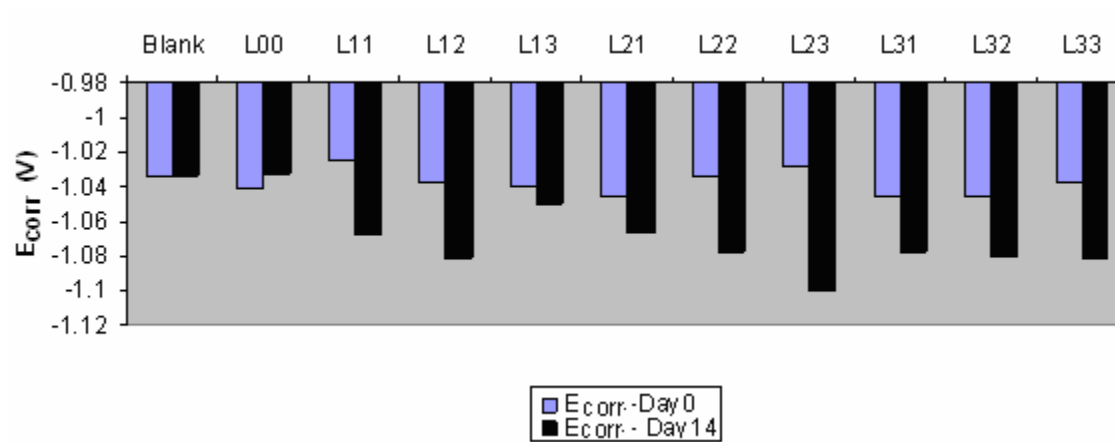
**Bis-[trimethoxysilylpropyl]amine****Vinyltriacetoxysilane**

Figure 2



**Figure 3**

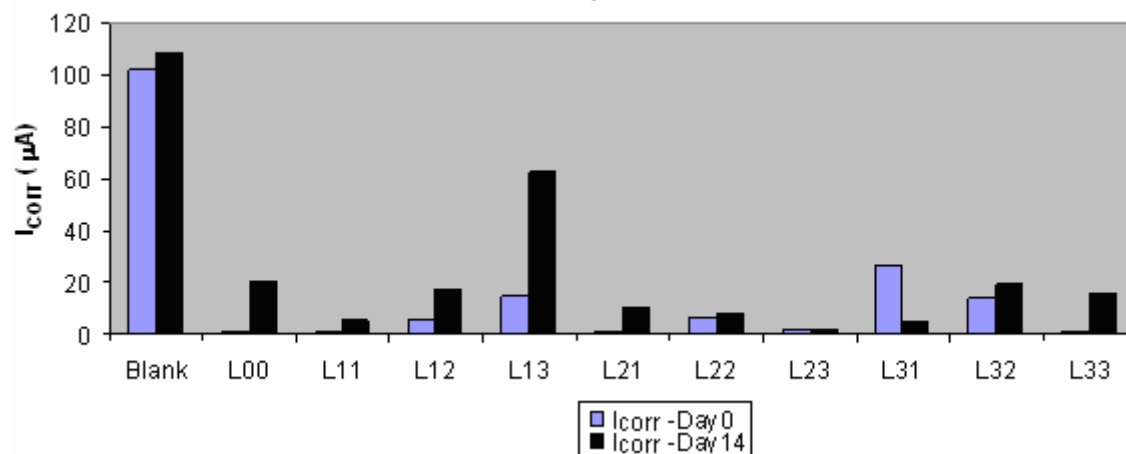
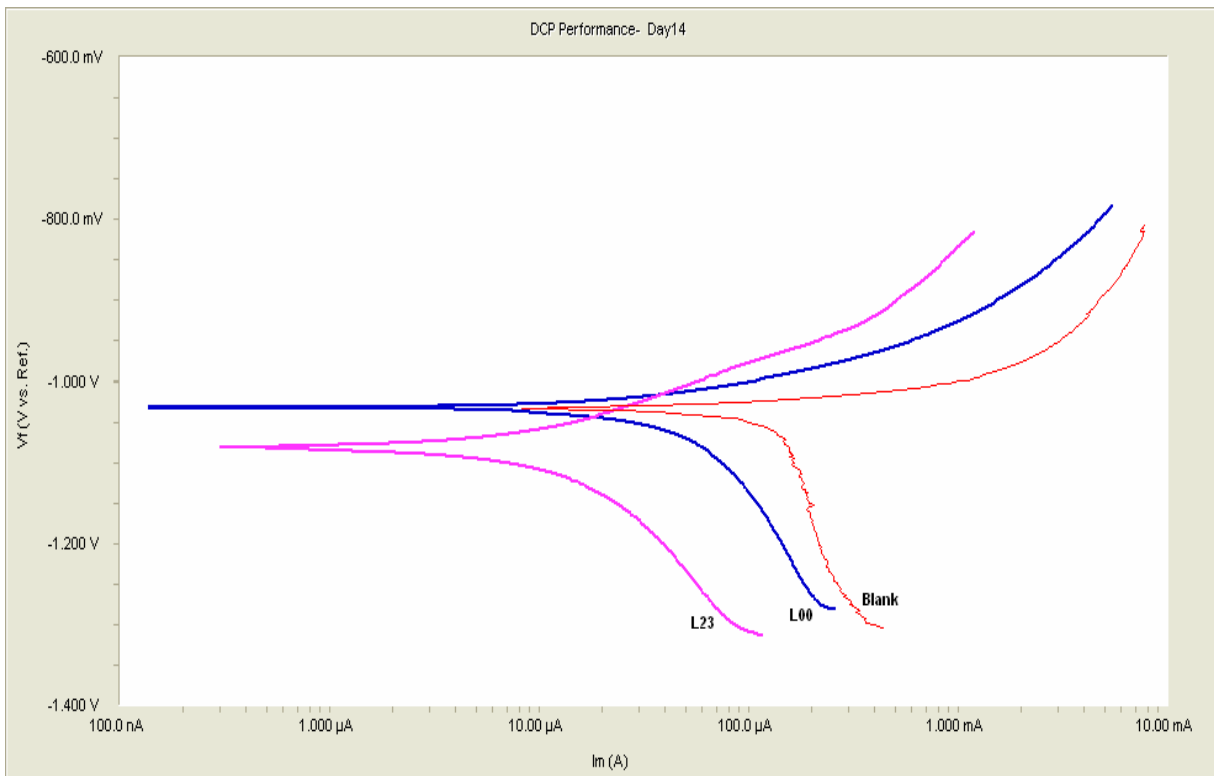
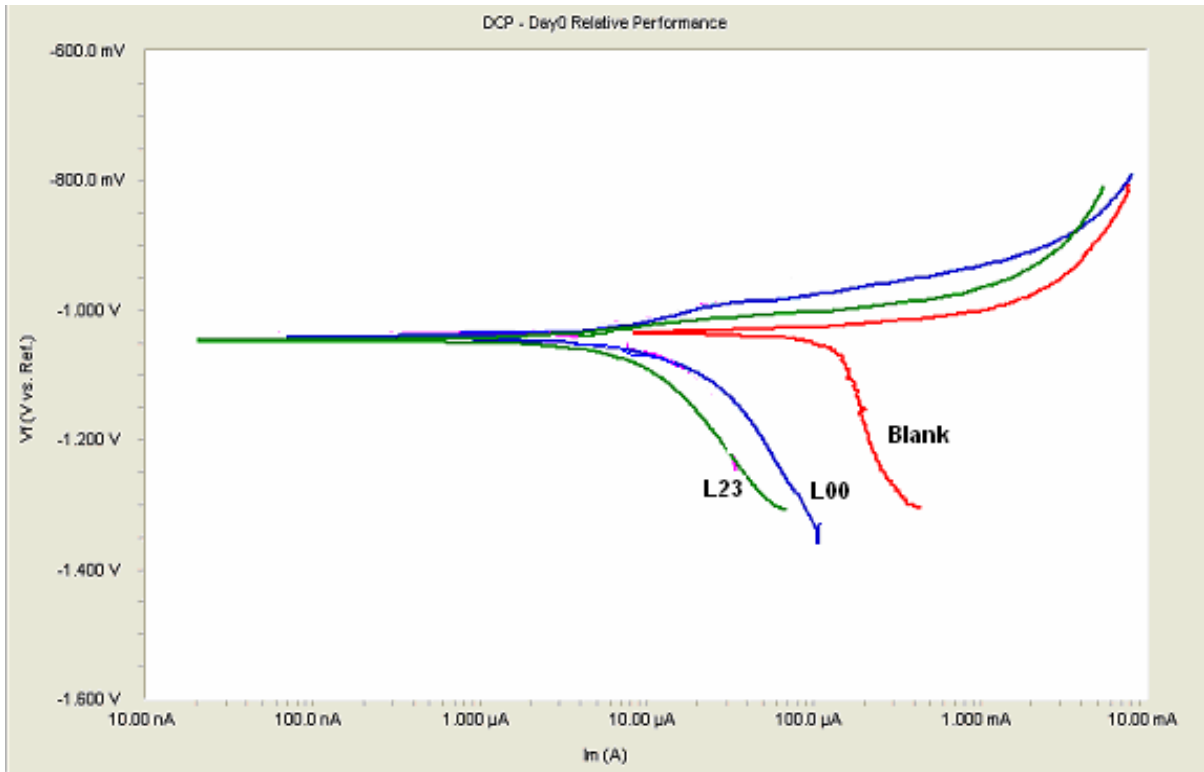


Figure 4



**Figure 5**

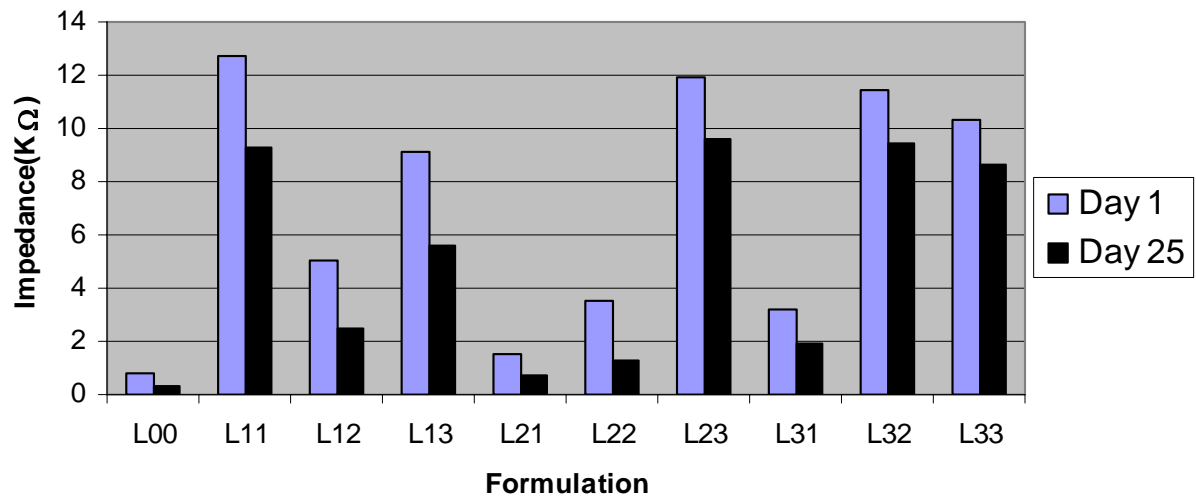
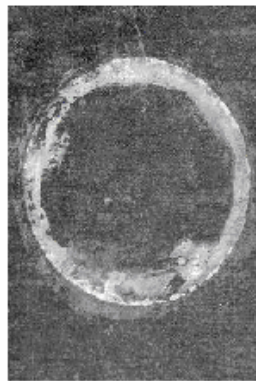
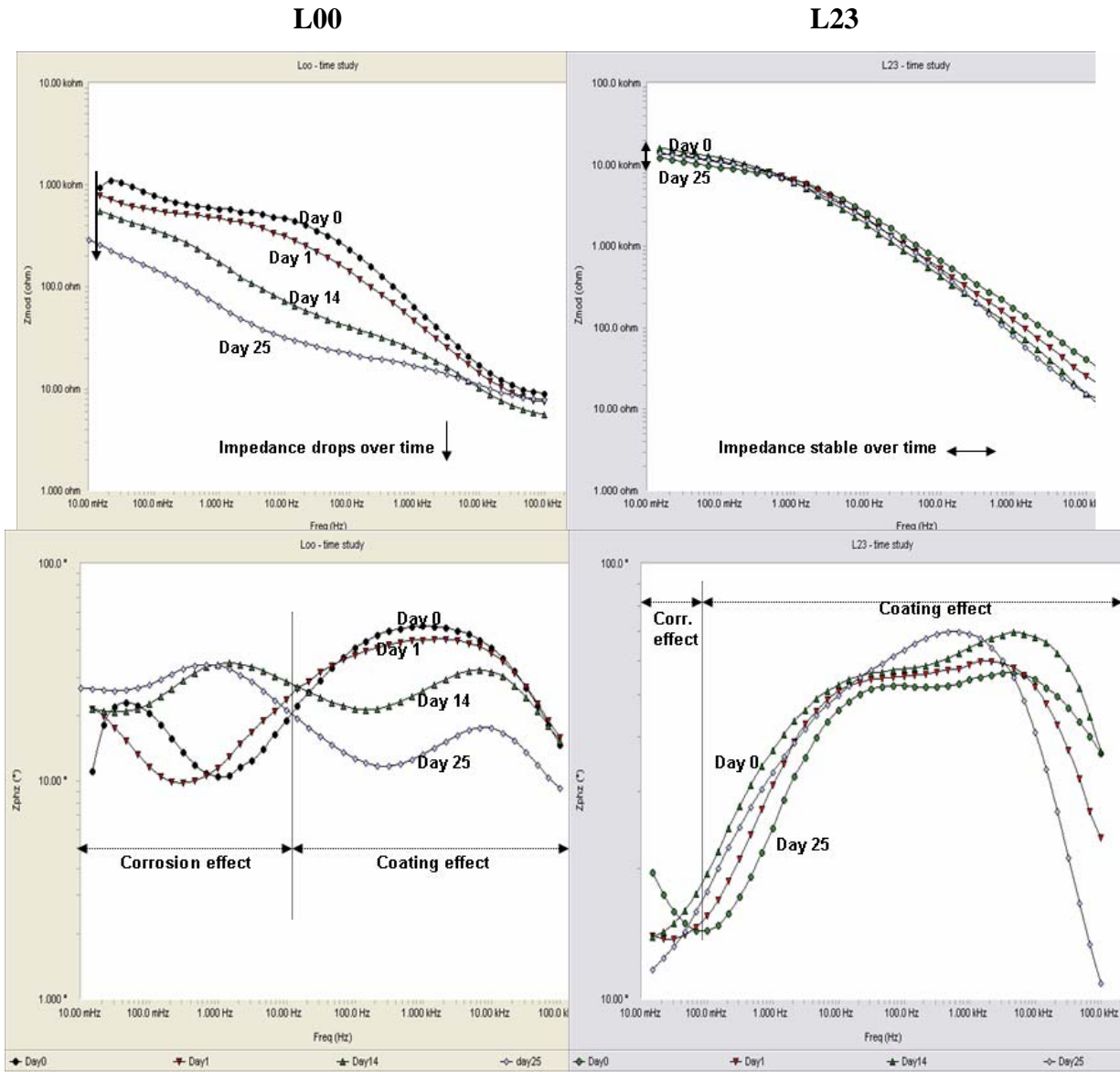
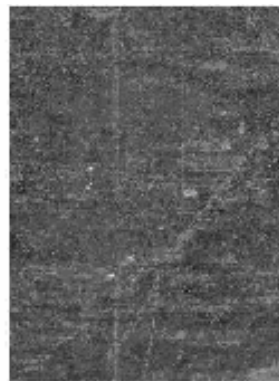


Figure 6



Panel under the O ring - after 25 days



Panel under O ring - After 30 days

Figure 7

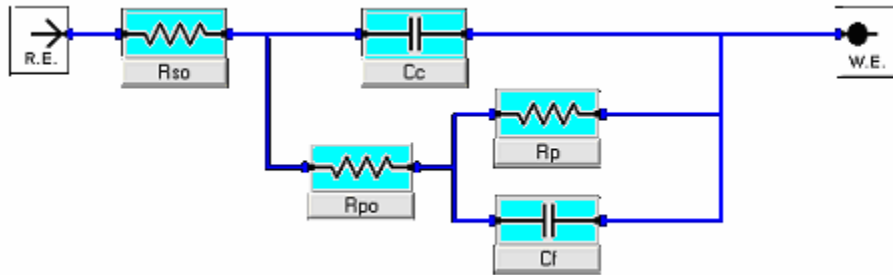


**Figure 8**



**Blank**



**L<sub>00</sub>**



**L<sub>23</sub>**



**L<sub>11</sub>**



**L<sub>33</sub>**



**L<sub>32</sub>**

**Figure 9 a**

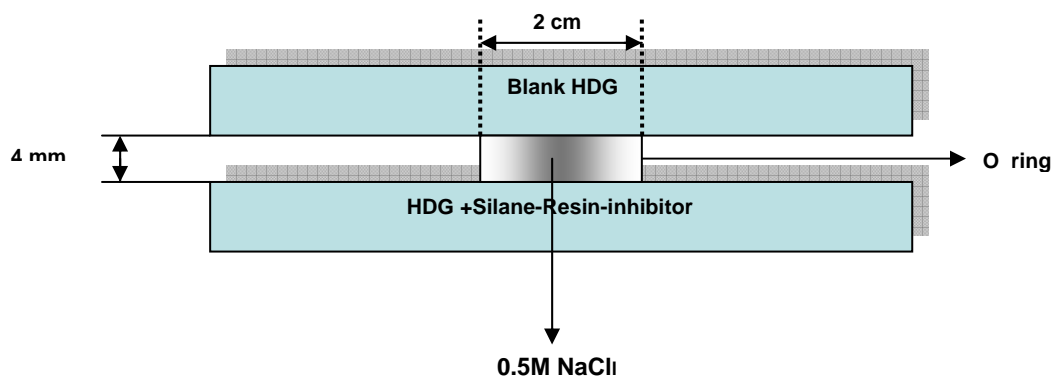


**Figure 9 b**



**Blank-on-Blank**



**Blank on L<sub>00</sub>**



**Blank on L<sub>23</sub>**



**HDG blank**



**L<sub>00</sub>**



**L<sub>23</sub>**

Figure 10 a



L00



L23

**Figure 10 b**

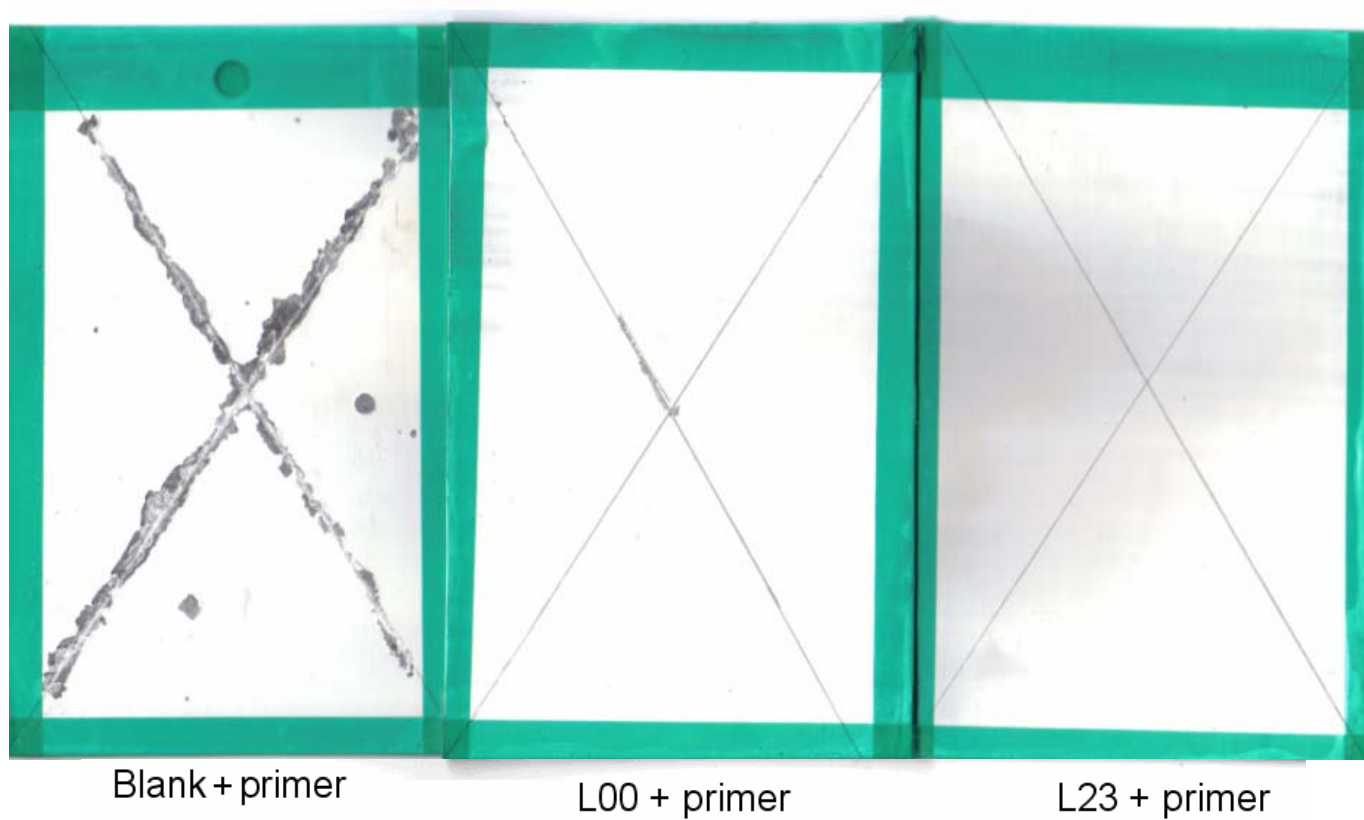


**Figure 11**



**L00  
8 hours**

**L03  
25 hours**

**L23  
100 hours**

Figure 12

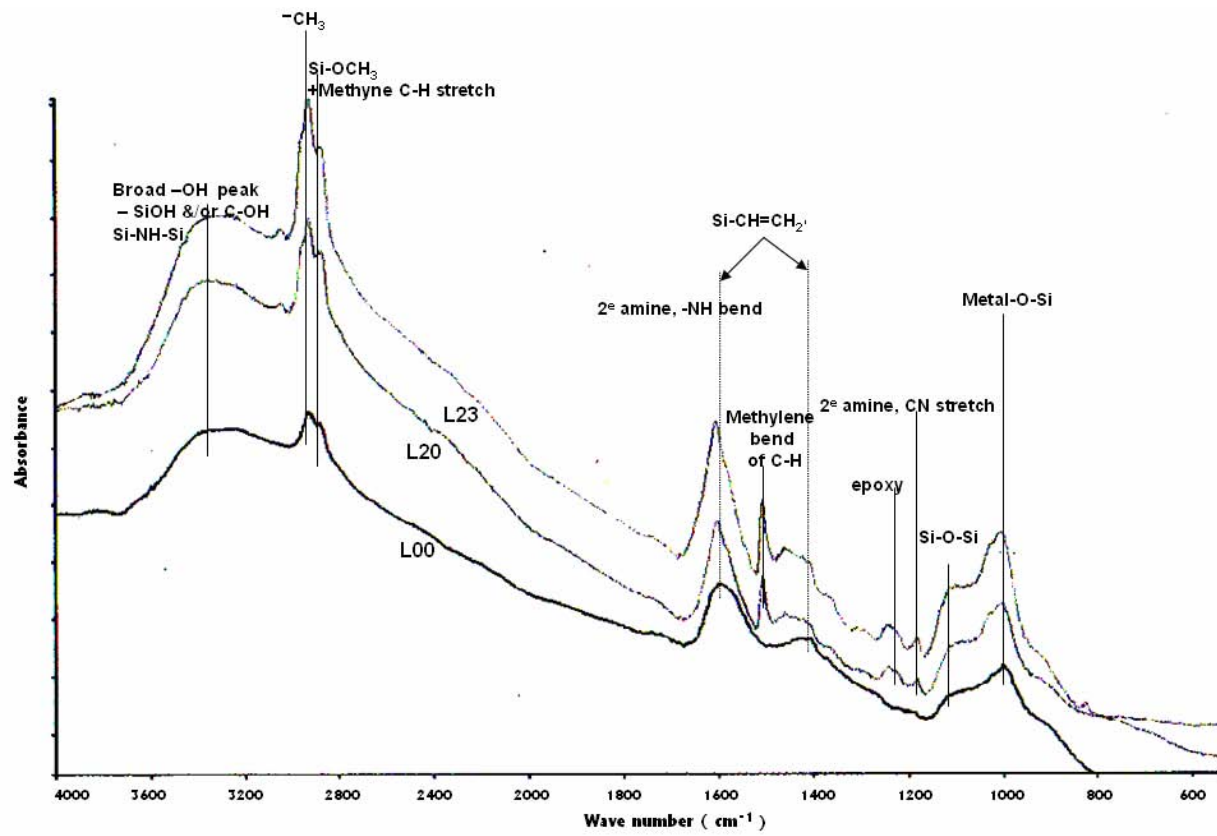
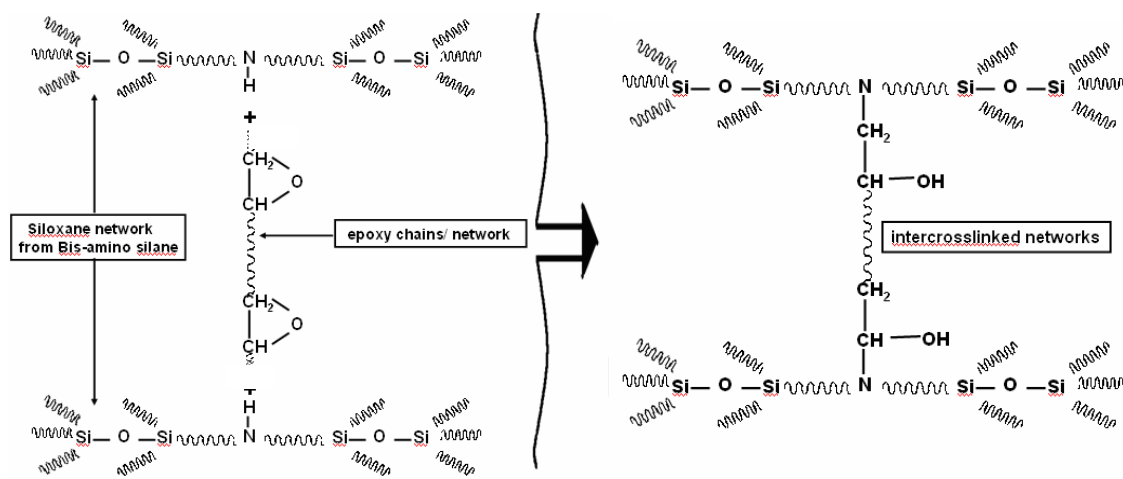


Figure 13



# UNIVERSITY OF CINCINNATI

**Date:** 06/23/2006

**I,** AKSHAY ASHIRGADE,

**hereby submit this work as part of the requirements for the degree of:**

MASTER OF SCIENCE

**in:**

MATERIALS SCIENCE AND ENGINEERING

**It is entitled:**

ENVIRONMENTALLY-COMPLIANT NOVOLAC SUPERPRIMERS FOR

CORROSION PROTECTION OF ALUMINUM ALLOYS

**This work and its defense approved by:**

**Chair:** Dr. W. J. van Ooij (Chair)

Dr. Relva C. Buchanan

Dr. Stephen J. Clarson

# **Environmentally-Compliant Novolac Superprimers for Corrosion Protection of Aluminum Alloys**

A thesis submitted to the  
Division of Research and Advanced Studies  
at the University of Cincinnati  
in partial fulfillment of  
the requirements for the degree of

**MASTER OF SCIENCE**

in the Department of Chemical and Materials Engineering  
of the College of Engineering

June, 2006

By

**Akshay Ashirgade**

B.E., Visvesvaraya National Institute of Technology, Nagpur, India, 2003

Committee Chair: Dr. W. J. van Ooij

## **ABSTRACT**

The Environmental Protection Agency (EPA) in the US has imposed legislations on the use of hexavalent chromium and solvents contributing to emission of volatile organic compounds in primer coatings. This has led researchers to pursue development of alternative environmentally-friendly coatings which would eliminate chromate conversion coatings (CCC). This thesis discusses the work done towards the development of a novel, chromate-free, low-VOC, water-based, organic coating system for corrosion protection of AA 2024-T3 aerospace alloy. These special coatings which can be applied directly to the metal are termed as ‘superprimers’ and consist of novolac epoxy binder, silanes, polyurethane and non-chromate inhibitors. Coating evaluation tests were employed to compare the performance of the superprimer coatings with controls. SEM, FTIR and NMR were carried out to understand the chemistry of the coatings. The requirement for a conversion coating was obviated and the coating system developed was on par with the chromate-based control coating in terms of performance.



## ACKNOWLEDGMENTS

I would like to express my sincere gratitude to all those who have been involved in the successful completion of this work. I am grateful to the University of Cincinnati and the Department of Chemical and Materials Engineering for presenting me with the opportunity and the facilities for research work in this exciting field.

I am exceptionally grateful to my academic advisor, Dr. William J. van Ooij, for introducing me to this new and fascinating field of scientific research. I am also grateful to him for his precious advice and guidance throughout the coursework. I am thankful to my thesis committee members, Dr. Relva C. Buchanan and Dr. Stephen J. Clarson for taking the time to review my thesis. I am also thankful to Dr. Dale W. Schaefer for the helpful interactions I have had with him during the course of this project.

I gratefully acknowledge the Strategic Environmental Research and Development Program (SERDP) for providing financial support for this study and Donna Ballard of the Air Force Research laboratories for providing progress reviews and suggestions during the project. I am also thankful to Dr. Guy Davis of DACCO SCI, INC., Columbia, MD, for the help with performance testing of coatings and Dr. Tammy Metroke of the Department of Chemistry, Oklahoma State University, for her valuable help with NMR studies.

I am particularly grateful to Dr, Paula Puomi for the help with IR studies and reviewing this thesis. I am also thankful to Sumeet Bhargava and Sachit Chopra for the help in carrying out the characterization studies. I express my appreciation to all of my research

group members, past and present, for their support and encouragement. My special thanks to Chetan, Anuj, Karthik and Trilok for their helpful suggestions during this research work.

My friends, Abhay, Amit, Ankur, Ashwini, Deepti, Girish, Parag, Prasan, Ramakrishna and many others for the wonderful times I had with them and for making my UC experience a memorable one.

Finally, I am obliged to my parents and my brother for inculcating strong beliefs in me and for their unswerving love and support throughout my life. I dedicate this thesis to my family.

# TABLE OF CONTENTS

<b>LIST OF TABLES</b> .....	1
<b>LIST OF FIGURES</b> .....	2
<b>1. INTRODUCTION</b> .....	8
1.1 Aerospace aluminum alloys .....	8
1.2 Corrosion of metals .....	9
1.3 AA 2024-T3 aluminum alloy and its susceptibility to corrosion .....	11
1.4 Significance of corrosion control .....	12
1.5 Corrosion protection by organic coatings .....	13
1.6 Silanes .....	17
1.7 Resins for organic coatings .....	19
1.8 Superprimer: A silane-resin based primer system .....	21
1.9 Objective of the thesis .....	22
1.10 References .....	24
<b>2. EXPERIMENTAL</b> .....	27
2.1 Chemicals and Materials .....	27
2.1.1 Metal Substrate .....	27
2.1.2 Water-based Resin Dispersions .....	27
2.1.3 Silanes .....	29
2.1.4 Crosslinkers and Curing Agents .....	29
2.1.5 Corrosion Inhibitors .....	30
2.1.6 Other Pigments and Fillers .....	31
2.1.7 Surfactants and Dispersants .....	31
2.1.8 Solvents and cleaners .....	31
2.1.9 Topcoats and Control Primers .....	32
2.2 Metal Surface Preparation .....	32
2.3 Formulation of Superprimer .....	33
2.3.1 High-shear Blender .....	33
2.4 Coating Methods .....	33
2.4.1. Draw-down Bar .....	34
2.4.2 Spray Painting .....	34

<i>2.5 Performance evaluation tests and characterization techniques</i> .....	34
2.5.1 Saltwater Immersion Test .....	35
2.5.2 Electrochemical Impedance Spectroscopy .....	35
2.5.3 ASTM B117 Salt Spray Test .....	37
2.5.4 The Ford AGPE Test .....	38
2.5.5 Outdoor Exposure Test .....	38
2.5.6 Tape Adhesion Test .....	39
2.5.7 MEK Double Rub Test .....	39
2.5.8 Chemical Resistance Test .....	40
2.5.9 Pencil Hardness Test .....	40
2.5.10 Bend Test .....	40
2.5.11 Contact Angle Measurements .....	41
2.5.12 Infrared Spectroscopy .....	42
2.5.13 Nuclear Magnetic Resonance Spectroscopy .....	43
2.5.14 Scanning Electron Microscopy and Energy Dispersive X-ray Spectroscopy .....	46
2.5.15 Thermogravimetric analysis .....	48
<i>2.6 References</i> .....	49

### **3. SUPERPRIMER FORMULATIONS AND THEIR PERFORMANCE**

<b>EVALUATION</b> .....	51
<i>3.1 Novolac epoxy based superprimer</i> .....	52
3.1.1 Novolac epoxy resin and curing agent .....	52
3.1.2 Addition of polyurethane resin .....	53
3.1.3 Appropriate choice of silane .....	55
3.1.4 Corrosion inhibitors .....	58
3.1.5 Other filler pigments .....	59
3.1.6 Minor additives .....	60
3.1.7 Co-solvents .....	61
3.1.8 Formulation for spray coating .....	61
<i>3.2 Control coatings</i> .....	62
<i>3.3 Performance Test results and evaluation</i> .....	62
3.3.1 Salt water immersion test .....	62
3.3.2 Electrochemical Impedance Spectroscopy .....	63
3.3.3 Tape adhesion test .....	66

3.3.4 Chemical Resistance test .....	66
3.3.5 ASTM B117 and Ford tests .....	67
3.3.6 Bend test .....	70
3.4 Summary .....	71
3.5 References .....	72
<b>4. CHARACTERIZATION STUDY OF SUPERPRIMERS .....</b>	<b>73</b>
4.1 NMR Spectroscopy .....	73
4.1.1 Sample Preparation .....	73
4.1.2 Liquid state <sup>13</sup> C NMR .....	74
4.1.3 Solid state <sup>13</sup> C NMR .....	77
4.2 Infrared Spectroscopy .....	79
4.2.1 ND-20 base formulation .....	81
4.2.2 N-1 superprimer .....	81
4.2.3 NP-1 superprimer .....	83
4.2.4 Polyurethane and silane .....	83
4.3 SEM/EDS analysis .....	84
4.3.1 Effectiveness of inhibitor .....	84
4.3.2 Cross-sectional analysis .....	86
4.4 Thermogravimetric analysis .....	86
4.5 Summary .....	88
4.6 References .....	89
<b>5. CONCLUSIONS AND SCOPE FOR FUTURE RESEARCH .....</b>	<b>91</b>
<b>TABLES .....</b>	<b>95</b>
<b>FIGURES .....</b>	<b>113</b>

## LIST OF TABLES

- 2.1 Physical properties of resins and curing agent used in the superprimer
- 2.2 Experimental cycle in the Ford AGPE test
- 3.1 Various formulations of novolac epoxy resin and curing agent
- 3.2 Properties of novolac epoxy resin and curing agent formulations
- 3.3 Formulations for various novolac-based superprimers with silanes and polyurethane
- 3.4 Properties for various novolac-based superprimer formulations
- 3.5 Formulations of superprimers with different corrosion inhibitors
- 3.6 MEK double-rub values and water contact angles for superprimers with corrosion inhibitors
- 3.7 Formulations for superprimers with filler pigments
- 3.8 Formulations for superprimer for spray coating experiment
- 3.9 Formulations for control coatings and topcoat
- 3.10 Properties of the NP-1 formulation
- 4.1 RAIR peak assignments for pure bis-sulfur silane film
- 4.2 RAIR peak assignments for the film of epoxy-amine adduct curing agent EPKURE 6870
- 4.3 RAIR peak assignments for the film of polyurethane resin dispersion NeoRez R-972
- 4.4 RAIR peak assignments for ND-20 time-based spectra
- 4.5 RAIR peak assignments for N-1 time-based spectra

- 4.6** RAIR peak assignments of time-based spectra for bis-sulfur silane and polyurethane resin films

## **LIST OF FIGURES**

- 1.1** Pourbaix diagrams for pure Al
- 1.2** General chemical structure of a silane compound
- 1.3** Sketches showing hydrolysis and condensation of silanes
- 1.4** Bonding mechanisms during a silane pretreatment process
- 1.5** Structure of a (a) mono-silane and (b) bis-silane
- 1.6** Structure of DGEBA resin
- 1.7** Epoxide ring opening (cross-linking) reactions
- 1.8** Chemical structure of a generic novolac resin
- 1.9** Chemical structure of epoxy amine curing agent
- 1.10** Chemical structure of some silanes used in a superprimer
- 1.11** Generic structure of polyurethane
- 1.12** Comparison of conventional coating system with superprimer technology
- 2.1** Schematic sketch of the High Shear Mixer
- 2.2** SoftSpray HVLP conversion gun for spray painting
- 2.3 (a)** Bode plots for a failed coating
- 2.3 (b)** A Nyquist plot for a failed coating
- 2.3 (c)** An equivalent circuit for a failed coating
- 2.4** EIS cell arrangement for impedance measurements
- 2.5** The salt spray chamber at DACCO SCI, INC.

- 2.6 The experimental set-up of the Ford AGPE test
- 2.7 Interfacial forces acting on a liquid droplet on a solid surface
- 2.8 The contact angle goniometer, VCA Optima 2000
- 2.9 (a) Stretching and bending vibrational modes for H<sub>2</sub>O
- 2.9 (b) Stretching and bending vibrational modes for CO<sub>2</sub>
- 2.10 Optical arrangement for a reflection-absorption IR sampling accessory
- 2.11 Possible spin states of nuclei with ½ and 1 integer spins in NMR
- 2.12 Typical ranges of chemical shifts for protons in different groups in NMR
- 2.13 Principle of working of SEM
- 2.14 Interaction volume of the electron beam and the specimen in SEM
- 2.15 Denton Vacuum Bench top cold sputter/etch unit used for preparing samples
- 2.16 Experimental set-up for TGA
- 3.1 ND-20 coating formulation without silane and inhibitors after 30 days of salt water immersion
- 3.2 N-1 coating formulation without corrosion inhibitors after 30 days of salt water immersion
- 3.3 NP-1 coating formulation (a) without corrosion inhibitors and (b) with zinc phosphate after 60 days of salt water immersion
- 3.4 Comparison of EIS impedance plots for ND-20 and N-1 coating formulations after 14 days of EIS testing
- 3.5 Bode impedance plot for NP-1 formulation
- 3.6 Bode impedance plot for N-2 formulation

- 3.7** Samples of (a) ND-20 and (b) NP-1 coating formulations after exposure in EIS test
- 3.8** Low-frequency impedance plots for control coatings exposed to ASTM B117 test
- 3.9** Low-frequency impedance plots for N-1 and NP-1 superprimers coatings exposed in ASTM B117 test
- 3.10** Low-frequency impedance plots for superprimer coatings with different inhibitors, exposed in ASTM B117 test
- 3.11** Adhesion test samples of some novolac-based superprimer formulations
- 3.12** Samples of ND-20 and N-1 superprimers exposed to ASTM B117 test for 1000 hrs and 1500 hrs respectively
- 3.13** Samples of N-1 superprimer with zinc phosphate and CZM corrosion inhibitors, exposed to ASTM B117 test for 2000 hrs
- 3.14** Samples of NP-1 superprimer with different corrosion inhibitors, exposed to ASTM B117 test for 2500 hrs
- 3.15** Samples of NP-1 superprimer different additives, exposed to ASTM B117 test for 1000 hrs
- 3.16** Samples of topcoated NP-1 and control formulations after exposure to ASTM B117 test
- 3.17** Samples of topcoated NP-1 after exposure to Ford AGPE test
- 3.18** Samples of bend tested coatings after exposure to salt water immersion
- 4.1** Chemical structure of DGEBA resin with calculated peak positions in <sup>13</sup>C NMR

- 4.2** Chemical structure and spectrum of EPIREZ 5003 novolac resin with calculated peak positions in liquid  $^{13}\text{C}$  NMR
- 4.3** Chemical structure and spectrum of EPIKURE 6870 curing agent with calculated peak positions in liquid  $^{13}\text{C}$  NMR
- 4.4** Chemical structure and spectrum of Bis-sulfur silane with calculated peak positions in liquid  $^{13}\text{C}$  NMR
- 4.5** Chemical structure and spectrum of NeoRez R-972 with calculated peak positions in liquid  $^{13}\text{C}$  NMR
- 4.6** Chemical structure and spectrum of CX-100 crosslinker with calculated peak positions in liquid  $^{13}\text{C}$  NMR
- 4.7** Spectrum of L-1 formulation and potential reaction product with calculated peak positions in liquid  $^{13}\text{C}$  NMR
- 4.8** Spectrum of L-2 formulation in liquid  $^{13}\text{C}$  NMR
- 4.9** Spectrum of L-3 formulation and potential reaction product with calculated peak positions in liquid  $^{13}\text{C}$  NMR
- 4.10** Spectrum of S-1 sample in solid state  $^{13}\text{C}$  NMR
- 4.11** Spectrum of S-2 sample in solid state  $^{13}\text{C}$  NMR
- 4.12** RAIR spectrum of a pure bis-sulfur silane film with annotated peaks after room temperature curing
- 4.13** RAIR spectrum of EPIKURE 6870 with annotated peaks after room temperature curing

- 4.14 RAIR spectrum of NeoRez-R-972 with annotated peaks after room temperature curing
- 4.15 RAIR spectra of ND-20 at specified time intervals of room temperature curing
- 4.16 RAIR spectra of N-1 at specified time intervals of room temperature curing
- 4.17 Comparison of RAIR spectra of N-1 after (a) room-temperature and (b) high-temperature curing
- 4.18 RAIR spectra of NP-1 at specified time intervals of room temperature curing
- 4.19 RAIR spectra of bis-sulfur silane and polyurethane resin films at specified time intervals of room temperature curing
- 4.20 Backscattered SEM image of Coating A with the elemental distribution across the scribe
- 4.21 EDS scan at the indicated spot on Coating A with the elemental distribution
- 4.22 EDS scan at the indicated spot on Coating A with the elemental distribution
- 4.23 EDS scan at the indicated spot on Coating A with the elemental distribution
- 4.24 EDS scan at the indicated spot on Coating A along with the elemental distribution

- 4.25 Backscattered SEM image of Coating B with the elemental distribution across the scribe
- 4.26 EDS scan at the indicated spot on Coating B with the elemental distribution
- 4.27 EDS scan at the indicated spot on Coating B with the elemental distribution
- 4.28 EDS scan at the indicated spot on Coating B with the elemental distribution
- 4.29 EDS scan at the indicated spot on Coating B with the elemental distribution
- 4.30 Backscattered SEM image of the cross-section of coating A on AA 2024-T3
- 4.31 Elemental distributions along the cross-section of coating A on AA 2024-T3
- 4.32 EDS scan at the indicated spot on Coating B cross-section with the elemental distribution
- 4.33 EDS scan at the indicated spot on Coating B cross-section with the elemental distribution
- 4.34 EDS scan at the indicated spot on Coating B cross-section with the elemental distribution
- 4.35 EDS scan at the indicated spot on Coating B cross-section with the elemental distribution
- 4.36 TGA curves for various superprimer coatings

# 1. INTRODUCTION

The work discussed in this thesis focuses on the development of a novel, chromate-free, environmentally-benign primer system for corrosion protection of aerospace aluminum alloys; AA 2024-T3 alloy in particular. The introductory chapter discusses the aerospace aluminum alloys, their susceptibility to corrosion and the existing coating technologies such as organic coatings, pretreatments and primer systems that offer corrosion protection for aluminum alloys. The chapter also overviews the role of silanes in corrosion protection of metals followed by the concept of superprimer and, ultimately, the purpose of the thesis.

## 1.1 Aerospace aluminum alloys

Aluminum is a relatively light, silver white metal and, to a certain extent, malleable. Aluminum is one of the most versatile metals and can be cast in any known form. It can be rolled, stamped, drawn, spun, roll-formed, hammered, forged and extruded into a variety of shapes. It can also be riveted, welded, brazed, or resin-bonded. Because of its machinability, aluminum can have a wide variety of surface finishes. For most applications, aluminum needs no protective coating. However, it is often anodized to enhance color and strength. It has good electrical and thermal conductivities and is highly reflective to heat and light. Aluminum alloys tend to lose some of their strength at extremely high temperatures (200-250°C). However, at subzero temperatures, their strength improves without impairing the ductility. This property makes aluminum an extremely useful low-temperature alloy. Aluminum alloys have a relatively strong resistance to corrosion as a result of an oxide skin formed due to reactions with the

atmosphere. This oxide layer protects aluminum from most chemicals, weathering conditions, and even many acids, but alkaline substances are known to penetrate the protective skin and corrode the metal. Figure 1.1 shows the Pourbaix diagram for pure aluminum [1, 2].

The aerospace industry is extremely demanding for the materials it employs. Demands include improved toughness, low weight, increased resistance to fatigue and corrosion. The limits of material properties are being constantly extended as manufacturers endeavor to give the next generation of aircrafts superior performance and efficiency. Aluminum is one of the key materials confronting these challenges. Aluminum and aluminum alloys have been used as aerospace materials especially in commercial airplanes due to their high strength (or stiffness) to weight ratio, all-around mechanical properties and better corrosion resistance. Aluminum alloy plate is used in a large number of aerospace applications, varying in complexity and performance requirements from simple components through to primary load bearing structures in the passenger as well as military aircrafts [1, 2]. Aluminum grades 2024, 2219, 6061, 7050 and 7075 are some of the commonly used alloys in aircrafts.

## **1.2 Corrosion of metals**

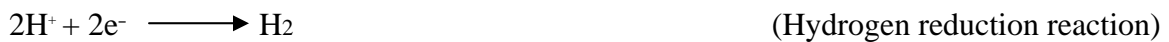
Corrosion is defined as the continuous destruction or deterioration of a material by chemical or electrochemical attack [3]. Uhlig defines corrosion as a destructive attack of a metal by a chemical or electrochemical reaction with its environment. Physical causes (erosion, galling, wear) are not considered corrosion in this definition. According to

Fontana, corrosion is the deterioration of a substance (usually a metal) or its properties as a result of a reaction with its environment [4]. The atmospheric corrosion of iron and its alloys (e.g. steel) is termed rusting. Corrosion of zinc or aluminum (alloys) is referred to as white rusting.

Corrosion occurs because most metals are thermodynamically unstable [3]. The corrosion reaction is termed electrochemical as the overall corrosion reaction can be split in to two partial reactions. The anodic or oxidation reaction involves the metal going into dissolution by releasing electrons.



where M is the metal,  $M^{n+}$  is the oxidized metal ion and n is the number of electrons produced during the anodic process. The consumption of these electrons from the anodic reaction signifies a reduction or cathodic reaction. There are several cathodic reactions that occur in metallic corrosion, some common cathodic reactions are:



The hydrogen reduction reaction occurs when a metal is exposed to an acid medium, whereas the oxygen reduction reaction is most commonly seen in aqueous solutions in contact with air. The anodic and the cathodic reactions occur simultaneously on the metal surface [4].

### **1.3 AA 2024-T3 aluminum alloy and its susceptibility to corrosion**

AA 2024-T3 is an Al-Cu alloy with the composition of 93.50 wt % Al, 4.4 wt % Al, 0.6 wt % Mn and 1.5 wt % Mg. The term T3 signifies the heat treatment that the alloy undergoes and is applicable to alloys which are cold worked to improve strength after solution heat treatment, or in which the effect of cold work in flattening or straightening is significant in mechanical property limits. AA 2024-T3 alloy is one of the most extensively used materials in the aerospace industry owing to its excellent mechanical properties. Strength is a crucial requirement of any alloy playing a load-bearing role in aerospace applications. The high strength of the AA 2024-T3 alloy is mainly due to the presence of uniformly distributed second phase particles in the Al matrix. These embedded second-phase particles, which largely consist of Al-Cu-Mg and Al-Cu-Fe-Mn intermetallics, lead to good mechanical properties of the alloy by strengthening the Al matrix [2].

Aluminum and its alloys have a high corrosion resistance in non-complex aqueous solutions due to the passive oxide film formation on the surface which can be predicted from the Pourbaix diagram of pure aluminum as shown in Figure 1.1. This passive oxide film is vulnerable to localized breakdown leading to loss of the underlying metal. When exposed to aggressive environments, aluminum and its alloys react with oxygen and chloride ions to form complex interfaces [5]. In case of the localized attack occurring at an open surface, pitting corrosion occurs which leads to structural breakdown. The pits act as sites of crack initiation. Pitting corrosion is, in fact, the main form of corrosion observed in aircraft aluminum alloys [3, 4]. AA 2024-T3 is prone to corrosion forms such

as pitting, intergranular corrosion and stress corrosion due to the presence of second phase intermetallic particles. Additionally, researchers have found that the T3 condition worsens the corrosion resistance of the alloy. With the desire to find an efficient solution to improve its corrosion behavior, several efforts have been made to understand corrosion phenomena in AA 2024-T3. Frankel suggested various stages of pitting corrosion such as passive film breakdown, growth of metastable pits and growth of larger stable pits. He also suggested that localized corrosion is controlled by factors relating to stabilization and growth of pits while the influence of the passive film being secondary in nature [6]. Kagwade et al. found that acetone, commonly used as a degreasing agent for metal cleaning, remaining on the Cu-containing second-phase particles can react slowly with water vapor under ambient light to form acetic acid and together with chloride ions cause severe corrosion [6]. To eliminate this unsolicited source of corrosion, acetone was not used for any metal cleaning purposes in this study.

#### **1.4 Significance of corrosion control**

Corrosion is one of the largest causes of revenue loss in the industrial world. The enormous costs of corrosion in monetary terms and in terms of safety have been long known. According to a National Association of Corrosion Engineers (NACE) study, the cost of corrosion control of metals in various industries exceeds over \$300 billion dollars annually in the United States alone. The annual (1996) corrosion cost to the U.S. aircraft industry alone was estimated at \$2.2 billion, which includes the cost of design and manufacturing [7]. Corrosion occurs in aircrafts, automobiles, pipelines and even household appliances. Though corrosion is inevitable, the costs involved can be

considerably reduced by protecting the metal surface. The important parameters to be considered in the corrosion process are the material that needs to be protected and the environment that it is exposed to. The corrosion process can be controlled by either protecting the material or controlling the corrosiveness of the environment or both. The first option emerges as more plausible of the two. By controlling the rate of either the anodic or the cathodic reaction, one can reduce the overall corrosion rate. Corrosion protection by organic or inorganic coatings has been successfully used over the years to minimize the corrosion process. Barrier coatings are used to protect metals from corrosion by preventing the interaction between the metal and the corrosive environment. Currently, the aerospace industry employs a chromate-containing, solvent based, two-step (primer and topcoat) coating technology for protection of the alloys used [8].

### **1.5 Corrosion protection by organic coatings**

Over the years, organic coatings have played an important role in corrosion protection of metals and have been used in a large scale in many industries. These coatings form a protective layer over the metal substrates and prevent them from oxidation which could affect the function and appearance of the object. They act as a barrier to the passage of current necessary for the completion of the corrosion cell connecting the areas of anodic and cathodic activity on the metal substrate. This is possible only if the coatings are able to wet the substrate surface adequately and provide good adhesion in the presence of water and electrolyte. Good interfacial adhesion at the metal/coating interface is an absolutely crucial element in good corrosion performance because most failures of the organic coatings are caused by the delamination of the coating from the metal surface [9].

Hence, performance of protective organic coatings is heavily dependent on the physical or chemical bonds formed at the metal/coating interface. Good coatings do not actually stop oxygen or water encroachment, but sufficiently limit water and electrolyte diffusion in order to impede the corrosion rate. The advantages of using organic coatings are that they have been economical to use and single application on the substrate is sufficient to achieve the desired performance maintaining the appearance and function at the same time [8].

In the aerospace industry, organic coatings are applied frequently as multi-layer coating systems known as finishing systems. A complete finishing system consists of a metal pretreatment or conversion coating, a primer coating and a topcoat. A conversion coating or a pretreatment is a unique formulation of inorganic chemicals that reacts with the metal surface to create a strongly adherent, anti-corrosive coating and provides a better surface than the original metal oxide layer for attaining good adhesion of the successive paint layers. Most commonly used conversion coatings consist of phosphates and chromates. A primer system, which is coated over the pretreatment, enhances corrosion protection, improves mechanical properties and provides adequate adhesion. Pigments and inhibitors such as chromates, which leach out to protect cracks and defects that develop when a coating is damaged during service, are incorporated into the primer. Epoxy resins, polyurethanes, alkyds, polysiloxanes, acrylates are most commonly used resins used as primers. The primer may also contain UV absorbers and other fillers or a separate coating called the undercoat containing these additives may be applied on the top of the primer. A topcoat gives the system a final finish and provides an aesthetic

appearance. A finishing system may or may not use all of the above mentioned layers dependent on aspects such as size and shape of article, protection required, severity of exposure and cost of production [6, 8].

Chromate and phosphate conversion coatings are pretreatments that demonstrate excellent adhesion and corrosion protection of the metal substrate. However, pretreatment processes are cumbersome, expensive and often produce enormous toxic wastes. The conversion coatings mainly consist of inorganic inhibitors that undergo reduction at active corrosion sites (pits, precipitates or inclusions) to form insoluble oxides. The inhibitors leach out to the exposed defects in the coating to form a passivating oxide film and suppress the cathodic reaction by limiting the diffusion of the electrolyte, oxygen and water to the substrate. Chromate pigments possess a unique 'self-healing' ability which has not been duplicated to such precision and consistency by any other pigments till date. Chromate conversion coatings consist of chromate salts which contain the  $\text{CrO}_4^{-2}$  and  $\text{Cr}_2\text{O}_7^{-2}$  ions. In both these ions, the chromium atom is in the oxidation state of +6. This hexavalent chromium has the ability to leach out into defects in a coating and form insoluble chromium compounds which prevent further ingress of the electrolyte and protect the metal from corrosion. However, hexavalent chromium (CrVI) compounds eventually leach out into the environment and are considered potential carcinogens [8, 9]. Their use has already been restricted by the Environmental Protection Agency (EPA) in the USA while the European Union (EU) has begun phasing out of chromate from most industrial applications. Researchers all over the world have been looking for chromate alternatives for more than a decade now. Several alternatives to chromates have been

investigated, some of them are molybdates, vanadates, silicates, rare earth metals such as Ce, acids of Ti and Zr, silanes and polymer-based film-forming treatments [6]. It has been established that organofunctional silane pretreatments perform equivalent to chromates and are seen as potential replacements to chromating.

Most industrial primers are either organic solvent-based or water-based. Organic solvents contain compounds classified as volatile organic compounds (VOC) and release hazardous air pollutants (HAP) which can be detrimental to both human health and the environment. Consequently, EPA has imposed restrictions on VOC and HAP emissions which have forced paint makers to opt for safer, environmentally friendly alternatives. But solvent-based primers are still used widely because they are formulated with a high molecular weight polymer which provide superior chemical, water and corrosion resistance [10].

Water-based primers have become popular because of their environmentally benign nature, low VOC content, low viscosity, higher pot life, ease of application and curing [11]. Being formulated from low molecular weight polymers, they are hydrophilic and provide inferior chemical and corrosion resistance compared to high solids solvent-based coatings. The polar nature of water causes wettability issues at the substrate surface leading to inferior adhesion [12]. Longer drying times and incompatibility with some paint components are also some of the weak points. In spite of these limitations, water-borne coatings remain the most probable alternatives as commercial replacements for solvent-borne coatings. Water is a universal solvent which is easily available,

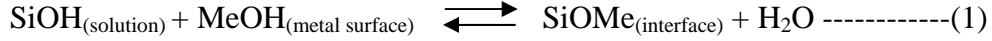
inexpensive and non-toxic. Specific additives, fillers, corrosion inhibitors and other pigments are mostly dispersible in water and improve the performance of these coatings with regards to corrosion resistance [11, 12]. Various surfactants and dispersants can be used to surmount some of the dispersion problems. As a result continuous improvements in technology, a whole array of water-based emulsions and paints for different substrates has spawned and already substituted solvent-based coatings in many applications [13]. The coatings developed in this work are water-based, low-VOC coatings for corrosion protection of aerospace aluminum alloys.

## **1.6 Silanes**

Organofunctional silanes have recently emerged as outstanding, environmentally friendly anti-corrosion treatments for metal substrates and have shown the potential to replace the conventional chromate pretreatment. Organofunctional silanes are hybrid organic-inorganic compounds having the structure  $X_3Si(CH_2)_nR$ , as shown in Figure 1.2. X represents a hydrolyzable group such as alkoxy, acyloxy, halogen or amine and R is a non-hydrolyzable organic group that may possess a functionality which imparts the desired characteristics [14].

The hydrolysis of silanes is an important step in the pretreatment of metals. A silane hydrolyzes and condenses to form covalent bond with the substrate as shown in Figure 1.3 (a) and (b). It is generally assumed that upon drying, silane molecules bond tightly to metals through the condensation reaction between silanols (SiOH) from the silane

solution and the metal hydroxyls (MeOH) from the metal surface hydroxides, forming covalent metallo-siloxane bonds (MeOSi) according to,



The excess SiOH groups adsorbed on the metals would also condense among themselves to form a siloxane (SiOSi) as shown below [15].



The as-formed MeOSi and SiOSi covalent bonds are assumed to be responsible for the excellent bonding of the silane film to the metal substrate as demonstrated in Figure 1.4 [6, 14].

Based on this hydrolysis and condensation mechanism silanes have been used as adhesion promoters for several years. The mechanism of adhesion and bonding of silanes was first studied as a pretreatment application for corrosion protection by Van Ooij et al. at the University of Cincinnati [16]. They showed silane pretreatments protected metals, especially aluminum and steel, against uniform, galvanic, pitting, crevice and stress corrosion. They also proved that silane pretreatments performed equal to chromates in terms of corrosion protection and paint adhesion. It was found by Van Ooij et al. that bis-type organofunctional silanes, which have two silicon atoms in its molecule, provided better corrosion inhibition performance on a wide range of metals and alloys as compared to mono-silanes [17]. The improved corrosion inhibition performance was attributed to the fact that the bis-silanes formed denser films mono-silanes. The bis-silanes, especially bis-sulfur silane, provide excellent adhesion of coatings to metal substrates and better

corrosion protection under severe corrosive conditions and the corrosion behavior is found to be comparable to chromates. Figure 1.5 shows a general chemical structure of a mono- silane and a bis-silane respectively. The coating systems studied in this work are silane-based selected because of their wide-ranging advantages over the existing metal pretreatments. Some of the advantages include ease of application, room temperature curing, fast treatment time, non-toxic nature of the process and excellent corrosion protection to metal.

## **1.7 Resins for organic coatings**

The organic coatings industry uses epoxy-based resins as binders on a large scale. Epoxy resins are the reaction products of epichlorohydrin and bisphenol A (BPA). Diglycidyl ether of bisphenol A (DGEBA) is a common example of BPA-type epoxy resin used in the coating industry. The chemical structure of a DGEBA resin monomer is shown in Figure 1.6. BPA epoxy resin-based coatings exhibit superior adhesion compared to other resins used in primers. Protective coatings, adhesives, electrical laminates, reinforced plastics and commercial flooring systems are some the applications illustrating the versatility and high performance characteristics of these materials.

Epoxy resins are incapable of forming good coatings by themselves and have to be reacted with a curing agent or another resin to get a cured film. The curing of an epoxy resin system normally takes place in various steps [18]. The epoxy resin, a viscous liquid, first reacts with the curing agent, a liquid or a low-melting solid. Heat released during the reaction accelerates the curing process. As a result, linear chains of combined epoxy resin

and curing agent are formed, with the viscosity increasing rapidly. The linear chains then form a cross-linking network to produce a solid gel of an extremely high molecular weight polymer system. Epoxide ring opening reactions, as demonstrated in Figure 1.7, lead to coatings with low shrinkage, which is especially important when the polymerization reaction is the final curing step in the coating process. In addition to the epoxide groups, an epoxy resin molecule also has reactive hydroxyl (-OH) groups. Overall coating performance will depend on the epoxide/OH mole ratio, amount of catalyst, cure time and temperature, and epoxide functionality [19]. In this study, a novel resin called novolac is used as the binder for the primer system. Novolac resins are formulated from bisphenol F or BPA novolac epoxy resins as compared to an ordinary BPA epoxy resins. Novolac epoxies provide an increase in chemical resistance over regular epoxies while the resistance to heat also increases. The chemical structure for a generic novolac resin is shown in Figure 1.8.

Curing agent or hardener is the chemical that reacts with the epoxide functionalities in the epoxy resin, i.e., it cures the resin. The selection of the curing agent depends on many parameters and will determine the final properties of the primer. Aliphatic or aromatic amine curing agents are commonly used as they have enough reactive sites per molecule to facilitate the formation of a three-dimensional polymer network when mixed with the epoxy resin. The chemical structure of an epoxy amine curing agent used in this study is shown in Figure 1.9. In addition to the above types of curing agents there are also non-amine based curing agents such as aromatic or aliphatic isocyanates. The isocyanates react through the hydroxyl groups of the epoxy resin and provide very good low

temperature curing, good flexibility, good impact and abrasion resistance as well as good adhesion. Urethane and urea groups are formed in the interphase depending on the functional groups available in the epoxy resin. Silanes can also be incorporated in the epoxy primer system to have enhanced adhesion and corrosion protection. Silanes will be more effective when the epoxy resin does not react completely with the silanes leaving some of the hydrolyzable functionalities in the silane unreacted. Such a system, which will produce a better performance coating, is explained in the following section.

### **1.8 Superprimer: A silane-resin based primer system**

Silanes have efficiently demonstrated corrosion protection of AA 2024-T3 in the form of pretreatments and proved to be viable replacements for chromate conversion coatings. However, a silane film alone, usually around 200-500 nm thick, is incapable of providing long-term protection without the presence of a primer or a topcoat on the pretreated metal substrate [20]. Alternatively, a self-priming coating termed “superprimer” can be obtained by integrating silanes with resins. Van Ooij introduced the idea of superprimers at the University of Cincinnati, Cincinnati, OH [21]. The inspiration to develop superprimers originated from the work done by Van Ooij et al. in the field of silane pretreatments for metals. The concept of the superprimer is to combine a two-step process of pretreatment and primer coating of metal into a single step. A silane is believed to form a crosslinking/interpenetrating network with the resin which effectively increases the thickness of coating to the order of 20-50  $\mu\text{m}$  [21]. The silanes used in this study were bis-silanes which have demonstrated better performance than mono-silanes because organofunctional bis-silanes have a higher number of hydrolyzable groups per

molecule. The good adhesion of the silane to the polymer is attributed to the chemical reactions that occur between the functional group in the silane and the reactive functional group in the polymer. A partially reacted silane leaves a large number of unsatisfied reactive groups especially at the surface which results in excellent adhesion to the subsequent topcoat. Some of the commonly used silanes in superprimers are shown in Figure 1.10.

Superprimer coatings have demonstrated good corrosion resistance and improved mechanical properties compared to a silane coating alone. The superprimer also has good adhesion and is compatible with various types of topcoats [21, 22]. In this study, water-based, low-VOC, chromate-free superprimer coatings are being considered as capable replacements for the conventional high-solids, chromate-containing, solvent-based commercial primers. The resulting superprimer consists primarily of an organic binder resin (novolac epoxy resin dispersions), a cross-linker or curing agent (water-borne epoxy-amine adduct), silanes, minor additives (polyurethane, surfactants, wetting and dispersing agents, defoamers), pigments and fillers (calcium zinc molybdate, zinc phosphate, calcium silicate, titania, sodium metavanadate) and solvents (acetone and water) [23, 24]. The resins and silanes used essentially affect the final properties of the superprimer. All of these components and various formulations and testing procedures towards the development of the superprimer are described in details in the next chapter.

## **1.9 Objective of the thesis**

The purpose of this thesis is development, testing and characteristic study of a novel primer system which will integrate properties of silanes and novolac epoxy resins for the

corrosion protection of AA 2024-T3 aerospace alloy. Organofunctional bis-silanes are used in non-hydrolyzed forms to ensure better performance in terms of adhesion and corrosion protection. The surface pretreatment step is eliminated with the use of superprimer technology. The superprimer under study is a novolac epoxy-based incorporated with bis-silanes, cross-linkers and other additives such as inhibitor pigments, surfactants and dispersants. The water-insoluble bis-silane addition imparts corrosion protection and the hydrophobicity to lend the system water-resistant properties. Due to the requirement of good low-temperature performance, polyurethane resin is added to the superprimer to impart flexibility. Generic structure of polyurethane is shown in Figure 1.11. Cross-linkers to boost room temperature curing, surfactants to improve adhesion and dispersants to improve pot-life form an integral part of the superprimer system. Corrosion inhibitor pigments, nanoparticles and colorants are also incorporated in order to get a complete paint system. The sketch in Figure 1.12 gives a comparison between conventional paint system and the superprimer system.

In summary, this study deals with the development and evaluation of a superprimer coating with the following benefits:

- 1) Excellent corrosion protection and outstanding adhesion to the substrate as well as topcoats
- 2) Capable of replacing conventional chromate-based inhibitors with inorganic, non-toxic inhibitors
- 3) Able to eliminate the chromate conversion coating and other pretreatments on the AA 2024-T3 alloy
- 4) Excellent chemical resistance, water resistance and solvent resistance

- 5) Room-temperature curing with good high-temperature performance
- 6) Water-based, low-VOC and HAP free
- 7) Exceptional low-temperature properties such as flexibility

The subsequent chapters (Chapter 2 and 3) will discuss the formulation, experimental study, performance tests of the superprimer using standard ASTM paint evaluation tests. An effort has been made to investigate the chemistry and bonding mechanisms underlying the anti-corrosive properties of the superprimer employing various characterization techniques (Chapter 4). Chapter 5 discusses the conclusions and scope for future work regarding this developmental work.

## **1.10 References**

1. Davis J.R., *Corrosion of aluminum and aluminum alloys*, 4<sup>th</sup> Ed., ASM International, Materials Park, OH (1999)
2. Vargel C., *Corrosion of Aluminum*, 1<sup>st</sup> Ed., Elsevier SAS, Paris, France (2004)
3. Jones D.A., *Principles and Prevention of Corrosion*, Prentice-Hall Inc., Upper Saddle River, NJ (1996)
4. Fontana M. G., *Corrosion Engineering*, 3<sup>rd</sup> Ed., McGraw-Hill, Denver, CO (1986)
5. La Que F.L. and Copson H.R., *Corrosion Resistance of Metals and Alloys*, 2<sup>nd</sup> Ed., ACS Monograph series, San Francisco, CA (1963)
6. Zhu D.Q., Ph.D. Dissertation, Department of CME, University of Cincinnati (2002)
7. CC Technologies Laboratories Inc., *Corrosion Costs and Preventive Strategies in the United States*, Report FHWA-RD-01-156 (2001)
8. Suryanarayanan K., M.S. Thesis, Department of CME, University of Cincinnati (2005)

9. Bierwagen G.P., *Organic Coatings for Corrosion Control*, ACS Symposium series, New Orleans, LA (1998)
10. Seth A., Van Ooij W. J., *J. Mat. Engg. Perf.* 13, 292 (2004)
11. Dören K., Frietag W., Stoye D., *Water-borne coatings: the Environmentally Friendly Alternative*, Hanser publishers, Munich, Germany (1994)
12. Shivane C., M.S. Thesis, Department of CME, University of Cincinnati (2006)
13. Osborne J.H., *Prog. Org. Coat.*, 41, 217 (2001)
14. Van Ooij W.J., Zhu D.Q., Prasad G., Jayaseelan S., Fu Y., and Teredesai N., *Surface Eng.*, 16, 386 (2000)
15. Plueddemann E.P., *Silane Coupling Agents*, 2<sup>nd</sup> Ed., Plenum Press, New York, NY (1991)
16. Van Ooij W.J., Song J. and Subramanian V., *ATB Métallurgie*, 37, 137 (1997)
17. Subramanian V. and Van Ooij W.J., 2<sup>nd</sup> *International Symposium on Silanes and other Adhesion Promoters*, Newark Airport, New Jersey (1998)
18. Mugada T., M.S. Thesis, Department of CME, University of Cincinnati, to be published in 2006
19. Sinko J., *Prog. Org. Coat*, 42, 267, (2001)
20. Seth A., Van Ooij W.J., *submitted for publication in 5<sup>th</sup> International Symposium on Silanes and Other Coupling Agents*, Toronto, Canada (2005)
21. Seth A. and Van Ooij W.J., 2<sup>nd</sup> *International Surface Engineering Congress*, Indianapolis (2003)
22. Ashirgade A., Mugada T., Van Ooij W.J., *submitted for publication in 5<sup>th</sup> International Symposium on Silanes and Other Coupling Agents*, Toronto, Canada (2005)

23. Palanivel V., Huang Y., Van Ooij W.J., *Prog. Org. Coat.*, 53, 153 (2005)
24. Yang L., Seth A., Simhadri N., Van Ooij W. J., *5<sup>th</sup> International Symposium on Silanes and Other Coupling Agents*, Toronto, Canada (2005)

## **2. EXPERIMENTAL**

This chapter discusses the chemicals and materials used and the experimental procedures employed for the formulation and development of the novel superprimer system for AA 2024-T3 substrate. The substrate preparation method, performance evaluation tests and characterization techniques used during the course of the coating development are also discussed. The prime objective of the formulation development experiments was to optimize the process parameters to obtain the best-performing primer system in terms of the corrosion protection and adhesion to metal substrate.

### **2.1 Chemicals and Materials**

#### **2.1.1 Metal Substrate**

Aluminum AA 2024-T3 alloy substrates of 0.81 mm thickness were acquired from Stillwater Steel and Supply, Stillwater, OK. Chromate conversion coating (CCC) pretreated AA 2024-T3 substrates were obtained from ACT laboratories, Inc., Hillsdale, MI. Chromated substrates were used as controls to compare the performance of the coatings.

#### **2.1.2 Water-based Resin Dispersions**

**EPI-REZ™ 5003-W-55** resin, a nonionic aqueous dispersion of a polyfunctional aromatic epoxy resin with an average functionality of three, was acquired from Resolution Performance Products, Houston, TX. It is also known as the bisphenol A novolac epoxy resin. EPI-REZ 5003-W-55 contains reactive epoxide functionalities and

is intended for high performance applications which require maximum chemical and solvent resistance and/or elevated temperature service. This thixotropic dispersion contains no organic solvent and is completely water reducible. Upon evaporation of water, EPI-REZ 5003-W-55 coalesces to form a clear, continuous, tacky film at ambient temperature, while in combination with a suitable crosslinking agent, it will form a clear, highly crosslinked, tough, chemical resistant film. Advantages associated with EPI-REZ 5003-W-55, compared to a standard bisphenol A epoxy resin, include improved elevated temperature performance, increased water and solvent resistance, and improved chemical resistance [1].

**NeoRez® R-972**, a colloidal dispersion of aliphatic polyurethane, was acquired from DSM Neo-Resins, Wilmington, MA. It has good abrasion and chemical resistance. Key benefits of using this resin in a coating include plasticizer migration resistance, adhesion to flexible films and UV resistance. It is completely water reducible and contains 10 wt % VOC [2].

**NeoRez® R-960** is an air-dry, water-borne aliphatic polyurethane dispersion similar to NeoRez R-972. It has 40 wt % VOC and is specifically designed for high performance uses, where hardness, flexibility, chemical and abrasion resistance are required. The aliphatic backbone of NeoRez R-960 results in excellent UV resistance, permitting its use in exterior coating applications. Other benefits include solvent resistance, water resistance and impact resistance [3]. Table 2.1 mentions some of the physical properties of the resins discussed above.

### 2.1.3 Silanes

Organofunctional bis-silanes were used in this study for corrosion protection of AA 2024-T3 and to obtain good adhesion to substrate as well as the topcoat. Some of the silanes were used in unhydrolyzed or neat state with the presumption that water present in the resin formulation would eventually hydrolyze the silanes over a period of time.

**Silquest<sup>®</sup> A-1289** bis-[3-(triethoxysilyl) propyl] tetrasulfide or bis-sulfur silane  $((OC_2H_5)_3Si(CH_2)_3S_4(CH_2)_3Si(OC_2H_5)_3)$ , **Silquest<sup>®</sup> Y 9805** bis-[triethoxysilyl] ethane or BTSE  $((OC_2H_5)_3Si(CH_2)_2Si(OC_2H_5)_3)$  and **Silquest<sup>®</sup> A-1170** bis-(trimethoxysilylpropyl) amine or bis-amino silane  $(OCH_3)_3Si(CH_2)_3NH(CH_2)_3Si(OCH_3)_3$ , were obtained from GE Silicones, South Charleston, WV. **VTAS<sup>®</sup>** vinyltriacetoxysilane  $(CH_2=CHSi(COCH_3)_3)$  was acquired from Gelest Inc., Morrisville, PA. A synergistic ratio of bis-amino silane and VTAS known as AV5 was used in the superprimer formulation in hydrolyzed state while the bis-sulfur and bis-amino silanes were used in pure or unhydrolyzed states. The structural formulae of these silanes have been shown in Figure 1.5.

### 2.1.4 Crosslinkers and Curing Agents

Cross-linkers and curing agents were used to obtain tough, dry and highly cross-linked polymer films of novolac epoxy resin. Water dispersion or water-soluble curing agents such as dicyandiamide, polyamides, and aliphatic and aromatic amines that react with epoxide groups or promote self-polymerization, have been recommended as crosslinking agents for the novolac epoxy resin.

Silquest<sup>®</sup> is a registered trademark of GE Silicones. VTAS<sup>®</sup> is a registered trademark of Gelest Inc.

**EPIKURE<sup>®</sup>™ Curing Agent 6870-W-53**, a 53% solids, non-ionic aqueous dispersion of a modified polyamine adduct curing agent, was acquired from Resolution Performance Products, Houston, TX. This high molecular weight curing agent contains no solvents and is designed to provide the high performance of traditional epoxy coatings in low-VOC, non-HAP waterborne epoxy coatings [4]. **NeoCryl<sup>®</sup>** Crosslinker CX-100 is a 100% active polyfunctional aziridine liquid crosslinker. Addition of one to three percent Crosslinker CX-100 to NeoRez R-972 or NeoRez R-960 produces a marked improvement in water, chemical, abrasion and humidity resistance. The use of CX-100 also improves the adhesion to metal substrates [5]. **Dibutyltin dilaurate** or **DBTL** (95% pure, C<sub>32</sub>H<sub>64</sub>O<sub>4</sub>Sn) was obtained from Sigma-Aldrich Co., Milwaukee, WI. It was used as a catalyst for the silane in very small amount of about 0.5 wt % or less of the coating formulation. Tin salts are widely used in the coating industry as catalysts and to accelerate drying and curing.

### 2.1.5 Corrosion Inhibitors

Non-chromate inhibitors were used in this study to impart self-healing or corrosion inhibiting properties to the superprimer. **Molywhite CZM**, a calcium zinc molybdate corrosion inhibitor pigment was procured from Molywhite Pigments Group, Cleveland, OH. **Corrostatin 228**, a corrosion inhibitor pigment containing Ca, Zn, P, Si and O, was procured from Wayne Pigment Corp., Milwaukee, WI. **Alfa Aesar zinc phosphate**, a technical grade zinc phosphate corrosion inhibitor was procured from Johnson Matthey, Ward Hill, MA.

EPIKURE<sup>®</sup>™ is a registered trademark of Resolution Performance Products, LLC. NeoCryl<sup>®</sup> is a registered trademark of DSM NeoResins Inc.

**Phosguard J0806**, a micronized zinc phosphate/molybdate corrosion inhibitor from Rockwood Pigments, Beltsville, MD. **Sodium meta-vanadate** of chemical grade was procured from Fluka Industries, Switzerland.

### **2.1.6 Other Pigments and Fillers**

**Nanoactive titanium dioxide**, obtained from NanoScale Materials Inc., Manhattan, KS was used as filler pigment in the superprimer. Stapa Hydrolac, a **leafy aluminum paste** containing petroleum distillate, obtained from Eckart America, Louisville, KY was also used as a filler material.

### **2.1.7 Surfactants and Dispersants**

**Surfynol MD 20** and **Surfynol DF 110L defoamers** were obtained from Air Products and Chemicals, Inc., Allentown, PA. **BYK<sup>®</sup> P 104 S**, a wetting and dispersing agent, which enhanced pigment dispersion was obtained from BYK-Chemie GmbH, Wesel, Germany. It is used in neutral aqueous coatings and it prevents flooding of pigments. It is a solution of a lower molecular weight unsaturated polycarboxylic acid polymer with a polysiloxane copolymer in xylene and 2,6-dimethyl-4-heptanone.

### **2.1.8 Solvents and cleaners**

**De-ionized water** was acquired from the University of Cincinnati lab supplies. **Acetone**, 99.5% pure was acquired from Tedia Company, Inc., Fairfield, OH. **Methyl ethyl ketone** (MEK) was acquired from Fisher Scientific, Fair Lawn, NJ. **Okemclean** alkaline cleaner was supplied by Chemetall Oakite, Romulus, MI.

BYK<sup>®</sup> is a registered trademark of BYK-Chemie GmbH, Germany.

### 2.1.9 Topcoats and Control Primers

The following military topcoats and primers, used in the US Navy and Air Force for vehicles and equipments, were used as controls for the superprimer coatings. **CA 7233 High solids** chromated epoxy standard military primer and its activator component CA 7233 B, were procured from PRC DeSoto, Glendale, CA. It conforms to military specification MIL-PRF-23377 H (Type I, class C). **Desothane HS** CA-8214/F36173, solvent-based camouflage gray polyurethane topcoat with a base component and an activator was also procured from PRC DeSoto, Glendale, CA. **Defthane ELT** MIL-PRF 85285 D, a gray military topcoat with a base component and an activator was procured from Deft Chemical Coatings, Irvine, CA.

### 2.2 Metal Surface Preparation

Substrate surface preparation is a very important step in any coating process. The metal surface has to be free of any grease, oil or other impurities as they affect the wettability of the surface by the coating. Poor wetting leads to adhesion problems and delamination of the coating [6, 7]. Before primer coating, AA 2024-T3 panels were prepared by carrying out following cleaning steps:

- Dry scrubbing using scotch brite® for removal of superficial impurities and oxides
- Ultrasonic cleaning in ethanol for 8 minutes at room temperature to remove grease and oil
- Alkaline cleaning in Okemclean alkaline cleaner for 3-5 minutes or 0.5 M NaOH solution for 3-6 seconds at 60-65° C

to enhance formation of aluminum hydroxide which helps adhesion to silane-based coatings

- Thorough rinsing in DI water till water break-free
- Blow-air drying

## **2.3 Formulation of Superprimer**

The formulation methods for the superprimer evolved as the coating development process progressed. The details of all the formulations prepared and modifications done will be discussed in Chapter 3 along with performance test results for each one of them.

### **2.3.1 High-shear Blender**

A high shear blender/mixer manufactured by Ross Mixing Inc., Port St. Lucie, FL was used to mix the superprimer formulation. The micro-mixer/rotor assembly was used at speeds of 1000 rpm to 3000 rpm especially to obtain good dispersion of pigments in the superprimer formulation. The shearing effect produced by the micro-mixer helped in de-agglomeration of pigments and avoided precipitation. It also helped the blending of resin, silane and cross-linkers to form a macroscopically homogenous formulation. A schematic sketch of the high shear mixer used in this study is shown in Figure 2.1.

## **2.4 Coating Methods**

The coating techniques and equipments utilized to coat the superprimer on AA 2024-T3 substrate are discussed in this section.

### **2.4.1. Draw-down Bar**

The cleaned substrate samples were coated with the primer using a draw-down bar number R 14, which gave an average wet-film thickness of 25  $\mu\text{m}$ . The coating thickness can be controlled by varying the profile of the draw-down bar. The topcoat and control primers were also applied using the same draw-down bar.

### **2.4.2 Spray Painting**

The superprimer formulations were sprayed using a SoftSpray HVLP Conversion Gun acquired from Wagner Spray Tech Corporation, Minneapolis, MN. The spray equipment set up consists of a spray gun, material and air hoses, a pressure pot containing the formulation and an air compressor. The viscosity of the formulation needs to be adjusted to enable spraying and avoid sagging. To avoid irregularities in the coating finish, the axis of the spray gun hose should always remain perpendicular to the substrate surface. The spraying pattern can be adjusted according to the application by turning the ears of the air cap into various positions. Multiple coats may be applied after the previous coats have been allowed to dry. A picture of the spray gun is shown in Figure 2.2.

## **2.5 Performance evaluation tests and characterization techniques**

Superprimer and control coatings were subjected to various corrosion and characterization tests after a period of 14 days of room temperature curing, a norm followed commonly in the coatings industry. The results of all the tests will be discussed in Chapter 4.

### **2.5.1 Saltwater Immersion Test**

Salt water immersion is a simple laboratory test for initial screening of coatings in terms of corrosion resistance offered to metal substrates. This test gives a good measure of resistance to blistering and water ingress in the organic film protecting the metal. In this study, the superprimer coated AA 2024-T3 samples were cross-scribed and partially immersed in 0.6 M NaCl (3.5 wt %) solution and their performance was monitored over a period of 30 days. After regular intervals, the coatings were inspected for corrosion, blistering, scribe creep or delamination in accordance with the ASTM D714 standard. For coatings that did not show considerable deterioration, the test was continued until 60 days.

### **2.5.2 Electrochemical Impedance Spectroscopy**

Electrochemical Impedance Spectroscopy (EIS) is an electrochemical technique which yields a high amount of information about the characteristics of paints and corrosion. EIS provides a more thorough understanding of an electrochemical system than any other electrochemical technique. Electrochemical impedance is usually measured by applying a sinusoidal AC potential to an electrochemical cell and measuring the current through the cell over a wide range of frequencies. The response to this potential is an AC current signal, containing the excitation frequency and its harmonics which can be analyzed as a sum of sinusoidal functions (a Fourier series). In case of a corroding metal in an electrolyte, a steady-state electrical double layer (EDL) is formed at the metal/electrolyte interface. This EDL acts as a capacitor whereas the adsorbed water acts as a dielectric

and the electrolyte as a resistor [8]. The presence of one or more coatings on the metal surface creates more interfaces and consequently more resistance to the passage of current, thereby impeding the corrosion reaction. The overall resistance offered by the coating is termed the impedance of the coating and depends on the characteristics of the coating such as porosity and cross-link density. Such a system can be represented in the form of an electrical circuit consisting of capacitors and resistors. This impedance value gives a good measure of the corrosion resistance offered by the coating to the metal substrate. EIS is also a useful tool to measure the nature and the degree of degradation such as electrolytic diffusion, delamination, blistering, discoloration and pitting in paint coatings and to study the mechanism of corrosion of metals [9]. The electrical data obtained from EIS is presented as Bode and Nyquist plots. Figures 2.3 (a), (b) and (c) show an example of a Bode plot, a Nyquist plot and an equivalent circuit, respectively, for a failed coating [10]. In this study, only the Bode magnitude plots were considered for comparison of the performance of superprimer coatings.

Figure 2.4 shows an EIS cell arrangement for a superprimer coating on AA 2024-T3 sample. The cell consisted of a saturated calomel reference electrode, a metal substrate as working electrode, a graphite counter electrode, the superprimer coating as the dielectric material and the NaCl solution as electrolyte. A coating area of 5.18 cm<sup>2</sup> was exposed to aerated 0.6 M NaCl solution. EIS measurements were carried out using an SR810 frequency response analyzer connected to a Gamry CMS100 potentiostat over a frequency range of 10<sup>-2</sup> to 10<sup>5</sup> Hz. Using Gamry Framework software, the EIS spectra were collected and the results were analyzed and correlated to the performance characteristics of the superprimer coatings.

### **2.5.3 ASTM B117 Salt Spray Test**

ASTM B117 salt spray test is a valuable accelerated test method for evaluation and quality control of paint coatings for corrosion protection of metals used in automotive, aircraft and other industries. It consists of a closed compartment where specimens are exposed to specific concentration of salt (NaCl) spray or fog at specific locations and angles. A wide range of chamber designs and sizes including walk-in rooms, capable of performing this test, are available in the market. There has been some skepticism over the authenticity of the test results and it is debated whether the conditions in this test represent actual service conditions. However, ASTM B117 salt spray test is still one of the most widely used cabinet tests used in the coatings industry.

In this study, the ASTM B117 test was carried out at DACCO SCI, Inc., Columbia, MD. Specimens coated with superprimers and control coating were cross-scribed and placed at 45° in a certified Singleton salt fog chamber with specifications of 5% NaCl solution (pH 7) atomized at 35°C. A picture of the salt spray chamber at DACCO SCI is shown in Figure 2.5. The specimens were removed periodically from the salt fog test and EIS measurements were taken using a handheld corrosion sensor developed at DACCO SCI, Inc [11]. These sensors allowed the EIS measurements to be taken under ambient conditions unlike the measurements of traditional EIS. A geometric mean of the impedance values from the 0.1 to 1 Hz frequency decade was reported along with an image of the exposed coating at regular time intervals. The EIS measurements have been correlated to long term performance of coatings [12-16].

#### **2.5.4 The Ford AGPE Test**

The Ford AGPE test is an accelerated cyclic corrosion test developed for the evaluation of resistance to perforation of painted automotive metal substrates [17]. Ford test was performed on cross-scribed coatings on AA 2024-T3 substrates with or without topcoat at DACCO SCI, Inc., Columbia, MD by using a Blue M VP100 Humidity Chamber. During weekends, the panels were kept in the humidity chamber. The exposure for different coatings was continued till failure. During the exposure, specimens were removed and EIS measurements were taken at regular intervals using the sensor equipment described in the previous section. The Ford AGPE test is the one of the most aggressive corrosion tests. An image of the Ford AGPE set-up at DACCO SCI is shown in Figure 2.6 and the test cycle is listed in Table 2.2.

#### **2.5.5 Outdoor Exposure Test**

Outdoor exposure test is being carried out on AA 2024-T3 specimens coated with superprimer formulations and topcoat at Kennedy Space Center, Ft Lauderdale, FL, an outdoor site where the annual temperatures range from 20 to 25°C with high humidity. At regular intervals during the exposure, EIS measurements will be taken using the corrosion sensors described earlier. This test gives a fair idea about the performance of the coating system in actual service conditions, however, the duration of the test is usually between 2-4 years. This test is in progress at the above mentioned location and the results for are not included in this thesis.

### **2.5.6 Tape Adhesion Test**

AA 2024-T3 specimens coated with superprimer and/or topcoat were subjected to dry and wet tape adhesion tests according to the ASTM D3359-97 standard. In this test, a cross-hatched grid area of the coated sample is taped. The tape is applied for at least 30 seconds and pulled off. The amount of coating delamination or removal is determined and the classification of coating quality is done according to the test standard. The classification varies from 5A for no peeling or removal to 0A for removal beyond the test area. The test is performed on dry test samples and then repeated on samples immersed in de-ionized water for 24 hours. The test gives a good measure of the adhesion between the superprimer and the metal substrate as well as the adhesion between the topcoat and the superprimer.

### **2.5.7 MEK Double Rub Test**

The MEK (methyl ethyl ketone) double rub test is a type of solvent resistance test to determine the degree of curing or cross-linking density of coatings. A cloth soaked in MEK is rubbed repetitively on the coating. One stroke of a back and forth movement constitutes a double rub. Repetitive double rubs are performed till the coating is removed or the substrate is visible and the number of double rubs required is reported. This test gives an idea about the quality of coatings cured at room temperature. A high MEK double rub value indicates a high degree of curing and cross-linking of the coating. A high degree of cross-linking generally results in high hydrophobicity of the coating and low permeability towards electrolytes and good corrosion resistance. In this study, the MEK double rub test was carried out on cured superprimer formulations according to the

ASTM D4752-03 standards and the number of double rubs for each individual superprimer formulation were reported.

### **2.5.8 Chemical Resistance Test**

The chemical resistance test is a measure of acidic and alkaline chemical resistance of a coating. This test involves exposure of a cured coating to acidic and basic solutions for a certain period of time. After exposure, any deterioration in the form of blistering, discoloration or corrosion is reported. In this study, superprimer coatings on AA 2024-T3 were exposed to a drop of 6 N HCl and 6 N NaOH for one day in accordance with the ASTM D3912 standard.

### **2.5.9 Pencil Hardness Test**

The pencil test is commonly used in the coatings industry to determine the mechanical hardness and scratching resistance of the coatings. Pencils with hardness ranging from 6B (softest) to 6H (hardest) were used in this study to scratch superprimer and control primer coatings on AA 2024-T3. The test was carried out in accordance with the ASTM D3363 standard. The first pencil to gouge the coating was reported. This test reflected the impact and scratch resistance properties of the superprimer coatings.

### **2.5.10 Bend Test**

The bend test was carried out on superprimer coatings, containing polyurethane resins as one of the components, at room temperature and sub-zero temperatures according to the ASTM D522 standard for mandrel bend test (mandrel diameter 3.2 mm). The coated samples were bent using a mandrel through 180° at room temperature. Some samples

were bent in slurry of dry ice and ethanol for sub-zero temperature testing. The bent samples were then exposed to 0.6 M NaCl solution for a period of 30 days. Observations were made for any corrosion products or delamination at the cracks in the coatings. The results gave an indication of the superprimer's flexibility and resistance to cracking.

### **2.5.11 Contact Angle Measurements**

Contact angle goniometry is the study of geometry of a liquid drop on a solid surface. The interfacial tension between a solid and a liquid and the contact angle reveals a great amount of information about the surface properties of a solid. The geometry of a liquid droplet on a solid surface is regulated by interfacial forces as given by Young's equation:

$$\gamma_{SL} = \gamma_S - \gamma_L \cos \theta \quad (0 \leq \theta < \pi)$$

Where  $\gamma_{SL}$  = interfacial free energy,  $\gamma_S$  = surface free energy of solid,  $\gamma_L$  = surface free energy of liquid and  $\theta$  = contact angle. Figure 2.7 shows a schematic sketch of forces acting on a liquid droplet on a solid surface. The contact angle measurements are a function of the surface tension, droplet diameter, viscosity and density of the liquid [18]. These factors need to be controlled in order to have consistent and accurate results.

In this study, contact angle measurements were performed on a contact angle goniometer VCA Optima 2000 manufactured by AST Products, Inc., Billerica, MA. The equipment is shown in Figure 2.8. A water droplet was delicately placed on superprimer coated on AA 2024-T3 using a syringe. A camera captured images of the water droplet. The contact angle between the liquid and solid was measured from the images using the software for operating the equipment. Contact angles for different coating systems were compared. The contact angle data provided information about the hydrophobicity which in turn

determines the corrosion resistance of the coatings. Surface energy calculations were not carried out and the conclusions were based only on the contact angle values.

### **2.5.12 Infrared Spectroscopy**

Infrared (IR) Spectroscopy is a type of absorption spectroscopy that uses the Infrared part of the electromagnetic spectrum. As with all spectroscopic techniques, it can be used to identify a compound and to investigate the composition of a sample. Infrared spectroscopy works because chemical bonds have specific frequencies at which they vibrate corresponding to energy levels. The resonant frequencies are determined by the shape of the molecular potential energy surfaces, the masses of the atoms and, eventually by the associated vibronic coupling. In order to be IR active, a molecule needs to have a changing dipole [19]. In the Born-Oppenheimer and harmonic approximations, the resonant frequencies are determined by the normal modes corresponding to the molecular electronic ground state potential energy surface. Nevertheless, the resonant frequencies can in a first approach be related to the length of the bond, and the mass of the atoms at either end of it. Thus, the frequency of the vibrations can be associated with a particular bond type. Bonds can vibrate in six different ways; symmetrical and asymmetrical stretching, scissoring, rocking, wagging and twisting. Some of the vibrations in H<sub>2</sub>O and CO<sub>2</sub> molecules are shown in Figure 2.9 (a) and (b) respectively. In order to measure a sample, a beam of monochromatic infrared light is passed through the sample, and the amount of energy absorbed is recorded. By repeating this operation across a range of interest (usually no more than 4000 cm<sup>-1</sup> or 0.5-0.6eV), a chart or spectrum can be built up. When looking at an IR spectrum of a substance, an experienced user can identify the

substance from the information in it. This technique works almost exclusively on covalent bonds, and as such is of most use in organic chemistry. Clear spectra will be produced by samples with high levels of purity of one substance [19]. However, the technique has been used for the characterization of very complex mixtures.

In the present study, the chemical structures of the various cured superprimer coatings on AA 2024-T3 were studied using reflection absorption infrared (RAIR) spectroscopy. A Spectrum One FTIR spectrometer manufactured by Perkin Elmer, Wellesley, MA was used to obtain the IR spectra. The spectra were collected with a fixed-angle (45°) specular reflectance accessory by taking 256 scans of the coating films in the IR frequency range of 4000  $\text{cm}^{-1}$  to 450  $\text{cm}^{-1}$ . Figure 2.10 shows a sketch of the optical arrangement for a reflection-absorption IR spectrometer sampling accessory.

### **2.5.13 Nuclear Magnetic Resonance Spectroscopy**

Nuclear Magnetic Resonance (NMR) Spectroscopy is a technique which exploits the magnetic properties of a nucleus. The two important techniques are proton NMR and carbon-13 NMR. In its simplest form NMR allows identification of individual atoms in a pure molecule. Analysis of a 1D NMR spectrum reveals information about the environment around an atom, structure of a chemical and reaction mechanisms [20]. Quantum mechanically subatomic particles, such as protons, neutrons and electrons, have a spin. In some atoms, such as  $^{12}\text{C}$ ,  $^{16}\text{O}$  and  $^{32}\text{S}$ , these spins are paired and cancel each other out so that the nucleus of the atom has no overall spin. However, in many atoms such as  $^1\text{H}$ ,  $^{13}\text{C}$ ,  $^{31}\text{P}$ ,  $^{15}\text{N}$  and  $^{19}\text{F}$  the nucleus does possess an overall spin. If the number of neutrons and the number of protons are both even, the nucleus has no spin. If the

number of neutrons plus the number of protons is odd, then the nucleus has a half-integer spin (i.e. 1/2, 3/2, 5/2). If the number of neutrons and the number of protons are both odd, then the nucleus has an integer spin (i.e., 1, 2, 3) [20].

When placed in a magnetic field, spinning nuclei behave like magnets as they have lower energy when aligned with the field than when opposed to it. This energy difference corresponds to radio frequencies hence the NMR active nuclei (like  $^1\text{H}$  or  $^{13}\text{C}$ ) resonate at a specific frequency. Figure 2.11 shows the possible spin states of some nuclei in an external magnetic field. Different nuclei resonate at a different frequency at the same field strength. The precise resonant frequency is dependent on the strength of the effective magnetic field at the nucleus that is affected by electron shielding and, in turn, dependent on the chemical environment. This frequency is converted into a field-independent value known as the chemical shift measured as a ratio of frequencies, usually in parts per million (ppm). So nuclei in different environments have different chemical shifts. In general, the more electropositive the nucleus, the larger its chemical shift. By understanding the different values of chemical shift we can assign each signal to an atom or group of atoms in the molecule under study [21]. Figure 2.12 shows typical ranges of chemical shifts for protons in different groups. For example, in a proton spectrum for ethanol ( $\text{CH}_3\text{CH}_2\text{OH}$ ) one would expect three specific signals at three specific chemical shifts, one for the  $\text{CH}_3$  group, one for the  $\text{CH}_2$  group and one for the OH. A typical  $\text{CH}_3$  group has a shift around 1 ppm, the  $\text{CH}_2$  attached to an OH has a shift of around 4 ppm and the OH has a shift around 2–3 ppm. The effective magnetic field is also affected by the orientation of neighboring nuclei. This effect is known as spin-spin coupling which can cause splitting of the signal for each type of nucleus into two or more lines. The size

of the splitting is independent of the magnetic field and is therefore measured as an absolute frequency (usually Hertz). The number of splitting indicates the number of chemically bonded nuclei in the vicinity of the observed nucleus [21].

An NMR spectrometer consists of four parts: magnet, RF generator, detector, and computer. The magnet surrounds the sample, generating a magnetic field of 1-20 Tesla. The RF generator emits a precise frequency of light (radio frequency). The detector (probe) measures the absorption of RF energy of the sample and the computer analyzes the signal from the detector to produce a spectrum [22]. In this study, NMR spectroscopy was conducted at the Department of Chemistry in Oklahoma State University, Stillwater, OK. Liquid-state and solid-state  $^{13}\text{C}$  and  $^{29}\text{Si}$  NMR studies were carried out on various superprimer formulations in collaboration with Dr. Tammy Metroke. Liquid-state  $^{13}\text{C}$  and  $^{29}\text{Si}$  NMR spectra were collected using a Varian Inova 400 MHz spectrometer. Spectra were collected using a Varian broadband probe and a single pulse sequence using a 10.2  $\mu\text{s}$  pulse width with a 3-second pulse delay and 2000 scans. Solid-state  $^{13}\text{C}$  NMR experiments were performed on cured superprimer samples using a Chemagnetics CMX-II 300 MHz (7.06 T) spectrometer. A Chemagnetics triple resonance probe was used for data collection. Resonance frequency for  $^{13}\text{C}$  NMR was 75.6 MHz. All chemical shifts (peaks) were referenced to tetramethyl silane (TMS). The spectra were collected using a quasi-adiabatic CP/MAS pulse sequence using a 1 s pulse delay, a 5  $\mu\text{s}$  pulse width, a 1 ms contact time, and 2000-3600 scans. Magic angle spinning was carried out in 5 mm zirconia rotors spinning at 5 kHz. Solid-state  $^{29}\text{Si}$  NMR results were not included in this thesis as the silane content in the superprimer formulations was found to be too low to be

detected in the  $^{29}\text{Si}$  NMR experiment. The acquired  $^{13}\text{C}$  NMR spectra were analyzed to observe the crosslinking between silane and resins and other curing reactions in the coatings.

#### **2.5.14 Scanning Electron Microscopy and Energy Dispersive X-ray Spectroscopy**

The scanning electron microscope (SEM) is a type of electron microscope capable of producing high resolution images of a sample surface. Due to the manner in which the image is created, SEM images have a characteristic three-dimensional appearance and are useful for judging the surface structure of the sample. Energy Dispersive Spectroscopy (EDS) is a standard procedure for identifying and quantifying elemental composition of sample areas as small as a few cubic micrometers. The characteristic X-rays are produced when a material is bombarded with electrons in an electron beam instrument, such as a scanning electron microscope. Detection of these x-rays can be accomplished by an energy dispersive spectrometer, which is a solid state device that discriminates among X-ray energies.

In a typical SEM, electrons are thermionically emitted from a tungsten or lanthanum hexaboride ( $\text{LaB}_6$ ) cathode and are accelerated towards an anode; alternatively electrons can be emitted via field emission (FE). Tungsten is used because it has the highest melting point and lowest vapor pressure of all metals, thereby allowing it to be heated for electron emission. The electron beam, which typically has an energy ranging from a few hundred eV to 50 keV, is focused by one or more condenser lenses into a beam with a very fine focal spot sized 1 nm to 5 nm. The beam passes through pairs of scanning coils

in the objective lens, which deflect the beam in a raster fashion over a rectangular area of the sample surface. A schematic sketch elucidating the principle of working of SEM is shown in Figure 2.13. As the primary electrons strike the surface, they are inelastically scattered by atoms in the sample. Through these scattering events, the primary electron beam effectively spreads and fills a teardrop-shaped volume, known as the interaction volume, extending about less than 100 nm to 5  $\mu\text{m}$  depths into the surface as shown in Figure 2.14. Interactions in this region lead to the subsequent emission of electrons which are then detected to produce an image [23].

X-rays, which are also produced by the interaction of electrons with the sample, may also be detected in an SEM equipped for energy dispersive X-ray spectroscopy or wavelength dispersive X-ray spectroscopy. The most common imaging mode monitors low energy (<50 eV) secondary electrons. Due to their low energy, these electrons originate within a few nanometers from the surface. The electrons are detected by a scintillator-photomultiplier device and the resulting signal is rendered into a two-dimensional intensity distribution that can be viewed and saved as a digital image. Using this technique, resolution less than 1 nm is possible. In addition to the secondary electrons, backscattered electrons can also be detected. Backscattered electrons may be used to detect contrast between areas with different chemical compositions. These can be observed especially when the average atomic number of the various regions is different [23].

A Philips XL 30 environmental scanning electron microscope (ESEM) equipped with an EDS unit was used. Superprimer coatings with different types and concentrations of

inhibitors were examined in the ESEM at 1.3 kPa of vapor pressure and an operating voltage of 25 kV. Back-scattered and secondary electron images along with EDS point and line scans were used to obtain chemical information about the coatings. Before the SEM/EDS analysis, the coatings were scribed and exposed to 3.5 wt % NaCl solution for 30 days. The scribed area of the coatings was studied for leaching of inhibitors and their role in corrosion protection. Cross-sectional study of the coating on AA 2024-T3 was also done to analyze any phase separation or layer formation in the superprimer. To avoid charging effects, a very thin layer of Au/Pd was deposited onto the samples using the Denton Vacuum Desk II Sputtering unit shown in Figure 2.15.

### **2.5.15 Thermogravimetric analysis**

Thermogravimetric analysis (TGA) is a technique in which changes in weight of a specimen are recorded as the specimen is heated in air or in a controlled atmosphere such as nitrogen. TGA curves or thermograms provide information regarding polymerization reactions, the efficiencies of stabilizers and activators, the thermal stability of materials, degradation temperatures and absorbed moisture content of materials, the level of inorganic and organic components in materials and decomposition points of chemicals [24]. In this study, TGA was performed on superprimer samples cured at room temperature. The aim was to assess the effect of silane and polyurethane resin additions on the thermal stability of the novolac-based superprimers. The study threw light on the extent of cross-linking reactions in the coating. TGA 2950 manufactured by TA Instruments, Newcastle, DE was used for this purpose. Predetermined amount of the powdered coating was placed on a platinum pan and heated over a temperature range of 25° C to 350° C at 10 °C /min with isothermal heating at 350° C for 5 minutes. A nitrogen

atmosphere was maintained inside the furnace. Figure 2.16 shows a general set-up for TGA instrumentation.

## 2.6 References

1. *SC:1553-01 / EPI-REZ™ 5003-W-55*, Resolution Performance Products LLC, Houston, TX (2001)
2. *Bulletin R-972*, DSM NeoResins Inc., Wilmington MA (2004)
3. *Bulletin R-972*, DSM NeoResins Inc., Wilmington MA (2006)
4. *SC: 2857 / EPIKURE™ 6870-W-53*, Resolution Performance Products LLC, Houston, TX (2005)
5. *Bulletin CX-100*, DSM NeoResins Inc., Wilmington MA (2004)
6. Nookala R., Wang Y. and Van Ooij W.J., submitted for publication in Fifth International Symposium on Silane and other Coupling Agents, Toronto, Canada, (2005).
7. Zhu D., Ph.D. Dissertation, Department of Chemicals and Materials Engineering, University of Cincinnati (2002)
8. Tait W. S., *An Introduction to Electrochemical Corrosion Testing for Practicing Engineers and Scientists*, Pair O Docs Publications, Racine, WI (1994)
9. Scully J.R., Silverman D.C. and Kendig M.W., *Electrochemical Impedance: Analysis and Interpretation*, , editors, ASTM (1993)
10. *Electrochemical Impedance Spectroscopy Primer*, Gamry Instruments Inc., Website: <http://www.gamry.com> (2005)

11. Davis G.D., Dacres C.M., U.S. Patent 5,859,537, January 12, 1999. Davis G.D. and Dacres C.M., U.S. Patent 6,054,038, April 25, 2000. Davis G.D. and Dacres C.M., U.S. Patent 6,313,646, November 6, 2001. Davis G.D., Dacres C.M., and Krebs L.A., U.S. Patent 6,328,878, December 11, 2001
12. Mansfeld F., *Corrosion* 37, 301 (1981)
13. Kendig M., Mansfeld F. and Tsai S., *Corrosion Sci.* 23, 317 (1983)
14. Kendig M. and Scully J., *Corrosion* 50, 527 (1989)
15. Scully J.R., *J. Electrochem. Soc.* 136, 979 (1989)
16. Tait W.S., *J. Coat. Technol.* 61, 57 (1989)
17. *Ford Laboratory Test Method*, BI-23-1 (1981)
18. Hartland S., *Surface and Interfacial Tension: measurement, theory and applications*, Basel Marcel Dekker, New York, NY (2004)
19. Socrates G., *Infrared Characteristic Group Frequencies*, John Wiley & Sons Inc., New York, NY (2001)
20. Macomber R.S., *NMR spectroscopy : basic principles and applications*, Harcourt Brace Jovanovich, San Diego, CA (1988)
21. Fawcett A. H. , *Polymer Spectroscopy*, John Wiley & Sons, West Sussex, England (1996)
22. Bauer H.H., Christian G.D., O'Reilly J.E., *Instrumental analysis*, Allyn & Bacon Inc., Boston, MA (1978)
23. Lee R.E., *Scanning electron microscopy and X-Ray microanalysis*, Prentice Hall, Englewood Cliffs, NY (1993)
24. Brown M.E., *Introduction to Thermal Analysis: Techniques and Applications*, Springer, Washington, DC (2001)

### **3. SUPERPRIMER FORMULATIONS AND THEIR PERFORMANCE EVALUATION**

This chapter focuses on the formulation and development of the superprimer coating system for AA 2024-T3. The formulations were developed as a part of the Strategic Environmental Research and Development Program (SERDP) project, a joint undertaking by Department of Defense (DoD), Department of Energy (DoE) and Environmental Protection Agency (EPA). This project which had a timeline of September 2003 to September 2007 was intended for development of chromate-free, low-VOC primer systems for DoD metals. I had the opportunity to work on this project from March 2005 to April 2006. Extensive work had been done by Van Ooij et al. on development of chromate-free, superprimer coating systems, cured at elevated temperatures, for hot-dip galvanized steel and aluminum alloys [1, 2]. Superprimer coatings had been devised for aluminum alloys which had excellent corrosion resistance, adhesion and durability. However, there was need for a superprimer coating system for aerospace aluminum alloys which had low-VOC content, cured at room temperature and possessed appreciable low temperature properties. The following sections give an overview of the process for selection of materials, some successful formulations, their properties and performance evaluation.

### **3.1 Novolac epoxy-based superprimer**

#### **3.1.1 Novolac epoxy resin and curing agent**

Epoxy novolac resins are produced by acid-catalyzed condensation of a phenolic precursor with formaldehyde, followed by glycidation with epichlorohydrin. The relatively high epoxide functionality of epoxy novolac resins leads to an increased cross-link density, which results in better chemical resistance and thermal properties compared to that achieved with standard Bisphenol A or Bisphenol F resins in parallel primer systems [3]. Epoxy novolac resins are therefore seen as high performance products for a broad range of applications. Most of the previous superprimer work in our research group was based on epoxy resins as major binders but the potential of novolac resins was hardly explored. With all the aspects of the final coating system taken into consideration, novolac epoxy resins were chosen as the major binder resins for this superprimer. EPI-REZ 5003-W-55, which is a water-based zero-VOC epoxy novolac resin, was used in this work as mentioned earlier in Chapter 2.

The novolac resin required the right type and amount of curing agent or hardener and temperature in order to form a cured film. EPIKURE 6870-W-53, a water-borne epoxy-amine adduct cross-linker with low VOC levels, was chosen as the curing agent based on the recommendations of the resin manufacturer. Properties obtained in cured coatings vary in accordance with the epoxy-to-hardener ratio. The amount of water absorbed or diffusing through the film depends on the amine content which can affect the corrosion-inhibiting properties of these films [4]. Hence, the ratio of resin to curing agent had to be chosen appropriately. Although the weight ratio of EPI-REZ 5003-W-55 and EPIKURE

6870-W-53 for a cured coating recommended by the manufacturer was 55:45, various combinations of the two components in weight ratios ranging from 90:10 to 50:50 were prepared. The two components were mixed in a beaker using a magnetic stirrer till the formulation became homogenous. Coatings were made using the formulation on AA 2024-T3 samples using a draw-down bar, as mentioned in Chapter 2. After curing for 14 days at room temperature, the coatings were examined in certain tests such as solvent resistance, and contact angle measurement. To observe the effect of high temperature curing, the solvent resistance test was also performed on coatings cured at 70° C (referred to as high-temperature curing from here onwards). The formulations of the two components are mentioned in Table 3.1 and their respective contact angle and MEK double-rub values are indicated in Table 3.2. The formulation ND-20 showed the best performance in terms of contact angle and MEK double-rub values. The ratio of the components in the ND-20 formulation seemed to have a beneficial effect on the cross-linking density and water-barrier properties. The pencil hardness for this formulation was found to be 1H which was decent for a room-temperature-cured coating. Based on these initial findings, ND-20 was chosen as the base formulation for further modifications.

### **3.1.2 Addition of polyurethane resin**

For applications on aircraft wings and other parts, coatings need to sustain cyclic stresses at low temperatures during flight. Since this was a prime area of concern in this project, a coating which had good flexibility at room temperature as well as sub-zero temperatures was desired. It was observed that the novolac epoxy resin formed a hard coating when combined with the curing agent and was brittle at low temperatures. Therefore, some sort

of modification in the formulation was required. During a project in 2004, Van Ooij et al. had developed a polyurethane-based superprimer which showed excellent sub-zero temperature behavior. Based on the encouraging results obtained in that work, the idea of incorporation of polyurethane into the novolac-based superprimer system occurred. After a thorough search, two aqueous polyurethane resin dispersions, NeoRez R-972 and NeoRez R-960, were used as minor additives to enhance the low-temperature properties and flexibility. The amount in which polyurethane was added in the formulations was carefully controlled to avoid gelling or precipitation. As the polyurethane resins had high reactivity, the addition of polyurethane was preferably done in the end during the preparation of all the formulations containing it.

The polyurethane resin was very reactive towards the EPIKURE curing agent. The amine groups in the curing agent seemed to react instantly with the urethane groups from the resin [4]. This caused a rise in the viscosity of the superprimer system. Based on a number of experiments, it was found that the formulations containing more than 15 wt.-% of polyurethane severely jeopardized the viscosity of the superprimer. Hence, the maximum amount of polyurethane addition was limited to 15 wt.-% of the formulation. Some formulations containing these polyurethane resins with silanes are cited in Table 3.3. Table 3.4 gives the contact angle and MEK double-rub values for these formulations. The polyurethane certainly seemed to improve the curing rate at room temperature by enhancing the solvent resistance as evident from the increased MEK double-rub values. Polyurethane additions between 10 to 15 wt.-% performed at similar levels with slight enhancement in performance with increasing polyurethane content. The water resistance

also improved to certain extent which was apparent from the slight increase in the water contact angle. The improvements in these properties of the superprimer coating can be attributed to the beneficial effect of polyurethanes and the presence of silanes, which will be discussed in the following section.

### **3.1.3 Appropriate choice of silane**

Silane is believed to be the core of the superprimer system and is the chief contributor of the corrosion resistance and adhesion characteristics of the coating. A silane can also enhance other properties such as hydrophobicity, hardness, solvent resistance and chemical resistance [5]. The type and amount of silane, its functionalities, molecular weight and the stability of siloxane bonds formed govern the extent of these properties. Therefore, the choice of silane has to be a calculated process. In this study, silanes were carefully chosen based on their properties and past applications in pretreatments for corrosion protection of metals. Only bis-silanes were considered because of their obvious advantages over mono-silanes in term of desired properties as discussed earlier in Chapter 2 [6]. Following is a brief account of the silanes used in this study and their effect on the performance of the superprimer coatings:

#### **(a) Bis-sulfur silane**

Bis-sulfur silane, a solvent-based silane insoluble in water, had been used successfully in many superprimer formulations by Van Ooij et al. at the University of Cincinnati [7]. Neutron reflectivity studies with bis-sulfur films showed that they are hydrophobic, resistant to the action of boiling water and seem to show reconstruction of the siloxane and metallo-siloxane bonds upon drying [8]. In this study, bis-sulfur silane was used in

the novolac-based superprimer formulations to impart better water-barrier properties and corrosion resistance. It was believed that a pure silane would consume some of the water of the resin to hydrolyze itself over a period of time. Pure bis-sulfur silane formed an emulsified solution when mixed with novolac resin after 2-3 hours of continuous stirring. However, stirring was continued over a period of 24 hours to ensure a high degree of emulsification. The curing agent was added to the mixture of novolac resin and bis-sulfur silane and stirred vigorously till a homogenous solution was obtained. Polyurethane resin was added as the last ingredient. The formulations were then applied on cleaned AA 2024-T3 panels using a draw-down bar. The superprimer formulations with bis-sulfur silane N-1, NP-1, NP-2 and NP-3 are cited in Table 3.3 and Table 3.4 gives the properties of these coatings. The increased contact angle values indicated an improved resistance against water penetration. In N-1 formulation, slight increase in MEK double-rub values at room temperature suggested improved solvent resistance due to addition of bis-sulfur silane. Though the polyurethane by itself formed a very soft coating of hardness 5B, it appeared to have produced a synergistic effect on the enhancing the hardness of the NP-1 coating to 2H. A similar effect was not observed in NP-2 or NP-3.

**(b) Bis-[triethoxysilyl] ethane (BTSE)**

Hydrolyzed BTSE had been used in superprimer formulations earlier by Van Ooij et al. In this study, unhydrolyzed BTSE was incorporated in some formulations as the silane component. It was believed that BTSE would possibly hydrolyze over a period of time using the water in the resin. This was just a trial formulation to see whether BTSE was able to perform to the same level as bis-sulfur silane. The procedure for preparing the formulations was similar to the one followed in the bis-sulfur formulations. The

formulation for BTSE is shown in Table 3.3. The polyurethane NeoRez R-960 was used in superprimer formulations with BTSE because of their better compatibility. BTSE, being highly hydrophobic and solvent-based, dispersed poorly in water-based formulations. Due to the higher solvent content in NeoRez R-960, BTSE mixed homogeneously into this formulation. The formulations were applied on the cleaned AA 2024-T3 panels. Table 3.3 shows the formulation NP-4 containing BTSE and Table 3.4 shows its properties. Increased water contact angle was the trait incorporated by the highly hydrophobic BTSE. Consequently, the films of this formulation took longer time than other coatings to cure at room temperature. A slight increase in MEK resistance was also observed.

#### **(c) AV5 silane mixture**

Bis-amino silane has hydrophilic secondary amino groups, which tend to be protonated in the presence of water. The resulting positive charge on these groups attracts detrimental ions like  $\text{Cl}^-$ ,  $\text{SO}_4^{2-}$ , etc., which accelerate corrosion of the metal substrate. Neutron reflectivity studies of bis-amino silanes films confirmed that they are very hydrophilic and tend to degrade in the presence of boiling water [8]. However, a synergistic ratio of bis-amino silane and vinyltriacetoxysilane or VTAS (5:1 by volume) known as AV5 is known to have unique properties and better performance than the individual silanes [5]. AV5 silane had been studied extensively by Van Ooij et al. at the University of Cincinnati. In this study, AV5 was used along with the novolac resins in some formulations. The formulations N-2 and N-3 presented in Table 3.3 are the two formulations with AV5 as the silane. Polyurethane resins were highly reactive towards

the AV5 silane and hence, were not used in N-2 and N-3 formulations. Curing of coatings was done at 70° C to ensure faster drying and crosslinking of these formulations.

Elevated temperature curing obviously did improve the crosslinking in the coating which was evident from the high MEK double-rub values. The water contact angle in these coatings was low due to the highly hydrophilic nature of the components, especially the AV5 silane.

### **3.1.4 Corrosion inhibitors**

In this study the focus was on a class of inhibitors which have the potential to be effective on AA 2024 such as zinc phosphate, calcium zinc molybdate and sodium meta-vanadate [9]. The commercially available non-chromate inhibitor pigments discussed in Chapter 2 were incorporated into the novolac-based superprimer coatings to impart defect healing and enhance corrosion resistance. Corrostatin 228, a commercially produced synergistic mixture of zinc phosphate and calcium silicate, was also used. Various formulations of superprimer coatings incorporated with these pigments are mentioned in Table 3.5.

The inhibitor pigments were added before the addition of curing agent to the silane-resin mixture. This ensured proper dispersion and prevented coagulation of the pigment particles. Initial mixing was done by mechanical stirring for 30 to 45 minutes. Following this, the formulations were subjected to vigorous mixing in the high-shear blender at 2000 rpm for 10-12 minutes. The high-shear blender aided in the micro-dispersion of the pigments. The formulations were then applied on the cleaned AA 2024-T3 panels. Solvent resistance data for these coatings is summarized in Table 3.6. From the observed

double-rub values, it was found that the addition of pigments to the superprimer slightly lowered its solvent resistance. However, a slender improvement in the values was observed with longer curing times. This behavior could be attributed to the pigments affecting the rate of the curing reaction. The water contact angle was also found to be reduced by some magnitude, which could be due to the formation of a rough surface. The effectiveness of these inhibitors will be discussed in more details later in this chapter.

### **3.1.5 Other filler pigments**

Titania was used in this study with the aim of improving the mechanical hardness and scratch-resistance and reducing the porous volume in the coatings. Titania was added at the same stage at which inhibitor pigments were added to the formulation. This particular formulation did not contain any inhibitors and polyurethane, as the aim was to observe the effect of titania on certain mechanical properties of the novolac-based coating. The high-shear blender was used to break down the aggregate titania particles which were insoluble in water. The scratch resistance and hardness (pencil hardness - HB) of the coating in the nickel test improved due to addition of titania.

Aluminum paste has been used regularly in topcoat formulations on automotive bodies as opalescent pigments which enhance the appearance. The lubricant layers impart low density which causes the aluminum particle to float and thereby form a layer at the top of the coating. Leafy aluminum paste, consisting of flat or spherical aluminum particles with fatty acid lubricant layers, was used as a filler material on a trial basis in superprimer formulations. It provided a metallic luster to the film and significantly increased its

barrier property [2]. Increase in the pencil hardness value (pencil hardness - 1H) confirms the effect of aluminum paste on the mechanical properties of the coating. Superprimer formulations containing filler pigments are shown in Table 3.7.

### **3.1.6 Minor additives**

Cross-linking of silanes typically proceeds slowly at room temperature. In order to accelerate this process, catalysts such as tin salts have been often used [10]. In this study, dibutyltin dilaurate (DBTL) was used as a crosslinker for solvent-based silanes such as bis-sulfur. N-1 formulation containing DBTL was prepared to observe its effect on curing and corrosion resistance imparted by the superprimers. DBTL was added in the amount of 0.5 wt % of the silane as the last component before the application of the coating. An increase in film hardness (pencil hardness - HB) was observed along with faster drying time at room temperature. These improvements indicated an improvement in the extent of cross-linking. The effect of DBTL on corrosion resistance will be discussed later in this chapter.

NeoCryl<sup>®</sup> Crosslinker CX-100, a polyfunctional aziridine, was used as a crosslinker for the polyurethane resins. It was especially helpful in spray-coat formulation which was very dilute compared to the original formulations. CX-100 addition further improved water and chemical resistance as well as enhanced adhesion to substrate [6]. Surfynol MD 20 and Surfynol DF 110L defoamers were used to avoid foaming and to drive out air bubbles from the formulations. Defoamers were added in the amount of 1-2 wt.-% of the wet formulation. A wetting and dispersing agent, BYK P 104 S, was used to aid uniform dispersion and prevent agglomeration of the various pigments.

### **3.1.7 Co-solvents**

Solvents are used in coating formulations to facilitate rheological changes and improve stabilization of the individual components. They are also meant to extend the pot-life of the formulation and control viscosity before the application of coating. In these experiments, the solvents used in the formulations had to be VOC-free in order to maintain a low-VOC system. Water was the most commonly used solvent for superprimer formulations in this study. During spray-coating, water was used to dilute the formulations to the desired viscosity. To facilitate room temperature drying, acetone, which is not considered as a VOC solvent, was used in some formulations. Many VOC-free co-solvents, which are commercially available, need to be explored to obtain a broader range of solvents for the novolac-based superprimer.

### **3.1.8 Formulation for spray coating**

The original NP-1 formulation had to be modified in terms of viscosity and pigment dispersion. Poor dispersion of the pigments and high viscosity of the formulation could have affected the quality of the spray coating and clogged the spray gun nozzle. The viscosity was adjusted using solvents such as water and acetone. But acetone being volatile, did not serve the purpose of reducing the viscosity to the desired level as done by water. Hence, water was the only solvent used in spraying formulations. A finer grade of zinc phosphate from Alfa Aesar was used as corrosion inhibitor pigment. This pigment had a good dispersion in the water-based formulation. Surfynol MD-20 defoamer, BYK P-104 dispersing agent and CX-100 crosslinker were added in minor amounts. The formulation for spray coating is shown in Table 3.8.

## **3.2 Control coatings**

CA 7233 High solids chromated epoxy standard military primer and its activator component CA 7233 B were mixed in the ratio 1:1 by volume and applied on chromate-pretreated AA 2024-T3 panels. The coatings were left to cure at room temperature. The topcoat Desothane HS CA-8214/F36173, mixed with its activator component in the volume ratio 3:1, was applied within 8-16 hr time frame after the application of the primer coating. This ensured good adhesion between primer and topcoat and avoided cracking of the topcoat. Both the control as well as the superprimer coatings was topcoated with Desothane topcoat. The topcoat Defthane ELT MIL-PRF 85285 D was used in coatings prepared for outdoor exposure test in Florida. The primer and the topcoat were applied using draw-down bars. Table 3.9 (a) and (b) shows the formulations for the control coatings.

## **3.3 Performance Test results and evaluation**

### **3.3.1 Salt Water Immersion Test**

Salt water immersion test was carried out on coatings as a screening test to determine formulations showing promising performance, as described earlier in Chapter 2. Figures 3.1 to 3.3 show images for coating formulations ND-20 (RT cured and HT cured), N-1 (RT cured and HT cured), and NP-1 with and without inhibitors after exposure in 3.5 wt.-% NaCl. The immersed coatings and the scribed surface were examined for evidence of corrosion or any other kind of deterioration. In the ND-20 formulations, blisters were observed in both coatings along with some corrosion products especially at the scribes. The rest of the coating remained mostly intact with no delamination but slight

discoloration in the coating cured at room temperature. The role of silane towards improvement in corrosion resistance of the coating was evident from the results for N-1 formulation. There were hardly any blisters along the scribes and no delamination was detected. White rust was visible in the scribes but that was expected as no corrosion inhibitors were incorporated in these coatings. The coatings with NP-1 formulation without inhibitors suffered only minor scale white rusting with no discoloration or delamination. In the NP-1 formulation with zinc phosphate as inhibitor, scribes were mostly clean even after 60 days of salt water immersion. The effect of corrosion inhibitors on scribe protection was obvious and also addition of polyurethane actually improved the performance of the coating. There was no delamination or blistering observed even on the scribed part. The salt water immersion test, thus, gave primary indications about the advantage of silane in enhancing corrosion resistance and water-barrier properties of the coating.

### **3.3.2 Electrochemical Impedance Spectroscopy**

In this study, EIS was used as a tool for electrochemical testing and characterization of superprimer coatings. EIS testing was conducted on superprimer coatings without corrosion inhibitors. Only Bode impedance plots will be discussed in this chapter since it is beyond the scope of this thesis to elucidate the complex nature of Bode phase and Nyquist plots. Figure 3.4 shows the Bode impedance plot for ND-20 and N-1 formulation after 14 days of EIS testing. The impedance value at 1 mHz frequency was higher for N-1 than for ND-20. This showed the improvement in the corrosion resistance due to silane addition. A gradual decreasing trend in the impedance values was observed in both cases. However, the decrement of the impedance values was considerably greater in case of

ND-20 formulation than in N-1 formulation. Also, at higher frequencies, the curve for ND-20 formulation shifted downwards which indicated electrolyte or water absorption by the coating possibly resulting in delamination. Occurrence of more than one time constant also confirmed that the coating layer was breached.

Figure 3.5 shows Bode impedance plots for NP-1 formulation. In these curves, the modulus at high frequency (1 MHz) remains almost constant which points to the conclusion that there was no change in solution resistance. It means there was hardly any absorption of water or electrolyte by the coatings. Figure 3.6 shows Bode impedance plots for the N-2 coating cured at high temperature. The extremely high impedance value of more than 100 M  $\Omega$  was a result of a high degree of crosslinking obtained from the high temperature curing. Even after 41 days of EIS testing, no major variation or shift in the curve pattern was observed. This confirmed that there was hardly any absorption of electrolyte by the coating and it remained intact throughout the course of the test. Figures 3.7(a) and (b) show images of ND-20 and NP-1 coatings after 30 days of exposure to EIS. The effect of silane was obvious from the appearance of the exposed parts of the coatings. There was considerable discoloration and a hint of corrosion in the ND-20 coating. On the other hand, the NP-1 coating showed no visible difference between the exposed and the unexposed part. No evidence of corrosion or discoloration was observed.

EIS curves depicting low-frequency impedance values of superprimer coatings subjected to salt spray test were obtained from DACCO SCI. These instantaneous readings were acquired using the EIS sensor which was mentioned earlier in Chapter 2. Figure 3.8 shows the low-frequency impedance plot for the control coatings C1 and C2 exposed to

salt spray test. The impedance values remain very high for these coatings as per expectations. Figures 3.9 and 3.10 show similar plots for superprimer coatings with and without corrosion inhibitors. The impedance values for various superprimer formulations dropped initially but stabilized later on. Even after more than 120 days, the impedance readings remained more or less constant. Similar impedance plots for superprimer coatings with a topcoat showed higher impedance values but essentially followed a trend similar to that of the superprimer coatings.

The low-frequency impedance curves apparently indicated that the controls performed better than the optimized superprimer formulations. However, we need to understand that the controls have high chromate pigment content and are solvent based. The superprimer coatings are water-based and contain much lower amount of inhibitor pigments compared to the controls. The mechanism of inhibitor leaching in the superprimer is dependent on the water that is being absorbed by the coating. The impedance data from EIS is a gauge for tendency of a coating to absorb water. Water-based coatings are prone to absorb water which does not essentially indicate failure or inferior performance [11]. It is believed that the superprimer coatings contain sizable amount of voids due to the interpenetrating network formed between the silane and the resins. When water is absorbed by the coating, it actually fills these voids and no swelling of the coating occurs. Hence, it does not affect the adhesion of the coating to the substrate or the topcoat. Furthermore, these readings were obtained during the course of the salt fog test. Hence, these impedance readings do not essentially pass a judgment about the performance of the coatings and should only be referred to observe possible trends in the performance. Probable

mechanism of inhibitor-leaching in water-based coatings and its advantages will be discussed in Chapter 4.

### **3.3.3 Tape Adhesion Test**

Tape adhesion tests were performed according to ASTM D 3359 standard on superprimer coatings to illustrate the role of silane in improving adhesion to the substrate and the topcoat. Figure 3.11 shows the images of some coatings subjected to the adhesion test. For ND-20 formulations, a slight delamination was observed in the dry adhesion test. The N-1 formulation did not show any delamination in the dry adhesion test. Even in wet adhesion test, no delamination was found which affirmed the effect of silane in improving the adhesion. According to the ASTM 3359 standard, the adhesion of the superprimer can be classified as 4A as compared to 5A for the control coating. Topcoat adhesion to the superprimer was also excellent (classification 4A) for all the novolac formulations. However, topcoat adhesion depended on the time interval between the application of superprimer and the succeeding topcoat.

### **3.3.4 Chemical Resistance Test**

The superprimer coatings were subjected to chemical resistance test using 6 N HCl and 6 N NaOH. The polyurethane resin by itself is very susceptible to chemical attack from acid or base. However, novolac resins are known for their excellent chemical resistance. This property did not lose any of its credibility even in the superprimer formulations such as N-1 and NP-1. All the novolac-based superprimer coatings passed the chemical resistance test without any difficulty [12]. The coatings showed no effect of any chemical attack.

### 3.3.5 ASTM B117 salt spray and Ford Cyclic Tests

ASTM B117 salt spray test was conducted on the novolac-based coatings and controls at DACCO SCI. Results for the superprimer formulations with corrosion inhibitors such as zinc phosphate (Phosguard), Corrostayn 228, Molywhite CZM, and sodium metavanadate and fillers such as titania and aluminum paste are discussed in this chapter. Figures 3.12(a) and (b) show the images for ND-20 and N-1 coatings after 1000 and 1500 hours of exposure in salt spray test respectively. The ND-20 formulation showed substantial blistering and corrosion. In case of N-1, initial blistering was observed but the extent of corrosion was much lower. Bis-sulfur silane improved the corrosion resistance of the coating. Figures 3.13(a) and (b) show the N-1 formulation with zinc phosphate and CZM as corrosion inhibitors after 2000 hours of salt spray test. There was an obvious improvement in the performance due to addition of zinc phosphate which acted in a beneficial way to protect the scribes from corrosion. The same effect was not observed for CZM as corrosion inhibitors. The coating failed miserably and consequently, CZM was no longer used in this study. These results suggested that corrosion inhibitors needed to be chosen carefully and were not guaranteed to be effective in all formulations.

Figure 3.14 (a) shows the NP-1 formulation coating after 2000 hours of salt spray exposure. The performance was improved due to the synergistic effect produced by the silane, novolac resin and polyurethane resin. There was considerable white rust in the scribes with a hint of blistering. The rest of the coating remained clear of any corrosion or delamination. Figures 3.14(b), (c) and (d) show the NP-1 formulation containing various inhibitors after 2500 hours of salt fog exposure. The effect of scribe protection or defect healing was generated by all three corrosion inhibitors. A hint of corrosion on scribes was

observed but large parts of the scribes remained clean and free from white rust. Some spots on the coatings which resembled blisters were actually due to poor dispersion of the pigments. This problem was later eliminated by the use of finer grades of pigments. Figure 3.15 shows images of N-1 formulation with DBTL, titania and aluminum paste as additives, exposed to ASTM B117 test. As these coatings did not contain any corrosion inhibitors, there was corrosion at the scribes and some parts of the coatings. However, the presence of filler pigments did not have any adverse effect on the performance. Moreover, a hiding effect was produced by the aluminum pigments. The onset of pitting was observed in unscribed samples containing aluminum paste and DBTL.

The topcoated NP-1 coating with zinc phosphate after 2000 hours of salt spray exposure is shown in figure 3.16 (a). The inhibitor seemed to be less effective in the presence of a topcoat as a lot of white rust was visible in the scribes. This issue needs to be investigated further in future. Figures 3.16 (b) and (c) show the control primer without (b) and with (c) topcoat after 2000 hours of salt spray test. The C1 coating showed no blistering or scribe creep which was expected. There was a slight hint of corrosion products on the scribes. The ineffectiveness of the chromate pigments in the presence of a topcoat was also clearly evident from the salt fog image for sample C2. A lot of white rust appeared on the scribes and the performance was very similar to a topcoated superprimer coating. Figure 3.17 show images of two topcoated superprimer coatings subjected to 25 cycles of the Ford AGPE test. The Ford test is more aggressive in comparison with the salt fog test and is recommended mainly for coatings on automotive substrates. Hence, a substantial amount of white rust was observed in the scribes of these topcoated superprimer coatings

with a hint of scribe creep. Still, it could be concluded that the coatings performed to a satisfactory level in this test.

Based on the observations from the B117 test results, it is fair to say that the performance of topcoated and non-topcoated superprimer formulations is on par if not better than that of chromated control primer. As per expectations, the chromated controls perform remarkably. The high VOC content (~340g/L) of the control primer and the chromate conversion coating on the substrate obviously play a major role in enhancing the corrosion resistance provided by the control samples. Furthermore, the control primer is solvent-based which aids in resistance against water penetration and better dissolution of binders. This results in a better cross-linked film [13]. A substantial amount of 30 wt.-% of the highly-efficient strontium chromate inhibitor imparts excellent defect healing properties. The superprimer formulations are water-based and contain lower quantity of corrosion inhibitors as compared to the chromate-based control. Water, being a polar solvent, can pose a threat to the stability of dispersions if added in excess. This, in turn, can lead to blistering, porous films and low cross-link density. In water-based coatings, there ought to be some amount of water absorption or penetration leading to swelling and delamination [11].

However, this excess water could also serve as an advantage especially for better leaching of pigments. The presence of silanes and other minor additives also help in using up this water in hydrolysis and other reactions and trap water in an interpenetrating crosslinked network. Silane also greatly enhances the adhesion to the substrate as well as to the topcoat. Moreover, the inhibitor pigments present in sufficient amounts can

actually use these water channels for effective leaching to the defects or the exposed metal substrate to prevent corrosion. This leaching effect has been observed in the ASTM B117 test results of the superprimer coatings. The low-VOC non-chromated superprimer coatings with zinc phosphate, Corrostayn 228 and sodium meta-vanadate show minimal scribe corrosion, and none of these formulations show any blistering or delamination in the scribes or the coating area.

### **3.3.6 Bend Test**

Figure 3.18 shows images of superprimer coatings subjected to a room-temperature bend test and then exposure to 3.5 wt.-% NaCl solution for a period of 30 days. The ND-20 formulation showed huge cracks after bending because of its extreme brittleness. It also suffered from extensive corrosion on the cracks as well as the rest of the coating. The N-1 formulation was slightly less brittle after bending and only the cracked part of the coating suffered from corrosion. The NP-1 formulation showed no cracking at room temperature bending and remained intact even after exposure to salt water immersion. The bend test results confirmed the role of silane in providing corrosion protection and the flexibility and resistance to cracking imparted by the addition of polyurethane to the novolac-based superprimer. Bending was also done at sub-zero temperature NP-1 coatings at  $-70^{\circ}$  C. There was some amount of cracking observed in the coating but still the coating performed well in salt water immersion test. Extensive low-temperature testing of these coatings could be the subject of emphasis for future work.

### 3.4 Summary

The experiments and performance test have demonstrated the following facts about the superprimer coatings:

- a) Incorporation of the silanes such as bis-sulfur, improves the anti-corrosion performance, water-barrier properties and adhesion characteristics of the novolac-based superprimer coatings.
- b) Corrostatin 228, zinc phosphate and sodium metavanadate have been effective in providing corrosion inhibition to the superprimer coatings on AA 2024-T3.
- c) The polyurethane resin enhances flexibility and low-temperature behavior of the novolac-based superprimer while further improving solvent resistance and adhesion.
- d) Titania and leafy aluminum paste increase the hardness of the N-1 superprimer while improving the water-barrier properties. DBTL accelerates room-temperature curing of the superprimer.
- e) The complete topcoated superprimer system performs competitively vis-à-vis the topcoated control coating. This can be verified from the ASTM B117 salt spray test results.

Some prominent properties of the NP-1 formulation are mentioned in Table 3.10. The next chapter gives the account of an effort made in this study to investigate the interaction of the superprimer components. A possible mechanism for the working of inhibitors in the superprimer was also investigated with the help of various characterization tools.

### 3.5 References

1. Mugada T., *M.S. Thesis*, Dept. of CME, University of Cincinnati (2006)
2. Shivane C. *M.S. Thesis*, Dept. of CME, University of Cincinnati (2006)
3. *SC:1553-01 / EPI-REZ™ 5003-W-55*, Resolution Performance Products LLC, Houston, TX (2001)
4. Bauer R.S., *Epoxy Resin Chemistry II*, ACS Symposium Series 221, Washington D.C. (1983)
5. Zhu D., *Ph.D. Thesis*, Dept. of CME, University of Cincinnati (2005)
6. Arkles B. and Larson G., *Silicon Compounds: Silanes and Silicones*, product catalogue by Gelest Inc., Morrisville, PA, 168 (2004)
7. Zhu D. and Van Ooij W.J., *Corrosion Science* 45, 2163 (2003)
8. Pan G. and Schaefer D.W., submitted for publication in *Silanes and Other Coupling Agents*, 4, K. L. Mittal, ed., 2005, Canada; June 22- 24, 2005
9. Van Ooij W.J., Zhu D., Palanivel V., Lamar, J.A. and Stacy M., *Silicon Chemistry* (September 2002)
10. Suryanarayanan K., *M.S. Thesis*, Dept. of CME, University of Cincinnati (2006 )
11. Satas D. and Tracton A.A., *Coatings Technology Handbook, 2<sup>nd</sup> Ed.*, Marcel Dekker, Inc., New York, NY (2001)
12. Wegmann A., *Prog. Org. Coat.*, 32, 231 (1997)
13. Athey R.D. *Testing Coatings for Solvent and Chemical Resistance*, Athey Technologies, El Cerrito, CA (August 2000)

## **4. CHARACTERIZATION STUDY OF SUPERPRIMERS**

An effort was made to understand the chemistry and bonding mechanisms in the superprimer using various characterization tools. NMR and FTIR spectroscopic studies were performed to investigate chemical and structural changes in the superprimer coatings. SEM/EDS analysis was performed to explore the role of corrosion inhibitors in corrosion protection of the substrate. TGA and DSC were used to study the thermal stability of the superprimer coatings. This chapter gives an account of the results and conclusion derived from the characterization of superprimer formulations discussed in earlier chapters.

### **4.1 NMR Spectroscopy**

#### **4.1.1 Sample Preparation**

NMR Spectroscopy was used to collect information on the chemical reactions taking place in the superprimer coating. NMR was carried out on liquid and solid samples of the superprimer. Individual components of the superprimer including the silanes and the resins were studied in as-obtained liquid form for reference using the  $^{13}\text{C}$  NMR technique. Certain combinations of the superprimer components were also studied in liquid state to understand their mutual interactions. Using the same technique, the superprimer coating system was studied in the liquid form as well as the solid or cured form. Cured superprimer samples for NMR were obtained by scraping a coated substrate using an ordinary blade. The residue was ground to a powder form using mortar and pestle. Ethanol was added to all the formulations to prepare the NMR samples. The NMR

spectra thus obtained were analyzed for the appearance of new peaks and changes in the peak position with time which could possibly indicate some chemical interaction between the components of the superprimer.  $^{29}\text{Si}$  NMR was not considered for the superprimer coatings because initial studies showed that the silicon (or silane) content was too low to be detected by this technique.

#### 4.1.2 Liquid State $^{13}\text{C}$ NMR

All the individual components of the superprimer were first analyzed in liquid state  $^{13}\text{C}$  NMR. Based on the information obtained from the manufacturer and literature, representative chemical structures for all the superprimer components were made. Approximate  $^{13}\text{C}$  NMR peak positions were calculated using ChemWindow software at Oklahoma State University. For all these materials, the observed NMR spectra correlated well with the resonances calculated by the software. Due to the rapid isotropic motion of molecules in the liquid, narrow spectral resonances usually constitute a liquid-state NMR spectrum.

The DGEBA resin is the base component of the novolac epoxy resin, as mentioned in the product data sheet provided by the manufacturer of the resin. The chemical structure and  $^{13}\text{C}$  NMR peak positions of the typical DGEBA water-based epoxy resin with 2-propoxyethanol as a co-solvent is shown in Figure 4.1. The  $^{13}\text{C}$  NMR spectra and the representative structures of various superprimer components along with their calculated peak positions for resonance of each type of carbon atom are shown in Figures 4.2 to 4.6.

Peaks assigned to ethanol added to prepare NMR samples are marked so that they can be distinguished from the peaks due to the components [1].

EPI-REZ 5003 is a nonionic aqueous dispersion of a polyfunctional aromatic epoxy resin. It contained a lot of epoxide groups as characterized by the two peaks at approximately 50 and 44 ppm (refer Figure 4.2). The intensities of these peaks assigned to the epoxide functionality appeared much more intense than in any of the other resin systems that have been investigated pertaining to the superprimer. The C-OH peak at approximately 69 ppm was the other reactive peak of interest in the spectrum. Peaks corresponding to the phenyl carbons of the novolac resin also appeared prominently in the spectrum. The rest of the peaks could be assigned to the DGEBA backbone. The NMR spectrum indicates that the novolac resin can be combined with dicyandiamide, polyamides, and aliphatic and aromatic amines to obtain a cured coating. EPIKURE 6870 is a 53% solids, non-ionic aqueous dispersion of a modified polyamine adduct curing agent with a high molecular weight and no solvents. The C-OH peak appeared prominently at approximately 69 ppm (refer Figure 4.3). Epoxide peaks with low intensities were visible in the region between 40 and 50 ppm.

The spectrum for bis-sulfur silane shows distinguished peaks corresponding to the ethoxy groups at around 58 ppm (refer Figure 4.4). Peak positions in the spectrum correlated well with the calculated peaks. NeoRez R-972 is a polyurethane resin, containing urethane polymer, water, N-methyl-2-pyrrolidone (NMP), triethylamine (TEA) and surfactant. The peaks assigned to the solvent NMP appeared distinguishingly in the

spectrum (refer Figure 4.5). Small peaks corresponding to carbon atoms in urethane group and TEA were also visible. CX-100 crosslinker, which is a polyfunctional aziridine liquid crosslinker used with waterborne urethane polymers, had an eminent peak at approximately 34-35 ppm assigned to aziridine as seen in its NMR spectrum in Figure 4.6. The rest of the peaks corresponded to a propylene imine backbone.

In order to investigate initial reactions at the stage of mixing of the superprimer components, the formulations mentioned below were also analyzed using liquid state  $^{13}\text{C}$  NMR. Inhibitor pigments were not added to any of the formulations to avoid complications.

(1) **L-1:** EPI-REZ 5003 + NeoRez R-972 (1:1 by wt.)

This formulation was analyzed to determine whether there is any interaction between the epoxide and the urethane groups. The concern was whether these two resins could react in a way to affect the viscosity and thereby the pot-life of the superprimer. As shown in Figure 4.7, the NMR spectrum suggested that there were no significant changes in the intensities of the C-OH, C-O-C, epoxide, or urethane group intensities. Also, there was no appearance of any new C-OH peaks. This analysis suggested no vigorous reaction between the two components.

(2) **L-2:** EPI-REZ 5003 + DPC 6870 (4:1wt.)

This is the basic ND-20 formulation of the novolac resin and curing agent. This formulation was chosen for NMR analysis to determine the reaction between the two components and the starting point of the curing reaction. As seen in Figure 4.8, there was

no clear evidence of the reaction product as the peaks from the epoxide and the curing agent overlapped making them indistinguishable. It was believed that the components did not react immediately but curing occurred with time which will be demonstrated later from solid state NMR and FTIR results.

(3) **L-3:** Bis-sulfur silane + NeoRez R-972 (1:3 by wt.) + CX100 (5 wt.-% of NeoRez R-972)

This formulation was of interest mainly to observe if bis-sulfur silane reacts at all when mixed with the polyurethane resin. As observed in Figure 4.9, bis-sulfur silane did not appear to have reacted with the polyurethane at all. The two peaks corresponding to ethoxy groups in bis-sulfur silane remained intact. This suggested that the silane only reacted with the novolac epoxy resin and not the polyurethane which will also be evident later in this chapter. There was clear evidence of reaction between the resin and the crosslinker as expected. The C=C linkage disappeared indicating reaction at the double bond. The aziridine peaks at approximately 34 ppm had significantly decreased in intensity. The carboxylic acid peak at approx. 172 resulting from CX-100 reacted probably with the amine. A new peak at 55ppm was observed due to aziridine crosslinking product. The potential reaction product is also shown in Figure 4.9.

### 4.1.3 Solid State <sup>13</sup>C NMR

In contrast to liquid state NMR, solid-state NMR spectra comprise of relatively broad resonances due to chemical shift anisotropy caused by averaging of molecular structures and the static nature of the sample. As the solid state NMR spectra obtained were broad and overlapping, peak assignments were made based on the observed resonances in the

liquid-state spectra. Time-based solid-state  $^{13}\text{C}$  NMR analysis was performed on two coatings cured at room temperature as mentioned below. The primary objective was to determine the extent of hydrolysis of the silane with time and the rate of curing reactions.

(1) **S-1:** EPI-REZ 5003 (8 g) + EPIKURE 6870 (2 g) + Bis-sulfur silane (1.15 g)

This was the N-1 formulation without any inhibitors. The goal here was to obtain evidence for the hydrolysis of silane, if any.  $^{13}\text{C}$  NMR was done on solid samples of S-1 over a period of 30 days of curing at room temperature. Figure 4.10 shows the spectra for S-1 sample on day 1, day 15 and day 30. The peaks assigned to C-OH (64.5 ppm) and epoxide (53, 44 ppm) appeared to have significantly reduced in intensity with increasing curing times. This indicated reaction at the epoxide functionality due to the reaction between the novolac epoxy resin and the curing agent with time [2]. A new peak that grew at 62.5 ppm, which is assigned to C-O-Si bond formation, was also visible. It continued to grow in the curing period. This peak could have been the result of condensation reaction between Si-OH group from the silane and C-OH group on the novolac resin. This pointed to the possible conclusion about the hydrolysis of silane in the superprimer coating taking place with time.

Two unassigned peaks at 35 and 25 ppm possibly due to some reactants (R) were also observed which reduced in intensity with increasing curing time. New peaks at 42, 34, and 23 ppm grew in intensity during the curing period. These peaks were unassigned and were assumed to be reaction products (P) of the curing reactions between EPI-REZ 5003 and EPIKURE 6870, primarily epoxide-amine reactions. There were several possible reactions which could have resulted in these unassigned peaks. Epoxy group and an

amine could react to generate C-OH and N-H (secondary amine) functionalities. Also a reaction between the ethoxy groups of the bis-sulfur silane and the secondary amine from the novolac resin and curing agents could not be ruled out. The reaction between the secondary amine and epoxy groups also contributed to these peaks.

(2) **S-2:** EPI-REZ 5003 (8 g) + EPIKURE 6870 (2 g) + Bis-sulfur silane (1.5 g) + NeoRez R-972 (3 g)

This was the NP-1 formulation without any inhibitors and other minor additives. Figure 4.11 shows the solid state  $^{13}\text{C}$  NMR spectra of S-2 sample over a period of 30 days of room temperature curing. The reaction patterns and peaks are similar to those seen in S-1.

There was evidence of linkage between the novolac resin and the bis-sulfur silane as seen from the growth of the peak assigned to C-O-Si. The epoxide group peaks reduced in intensity indicating curing reaction of the novolac resin. However, the higher intensities of C-O-Si and some unassigned peaks could be attributed to the catalytic crosslinking reaction between the TEA present in NeoRez R-972 and the novolac epoxy resin. Further tests using the IR technique were conducted to corroborate these observations.

## 4.2 Infrared Spectroscopy

Infrared Spectroscopy was performed on superprimer coatings in order to obtain a picture of the chemical interaction between the different components of the superprimer. Coatings were made on AA 2024-T3 panels and the IR absorbance spectra were obtained using RAIR instrumentation at different curing times. IR spectra of some individual

components were also obtained for reference and peak assignment. References 3-8 were helpful in peak assignments for the IR spectra.

Fig. 4.12 shows the IR absorption spectrum of pure, non-hydrolyzed bis-sulfur silane. The peak assignments for bis-sulfur silane are given in Table 4.1. The  $(\text{C}_2\text{H}_5\text{O})_3\text{Si}$  functional groups are the most likely species for reaction. These groups can hydrolyze and form silanols (Si-OH) which further condense to form an -Si-O-Si- network. However, this reaction occurs only in the presence of water. The reaction between epoxy resin and bis-sulfur silane is also possible. The peak at  $960\text{ cm}^{-1}$ , which is assigned to asymmetric stretching of Si-O- in  $\text{Si}(\text{OC}_2\text{H}_5)_3$ , is a critical peak. RAIR was not performed on EPI-REZ 5003 as its films fails to cure without adding a curing agent.

Figure 4.13 shows a RAIR spectrum of EPIKURE 6870 and Table 4.2 gives the peak assignments for the same. The spectra for EPIKURE 6870 are very complex with the peaks due to primary and secondary amines overlapping with benzene overtones ( $2000\text{-}1600\text{ cm}^{-1}$ ). It was not easy to distinguish whether these peaks denote 1, 4 di-substituted benzene or 1, 2 and 1, 3 di-substituted benzene. The aromatic groups are, however, not of interest as they usually do not take part in curing reactions and require higher curing temperature. Peaks corresponding to primary and secondary amines are seen in the region  $3550\text{ to }3250\text{ cm}^{-1}$ . Primary amines ( $-\text{NH}_2$ ) are known to react with the epoxide group to form reaction products containing secondary amines ( $-\text{NH}$ ) and hydroxyl groups ( $-\text{OH}$ ). The  $-\text{OH}$  groups can also react to open the epoxide ring and form more  $-\text{OH}$  groups. Figure 4.14 shows the RAIR spectrum for NeoRez R-972 polyurethane resin and Table 4.3 shows the corresponding peak assignments. Peaks corresponding to N-H deformation

and C-N starch vibrations were visible. The broad peaks in the 2400 to 2700  $\text{cm}^{-1}$  can be attributed to various additives in the resins such as surfactants and dispersants.

#### **4.2.1 ND-20 Base Formulation**

Figure 4.15 shows the time-based RAIR spectra for the ND-20 coating cured at room temperature while Table 4.4 shows the peak assignments for these spectra. There was not much shifting or deformation in the peaks even after 40 days of room temperature. In this case also, overlapping of peaks due to secondary amines and di-substituted benzene and aliphatic chain vibrations was observed and no clear differentiation was possible. It was difficult to claim from the spectra whether there were any primary amines left in the coating. It could be said that a lot of  $-\text{OH}$  groups were present in the coating resulting from various curing reactions [9]. There was a hint of an epoxy peak at around  $920 \text{ cm}^{-1}$ . However, a presence of a large amount of epoxy groups was ruled out. This indicated a curing reaction between the epoxy groups present in the novolac resin and amines present in the curing agent. Peaks corresponding to aromatic compounds were mainly because the non-reaction of the di-substituted benzene rings present in the novolac resin [10].

#### **4.2.2 N-1 Superprimer**

Figure 4.16 shows the time-based RAIR spectra for N-1 coating cured at room temperature. The peak assignments are shown in Table 4.5. The peaks in the region to the left of  $3000 \text{ cm}^{-1}$  were very similar to the overlapping of peaks corresponding to benzoic overtones, primary and secondary amines and  $-\text{OH}$  groups as seen in the spectra for ND-20 coating. Some of the  $-\text{OH}$  peaks could be due to silanol ( $\text{SiOH}$ ) formation. An

epoxide peak at 916  $\text{cm}^{-1}$  of medium intensity was also observed. The peaks at 1134 and 1052 were seen to increase in intensity with time. The peaks were due to Si-O-Si and Si-O-C. Also peaks due to unreacted ethoxy groups in  $\text{Si}(\text{OC}_2\text{H}_5)_3$  at 475  $\text{cm}^{-1}$  were found to be diminishing with time. Thus, there was evidence of siloxane formation in the coating which was due to slow hydrolysis of the bis-sulfur silane. It was assumed that the silane used the water entrapped in the coating or the absorbed moisture to undergo hydrolysis. Some peaks in the range of 1150-1050  $\text{cm}^{-1}$  might also be due to an alkyl substituted C-O-C stretch resulting from the crosslinking of epoxy groups. Condensation reactions between silanol SiOH and C-OH groups (Si-O-C) could have resulted in some peaks at around 950  $\text{cm}^{-1}$ .

Figure 4.17 shows comparative RAIR spectra of ND-20 coatings cured at room temperature and high temperature, respectively. Only the region below 1300  $\text{cm}^{-1}$  was chosen for comparison due to their dissimilarities. The peak around 575  $\text{cm}^{-1}$  was broader in the high-temperature cured ND-20 coating. Also the peaks corresponding to siloxane were sharper and stronger in case of high-temperature cured ND-20. Peak (around 475  $\text{cm}^{-1}$ ) assigned to unreacted  $\text{Si}(\text{OC}_2\text{H}_5)_3$  was visible in room-temperature cured ND-20 which was absent in the other case. This finding only confirmed that curing temperature actually accelerated the siloxane formation. Hydrolysis of silane proceeded slowly in a coating left to cure at room temperature [12].

### 4.2.3 NP-1 Superprimer

Figure 4.18 shows the time-based RAIR spectra for N-1 coating cured at room temperature. It could not be distinguished whether the peaks in the range of 1180 to 1050  $\text{cm}^{-1}$  were due to ethoxy group bending or siloxane. A lot of overlapping of peaks due to polyurethane and novolac were seen in the region below 2000  $\text{cm}^{-1}$ . Hence, any evidence of siloxane formation was not clearly visible as it was in case of ND-20. However, siloxane formation could not be ruled out. Peaks corresponding to reaction between the epoxy groups and the secondary amine groups in the polyurethane were observed in the region of 2400 to 2600  $\text{cm}^{-1}$ . The broad overlapping peaks in the region above 3000  $\text{cm}^{-1}$  indicated extensive formation of  $-\text{OH}$  due to epoxy-amine reaction or formation of silanols [13].

### 4.2.4 Polyurethane and silane

Figure 4.19 shows the time-based RAIR spectra for a coating of bis-sulfur silane and NeoRez R-972 (1:3 by wt.) cured at room temperature. The peak assignments are shown in Table 4.6. The goal here was to see whether there was any siloxane formation in this formulation. All peaks characteristic of polyurethane resin and bis-sulfur silane were seen. It signified that a large amount of bis-sulfur silane remained unreacted in the coating. The only interaction expected could be hydrogen bonding between the hydroxyl group in silanol and the amine and carbonyl groups in the polyurethane. The fact the bis-sulfur silane did not hydrolyze in the presence of polyurethane could well be an advantage for the packaging study and shelf life of this superprimer.

### 4.3 SEM/EDS Analysis

Scanning electron microscopy and energy dispersive X-ray analysis was carried out on superprimer formulations containing corrosion inhibitor pigments in order to test the effectiveness of pigments in terms of corrosion protection of the aluminum substrate. Cross-sectional analysis of a coated sample was also done to determine the phase distribution of the superprimer.

#### 4.3.1 Effectiveness of Inhibitor

The NP-1 superprimer coating with zinc phosphate inhibitor (**Coating A**) was chosen for SEM analysis as zinc phosphate was found to be the most effective inhibitor pigment from various corrosion tests. The NP-1 coating was used as reference or control (**Coating B**). The coatings were cured at room temperature for 14 days. The coatings were scribed and exposed to 3.5 wt.-% salt water immersion test for a period of 30 days. The coatings were then washed to remove salt deposits and 1 mm x 1 mm samples of the scribed panels were prepared. Corrosion products, if present on the exposed sample, cannot be washed off by water easily. The samples were sputtered with an Au-Pd target and analyzed using SEM/EDS.

Figures 4.20 (a) and (b) show the backscattered SEM images of the scribed part of coating A with the distribution of various elements across the scribe obtained from a line scan. This sample had a visually clean scribe as seen from the SEM image with hardly any corrosion products on the scribe. Figures 4.21 to 4.24 show the EDS scans at various spots across the scribe on coating A. The respective SEM images showing the spot of scan and the elemental distribution are also shown. Scans on the scribed part revealed

high peaks of aluminum and oxygen and low peaks of zinc and chlorine. The amount of chlorine in the scribe is directly proportional to the amount of chloride corrosion product formed in NaCl solutions [13]. In this case, the corrosion product if present would most probably be some complex of aluminum or copper or zinc hydroxy chloride. As the scribed part was approached in the scan, the chlorine content was actually found to be decreasing. The novolac resin had some amount of chlorine present due to epichlorohydrin. Based on the low amounts of chlorine and zinc in the scribe, it was concluded that the inhibitor was effective in protecting the scribe from corrosion keeping it free of corrosion products.

Figure 4.25 shows the backscattered SEM images of the scribe region in coating B which did not contain any inhibitor. The SEM image showed that the scribe was very unclean with some deposits over the scribed part. Figures 4.26 to 4.29 show EDS scans at various spots across the scribe on coating B along with the respective SEM images and elemental distribution. High amount of chlorine was observed along the scribe. The low peaks for aluminum indicated that corrosion products were deposited on top of the exposed metals in the scribe. The absence of inhibitors led to corrosion of in the scribe. It can be certainly claimed that zinc phosphate works well in these water-based coatings. Inclusion of silane and other curing agents may lead to ineffective leaching in primers. However, in water-based coatings, this aspect can be neglected as these coating tend to absorb water which facilitate leaching of inhibitors. The leaching of the inhibitors might be facilitated by the creation of water channels in these coatings. The exact mechanism for the leaching of zinc phosphate still needs to be investigated further.

### **4.3.2 Cross-sectional Analysis**

Figure set 4.30 (a) and (b) provides cross-sectional view of the coating A, i.e. NP-1 coating with zinc phosphate inhibitors on AA 2024-T3. Elemental distribution information along the cross-section is shown in Figure 4.31. Figures 4.32 to 4.35 show EDS scans at various spots along the cross-section of the coating. The line scan revealed that the distribution of the silane (Si) was fairly even along the cross-section. The SEM images also did not reveal any visible phase separation along the cross-section. The EDS scans and spot analysis also directed to the conclusion that the distribution of components was even. Huge chunks of inhibitor pigments were visible throughout the cross-section. However, the distribution of the pigments was uniform on a large scale.

### **4.4 Thermogravimetric Analysis**

Thermogravimetric analysis was carried out on novolac-based superprimer coatings with the point of view of determining the effect of silane on the thermal behavior of the coatings. Pigments were not included in the coatings for this study. ND-20, N-1 and NP-1 superprimer coatings cured at room temperature were analyzed using TGA. Weight loss was recorded for predetermined amounts of coating samples heated from room temperature to 350° C at the rate of 10° C/min. The samples were then held isothermally at 350° C for 5 minutes. Figure 4.36 shows the TGA curves for these coatings in terms of weight loss and percentage weight loss. The weight loss in a material upon heating is due to the evaporation of water and other solvents and degradation of chemical bonds. Water and solvents which may be entrapped in a crosslinked network, account for the initial

weight loss. The weight loss at later stages is mainly caused by the degradation of chemicals and release of gaseous compounds [14-16].

The cross-linked ND-20 had higher thermal stability than N-1 and NP-1 coatings. There was not much difference between the thermal behavior of N-1 and NP-1 suggesting that the polyurethane resin did not exert a negative effect on the thermal stability of the coating. From the nature of the curves, it was observed that the thermal stability of the coatings decreased with the addition of silane. However, this could not be concluded with certainty. It is known from literature that the bis-sulfur silane degrades at a temperature of around 150° C due to the low bond strength of the S-S bonds. Degradation of bis-sulfur silane could have accounted for some of the weight loss. The weight loss could also be attributed mainly to loss of water from the coatings. As explained earlier, water is absorbed by the superprimer coating in sizable amounts due to the voids in the coatings. It could have accounted for all of the weight loss observed in the thermograms. Also, IR and NMR studies had suggested a slow hydrolysis of bis-sulfur silane in the superprimer. These could have caused water absorption in the coating. The coating, being water-based, was prone to absorb more water than a solvent-based coating. Curing time was a major factor affecting the thermal stability of the coating. Study of the effluents released during heating in the TGA experiment is expected to give a better understanding about the thermal behavior of these coating.

## 4.5 Summary

Based on the results from NMR and IR studies, the formation of siloxane network in the superprimer coatings studied was evident. Time-based analysis indicated slow hydrolysis of the bis-sulfur silane. There was evidence of siloxane linkages to metal suggesting adhesive bonding due to silane. Si-O-C linkage between the novolac epoxy and silane was also a possibility but a clear indication could not be obtained because of overlapping of various peaks. It was understood that high-temperature curing of the superprimer accelerated the siloxane formation by crosslinking of the silane. The reaction between the novolac resin and curing agent occurred almost instantly and almost all of the epoxide in the resins was used up in this reaction. However, the instant curing of the novolac resins did not seem to affect the siloxane formation.

SEM/EDS analysis verified the effectiveness of inhibitors in protecting exposed metal against corrosion. No corrosion products were observed in the scribe of NP-1 coating with inhibitors. High amount of crosslinking of the novolac resins and curing agent did not seem to affect leaching of inhibitors. Cross-sectional examination did not reveal any phase separation between the superprimer components suggesting an obvious interaction between them. The TGA curves of superprimers appeared to be affected by the addition of silane. However, it did not necessarily indicate thermal instability. The shifts in the thermal behavior were due to unhydrolyzed silane still present in the coating. Longer curing times were expected to improve thermal behavior.

## 4.6 References

1. Maria Ines B., Tavares, D'Almeida J.R.M., and Monteiro S.N., *J. App. Pol. Sci.*, 78, 2358 (2000)
2. Adriaensens P., Rego R., Carleer R., Ottenbourgs B. and Gelan J., *Poly. Int.* 52, 1647 (2003)
3. Socrates G., *Infrared Characteristic Group Frequencies*, John Wiley & Sons Inc., New York, USA (2001)
4. Coates J., *Encyclopedia of Analytical Chemistry* (Ed) R. A. Meyers, John Wiley & Sons Ltd, New York , 10815 (2000)
5. IR wizard of University of Potsdam, available at <http://www.chem.uni-potsdam.de/cgi-bin/irwiz2.pl>
6. Matinlinna J.P., Areva S., Lassila L.V.J., Vallittu P.K., *Surf. Interface Anal.*; 36, 1314 (2004)
7. Cherdoud-Chihani A., Mouzali M., Abadie M. J. M., *J. App.Poly. Sci.*, 87, 2033 (2003)
8. Puomi P., Fagerholm H. M., *J. Adhes. Sci. Technol*, 15, 509 (2001)
9. Hung A.Y.C., Wang F.Y., Ma C.M. and Sun Y.M., *J. App. Pol. Sci.*, 86, 984 (2002)
10. Sherzer T., *J. App. Pol. Sci.*, 70, 247 (1998)
11. Antonucci J., *J. Res. Natl. Inst. Stand. Technol.*, 110, 541 (2005)
12. Wicks D.A., Yeske P.E., *Prog. Org. Coat*, 30, 265 (1997)
13. Seth A., *Ph.D.Thesis, Dept. of CME, University of Cincinnati*, to be published in 2006

14. Nair C.P.R., Bindu R.L. and Ninan K.N., *J. Poly. Degrn. and Stab.*, 73, 251  
(2001)
15. Chiang C., Ma C.M., Wang F., Kuan H., *Euro. Poly. Jour.*, 39, 825 (2003)
16. Rodriguez M.T., Gracenea J.J., Kudama A.H., Suay J.J. *Prog. Org. Coat.*, 50, 62  
(2004)

## 5. CONCLUSIONS AND SCOPE FOR FUTURE WROK

Silanes were successfully blended with resins to develop a ‘superprimer’ coating system worthy of providing corrosion protection to AA 2024-T3. A new family of water-based epoxy resins called the ‘novolacs’ was explored. Formulations were developed for various concentrations of novolac resin, curing agent and silane and evaluated in various corrosion and chemical tests. A polyurethane resin was incorporated in amounts up to 15 wt.-percent with the solitary aim of improving low-temperature behavior of the superprimer coatings and accelerating room-temperature curing. Non-chromate corrosion inhibitors were added in the form of pigments to impart self-healing ability in the superprimer. No solvents other than water were used to mix the components. As a result, a chromate-free, low-VOC, water-based superprimer formulation was developed which possessed the capability to serve as a replacement for commercial chromate-containing, solvent-based primers.

The integration of hydrophobic bis-sulfur silane into the formulation improved the hydrophobicity and anti-corrosion performance of the superprimer. Salt water immersion and EIS tests showed that the silane had a very positive effect on the anti-corrosion properties of the superprimer. Improvement in solvent resistance and hardness was also observed. Bis-sulfur silane undeniably enhanced the adhesion of the superprimer to the substrate as well as the topcoat as was evident from the adhesion tests. Incorporation of small amounts of the water-borne polyurethane was instrumental in improving the performance of the coatings in bend test. These coatings survived 180° of bending at room temperature without cracking and showed excellent corrosion resistance in salt

water immersion tests. Pigments such as phosphate, molybdate and vanadate based non-chromate corrosion inhibitors were successfully incorporated into the superprimer. Some inhibitors such as zinc phosphate were identified for possessing the capability to instill a self-healing ability to the superprimer, i.e., protecting the exposed substrate due to defects in coatings from corrosion. DBTL addition improved curing rate of the superprimer at room temperature but did not enhance its corrosion resistance. Filler particles such as aluminum paste and titania were found to improve water-barrier properties to some extent. A variety of additives such as dispersants, wetting agents, defoamers and surfactants were also included in the superprimer system to perk up properties such as pot-life, wettability and sprayability.

The complete superprimer system successfully completed more than 2000 hours of ASTM B 117 salt spray test. The coatings also showed good performance in the Ford AGPE test. The superprimer performed excellently in chemical resistance and solvent resistance tests. The final superprimer formulations had very low VOC levels (~30 g/L) and were also entirely chromate-free and water-based. No conversion coating was required for this system. This superprimer system was able to perform at similar levels if not better than the chromate-containing controls in terms of corrosion protection of AA 2024-T3. The formulations were also modified for spraying. The spray coating formulations still needed some optimization as the dilution of the formulation was expected to have an adverse effect on its performance. Characterization study of the superprimers revealed a lot of information about the chemistry of the coatings. NMR and IR spectroscopic studies indicated that the hydrolysis of silane proceeded slowly with

time. It was believed that silane used water from the coating for hydrolysis. SEM/EDS studies elucidated the self-healing effect of the corrosion inhibitors. These studies also unveiled the homogeneous distribution of the components in superprimer films with hardly any phase separation. Thermal behavior of superprimers was studied which suggested that the silane could potentially decrease the thermal stability of the superprimer to some extent. However, it was understood that the high water content of the coatings was responsible for most of the weight loss observed in the TGA thermograms.

Though most of the objectives of this study have been achieved by the development of a novel superprimer system, there is always scope for further improvement. In the case of the superprimer developed in this study, the amount of inhibitors added is much lower compared to the chromate pigment content in commercially available paints. Using effective dispersants and high shear blender, larger amounts of non-chromate pigments can be added to attain a higher degree of corrosion inhibition. Also, newer pigments and their combinations can be incorporated in the superprimer. Inductively Coupled Plasma - Mass spectroscopy studies (ICP-MS) can be performed in order to determine the leaching rate of various inhibitors in different conditions in superprimer formulations. Interfacial studies using Time-of-Flight Secondary Ion Mass Spectrometry (TOF-SIMS) can be performed for a better understanding of the bonding mechanism at the coating-metal interface. As a step towards commercialization of these systems, a packaging study needs to be performed. The superprimer needs to be separated into packs or components which should remain stable for a definite amount of time. <sup>29</sup>Si NMR studies can further

elucidate the siloxane crosslinking reactions and factors influencing it. Rheological studies can be carried out to study the viscoelastic behavior of the superprimer. Modifications can be done to the spray coating formulation to improve pigment dispersion. For this purpose, commercially available VOC-free solvents can be used.

## TABLES

**Table 2.1** Physical properties of resins and curing agent used in the superprimer

<b>Product name</b>	<b>Type</b>	<b>Wt % solids</b>	<b>Viscosity at 25° C (cP)</b>	<b>VOC (g/L)</b>
<b>EPI-REZ 5003-W-55</b>	Novolac bisphenol A epoxy	55	2000-15000	0
<b>EPIKURE 6870-W-53</b>	Polyamine adduct	53	8000	0
<b>NeoRez R-972</b>	Aliphatic polyurethane	34	150	100
<b>NeoRez R-960</b>	Aliphatic polyurethane	33	300	400

**Table 2.2** Experimental cycle in the Ford AGPE test

(Refer Figure 2.6)

<b>Step</b>	<b>Test</b>
<b>1</b>	15 minutes immersion in 5% NaCl solution at room temperature
<b>2</b>	105 minutes ambient drying
<b>3</b>	22 hours in 90% humidity at 60 °C

## TABLES

**Table 3.1** Various formulations of novolac epoxy resin and curing agent

Formulation	EPI-REZ 5003-W-55 (g)	EPIKURE 6870-W-53 (g)
ND-10	90	10
<b>ND-20</b>	<b>80</b>	<b>20</b>
ND-30	70	30
ND-45	55	45
ND-50	50	50

**Table 3.2** Properties of novolac epoxy resin and curing agent formulations

Formulation	Contact angle with water in degrees (room temperature curing)	MEK double rub value (room temperature curing)	MEK double rub value (high temperature curing)	Pencil Hardness (room temperature curing)
ND-10	49.3	30	200	2B
<b>ND-20</b>	<b>58.7</b>	<b>60</b>	<b>300</b>	<b>1H</b>
ND-30	53.5	40	300	1H
ND-45	50.2	15	150	2H
ND-50	45.6	8	50	2H

**Table 3.3** Formulations for various novolac-based superprimers with silanes and polyurethane

Formulation	EPI- REZ-W- 55 5003 (g)	EPIKURE 6870-W-53 (g)	Bis- sulfur silane (g)	BTSE (g)	AV5 (g)	NeoRez R-972 (g)	NeoRez R-960 (g)
<b>N-1</b>	<b>72</b>	<b>18</b>	<b>10</b>	-	-	-	-
N-2	72	18	-	-	10	-	-
N-3	64	16	-	-	20	-	-
<b>NP-1</b>	<b>60</b>	<b>15</b>	<b>10</b>	-	-	<b>15</b>	-
NP-2	56	14	10	-	-	20	-
NP-3	64	16	10	-	-	10	-
NP-4	60	15	-	10	-	-	15

**Table 3.4** Properties for various novolac-based superprimer formulations

Formulation	Contact angle with water in degrees (room temperature cured)	MEK double rub value (room temperature cured)	MEK double rub value (high temperature cured)	Pencil Hardness (room temperature cured)
<b>N-1</b>	<b>76.2</b>	<b>60</b>	<b>300</b>	<b>1B</b>
N-2	64.6	25	250	1H
N-3	60.1	15	150	2H
<b>NP-1</b>	<b>79.3</b>	<b>100</b>	<b>300</b>	<b>2H</b>
NP-2	76.4	90	-	HB
NP-3	73.2	10	-	2B
NP-4	81.2	70	-	2B

**Table 3.5** Formulations of superprimers with different corrosion inhibitors

Formulation	EPI-REZ 5003-W-55 (g)	EPIKURE 6870-W-53 (g)	Bis-sulfur silane	NeoRez R-972	Phosguard Zinc phosphate	CZM	Corrostayn 228	Sodium metavanadate
N-1 with 10% zinc phosphate	56	14	8	12	10	-	-	-
NP-1 with 15% zinc phosphate	52	13	8	12	15	-	-	-
NP-1 with CZM	56	14	8	12	-	10	-	-
NP-1 with Corrostayn 228	56	14	8	12	-	-	10	-
NP-1 with sodium metavanadate	60	15	9	13	-	-	-	3

**Table 3.6** MEK double-rub values and water contact angles for superprimers with corrosion inhibitors

Formulation	MEK double rub value (room temperature curing)	Water contact angle in degrees
N-1 with 10% zinc phosphate	40	63.1
NP-1 with 10% zinc phosphate	60	66.2
NP-1 with 15% zinc phosphate	50	61.5
NP-1 with CZM	40	57.5
NP-1 with Corrostatin 228	55	62.4
NP-1 with sodium metavanadate	50	65.3

**Table 3.7** Formulations for superprimers with filler pigments

Formulation	EPI-REZ 5003 (g)	EPIKURE 6870 (g)	Bis-sulfur silane (g)	Titania (g)	Leafy Aluminum paste (g)
N-1 with Titania	68	17	10	5	-
N-1 with leafy aluminum paste	68	17	10	-	5

**Table 3.8** Formulations for superprimer for spray coating experiment

Formulation	EPI-REZ 5003 (g)	EPIKURE 6870 (g)	Bis-sulfur silane (g)	NeoRez R- 972 (g)	Alfa Aesar zinc phosphate (g)
NP-1 for spraying	55	14	8	8	15

**Table 3.9** Formulations for control coatings and topcoat

**(a)**

Formulation	CA 7233 High solids primer (ml)	CA 7233 B Activator (ml)
<b>Chromated Control Primer</b>	1	1

**(b)**

Formulation	Desothane HS CA-8214/F36173 (ml)	CA-8214/F36173 Activator (ml)
<b>Topcoat</b>	3	1

**Table 3.10** Properties of the NP-1 formulation

VOC content	Pot Life	Dry-to-tape Time	Top-coat adhesion	Chemical Resistance	Solvent Resistance (MEK double rubs)	Hardness
~30 g/L	3-4 hrs	4-5 hrs	4A	Passed 6N HCl and 6N NaOH test	90	2H

## TABLES

**Table 4.1** RAIR peak assignments for pure bis-sulfur silane film (refer Figure 4.12)

Wave number	Group Assignment
2974	CH <sub>3</sub> asymmetric stretching
2926	CH <sub>2</sub> asymmetric stretching
2886	CH <sub>3</sub> symmetric stretching
1482	CH <sub>2</sub> symmetric bending
1442	CH <sub>2</sub> asymmetric bending
1390	CH <sub>3</sub> symmetric bending
1296	CH <sub>2</sub> wagging
1243	CH <sub>2</sub> -S wagging
1167	O-C <sub>2</sub> H <sub>5</sub> bending
1123	<i>-Si-O-Si- small chains</i> + Si-O-C asymmetric deformation
1085	Si-O-C asymmetric stretching + Si-O-Zn bond + <i>-Si-O-Si- small chains</i>
960, 787	Si- O-C <sub>2</sub> H <sub>5</sub> symmetric stretching
479	Inorganic silicates + S-S stretch in polysulfide +Si- O- C <sub>2</sub> H <sub>5</sub> symmetric deformation

**Table 4.2** RAIR peak assignments for the film of epoxy-amine adduct curing agent EPKURE

6870 (refer Figure 4.13)

Wavenumber (cm <sup>-1</sup> )	Group Assignment
3590 - 3400	Intramolecular hydrogen bonding between hydroxyl groups
3550 - 3230	Intermolecular hydrogen bonding between hydroxyl groups
3500 - 3300	O-H stretch
3450 - 3200	N-H stretch (from the amines)
3000-2850	C-H stretch from the alkanes or aliphatic chains, CH <sub>3</sub> asymmetric stretching
2700-2400	Peaks not visible in this region. Due to the hydrides in the proprietary surfactants/dispersants
2000 - 1600	Weak overtone and combination bands from di-substituted benzene (benzene fingers)
1613	C=C stretching in the benzene ring
1516	C=C stretching in the benzene ring (goes along with the 1613 peak)
1474	CH <sub>2</sub> scissoring / CH <sub>3</sub> asymmetric / C=C stretching of the 1,4-substituted benzene
1313	CH <sub>2</sub> twisting and wagging + C-H deformation vibration from secondary alcohol bounded (CHOH in the epoxy part of the adduct)
1259	Asymmetric C-O-C stretching of the aromatic ether and vibration of the epoxide ring
1191	C-H bending (benzoic)
1056	C-H bending of the 1,4 substituted benzene + symmetric C-O-C stretching of the aromatic ether
1127	C-N stretching of the aliphatic secondary amine
840	C-H stretching of the 1,4 substituted benzene + CH <sub>2</sub> rocking of the epoxide group + N-H wag of the aliphatic secondary amine

**Table 4.3** RAIR peak assignments for the film of polyurethane resin dispersion NeoRez R-972

(refer Figure 4.14)

Wavenumber (cm <sup>-1</sup> )	Associated structure
3590 - 3400	Intramolecular hydrogen bonding between hydroxyl /secondary amine groups
3550 - 3230	Intermolecular hydrogen bonding between hydroxyl groups / secondary amine groups
3500 - 3300	O-H stretching (free / adsorbed water)
3450 - 3200	N-H stretch (from the amines)
2700-2400	From hydride vibrations, such as from silanes (Si-H), thiols and sulfides (S-H), phosphines (P-H), arsines (As-H), boranes (B-H), etc. possibly due to surfactants/dispersants used in the resin dispersion, exact chemistry unknown
1747	C=O stretch
1558	Weak N-H deformation vibrations
1470	CH <sub>2</sub> scissoring / CH <sub>3</sub> asymmetric stretching
1273	Asymmetric C-O-C stretching + CH <sub>2</sub> wagging
1200	C-N stretch (TEA) + strong C-O stretch
1150	C-O stretching vibration in ester groups
1085	-O-CH <sub>3</sub> out of plane deformation
786	C-O-C deformation vibration + C-C rocking in CH <sub>2</sub>

**Table 4.4** RAIR peak assignments for ND-20 time-based spectra (refer Figure 4.15)

Wavenumber (cm <sup>-1</sup> )	Group Assignment
3377	Peak shape suggests: -OH ( may mask -NH, -NH <sub>2</sub> , however NH <sub>2</sub> makes two peaks)
3058	vC-H aromatic
2966	vC-H aliphatic
2932	vC-H aliphatic
2873	vC-H aliphatic
2070	substituted benzoic overtones
1889	substituted benzoic overtones
1607	C=C vibration of the substituted benzene
1582	C=C vibration of the substituted benzene
1517	C=C stretching in the benzene ring (goes along with the ~1610 peak)
1463	δCH <sub>2</sub> (scissoring) + δ <sub>asym</sub> CH <sub>3</sub> + C=C of the 1,4 substituted benzene
1384	δ <sub>sym</sub> CH <sub>3</sub> , doublet in case of gem-dimethyl groups
1362	δ <sub>sym</sub> CH <sub>3</sub> , doublet in case of gem-dimethyl groups
1297	v symmetric of the epoxide ring + v asymmetric C-O-C in the case of aromatic ether
1185	δC-H benzoic
1045	δC-H of the di-substituted benzene + v symmetric C-O-C aromatic ether
937	A hint of epoxy peak
832	Stretching, C-H of the di-substituted benzene + CH <sub>2</sub> of the epoxide group

**Table 4.5** RAIR peak assignments for N-1 time-based spectra (refer Figure 4.16)

Wavenumber (cm <sup>-1</sup> )	Group Assignment
3431	-OH (overlapping with -NH, -NH <sub>2</sub> , NH <sub>2</sub> has two peaks)
3056	vC-H aromatic
3037	vC-H aromatic
2973	CH <sub>2</sub> , -CH <sub>3</sub> , also ethoxy groups from BS
2068	substituted benzoic overtones
1888	substituted benzoic overtones
1734	substituted benzoic overtones
1611	Stretching, C=C of the substituted benzene
1582	Stretching, C=C of the substituted benzene
1472	broader than in the RT cured, looks like in N1+BS
1384	δsymCH <sub>3</sub> , doublet in case of gem-dimethyl groups as in DGEBA
1362	δsymCH <sub>3</sub> , doublet in case of gem-dimethyl groups as in DGEBA
1307	v symmetrical of the epoxide ring + v asymmetrical C-O-C in the case of aromatic ether
1190	δC-H benzoic
1135	Si-O-Si, could also be Si-O-C
1051	Si-O-Si, could also be Si-O-C
1010	Like the shoulder in spectrum of N1 RT cured
971	Si-O-C <sub>2</sub> H <sub>5</sub> symmetric stretching,
916	Epoxide
842	Stretching, C-H of the di-substituted benzene + γCH <sub>2</sub> r of the epoxide group
475	Si-(OC <sub>2</sub> H <sub>5</sub> ) <sub>3</sub> , unreacted leg

**Table 4.6** RAIR peak assignments of time-based spectra for bis-sulfur silane and polyurethane resin films (refer Figure 4.16)

Wavenumber (cm <sup>-1</sup> )	Group Assignment
3344 broad	-OH, overlapping with peaks from -NH, 3450-3390 cm <sup>-1</sup> , (unassociated) secondary urethanes
2971	Stretching, C-H aliphatic, i.e. -CH <sub>2</sub> , -CH <sub>3</sub> , also ethoxy groups from BS
2934	Stretching, C-H aliphatic, i.e. -CH <sub>2</sub> , -CH <sub>3</sub> , also ethoxy groups from BS
2857	Stretching, C-H aliphatic, i.e. -CH <sub>2</sub> , -CH <sub>3</sub> , also ethoxy groups from BS
1740-1680	-C=O, stretching, from the ureido group (polyurethane)
1528	Urethane combination N-H deformation and C-N stretching vibrations
1452	-CH <sub>2</sub> -, deformation vibrations, -CH <sub>3</sub> asymmetric
1390	-CH <sub>3</sub> symmetrical
1244	CH <sub>2</sub> -S wagging and -C(=O)-O-C-
1171	O-C <sub>2</sub> H <sub>5</sub> bending and -C-O-C-
1107	unreacted ethoxy attached to Si, could be small amount of -Si-O-Si-
1087	Si-O-C asymmetric stretching, could mean small amount of -Si-O-Si-
962	Si-O-C <sub>2</sub> H <sub>5</sub> symmetric stretching
787	Si-O-C <sub>2</sub> H <sub>5</sub> symmetric stretching
479	Si-(OC <sub>2</sub> H <sub>5</sub> ) <sub>3</sub> , unreacted leg

# FIGURES

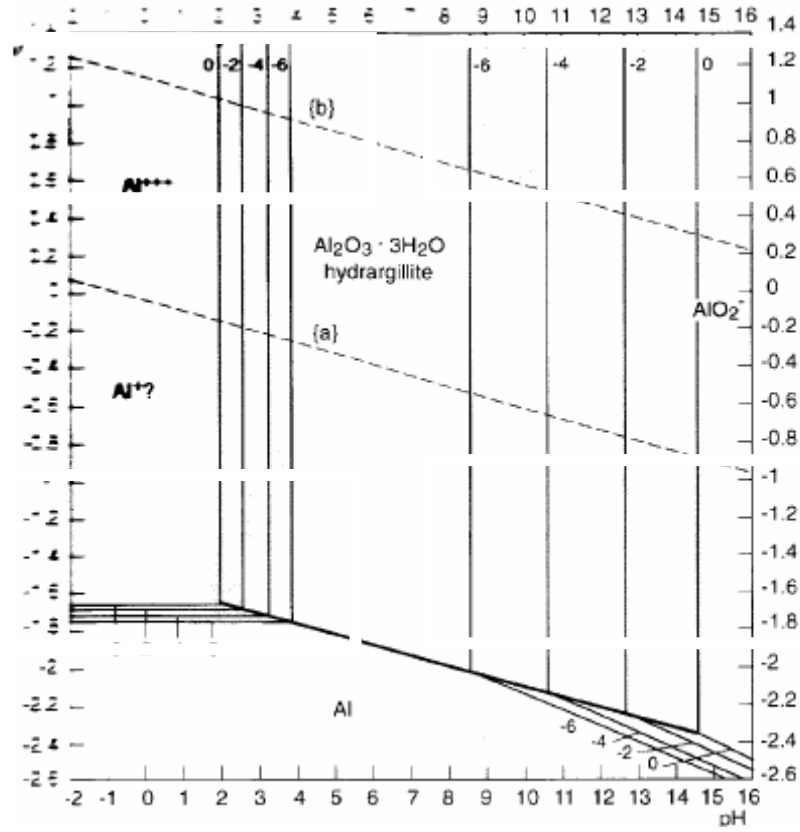


**Figure 1.1** Pourbaix diagrams for pure Al

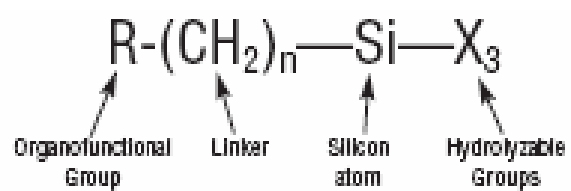


**Figure 1.2** General chemical structure of a silane compound

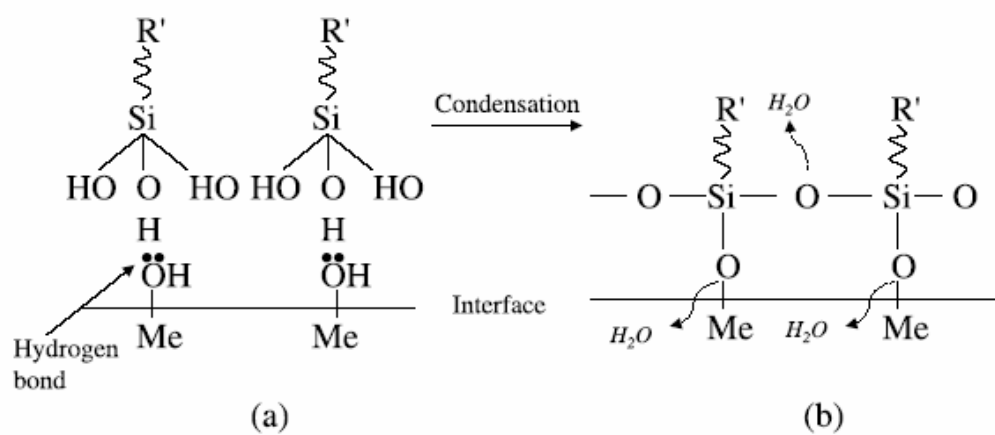


**Figure 1.3** Sketches showing hydrolysis and condensation of silanes

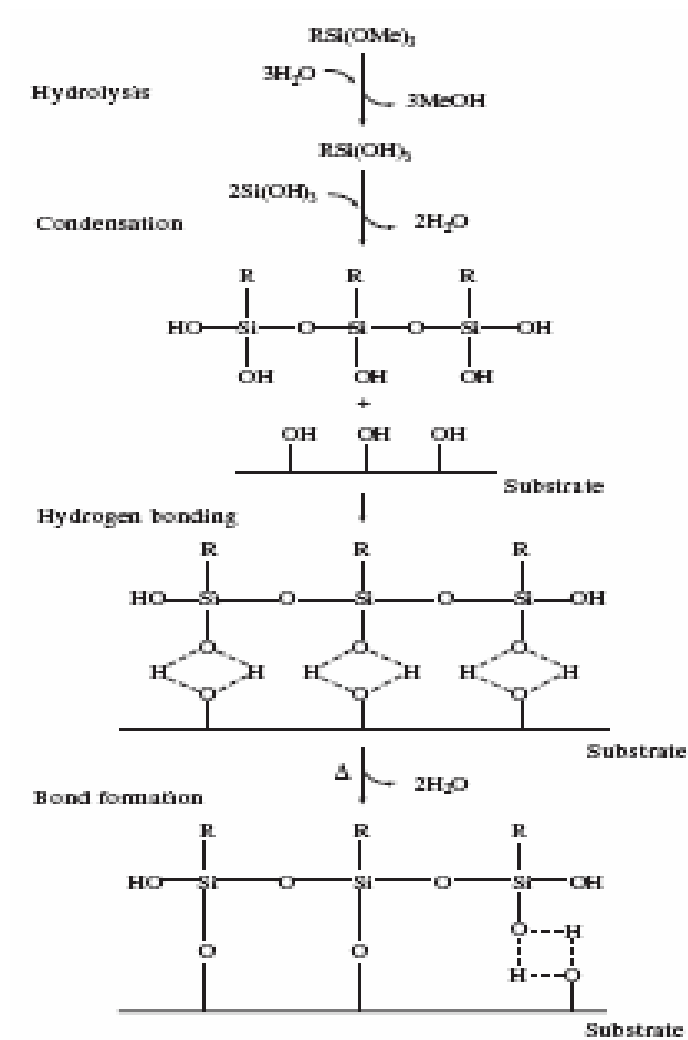
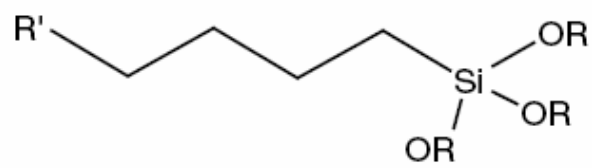
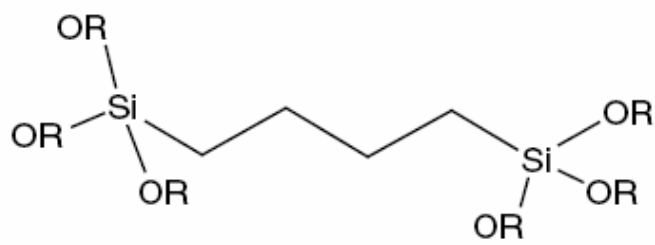


**Figure 1.4** Bonding mechanisms during a silane pretreatment process [Ref. B. Arkles, Chemtech, 7, 705, 1977]



(a)



(b)

**Figure 1.5** Structure of a (a) mono-silane and (b) bis-silane

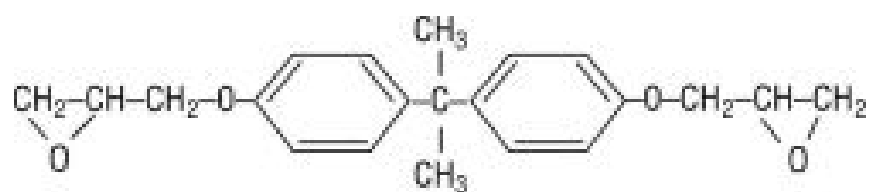


**Figure 1.6** Structure of a DGEBA resin monomer



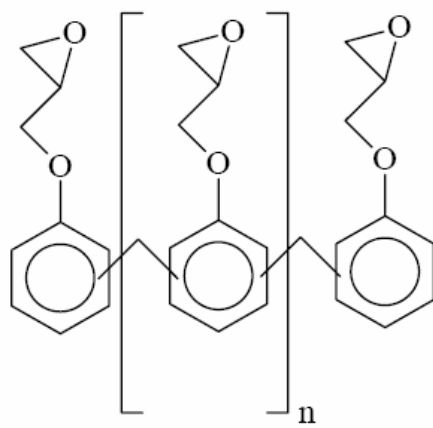


**Figure 1.8** Chemical structure of a generic novolac resin

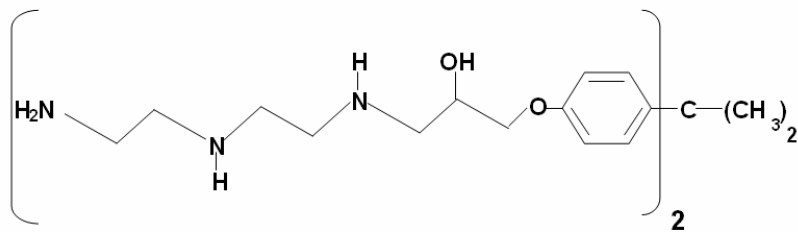
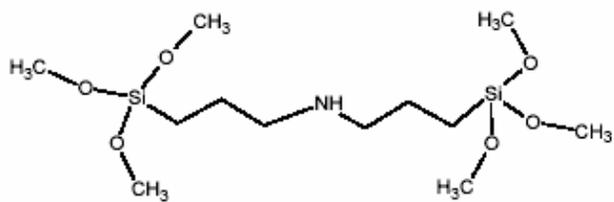
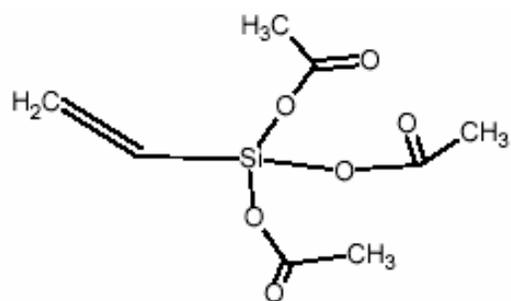


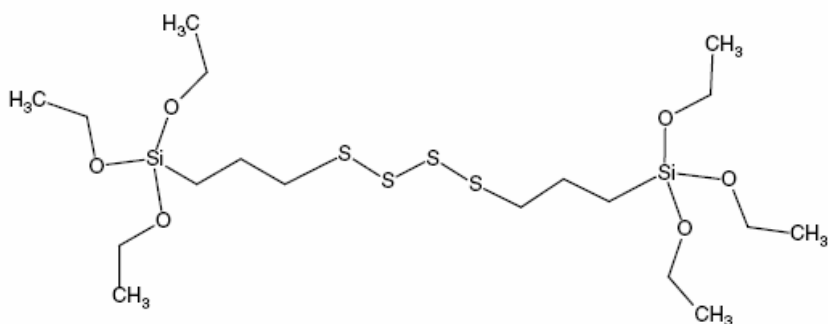
**Figure 1.9** Chemical structure of epoxy amine curing agent



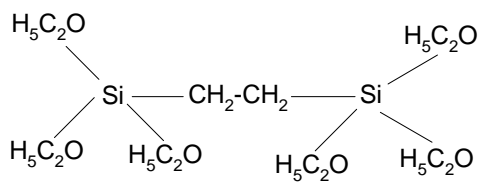
Bis-amino silane



Vinyl triacetoxysilane



Bis-sulfur silane



BTSE

**Figure 1.10** Chemical structure of some silanes used in a superprimer

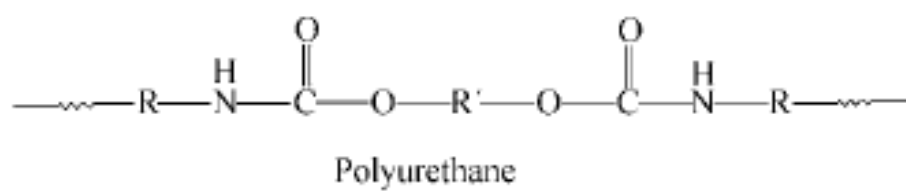


**Figure 1.11** Generic structure of polyurethane

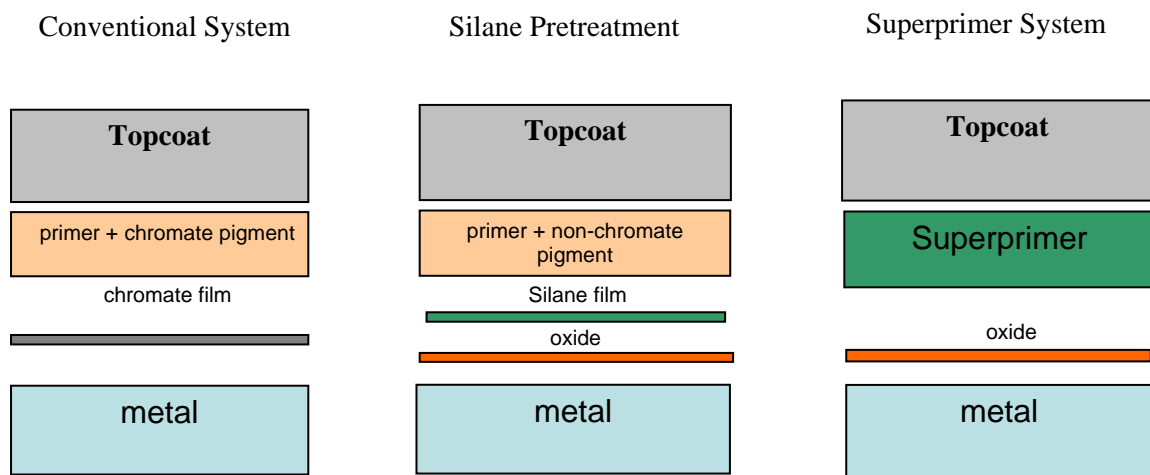


**Figure 1.12** Comparison of conventional coating system with superprimer technology

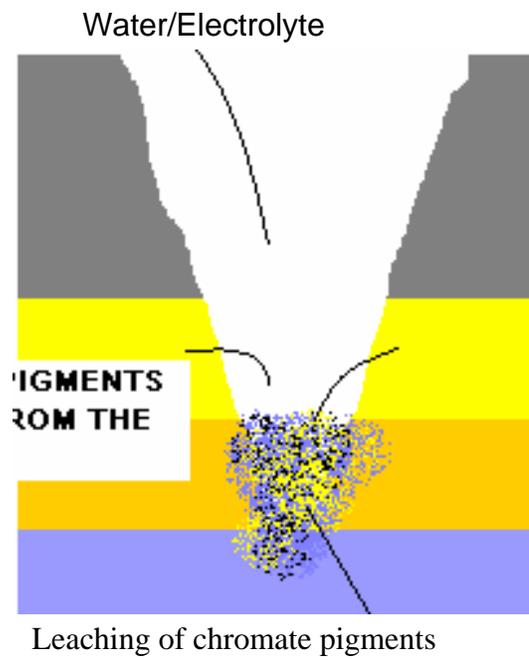


**Figure 1.12** Sketch showing the leaching of hexavalent chromate pigments in the conventional coating system

## FIGURES

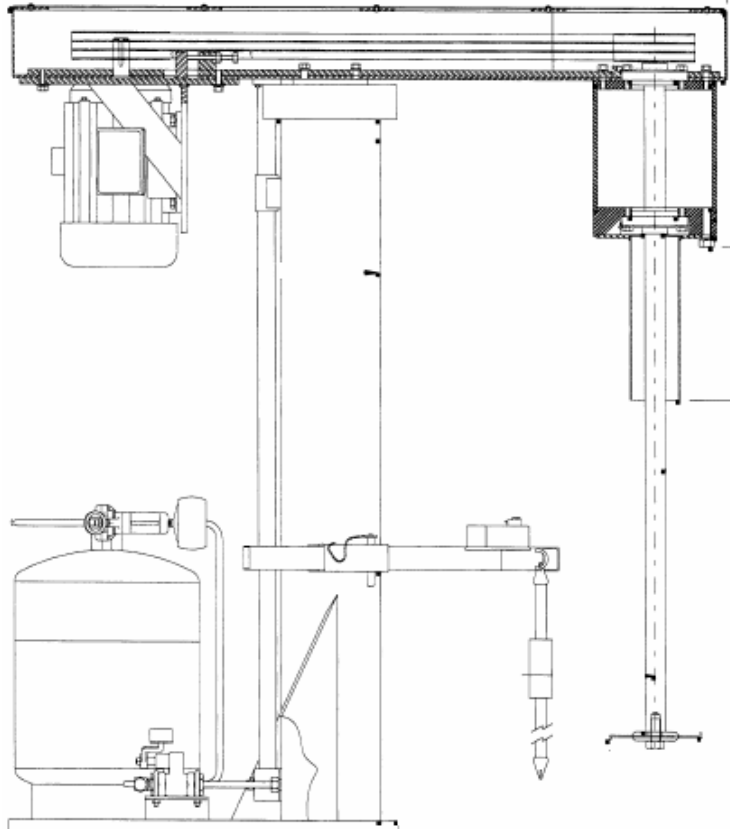


**Figure 2.1** Schematic sketch of the High Shear Mixer



**Figure 2.2** SoftSpray HVLP conversion gun for spray painting

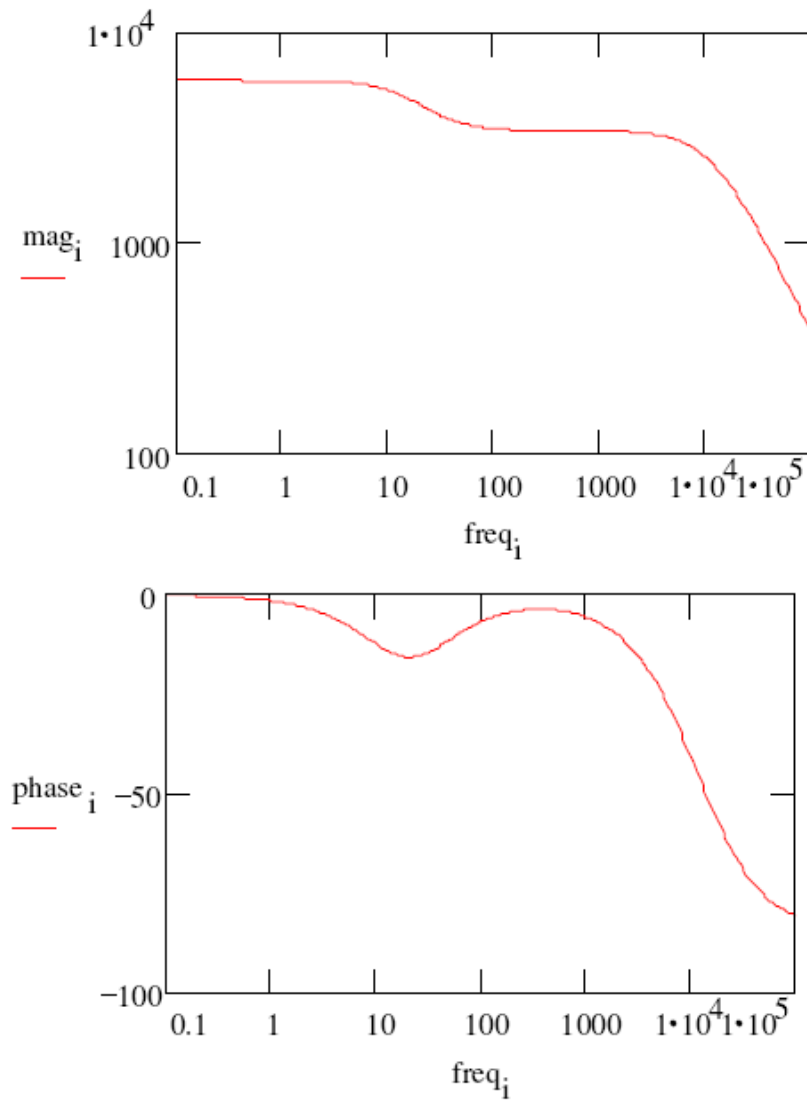


**Figure 2.3 (a)** Bode plots for a failed coating

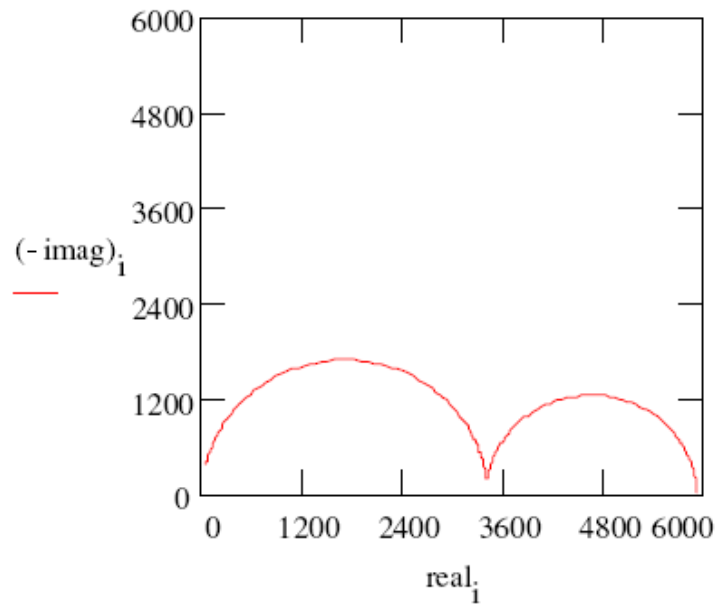


**Figure 2.3 (b)** A Nyquist plot for a failed coating

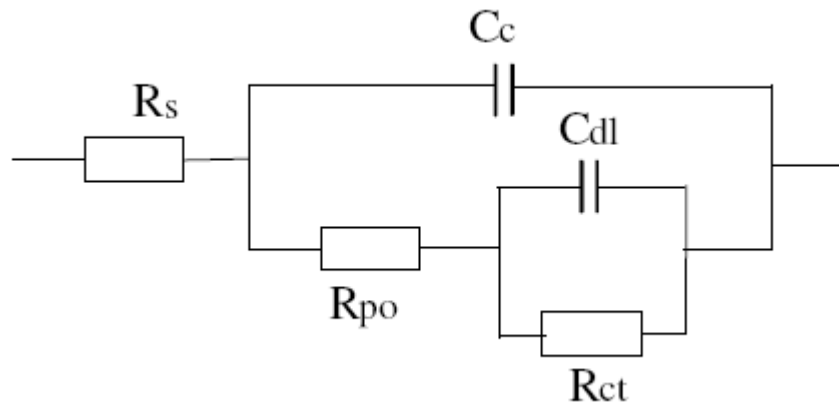


**Figure 2.3 (c)** An equivalent circuit for a failed coating



**Figure 2.4** EIS cell arrangement for impedance measurements



**Figure 2.5** The salt spray chamber at DACCO SCI, INC.

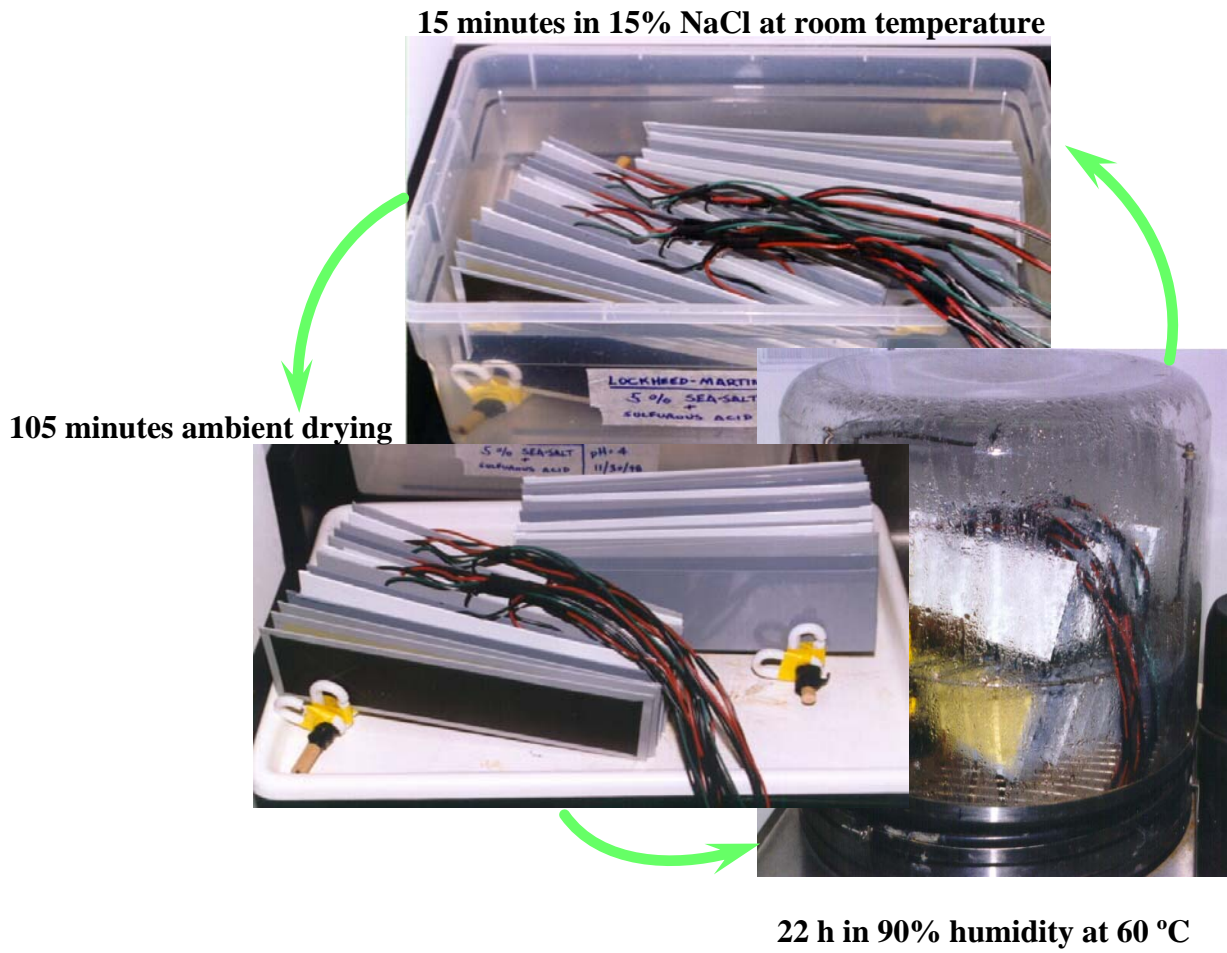


**Figure 2.6** The experimental set-up of the Ford AGPE test

(Refer Table 2.2)

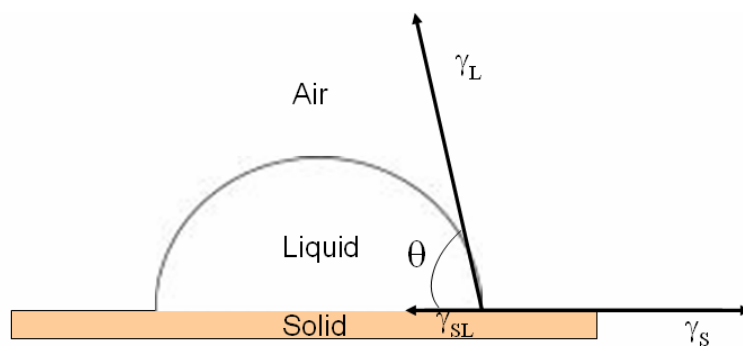


**Figure 2.7** Interfacial forces acting on a liquid droplet on a solid surface



**Figure 2.8** The contact angle goniometer, VCA Optima 2000

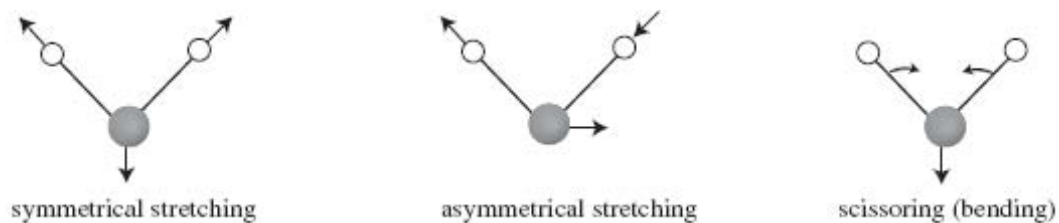


**Figure 2.9 (a)** Stretching and bending vibrational modes for H<sub>2</sub>O

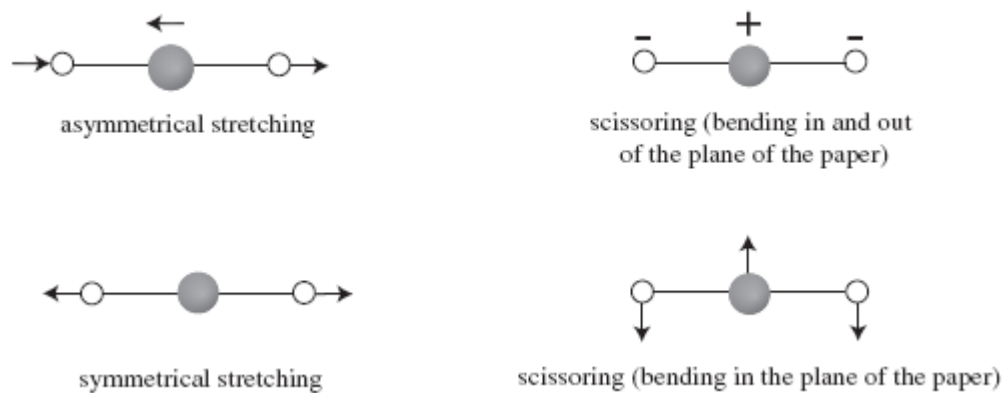


**Figure 2.9 (b)** Stretching and bending vibrational modes for CO<sub>2</sub>

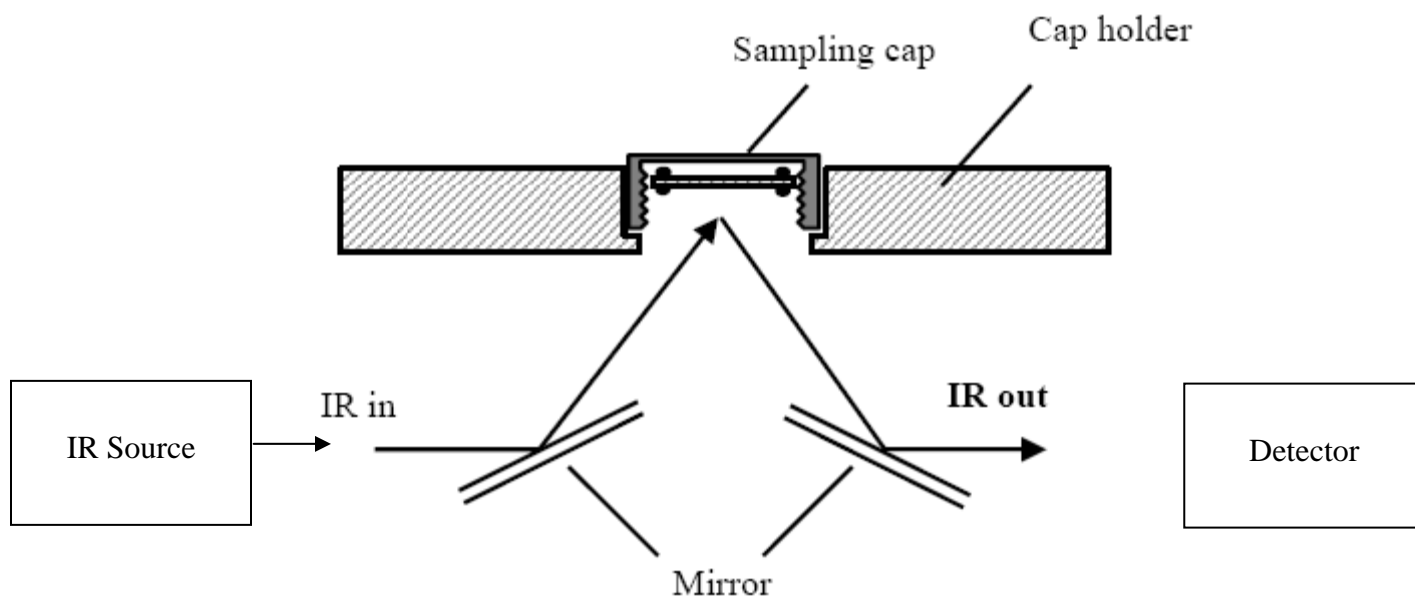


**Figure 2.10** Optical arrangement for a reflection-absorption IR sampling accessory

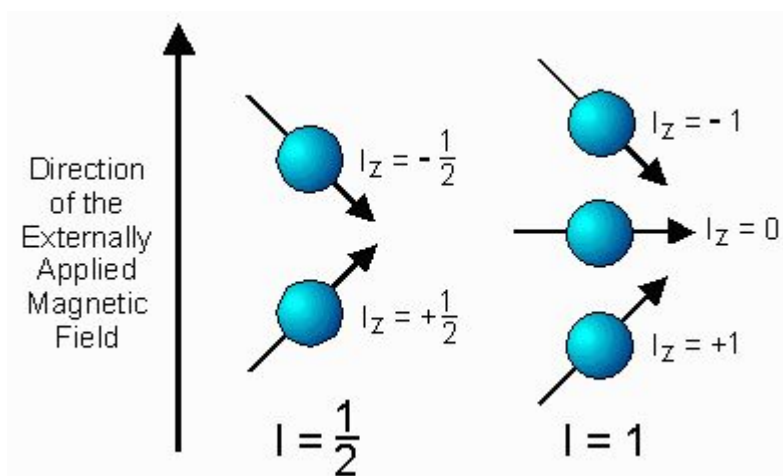


**Figure 2.11** Possible spin states of nuclei with  $\frac{1}{2}$  and 1 integer spins in NMR

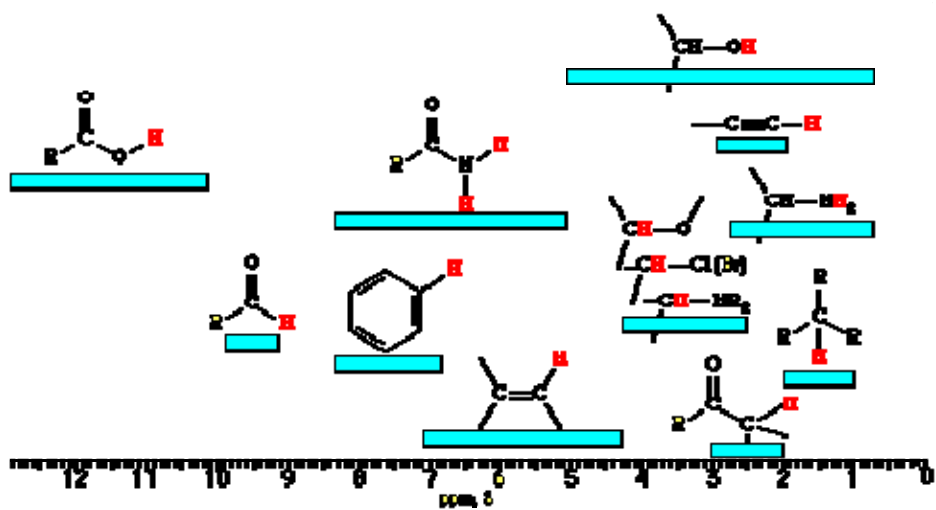


**Figure 2.12** Typical ranges of chemical shifts for protons in different groups in NMR

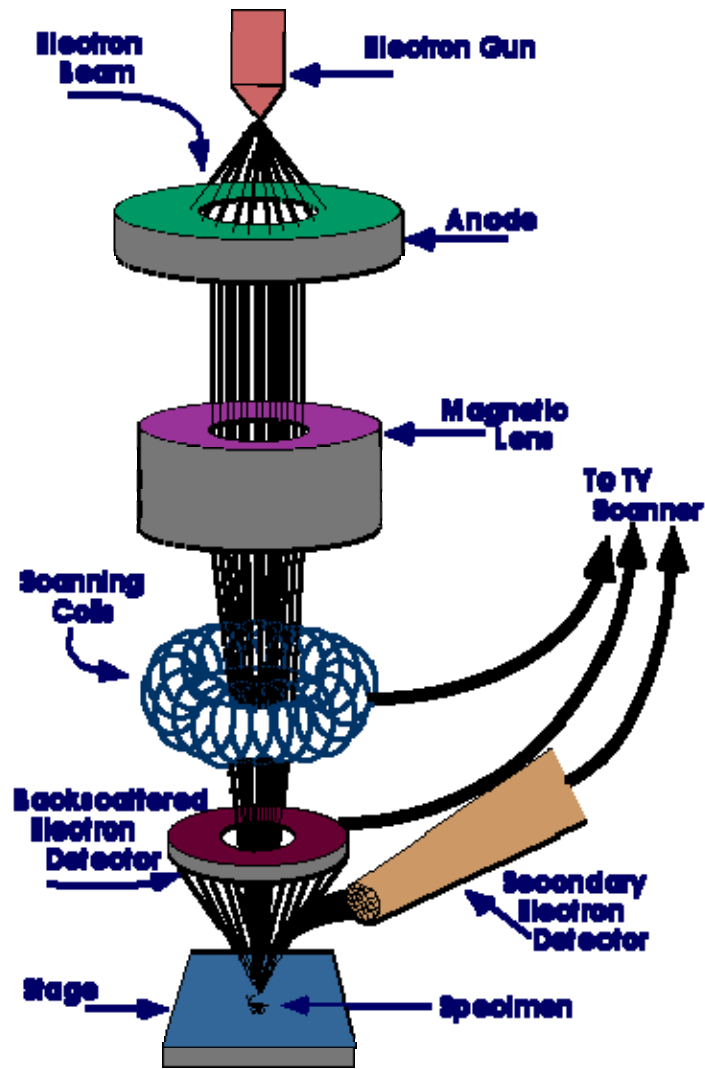


**Figure 2.13** Principle of working of SEM

[<http://surf.eng.iastate.edu/~karie/Documentation>]

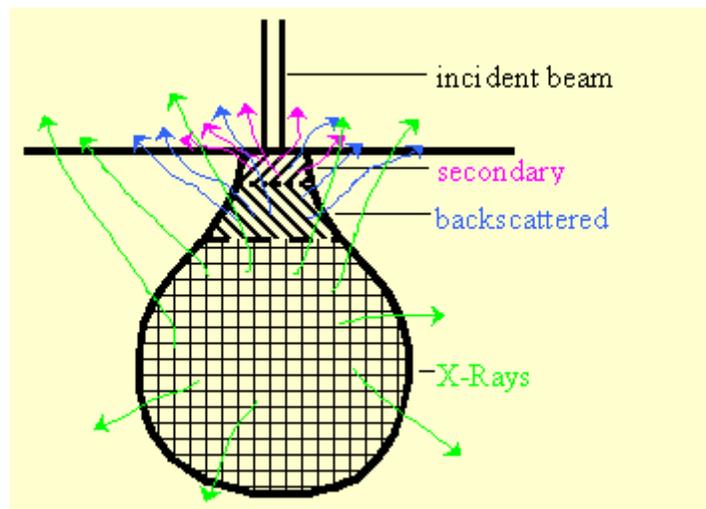


**Figure 2.14** Interaction volume of the electron beam and the specimen in SEM



**Figure 2.15** Denton Vacuum Bench top cold sputter/etch unit used for preparing samples for SEM [Denton Vacuum]

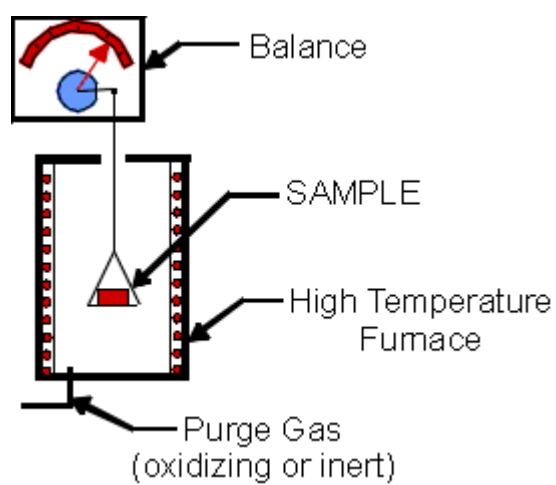
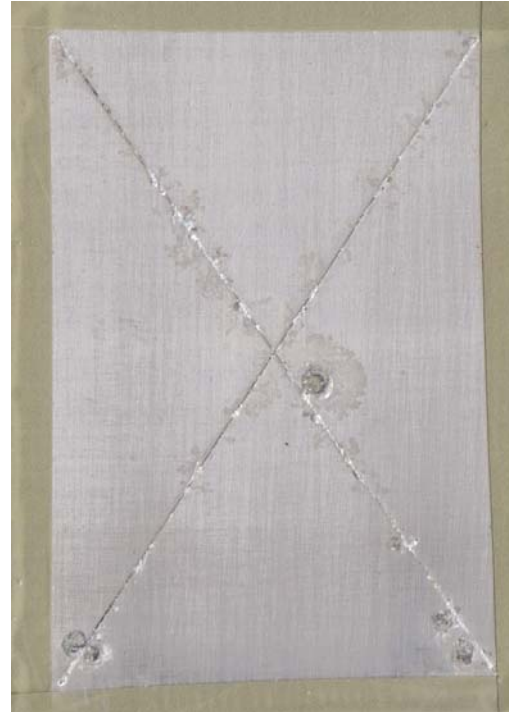


**Figure 2.16** Experimental set-up for TGA

## FIGURES

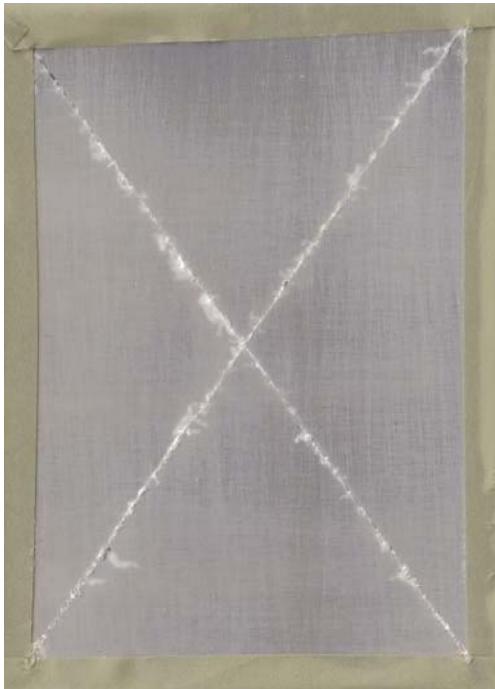


**(a) RT cured**



**(b) HT cured**

**Figure 3.1** ND-20 coating formulation (Refer Table 3.1) without silane and inhibitors after 30 days of salt water immersion



**(a) RT cured**



**(b) HT cured**

**Figure 3.2** N-1 coating formulation (Refer Table 3.3) without corrosion inhibitors after 30 days of salt water immersion



**(a) No corrosion inhibitor**



**(b) with zinc phosphate inhibitor**

**Figure 3.3** NP-1 coating formulation (a) without corrosion inhibitors and (b) with zinc phosphate (Refer Table 3.3 and 3.4) after 60 days of salt water immersion

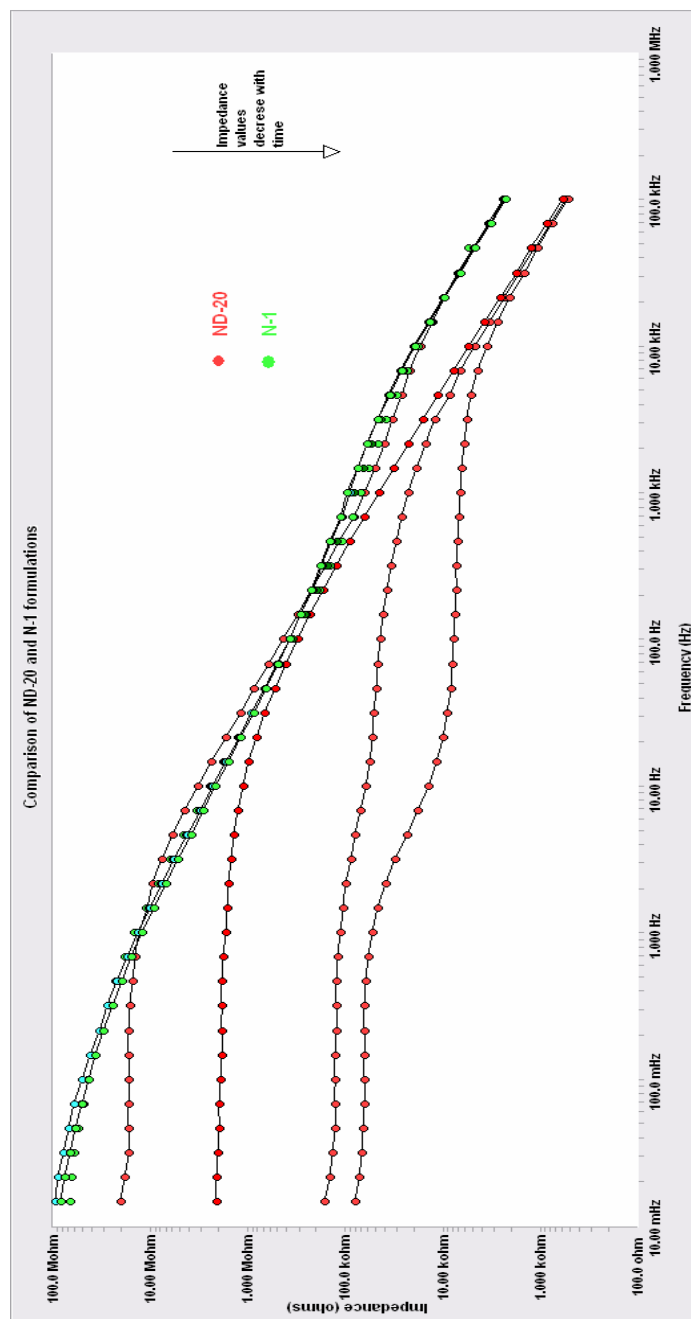


**Figure 3.4** Comparison of EIS impedance plots for ND-20 and N-1 coating formulations after 14 days of EIS testing

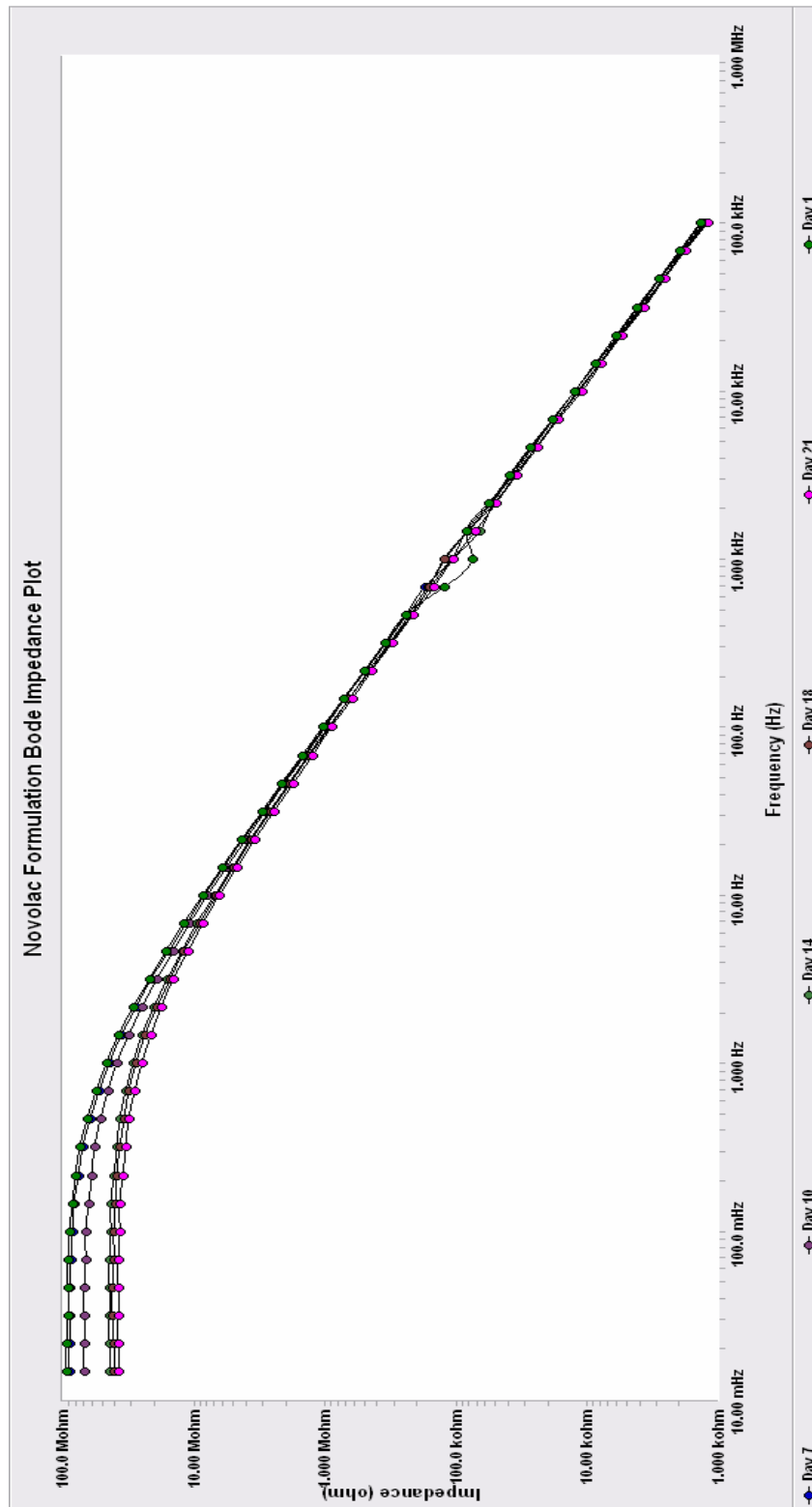


**Figure 3.5** Bode impedance plot for NP-1 formulation

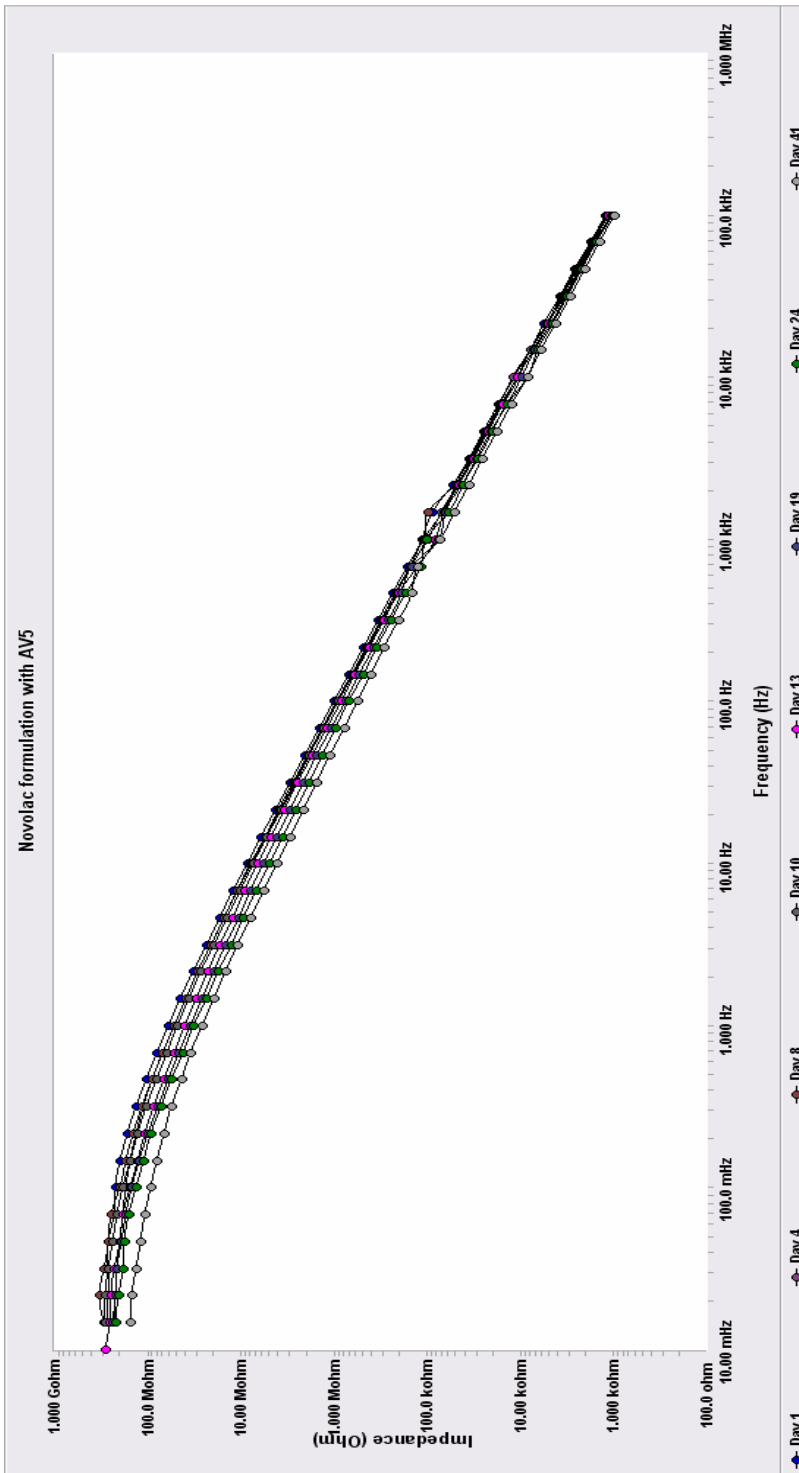
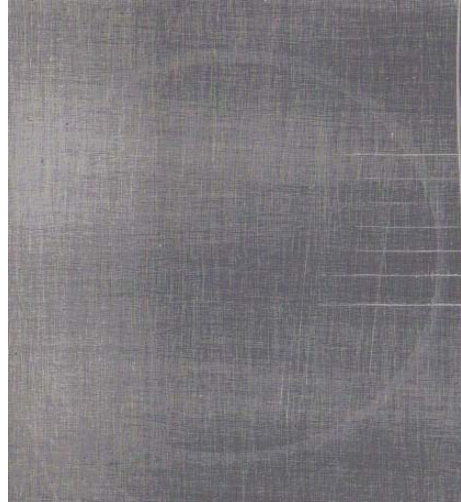


Figure 3.6 Bode impedance plot for N-2 formulation



**(a)**



**(b)**

**Figure 3.7** Samples of (a) ND-20 and (b) NP-1 coating formulations after exposure in EIS test

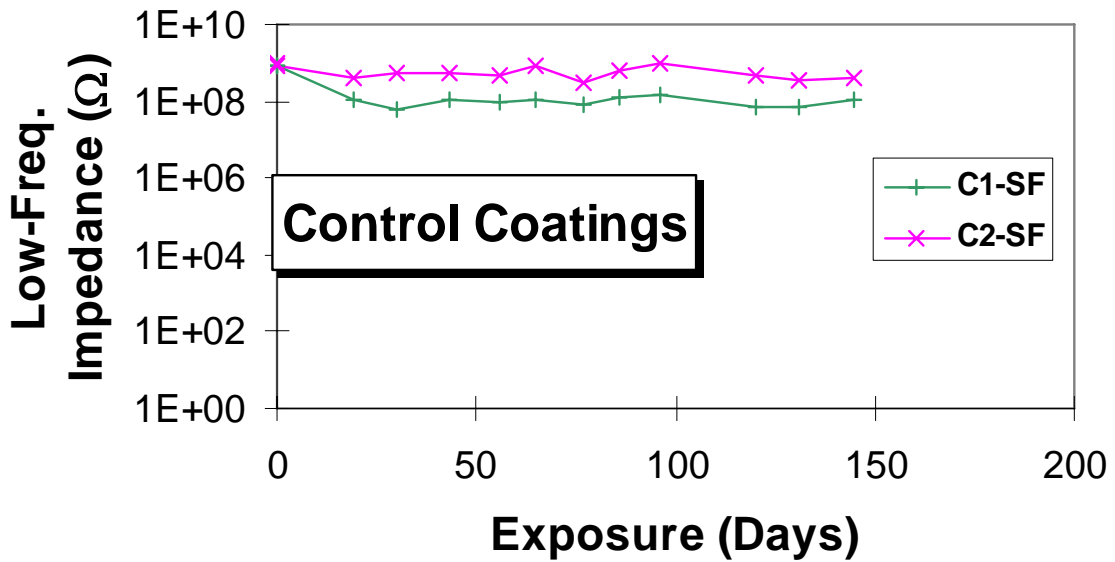


Figure 3.8 Low-frequency impedance plots for control coatings exposed to ASTM B117 test

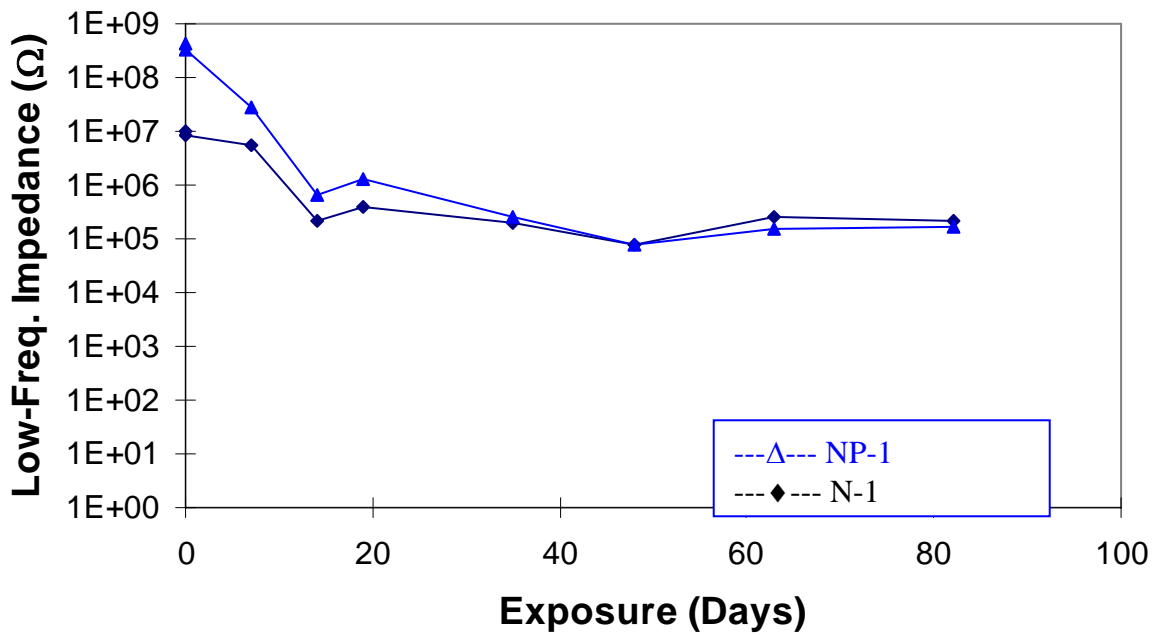
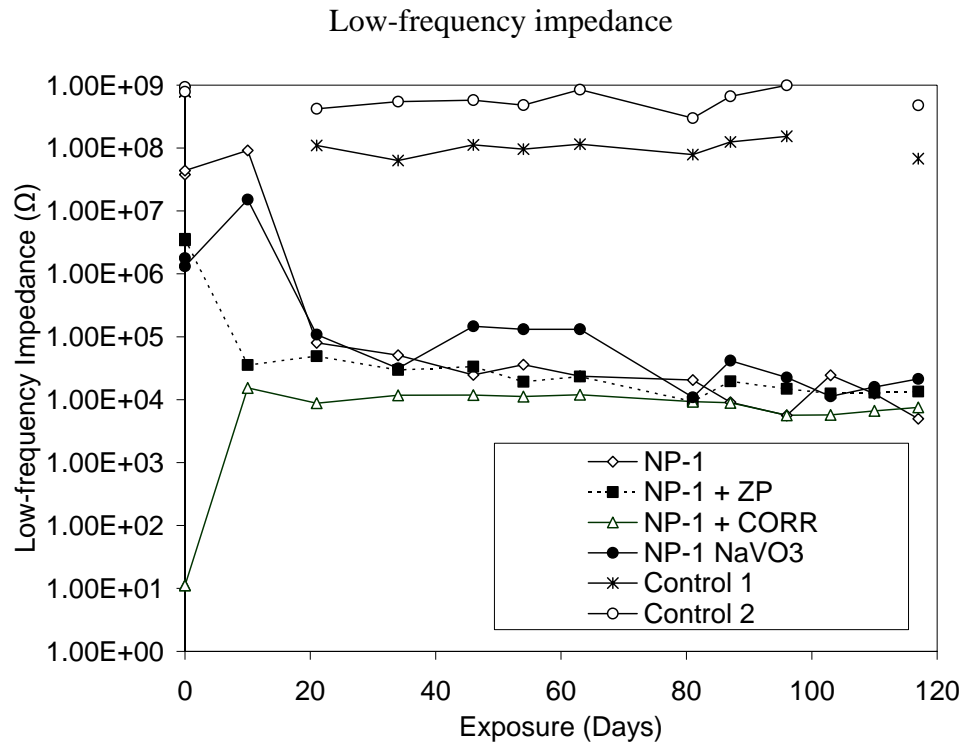


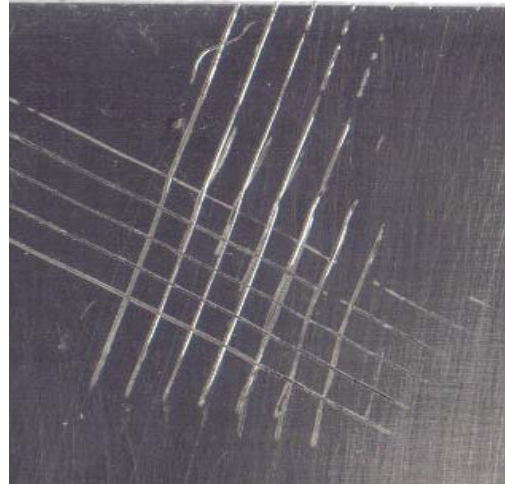
Figure 3.9 Low-frequency impedance plots for N-1 and NP-1 superprimers coatings exposed in ASTM B117 test



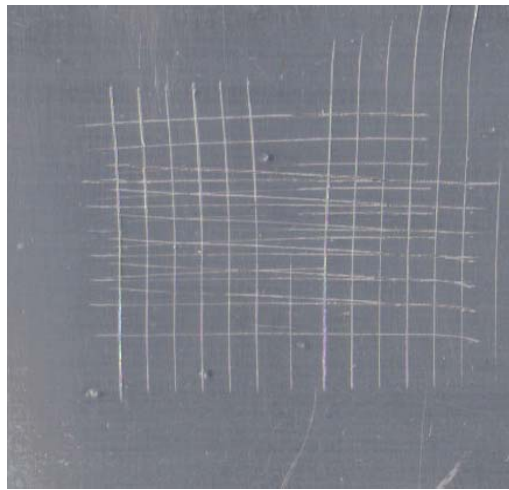
**Figure 3.10** Low-frequency impedance plots for superprimer coatings with different inhibitors, exposed in ASTM B117 test



**(a) ND-20**

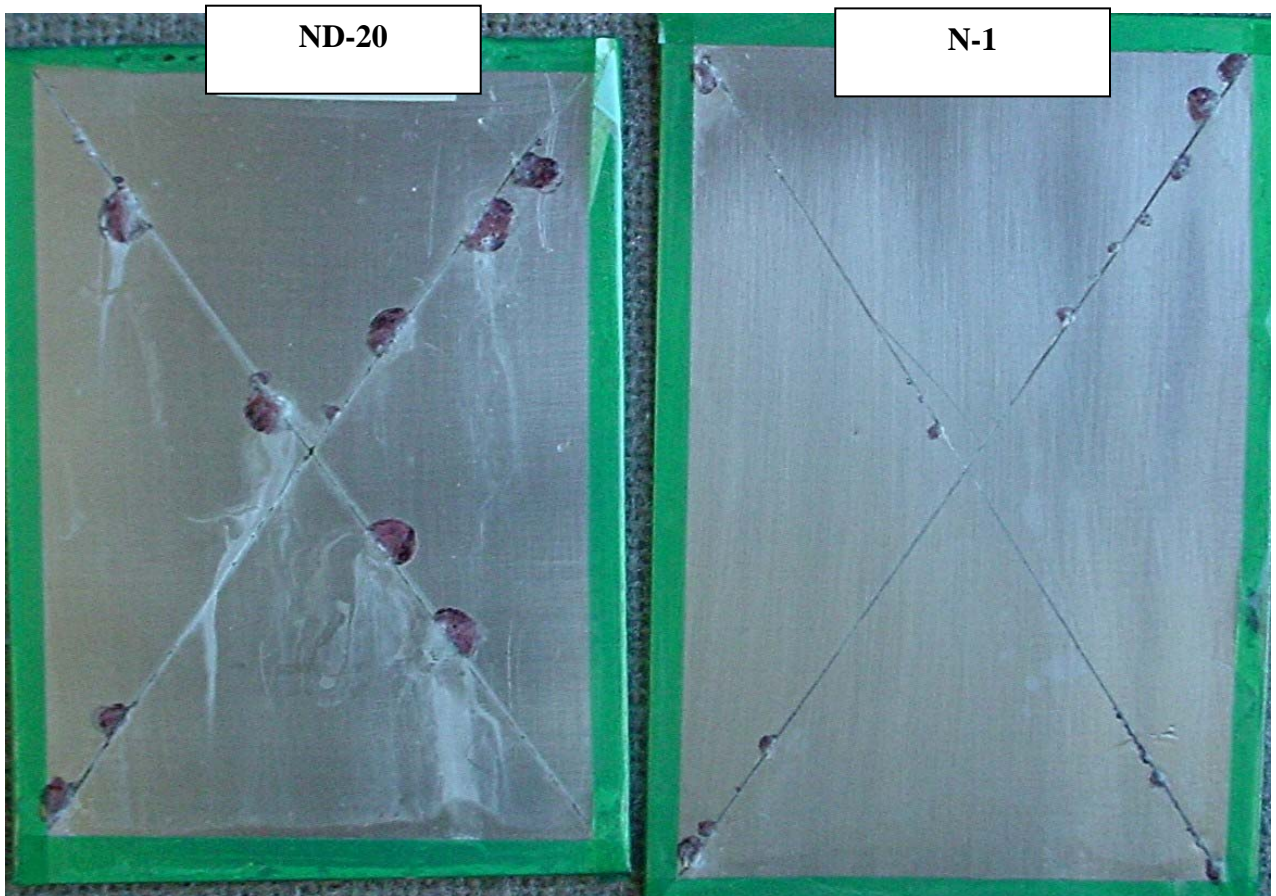


**(b) N-1**



**(c) NP-1**

**Figure 3.11** Adhesion test samples of some novolac-based superprimer formulations



(a)

(b)

**Figure 3.12** Samples of ND-20 and N-1 superprimers exposed to ASTM B117 test for 1000 hrs and 1500 hrs respectively

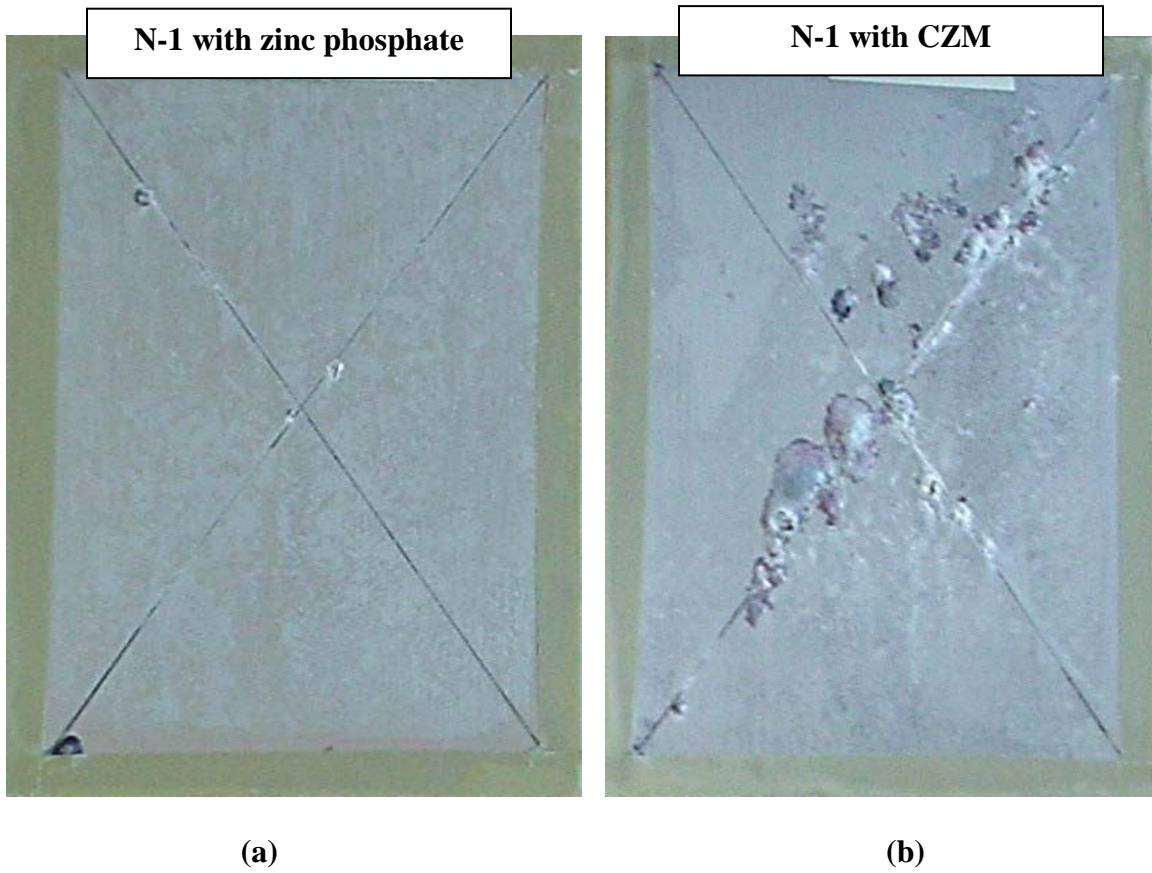


**Figure 3.13** Samples of N-1 superprimer with zinc phosphate and CZM corrosion inhibitors, exposed to ASTM B117 test for 2000 hrs

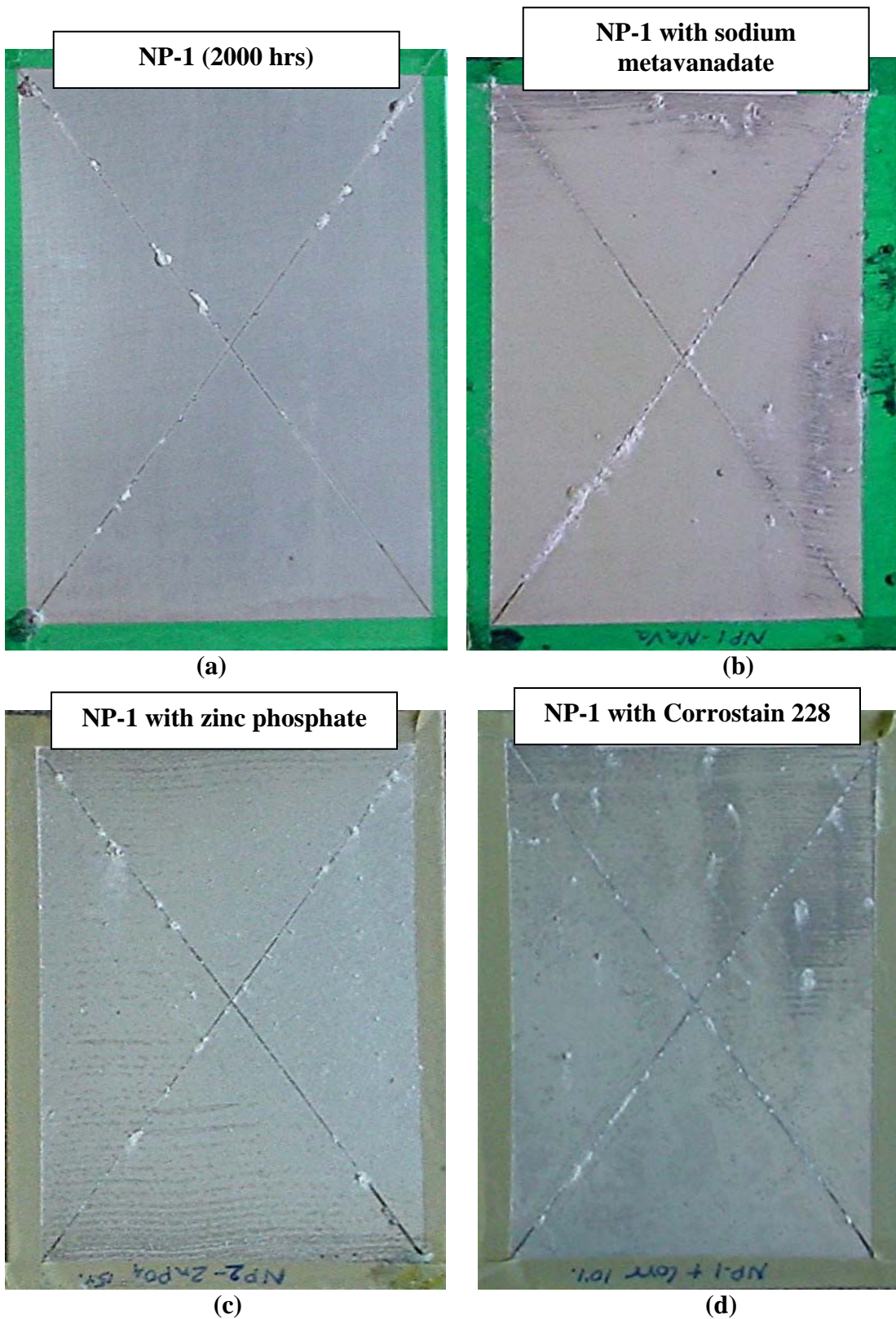


**Figure 3.14** Samples of NP-1 superprimer with different corrosion inhibitors, exposed to ASTM B117 test for 2500 hrs

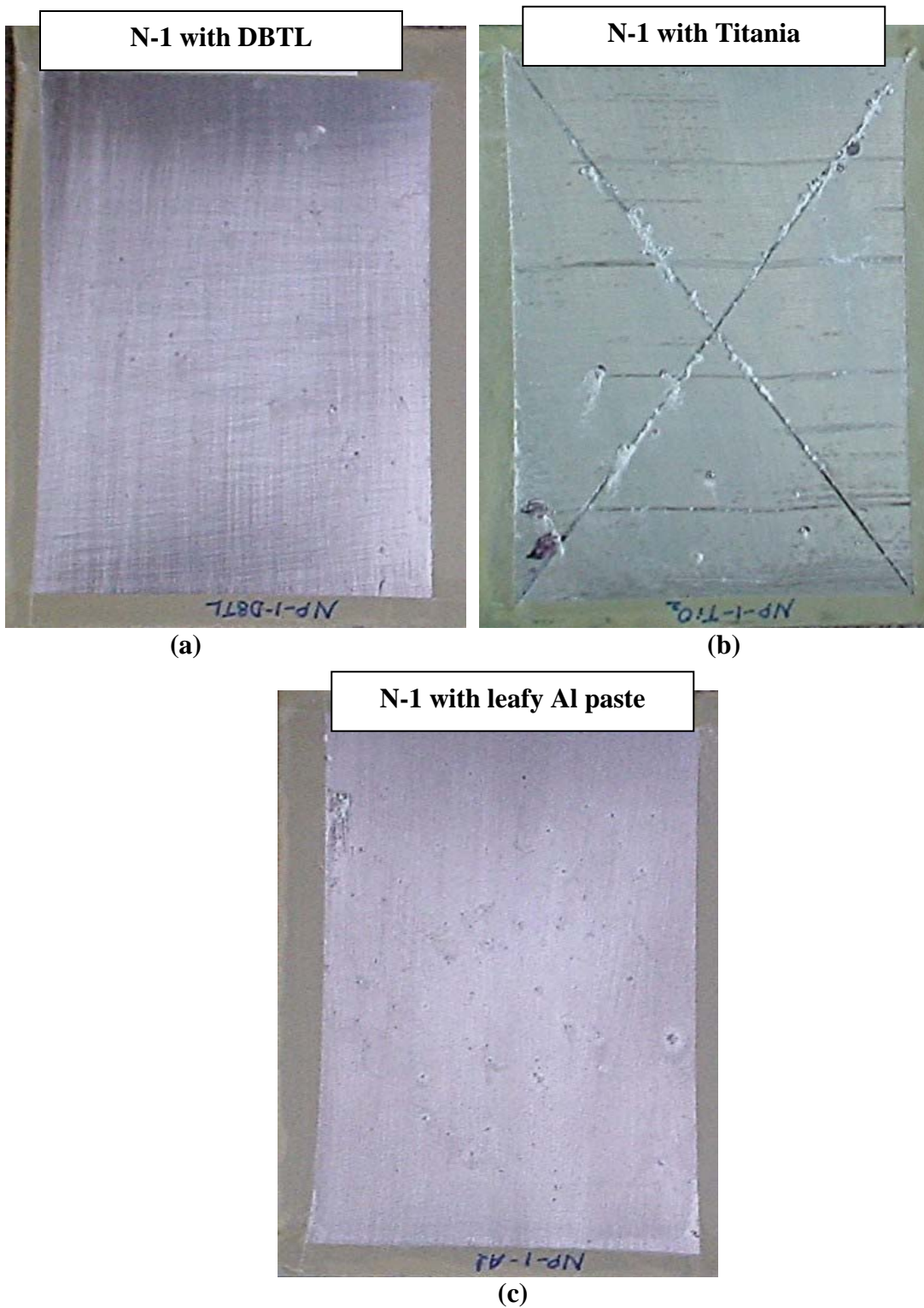
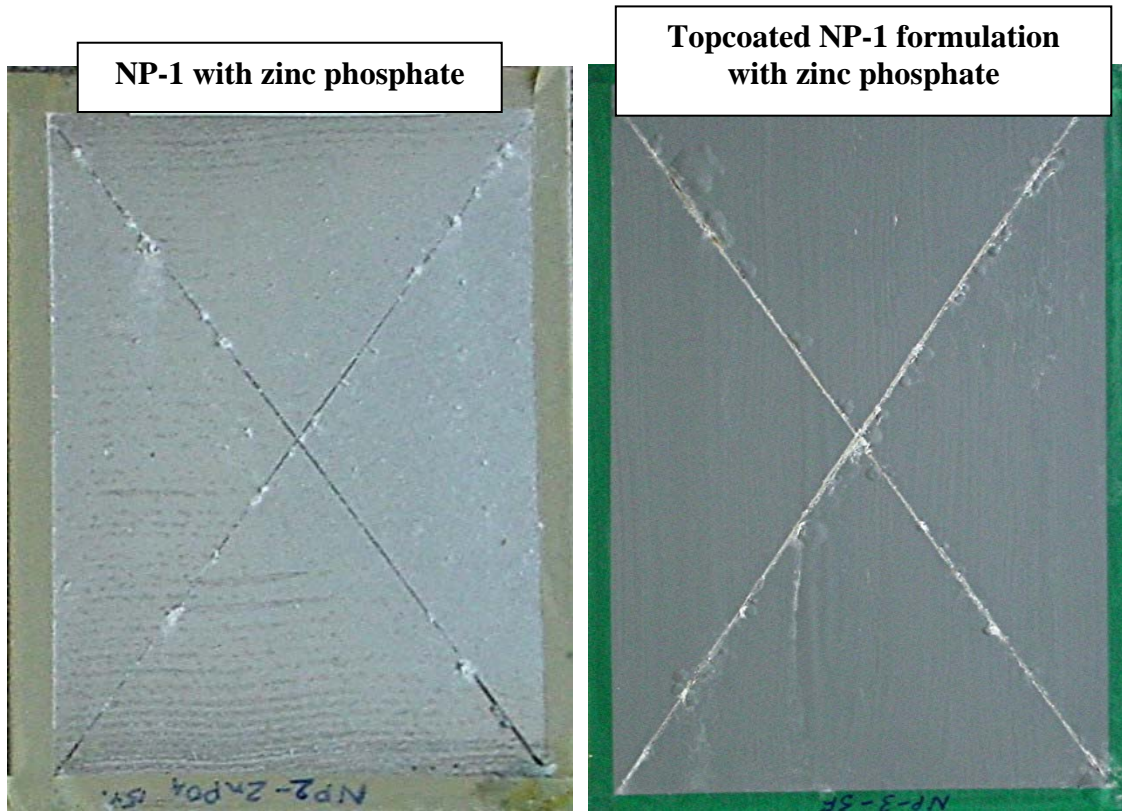
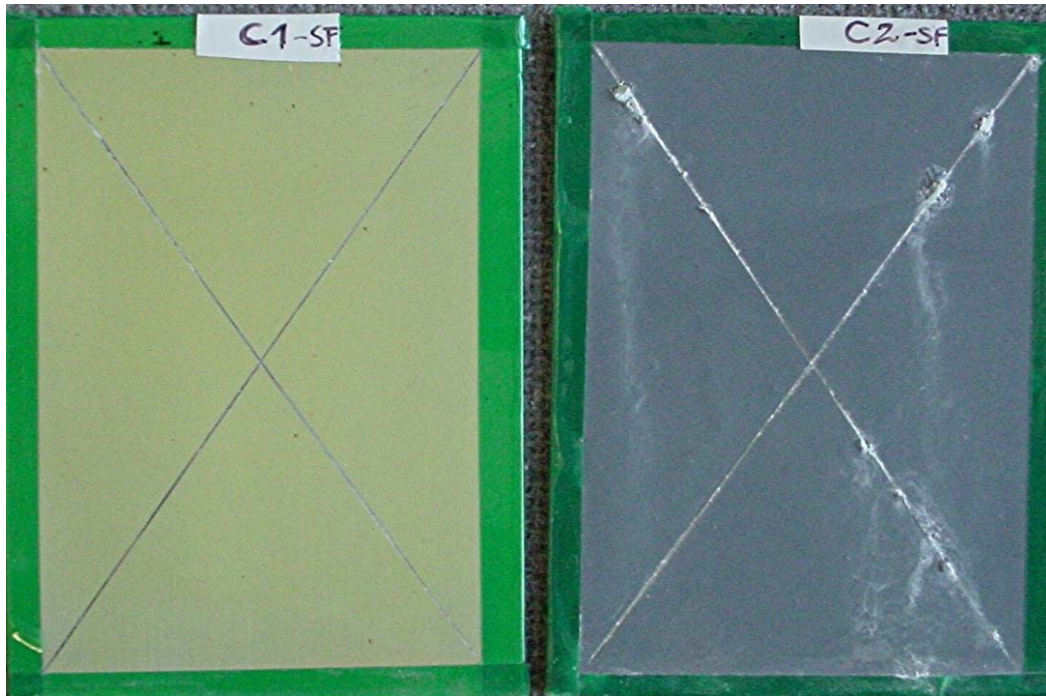


**Figure 3.15** Samples of NP-1 superprimer different additives, exposed to ASTM B117 test for 1000 hrs



(a)



(b)

(c)

**Figure 3.16** Samples of topcoated NP-1 and control formulations after exposure to

ASTM B117 test

Topcoated NP-1 formulation with zinc phosphate



(a)

Topcoated NP-1 formulation with Corrostatin 228

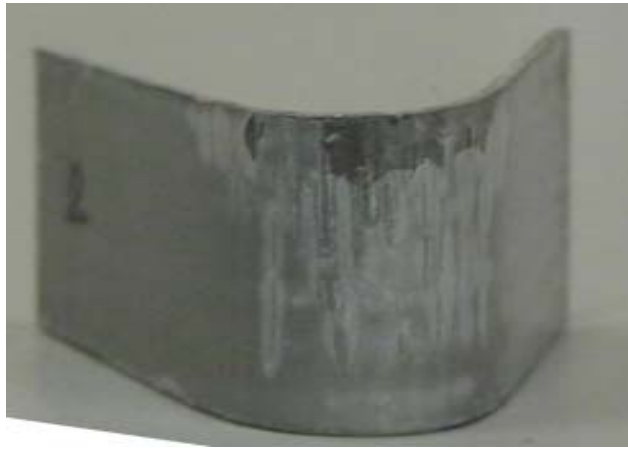


(b)

**Figure 3.17** Samples of topcoated NP-1 after exposure to Ford AGPE test



**(a) ND-20 coating**



**(b) N-1 coating**



**(c) NP-1 coating**

**Figure 3.18** Samples of bend tested coatings after exposure to salt water immersion

## FIGURES

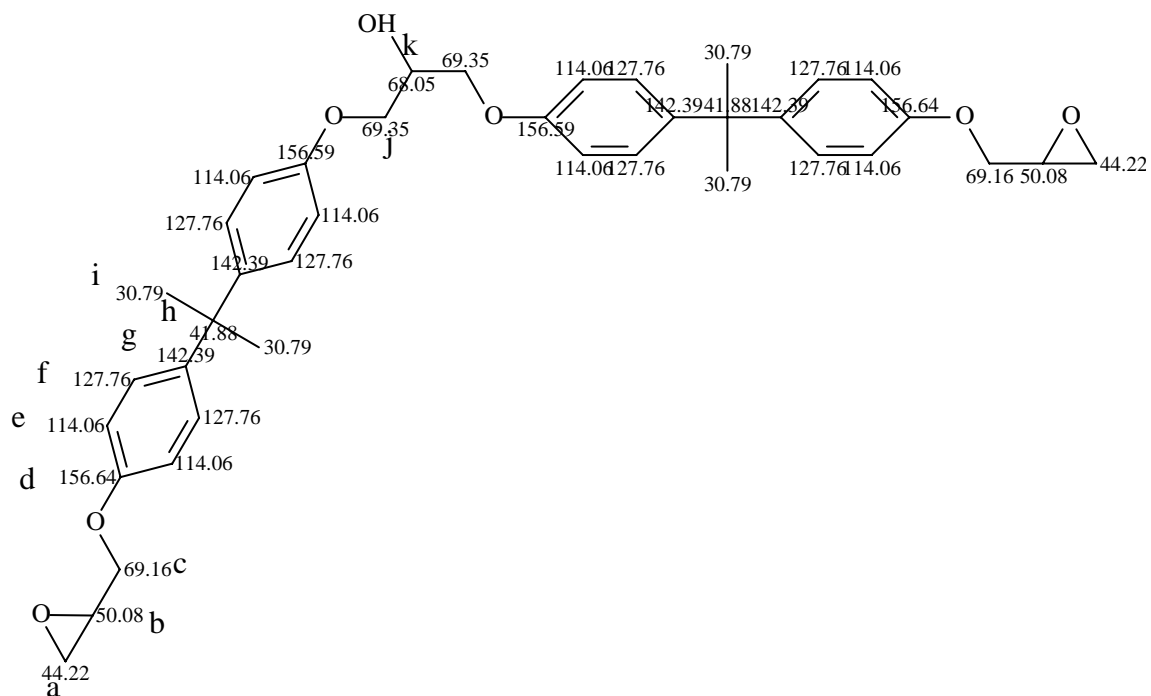


**Figure 4.1** Chemical structure of DGEBA resin with calculated peak positions in <sup>13</sup>C NMR

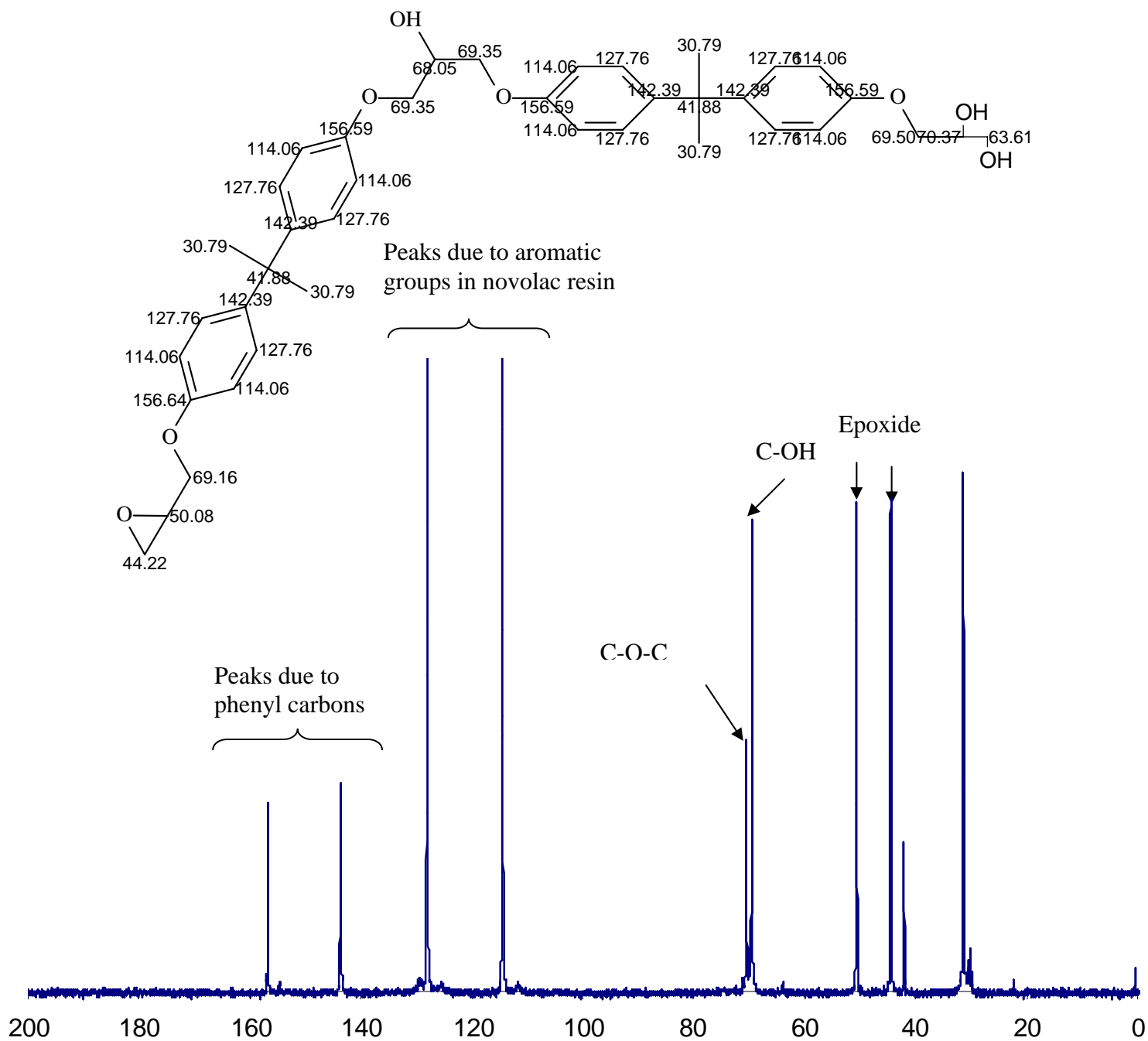


**Figure 4.2** Chemical structure and spectrum of EPIREZ 5003 novolac resin

with calculated peak positions in liquid  $^{13}\text{C}$  NMR



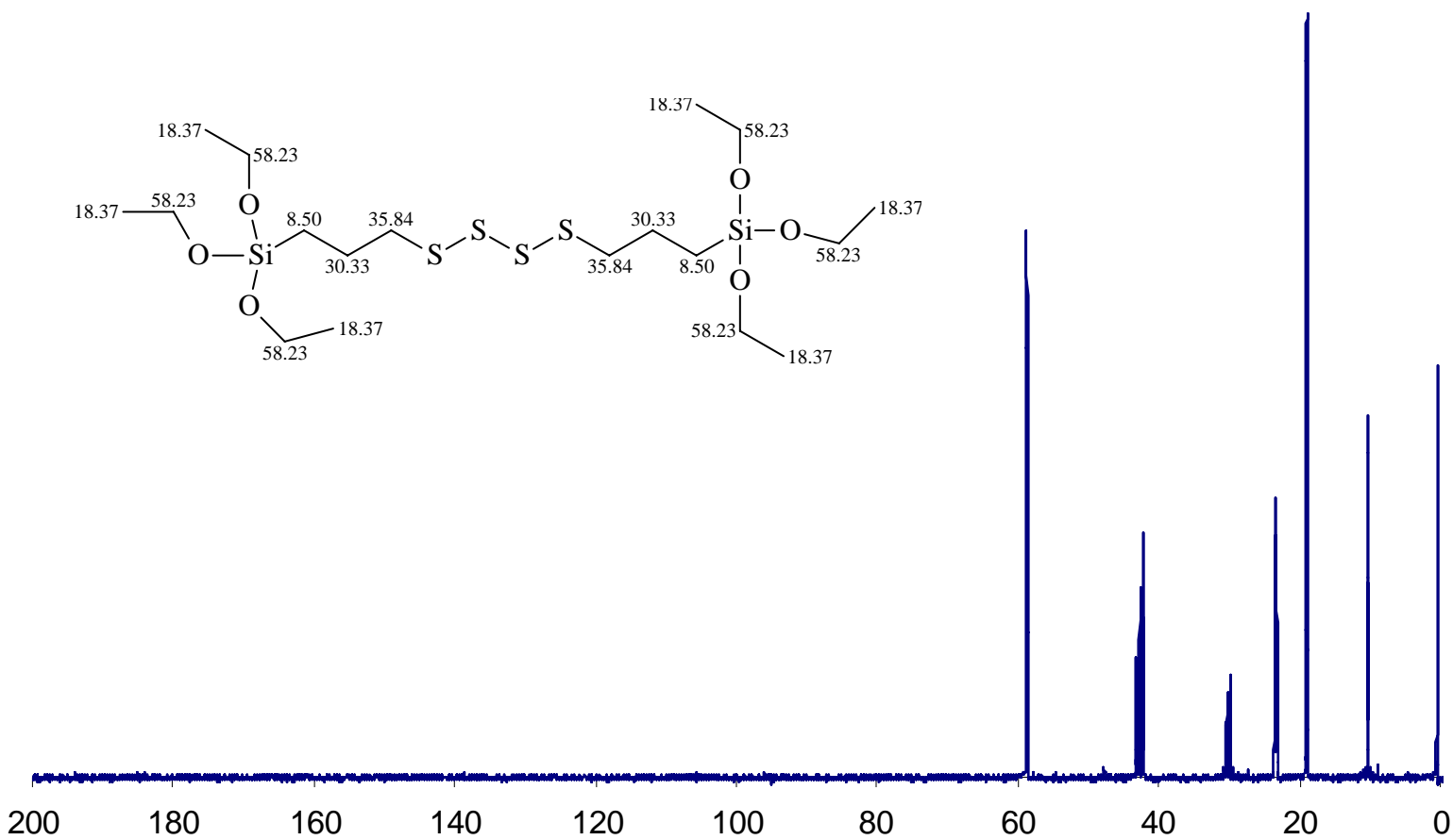


**Figure 4.4** Chemical structure and spectrum of Bis-sulfur silane

with calculated peak positions in liquid  $^{13}\text{C}$  NMR

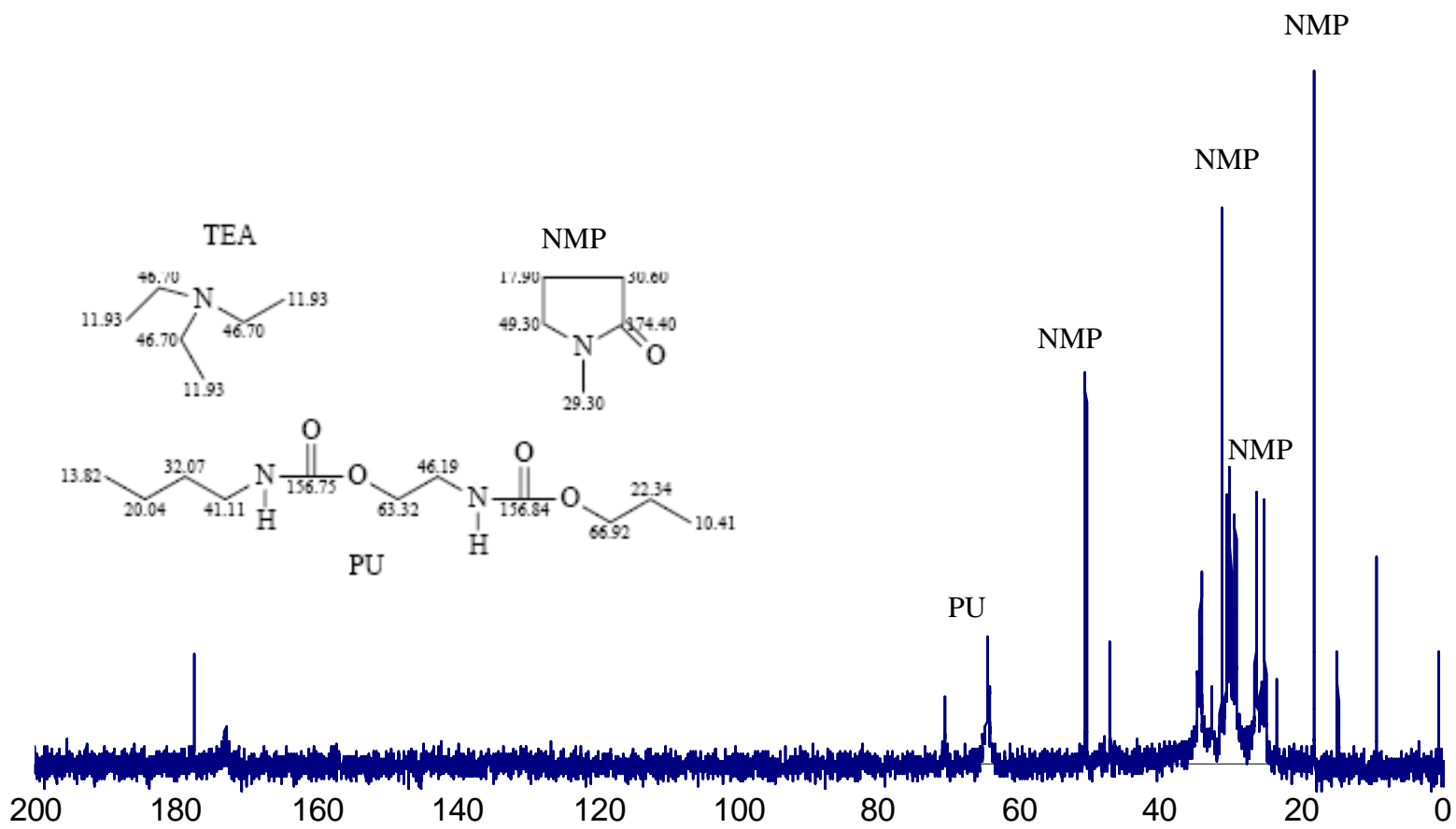


**Figure 4.5** Chemical structure and spectrum of NeoRez R-972  
with calculated peak positions in liquid  $^{13}\text{C}$  NMR





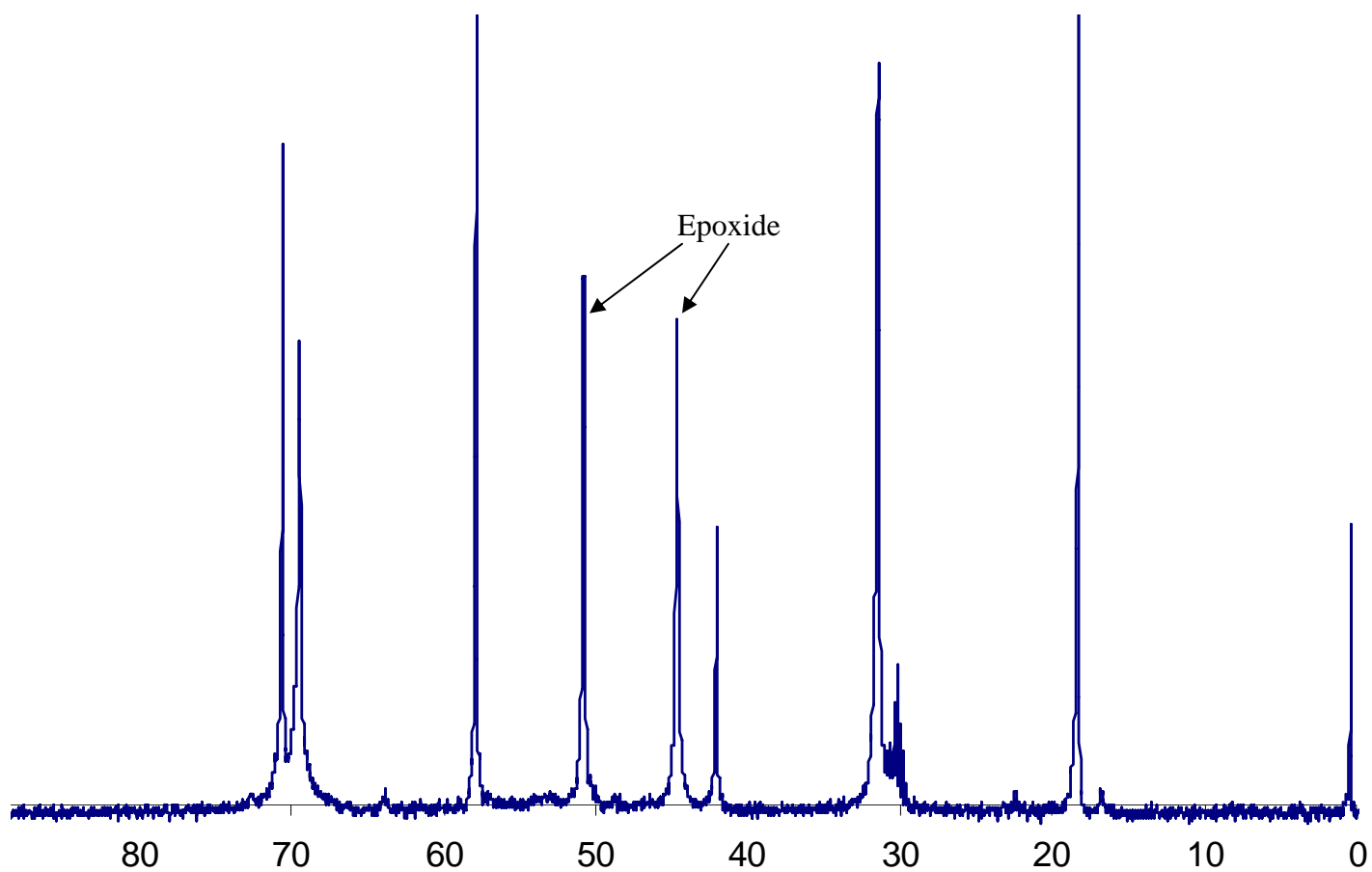
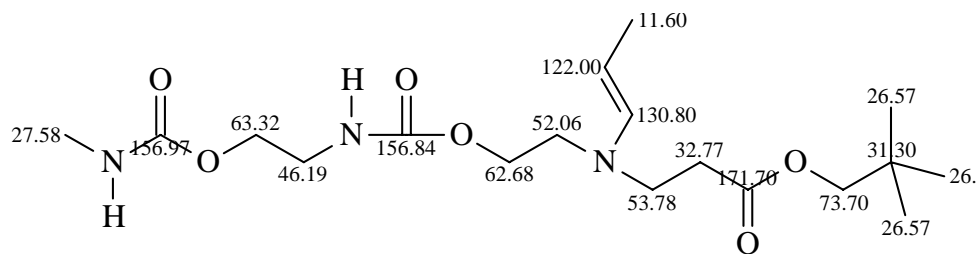


**Figure 4.8** Spectrum of L-2 formulation in liquid  $^{13}\text{C}$  NMR



**Potential reaction product of polyurethane and crosslinker**

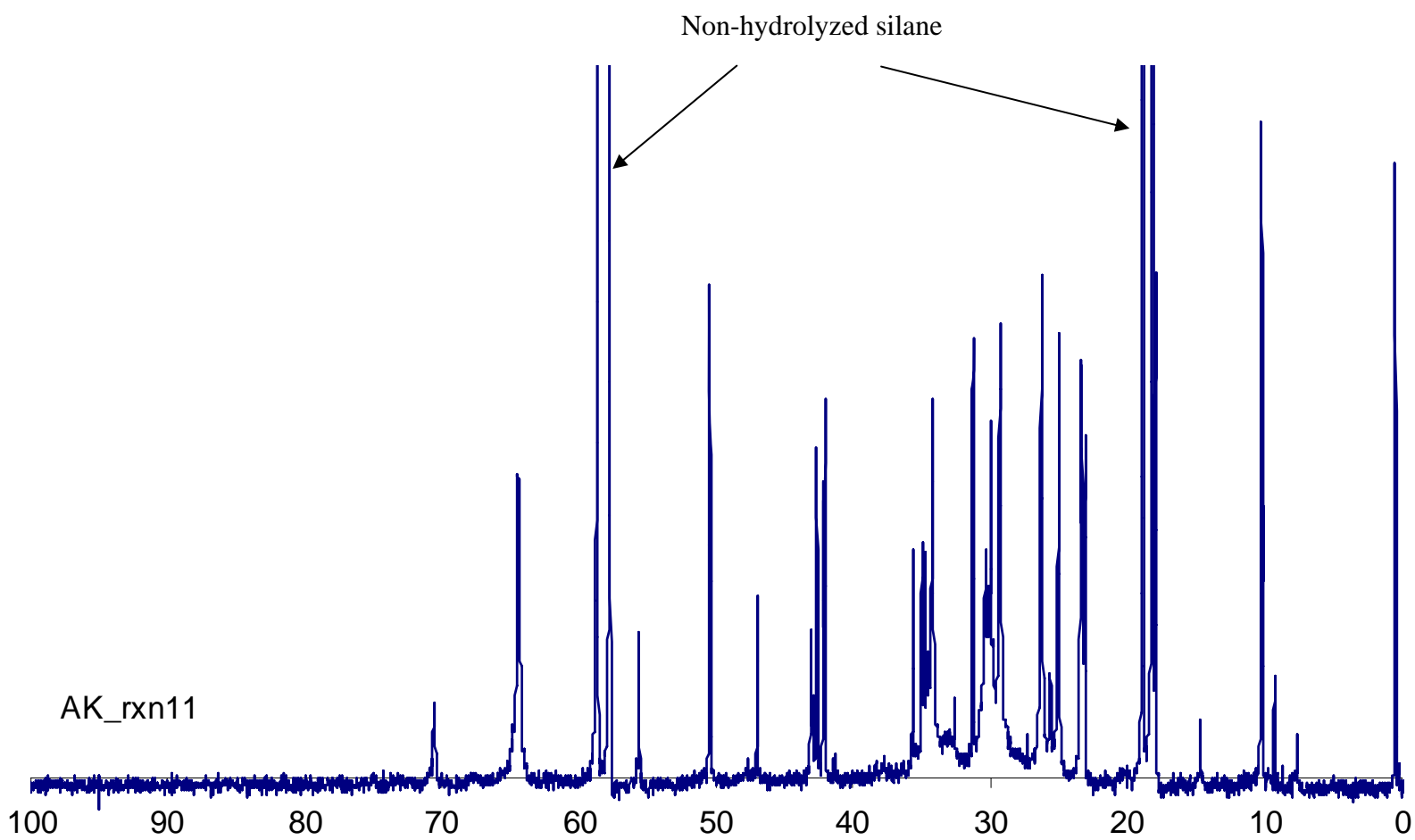


**Figure 4.9** Spectrum of L-3 formulation and potential reaction product

with calculated peak positions in liquid  $^{13}\text{C}$  NMR

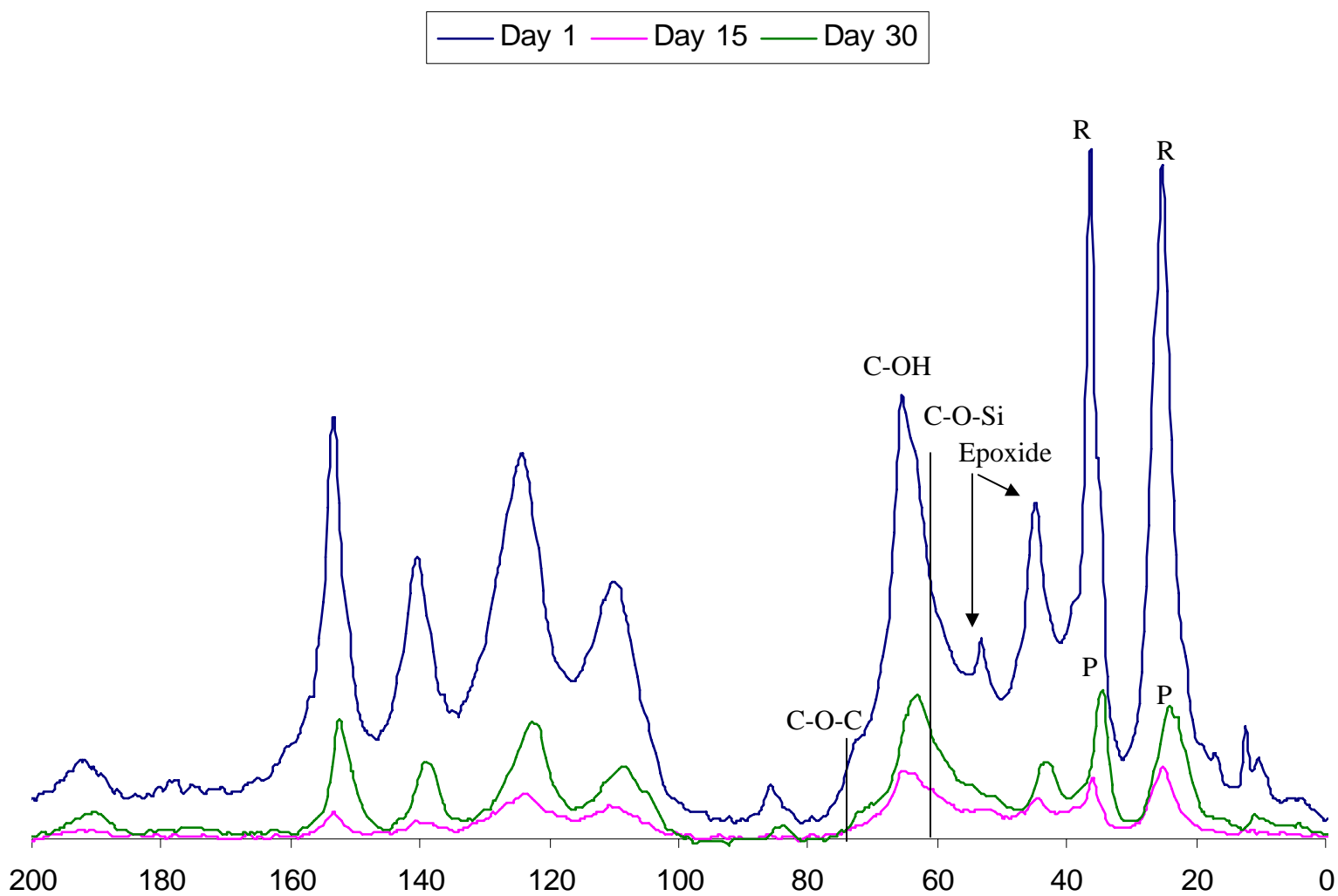


**Figure 4.10** Spectrum of S-1 sample in solid state  $^{13}\text{C}$  NMR

— Day 1 — Day 15 — Day 30

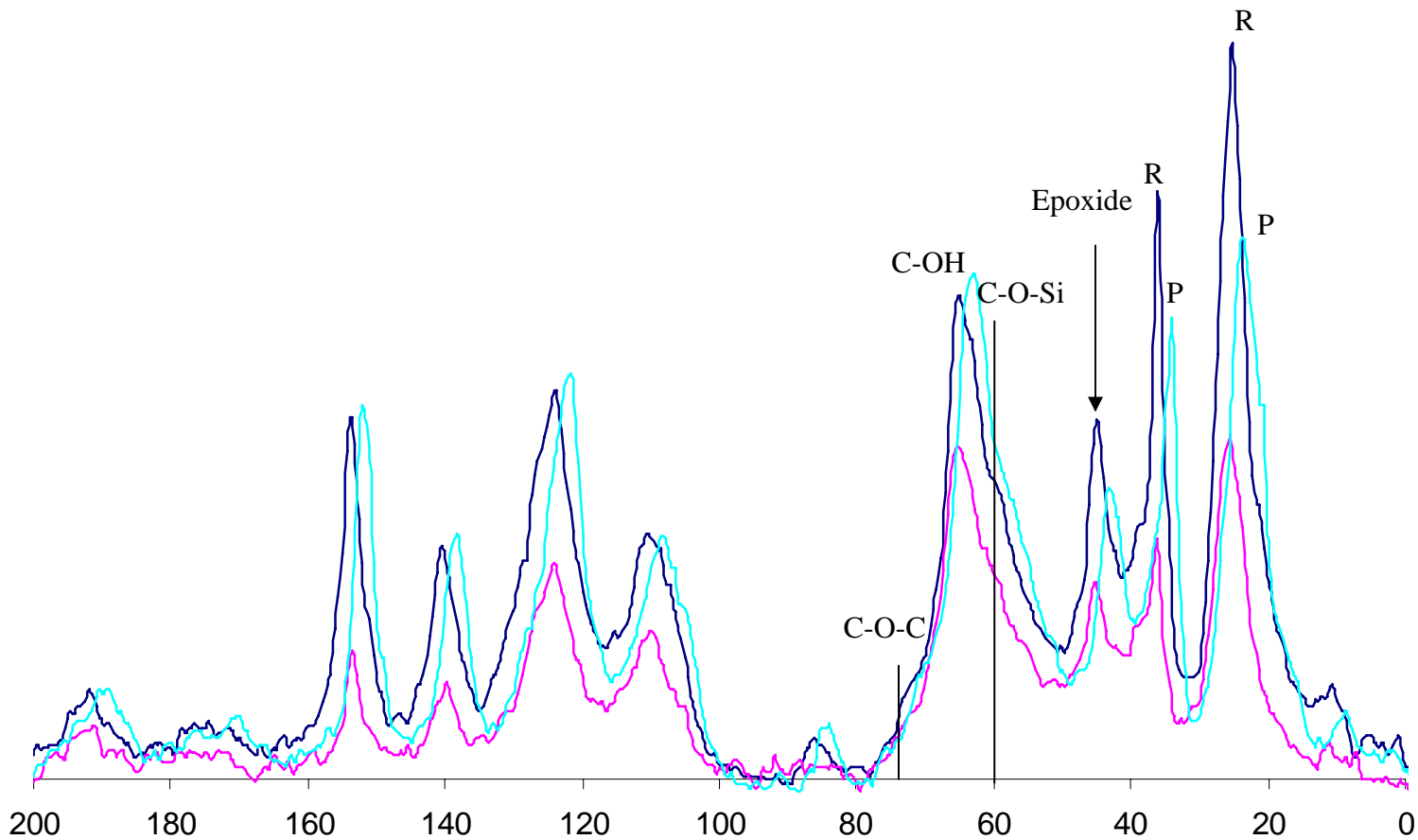


**Figure 4.11** Spectrum of S-2 sample in solid state  $^{13}\text{C}$  NMR

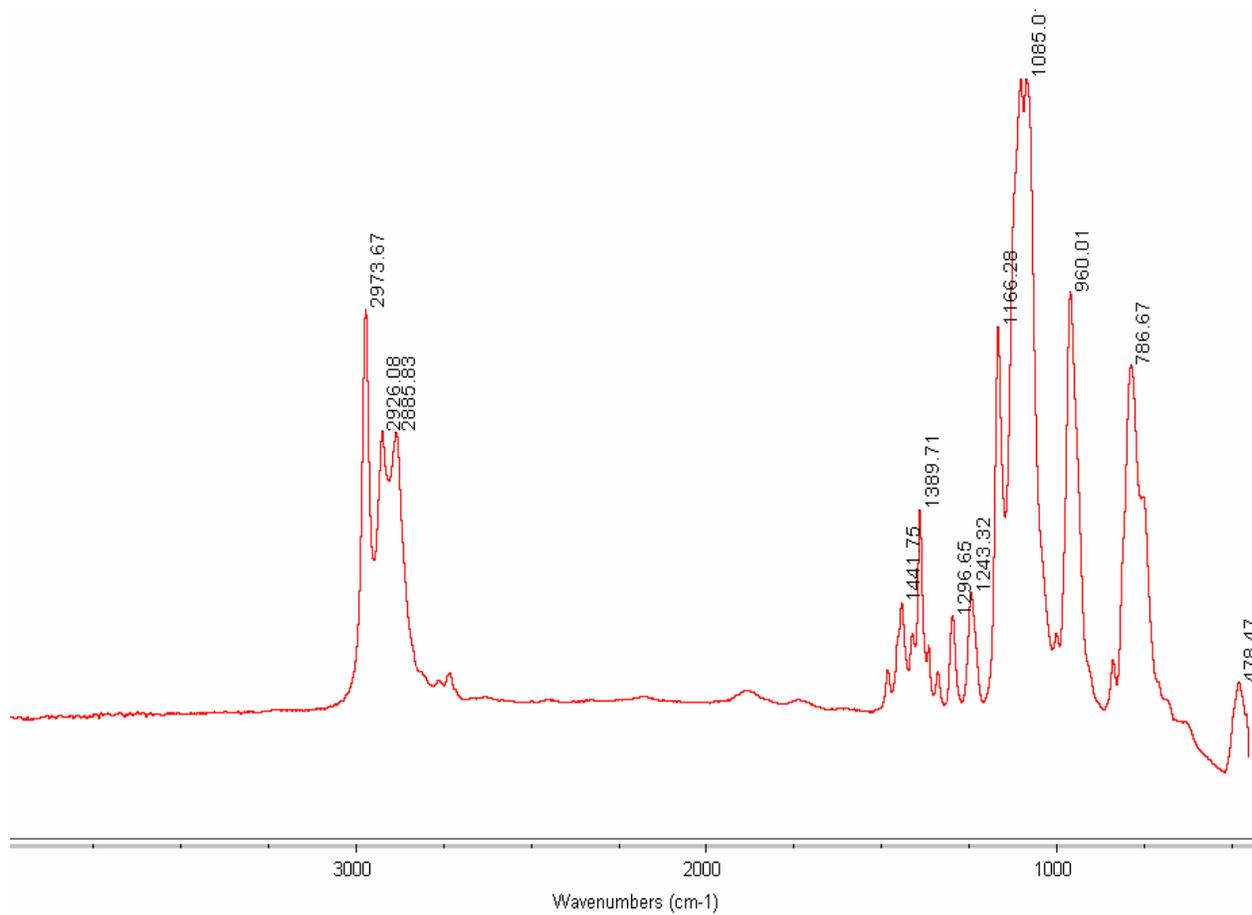


**Figure 4.12** RAIR spectrum of a pure bis-sulfur silane film with annotated peaks after room temperature curing

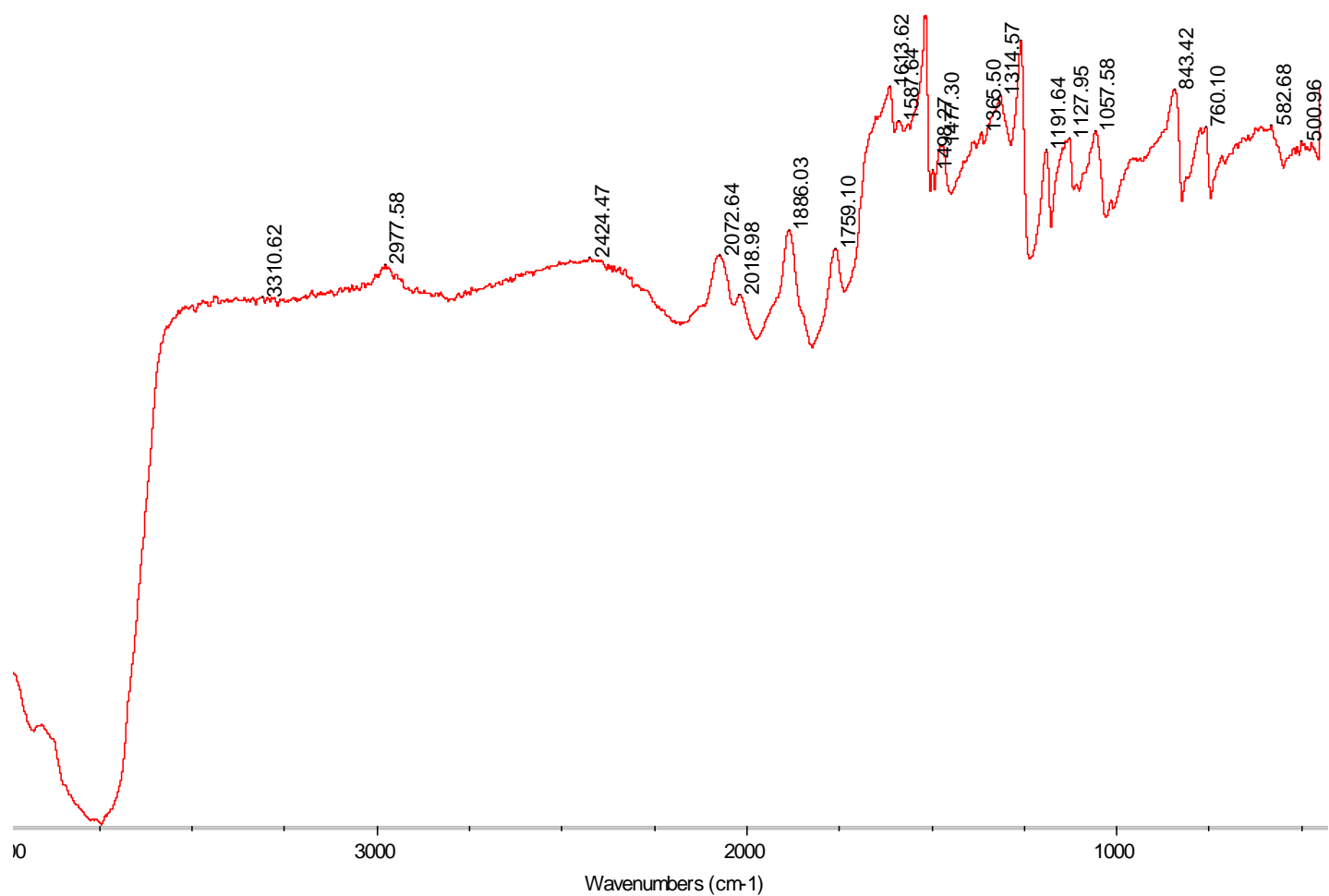


**Figure 4.13** RAIR spectrum of EPIKURE 6870 with annotated peaks after room temperature curing

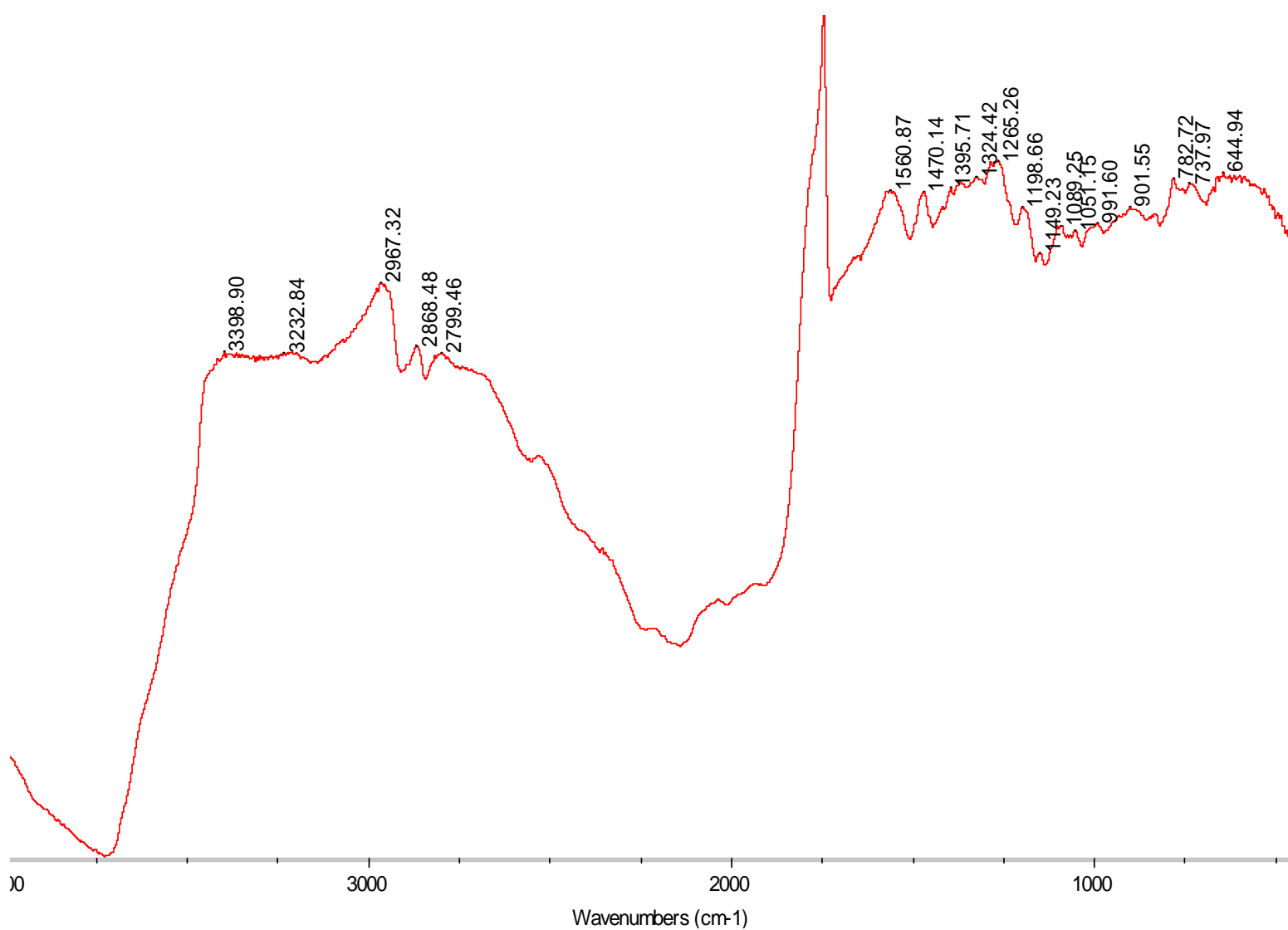


**Figure 4.14** RAIR spectrum of NeoRez-R-972 with annotated peaks after room temperature curing

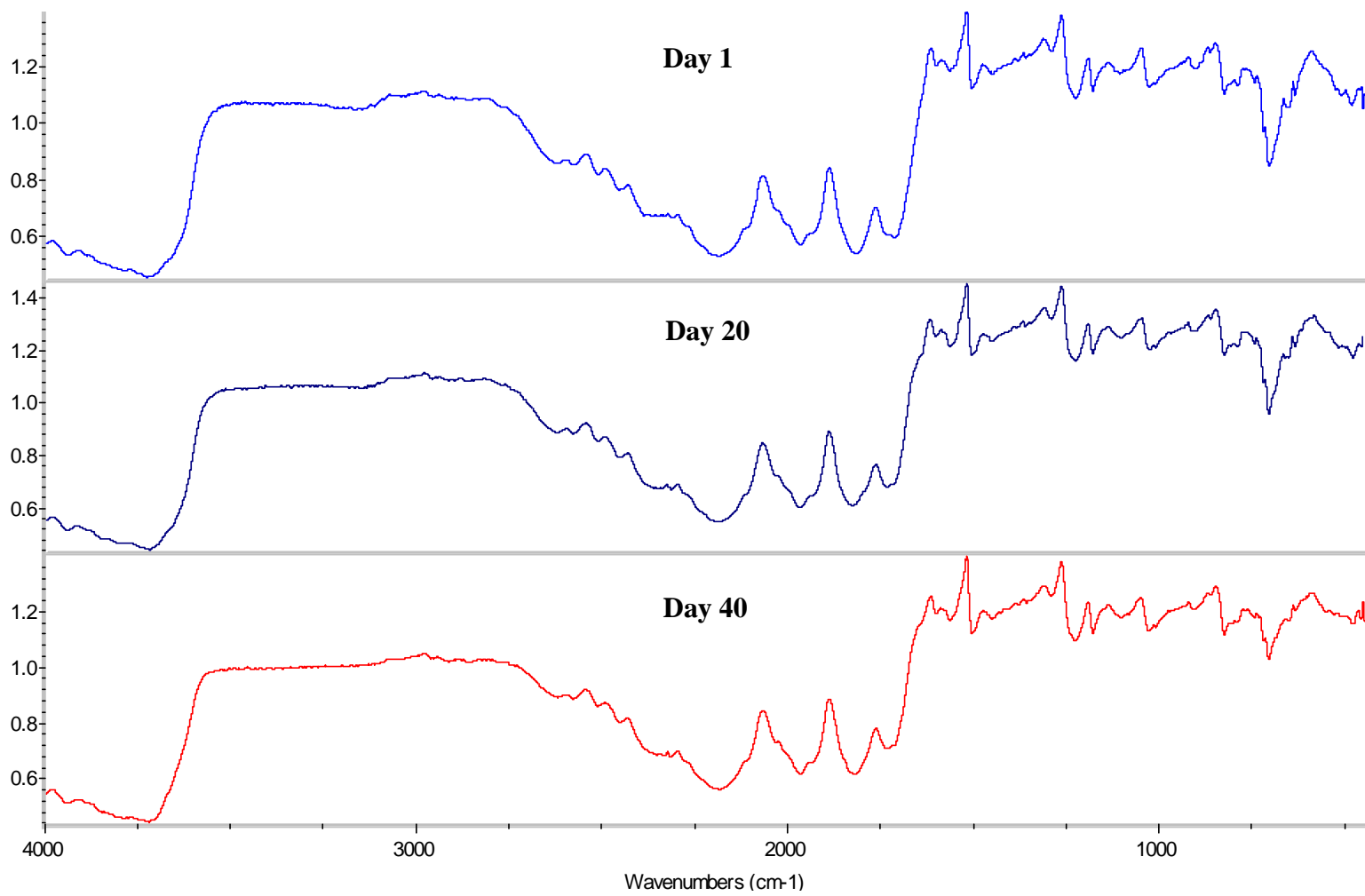


**Figure 4.15** RAIR spectra of ND-20 at specified time intervals of room temperature curing

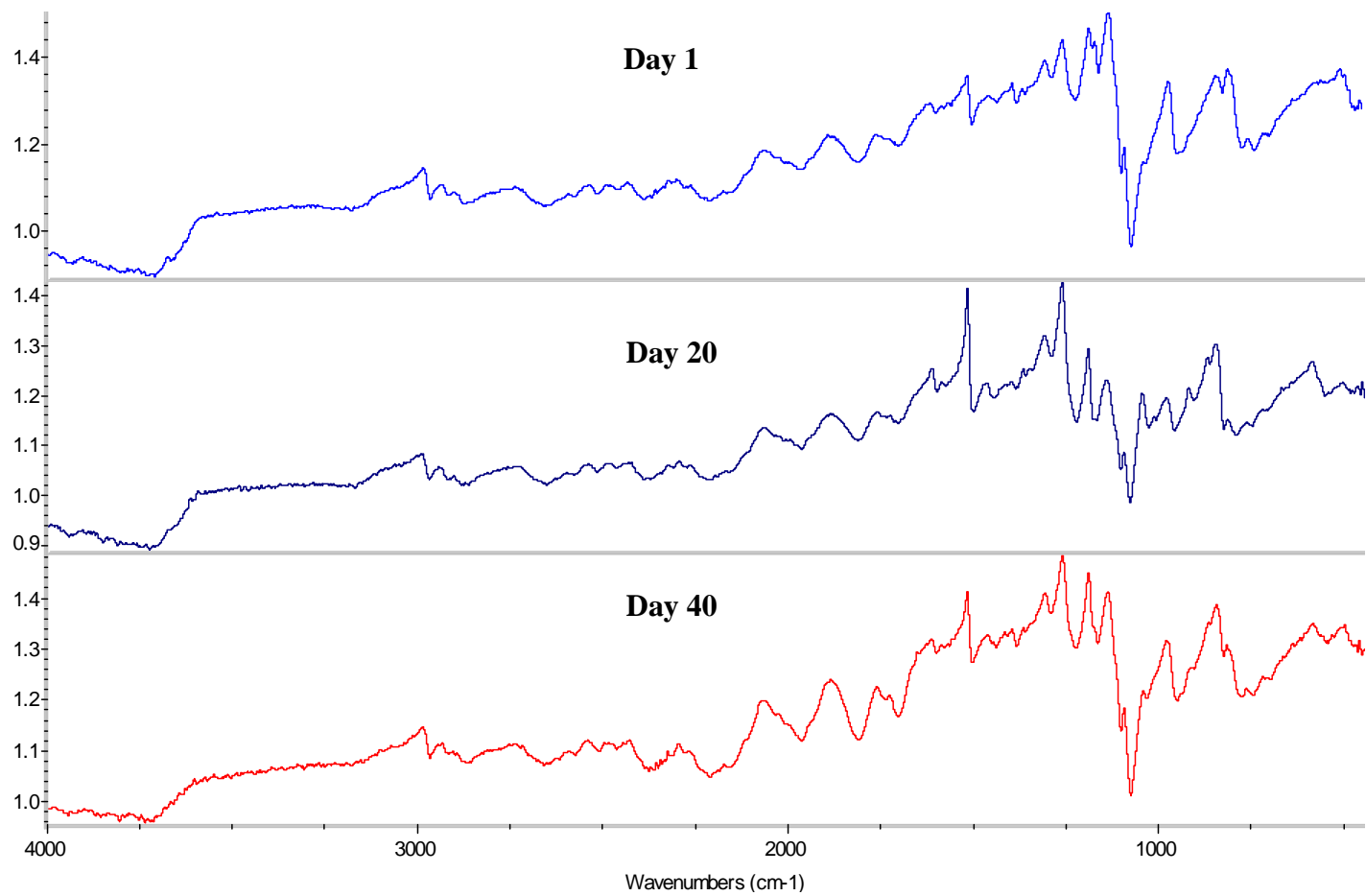
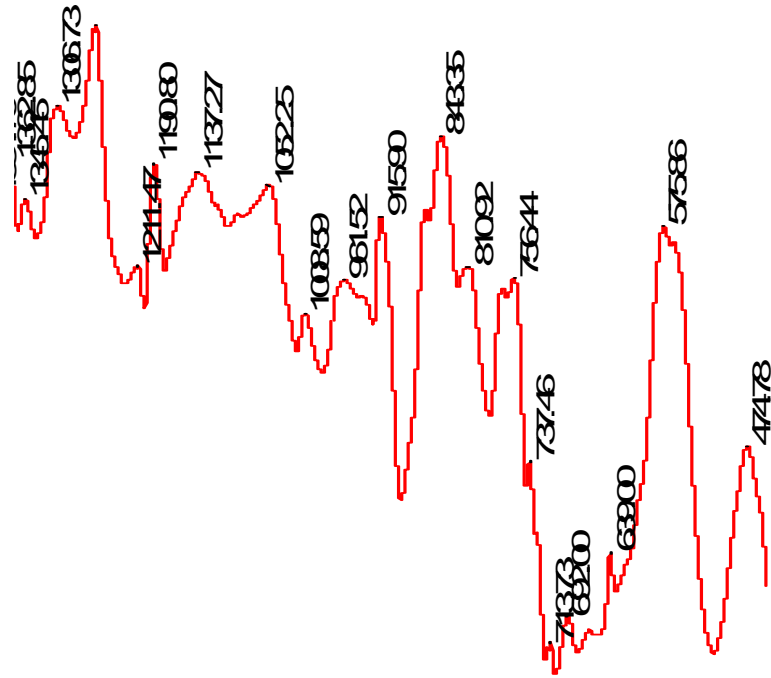
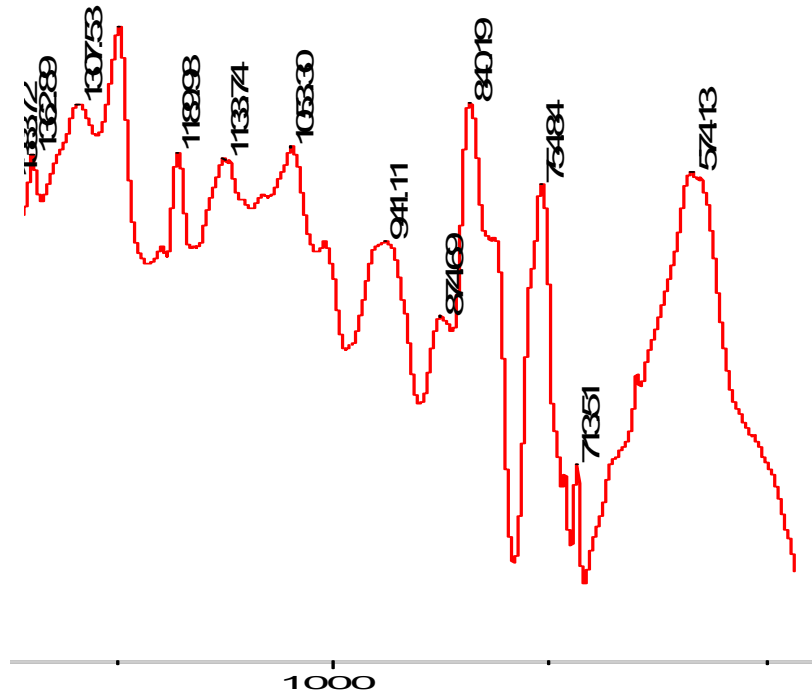


**Figure 4.16** RAIIR spectra of N-1 at specified time intervals of room temperature curing



(a) Room-temperature curing



(b) High-temperature curing

**Figure 4.17** Comparison of RAIR spectra of N-1 after (a) room-temperature and (b) high-temperature curing

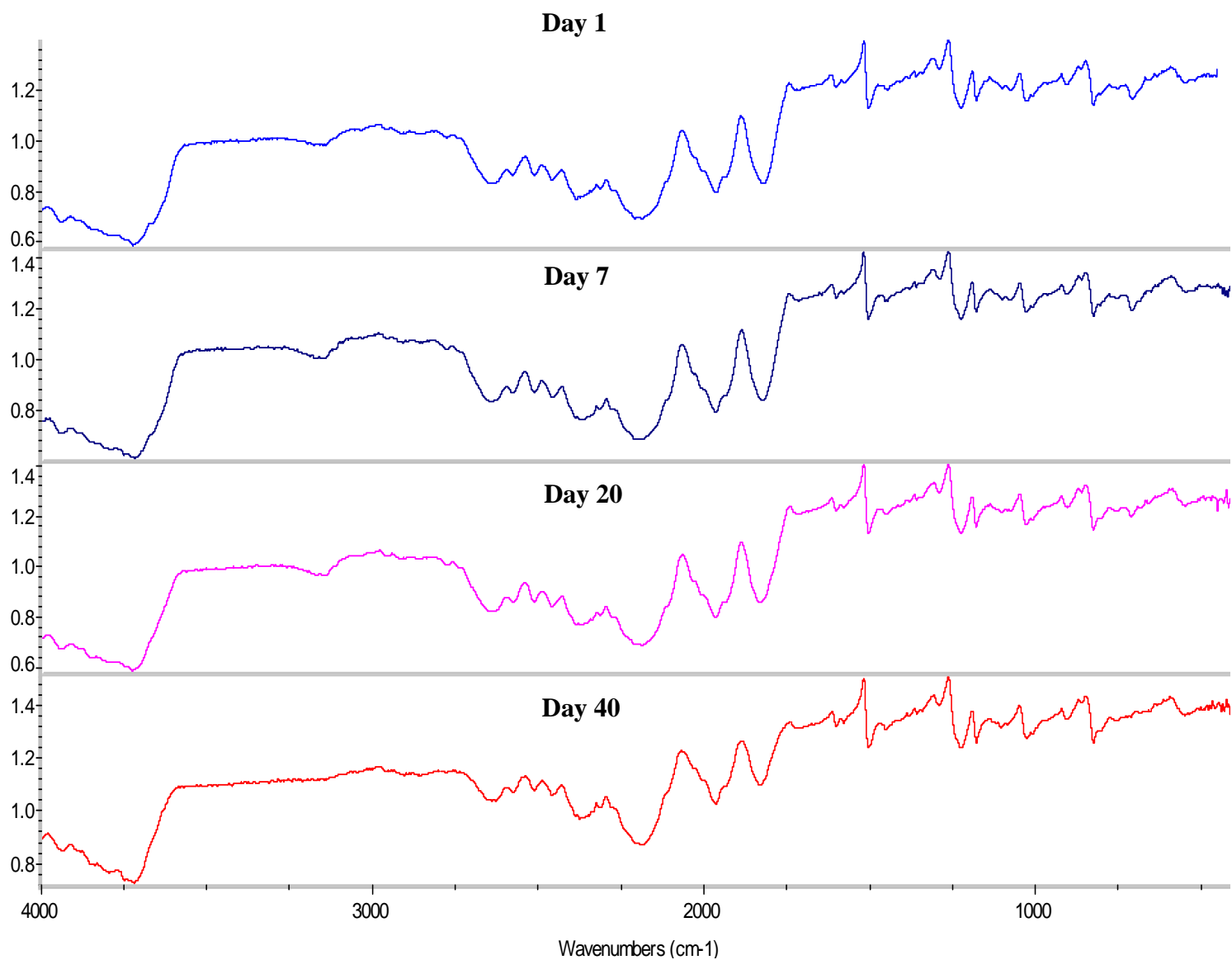


**Figure 4.18** RAIR spectra of NP-1 at specified time intervals of room temperature curing

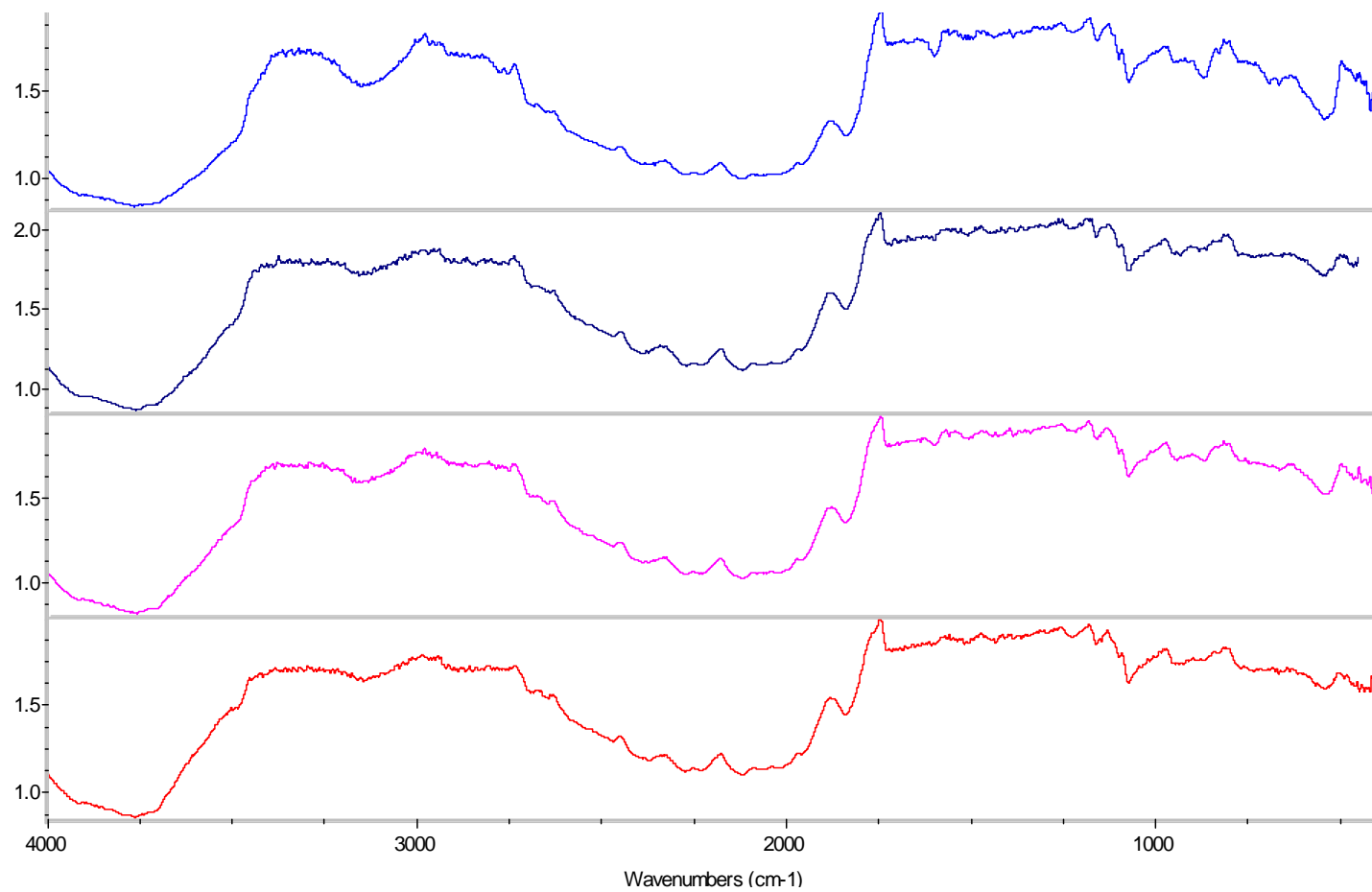
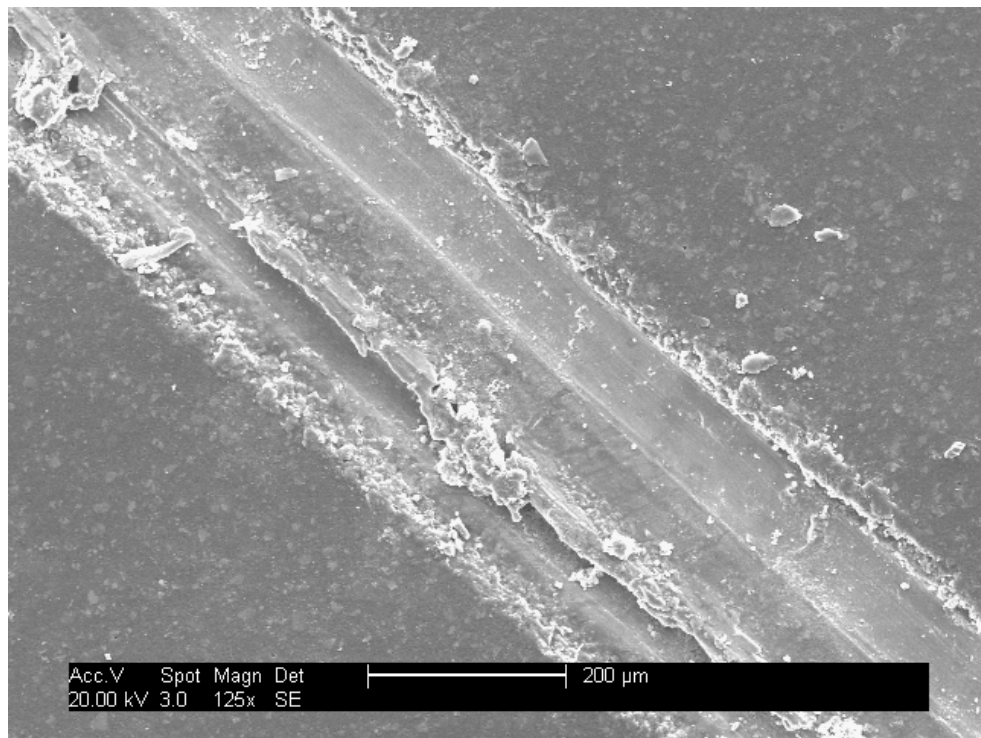
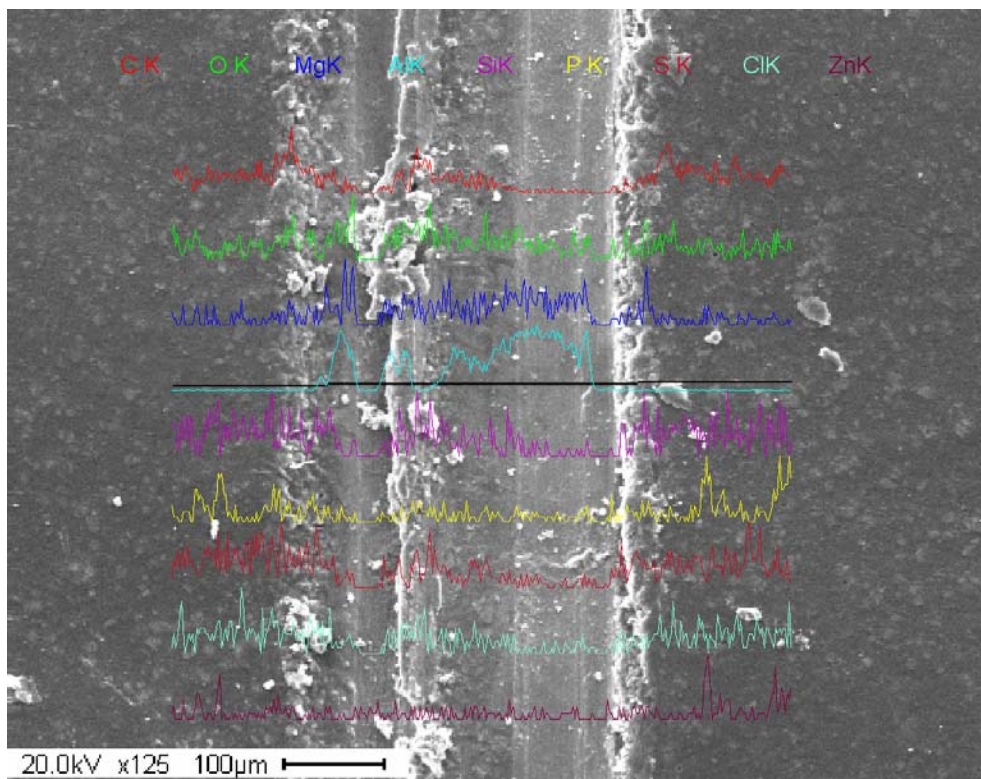


**Figure 4.19** RAIR spectra of bis-sulfur silane and polyurethane resin films  
at specified time intervals of room temperature curing

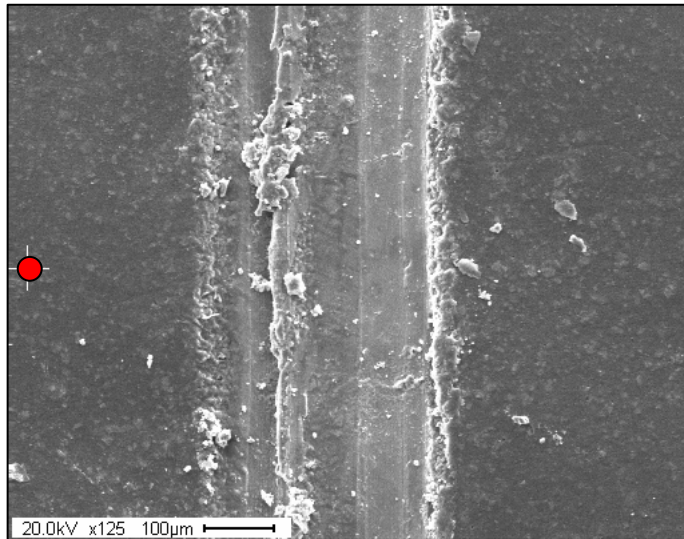
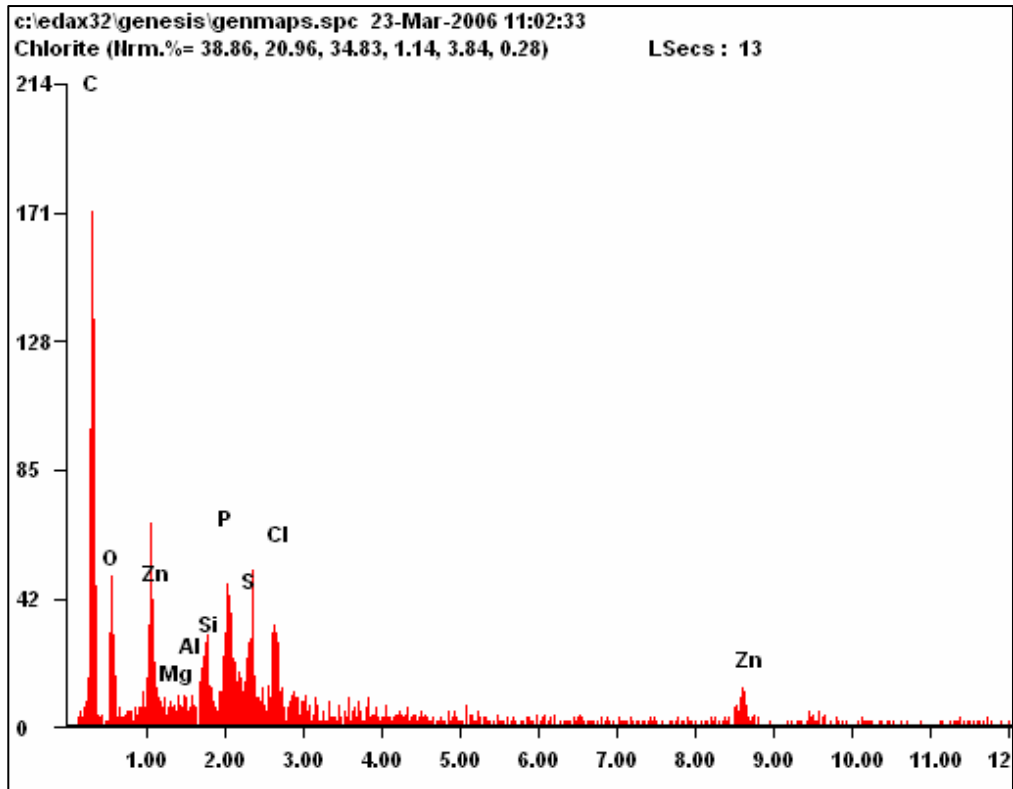


(a)



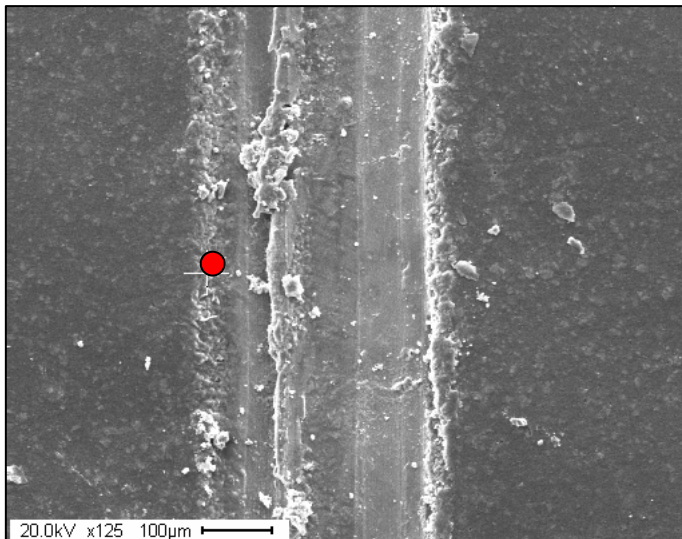
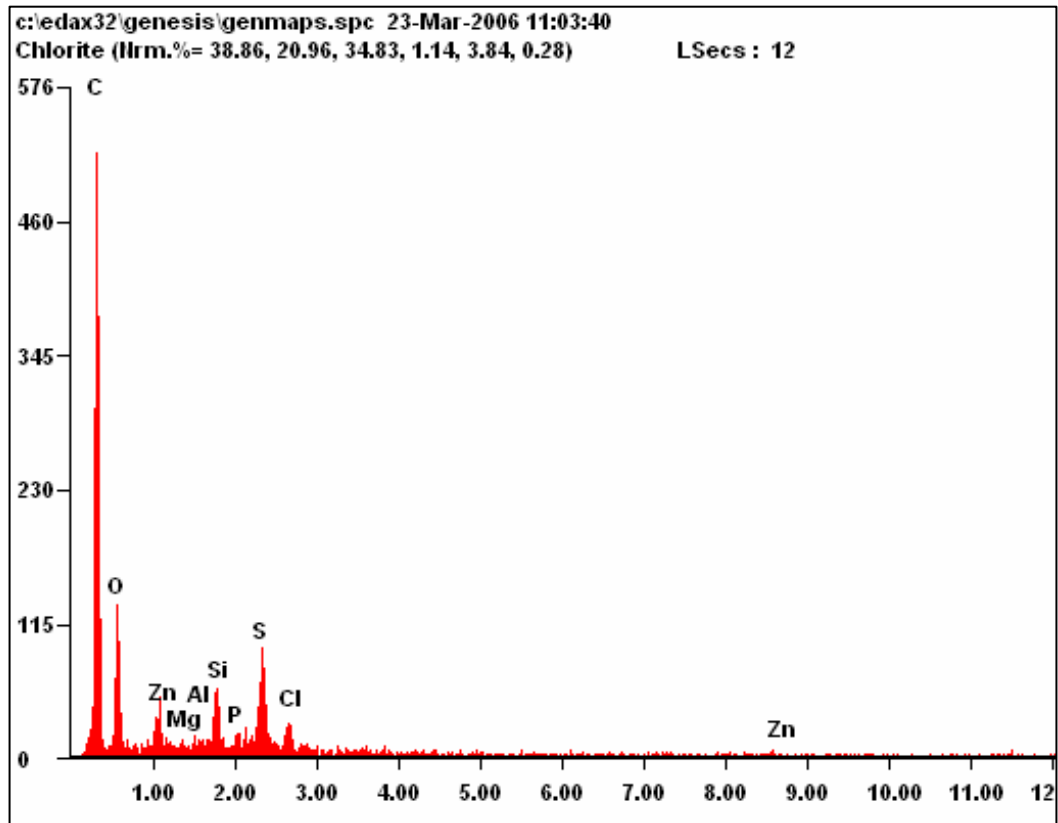
(b)

**Figure 4.20** Backscattered SEM image of Coating A with the elemental distribution across the scribe



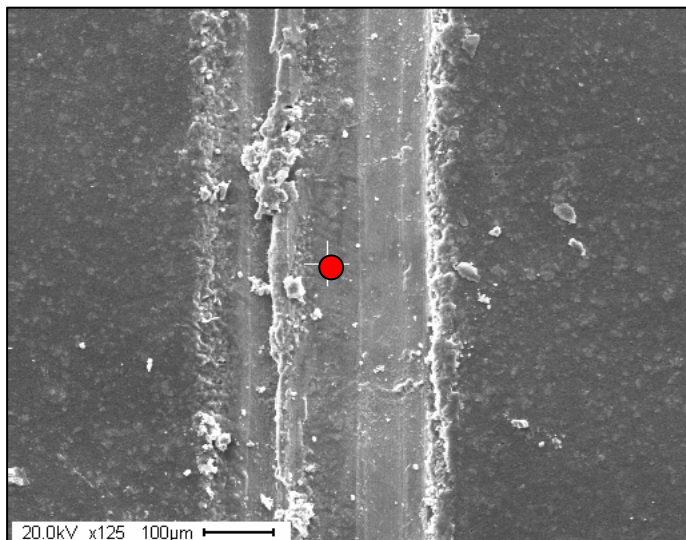
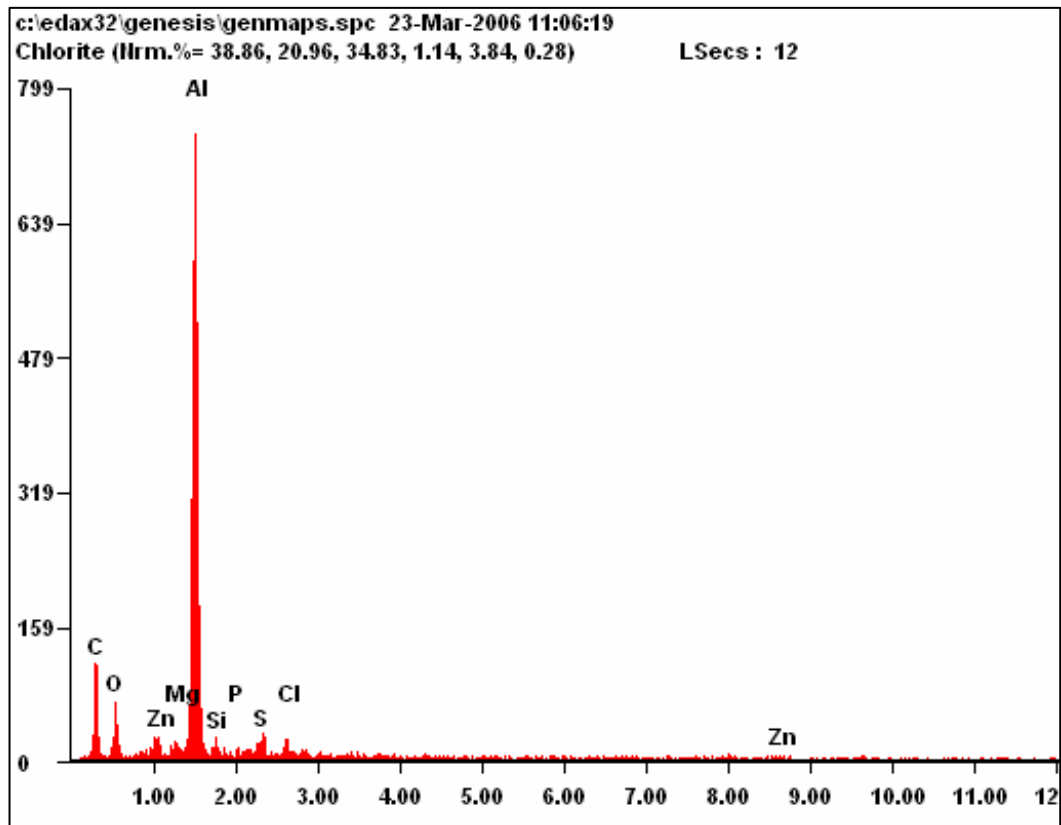
<i>Element</i>	<i>Wt%</i>	<i>At%</i>
<i>C</i>	70.35	83.68
<i>O</i>	10.75	09.60
<i>Mg</i>	00.30	00.18
<i>Al</i>	00.40	00.21
<i>Si</i>	01.45	00.74
<i>P</i>	03.15	01.45
<i>S</i>	02.91	01.30
<i>Cl</i>	02.74	01.10
<i>Zn</i>	07.94	01.74

Figure 4.21 EDS scan at the indicated spot on Coating A with the elemental distribution



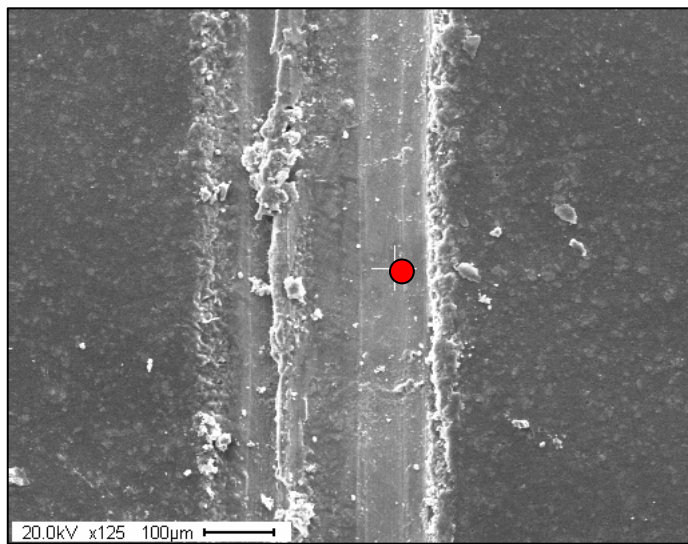
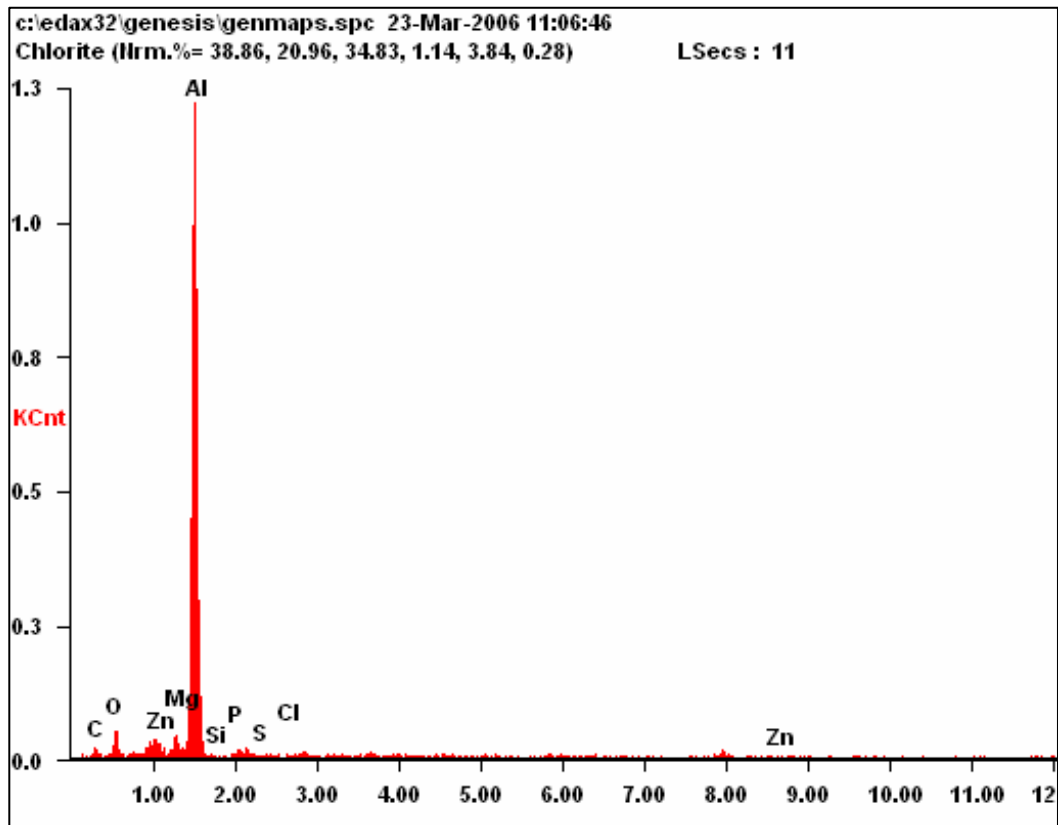
<i>Element</i>	<i>Wt%</i>	<i>At%</i>
<i>C</i>	74.92	82.36
<i>O</i>	17.76	14.66
<i>Mg</i>	00.25	00.13
<i>Al</i>	00.42	00.21
<i>Si</i>	01.68	00.79
<i>P</i>	00.13	00.06
<i>S</i>	03.06	01.26
<i>Cl</i>	01.01	00.38
<i>Zn</i>	00.77	00.16

**Figure 4.22** EDS scan at the indicated spot on Coating A with the elemental distribution



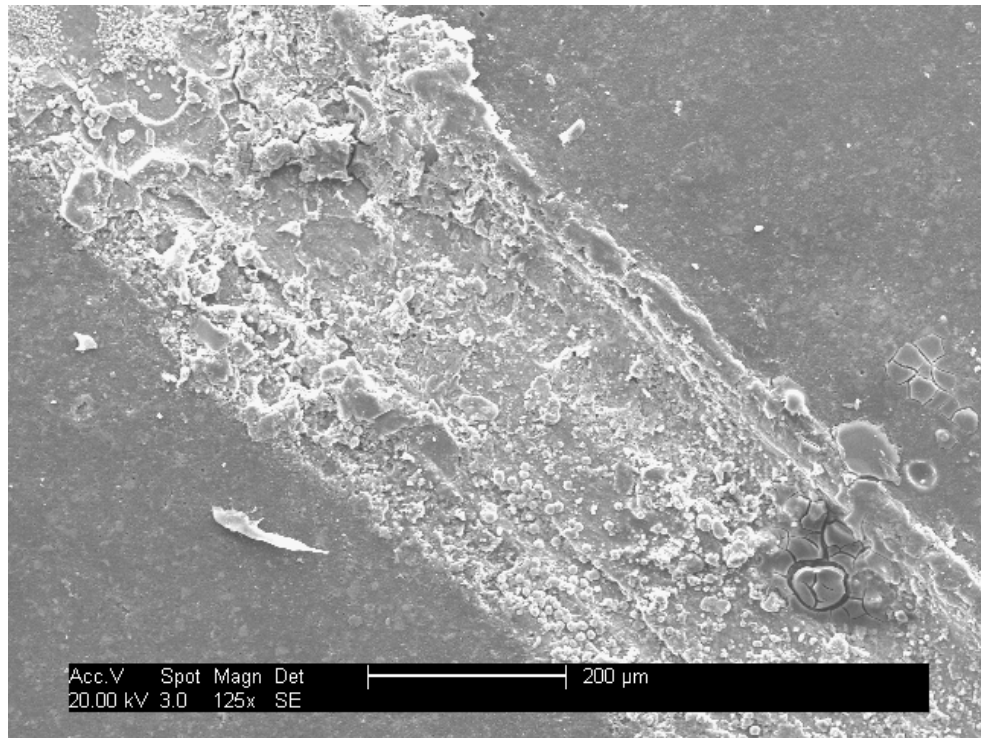
<i>Element</i>	<i>Wt%</i>	<i>At%</i>
<i>C</i>	48.49	65.10
<i>O</i>	11.65	11.74
<i>Mg</i>	00.81	00.53
<i>Al</i>	35.01	20.92
<i>Si</i>	00.82	00.47
<i>P</i>	00.00	00.00
<i>S</i>	01.01	00.51
<i>Cl</i>	00.87	00.40
<i>Zn</i>	01.34	00.33

**Figure 4.23** EDS scan at the indicated spot on Coating A with the elemental distribution

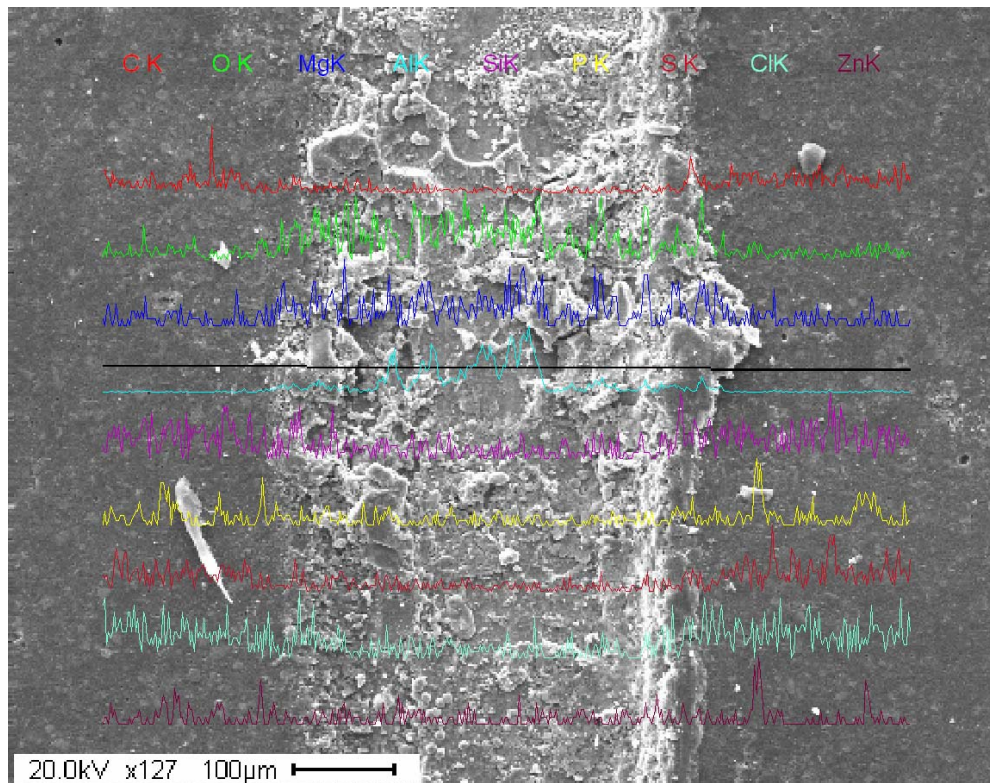


<i>Element</i>	<i>Wt%</i>	<i>At%</i>
<i>C</i>	17.42	30.91
<i>O</i>	09.31	12.41
<i>Mg</i>	02.18	01.92
<i>Al</i>	66.47	52.52
<i>Si</i>	00.36	00.27
<i>P</i>	00.78	00.53
<i>S</i>	00.59	00.39
<i>Cl</i>	00.36	00.22
<i>Zn</i>	02.52	00.82

**Figure 4.24** EDS scan at the indicated spot on Coating A along with the elemental distribution

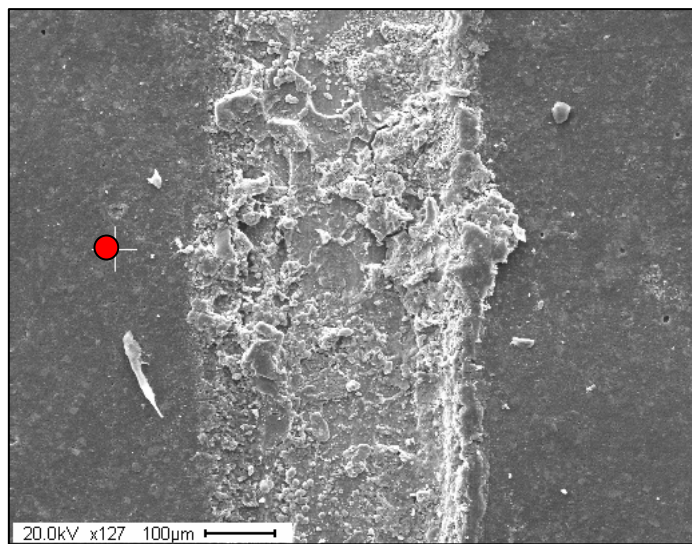
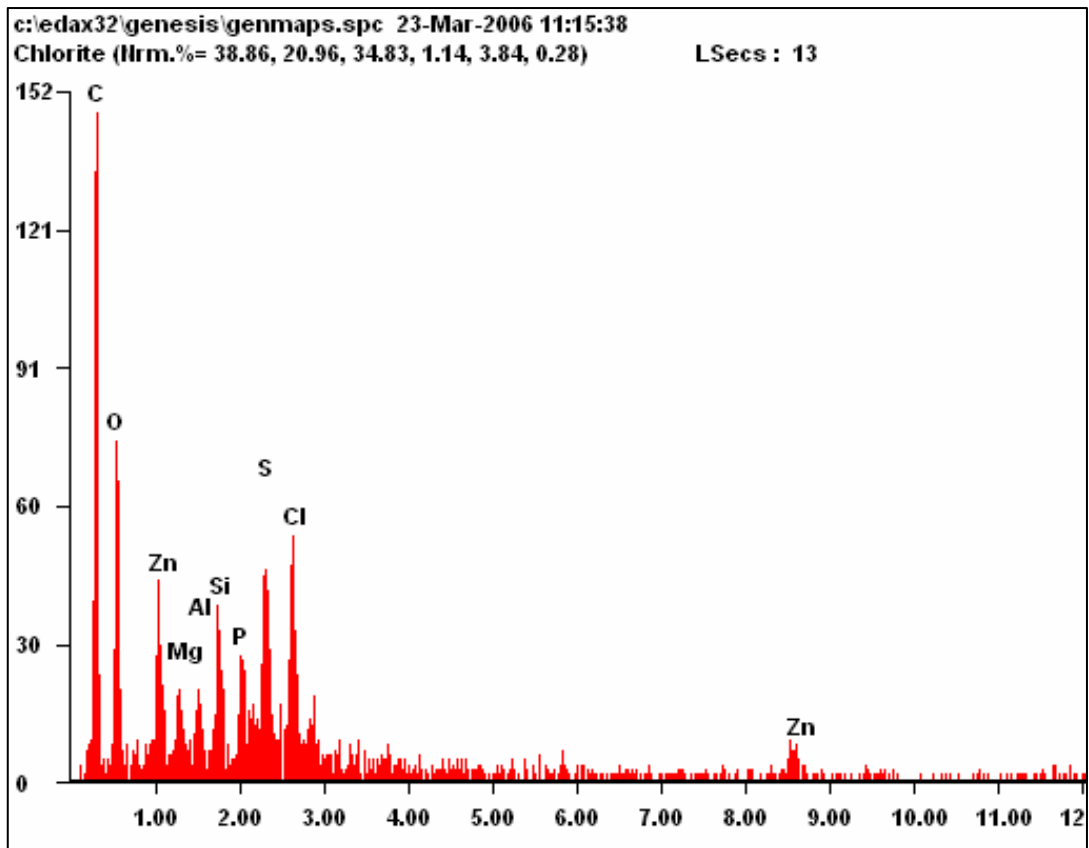


(a)



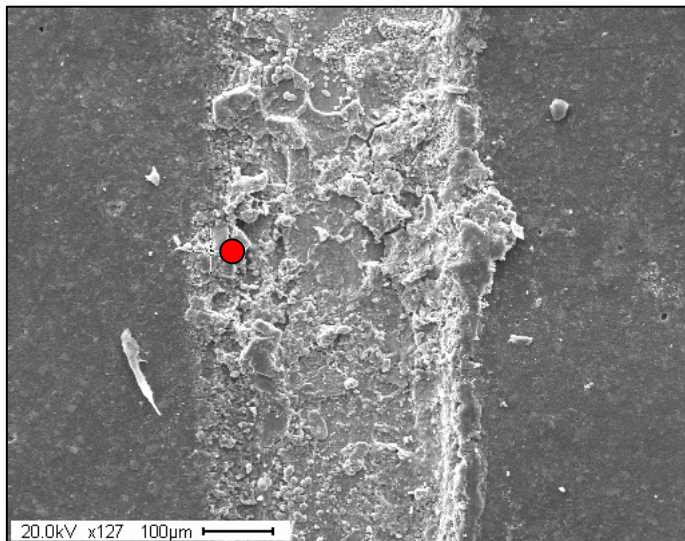
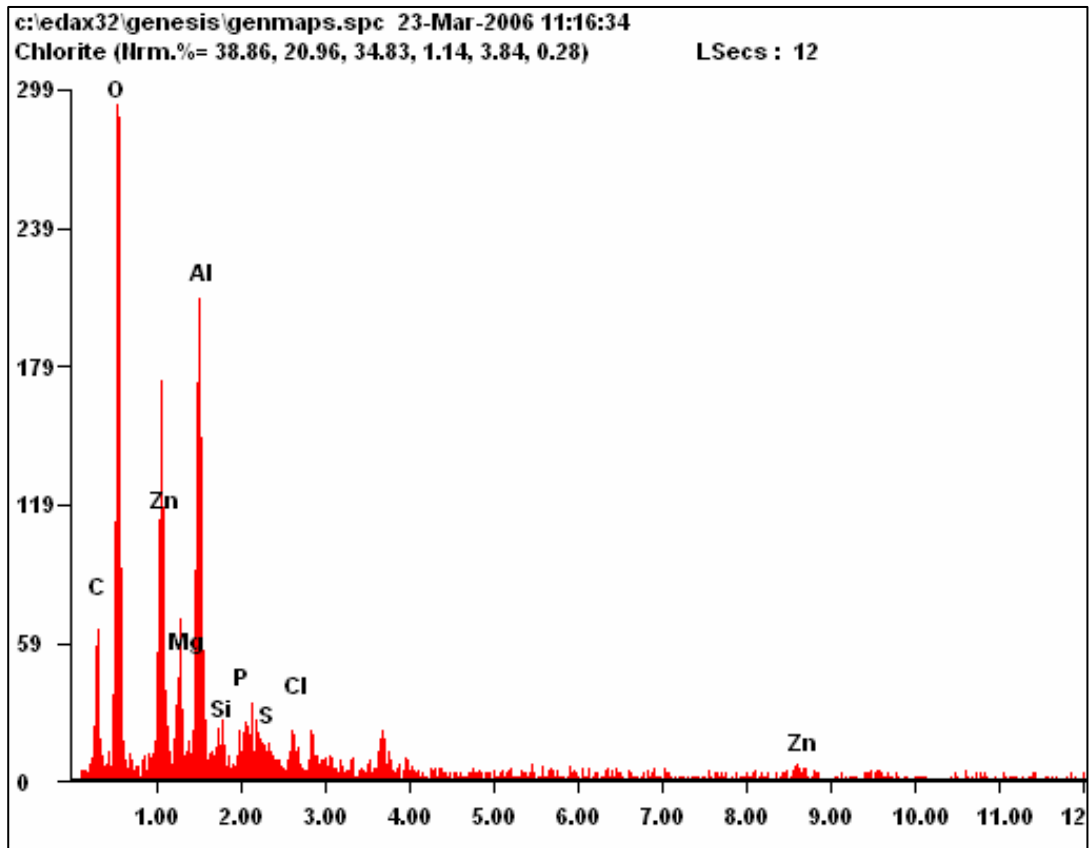
(b)

**Figure 4.25** Backscattered SEM image of Coating B with the elemental distribution across the scribe



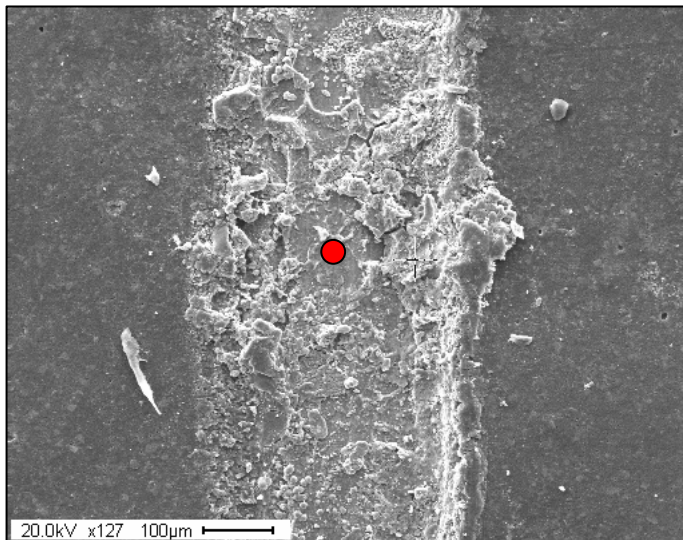
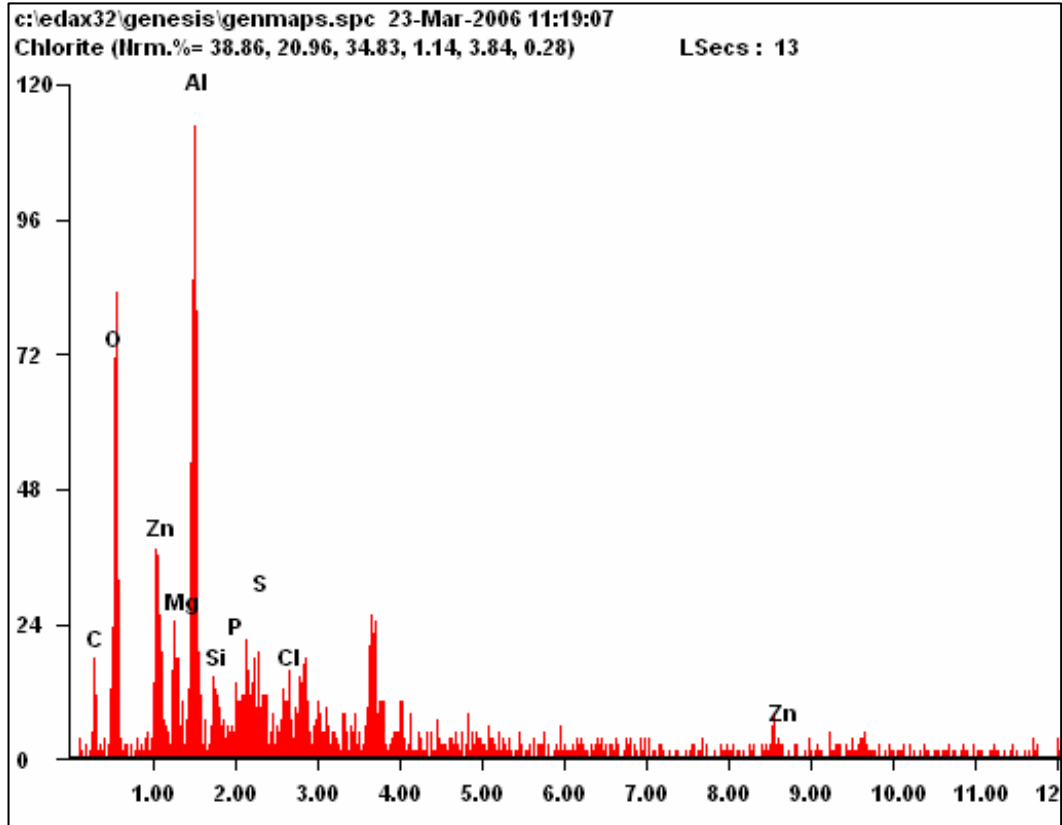
<i>Element</i>	<i>Wt%</i>	<i>At%</i>
<i>C</i>	63.19	75.20
<i>O</i>	20.21	18.05
<i>Mg</i>	01.10	00.65
<i>Al</i>	00.78	00.41
<i>Si</i>	01.61	00.82
<i>P</i>	01.28	00.59
<i>S</i>	04.04	01.80
<i>Cl</i>	04.21	01.70
<i>Zn</i>	03.59	00.79

**Figure 4.26** EDS scan at the indicated spot on Coating B with the elemental distribution



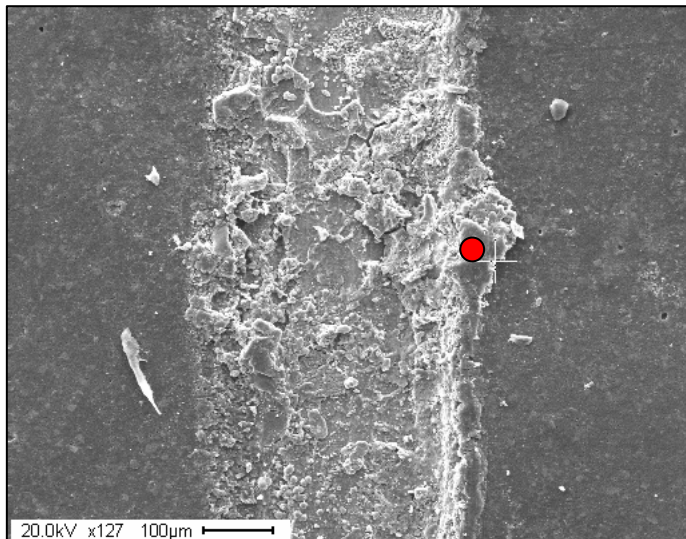
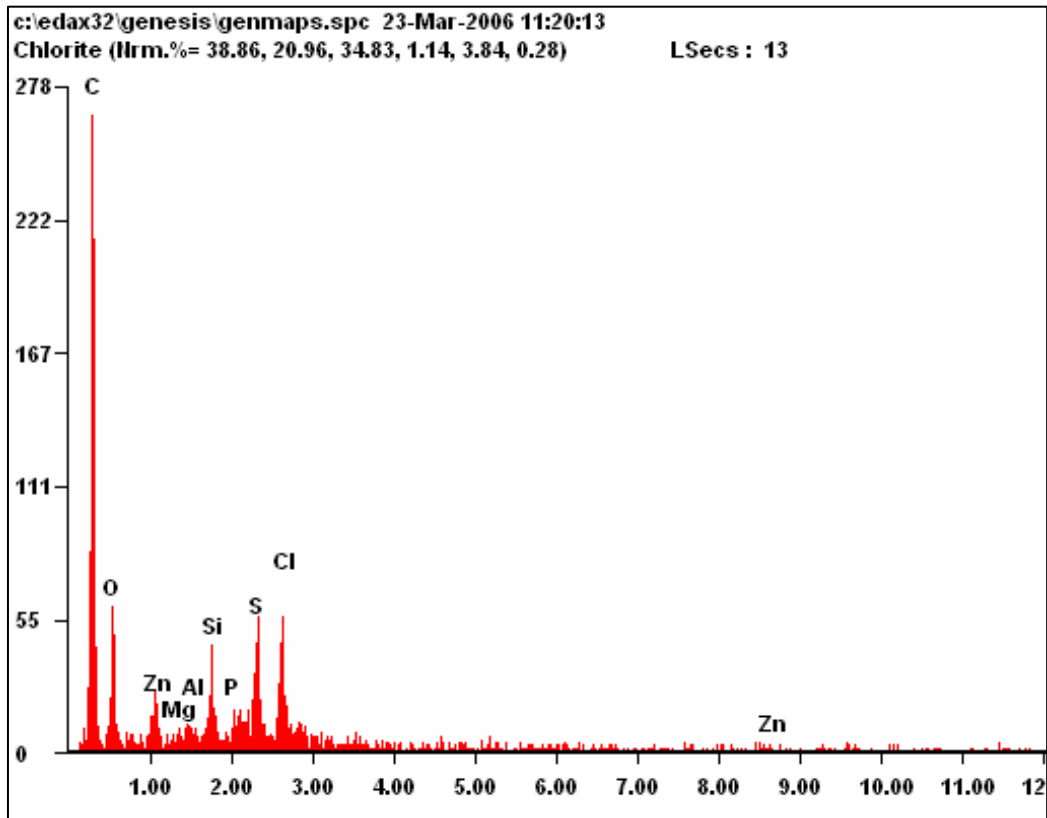
<i>Element</i>	<i>Wt%</i>	<i>At%</i>
<i>C</i>	31.01	41.96
<i>O</i>	43.01	43.69
<i>Mg</i>	04.07	02.72
<i>Al</i>	13.39	08.06
<i>Si</i>	01.57	00.91
<i>P</i>	01.20	00.63
<i>S</i>	01.24	00.63
<i>Cl</i>	01.35	00.62
<i>Zn</i>	03.17	00.79

**Figure 4.27** EDS scan at the indicated spot on Coating B with the elemental distribution



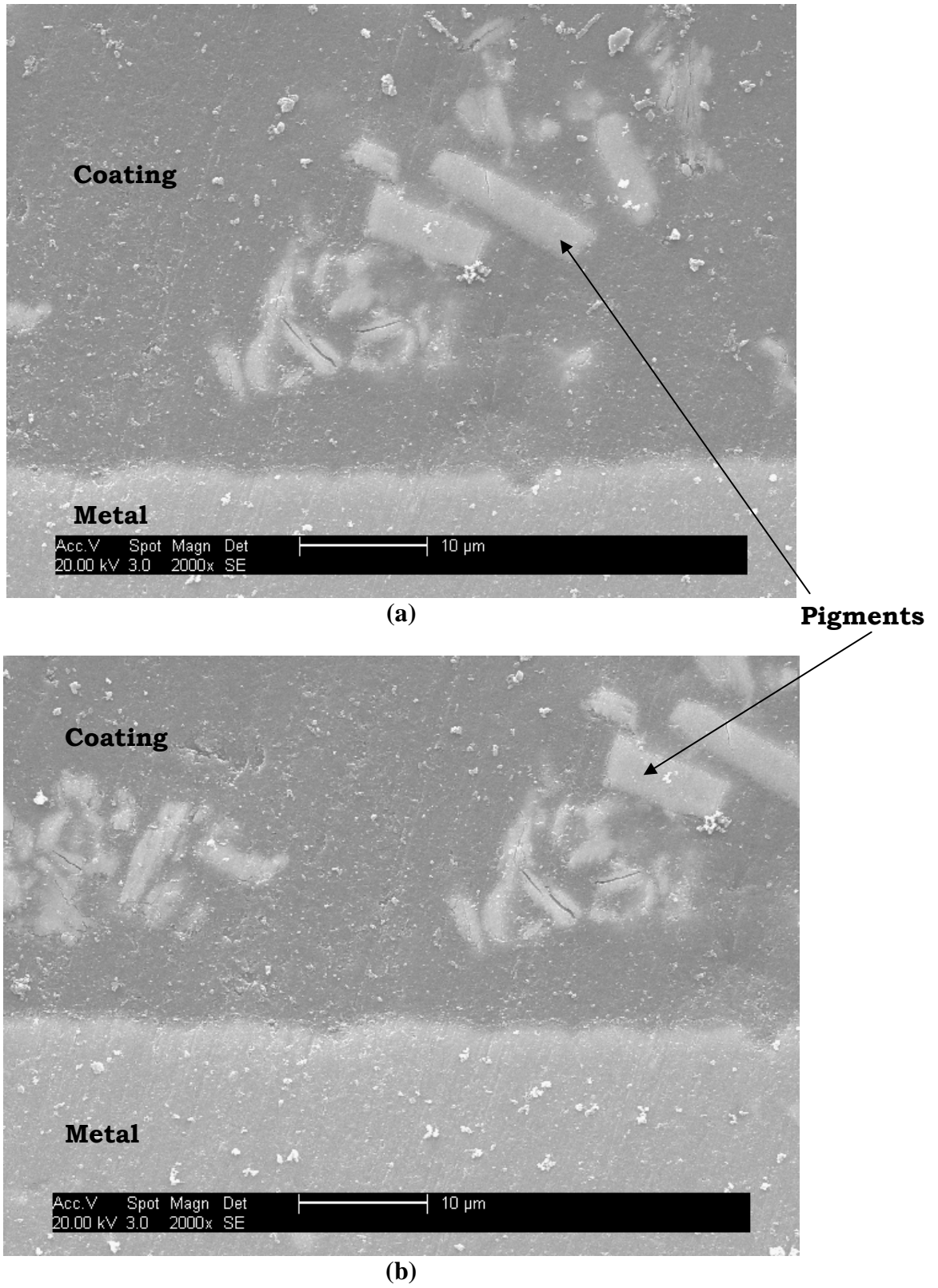
<i>Element</i>	<i>Wt%</i>	<i>At%</i>
<i>C</i>	23.20	36.08
<i>O</i>	30.66	35.78
<i>Mg</i>	05.37	04.12
<i>Al</i>	23.05	15.95
<i>Si</i>	02.46	01.64
<i>P</i>	02.50	01.51
<i>S</i>	02.23	01.30
<i>Cl</i>	02.52	01.33
<i>Zn</i>	08.00	02.28

Figure 4.28 EDS scan at the indicated spot on Coating B with the elemental distribution



<i>Element</i>	<i>Wt%</i>	<i>At%</i>
<i>C</i>	75.69	84.13
<i>O</i>	13.97	11.66
<i>Mg</i>	00.36	00.20
<i>Al</i>	00.38	00.19
<i>Si</i>	01.58	00.75
<i>P</i>	00.64	00.27
<i>S</i>	03.33	01.38
<i>Cl</i>	03.42	01.29
<i>Zn</i>	00.63	00.13

Figure 4.29 EDS scan at the indicated spot on Coating B with the elemental distribution



**Figure 4.30** Backscattered SEM image of the cross-section of coating A on AA 2024-T3

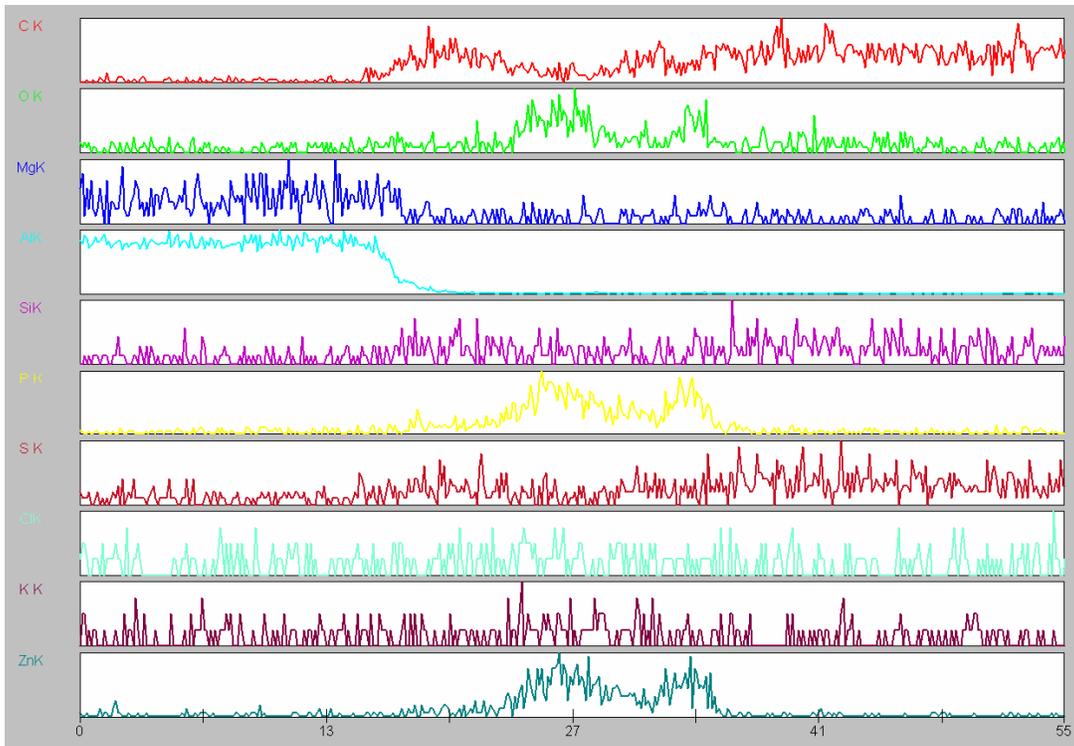
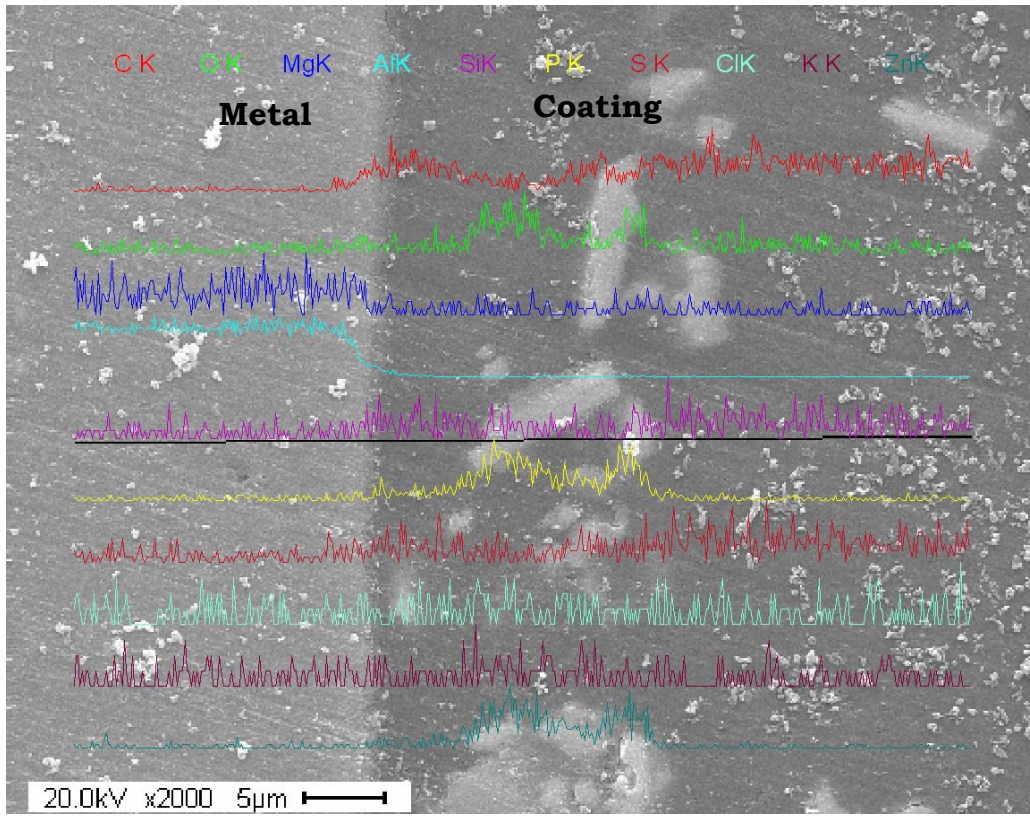
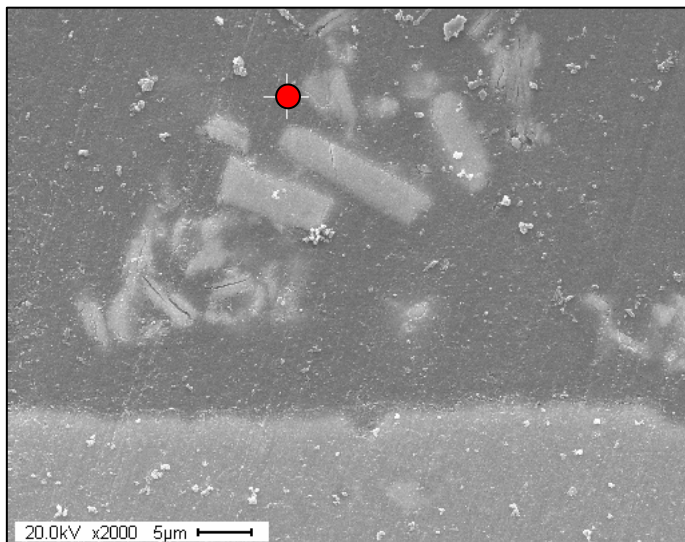
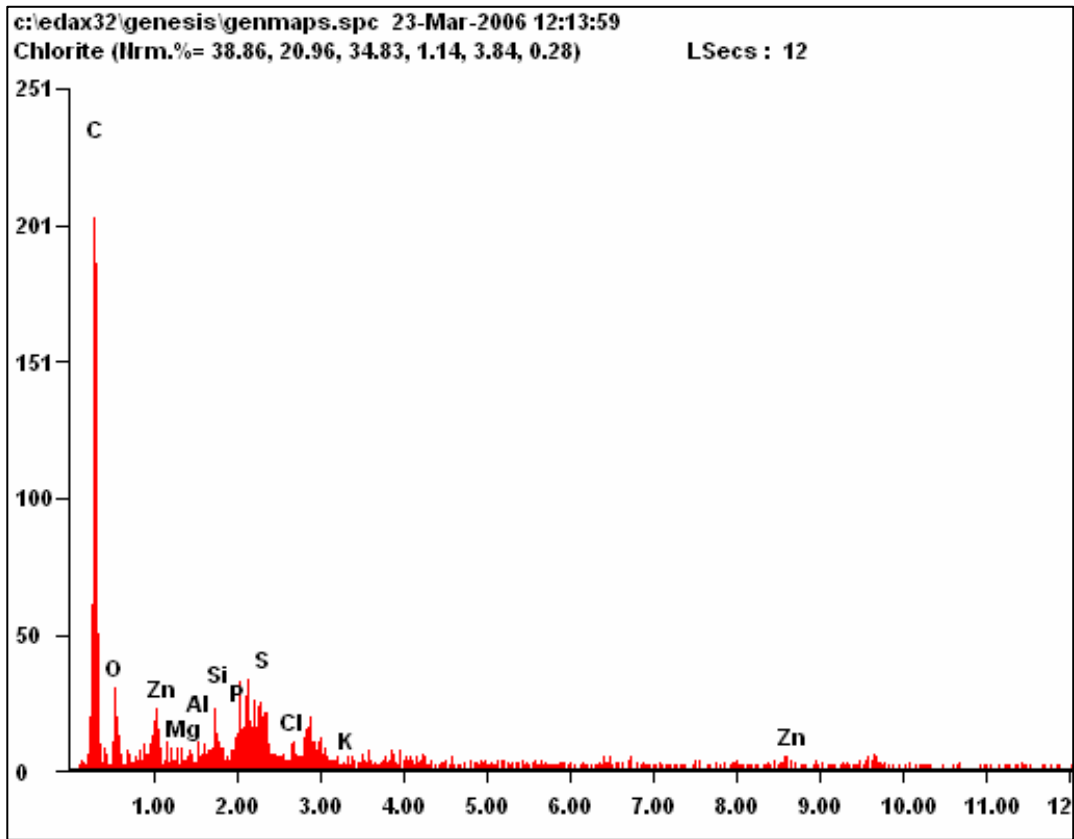
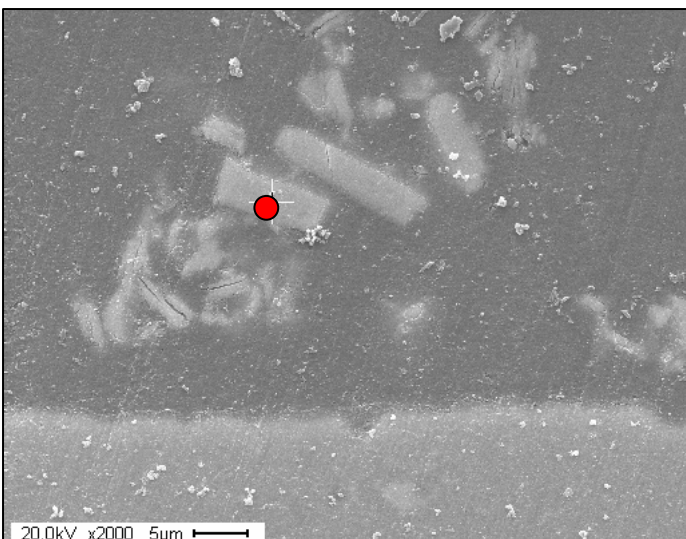
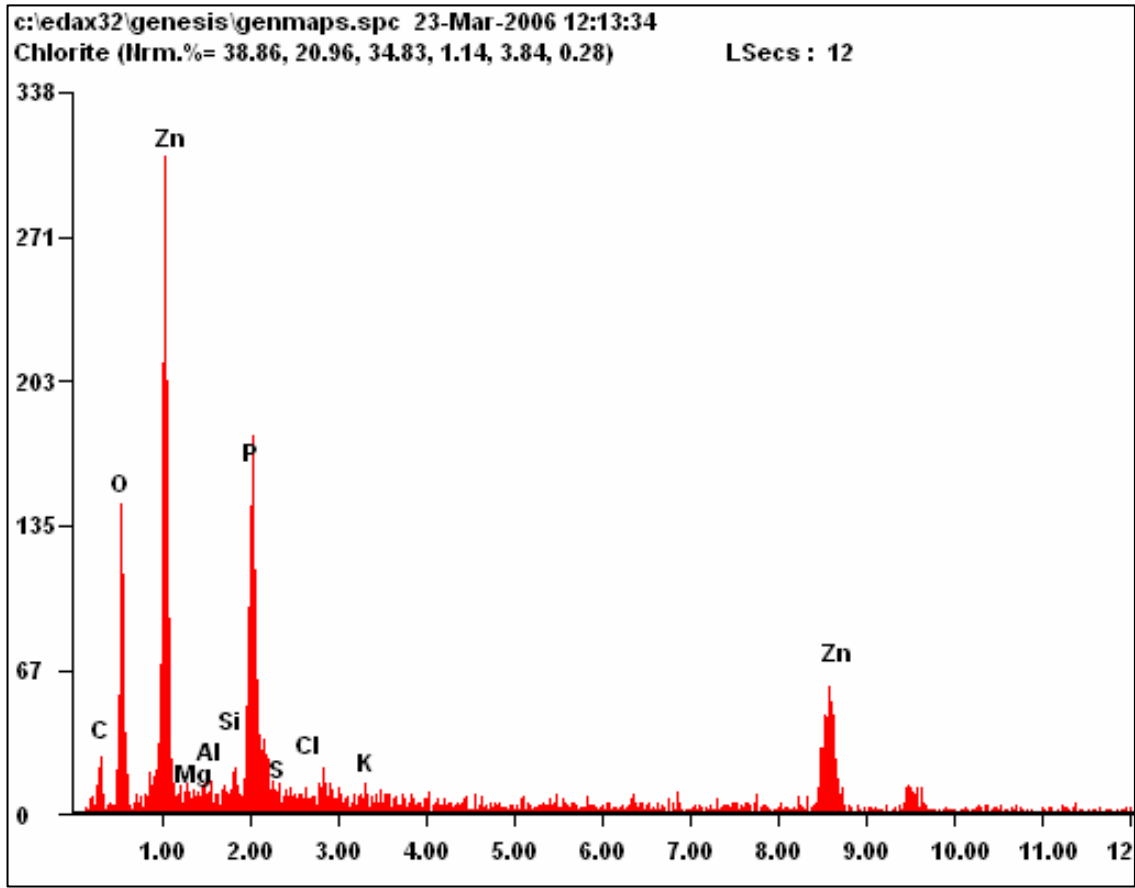


**Figure 4.31** Elemental distributions along the cross-section of coating A on AA 2024-T3



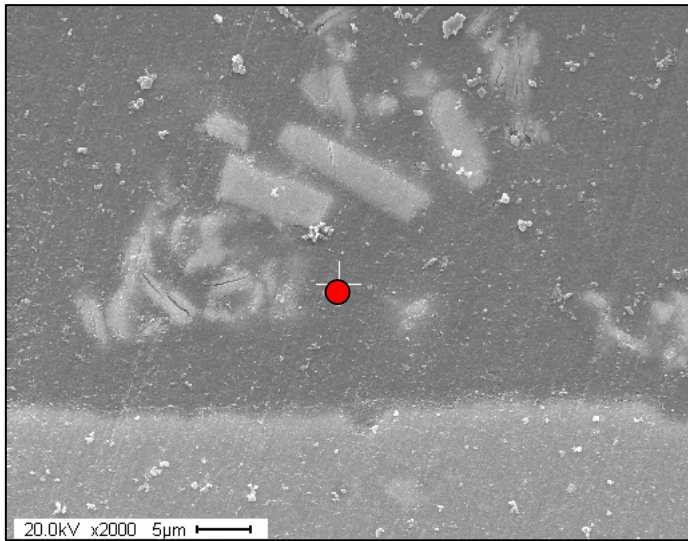
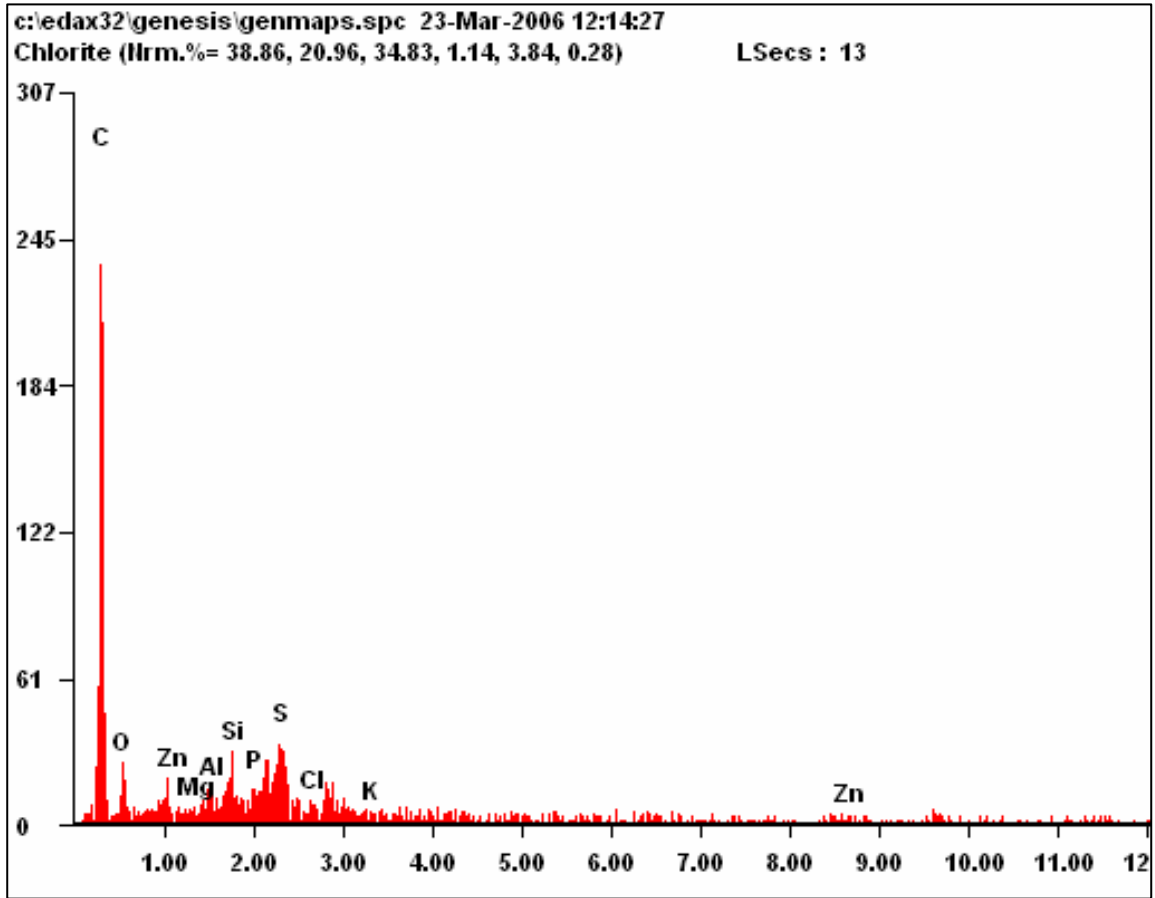
<i>Element</i>	<i>Wt%</i>	<i>At%</i>
<i>C</i>	78.06	86.24
<i>O</i>	12.51	10.38
<i>Mg</i>	00.44	00.24
<i>Al</i>	00.12	00.06
<i>Si</i>	01.40	00.66
<i>P</i>	01.90	00.81
<i>S</i>	02.24	00.93
<i>Cl</i>	00.00	00.00
<i>K</i>	00.00	00.00
<i>Zn</i>	03.31	00.67

**Figure 4.32** EDS scan at the indicated spot on Coating B cross-section with the elemental distribution



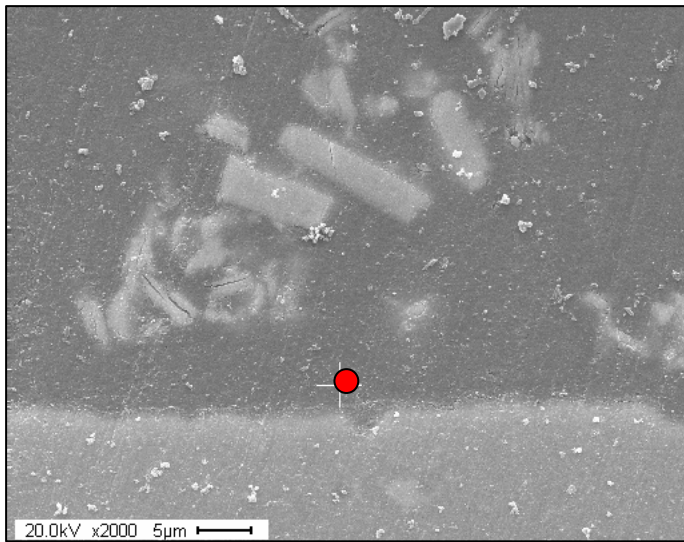
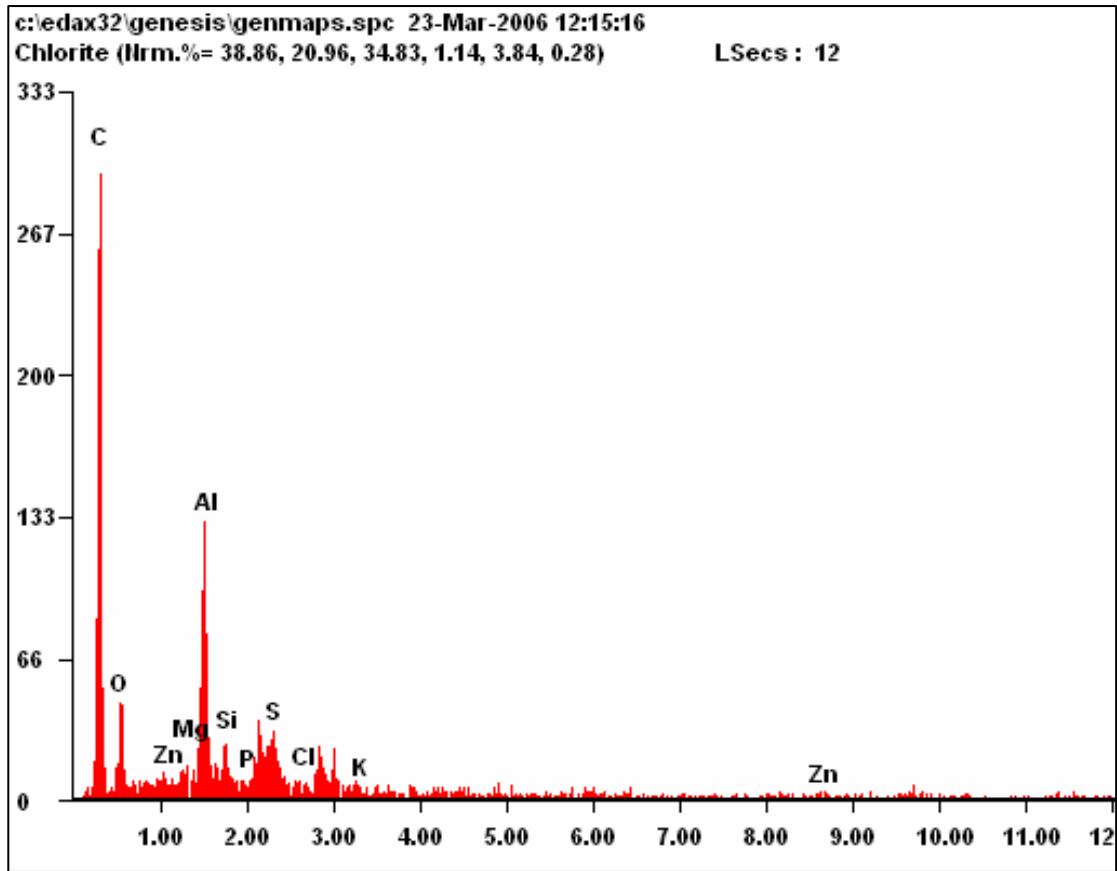
<i>Element</i>	<i>Wt%</i>	<i>At%</i>
<i>C</i>	18.15	37.15
<i>O</i>	21.00	32.28
<i>Mg</i>	00.66	00.67
<i>Al</i>	01.27	01.15
<i>Si</i>	00.70	00.61
<i>P</i>	14.35	11.39
<i>S</i>	00.45	00.34
<i>Cl</i>	00.00	00.00
<i>K</i>	00.26	00.16
<i>Zn</i>	43.17	16.24

**Figure 4.33** EDS scan at the indicated spot on Coating B cross-section with the elemental distribution



<i>Element</i>	<i>Wt%</i>	<i>At%</i>
<i>C</i>	81.86	88.60
<i>O</i>	09.68	07.87
<i>Mg</i>	00.39	00.21
<i>Al</i>	00.86	00.41
<i>Si</i>	01.73	00.80
<i>P</i>	01.25	00.52
<i>S</i>	03.49	01.42
<i>Cl</i>	00.00	00.00
<i>K</i>	00.21	00.07
<i>Zn</i>	00.53	00.11

**Figure 4.34** EDS scan at the indicated spot on Coating B cross-section with the elemental distribution



<i>Element</i>	<i>Wt%</i>	<i>At%</i>
<i>C</i>	77.15	85.24
<i>O</i>	11.11	09.21
<i>Mg</i>	00.77	00.42
<i>Al</i>	06.75	03.32
<i>Si</i>	01.31	00.62
<i>P</i>	00.40	00.17
<i>S</i>	02.15	00.89
<i>Cl</i>	00.25	00.09
<i>K</i>	00.11	00.04
<i>Zn</i>	00.00	00.00

**Figure 4.35** EDS scan at the indicated spot on Coating B cross-section with the elemental distribution

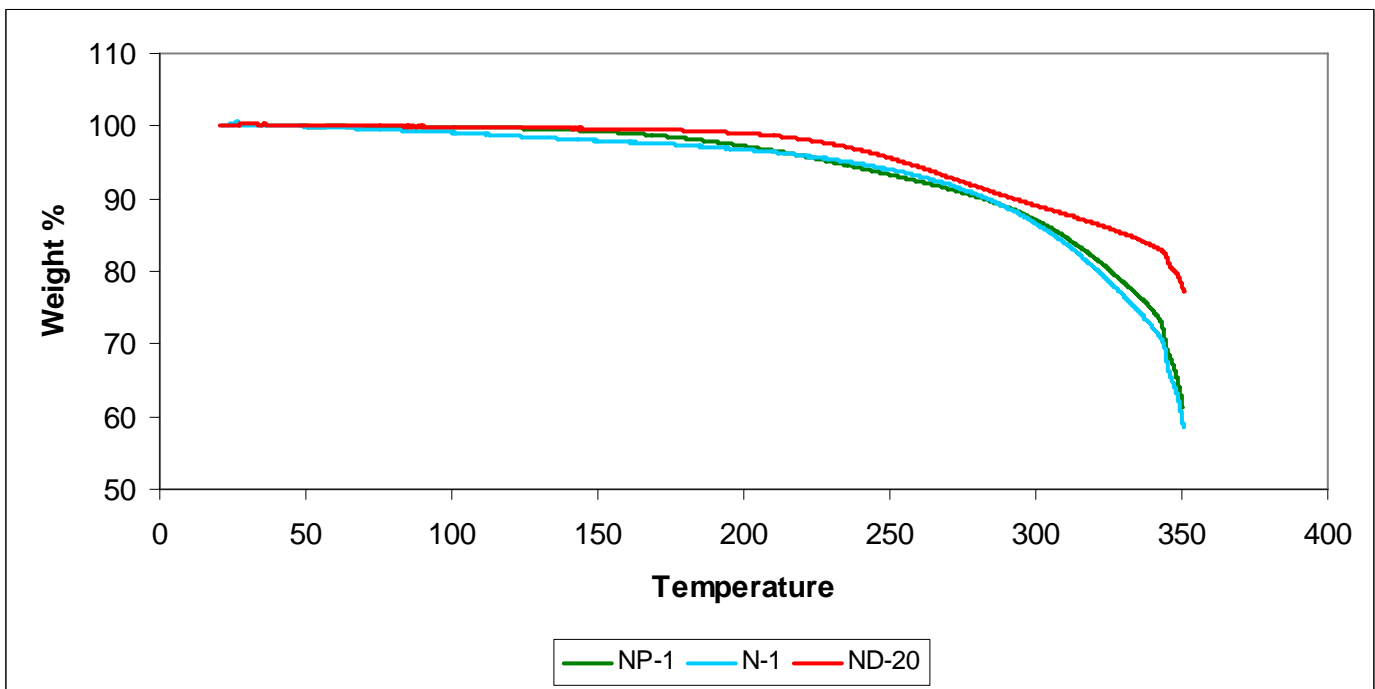
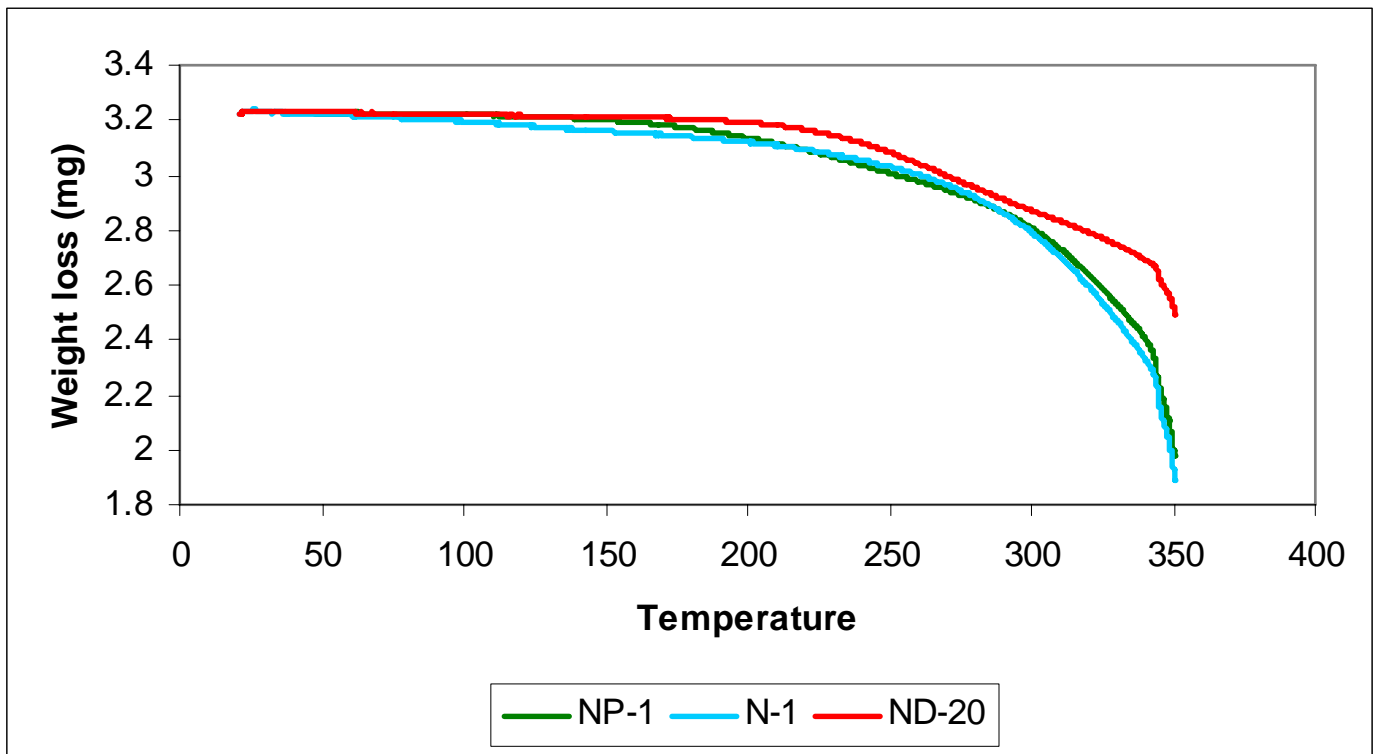


Figure 4.36 TGA curves for various superprimer coatings

# Hydrothermal Degradation of Hydrophobic Organosilane Films Determined by Neutron Reflectometry

PENG WANG<sup>1</sup>, GUIRONG PAN<sup>1</sup>, WILLIAM A. HAMILTON<sup>2</sup> and DALE W. SCHAEFER<sup>1,\*</sup>

<sup>1</sup>Department of Chemical and Materials Engineering, University of Cincinnati, Cincinnati, OH 45221-0012, USA

<sup>2</sup>Condensed Matter Sciences Division, Oak Ridge National Laboratory, Oak Ridge National Laboratory, Oak Ridge, TN 37831, USA (Current address: Bragg Institute, Australian Nuclear Science and Technology Organisation, Lucas Heights, NSW 2234, Australia)

**Abstract** - The structure and hydrothermal degradation behavior of bis[3-(triethoxysilyl)propyl]tetrasulfide (bis-sulfur silane) film were studied by specular neutron reflectivity (NR). The degradation process was investigated by comparing the NR data of the as-prepared dry film with the re-dried film after 10 and 24 hours exposure to 80°C liquid water. The hydrophobic sulfur (S<sub>4</sub>) bridging group of bis-sulfur silane is the key factor determining the hydrothermal stability, but thickness is also important. When the thickness is below 200 Å, the film-substrate interface degrades whereas thicker films (above 1000 Å) are robust. Although elevated curing temperature (180°C) can give a more condensed film (higher crosslink density), 80°C is sufficient to provide good hydrothermal stability.

*Keywords:* Silane film; neutron reflectivity; hydrothermal degradation, anti-corrosion, hydrophobic, hydrophobicity, aging

## 1. INTRODUCTION

Organofunctional silanes are hybrid organic-inorganic compounds, functionalized on the organic group and bearing hydrolyzable groups on silicon. The commercial use of organosilanes has developed steadily since the 1950's.[1] Recent studies demonstrate the use of organosilanes as corrosion inhibitors for a range of metals.[2-8]

Films containing bis[3-(triethoxysilyl)propyl]tetrasulfide (bis-sulfur silane) with a 4-atom sulfur chain (S<sub>4</sub>) bridging group are effective anti-corrosion coatings especially for aluminum alloys.[9] Effective corrosion protection is related to the nature of bridging group and high crosslink density. Interestingly, however, strict hydrophobicity is not required for good protection.[10-12]

The condensation reactions of silane between itself and the metal substrate are reversible.[1] The hydrolysis of siloxane (Si-O-Si) network bonds or Me-O-Si bonds is believed to be the primary degradation mechanism when organosilane films are exposed to the environment. Hydrolysis rate of siloxane bonds can be modeled by: [13]

---

\*To whom correspondence should be addressed. E-mail: dale.schaefer@uc.edu

$$V = k[\text{Si-O-Si}][\text{H}_2\text{O}] \quad [1]$$

Where  $V$  is the rate of hydrolysis,  $k = k_0 \exp(-E_a/RT)$ , and  $E_a$  is the activation energy. According to eq. 1, the hydrolysis rate increases exponentially with temperature. Elevated temperature also increases the solubility of oligomers generated from hydrolysis, which accelerates the degradation.[13] Therefore, when silane films are exposed to the environment, especially at high humidity or/and elevated temperature, degradation may be accelerated leading to protection failure.

This study seeks to understand the principles of hydrothermal degradation and to determine the key factors that control the hydrothermal stability. Bis-sulfur silane films of varying thicknesses and curing temperatures were spin-coated onto the silicon wafer substrates. Neutron reflectivity (NR) was used to trace the changes in the films after exposure to 80°C liquid water ( $\text{H}_2\text{O}$ ).

NR can easily examine interfaces that are buried well within a sample. NR can elucidate film composition normal to the film surface on scales from 10 Å to 2000 Å. Contrast over the depth of the film arises from differences in the neutron scattering length density (SLD), which is determined by the material's local density and chemical composition. The SLD represents the scattering power of a substance and can be calculated if chemical composition and density are known. The structure of the film normal to the surface is captured by the SLD profile (SLD vs. distance from the substrate surface) as determined by fitting the measured specular neutron reflectivity. By analyzing changes of the SLD and thickness of each layer, we establish the course of hydrothermal degradation.

## 2. EXPERIMENTAL

### 2.1. Materials

Bis[3-(triethoxysilyl)propyl]tetrasulfide was provided by OSi Specialties (Tarrytown, NY). The molecular structure is shown in Figure. 1. The silane was used without further purification. The silicon wafers used as substrates were polished 3-inch diameter single crystal (111) wafers obtained from Wafer World, Inc. (West Palm Beach, FL. USA). Sulfuric acid and hydrogen peroxide were obtained from Aldrich and used as received.

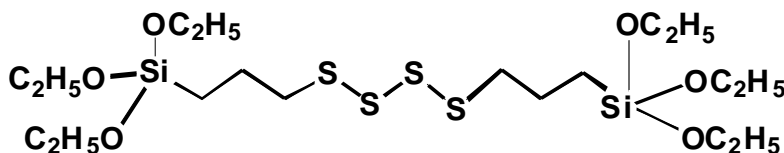


Figure 1. Molecular structure of Bis[3-(triethoxysilyl)propyl]tetrasulfide (bis-sulfur silane)

### 2.2 Procedure

The silicon wafers were cleaned by immersion in a freshly prepared “Piranha” solution at

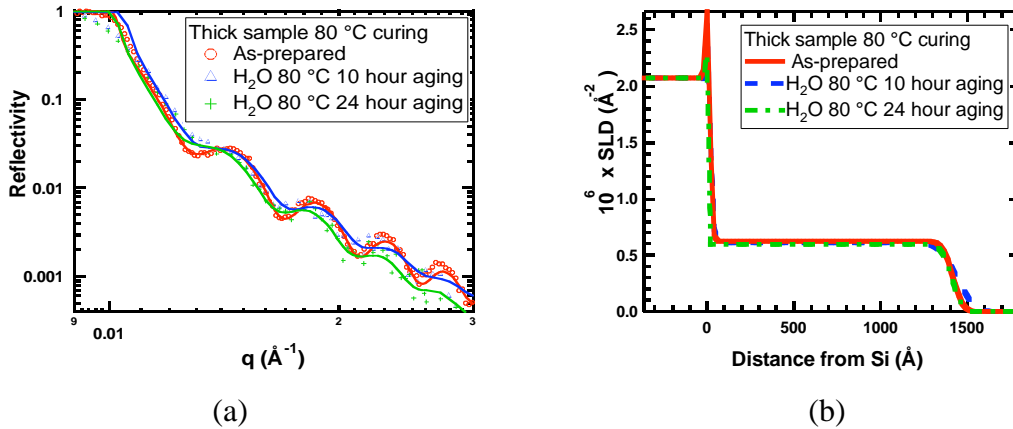


Figure 2. (a) Neutron reflectivity data from thick bis-sulfur silane cured at 80°C, as-prepared and after aging in 80°C liquid H<sub>2</sub>O for 10 and 24 hours. The curves through the data points correspond to the best fits using model SLD profiles. (b) Best-fit SLD profiles corresponding to the curves through the data in (a). The data indicate minor alteration of the surface region on accelerated aging.

room temperature for at least 30 minutes. Piranha solution is a mixture of H<sub>2</sub>SO<sub>4</sub> and 30% H<sub>2</sub>O<sub>2</sub> at a volume ratio of 7:3. After immersion, the substrates were rinsed repeatedly with de-ionized (DI) water. After desiccation, the silicon wafers are ready for spin coating.

The thickness of bis-sulfur silane film can be controlled by either the concentration of precursor solution or the spin-coating speed. Here, the concentration of the precursor solution was varied from 1% to 5% (by weight) to control the thickness of the film, while the spinning speed is fixed at 2000 rpm. The bis-sulfur silane solution was prepared by adding the silane to a mixture of DI water and ethanol. The weight ratio of bis-sulfur silane/water/ethanol was 1/9/90 for the 1% solution, and 5/5/90 for the 5% solution. The solutions need to be properly aged to pre-hydrolyze the ethoxy groups before spin-coating.[14]

The coating procedure was carried out using a Laurell single-wafer spin processor (WS-400A-6NPP-Lite, North Wales, PA, USA). The silane solution is pipetted onto the wafers covering the whole surface. After one minute, the sample is spun at 2000 rpm for 30 seconds. The sample is then dried and cured in an oven at 80°C or 180°C for 1 hour. Samples are kept in a desiccated environment before measurement.

Our measurements were performed on the MIRROR neutron reflectometer at Oak Ridge National Laboratory and SPEAR at Los Alamos National Laboratory.

Samples were first measured as-prepared to establish the virgin state. A sealed Teflon can containing water at 80°C was used to carry out accelerated aging. The samples were conditioned for 10 and 24 hours, and then measured in the re-dried state after each aging stage. The re-dry process takes about 12 hours in the presence of a desiccant.

### 3. RESULTS AND DISCUSSION

#### 3.1 Effect of curing temperature

Two thick films deposited from 5% bis-sulfur silane solution and cured at different temperatures (180°C and 80°C) were measured to investigate the influence of curing temperature. The reflectivity data after each aging stage for the sample cured at 80°C are shown in Figure 2a. The SLD profiles associated with each fit are plotted in Figure 2b. The corresponding data for 180°C-cured sample are shown in Figure 3.

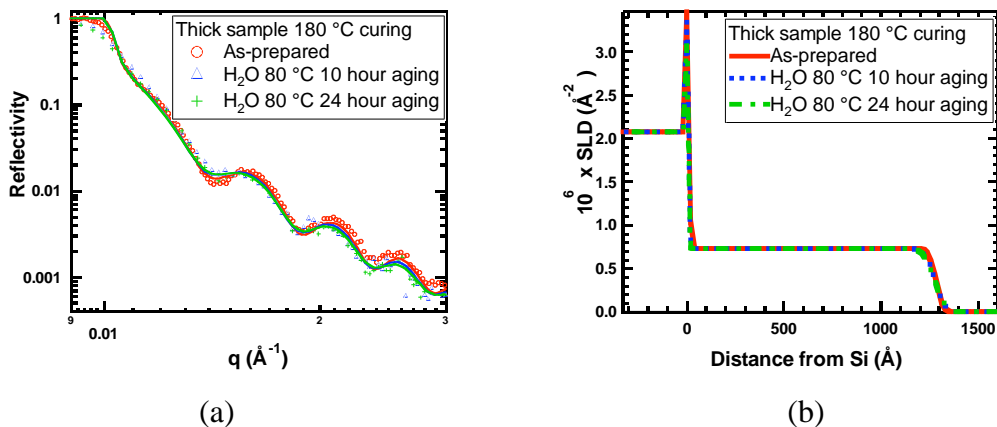


Figure 3. (a) Reflectivity data from thick bis-sulfur silane film cured at 180°C, as-prepared and after aging in 80°C after aging in 80°C liquid H<sub>2</sub>O for 10 and 24 hours. The curves through the data points correspond to the best fits using model SLD profiles. (b) Best-fit SLD profiles corresponding to the curves through the data in (a). The data indicate that the films are robust.

##### 3.1.1 Structure of as-prepared thick films

As-prepared bis-sulfur films cured at different temperatures have a similar one-uniform-layer structure. The SLD profile and the smaller fringe spacing of 80°C-cured sample indicate that lower curing temperature leads to a thicker film. The film thickness of the sample cured at 80°C is  $1390 \pm 5 \text{ \AA}$ , which is 9.4% thicker than the film cured at 180°C. By contrast, the SLD value of the 80°C-cured sample is  $(6.3 \pm 0.3) \times 10^{-7} \text{ \AA}^{-2}$ , which is 13.7% lower than 180°C-cured sample  $(7.3 \pm 0.3 \times 10^{-7})$ . The SLDs of both the as-prepared films are substantially higher than the SLD of the bis-sulfur monomer ( $2.1 \times 10^{-7} \text{ \AA}^{-2}$ ). The difference is due to the fact that Si-O-Si is formed by hydrolysis and condensation, replacing the ethoxy groups, which have a low SLD. Assuming the fully condensed bis-sulfur silane film has the same density as its monomer ( $1.1\text{g/cm}^3$ ), the calculated SLD is  $6.7 \times 10^{-7} \text{ \AA}^{-2}$ . Since the bulk density of the film should increase after condensation, the SLD of 180°C-cured sample indicates full condensation. Therefore, 80°C is not sufficient to reach the fully condense state. [10-12] Unhydrolyzed ethoxy groups or uncondensed silanol groups must present.

Compared with the 80°C-cured film, the increase of SLD of the 180°C-cured film is

larger than expected based on a density increase due to condensation. According to previous work of our group, the 180°C-cure eliminates water and ethanol sequestered in the film, further condenses the residual silanol groups and breaks down the tetrasulfide bonds into shorter linkages. All those effects result in a higher crosslink density and lower thickness, thereby, increasing the SLD. [15]

For the fully condensed bis-sulfur silane films, the network structure can be simplified as in Figure 4. Based on this structure, the SLD can be calculated using eq. 2 below. [16] In this equation,  $b_i$  is the coherent scattering length of the  $i^{\text{th}}$  of atom,  $\rho$  is the density,  $M$  is the molecular weight, and  $N_A$  is Avogadro's number.

$$SLD_{neutron} = \rho \frac{N_A}{M} \sum_{i=1}^{atoms} b_i \quad [2]$$

According to eq. 2, the SLD is proportional to density assuming a fully condensed film. Therefore, the density of the 180°C-cured film can be calculated to be  $1.2 \pm 0.04 \text{ g/cm}^3$ , which is marginally greater than that of the bis-sulfur monomer.

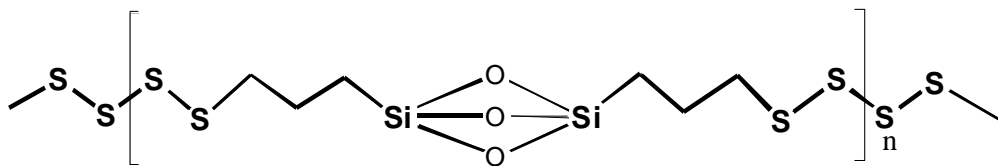


Figure 4. Simplified molecular structure of fully condensed bis-sulfur silane.

Because both the 80°C and 180°C-cured, thick films are deposited from the same solution and spun at the same speed, the as-prepared films should have the same thickness and density before cure. After cure, assuming the silane backbone (not including molecular level free space) maintains constant density despite the chemical differences, the density of cured film is inversely proportional to thickness. Therefore, the density of the 80°C-cured film is  $1.1 \pm 0.04 \text{ g/cm}^3$ , since the 180°C-cured film is fully condensed. If degree of condensation is  $\delta$  and only uncondensed silanol groups (Si-OH) are left in the 80°C-cured film, then  $SLD_{80^\circ\text{C}} = SLD_{180^\circ\text{C}}\delta + SLD_{silanol}(1-\delta)$ . Taking the density increase when cured at 180°C into account, the degree of condensation can be calculated according to eq. 3:

$$SLD_{80^\circ\text{C}} = (SLD_{180^\circ\text{C}}\delta + SLD_{silanol}(1-\delta)) \times \frac{1.1}{1.2} \quad [3]$$

Based on the above calculation,  $88 \pm 5 \%$  silanol groups are condensed for the 80°C-cured virgin film.

### 3.1.2 Hydrothermal stability

For the 80°C-cured film, the fringes are less distinct after 10 and 24 hours aging, which indicates an increase of roughness. The SLD profiles show a broader SLD transitional region at the film-air interface also. However, the thickness and SLD of middle of the film remain unchanged, which indicates that the bulk of the film is robust under accelerated aging. The aging process neither hydrolyzes nor densifies the film.

For the 180°C-cured film, there are no noticeable changes even after 24-hours aging. Neither the thickness nor SLD of bulk film changes. Even the top surface remains as smooth as the virgin state.

Although it is expected that 80°C-cured films are vulnerable because of the insufficient condensation, [15] our observations show that the 80°C-cure is sufficient to provide good hydrothermal stability to bis-silane films except for the top surface. The elevated curing temperature leads to increased condensation, and therefore, further enhances the durability of both the bulk film and the surface.

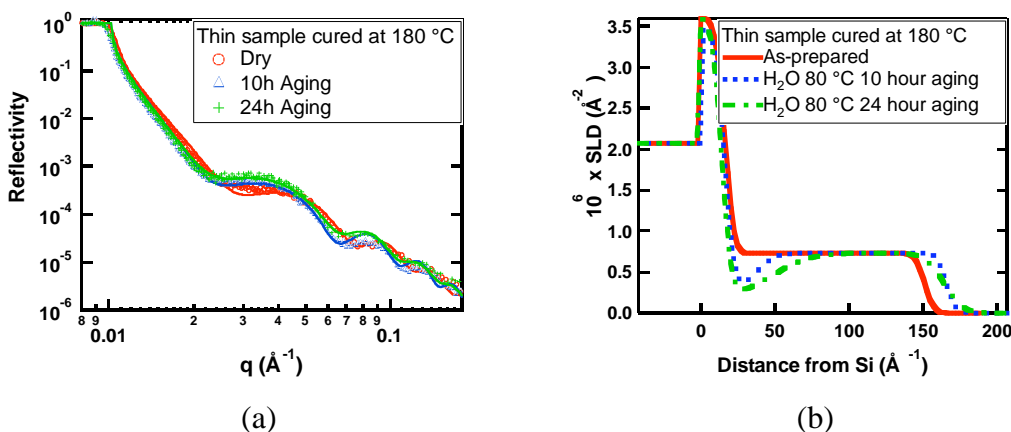


Figure 5. (a) Neutron reflectivity data from thin bis-sulfur silane film cured at 180°C, as-prepared and after aging in 80°C liquid H<sub>2</sub>O for 10 and 24 hours. The curves through the data points correspond to the best fits using model SLD profiles. (b) Best-fit SLD profiles corresponding to the curves through the data in (a). The data indicate considerable reconstruction of the film-substrate interface. The fits are not particularly good. A number of different structures were evaluated before settling on the two-layer-film model, which is the simplest structure that adequately represents the data.

### 3.2 Effect of film thickness

Films of two different thicknesses, deposited from 1% and 5% bis-sulfur silane solution and cured at 180°C, were measured to investigate the influence of film thickness on the hydrothermal stability. The reflectivity data at each aging stage of the thin sample (deposited from a 1% bis-sulfur silane solution) are plotted in Figure 5. The results for thick sample (deposited from a 5% bis-sulfur silane solution) are shown in Figure 3.

For the thin sample cured at 180°C (Figure 5a), one-uniform-layer structure was observed. The thickness of thin film is  $135 \pm 5$  Å, which is 10% of the thickness of the thick film. The SLD of thin film is  $(7.3 \pm 0.3) \times 10^{-7}$  Å<sup>-2</sup>, which indicates a fully

condensed state. However, after aging, changes occur near the film-silicon interface and at the top surface. After 10-hours aging, the total thickness of the film increases 10% due to the degradation and swelling of the film-silicon interface. Although most of the film retains its original SLD, a low SLD ( $2.8 \pm 0.5 \times 10^{-7} \text{ \AA}^{-2}$ ) region appears at the film-substrate interface. The width of this region is  $20 \pm 5 \text{ \AA}$ . The gradient between this region and bulk film indicates that this is a transitional region rather than a sharp interface. If the density decrease is the only cause of the SLD drop, the 62% SLD drop means that 62% of interfacial material is lost after 10 hours aging.

After 24 hours aging, the width of affected interfacial area increases from  $20 \pm 5 \text{ \AA}$  to  $35 \pm 5 \text{ \AA}$ . The SLD decreases further to  $2.0 \pm 0.3 \times 10^{-7} \text{ \AA}^{-2}$ , which indicates the density of interface drops another 11%. At the same time, the top surface becomes rough.

These phenomena indicate that for thin bis-sulfur film, the film-substrate interface is more vulnerable than bulk film. The interface is damaged during the hydrothermal degradation process and about 73 % of the material is lost after 24-hours aging. It is reasonable to believe that the failure will occur at the substrate interface for thin bis-sulfur film under hydrothermal conditions.

Compared with the stability of thick, high-temperature-cured bis-sulfur film, we conclude that a thickness greater than  $1000 \text{ \AA}$  is essential to achieve hydrothermal stability of bis-silane films.

#### 4. CONCLUSIONS

Neutron reflection has been used to study the hydrothermal degradation of different types of bis-sulfur silane films. Thickness is a key factor controlling hydrothermal stability. When the thickness is below  $200 \text{ \AA}$ , the film-substrate interface degrades. On the other hand, thicker films (above  $1000 \text{ \AA}$ ) are robust. Elevated curing temperature ( $180^\circ\text{C}$ ) gives improved hydrothermal stability to bis-sulfur films, by increasing the durability of top surface.

#### *Acknowledgments*

The neutron reflectivity data were collected with the use of the MIRROR reflectometer at the High Flux Isotope High Reactor at Oak Ridge National Laboratory and SPEAR reflectometer at the Lujan Center at Los Alamos National Laboratory. We thank Dr. Jaraslaw Majewski, and Mr. Erik Watkins for their help experiment and data analysis. Work at University of Cincinnati was sponsored by the Strategic Environmental Research and Development Program ([www.serdp.org](http://www.serdp.org)).

#### REFERENCES

1. E.P. Plueddemann, *Silane Coupling Agents*. 2nd ed., New York: Plenum Press. (1991)
2. W.J. van Ooij and T. Child, *Protecting metals with silane coupling agents*. Chemtech, **28**(2), pp.

- 26-35. (1998)
3. W.J. van Ooij and D. Zhu, *Electrochemical impedance spectroscopy of bis- triethoxysilylpropyl tetrasulfide on Al 2024-T3 substrates*. Corrosion, **57**(5), pp. 413-427. (2001)
  4. V. Schaftinghen , P. C. Le, H. Terryn, F. Horzenberger, *Investigation of the barrier properties of silanes on cold rolled steel*. Electrochimica Acta, **49**(17-18), pp. 2997-3004. (2004)
  5. D. Susac, X. Sun and K. A. R. Mitchell, *Adsorption of BTSE and gamma-APS organosilanes on different microstructural regions of 2024-T3 aluminum alloy*. Appli. Surface Sci., **207**(1-4), pp. 40-50. (2003)
  6. D. Zhu and W.J. van Ooij, *Corrosion protection of AA 2024-T3 by bis- 3- (triethoxysilyl)propyl tetrasulfide in sodium chloride solution. Part 2: mechanism for corrosion protection*. Corrosion Science, **45**(10): pp. 2177-2197. (2003)
  7. D. Zhu, W.J. van Ooij, *Surface Modification of Metals by Silanes*. in: *Adhesion Aspects of Polymeric Coatings*. Newark, NJ. (2000)
  8. A. Franquet, J. De Laet, T. Schram, H. Terryn, *Determination of the thickness of thin silane films on aluminium surfaces by means of spectroscopic ellipsometry*. Thin Solid Films, **384**(1), pp. 37-45. (2001)
  9. W.J. van Ooij, D. Zhu, G. Prasad, S. Jayaseelan, Y. Fu, N. Teredesai, *Silane based chromate replacements for corrosion control, paint adhesion, and rubber bonding*, Surf. Eng., **16** pp. 386-396. (2000)
  10. G. Pan, *Morphology and Properties of Anti-Corrosion Organosilane Films*, Ph.D. thesis in *Chemical and Materials Engineering*, University of Cincinnati: Cincinnati, OH. (2006)
  11. G. Pan and D. W. Schaefer, *Morphology and Water-Barrier Properties of Silane Films on Aluminum and Silicon*. Thin Solid Films, **503**: pp. 259-267. (2006)
  12. G. Pan, H. Yim, M.S. Kent, J. Majewski and D.W. Schaefer, *Effect of bridging group on the structure of bis-silane water-barrier films*. in *Silanes and Other Coupling Agents*, K.L. Mittal, Editor, V3, VSP: Utrecht, Netherlands. p. 39-50. (2004)
  13. H. Yim, M. Kent, W. F. McNamara, R. Ivkov, S. Satija, J. Majewski, *Hygrothermal degradation of (3-glycidoxypropyl)trimethoxysilane films studied by neutron and X-ray reflectivity and attenuated total reflection infrared spectroscopy*. Langmuir, **21**(10), pp. 4382. (2005)
  14. G. Pan, D. W. Schaefer, W.J. van Ooij, M. Kent, J. Majewski, H. Yim, *Morphology and Water Resistance of Mixed Silane Films of Bis[3-(triethoxysilyl) propyl]tetrasulfide and Bis-[trimethoxysilylpropyl]amine*. Thin Solid Films, **515**, pp. 2771-2780. (2006)
  15. G. Pan, D. W. Schaefer, J. Ilavsky, *Morphology and Water Barrier Properties of Organosilane Films: The Effect of Curing Temperature*. Journal of Colloid and Interface Science, **302**(1), pp. 287-293. (2006)
  16. R.J. Roe, *Methods of X-ray And Neutron Scattering In Polymer Science*. New York: Oxford University Press. pp. 1-34. (2000)

## XI. TECHNICAL PUBLICATIONS

### Published

T. Metroke, Y. Wang, W.J. van Ooij and D.W. Schaefer, “*Investigation of the Reaction Mechanism between Bis-[trimethoxysilypropyl]amine and Vinyltriacetoxysilane using NMR Spectroscopy*”. Chemistry of Materials, 2008

D.W. Schaefer, Y. Wang and T. Metroke, “*Metal Protective Films Based on Silane Coupling Agents, in Silanes and Other Coupling Agents*”, Vol. 5, K.L. Mittal, Editor. 2008, VSP: Leiden, Netherlands

P. Wang, G. Pan, W.A. Hamilton and D.W. Schaefer, “*Hydrothermal Degradation of Hydrophobic Organosilane Films Determined by Neutron Reflectometry*”, in Silanes and Other Coupling Agents, Vol. 5, K.L. Mittal, Editor. 2008, VSP: Leiden, Netherlands

Y. Wang, P. Wang, D. Kohls, W.A. Hamilton and D.W. Schaefer, “*Water absorption and transport in bis-amino silane films*”, in Silanes and Other Coupling Agents, Vol. 5, K.L. Mittal, Editor. 2008, VSP: Leiden, Netherlands

Y. Wang, P. Wang, D. Kohls, D.W. Schaefer and W.A. Hamilton, “*Water absorption and transport in bis-silane films*”. Langmuir, 2008. **Submitted**.

Y. Wang, E. Watkins, J. Ilavsky, T.L. Metroke, P. Wang, B. Lee and D.W. Schaefer, “*Water-Barrier Properties of Mixed Bis-[trimethoxysilypropyl]amine and Vinyl Triacetoxysilane Films*”, J. Phys. Chem. B, 2007. **111**: p. 7041-7051.

Seth, W.J. van Ooij, P. Puomi, T. Metroke, A. Apblett, “*Characterization of one-step, chromate-free, primer systems using liquid-state  $^{29}\text{Si}$  and  $^{13}\text{C}$  NMR*”, submitted to Progr. Org. Coat.

Yimin Wang, Paula Puomi and Wim J. van Ooij, “*Effect of Substrate Cleaning Solution pH on the Corrosion Performance of Silane-Coated Cold-Rolled Steel*”, J. Adhesion Sci. Technol., 21, 935-960 (2007)

Lin Yang, Naveen Simhadri, Anuj Seth and Wim J. van Ooij, “*Novel Corrosion Inhibitors for Silane Systems on Metals*”. Presented at the Fifth International Symposium on Silane and other Coupling Agents. Toronto, Canada, June 22-24, 2005; published in K.L. Mittal, editor, “Silanes and other Coupling Agents”, Volume 4, VSP, Leiden, 2007, pp. 287-306

Wim J. van Ooij, Karthik Suryanarayan, Tammy L. Metroke, “*Integral Epoxy Resin-Silane Primer System for Hot-dip Galvanized Steel*”. Presented at the Fifth International Symposium on Silane and other Coupling Agents. Toronto, Canada, June 22-24, 2005; published in K.L. Mittal, editor, “Silanes and other Coupling Agents”, Volume 4, VSP, Leiden, 2007, pp. 275-286

Akshay Ashirgade, Trilok Mugada, W J van Ooij, “*An ultra-flexible, chromate-free, low-VOC, Silane-based finishing and coating system for Corrosion Protection of Aluminum Alloys*”. Presented at the Fifth International Symposium on Silane and other Coupling Agents. Toronto, Canada, June 22-24, 2005; published in K.L. Mittal, editor, “Silanes and other Coupling Agents”, Volume 4, VSP, Leiden, 2007, pp. 331-354

Senthilkumar Chandrasekaran, W J van Ooij, Tammy L Metroke, “*Electrodeposition of Aromatic Bis-silanes for pretreatment of Al Alloys*”. Presented at the Fifth International Symposium on Silane and other Coupling Agents. Toronto, Canada, June 22-24, 2005; published in K.L. Mittal, editor, “Silanes and other Coupling Agents”, Volume 4, VSP, Leiden, 2007, pp. 219-230

Anuj Seth and Wim J. van Ooij, “*A novel low-VOC, Chromate free, One-step Primer System for the Corrosion Protection of Metals and Alloys*”. Presented at the Fifth International Symposium on Silane and other Coupling Agents. Toronto, Canada, June 22-24, 2005; published in K.L. Mittal, editor, “Silanes and other Coupling Agents”, Volume 4, VSP, Leiden, 2007, pp. 307-330

Ramakrishna Nookala, Yimin Wang and Wim J. van Ooij, “*Performance of Silanes in protecting Metals from Corrosion Effect of Substrate Cleaning*”. Presented at the Fifth International Symposium on Silane and other Coupling Agents. Toronto, Canada, June 22-24, 2005; published in K.L. Mittal, editor, “Silanes and other Coupling Agents”, Volume 4, VSP, Leiden, 2007, pp. 231-252

Chetan Shivane, Naveen B. Simhadri and W. J. van Ooij, “*Improved water-based silane pretreatment for HDG substrates*”. Presented at the Fifth International Symposium on Silane and other Coupling Agents. Toronto, Canada, June 22-24, 2005; published in K.L. Mittal, editor, “Silanes and other Coupling Agents”, Volume 4, VSP, Leiden, 2007, pp. 253-274

A. Seth, W.J. van Ooij, P. Puomi, Z. Yin, A. Ashirgade, S. Bafna and C. Shivane, “*Novel, One-Step, Chromate-free Coatings containing Anticorrosion Pigments for Metals – An Overview and Mechanistic Study*”, Prog. Org Coat., **58**, 136-145 (2007)

G. Pan and D.W. Schaefer, “*Are Silane Films Water Barriers?*”, in Silanes and Other Coupling Agents, Vol. 4, K.L. Mittal, Editor. 2007, VSP: Leiden, Netherlands. p. 3-16

G. Pan, E. Watkins, J. Majewski and D.W. Schaefer, “*Effect of Thickness on the Water-Barrier Properties of Silane Films*”. Journal of Physical Chemistry C, 2007. **111**: p. 15325-15330

Y. Wang, E. Watkins, J. Ilavsky, T.L. Metroke, P. Wang, B. Lee and D.W. Schaefer, “*Water-Barrier Properties of Mixed Bis-[trimethoxysilylpropyl]amine and Vinyl Triacetoxysilane Films*”, J. Phys. Chem. B, 2007. **111**: p. 7041-7051

Wang Y., Puomi P. and Van Ooij W.J., “*Effect of Cleaning Solution pH on the Corrosion Performance of Silane-coated Cold-rolled Steel*”, accepted for publication in J.A.S.T. (2007)

Ashirgade, T. Mugada and W. J. van Ooij, “*An ultra-flexible, chromate-free, low-VOC, silane-based finishing and coating system for corrosion protection of aluminum alloys*”, in Silanes and Other Coupling Agents, ed. K.L. Mittal. Vol. 4. 2006, VSP: Utrecht, Netherlands

Schaefer, D.W., G. Pan and W.J. van Ooij, “*Chromate-Free Coatings for Corrosion Protection*”. Los Alamos Science, 2006. 30: p. 172-177

Shivane, Naveen BV Simhadri and Wim J. van Ooij, “*Improved Water-based Silane Pretreatment for Hot-Dip Galvanized Steel Substrates*”, in Silanes and Other Coupling Agents, ed. K.L. Mittal. Vol. 4. 2006, VSP: Utrecht, Netherlands

G. Pan and D.W. Schaefer, “*Morphology and Water-Barrier Properties of Silane Films on Aluminum and Silicon*”. Thin Solid Films, 2006. **503**: p. 259-267.

G. Pan, D.W. Schaefer and J. Ilavsky, “*Morphology and Water Barrier Properties of Organosilane Films: The Effect of Curing Temperature*”, Journal of Colloid and Interface Science, 2006. **302**(1): p. 287-293.

G. Pan, D.W. Schaefer, W.J. van Ooij, M.S. Kent, J. Majewski and H. Yim, “*Morphology and Water Resistance of Mixed Silane Films of Bis[3-(triethoxysilyl) propyl] tetrasulfide and Bis-[trimethoxysilylpropyl]amine*”. Thin Solid Films, 2006. **515**: p. 2771-2780.

D.W. Schaefer, G. Pan and W.J. van Ooij, “*Chromate-Free Coatings for Corrosion Protection*”. Los Alamos Science, 2006. **30**: p. 172-177.

Pan, G., E. Watkins, D.W. Schaefer and J. Majewski, “*Effect of thickness on the water-barrier properties of silane films*”, Journal of Colloid and Interface Science, 2006: p. submitted

W.J. van Ooij, A. Seth, T. Maguda, G. Pan and D.W. Schaefer. “*A Novel Self-priming Coating for Corrosion Protection*”. in *International Surface Engineering Congress and Exposition*. 2005.

G. Pan, H. Yim, M.S. Kent, J. Majewski and D.W. Schaefer, “*Effect of bridging group on the structure of bis-silane water-barrier films*”, in *Silanes and Other Coupling Agents Vol. 3*, K.L. Mittal, Editor. 2004, VSP: Utrecht, Netherlands. p. 39-50.

G. Pan, H. Yim, M.S. Kent, J. Majewski and D.W. Schaefer, “*Neutron reflectivity investigation of bis-amino silane films*”. Journal of Adhesion Science and Technology, 2003. **17**(16): p. 2175-2189.

### **Conference Proceedings**

Van Ooij, W.J. and Puomi P., “*Corrosion Protection of Automotive Steels by Novel Water-borne Primer Systems*”, to be published in Proceedings of International Corrosion Engineering Conference, Seoul, Korea, May 20-24, 2007

Yin Z., Van Ooij, W.J. and Puomi P., “*Replacements for Chromate Pigments in Anticorrosion Primers for Aluminum Alloys*”, to be published in Proceedings of International Corrosion Engineering Conference, Seoul, Korea, May 20-24, 2007

Yin Z., Van Ooij W.J., Puomi P., Seth A. and Shivane C., “*A Novel Series of Low-VOC, Chromate-free Metal Primers*”, 14th Asian-Pacific, Corrosion Control Conference, October 21-24, Shanghai, China, 2006

Shivane C., Puomi P. and Van Ooij W.J., “*Environmentally Friendly Anti-Corrosion Primers for HDG steel*”, 15th IFHSTE and SMT20, 25-29 September, Vienna, Austria, Europe, 2006.

Hansal S., Hansal W.E.G, Van Ooij W.J and Puomi P., “*Chromate replacement in aluminum corrosion protection coatings*”, 15th IFHSTE and SMT20, 25-29 September, Vienna, Austria, Europe, 2006

Shivane C., Puomi P. and Van Ooij W.J., “*Novel coating systems for automotive steels*”, paper published on a conference CD, Eurocorr 2006 in Maastricht, Sep 24-28, 2006

Ashirgade A., Puomi P, Van Ooij W.J., Bafna S., Seth A., Shivane C. and Yin Z., “*Novel, One-step, Chromate-free Coatings Containing Anticorrosion Pigments for Metals that can be used in a Variety of Industries*”, paper published on a conference CD, Eurocorr 2006 in Maastricht, Sep 24-28, 2006

Van Ooij W.J., Puomi P., Ashirgade A., Bafna S., Seth A., Shivane C. and Yin Z., “*Low-VOC, Chromate-free, Anti-corrosion Primers for Aluminum Alloys and HDG steel*”, presented at Megarust 2006, June 12-15, Norfolk, Virginia,

### **Published Technical Abstracts**

Puomi P., Van Ooij W.J., Seth A., Yin Z., Ashirgade A., Bafna S. and Shivane C., Novel, “*One-step, Chromate-free Coatings Containing Anticorrosion Pigments for Metals*”, Extended Abstract in the Book of Abstracts of Coatings Science International, Noordwijk, The Netherlands, 26-30 June (2006) 74-78

Ashirgade, P. Puomi, P. Wang, Y. Wang, Z. Yin, W.J. van Ooij and D. Schaefer, “*Superprimers: Chromate-free coating systems for DoD applications*”, SERDP Annual Symposium, November 28-30, Washington D.C., Washington, 2006.

### **Presentations at Conferences by Wim J. van Ooij**

#### **International Corrosion Engineering Conference, Seoul, Korea, 20-24 May 2007**

William J. van Ooij and Paula Puomi, “Corrosion Protection of Automotive steel by Novel Water-Borne Primer Systems”

Zhangzhang Yin, Wim van Ooij and Paula Puomi, “Replacement for Chromate Pigments in Anticorrosion Primers for Aluminum Alloys”

Wim van Ooij, Paula Puomi, Zhangzhang Yin and Anuj Seth, “Replacement of Zinc Phosphating and e-coating by a one step Primer”

#### **International Symposium On Silanes and other Coupling Agents, Cincinnati, OH, 13-15 June 2007**

W.J. van Ooij, “Overview of Potential of Silanes to Protect Metals against Corrosion Phenomena”

Paula Puomi, Zhangzhang Yin, Wim J. van Ooij, Akshay Ashirgade and Anuj Seth, “Novel Chromate-Free Silane-Containing SUPERprimer Technology”

Danqing Zhu, Man Xu and Wim J. van Ooij, “Corrosion Protection of Galvanized steel with water-borne silane-based systems”

Zhangzhang Yin, Akshay Ashirgade, Anuj Seth, Paula Puomi and W.J. van Ooij, “Zinc Phosphate as an Effective Anticorrosion Pigment in Silane-based Waterborne Primers”

**Materials Science and Technology (MS&T07), Detroit, MI, 16-20 September 2007**

W.J. Van Ooij, Paula Puomi, Zhangzhang Yin and Anuj Seth, “An Attempt to Simplify the Metal Pretreatments prior to Painting in the Automotive Industry”

**Future Coat, Toronto, Canada, 3-5 October 2007**

W.J. Van Ooij, Paula Puomi, Zhangzhang Yin and Anuj Seth, “A Two-Pack Epoxy-Acrylate Primer for Corrosion Protection of Metals”

**Published Text Books or Book Chapters**

Van Ooij W.J. and Puomi P., “*Environmental and Solubility Issues Related to Novel Corrosion Control*”, chapter 6 in THERMODYNAMICS, SOLUBILITY AND ENVIRONMENTAL ISSUES, Edited by Trevor Letcher, Stratton on the Fosse, UK, Elsevier B.V., in print, 2007

**Invention disclosures filed by Wim van Ooij with the University of Cincinnati and licensed to ECOSIL Technologies LLC**

107-086 Treatment of Batch HDG for White Rust Protection

107-108 Enhanced Performance of Superprimers by Electrodeposition

108-001 A new, anti-corrosion Pigment for Water-borne Primers on cold-rolled Steel

108-021 A borosilicate Pigment for Primers on Steel

**Awards**

Collano Innovation Award 2008 for Superprimer Technology (Horw, Switzerland)

## **XII. OTHER TECHNICAL MATERIAL**

### **Patents**

William J. van Ooij, Karthik Suryanarayanan, Jaspreet Singh Gandhi, Naveen Simhadri, Chetan Shivane, Matthew Stacy and Danqing Zhu, US Pat. Application, March 2, 2006, "Silane Coating Compositions and Methods of Use Thereof"

W.J. van Ooij, Max Sorenson, Charles Smith, Ramakrishna Nookala and Kevin Williams, US Pat. Application, March 2, 2006, Method of Applying Silane to Metal Composition"

W.J. van Ooij and Karthik Suryanarayanan, US Pat. Appl., 31 January 2005, "Integral Resin-Coating System"

W.J. van Ooij, A. Seth, T. Mugada and K. Suryanarayanan, Provisional US Pat. Application, December 22, 2004, "Improved Superprimer"

W.J. van Ooij and Matt Stacy, PCT Application, July 24, 2003, "Superprimer"

**Protocols** – none

**EPA/State Regulatory Permits** - none

### **Awards** -

a) Wim van Ooij - PI

- Collano Innovation Award 2007; this is an annual award by Collano AG, a Swiss resin company; they award two innovative technologies on a worldwide basis; for 2008 they selected the superprimer technology, the first time an award was given to a non-European technology
- UC Special Achievement Award 2006; the PI received this Special Award from the University of Cincinnati for Submitting his 100th Invention Disclosure, a record at this University
- UC Emerging Entrepreneur Award 2005 for founding ECOSIL Technologies LLC

**Scientific/Technical honors** - see Awards